

Onkar N. Tripathi
Ursula Ravens
Michael C. Sanguinetti
Editors

Heart Rate and Rhythm

Molecular Basis,
Pharmacological Modulation
and Clinical Implications



Heart Rate and Rhythm

Onkar N. Tripathi • Ursula Ravens •
Michael C. Sanguinetti
Editors

Heart Rate and Rhythm

Molecular Basis, Pharmacological
Modulation and Clinical Implications



Springer

Editors

Prof. Dr. Onkar N. Tripathi
Life Sciences Academy
103 Usman Enclave
Aliganj Sector "O"
Lucknow 226024
India
onkar.tripathi@gmail.com

Prof. Dr. Ursula Ravens
Department of Pharmacology and
Toxicology
Fetscherstraße 74
01307 Dresden
Germany
ravens@rcs.urz.tu-dresden.de

Prof. Dr. Michael C. Sanguinetti
Department of Physiology
Nora Eccles Harrison Cardiovascular
Research & Training Institute
University of Utah
95 South 2000 East
Salt Lake City, Utah 84112
USA
sanguinetti@cvrti.utah.edu

ISBN 978-3-642-17574-9 e-ISBN 978-3-642-17575-6
DOI 10.1007/978-3-642-17575-6
Springer Heidelberg Dordrecht London New York

Library of Congress Control Number: 2011924778

© Springer-Verlag Berlin Heidelberg 2011

This work is subject to copyright. All rights are reserved, whether the whole or part of the material is concerned, specifically the rights of translation, reprinting, reuse of illustrations, recitation, broadcasting, reproduction on microfilm or in any other way, and storage in data banks. Duplication of this publication or parts thereof is permitted only under the provisions of the German Copyright Law of September 9, 1965, in its current version, and permission for use must always be obtained from Springer. Violations are liable to prosecution under the German Copyright Law.

The use of general descriptive names, registered names, trademarks, etc. in this publication does not imply, even in the absence of a specific statement, that such names are exempt from the relevant protective laws and regulations and therefore free for general use.

Cover design: deblik, Berlin

Printed on acid-free paper

Springer is part of Springer Science+Business Media (www.springer.com)

Preface

The heart is a remarkable electrically activated rhythmic muscular pump responsible for distributing blood to the lungs, brain visceral organs, skeletal muscle other organs and to itself. The intrinsic pumping rate is normally set by pacemaker cells in the sinoatrial node, but the resulting physiological rhythm is variable and highly modulated by the autonomic nervous system and humoral factors. Pathological heart rhythm is a major health issue. Sudden death caused by cardiac arrhythmias is a significant cause of mortality worldwide. In the USA alone, it has been estimated that nearly 300,000 emergency medical services-treated cardiac arrests occur outside a hospital setting each year. In young adults, cardiac arrests are often associated with cardiac abnormalities (either structural or electrical) and can be triggered by intense physical activity or emotion. In adults, the most common underlying cause of lethal arrhythmias (ventricular tachycardia or fibrillation) is coronary artery disease. A minority of cardiac arrests are due to extreme bradycardia or side effects of drug therapy or abuse. Treatment for cardiac arrhythmia includes drugs, implantable pacemakers or cardioverter/defibrillator devices, catheter ablation or surgical resection.

Due to the primary importance of the heart in the life of vertebrates, it is only natural that the molecular and cellular basis of normal and pathophysiological heart rhythms is an intense area of both basic and biomedical research. During the past 50 years, biophysical approaches such as microelectrode recording of intracellular action potentials of isolated cardiac tissue and the voltage clamp technique used to record ionic currents in isolated myocytes led to the remarkable insights into our understanding of the electrical basis of cardiac pacemaking, impulse conduction and myocardial contraction. In the past few decades, molecular biology, genetics, and biochemical approaches have defined the molecular basis, as well as the specific cellular location, of the plethora of ion channels and transporters that underlie the ionic currents identified by voltage clamp techniques and how their synchronized activity controls the basic rate and rhythm of the heart. The resulting information explosion has made it difficult for investigators to keep abreast of new findings in fields outside their areas of expertise and served as motivation for this volume. Here we have endeavored to bring together experts from various fields who share a passion for understanding the mechanisms of cardiac pacemaking and arrhythmogenesis. Individual chapters cover a full range of topics, including the

ionic basis of pacemaking, the role of specific channels and transporters in sinoatrial node pacemaking, altered intracellular Ca^{2+} handling in response to disease, computer modeling of the action potentials of pacemaker and working cardiomyocytes, genetic and molecular basis of inherited arrhythmias, development of cardiac conduction system and a review of novel antiarrhythmic agents. Due to the key importance of the specialized pacemaker cells and tissue (sinoatrial and atrioventricular nodes, Purkinje fibers) in maintaining heart rate and rhythm, special emphasis is placed on the peculiar electrophysiology of these cells. The intended audience for this book includes investigators in the fields of cardiac electrophysiology and arrhythmia, advanced graduate students, cardiologists and pharmaceutical industry. It is our hope that the topics and unresolved issues highlighted here will serve to both educate and motivate continued interest in research of the complicated molecular and cellular mechanisms that underlie normal and pathophysiological cardiac rhythms.

We thank all the experts who contributed chapters on various specialized topics for this book despite their very busy schedule. It has been a pleasure working with colleagues at Springer; Jutta Lindenborn offered sustained help and support at all the stages of preparation of this book. We appreciate the art work by Mr. Ali Kausar on several illustrations included in this book.

Lucknow, Uttar Pradesh, India
Dresden, Germany
Salt Lake City, UT, USA

Onkar N. Tripathi
Ursula Ravens
Michael C. Sanguinetti

Contents

Part I Normal Cardiac Rhythm and Pacemaker Activity

1 Cardiac Ion Channels and Heart Rate and Rhythm	3
Onkar Nath Tripathi	
2 Ionic Basis of the Pacemaker Activity of SA Node Revealed by the Lead Potential Analysis	33
Yukiko Himeno, Chae Young Cha, and Akinori Noma	
3 The “Funny” Pacemaker Current	59
Andrea Barbuti, Annalisa Bucchi, Raffaella Milanesi, Georgia Bottelli, Alessia Crespi, and Dario DiFrancesco	
4 Novel Perspectives on Cardiac Pacemaker Regulation: Role of the Coupled Function of Sarcolemmal and Intracellular Proteins	83
Victor A. Maltsev, Tatiana M. Vinogradova, and Edward G. Lakatta	
5 Pacemaker Activity of the SA Node: Insights from Dynamic-Clamp Experiments	101
Ronald Wilders, Antoni C.G. van Ginneken, and Arie O. Verkerk	
6 Heart Rate Variability: Molecular Mechanisms and Clinical Implications	119
Kishore K. Deepak	
7 Mechano-Electric Feedback in the Heart: Effects on Heart Rate and Rhythm	133
T. Alexander Quinn, Rebecca A. Bayliss, and Peter Kohl	

Part II Modeling

- 8 A Historical Perspective on the Development of Models of Rhythm in the Heart** 155
Penelope J. Noble and Denis Noble
- 9 Simulation of Cardiac Action Potentials** 175
Jonathan D. Moreno and Colleen E. Clancy

Part III Cardiac Development and Anatomy

- 10 Development of Pacemaker Activity in Embryonic and Embryonic Stem Cell-Derived Cardiomyocytes** 197
Huamin Liang, Michael Reppel, Ming Tang, and Jürgen Hescheler
- 11 Molecular Basis of the Electrical Activity of the Atrioventricular Junction and Purkinje Fibres** 211
Halina Dobrzynski, Oliver Monfredi, Ian D. Greener, Andrew Atkinson, Shin Inada, Mary-Anne Taube, Joseph Yanni, Olga Fedorenko, Peter Molenaar, Robert H. Anderson, Igor R. Efimov, and Mark R. Boyett
- 12 Molecular Basis and Genetic Aspects of the Development of the Cardiac Chambers and Conduction System: Relevance to Heart Rhythm** 231
Martijn L. Bakker, Vincent M. Christoffels, and Antoon F.M. Moorman
- 13 Role of the T-Tubules in the Response of Cardiac Ventricular Myocytes to Inotropic Interventions** 255
C.H. Orchard, F. Brette, A. Chase, and M.R. Fowler

Part IV Mechanisms of Acquired Arrhythmia

- 14 An Overview of Spiral- and Scroll-Wave Dynamics in Mathematical Models for Cardiac Tissue** 269
Rupamanjari Majumder, Alok Ranjan Nayak, and Rahul Pandit
- 15 Post-infarction Remodeling and Arrhythmogenesis: Molecular, Ionic, and Electrophysiological Substrates** 283
Nabil El-Sherif

16 The Role of Intracellular Ca²⁺ in Arrhythmias in the Postmyocardial Infarction Heart	305
Wen Dun, Henk ter Keurs, and Penelope A. Boyden	
17 Molecular and Biochemical Characteristics of the Intracellular Ca²⁺ Handling Proteins in the Heart	323
Yasser Abdellatif, Vijayan Elimban, Delfin Rodriguez-Leyva, and Naranjan S. Dhalla	
18 Pharmacological Modulation and Clinical Implications of Sarcolemmal Ca²⁺-Handling Proteins in Heart Function	337
Yasser Abdellatif, Adriana Adameova, and Naranjan S. Dhalla	
19 Calmodulin Kinase II Regulation of Heart Rhythm and Disease ...	351
Thomas J. Hund	
20 MicroRNA and Pluripotent Stem Cell-Based Heart Therapies: The Electrophysiological Perspective	365
Ellen Poon, Deborah K. Lieu, and Ronald A. Li	

Part V Mechanisms of Inherited Arrhythmia

21 Intracellular Calcium Handling and Inherited Arrhythmogenic Diseases	387
Nicola Monteforte, Carlo Napolitano, Raffaella Bloise, and Silvia G. Priori	
22 Molecular Mechanisms of Voltage-Gated Na⁺ Channel Dysfunction in LQT3 Syndrome	409
Thomas Zimmer and Klaus Benndorf	
23 The Short QT Syndrome	431
Jules C. Hancox, Mark J. McPate, Aziza El Harchi, Rona S. Duncan, Chris E. Dempsey, Harry J. Witchel, Ismail Adeniran, and Henggui Zhang	
24 Adrenergic Regulation and Heritable Arrhythmias: Key Roles of the Slowly Activating Heart I_{Ks} Potassium Channel	451
David Y. Chung, Kevin J. Sampson, and Robert S. Kass	

25 Defects in Ankyrin-Based Protein Targeting Pathways in Human Arrhythmia	461
Hjalti Gudmundsson, Francis Jareczek, and Peter J. Mohler	
26 Genetically Modified Mice: Useful Models to Study Cause and Effect of Cardiac Arrhythmias?	473
Gregor Sachse, Martin Kruse, and Olaf Pongs	
27 Genetics of Atrial Fibrillation	485
Saagar Mahida, Michiel Rienstra, Moritz F. Sinner, Steven A. Lubitz, Patrick T. Ellinor, and Stefan Kääb	

Part VI Role of Specific Channels and Transporters in Arrhythmia

28 The Role of Gap Junctions in Impulse Propagation in the Heart: New Aspects of Arrhythmogenesis and New Antiarrhythmic Agents Targeting Gap Junctions	503
Stefan Dhein, Joanna Jozwiak, Anja Hagen, Thomas Seidel, Anna Dietze, Aida Salameh, Martin Kostelka, and Friedrich Wilhelm Mohr	
29 Possible Mechanisms of the Acute Ischemia-Induced Ventricular Arrhythmias: The Involvement of Gap Junctions	525
Ágnes Végh and Rita Papp	
30 Role of NCX1 and NHE1 in Ventricular Arrhythmia	543
András Tóth and András Varró	
31 TRP Channels in Cardiac Arrhythmia: Their Role During Purinergic Activation Induced by Ischemia	563
Guy Vassort and Julio Alvarez	
32 Cardiac Aquaporins: Significance in Health and Disease	581
Tanya L. Butler and David S. Winlaw	

Part VII Drugs and Cardiac Arrhythmia

33 Ion Channels as New Drug Targets in Atrial Fibrillation	599
Ursula Ravens	
34 hERG1 Channel Blockers and Cardiac Arrhythmia	611
Michael C. Sanguinetti and Matthew Perry	

Contents	xi
35 Preclinical Drug Safety and Cardiac Ion Channel Screening	627
Zhi Su and Gary Gintant	
36 QT Prolongation Is a Poor Predictor of Proarrhythmia Liability: Beyond QT Prolongation!	639
Luc M. Hondeghem	
37 K Channel Openers as New Anti-arrhythmic Agents	655
Nathalie Strutz-Seebohm and Guiscard Seebohm	
Index	669

Contributors

Yasser Abdellatif Institute of Cardiovascular Sciences, St. Boniface General Hospital Research Centre, Winnipeg, MB, Canada; Department of Physiology, Faculty of Medicine, University of Manitoba, Winnipeg, MB, Canada

Adriana Adameova Institute of Cardiovascular Sciences, St. Boniface General Hospital Research Centre, Winnipeg, MB, Canada; Department of Physiology, Faculty of Medicine, University of Manitoba, Winnipeg, MB, Canada

Ismail Adeniran Biological Physics Group, School of Physics and Astronomy, University of Manchester, Manchester M13 9PL, UK

T. Alexander Quinn Department of Physiology, Anatomy and Genetics, Cardiac Mechano-Electric Feedback Group, University of Oxford, Oxford, UK, alex.quinn@dpag.ox.ac.uk

Julio Alvarez Laboratorio de Electrofisiologia, Instituto de Cardiología, La Habana, Cuba

Robert H. Anderson University of Manchester, Manchester, UK

Andrew Atkinson University of Manchester, Manchester, UK

Martijn L. Bakker Heart Failure Research Center, Academic Medical Center, Meibergdreef 15, 1105 AZ Amsterdam, The Netherlands

Andrea Barbuti Department of Biomolecular Sciences and Biotechnology, University of Milano, Via Celoria 26, 20133 Milano, Italy, andrea.barbuti@unimi.it

Rebecca A. Bayliss Balliol College, University of Oxford, Oxford, UK

Klaus Benndorf Institute of Physiology II, University Hospital Jena, Friedrich Schiller University Jena, Kollegiengasse 9, Jena 07743, Germany

Raffaella Bloise Molecular Cardiology, Fondazione S. Maugeri IRCCS, Via Salvatore Maugeri 10/10A, 27100 Pavia, Italy

Georgia Bottelli Department of Biomolecular Sciences and Biotechnology, University of Milano, Via Celoria 26, 20133 Milano, Italy

Penelope A. Boyden Department of Pharmacology, Center for Molecular Therapeutics, Columbia University, New York, NY, USA, pab4@columbia.edu

Mark R. Boyett University of Manchester, Manchester, UK

F. Brette Faculty of Life Sciences, University of Manchester, Manchester, M13 9NT, UK

Annalisa Bucchi Department of Biomolecular Sciences and Biotechnology, University of Milano, Via Celoria 26, 20133 Milano, Italy

Tanya L. Butler Kids Heart Research, The Children's Hospital at Westmead, Locked Bag 4001, Westmead NSW 2145, Sydney, Australia, TanyaB@chw.edu.au

A. Chase School of Physiology and Pharmacology, Medical Sciences Building, University of Bristol, Bristol BS8 1TD, UK,

Vincent M. Christoffels Heart Failure Research Center, Academic Medical Center, Meibergdreef 15, 1105 AZ Amsterdam, The Netherlands

David Y. Chung Department of Pharmacology, College of Physicians and Surgeons of Columbia University, 630 W. 168th St., New York, NY 10032, USA

Colleen E. Clancy Department of Pharmacology, University of California, Genome Building Rm 3503, Davis, CA 95616-8636, USA, ceclancy@ucdavis.edu

Alessia Crespi Department of Biomolecular Sciences and Biotechnology, University of Milano, Via Celoria 26, 20133 Milano, Italy

Kishore K. Deepak Autonomic Function Laboratory, Department of Physiology, All India Institute of Medical Sciences, New Delhi, Delhi 110608, India, kkdeepak@gmail.com

Chris E. Dempsey Department of Biochemistry, School of Medical Sciences, University Walk, Bristol BS8 1TD, UK

Naranjan S. Dhalla Institute of Cardiovascular Sciences, St. Boniface General Hospital Research Centre, Winnipeg, MB, Canada; Department of Physiology, Faculty of Medicine, University of Manitoba, Winnipeg, MB, Canada, nsdhalla@sbrc.ca

Stefan Dhein Heart Centre Leipzig, Clinic for Cardiac Surgery, University of Leipzig, Struempellstr. 39, 04289 Leipzig, Germany, dhes@medizin.uni-leipzig.de

Anna Dietze Heart Centre Leipzig, Clinic for Cardiac Surgery, University of Leipzig, Struempellstr. 39, 04289 Leipzig, Germany

Dario Di Francesco Department of Biomolecular Sciences and Biotechnology, University of Milano, Via Celoria 26, 20133 Milano, Italy

Halina Dobrzynski University of Manchester, Manchester, UK, halina.dobrzynski@manchester.ac.uk

Wen Dun Department of Pharmacology, Center for Molecular Therapeutics, Columbia University, New York, NY, USA

Rona S. Duncan Department of Physiology and Pharmacology, School of Medical Sciences, University Walk, Bristol BS8 1TD, UK

Igor R. Efimov Washington University, St. Louis, MO, USA

Vijayan Elimban Institute of Cardiovascular Sciences, St. Boniface General Hospital Research Centre, Winnipeg, MB, Canada; Department of Physiology, Faculty of Medicine, University of Manitoba, Winnipeg, MB, Canada

Patrick T. Ellinor Cardiovascular Research Center, Massachusetts General Hospital, Charlestown, MA, USA; Cardiac Arrhythmia Service, Massachusetts General Hospital, Boston, MA, USA

Nabil El-Sherif State University of New York, Downstate Medical Center, VA New York Harbor Healthcare System, Brooklyn, NY, USA, nelsherif@aol.com

Olga Fedorenko University of Manchester, Manchester, UK

M.R. Fowler Cardiovascular Physiology, University of Glasgow, Glasgow G12 8QQ, UK

Gary Gintant Department of Integrative Pharmacology, Global Pharmaceutical Research and Development, Abbott Laboratories, 100 Abbott Park Road, Abbott Park, IL 60064, USA, gary.gintant@abbott.com

Ian D. Greener University of Manchester, Manchester, UK

Hjalti Gudmundsson Department of Internal Medicine, Division of Cardiovascular Medicine, University of Iowa, Iowa City, IA, USA

Anja Hagen Heart Centre Leipzig, Clinic for Cardiac Surgery, University of Leipzig, Struempellstr. 39, 04289 Leipzig, Germany

Jules C. Hancox Department of Physiology and Pharmacology, School of Medical Sciences, University Walk, Bristol BS8 1TD, UK, Jules.Hancox@bristol.ac.uk

Aziza El Harchi Department of Physiology and Pharmacology, School of Medical Sciences, University Walk, Bristol BS8 1TD, UK

Jürgen Hescheler Institute of Neurophysiology, University of Cologne, Cologne, Germany, j.hescheler@uni-koeln.de

Yukiko Himeno Biosimulation Project, Faculty of Medicine, Kyoto University, 54 Kawara-cho, Shogoin, Sakyo-ku, Kyoto 606-8507, Japan, himeno@biosim.med.kyoto-u.ac.jp

Luc M. Hondeghem Pharmacology, Catholic University Leuven, Westlaan 85, 8400 Oostende, Belgium, Luc.Hondeghem@screenQT.com

Thomas J. Hund Department of Internal Medicine, University of Iowa Carver College of Medicine, 285 Newton Rd. 2269 CBRB, Iowa City, IA 52242, USA, thomas-hund@uiowa.edu

Shin Inada University of Manchester, Manchester, UK, thomas-hund@uiowa.edu

Francis Jareczek Department of Internal Medicine, Division of Cardiovascular Medicine, University of Iowa, Iowa City, IA, USA

Joanna Jozwiak Heart Centre Leipzig, Clinic for Cardiac Surgery, University of Leipzig, Struempellstr. 39, 04289 Leipzig, Germany

Stefan Käab Department of Medicine I, Ludwig-Maximilians-University Munich, Klinikum Grosshadern, Marchioninstr. 15, Munich 81377, Germany, stefan.kaab@med.uni-muenchen.de

Robert S. Kass Department of Pharmacology, College of Physicians and Surgeons of Columbia University, 630 W. 168th St., New York, NY 10032, USA, rsk20@columbia.edu

Henk terKeurs University of Calgary, Calgary, AB, Canada

Peter Kohl National Heart and Lung Institute, Imperial College of Science, Technology and Medicine, London, UK

Martin Kostelka Heart Centre Leipzig, Clinic for Cardiac Surgery, University of Leipzig, Struempellstr. 39, 04289 Leipzig, Germany

Martin Kruse Institut für Neurale Signalverarbeitung, ZMNH, University Hospital Hamburg-Eppendorf, Martinistr. 52, 20246 Hamburg, Germany

Edward G. Lakatta Laboratory of Cardiovascular Science, NIA Intramural Research Program, NIH, 5600 Nathan Shock Drive, Baltimore, MA 21224, USA

Ronald A. Li Stem Cell and Regenerative Medicine Program, Heart, Brain, Hormone and Healthy Ageing Research Center and Department of Medicine, University of Hong Kong, Hong Kong, China; Center of Cardiovascular Research, Mount Sinai School of Medicine, Atran Berg Laboratory Building Floor 3 Room 3-22, 1428 Madison Avenue, New York, NY 10029, USA, ronaldli@mssm.edu

Huamin Liang Institute of Neurophysiology, University of Cologne, Cologne, Germany; Department of Physiology, Tongji Medical College, Huazhong University of Science and Technology, Wuhan, Hubei, China

Deborah K. Lieu Center of Cardiovascular Research, Mount Sinai School of Medicine, Atran Berg Laboratory Building Floor 3 Room 3-22, 1428 Madison Avenue, New York, NY 10029, USA

Steven A. Lubitz Cardiovascular Research Center, Massachusetts General Hospital, Charlestown, MA, USA; Cardiac Arrhythmia Service, Massachusetts General Hospital, Boston, MA, USA

Saagar Mahida Cardiovascular Research Center, Massachusetts General Hospital, Charlestown, MA, USA

Rupamanjari Majumder Centre for Condensed Matter Theory, Department of Physics, Indian Institute of Science, Bangalore, Karnataka 560012, India

Victor A. Maltsev Laboratory of Cardiovascular Science, NIA Intramural Research Program, NIH, 5600 Nathan Shock Drive, Baltimore, MA 21224, USA, MaltsevVi@grc.nia.nih.gov

Mark J. McPate Department of Physiology and Pharmacology, School of Medical Sciences, University Walk, Bristol BS8 1TD, UK

Raffaella Milanesi Department of Biomolecular Sciences and Biotechnology, University of Milano, Via Celoria 26, 20133 Milano, Italy

Peter J. Mohler Department of Internal Medicine, Division of Cardiovascular Medicine, University of Iowa, Iowa City, IA, USA; Department of Molecular Physiology and Biophysics, University of Iowa, Iowa City, IA, USA, peter-mohler@uiowa.edu

Peter Molenaar Quneensland University, Brisbane, QLD 4072, Australia

Oliver Monfredi University of Manchester, Manchester, UK

Nicola Monteforte Molecular Cardiology, Fondazione S. Maugeri IRCCS, Via Salvatore Maugeri 10/10A, 27100 Pavia, Italy

Antoon F.M. Moorman Heart Failure Research Center, Academic Medical Center, Meibergdreef 15, 1105 AZ Amsterdam, The Netherlands, a.f.moorman@amc.uva.nl

Jonathan D. Moreno Tri-Institutional MD-PhD Program, Physiology, Biophysics and Systems Biology Graduate Program; Weill Cornell Medical College/The Rockefeller University/Sloan-Kettering Cancer Institute; Weill Medical College of Cornell University, 1300 York Avenue, New York, NY 10021, USA

Carlo Napolitano Molecular Cardiology, Fondazione S. Maugeri IRCCS, Via Salvatore Maugeri 10/10A, 27100 Pavia, Italy; Cardiovascular Genetics Program; Leon H. Charney Division of Cardiology, New York University, New York, NY, USA

Alok Ranjan Nayak Centre for Condensed Matter Theory, Department of Physics, Indian Institute of Science, Bangalore, Karnataka 560012, India

Penelope J. Noble Department of Physiology, Anatomy and Genetics, Oxford University, Sherrington Building, Parks Rd, Oxford, OX1 3PT, UK

Denis Noble Department of Physiology, Anatomy and Genetics, Oxford University, Sherrington Building, Parks Rd, Oxford, OX1 3PT, UK, denis.noble@dpag.ox.ac.uk

Akinori Noma Biosimulation Project, Faculty of Bioinformatics, College of Life Science, Ritsumeikan University, 1-1-1 Noji Higashi, Kusatsu 525-8577, Japan, noma@sk.ritsumei.ac.jp

C. H. Orchard School of Physiology and Pharmacology, Medical Sciences Building, University of Bristol, Bristol BS8 1TD, UK, clive.orchard@bristol.ac.uk

Rahul Pandit Centre for Condensed Matter Theory, Department of Physics, Indian Institute of Science, Bangalore, Karnataka 560012, India, rahul@physics.iisc.ernet.in

Rita Papp Department of Pharmacology and Pharmacotherapy, University of Szeged, 6720 Szeged, Dóm tér 12, Szeged, Hungary

Matthew Perry Department of Physiology, Nora Eccles Harrison Cardiovascular Research and Training Institute, University of Utah, 95 South 2000 East, Salt Lake City, UT 84112, USA

Olaf Pongs Institut für Neurale Signalverarbeitung, ZMNH, University Hospital Hamburg-Eppendorf, Martinistr. 52, 20246 Hamburg, Germany, morin@zmnh.uni-hamburg.de

Ellen Poon Stem Cell and Regenerative Medicine Program, Heart, Brain, Hormone and Healthy Ageing Research Center and Department of Medicine, University of Hong Kong, Hong Kong, China

Silvia G. Priori Molecular Cardiology, Fondazione S. Maugeri IRCCS, Via Salvatore Maugeri 10/10A, 27100 Pavia, Italy; Cardiovascular Genetics Program; Leon H. Charney Division of Cardiology, New York University, New York, NY, USA; Department of Cardiology, Università degli Studi di Pavia, Pavia, Italy, silvia.priori@fsm.it

Ursula Ravens Department of Pharmacology and Toxicology, Medical Faculty Carl Gustav Carus, Dresden University of Technology, Fetscherstrasse 74, 01307 Dresden, Germany, ravens@rcs.urz.tu-dresden.de

Michael Reppel Medizinische Klinik II, Medical University of Lübeck, Lübeck, Germany

Michiel Rienstra Cardiovascular Research Center, Massachusetts General Hospital, Charlestown, MA, USA; University Medical Center Groningen, University of Groningen, Groningen, The Netherlands

Delfin Rodriguez-Leyva Institute of Cardiovascular Sciences, St. Boniface General Hospital Research Centre, Winnipeg, MB, Canada; Department of Physiology, Faculty of Medicine, University of Manitoba, Winnipeg, MB, Canada

Gregor Sachse Institut für Neurale Signalverarbeitung, ZMNH, University Hospital Hamburg-Eppendorf, Martinistr. 52, 20246 Hamburg, Germany

Aida Salameh Heart Centre Leipzig, Clinic for Cardiac Surgery, University of Leipzig, Struempellstr. 39, 04289 Leipzig, Germany

Kevin J. Sampson Department of Pharmacology, College of Physicians and Surgeons of Columbia University, 630 W. 168th St., New York, NY 10032, USA

Michael C. Sanguinetti Department of Physiology, Nora Eccles Harrison Cardiovascular Research and Training Institute, University of Utah, 95 South 2000 East, Salt Lake City, UT 84112, USA, sanguinetti@cvrti.utah.edu

Guiscard Seeböhm Lehrstuhl für Biochemie I, Cation Channel Group, Ruhr University Bochum, Room NC6/132, Universitätsstr. 150, 44780 Bochum, Germany, guiscard.seebohm@rub.de

Thomas Seidel Heart Centre Leipzig, Clinic for Cardiac Surgery, University of Leipzig, Struempellstr. 39, 04289 Leipzig, Germany

Moritz F. Sinner Cardiovascular Research Center, Massachusetts General Hospital, Charlestown, MA, USA; Department of Medicine I, Ludwig-Maximilians-University Munich, Klinikum Grosshadern, Marchioninistr. 15, Munich 81377, Germany; The NHLBI's Framingham Heart Study, Framingham, MA, USA

Nathalie Strutz-Seeböhm Lehrstuhl für Biochemie I, Cation Channel Group, Ruhr University Bochum, Room NC6/132, Universitätsstr. 150, 44780 Bochum, Germany

Zhi Su Department of Integrative Pharmacology, Global Pharmaceutical Research and Development, Abbott Laboratories, 100 Abbott Park Road, Abbott Park, IL 60064, USA

András Tóth Department of Pharmacology and Pharmacotherapy, University of Szeged, 6720 Szeged, Dóm tér 12, Szeged, Hungary

Ming Tang Department of Physiology, Tongji Medical College, Huazhong University of Science and Technology, Wuhan, Hubei, China

Mary-Anne Taube University of Manchester, Manchester, UK

Onkar Nath Tripathi Cardiac Electrophysiology Division, Ion Channel Study Center, Life Sciences Academy, 103 Usman Enclave, Aliganj Sector “O”, Lucknow 226024, India, onkar.tripathi@gmail.com; onkar_t@yahoo.com

Antoni C. G. vanGinneken Heart Failure Research Center, Academic Medical Center, University of Amsterdam, Amsterdam, The Netherlands,

András Varró Department of Pharmacology and Pharmacotherapy, University of Szeged, 6720 Szeged, Dóm tér 12, Szeged, Hungary; Division of Cardiovascular Pharmacology, Hungarian Academy of Sciences, Szeged, Hungary, a.varro@phcol.szote.u-szeged.hu

Guy Vassort INSERM U-637 Physiopathologie cardiovasculaire, CHU Arnaud de Villeneuve, Montpellier, France, guy.vassort@inserm.fr

Ágnes Végh Department of Pharmacology and Pharmacotherapy, University of Szeged, 6720 Szeged, Dóm tér 12, Szeged, Hungary, vegh@phcol.szote.u-szeged.hu

Arie O. Verkerk Heart Failure Research Center, Academic Medical Center, University of Amsterdam, Amsterdam, The Netherlands; Department of Anatomy, Embryology and Physiology, Academic Medical Center, University of Amsterdam, Meibergdreef 15, 1105 AZ Amsterdam, The Netherlands, a.o.verkerk@amc.uva.nl

Tatiana M. Vinogradova Laboratory of Cardiovascular Science, NIA Intramural Research Program, NIH, 5600 Nathan Shock Drive, Baltimore, MA 21224, USA

Ronald Wilders Heart Failure Research Center, Academic Medical Center, University of Amsterdam, Amsterdam, The Netherlands

Friedrich Wilhelm Mohr Heart Centre Leipzig, Clinic for Cardiac Surgery, University of Leipzig, Struempellstr. 39, 04289 Leipzig, Germany

David S. Winlaw Kids Heart Research, The Children’s Hospital at Westmead, Locked Bag 4001, Westmead NSW 2145, Sydney, Australia, DavidW@chw.edu.au

Harry J. Witchel Department of Physiology and Pharmacology, School of Medical Sciences, University Walk, Bristol BS8 1TD, UK; Medical Research Building, Brighton and Sussex Medical School, University of Sussex, Falmer, Brighton BN1 9PS, UK

Joseph Yanni University of Manchester, Manchester, UK

Chae Young Cha Biosimulation Project, Faculty of Bioinformatics, College of Life Science, Ritsumeikan University, 1-1-1 Noji Higashi, Kusatsu 525-8577, Japan, chacy@biosim.med.kyoto-u.ac.jp

Henggui Zhang Biological Physics Group, School of Physics and Astronomy, University of Manchester, Manchester M13 9PL, UK

Thomas Zimmer Institute of Physiology II, University Hospital Jena, Friedrich Schiller University Jena, Kollegiengasse 9, Jena 07743, Germany, thomas.zimmer@mti.uni-jena.de

Part I

Normal Cardiac Rhythm and

Pacemaker Activity

Chapter 1

Cardiac Ion Channels and Heart Rate and Rhythm

Onkar Nath Tripathi

1.1 Introduction

The heart beat originates in the form of spontaneous electrical activity of the primary pacemaker cells of sino-atrial node (SAN). An efficient propagation of the electrical waveform initiated by this spontaneous electrical activity (action potentials, AP) to the atria and, via the cardiac conduction system, viz., atrio-ventricular node (AVN), Bundle of His, Bundle branches, and Purkinje fibre network, to the rest of the heart brings about a highly coordinated rhythmic mechanical activity characterised by synchronised contraction and relaxation of different regions of heart. The cardiac cycle repeats itself throughout the life of an organism with a high level of efficiency and determines the heart rate and rhythm. The classical work of Carl Wiggers [see 1] on cardiac cycle identified the correlation between the electrical activity (electrocardiogram, ECG) and different parameters of mechanical activity, making it evident that the electrical cycle initiates the mechanical cycle. Excitation–contraction (E–C) coupling plays a crucial role in this process, through influx of Ca^{2+} ions, facilitating conversion of the electrical energy into chemical energy required for myocardial contraction [2]. The two phases of the electrical cycle, viz. electrical systole and diastole, are clinically examined to assess the cardiac functions in the normal and diseased heart.

The electrical cycle, recorded with an ECG, begins with the P wave, reflecting the atrial depolarisation (Fig. 1.1). The PR interval, the time taken for atrial depolarisation to reach the AVN and beyond, is characteristically well preserved in different mammals. The PR interval is only one order of magnitude longer in humpback whales, the largest mammal, compared to the mouse even though their body mass differs by six orders of magnitude ([3]; Table 1.1). The QRS complex represents entry of the wave of excitation via the cardiac conduction system into the ventricles and depolarisation of ventricular myocytes. Subsequent repolarisation of

O.N. Tripathi

Cardiac Electrophysiology Division, Ion Channel Study Center, Life Sciences Academy, 103 Usman Enclave, Aliganj Sector “O”, Lucknow 226024, India
e-mail: onkar.tripathi@gmail.com; onkar_t@yahoo.com

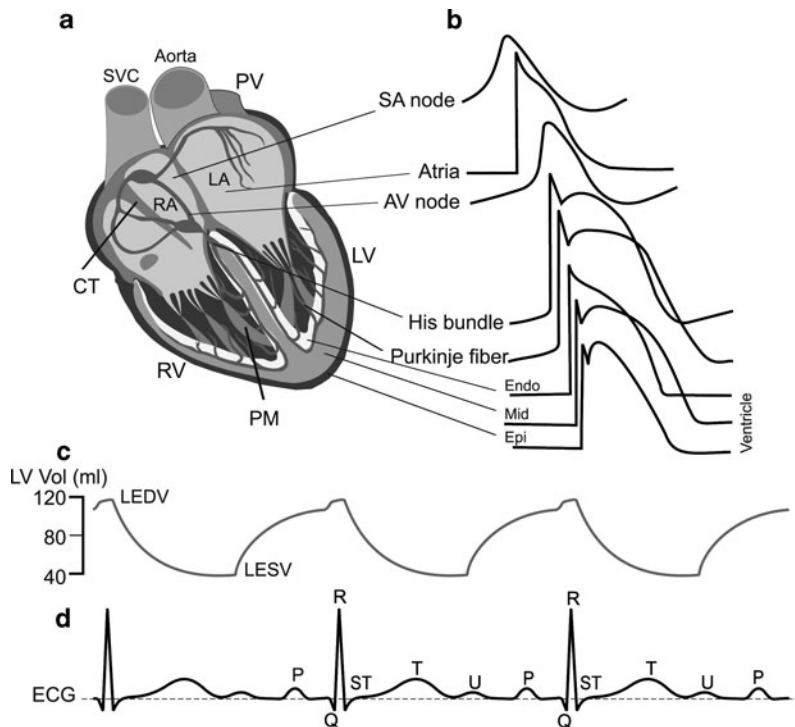


Fig. 1.1 Diagrammatic representation of the salient electrical events in different regions of heart during a cardiac cycle. (a) Heart showing SA node, conducting system and the working cardiac tissues. SVC, superior vena cava; PV, pulmonary vein; CT, crista terminalis; RA, right atrium, LA, left atrium; RV, right ventricle; LV, left ventricle; Endo, endocardium; Epi, epicardium; Mid, midmyocardium; PM, papillary muscle. (b) APs in the cells of different regions of heart roughly corresponding to different phases of ECG. (c) Left ventricular volume (LV) indicating left ventricular contraction and relaxation; LEDV, Left ventricular end-diastolic volume; LESV, Left ventricular end-systolic volume. (d) Surface ECG showing the classical P, Q, R, S, T, and U waves; ST indicates end of S and beginning of T waves

Table 1.1 Heart rate and PR interval vary as a function of body size in mammals (values taken from [3])

Species	Heart rate (beats per minute)	PR interval (ms)	Heart weight (g)	Body weight (kg)
Mouse	376 ± 49	43 ± 4	0.192	0.029 ± 0.04
Human (male)	80	164 ± 0.16	390	66 ± 3
Humpback whale	30	400	180,000	30,000

the ventricles is reflected in the T wave which is often followed by U wave, the cause of which is still unclear [4]. QT interval is the time required for repolarisation of the ventricles and corresponds roughly to the duration of ventricular APs. It serves as an important indicator for arrhythmogenic propensity of heart associated with congenital or acquired long QT syndrome.

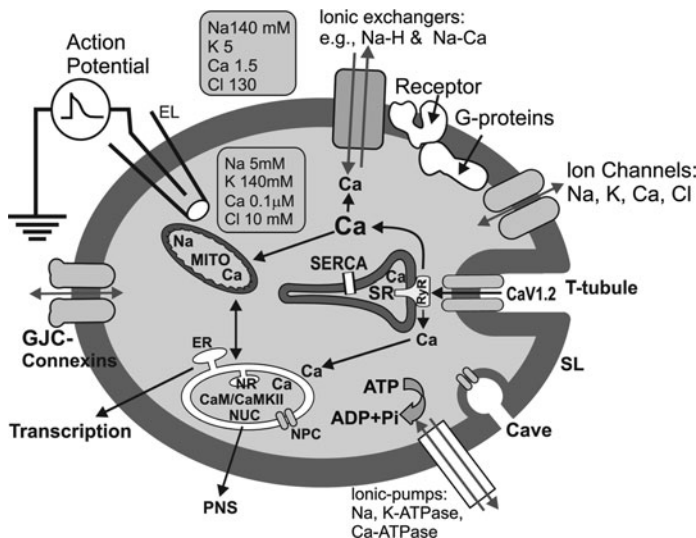


Fig. 1.2 Cartoon diagram of a cardiac myocyte grossly depicting various categories of ion transporters in sarcolemma and intracellular organelles. Extracellular and cytosolic concentrations of Na^+ , K^+ , Ca^{2+} , and Cl^- ions which offer passive electrochemical gradient for the flow of ionic currents through ion channels are shown. The ionic currents underlie APs which can be recorded using classical glass microelectrode (El) techniques. SL, sarcolemma; Cave, caveolae; SR, sarcoplasmic reticulum; MITO, mitochondria; NUC, nucleus; ER, endoplasmic reticulum; PNS, perinuclear space; NR, nuclear reticulum; NPC, nuclear pore complex; GJC, gap junction channel; RyR, ryanodine receptor; SERCA, SR Ca^{2+} -ATPase

The cardiac electrical cycle is initiated and maintained by transmembrane flux of ions via ion channels, exchangers, and pumps (Fig. 1.2). The specific tissue and subcellular distribution of a wide spectrum of ion channel types determines the AP shape and spread of the wave of excitation in the heart. Notable advances in the molecular basis of cardiac excitation and conduction are well covered in several recent reviews [5–8]. Fascinating aspects of development of the cardiac conduction system (Chap. 12) and its structural and molecular characteristics (Chap. 11) are presented in this book. This chapter provides an overview of some basic features of ion channels expressed in the heart, their likely contributions to ionic currents and APs, and their proposed role in cardiac activity.

1.2 Molecular Basis of Cardiac Electrical Activity

The cardiac AP is typically described with five distinct phases, namely phase 0 (upstroke), phase 1 (early repolarisation – notch), phase 2 (plateau), phase 3 (repolarisation), and phase 4 (resting potential or pacemaker potential or diastolic depolarisation). Ionic currents through electrogenic membrane ion transport

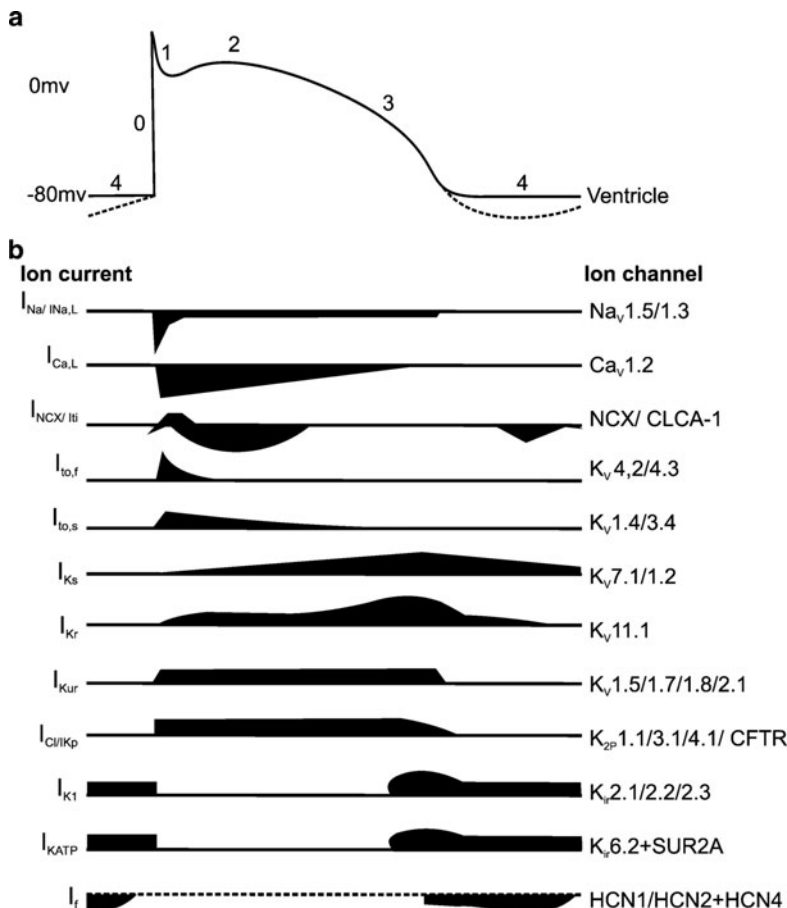


Fig. 1.3 Diagram showing different phases of ventricular AP and the underlying ionic currents. (a) AP showing rapid depolarization (upstroke- phase 0) followed by rapid repolarization (notch- phase 1), slow repolarization (plateau-phase 2) and then faster smooth repolarization (phase 3) terminating into resting potential (phase 4). The cells of SAN, AVN and Purkinje fiber exhibit slow diastolic depolarization (DD, dotted lines). (b) Various inward and outward ionic currents depicted by downward and upward deflections respectively relative to the baseline are shown along with the ion channels/transporters generating the currents. N.B.: K_v1.2 contributes to $I_{K,slow}$. The bottom recording shows inward (dotted line) pacemaker current, I_f/I_h , that contributes to DD in the pacemaker cells of SAN, AVN and Purkinje fiber (Modified from [172] with permission)

proteins form the basis of the different phases of the AP (Fig. 1.3). These proteins are heterogeneously distributed in different types of heart cells endowed with specific functions, and their superbly orchestrated activity determines the characteristic configuration of the AP. Ion channels allow passive flux of Na⁺, K⁺, Ca²⁺, and Cl⁻ in a direction dictated by their concentration gradient across the membrane, and the resulting ionic currents contribute to maintenance of resting potential and generation and conduction of APs (Fig. 1.2); for modeling of cardiac AP see Chap. 9.

Palettes of ion channels in sarcolemma (SL) and sarcoplasmic reticular (SR), mitochondrial (MT), and nuclear (NUC) membranes differ significantly in the same cell and in different types of heart cells. The SL electrogenic proteins primarily determine the shape of cardiac APs. However, the SR ion transport proteins have crucial roles in cardiac pacemaker activity, E–C coupling, and intracellular Ca homeostasis. MT ion channels contribute to the metabolic state of heart cells via excitation–metabolism coupling. NUC ion channels contribute to the transcriptional regulation of SL and MT ion transport and signalling proteins (excitation–transcription coupling), thereby contributing indirectly to heart rate and rhythm. Altered ion channel activity is frequently associated with arrhythmias and mutations in ion channel genes, in particular, cause several cardiac channelopathies.

On the basis of the primary gating (activating) factor, two major groups of ion channels have been identified: voltage-gated (VGIC) and ligand-gated (LGIC) ion channels. The VGICs, activated by change in membrane potential, contribute maximally to cardiac APs, and information on their genes, amino acid residues, conductance, kinetics, etc. is presented with respect to adult heart cells [22, 171].

1.3 Sarcolemmal Ion Channels

1.3.1 *Voltage-Gated Na Channels*

Nine different types of mammalian voltage-gated sodium channels (VGSCs) have been identified and are named after their α -subunits as $\text{Na}_V1.1$ – $\text{Na}_V1.9$. Heart primarily expresses $\text{Na}_V1.5$ (cardiac type), but is also reported to express the brain type Na channels, $\text{Na}_V1.1$, $\text{Na}_V1.3$, and $\text{Na}_V1.6$ [9, 10]. The VGSCs carry a fast inward Na current, I_{Na} , that underlies the fast upstroke (phase 0) of AP in most cardiac cells.

VGSCs are heteromultimeric membrane proteins composed of four subunits: α , β , γ , and δ . The α -subunit is the primary functional unit and contains the pore, ion selectivity filter, voltage sensor, and the drug and toxin binding sites. An α -subunit has four domains (DI–DIV) each comprising of six TM segments (S1–S6). The four domains are arranged concentrically to form collectively a water-filled, open-ended central cavity. An inverted loop (P) between extracellular ends of S5 and S6 of each domain forms the selectivity filter and outer vestibule of the channel. S4 acts as the voltage sensor, due to its many positively charged amino acids. A short intracellular loop between DIII and DIV serves as an inactivation gate that is proposed to occlude the inner vestibule. The N and C termini of α -subunits are intracellular. Four β -subunits, β_1 – β_4 , are reported for VGSCs and are formed of one TM segment. The β -subunit regulates the localisation and functions of α -subunit and is involved in its interaction with the extracellular matrix, cytosolic linker proteins, and cell adhesion molecules (CAM). The following VGSCs have been identified in heart.

$\text{Na}_V1.1$ (BrainI, Gene - *SCN1A*, 1998 amino acids (aa)) is expressed in ventricular myocytes [9] and SAN cells [10] and conducts a small or negligible I_{Na} . Two subunits, $\beta 1$ and $\beta 2$, are identified for this channel. The macroscopic $I_{\text{NaV}1.1}$ has a

voltage for 1/2 maximal ($V_{0.5}$) activation of -19.6 to -13.7 mV and inactivation $V_{0.5}$ of -41.9 to -37.9 mV. $\text{Na}_V1.1$ is localised in the T-tubules of ventricular myocytes and is involved in E-C coupling in ventricles [9]. In SAN it is homogeneously distributed on SL and is associated with AP firing frequency [10, 11]. $\text{Na}_V1.1$ is blocked by tetrodotoxin (TTX) with high sensitivity and is activated by β scorpion toxin, CssIV [10].

$\text{Na}_V1.3$ (Brain III, Gene - *SCN3A*, 2000 aa) is expressed in foetal and adult heart, ventricular myocytes [9], and in SAN cells [10]. It is reported to have two subunits, $\beta 1$ and $\beta 3$. $\text{Na}_V1.3$ carries a small macroscopic $I_{\text{Na}V1.3}$ having activation $V_{0.5}$ of -12 mV and inactivation $V_{0.5}$ of -47.5 mV. $\text{Na}_V1.3$ is also localised on T-tubules and plays a role in E-C coupling in ventricles [9] and mediates AP firing in SAN cells [10]. It is blocked by TTX with high sensitivity and is stimulated by CssIV.

$\text{Na}_V1.5$ (h1, Cardiac, Gene - *SCN5A*, 2016 aa, ~ 20 pS) is the cardiac-specific VGSC and has four subunits, $\beta 1$, $\beta 2$, $\beta 3$, and $\beta 4$. $\text{Na}_V1.5$ is localised on the intercalated discs in ventricles [9] and has important role in cell-to-cell conduction of impulse in heart. $\text{Na}_V1.5$ is also present in peripheral cells of SAN and is involved in conduction of SAN APs to atria [11]. A fast, transient inward Na current, I_{Na} , with rapid kinetics of activation ($V_{0.5} = -44$ mV) and inactivation ($V_{0.5} = -87$ mV) is mediated by $\text{Na}_V1.5$ and contributes significantly to the fast upstroke of AP in atria, ventricles, and Purkinje fibres. $\text{Na}_V1.5$ is reported to contribute significantly to the late Na current, I_{NaL} [12]. $\text{Na}_V1.5$ is relatively insensitive to the blocking effect of TTX and is more sensitive to STX. Class I antiarrhythmics, e.g. lidocaine, procainamide, flecainide, propafenone, etc. act by blocking $\text{Na}_V1.5$. Ranolazine, a new antiarrhythmic drug, targets I_{NaL} [12]. $\text{Na}_V1.5$ is implicated in sick sinus syndrome, Brugada syndrome and other cardiac arrhythmias [13]. As described in Chap. 22, gain of function mutations in *SCN5A* cause type 3 long QT (LQT3) syndrome.

$\text{Na}_V1.6$ (Gene - *SCN8A*, 1980 aa) is expressed in the T-tubules of ventricular myocytes [9]. It mediates a small current with activation $V_{0.5}$ of -28.7 mV and inactivation $V_{0.5}$ of -71.9 mV [14]. All four β subunits, $\beta 1$ - $\beta 4$, are associated with $\text{Na}_V1.6$. It is activated by β scorpion toxins and blocked by TTX. $\text{Na}_V1.6$ is suggested to be involved in E-C coupling [9].

Interestingly, TTX is a potent inhibitor of the chick and fish heart I_{Na} as evident from studies on isolated fish ventricular myocytes and isolated chick ventricular tissue which indicates a predominant role of other TTX-sensitive isoforms of VGSCs in non-mammalian heart [15, 16].

1.3.2 Voltage-Gated Ca Channels

The voltage-gated calcium channels (VGCCs) conduct an inward Ca current (I_{Ca}), which leads to elevation of intracellular Ca, a second messenger necessary for a large variety of cellular functions including cardiac contraction, impulse generation, secretion, neurotransmission, gene expression, development, and differentiation etc.

VGCCs facilitate conversion of the electrical energy into chemical energy for execution of cellular functions.

Three families of VGCCs are identified and are generally grouped under two categories depending on their activation voltage, viz. high voltage-activated (HVA) and low voltage-activated (LVA) Ca channels. The HVA Ca channels are activated at higher membrane voltages (i.e. more depolarised potentials) and include $\text{Ca}_V1.x$ (L, N, and P/Q type) and $\text{Ca}_V2.x$ (R type) VGCCs. The LVA Ca channels, $\text{Ca}_V3.x$ (T type) VGCCs, are activated at low membrane voltages (i.e. more negative potentials). VGCCs are heteromultimeric membrane protein complexes of 4–5 subunits, viz. $\alpha 1$, $\alpha 2$, β , γ , and δ . The $\alpha 1$ (Ca_V) subunits of 150–250 kDa have essentially the same structure as Na_V containing the pore, the voltage sensor, and binding sites for most of the pharmacological modulators [17]. The auxiliary subunits of VGCCs, $\alpha 2$, β , γ , and δ , are smaller proteins compared to $\alpha 1$; $\alpha 2$ is a 140 kDa extracellular protein and δ a 27 kDa TM glycoprotein. The β subunits, $\beta 1$ – $\beta 4$, are located intracellularly, have specific tissue distribution, and play important regulatory roles in surface expression and activation/inactivation kinetics of $\alpha 1$ subunit. The γ subunit, formed of 4TM segments, is involved in assembly and surface expression of $\alpha 1$ subunit and other membrane signalling proteins.

Some of the salient features of the VGCCs expressed in heart are described below.

$\text{Ca}_V1.2$ (Cardiac L-type Ca channel, $\alpha 1C$, Gene - *CACNA1C*, 2138 aa, 8 pS with Ca) is strongly expressed in all regions of heart and is localised in the T-tubules of ventricular myocytes [18]-see Chap. 13. A cardiac-specific isoform, $\text{Ca}_V1.2a$, has been identified [19]. $\beta 1$ – $\beta 4$ accessory subunits are differentially distributed at the subcellular level. Four $\alpha 2\delta$ isoforms are also reported as the auxiliary subunits of $\text{Ca}_V1.2$ [20].

$\text{Ca}_V1.2$ current, $I_{\text{Ca,L}}$, contributes to the plateau phase (phase 2) of ventricular APs and plays a key role in E–C coupling [2]. In SAN, $I_{\text{Ca,L}}$ underlies the slow upstroke of APs and is also considered to contribute to pacemaker potential [21]. The ventricular macroscopic $I_{\text{Ca,L}}$ has activation $V_{0.5}$ of -4.8 mV and τ of 5–7 ms; the inactivation $V_{0.5}$ is -20.4 mV and τ_f and τ_s are 20.4 ms and 61–133 ms, respectively [22].

The organic Ca channel blockers (CCBs), dihydropyridines (DHP; e.g. nifedipine), phenylalkylamines (e.g. verapamil), diphenylalkylamines (e.g. fendiline), and benzothiazepines (e.g. diltiazem), inhibit $\text{Ca}_V1.2$ activity. Several Ca channel activators (CCA), e.g. Bay K 8644 and FPL 64176, activate $\text{Ca}_V1.2$ [23].

$\text{Ca}_V1.2$ is strongly modulated by phosphorylation via β_2 -adrenergic receptor-induced increase in cAMP level and PKA activation, which is terminated by PP2A [24]. This β_2 -AR pathway has an important role in sympathetic nerve-induced positive chronotropy and inotropy invoked during “fight-or-flight” response of the heart. $\text{Ca}_V1.2$ and its auxiliary subunits are associated with inherited (Timothy syndrome- LQT8, see Chap. 21) and acquired cardiac arrhythmias. Calmodulin and CaMKII that regulate the activity of L-type Ca channels are suggested to contribute to arrhythmogenesis [25].

$\text{Ca}_V1.3$ ($\alpha 1D$, L-type Ca channel, Gene - *CACNA1D*, 2181 aa) is expressed in SAN, AVN, Purkinje fibers and right atrial cells [26–28]. $\text{Ca}_V1.3$ is reported to have

two auxiliary subunits, β and $\alpha_2\delta$. The macroscopic $I_{CaV1.3}$ has activation $V_{0.5} = -12.9$ mV and $\tau = 0.5\text{--}2.5$ ms and inactivation $V_{0.5} = -42.7$ mV and $\tau = 3.8\text{--}74$ ms [29]. It contributes to normal pacemaking in SAN and is implicated in SAN dysfunction [26, 27, 30]. Channel phosphorylation following β_2 -AR stimulation brings about positive chronotropy accounting for part of the effects of increased sympathetic discharge. The CCBs and CCAs have profound effects on $CaV1.3$.

$CaV2.3$ ($\alpha 1E$, R-type Ca channel, Gene - *CACNA1E*, 2270 aa, 20 pS) is associated with β and $\alpha_2\delta$ subunits. $CaV2.3$ channel allows the flow of a residual inward Ca current ($I_{Ca,R}$) at high membrane voltages when $I_{Ca,L}$ is blocked by CCBs. The macroscopic $I_{Ca,R}$ has an activation $V_{0.5}$ of -29 mV, $\tau = 2.4$ ms, and inactivation $V_{0.5}$ of -54 mV and $\tau = 16\text{--}655$ ms [22]. $CaV2.3$ is expressed in atrial cells [31]. It is insensitive to CCBs and CCAs and is inhibited by Ni^{2+} and Cd^{2+} [22].

$CaV3.1$ ($\alpha 1G$, T-type Ca channel, Gene - *CACNA1G*, 2377 aa, 7.3 pS) is expressed predominantly in the conduction system, viz. SAN, AVN and Purkinje fibres [32]. $CaV3.1$ elicits $I_{Ca,T}$, a transient inward Ca current activated at low (more negative) membrane voltages, suggested to play a key role in the pacemaker activity of SAN and in AVN conduction [27, 32]. The macroscopic $I_{Ca,T}$ exhibits activation $V_{0.5} = -50$ mV, $\tau = 1\text{--}7$ ms, inactivation $V_{0.5} = -68$ mV, and $\tau = 15\text{--}40$ ms [33]. $CaV3.1$ is insensitive to CCBs and CCAs and is blocked by Ni and mibepradil [22, 34].

$CaV3.2$ ($\alpha 1H$, T-type Ca channel, gene - *CACNA1H*, 2353 aa, 9.1 pS) are most abundant in the conduction system of heart and are not expressed in adult mammalian ventricles [32, 35]. The macroscopic $I_{CaV3.2}$ shows activation $V_{0.5}$ of -41.9 mV and τ of $2\text{--}10$ ms. The inactivation $V_{0.5}$ is in the range of -50.9 mV and τ of $20\text{--}120$ ms [22]. $I_{CaV3.2}$ is inhibited by mibepradil, Ni, pimozol, and anandamide [22, 34]. $CaV3.2$ is re-expressed in atria and ventricles during cardiac pathologies like HF and cardiac hypertrophy and associated ventricular arrhythmias [32, 36].

1.3.3 Voltage-Gated K Channels (K_V)

K channels contribute to maintenance of resting membrane potential and repolarisation of cardiac APs and, therefore, determine excitability, AP duration, and refractoriness of myocardium. K channels are the most diverse groups of ion channels encoded by about 70 genes in mammals and include six TM voltage-gated (K_V), 6/7 TM Ca- and Na-activated (K_{Ca} , K_{Na}), two TM inwardly-rectifying (K_{ir}), and two pore (K_{2p}) K channel families [22].

Voltage-gated potassium channels (VGPCs) are the largest family of K channels encoded by 40 genes in human genome and are, therefore, extremely diverse. VGPCs are comprised of a primary pore-forming α -subunit each with six TM segments. α -subunits co-assemble to form a homo- or hetero-tetramer that has the pore for K^+ flux, selectivity filter, voltage sensor, activation and inactivation gates, and sites for action of pharmacological agents. Presently 12 subfamilies of VGPCs are identified and are named, $K_V1.x$ - $K_V12.x$.

The members of Kv5.x, Kv6.x, Kv8.x, and Kv9.x form “modifiers” and are non-functional ion channels upon formation of homotetramers. Auxiliary β -subunits, Kv β 1.x, Kv β 2.x, and Kv β 3.x, and other associated proteins are also identified for several VGPCs and modulate their functions.

Kv1.1 (Gene - *KCNA1*, 495 aa, 10 pS) is associated with two heteromeric pore-forming subunits, Kv β 1 and Kv β 2 [22]. Kv1.1 mediates an outward I_K contributing to delayed rectifier K current which maintains the resting potential and cellular excitability [37, 38]. The kinetics of macroscopic $I_{KV1.1}$ is characterised by activation $V_{0.5}$ of -29.7 mV and τ 15.5 ms, and inactivation $V_{0.5} = -47$ mV and τ 83.4 ms [37]. SA node is reported to over-express Kv1.1 in mice exhibiting chronic bradycardia [39].

Kv1.2 (Gene - *KCNA2*, 499 aa, 14–18 pS) has two heteromeric pore-forming units, Kv β 1 and Kv β 2, and co-assembles with other Kv channels. The outward $I_{KV1.2}$ contributes to delayed rectifier I_K and restores resting potential and excitability [40, 41]. The macroscopic $I_{KV1.2}$ has activation $V_{0.5}$ of 5–27 mV and τ of 6 ms, and inactivation $V_{0.5}$ of -15 mV [41]. It is expressed in SAN, atria, and ventricles [42] and is associated with right ventricular hypertrophy [43].

Kv1.4 (Gene - *KCNA4*, 653 aa, 5 pS) forms heteromeric pore with Kv β and co-assembles with other Kv channels. They are expressed in SAN, AVN, Purkinje fibres, and ventricles [38, 44–47]. Kv1.4 is responsible for the slow transient outward K current, $I_{to,s}$, involved in early repolarisation that shapes the configuration of APs in different types of heart cells [48, 49] and is altered in post-myocardial infarction (MI) ventricular myocardium in a differential manner [50]. Kv1.4 is associated with cardiac hypertrophy and heart failure (HF) [49, 55].

Kv1.5 (Gene - *KCNA5*, 613 aa, 8 pS) forms heteromeric channel with Kv β 1 and Kv β 2. It is expressed in SAN, AVN, atria, and ventricles, being more predominant in atria [38, 44, 51, 52] and is a major contributor to ultra-rapidly activating delayed rectifier outward K current (I_{Kur}). The macroscopic $I_{KV1.5}$ shows activation $V_{0.5}$ of -14 mV and τ of 23 ms which are in the range of those for I_{Kur} . I_{Kur} participates in repolarisation and maintenance of resting potential [53, 54]. Kv1.5 expression levels and I_{Kur} are associated with cardiac rhythm disorders like atrial fibrillation (AF; see Chap. 33) and with ventricular hypertrophy [54, 55].

Kv1.7 (Gene - *KCNA7*, 456 aa, 21 pS) co-assembles with other Kv1 channels. It is expressed in heart [56] and is responsible for an I_{Kur} like current. The macroscopic $I_{KV1.7}$ has activation $V_{0.5}$ of -4.3 mV and inactivation $V_{0.5}$ of -21 mV and τ of 181.8 ms [57]. Kv1.7 is suggested to contribute significantly to I_{Kur} and facilitates repolarisation. *KCNA7* is considered a candidate gene for inherited cardiac disorders [58].

Kv1.8 (Gene - *KCNA10*, 511 aa, 11 pS) co-assembles with other members of Kv1 and KCNA4B acts as a novel β subunit of this channel to form a heteromeric channel [59]. Kv1.8 is activated by cGMP and not by cAMP [60]. Kv1.8 is expressed in heart, contributes to I_{Kur} , and facilitates repolarisation and restoration of resting potential and has a potential role in acquired arrhythmias [60, 61].

Kv2.1 (Gene - *KCNB1*, 858 aa, 8 pS) is associated with several “modifier” heteromeric pore-forming subunits, viz. Kv5.1, Kv6.1–Kv6.3, Kv8.1, and

$Kv9.1-Kv9.3$. Expression level of $Kv2.1$ is high in ventricles and atria [47, 52]. $Kv2.1$ causes a delayed rectifier outward current $I_{K,slow2}$ and contributes significantly to I_{Kur} , facilitating repolarisation [47, 66]. It is associated with arrhythmias and left ventricular remodelling [47, 62].

$Kv3.4$ (Gene - *KCNC4*, 635 aa, 14 pS) co-assembles with heteromeric pore-forming subunit MiRP2. It is expressed in Purkinje fibres and ventricles [52, 63] and mediates a K outward current that facilitates repolarisation. $Kv3.4$ is associated with conduction abnormalities in congestive HF [63].

$Kv4.1$ (Gene - *KCND1*, 647 aa, 6 pS) forms heteromeric pore with KChIP1 and DPPX [22]. It is differentially expressed in heart [45, 64].

$Kv4.2$ (Gene - *KCND2*, 630 aa, 7.5 pS) forms heteromeric pore with the subunits KChIP1, 2, 3, and 4 and $Kv\beta$. It is asymmetrically expressed in heart and is localised in the T-tubules in ventricles [65]. $Kv4.2$ contributes to $I_{to,f}$ and participates in repolarisation during phase 1 of cardiac AP [49]. However, its expression level is low in the ventricles of higher mammals allowing appearance of prominent notch phase of AP [66]. $Kv4.2$ is implicated in diabetic cardiomyopathy [67, 68].

$Kv4.3$ (Gene - *KCND3*, 655 aa, 5 pS) is associated with KChIP2, a heteromeric pore-forming subunit. $Kv4.3$ is expressed in heart with profound differences in regional distribution and between different species [66, 69]. It also mediates a transient outward K current and contributes to $I_{to,f}$ which determines AP duration in different types of heart cells. $Kv4.3$ is associated with several cardiac rhythm disorders [49, 68, 70, 71].

$Kv7.1$ ($KvLQT1$, Gene - *KCNQ1*, 676 aa; 5.8 pS) has several auxiliary subunits, viz. MinK (KCNE1), and MiRP1–MiRP4 [72]. It is expressed in atria and ventricles and mediates the slowly activating delayed rectifier outward K current, I_{Ks} , contributing to repolarisation during the “plateau” phase of the AP [73]. Mutation in $Kv7.1$ is the most common cause of LQT syndrome [74] and, very rarely, SQT syndrome ([75, 76]- see Chap. 23) and is associated with AF (see Chap. 27).

$Kv11.1$ (Gene - *KCNH2* or *HERG*, 1159 aa; 12 pS) is proposed to co-assemble with the accessory subunit MiRP1 [77]. They are abundantly and asymmetrically expressed in SAN, atria and ventricles [78, 79]. $Kv11.1$ channel underlies the rapidly activating delayed rectifier outward K current, I_{Kr} , having strong inwardly rectifying properties [79]. I_{Kr} determines the time course of later phase of repolarisation of AP. hERG channels are associated with both inherited (LQT and SQT) and acquired (drug-induced) arrhythmias [79]. A number of chemically unrelated drugs and several of those intended for non-cardiac use are reported to block hERG channel causing ventricular arrhythmias, torsades de pointes (TDP), and sudden cardiac death (SCD) (see Chaps. 34 and 35).

1.3.4 Ca- and Na-Activated K Channels (K_{Ca}/K_{Na})

Five families of K_{Ca} channels (including K_{Na} channels), namely, $K_{Ca}1.x$, $K_{Ca}2.x$, $K_{Ca}3.x$, $K_{Ca}4.x$, and $K_{Ca}5.x$ have been identified [22]. The K_{Ca} channels, activated

by intracellular Ca, are also grouped as small conductance (SK), intermediate conductance (IK), and big conductance (BK) channels on the basis of their conductance and pharmacological sensitivity. $K_{Ca1.x}$ has one member, i.e. $K_{Ca1.1}$ (BK, slo1), and belongs to BK group. $K_{Ca5.x}$ also has one member ($K_{Ca5.1}$, slo3) and is related to $K_{Ca1.x}$. $K_{Ca2.x}$ has three members, viz. $K_{Ca2.1}$, $K_{Ca2.2}$, and $K_{Ca2.3}$, and belongs to SK group. $K_{Ca3.1}$ is the only member of $K_{Ca3.x}$ (IK) group.

The Na-activated K (K_{Na}) channels are named $K_{Ca4.x}$ by IUPHAR and have two members, i.e. $K_{Ca4.1}$ (slack, slo2.2) and $K_{Ca4.2}$ (slick, slo2.1). The $K_{Ca4.x}$ channels are activated by intracellular Na and not Ca.

The following K_{Ca} and K_{Na} channels are reported to be expressed in heart.

$K_{Ca2.1}$ (SK1, Gene - *KCNN1*, 543 aa, 9.2 pS) is formed of six TM segments, and calmodulin serves as its auxiliary subunit. They are activated by intracellular Ca and are voltage-dependent. $K_{Ca2.1}$ is reported in atria and ventricles [80], and is blocked by apamin and leurotoxin I [22, 81].

$K_{Ca2.2}$ (SK2, Gene - *KCNN2*, 579 aa, 9.5 pS) has no auxiliary subunits and is present in heart its expression being higher in atria than in ventricles [82–84]. $K_{Ca2.2}$ is voltage-independent and facilitates repolarisation in atrial cells; their deletion in mice results in AF [84]- See also Chap. 33. Apamin and leurotoxin I are its pore blockers [22, 81].

$K_{Ca2.3}$ (SK3, Gene - *KCNN3*, 731 aa) is voltage-independent, and no auxiliary subunits are reported. $K_{Ca2.3}$ is expressed in atria and ventricles [83] with a role in AF (See Chap. 27). Apamin and leurotoxin I are its pore blockers [22, 81].

$K_{Ca4.2}$ (Slick/Slo2.1/ K_{Na} , Gene - *KCNT2*, 1138 aa, 141 pS [85], and 220 pS [86]). First reported in guinea pig ventricular myocytes, these channels are ubiquitously distributed [87]. K_{Na} channels in ventricular myocytes show complex bursting behaviour [86] with several stable subconductance levels [88]. $K_{Ca4.2}$ is reported to form heteromers with $K_{Ca4.1}$ in neurones [89]. $K_{Ca4.2}$ channels are believed to protect from hypoxic insults [90]. They are blocked by several antiarrhythmic drugs [91] and activated (Slo2.1) by niflumic acid [92].

1.3.5 *Leak K Channels ($K_{2P}/4$ TM)*

Leak K channels in part mediate a background leak of K across the SL, and maintain the membrane potential to subthreshold resting levels, thus modulating cellular excitability [93, 94]. The primary pore-forming α -subunits of these K channels have two pores formed with four TM segments arranged usually as homodimers or heterodimers. Fifteen types of K_{2P} channels have been identified [22]. K_{2P} channels remain open in the range of resting potential and carry time- and voltage-independent outward K currents. A variety of factors are known to modulate the activity of K_{2P} channels, including temperature, pO_2 , pH, lipids, neurotransmitters, G-protein-coupled receptors, and mechanical stimuli.

The cardiac K_{2P} family members underlie K currents somewhat similar to the “plateau current” and steady-state K current, ISS [94, 95], and are described below:

K_{2P}1.1 (TWIK-1, Gene - *KCNK1*, 336 aa, 34 pS) is expressed more abundantly in ventricles and Purkinje fibres than in atria [96, 97]. These channels conduct an inwardly rectifying outward K current and have been implicated in cardiac arrhythmias, e.g. Brugada syndrome and right ventricular arrhythmia [71].

K_{2P}2.1 (TREK-1, Gene - *KCNK2*, 426 aa, 100 pS) [98, 99] is a TWIK-related channel and is expressed differentially in the three layers of left ventricle, being higher in epicardium than in endocardium [93]. It is present in longitudinal stripes in SL of ventricular myocytes [99]. K_{2P}2.1 channel underlies an outward K current with weak inward rectification and exhibits mechano-sensitivity [99]. The transmural gradient of K_{2P}2.1 has been proposed to contribute to AP duration and dispersion of repolarisation [93, 99].

K_{2P}3.1 (TASK-1, Gene - *KCNK3*, 394 aa, 14 pS) is a TWIK-related acid-sensitive K channel that is expressed strongly in heart. The outward K current mediated by these channels facilitates repolarisation [98, 100]. K_{2P}3.1 level in left ventricular myocytes is increased in experimental Left ventricular hypertrophy [62]. I_{TASK-1} is suggested to mediate α 1-adrenergic receptor-mediated prolongation of cardiac repolarisation that is inhibited by A293 [100].

1.3.6 Inwardly Rectifying K Channels (2 TM)

The inwardly rectifying K channels allow larger inward currents at potentials negative to E_K than outward currents positive to E_K . They are comprised of pore-forming two TM α -subunits, K_{ir}, which form homotetramers although some members also form heterotetramers. Seven subfamilies of K_{ir} channels have been identified: K_{ir}1.x–K_{ir}7.x. K_{ir}2.x families have four subfamilies, K_{ir}2.1–K_{ir}2.4, and their inwardly rectifying K currents contribute significantly to I_{K1} [101]. K_{ir}3.x family has four channel types identified as K_{ir}3.1, K_{ir}3.2, K_{ir}3.3, and K_{ir}3.4, also called GIRK1, GIRK2, GIRK3, and GIRK4, respectively. The K_{ir}3 channels are coupled to G-proteins. K_{ir}6.x (K_{ATP}) family has two members, K_{ir}6.1 and K_{ir}6.2. Functional K_{ir}6.x channels form heteromultimers of octameric conformation with four auxiliary subunits, the sulfonylurea receptors (SUR) that serve as binding sites for glibenclamide and diazoxide.

The following K_{ir} family members are expressed in heart.

K_{ir}2.1 (IRK1, Gene - *KCNJ2*, 427 aa, 21 pS) has a higher expression in ventricles than in atria. Other K_{ir}2.x members and K_{ir}4.1 serve as its heteromeric pore-forming domain. K_{ir}2.1 channel K outward current is the major contributor to I_{K1} and contributes to the repolarisation phase of the AP and maintenance of resting potential in ventricles and atria [102, 103]. K_{ir}2.1 is associated with several rhythm disorders, including AF, left ventricular hypertrophy, and Andersen–Tawil syndrome (LQT7) [62, 63, 104] and SQT3 (see Chap. 23).

K_{ir}2.2 (IRK2, Gene - *KCNJ2*, 433 aa, 34.2 pS) is expressed in ventricles and atria [22, 102, 105]. K_{ir}2.1 serves as a heteromeric pore-forming subunit for K_{ir}2.2. K outward current due to K_{ir}2.2 contributes partly to I_{K1} and facilitates repolarisation of AP and maintenance of resting potential [102].

K_{ir}2.3 (IRK3, Gene - *KCNJ4*, 445 aa, 13 pS) forms complexes with other K_{ir}2.x subunits [22, 106–108]. It also contributes to I_{K1} and thus to repolarisation phase and resting potential. K_{ir}2.3 is associated with several types of cardiac arrhythmias including Andersen's syndrome [101, 107].

K_{ir}3.1 (GIRK1, Gene - *KCNJ3*, 501 aa, 42 pS) is abundant in SA node, AV node, and atria [109, 110]. K_{ir}3.1 is electrically silent and forms functional heteromers with the pore-forming subunits, K_{ir}3.2, K_{ir}3.3, or K_{ir}3.4 with virtually identical conductances, kinetics, and $G_{\beta\gamma}$ sensitivities [110]. M2R stimulation leads to $G_{\beta\gamma}$ -mediated activation of heteromeric K_{ir}3.1 channel causing an outward K current (I_{KACH}), which brings about SA nodal cellular hyperpolarisation, AV conduction delay, atrial hyperpolarisation, and negative chronotropy [111].

K_{ir}3.2 (GIRK2, Gene - *KCNJ6*, 423 aa, 30 pS) is primarily a brain-type channel but its splice variants are also reported in SA node and atria [112]. K_{ir}3.2 is activated by M2R-mediated $G_{\beta\gamma}$ and RGS4 pathways, and induces I_{KACH} causing bradycardia due to hyperpolarisation of SAN cells [112].

K_{ir}3.4 (GIRK4, Gene - *KCNJ5*, 419 aa, 15–30 pS) can form homomeric channels but usually forms heteromers with K_{ir}3.1, K_{ir}3.2, and K_{ir}3.3. It assembles in heart as heterotetramers with K_{ir}3.1 [113]. The K_{ir}3.4/K_{ir}3.1 heteromeric channels are strongly activated by $G_{\beta\gamma}$ subunits of G protein that mediate the M2 receptor stimulation by ACh resulting in activation of I_{KACH} [110]. A decrease in I_{KACH} prevents, while its increase favours occurrence of AF in GIRK4 K/O mice [54, 114–116]. It is, therefore, suggested that I_{KACH} has a potential role in clinical AF ([117], Chap. 33).

K_{ir}6.1 (K_{ATP}, Gene - *KCNJ8*, 424 aa, 33 pS) forms heteromultimeric complex with four auxiliary subunits, SUR2B. These channels are activated by low ($<10^{-5}$ M) concentrations of intracellular ATP but inhibited by its higher ($>10^{-4}$ M) concentrations [118]. K_{ir}6.1 channels are reported in atria and ventricles, are distributed in the sarcolemma of cardiac myocytes and are associated with cardiac maladaptive remodelling [119].

K_{ir}6.2 (K_{ATP}, Gene - *KCNJ11*, 390 aa, 79 pS) forms heteromultimers with SUR2A in heart and causes the repolarising I_{KATP} [120]. K_{ir}6.2 and SUR2A subunits predominate in the sarcolemma of ventricular and atrial myocytes [121]. While K_{ir}6.2 is the K channel, SUR2A acts as the sensor for intracellular ATP and ADP levels and modulates the activity of the former, thereby determining the amplitude of I_{KATP} , membrane potential, and APD. K_{ATP} channels play important roles in normal myocardial function and in several acquired and inherited cardiac disorders, viz. AF, cardiomyopathy, HF, and poor adaptability to stress-induced cardiac dysfunction [122]. The sarcolemmal Kir6.2/SUR2A is reported to facilitate protection from ischemia–reperfusion cardiac injury [123].

1.3.7 Cyclic Nucleotide-Regulated Channels

Two groups of channels belong to the superfamily of cyclic nucleotide-regulated channels: (1) Cyclic nucleotide-gated (CNG) channels and (2) hyperpolarisation-activated, cyclic nucleotide-gated (HCN) channels [22].

CNG Channels: These cation channels are expressed as heterotetramers comprised of homologous six TM A subunits (CNGA1–CNGA4) with six TM B subunits (CNGB1 and CNGB3). A cyclic nucleotide binding domain (CNBD) located on the cytosolic C terminal serves as the site for activation by cAMP or cGMP. CNG channels are permeable to monovalent cations Na and K and also Ca.

CNGA2 (Gene - *CNGA2*, 664 aa, 35 pS) is expressed, though feebly, in myocardial sarcolemma [124]. CNGA2 is permeable to Ca^{2+} but its physiological significance is unknown.

HCN channels: Four types of HCN channels, HCN1–HCN4, are identified in cardiac and neuronal tissues [125]. HCN channels are homo- or hetero-tetramers of subunits comprised of six TM segments, S1–S6, with S4 acting as the voltage sensor. The four monomeric subunits are arranged around a central pore lined by their S6 TM segments. The N and C termini of the subunits are cytosolic, the latter having a crucial role in channel regulation by cAMP. A cyclic nucleotide-binding domain on the C terminus serves as the binding site for cAMP and has a key role in the channel activity. Membrane potentials in the hyperpolarised range (negative to resting potential) activate these channels. HCN channels are permeable to monovalent cations, K and Na, which upon channel opening carry an inward depolarising cation current, contributing to funny (I_f) or hyperpolarising (I_h) currents. I_f contributes significantly to diastolic depolarisation in the pacemaker cells of SAN, AVN and Purkinje fibers and modulates heart rate and rhythm. Therefore, HCN channels are often called “pacemaker channels”. Sympathetic neurotransmitters, epinephrine and norepinephrine, stimulate the activity of HCN channels through β_2 AR-mediated increase in intracellular cAMP level and induce positive chronotropy. The parasympathetic neurotransmitter, ACh, is reported to cause negative chronotropy partly by inhibiting HCN channel activity. Several specific blockers of I_f (bradycardiac agents) have been discovered, exemplified by ivabradine, offering new therapeutic agents to treat sinus tachycardias.

HCN1 (Gene - *HCN1*, 890 aa, 12.9 pS) is expressed feebly in SAN and embryonic ventricular myocytes [22, 125]. MiRP1 serves as an auxiliary subunit.

HCN2 (Gene - *HCN2*, 889 aa, 1.5–35 pS) is also expressed in SAN and is considered to be complimentary to HCN4. HCN2 channels contribute up to 20% to I_f current in mice SAN cells [125, 126]. HCN2 channels are permeable to Na and K. Dysfunction of HCN2 is associated with sinus dysrhythmia [126].

HCN4 (Gene - *HCN4*, 1203 aa, 17.5 pS) is expressed predominantly in SAN [127]. MiRP1 is a potential auxiliary subunit. HCN4 has an activation $V_{0.5}$ of -82 mV and τ of ~ 2 s when expressed in HEK293 cells [22]. HCN4 contributes up to 80% to I_f in SAN. HCN4 is associated with sick sinus syndrome and other disorders of SAN and AVN and has also been implicated in AF, ventricular tachycardia (VT), and HF [128–131].

The HCN channels are extensively covered in Chaps. 3 and 5. Mathematical modeling of the role of HCN channels in pacemaker activity of SAN cells is also covered extensively in Chaps. 2 and 8.

1.3.8 Transient Receptor Potential Channels

The mammalian transient receptor potential (TRP) ion channel superfamily is comprised of six protein families, the classical TRP (TRPC), vallinoid receptor (TRPV), melastatin (TRPM), mucolipin (TRPML), polycystin (TRPP), and ankyrin (TRPA1) protein channels. TRP channel subunits are formed of six TM α helical segments (S1–S6), the loop between S5 and S6 making the pore. Although S4 in these ion channels lacks classical voltage sensors several members of TRP family show voltage-dependent gating [133, 171]. Most of the TRP channels are non-selectively cation permeant, except TRPV5 and TRPV6 which are Ca selective, and TRPM4 and TRPM5 which are monovalent cation selective. TRP channels when in open state allow increase in cytosolic Ca and Na concentrations and depolarise the cell; they are also considered to act as store-operated Ca channels (SOCCs), contribute to cellular Ca homeostasis and are implicated in SAN automaticity and hypertrophy [132, 167]. Several TRP channels are activated by stretch and contribute to mechano-electrical feedback. Chapter 31 covers TRP channels.

1.3.9 Chloride Channels

The chloride channels are functionally and structurally diverse with ubiquitous distribution both on the plasma membrane as well as on intracellular organelles [134, 135, 171]. A surge of research on Cl channels during the past decade has led to identification of a large variety of these anion channels and their prospective roles in various cellular functions in health and disease. As a consequence Cl channels are emerging as important targets for new drug discovery for a number of diseases. The mammalian Cl channels identified so far are grouped into five families: Voltage-sensitive Cl channels (CIC), Cystic fibrosis transmembrane conductor regulator (CFTR), Ca-activated Cl channels (CaCC), Maxi Cl channels (Maxi Cl), and Volume-regulated Cl channels (VRC, VRAC) [171].

Several types of Cl channels have been described in heart cells, and their special features and roles in cardiac activity are well described in a recent review [134]. Some salient features of these channels and their relevance to cardiac electrical activity and heart rate and rhythm are discussed below.

CIC-2 channels are responsible for a voltage-activated inwardly rectifying chloride current, $I_{Cl,ir}$, and are likely to contribute to cell swelling. CLC-2 is expressed in SAN pacemaker cells, Purkinje fibers and atrial and ventricular myocytes [135].

CIC-3 channels elicit a volume-regulated outwardly rectifying Cl current, $I_{Cl,vol}$, with two components, the swelling-activated one, $I_{Cl,swell}$, and basally activated one, $I_{Cl,b}$. CIC-1,-2, and -3 channels are expressed in atria and ventricles and $I_{Cl,Swell}$ is reported in SAN, and atrial and ventricular myocytes [134, 136, 137]. $I_{Cl,Swell}$ is stretch-sensitive and is thought to play a role in regulating membrane potential, APD, and excitability and has arrhythmogenic potentials [137]. They are implicated

in VF dynamics in isolated guinea pig heart and exert a protective role in cardiac hypertrophy and HF [138].

CFTR channels are expressed in atria and ventricles and give rise to slightly outwardly rectifying currents named after their activators, namely $I_{\text{Cl,PKA}}$, $I_{\text{Cl,PKC}}$, and $I_{\text{Cl,ATP}}$ [139]. The cAMP/PKA-induced current, $I_{\text{Cl,PKA}}$, was the first Cl channel current recorded in heart cells. The PKC-activated current, $I_{\text{Cl,PKC}}$, has been recorded from ventricular myocytes [140–142]. The extracellular ATP-activated [134] CFTR current, $I_{\text{Cl,ATP}}$, has also been recorded from atria and ventricles. CFTR responsible for $I_{\text{Cl,PKA}}$ are clustered on the z-groove but are not seen on the mouth of T-tubules [142]. I_{CFTR} is associated with early afterdepolarizations (EAD) [137], is reported to modulate ventricular myocyte contraction rate and is associated with changes in HF [143]. An epicardium to endocardium gradient is suggested to exist for CFTR ($I_{\text{Cl,PKA}}$) which is lost in cardiac hypertrophy [144]. The channel is blocked by GaTx-1 and activated by nicorandil [145, 171].

CLCA-1 channel-mediated current, $I_{\text{Cl,Ca}}$, has been recorded from Purkinje fibers and ventricular myocytes [146]. $I_{\text{Cl,Ca}}$ has a role in determining membrane potential and membrane excitability in heart cells and contributes to I_t in addition to I_{NCX} (Fig. 1.3). An increase in $I_{\text{Cl,Ca}}$ is reported to be associated with delayed afterdepolarization (DAD) in ventricular myocytes [146] and with left ventricular hypertrophy exhibiting APD prolongation, AP alternans, and T wave alternans, indicating a role of CLCA-1 in arrhythmogenesis [147].

Bestrophin, a member of CaCC group, has several homologues, expressed in a wide variety of cells including myocardium [134, 148] where Best-3 is more predominant than Best-1 and Best-2 [149]. mBest-3 is widely distributed in mouse heart and has a sarcolemmal localisation [149]. It is shown to have a putative pore domain and to function like a channel. The bestrophin-induced $I_{\text{Cl,Ca}}$ is time- and voltage-independent and displays slight outward rectification. It is inhibited by niflumic acid and DIDS [149, 171].

THEM16 (Anoctamin, ANO), another member of Ca-activated Cl channels, has 10 homologues, and THEM16A is expressed in heart [134, 150].

VDAC1, the voltage-dependent anion channel 1, having very high conductance (280–430 pS; [171]) and normally localised on the outer mitochondrial membrane in ventricular myocytes is also expressed on SL [134].

$I_{\text{Cl,acid}}$, activated by acidic extracellular pH [151], has also been reported in atrial and ventricular myocytes showing outward rectification. Its activation is independent of $[\text{Ca}^{2+}]_i$. Since high extracellular pH increases APD and extracellular acidosis accompanies MI-induced arrhythmias it is likely that $I_{\text{Cl,acid}}$ has a role in pathophysiology of such arrhythmias [152].

1.3.10 Stretch-Activated Channels

Mechano-sensitive (MSC), mechano-gated (MGC), or stretch-activated (SAC) channels are activated primarily by mechanical stress (mechanical tension) in the

membrane [153]. Membrane cytoskeleton is considered to mediate the mechanical stress to the channel protein bringing about the required changes in channel conformation to induce channel opening. Although several members of VGIC and LGIC superfamilies do respond to mechanical stress they are not categorised as SACs. However, a few members of TRPC and K₂P (TWIK) families indeed respond to primary mechanical stimulus and are, therefore, identified as SACs. In the strict sense of SACs no specific protein has yet been identified as a representative of these channels [153]. It is well recognised that mechano-electric feedback has important roles in the cardiac cycle and is involved in maintaining the heart rate and rhythm under physiological conditions and cardiac rhythm disturbances (see Chap. 7). The mechano-sensitive channels include TREK-1, TRPC1, and TRPV2. These SACs are implicated in AF, DADs, cardiomyopathy, and ventricular arrhythmia [99, 154].

Gadolinium and streptomycin inhibit the activity of SACs, but GsMTx4, a peptide isolated from tarantula venom, is a more specific blocker of SACs and inhibits stretch-induced AF [153].

1.3.11 Gap Junction Channels

The intercalated discs (ICD) on SL between adjacent cardiac myocytes connect the two neighbouring cells. Gap junction (GJ) channels are one of the three components of ICDs, the other two being fascia adherens and desmosomes, and provide electrical coupling between adjacent cells. GJ channels are composed of two hemichannels, each one, called connexons, inserted in the SL of two adjoining cells. Each connexon comprises of six domains of connexins arranged concentrically to form a central pore. The connexins themselves are made up of four TM segments, M1–M4 with their N and C termini located intracellularly. Two loops connecting M1 with M2 and M3 with M4 are extracellular, while an intracellular loop connects M2 to M3. Normally GJ channels are located at the terminal poles of myocardial cells and bring about cell-to-cell electrical coupling facilitating impulse conduction along cardiac fibres. GJ channels allow passive diffusion of molecules <1 kDa, e.g. anions, cations, nutrients, metabolites, and second messengers (IP₃). Connexins, e.g. Cx43, have a short half-life that may have implications in myocardial excitability [155].

GJ channels are named after their constituent connexin (Cx) followed by numerals that denote its molecular weight, e.g. Cx40 meaning connexin of 40 kDa. Twenty one connexins are expressed in humans, only a few being expressed in heart, viz. Cx30, Cx30.2, Cx 40, Cx43, and Cx 45 [156, 157]. Cx30 and Cx30.2 are expressed in SAN center and contribute to regulation of pacemaker activity and heart rate [156, 158]. Cx40 is expressed in Purkinje fibers, SAN periphery and atria [155–157, 159]. Cx43 is a ventricular-specific protein and is also expressed in atria and the periphery of SAN [156, 157]. Cx45 is expressed in AVN and is reported in the SAN center. Cx30.2, Cx40, and Cx45 are expressed in AVN and His-bundle and contribute differentially to supra-Hisian and infra-Hisian impulse conduction in mice, as evident from ECG changes in Cx30.2/Cx40 deficient animals [159].

Connexins play a key role in impulse conduction in the entire heart maintaining specific regional conduction requirements necessary for a co-ordinated cardiac contraction underlying normal heart rate. Alterations in expression pattern of specific connexins herald several cardiac rhythm disorders including AF (see Chap. 27), ischemia–reperfusion injury, and congestive heart failure (CHF) [63].

Chapter 28 provides an account of GJ channels in cardiac disorders. Chapter 29 discusses the role of connexins in ischemia–reperfusion-induced arrhythmias.

1.4 Sarcoplasmic Reticulum Membrane Ion Channels

SR membrane is endowed with the capability of contributing to fine maintenance of cytosolic free Ca ion concentration and to make free Ca available at strategic locations necessary for performance of cellular functions. To this end, the SR membrane possesses two major types of Ca release channels, ryanodine receptor channels (RyR) and inositol triphosphate receptor channels (InsP3R). The SR membrane Ca-ATPase (SERCA2) takes up excess Ca from cytosol and fills the SR Ca stores. This topic is covered in Chap. 17.

1.4.1 Ryanodine Receptor Channels

The RyRs are ubiquitously distributed. Three types of RyRs have been identified, namely RyR1, RyR2, and RyR3, which represent large (~558 kDa) structurally related tetrameric membrane-spanning proteins, which co-assemble with four calstabin (FKBP12) proteins [160, 171]. The RyR channels form a mushroom-like structure and bulk of their protein lies on the cytosolic surface of SR. Significant advances have been made in resolving the pore structure of RyRs using high-resolution cryo-electron microscopy [161]. RyR2, the main cardiac Ca release channel, plays a key role in E–C coupling by releasing required amount of Ca in the cytosol following SL influx of Ca through Cav1.2 channels localised in T-tubules (Fig. 1.2). RyR2 and RyR3 are also expressed in SAN and Purkinje fibre cells, contributing to the pacemaker activity of the former [162, 163], and impulse conduction in the latter, thereby contributing to regulation of heart rate and rhythm. RyR2 is implicated in several acquired and inherited cardiac rhythm disorders, e.g. arrhythmogenic right ventricular cardiomyopathy type 2 (ARVC2), CPVT, AF, and abnormal sinus rhythm [164, 165]. It is suggested that changes in RyR2 in the His-Purkinje system underlie CPVT [163].

RyR2 channels are blocked by ryanodine, dantrolene, ruthenium red, tetracaine, and lidocaine and are activated by caffeine. Treatability of CPVT-like condition by tetracaine in mice shows that RyR2 is a promising target for developing novel antiarrhythmic drugs [163, 166].

Chapter 21 gives an account of the role of RyR2 in CPVT and Chapter 4 describes the role of RyRs in the pacemaker activity of SA node.

1.4.2 SR Inositol Triphosphate Receptor Channels

Out of several isoforms of InsP3R, heart expresses InsP3R2, a 300 kDa protein that co-assembles to form a tetrameric channel. InsP3R2 is expressed in atria, ventricles, and Purkinje fibres albeit at lower density than RyR2. InsP3R2 is suggested to fine tune the perinuclear Ca and activate CaMKII to modulate transcription mechanisms of nucleus [169, 173]. Such a role of InsP3R2 in excitation–transcription coupling may be involved in gene expression alterations during cardiac disorders like ventricular hypertrophy and HF. RyR2 and InsP3R2 have distinct functions to perform in heart and modulate heart rhythm via altogether different mechanisms (see Chap. 17).

1.5 Mitochondrial and Nuclear Channels

Mitochondria serve as the energy centre of heart cells and also regulate cardiac electrical activity by modulating the SL ion channel kinetics. The mitochondrial membranes express several ion channels with crucial roles in the normal and pathological cardiac activity including arrhythmogenesis [168]. Given below are some of the predominant mitochondrial and nuclear ion channels (see also Chap. 17).

K_{Ca}1.1 (Slo, BK, Gene - KCNMA1, 1182 aa, 200–220 pS) has Slack as its heteromeric pore-forming subunit and β1–β4 serve as auxiliary subunits [22]. It is activated both by voltage and intracellular Ca and is blocked by TEA, charybdotoxin, and iberiotoxin. K_{Ca}1.1 is expressed in inner mitochondrial membrane in heart and plays a significant role in myocardial energetics. Openers of K_{Ca}1.1 are reported to protect the ventricles from ischemia–reperfusion injury and open the possibilities of developing new drug for treatment of cardiac disorders [168].

K_ir6.1, K_ir6.2 (K_{ATP}), and SUR2A subunits are expressed in mitochondria and are associated with protection from ischemia–reperfusion injuries [123].

Voltage-dependent anion channels, VDAC, are expressed prominently in mitochondrial outer membrane.

The nucleus in cardiomyocytes serves as the seat of transcription and the nuclear membrane and nucleoplasmic reticulum have key roles in excitation–transcription coupling [169]. Both the nuclear membrane and the nucleoplasmic reticulum express several ion channels, including RyR, InsP3R, R-type Ca channels, and K channels [170] (see Sec. 1.4.2 and Chap. 17).

1.6 Conclusions

Our present knowledge of the molecular basis of electrical activity of heart owes greatly to the analytical approach in identifying the ion channels and other transport proteins expressed at mRNA and protein levels in the sarcolemma of different types of heart cells. The roles of SR, mitochondrial and nuclear membrane ion transport proteins in cardiac cellular activity during normal and abnormal cardiac rhythm are also better understood now. Future research on analytical and integrative aspects of “ion channels, ion transporters, signaling cascades, mechanical function, energy metabolism, transcription, translation and targeting” [173] (Fig. 1.2) is expected to provide a better picture of the molecular basis of ionic mechanisms underlying electrical activity during a cardiac cycle in health and disease. Because most of the studies on cardiac ion channels in SR, mitochondria and nucleus have been carried out on ventricular myocytes the need for research on these aspects of cells from other regions of heart cannot be overemphasized. An important problem, however, concerns differences in the ion channel compliments of the same type of cardiac tissue in different mammalian species limiting extrapolation of data from laboratory animals to humans. It is hoped that future research will overcome this issue by identifying the entire compliment of human cardiac ion channel signature and also establish their role in arrhythmias including channelopathies. The other problem concerns reported disparities between the ion channel mRNA and protein expression levels in different regions of heart and functional aspects of the expressed channel proteins. Thus, for example, we do not yet fully know about the molecular components of all the ionic currents recorded in different types of heart cells in higher mammals, including humans, let alone their precise contributions to AP configuration and ECG waveform. Ongoing research is expected to provide a better understanding of these important aspects. This will also help identification and validation of new target molecules that could be explored, by employing the newly developed ion channel-high throughput screening (HTS) and related technologies, for discovery of novel and better antiarrhythmic drugs (see Chap. 35).

Acknowledgements The author is thankful to the generous financial support from Life sciences Academy, Lucknow, India for preparation of this manuscript. My research work included in this chapter was supported by CSIR, DST and DBT, India. I am very grateful to Prof. M. C. Sanguinetti for critically going through this manuscript and for making valuable suggestions. I thank Mr. Ali Kausar for preparing the illustrations.

References

1. Landes EM. Carl John Wiggers: A Biographical Memoir. National Academy of Sciences, Washington DC, 1976.
2. Trautwein W, McDonald TF, Tripathi O. Calcium conductance and tension in mammalian ventricular muscle. *Pflugers Arch.* 1975;354:55–74.
3. Noujaim SF, Lucca E, Munoz V, Persaud D, Berenfeld O, Meijler FL, et al. From mouse to whale: a universal scaling relation for the PR Interval of the electrocardiogram of mammals. *Circulation.* 2004;110:2802–8.

4. Postema PG, Ritsema van Eck HJ, Ophof T, van Herpen G, van Dessel PF, Priori SG, et al. I_{K1} modulates the U-wave: insights in a 100-year-old enigma. *Heart Rhythm.* 2009;6:393–400.
5. Nerbonne JM, Kass RS. Molecular physiology of cardiac repolarization. *Physiol Rev.* 2005;85(4):1205–53.
6. Gaborit N, Le Bouter S, Szuts V, Varro A, Escande D, Nattel S, et al. Regional and tissue specific transcript signatures of ion channel genes in the non-diseased human heart. *J Physiol.* 2007;582(Pt 2):675–93.
7. Amin AS, Tan HL, Wilde AA. Cardiac ion channels in health and disease. *Heart Rhythm.* 2010;7(1):117–26.
8. Michael G, Xiao L, Qi XY, Dobrev D, Nattel S. Remodelling of cardiac repolarization: how homeostatic responses can lead to arrhythmogenesis. *Cardiovasc Res.* 2009;81(3):491–9.
9. Maier SK, Westenbroek RE, Schenkman KA, Feigl EO, Scheuer T, Catterall WA. An unexpected role for brain-type sodium channels in coupling of cell surface depolarization to contraction in the heart. *Proc Natl Acad Sci USA.* 2002;99(6):4073–8.
10. Maier SK, Westenbroek RE, Yamanishi TT, Dobrzynski H, Boyett MR, Catterall WA, Scheuer T. An unexpected requirement for brain-type sodium channels for control of heart rate in the mouse sinoatrial node. *Proc Natl Acad Sci USA.* 2003;100(6):3507–12.
11. Lei M, Jones SA, Liu J, Lancaster MK, Fung SS, Dobrzynski H, et al. Requirement of neuronal- and cardiac-type sodium channels for murine sinoatrial node pacemaking. *J Physiol.* 2004;559:835–48.
12. Maltsev VA, Kyle JW, Undrovinas A. Late Na^+ current produced by human cardiac Na^+ channel isoform Nav1.5 is modulated by its beta1 subunit. *J Physiol Sci.* 2009;59(3):217–25.
13. Lei M, Huang CL, Zhang Y. Genetic Na^+ channelopathies and sinus node dysfunction. *Prog Biophys Mol Biol.* 2008;98:171–8.
14. Burbidge SA, Dale TJ, Powell AJ, Whitaker WR, Xie XM, Romanos MA, et al. Molecular cloning, distribution and functional analysis of the Nav1.6. Voltage-gated sodium channel from human brain. *Brain Res Mol Brain Res.* 2002;103:80–90.
15. Prakash P, Tripathi O. Verapamil and TTX inhibit +V_{max} but differentially alter the duration of action potential of adult chicken ventricular myocardium. *Indian J Biochem Biophys.* 1998;35(2):123–30.
16. Haverinen J, Hassinen M, Vornanen M. Fish cardiac sodium channels are tetrodotoxin sensitive. *Acta Physiol.* 2007;191(3):197–204.
17. Hofmann F, Biel M, Flockerzi V. Molecular basis for Ca^{2+} channel diversity. *Annu Rev Neurosci.* 1994;17:399–418.
18. Gu Y, Gorelik J, Spohr HA, Shevchuk A, Lab MJ, Harding SE, et al. High-resolution scanning patch-clamp: new insights into cell function. *FASEB J.* 2002;16(7):748–50.
19. Murakami M, Ohba T, Takahashi Y, Watanabe H, Miyoshi I, Nakayama S, et al. Identification of a cardiac isoform of the murine calcium channel alpha1C (Cav1.2-a) subunit and its preferential binding with the beta2 subunit. *J Mol Cell Cardiol.* 2006;41(1):115–25.
20. Foell JD, Balijepalli RC, Delisle BP, Yunker AM, Robia SL, Walker JW, et al. Molecular heterogeneity of calcium channel beta-subunits in canine and human heart: evidence for differential subcellular localization. *Physiol Genomics.* 2004;17(2):183–200.
21. Irisawa H, Brown HF, Giles W. Cardiac pacemaking in the sinoatrial node. *Physiol Rev.* 1993;73(1):197–227.
22. IUPHAR database of G protein coupled receptors and ion channels (2009). <http://www.iuphar-db.org/DATABASE/>.
23. McDonald TF, Pelzer S, Trautwein W, Pelzer DJ. Regulation and modulation of calcium channels in cardiac, skeletal, and smooth muscle cells. *Physiol Rev.* 1994;74(2):365–507.
24. Dai S, Hall DD, Hell JW. Supramolecular assemblies and localized regulation of voltage-gated ion channels. *Physiol Rev.* 2009;89(2):411–52.
25. Wu Y, Temple J, Zhang R, Dzhura I, Zhang W, Trimble R, et al. Calmodulin kinase II and arrhythmias in a mouse model of cardiac hypertrophy. *Circulation.* 2002;106:1288–93.

26. Zhang Z, Xu Y, Song H, Rodriguez J, Tuteja D, Namkung Y, et al. Functional roles of $\text{Ca}_v1.3$ (alpha(1D)) calcium channel in sinoatrial nodes: insight gained using gene-targeted null mutant mice. *Circ Res.* 2002;90(9):981–7.
27. Mangoni ME, Nargeot J. Genesis and regulation of the heart automaticity. *Physiol Rev.* 2008;88(3):919–82.
28. Qu Y, Baroudi G, Yue Y, El-Sherif N, Boutjdir M. Localization and modulation of {alpha} 1D ($\text{Ca}_v1.3$) L-type Ca channel by protein kinase A. *Am J Physiol Heart Circ Physiol.* 2005;288(5):H2123–30.
29. Singh A, Gebhart M, Fritsch R, Sinnegger-Brauns MJ, Poggiani C, Hoda JC, et al. Modulation of voltage- and Ca^{2+} -dependent gating of $\text{Ca}_v1.3$ L-type calcium channels by alternative splicing of a C-terminal regulatory domain. *J Biol Chem.* 2008;283(30):20733–44.
30. Platzer J, Engel J, Schrott-Fischer A, Stephan K, Bova S, Chen H, et al. Congenital deafness and sinoatrial node dysfunction in mice lacking class D L-type Ca^{2+} channels. *Cell.* 2000; 102(1):89–97.
31. Mitchell JW, Larsen JK, Best PM. Identification of the calcium channel alpha 1E ($\text{Ca}_v2.3$) isoform expressed in atrial myocytes. *Biochim Biophys Acta.* 2002;1577(1):17–26.
32. Ono K, Iijima T. Cardiac T-type Ca^{2+} channels in the heart. *J Mol Cell Cardiol.* 2010; 48(1):65–70.
33. Emerick MC, Stein R, Kunze R, McNulty MM, Regan MR, Hanck DA, et al. Profiling the array of $\text{Ca}_v3.1$ variants from the human T-type calcium channel gene CACNA1G: alternative structures, developmental expression, and biophysical variations. *Proteins.* 2006;64(2):320–42.
34. McGivern JG. Pharmacology and drug discovery for T-type calcium channels. *CNS Neurol Disord Drug Targets.* 2006;5(6):587–603.
35. Cribbs LL, Lee JH, Yang J, Satin J, Zhang Y, Daud A, et al. Cloning and characterization of alpha1H from human heart, a member of the T-type Ca^{2+} channel gene family. *Circ Res.* 1998;83(1):103–9.
36. Maturana A, Lenglet S, Python M, Kuroda S, Rossier MF. Role of the T-type calcium channel $\text{Ca}_v3.2$ in the chronotropic action of corticosteroids in isolated rat ventricular myocytes. *Endocrinology.* 2009;150(8):3726–34.
37. Stühmer W, Ruppertsberg JP, Schröter KH, Sakmann B, Stocker M, Giese KP, et al. Molecular basis of functional diversity of voltage-gated potassium channels in mammalian brain. *EMBO J.* 1989;8(11):3235–44.
38. Robards SL, Tamkun MM. Cloning and tissue-specific expression of five voltage-gated potassium channel cDNAs expressed in rat heart. *Proc Natl Acad Sci USA.* 1991;88(5): 1798–802.
39. Leoni AL, Marionneau C, Demolombe S, Le Bouter S, Mangoni ME, Escande D, et al. Chronic heart rate reduction remodels ion channel transcripts in the mouse sinoatrial node but not in the ventricle. *Physiol Genomics.* 2005;24(1):4–12.
40. Matsubara H, Liman ER, Hess P, Koren G. Pretranslational mechanisms determine the type of potassium channels expressed in the rat skeletal and cardiac muscles. *J Biol Chem.* 1991;266(20):13324–8.
41. Grissmer S, Nguyen AN, Aiyar J, Hanson DC, Mather RJ, Gutman GA, et al. Pharmacological characterization of five cloned voltage-gated K^+ channels, types Kv1.1, 1.2, 1.3, 1.5, and 3.1, stably expressed in mammalian cell lines. *Mol Pharmacol.* 1994;45(6):1227–34.
42. Brahmajothi MV, Morales MJ, Rasmusson RL, Campbell DL, Strauss HC. Heterogeneity in K^+ channel transcript expression detected in isolated ferret cardiac myocytes. *Pacing Clin Electrophysiol.* 1997;20(2 Pt 2):388–96.
43. Lee JK, Nishiyama A, Kambe F, Seo H, Takeuchi S, Kamiya K, et al. Downregulation of voltage-gated K^+ channels in rat heart with right ventricular hypertrophy. *Am J Physiol.* 1999;277(5 Pt 2):H1725–31.
44. Tamkun MM, Knoth KM, Walbridge JA, Kroemer H, Roden DM, Glover DM. Molecular cloning and characterization of two voltage-gated K^+ channel cDNAs from human ventricle. *FASEB J.* 1991;5(3):331–7.

45. Brahmajothi MV, Morales MJ, Liu S, Rasmusson RL, Campbell DL, Strauss HC. In situ hybridization reveals extensive diversity of K^+ channel mRNA in isolated ferret cardiac myocytes. *Circ Res.* 1996;78(6):1083–9.
46. Han W, Wang Z, Nattel S. A comparison of transient outward currents in canine cardiac Purkinje cells and ventricular myocytes. *Am J Physiol Heart Circ Physiol.* 2000;279(2):H466–74.
47. O'Connell KM, Whitesell JD, Tamkun MM. Localization and mobility of the delayed-rectifier K^+ channel Kv2.1 in adult cardiomyocytes. *Am J Physiol Heart Circ Physiol.* 2008;294(1):H229–37.
48. Roberds SL, Knoth KM, Po S, Blair TA, Bennett PB, Hartshorne RP, et al. Molecular biology of the voltage-gated potassium channels of the cardiovascular system. *J Cardiovasc Electrophysiol.* 1993;4(1):68–80.
49. Niwa N, Nerbonne JM. Molecular determinants of cardiac transient outward potassium current (I_{to}) expression and regulation. *J Mol Cell Cardiol.* 2010;48(1):12–25.
50. Huang B, Qin D, El-Sherif N. Spatial alterations of Kv channels expression and K^+ currents in post-MI remodeled rat heart. *Cardiovasc Res.* 2001;52(2):246–54.
51. Dobrzynski H, Rothery SM, Marples DD, Coppen SR, Takagishi Y, Honjo H, et al. Presence of the Kv1.5 K^+ channel in the sinoatrial node. *J Histochem Cytochem.* 2000;48(6):769–80.
52. Ordóñez B, Brutýo E, Puskás LG, Papp JG, Varró A, Szabad J, et al. Gene expression profiling of human cardiac potassium and sodium channels. *Int J Cardiol.* 2006;111(3):386–93.
53. Snyders DJ, Tamkun MM, Bennett PB. A rapidly activating and slowly inactivating potassium channel cloned from human heart. Functional analysis after stable mammalian cell culture expression. *J Gen Physiol.* 1993;101(4):513–43.
54. Van Wagoner DR, Pond AL, McCarthy PM, Trimmer JS, Nerbonne JM. Outward K^+ current densities and Kv1.5 expression are reduced in chronic human atrial fibrillation. *Circ Res.* 1997;80(6):772–81.
55. Matsubara H, Suzuki J, Inada M. Shaker-related potassium channel, Kv1.4, mRNA regulation in cultured rat heart myocytes and differential expression of Kv1.4 and Kv1.5 genes in myocardial development and hypertrophy. *J Clin Invest.* 1993;92:1659–66.
56. Kalman K, Nguyen A, Tseng-Crank J, Dukes ID, Chandy G, Hustad CM, et al. Genomic organization, chromosomal localization, tissue distribution, and biophysical characterization of a novel mammalian Shaker-related voltage-gated potassium channel, Kv1.7. *J Biol Chem.* 1998;273(10):5851–7.
57. Finol-Urdaneta RK, Strüver N, Terlau H. Molecular and functional differences between heart mKv1.7 channel isoforms. *J Gen Physiol.* 2006;128(1):133–45.
58. Bardien-Kruger S, Wulff H, Arieff Z, Brink P, Chandy KG, Corfield V. Characterisation of the human voltage-gated potassium channel gene, KCNA7, a candidate gene for inherited cardiac disorders, and its exclusion as cause of progressive familial heart block I (PFHBI). *Eur J Hum Genet.* 2002;10(1):36–43.
59. Tian S, Liu W, Wu Y, Rafi H, Segal AS, Desir GV. Regulation of the voltage-gated K^+ channel KCNA10 by KCNA4B, a novel beta-subunit. *Am J Physiol Renal Physiol.* 2002;283(1):F142–9.
60. Yao X, Liu Y, Tung F, Desir GV. Genomic structure and regulation of Kcn1, a cGMP-gated potassium channel. *Am J Physiol.* 1996;271(1 Pt 2):F37–41.
61. Iwasa H, Kurabayashi M, Nagai R, Nakamura Y, Tanaka T. Genetic variations in five genes involved in the excitability of cardiomyocytes. *J Hum Genet.* 2001;46(9):549–52.
62. Marionneau C, Brunet S, Flagg TP, Pilgram TK, Demolombe S, Nerbonne JM. Distinct cellular and molecular mechanisms underlie functional remodeling of repolarizing K^+ currents with left ventricular hypertrophy. *Circ Res.* 2008;102(11):1406–15.
63. Maguy A, Le Bouter S, Comtois P, Chartier D, Villeneuve L, Wakili R, et al. Ion channel subunit expression changes in cardiac Purkinje fibers: a potential role in conduction abnormalities associated with congestive heart failure. *Circ Res.* 2009;104(9):1113–22.

64. Suzuki H, Momoi N, Ono T, Maeda S, Shikama Y, Matsuoka I, Suzuki H, Kimura J, et al. Inhibitory effect of thiopental on ultra-rapid delayed rectifier K⁺ current in H9c2 cells. *J Pharmacol Sci.* 2005;99(2):177–84.
65. Takeuchi S, Takagishi Y, Yasui K, Murata Y, Toyama J, Kodama I. Voltage-gated K⁺ channel, Kv4.2, localizes predominantly to the transverse-axial tubular system of the rat myocyte. *J Mol Cell Cardiol.* 2000;32(7):1361–9.
66. Rosati B, Dong M, Cheng L, Liou SR, Yan Q, Park JY, et al. Evolution of ventricular myocyte electrophysiology. *Physiol Genomics.* 2008;35:262–72.
67. Postma AV, Bezzina CR, de Vries JF, Wilde AA, Moorman AF, Mannens MM. Genomic organisation and chromosomal localisation of two members of the KCND ion channel family, KCND2 and KCND3. *Hum Genet.* 2000;106(6):614–9.
68. Birnbaum SG, Varga AW, Yuan LL, Anderson AE, Sweatt JD, Schrader LA. Structure and function of Kv4-family transient potassium channels. *Physiol Rev.* 2004;84(3):803–33.
69. Dilks D, Ling HP, Cockett M, Sokol P, Numann R. Cloning and expression of the human kv4.3 potassium channel. *J Neurophysiol.* 1999;81(4):1974–7.
70. Kääb S, Dixon J, Duc J, Ashen D, Näbauer M, Beuckelmann DJ, et al. Molecular basis of transient outward potassium current downregulation in human heart failure: a decrease in Kv4.3 mRNA correlates with a reduction in current density. *Circulation.* 1998;98(14):1383–93.
71. Gaborit N, Wichter T, Varro A, Szuts V, Lamirault G, Eckardt L, et al. Transcriptional profiling of ion channel genes in Brugada syndrome and other right ventricular arrhythmic diseases. *Eur Heart J.* 2009;30(4):487–96.
72. Abbott GW, Xu X, Roepke TK. Impact of ancillary subunits on ventricular repolarization. *J Electrocardiol.* 2007;40(6 Suppl):S42–6.
73. Sanguinetti MC, Curran ME, Zou A, Shen J, Spector PS, Atkinson DL, et al. Coassembly of K(V)LQT1 and minK (IsK) proteins to form cardiac I_{Ks} potassium channel. *Nature.* 1996;384(6604):80–3.
74. Keating MT, Sanguinetti MC. Molecular and cellular mechanisms of cardiac arrhythmias. *Cell.* 2001;104(4):569–80.
75. Bellocq C, van Ginneken AC, Bezzina CR, Alders M, Escande D, Mannens MM, et al. Mutation in the KCNQ1 gene leading to the short QT-interval syndrome. *Circulation.* 2004;109(20):2394–7.
76. Hong K, Piper DR, Diaz-Valdecantos A, Brugada J, Oliva A, Burashnikov E, et al. De novo KCNQ1 mutation responsible for atrial fibrillation and short QT syndrome in utero. *Cardiovasc Res.* 2005;68(3):433–40.
77. Abbott GW, Sesti F, Splawski I, Buck ME, Lehmann MH, Timothy KW, et al. MiRP1 forms IKr potassium channels with HERG and is associated with cardiac arrhythmia. *Cell.* 1999;97(2):175–87.
78. Jones EM, Roti Roti EC, Wang J, Delfosse SA, Robertson GA. Cardiac I_{Kr} channels minimally comprise hERG 1a and 1b subunits. *J Biol Chem.* 2004;279(43):44690–4.
79. Sanguinetti MC, Tristani-Firouzi M. hERG potassium channels and cardiac arrhythmia. *Nature.* 2006;440(7083):463–9.
80. Tuteja D, Xu D, Timofeyev V, Lu L, Sharma D, Zhang Z, et al. Differential expression of small-conductance Ca²⁺-activated K⁺ channels SK1, SK2, and SK3 in mouse atrial and ventricular myocytes. *Am J Physiol Heart Circ Physiol.* 2005 Dec;289(6):H2714–23.
81. Wulff H, Kolski-Andreaco A, Sankaranarayanan A, Sabatier JM, Shakkottai V. Modulators of small- and intermediate-conductance calcium-activated potassium channels and their therapeutic indications. *Curr Med Chem.* 2007;14(13):1437–57.
82. Xu Y, Tuteja D, Zhang Z, Xu D, Zhang Y, Rodriguez J, et al. Molecular identification and functional roles of a Ca²⁺-activated K⁺ channel in human and mouse hearts. *J Biol Chem.* 2003;278(49):49085–94.
83. Chen MX, Gorman SA, Benson B, Singh K, Hieble JP, Michel MC, et al. Small and intermediate conductance Ca²⁺-activated K⁺ channels confer distinctive patterns of

- distribution in human tissues and differential cellular localisation in the colon and corpus cavernosum. *Naunyn Schmiedebergs Arch Pharmacol.* 2004;369(6):602–15.
- 84. Li N, Timofeyev V, Tuteja D, Xu D, Lu L, Zhang Q, et al. Ablation of a Ca^{2+} -activated K^+ channel (SK2 channel) results in action potential prolongation in atrial myocytes and atrial fibrillation. *J Physiol.* 2009;587(Pt 5):1087–100.
 - 85. Bhattacharjee A, Joiner WJ, Wu M, Yang Y, Sigworth FJ, Kaczmarek LK. Slick (Slo2.1), a rapidly-gating sodium-activated potassium channel inhibited by ATP. *J Neurosci.* 2003; 23(37):11681–91.
 - 86. Mistry DK, Tripathi O, Chapman RA. Kinetic properties of unitary Na^+ -dependent K^+ channels in inside-out patches from isolated guinea-pig ventricular myocytes. *J Physiol.* 1997; 500(Pt 1):39–50.
 - 87. Kameyama M, Kakei M, Sato R, Shibasaki T, Matsuda H, Irisawa H. Intracellular Na^+ activates a K^+ channel in mammalian cardiac cells. *Nature.* 1984;309(5966):354–6.
 - 88. Mistry DK, Tripathi O, Chapman RA. The occurrence of stable subconductance levels in Na^+ -activated K^+ channels in excised membrane patches from guinea-pig ventricular myocytes. *Exp Physiol.* 1996;81(6):899–907.
 - 89. Chen H, Kronengold J, Yan Y, Gazula VR, Brown MR, Ma L, et al. The N-terminal domain of Slack determines the formation and trafficking of Slick/Slack heteromeric sodium-activated potassium channels. *J Neurosci.* 2009;29(17):5654–65.
 - 90. Yuan A, Santi CM, Wei A, Wang ZW, Pollak K, Nonet M, et al. The sodium-activated potassium channel is encoded by a member of the Slo gene family. *Neuron.* 2003;37(5):765–73.
 - 91. Mori K, Kobayashi S, Saito T, Masuda Y, Nakaya H. Inhibitory effects of class I and IV antiarrhythmic drugs on the Na^+ -activated K^+ channel current in guinea pig ventricular cells. *Naunyn Schmiedebergs Arch Pharmacol.* 1998;358(6):641–8.
 - 92. Dai L, Garg V, Sanguinetti MC. Activation of Slo2.1 channels by niflumic acid. *J Gen Physiol.* 2010;135(3):275–95.
 - 93. Tan JH, Liu W, Saint DA. Differential expression of the mechanosensitive potassium channel TREK-1 in epicardial and endocardial myocytes in rat ventricle. *Exp Physiol.* 2004; 89(3):237–42.
 - 94. Gurney A, Manoury B. Two-pore potassium channels in the cardiovascular system. *Eur Biophys J.* 2009;38(3):305–18.
 - 95. Charpentier F. Understanding the cardiac role of K2P channels: a new TASK for electrophysiologists. *Cardiovasc Res.* 2007;75(1):5–6.
 - 96. Lesage F, Guillemaire E, Fink M, Duprat F, Lazdunski M, Romey G, et al. TWIK-1, a ubiquitous human weakly inward rectifying K^+ channel with a novel structure. *EMBO J.* 1996;15(5):1004–11.
 - 97. Wang Z, Yue L, White M, Pelletier G, Nattel S. Differential distribution of inward rectifier potassium channel transcripts in human atrium versus ventricle. *Circulation.* 1998;98(22):2422–8.
 - 98. Lesage F, Lazdunski M. Molecular and functional properties of two-pore-domain potassium channels. *Am J Physiol Renal Physiol.* 2000;279(5):F793–801.
 - 99. Li XT, Dyachenko V, Zuzarte M, Putzke C, Preisig-Müller R, Isenberg G, et al. The stretch-activated potassium channel TREK-1 in rat cardiac ventricular muscle. *Cardiovasc Res.* 2006;69(1):86–97.
 - 100. Putzke C, Wemhöner K, Sachse FB, Rinné S, Schlächter G, Li XT, et al. The acid-sensitive potassium channel TASK-1 in rat cardiac muscle. *Cardiovasc Res.* 2007;75(1):59–68.
 - 101. Dhamoon AS, Jalife J. The inward rectifier current (I_{K_1}) controls cardiac excitability and is involved in arrhythmogenesis. *Heart Rhythm.* 2005;2(3):316–24.
 - 102. Zaritsky JJ, Redell JB, Tempel BL, Schwarz TL. The consequences of disrupting cardiac inwardly rectifying K^+ current (I_{K_1}) as revealed by the targeted deletion of the murine Kir2.1 and Kir2.2 genes. *J Physiol.* 2001;533(Pt 3):697–710.
 - 103. Hibino H, Inanobe A, Furutani K, Murakami S, Findlay I, Kurachi Y. Inwardly rectifying potassium channels: their structure, function, and physiological roles. *Physiol Rev.* 2010; 90(1):291–366.

104. Ma D, Tang XD, Rogers TB, Welling PA. An andersen-Tawil syndrome mutation in Kir2.1 (V302M) alters the G-loop cytoplasmic K⁺ conduction pathway. *J Biol Chem.* 2007;282(8):5781–9.
105. Takahashi N, Morishige K, Jahangir A, Yamada M, Findlay I, Koyama H, et al. Molecular cloning and functional expression of cDNA encoding a second class of inward rectifier potassium channels in the mouse brain. *J Biol Chem.* 1994;269(37):23274–9.
106. Périer F, Radeke CM, Vandenberg CA. Primary structure and characterization of a small-conductance inwardly rectifying potassium channel from human hippocampus. *Proc Natl Acad Sci USA.* 1994;91(13):6240–4.
107. Preisig-Müller R, Schlichthörl G, Goerge T, Heinen S, Brüggemann A, Rajan S, et al. Heteromerization of Kir2.x potassium channels contributes to the phenotype of Andersen's syndrome. *Proc Natl Acad Sci USA.* 2002;99(11):7774–9.
108. Dhamoon AS, Pandit SV, Sarmast F, Parisian KR, Guha P, Li Y, et al. Unique Kir2.x properties determine regional and species differences in the cardiac inward rectifier K⁺ current. *Circ Res.* 2004;94(10):1332–9.
109. Dascal N, Schreibmayer W, Lim NF, Wang W, Chavkin C, DiMagno L, et al. Atrial G protein-activated K⁺ channel: expression cloning and molecular properties. *Proc Natl Acad Sci USA.* 1993;90(21):10235–9.
110. Kravivinsky G, Gordon EA, Wickman K, Velimirović B, Kravivinsky L, Clapham DE. The G-protein-gated atrial K⁺ channel IKACH is a heteromultimer of two inwardly rectifying K⁺-channel proteins. *Nature.* 1995;374(6518):135–41.
111. Kurachi Y. G protein regulation of cardiac muscarinic potassium channel. *Am J Physiol.* 1995;269(4 Pt 1):C821–30.
112. Lignon JM, Bichler Z, Hivert B, Gannier FE, Cosnay P, del Rio JA, et al. Altered heart rate control in transgenic mice carrying the KCNJ6 gene of the human chromosome 21. *Physiol Genomics.* 2008;33:230–9.
113. Corey S, Clapham DE. Identification of native atrial G-protein-regulated inwardly rectifying K⁺ (GIRK4) channel homomultimers. *J Biol Chem.* 1998;273(42):27499–504.
114. Wickman K, Nemec J, Gandler SJ, Clapham DE. Abnormal heart rate regulation in GIRK4 knockout mice. *Neuron.* 1998;20(1):103–14.
115. Kovoov P, Wickman K, Maguire CT, Pu W, Gehrmann J, Berul CI, et al. Evaluation of the role of I_{KACH} in atrial fibrillation using a mouse knockout model. *J Am Coll Cardiol.* 2001;37(8):2136–43.
116. Ehrlich JR, Nattel S. Atrial-selective pharmacological therapy for atrial fibrillation: hype or hope? *Curr Opin Cardiol.* 2009 Jan;24(1):50–5.
117. Dobrev D, Wettwer E, Kortner A, Knaut M, Schüller S, Ravens U. Human inward rectifier potassium channels in chronic and postoperative atrial fibrillation. *Cardiovasc Res.* 2002;54(2):397–404.
118. Yamada M, Isomoto S, Matsumoto S, Kondo C, Shindo T, Horio Y, et al. Sulphonylurea receptor 2B and Kir6.1 form a sulphonylurea-sensitive but ATP-insensitive K⁺ channel. *J Physiol.* 1997;499(Pt 3):715–20.
119. Kane GC, Lam CF, O'Cochlain F, Hodgson DM, Reyes S, Liu XK, et al. Gene knockout of the KCNJ8-encoded Kir6.1 K(ATP) channel imparts fatal susceptibility to endotoxemia. *FASEB J.* 2006;20(13):2271–80.
120. Inagaki N, Gono T, Clement JP, Wang CZ, Aguilar-Bryan L, Bryan J, et al. A family of sulfonylurea receptors determines the pharmacological properties of ATP-sensitive K⁺ channels. *Neuron.* 1996;16(5):1011–7.
121. Morrissey A, Rosner E, Lanning J, Parachuru L, Dhar Chowdhury P, Han S, et al. Immunolocalization of KATP channel subunits in mouse and rat cardiac myocytes and the coronary vasculature. *BMC Physiol.* 2005;5(1):1.
122. Olson TM, Terzic A. Human KATP channelopathies: diseases of metabolic homeostasis. *Pflugers Arch.* 2010;460(2):295–306.
123. Suzuki M, Sasaki N, Miki T, Sakamoto N, Ohmoto-Sekine Y, Tamagawa M, et al. Role of sarcolemmal K(ATP) channels in cardioprotection against ischemia/reperfusion injury in mice. *J Clin Invest.* 2002;109(4):509–16.

124. Ruiz ML, London B, Nadal-Ginard B. Cloning and characterization of an olfactory cyclic nucleotide-gated channel expressed in mouse heart. *J Mol Cell Cardiol.* 1996;28(7):1453–61.
125. Moosmang S, Stieber J, Zong X, Biel M, Hofmann F, Ludwig A. Cellular expression and functional characterization of four hyperpolarization-activated pacemaker channels in cardiac and neuronal tissues. *Eur J Biochem.* 2001;268(6):1646–52.
126. Ludwig A, Budde T, Stieber J, Moosmang S, Wahl C, Holthoff K, et al. Absence epilepsy and sinus dysrhythmia in mice lacking the pacemaker channel HCN2. *EMBO J.* 2003;22(2):216–24.
127. Shi W, Wymore R, Yu H, Wu J, Wymore RT, Pan Z, et al. Distribution and prevalence of hyperpolarization-activated cation channel (HCN) mRNA expression in cardiac tissues. *Circ Res.* 1999;85(1):e1–6.
128. Nguyen BL, Fishbein MC, Chen LS, Chen PS, Masroor S. Histopathological substrate for chronic atrial fibrillation in humans. *Heart Rhythm.* 2009;6(4):454–60.
129. Stieber J, Hofmann F, Ludwig A. Pacemaker channels and sinus node arrhythmia. *Trends Cardiovasc Med.* 2004;14(1):23–8.
130. Stillitano F, Lonardo G, Zicha S, Varro A, Cerbai E, Mugelli A, et al. Molecular basis of funny current (If) in normal and failing human heart. *J Mol Cell Cardiol.* 2008;45(2):289–99.
131. Chandler NJ, Greener ID, Tellez JO, Inada S, Musa H, Molenaar P, et al. Molecular architecture of the human sinus node: insights into the function of the cardiac pacemaker. *Circulation.* 2009;119(12):1562–75.
132. Ju YK, Chu Y, Chaulet H, Lai D, Gervasio OL, Graham RM, et al. Store-operated Ca²⁺ influx and expression of TRPC genes in mouse sinoatrial node. *Circ Res.* 2007 Jun 8;100(11):1605–14.
133. Watanabe H, Murakami M, Ohba T, Ono K, Ito H. The pathological role of transient receptor potential channels in heart disease. *Circ J.* 2009;73(3):419–27.
134. Duan D. Phenomics of cardiac chloride channels: the systematic study of chloride channel function in the heart. *J Physiol.* 2009;587(Pt 10):2163–77.
135. Huang ZM, Prasad C, Britton FC, Ye LL, Hatton WJ, Duan D. Functional role of CLC-2 chloride inward rectifier channels in cardiac sinoatrial nodal pacemaker cells. *J Mol Cell Cardiol.* 2009;47(1):121–32.
136. Choi BR, Hatton WJ, Hume JR, Liu T, Salama G. Low osmolarity transforms ventricular fibrillation from complex to highly organized, with a dominant high-frequency source. *Heart Rhythm.* 2006;3(10):1210–20.
137. Hiraoka M, Kawano S, Hirano Y, Furukawa T. Role of cardiac chloride currents in changes in action potential characteristics and arrhythmias. *Cardiovasc Res.* 1998;40(1):23–33.
138. Xiong D, Heyman NS, Airey J, Zhang M, Singer CA, Rawat S, et al. Cardiac-specific, inducible CIC-3 gene deletion eliminates native volume-sensitive chloride channels and produces myocardial hypertrophy in adult mice. *J Mol Cell Cardiol.* 2010;48(1):211–9.
139. Hume JR, Duan D, Collier ML, Yamazaki J, Horowitz B. Anion transport in heart. *Physiol Rev.* 2000;80(1):31–81.
140. Walsh KB, Long KJ. Properties of a protein kinase C-activated chloride current in guinea pig ventricular myocytes. *Circ Res.* 1994;74(1):121–9.
141. Collier ML, Hume JR. Unitary chloride channels activated by protein kinase C in guinea pig ventricular myocytes. *Circ Res.* 1995;76(2):317–24.
142. James AF, Sabirov RZ, Okada Y. Clustering of protein kinase A-dependent CFTR chloride channels in the sarcolemma of guinea-pig ventricular myocytes. *Biochem Biophys Res Commun.* 2010;391(1):841–5.
143. Sellers ZM, De Arcangelis V, Xiang Y, Best PM. Cardiomyocytes with disrupted CFTR function require CaMKII and Ca²⁺-activated Cl⁻ channel activity to maintain contraction rate. *J Physiol.* 2010;588(Pt 13):2417–29.

144. Wong KR, Trezise AE, Vandenberg JI. Developmental regulation of the gradient of cfr expression in the rabbit heart. *Mech Dev.* 2000;94:195–7.
145. Nishimura N, Reien Y, Matsumoto A, Ogura T, Miyata Y, Suzuki K, et al. Effects of nicorandil on the cAMP-dependent Cl⁻ current in guinea-pig ventricular cells. *J Pharmacol Sci.* 2010;112(4):415–23.
146. Zygmont AC, Goodrow RJ, Weigel CM. I_{NaCa} and I_{ClCa} contribute to isoproterenol-induced delayed after depolarizations in midmyocardial cells. *Am J Physiol.* 1998;275(6 Pt 2): H1979–92.
147. Guo D, Young L, Patel C, Jiao Z, Wu Y, Liu T, et al. Calcium-activated chloride current contributes to action potential alternations in left ventricular hypertrophy rabbit. *Am J Physiol Heart Circ Physiol.* 2008;295(1):H97–104.
148. Kunzelmann K, Kongsuphol P, Aldehni F, Tian Y, Ousingsawat J, Warth R, et al. Bestrophin and TMEM16-Ca²⁺ activated Cl⁻ channels with different functions. *Cell Calcium.* 2009;46(4):233–41.
149. O'Driscoll KE, Hatton WJ, Burkin HR, Leblanc N, Britton FC. Expression, localization, and functional properties of Bestrophin 3 channel isolated from mouse heart. *Am J Physiol Cell Physiol.* 2008;295(6):C1610–24.
150. Galietta LJ. The TMEM16 protein family: a new class of chloride channels? *Biophys J.* 2009;97(12):3047–53.
151. Lambert S, Oberwinkler J. Characterization of a proton-activated, outwardly rectifying anion channel. *J Physiol.* 2005;567(Pt 1):191–213.
152. Komukai K, Brette F, Orchard CH. Electrophysiological response of rat atrial myocytes to acidosis. *Am J Physiol Heart Circ Physiol.* 2002;283(2):H715–24.
153. Sachs F. Stretch-activated ion channels: what are they? *Physiology.* 2010;25(1):50–6.
154. Watanabe H, Murakami M, Ohba T, Ono K, Ito H. The pathological role of transient receptor potential channels in heart disease. *Circ J.* 2009;73(3):419–27.
155. Saffitz JE, Laing JG, Yamada KA. Connexin expression and turnover: implications for cardiac excitability. *Circ Res.* 2000;86(7):723–8.
156. Boyett MR, Inada S, Yoo S, Li J, Liu J, Tellez J, et al. Connexins in the sinoatrial and atrioventricular nodes. *Adv Cardiol.* 2006;42:175–97.
157. Lin X, Gemel J, Glass A, Zemlin CW, Beyer EC, Veenstra RD. Connexin40 and connexin43 determine gating properties of atrial gap junction channels. *J Mol Cell Cardiol.* 2010 Jan; 48(1):238–45.
158. Gros D, Théveniau-Ruissy M, Bernard M, Calmels T, Kober F, Söhl G, et al. Connexin 30 is expressed in the mouse sino-atrial node and modulates heart rate. *Cardiovasc Res.* 2010; 85(1):45–55.
159. Schricker JW, Kreuzberg MM, Ghanem A, Kim JS, Linhart M, Andrié R, et al. Normal impulse propagation in the atrioventricular conduction system of Cx30.2/Cx40 double deficient mice. *J Mol Cell Cardiol.* 2009;46(5):644–52.
160. Zalk R, Lehnart SE, Marks AR. Modulation of the ryanodine receptor and intracellular calcium. *Annu Rev Biochem.* 2007;76:367–85.
161. Hamilton SL, Serysheva II. Ryanodine receptor structure: progress and challenges. *J Biol Chem.* 2009;284(7):4047–51.
162. Marionneau C, Couette B, Liu J, Li H, Mangoni ME, Nargeot J, et al. Specific pattern of ionic channel gene expression associated with pacemaker activity in the mouse heart. *J Physiol.* 2005;562(Pt 1):223–34.
163. Kang G, Giovannone SF, Liu N, Liu FY, Zhang J, Priori SG, et al. Purkinje cells from RyR2 mutant mice are highly arrhythmogenic but responsive to targeted therapy. *Circ Res.* 2010; 107(4):512–9.
164. Thomas NL, George CH, Williams AJ, Lai FA. Ryanodine receptor mutations in arrhythmias: advances in understanding the mechanisms of channel dysfunction. *Biochem Soc Trans.* 2007;35(Pt 5):946–51.

165. Eisner DA, Kashimura T, Venetucci LA, Trafford AW. From the ryanodine receptor to cardiac arrhythmias. *Circ J.* 2009;73(9):1561–7.
166. Mackrill JJ. Ryanodine receptor calcium channels and their partners as drug targets. *Biochem Pharmacol.* 2010;79(11):1535–43.
167. Wu X, Eder P, Chang B, Molkentin JD. TRPC channels are necessary mediators of pathologic cardiac hypertrophy. *Proc Natl Acad Sci USA.* 2010;107(15):7000–5.
168. Aon MA, Cortassa S, Akar FG, Brown DA, Zhou L, O'Rourke B. From mitochondrial dynamics to arrhythmias. *Int J Biochem Cell Biol.* 2009;41(10):1940–8.
169. Wu X, Zhang T, Bossuyt J, Li X, McKinsey TA, Dedman JR, et al. Local InsP₃-dependent perinuclear Ca²⁺ signaling in cardiac myocyte excitation-transcription coupling. *J Clin Invest.* 2006;116(3):675–82.
170. Bkaily G, Avedanian L, Jacques D. Nuclear membrane receptors and channels as targets for drug development in cardiovascular diseases. *Can J Physiol Pharmacol.* 2009;87(2):108–19.
171. Alexander SP, Mathie A, Peters JA. Guide to receptors and channels (GRAC), 4th edn. *Br J Pharmacol.* 2009;158 Suppl 1:S1–254.
172. Snyders DJ. Structure and function of cardiac potassium channels. *Cardiovasc Res.* 1999;42(2):377–90.
173. Rudy Y, Ackerman MJ, Bers DM, Clancy CE, Houser SR, London B, et al. Systems approach to understanding electromechanical activity in the human heart: a national heart, lung, and blood institute workshop summary. *Circulation.* 2008;118(11):1202–11.

Chapter 2

Ionic Basis of the Pacemaker Activity of SA Node Revealed by the Lead Potential Analysis

Yukiko Himeno, Chae Young Cha, and Akinori Noma

2.1 Introduction

The ionic mechanisms underlying SA node pacemaker activity have been discussed for decades based on findings of voltage clamp experiments using the isolated single pacemaker cells as well as the SA node tissue preparation. It is now well established that there is no single “pacemaker current,” instead multiple ion channels and electrogenic ion transporter currents generate the pacemaker potential. Thus, although technically challenging, the key issue is to clarify the quantitative as well as qualitative role of individual ionic currents in the pacemaker potential generation. In experiments, a given current of interest is often blocked or depressed using a channel-specific drug. The interpretation of the results or quantitative measure of the contribution is largely interfered with secondary changes in other current systems via modified time course of membrane potential change or ionic concentrations within a cell. This difficulty is largely solved by the recent progress in developing the electrophysiological cardiac cell model. Indeed the pacemaker activity has been well reproduced by a variety of mathematical cell models which integrate experimental findings [1].

In this chapter, we will introduce an analytical tool, the lead potential (V_L) analysis, to estimate the quantitative contribution of each ionic current and ion exchanger to the pacemaker potential based on mathematical SA node cell models. We will apply this new method to six mathematical models published by Wilders et al. [2], Demir et al. [3], Kurata et al. [4], Sarai et al. [5], Himeno et al. [6] and Maltsev and Lakatta [7]. This analysis allows us to indicate common mechanisms

Y. Himeno (✉)

Biosimulation Project, Graduate School of Medicine, Kyoto University, 54 Kawahara-cho, Shogoin, Sakyo-ku, Kyoto 606-8507, Japan
e-mail: himeno@biosim.med.kyoto-u.ac.jp

C.Y. Cha and A. Noma

Biosimulation Project, Faculty of Bioinformatics, College of Life Science, Ritsumeikan University, 1-1-1 Noji Higashi, Kusatsu 525-8577, Japan
e-mail: chacy@fc.ritsumei.ac.jp, noma@sk.ritsumei.ac.jp

shared by all these models. Further analyses are used to clarify the reasons for discrepancies between these models.

2.2 The Lead Potential (V_L) Analysis

The concept of the V_L analysis has recently been refined to measure the contribution of individual currents to changes in membrane potential [8]. To facilitate understanding of this method, we first explain the preliminary version of the method introduced by Sarai et al. (2003) [5] before describing the latest version.

2.2.1 The Primary Concept of V_L

The ionic mechanisms underlying the spontaneous action potential in SA node cells can be explained as follows. The rising phase of the action potential is mainly due to the rapid activation of the L-type Ca^{2+} current (I_{CaL}). A positive feedback mechanism is well established that the depolarization by the activation of inward I_{CaL} causes more activation of I_{CaL} itself, culminating in the overshoot potential. The resulting membrane depolarization and Ca^{2+} influx causes inactivation of I_{CaL} and activation of the delayed rectifier K^+ currents (I_{Kr} and I_{Ks}), which together promotes repolarization of the cell to the maximum diastolic potential. Then, the negative potential progressively deactivates I_{Kr} and I_{Ks} in the presence of background inward currents, resulting in the gradual depolarization during the early diastolic period that finally triggers the next action potential through the activation of I_{CaL} . The slow diastolic depolarization is also influenced by $\text{Na}^+/\text{Ca}^{2+}$ exchanger current (I_{NaCa}) and Na^+/K^+ pump current (I_{NaK}) to an extent that depends on the concentrations of intracellular Ca^{2+} and Na^+ , respectively.

In general, the spontaneous changes of the membrane potential are generated by variations in the conductances of individual channel currents by membrane potential, the chemical gating, or the intracellular ion concentrations, and also in the transporter currents such as I_{PMCA} and I_{NaK} . Accordingly, development of the V_L analysis method started from reducing the membrane system consisting of more than ten ion channels into a single whole cell membrane conductance (G_m). Irrespective of the conductance properties of each channel, G_m is defined as a sum of the whole cell conductance of K^+ (G_K), Na^+ (G_{Na}), Ca^{2+} (G_{Ca}), and Cl^- (G_{Cl}) (Fig. 2.1a):

$$G_m = G_K + G_{\text{Na}} + G_{\text{Ca}} + G_{\text{Cl}}, \quad (2.1)$$

$$G_K = \frac{I_K}{V_m - E_K} = \frac{I_{\text{netK}} + 2I_{\text{NaK}}}{V_m - E_K}, \quad (2.2)$$

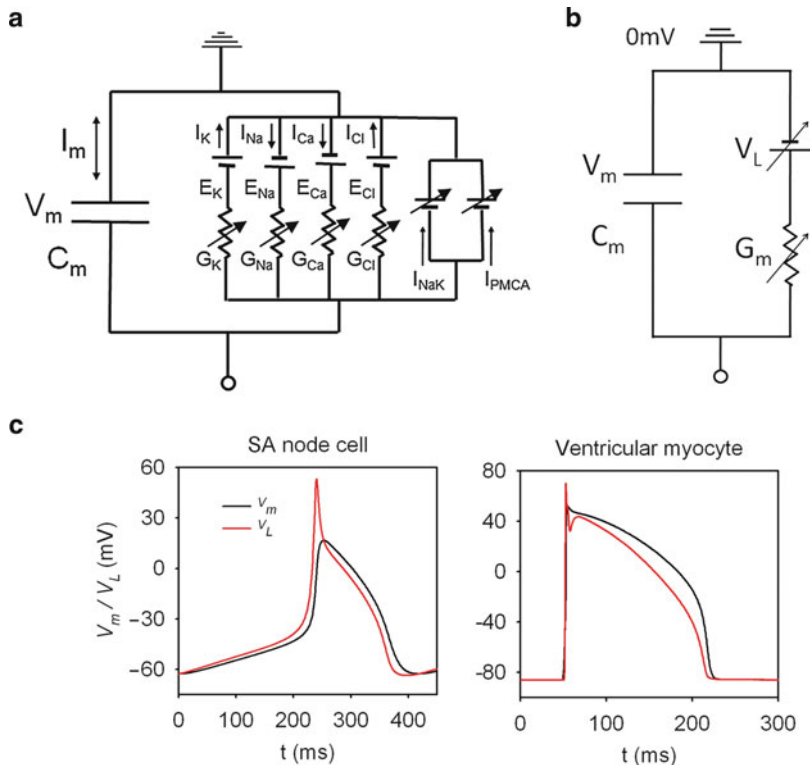


Fig. 2.1 The equivalent electrical circuit of a pacemaker cell membrane excitation (a) and a reduced circuit (b). C_m , cell membrane capacitance; V_m , membrane potential; G_m , membrane conductance; I_m , total membrane current; I_X , current carried by ion X; E_x , reversal potential for ion X; G_x , conductance for ion X; V_L , lead potential, which is replacement of E_0 in (2.8). (c) The time course of V_L (red curve, old V_L analysis) superimposed on V_m (black) in the SA node cell (left) and ventricular cell model (right)

$$G_{Na} = \frac{I_{Na}}{V_m - E_{Na}} = \frac{I_{netNa} - 3I_{NaK}}{V_m - E_{Na}}, \quad (2.3)$$

$$G_{Ca} = \frac{I_{Ca}}{V_m - E_{Ca}} = \frac{I_{netCa} - I_{PMCA}}{V_m - E_{Ca}}, \quad (2.4)$$

$$G_{Cl} = \frac{I_{Cl}}{V_m - E_{Cl}} = \frac{I_{netCl}}{V_m - E_{Cl}}, \quad (2.5)$$

Here, V_m is membrane potential and E_x stands for reversal potential for ion X, which can be defined by the Nernst equation. I_{netX} , the whole cell net current for ion X, is calculated according to the ion species irrespective of the passage through specific channel types. For example, the Ca^{2+} , Na^+ , and K^+ current components

through the L-type Ca^{2+} channel were involved in $I_{\text{net}}\text{Ca}$, $I_{\text{net}}\text{Na}$, and $I_{\text{net}}\text{Ca}$, respectively. The Na^+ and Ca^{2+} fluxes through the $\text{Na}^+/\text{Ca}^{2+}$ exchanger are included in $I_{\text{net}}\text{Na}$ and $I_{\text{net}}\text{Ca}$, since this ion exchange is driven by the passive electrochemical driving force like for the ion channel flux. On the other hand, for the ion fluxes through active transporter, such as I_{NaK} and I_{PMCA} , are excluded from $I_{\text{net}}\text{X}$ because they are driven by the energy through ATP hydrolysis. In this sense, the electrical property of the model can be reduced to an equivalent circuit consisting of a capacitor, a single variable resistor, and a battery, as shown in Fig. 2.1b. The battery is defined as a zero current potential E_0 , which satisfies the following equation:

$$I_{\text{net}}\text{K} + I_{\text{net}}\text{Na} + I_{\text{net}}\text{Ca} + I_{\text{net}}\text{Cl} = 0. \quad (2.6)$$

E_0 is solved by substituting net ionic currents in (2.2)–(2.5) into (2.6);

$$E_0 = \frac{G_{\text{K}}E_{\text{K}} + G_{\text{Na}}E_{\text{Na}} + G_{\text{Ca}}E_{\text{Ca}} + G_{\text{Cl}}E_{\text{Cl}} - I_{\text{NaK}} - I_{\text{PMCA}}}{G_{\text{K}} + G_{\text{Na}} + G_{\text{Ca}} + G_{\text{Cl}}}. \quad (2.7)$$

In the reduced circuit, the membrane current is driven by the difference between V_m and E_0 . Thus, the time-dependent change in V_m is given by,

$$\frac{dV_m}{dt} = -\frac{I_m}{C_m} = -\frac{G_m \times (V_m - E_0)}{C_m}. \quad (2.8)$$

Equation (2.8) indicates that V_m always moves toward E_0 with a time constant given by C_m/G_m . In Fig. 2.1c, the time course of E_0 is superimposed on that of V_m . Indeed, E_0 is always more positive than V_m during the depolarizing phase and vice versa during the hyperpolarizing phase. E_0 continuously changes in the SA node cell and V_m crosses E_0 when $dV_m/dt = 0$ at the maximum diastolic potential and at the peak of the action potential. In the ventricular myocyte model, V_m remains constant at the resting membrane potential, but once the action potential is triggered, E_0 changes in advance of V_m in the repolarizing phase. Since E_0 leads the change in V_m , we named E_0 as lead potential (V_L).

Note that the spontaneous change in V_L is caused by the time-dependent changes in the ion channel conductance or the time-dependent change in the electrogenic ion pumps. If changes in these membrane conductances are all stopped, the time-dependent changes in V_m level off at V_L , and the spontaneous activity disappears. The nongating background ion currents scarcely contribute to the time-dependent changes in V_L because their conductance remains constant.

2.2.2 Contribution of Each Ionic Current Estimated Using the Primary V_L Analysis

The application of the preliminary V_L method to the Sarai et al. model [5], Wilders et al. model [2], and Demir et al. model [3] provided a clear general view of ionic mechanisms as compared in Fig. 2.2. In this method, $p(o)$ of a given channel was

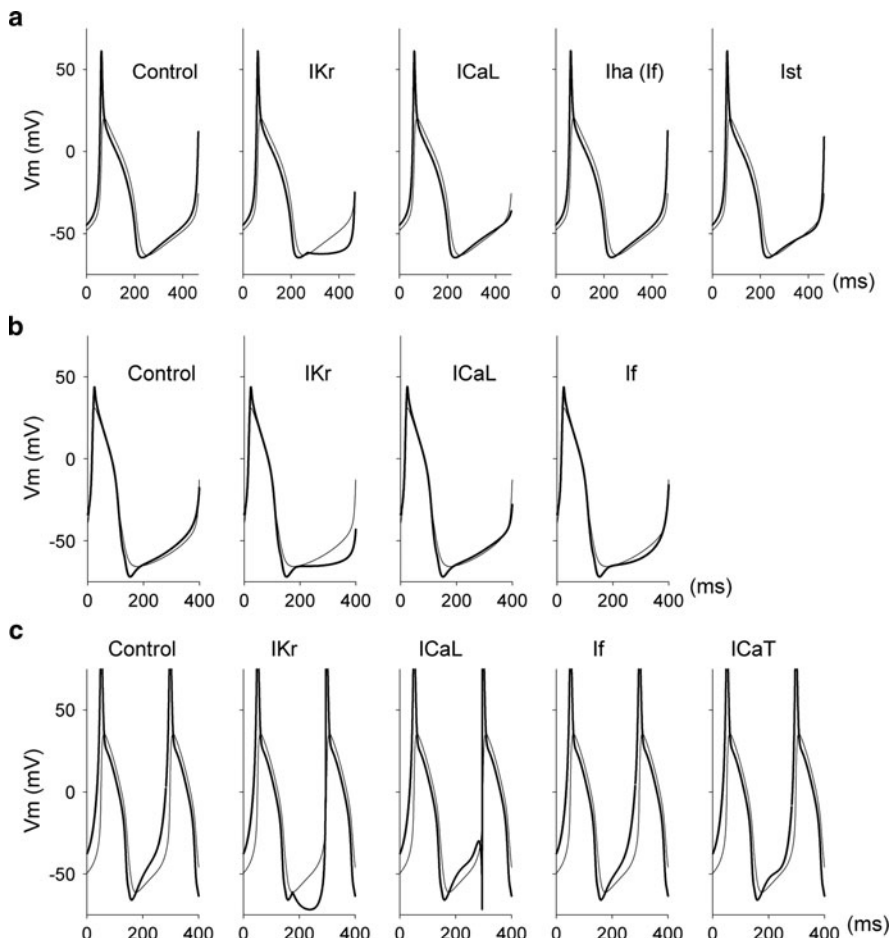


Fig. 2.2 Contribution of each current component to time-dependent changes in V_L examined by the old V_L analysis. (a) Sarai et al. model (Kyoto model), (b) Wilders et al. model, and (c) Demir et al. model. The thin trace is the V_m record and the thick trace is V_L , which is calculated during the interval from the maximum diastolic potential to the beginning of the upstroke of the action potential. In calculating V_L , the $p(o)$ of indicated current was fixed at the value obtained at the maximum diastolic potential

suddenly fixed at the maximum diastolic potential. In all models, fixation of $p(o)$ of I_{Kr} almost suppresses the diastolic depolarization in V_L , indicating that the time-dependent deactivation of I_{Kr} is the basal mechanism to drive the slow diastolic depolarization. Fixing $p(o)$ of I_{CaL} results in a slight downward deflection of V_L in the late diastolic phase, indicating that the activation of I_{CaL} is responsible for initiating the next action potential. It is obvious that the deactivation of I_{Kr} and the activation of I_{CaL} are the primary mechanism of the pacemaker depolarization in all three models.

Differences among these three models are observed in the contributions of the hyperpolarization-activated current (I_h , I_{ha} , or I_f), the sustained inward current (I_{st}), and the T-type calcium current (I_{CaT}). Fixing $p(o)$ of these currents all hinders the slow diastolic depolarization, but the effects are rather small if compared to that of I_{Kr} in these three models. In this respect, these currents might be categorized as “supplemental” currents. Namely, fixing $p(o)$ of I_f is modest in the Sarai et al. model and Demir et al. model. On the other hand, fixing $p(o)$ of I_f in the Wilders model caused a significant downward deflection throughout the diastolic depolarization as if it substitutes the effects of I_{st} in the Sarai et al. model or I_{CaT} in the Demir et al. model. It is evident that the difference among currents in these three models is caused by the different experimental findings used for developing the model as described below.

I_{CaT} is the low voltage-activated “transient” calcium current, but its window current acts as a sustained current in the Demir et al. model. Steady-state activation and inactivation curves in the two models are shown and compared in Fig. 2.3. In the Sarai et al. model, the description of the current is based on data obtained by Hagiwara et al. [9]. On the other hand, Demir et al. modeled the current based on experimental data obtained by Fermini and Nathan [10], whose inactivation was slower and occurred at more positive voltage range. It might be noted that the experimental data points suggest even larger window current than the activation curve used for I_{CaT} modeling (Fig. 2.3a, right panel). In contrast, the fast inactivation kinetics hinders I_{CaT} to exhibit an obvious contribution in the Sarai et al. model. These differences in the inactivation kinetics resulted in an obvious difference in the I_{CaT} contributions between the two models. It should be finally clarified if a different subgroup of cells in the SA node region or different experimental protocols caused different results in each study.

The I_{st} assumed in Sarai et al.’s model is not always used in other SA node modeling, but plays a substantial role in the pacemaker depolarization especially in the late phase of the depolarization (Fig. 2.2a). I_{st} is a sustained inward current, whose reversal potential ranged between +10 and +30 mV. It was first reported by Guo et al. in rabbit [11] and then in guinea pig [12, 13] (Fig. 2.4), mouse [14] and rat [15]. Although its molecular basis is still unclear, the nicardipine sensitive single channel current as well as whole cell current has been recorded as shown in Fig. 2.4 [12, 13]. Furthermore, its physiological response to autonomic agonists is also observed in guinea pig [16]. Thus, there is no doubt about its existence in some population of SA node cells.

2.3 Sophistication of the V_L Analysis

Although the original V_L analysis enabled us to conclude which ionic channel has relatively large or small contribution to pacemaker activity, it was still intuitive and qualitative. The goal of improving the V_L analysis method was to perform quantitative measurement of the contribution of individual current components during the

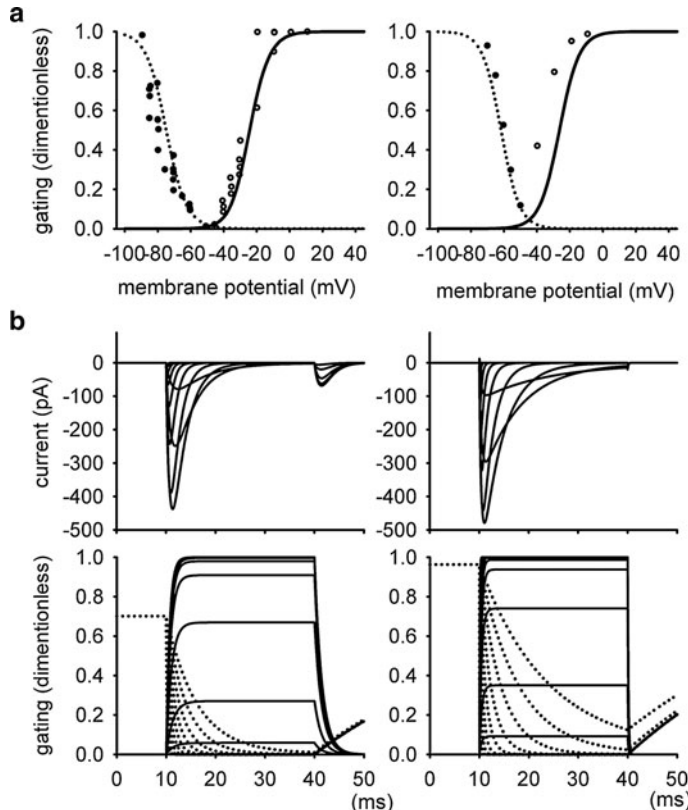


Fig. 2.3 A comparison between the two I_{CaT} models in Sarai et al. (left) and in Demir et al. (right). **(a)** Steady-state voltage dependence of the models (continuous curves). Filled circles and open circles indicate experimental data of steady-state inactivation and activation, respectively, taken from Hagiwara et al. [9] (left) and Fermini and Nathan [10] (right). **(b)** Superimposed traces of simulated currents activated by various test pulses to the range between -40 and 50 mV from a holding potential of -80 mV (top). Time courses of inactivation (dotted lines) and activation (solid lines) gating parameters are shown at the bottom

time course of the slow diastolic depolarization. Toward this end, we refined the mathematical derivation of V_L .

2.3.1 Derivation of the Refined V_L

The temporal change of V_m is described with the following fundamental equation in a single cell:

$$\frac{dV_m}{dt} = - \frac{I_m}{C_m}, \quad (2.9)$$

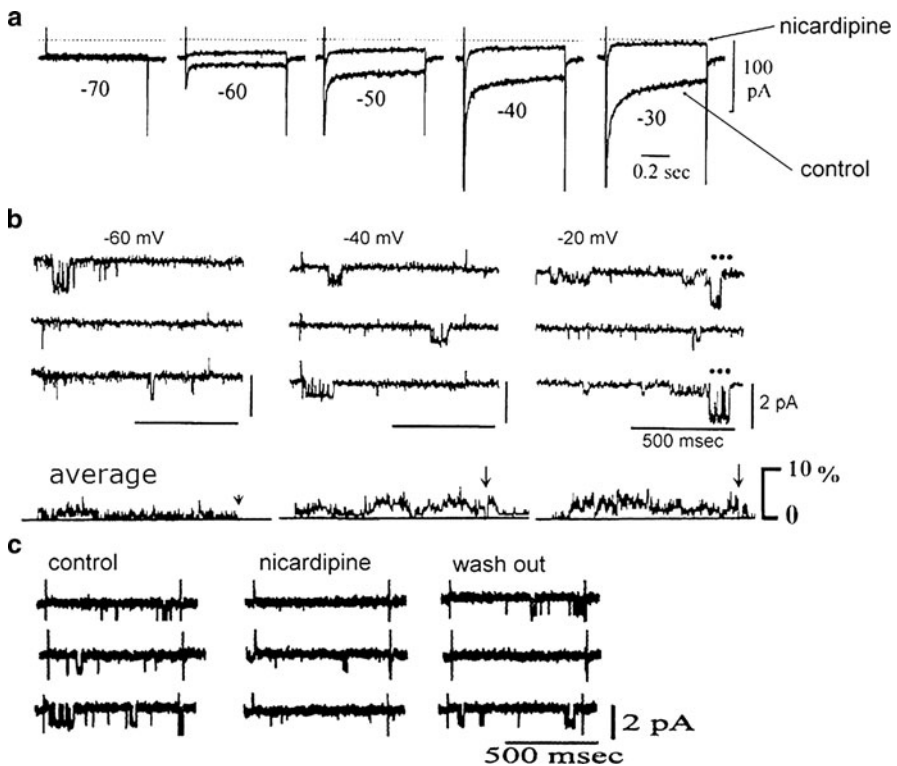


Fig. 2.4 Recordings of I_{st} . (a) Whole cell current traces elicited by depolarization pulses in 10 mV steps from -70 to -30 mV from a holding potential of -80 mV. Superimposed traces were recorded with and without $1 \mu\text{M}$ nicardipine [12]. (b) Single channel current (I_{st}) traces (cell attached patches) evoked by sequential test pulses to -60 , -40 , and -20 mV from a holding potential of -100 mV and their averages of 70 – 120 sequential sweeps. (c) I_{st} recordings before, during, and after the application of $5 \mu\text{M}$ nicardipine [13]

where C_m is the whole cell membrane capacitance, and I_m is the sum of membrane currents through all ion channels and electrogenic transporters in a single cell. In most mathematical models, current conducted by a channel X (I_X) is described by Ohm's law:

$$I_X = g_{\max} \times p(o) \times (V_m - E_{rev}), \quad (2.10)$$

or the Goldman–Hodgkin–Katz (GHK) current equation with a constant field approximation,

$$I_X = p_{\max} \times p(o) \times \frac{V_m z_s^2 F^2}{RT} \frac{[S]_i - [S]_o \exp(-z_s F V_m / RT)}{1 - \exp(-z_s F V_m / RT)}. \quad (2.11)$$

$$= p_{\max} \times p(o) \times f(V_m)$$

E_{rev} is the reversal potential for the channel in (2.10), and $f(V_m)$ is the nonlinear part of the GHK equation in (2.11). g_{\max} , the maximum conductance in (2.10) and p_{\max} , the maximum permeability, are defined as constant parameters in (2.11). $[S]$ is the concentration of ion S , and F , R , T and z_s are the usual thermodynamic parameters. $p(o)$ stands for the open probability of the channel, which is a time- and voltage-dependent variable determined by V_m - and/or ligand-dependent gating of the channel. For example, pore block of the I_{K1} channel by polyamines or Mg^{2+} [17], or unspecified mechanisms underlying the rectifying properties of I_{Kpl} , was attributed to changes in $p(o)$ in this V_L analysis.

When aiming to quantitatively determine the contribution of ionic systems to the pacemaker depolarization, neglecting nonlinearity of $f(V_m)$ in the old V_L method is a fatal error. The new V_L method solves this problem by restricting the following argument only at the moment of observation ($t = t_{\text{ob}}$). That is, $f(V_m)$ can be described as a tangential line at $t = t_{\text{ob}}$ as follows:

$$f(V_m) = f'(V_m) \times (V_m - E), \quad (2.12)$$

where E is the value of intersection of the tangential line with the voltage axis. Then, all the channel currents can be expressed in the common form of $G_X(V_m - E_X)$, where

$$G_X = g_{\max} \times p(o).$$

in (2.10), and,

$$G_X = p_{\max} \times p(o) \times f'(V_m)$$

in (2.11). Thus, (2.1) can be described as follows:

$$\frac{dV_m}{dt} = -\frac{1}{C_m} \left(\sum_X G_X \cdot (V_m - E_X) + \sum_Y I_Y \right), \quad (2.13)$$

where X and Y are labels for a channel current and an ion transporter current, respectively. Thus, an individual channel is expressed with one battery (E_X) and one conductance (G_X), and each transporter is represented by a current source (I_Y). Equation (2.13) can be rearranged as follows:

$$\begin{aligned} \frac{dV_m}{dt} &= -\frac{1}{C_m} \left(\sum_X G_X \cdot (V_m - E_X) + \sum_Y I_Y \right) \\ &= -\frac{1}{C_m} \left(V_m \cdot \sum_X G_X - \sum_X G_X E_X + \sum_Y I_Y \right) \\ &= -\frac{\sum_X G_X}{C_m} \cdot \left(V_m - \frac{\sum_X G_X E_X - \sum_Y I_Y}{\sum_X G_X} \right), \end{aligned} \quad (2.14)$$

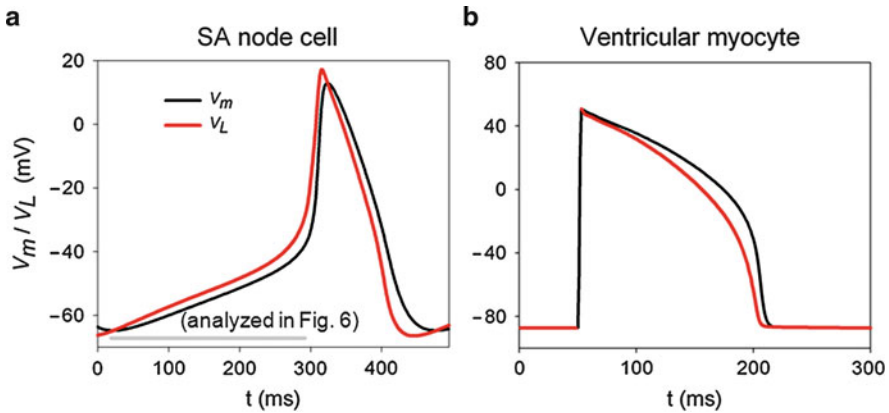


Fig. 2.5 V_L (red) obtained by the new V_L analysis method superimposed on V_m (black) in SA node cell model (a) and ventricular myocyte model (b). The gray bar in (a) indicates the time spans analyzed in Fig. 2.6

(2.14) is described as:

$$\frac{dV_m}{dt} = -\frac{1}{\tau}(V_m - V_L), \quad (2.15)$$

then,

$$V_L = \frac{\sum_X G_X E_X - \sum_Y I_Y}{\sum_X G_X}, \quad (2.16)$$

$$\tau = \frac{C_m}{\sum_X G_X}. \quad (2.17)$$

Until the derivation for (2.9)–(2.17), we fixed all the time-dependent variables by the values at $t = t_{ob}$. Now, if we consider V_m as a free variable, (2.15) corresponds to Fig. 2.1b. Therefore, V_m tends to approach V_L with a time constant τ at each time point. Figure 2.5a, b shows temporal changes of V_L and V_m during an action potential in the SA node cell model [6] and ventricular myocyte model [17] obtained by calculating (2.16) at every moment. Note that V_L of the new version (Fig. 2.5a) is slightly different from the old one (Fig. 2.1c, left).

2.3.2 Estimation of Contributions of Each Ionic Component

According to Fig. 2.1b and (2.15), it can be interpreted that the automatic change of V_m is driven by the time-dependent change in V_L , and τ represents the passive

property of the membrane. Therefore, automaticity can be expressed in terms of “ dV_L/dt ” with complete exclusion of τ .

$$\frac{dV_L}{dt} = \frac{\left(\sum_X \dot{G}_X \cdot E_X + \sum_X G_X \cdot \dot{E}_X - \sum_Y \dot{I}_Y \right) \cdot \sum_X G_X - \left(\sum_X G_X \cdot E_X - \sum_Y I_Y \right) \cdot \sum_X \dot{G}_X}{\left(\sum_X G_X \right)^2}. \quad (2.18)$$

Here, we will calculate the extent to which a component of interest affects dV_L/dt . To evaluate the contribution of a single component, we determine dV_{L_Fix}/dt after eliminating its time-dependent change (i.e., $\dot{G}_i = 0$, $\dot{E}_i = 0$, or $\dot{I}_i = 0$), leaving all the other components intact. We refer to this process of eliminating the time-dependent change as “fixing.” For example, when we fix G_i , we set $\dot{G}_i = 0$ in (2.18):

$$\frac{dV_{L_Fix}}{dt} = \frac{\left(\sum_{X \neq i} \dot{G}_X \cdot E_X + \sum_X G_X \cdot \dot{E}_X - \sum_Y \dot{I}_Y \right) \cdot \sum_X G_X - \left(\sum_X G_X \cdot E_X - \sum_Y I_Y \right) \cdot \sum_{X \neq i} \dot{G}_X}{\left(\sum_X G_X \right)^2}. \quad (2.19)$$

The relative contribution, r_c , is defined as follows:

$$r_c = \frac{\frac{dV_L}{dt} - \frac{dV_{L_Fix}}{dt}}{\frac{dV_L}{dt}} \quad (\text{when } \frac{dV_L}{dt} \neq 0), \quad (2.20)$$

and r_c satisfies the following equation:

$$\sum r_c = 1, \quad (2.21)$$

for all components. An r_c of positive sign means that the component is operating to drive dV_L/dt in the same direction as the control dV_L/dt . On the other hand, an r_c of negative sign means that the component interferes with the change of V_L by inclining dV_L/dt in the opposite direction.

2.3.3 Contribution of Each Ionic Component to the Pacemaker Potential Quantified by the V_L Analysis

Using the refined V_L method, the description of the contribution of each ionic component has been improved dramatically. Figure 2.6 shows the result of the V_L

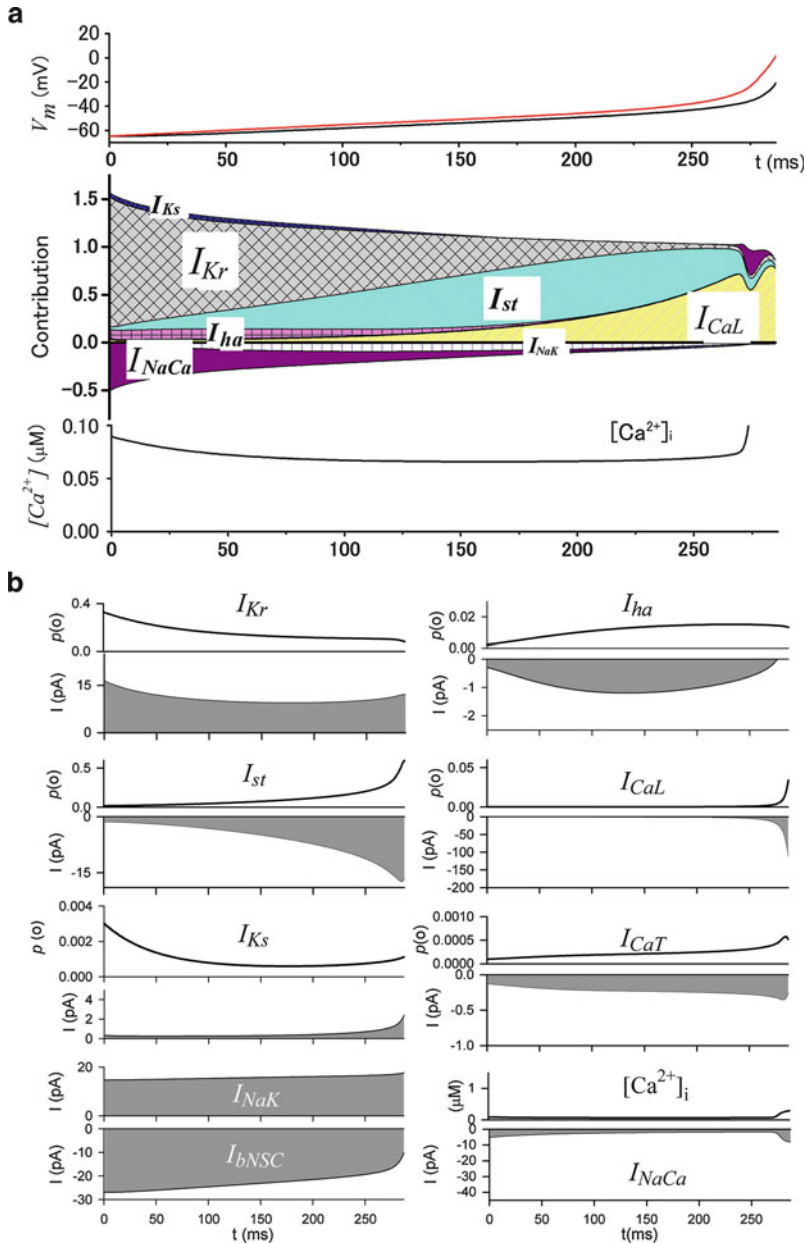


Fig. 2.6 The time profile of r_c (defined by 2–12) during the slow diastolic depolarization in Himeno et al. model. **(a)** The time-dependent changes of r_c of the major current components during changes of V_L (red) and V_m (black) shown at the top and $[Ca^{2+}]_i$ at the bottom. The analyzed section of the action potential is shown by gray bar in Fig. 2.5a. **(b)** Changes of $p(o)$ s and amplitudes of individual currents indicated in the graph, and $[Ca^{2+}]_i$

analysis performed on the same SA node model illustrated in Fig. 2.5a. Transition of the relative contribution is shown along the time axis, and the mechanisms of contribution are explained based on the time-dependent variations of $p(o)$ and the current amplitude shown in Fig. 2.6b. The magnitude of dV_L/dt remained nearly constant around 0.09 mV ms^{-1} during the initial 200 ms after the maximum diastolic potential and increased exponentially thereafter, as shown in Fig. 2.6a. At the beginning of depolarization, dV_L/dt is largely determined by the deactivation of the outward I_{Kr} (i.e., the decrease in $p(o)$ of I_{Kr} in Fig. 2.6b). As r_c of I_{Kr} decreases, it is substituted by those of the inward currents, I_{st} and I_{CaL} , via depolarization-dependent activation. r_c of I_{st} reached a peak of ~ 0.63 and then decreased after 220 ms, which is simply biased by the much larger increase in r_c of I_{CaL} . Although the increase of $p(o)$ in I_{CaL} is tiny (< 0.002) during the late diastolic period, it is the main current in the upstroke of the action potential and also affects dV_L/dt . Inward I_h also plays a positive role at the early stage with an r_c of ~ 0.1 . This is relatively small because the increase of $p(o)$ saturates around 220 ms and the amplitude of I_h is small. Similarly, relatively small contribution of I_{Ks} is explained by a little change in $p(o)$ (~ 0.002), which is attributable to a limited activation during the preceding action potential. The lead potential analysis clearly separates the role of the nonselective cation current (I_{bNSC}) from that of V_m -gated channel currents. It has been reported that I_{bNSC} , the largest inward current of $\sim -25 \text{ pA}$, plays a role in diastolic depolarization by driving V_m toward its reversal potential of $\sim 0 \text{ mV}$ [18]. However, r_c of I_{bNSC} is zero because I_{bNSC} has neither gating nor rectification in its channel kinetics.

The amplitude of inward going I_{NaCa} gradually decreases during the diastolic depolarization period due to a decrease of $[Ca^{2+}]_i$ in the first two-thirds of the depolarization phase and a continuous increase in V_m . Thereby, r_c of I_{NaCa} is negative for the slow diastolic depolarization. I_{NaK} also has a negative r_c because the outward I_{NaK} increases with depolarizing V_m . Because of these negative contributions of I_{NaCa} and I_{NaK} , the sum of positive contributions in the profile is larger than 1.0 in this model. As far as we are aware, the concept of this negative contribution is introduced for the first time in this V_L analysis and is clearly defined by (2.20).

2.4 Variations in the Ionic Mechanisms Hypothesized by Different Mathematical Pacemaker Cell Models

It has long been suggested that the configuration of the spontaneous action potentials shows variations according to the recording location within the SA node regions. This issue has been thoroughly investigated by Prof. Boyett's group by examining the ion channel expression in different cells isolated from different locations within the SA node [19]. This kind of variation may partly correspond to variable weight of individual channel current contribution among different mathematical models as demonstrated in Fig. 2.2.

Variations in the ionic mechanisms have also been explained by modifying the model structure. Especially the intracellular Ca^{2+} distribution within the cell has recently been examined in the pacemaker mechanism by assuming a subsarcolemmal space. It might be noted that SA node cells have no transverse tubules within the cell, and therefore the EC coupling may occur at the junction of subsarcolemmal cisterna of sarcoplasmic reticulum (SR) with the surface membrane [20]. For the sake of simplicity, a uniform subsarcolemmal space was first assumed in the SA node cell model [4]. Later, this model was further modified and used by Maltsev and Lakatta [7], focusing on the contribution of intracellular Ca^{2+} concentration to the pacemaker mechanisms. In the following section, we will apply the V_L method to the Kurata et al. model and the Maltsev and Lakatta model to compare with the Himeno et al. model.

2.4.1 Contribution of I_{NaCa} Intensified by the Localized Ca^{2+} in Kurata Model

In the Kurata model, a subsarcolemmal space of 20 nm in depth is introduced underneath the surface membrane, and occupies only 1% of the cytosolic space. Since it is assumed that the Ca^{2+} flux through both the I_{CaL} channel as well as the ryanodine receptor (RyR) channel on the SR are directed into this limited subsarcolemmal space, the transient increase in subsarcolemmal Ca^{2+} ($[\text{Ca}^{2+}]_{\text{sub}}$) is much larger than that in intracellular bulk Ca^{2+} ($[\text{Ca}^{2+}]_i$) in other SA node cell models, where $[\text{Ca}^{2+}]_i$ is assumed to be homogeneous throughout the cell. Figure 2.7a shows the results of V_L analysis as well as Ca^{2+} concentrations ($[\text{Ca}^{2+}]_{\text{sub}}$ and $[\text{Ca}^{2+}]_i$) in the Kurata et al. model. Except for the Ca^{2+} -related events, the general view of the mechanism is in good agreement with Himeno et al. model. Namely, the successive shift of the major role from I_{Kr} to I_{st} and the following significant increase in the contribution of I_{CaL} are essentially the same in the other pacemaker cell models described previously. A gradual decrease in the negative contribution of I_{NaCa} caused by dissipation of the Ca^{2+} transient is also a common mechanism observed in other models. The prominent difference is the timing of conversion of the sign of I_{NaCa} contribution from negative to positive in the last one-third of the diastolic period in this model. This conversion is caused by voltage-dependent activation of I_{CaT} as well as I_{CaL} over the corresponding time period in Kurata et al.'s model. $[\text{Ca}^{2+}]_{\text{sub}}$ increased twice as much as that in myoplasm at 125 ms and yielded a peak of $\sim 1.8 \mu\text{M}$ at its maximum as reported by Glukhovsky et al. [21] and Snyder et al. [22] in their simulation studies. The activation of I_{CaT} starts soon after the maximum diastolic potential, and thereby favors the early contribution of I_{NaCa} through the Ca^{2+} accumulation in the subsarcolemmal space. The r_c of I_{NaCa} , which is accelerated by the Ca^{2+} released from the SR is still minor (27%) in this model at the end of the V_L profile. The r_c of I_{CaT} is enlarged in this model (22%) compared to that in Himeno et al.'s model (12%). The maximum amplitude of I_{CaT} reached to $\sim -7 \text{ pA}$ in the late diastolic depolarization in the Kurata et al. model (Fig. 2.7), whereas it is

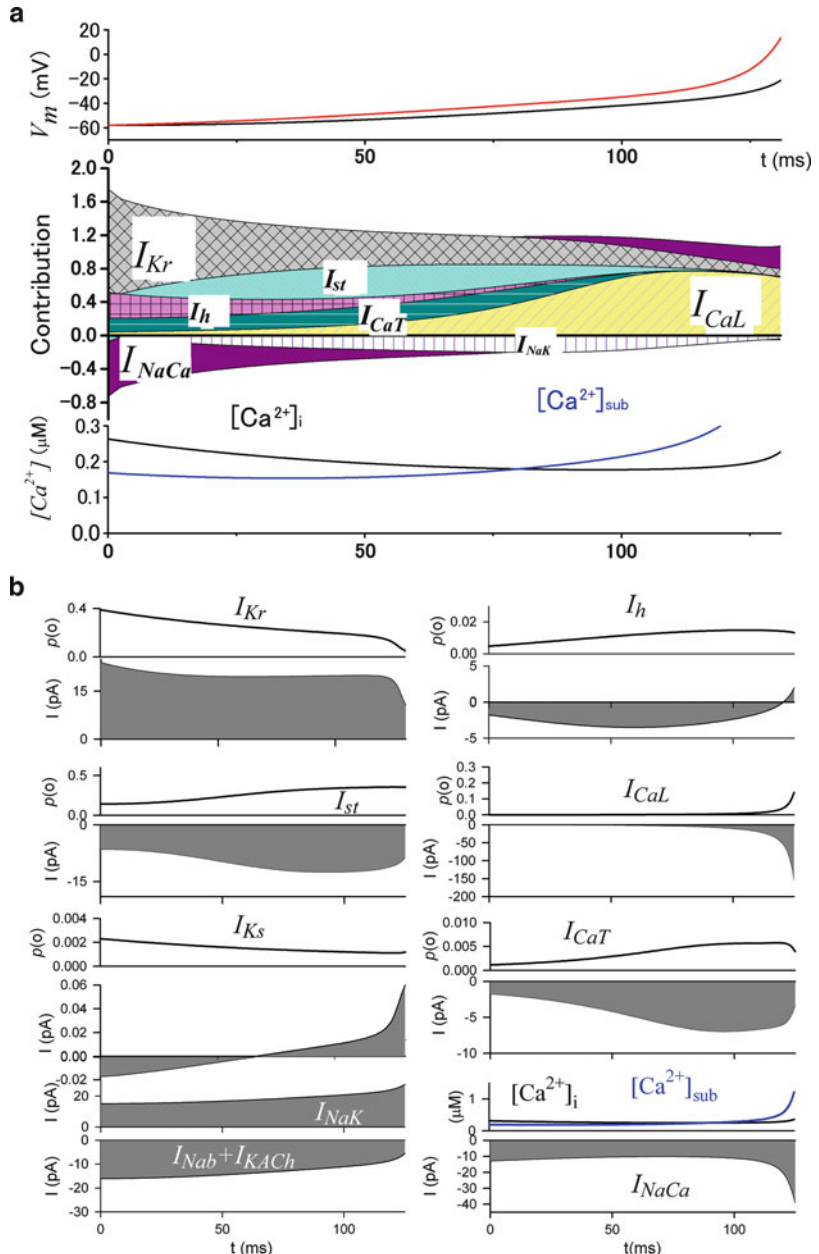


Fig. 2.7 The time profile of r_c during the slow diastolic depolarization in Kurata et al. model. (a) and (b) are shown in the same style as in Fig. 2.7 except for the presence of green line, which represents $[Ca^{2+}]_{sub}$

only -0.2 pA in Himeno et al.'s model (Fig. 2.6). The difference is attributable to the different experimental data referred to in each model as explained in Sect. 2.3 above and Fig. 2.3. Kurata et al. assumed a larger contribution of I_{CaT} to the pacemaker depolarization based on an experimental observation by Doerr et al. [23] and adopted equations from model by Demir et al.

2.4.2 Intracellular Ca^{2+} Clock in Maltsev and Lakatta Model

A new pacemaker mechanism was recently proposed by Prof. Lakatta's group (the intracellular Ca^{2+} clock [24–26]). This mechanism is quite comparable to the "triggered activity," which is well established in the ventricular myocytes. If ventricular myocytes are superfused with solution containing moderate concentrations of cardiotonic steroids and a high concentration of extracellular Ca^{2+} ($75\text{--}200 \text{ ng ml}^{-1}$ acetylstrophantidin and 2.5 mM Ca^{2+} in Ferrier and $2\text{--}10 \mu\text{M}$ ouabain and 5.4 mM Ca^{2+} in Matsuda et al., respectively) [27, 28], the Ca^{2+} content in the SR is increased and the spontaneous Ca^{2+} release is accelerated. By applying conditional depolarizing pulses under the voltage clamp condition, this spontaneous Ca^{2+} release can be detected by the oscillatory transient inward current, I_{NaCa} . Without the voltage clamp, repetitive Ca^{2+} transients or inward I_{NaCa} are evoked after conditional repetitive electrical stimulation. When the increase in the amplitude of transient depolarization was sufficient to bring the membrane potential to the threshold, a spontaneous full-amplitude action potential was elicited, especially with β -adrenergic stimulation. This triggered activity disappears if the ventricular myocytes are relieved from the Ca^{2+} -overload. Healthy myocytes do not show the transient depolarization or inward current.

In SA node pacemaker cells, repetitive Ca^{2+} transients were recorded by Prof. Lakatta's group when the spontaneous action potential was stopped by the voltage clamp even under normal physiological conditions. Vinogradova et al. observed repetitive spontaneous inward currents, which were largely dependent on the spontaneous Ca^{2+} release from SR [24]. Despite only a limited number of studies have described this repetitive spontaneous inward current under normal physiological conditions, this hypothesis has provoked a lot of discussion and was recently explained with a concrete SA node pacemaker cell model [7]. The significant modifications from the Kurata et al. model [4] were reductions of conductances in major inward currents, g_{CaL} , g_{CaT} , g_h and g_{st} , by 20, 60, 60 and 80% respectively, which interfered spontaneous generation of the action potential by plasma membrane currents. In addition, the Ca^{2+} -dependent mechanisms were enhanced by increasing the maximum amplitude of I_{NaCa} by 50% and adding the background Ca^{2+} influx (I_{bca}). Parameters for the SR Ca^{2+} dynamics, such as the time constant of Ca^{2+} transfer from the network SR (uptake site) to junctional SR (release site) and rate constant for Ca^{2+} uptake by Ca^{2+} pump and Ca^{2+} release flux via RyR, are also modified to strengthen the effect of the SR based on their experimental results [25]. Consequently, it is noted that $[\text{Ca}^{2+}]_{\text{sub}}$ starts increasing almost from the beginning

of the slow diastolic depolarization and activates I_{NaCa} significantly to contribute to V_m change throughout the slow diastolic depolarization, as revealed by the V_L analysis (Fig. 2.8).

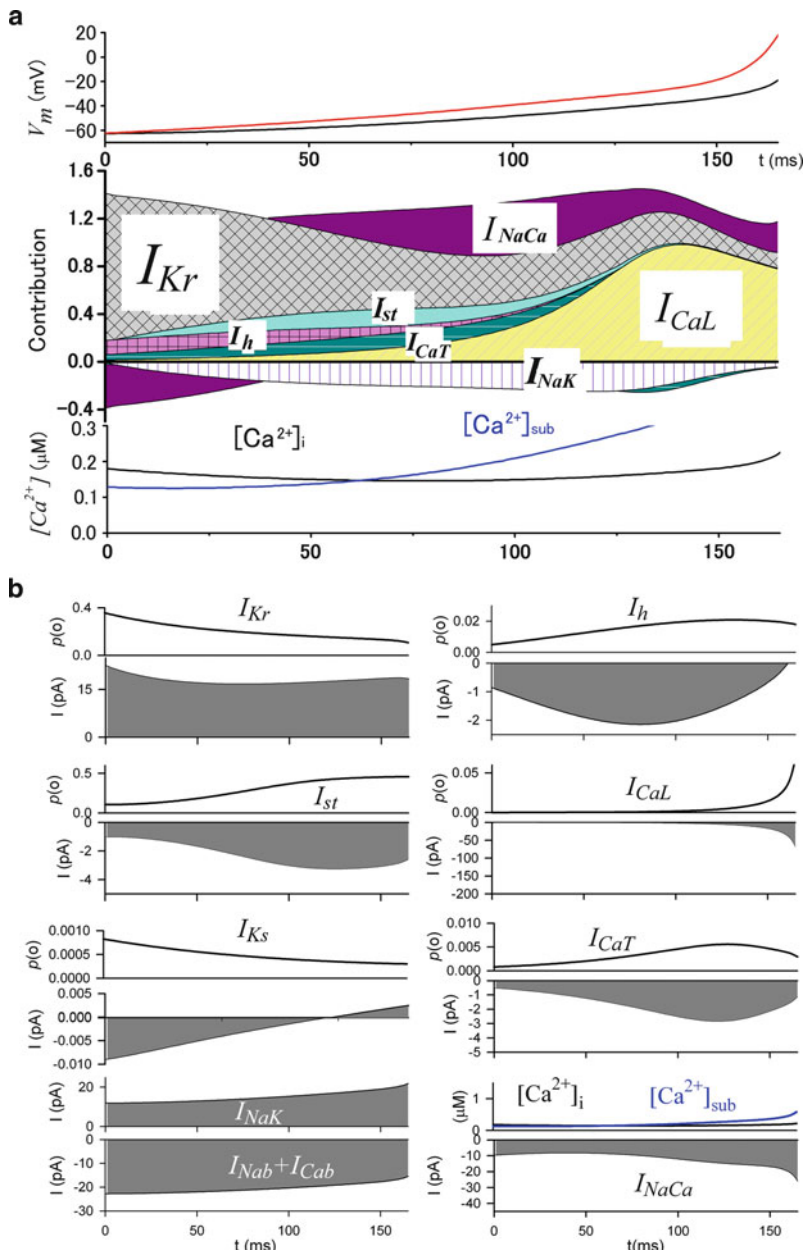


Fig. 2.8 The time profile of r_c during the slow diastolic depolarization in Maltsev and Lakatta model. (a) and (b) are shown in the same style as in Fig. 2.8

2.5 Ionic Mechanisms Underlying the Positive Chronotropy Induced by Catecholamine Stimulation

In the working heart, pacemaker cells are always under the influence of humoral and neural regulation and their activity is modified every moment. In this chapter, we focus specifically on regulation by catecholamines, simulating the effect of sympathetic nerve input. Although sympathetic regulation is crucial in understanding positive chronotropy, the complex signal transduction process that occurs within a cell hinders us from intuitive comprehension of the acceleration mechanism. Therefore, we will introduce a mathematical SA node cell model with an adrenergic signaling cascade to clarify the contribution of each ionic component to the pacemaker activity during catecholamine stimulation.

2.5.1 Revision of the Kyoto Model: From Sarai et al. Model to Himeno et al. Model

The Kyoto model was first published in 2003 [5, 29] and reproduced action potential generation, intracellular ion homeostasis, and Ca^{2+} dynamics in ventricular myocyte and SA node pacemaker cells. Since then, the model has been improved continuously by refining the mitochondria portion of the model [29], updating ion channel representations [30], modeling volume regulation [17], and adding a β 1-adrenergic signaling module [31]. In 2008, we revised our Sarai et al. SA node model [5] to include the above components developed mainly for the ventricular myocyte model to analyze the role of each ion current in the positive chronotropy during β 1-adrenergic stimulation (Himeno et al. model) [6]. Our new model is based on experimental findings in guinea pig SA node cells, which show relatively large I_{Ks} as a target of the β 1-adrenergic stimulation. We also included an alteration of Ca^{2+} dynamics caused by a modification of the Ca^{2+} pump (SERCA) on the sarcoplasmic membrane to gain new insights into possible effect of β 1-adrenergic stimulation on Ca^{2+} handling in pacemaker cells.

2.5.2 Modeling the Catecholamine Effects on Individual Current Systems

The β 1-adrenergic cascade model shown in Fig. 2.9 is basically taken from the Kuzumoto et al. model [31], which is mostly a derivation of the Saucerman et al. model [30]. Briefly, the decoupling of the α -subunit of the G_s protein ($G_{s\alpha}$) from $G_{s\beta\gamma}$ occurs after the activation of the β 1-adrenergic receptor ($\beta_1\text{AR}$), which is stimulated by giving a concentration of β 1-specific agonist isoprenaline (ISO) and partly inactivated by phosphorylation at S301 by protein kinase A (PKA) and at S464 by β -adrenergic receptor kinase ($\beta\text{-ARK}$). Then, the activated $G_{s\alpha}$ enhances cAMP

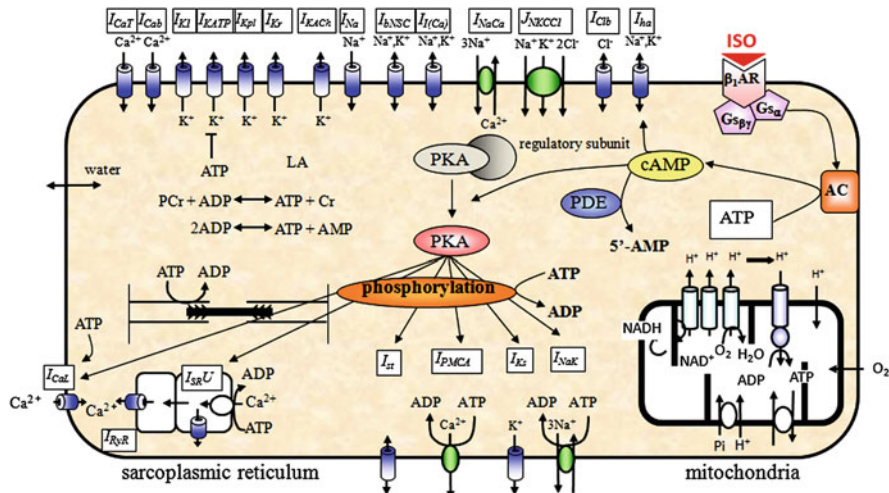


Fig. 2.9 A schematic diagram of pacemaker cell model. The model includes the 15 kinds of ion channels, the sarcolemmal Na^+/K^+ pump, Ca^{2+} -ATPase, $\text{Na}^+/\text{K}^+/2\text{Cl}^-$ cotransporter, and the $\text{Ca}^{2+}/\text{Na}^+$ exchange. The model is also consist of sarcoplasmic reticulum including the Ca^{2+} -release channels (RyR and leak channels) and the Ca^{2+} pump, the contraction model and the oxidative phosphorylation model, as well as the $\beta 1$ -adrenergic signaling cascade (figure taken from Himeno et al. 2008 [6])

synthesis by activating adenylate cyclase (AC). The amount of free cAMP is determined by the balance between the synthesis and degradation by phosphodiesterase (PDE). The unleashing of catalytic subunits of PKA is partially calculated as a function of the concentration of cAMP. The catalytic subunit of PKA is inactivated by protein kinase inhibitor (PKI). Applying $0.01 \mu\text{M}$ ISO to the model cell increases the activated catalytic subunit of PKA by about 2.3-fold. The concentrations of cAMP and PKA reach a peak about 20 s after the application and then slowly decrease. The equations for describing these reactions may be referred to in the original papers.

The targets of PKA in our SA node model are ion channels on the plasma membrane that conduct I_{CaL} , I_{st} , I_h and I_{Ks} , and ion transporters such as the Na^+/K^+ pump, sarcolemmal Ca^{2+} -ATPase (PMCA) and sarcoplasmic reticulum SERCA. For convenience, the ion fluxes of these ion transporters are all expressed as currents such as I_{NaK} , I_{PMCA} , and I_{SRU} , respectively. I_{CaL} , I_{st} , I_h , I_{Ks} , I_{NaK} , I_{PMCA} , and I_{SRU} are modulated as a function of the concentration of PKA catalytic subunits ($[{\text{PKA}}]$) or cAMP ($[{\text{cAMP}}]$). Mathematical descriptions of PKA- or cAMP-dependent activations of these proteins, which are newly introduced in our model, are provided as follows.

2.5.2.1 I_{Ks} , I_{SRU} and I_{PMCA}

Essentially the same equations as those in the ventricular cell model by Kuzumoto et al. [31] are used in the $\beta 1$ -adrenergic stimulation of I_{Ks} , I_{SRU} , and I_{PMCA} . For I_{Ks} , phosphorylation of the main subunit KCNQ1 by catalytic PKA is

modeled based on Saucerian et al. [32] to reproduce the increase of the current. As to $I_{SR}U$, the dissociation constant of SERCA for intracellular Ca^{2+} is assumed to be regulated by catalytic PKA via phosphorylation of phospholamban [30]. The maximum pumping rate of PMCA is augmented by an increase in the concentration of catalytic PKA, whose activity is augmented by cAMP by 2.4 times as observed experimentally. The model equations for these reactions may be referred to the original papers.

2.5.2.2 I_{CaL}

To reproduce amplification of p_{\max} and negative shift in the voltage-dependent activation of I_{CaL} induced by the β 1-adrenergic stimulation [33, 34], a mathematical representation is determined according to (2.11) as follows:

$$I_{\text{CaL}} = p_{\max} \cdot f_{\text{PKA}} \cdot p(o) \cdot f(V_m + V_{\text{shift}}). \quad (2.22)$$

Namely, the permeability of I_{CaL} ($p_{\max} = 31.5 \text{ pA mM}^{-1}$) is multiplied by a factor.

f_{PKA} , which increases as the concentrations of catalytic subunit of PKA elevate from its basal concentration ($\text{PKA}_0 = 0.136 \mu\text{M}$):

$$f_{\text{PKA}} = \text{max_}f \frac{([\text{PKA}] - \text{PKA}_0)^{\text{nH}}}{([\text{PKA}] - \text{PKA}_0)^{\text{nH}} + K_m \text{PKA}^{\text{nH}}} + 1, \quad (2.23)$$

where the value for the maximum amplitude ($\text{max_}f$), Hill coefficient (nH), and the equilibrium constant for PKA ($K_m \text{PKA}$) are 17.5, 1, and $6.5 \mu\text{M}$, respectively.

The rate constants of all voltage-dependent gates for I_{CaL} are biased with V_{shift} , which is determined by the difference between concentrations of catalytic PKA before and after the β -adrenergic stimulation:

$$V_{\text{shift}} = \text{max_}v \cdot \frac{([\text{PKA}] - \text{PKA}_0)^{\text{nH}}}{([\text{PKA}] - \text{PKA}_0)^{\text{nH}} + K_m \text{PKA}^{\text{nH}}}, \quad (2.24)$$

where $\text{max_}v$ is 62.5 mV. As a result, the current amplitude was nearly doubled and the voltage dependency of the peak current–voltage relationship was shifted negatively by $\sim 7 \text{ mV}$ in response to $0.1 \mu\text{M}$ ISO as observed in experiments.

2.5.2.3 I_{st}

The increase of I_{st} induced by the β -adrenergic stimulation is reconstructed by fitting the following equation to experimental data obtained by Toyoda et al. [16].

$$I_{\text{st}} = p_{\max} \cdot f_{\text{PKA}} \cdot p(o) \cdot f(V_m). \quad (2.25)$$

The same (2.23) is applied to I_{PKA} , where values of p_{max} , $\text{max_}f$, nH , and K_m^{PKA} are $62.5 \mu\text{M mM}^{-1}$, 1, 1, and $0.065 \mu\text{M}$, respectively. V_{shift} is not included in this I_{st} model for simplicity.

2.5.2.4 I_h , I_{ha} or I_f

The β -agonists shift the activation curve of I_h , I_{ha} or I_f positively on the voltage axis [35]. Representation of I_{ha} in our model is:

$$I_{ha} = p_{\text{max}} \cdot p(o) \cdot f(V_m + V_{\text{shift}}). \quad (2.26)$$

A similar Michaelis–Menten equation as in (2.24) is used to define V_{shift} as a function of concentration of free cAMP:

$$V_{\text{shift}} = \text{max_}v \frac{([c\text{AMP}] - c\text{AMP}_0)^{nH}}{([c\text{AMP}] - c\text{AMP}_0)^{nH} + K_m^{\text{cAMP}}}, \quad (2.27)$$

where values for $\text{max_}v$, the concentration of cAMP in the absence of $\beta 1$ -adrenergic stimulation ($c\text{AMP}_0$), nH , and the equilibrium constant for cAMP (K_m^{cAMP}) are -15 mV , $0.200 \mu\text{M}$, 1, and $0.294 \mu\text{M}$, respectively.

2.5.2.5 I_{NaK}

Na^+/K^+ pump is regulated by phospholemman, one of the members of FXYD proteins. We assumed that Na^+ affinity ($K_m^{\text{Na}_i}$) is increased by catalytic PKA (35% decrease in the half maximum concentration for Na^+) to fit to the experimental data by Despa et al. [36].

$$K_d^{\text{Na}_i} = K_m^{\text{Na}_i} \cdot \left(\frac{0.35}{1 + \left(\frac{[\text{PKA}]}{K_m^{\text{PKA}}} \right)^{nH}} + 0.65 \right), \quad (2.28)$$

where values of $K_m^{\text{Na}_i}$, nH , and K_m^{PKA} are 4.05 mM , 5, and $0.500 \mu\text{M}$, respectively.

2.5.3 Modification of Membrane Potential, Ionic Currents and Ca^{2+} Transient During the Catecholamine Stimulation

The effects of $\beta 1$ -adrenergic stimulation are shown in Fig. 2.10. In each panel, two traces obtained before and during the stimulation (20 s from the onset) are superimposed by referring to the maximum rate of rise of the action potential. The slope

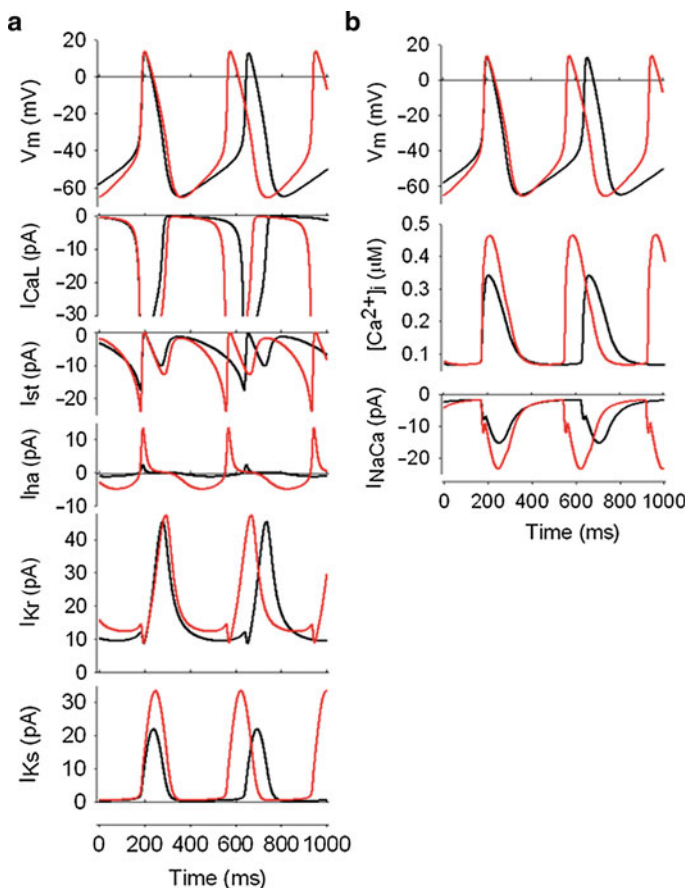


Fig. 2.10 (a) Comparison of V_m , ionic currents (I_{CaL} , I_{st} , I_h , I_{Kr} , I_{Ks} , and I_{NaCa}) and Ca^{2+} transient before and 30 s after the application of 0.01 μM ISO. The black traces are control and red traces ISO traces superimposed at the time point of the maximum rate of rise of the action potential. The peak of I_{CaL} is out of the scale. (b) Modulation of I_{NaCa} , intracellular Ca^{2+} concentration, and I_{NaCa} by $\beta 1$ -adrenergic stimulation

of slow diastolic depolarization was significantly increased by 0.01 μM ISO from 0.087 to 0.126 $mV\ ms^{-1}$, when measured over the linear portion of the diastolic depolarization. This increase in the depolarizing rate decreases the duration taken for ~ 25 mV depolarization from the maximum diastolic potential (-65 mV) to the take-off potential of the action potential (~ 40 mV) by approximately 88 ms. Although the peak amplitude of I_{CaL} increased significantly from 158 to 184 pA, the increase of I_{CaL} during the slow diastolic depolarization is small if compared with that of I_{st} . To estimate the relative importance of I_{st} and I_h during the diastolic depolarization, the time-integral of I_{st} and I_h was measured over the initial period of 280 ms from the maximum diastolic potential. The increases in electrical charge carried by I_{st} and I_h induced by the $\beta 1$ -adrenergic stimulation were nearly equal

(the ratio $\Delta I_{st}/\Delta I_h = 1.19$), indicating that I_{st} and I_h almost equally contribute to the positive chronotropy.

Since outward I_{Kr} is not a target of PKA, its increase during diastole is secondary to the modification of the membrane potential. The amplitude of I_{Ks} is increased by up to 150% at the peak. Although I_{Ks} is enhanced by both PKA and increased Ca^{2+} transients, the amplitude of I_{Ks} during diastolic depolarization remained negligibly small. The increase in I_{Ks} , however, is useful in compromising the effect of I_{CaL} to elongate the action potential under the β 1-adrenergic stimulation.

The PKA-dependent activation of Ca^{2+} uptake by SERCA accelerated the decay of the Ca^{2+} transient, and increased the Ca^{2+} content within the SR, supplemented by the increased Ca^{2+} influx through I_{CaL} . Thus, the peak amplitude of the Ca^{2+} transient was increased by 56% (Fig. 2.10b). The magnitude of inward I_{NaCa} was almost equal to that observed in control during diastolic depolarization (Fig. 2.10b, bottom panel). Thus, modulation of I_{NaCa} does not seem to contribute to the slow diastolic depolarization. On the contrary, the increase in I_{NaCa} during the action potential hampered the positive chronotropic effect of β 1-adrenergic stimulation by prolonging the action potential duration.

2.5.4 Contribution of Each Ionic Component to the Pacemaker Depolarization During Catecholamine Stimulation

Figure 2.11 compares results of the V_L analysis obtained before (bottom panel) and 20 s after the onset of ISO application (top panel). The time axis of the control profile at the bottom is reduced to $\sim 2/3$ and the membrane potentials obtained before (black) and after ISO application (red) are superimposed in the middle panel. In general, the contribution profile remained very similar after the β -adrenergic stimulation when the time axis is normalized with the time course of the profile obtained in the presence of ISO. Namely, the early contribution of I_{Kr} deactivation is finally connected to the I_{CaL} activation near the foot of the action potential via the contribution by both I_{st} and I_h activation in the intermediate phase. The contribution of I_h is enlarged from ~ 0.1 in the control to 0.33 after the ISO application, because of the positive voltage shift of I_h activation. These common profiles are well explained by the overlapping time course of membrane depolarization. The negative contribution of I_{NaCa} is also common for both the control and the β -adrenergic stimulation. Although the positive contribution of I_{NaCa} at the end of the slow diastolic depolarization, corresponding to the Ca^{2+} transient increased from 0.26 in control to 0.35 with 0.01 μM ISO application, the contribution was only transient. Therefore, it may be concluded that I_{NaCa} is scarcely involved in the positive chronotropy in our model.

As to the role of I_{Ks} in the pacemaker depolarization, there might be species difference. In the present V_L analysis, only a little contribution is disclosed in I_{Ks} as shown in Fig. 2.11 in the guinea pig model. However, a larger contribution of I_{Ks} has been supposed in the porcine and human SA node cell, which has dominant

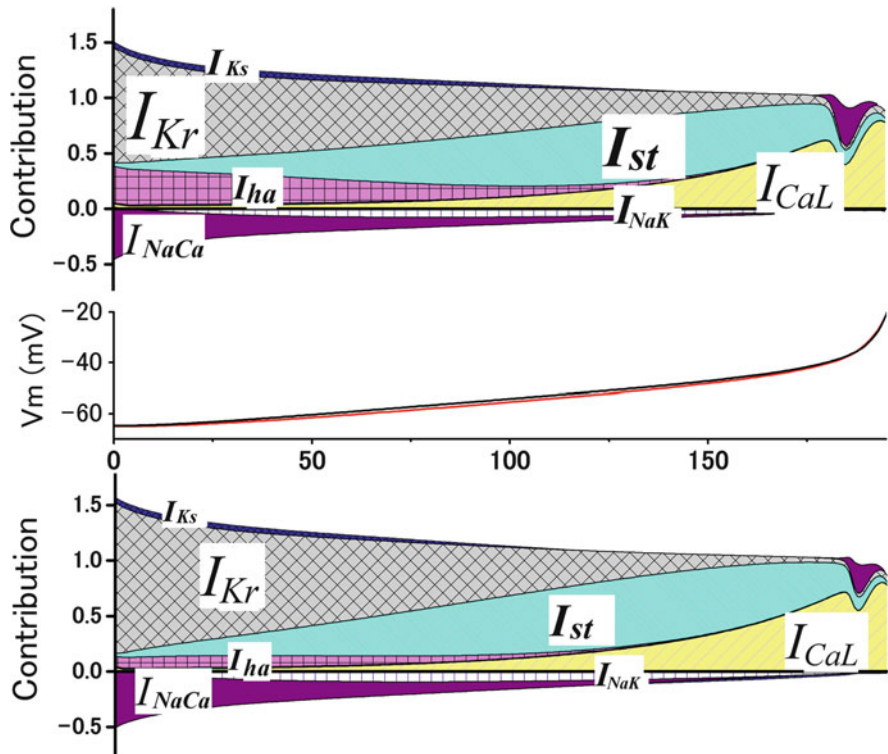


Fig. 2.11 Comparison of the time profile of r_c between the control (bottom) and that in the presence of $0.01 \mu\text{M}$ ISO (top) in Himeno et al. model. The time scale for the control is reduced to $\sim 2/3$ to superimpose the V_m traces (red; ISO and black; control) to facilitate the comparison of the time-dependent change of r_c

expression of I_{Ks} and very low heart rate ($\sim 80 \text{ min}^{-1}$) compared to the small mammals [35, 37].

2.6 Conclusions

The lead potential analysis revealed a common profile of contributions of ionic channels and transporters among variety of pacemaker cell models of small mammals. That is, the transition of the main contributor current from I_{Kr} to I_{CaL} transmitted by a set of inward currents, such as I_{st} , I_{h} , and I_{CaT} . As to the role of I_{NaCa} , although the extent of the contribution may differ, the contribution of I_{NaCa} is no more than substitution of some contribution of the set of inward currents. It should be noted that the variations among models arise from the different weights of each ionic current in the set of inward currents, leaving the common feature intact. To our surprise, the common feature was maintained even when the

spontaneous rate is increased after β -adrenergic stimulation, where activities of all channels and transporters are modulated directly by PKA/cAMP or secondarily by modified membrane potentials and intracellular ionic concentrations. For further development of this research on pacemaker mechanisms, see Himeno Y et al. (2011) “Minor contribution of cytosolic Ca^{2+} transients to the pacemaker rhythm in guinea pig sinoatrial node cells” [38].

Acknowledgments This work was supported by the Biomedical Cluster Kansai project of Ministry of Education, Culture, Sports, Science and Technology Japan and Ritsumeikan-Global Innovation Research Organization in Ritsumeikan University.

References

1. Wilders R. Computer modelling of the sinoatrial node. *Med Biol Eng Comput*. 2007;45:189–207.
2. Wilders R, Jongsma HJ, van Ginneken AC. Pacemaker activity of the rabbit sinoatrial node. A comparison of mathematical models. *Biophys J*. 1991;60:1202–16.
3. Demir SS, Clark JW, Murphrey CR, Giles WR. A mathematical model of a rabbit sinoatrial node cell. *Am J Physiol*. 1994;266:C832–52.
4. Kurata Y, Hisatome I, Imanishi S, Shibamoto T. Dynamical description of sinoatrial node pacemaking: improved mathematical model for primary pacemaker cell. *Am J Physiol Heart Circ Physiol*. 2002;283:H2074–101.
5. Sarai N, Matsuoka S, Kuratomi S, Ono K, Noma A. Role of individual ionic current systems in the SA node hypothesized by a model study. *Jpn J Physiol*. 2003;53:125–34.
6. Himeno Y, Sarai N, Matsuoka S, Noma A. Ionic mechanisms underlying the positive chronotropy induced by beta1-adrenergic stimulation in guinea pig sinoatrial node cells: a simulation study. *J Physiol Sci*. 2008;58:53–65.
7. Maltsev VA, Lakatta EG. Synergism of coupled subsarcolemmal Ca^{2+} clocks and sarcolemmal voltage clocks confers robust and flexible pacemaker function in a novel pacemaker cell model. *Am J Physiol Heart Circ Physiol*. 2009;296:H594–615.
8. Cha CY, Himeno Y, Shimayoshi T, Amano A and Noma A. A Novel Method to quantify contribution of channels and transporters to membrane potential dynamics. *Biophys J*. 2009;97(12):3086–94.
9. Hagiwara N, Irisawa H, Kameyama M. Contribution of two types of calcium currents to the pacemaker potentials of rabbit sino-atrial node cells. *J Physiol*. 1988;395:233–53.
10. Fermini B, Nathan RD. Removal of sialic acid alters both T- and L-type calcium currents in cardiac myocytes. *Am J Physiol*. 1991;260:H735–43.
11. Guo J, Ono K, Noma A. A sustained inward current activated at the diastolic potential range in rabbit sino-atrial node cells. *J Physiol*. 1995;483(Pt 1):1–13.
12. Guo J, Mitsuiye T, Noma A. The sustained inward current in sino-atrial node cells of guinea-pig heart. *Pflugers Arch*. 1997;433:390–6.
13. Mitsuiye T, Guo J, Noma A. Nicardipine-sensitive Na^+ -mediated single channel currents in guinea-pig sinoatrial node pacemaker cells. *J Physiol*. 1999;521(Pt 1):69–79.
14. Cho HS, Takano M, Noma A. The electrophysiological properties of spontaneously beating pacemaker cells isolated from mouse sinoatrial node. *J Physiol*. 2003;550:169–80.
15. Shinagawa Y, Satoh H, Noma A. The sustained inward current and inward rectifier K^+ current in pacemaker cells dissociated from rat sinoatrial node. *J Physiol*. 2000;523(Pt 3):593–605.
16. Toyoda F, Ding WG, Matsura H. Responses of the sustained inward current to autonomic agonists in guinea-pig sino-atrial node pacemaker cells. *Br J Pharmacol*. 2005;144:660–8.

17. Ishihara H, Ozaki H, Sato K, et al. Calcium-independent activation of contractile apparatus in smooth muscle by calyculin-A. *J Pharmacol Exp Ther.* 1989;250:388–96.
18. Hagiwara N, Irisawa H, Kasanuki H, Hosoda S. Background current in sino-atrial node cells of the rabbit heart. *J Physiol.* 1992;448:53–72.
19. Tellez JO, Dobrzynski H, Greener ID, et al. Differential expression of ion channel transcripts in atrial muscle and sinoatrial node in rabbit. *Circ Res.* 2006;99:1384–93.
20. Irisawa A. Fine structure of the small sinoatrial node specimen used for voltage clamp experiment. In: The sinusnode, structure, function and clinical relevance. (F.I.M. Bonke, ed.) The Hague: Martinus Nijhoff Medical Division, 1978, pp. 311–319.
21. Glukhovsky A, Adam DR, Amitzur G, Sideman S. Mechanism of Ca⁺⁺ release from the sarcoplasmic reticulum: a computer model. *Ann Biomed Eng.* 1998;26:213–29.
22. Snyder SM, Palmer BM, Moore RL. A mathematical model of cardiocyte Ca(2+) dynamics with a novel representation of sarcoplasmic reticular Ca(2+) control. *Biophys J.* 2000;79:94–115.
23. Doerr T, Denger R, Trautwein W. Calcium currents in single SA nodal cells of the rabbit heart studied with action potential clamp. *Pflugers Arch.* 1989;413:599–603.
24. Vinogradova TM, Zhou YY, Maltsev V, Lyashkov A, Stern M, Lakatta EG. Rhythmic ryanodine receptor Ca²⁺ releases during diastolic depolarization of sinoatrial pacemaker cells do not require membrane depolarization. *Circ Res.* 2004;94:802–9.
25. Lyashkov AE, Juhaszova M, Dobrzynski H, et al. Calcium cycling protein density and functional importance to automaticity of isolated sinoatrial nodal cells are independent of cell size. *Circ Res.* 2007;100:1723–31.
26. Maltsev VA, Lakatta EG. Dynamic interactions of an intracellular Ca²⁺ clock and membrane ion channel clock underlie robust initiation and regulation of cardiac pacemaker function. *Cardiovasc Res.* 2008;77:274–84.
27. Ferrier GR. The effects of tension on acetylstrophantidin-induced transient depolarizations and aftercontractions in canine myocardial and Purkinje tissues. *Circ Res.* 1976;38:156–62.
28. Matsuda H, Noma A, Kurachi Y, Irisawa H. Transient depolarization and spontaneous voltage fluctuations in isolated single cells from guinea pig ventricles. Calcium-mediated membrane potential fluctuations. *Circ Res.* 1982;51:142–51.
29. Matsuoka S, Sarai N, Jo H, Noma A. Simulation of ATP metabolism in cardiac excitation–contraction coupling. *Prog Biophys Mol Biol.* 2004;85:279–99.
30. Saucerman JJ, Brunton LL, Michailova AP, McCulloch AD. Modeling beta-adrenergic control of cardiac myocyte contractility in silico. *J Biol Chem.* 2003;278:47997–8003.
31. Kuzumoto M, Takeuchi A, Nakai H, Oka C, Noma A, Matsuoka S. Simulation analysis of intracellular Na⁺ and Cl⁻ homeostasis during beta 1-adrenergic stimulation of cardiac myocyte. *Prog Biophys Mol Biol.* 2008;96:171–86.
32. Saucerman JJ, Healy SN, Belik ME, Puglisi JL, McCulloch AD. Proarrhythmic consequences of a KCNQ1 AKAP-binding domain mutation: computational models of whole cells and heterogeneous tissue. *Circ Res.* 2004;95:1216–24.
33. Kameyama M, Hofmann F, Trautwein W. On the mechanism of beta-adrenergic regulation of the Ca channel in the guinea-pig heart. *Pflugers Arch.* 1985;405:285–93.
34. Zaza A, Robinson RB, DiFrancesco D. Basal responses of the L-type Ca²⁺ and hyperpolarization-activated currents to autonomic agonists in the rabbit sino-atrial node. *J Physiol.* 1996;491(Pt 2):347–55.
35. Ono K, Shibata S, Iijima T. Pacemaker mechanism of porcine sino-atrial node cells. *J Smooth Muscle Res.* 2003;39:195–204.
36. Despa S, Bossuyt J, Han F, et al. Phospholemman-phosphorylation mediates the beta-adrenergic effects on Na/K pump function in cardiac myocytes. *Circ Res.* 2005;97:252–9.
37. Ono K, Shibata S, Iijima T. Properties of the delayed rectifier potassium current in porcine sino-atrial node cells. *J Physiol.* 2000;524(Pt 1):51–62.
38. Himeno Y, Toyoda F, Satoh H, Amano A, Cha CY, Matsuura H, Noma A. Minor contribution of cytosolic Ca²⁺ transients to the pacemaker rhythm in guinea pig sinoatrial node cells. *Am J Physiol Heart Circ Physiol.* 2011;300:H251–61.

Chapter 3

The “Funny” Pacemaker Current

**Andrea Barbuti, Annalisa Bucchi, Raffaella Milanesi, Georgia Bottelli,
Alessia Crespi, and Dario DiFrancesco**

3.1 Introduction: The Mechanism of Cardiac Pacemaking

The spontaneous activity of the heart has been known for a long time. In the second century AD, the physician Claudius Galenus (Galen of Pergamum AD ca 130–ca 200) realized that when extracted from the chest the heart keeps beating for a long period. Several more centuries were necessary, however, for Keith and Flack to discover, in 1907, a structure responsible for the initiation of the heartbeat, the sinoatrial node (SAN) [1, 2]. More than 100 years later, the electrical and molecular mechanisms responsible for the intrinsic automaticity of the SAN are still debated [3].

The shape and duration of action potentials (APs) of SAN cells are different from those of atrial and ventricular myocytes, most notably for the presence of the diastolic phase (pacemaker or diastolic depolarization, DD) which drives the membrane potential from the maximum diastolic potential (MDP, around -60 mV) up to threshold (around -40 mV) for another AP, thus generating autorhythmicity.

The pacemaker phase is the result of a concerted interplay of several mechanisms comprising ionic currents, pumps and exchangers. Activation of the “funny” current (I_f or “pacemaker” current) drives early DD up to a point where Ca^{2+} -dependent mechanisms, involving first the T-type calcium current and the $\text{Na}-\text{Ca}$ exchanger, and then the L-type Ca^{2+} current, kick in to determine the late fraction of DD and help reaching the threshold of a new AP. The events leading to the discovery of the funny current and its main properties in SAN tissue/cells are described below.

A. Barbuti (✉), A. Bucchi, R. Milanesi, G. Bottelli, A. Crespi, and D. DiFrancesco
Department of Biomolecular Sciences and Biotechnology, University of Milano, Via Celoria 26,
20133 Milano, Italy
e-mail: andrea.barbuti@unimi.it

3.1.1 Historical Background and Basic Biophysical Properties of I_f

In 1979 a new pacemaking mechanism was proposed to explain the spontaneous activity of SAN myocytes. This mechanism was based on the activation, upon hyperpolarization to the diastolic (pacemaker) voltage range, of an inward current, responsive to stimulation by noradrenaline. The current was dubbed “funny” (I_f) because of its unusual properties [4]. Prior to the discovery of I_f , pacemaking had been largely investigated in Purkinje fibers and attributed to a completely different mechanism, the decay of a K^+ current (I_{K2}). However, some I_{K2} properties, such as a strong dependence on external Na^+ and a very negative reversal potential, did not reconcile with those of a pure K^+ current. The pacemaking mechanism proposed for SAN myocytes based on I_f was actually opposite to that involving I_{K2} deactivation suggested for Purkinje fibers. This puzzle was solved in 1981, with the demonstration that I_{K2} was the same I_f current just discovered in the SAN [5, 6].

The I_f current had several unusual features. It was the first voltage-and time-dependent current found to be activated on membrane hyperpolarization rather than on depolarization and had a reversal potential around $-10/-20$ mV, due to a mixed Na^+ and K^+ permeability [5–8]. Although the Na^+/K^+ permeability ratio is about 0.27–0.33, implying a preferential permeability of K^+ over Na^+ , Na^+ permeation is functionally important because it renders the current inward and depolarizing at diastolic voltages (about -40 to -60 mV in the SAN). Finally, I_f had a dual modulation by voltage and cyclic nucleotides [9].

3.1.2 Voltage Dependence of f-Channel Activation

According to data from the literature, the voltage range of activation of I_f in the SAN has a large variability with threshold values ranging between -32 and -70 mV, and half-activation voltages ($V_{1/2}$) in the range $-50/-120$ mV [10]. These differences can be explained partly by the different experimental conditions and partly by the high sensitivity of this channel to the cellular “environment.” For example, cAMP concentration and “run-down” can influence the open probability of f-channels [11]. Run-down causes a rapid negative shift of the f-channels activation curve during whole-cell patch clamp recordings and can induce a substantial underestimation of the I_f contribution [12], which might explain the highly negative threshold or $V_{1/2}$ values reported in some studies. Other mechanisms modulating f-channel function include phosphorylation [13, 14], interaction with auxiliary subunits [15–19], and interaction with lipids and/or structural proteins [20, 21].

The variability in the activation range of I_f becomes even greater when considering that f-channels are also expressed in other autorhythmic cardiac regions such as the atrioventricular node (AVN) and the His-Purkinje system [22], where I_f activates at more negative voltages compared to SAN myocytes [23, 24].

Expression of f-channels has also been reported in working myocardium (atrial and ventricular muscle), although their physiological relevance is negligible due to the low expression and to the too negative range of activation [25, 26]. Interestingly, pathological conditions such as cardiac hypertrophy may lead to an increased f-channel expression in the working myocardium, with associated increased propensity to ventricular arrhythmias [27].

3.1.3 *I_f*-Mediated Autonomic Modulation of Cardiac Rate

The heart rate needs to be promptly adjusted to the physical and emotional state of the organism. Since the duration of DD is a main determinant of heart rate, its fine modulation is achieved by precise control of the steepness of DD by autonomic neurotransmitters (Fig. 3.1c). Sympathetic stimulation accelerates, and parasympathetic stimulation slows heart rate, through activation of β -adrenergic (β -ARs) and muscarinic M2 receptors, respectively. β -ARs (coupled to stimulatory G-protein, $G\alpha s$) and M2 receptors (coupled to inhibitory G-proteins, $G\alpha i$) exert opposite effects on adenylate cyclase thus controlling, together with cAMP-phosphodiesterase, the cytosolic concentration of cAMP.

cAMP directly binds to f-channels and shifts their activation curve towards more positive potentials [28]. This mechanism increases the net inward current flowing

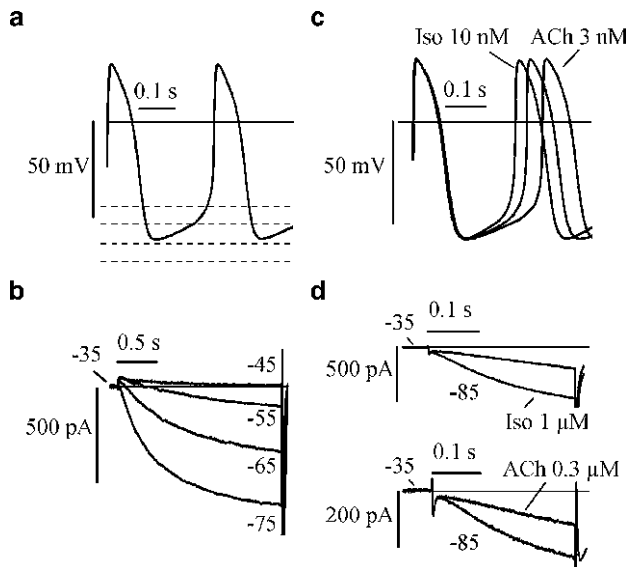


Fig. 3.1 Properties of the funny current. (a, b) Action potentials (a) and I_f current recorded during steps to the voltages indicated (b) from a rabbit SAN cell; the same voltages are indicated in (a) by broken lines. (c) Low doses of the β -AR-agonist isoprenaline (Iso) and muscarinic agonist acetylcholine (ACh) accelerate and slow rate, respectively, of a SAN cell by changing the rate of diastolic depolarization. (d) These changes are due to I_f increase/decrease caused by Iso/ACh, respectively

during the DD, and results in the steepening of DD slope and consequent cardiac acceleration [29]; slowing of heart rate is obtained by an opposite set of events initiated by M2-receptor-mediated decrease in cAMP.

Both $\beta 1$ and $\beta 2$ subtypes of β -ARs are expressed in the heart and although $\beta 1$ -ARs are predominant, the SAN has the highest expression of $\beta 2$ -ARs among cardiac tissues [30]. Interestingly, in rabbit SAN myocytes stimulation of $\beta 2$ -ARs causes a larger shift of I_f activation curve and a more pronounced positive chronotropy than $\beta 1$ -AR stimulation. This is due to co-localization of $\beta 2$ -ARs and f-channels in specific membrane microdomains (caveolae, see also Sect. 3.2.2.3.1) [21].

3.2 Molecular Structure of Pacemaker Channels

The genes encoding the molecular correlates of f-channels were cloned in the late 1990s [31]. Based on structure homology, the f-channel α -subunits, termed Hyperpolarization-activated Cyclic Nucleotide-gated (HCN) channels, were included in the superfamily of voltage-dependent K⁺ and CNG channels. HCN channels have been cloned from vertebrates, invertebrates and urochordates; in mammals four different isoforms were found (HCN1–4) [32, 33].

HCN isoforms are widely expressed both in excitable (heart and nervous system, and also smooth muscle) and non-excitable tissues (testes, pancreatic β -cells) [33]. The various subunits can assemble to form functional homomeric and/or heteromeric channels (with the exception of HCN2–HCN3 heteromers) which are tetramers [33, 34].

The overall structure of HCN channels includes: a conserved core region formed by six transmembrane (S1–S6) domains, with a positively charged S4 segment; a pore (P) region involving S5, S6 and their connecting loop; a relatively short intracellular N-terminus and a relatively long intracellular C-terminus which are less conserved among isoforms. All HCN isoforms exhibit, within the permeation pathway, a selectivity filter including the GYG triplet typical of K⁺ channels, although partially hydrated Na⁺ ions can also accommodate in the not-too-rigid structure of the inner pore of HCN channels [35].

The N-terminus contains a sequence which appears to be important in mediating channel trafficking to the plasma membrane [36, 37]. In the C-terminus, three separate structural elements can be recognized: the C-linker, organized in six α -helices, the Cyclic Nucleotide Binding Domain (CNBD), and the actual C-terminus. The CNBD and the C-linker act as a functional unit that modulates the open probability of a pacemaker channel. When cAMP is bound the α -helices of the C-linker of one subunit interact with the α -helices of the adjacent subunit, a conformation favoring the open state of the channel. The removal of cAMP favors a rearrangement of the structure leading to channel closing [38–40].

The overall molecular structure confers to all HCN isoforms the specific functional properties typical of f-channels described above; there are nonetheless important differences in the rates of channel opening/closing and cAMP sensitivities.

HCN1 is by far the fastest activating/deactivating isoform, followed by HCN2 and HCN3, while HCN4 has the slowest kinetics [41, 42]. HCN1 is weakly affected by cAMP (4.3–5.8 mV maximal shift), HCN2 and HCN4 display a larger response (shifts of 16.9–19.2 and 11–23 mV respectively), and the activation curve of HCN3 is shifted to the negative direction (from -2.9 to -5 mV) [38, 43]. The voltage dependence of activation also varies: HCN1 has the most positive $V_{1/2}$ followed by HCN4, HCN3 and HCN2 [42]. Finally, the functional properties of these channels depend on several factors, referred to as “context dependence”, which can significantly offset the position of the activation curve [44].

3.2.1 *HCN Composition of Native Pacemaker Channels*

The existence of four different HCN isoforms was initially seen as a possible basis for tissue-specific differences in I_f properties. However, none of the four isoforms, when heterologously expressed as homomeric channels, could generate currents with properties identical to those of native I_f current in specific cardiac tissues. This finding raised the question whether native pacemaker channels could be heteromers of different subunits, and prompted the study of the distribution of HCN channels in different cardiac regions. Analysis of HCN distribution indicated that the HCN4 isoform represents the major component of pacemaker channels in the SAN (Table 3.1). In fact, from early cardiac development up to adulthood, HCN4 expression delineates the pacemaker region/conduction system of the heart [54, 55, 61, 62]. Species-dependent expression of HCN1 and HCN2 has also been reported in the SAN, but always at a much lower level than HCN4 expression [34]. In the working myocardium, HCN2 is the predominant isoform even though at a low level of expression compared to SAN and conduction system. The HCN3 isoform has been found both in mouse SAN and ventricle at the mRNA level, with higher expression during embryogenesis, but protein expression has never been shown [34].

As a consequence of the finding that more than one HCN subunit is co-expressed in a specific cardiac region, the ability of the various subunits to co-assemble in heterotetramers was evaluated. Co-expression of various subunits often results in functional channels displaying kinetic and modulatory characteristics intermediate between those of the individual components; nevertheless, heterotetramers often failed to fully recapitulate native I_f [33, 63, 64].

3.2.2 *Regulation of HCN Channels*

When HCN2 channels are heterologously expressed in neonatal and adult ventricular myocytes, they generate similar currents, but the voltage range of activation in neonatal cells is some 18 mV more positive than in the adult [65]. A 22 mV difference is also found when comparing native I_f activation curves in newborn

Table 3.1 HCN isoform distribution in different cardiac regions: SAN sinoatrial node, *PF* Purkinje Fibers, *AVN* atrioventricular node, *NM* not measured, – below detection level, +/- very low expression at the limit of detection, from + to ++++ increasing levels of expression

Tissue		Species	Method(s)	HCN1	HCN2	HCN3	HCN4	Ref
SAN	mRNA	Human	qPCR	++	+	–	++++	[45]
		Human	RT-PCR	+	+	–	++++	[46]
		Dog	C RT-PCR	–	++	NM	+++	[47]
		Rabbit	RNase PAs	++	+	–	++++	[48]
		Rabbit	NB, <i>isH</i>	+	NM	NM	NM	[49]
		Mouse	qRT-PCR	++	+	+/-	++++	[50]
		Mouse	<i>isH</i>	+	++	NM	++++	[51]
		Rat	qRT-PCR	–	+	–	+	[52]
	Protein	Human	Immuno	NM	NM	NM	++	[45]
		Dog	WB/immuno	NM	++	NM	+++	[47]
Atrium	mRNA	Rabbit	WB/immuno	+	NM	NM	NM	[49]
		Rabbit	WB/immuno	+/-	–	NM	++	[53]
		Mouse	Immuno	–	–	NM	+	[54]
		Rat	Immuno	NM	NM	NM	+	[55]
		Human	qPCR	+	+++	–	++	[45]
	Protein	Human	rt RT-PCR	++	+++	–	++++	[56]
		Human	C RT-PCR	+	+	NM	++	[57]
		Dog	C RT-PCR	–	+	NM	++	[47]
		Mouse	qRT-PCR	+	+	–	+	[50]
		Rat	Immuno	NM	NM	NM	–	[45]
Ventricle	mRNA	Human	WB	–	+	NM	++	[57]
		Dog	WB/immuno	NM	+	NM	++	[47]
		Rabbit	Immuno	NM	NM	NM	–	[58]
		Mouse	Immuno	–	–	NM	–	[54]
		Rat	Immuno	NM	NM	NM	–	[55]
	Protein	Human	rt RT-PCR	+	++	–	+++	[56]
		Human	C RT-PCR	–	++	NM	+	[57]
		Dog	C RT-PCR	–	++	NM	–	[59]
		Rabbit	RNase PAs	–	+	–	–	[48]
		Mouse	qRT-PCR	+	++	–	+	[50]
PF	mRNA	Rat	RNase PAs	–	++++	NM	+	[48]
		Rat	qRT-PCR	–	+	NM	+	[60]
		Human	WB	–	++	NM	+	[57]
	Protein	Dog	WB	–	+	NM	–	[59]
		Rabbit	Immuno	NM	NM	NM	–	[58]
		Human	rt RT-PCR	+	+	+	++	[56]
AVN	mRNA	Dog	C RT-PCR	+/-	++	NM	+++	[59]
		Rabbit	RNase PAs	–	+	–	–	[48]
	Protein	Dog	WB	–	++	–	+++	[59]
	mRNA	Rabbit	NB, <i>isH</i>	–	NM	NM	NM	[49]
	Protein	Mouse	qRT-PCR	+	+	–	+	[50]
	Protein	Rabbit	Immuno	–	NM	NM	+	[58]
	Protein	Rat	Immuno	NM	NM	NM	+	[55]

The + symbols do not refer to absolute values and can be compared only within the same group. *qPCR* quantitative polymerase chain reaction (PCR), *RT-PCR* reverse transcriptase PCR, *C RT-PCR* competitive RT-PCR, *rt RT-PCR* real-time RT-PCR, *NB* Northern Blot, *WB* Western Blot, *immuno* immunolabeling, *isH* in situ hybridization, *RNase PAs* RNase protection assays

and adult ventricular myocytes [66]. These differences cannot be readily explained in terms of different channel-bound cAMP concentrations. Indeed HCN channels are also regulated by several other factors such as Src-kinases [13, 67], membrane phospholipids (phosphatidylinositol 4,5-bisphosphate PI(4,5)P₂) [68, 69], cholesterol [20] and by interaction with transmembrane/intracellular proteins (KCNE2, caveolin 3, KCR1, SAP97) [15, 16, 18, 19, 21, 70, 71]. As mentioned above, these and perhaps other modulatory factors generate a “context dependence” of funny channels.

3.2.2.1 Src-Kinases

Src forms complexes with HCN2 and HCN4 channels and phosphorylates HCN4 in at least two different highly conserved tyrosine residues in the C-linker (Tyr 531 and Tyr 554) [13, 14]; this increases channel open probability and speeds activation kinetics [13].

3.2.2.2 Cholesterol and Membrane Phospholipids

Phospholipids are not uniformly distributed in the membrane but form distinct microdomains, called lipid rafts, enriched in cholesterol and sphingolipids [72]. In rabbit SAN myocytes, HCN4 localizes in caveolar lipid rafts and their disruption strongly affects f-channel kinetics, shifting the activation curve toward more positive potentials and slowing deactivation kinetics, which leads to acceleration of spontaneous activity [20].

Funny channels are also modulated by PI(4,5)P₂ whose depletion can partially explain the I_f run-down phenomenon [69]. Furthermore, the increase of PI(4,5)P₂ mediated by activation of phospholipase C-coupled receptors (bradykinin BK2 receptor and muscarinic M1 receptor) can modulate channel gating; specifically, stimulation of BK2 receptors induces a large positive shift of the activation curve of HCN2, HCN1 and SAN f-channels [68].

3.2.2.3 Protein–Protein Interactions

A well established function of lipid rafts is to confine in a discrete membrane domain proteins involved in the same signal transduction pathway, so as to favor their functional interaction [72]. Functional interactions able to alter channel properties have been demonstrated between cardiac HCN channels and caveolin 3, MiRP1, KCR1 and SAP97 (Fig. 3.2).

Caveolin 3

Caveolae are a type of lipid raft characterized by the presence of the scaffold protein caveolin. In rabbit SAN cells, particularly rich in caveolae [73], HCN4

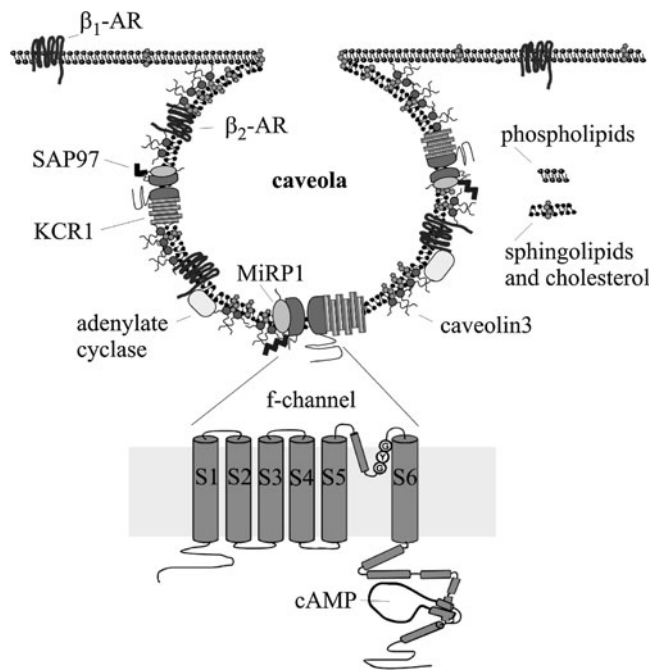


Fig. 3.2 Cartoon illustrating the caveolar localization of f-channels and other elements of the f-channel modulatory pathway. Further explanation in text

co-localizes and interacts with caveolin 3 [21, 71]. Disorganization of caveolae strongly affects f-channel kinetics, by shifting the activation curve toward more positive potentials, slowing deactivation kinetics and altering adrenergic modulation [20, 21].

MiRP1

Mink-related protein 1 (MiRP1 or KCNE2) is a single transmembrane domain protein that acts as β -subunit of hERG and HCN channels. It has been shown that MiRP1 interacts with HCN2 channels in SAN and ventricular myocytes. In heterologous expression systems, MiRP1 increases HCN1, HCN2 and HCN4 current densities and alters activation kinetics; this latter effect, however, depends on the specific isoform tested and on the expression system used [15–17].

KCR1

This is another membrane spanning protein shown to interact in heterologous expression systems with HCN2 channels. It causes a significant decrease of current

density, and a negative shift of the activation curve when both proteins are co-expressed in CHO cells. Exogenous expression of KCR1 in neonatal ventricular myocytes decreased current density, while down-regulation of KCR1 by specific siRNA (small interfering RNA) increased current density. Interestingly, in pig and rat hearts, the SAN has the lowest level of KCR1 mRNA, in agreement with the relevant role of I_f in this tissue [18].

SAP97

In rabbit SAN, HCN2 and HCN4 channels co-localize with the Synapse Associated Protein-97 (SAP97), a scaffold protein which clusters proteins at the cell membrane. In heterologous expression systems, SAP97 functionally interacts with HCN2 and HCN4 channels through a PDZ domain and alters the current density, though in a context-(in CHO cells but not in HEK cells) and isoform-specific manner (increases HCN2 and decreases HCN4 current) [19].

While a general picture of all the relative interactions among these proteins is still lacking, the above data, together with evidence that in heart MiRP1, SAP97 and other voltage-gated ion channels are also associated with caveolin 3-rich membrane microdomains [74, 75], suggest the formation of a macromolecular complex important for the proper activity and modulation of HCN channels and for the correct electrical function of SAN pacemaker myocytes.

3.3 Pacemaker Channels in Cardiac Development

In the chick embryonic heart, pacemaker activity initiates from the sinus venosus (the prospective SAN) before the first contraction takes place [76–78]. In mice, the first cardiac contraction is visible around embryonic day 8.5 (ED8.5) when the heart is a linear tube; at this stage all cardiomyocytes, when isolated, are autorhythmic and express the I_f current [79]. Towards the end of gestation (ED18), the number of spontaneously active myocytes decreases to 33%. Interestingly this occurs in parallel with an 82% decrease of I_f current density and a concomitant large down-regulation of HCN1 and HCN4 mRNAs, by far the predominant HCN isoforms at early stages of development [79].

3.3.1 *f/HCN Channels During Embryonic Cardiac Development*

A detailed analysis of HCN4 localization during mouse cardiac development, by *in situ* hybridization, indicates that HCN4 mRNA is already expressed in the cardiac mesoderm at ED7.5 (in the cardiac crescent), and its expression remains confined to the sinus venosus [61]. Studies addressing the molecular development of mouse

SAN have elucidated the critical role of the transcription factors Tbx18, Shox2 and Tbx3. From ED9.5, Tbx18-expressing cells proliferate to form the future SAN, and expression of Shox2 and Tbx3 represses atrial differentiation of primary pacemaker myocardium, thus limiting down-regulation of HCN4. Co-expression of Shox2, Tbx3 and HCN4 specifically delineates the developing SAN [62, 80, 81]. Interestingly, constitutive deletion of the transcription factor Shox2, an intervention leading to embryonic death at mid-gestation (ED11.5–ED12.5), prevents the expression of both HCN4 and Tbx3 and causes formation of an underdeveloped SAN and significant bradycardia [80]. These data show that pacemaker activity, development of the SAN and expression of HCN4 are strictly related and, together with the evidence of embryonic lethality of HCN4 knockout mice, strongly support the essential role of HCN4 in the correct development of the SAN [82].

3.3.2 *f/HCN Channels in Embryonic Stem Cell Differentiation*

An alternative approach to study early events in cardiac development involves in vitro differentiation of embryonic stem cells (ESCs). ESCs can be differentiated into spontaneously contracting myocytes [83]. ESC-derived autorhythmic cardiomyocytes display SAN-like APs and express I_f [84–86]. Involvement of I_f in the generation and modulation of rate in this cellular system has been confirmed using specific I_f inhibitors (see below). 3 μ M ivabradine, for example, slowed beating rate by 25% and reduced I_f by about 50% [86]; these effects are quantitatively similar to those reported in SAN myocytes. ZD7288 (0.3 μ M) also slowed the beating rate by about 50% and reduced I_f by 15% [85]. Furthermore, the rate of spontaneously beating human ES-derived cardiomyocytes, which express a robust I_f current, is slowed by zatebradine, another I_f blocker [87, 88].

Several reports indicate that both murine and human ESC-derived cardiomyocytes express HCN channels (Fig. 3.3) [85, 86, 88–90]. Despite some variability in the isoform composition, likely arising from different ES clones and techniques employed, these reports indicate that I_f and the underlying HCN channels contribute significantly to cardiac cellular autorhythmicity.

3.4 f-Channels Blockers

Given the importance of I_f in generation of pacemaker activity, it is not surprising that f-channels have been considered as a main target in the search for drugs able to control heart rate specifically. The underlying reason is that a specific (and moderate) reduction of I_f will affect only the slope of DD and thus cardiac rate, without undesired effects on AP duration and/or inotropism associated with altered K⁺ and/or Ca²⁺ channel activities.

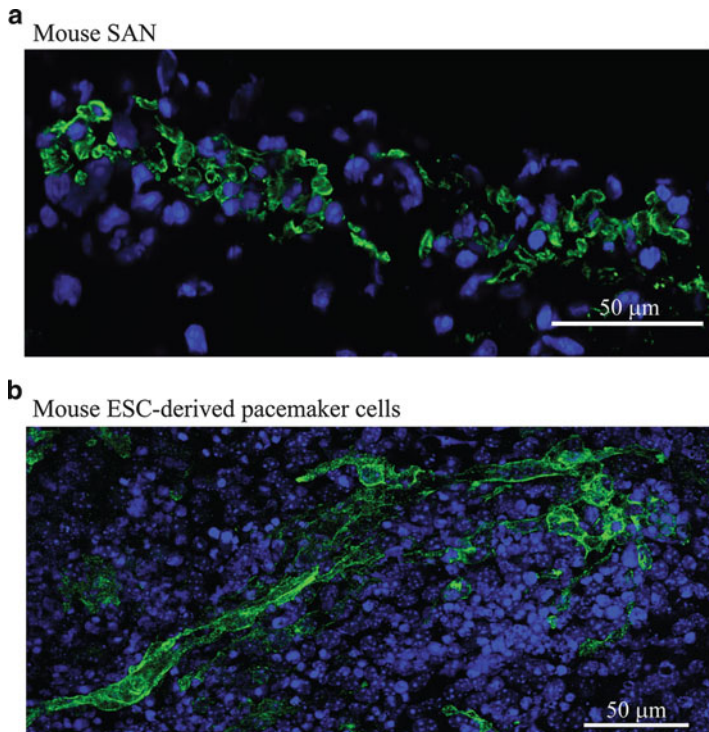


Fig. 3.3 Confocal images showing HCN4 expression (green) in the central part of the mouse SAN tissue (a) and in ESC-derived cardiac myocytes in culture (b); nuclei stained with DAPI (blue)

Drugs able to selectively reduce I_f have, therefore, been long regarded as important tools in the search for a novel therapeutic approach to ischemic heart disease (IHD), normally due to unbalanced myocyte oxygen demand and supply. Slowing of heart rate is beneficial under these conditions because it causes both a reduction in oxygen consumption and an increase in the duration of diastole and coronary perfusion. β -blockers, Ca^{2+} channel inhibitors and nitrates all reduce heart rate, but also cause side-effects such as reduced cardiac inotropism and are, therefore, not entirely satisfactory in terms of efficacy and tolerance.

Substances able to reduce specifically heart rate, initially termed “specific bradycardic” and later “pure heart rate reducing” agents, were developed since the late 1970s, starting with a clonidine derivative (alnididine, ST 567) [10]. This family includes falepamil (AQ-A39), zatebradine (UL-FS49), cilobradine (DK-AH26), ZD-7288, and ivabradine (S16257) [10, 34]. Investigation in Purkinje fibers and SAN revealed that these substances reduce the slope of DD and slow heart rate by blocking the I_f current [91, 92]. With the exception of ivabradine, clinical use of these drugs was hampered by the presence of side-effects at therapeutic concentrations (i.e., concentrations blocking I_f) caused by partial block of K^+ and/or Ca^{2+} channels, and by block of the neuronal I_h current (equivalent to the cardiac I_f).

Undesired visual effects were reported in patients treated with zatebradine due to block of I_h in photoreceptors [10].

Ivabradine is the only member of this family of compounds presently available on the market and is used for treatment of chronic stable *angina* in patients with a normal sinus rhythm and with contraindication or intolerance to treatment with β -blockers [93].

At low/moderate doses, ivabradine is a highly specific I_f inhibitor (Fig. 3.4). In rabbit SAN, 3 μM ivabradine decreased spontaneous firing by 24%, mainly by reducing DD slope (-67%) and with only a minor effect on AP duration (+9%) [94]. Studies in rabbit isolated SAN myocytes showed that ivabradine (3 μM) blocks I_f substantially (about 60%) without altering either T- and L-type Ca^{2+} currents, or delayed outward rectifying K^+ currents [95]. Additional studies showed that ivabradine acts from the cytoplasmic side [95] and that drug binding/unbinding to f-channels were constrained to open channel states [96]; also, the block has the unique feature of being determined by the direction of current flow (current dependence). According to this mechanism, drug molecules are “kicked-in” to their blocking site within the pore by the outward ion flow during depolarization, and “kicked off” by the inward ion flow during hyperpolarization [96]. The overall block properties determine use-dependence, implying that block is favored by frequent cycling between open and closed states [97].

The bradycardic action of ivabradine has been confirmed in both pre-clinical and clinical studies [34, 98, 99]. In healthy volunteers a single oral dose of ivabradine (20 mg) induced a decrease of heart rate by $18 \pm 6\%$ during physical exercise [100]. Trials in patient with stable *angina* showed that the anti-anginal effects of ivabradine are comparable to those of β -blockers but without side effects such as

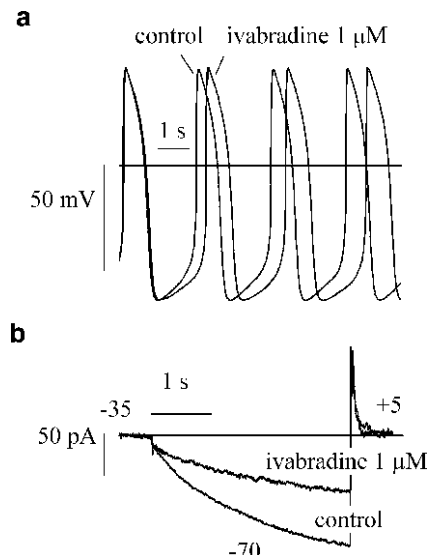


Fig. 3.4 Ivabradine slows heart rate by partial block of I_f . (a) Spontaneous activity recorded from a SAN cell before and during perfusion with ivabradine 1 μM . Note that slowing is due to a reduced steepness of the diastolic depolarization. (b) Inhibition by ivabradine 1 μM of I_f recorded from a SAN cell during steps to -70 mV

sexual disturbances, respiratory problems, and rebound phenomena; the only adverse events linked to ivabradine treatment were a limited reduction of blood pressure and mild, well-tolerated visual symptoms (phosphenes). The visual disturbances are due to the action of ivabradine on HCN channels in the retina [101, 102]. Ivabradine was eventually marketed at the end of 2005. A large clinical trial (BEAUTIFUL), ended in 2008, was promoted to investigate the efficacy of ivabradine in patients with coronary artery disease (CAD) and LV dysfunction. The trial outcome was that ivabradine improves coronary endpoints (i.e., hospitalization for myocardial infarction, revascularization) in CAD patients with heart rate ≥ 70 bpm [103, 104].

3.4.1 Effects of Heart Rate Reducing Agents on HCN Isoforms

Investigation of the molecular interactions between heart rate-reducing agents and HCN channels is in progress. Emerging data indicate that mislocalization and/or altered expression of HCN channels may be involved in cardiac and non-cardiac pathological conditions (arrhythmias, pain associated with nerve injury, epileptic seizure disorders and others) [105–107]. An important goal of these studies is to provide information useful to the development of HCN isoform-specific agents as innovative antiarrhythmic, analgesic and antiepileptic drugs.

Some of the knowledge gained so far in relation to different pure heart rate-reducing agents can be summarized as follows: cilobradine, ivabradine and zatebradine block HCN1, HCN2 and HCN4 isoforms expressed in HEK293 cells, with a similar IC_{50} (close to 1 μ M) and Hill slope factors close to 1; these values are similar to those reported for native f-channels in SAN [10]. Ivabradine blocks HCN4 and HCN1 differently; it is an open channel blocker of HCN4 channels, and a closed-channel blocker of HCN1 channels [97]. Residues important in ZD7288-block of two HCN isoforms have been identified. In one study, binding of ZD7288 to the mHCN1 isoform was shown to depend critically on residues Y355, M357, and V359 in the S6 domain [10]. In another study, residues A425 and I432 in the S6 domain of mHCN2 were found to be critical for ZD7288 and cilobradine binding [108].

3.5 Genetics of HCN Channels

In a large-scale screen for mutations that affect the development of heart in the embryo of zebrafish *Danio rerio*, a mutant (*slow-mo*) showed a substantially reduced heart rate compared to wild type animals [109]. The bradycardic phenotype was evident also in the isolated heart and patch clamp experiments showed that the only current greatly reduced (85%) was I_f . The *slow-mo* mutant was the first genetic model showing the importance of I_f for generation of cardiac pacemaker activity *in vivo*.

3.5.1 Transgenic Animal Models

In recent years, four HCN4 knockout mouse models have been developed to evaluate in vivo the functional contribution of this isoform to pacemaking [82, 110, 111]. Both global and cardiac-specific constitutive knockouts of the HCN4 gene cause premature death of mice at mid-gestation (ED9.5–ED11.5), a developmental stage when regular contractile activity normally develops [82]. SAN myocytes isolated from knockout embryos at day ED9.5 showed reduced spontaneous rate (-36.7%) and I_f current (-85%) compared to controls. The knockout process also led to the complete loss of cAMP-mediated β -adrenergic modulation, suggesting that the residual I_f current might be carried by the HCN1 and HCN3 isoforms which are almost insensitive to cAMP stimulation [42, 43, 49]. These data show that HCN4 expression is necessary for proper embryonic heart development, although they do not provide evidence for the role of the HCN4 current in the adult animal.

To avoid the limitations due to constitutive HCN4 knockout, inducible knockout animals were generated [110, 111]. In one model, ECGs recorded from freely moving knockout animals showed sinus pauses followed by normal rhythmic activity; β -modulation of rate was not lost, and any acceleration in heart rate led to a reduction of sinus pauses [110]. In another model, the induction of the HCN4 knockout was under the control of a regulatory region of the HCN4 gene. ECG recordings from these animals also showed sinus pauses (mean frequency 16.1 per minute) [111]. Since 90% of the global knockout-derived and 50% of the HCN4-targeted knockout-derived SAN myocytes were quiescent and the I_f current was reduced by about 75–80% [110, 111], further investigation will be required to understand the difference between the effects of knockout process on SAN automaticity in vivo and in vitro conditions.

3.5.2 Pathologies Associated with HCN Dysfunctions

To date, four different mutations in the coding sequence of the *hHcn4* gene, associated with alterations of cardiac rhythm in humans, have been identified [112–115]. One patient with idiopathic sinus node dysfunction (SND) characterized by severe bradycardia (41 bpm), intermittent atrial fibrillation and chronotropic incompetence, had a deletion of a single nucleotide in exon 5 of *hHcn4*. This alteration caused a sequence frameshift resulting in a premature stop codon and thus in a truncated protein (HCN4-573X) lacking the CNBD [112]. In vitro expression of the mutation led to altered channel kinetics and lack of sensitivity to cAMP [112]. In another study, a missense mutation (D553N) was identified in members of a family with a complex phenotype characterized by recurrent syncope, QT prolongation and polymorphic ventricular tachycardia. Heterologous expression experiments indicated that this mutation causes a dominant-negative trafficking defect of HCN4 channels, and concomitant reduction of I_f [113]. However, the complexity of the arrhythmic phenotype precluded a clear link between mutation and the phenotype.

A direct functional correlation between defective HCN4 and arrhythmia was reported in 2006 [114] from a study on a large Italian family spanning three generations. A point mutation (S672R) in a highly conserved residue of CNBD was found to be associated with inherited asymptomatic sinus bradycardia according to an autosomal dominant pattern. The heart rate of family members carrying the mutation was significantly slower (52.2 ± 1.4 bpm, $n = 15$) than that of wild-type members (73.2 ± 1.6 bpm, $n = 12$). Co-segregation of bradycardia with the *hHcn4* gene was strong, as shown by the high LOD score value (5.47). In vitro electrophysiological analysis of S672R channels showed a more negative activation curve (-4.9 mV shift) and faster deactivation kinetics than the wild-type. The effect of the S672R mutation, in heterozygosis, is therefore analogous to a mild vagal stimulation corresponding to a low concentration of acetylcholine (about 20 nM); this action leads to a reduced net inward current during DD and negative chronotropy [114].

Another missense mutation, leading to the substitution G480R in the pore region of HCN4, has also been identified in a family with asymptomatic sinus bradycardia [115]. In vitro experiments showed that G480R channels are activated at more negative voltages and their membrane density is reduced compared to wild-type.

These findings support the idea that mutated HCN4 channels can be responsible for rhythm disturbances of various degrees of severity.

3.6 Biological Pacemaker

Normal generation and propagation of heart rhythm can be affected by several cardiac diseases such as Sick Sinus Syndrome, AV block and severe bradycardia, requiring implantation of an electronic pacemaker. Therefore, there is an increasing interest in biological pacemakers, which consist of cellular substrates able to drive a quiescent tissue and to respond to autonomic modulation. The first attempts to induce autorhythmic activity in a quiescent substrate used viruses to over-express $\beta 2$ -adrenergic receptors or to inhibit inwardly rectifying K^+ currents [116]. HCN channels, however, are more suitable candidates for gene transfer technology because, (1) they are active only during, and thus contribute solely to, the diastolic phase of APs, and (2) they are responsive to autonomic regulation [11, 28].

3.6.1 HCN-Gene Strategies

“Proof of principle” evidence that HCN overexpression can induce spontaneous activity was provided by experiments showing that in vitro infection of primary cultures of neonatal rat myocytes with adenoviruses carrying the mouse HCN2

channel leads to a significant increase of their beating rate (83%) [65]. Further, in vivo over-expression of HCN2 in left atrium or in left bundle branch of dogs increased the I_f current density and generated stable, spontaneous activity following sinus arrest or AV block [116]. Similar strategies using HCN1 and HCN4 isoforms also successfully induced stable ectopic rhythm in an animal model [117]. To overcome the limitation of low rate at which these biological pacemakers drove the heart, either mutated HCN2 constructs, with more depolarized activation curve and faster kinetics, or HCN1–HCN2 chimeric constructs characterized by fast activation kinetics (provided by HCN1) and cAMP modulation (provided by HCN2) were used. In vivo experiments showed that the former construct improves catecholamine sensitivity but not basal heart rate, and the latter construct causes episodes of ventricular tachycardia interrupted by pauses of variable length [116].

In an alternative approach synthetic HCN channels obtained by mutating human Kv1.4 channels in four specific residues, were used. In vivo expression of the engineered channels in guinea pig ventricle generated an HCN-like inward current and an ectopic rhythm [116].

3.6.2 Stem Cell-Based Biological Pacemakers

Because of teratogenic risk, viral vectors, even if efficient, are unlikely to be the delivery system of choice for HCN channels. Cell-based biological pacemakers have therefore been considered with growing interest. Progress in this direction came from use of human adult mesenchymal stem cells (MSCs) over-expressing mouse HCN2 gene [118]. MSCs express endogenously gap junctions and when electrically coupled to ventricular myocytes their membrane hyperpolarizes, leading to large activation of the HCN2 channels and spontaneous rhythm generation in the surrounding tissue [118]. MSCs engineered with HCN4 channels were also effective in pacing a ventricular substrate [119]. A different approach was based on HCN1-expressing fibroblasts induced to fuse (by PolyEthylene Glycol) with guinea pig ventricular myocytes. The heterokaryons displayed spontaneous APs with a slow depolarization phase and expressed I_f -like pacemaker current sensitive to the I_f blocker ZD7288. Surprisingly, heterokaryons were responsive to β -adrenergic but not to cholinergic agonists [116].

Embryonic stem cells (ESCs), known to differentiate into spontaneously beating SAN-like cells expressing I_f [84–86, 88, 90] have also been used to develop a cell-based biological pacemaker. Two separate studies have demonstrated that spontaneously beating ESC-derived myocytes can pace cultures of neonatal rat cardiac myocytes and generate an ectopic rhythm when injected in the ventricle of animal models after AV ablation [87, 120]. Although the presence of f/HCN channels was not directly addressed in these studies, their involvement in the generation of the rhythmic was apparent, based on evidence for rate increase by β -adrenergic activation and rate decrease by f-channel blocker ZD7288 [87, 120].

3.7 Conclusions

Although the biophysical properties of the “funny” current fit well with an important role in pacemaking, the idea of this bizarre but essentially simple mechanism having a relevant part in the governance of cardiac rhythm took time to be accepted and is still hotly debated [3, 121–123]. In the late 1990s, after the cloning of the HCN genes, strong evidence in favor of f/HCN channels as key players in the pacemaking process was gathered. Analysis of HCN isoform distribution highlighted the selective expression of HCN4 channels in SAN and the conduction system of various species including humans. Embryological studies of mice showing an early onset of HCN4 expression specifically in the prospective SAN and conduction system, together with the evidence that transgenic mice lacking HCN4 gene die early during embryogenesis strengthened the functional role of f-channels in the generation of cardiac pacemaker activity. Finally, the development of f-channel blockers for the therapeutic control of heart rate in humans, and the discovery of HCN4 mutations in patients affected by rhythm disturbances, has further established the importance of f-channels in pacemaking.

References

1. Silverman ME, Grove D, Upshaw Jr CB. Why does the heart beat? The discovery of the electrical system of the heart. *Circulation*. 2006;113(23):2775–81.
2. Keith A, Flack M. The form and nature of the muscular connections between the primary divisions of the vertebrate heart. *J Anat Physiol*. 1907;41(Pt 3):172–89.
3. Lakatta EG, DiFrancesco D. What keeps us ticking: A funny current, a calcium clock, or both? *J Mol Cell Cardiol*. 2009;47(2):157–70.
4. Brown HF, DiFrancesco D, Noble SJ. How does adrenaline accelerate the heart? *Nature*. 1979;280(5719):235–6.
5. DiFrancesco D. A new interpretation of the pace-maker current in calf Purkinje fibres. *J Physiol*. 1981;314:359–76.
6. DiFrancesco D. A study of the ionic nature of the pace-maker current in calf Purkinje fibres. *J Physiol*. 1981;314:377–93.
7. Frace AM, Maruoka F, Noma A. External K⁺ increases Na⁺ conductance of the hyperpolarization-activated current in rabbit cardiac pacemaker cells. *Pflugers Arch*. 1992;421(2–3):97–9.
8. Wollmuth LP, Hille B. Ionic selectivity of Ih channels of rod photoreceptors in tiger salamanders. *J Gen Physiol*. 1992;100(5):749–65.
9. DiFrancesco D. Dual allosteric modulation of pacemaker (f) channels by cAMP and voltage in rabbit SA node. *J Physiol*. 1999;2:367–76.
10. Baruscotti M, Bucchi A, DiFrancesco D. Physiology and pharmacology of the cardiac pacemaker (“funny”) current. *Pharmacol Ther*. 2005;107(1):59–79.
11. DiFrancesco D, Ferroni A, Mazzanti M, Tromba C. Properties of the hyperpolarizing-activated current (i_f) in cells isolated from the rabbit sino-atrial node. *J Physiol*. 1986;377:61–88.
12. DiFrancesco D. The contribution of the ‘pacemaker’ current (i_f) to generation of spontaneous activity in rabbit sino-atrial node myocytes. *J Physiol*. 1991;434:23–40.

13. Arinsburg SS, Cohen IS, Yu HG. Constitutively active Src tyrosine kinase changes gating of HCN4 channels through direct binding to the channel proteins. *J Cardiovasc Pharmacol.* 2006;47(4):578–86.
14. Li CH, Zhang Q, Teng B, Mustafa SJ, Huang JY, Yu HG. Src tyrosine kinase alters gating of hyperpolarization-activated HCN4 pacemaker channel through Tyr531. *Am J Physiol Cell Physiol.* 2008;294(1):C355–62.
15. Qu J, Kryukova Y, Potapova IA, Doronin SV, Larsen M, Krishnamurthy G, et al. MiRP1 modulates HCN2 channel expression and gating in cardiac myocytes. *J Biol Chem.* 2004;279(42):43497–502.
16. Decher N, Bundis F, Vajna R, Steinmeyer K. KCNE2 modulates current amplitudes and activation kinetics of HCN4: influence of KCNE family members on HCN4 currents. *Pflugers Arch.* 2003;446(6):633–40.
17. Brandt MC, Endres-Becker J, Zagidullin N, Motloch LJ, Er F, Rottlaender D, et al. Effects of KCNE2 on HCN isoforms: distinct modulation of membrane expression and single channel properties. *Am J Physiol Heart Circ Physiol.* 2009;297(1):H355–63.
18. Michels G, Er F, Khan IF, Endres-Becker J, Brandt MC, Gassanov N, et al. K^+ channel regulator KCR1 suppresses heart rhythm by modulating the pacemaker current If. *PLoS One.* 2008;3(1):e1511.
19. Peters CJ, Chow SS, Angoli D, Nazzari H, Cayabyab FS, Morshedian A, et al. In situ co-distribution and functional interactions of SAP97 with sinoatrial isoforms of HCN channels. *J Mol Cell Cardiol.* 2009;46(5):636–43.
20. Barbuti A, Gravante B, Riolfo M, Milanesi R, Terragni B, DiFrancesco D. Localization of pacemaker channels in lipid rafts regulates channel kinetics. *Circ Res.* 2004;94(10):1325–31.
21. Barbuti A, Terragni B, Brioschi C, DiFrancesco D. Localization of f-channels to caveolae mediates specific beta2-adrenergic receptor modulation of rate in sinoatrial myocytes. *J Mol Cell Cardiol.* 2007;42(1):71–8.
22. DiFrancesco D. Cardiac pacemaker: 15 years of “new” interpretation. *Acta Cardiol.* 1995;50(6):413–27.
23. Munk AA, Adjemian RA, Zhao J, Ogbaghebriel A, Shrier A. Electrophysiological properties of morphologically distinct cells isolated from the rabbit atrioventricular node. *J Physiol.* 1996;493(3):801–18.
24. Yuill KH, Hancox JC. Characteristics of single cells isolated from the atrioventricular node of the adult guinea-pig heart. *Pflugers Arch.* 2002;445(3):311–20.
25. Cerbai E, Barbieri M, Mugelli A. Characterization of the hyperpolarization-activated current, I(f), in ventricular myocytes isolated from hypertensive rats. *J Physiol.* 1994;481(3):585–91.
26. Yu H, Chang F, Cohen IS. Phosphatase inhibition by calyculin A increases i(f) in canine Purkinje fibers and myocytes. *Pflugers Arch.* 1993;422(6):614–6.
27. Cerbai E, Barbieri M, Mugelli A. Occurrence and properties of the hyperpolarization-activated current If in ventricular myocytes from normotensive and hypertensive rats during aging. *Circulation.* 1996;94(7):1674–81.
28. DiFrancesco D, Tortora P. Direct activation of cardiac pacemaker channels by intracellular cyclic AMP. *Nature.* 1991;351:145–7.
29. Barbuti A, Baruscotti M, DiFrancesco D. The pacemaker current: from basics to the clinics. *J Cardiovasc Electrophysiol.* 2007;18(3):342–7.
30. Rodefeld MD, Beau SL, Schuessler RB, Boineau JP, Saffitz JE. Beta-adrenergic and muscarinic cholinergic receptor densities in the human sinoatrial node: identification of a high beta 2-adrenergic receptor density. *J Cardiovasc Electrophysiol.* 1996;7(11):1039–49.
31. Santoro B, Grant SG, Bartsch D, Kandel ER. Interactive cloning with the SH3 domain of N-src identifies a new brain specific ion channel protein, with homology to eag and cyclic nucleotide-gated channels. *Proc Natl Acad Sci USA.* 1997;94(26):14815–20.

32. Jackson HA, Marshall CR, Accili EA. Evolution and structural diversification of hyperpolarization-activated cyclic nucleotide-gated channel genes. *Physiol Genomics*. 2007;29(3):231–45.
33. Biel M, Wahl-Schott C, Michalakis S, Zong X. Hyperpolarization-activated cation channels: from genes to function. *Physiol Rev*. 2009;89(3):847–85.
34. Baruscotti M, Barbuti A, Bucchi A. The cardiac pacemaker current. *J Mol Cell Cardiol*. 2010;48(1):55–64.
35. Giorgetti A, Carloni P, Mistrik P, Torre VA. Homology model of the pore region of HCN channels. *Biophys J*. 2005;89(2):932–44.
36. Proenza C, Tran N, Angoli D, Zahynacz K, Balcar P, Accili EA. Different roles for the cyclic nucleotide binding domain and amino terminus in assembly and expression of hyperpolarization-activated, cyclic nucleotide-gated channels. *J Biol Chem*. 2002;277(33):29634–42.
37. Tran N, Proenza C, Macri V, Petigara F, Sloan E, Samler S, et al. A conserved domain in the NH₂ terminus important for assembly and functional expression of pacemaker channels. *J Biol Chem*. 2002;277(46):43588–92.
38. Zagotta WN, Olivier NB, Black KD, Young EC, Olson R, Gouaux E. Structural basis for modulation and agonist specificity of HCN pacemaker channels. *Nature*. 2003;425(6954):200–5.
39. Wainger BJ, DeGennaro M, Santoro B, Siegelbaum SA, Tibbs GR. Molecular mechanism of cAMP modulation of HCN pacemaker channels. *Nature*. 2001;411(6839):805–10.
40. Craven KB, Zagotta WN. Salt bridges and gating in the COOH-terminal region of HCN2 and CNGA1 channels. *J Gen Physiol*. 2004;124(6):663–77.
41. Accili EA, Proenza C, Baruscotti M, DiFrancesco D. From funny current to HCN channels: 20 years of excitation. *News Physiol Sci*. 2002;17:32–7.
42. Stieber J, Stockl G, Herrmann S, Hassfurth B, Hofmann F. Functional expression of the human HCN3 channel. *J Biol Chem*. 2005;280(41):34635–43.
43. Mistrik P, Mader R, Michalakis S, Weidinger M, Pfeifer A, Biel M. The murine HCN3 gene encodes a hyperpolarization-activated cation channel with slow kinetics and unique response to cyclic nucleotides. *J Biol Chem*. 2005;280(29):27056–61.
44. Qu J, Altomare C, Bucchi A, DiFrancesco D, Robinson RB. Functional comparison of HCN isoforms expressed in ventricular and HEK 293 cells. *Pflugers Arch*. 2002;444(5):597–601.
45. Chandler NJ, Greener ID, Tellez JO, Inada S, Musa H, Molenaar P, et al. Molecular architecture of the human sinus node: insights into the function of the cardiac pacemaker. *Circulation*. 2009;119(12):1562–75.
46. Thollon C, Bedut S, Villeneuve N, Coge F, Piffard L, Guillaumin JP, et al. Use-dependent inhibition of hHCN4 by ivabradine and relationship with reduction in pacemaker activity. *Br J Pharmacol*. 2007;150(1):37–46.
47. Zicha S, Fernandez-Velasco M, Lonardo G, L’Heureux N, Nattel S. Sinus node dysfunction and hyperpolarization-activated (HCN) channel subunit remodeling in a canine heart failure model. *Cardiovasc Res*. 2005;66(3):472–81.
48. Shi W, Wymore R, Yu H, Wu J, Wymore RT, Pan Z, et al. Distribution and prevalence of hyperpolarization-activated cation channel (HCN) mRNA expression in cardiac tissues. *Circ Res*. 1999;85(1):e1–6.
49. Moroni A, Gorza L, Beltrame M, Gravante B, Vaccari T, Bianchi ME, et al. Hyperpolarization-activated cyclic nucleotide-gated channel 1 is a molecular determinant of the cardiac pacemaker current I(f). *J Biol Chem*. 2001;276(31):29233–41.
50. Marionneau C, Couette B, Liu J, Li H, Mangoni ME, Nargeot J, et al. Specific pattern of ionic channel gene expression associated with pacemaker activity in the mouse heart. *J Physiol*. 2005;562(Pt 1):223–34.
51. Moosmang S, Stieber J, Zong X, Biel M, Hofmann F, Ludwig A. Cellular expression and functional characterization of four hyperpolarization-activated pacemaker channels in cardiac and neuronal tissues. *Eur J Biochem*. 2001;268(6):1646–52.

52. Huang X, Yang P, Du Y, Zhang J, Ma A. Age-related down-regulation of HCN channels in rat sinoatrial node. *Basic Res Cardiol.* 2007;102(5):429–35.
53. Brioschi C, Micheloni S, Tellez JO, Pisoni G, Longhi R, Moroni P, et al. Distribution of the pacemaker HCN4 channel mRNA and protein in the rabbit sinoatrial node. *J Mol Cell Cardiol.* 2009;47(2):221–7.
54. Liu J, Dobrzynski H, Yanni J, Boyett MR, Lei M. Organisation of the mouse sinoatrial node: structure and expression of HCN channels. *Cardiovasc Res.* 2007;73(4):729–38.
55. Yamamoto M, Dobrzynski H, Tellez J, Niwa R, Billeter R, Honjo H, et al. Extended atrial conduction system characterised by the expression of the HCN4 channel and connexin45. *Cardiovasc Res.* 2006;72(2):271–81.
56. Gaborit N, Le Bouter S, Szuts V, Varro A, Escande D, Nattel S, et al. Regional and tissue specific transcript signatures of ion channel genes in the non-diseased human heart. *J Physiol.* 2007;582(2):675–93.
57. Stillitano F, Lonardo G, Zicha S, Varro A, Cerbai E, Mugelli A, et al. Molecular basis of funny current (If) in normal and failing human heart. *J Mol Cell Cardiol.* 2008;45(2):289–99.
58. Dobrzynski H, Nikolski VP, Sambelashvili AT, Greener ID, Yamamoto M, Boyett MR, et al. Site of origin and molecular substrate of atrioventricular junctional rhythm in the rabbit heart. *Circ Res.* 2003;93(11):1102–10.
59. Han W, Bao W, Wang Z, Nattel S. Comparison of ion-channel subunit expression in canine cardiac Purkinje fibers and ventricular muscle. *Circ Res.* 2002;91(9):790–7.
60. Fernandez-Velasco M, Goren N, Benito G, Blanco-Rivero J, Bosca L, Delgado C. Regional distribution of hyperpolarization-activated current (If) and hyperpolarization-activated cyclic nucleotide-gated channel mRNA expression in ventricular cells from control and hypertrophied rat hearts. *J Physiol.* 2003;553(2):395–405.
61. Garcia-Frigola C, Shi Y, Evans SM. Expression of the hyperpolarization-activated cyclic nucleotide-gated cation channel HCN4 during mouse heart development. *Gene Expr Patterns.* 2003;3(6):777–83.
62. Mommersteeg MT, Hoogaars WM, Prall OW, Gier-de Vries C, Wiese C, Clout DE, et al. Molecular pathway for the localized formation of the sinoatrial node. *Circ Res.* 2007;100(3):354–62.
63. Ishii TM, Takano M, Ohmori H. Determinants of activation kinetics in mammalian hyperpolarization-activated cation channels. *J Physiol.* 2001;537(1):93–100.
64. Xue T, Marban E, Li RA. Dominant-negative suppression of HCN1- and HCN2-encoded pacemaker currents by an engineered HCN1 construct: insights into structure-function relationships and multimerization. *Cir Res.* 2002;90(12):1267–73.
65. Qu J, Barbuti A, Protas L, Santoro B, Cohen IS, Robinson RB. HCN2 overexpression in newborn and adult ventricular myocytes: distinct effects on gating and excitability. *Circ Res.* 2001;89(1):E8–14.
66. Robinson RB, Yu H, Chang F, Cohen IS. Developmental change in the voltage-dependence of the pacemaker current, if, in rat ventricle cells. *Pflugers Arch.* 1997;433(4):533–5.
67. Zong X, Eckert C, Yuan H, Wahl-Schott C, Abicht H, Fang L, et al. A novel mechanism of modulation of hyperpolarization-activated cyclic nucleotide-gated channels by Src kinase. *J Biol Chem.* 2005;280(40):34224–32.
68. Pian P, Bucchi A, Decostanzo A, Robinson RB, Siegelbaum SA. Modulation of cyclic nucleotide-regulated HCN channels by PIP(2) and receptors coupled to phospholipase C. *Pflugers Arch.* 2007;455(1):125–45.
69. Pian P, Bucchi A, Robinson RB, Siegelbaum SA. Regulation of gating and rundown of HCN hyperpolarization-activated channels by exogenous and endogenous PIP2. *J Gen Physiol.* 2006;128(5):593–604.
70. Yu H, Wu J, Potapova I, Wymore RT, Holmes B, Zuckerman J, et al. MinK-related peptide 1: A beta subunit for the HCN ion channel subunit family enhances expression and speeds activation. *Circ Res.* 2001;88(12):E84–7.

71. Ye B, Balijepalli RC, Foell JD, Kroboth S, Ye Q, Luo YH, et al. Caveolin-3 associates with and affects the function of hyperpolarization-activated cyclic nucleotide-gated channel 4. *Biochemistry*. 2008;47(47):12312–8.
72. Simons K, Toomre D. Lipid rafts and signal transduction. *Nat Rev Mol Cell Biol*. 2000;1(1): 31–9.
73. Masson-Pevet M, Gros D, Besselsen E. The caveolae in rabbit sinus node and atrium. *Cell Tissue Res*. 1980;208(2):183–96.
74. Folco EJ, Liu GX, Koren G. Caveolin-3 and SAP97 form a scaffolding protein complex that regulates the voltage-gated potassium channel Kv1.5. *Am J Physiol Heart Circ Physiol*. 2004;287(2):H681–90.
75. Balijepalli RC, Delisle BP, Balijepalli SY, Foell JD, Slind JK, Kamp TJ, et al. Kv11.1 (ERG1) K⁺ channels localize in cholesterol and sphingolipid enriched membranes and are modulated by membrane cholesterol. *Channels*. 2007;1(4):263–72.
76. DeHaan RL. Development of pacemaker tissue in the embryonic heart. *Ann N Y Acad Sci*. 1965;127(1):7–18.
77. Van Mierop LH. Location of pacemaker in chick embryo heart at the time of initiation of heartbeat. *Am J Physiol*. 1967;212(2):407–15.
78. Pennisi DJ, Rentschler S, Gourdie RG, Fishman GI, Mikawa T. Induction and patterning of the cardiac conduction system. *Int J Dev Biol*. 2002;46(6):765–75.
79. Yasui K, Liu W, Ophof T, Kada K, Lee JK, Kamiya K, et al. If(f) current and spontaneous activity in mouse embryonic ventricular myocytes. *Circ Res*. 2001;88(5):536–42.
80. Espinoza-Lewis RA, Yu L, He F, Liu H, Tang R, Shi J, et al. Shox2 is essential for the differentiation of cardiac pacemaker cells by repressing Nkx2-5. *Dev Biol*. 2009;327(2): 376–85.
81. Wiese C, Grieskamp T, Airik R, Mommersteeg MT, Gardiwal A, Gier-de Vries C, et al. Formation of the sinus node head and differentiation of sinus node myocardium are independently regulated by Tbx18 and Tbx3. *Circ Res*. 2009;104(3):388–97.
82. Stieber J, Herrmann S, Feil S, Loster J, Feil R, Biel M, et al. The hyperpolarization-activated channel HCN4 is required for the generation of pacemaker action potentials in the embryonic heart. *Proc Natl Acad Sci USA*. 2003;100(25):15235–40.
83. Hescheler J, Fleischmann BK, Lentini S, Maltsev VA, Rohwedel J, Wobus AM, et al. Embryonic stem cells: a model to study structural and functional properties in cardiomyogenesis. *Cardiovasc Res*. 1997;36(2):149–62.
84. Abi-Gerges N, Ji GJ, Lu ZJ, Fischmeister R, Hescheler J, Fleischmann BK. Functional expression and regulation of the hyperpolarization activated non-selective cation current in embryonic stem cell-derived cardiomyocytes. *J Physiol*. 2000;523(2):377–89.
85. Qu Y, Whitaker GM, Hove-Madsen L, Tibbets GF, Accili EA. Hyperpolarization-activated cyclic nucleotide-modulated ‘HCN’ channels confer regular and faster rhythmicity to beating mouse embryonic stem cells. *J Physiol*. 2008;586(3):701–16.
86. Barbuti A, Crespi A, Capilupo D, Mazzocchi N, Baruscotti M, DiFrancesco D. Molecular composition and functional properties of f-channels in murine embryonic stem cell-derived pacemaker cells. *J Mol Cell Cardiol*. 2009;46(3):343–51.
87. Kehat I, Khimovich L, Caspi O, Gepstein A, Shofti R, Arbel G, et al. Electromechanical integration of cardiomyocytes derived from human embryonic stem cells. *Nat Biotechnol*. 2004;22(10):1282–9.
88. Sartiani L, Bettoli E, Stillitano F, Mugelli A, Cerbai E, Jaconi ME. Developmental changes in cardiomyocytes differentiated from human embryonic stem cells: a molecular and electrophysiological approach. *Stem Cells*. 2007;25(5):1136–44.
89. van Kempen M, van Ginneken A, de Grijis I, Mutsaers N, Ophof T, Jongsma H, et al. Expression of the electrophysiological system during murine embryonic stem cell cardiac differentiation. *Cell Physiol Biochem*. 2003;13(5):263–70.

90. Yanagi K, Takano M, Narasaki G, Uosaki H, Hoshino T, Ishii T, et al. Hyperpolarization-activated cyclic nucleotide-gated channels and T-type calcium channels confer automaticity of embryonic stem cell-derived cardiomyocytes. *Stem Cells*. 2007;25(11):2712–9.
91. Van Bogaert PP, Goethals M. Pharmacological influence of specific bradycardic agents on the pacemaker current of sheep cardiac Purkinje fibres. A comparison between three different molecules. *Eur Heart J*. 1987;8(Suppl L):35–42.
92. DiFrancesco D. Some properties of the UL-FS 49 block of the hyperpolarization-activated current ($I(f)$) in sino-atrial node myocytes. *Pflugers Arch*. 1994;427(1–2):64–70.
93. DiFrancesco D, Camm JA. Heart rate lowering by specific and selective $I(f)$ current inhibition with ivabradine: a new therapeutic perspective in cardiovascular disease. *Drugs*. 2004;64(16):1757–65.
94. Thollon C, Cambarat C, Vian J, Prost JF, Peglion JL, Vilaine JP. Electrophysiological effects of S 16257, a novel sino-atrial node modulator, on rabbit and guinea-pig cardiac preparations: comparison with UL-FS 49. *Br J Pharmacol*. 1994;112(1):37–42.
95. Bois P, Bescond J, Renaudon B, Lefrant J. Mode of action of bradycardic agent, S 16257, on ionic currents of rabbit sinoatrial node cells. *Br J Pharmacol*. 1996;118(4):1051–7.
96. Bucchi A, Baruscotti M, DiFrancesco D. Current-dependent block of rabbit sino-atrial node $I(f)$ channels by ivabradine. *J Gen Physiol*. 2002;120(1):1–13.
97. Bucchi A, Tognati A, Milanesi R, Baruscotti M, DiFrancesco D. Properties of ivabradine-induced block of HCN1 and HCN4 pacemaker channels. *J Physiol*. 2006;572(2):335–46.
98. Borer JS, Heuzey JY. Characterization of the heart rate-lowering action of ivabradine, a selective $I(f)$ current inhibitor. *Am J Ther*. 2008;15(5):461–73.
99. Lopez-Bescos L, Filipova S, Martos R. Long-term safety and efficacy of ivabradine in patients with chronic stable angina. *Cardiology*. 2007;108(4):387–96.
100. Ragueneau I, Laveille C, Jochemsen R, Resplandy G, Funck-Brentano C, Jaillon P. Pharmacokinetic-pharmacodynamic modeling of the effects of ivabradine, a direct sinus node inhibitor, on heart rate in healthy volunteers. *Clin Pharmacol Ther*. 1998;64(2):192–203.
101. Cervetto L, Demontis GC, Gargini C. Cellular mechanisms underlying the pharmacological induction of phosphenes. *Br J Pharmacol*. 2007;150(4):383–90.
102. Demontis GC, Gargini C, Paoli TG, Cervetto L. Selective $Hcn1$ channels inhibition by ivabradine in mouse rod photoreceptors. *Invest Ophthalmol Vis Sci*. 2009;50(4):1948–55.
103. Fox K, Ford I, Steg PG, Tendera M, Robertson M, Ferrari R. Heart rate as a prognostic risk factor in patients with coronary artery disease and left-ventricular systolic dysfunction (BEAUTIFUL): a subgroup analysis of a randomised controlled trial. *Lancet*. 2008;372(9641):817–21.
104. Fox K, Ford I, Steg PG, Tendera M, Ferrari R. Ivabradine for patients with stable coronary artery disease and left-ventricular systolic dysfunction (BEAUTIFUL): a randomised, double-blind, placebo-controlled trial. *Lancet*. 2008;372(9641):807–16.
105. Cerbai E, Mugelli A. $I(f)$ in non-pacemaker cells: role and pharmacological implications. *Pharmacol Res*. 2006;53(5):416–23.
106. Jiang YQ, Sun Q, Tu HY, Wan Y. Characteristics of HCN channels and their participation in neuropathic pain. *Neurochem Res*. 2008;33(10):1979–89.
107. Reid CA, Berkovic SF, Petrou S. Mechanisms of human inherited epilepsies. *Prog Neurobiol*. 2009;87(1):41–57.
108. Cheng Y, George I, Yi GH, Reiken S, Gu A, Tao YK, et al. Bradycardic therapy improves left ventricular function and remodeling in dogs with coronary embolization-induced chronic heart failure. *J Pharmacol Exp Ther*. 2007;321(2):469–76.
109. Baker K, Warren KS, Yellen G, Fishman MC. Defective “pacemaker” current (I_h) in a zebrafish mutant with a slow heart rate. *Proc Natl Acad Sci USA*. 1997;94(9):4554–9.
110. Herrmann S, Stieber J, Stockl G, Hofmann F, Ludwig A. HCN4 provides a ‘depolarization reserve’ and is not required for heart rate acceleration in mice. *EMBO J*. 2007;26(21):4423–32.

111. Hoesl E, Stieber J, Herrmann S, Feil S, Tybl E, Hofmann F, et al. Tamoxifen-inducible gene deletion in the cardiac conduction system. *J Mol Cell Cardiol.* 2008;45(1):62–9.
112. Schulze-Bahr E, Neu A, Friederich P, Kaupp UB, Breithardt G, Pongs O, et al. Pacemaker channel dysfunction in a patient with sinus node disease. *J Clin Invest.* 2003;111(10):1537–45.
113. Ueda K, Nakamura K, Hayashi T, Inagaki N, Takahashi M, Arimura T, et al. Functional characterization of a trafficking-defective HCN4 mutation, D553N, associated with cardiac arrhythmia. *J Biol Chem.* 2004;279(26):27194–8.
114. Milanesi R, Baruscotti M, Gnechi-Ruscone T, DiFrancesco D. Familial sinus bradycardia associated with a mutation in the cardiac pacemaker channel. *N Engl J Med.* 2006;354(2):151–7.
115. Nof E, Luria D, Brass D, Marek D, Lahat H, Reznik-Wolf H, et al. Point mutation in the HCN4 cardiac ion channel pore affecting synthesis, trafficking, and functional expression is associated with familial asymptomatic sinus bradycardia. *Circulation.* 2007;116(5):463–70.
116. Rosen MR, Brink PR, Cohen IS, Robinson RB. Cardiac pacing: from biological to electronic ... to biological? *Circ Arrhythm Electrophysiol.* 2008;1(1):54–61.
117. Cai J, Yi FF, Li YH, Yang XC, Song J, Jiang XJ, et al. Adenoviral gene transfer of HCN4 creates a genetic pacemaker in pigs with complete atrioventricular block. *Life Sci.* 2007;80(19):1746–53.
118. Rosen MR, Brink PR, Cohen IS, Robinson RB. The utility of mesenchymal stem cells as biological pacemakers. *Congest Heart Fail.* 2008;14(3):153–6.
119. Yang XJ, Zhou YF, Li HX, Han LH, Jiang WP. Mesenchymal stem cells as a gene delivery system to create biological pacemaker cells in vitro. *J Int Med Res.* 2008;36(5):1049–55.
120. Xue T, Cho HC, Akar FG, Tsang SY, Jones SP, Marban E, et al. Functional integration of electrically active cardiac derivatives from genetically engineered human embryonic stem cells with quiescent recipient ventricular cardiomyocytes: insights into the development of cell-based pacemakers. *Circulation.* 2005;111(1):11–20.
121. DiFrancesco D. Considerations on the size of currents required for pacemaking. *J Mol Cell Cardiol.* 2010;48(4):802–803.
122. Maltsev VA, Lakatta EG. Funny current provides a relatively modest contribution to spontaneous beating rate regulation of human and rabbit sinoatrial node cells. *J Mol Cell Cardiol.* 2010;48(4):804–6.
123. Verkerk AO, Wilders R. Relative importance of funny current in human versus rabbit sinoatrial node. *J Mol Cell Cardiol.* 2010;48(4):799–801.

Chapter 4

Novel Perspectives on Cardiac Pacemaker Regulation: Role of the Coupled Function of Sarcolemmal and Intracellular Proteins

Victor A. Maltsev, Tatiana M. Vinogradova, and Edward G. Lakatta

4.1 Introduction

Recent experimental and theoretical studies demonstrate that sinoatrial node cells (SANCs) operate as a system of dynamically coupled molecules residing both in the surface membrane and within the pacemaker cell (Fig. 4.1). The system is comprised of several levels of complexity and integration of its components. The sarcolemmal (SL) ion currents (Fig. 4.1, blue) have been extensively studied in the past [29]; and the ensemble of these currents recreated in silico from the voltage-clamp data can generate spontaneous action potentials (APs) in at least 12 SANC models [50]. Thus, the subsystem of SL molecules forms a membrane clock (M clock) [27]. However, during spontaneous SANC beating M clock is dynamically coupled to Ca^{2+} cycling (Fig. 4.1, gray area) [17, 23]. SANC SR, however, can generate its own spontaneous rhythmic signals, local (submembrane) Ca^{2+} releases, in isolation from M clock in chemically skinned cells [45, 49], under voltage-clamp [45, 49], and also in silico [25]. Thus, similar to M clock, the SR subsystem is also envisioned as an oscillator or a clock, i.e., Ca^{2+} clock [27]. During spontaneous SANC beating, the M clock and Ca^{2+} clock do not exist as separate entities: they not only mutually entrain each other but this entrainment substantially changes the properties of each clock forming a robust pacemaker system [25]. This chapter reviews perspectives on pacemaker clock system of SANCs gleaned from recent experimentation and novel numerical modeling that embraces complex, dynamic, and functional integration of SL and intracellular proteins.

V.A. Maltsev (✉), T.M. Vinogradova, and E.G. Lakatta

Laboratory of Cardiovascular Science, NIA Intramural Research Program, NIH, 5600 Nathan Shock Drive, Baltimore, MA 21224, USA

e-mail: MaltsevVi@grc.nia.nih.gov

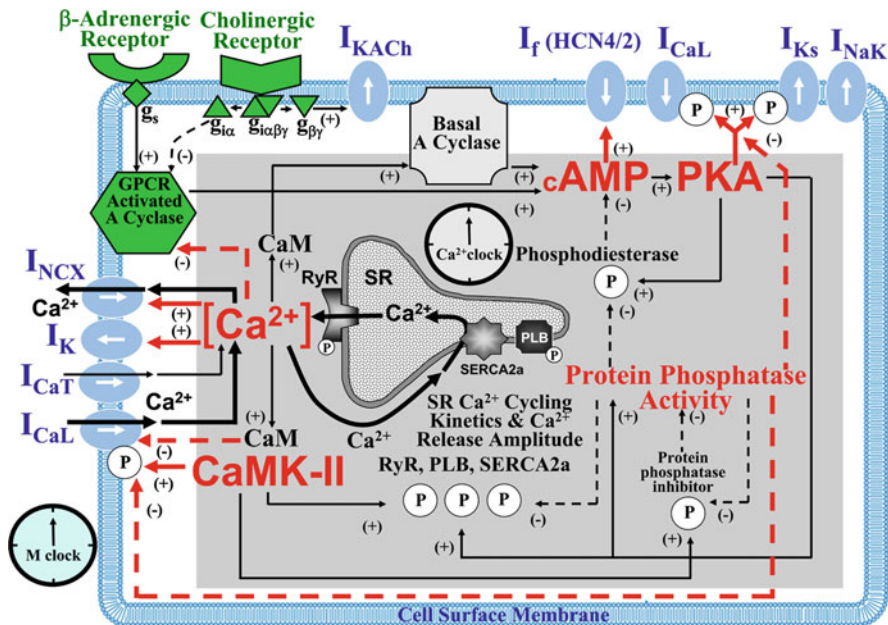


Fig. 4.1 Schematic illustration of complex interactions of molecules comprising the SANC pacemaker system. See text for details. Modified from [16]

4.2 Interactions and Entrainment of SL Electrogenic Function and $[Ca^{2+}]_i$ Cycling During the SANC Spontaneous Cycle

Spontaneous diastolic depolarization (DD) is the essence of cardiac pacemaker cell automaticity because it controls the time between consecutive APs. Since, by definition, DD is an electrical event, it was initially thought to be autonomously controlled by SL ion channels [33]. Subsequent studies, however, showed that functions of ion channels and electrogenic ion transporters are strongly and dynamically modulated by intracellular processes that involve Ca^{2+} , cAMP, and protein phosphorylation (reviews [17, 23, 44]). Thus, subcellular events, via modulation of the characteristics of SL electrogenic molecules, can influence DD as much as the ion channels themselves.

4.2.1 Interactions During Late Diastolic Depolarization

SANCs exhibit strong SERCA2 and RyR immunolabeling [21, 35] (but see also [32]). Confocal imaging of Ca^{2+} in SANCs and atrial subsidiary pacemaker cells, combined with noninvasive perforated patch-clamp recording [3, 10] and imaging

of toad sinus venosus cells [14], have discovered a crucial function of these expressed Ca^{2+} cycling proteins: the generation of subsarcolemmal Local Ca^{2+} Releases (LCRs) via RyRs during the late DD following dissipation of the global systolic Ca^{2+} transient brought about by the prior AP (Fig. 4.2a). LCRs in the form of 4–10 μm Ca^{2+} wavelets (Fig. 4.2a), or the integral of LCRs (Fig. 4.2b), i.e., late

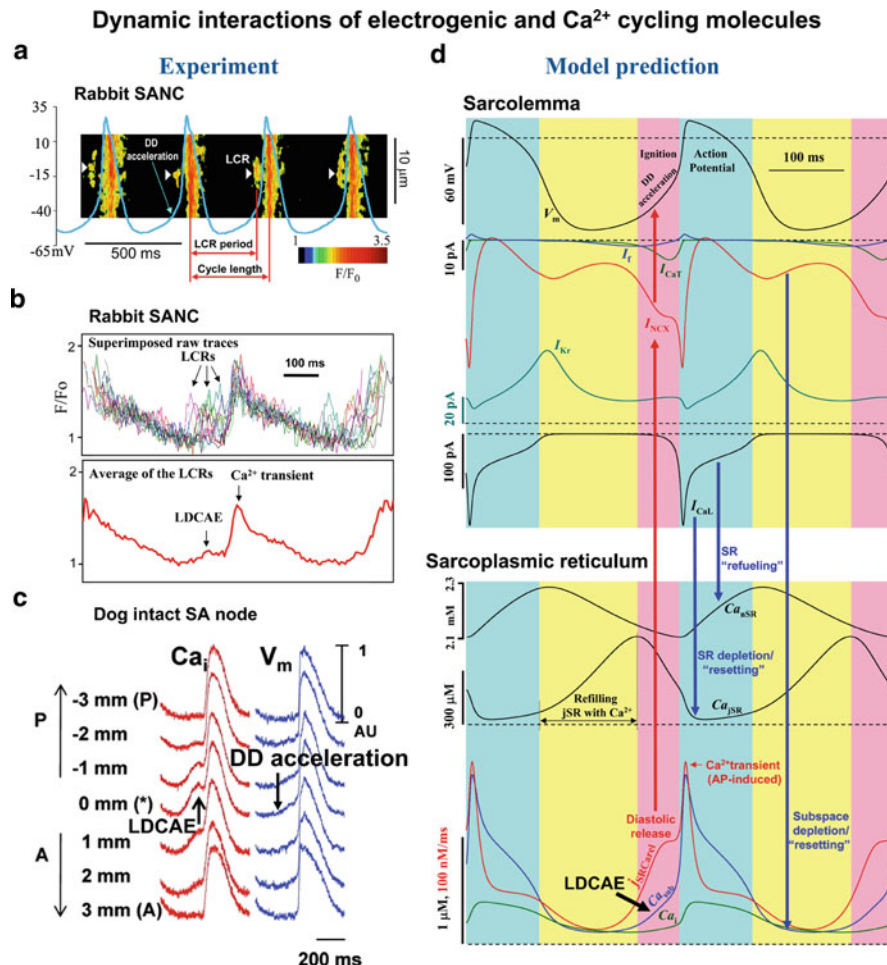


Fig. 4.2 (a) Line-scan image of LCRs with superimposed spontaneous APs in rabbit SANCs. White arrowheads show LCRs. The LCR period is defined as indicated. Modified from [2]. (b) Confocally measured subsarcolemmal LCRs (*upper panel*) in rabbit SANCs. The temporal average of the individual LCRs within each cycle (*lower panel*) generates Late Diastolic Ca^{2+} Elevation (LDCAE) that precedes Ca^{2+} transient induced by AP. Modified from [26]. (c) LDCAE in intact SA node detected in the leading pacemaker site (0 mm) simultaneously with DD acceleration in membrane potential recording. From [12] with permission. (d) Simultaneous numerical simulations of dynamics of important system parameters of SL (*top*) and SR (*bottom*) and their interactions (*vertical arrows*). Modified from [25]

diastolic Ca^{2+} elevations (LDCAE) (Fig. 4.2c), have now been documented in several species [3, 6, 10, 12, 14, 41, 51] and predicted by numerical modeling [25] (Fig. 4.2d, bottom panel).

LCRs do not require membrane depolarization in rabbit SANCs and occur spontaneously [45, 49]. Rhythmic LCRs are observed in saponin-skinned rabbit SANCs, in which $[\text{Ca}^{2+}]_i$ is buffered at a constant physiological level [45, 49]. Persistent rhythmic LCRs are also documented during acute voltage-clamp at a potential that prevents Ca^{2+} loss from the cell and are accompanied by membrane current fluctuations of the same periodicity [49]. These spontaneous rhythmic SR Ca^{2+} releases of rabbit SANCs have been recently reproduced in silico [25]. The numerical SR Ca^{2+} oscillator of SANCs generates Ca^{2+} releases over a wide range of frequencies (1.3–6.1 Hz) in the context of wide range of model parameters (SR Ca^{2+} pumping and release rates).

In addition to SERCA and RyRs, SANCs also exhibit strong $\text{Na}^+/\text{Ca}^{2+}$ exchanger (NCX) immunolabeling [21]. At the resolution of the confocal microscope [21], RyR and NCX molecules colocalize across the ~12 nm subsarcolemmal gap between RyRs on the SR and NCX molecules on the sarcolemma. Therefore, diastolic LCRs (or LDCAE) activate inward NCX current (I_{NCX} , Fig. 4.2d). This inward I_{NCX} is sufficient to strongly accelerate the DD [2, 25, 47] (“DD acceleration” in Fig. 4.2a, c, d). This leads to activation of L-type Ca^{2+} channel (LTCC) current (I_{CaL}) during the late DD (“Ignition” in Fig. 4.2d) that culminates in the generation of the rapid upstroke of the AP.

4.2.2 *Interactions During the AP*

Ca^{2+} influx via LTCCs during the AP induces Ca^{2+} release from SR via RyRs, i.e., Ca^{2+} -induced Ca^{2+} release (CICR) [1] (“ Ca^{2+} transient” in Fig. 4.2b, d). Ca^{2+} that accumulates within the subsarcolemmal space binds to calmodulin to inactivate I_{CaL} and modulates the NCX throughout the AP (red trace in Fig. 4.2d), contributing to the Ca^{2+} transient decay, by causing Ca^{2+} efflux from the cell. The occurrence of AP-triggered Ca^{2+} release from the SR (via CICR) synchronizes the global SR function (i.e., all parts of SR) in a relatively Ca^{2+} -depleted state (“SR depletion/resetting” in Fig. 4.2d) that temporarily suspends generation of spontaneous LCRs during early DD (described below). SR Ca^{2+} ATPase pumps Ca^{2+} at a rate modulated by the amount of Ca^{2+} to be pumped. A substantial component of Ca^{2+} influx via LTCCs is pumped by SR Ca^{2+} ATPase directly into the SR [11], and replenishes cell Ca^{2+} load (“SR refueling” in Fig. 4.2d). Ca^{2+} influx via LTCCs [and perhaps via Ca^{2+} store-operated TRPC channels (15)] balances cell Ca^{2+} efflux via NCX.

Membrane depolarization during AP activates ERG K^+ channels (see simulated rapid delayed rectifier current I_{Kr} in Fig. 4.2d) resulting in AP repolarization. Intracellular Ca^{2+} also modulates ERG K^+ channel gating [40] (Fig. 4.1). As NCX flux is both voltage- and Ca^{2+} -dependent, ERG K^+ channels, via AP repolarization,

modulate the activation of forward mode NCX (Fig. 4.2d). The membrane repolarization by I_{Kr} activation also inactivates LTCCs (Fig. 4.2d), limiting Ca^{2+} influx and thus also modulates Ca^{2+} balance.

4.2.3 Interactions During Early and Mid Diastolic Depolarization

Ca^{2+} ion concentration $[\text{Ca}^{2+}]$ within the cytosolic and subsarcolemmal compartments decays, due to $\text{Na}^+-\text{Ca}^{2+}$ exchange and SR Ca^{2+} pumping, to a nadir near the end of early DD (Fig. 4.2d, bottom panel, Ca_i and Ca_{sub} , respectively). Inward I_{NCX} activated by the AP-induced global Ca^{2+} transient concomitantly decays, and also reaches its nadir near the end of early DD, just before LCRs emerge (Fig. 4.2d, simulated I_{NCX} and SR Ca^{2+} release flux, j_{SRCrel}). Following achievement of the maximum diastolic potential (MDP), I_{Kr} conductance (g_{Kr}) decreases and this I_{Kr} deactivation is one mechanism of the early DD in pacemaker cells (green trace in Fig. 4.2d). This “ g_K decay” is thought to unmask an inward current, initially described as a background Na^+ current ($I_{b\text{Na}}$) [33]. A nonselective, sustained current (I_{st}) [8] has also been suggested as a mechanism for DD, but so far, it has no molecular identity or specific blockers. Since I_{st} exhibits some characteristics of I_{CaL} and I_{NCX} , combined effects of these two currents could possibly reflect in I_{st} [17]. The later repolarization phase of AP also activates I_f (Fig. 4.2d), a nonselective Na^+/K^+ current. Since the reversal potential of I_f is about -25 mV, it generates an inward current during DD, and is yet another early-mid DD mechanism (Fig. 4.2d, blue trace) [7, 31]. It is important to note that $[\text{Ca}^{2+}]_i$ does not directly regulate I_f [30] and that during late DD LCR/ I_{NCX} and I_{CaL} contributions wax but the I_f contribution wanes, as membrane potential approaches the I_f reversal potential (Fig. 4.2d). A new cycle begins with the late DD and AP ignition by the LCR/ I_{NCX} /DD-acceleration/ I_{CaL} -activation mechanism (Fig. 4.2d, “Ignition”), and the events described above recur.

4.3 Importance of Entrainment of SL and SR Function in SANC Basal AP Firing

The aforementioned interactions result in a mutual entrainment of the SL electrogenic molecules and Ca^{2+} cycling molecules of the system (Fig. 4.1). The entrainment of DD/APs and spontaneous Ca^{2+} releases is documented in rabbit SANCs during the transition from voltage-clamp (e.g., at -63 mV) to current-clamp (Fig. 4.3a) [49]. The SR of voltage-clamped SANCs becomes Ca^{2+} depleted via NCX [49]. During the recovery after voltage-clamp the LCR signal mass (i.e., the product of LCR size, amplitude, duration, and number per cycle within the confocal scanline) gradually increases after each subsequent AP and cycle length

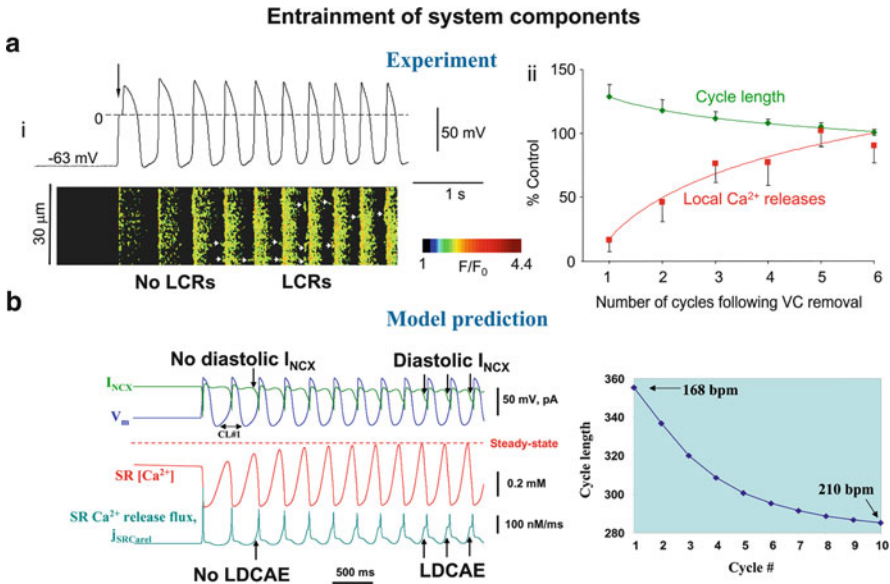


Fig. 4.3 (a) (i) An example of entrainment of electrophysiology and Ca^{2+} cycling in transition of rabbit SANCs from voltage clamp (VC) at -63 mV to rhythmic beating. *Top and bottom traces* are simultaneous recordings of membrane potential and subsarcolemmal Ca^{2+} signals, respectively, in a perforated patch clamp experiment. White arrows indicate LCRs. (ii) Average data on the dynamics of cycle length and LCR signal mass (“Local Ca^{2+} releases”). From [49]. (b) Simulations of a new SANC model [25]

(CL) concomitantly shortens, so that after several cycles SANCs resume rhythmic beating at the prevoltage-clamp CL. Simulations reproduce this experimental result and provide further insights into the mechanisms of entrainment (Fig. 4.3b): Upon switching to current-clamp, SR becomes replenished with Ca^{2+} (red curve in Fig. 4.3b) via Ca^{2+} influx during repetitive I_{CaL} activation. As the SR Ca^{2+} load increases, the system begins to generate LDCAE of increasing amplitude (Fig. 4.3b) concomitantly with increasing diastolic I_{NCX} and DD acceleration, which were initially missing.

The issue of entrained SL and SR function has been addressed in numerous pharmacological, ion substitution, genetic, and simulation studies (review [17]). Pioneering studies of 1980s and 1990s which discovered the importance of Ca^{2+} cycling or NCX in cardiac pacemaker function [13, 19, 36, 37, 53] attempted to make the system fail by inhibition of either the SR Ca^{2+} cycling per se or NCX, the critical link of entrainment. Three popular types of perturbations include (1) ryanodine which locks RyRs in an open subconductance state and thereby interferes with normal Ca^{2+} release; (2) cyclopiazonic acid (CPA) that inhibits SR Ca^{2+} pumping; and (3) Na^+ -free medium, disabling NCX function.

Oscillatory I_{NCX} was shown to occur during DD [3, 20, 47]. In our opinion the effect of acutely disabling NCX provides the most convincing evidence for the

importance of entrainment of Ca^{2+} cycling and SL electrogenic function. When Na^+ is acutely removed from the bathing milieu following a prior AP of rabbit [3] or guinea pig [38] SANCs, generation of the subsequent AP acutely fails, while LCRs persist [3] (Fig. 4.4a). We interpret this result to indicate that (1) forward mode NCX, by generating inward I_{NCX} , couples LCRs to the late DD acceleration [2, 3] and (2) entrainment of Ca^{2+} cycling and DD/APs (via the NCX link) is crucial for SANC function. This interpretation is fully supported by simulations [25] (Fig. 4.4b). Since acute augmentation of I_{NCX} during DD requires an acute increase in subsarcolemmal $[\text{Ca}^{2+}]$, buffering subsarcolemmal Ca^{2+} in rabbit or guinea pig SANCs severely impairs or blocks spontaneous AP firing [21, 38, 48].

The results of ryanodine effects on isolated SA node tissue, isolated SANCs, or the intact heart have been extensively reviewed recently [17, 44]. The extent of ryanodine-induced suppression of AP firing rate in these studies varies from 12% to 100%, average ~40%. Ryanodine eliminates a substantial late DD inward NCX current in SANCs [3, 19, 47], with the current density during DD varying in rabbit SANCs from 0.3 pA/pF [47] to 1.6 pA/pF [3]. As illustrated in Fig. 4.5a ryanodine suppresses the exponential character of the late DD [2, 18], and the AP firing becomes often dysrhythmic (Fig. 4.5b). A small suppression of the SAN beating rate by ryanodine in some studies may be due to an insufficient ryanodine

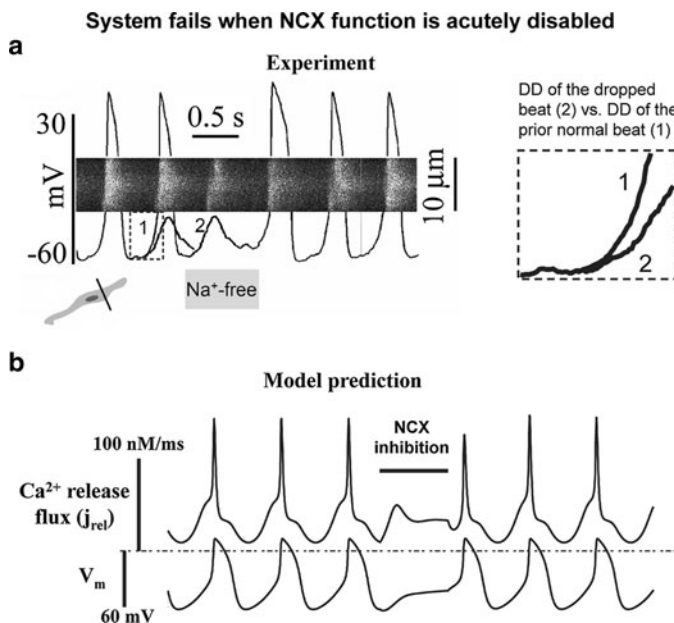


Fig. 4.4 (a) Linescan image of Ca^{2+} release with superimposed simultaneous AP records during rapid, brief superfusion in the diastolic period with a Na^+ -free solution. *Curve 2* was superimposed on *curve 1* of the last AP, preceding Na^+ -free solution (zoomed in right inset). Scanned line was oriented perpendicular to long cell axis (left inset). Modified from [3]. (b) Simulations predict the experimental result in (a). Modified from [25]

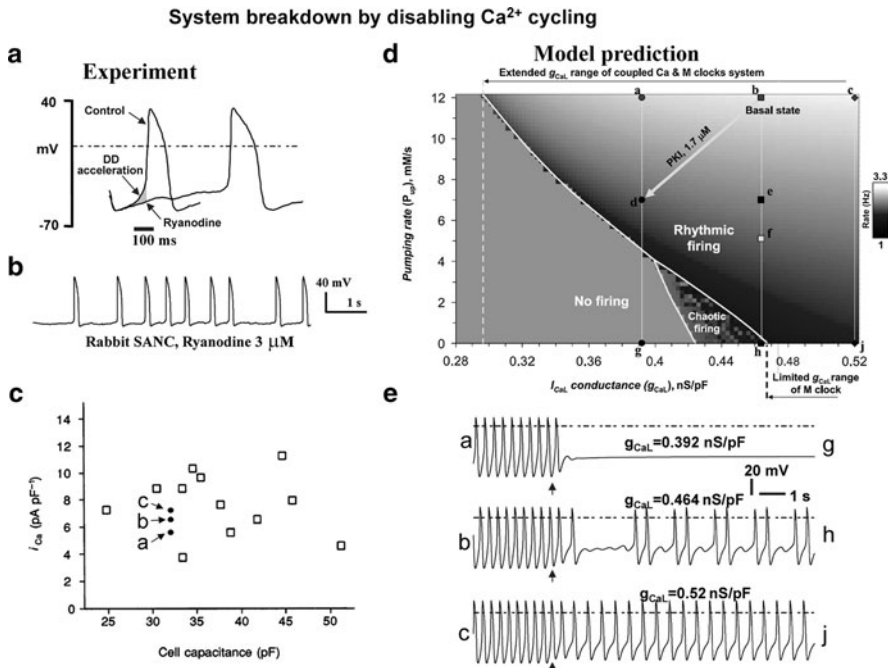


Fig. 4.5 (a) Superimposed APs of representative rabbit SANCs before and after treatment with 3 μM ryanodine (from [18]). (b) An example of irregular beating of SANCs after treatment with ryanodine (Lyashkov et al., unpublished data). (c) Substantial variations of I_{CaL} peak density in rabbit SANCs versus cell capacitance (squares). Circles show the current peak values of I_{CaL} simulations using the respective conductances in panel (e) (a–c) and the same voltage protocol as in experiments. From [9] with permission. (d) The steady-state AP firing rates and bifurcation transition lines predicted by numerical model simulations of rabbit SANCs with various combinations of g_{CaL} and P_{up} . From [25]. (e) Simulations of membrane potentials in transitions when model parameters acutely change (arrows) as marked in panel D by respective small cap letters (see text for details). From [25]

concentration, or insufficient time of exposure. The kinetics of the ryanodine effect are especially important, because a rapid application of ryanodine to isolated SANCs or SAN tissue initially increases RyR Ca^{2+} release, and the spontaneous beating rate concomitantly increases; then as SR becomes depleted with time, the spontaneous beating slows [4, 37].

In guinea pig SANCs partial disabling of the SR Ca^{2+} cycling by CPA substantially reduced the frequency of AP-induced Ca^{2+} transients by $80 \pm 6\%$ and this was associated with a reduction in the amplitude of the transients by $53 \pm 9\%$ [35]. More recent studies in guinea pig [38] and rabbit [43] SANCs also demonstrate that SANC CL is substantially increased by CPA, up to $\sim 50\%$ (Fig. 4.6a). Simulations showed that the documented effect of CPA on beating rate is achieved when the pumping rate is inhibited to 1/3 of its basal rate [25] (Fig. 4.6c, “Cycle length increase” in bottom panel versus “SR Ca^{2+} pumping rate” in top panel).

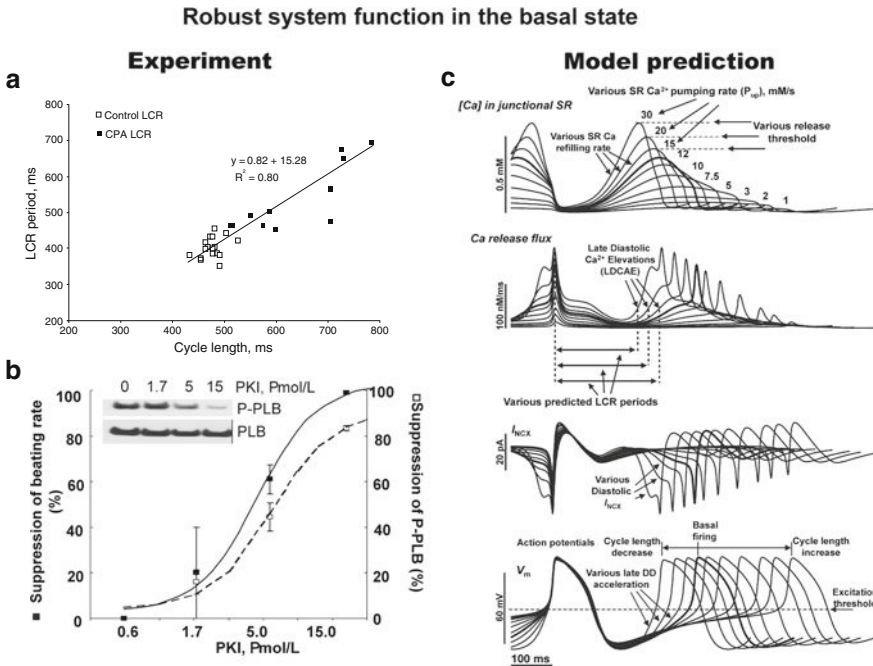


Fig. 4.6 (a) When SR Ca^{2+} pump is inhibited by cyclopiazonic acid (CPA, 3 μM), the prolongation of the LCR period is highly correlated with the spontaneous CL. Line and equation represent the best fit to the data points. Modified from [43]. (b) The relationship of suppression of SANC beating rate (solid line) and phospholamban (PLB) phosphorylation of SANC suspensions (dashed line) by suppression of PKA signaling by PKI. Inset shows Western blots of phosphorylated PLB and total PLB in response to increasing PKI concentrations. Error bars indicate standard error of mean. From [45]. (c) Simulations predict the wide range of pacemaker rate regulation via variations in the maximum SR Ca^{2+} pumping rate (P_{up} , reflecting the number of functional SERCA molecules and phospholamban phosphorylation by PKA, 1–30 mM/s). Shown are simulations of SR $[\text{Ca}^{2+}]$, SR Ca^{2+} release flux, I_{NCX} , and V_m . Simulations for basal state AP firing ($P_{\text{up}} = 12 \text{ mM/s}$) are illustrated by bold curves. Modified from [25]

It is difficult to halt spontaneous SANC beating by incomplete pharmacological inhibition of Ca^{2+} cycling because the SANC robust pacemaker system (Fig. 4.1) has redundancies and substantial safety reserves (see more about robustness below). For example, when diastolic LCR/ I_{NCX} signals become inhibited and SANC beating rate is reduced, I_f increases because it has more time to active. An explanation of variability or incompleteness of the effects of Ca^{2+} cycling inhibition, e.g., by ryanodine or CPA, in individual SANCs (having various electrophysiological characteristics [9]) is gleaned from simulation studies. Figure 4.5d illustrates the results of 5917 model simulations of steady-state AP firing with various combinations of basal I_{CaL} conductance (g_{CaL}) and maximum SR Ca^{2+} pumping rate (P_{up}), reflecting the number of functional LTCC and SERCA molecules, respectively. This parametric sensitivity analysis demonstrates the crucial importance of combined function of LTCCs and SERCA to define DD and cell Ca^{2+} handling: both

determine not only the resultant steady-state firing rate (shade-coded), but also boundaries of fail-safe system function, i.e., the bifurcation curve separating “rhythmic firing” from “Chaotic firing” or “No firing” in Fig. 4.5d. Note that the boundaries are broader when Ca^{2+} cycling is intact (top horizontal arrow versus bottom horizontal arrow in Fig. 4.5d). Thus, when Ca^{2+} cycling is partially disabled (e.g., by a pharmacologic perturbation), those boundaries are compressed, and the system may fail if it crosses the bifurcation line. Thus, the outcome depends on both the effectiveness of Ca^{2+} cycling suppression and g_{CaL} , with the latter exhibiting intrinsic cell-to-cell variations [9] (Fig. 4.5c, squares). Thus, in the extreme case of complete Ca^{2+} cycling inhibition (Fig. 4.5e), SANCs with a relatively high g_{CaL} ($c \rightarrow j$) exhibit rate slowing, but in SANCs with smaller g_{CaL} the effect of SR Ca^{2+} cycling disabling exaggerates, culminating in irregular beating ($b \rightarrow h$) and complete halt ($a \rightarrow g$).

4.4 Phosphorylation of Ca^{2+} Cycling and Membrane Proteins Is Required for Basal SAN Automaticity

Another part of the complex SANC system conundrum is “what drives the LCR occurrence in basal state?” This problem has been studied recently [30, 45, 46, 52] and reviewed [17, 44]. In short, the discoveries of Ca^{2+} -activated adenylyl cyclase (AC) types, i.e., AC1 and AC8, in rabbit and guinea-pig SANCs [30, 46, 52], and localization of the basal Ca^{2+} -activated AC activity within lipid raft microdomains [52], link Ca^{2+} to localized cAMP production (Fig. 4.1). Ca^{2+} binds to calmodulin to activate AC, leading to a high basal level of cAMP-mediated, PKA-dependent phosphorylation of SL and intracellular proteins involved in cell Ca^{2+} balance and SR Ca^{2+} cycling [45, 52] (Fig. 4.1). Phosphorylated proteins include phospholamban [22, 45] (Fig. 4.6b), RyR [45], and possibly SERCA, LTCC [34], and K^+ channels (Fig. 4.1). Thus, PKA, and likely CaMKII, can be envisioned as coupling factors [17, 25], which enzymatically (via phosphorylation) couple function of numerous sarcolemmal and intracellular proteins within the SANC complex system (Fig. 4.1). This protein phosphorylation is *required* for LCR generation and normal basal function of SANC system, because both LCRs and spontaneous AP firing cease when either kinase is inhibited [39, 45, 48]. While the kinases drive the enhanced system function, their actions are kept in check by PDEs [47] and likely phosphatases [22] (Fig. 4.1).

Although a detailed biochemical model of SANC function is presently lacking, some crucial aspects of basal PKA and CaMKII signaling have been incorporated into a recent numerical model of SANCs [25]. The model mimics basal phosphorylation of phospholamban and RyR by enabling higher rates of SR Ca^{2+} pumping and release versus prior SANC models and models of cardiac muscle cells. This enhanced Ca^{2+} cycling in the model is required to reproduce the effect of LCR occurrence in the basal state beating (“LDCAE” in Fig. 4.6c).

4.5 Coupled-Clock System Robustness: LCR Period Regulation by Ca^{2+} , PKA, and CaMKII Signaling

The delay between the onset of the global SR Ca^{2+} depletion triggered by an AP (via CICR) and the spontaneous emergence of an LCR during the subsequent DD is the LCR period (Fig. 4.2a). It may seem paradoxical that the LCR period does *not* report Ca^{2+} clock function, *per se*, but reports the integrated function of the *entire system*, because of intimate interactions of the electrogenic SL molecules with the Ca^{2+} cycling apparatus described above and depicted in Fig. 4.1. In other words, NCX and even SL Ca^{2+} and K^+ channels contribute (albeit indirectly) to the LCR period as much as SR Ca^{2+} pumping or release does! Importantly, after integrating the functions of various system components, the LCR period determines the “ticking speed” of the coupled-clock system, because LCRs prompt each AP occurrence (via I_{NCX} and DD acceleration, see above).

If LCR period were indeed such a crucial parameter of the system, then how is it specifically determined and regulated? As noted above, a strong Ca^{2+} depletion of SR, triggered during the AP via CICR, causes spontaneous LCRs to stop (Fig. 4.2). Then SR Ca^{2+} pumping and intraSR diffusion refill and redistribute Ca^{2+} within SR towards release sites within junctional SR. When threshold conditions for spontaneous Ca^{2+} release are achieved, SR begins to generate LCRs again. Thus, the LCR period is determined, at least in part, by the duration of this restitution process, and SR Ca^{2+} pumping rate certainly contributes to the restitution kinetics. Indeed, the LCR period and CL concomitantly increase when SR Ca^{2+} pump is inhibited by CPA [43] (Fig. 4.6a) or when basal phospholamban phosphorylation is decreased by PKA inhibition [45] (Fig. 4.6b). But the issue is complicated by the fact that instantaneous rates of SR Ca^{2+} pumping are determined not only by the number of functional (or phospholamban-free) SERCA molecules, but also by the amount of Ca^{2+} , i.e., the oscillatory substrate, available for pumping, which, in turn, is controlled by the coupling factors, i.e., PKA- and CaMKII-dependent phosphorylation of the system proteins other than SERCA and phospholamban, i.e., RyR and SL ion channels [17, 44] (Fig. 4.1). Another crucial process that determines the duration of the restitution is spontaneous activation of RyRs (completing the restitution), which, in turn, depends on both the regulation of RyRs by intra SR $[\text{Ca}^{2+}]$ (luminal regulation) and the residual Ca^{2+} in subsarcolemmal space [25].

Simulation studies [25] provide mechanistic insights into the complex SR restitution process and how it controls CL. Simulations in Fig. 4.6c were performed for different values of model constant P_{up} that determines the capability of SR Ca^{2+} pumping (mimicking the number of functional SERCA molecules and the state of phospholamban phosphorylation by PKA). While SL molecules affect cell Ca^{2+} balance and Ca^{2+} available for pumping directly via Ca^{2+} influx and efflux, P_{up} also affects cell Ca^{2+} balance because it determines how much Ca^{2+} is retained within the SR, and therefore not extruded via NCX during each cycle. Indeed the integrated effect of increased P_{up} and changes in Ca^{2+} balance affect not only SR Ca^{2+} refilling kinetics, but also the apparent threshold for spontaneous diastolic

releases (Fig. 4.6c, top panel). A higher threshold for spontaneous release results in a larger SR Ca^{2+} loading and stronger Ca^{2+} releases. This relationship ideally fits the purpose of robust firing at various basal rates: higher release amplitudes at higher rates provide faster depolarizations to reach AP threshold in shorter times (via waxing LCR– I_{NCX} mechanism, Fig. 4.6c).

The robust, coupled-clock SANC pacemaker system exhibits broader margins for fail-safe parameter variations versus M clock alone (top horizontal arrow versus bottom horizontal arrow in Fig. 4.5d) due to functional synergism of the entrained molecules [25]. An example of such synergism is illustrated by simulations of the effects of a moderate PKA inhibition by 1.7 μM PKI (Fig. 4.5d). The reported rate reduction is achieved in the model with a much smaller P_{up} decrease when it is combined with a small (15.5%) decrease in g_{CaL} (vectors b→d versus b→f). The synergism among SANC functional components provides a substantial safety reserve to safely handle extreme perturbations by the pacemaker system [25]. This simulation of robust SANC function closely predicts the autonomic rate regulation [24] (see next section for details) and more extreme rate increases or decreases in SANC responses to inhibition of PDEs [47] or PKA [45], respectively.

4.6 System Flexibility: Pacemaker Rate Modulation via G Protein-Coupled receptor (GPCR) Signaling

In addition to robustness or “fail-safe,” stable basal operation, the heart’s pacemaker clock must tick over a wide range of frequencies that encompasses the physiological range of heart rates. This flexibility of the “throttle” of the pacemaker clock is achieved via modulation of the LCR period by GPCR signaling (reviews [17, 18, 23, 44]). Robust modulation of the beating rate of SANCs by G protein-coupled receptors (GPCR; Fig. 4.1) is achieved by impacting the very same factors (Ca^{2+} and protein phosphorylation) of the system that regulate basal SANC function (described in the previous section; Fig. 4.1, red). Specifically, β adrenergic receptor (β -AR) stimulation further increases, and muscarinic receptor ($M_2\text{R}$) stimulation reduces basal levels of phosphorylation of proteins of the system, leading to an increase or a reduction, respectively, in LCR period [22, 45].

Effects of β -AR stimulation: In addition to the reduction in the LCR period, β -AR stimulation also increases the integrated LCR Ca^{2+} release signal mass because RyR activation becomes more synchronized via local recruitment [42, 47]. This earlier and stronger local Ca^{2+} release into the submembrane space results in earlier and stronger I_{NCX} and DD acceleration, causing a reduction in CL. Thus, pacemaker rate acceleration by β -AR stimulation is linked to both the early and late DD phases [2, 5, 16]. This experimental result is fully reproduced in silico [24] by a doubling of P_{up} complemented by the well-known changes in I_{CaL} , I_f , and I_{Kr} upon β -AR stimulation. The simulations predict that β -AR stimulation is mainly mediated by diastolic I_{NCX} that occurs earlier in the cycle and doubles in amplitude, due to both an earlier occurrence and a concomitant increase in the magnitude of diastolic Ca^{2+} release flux. It is also important to note that the system interactions

remain well balanced during β -AR stimulation: increased Ca^{2+} influx via increased I_{CaL} supports the larger Ca^{2+} releases and larger Ca^{2+} efflux via the doubled I_{NCX} .

Recent studies have shown that in order to increase the beating rate, β -AR stimulation (or PDE inhibition) indeed requires a link between β -AR-induced increases in PKA or CaMKII modulation of SL molecules and SR Ca^{2+} cycling molecules within the system [42, 45, 47, 53]. The requirement of intact Ca^{2+} cycling within the system for β -AR stimulation-induced positive chronotropic effect has been demonstrated in studies involving ryanodine-induced disabling of RyR function and depletion of SR Ca^{2+} in both single SANC and intact SA node of several species (Reviews [17, 44]). In these experiments β -AR stimulation still showed its normal effects on SL Ca^{2+} and K^+ channels but this is insufficient to cause the normal increase in SANC AP firing rate.

Effects of M₂R stimulation: Two recent studies of rabbit SANCs [22, 41] have demonstrated that M₂R stimulation suppresses LCRs (or LDCAE), which contributes substantially (35–75%) to the slowing of the beating rate. At a low carbachol concentration causing 30% max rate inhibition, I_{KACH} activation is not evident, and the negative chronotropic effect is almost fully attributable to a suppression of cAMP-mediated, PKA-dependent Ca^{2+} signaling. At IC₅₀ of 100 nM carbachol for rate reduction, a 50% reduction in phospholamban phosphorylation is accompanied by ~60% prolongation of LCR period that is linked to the 50% prolongation in CL. While at this [carbachol] a moderate I_{KACH} activation was found, phosphatase inhibition reverses almost completely the effect of carbachol on SANC LCR period and cycle length [22], demonstrating an important role of protein dephosphorylation in the rate reduction due to moderate M₂R stimulation. At higher carbachol concentrations, more marked I_{KACH} activation underlies a more pronounced reduction in the beating rate [22].

Simulations of the effect of a physiological M₂R stimulation with 100 nM of carbachol [24] with documented changes in SL ion currents and SR Ca^{2+} pump inhibition by 36.8% [22] show that the effective and synergistic rate reduction indeed includes two major mechanisms that act on membrane potential: I_{NCX} and I_{KACH} . The diastolic LCRs/ I_{NCX} mechanism is basically the same mechanism as described above for β -AR stimulation, but works in opposite direction. The predicted beating rate decrease is directly due to a smaller and delayed diastolic I_{NCX} , because of a reduced amplitude and later occurrence of LDCAE. The later occurrence of LDCAE reproduces the experimentally documented increase of the LCR period effected by M₂R stimulation [22]. The smaller LDCAE, in turn, reproduces the experimentally documented decrease in LCR signal mass [22].

4.7 Clinical Implications

In the light of our novel pacemaker concept presented herein, mechanisms of action of pharmacological agents on SA node and clinical implications (e.g., in sick sinus syndrome etc.) cannot be simple, i.e., based on one specific parameter change, such as I_f , but, in fact, involve numerous interactions within the complex robust SANC

system (Fig. 4.1). For example, the complex system response to a pharmacological or disease perturbation can be explored using a numerical bifurcation analysis that includes both SL and SR components (e.g., PKI in Fig. 4.5d). A novel type of biological pacemaker [28] targets coupling factors, such as PKA and CaMKII, that orchestrate the function of numerous SL and SR system components (Fig. 4.1), which would allow to control rhythmic pacemaker function in the same way as it naturally occurs in healthy SANCs.

4.8 Conclusions

Based on the experimental results and novel type of numerical modeling of SANCs presented here, the heart's pacemaker clock can be envisioned as a complex *system* of dynamically interacting sarcolemmal and intracellular proteins (Fig. 4.1). The functional entrainment of electrogenic proteins and Ca^{2+} cycling proteins (Figs. 4.2 and 4.3) within the system is regulated by protein phosphorylation (Figs. 4.1 and 4.6b) and is required for the SANC function (Figs. 4.4 and 4.5). The system has redundancies and a substantial safety reserve, as it allows large-scale parameter variation without comprising the system performance (Fig. 4.6). The regulation of beating rate of SANCs by autonomic nerves via GPCR is also robust, because it acts upon the same coupling factors, such as PKA and CaMKII (Fig. 4.1) that ensure robustness of the coupled system function in the basal state (Fig. 4.6). In summary, we believe that further progress in our exploration of pacemaker function and clinical implications requires intertwining of novel experimentation with this novel type numerical modeling that embraces complex, dynamic, and functional integration of SL and intracellular proteins.

Acknowledgments This research was supported entirely by the Intramural Research Program of the NIH, National Institute on Aging.

References

1. Bers DM. Excitation-contraction coupling and cardiac contractile force. 2nd ed. Norwell, MA: Kluwer Academic; 2001.
2. Bogdanov KY, Maltsev VA, Vinogradova TM, Lyashkov AE, Spurgeon HA, Stern MD, et al. Membrane potential fluctuations resulting from submembrane Ca^{2+} releases in rabbit sino-atrial nodal cells impart an exponential phase to the late diastolic depolarization that controls their chronotropic state. *Circ Res*. 2006;99:979–87.
3. Bogdanov KY, Vinogradova TM, Lakatta EG. Sinoatrial nodal cell ryanodine receptor and $\text{Na}^+ \text{-Ca}^{2+}$ exchanger: molecular partners in pacemaker regulation. *Circ Res*. 2001;88:1254–8.
4. Buchi A, Baruscotti M, Robinson RB, DiFrancesco D. I_f -dependent modulation of pacemaker rate mediated by cAMP in the presence of ryanodine in rabbit sino-atrial node cells. *J Mol Cell Cardiol*. 2003;35:905–13.

5. Bucchi A, Baruscotti M, Robinson RB, DiFrancesco D. Modulation of rate by autonomic agonists in SAN cells involves changes in diastolic depolarization and the pacemaker current. *J Mol Cell Cardiol.* 2007;43:39–48.
6. Chen B, Wu Y, Mohler PJ, Anderson ME, Song LS. Local control of Ca^{2+} -induced Ca^{2+} release in mouse sinoatrial node cells. *J Mol Cell Cardiol.* 2009;47:706–15.
7. DiFrancesco D. The contribution of the ‘pacemaker’ current (i_p) to generation of spontaneous activity in rabbit sino-atrial node myocytes. *J Physiol.* 1991;434:23–40.
8. Guo J, Ono K, Noma A. A sustained inward current activated at the diastolic potential range in rabbit sino-atrial node cells. *J Physiol.* 1995;483(Pt 1):1–13.
9. Honjo H, Boyett MR, Kodama I, Toyama J. Correlation between electrical activity and the size of rabbit sino-atrial node cells. *J Physiol.* 1996;496(Pt 3):795–808.
10. Huser J, Blatter LA, Lipsius SL. Intracellular Ca^{2+} release contributes to automaticity in cat atrial pacemaker cells. *J Physiol.* 2000;524(Pt 2):415–22.
11. Janczewski AM, Lakatta EG. Buffering of calcium influx by sarcoplasmic reticulum during the action potential in guinea-pig ventricular myocytes. *J Physiol.* 1993;471:343–63.
12. Joung B, Tang L, Maruyama M, Han S, Chen Z, Stucky M, et al. Intracellular calcium dynamics and acceleration of sinus rhythm by beta-adrenergic stimulation. *Circulation.* 2009;119:788–96.
13. Ju YK, Allen DG. Intracellular calcium and $\text{Na}^+-\text{Ca}^{2+}$ exchange current in isolated toad pacemaker cells. *J Physiol.* 1998;508(Pt 1):153–66.
14. Ju YK, Allen DG. The distribution of calcium in toad cardiac pacemaker cells during spontaneous firing. *Pflugers Arch.* 2000;441:219–27.
15. Ju YK, Chu Y, Chaulet H, Lai D, Gervasio OL, Graham RM, et al. Store-operated Ca^{2+} influx and expression of TRPC genes in mouse sinoatrial node. *Circ Res.* 2007;100:1605–14.
16. Lakatta EG, DiFrancesco D. What keeps us ticking: a funny current, a calcium clock, or both? *J Mol Cell Cardiol.* 2009;47:157–70.
17. Lakatta EG, Maltsev VA, Vinogradova TM. A coupled SYSTEM of intracellular Ca^{2+} clocks and surface membrane voltage clocks controls the timekeeping mechanism of the heart’s pacemaker. *Circ Res.* 2010;106:659–73.
18. Lakatta EG, Vinogradova T, Lyashkov A, Sirenko S, Zhu W, Ruknudin A, et al. The integration of spontaneous intracellular Ca^{2+} cycling and surface membrane ion channel activation entrains normal automaticity in cells of the heart’s pacemaker. *Ann NY Acad Sci.* 2006;1080:178–206.
19. Li J, Qu J, Nathan RD. Ionic basis of ryanodine’s negative chronotropic effect on pacemaker cells isolated from the sinoatrial node. *Am J Physiol.* 1997;273:H2481–9.
20. Lipsius SL, Huser J, Blatter LA. Intracellular Ca^{2+} release sparks atrial pacemaker activity. *News Physiol Sci.* 2001;16:101–6.
21. Lyashkov AE, Juhaszova M, Dobrzynski H, Vinogradova TM, Maltsev VA, Juhasz O, et al. Calcium cycling protein density and functional importance to automaticity of isolated sino-atrial nodal cells are independent of cell size. *Circ Res.* 2007;100:1723–31.
22. Lyashkov AE, Vinogradova TM, Zahanich I, Li Y, Younes A, Nuss HB, et al. Cholinergic receptor signaling modulates spontaneous firing of sinoatrial nodal cells via integrated effects on PKA-dependent Ca^{2+} cycling and I_{KACH} . *Am J Physiol Heart Circ Physiol.* 2009;297:H949–59.
23. Maltsev VA, Lakatta EG. Dynamic interactions of an intracellular Ca^{2+} clock and membrane ion channel clock underlie robust initiation and regulation of cardiac pacemaker function. *Cardiovasc Res.* 2008;77:274–84.
24. Maltsev VA, Lakatta EG. A novel quantitative explanation for autonomic modulation of cardiac pacemaker cell automaticity via a dynamic system of sarcolemmal and intracellular proteins. *Am J Physiol Heart Circ Physiol.* 2010;298:H2010–H2023.
25. Maltsev VA, Lakatta EG. Synergism of coupled subsarcolemmal Ca^{2+} clocks and sarcolemmal voltage clocks confers robust and flexible pacemaker function in a novel pacemaker cell model. *Am J Physiol Heart Circ Physiol.* 2009;296:H594–615.

26. Maltsev VA, Vinogradova TM, Bogdanov KY, Lakatta EG, Stern MD. Diastolic calcium release controls the beating rate of rabbit sinoatrial node cells: numerical modeling of the coupling process. *Biophys J.* 2004;86:2596–605.
27. Maltsev VA, Vinogradova TM, Lakatta EG. The emergence of a general theory of the initiation and strength of the heartbeat. *J Pharmacol Sci.* 2006;100:338–69.
28. Maltsev VA et al. Engineered biological pacemakers (U.S. Provisional Patent Application No. 61/180, 491). *Fed Regist.* 2009;74(199):53268.
29. Mangoni ME, Nargeot J. Genesis and regulation of the heart automaticity. *Physiol Rev.* 2008;88:919–82.
30. Mattick P, Parrington J, Odia E, Simpson A, Collins T, Terrar D. Ca^{2+} -stimulated adenylyl cyclase isoform AC1 is preferentially expressed in guinea-pig sino-atrial node cells and modulates the I_f pacemaker current. *J Physiol.* 2007;582:1195–203.
31. Maylie J, Morad M, Weiss J. A study of pace-maker potential in rabbit sino-atrial node: measurement of potassium activity under voltage-clamp conditions. *J Physiol.* 1981;311: 161–78.
32. Musa H, Lei M, Honjo H, Jones SA, Dobrzynski H, Lancaster MK, et al. Heterogeneous expression of Ca^{2+} handling proteins in rabbit sinoatrial node. *J Histochem Cytochem.* 2002;50:311–24.
33. Noble D. Cardiac action and pacemaker potentials based on the Hodgkin-Huxley equations. *Nature.* 1960;188:495–7.
34. Petit-Jacques J, Bois P, Bescond J, Lenfant J. Mechanism of muscarinic control of the high-threshold calcium current in rabbit sino-atrial node myocytes. *Pflugers Arch.* 1993;423:21–7.
35. Rigg L, Heath BM, Cui Y, Terrar DA. Localisation and functional significance of ryanodine receptors during beta-adrenoceptor stimulation in the guinea-pig sino-atrial node. *Cardiovasc Res.* 2000;48:254–64.
36. Rigg L, Terrar DA. Possible role of calcium release from the sarcoplasmic reticulum in pacemaking in guinea-pig sino-atrial node. *Exp Physiol.* 1996;81:877–80.
37. Rubenstein DS, Lipsius SL. Mechanisms of automaticity in subsidiary pacemakers from cat right atrium. *Circ Res.* 1989;64:648–57.
38. Sanders L, Rakovic S, Lowe M, Mattick PA, Terrar DA. Fundamental importance of $\text{Na}^+-\text{Ca}^{2+}$ exchange for the pacemaking mechanism in guinea-pig sino-atrial node. *J Physiol.* 2006;571: 639–49.
39. Sirenko S, Li Y, Yang D, Lukyanenko Y, Lakatta EG, Vinogradova TM. Basal phosphorylation of Ca^{2+} cycling proteins by both PKA and CAMKII is required for robust generation of local subsarcolemmal Ca^{2+} releases to drive sinoatrial node cell automaticity. *Circulation.* 2008;118 Suppl 2:S346.
40. Tohse N. Calcium-sensitive delayed rectifier potassium current in guinea pig ventricular cells. *Am J Physiol.* 1990;258:H1200–7.
41. van Borren MM, Verkerk AO, Wilders R, Hajji N, Zegers JG, Bourier J, et al. Effects of muscarinic receptor stimulation on Ca^{2+} transient, cAMP production and pacemaker frequency of rabbit sinoatrial node cells. *Basic Res Cardiol.* 2010;105:73–87.
42. Vinogradova TM, Bogdanov KY, Lakatta EG. beta-Adrenergic stimulation modulates ryanodine receptor Ca^{2+} release during diastolic depolarization to accelerate pacemaker activity in rabbit sinoatrial nodal cells. *Circ Res.* 2002;90:73–9.
43. Vinogradova TM, Brochet DX, Sirenko SG, Lyashkov AE, Maltsev VA, Yang D, et al. Sarcoplasmic reticulum (SR) Ca^{2+} refilling kinetics controls the period of local subsarcolemmal Ca^{2+} releases (LCR) and the spontaneous beating rate of sinoatrial node cells (SANC). *Biophys J Suppl.* 2007;2007:31a (Abstract).
44. Vinogradova TM, Lakatta EG. Regulation of basal and reserve cardiac pacemaker function by interactions of cAMP mediated PKA-dependent Ca^{2+} cycling with surface membrane channels. *J Mol Cell Cardiol.* 2009;47:456–74.

45. Vinogradova TM, Lyashkov AE, Zhu W, Ruknudin AM, Sirenko S, Yang D, et al. High basal protein kinase A-dependent phosphorylation drives rhythmic internal Ca^{2+} store oscillations and spontaneous beating of cardiac pacemaker cells. *Circ Res.* 2006;98:505–14.
46. Vinogradova TM, Ruknudin AM, Zhu W, Lyashkov AE, Volkova M, Boheler KR, et al. High basal cAMP content markedly elevates PKA-dependent protein phosphorylation and sustains spontaneous beating in rabbit sinoatrial nodal pacemaker cells (SANC). *Biophys J.* 2006; 90:155a (Abstract).
47. Vinogradova TM, Sirenko S, Lyashkov AE, Younes A, Li Y, Zhu W, et al. Constitutive phosphodiesterase activity restricts spontaneous beating rate of cardiac pacemaker cells by suppressing local Ca^{2+} releases. *Circ Res.* 2008;102:761–9.
48. Vinogradova TM, Zhou YY, Bogdanov KY, Yang D, Kuschel M, Cheng H, et al. Sinoatrial node pacemaker activity requires Ca^{2+} /calmodulin-dependent protein kinase II activation. *Circ Res.* 2000;87:760–7.
49. Vinogradova TM, Zhou YY, Maltsev V, Lyashkov A, Stern M, Lakatta EG. Rhythmic ryanodine receptor Ca^{2+} releases during diastolic depolarization of sinoatrial pacemaker cells do not require membrane depolarization. *Circ Res.* 2004;94:802–9.
50. Wilders R. Computer modelling of the sinoatrial node. *Med Biol Eng Comput.* 2007;45: 189–207.
51. Wu Y, Gao Z, Chen B, Koval OM, Singh MV, Guan X, et al. Calmodulin kinase II is required for fight or flight sinoatrial node physiology. *Proc Natl Acad Sci USA.* 2009;106:5972–7.
52. Younes A, Lyashkov AE, Graham D, Sheydina A, Volkova MV, Mitsak M, et al. Ca^{2+} -stimulated basal adenylyl cyclase activity localization in membrane lipid microdomains of cardiac sinoatrial nodal pacemaker cells. *J Biol Chem.* 2008;283:14461–8.
53. Zhou Z, Lipsius SL. $\text{Na}^+-\text{Ca}^{2+}$ exchange current in latent pacemaker cells isolated from cat right atrium. *J Physiol.* 1993;466:263–85.

Chapter 5

Pacemaker Activity of the SA Node: Insights from Dynamic-Clamp Experiments

Ronald Wilders, Antoni C.G. van Ginneken, and Arie O. Verkerk

5.1 Introduction

The sinoatrial node (SAN) is the normal pacemaker of the mammalian heart and generates the electrical impulse for its regular, rhythmic contraction. Pacemaker activity (or spontaneous electrical activity) of single SAN cells is based on the spontaneous diastolic depolarization (DD), during which SAN cells depolarize spontaneously toward the action potential (AP) threshold (Fig. 5.1b), and which is due to a very small net inward current across the cell membrane (Fig. 5.1c). Experimental studies have identified that this net inward current is the result of a complex interaction of multiple inwardly and outwardly directed ion currents (for reviews, see [1–4]).

The set of inward currents contributing to DD is thought to include the hyperpolarization-activated “funny current” (I_f), also known as “pacemaker current”, the background current carried by Na^+ ($I_{\text{b},\text{Na}}$), the sustained inward current (I_{st}), the L- and T-type Ca^{2+} currents ($I_{\text{Ca,L}}$ and $I_{\text{Ca,T}}$, respectively), and the Ca^{2+} -release-activated $\text{Na}^+–\text{Ca}^{2+}$ exchange current (I_{NCX}), whereas outward currents flowing during DD may include the rapid delayed rectifier K^+ current (I_{Kr}) and the slow delayed rectifier K^+ current (I_{Ks}) (which both deactivate during DD and together form the delayed rectifier K^+ current (I_K)), the ACh-activated K^+ current ($I_{\text{K,ACh}}$), and the net outward current generated by the electrogenic $\text{Na}-\text{K}$ pump (I_{NaK}) (see [5] and primary references cited therein). Whether these currents really contribute to DD depends on the channel properties (i.e., voltage dependency of (in)

R. Wilders, A.C.G. van Ginneken, and A.O. Verkerk (✉)
Heart Failure Research Center, Academic Medical Center, University of Amsterdam, Amsterdam,
The Netherlands
and

Department of Anatomy, Embryology and Physiology, Academic Medical Center, University of
Amsterdam, Meibergdreef 15, 1105 AZ Amsterdam, The Netherlands
e-mail: a.o.verkerk@amc.uva.nl

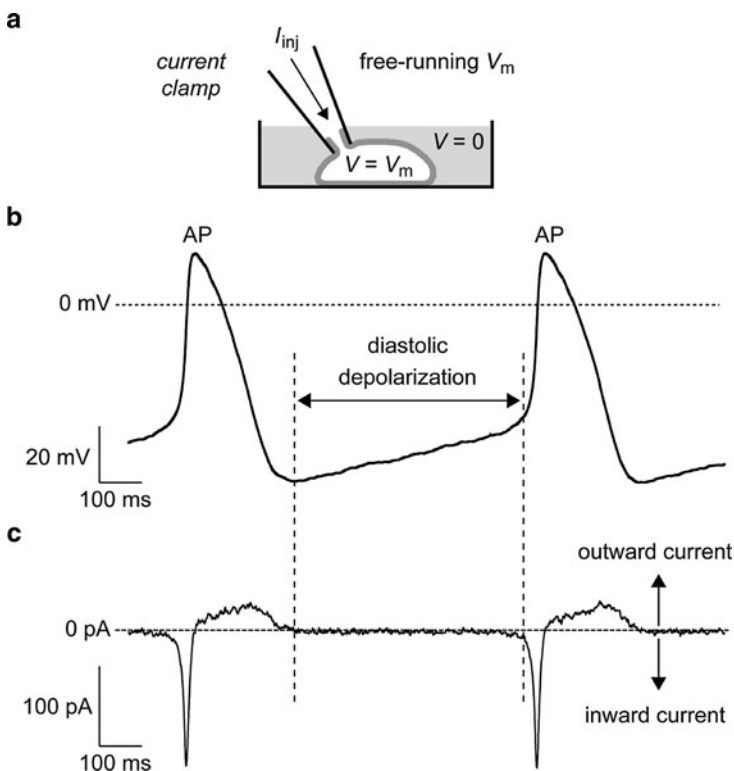


Fig. 5.1 Electrical activity of a human sinoatrial node (SAN) pacemaker cell. (a) Experimental configuration: whole-cell patch-clamp configuration in current-clamp mode with free-running transmembrane potential (V_m) and zero injected current (I_{inj}). (b) Typical action potentials (APs) of an isolated human SAN pacemaker cell with a membrane capacitance (C_m) of 52 pF. (c) Associated net membrane current (I_{net}) calculated from $I_{net} = -C_m \times dV_m/dt$. Note the small net inward current underlying diastolic depolarization

activation, recovery from inactivation, reversal potential, and the time constants of activation and deactivation) and the voltage range of DD. For example, the relatively negative half-maximum activation voltage and relatively slow activation kinetics of I_f have traditionally raised questions as to its functional significance in adult primary SAN cell pacemaking (see [5] and primary references cited therein).

Furthermore, single SAN cells display a large variety of AP waveforms, discharge irregularly, and have intrinsically different rhythms [2, 6]. For the SAN to maintain a stable and regular discharge pattern, individual cells have to interact electrically such that their activation times are synchronized, producing APs at a regular rate [7]. The mechanism by which SAN cells, with different intrinsic rates of spontaneous activity, maintain this synchronization has been the subject of numerous studies.

In this chapter, we first describe the “dynamic-clamp” technique and subsequently demonstrate how this technique can provide insights into (1) the role of

membrane currents, and especially I_f , in SAN pacemaker activity, and (2) the role of intercellular coupling current in SAN pacemaker synchronization.

5.2 Dynamic-Clamp Methodology

In today's cardiac cellular electrophysiology, patch-clamp is the common technique to record the electrical activity of single cells. In this section, we discuss the well-known recording modes of the whole-cell patch-clamp configuration, i.e., current-clamp, voltage-clamp, and AP-clamp, as well as "dynamic-clamp", a technique less well-known to cardiac electrophysiologists.

5.2.1 Current-Clamp and Voltage-Clamp

Traditionally, the main recording modes of the whole-cell patch-clamp configuration are current-clamp (Fig. 5.1a) and voltage-clamp (Fig. 5.2a). In either case, the bath solution is grounded to earth, as indicated by "V = 0" in Fig. 5.1a. In current-clamp mode, the free-running membrane potential of the cell (V_m) is recorded (Fig. 5.1a). When recording from SAN cells, spontaneous APs, as in Fig. 5.1b, can be acquired. In the voltage-clamp mode, V_m is held at a set level through a feedback circuit in the patch-clamp amplifier. Consequently, there is no (dis) charging of the cell membrane capacitance and the current that enters the cell through the recording pipette (I_{inj}) matches the current that leaves the cell through its membrane (I_m) (Fig. 5.2a). This way, ion current densities and gating properties can be studied under carefully controlled conditions, applying dedicated voltage-clamp protocols.

Figure 5.2 shows data from typical whole-cell voltage-clamp experiments carried out on HEK-293 cells expressing HCN4 channels. In SAN, HCN4 is the dominant isoform of the hyperpolarization-activated cyclic nucleotide-modulated (HCN) gene family [3, 5], which encodes the ion channels that conduct I_f . Figure 5.2b shows representative HCN4 current recordings. The average current-voltage relationship of the steady-state HCN4 current at the end of the 6-s hyperpolarizing steps is shown in Fig. 5.2c. The amplitude of the tail current immediately following the 6-s hyperpolarizing step reflects the amount of channels that activated during the preceding hyperpolarizing step. To characterize the voltage dependence of activation of the HCN4 current, we therefore plotted the normalized tail current amplitude versus the preceding hyperpolarizing potential (Fig. 5.2d). A mono-exponential fit to the current traces revealed the HCN4 activation time constant (Fig. 5.2g, closed symbols). The HCN4 current deactivation kinetics and reversal potential were studied as illustrated in Fig. 5.2e, resulting in the normalized fully-activated current of Fig. 5.2f and the deactivation time constant, obtained from mono-exponential fits, of Fig. 5.2g (open symbols).

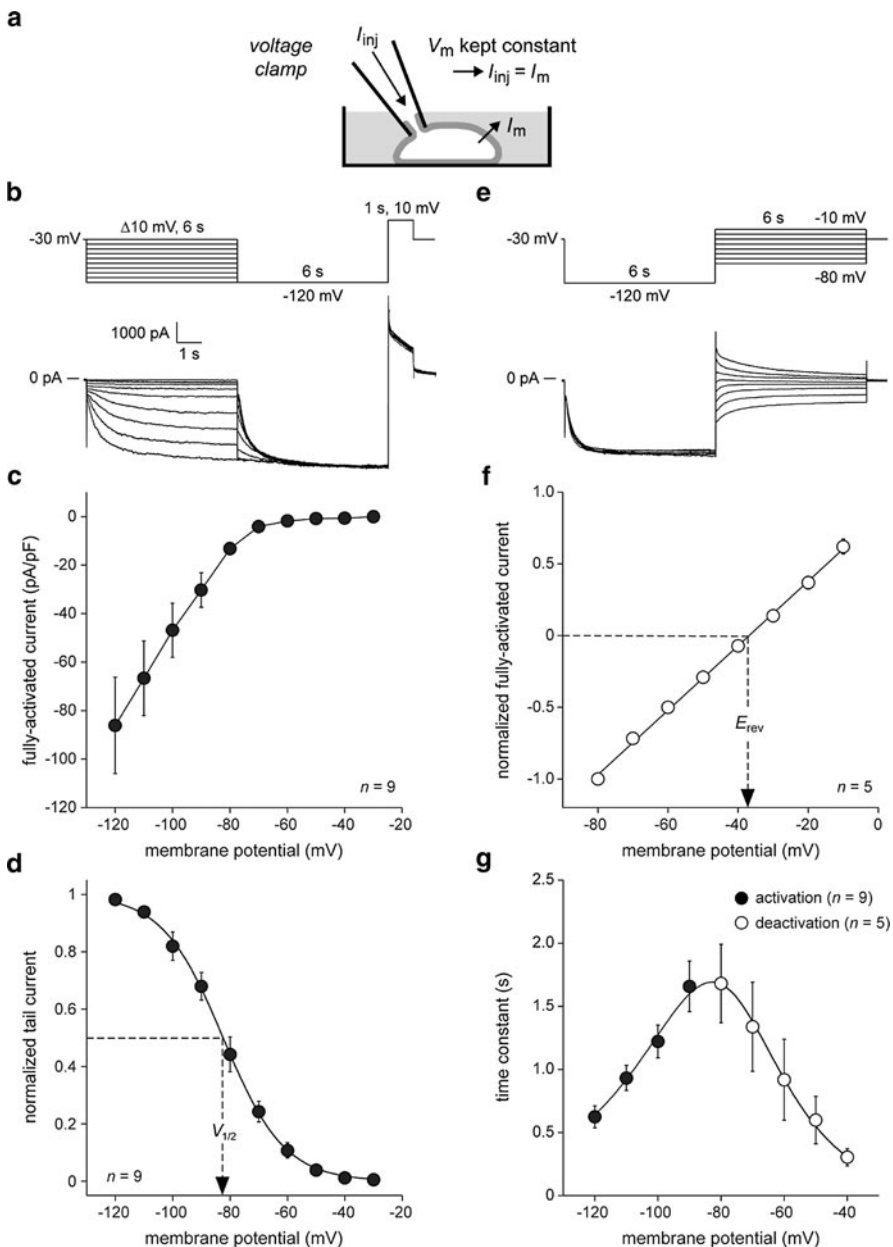


Fig. 5.2 Voltage-clamp recordings of HCN4 current expressed in HEK-293 cells. (a) Experimental configuration: whole-cell patch-clamp configuration in voltage-clamp mode with the transmembrane potential (V_m) held at constant preset levels through injection of a current (I_{inj}) that cancels the membrane current (I_m). (b) Voltage pulse protocol to measure activation properties (top) and typical HCN4 current traces in response to this protocol (bottom). (c) Average current–voltage relationship of steady-state HCN4 current at the end of the hyperpolarizing steps. Currents are normalized to cell

Thus, voltage-clamp experiments are useful to determine biophysical properties of specific ion channels. However, despite detailed knowledge of kinetic properties, contribution of a specific ion channel to the electrical activity of cardiac cells still might be difficult to predict. For example, the intrinsically slow activation kinetics and negative activation profile of I_f /HCN4 current (Fig. 5.2), relative to the time scale and voltage range of DD in the SAN (Fig. 5.1b), have led to the questioning of the role of I_f in SAN pacemaker activity (see [5] and primary references cited therein). As for other ion channels, pharmacological tools and mathematical models of cardiac cells (see Chap. 2 by Himeno et al.) have been used to elucidate the functional role of I_f . However, specific blockers with blocking effects in the complete voltage range of I_f are lacking. In addition, despite advances in mathematical modeling, the role of I_f in SAN pacemaker formation revealed with mathematical models remains obscure, as illustrated by the 0.9–30% increase in cycle length upon blockade of I_f in the various rabbit SAN cell models [8].

5.2.2 Action Potential-Clamp Technique

A refinement of voltage-clamp is the “action potential-clamp” technique (Fig. 5.3a). Instead of the traditional step protocols (cf. Fig. 5.2b and e), a pre-recorded AP waveform is used as voltage-clamp command potential (cf. Fig. 5.3b), as first applied to SAN cells by Doerr et al. [9]. The current in response to a voltage-clamp command potential with the shape of an AP then reflects the behavior of particular channels during that AP.

Figure 5.3c shows a typical example of AP-clamp recordings of HCN4 current. With the availability of HEK-293 cells expressing HCN4 channels (Fig. 5.2), it is possible to record the HCN4 current that would flow during a prerecorded SAN AP. We used the Wilders et al. [10] rabbit SAN cell model with I_f set to zero to generate an AP waveform and, in a 10-s run, continuously applied this waveform to the HEK-293 cell as voltage-clamp command potential (Fig. 5.3b). Figure 5.3c shows the associated HCN4 current recorded from the HEK-293 cell. There are several differences between the recorded HCN4 current (Fig. 5.3c) and I_f of SAN cell

Fig. 5.2 (continued) membrane capacitance. (d) Voltage dependence of HCN4 current activation. *Solid line*: Boltzmann fit to the data, with a half-maximum activation voltage ($V_{1/2}$) and slope factor of -87.7 ± 2.4 and 11.5 ± 2.4 mV (mean \pm SEM, $n = 9$), respectively. (e) Voltage pulse protocol to measure deactivation properties (top) and typical HCN4 current traces in response to this protocol (bottom). (f) Current–voltage relationship of the fully-activated HCN4 current at the beginning of the depolarizing steps. *Solid line*: linear fit to the data normalized to the value at -80 mV, with a reversal potential (E_{rev}) of -36.8 ± 1.0 mV ($n = 5$). (g) Time constants of (de)activation. *Bell-shaped curve*: fit to the data according to $\tau = 1/[A_1 \times \exp(-V_m/B_1) + A_2 \times \exp(V_m/B_2)]$, where τ is the (de)activation time constant, V_m is membrane potential, and A_1 , A_2 , B_1 , and B_2 are fitting parameters

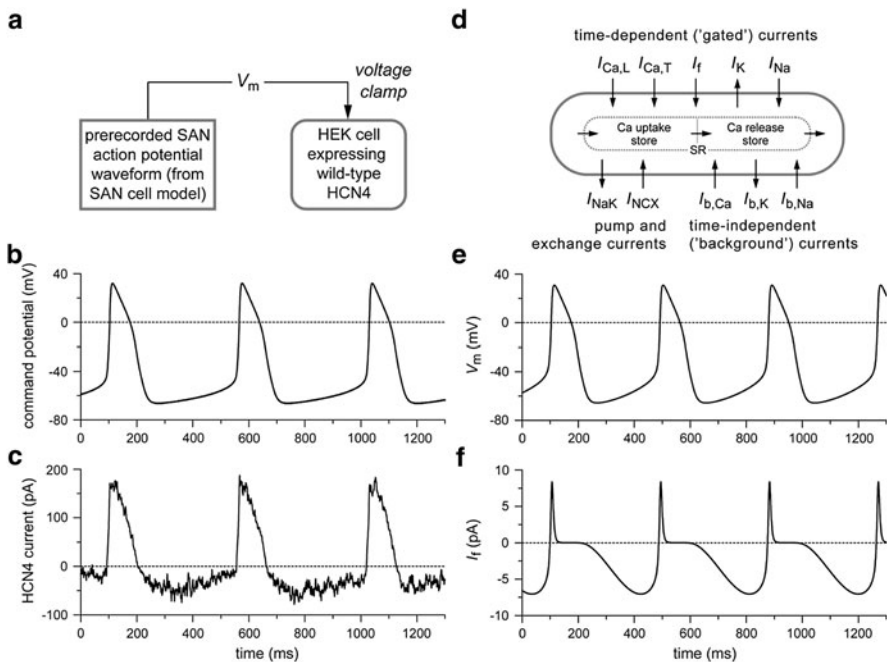


Fig. 5.3 Traditional AP-clamp experiment with a HEK-293 cell expressing HCN4 channels. (a) Experimental configuration. (b) SAN AP waveform of the Wilders et al. [10] SAN cell model with hyperpolarization-activated “funny current” (I_f) set to zero, applied to the HEK-293 cell as voltage-clamp command potential. (c) HCN4 current recorded from the HEK-293 cell. (d) Diagram of the Wilders et al. [10] SAN cell model. In addition to the currents mentioned in Sect. 5.1, the model contains small background Ca^{2+} and K^+ currents ($I_{b,\text{Ca}}$ and $I_{b,\text{K}}$, respectively). (e) AP and (f) associated I_f of the Wilders et al. [10] SAN cell model with default I_f setting

models. For example, Fig. 5.3e, f shows spontaneous APs and associated I_f of a rabbit SAN cell, according to the mathematical model of such cells by Wilders et al. [10] (Fig. 5.3d). In this model, I_f is computed from the Hodgkin and Huxley-type kinetic scheme described by van Ginneken and Giles [11], based on their voltage-clamp data on I_f obtained from rabbit SAN cells. The most striking differences between the recorded HCN4 current and calculated I_f are that the HCN4 current has a large outward component, partly due to the more negative reversal potential of the HCN4 current (-43 mV in this particular cell, compared to -24 mV for the model I_f), and is available early during DD. Interestingly, the more pronounced outward component and early availability during diastole are in agreement with AP-clamp data from rabbit SAN cells by Zaza et al. [12], who studied I_f as the current sensitive to $2\text{ mM } \text{Cs}^+$, and our recent numerical reconstructions of I_f in human SAN cells [5, 13, 14].

Although there are differences between HCN4 current recorded from HEK-293 cells and I_f recorded from freshly isolated rabbit SAN cells [15], the experiment of Fig. 5.3 underscores the importance of carrying out AP-clamp experiments in

addition to traditional voltage-clamp experiments and computer simulations. However, despite the demonstration by AP-clamp that HCN4 current may flow both during DD and AP, the net effect of the HCN4 current on DD and AP is not known. This is where dynamic-clamp, and especially the dynamic AP-clamp technique, can provide a direct and unambiguous answer.

5.2.3 *Dynamic-Clamp*

Dynamic-clamp is a collection of closely related electrophysiological tools to add artificial membrane, synaptic, or gap junctional conductances to the free-running membrane conductance of neurons or cardiac cells. In cardiac electrophysiology, it is used to provide direct answers to numerous research questions regarding basic cellular mechanisms of AP formation, AP transfer, and AP synchronization in health and disease (see reviews by Goaillard and Marder [16] and Wilders [17], and the comprehensive book edited by Destexhe and Bal [18]). In cardiac electrophysiology, the dynamic-clamp technique has been used in three different experimental configurations, i.e., “coupling-clamp”, “model-clamp”, and “dynamic AP-clamp” [17].

5.2.3.1 *Coupling-Clamp*

Originally, dynamic-clamp was used to electrically couple two cells, not in physical contact with each other, at any desired value of intercellular conductance by means of an analog external circuit that continuously applies time-varying currents to each cell with a sign and magnitude that would have been present if the cells had been physically coupled [19, 20]. Figure 5.4a illustrates how “coupling-clamp” is accomplished today, using a PC instead of the analog circuit. Electrical recordings are made from two freshly isolated cells, both in current-clamp mode, thus requiring two patch-clamp amplifiers. These cells can either be in one cell chamber on a single electrophysiological setup or in separate recording chambers on two different electrophysiological setups. The membrane potentials $V_{m,1}$ and $V_{m,2}$ of the two cells are sampled into a personal computer (PC). This computer then computes the coupling current I_c flowing from cell 1 to cell 2, based on $V_{m,1}$ and $V_{m,2}$, i.e.,

$$I_c = G_c \times (V_{m,1} - V_{m,2}), \quad (5.1)$$

where G_c is the intercellular coupling conductance, and sends command potentials to the amplifiers such that the appropriate current is injected into each of the cells, where it contributes to net membrane current and thus affects the membrane potential.

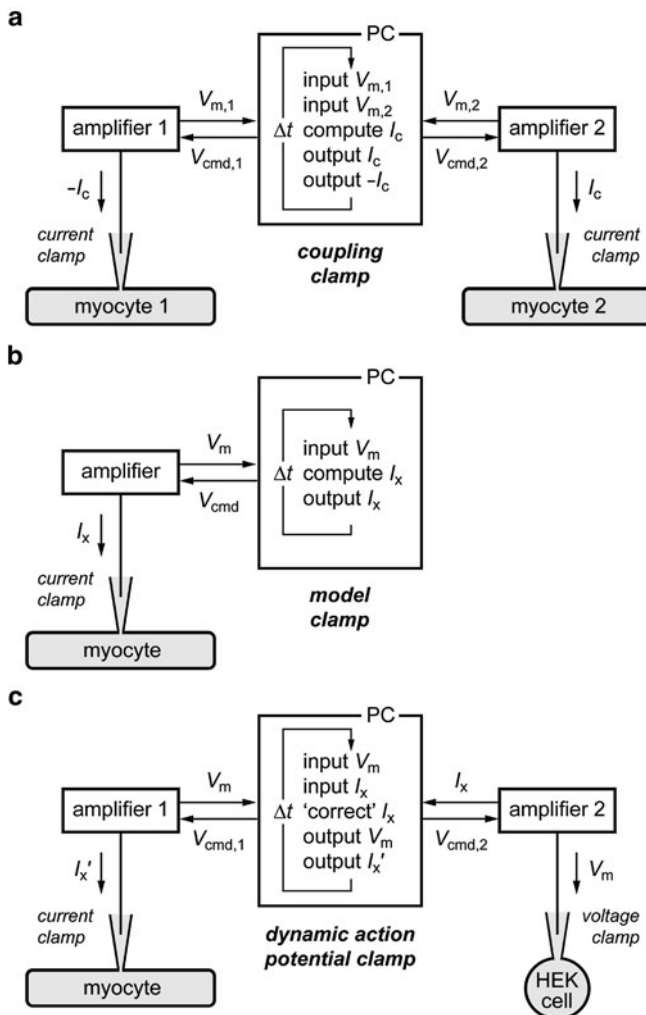


Fig. 5.4 Experimental design of dynamic-clamp experiments in cardiac cellular electrophysiology. (a) “Coupling-clamp” configuration. The membrane potentials of two isolated cells ($V_{m,1}$ and $V_{m,2}$), both in current-clamp mode, are sampled by a PC and a coupling current (I_c) is computed, based on $V_{m,1}$ and $V_{m,2}$. Command potentials (V_{cmd}) are then sent to the patch-clamp amplifiers to inject this current into the cells as additional membrane current via the recording patch pipettes. The time step for updating input and output values is Δt . (b) “Model-clamp” configuration. The free-running membrane potential of a single isolated cell in current-clamp mode (V_m) is sampled by a PC. An additional V_m -dependent membrane current (I_x) is computed and injected into the cell via the recording patch pipette. (c) “Dynamic AP-clamp” configuration. The free-running membrane potential of a single isolated cell is recorded in current-clamp mode and used to voltage-clamp a HEK-293 cell, in which a specific ion current is expressed. This ion current (I_x) is fed back to the PC and, after online “correction” (i.e., subtraction of endogenous background current of the HEK cell and appropriate scaling of the remaining current), injected into the cell as additional membrane current (I_x')

The coupling-clamp configuration of the dynamic-clamp technique has been used in studies of the modulation of AP conduction between two isolated guinea pig ventricular cells by $I_{Ca,L}$, electrotonic modulation of SAN pacemaker activity by atrial muscle, synchronization of SAN cells or atrioventricular node cells, interactions between Purkinje and ventricular cells, beat-to-beat repolarization variability in ventricular cells, and effects of transient outward current inhibition on conduction between ventricular cells (see [17] and primary references cited therein). In some of these studies, one of the real cells of Fig. 5.4a was replaced with an RC circuit as a model of an atrial or ventricular cell. An application of the coupling-clamp technique is shown in Sect. 5.4 below.

5.2.3.2 Model-Clamp

Model-clamp has been used to simulate the presence of an additional conductance in the membrane of a single isolated cell. In this configuration (Fig. 5.4b), the membrane potential V_m of the cell is continuously sampled by a PC, which calculates the V_m -dependent current I_x and sends a command potential to the amplifier to inject this current into the cell. This configuration has been referred to as “model clamp” [7], because a model-based current is injected into the cell.

The model-clamp configuration of Fig. 5.4b has been used to introduce a specific membrane current into cardiac cells, e.g., a stretch-activated current in rat atrial cells, an injury current flowing from normal myocardium to ischemic tissue in human and sheep ventricular cells, and a transient outward current in guinea pig and canine endocardial ventricular cells (see [17] and primary references cited therein). The current that is injected into a cell can also represent gap junctional current flow to a second cell, with both junctional current and the second cell simulated in real time (e.g., [7]). The geometry can even be made more complex with the real cell embedded in a virtual network of atrial or ventricular cells (e.g., [21]). The injected current is then the net current flowing between the real cell and the virtual cells to which it is connected.

A relatively simple application of the model-clamp technique is shown in Fig. 5.5, and is related to the question whether an artificial biological pacemaker (“bio-pacemaker”) can be created with gating-engineered HCN channels [22, 23]. Proof-of-principle experiments have demonstrated that overexpression of gating-engineered HCN channels with fast activation properties may convert quiescent ventricular cells into spontaneously active pacemaker-like cells [22, 23]. In Fig. 5.5, we simulated such an approach using the model-clamp methodology by which we were able to inject an ohmic current with a reversal potential of -20 mV, representing the reversal potential of HCN channels, and an adjustable conductance G_x into an isolated human ventricular cell (Fig. 5.5a; see [24] for cell and electrophysiological recording details). In the absence of simulated HCN current, the ventricular cell stimulated at 0.5 Hz had a resting potential of approximately -80 mV and AP duration of approximately 800 ms (Fig. 5.5b). Upon the introduction of HCN current, the AP shortened and the resting potential depolarized, and these effects

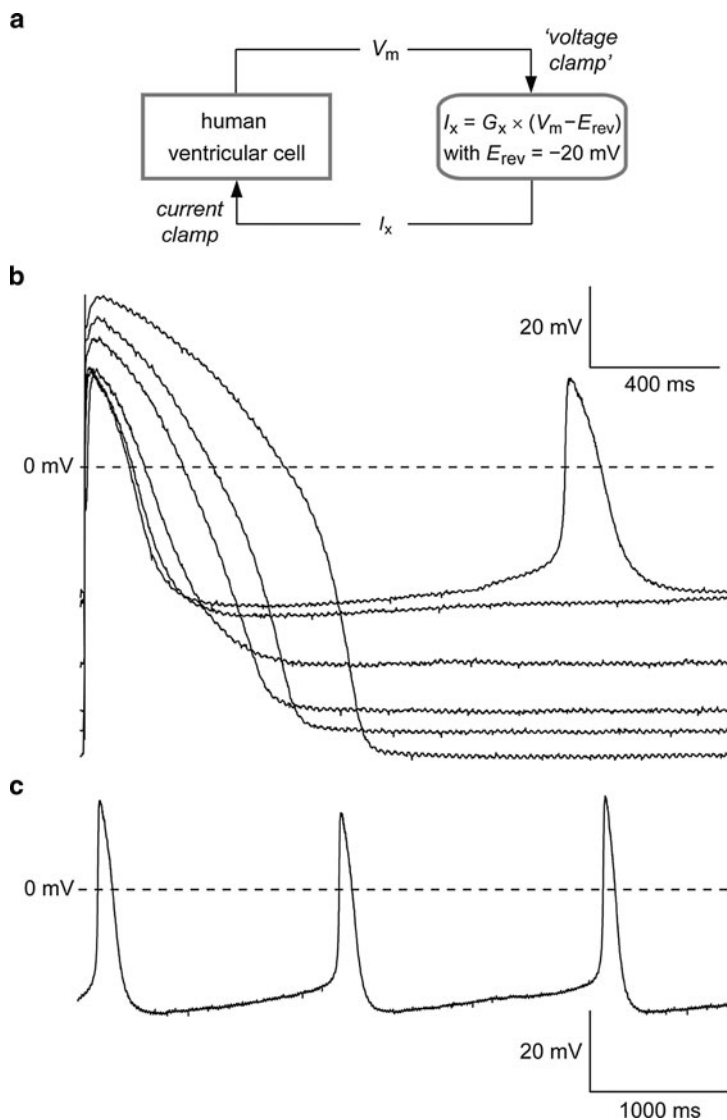


Fig. 5.5 Effect of simulated gating-engineered HCN channels with fast activation properties on human left ventricular APs. **(a)** Experimental configuration. The dynamic-clamp technique was used to inject a time-varying, ohmic current (I_x) with a user selectable conductance (G_x) and a reversal potential (E_{rev}) of -20 mV into an isolated human left ventricular cell. **(b)** Superimposed APs of the cell, recorded at six different values of G_x . The cell was stimulated at 0.5 Hz. **(c)** APs of the cell at high G_x in nonstimulated conditions

increased with increasing HCN currents, i.e., with increasing G_x . At a resting membrane potential of approximately -30 mV, the cell started to show a slow DD, which resulted in a spontaneous AP (Fig. 5.5b). Interestingly, after switching

off the 0.5-Hz stimulation, the cell showed slow, but regular spontaneous activity (Fig. 5.5c), suggesting that gating-engineered HCN channels may be suitable for pacemaker formation also in human tissue.

5.2.3.3 Dynamic AP-Clamp

As a novel application of dynamic-clamp, we recently developed the “dynamic AP-clamp” technique, which we used to study the effects of ion channel mutations by effectively replacing a native ionic current of a cardiac cell with wild-type or mutant current expressed in HEK-293 cells [17, 25]. Dynamic AP-clamp differs from traditional dynamic-clamp and AP-clamp in that it combines current-clamp, as used in dynamic-clamp, and voltage-clamp, as used in AP-clamp.

The diagram of Fig. 5.4c illustrates the concept of dynamic AP-clamp. Wild-type or mutant channels are expressed in HEK-293 cells, and measured in voltage-clamp mode. This time, however, the voltage-clamp command potential is not a distinct voltage-clamp step or prerecorded AP but the free-running membrane potential of a freshly isolated, patch-clamped ventricular cell (or cell model), with the native current of interest blocked by a pharmacological agent (or set to zero in case of a model cell). The measured HEK-293 cell current is injected into the ventricular cell in real time. Thus, there is continuous feedback between AP and expressed current. The wild-type or mutant channels are allowed to follow the natural time course of the ventricular AP (through the voltage-clamp), upon being simultaneously allowed to contribute current for the generation of this AP as if they were incorporated into the membrane of the cell (through injection of the expressed current into the current-clamped cell).

The dynamic AP-clamp technique has been used to study the effects of mutant channels in the long-QT syndrome types 2 [26] and 3 [27], and to mimic the gene therapy strategy to create a bio-pacemaker by downregulation of the inward rectifier current (I_{K1}) and (over)expression of I_f [13, 28]. A recent application of the dynamic AP-clamp technique is shown in Sect. 5.3 below.

5.3 Role of I_f in SAN Pacemaker Activity Studied with Dynamic-Clamp Methodology

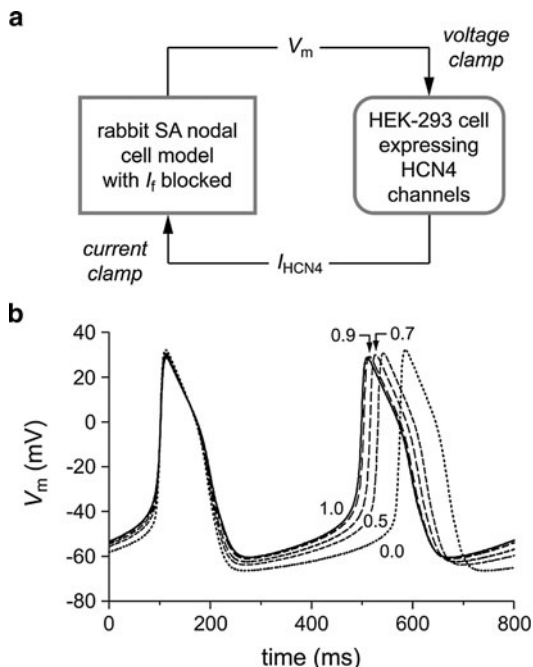
As mentioned in Sect. 5.1, the net inward current responsible for the DD phase in SAN cells (Fig. 5.1) is the result of a complex interaction of multiple inwardly and outwardly directed ion currents [1–4]. Despite a large body of experimental data from voltage-clamp experiments, the contribution of I_f to pacemaker activity in the adult SAN is still controversial and not fully established. I_f has been proposed as the principal pacemaker current [29], while this role has been questioned in other studies which assign only a minor role, if any, of I_f in generation of SAN pacemaker

depolarization [1, 30–35]. The continuing debate on the physiologic significance of I_f in SAN pacemaking is strongly related to the intrinsically slow activation kinetics and negative activation profile of I_f relative to the time scale and voltage range of DD in the SAN.

The AP-clamp experiment of Fig. 5.3 reveals the HCN4 current that would flow during the prerecorded SAN AP of Fig. 5.3b. However, it does not show how this current modulates the SAN AP. Therefore, we carried out a dynamic AP-clamp experiment with an HCN4-transfected HEK-293 cell in combination with the Wilders et al. [10] model of a rabbit SAN pacemaker cell with its native I_f set to zero, as illustrated here in Fig. 5.6 and published elsewhere in the context of engineering a gene-based biological pacemaker [13, 28].

In the Wilders et al. [10] model, as in other (rabbit) SAN cell models [8], the cycle length increases significantly upon blockade of I_f , mainly due to a decrease in the rate of DD. Figure 5.6a depicts a simplified diagram of Fig. 5.4c. As diagrammed in Fig. 5.6a, we used the AP of the model cell – with its I_f set to zero – to voltage-clamp the HEK-293 cell and fed the recorded HCN4 current back into the current-clamped model cell, thus establishing the dynamic AP-clamp configuration. Given the large HCN4 currents expressed in HEK-293 cells (Fig. 5.2), we applied scaling factors of 0.0–1.0% to the recorded HCN4 current before adding it to the model. Any endogenous current included in the current recorded from the

Fig. 5.6 Dynamic AP-clamp experiment with real-time simulation of a SAN pacemaker cell and a HEK-293 cell expressing HCN4 channels. (a) Experimental configuration. A SAN pacemaker cell is simulated in real time using the Wilders et al. [10] model of a rabbit SAN cell. I_f of the model cell was set to zero and replaced with HCN4 current recorded from the HEK-293 cell (I_{HCN4}). (b) Effect of adding increasing amounts of HCN4 current to the SAN cell with its native I_f set to zero. A scaling factor of 0.0, 0.5, 0.7, 0.9, or 1.0%, as indicated by numbers near traces, was applied to the HCN4 current recorded from the HEK-293 cell



HEK-293 cell [36, 37] is then also scaled down, so that this endogenous current becomes negligible. With the scaling factor set to zero (Fig. 5.6b, dotted line labeled “0.0”), the resulting AP is identical to that of the model cell with its I_f set to zero (Fig. 5.3b). With a scaling factor of 1.0% (Fig. 5.6b, solid line labeled “1.0”), the cycle length shortens and becomes almost identical to that of the original model with its default I_f (Fig. 5.3e). Intermediate shortening occurs with intermediate values for the scaling factor (Fig. 5.6b, dashed lines labeled “0.5”, “0.7”, and “0.9”).

The data of Fig. 5.6 indicate that the HCN4 current can functionally, in terms of modulating pacemaker frequency, replace the native I_f . However, unlike I_f , increasing the HCN4 current not only increases the rate of DD, but also clearly depolarizes the maximum diastolic potential (MDP) to less negative values. This emphasizes that the kinetics of HCN4 channels need not be identical to those of native I_f channels [15] and that HCN4 channels should not simply be regarded as a replacement of I_f “pacemaker channels” in gene therapy strategies. In addition, it stresses that the behavior of HCN4 channels is more complex than reflected in the description of I_f in currently available SAN cell models [8]. A caveat is that the depolarization of the MDP may, at least to some extent, be due to inward “leakage current” of the HEK-293 cell, although the scaling factor of 0.01 or less also applies to this current.

5.4 SAN Cell Synchronization Studied with Dynamic-Clamp Methodology

In the intact SAN, synchronization of the activation of electrically coupled, spontaneously pacing cells is a required attribute of normal AP initiation. However, individual isolated SAN cells display a large variety in AP waveforms and have irregular firing patterns, with a varying cycle length [2, 6], most likely due to differences in the composition of the set of membrane currents [2]. For the SAN to maintain a stable and regular discharge pattern, individual cells have to interact electrically such that their activation times are synchronized, producing APs at a regular rate. The mechanisms by which SAN cells with different intrinsic rates of automaticity maintain this synchronization has been the subject of numerous studies using a variety of experimental and model systems.

The mutual entrainment of rabbit SAN cells has been studied in the isolated node that was “partly divided into two parts by a cut in the middle portion” [38] and in thin SAN strips using the “sucrose gap” technique [39, 40]. The latter studies demonstrated that SAN strips with the central region of the strip sealed off in a compartment containing either ion-free sucrose solution or perfusion solution containing heptanol showed synchronization of the proximal and distal regions of the strand after electrical coupling had been established. Several attempts have been made to estimate the minimal amount of coupling conductance required for SAN

pacemaker synchronization. Anumonwo et al. [41] observed a single-channel junctional conductance of ≈ 50 pS in real SAN cell pairs. Using this value, they estimated that approximately three gap junction channels between the cells would allow pacemaker synchronization. In a model study, Cai et al. [42] determined that approximately four 50-pS gap junction channels are required for frequency entrainment. In addition, using a freshly isolated SAN cell and a SAN model in the model-clamp configuration, we showed that the critical amount of coupling depends on the difference in the intrinsic interbeat interval of both cells [7]. At an interbeat interval difference of $\approx 10\%$, the critical coupling conductance became as low as 75 pS.

In Figure 5.7, we show data of a coupling-clamp experiment with two real, freshly isolated SAN cells [43]. The cells were simultaneously studied in two

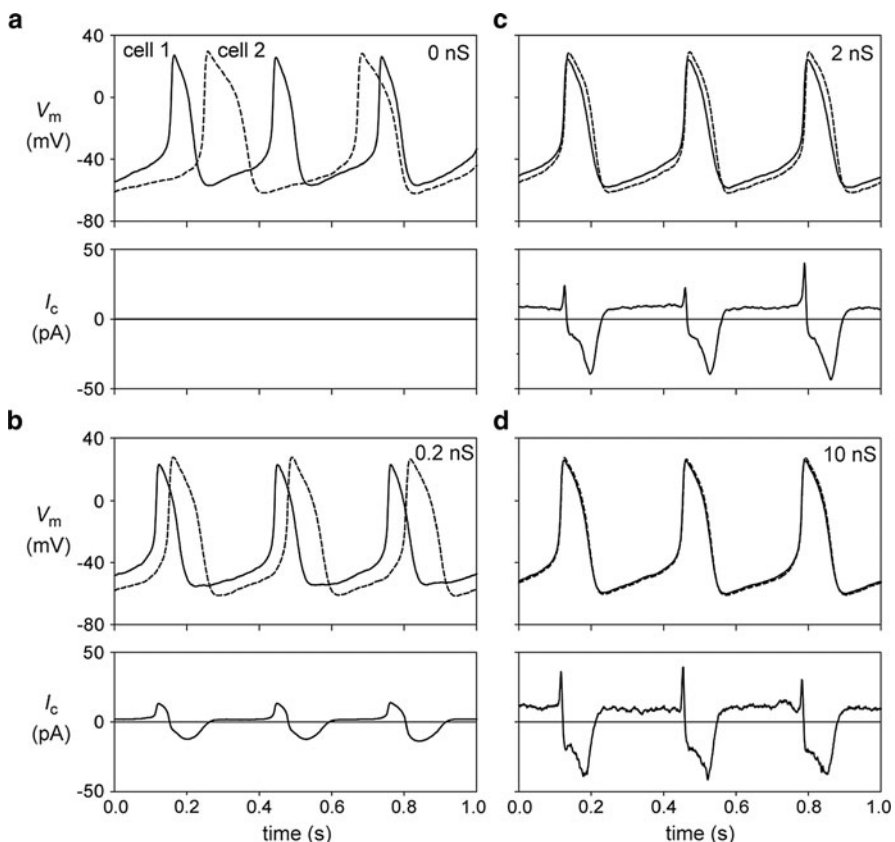


Fig. 5.7 Mutual synchronization of two adult pacemaker cells isolated from the rabbit SAN. The coupling-clamp configuration of Fig. 5.4a was used to introduce an ohmic coupling conductance of 0–10 nS between the two cells, thus simulating gap junctional conductance. Membrane potential of the two cells (V_m) and coupling current flowing in the direction from cell 1 to cell 2 (I_c). Data from Verheijck et al. [43]. (a) Cells not coupled. (b) Cells coupled by 0.2 nS. (c) Cells coupled by 2 nS. (d) Cells coupled by 10 nS

separate microscope setups, thus precluding any electrical contact between the cells except that provided by the coupling circuit. Figure 5.7 shows simultaneous recordings from the two amphotericin-perforated patch-clamped SAN cells, with the membrane potential recordings of the two cells distinguished by a solid (for cell 1) or dashed (for cell 2) line. If uncoupled (Fig. 5.7a; zero coupling conductance), APs of the two cells are clearly different in shape, with the spontaneous activity of cell 1 occurring at a shorter interbeat interval (310 ms) than the spontaneous activity of cell 2 (390 ms). The coupling current is, of course, zero (Fig. 5.7a, bottom).

Figure 5.7b–d shows data from the same two cells, using coupling conductance values of 0.2 nS (Fig. 5.7b), 2 nS (Fig. 5.7c), and 10 nS (Fig. 5.7d). Already at 0.2 nS, equivalent to the conductance of only a few gap junctional channels, a stable pattern of entrainment of APs of cells 1 and 2 is established. Both at 0.2 and 2 nS, the APs of cells 1 and 2 are entrained at a common interbeat interval, but the shapes of the APs are still different for cell 1 and cell 2, with cell 2 retaining a more negative MDP and a longer AP duration (APD): the cells show “frequency entrainment”, but not “waveform entrainment”. Upon further increasing coupling conductance to 10 nS (Fig. 5.7d), the APs of cells 1 and 2 become nearly synchronous, with nearly identical AP shapes: the cells now show both frequency and waveform entrainment. The common interbeat interval is 333 ms, which is closer to that of the faster beating cell, as expected on theoretical grounds [43]. The coupling current, which is plotted as a positive current in the direction from cell 1 to cell 2, increases in magnitude from Fig. 5.7b to Fig. 5.7c to Fig. 5.7d as the coupling conductance increases, but not in a linear fashion because it is not only dependent on coupling conductance but also on driving force, i.e., the difference in membrane potential between the two cells (cf. (5.1)), which decreases with increasing coupling conductance. There is a significant negative component of coupling current (flowing from cell 2 to cell 1) due to the intrinsically longer APD of cell 2. During DD, a sustained “tonic” component of coupling current is flowing from cell 1 to cell 2.

5.5 Conclusion

In this chapter we have shown that the dynamic-clamp technique, including further refinements (dynamic AP-clamp technique), is a very powerful electrophysiological technique which can provide important insights into the ionic mechanisms underlying intrinsic pacemaker activity of SAN cells and pacemaker cell synchronization. Without making assumptions with regard to kinetic properties of HCN4 channels, we demonstrate that HCN4 current can contribute not only to SAN DD but also to the SAN AP. In addition, we show that at low coupling conductance, mutual pacemaker synchronization results mainly from the phase-resetting effects of the AP of one cell on the depolarization phase of the other, whereas at higher coupling conductance the tonic, diastolic interaction prevails.

References

1. Irisawa H, Brown HF, Giles W. Cardiac pacemaking in the sinoatrial node. *Physiol Rev.* 1993;73:197–227.
2. Boyett MR, Honjo H, Kodama I. The sinoatrial node, a heterogeneous pacemaker structure. *Cardiovasc Res.* 2000;47:658–87.
3. Dobrzynski H, Boyett MR, Anderson RH. New insights into pacemaker activity: promoting understanding of sick sinus syndrome. *Circulation.* 2007;115:1921–32.
4. Mangoni ME, Nargeot J. Genesis and regulation of the heart automaticity. *Physiol Rev.* 2008;88:919–82.
5. Verkerk AO, van Ginneken ACG, Wilders R. Pacemaker activity of the human sinoatrial node: role of the hyperpolarization-activated current, I_f . *Int J Cardiol.* 2009;132:318–36.
6. Wilders R, Jongasma HJ. Beating irregularity of single pacemaker cells isolated from the rabbit sinoatrial node. *Biophys J.* 1993;65:2601–13.
7. Wilders R, Verheijck EE, Kumar R, Goolsby WN, van Ginneken ACG, Joyner RW, et al. Model clamp and its application to synchronization of rabbit sinoatrial node cells. *Am J Physiol.* 1996;271:H2168–82.
8. Wilders R. Computer modelling of the sinoatrial node. *Med Biol Eng Comput.* 2007;45:189–207.
9. Doerr T, Denger R, Trautwein W. Calcium currents in single SA nodal cells of the rabbit heart studied with action potential clamp. *Pflügers Arch.* 1989;413:599–603.
10. Wilders R, Jongasma HJ, van Ginneken ACG. Pacemaker activity of the rabbit sinoatrial node: a comparison of mathematical models. *Biophys J.* 1991;60:1202–16.
11. van Ginneken ACG, Giles W. Voltage clamp measurements of the hyperpolarization-activated inward current I_f in single cells from rabbit sino-atrial node. *J Physiol.* 1991;434:57–83.
12. Zaza A, Micheletti M, Brioschi A, Rocchetti M. Ionic currents during sustained pacemaker activity in rabbit sino-atrial myocytes. *J Physiol.* 1997;505:677–88.
13. Verkerk AO, Zegers JG, van Ginneken ACG, Wilders R. Dynamic action potential clamp as a powerful tool in the development of a gene-based bio-pacemaker. *Conf Proc IEEE Eng Med Biol Soc.* 2008;1:133–6.
14. Verkerk AO, Wilders R. Relative importance of funny current in human versus rabbit sinoatrial node. *J Mol Cell Cardiol.* 2010;48:799–801.
15. Altomare C, Terragni B, Brioschi C, Milanesi R, Pagliuca C, Visconti C, et al. Heteromeric HCNI–HCN4 channels: a comparison with native pacemaker channels from the rabbit sinoatrial node. *J Physiol.* 2003;549:347–59.
16. Goillard J-M, Marder E. Dynamic clamp analyses of cardiac, endocrine, and neural function. *Physiology.* 2006;21:197–207.
17. Wilders R. Dynamic clamp: a powerful tool in cardiac electrophysiology. *J Physiol.* 2006;576:349–59.
18. Destexhe A, Bal T, editors. *Dynamic-clamp: from principles to applications.* New York: Springer; 2009.
19. Tan RC, Joyner RW. Electrotonic influences on action potentials from isolated ventricular cells. *Circ Res.* 1990;67:1071–81.
20. Joyner RW, Sugiyama H, Tan RC. Unidirectional block between isolated rabbit ventricular cells coupled by a variable resistance. *Biophys J.* 1991;60:1038–45.
21. Joyner RW, Wang YG, Wilders R, Golod DA, Wagner MB, Kumar R, et al. A spontaneously active focus drives a model atrial sheet more easily than a model ventricular sheet. *Am J Physiol Heart Circ Physiol.* 2000;279:H752–63.
22. Tse HF, Xue T, Lau CP, Siu CW, Wang K, Zhang QY, et al. Bioartificial sinus node constructed via *in vivo* gene transfer of an engineered pacemaker HCN channel reduces the dependence on electronic pacemaker in a sick-sinus syndrome model. *Circulation.* 2006;114:1000–11.

23. Xue T, Siu CW, Lieu DK, Lau CP, Tse HF, Li RA. Mechanistic role of I_f revealed by induction of ventricular automaticity by somatic gene transfer of gating-engineered pacemaker (HCN) channels. *Circulation*. 2007;115:1839–50.
24. Verkerk AO, Veldkamp MW, de Jonge N, Wilders R, van Ginneken ACG. Injury current modulates after depolarizations in single human ventricular cells. *Cardiovasc Res*. 2000;47: 124–32.
25. Berecki G, Zegers JG, Wilders R, van Ginneken ACG. Cardiac channelopathies studied with the dynamic action potential-clamp technique. *Methods Mol Biol*. 2007;403:233–50.
26. Berecki G, Zegers JG, Verkerk AO, Bhuiyan ZA, de Jonge B, Veldkamp MW, et al. HERG channel (dys)function revealed by dynamic action potential clamp technique. *Biophys J*. 2005;88:566–78.
27. Berecki G, Zegers JG, Bhuiyan ZA, Verkerk AO, Wilders R, van Ginneken ACG. Long-QT syndrome-related sodium channel mutations probed by the dynamic action potential clamp technique. *J Physiol*. 2006;570:237–50.
28. Verkerk AO, Zegers JG, van Ginneken ACG, Wilders R. Development of a genetically engineered cardiac pacemaker: insights from dynamic action potential clamp experiments. In: Destexhe A, Bal T, editors. *Dynamic-clamp: from principles to applications*. New York: Springer; 2009. p. 399–415.
29. DiFrancesco D. Serious workings of the funny current. *Prog Biophys Mol Biol*. 2006;90: 13–25.
30. Noma A, Morad M, Irisawa H. Does the “pacemaker current” generate the diastolic depolarization in the rabbit SA node cells? *Pflügers Arch*. 1983;397:190–4.
31. Vassalle M. The pacemaker current (I_f) does not play an important role in regulating SA node pacemaker activity. *Cardiovasc Res*. 1995;30:309–10.
32. Lipsius SL, Hüser J, Blatter LA. Intracellular Ca^{2+} release sparks atrial pacemaker activity. *News Physiol Sci*. 2001;16:101–6.
33. Herrmann S, Stieber J, Stöckl G, Hofmann F, Ludwig A. HCN4 provides a ‘depolarization reserve’ and is not required for heart rate acceleration in mice. *EMBO J*. 2007;26:4423–32.
34. Harzheim D, Pfeiffer KH, Fabritz L, Kremmer E, Buch T, Waisman A, et al. Cardiac pacemaker function of HCN4 channels in mice is confined to embryonic development and requires cyclic AMP. *EMBO J*. 2008;27:692–703.
35. Maltsev VA, Lakatta EG. Funny current provides a relatively modest contribution to spontaneous beating rate regulation of human and rabbit sinoatrial node cells. *J Mol Cell Cardiol*. 2010;48:804–6.
36. Yu SP, Kerchner GA. Endogenous voltage-gated potassium channels in human embryonic kidney (HEK293) cells. *J Neurosci Res*. 1998;52:612–7.
37. Jiang B, Sun X, Cao K, Wang R. Endogenous K_v channels in human embryonic kidney (HEK-293) cells. *Mol Cell Biochem*. 2002;238:69–79.
38. Sano T, Sawanobori T, Adaniya H. Mechanism of rhythm determination among pacemaker cells of the mammalian sinus node. *Am J Physiol*. 1978;235:H379–84.
39. Jalife J. Mutual entrainment and electrical coupling as mechanisms of synchronous firing of rabbit sino-atrial pace-maker cells. *J Physiol*. 1984;356:221–43.
40. Delmar M, Jalife J, Michaels DC. Effects of changes in excitability and intercellular coupling on synchronization in the rabbit sino-atrial node. *J Physiol*. 1986;370:127–50.
41. Anumonwo JMB, Wang H-Z, Trabka-Janik E, Dunham B, Veenstra RD, Delmar M, et al. Gap junctional channels in adult mammalian sinus nodal cells: immunolocalization and electrophysiology. *Circ Res*. 1992;71:229–39.
42. Cai D, Winslow RL, Noble D. Effects of gap junction conductance on dynamics of sinoatrial node cells: two-cell and large-scale networks. *IEEE Trans Biomed Eng*. 1994;41:217–31.
43. Verheijck EE, Wilders R, Joyner RW, Golod DA, Kumar R, Jongsma HJ, et al. Pacemaker synchronization of electrically coupled rabbit sinoatrial node cells. *J Gen Physiol*. 1998;111: 95–112.

Chapter 6

Heart Rate Variability: Molecular Mechanisms and Clinical Implications

Kishore K. Deepak

6.1 Introduction

Spontaneous oscillations in heart rate have been known for a long time and largely represent the variation with respiration (respiratory sinus arrhythmia, RSA). Lately, the interest in RSA and heart rate variability (HRV) has been augmented by a large number of studies to investigate the mechanism of sudden cardiac death and antiarrhythmic effect of mechanical stimulation (see Chap. 8: Mechano-electric Feedback in the Heart: Effect on Heart Rate and Rhythm). There has been an earnest desire to find out a reliable event predictor for sudden cardiac death. Digital signal processing technology has unraveled different types of variations that contain valuable information about control system.

HRV is an analysis of beat-to-beat variation in heart rate (i.e., in R–R intervals) under resting conditions. These beat-to-beat variations occur due to changes in the sympathetic and parasympathetic outflow to the heart. The variations are either quantified by simple statistical methods (time domain analysis) or by using computer algorithms to detect slow (low-frequency modulations) and fast (high-frequency modulations) changes occurring from beat to beat. HRV has been shown to be a good phenomenon that unravels the tonic drive of autonomic nervous system to the myocardium. It is influenced by several physiologic and disease conditions and also serves as a predictor for mortality after a first incidence of myocardial infarction (MI). HRV has been suggested as a bedside assessment procedure in both adults and children [1].

K.K. Deepak

Autonomic Function Laboratory, Department of Physiology, All India Institute of Medical Sciences, New Delhi, Delhi 110608, India
e-mail: kkdeepak@gmail.com

6.2 Heart Rate Variability as Indicator of Cardiac Autonomic Tone

The HRV spectrum shows parasympathetic modulation in the high-frequency (HF) range and the sympathetic modulation in the low-frequency (LF) range. This fact has been confirmed by a number of experiments. For example, vagotomy in decerebrated cats renders the HF peak to disappear suggesting that this peak is vagally mediated [2]. The concept was later reinforced by more studies in conscious dogs [3, 4]. Surprisingly, the pharmacologic blockade of vagal activity not only eliminated the power in the HF range, but it also reduced the power in LF range [3–6]. The LF peak that was supposed to be dependent on sympathetic activity was found to be mediated by both sympathetic and parasympathetic activity in canines and humans [3–5, 7]. In canine studies, total parasympathetic blockade was achieved with glycopyrrolate, and subsequent β -adrenergic blockade eliminated the residual LF fluctuations. Thus, it is believed that the LF is predominantly caused by sympathetic mediation. The LF:HF ratio is considered as a marker for sympathovagal drive to the myocardium. The evidence for “vagally mediated changes are faster” and “sympathetically mediated changes are slower” is substantial [8]. Parasympathetic nerve activity modulates heart rate on a beat-to-beat basis, while sympathetic nerve activity requires up to 20 s to elicit the effect [8].

The relationship between spectral components of HRV and direct measures of muscle sympathetic nerve activity has been studied in humans where there is a predominance of the LF oscillations of blood pressure, RR interval, and sympathetic nerve activity. During sympathetic inhibition, the HF component predominates [9]. Recently, the advent of newer technology has permitted measurement of plasma catecholamine and real time recording of concomitant HRV in the patients with pheochromocytoma undergoing laparoscopic removal of the tumor [10]. The study convincingly provided scientific evidence of a strong correlation between LF component (sympathetic) of HRV and plasma levels of norepinephrine.

6.3 The Quantification of Autonomic Drive to Myocardium

HRV can be measured from any length of recorded ECG, but at least 5 min is required to quantify sympathetic and parasympathetic tone as per the guidelines of the Task Force on HRV [11]. The ECG is recorded in supine position for 5 min after 15 min of supine rest, and at a comfortable room temperature, for short-term analysis of HRV. The acquired ECG signal is digitized and stored. The HRV software later detects R waves and computes an R–R interval plot (Tachogram, Fig. 6.1). The analysis of HRV is done by three methods: time domain, frequency domain, and nonlinear methods.

In *time domain methods*, statistical tools are applied to quantify the variations in R–R intervals and the parameters are computed. Most of the conventional time

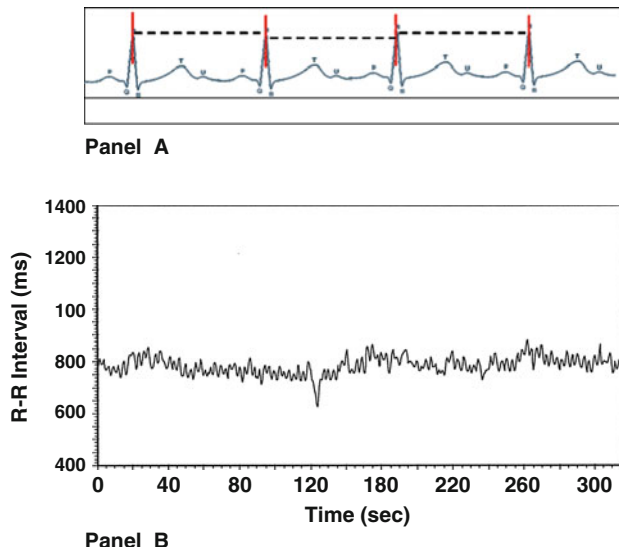


Fig. 6.1 ECG and tachogram. **(a)** ECG tracings with marked R waves. **(b)** Tachogram, a record of RR intervals plotted against time. By using Heart Rate Variability software, the tachogram is analyzed for generating time domain, frequency domain, and nonlinear parameters

domain parameters (i.e., SDNN, SDSD, RMSSD, NN50, and pNN50) are markers of parasympathetic activity. In *frequency domain methods*, frequency components of HRV are analyzed, commonly by Fast Fourier Transform (FFT). The power spectrum is subsequently divided into three frequency bands: VLF (very low frequency; 0.001–0.04 Hz), LF (0.040–0.15 Hz), and HF (0.15–0.4 Hz). Power spectral densities (PSD) are plotted in milliseconds square per Hertz against preset frequencies. The power of the spectral bands is calculated in milliseconds square (absolute power) and in normalized units (nu). For example, the normalized unit of LF is calculated by the formula: [LF/total power – VLF] × 100. There are several *nonlinear methods* available to analyze HRV [12]. The Poincaré plot is a scatter plot of the current R–R interval against the R–R interval immediately preceding it ($R-R_n$ vs. $R-R_{n+1}$). The R–R interval Poincaré plot typically appears as an elongated scatter of points oriented along the line of identity at 45° to the normal axis. The conventional parameters of nonlinear methods are given in Table 6.1.

6.4 Physiologic Factors Influencing HRV

The understanding of control systems has given wide acceptability to HRV. The knowledge of physiology is useful while collecting HRV data and interpreting the HRV results. Several physiological stimuli do serve as protocol in autonomic

Table 6.1 HRV parameters, their basis of calculation, and physiological interpretation

Name of the parameter	Unit	Statistical terms or basis of calculation	Physiological interpretation
<i>Time domain parameters</i>			
MeanNN	ms	Mean of RR interval of normal-to-normal beats	Denotes reverse of mean heart rate
SDNN (standard deviation of normal-to-normal intervals)	ms	Standard deviation of the R–R intervals	Reflects the influence of parasympathetic and sympathetic system on heart rate variability It reflects all the cyclic components responsible for variability in the recording period
COV (coefficient of variance)	Ratio	Coefficient of variance	Reflects the influence of parasympathetic and sympathetic system on heart rate variability It reflects all the cyclic components responsible for variability in the recording period
SDSD	ms	Standard deviation of differences between adjacent R–R intervals	Quantifies short-term variability; reflects parasympathetic activity
RMSSD (root mean square of successive differences)	ms	Root mean square of successive differences between adjacent R–R intervals	Reflects parasympathetic activity
NN50 (normal to normal RR intervals ≥ 50 ms)	Count	Number of R–R interval with difference ≥ 50 ms	Reflects absolute amount of parasympathetic activity
pNN50 (% of normal to normal RR intervals ≥ 50 ms)	Percentage	Percentage of number of R–R interval with difference ≥ 50 ms	Reflects parasympathetic activity
<i>Frequency domain parameters</i>			
TP (total power)	ms ²	Total power (0–0.4 Hz)	Reflects total variance
LF (low frequency)	ms ²	Power in the low-frequency band (0.04–0.15 Hz)	Reflects predominantly sympathetic
LFnu (normalized Low frequency)	Normalized units	Normalized unit low frequency = LF/ (TP – VLF) $\times 100$	Normalization of the data removes most of the interbeat and intersubject variability of the total raw HRV spectral power
HF (high frequency)	ms ²	Power in the high frequency (0.15–0.4 Hz)	Reflects the centrally mediated parasympathetic activity
HFnu (normalized high frequency)	Normalized units	Normalized unit high frequency = HF/ (TP – VLF) $\times 100$	Reflects the centrally mediated parasympathetic activity

(continued)

Table 6.1 (continued)

Name of the parameter	Unit	Statistical terms or basis of calculation	Physiological interpretation
LF/HF ratio	Ratio	Low- to high-frequency power ratio averaged for 5 min	Reflects sympathovagal balance
<i>Nonlinear parameters (Poincaré plot)</i>			
SD1 (standard deviation along axis 1)	ms	Standard deviation of the instantaneous R–R intervals (short axis of ellipse fitted around a Poincaré plot of N–N intervals)	Measures fast beat-to-beat variability; reflects parasympathetic activity
SD2 (standard deviation along axis 2)	ms	Standard deviation of the continuous long-term R–R intervals (long axis of an ellipse fitted around a Poincaré plot of N–N intervals)	Measures slow beat-to-beat variability; reflects sympathetic activity
SD1/SD2	Ratio	The ratio of the SD1 and SD2	Reflects the ratio of parasympathetic activity and sympathetic activity

function testing. There are several physiological factors that influence HRV as described later.

The mechanism of postprandial hypotension may lie in postprandial reduction in parasympathetic nervous system (PNS) activity. However, when the HRV was recorded four times: just before a meal, and 15 min, 1 h, and 2 h after a meal during a fixed time of the day, to our surprise we did not find any change in HRV. Thus, *prandial state* does not influence the HRV in healthy subjects [13]. We believe that the postprandial phenomenon is well tolerated in healthy subjects. It may manifest signs of postural hypotension in individuals where autonomic functions are compromised, e.g., long-standing diabetic autonomic neuropathy. The day-to-day consistency has been shown in autonomic parameters [14] and virtually serves as a signature for a given individual.

The *ambient temperature* influences the HRV as it initiates acclimation responses involving cardiovascular system. The discomfort levels of the subjects were found to correlate with temperatures and the subjects showed significantly higher levels of LF:HF ratio [15]. The study clearly showed involvement of sympathetic activity during thermal load, a well known fact to physiologists.

Posture is another very important physiological factor that influences autonomic functions [16]. In a recent study, the effect of postural change was reported on HRV and nasal airflow. The authors showed that the supine position (when compared with sitting position) resulted in decreased LF:HF ratio and nasal air flow [17]. The stimulus (change in posture, either by standing or head-up tilt) is quantifiable and controllable and its effect is quantifiable, precise, and predictable. It is interesting to note that there may be ethnic variations in this phenomenon. It was noted by Japanese that a large number of children have tendency to pass out (postural fall)

in schools. This triggered research in Japan during the 1950s; however, it remained confined in Japan because of language barriers. Mariko Nishikino et al. (2006) studied 149 young healthy Japanese males for their HRV in supine and standing postures. They confirmed that the cardiac autonomic function can be modulated by genetic polymorphism in renin-angiotensin system [18].

It has been observed that there is a rapid parasympathetic withdrawal in morning hours [19]. It, perhaps, is responsible for enhanced (unsuppressed) sympathetic excitation in the morning. Several authors have forwarded it as a reason for large incidences of cardiovascular morbidity and mortality in wee hours of the day. The heightened sympathoexcitation of morning (in fact parasympathetic inhibition) is a part of *circadian autonomic rhythm*. Various time domain parameters (except SDNN) and all frequency domain parameters have been shown to exhibit significant circadian variation [20].

It is a well-known fact that *physical training* results in lowering of heart rate. Physical training is a physiological way to achieve an increase in parasympathetic control of heart rate. Experimental studies have shown that exercise training increases autonomic markers and also provides a striking protection from ventricular fibrillation. Animal studies strongly indicate that increased parasympathetic activity due to physical training has a significant protective effect. Differences in duration and intensity of the physical training program (schedule) are likely to influence the outcome. However, the effect of physical training schedule on autonomic parameters has been debated. We have reported changes in autonomic functions after 2 weeks and 24 weeks of physical training in healthy individuals. The 2-week training schedule resulted in quick recovery of autonomic parameters with trends reflecting increased HRV [21], while the 24-week training resulted in decreased LF component of HRV [22]. It has been proposed that exercise is an effective and nonpharmacological way to enhance cardiac electrical stability which provides an antiarrhythmic intervention in humans [23]. In patients with myocardial infarction, even short-term aerobic training for 2 weeks may facilitate recovery of the activity of PNS [24]. A meta-analysis study reported that exercise results in significant increase in HF power vis-à-vis R-R interval and these changes are influenced by age [25]. Gender, age, and posture were found to be consistent and independent correlates of HRV in a European study. Respiratory rate, systolic blood pressure, body mass index, family history of hypertension explained not more than 8% of the total variance. This asserts the robustness of HRV toward physiological and environmental determinants [26].

6.5 HRV Alteration in Various Diseases

HRV may be deranged in diseases involving a very large number of conditions such as cardiovascular disorders, respiratory disorders, neurological disorders, gastrointestinal disorders, renal disease, immunological insults, hematological disorders, severe traumatic situation, functional disorders, etc. The spectrum of diseases covers

clinico-pathologically confirmed diseases (e.g., myocardial infarction), metabolically confirmed diseases (e.g., diabetes mellitus), and psychosomatic disorders. For diabetes mellitus, HRV has established itself as a diagnostic and prognostic parameter for autonomic neuropathy. Our lab has been involved in HRV research for two decades now and we have reported HRV abnormalities in various diseases, like hypertension [27], HIV-positive patients [28, 29], irritable bowel syndrome [30], lead poisoning [31], inflammatory bowel disease [12], and intractable epilepsy [32].

In recent past, there has been a surge of HRV studies in acute emergencies involving unstable hemodynamic situations, surgical stress, nonsurgical stress, and trauma. Respiratory insufficiency in infants seriously affects the relationship of sympathetic (LF) and parasympathetic (HF) components. One study showed that regression of respiratory insufficiency resulted in normalization of sympathetic and parasympathetic activity (LF:HF ratio) [33]. A study on acute traumatized patients has shown increased mortality in those patients who had lowered time domain measures of HRV [34]. Such changes have also been observed under acute septic shock situation [35]. Improved HRV measures were found to be associated with higher survival rates after glucocorticosteroid infusion in presumably adrenal insufficiency patients [36].

The studies have shown signs of increased sympathetic activity and/or impaired parasympathetic activity after myocardial infarction [37]. This increase in sympathetic nervous system activity enhances the ventricle's vulnerability to fibrillation and may predispose to sudden death. The association of higher risk of postinfarction mortality with reduced HRV has been shown [37]. Experimental and clinical studies analyzing HRV after myocardial infarction showed a correlation between a greater occurrence of sudden cardiac death and signs of increased sympathetic activity and/or of impaired vagal activity [9, 19, 38]. Several researchers have shown that all components of HRV are markedly reduced after myocardial infarction [37, 38]. The emerging concept is that the strategies which increase indirect markers of autonomic activity might be an important target for intervention in myocardial infarction.

6.6 The Relationship of HRV and QT Variability

The QT variability (QTV) is the study of variability of ventricular repolarization. It represents the extent of ventricular contractility. The large QT represents relaxed state and small QT represents sympathetically excited state. Less variability would mean that there is no excess strain on myocardium. The QT–RR relationship is dynamic and it shows hysteresis [39]. This means that QT interval adaptation to beat-to-beat changes is individualistic. This adaptability may show variable degree of coherence between QT dispersion and HRV. The gender differences in humans with reference to duration of QT interval showed differential tendency to induce arrhythmias [40]. Healthy women showed longer QT interval with enhanced tendency to manifest drug-induced pro-arrhythmia when compared to men. However, women do well on implantable cardioverter defibrillators. The women manifested

increased QTV which was not associated with HRV. This dissociation could be the reason for genesis of ventricular arrhythmia [40]. Lombardi et al. showed that alteration in HRV in acute myocardial infarction depends on the site of infarct and ejection fraction [41]. The collateral circulation to infarct area affects HRV and the development of ventricular arrhythmia [42]. The changes in HRV induced by coronary angioplasty have been found to be dependent on localization of coronary lesions [43]. Further investigations are required to determine whether regional anatomical patterns of circulation are responsible for this effect.

6.7 Molecular Basis of the Physiological and Pathophysiological Aspects of HRV

Autonomic receptors play an important role in the modulation of HRV [44]. Atropine when given alone or with atenolol abolishes all power in HF and LF bands and decreases VLF significantly. The β -adrenergic blockade (by using atenolol) has no significant effect on VLF or LF but increases HF power. The ACE blockade with enalaprilat has no significant effect on LF and HF component of HRV. However, the ACE blockade results in significant increase in VLF in supine position [44]. The α_2 -adrenoceptor blockade and α_2 -adrenoceptor stimulation suggest that α_2 -adrenoceptors exert a regulatory influence on HF component of HRV [45]. Further, by using moxonidine, the drug that stimulates imidazoline II-receptors, it has been suggested that central α_2 -adrenoceptors play a significant role in mediation of sympatholysis (in low doses) and parasympathomimetic effects (in high doses) [46]. The α_{2C} -adrenoceptors deletion does not affect resting HRV [47]. Animal studies using exercise as an ANS modulating agent have supported the link in autonomic receptors, myocardial function, and HRV. In rats, it has been shown that the exercise training reduces the density of myocardial β_1 -adrenergic receptors (AR) and enhances response of the SA node to sympathetic blockade [48]. Studies on genetic polymorphism involving autonomic receptors have further supported this link. One Japanese study on β -adrenoceptor polymorphism explored the relationship between HRV and four genetic polymorphisms of β -adrenoceptors (Ser49Gly and Arg389Gly in β_1 -AR, Arg16Gly and Gln27Glu in β_2 -AR) in healthy subjects. They found that Arg16Gly polymorphism of the β_2 -AR is related to the modulation of sympathovagal balance (LF:HF ratio), and β_2 -AR Glu27 allele carriers potentially have increased higher LF (sympathetic) power in HRV [49]. Knockout studies in mice have further confirmed that β -adrenergic receptor subtypes (β_1 , β_2 , and β_3) have differential role in regulating autonomic signaling [50]. In an experimental study, transgenic mice overexpressing atrial β_1 -adrenoceptors have been found to change LF and HF component of HRV without altering the heart rate. In these mice, the basal level of adenosine 3',5'-cyclic monophosphate production was found to be decreased [51].

Various ionic channels play a crucial role in regulating membrane potential and thus determine the rhythmicity of myocardium (see Chap. 8: Mechano-electric

Feedback in the Heart: Effect on Heart Rate and Rhythm). A pharmacologic study by Yamabe et al. (2007) elucidated the role of various ionic channels in HRV. They used three bradycardia inducing agents – zatebradine, diltiazem, and propranolol [52]. These agents exhibited different patterns in their modification of HRV and QT interval (Table 6.2). The study pointed toward specific role of ionic channels in modulation of HRV. It appears that L-type Ca channels mediate LF oscillations in HRV but nonselective β -receptors mediate HF oscillation (Table 6.2).

Vagal activity provides protection from arrhythmias. Possibly, the vagal effect involves activation of the G protein-coupled inward rectifying K⁺ channel (GIRK1/4) and results in an acetylcholine-sensitive K⁺ current (I_{KACH}) [53]. The G protein-coupled inward rectifying K⁺ channel appears to be responsible for reduction in HRV [53]. The sterol regulatory element binding protein-1 (SREBP-1) knockout mice exhibit certain interesting responses. First, there is reduction in the heart rate to parasympathetic stimulation. Second, the expression of G protein-coupled inward rectifying K⁺ channel (GIRK1) is also reduced. The production of myocardial infarction in SREBP-1 knockout mice results in doubling of the chances to develop ventricular tachycardia. These results also demonstrate a relationship between lipid metabolism and parasympathetic responses which are likely to play a role in arrhythmogenesis [53]. Further, the association of HRV with polymorphisms of mitochondrial uncoupling proteins UCP2 and UCP3 has recently been reported [54]. This fact could explain various factors that influence HRV, such as ethnicity, reactive oxygen species, and fatty acids. Thus, several studies point toward the fact that the ANS may have links with energy-regulating mechanisms.

In another study, the dysfunction of ankyrin-B channel-deficient mice exhibited bradycardia and patterns of HRV similar to human individuals who have ANK2 variant [55]. Their findings indicated that ankyrin-B serves as a critical function for channels and transporters which are important for sarcoplasmic reticulum calcium homeostasis as well as membrane depolarization in sinoatrial node. This notion has

Table 6.2 Comparative effect of three bradycardia-inducing pharmacologic agents on heart rate variability (HRV) and QT variability [52]

Drug	Mechanism	Effect on HRV parameters and QT interval			
		HF power (parasympathetic activity)	LF power (sympathetic activity)	LF:HF ratio (sympath- ovagal balance)	QT variability (ventricular function)
Zatebradine	Channel blocker of the hyperpolarization-activated inward current (I_f)	No effect	No effect	No effect	No effect
Diltiazem	Blocker of the L-type Ca channel (a nondihydropyridine I_{CaL} blocker)	Increased	Nil	Decreased	Increased
Propanolol	Nonselective β blocker	No effect	Decreased	Decreased	Decreased

been supported by another study which proved that the dysfunction in AnkB-based trafficking pathways causes abnormal sinoatrial node electrical activity and sinus node dysfunction. The findings associate abnormal channel targeting with human sinus node dysfunction and highlight the critical role of local membrane organization for sinoatrial node excitability [56]. According to the authors it appears that the AnkB is essential for normal membrane organization of sinoatrial node cell channels and transporters.

It has been demonstrated that the heterozygous disruption of the Akap10 (D-AKAP2) gene that disrupts the final 51aa increases the contractile response of cultured cardiac cells to cholinergic stimulation [57]. The same Akap10 disruption increases the cardiac response to cholinergic stimulation in both heterozygous and homozygous mutant mice derived from the mouse embryonic stem cells. This suggests a dominant interfering effect of the Akap10 mutant allele. This may produce cardiac arrhythmias in mice. The authors also found that a common variant of AKAP10 in humans (646V, 40% of alleles) was associated with increased basal heart rate and decreased HRV. Although the molecular mechanism remains unknown, their findings in mutant mouse embryonic stem cells, mice, and a common human AKAP10 SNP suggest a role of AKAP10 in the regulation of HRV [57].

Goncalves et al. investigated the role of leptin in mediating autonomic imbalance by using leptin receptor-deficient db/db mice [58]. They found that the resting blood pressure and heart rate were higher in db/db mice compared with db/+ mice. Blood pressure and heart rate amplitudes were lower in db/db mice compared with db/+ mice. Blood pressure response to trimetaphan and HR response to metoprolol were greater in db/db mice than in db/+ mice. The HRV and heart rate response to atropine were blunted in db/db mice. Enlarpril improved autonomic regulation in db/db mice. It appears that α -2-adrenoceptors and the renin–angiotensin system are involved in the increased sympathetic and decreased parasympathetic tones in db/db mice [58].

It would be interesting to see how cholinergic transmission integrates with ionic channels and regulates cardiac autonomic tone. A recent study found that the acetylcholine (ACh) inhibits the contractility and shortens the action potential duration of ventricular myocytes in mammals [59]. They proved the existence of muscarinic receptors and vagal innervation in ventricles. The ACh-activated potassium (K_{ACh}) channels have been found in the ventricles. The fade of I_{KACH} to ACh in atrium has been earlier reported by them [60]. It was related to the muscarinic receptors and phosphorylation of G protein or potassium channel. They demonstrated protective effects of the vagus nerve on the ischemic myocardium by increasing the vagal influence (ACh-induced preconditioning or postconditioning, aerobic exercise, β -receptor antagonist). Evaluating cardiac autonomic regulation and improving balance between sympathetic and vagal tone will provide an important basis for the prevention and treatment of cardiovascular diseases [59]. The autonomic tone testing may serve as a significant step in diagnosing people at risk of cardiac death. Exercise prescription along with monitoring of autonomic tone should be used routinely in health prevention programs.

6.8 Conclusions

Experimental and clinical evidence is accumulating that HRV is an independent physiological marker of autonomic tone. By analysis of HRV, the sympathetic tone, parasympathetic tone, and their interaction can be quantified separately.

Several studies document the reliability of HRV as moderate to poor. The HRV varies with certain physiological conditions. The alterations in HRV have been documented in several pathological conditions, including severe hemodynamic crisis, and thus has potential to serve as a predictor of these conditions. It also has the capability to predict the severity of prognosis for recovery in traumatic injury. A large amount of research has been carried out to relate HRV to cardiac abnormalities. It appears that the abnormality in autonomic tone appears first, and it serves as a leading factor to determine the shape and sequel of events in angina, myocardial infarction, and sudden cardiac death.

Various studies have provided the evidence for association in HRV, autonomic receptors, and ionic channels by using pharmacological manipulations, genetic markers, and physiological interventions (see also Chap. 8: Mechano-electric Feedback in the Heart: Effect on Heart Rate and Rhythm). There is a need to study the central HRV output and its modulation by the behavior of ionic channels of end organs. The understanding of such modulation carries significant implications to interpret the pathophysiological mechanism of autonomic dysfunction and management of diseases.

Newer technologies offer ways and means to decipher HRV in terms of their functional roles. Nonlinear analysis along with traditional linear approach will be useful for the studies using HRV as a dependent or independent parameter.

HRV analysis is useful in spite of a lack of full understanding of complexities involved in its genesis. The HRV measurements show acceptable interclass correlation and meet the criteria required to be used for diagnostic or classification purpose [61]. In conclusion, HRV analysis is simple, cost effective, noninvasive, and very useful technique for quantification of autonomic tone.

Acknowledgments The work in Autonomic Function Laboratory was supported by Government of India's funding agencies: Department of Science and Technology; Indian Council of Medical Research and Central Council for Research in Yoga and Naturopathy. The author gratefully acknowledges the help of Dr. Onkar N. Tripathi for his valuable inputs and critical evaluation of the manuscript.

References

1. Biswas AK, Scott WA, Sommerauer JF, Luckett PM. Heart rate variability after acute traumatic brain injury in children. *Crit Care Med.* 2000;28:3907–12.
2. Chess GF, Tam RM, Calaresu FR. Influence of cardiac neural inputs on rhythmic variations of heart period in the cat. *Am J Physiol.* 1975;228:775–80.

3. Akselrod S, Gordon D, Ubel FA, Shannon DC, Berger AC, Cohen RJ. Power spectrum analysis of heart rate fluctuation: a quantitative probe of beat-to-beat cardiovascular control. *Science*. 1981;213:220–2.
4. Akselrod S, Gordon D, Madwed JB, Snidman NC, Shannon DC, Cohen RJ. Hemodynamic regulation: investigation by spectral analysis. *Am J Physiol*. 1985;249:H867–75.
5. Pomeranz B, Macaulay RJ, Caudill MA, Kutz I, Adam D, Gordon D, et al. Assessment of autonomic function in humans by heart rate spectral analysis. *Am J Physiol*. 1985;248: H151–3.
6. Malliani A, Pagani M, Lombardi F, Cerutti S. Cardiovascular neural regulation explored in the frequency domain. *Circulation*. 1991;84:482–92.
7. Pagani M, Malfatto G, Pierini S, Casati R, Masu AM, Poli M, et al. Spectral analysis of heart rate variability in the assessment of autonomic diabetic neuropathy. *J Auton Nerv Syst*. 1988;23:143–53.
8. Spiers JP, Silke B, McDermott U, Shanks RG, Harron DW. Time and frequency domain assessment of heart rate variability: a theoretical and clinical appreciation. *Clin Auton Res*. 1993;3:145–58.
9. Pagani M, Lombardi F, Guzzetti S, Rimoldi O, Furlan R, Pizzinelli P, et al. Power spectral analysis of heart rate and arterial pressure variabilities as a marker of sympatho–vagal interaction in man and conscious dog. *Circ Res*. 1986;59:178–93.
10. Sesay M, Tazin-Fin P, Gosse P, Ballanger P, Maurette P. Real-time heart rate variability and its correlation with plasma catecholamines during laparoscopic adrenal pheochromocytoma surgery. *Anesth Analg*. 2008;106:164–70.
11. Task Force of the European Society of Cardiology and the North American Society of Pacing and Electrophysiology. Heart rate variability standards of measurement, physiological interpretation, and clinical use. *Circulation*. 1996;93:1043–65.
12. Sharma P, Makharia G, Ahuja V, Dwivedi SN, Deepak KK. Autonomic dysfunctions in patients with inflammatory bowel disease in clinical remission. *Dig Dis Sci*. 2009;54:853–61.
13. Ambarish V, Barde P, Vyas A, Deepak KK. Comparison between pre-prandial and post-prandial heart rate variability (HRV). *Indian J Physiol Pharmacol*. 2005;49:436–42.
14. Kleiger RE, Bigger JT, Bosner MS, Chung MK, Cook JR, Rolnitzky LM, et al. Stability over time of variables measuring heart rate variability in normal subjects. *Am J Cardiol*. 1991;68: 626–30.
15. Liu W, Lian Z, Liu Y. Heart rate variability at different thermal comfort levels. *Eur J Appl Physiol*. 2008;103:361–6.
16. Jahan N, Deepak KK, Kaushal N, Paudel BH. Effect of graded head-up tilt on parasympathetic reactivity. *Indian J Physiol Pharmacol*. 1996;40:309–17.
17. Ko JH, Kuo TB, Lee GS. Effect of postural change on nasal airways and autonomic nervous activity established by rhinomanometry and heart rate variability analysis. *Am J Rhinol*. 2008;22:159–65.
18. Nishikino M, Matsunaga T, Yasuda K, Adachi T, Moritani T, Tsujimoto G, et al. Genetic variation in the renin-angiotensin system and autonomic nervous system function in young healthy Japanese subjects. *J Clin Endocrinol Metab*. 2006;9:4676–81.
19. Wennerblom B, Lurje L, Karlsson T, Tygesen H, Vahisalo R, Hjalmarson A. Circadian variation of heart rate variability and the rate of autonomic change in the morning hours in healthy subjects and angina patients. *Int J Cardiol*. 2001;79:61–9.
20. Kardelen F, Akçurin G, Ertuğ H, Akçurin S, Bircan I. Heart rate variability and circadian variations in type 1 diabetes mellitus. *Pediatr Diabetes*. 2006;7:45–50.
21. Sharma RK, Deepak KK. A short duration of physical training benefits cardiovascular performance. *Indian J Physiol Pharmacol*. 2004;48:481–5.
22. Deepak KK, Kaushal N, Shaw D, Pandey RM, Paudel BH. Predictive value of autonomic parameters for outcome of physical training. *Clin Auton Res*. 1999;9:222.
23. Billman GE. Aerobic exercise conditioning: a nonpharmacological antiarrhythmic intervention. *J Appl Physiol*. 2002;92:446–54.

24. Oya M, Ito H, Kato K, Tanabe K, Murayama M. Effects of exercise training on the recovery of the autonomic nervous system and exercise capacity after acute myocardial infarction. *Jpn Circ J.* 1999;63:843–8.
25. Sandercock G. Normative values, reliability and sample size estimates in heart rate variability. *Clin Sci (Lond).* 2007;113:129–30. Comment on: *Clin Sci (Lond)* 2007;113:131–140.
26. Stolarz K, Staessen J, Kuznetsova T, Tikhonoff V, State D, Babeanu S, et al. Host and environmental determinants of heart rate and heart rate variability in four European populations. *J Hypertens.* 2003;21:525–35. on behalf of the European Project on Genes in Hypertension (EPOGH) Investigators.
27. Deepak KK, Bhargava B, Narang R, Paudel BH, Rai PK, Saxena S. Autonomic studies in hypertensive patient with unusual sexual dysfunction: response to reserpine. *Clin Auton Res.* 2000;10:313–5.
28. Mittal CM, Wig N, Mishra S, Deepak KK. Heart rate variability in human immunodeficiency virus positive individuals. *Int J Cardiol.* 2004;94:1–6.
29. Sakhuja A, Goyal A, Jaryal AK, Wig N, Vajpayee M, Kumar A, et al. Heart rate variability and autonomic function tests in HIV positive individuals in India. *Clin Auton Res.* 2007;17:193–6.
30. Taneja I, Deepak KK, Poojary G, Acharya I, Pandey RM, Sharma MP. Yogic versus conventional treatment in diarrhea-predominant irritable bowel syndrome: a randomized control study. *Appl Psychophysiol Biofeedback.* 2004;29:19–33.
31. Madan K, Sharma PK, Makharla G, Poojary G, Deepak KK. Autonomic dysfunction due to lead poisoning. *Auton Neurosci.* 2007;132:103–6.
32. Mukherjee S, Tripathi M, Chandra PS, Yadav R, Choudhary N, Sagar R, et al. Cardiovascular autonomic functions in well-controlled and intractable partial epilepsies. *Epilepsy Res.* 2009;85:261–9.
33. Gumprecht K, Sieroń-Rokicka B, Gumprecht J, Grzeszczak W. The influence of respiratory insufficiency on autonomic nervous system function in infants. *Wiad Lek.* 2002;55:373–81.
34. Norris PR, Anderson SM, Jenkins JM, Williams AE, Morris Jr JA. Heart rate multiscale entropy at three hours predicts hospital mortality in 3,154 trauma patients. *Shock.* 2008;30:17–22.
35. Korach M, Sharshar T, Jarrin I, Fouillot JP, Raphaël JC, Gajdos P, et al. Cardiac variability in critically ill adults: influence of sepsis. *Crit Care Med.* 2001;29:1380–5. Comments in: *Crit Care Med* 2001;29:1483–4.
36. Morris Jr JA, Norris PR, Waitman LR, Ozdas A, Guillamondegui OD, Jenkins JM. Adrenal insufficiency, heart rate variability and complex biologic systems: a study of 1, 871 critically ill trauma patient. *J Am Coll Surg.* 2007;204:885–92.
37. Wolf M, Varigos GA, Hunt D, Sloman JG. Sinus arrhythmia in acute myocardial infarction. *Med J Aust.* 1978;2:52–3.
38. Bigger Jr JT, Fleiss JL, Steinman RC, Rolnitzky LM, Kleiger RE, Rottman JN. Correlations among time and frequency domain measures of heart period variability two weeks after acute myocardial infarction. *Am J Cardiol.* 1992;69:891–8.
39. Malik M, Hnatkova K, Novotny T, Schmidt G. Subject specific profiles of QT/RR hysteresis. *Am J Physiol Heart Circ Physiol.* 2008;295:H2356–63.
40. Haigney MC, Zareba W, Nasir JM, McNitt S, McAdams D, Gentleski PJ, et al. MADIT II Investigators. Gender differences and risk of ventricular tachycardia or ventricular fibrillation. *Heart Rhythm.* 2009;6:180–6.
41. Lombardi F, Sandrone G, Mortara A, Torzillo D, La Rovere MT, Signorini MG, et al. Linear and nonlinear dynamics of heart rate variability after acute myocardial infarction with normal and reduced left ventricular ejection fraction. *Am J Cardiol.* 1996;77:1283–8.
42. Ozdemir O, Soylu M, Demir AD, Geyik B, Alyan O, Chan G, et al. Do collaterals affect heart rate variability in patients with acute myocardial infarction? *Coron Artery Dis.* 2004;15:405–11.
43. Janowska-Kulińska A, Torzyńska K, Markiewicz-Grochowalska A, Sowińska A, Majewski M, Olga J, et al. Changes in heart rate variability caused by coronary angioplasty depend on the localization of coronary lesions. *Kardiol Pol.* 2009;67:130–8.

44. Taylor JA, Carr DL, Myers CW, Eckberg DL. Mechanisms underlying very low frequency R-R interval oscillations in humans. *Circulation*. 1998;98:547–55.
45. Tank J, Jordan J, Diedrich A, Obst M, Plehm R, Luft FC, et al. Clonidine improves spontaneous baroreflex sensitivity in conscious mice through parasympathetic activation. *Hypertension*. 2004;43:1042–7.
46. Turcani M. Biphasic dose-dependent modulation of cardiac parasympathetic activity by moxonidine, an imidazoline II-receptor agonist. *J Cardiovasc Pharmacol*. 2008;52:524–35.
47. Kurnik D, Muszkat M, Friedman EA, Sofowora GG, Diedrich A, Xie HG, et al. Effect of the alpha2C-adrenoreceptor deletion 322–325 variant on sympathetic activity and cardiovascular measures in healthy subjects. *J Hypertens*. 2007;25:763–71.
48. Barber J, Rekand S, Ville N, Rannou-Bekono F, Wing S, Carré F. The effect of exercise training on myocardial adrenergic and muscarinic receptors. *Clin Auton Res*. 2006;16:61–5.
49. Matsunaga T, Yasuda K, Adachi T, Gu N, Yamamura T, Moritani T, et al. Association of beta-adrenoceptor polymorphisms with cardiac autonomic modulation in Japanese males. *Am Heart J*. 2007;154:759–66.
50. Ecker PM, Lin CC, Powers J, Kobilka BK, Dubin AM, Bernstein D. Effect of targeted deletions of beta1- and beta2-adrenergic-receptor subtypes on heart rate variability. *Am J Physiol Heart Circ Physiol*. 2006;290:H192–9.
51. Yang ZF, Sun Y, Li CZ, Wang HW, Wang XJ, Zheng YQ, et al. Reduced sinoatrial cAMP content plays a role in postnatal heart rate slowing in the rabbit. *Clin Exp Pharmacol Physiol*. 2006;33:757–62.
52. Yamabe M, Sanyal SN, Miyamoto S, Hadama T, Isomoto S, Ono K. Three Different bradycardic agents, zatebradine, diltiazem and propranolol, distinctly modify heart rate variability and QT-interval variability. *Pharmacology*. 2007;80:293–303.
53. Park HJ, Georgescu SP, Du C, Madias C, Aronovitz MJ, Welzig CM, et al. Parasympathetic response in chick myocytes and mouse heart is controlled by SREBP. *J Clin Invest*. 2008;118:259–71.
54. Matsunaga T, Gu N, Yamazaki H, Tsuda M, Adachi T, Yasuda K, et al. Association of UCP2 and UCP3 polymorphisms with heart rate variability in Japanese men. *J Hypertens*. 2009;27: 305–13.
55. Hund TJ, Mohler PJ. Ankyrin-based targeting pathway regulates human sinoatrial node automaticity. *Channels (Austin)*. 2008;2:404–6.
56. Le Scouarnec S, Bhasin N, Vieyres C, Hund TJ, Cunha SR, Koval O, et al. Dysfunction in ankyrin-B-dependent ion channel and transporter targeting causes human sinus node disease. *Proc Natl Acad Sci USA*. 2008;105:15617–22.
57. Tingley WG, Pawlikowska L, Zaroff JG, Kim T, Nguyen T, Young SG, et al. Gene-trapped mouse embryonic stem cell-derived cardiac myocytes and human genetics implicate AKAP10 in heart rhythm regulation. *Proc Natl Acad Sci U S A*. 2007;104:8461–6.
58. Goncalves AC, Tank J, Diedrich A, Hilzendeger A, Plehm R, Bader M, et al. Diabetic hypertensive leptin receptor-deficient db/db mice develop cardioregulatory autonomic dysfunction. *Hypertension*. 2009;53:387–92.
59. Zang WJ, Sun L, Yu XJ, Lv J, Chen LN, Liu BH. Vagal control of cardiac functions and vagal protection of ischemic myocardium. *Sheng Li Xue Bao*. 2008;60:443–52.
60. Shui Z, Boyett MR, Zang WJ. ATP-dependent desensitization of the muscarinic K⁺ channel in rat atrial cells. *J Physiol*. 1997;505:77–93.
61. Maestri R, Raczk G, Danilowicz-Szymanowicz L, Toruński A, Sukiennik A, Kubica J, et al. Reliability of heart rate variability measurements in patients with a history of myocardial infarction. *Clin Sci (Lond)* 2010;118:195–201. Available from: <http://www.clinsci.org/cs/118/cs1180195.htm>.

Chapter 7

Mechano-Electric Feedback in the Heart: Effects on Heart Rate and Rhythm

T. Alexander Quinn, Rebecca A. Bayliss, and Peter Kohl

7.1 Introduction

Cardiac electrical and mechanical activity are closely interrelated, not only via the chain of events that links electrical excitation to contraction (commonly referred to as excitation-contraction coupling, ECC), but equally via feedback from the heart's mechanical environment to the origin and spread of cardiac electrical excitation. The latter has been termed mechano-electric feedback (MEF), and complements ECC to form an intracardiac electro-mechanical regulatory loop. This chapter will review MEF effects on heart rate (HR, number of beats per unit time, usually 1 min) and rhythm (regularity of cardiac contractions), distinguishing between pro- and anti-arrhythmic effects, and elucidate the extent to which stretch-activated ion channels (SAC) may explain observed responses. A concluding section addresses current shortfalls in insight and presents theories regarding the physiological relevance of MEF in the heart.

T.A. Quinn (✉)

Department of Physiology, Anatomy and Genetics, Cardiac Mechano-Electric Feedback Group,
University of Oxford, Oxford, UK
e-mail: alex.quinn@dpag.ox.ac.uk

R.A. Bayliss

Balliol College, University of Oxford, Oxford, UK

P. Kohl

National Heart and Lung Institute, Imperial College of Science, Technology and Medicine,
London, UK

7.2 Mechanical Modulation of Heart Rate

7.2.1 *Background*

Modulation of HR through changes in venous return was reported about a century ago by Bainbridge, who attributed HR acceleration upon venous fluid injection in anaesthetised dogs to a predominantly vagal autonomic reflex [1]. His experiments established a correlation between HR response and central venous pressure (CVP), but not arterial pressure. Reconfirmation of this response in humans proved difficult, as most non-invasive interventions that change CVP also affect arterial pressure. The latter may trigger dominant baroreceptor responses that stimulate contrasting HR effects (e.g., via the depressor reflex). Donald and Shepherd finally circumvented this problem and established the equivalent of a “Bainbridge response” in humans, using passive leg elevation of volunteers in supine position to favour venous blood return to the trunk of the body. This raised CVP without measurably affecting arterial pressure, revealing a positive chronotropic effect on human HR [2].

The Bainbridge response has also been observed in isolated hearts, right atrial [3] and sino-atrial node (SAN) tissue [4], and even in single pacemaker cells [5]. Thus, local MEF mechanisms contribute to mechanical modulation of HR, involving mechanisms beyond the originally implied reflex.

7.2.2 *Clinical Observations*

Human studies of the Bainbridge response have focussed on the assessment of respiratory sinus arrhythmia (RSA) in normal subjects and in heart transplant recipients.

RSA is a “physiological arrhythmia”, where HR is modulated during the respiratory cycle, increasing during inspiration (when low intrathoracic pressure aids venous return), and decreasing during expiration (when output from the chest is favoured). It is reported to reduce pulmonary shunt effects and increase oxygen uptake, when compared to stable HR [6], indicating a possible role for mechanical HR modulation in normal physiology. It can be measured non-invasively by establishing respiratory rate-related frequency oscillations in the R–R intervals of the electrocardiogram. Two major peaks in HR frequency oscillations appear in healthy subjects at rest. A so-called high-frequency (HF) peak (0.15–0.3 Hz) is correlated with the respiratory cycle, and usually attributed to oscillations in “vagal tone”. It is this peak which is considered to represent RSA. A second, low-frequency (LF) peak (~ 0.1 Hz) is attributed to changes in “sympathetic tone” and is not modulated with the respiratory cycle.

As expected, transplant recipients (denervated heart) tend to lack the LF peak. However, a distinct HF peak is still discernible, albeit at reduced magnitude,

suggesting that mechanisms intrinsic to the heart may contribute to RSA [7]. Interestingly, tidal volume (and, therefore, venous return) modulates HR variability in these patients.

Intrinsic HR modulation is not unique to transplant recipients. In normal subjects, the magnitude of both LF and HF oscillations is reduced during early exercise. As workload increases, the LF component diminishes and all but disappears at maximal workloads, whereas the HF peak increases in magnitude, despite the loss of “vagal tone” associated with physical work [8]. This can be observed even after additional ganglion blockade [9], again suggesting intracardiac contributions to RSA. Interestingly, the delay between respiratory and HF oscillation peaks drops with exercise in normal subjects, rendering it similar to that in transplant recipients (in whom it remains unchanged), perhaps suggesting a switch from normally dominant longer-latency reflex loops to intrinsic cellular/tissue-level control [8].

Human studies, therefore, point towards the existence of an intracardiac mechano-sensitive HR control mechanism, contributing to HR modulation by venous return. Elucidation of the stimulus for, and mechanisms of, this response requires experimental manipulation that would be impractical and/or unethical in humans.

7.2.3 *Experimental Studies*

The HR changes observed in humans have been reproduced in intact anaesthetised dogs, where SAN-specific stretch (applied via a weight and pulley system in open-chest experiments) is capable of eliciting instantaneous HR acceleration by >20% [10]. This is not abolished by denervation or adrenergic and cholinergic blockade.

In the isolated heart, responses matching in time course and dynamics those of intact preparations were described by Blinks [3], who observed that progressive increases in atrial pressure (up to ~100 mmHg at constant flow) are accompanied by instantaneous HR acceleration in canine and rabbit. This response appears rapidly, plateaus by 2–3 min, and can be maintained for several hours. Further atrial pressure increases beyond this (already supra-physiological) range result in HR deceleration.

Adrenergic and cholinergic blockade, sufficient to alter HR by 50% from baseline, have no effect on the HR response to changes in filling pressure in rat. Neither the application of TTX (tetrodotoxin, fast Na⁺ channel blocker) nor neonatal capsaicin injections (ablation of intracardiac neurons) prevent mechanical modulation of HR [11]. This shows that neither external autonomic nor intracardiac neuronal signalling is necessary for the intrinsic HR response to stretch. Finally, the high solution flow rates used in atrial preparations [3] and the speed of response suggest that humoral factors are unlikely to be key contributors.

In the 1960s, Deck demonstrated an equivalent to HR changes, observing beating rate (BR) during distension of cat and rabbit isolated atrial tissue containing the SAN. Measuring the transmembrane potential (V_m) of SAN pacemaker cells, and the

contractile behaviour of the tissue during linear or equi-biaxial stretch [4], he observed a 15–20% BR acceleration upon stretch. This was accompanied by an instantaneous reduction in absolute amplitudes of both maximum systolic and maximum diastolic potentials (MSP and MDP, respectively), giving rise to a reduction in action potential (AP) amplitude and duration of the spontaneous diastolic depolarisation phase. These first direct electrophysiological observations of transmembrane potential changes in SAN tissue help in narrowing down the range of plausible molecular mechanisms involved, as their effect would appear to be linked to an electrophysiological mechanism with a net reversal potential (E_{rev}) between MDP and MSP of SAN pacemaker cells.

7.2.4 Underlying Mechanisms

Early single cell studies into the mechanisms underlying mechanical modulation of HR used cell swelling as the mechanical stimulus. This was shown to activate a chloride current ($I_{Cl,swell}$), whose E_{rev} near 0 mV would confer the capacity to augment pacemaker frequency [12]. However, $I_{Cl,swell}$ activates with a lag time of over 30 s in cardiac myocytes, rendering it too slow for acute beat-by-beat changes in HR.

Furthermore, cell swelling is associated with an increase in cell diameter and negligible axial elongation, or even shortening. Micro-mechanically, this is fundamentally different from axial stretch, where lengthening at constant cell volume is associated with a reduction in cell diameter. In addition to these biophysical differences in stimulus, hypo-osmotic swelling of rabbit spontaneously beating SAN pacemaker cells actually elicits BR reduction [13]. Cell swelling is not an ideal approach, therefore, to probe acute mechanical modulation of cardiomyocyte electrophysiology in normal physiological conditions, where cardiomyocytes are not assumed to change cell volume. That said, acute cell swelling mimics certain aspects of cell behaviour in ischaemia and reperfusion which, together with pathologically remodelled cells (e.g., in hypertrophy, where $I_{Cl,swell}$ can be persistently activated in working myocardium [14]), constitute highly relevant research targets for this technique.

Axial stretch can be applied to single myocytes using a range of techniques to attach probes for mechanical stimulation. One approach is to use carbon fibres that adhere to single cells without the need for gluing, tying, or suction [15]. Using this technique, Cooper et al. observed a significant increase in BR of rabbit single SAN cells during 5–10% stretch. This was accompanied by a reduction in absolute values of MSP and MDP [5], reproducing previous SAN tissue results [4]. Voltage clamp studies revealed that stretch activated a 6 nS/pF whole-cell current with an E_{rev} of –11 mV [5].

This SAC is similar to the mechanically induced cation non-selective current (SAC_{NS}) reported in many other eukaryotic cells. SAC_{NS} is carried by rapidly activating channels with E_{rev} approximately half-way between MDP and MSP [16].

SAC_{NS} opening will therefore depolarise diastolic, and repolarise systolic V_m , potentially explaining the observed changes in SAN cell and tissue MSP and MDP during stretch.

An apparent point of contention has been the observation that HR responses may differ between species. Most medium and large mammals respond to SAN stretch with HR acceleration, while smaller mammals may show HR deceleration [17]. Interestingly, this discrepancy is not incompatible with a major contribution of SAC_{NS} to both responses. Larger animals tend to have slower-beating SAN, with AP shapes that are characterised by a slow upstroke (carried largely by Ca^{2+} influx) and a prominent plateau-like phase (Fig. 7.1a), while smaller mammals with faster HR show faster upstrokes (with a significant contribution from fast Na^+ channels) and swift initial repolarisation, giving rise to a more triangular AP shape (Fig. 7.1b). Thus, “slow” SAN AP spend the majority of each cycle moving their V_m from MDP (or MSP) towards the E_{rev} of SAC_{NS}. Their faster counterparts spend a larger proportion of time moving their V_m away from the E_{rev} of SAC_{NS}. Thus, one and the same mechanism – activation of SAC_{NS} by SAN stretch – may speed-up slow HR and reduce already fast ones.

Ideally, the insight obtained by reduction of a problem from whole animal to tissues, cells, and channels should be complemented by reintegration, from putative mechanisms to systemic response. This can be achieved using conceptual consideration (or, better, quantitative mathematical models) or experimental investigation (e.g., via application of selective pharmacological probes). Modelling of stretch effects on SAN cell activity has confirmed the *plausibility* of SAC_{NS} contributions as a key to stretch-induced BR changes [5]. Experimental proof calls for selective inhibition (or activation) of SAC_{NS}. At present, available pharmacological tools are limited (e.g., no known SAC_{NS} activators). Gadolinium ions are potent SAC_{NS} blockers, but they also affect other ion channels and precipitate in physiological

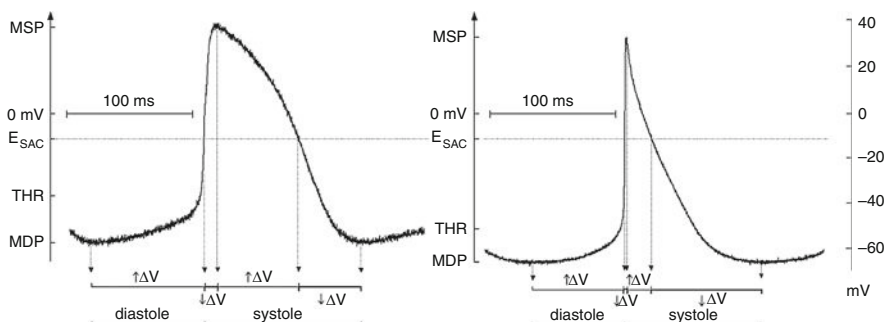


Fig. 7.1 Species differences in potential SAC_{NS} effects on SAN cell AP. Membrane potential recordings illustrate the interrelation of cell electrophysiological parameters (MSP; MDP; threshold for activation of AP, THR) and the SAC_{NS} reversal potential (E_{SAC}). Time periods during which SAC_{NS} activation would either accelerate ($\uparrow\Delta V$) or slow ($\downarrow\Delta V$) intrinsic changes in SAN cell membrane potential are labelled. Left: rabbit SAN cell; Right: mouse SAN cell. The rabbit SAN cell spends ~71% of cycle duration in $\uparrow\Delta V$, whereas in the mouse, this phase accounts for just ~46% (from [83] with permission)

buffers. At low concentrations ($<50\text{ }\mu\text{M}$), streptomycin is both potent and reasonably selective when used on isolated cells, but its utility for acute SAC_{NS} block in multicellular preparations has been called into question (if streptomycin did act as an acute SAC_{NS} blocker *in situ*, we could probably not prescribe it to patients) [17]. The most specific SAC_{NS} blocker, *Grammostola spatulata* mechanotoxin-4 (GsMTx-4) is a peptide, isolated from a tarantula toxin [18]. It has been found to reversibly block stretch-induced BR changes in guinea pig and mouse SAN tissue, without affecting background force [17]. Unfortunately, native GsMTx-4 is of limited availability, and synthesised forms are both expensive and, at least in some cases, of reduced potency.

The magnitude of mechanical effects on HR appears to decrease with reduction in structural complexity of the biological model (intact dog up to 30%, whole-heart/SAN tissue ~15%, isolated SAN cells ~5% [17]). Probable explanations include (1) the progressive loss of structures involved in transmission of mechanical stimuli to molecular effectors as one reduces the biological model system; (2) increasing deprivation of possible paracrine effects, such as may be mediated by endothelial cells which are prone to suffer from tissue isolation and are removed by cell separation; or (3) removal of inter-cellular electrotonic coupling between identical and/or different cell populations. Human fibroblasts, for example, have been found to contain SAC_{NS} [19]. Functional coupling via connexins has been established both at fibroblast–fibroblast and fibroblast–myocyte junctions [20], and computational modelling predicts that stretch modulation of fibroblast V_m has the potential to accelerate diastolic depolarisation in electrotonically coupled SAN myocytes by $>20\%$ [21].

Finally, intrinsic cellular MEF responses could be amplified *in vivo* by interaction with autonomic signalling. Atrial pressure increases of just 2 mmHg, for example, induce both HR acceleration and a significant reduction in the percentage response to vagal stimulation in intact rabbit [22], effectively reducing the influence of underlying vagal tone. Thus, local and systemic HR modulation occur in conjunction and may amplify, or dampen, each other's effect.

7.2.5 Summary

The intrinsic HR response to stretch, such as caused by changes in venous return, is demonstrable at physiologically relevant levels of mechanical stimulation, over multiple spatial scales. Intrinsic control has been estimated to contribute $>30\%$ of RSA during exercise in healthy individuals [9]. The evolutionary advantage of such a mechanism has been speculated to arise from earlier beat-induction in response to cardiac filling (haemodynamic benefit), from improved mechanical performance of the heart (which is more mechanically efficient when working at smaller radii), and from maximising gas exchange (with reduced shunt volume) [6]. Alternatively,

stretch effects on HR could be a side effect of mechanisms that underlie mechanical modulation of contractile force [23].

Future investigations should consider the mounting evidence suggesting that SAN pacemaker rate depends not only on trans-sarcolemmal ion conductances, but involves an intracellular Ca^{2+} “clock”, driven by release of Ca^{2+} from the sarcoplasmic reticulum (SR), followed by transsarcolemmal inward currents such as via the $\text{Na}^+/\text{Ca}^{2+}$ exchanger [24]. Of note, stretch has been shown to increase SR Ca^{2+} release in ventricular cells [25], which – if present in SAN – could be relevant for mechanical modulation of heart rate.

7.3 Proarrhythmic Effects of Mechanical Stimulation

7.3.1 *Background*

First observations that perturbation of the heart’s mechanical status could initiate deadly cardiac arrhythmias were published over 130 years ago, with reports of sudden cardiac death associated with non-penetrating impact to the precordium (*Commotio cordis*, CC; for review see [26]). More recently, rhythm disturbances due to internal mechanical stimulation with cardiac catheterisation have been observed [27]. It is now also believed that cardiac tachyarrhythmias, encountered in pathologies associated with volume or pressure overload are, in part, caused by electrophysiological responses to the altered mechanical environment [28]. Arrhythmogenic stretch effects on cardiac electrophysiology have been investigated in isolated whole heart, tissue, and cellular models, helping to elucidate underlying mechanisms.

7.3.2 *Clinical Observations*

Reports about proarrhythmic effects of acute external mechanical stimulation by CC [26], occasionally occurring during chest compressions soon after electrical defibrillation [29], together with cases of ectopy induction upon intracardiac catheter contact, suggest that heart rhythm disturbances can be related to intracardiac MEF effects [27]. Arrhythmogenic mechanical stimulation can be local or global, such as ventricular ectopy associated with balloon inflation during pulmonary valvuloplasty, where the electrophysiologically relevant mechanical stimulus acts via an increase in ventricular load [30]. The same is true for the atria, where acute changes in volume loading have been found to increase the incidence and sustenance of arrhythmias [31]. Changes in atrial electrophysiology have also been seen with acute drops in atrial pressure during balloon commissurotomy for mitral stenosis and atrial flutter, as well as with short-term dual chamber pacing [31].

Effects of chronic stretch are usually observed in patients with sustained ventricular pressure or volume overload. Hypertension, congestive heart failure, and dilated cardiomyopathy are all associated with a high incidence of arrhythmias [28]. It is difficult to assess, in these cases, whether the sustained mechanical stimulation may directly contribute to rhythm disturbances, or whether it acts via structural and functional tissue remodelling. However, the observation that acute temporary removal of ventricular overload (e.g., by the Valsalva manoeuvre) can terminate chronic ventricular tachycardia in patients suggests that mechanical factors may play a role in the chronic setting as well [32].

7.3.3 *Experimental Studies*

Depolarisation of V_m by acute diastolic stretch has been demonstrated in isolated heart, as well as in ventricular and atrial tissue and cell preparations [28]. In isolated hearts, a transient increase of intraventricular volume during diastole results in membrane depolarisation, which, if sufficiently large and rapid, can trigger premature ventricular excitation [33] and short periods of ventricular tachycardia (VT) [34].

The effects of acute systolic stretch are more complex. Both shortening and prolongation of the AP have been observed, along with early after-depolarisation-like events, both in isolated cardiomyocytes and multicellular experimental preparations [28]. In the setting of CC, non-penetrating precordial impacts can induce rhythm disturbances in the absence of structural damage to the heart. The severity of arrhythmias, including ventricular fibrillation (VF), changes in an impact magnitude- and timing-dependent manner. This was first investigated almost 80 years ago by Schlamka et al., who found that impacts to the precordial region of anaesthetised rabbits, cats, and dogs resulted in ectopic excitation and, in 20% of cases, VF [35, 36]. Importantly, they showed that mechanical induction of arrhythmias was not affected by bilateral vagotomy, indicating that this was not a result of a parasympathetic reflex. Furthermore, arrhythmia induction depended on the region of impact (mid and lower sternum were the most susceptible areas, especially for VF), the size of the contact area (smaller impact areas resulted in more severe rhythm disturbances), and the duration of the impact (rapid impacts were more arrhythmogenic). More recently, in a swine model of CC, Link et al. confirmed the importance of impact site, size, and severity, and showed that only impacts during the early T-wave result in VF, while impacts at other times in the cardiac cycle produce various other transient rhythm disturbances [37]. A similar response has been demonstrated with a rapid increase of intraventricular volume in isolated rabbit hearts [38]. Acute volume loading has been shown to decrease conduction velocity, both in ventricles [39] and atria [31], which can contribute to the initiation and maintenance of arrhythmias. With loading in the atria, a reduction in AP duration and refractoriness, and an increase in dispersion of refractoriness, have been demonstrated, with an associated increase in vulnerability to atrial fibrillation [31]. Interestingly, it has been shown (by one of the editors of this book under her maiden name Theophile) that stretch of Purkinje fibres speeds up their

rate of spontaneous diastolic depolarisation [40], increasing conduction velocity [41], potentially leading to stretch-induced ectopy [40]. Other cardiac cell types, such as fibroblasts [21], pulmonary vein muscle cells [42], chondrocytes, smooth muscle and endothelial cells [43], and intracardiac neurons, are also mechano-sensitive, suggesting that the interplay between different cell types in the heart may be relevant for stretch-induced arrhythmogenesis, an important concept that has been insufficiently explored.

The similarity of effects of precordial impact and rapid intraventricular pressure increase raise an interesting question about the relative contribution of local versus global stretch to electrophysiological responses. This is highlighted by the large change in intraventricular pressure (brief spikes of more than 500 mmHg) seen with precordial impact in the swine model, whose magnitude has been correlated with the probability of VF induction (maximum effects between 250 and 450 mm Hg) [44]. Myocardial compliance varies throughout the ventricle (which may also be affected by regional differences in coronary vascular pressure), so gross changes in intraventricular pressure or volume will result in a heterogeneous distribution of stretch. This is supported by the observation that intraventricular volume changes yield non-uniform depolarisation, with the origin of excitation most often in the posterolateral region of the left ventricle, typically a region of high compliance [33]. The only presently published data of intraventricular activation sequence during extra-corporeal CC impacts stem from a single pig experiment and suggest the presence of focal excitation of the ventricle immediately underneath the impact site [45]. This suggests a more directly impact-site related mechanism, and reemphasises the question as to the relative causal contributions of global and local stretch.

In isolated heart models, large intraventricular pressure pulses (between 208 and 280 mmHg) have been used to trigger VF [38]. At the same time, local low-energy non-traumatic (<2 mN) impacts, timed with the early T-wave, can induce VF in isolated guinea pig [46] and rabbit hearts [47]. Preliminary epicardial optical mapping, conducted in this setting, revealed focal activation and VF when there is spatio-temporal overlap of the mechanical stimulus with the trailing wave of repolarisation. This may give rise to the arrhythmogenic response [47] predicted in prior modelling work (see next section) [48].

The idea, that the structural heterogeneity of ventricular tissue modulates globally applied stretch to create heterogeneous strain distributions and focal sites of excitation that leads to initiation of reentrant arrhythmias is further supported by a recent study of Seo et al. [49]. Using optical mapping with stretch applied across a right ventricular tissue flap, they demonstrated that focal excitation originates at the point of largest strain differences, which can result in sustained reentrant tachyarrhythmias. Similarly, an increase in the probability of mechanically induced excitation in areas showing paradoxical segment lengthening has been observed in diseases with heterogeneous changes in ventricular compliance such as regional ischaemia [50] and infarction [51]. In acute regional ischaemia, the degree of dilation of the acutely ischaemic tissue is a strong predictor of the probability of arrhythmogenesis, including VF [52]. The role of heterogeneous stretch in VF

induction is further supported by experiments showing that acute localised stretch increases the complexity of VF activation maps, with more areas of conduction block and breakthrough patterns [53]. These heterogeneities in stress–strain distribution would result in significant differences in mechanical stimulation of cells, which could give rise to local ectopic foci and regions of functional block.

7.3.4 Underlying Mechanisms

Proarrhythmic effects of myocardial stretch can be explained, in part at least, by SAC activation. Two sub-categories of SAC can be distinguished in myocardium: SAC_{NS} , which allow passage of various cations (E_{rev} usually between 0 and -20 mV), and potassium-selective SAC_K (E_{rev} near -90 mV; for review see [54]). During diastolic stretch, V_m tends to show depolarisation (Fig. 7.2), which can be explained by a predominant contribution of SAC_{NS} (SAC_K would cause stretch-induced hyperpolarisation, which is not seen in cardiac cells). Systolic stretch primarily accelerates AP repolarisation, which could be caused by either SAC sub-type [55].

A predominant contribution to stretch-induced changes in V_m by SAC_{NS} is further supported by the observation that effects can be eliminated in the ventricle [56] and atrium [31] by pharmacological block of this channel. In turn, activation of SAC_{NS} is sufficient to trigger AP generation in isolated cardiomyocytes [57]. Interestingly, SAC_{NS} blockers do not prevent the drop in refractory period seen

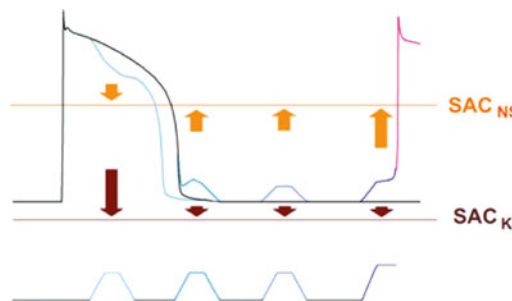


Fig. 7.2 Schematic representation of transient stretch effects on whole-cell membrane potentials (V_m), and indication of contributions by cation non-selective and K^+ -selective stretch-activated channels (SAC_{NS} and SAC_K , respectively). SAC_{NS} have a reversal potential about half-way between plateau and resting potential. Depending on the timing of mechanical stimuli (bottom curve), SAC_{NS} activation may shorten AP duration, cause early or delayed after-depolarisation-like behaviour or, if strong enough, trigger excitation. The reversal potential of SAC_K is negative to resting V_m . Their activation, during *any* part of the cardiac cycle, would tend to re- or hyperpolarise cardiac cells, in particular during the AP plateau (when their electrotonic driving force is largest; compare lengths of arrows indicating SAC effects). Given that diastolic stretch, if it causes any change in V_m at all, tends to depolarise resting cells, this response appears to be dominated by SAC_{NS} under normal circumstances (from [23] with permission)

with atrial pressure loading of the isolated heart, suggesting that SAC_K may contribute to responses in that setting [58].

Relative contributions of SAC_{NS} and SAC_K to impact-induced VF have remained controversial. The vulnerable window for VF induction coincides with a period of pronounced heterogeneity in ventricular V_m and refractoriness. Mechanical stimulation, in this setting, depolarises cells that have regained excitability (presumably a SAC_{NS} effect, potentially giving rise to ectopic foci), while in other cells that are still more depolarised, the time course of repolarisation is altered (possibly through both SAC_{NS} and/or SAC_K effects, increasing heterogeneity in refractoriness). The former may provide the trigger and the latter a sustaining mechanism for arrhythmias, including VF. Among experimentally established contributors is the ATP-dependent potassium channel (K_{ATP}), whose open probability is also modulated by stretch [59]. In the presence of glibenclamide (to block K_{ATP}), the incidence of VF upon precordial impact is significantly reduced in pig. At the same time, impacts during the T-wave still trigger premature ventricular contractions, highlighting the continued ability to mechanically induce an arrhythmogenic trigger [60]. Application of streptomycin in the same animal model did not affect VF inducibility [61], but as mentioned before, there is a potential for false-negative interpretation of data obtained with systemic streptomycin application. This question will require further investigation, presumably using more specific blockers in smaller preparations, such as the Langendorff-perfused heart.

The principal electrophysiological effects of cardiac MEF have been reproduced in various computational models of cardiomyocyte SAC effects [62]. These formulations have been integrated into two- [48] and three-dimensional models [63] of ventricular tissue, which suggest that sustained reentry is observed only if a mechanical stimulus (1) encounters tissue that has regained excitability (so that an ectopic focus can arise), (2) overlaps with the trailing wave of repolarisation (so that local AP prolongation gives rise to an area of functional block), and (3) extends into tissue that is still at more positive V_m levels (so that regional AP shortening may help to sustain the arrhythmia). This would help explain why the most severe expression of CC, sudden cardiac death, is rare in real life. Computational modelling has also been utilised to investigate whether ischaemic lengthening may be responsible for mechanically induced excitation and reentry, suggesting that premature ventricular excitation originates from the ischaemic border because of mechanically induced depolarisation [64]. These computational predictions form interesting targets for experimental assessment.

7.3.5 Summary

Stretch of the myocardium, whether acute or chronic, has pronounced effects on cardiac electrophysiology. This can contribute to induction and sustenance of cardiac arrhythmias. Experimental models have reproduced effects of stretch on heart rhythm in single cells, tissue preparations, isolated hearts, and whole animals,

demonstrating that a significant proportion of effects can be explained by intracardiac MEF. Experimental and computational work strongly suggests a role for SAC in these responses. In addition to SAC, most ion channels in the heart can be modulated by the mechanical environment [65], which complicates the picture, in particular as longer-term responses mediated via ion concentration changes are concerned. In addition, effects of heterogeneous stretch on myocardial Ca^{2+} handling have been shown to independently act as sources of ectopic excitation (for review see [66]). The molecular mechanisms by which ion channels (and Ca^{2+} handling proteins) sense mechanical changes, as well as their individual roles in the generation of arrhythmias may, in the long run, help to devise new pharmacological and device therapies to treat disease associated with stretch-induced changes in heart rhythm.

7.4 Antiarrhythmic Effects of Mechanical Stimulation

7.4.1 *Background*

Schott's observation that a forceful blow to the chest wall (precordial thump, PT) could restore a palpable pulse of a patient in ventricular standstill during a Stokes–Adams attack, published in 1920, is believed to have been the first report in the European medical literature on antiarrhythmic effects of mechanical stimulation [67]. Since then, mechanical resuscitation has been attempted using a range of interventions. However, even though PT has been a documented part of European clinical practice for much of the past century, there is little agreement on mechanisms and clinical utility of mechanical cardioversion.

7.4.2 *Clinical Observations*

Antiarrhythmic mechanical stimulation has been observed in various clinical settings. In his studies of “intracardiac therapy” in the 1930s, Hyman found that the mechanical interaction of a needle with the myocardium could induce contractile activity [68]. Similarly, direct myocardial contact of catheters can cause ectopic activity, with case reports illustrating termination of VT, ventricular bradycardia [27], and even atrial fibrillation [69]. Cardiac mechano-sensitivity is also exploited by cardiac surgeons when weaning the heart from cardio-pulmonary bypass, where finger-tapping of the heart may serve to restore rhythmic contractile activity, in particular after failed electrical defibrillation. Extra-corporeal mechanical stimuli can trigger contractions in ventricular standstill [70], for example to maintain consciousness in cardiac arrest victims [71], and (although less reliably) terminate VT and VF [72]. Several reports have also found a link between an abrupt increase in intrathoracic pressure (due to

coughing [73] or the Valsalva manoeuvre [32]) and termination of tachyarrhythmias, although contributions by the nervous system and/or improved coronary perfusion have not been differentially assessed.

7.4.3 Experimental Studies

The use of cardiac catheterisation to terminate sustained cardiac arrhythmias was systematically explored in patients by Befeler [27], who showed that catheter tip stimulation of atrial and ventricular muscle is effective in reverting various rhythm disturbances (24% of atrial tachycardia cases, 60% of junctional tachycardias, and 14% of VT).

The success rate of PT has been studied with highly variable results. In the study by Befeler, 27% of VT cases were successfully treated with PT [27], while other studies have shown success rates exceeding 40% [74]. Only two prospective studies on PT effects have been published, one assessing PT outcomes in the cardiac catheterisation lab [75], the other in the out-of-hospital cardiac arrest setting [76]. Both demonstrated vanishingly low success rates of tachyarrhythmia termination by PT (below 2%). However, the use of PT may be more promising in the asystolic heart, where PT-induced restoration of spontaneous circulation was found in 50% of resuscitated asystolic cardiac arrest victims (the study suffers from low *n*-numbers, so extrapolation to practice should be done with care [76]).

The (limited) clinical utility of PT in the setting of VF appears to be related to time since collapse, as all reported successful cases of PT-induced cardioversion occurred very early during the development of VF, either at the verge of VT deterioration [77] or within the first few seconds of VF [27]. Animal models of PT have shown a similar disparity of results, with success rates ranging from 0% in an asphyxiated dog model [78] to 95% in a post-infarction pig model [79], suggesting that the utility of PT may be related to myocardial tissue energy supply.

7.4.4 Underlying Mechanisms

The mechanisms underlying mechanical induction of ectopic excitation in the asystolic heart have been discussed earlier, and similar mechanisms may underlie PT pacing of patients in ventricular standstill. The dynamic interaction of SAC effects with ectopic foci and/or reentrant excitation in the tachycardiac heart is more complex.

During mechanical stimulation in VT and VF, cells in the excitable gap(s) will be near the resting V_m , while others will be at various stages of the AP (somewhat like in the setting of CC, only that there will be multiple waves that coexist in the tissue). Stretch of resting cells, if of sufficient amplitude, may cause excitation and obliterate the excitable gap. In cases where (1) no other reentrant circles survive and

(2) no new ones are created by the intervention, this may terminate the arrhythmia. Computational models have shown that this conceptual view is biophysically plausible, using two- [62] and three-dimensional models [80]. Interestingly, these models also highlight how reduced availability in energy substrates may render PT less efficient. This is mediated via an ATP-reduction induced “preconditioning” of K_{ATP} channels, which activate more readily upon mechanical stimulation in ischaemic conditions [81]. In the models, mechanical co-activation of K_{ATP} channels shifts the whole-cell “net” E_{rev} towards more negative potentials than would be encountered with SAC_{NS} activation alone. This shortens AP duration and reduces the ability of mechanical stimulation to render resting cells inexcitable, with eventual failure to terminate reentry, as observed in the setting of severe hypoxia [78].

7.4.5 Summary

The antiarrhythmic effects of mechanical stimulation in various settings have been known to medical practitioners for well over a century. PT can be utilised to pace the asystolic heart or, less successfully, to terminate tachyarrhythmias. These beneficial effects have been attributed to SAC_{NS} activation. However, reported success rates vary drastically, and even though PT can be quickly and easily applied, current international resuscitation guidelines have de-emphasised PT as an intervention for cardiac arrest. There is concern, also, regarding the timing of PT, due to potential proarrhythmic effects of mechanical stimulation. The idea, however, that ill-timed PT would easily convert VT to VF has not been confirmed in most studies, except in the setting of preexisting severe hypoxia [78]. Overall, reported PT side-effects have been rare and minor. The variable success rates of PT may be related to a lack of training and/or variability in energy delivery by individuals applying PT. The scarcity of prospective study data calls for further research, to help identify the clinical utility of PT, and to explore the potential for more sophisticated mechanical interventions in antiarrhythmic therapy.

7.5 Conclusion

The heart is an integrated electro-mechanical system. Firmly established mechanisms underlying cardiac MEF effects include mechanical modulation of transsarcolemmal ion fluxes and intracellular Ca^{2+} handling. MEF affects heart rate and rhythm, from venous return-mediated changes in SAN pacemaker rate to stretch-induced induction or termination of arrhythmias.

What is less clear is the physiological relevance of MEF. Of course, from a regulation theory point of view, ECC *should* be complemented by an intracardiac feedback pathway from mechanics to electrics [82]. But perhaps many of the “most striking” examples of MEF on electrophysiology are, in fact, secondary to mechanisms

involved in mechanical modulation of contractility. Strategies successfully employed in skeletal muscle force grading, such as spatial recruitment or temporal summation of muscle fibre contractility, are ill-suited for the heart where all muscle cells contract on every cycle of the heart, where long AP plateaus cover most or all of the period during which cytosolic free Ca^{2+} is elevated, and where neuromuscular junctions for individual cells are missing. Thus, cardiac myocytes must be able to actively adjust their contractility to locally prevailing, and temporally changing, mechanical demands. If this involved mechanisms (such as SAC) that – in response to distension (or reduced cell shortening) – allowed a cardiomyocyte to preserve or gain Ca^{2+} (whether directly, or indirectly via Na^+ influx with knock-on effects on $\text{Na}^+/\text{Ca}^{2+}$ exchanger flux balance), then that would offer an evolutionary advantage. This advantage for mechanics may well be more important than the associated “side effect” of inward currents, which carry a risk of triggering ectopic excitation or contributing to the sustenance of tachyarrhythmias.

Clearly, this is an area for further study. What is without question is that the heart is an exquisitely mechano-sensitive organ, and that this mechano-sensitivity has direct effects on heart rate and rhythm.

Acknowledgement Work in the authors' laboratory is supported by the British Heart Foundation, the UK's Medical Research Council, Biotechnology and Biological Sciences Research Council, Engineering and Physical Sciences Research Council, and by funding from the EU FP6 and FP7 framework programmes.

References

1. Bainbridge FA. The influence of venous filling upon the rate of the heart. *J Physiol.* 1915;50: 65–84.
2. Donald DE, Shepherd JT. Reflexes from the heart and lungs: physiological curiosities or important regulatory mechanisms. *Cardiovasc Res.* 1978;12:446–69.
3. Blinks JR. Positive chronotropic effect of increasing right atrial pressure in the isolated mammalian heart. *Am J Physiol.* 1956;186:299–303.
4. Deck KA. Dehnungseffekte am spontanschlagendenen, isolierten Sinusknoten [effects of stretch on the spontaneously beating, isolated sinus node]. *Pflugers Arch Gesamte Physiol Menschen Tiere.* 1964;280:120–30.
5. Cooper PJ, Lei M, Cheng LX, Kohl P. Selected contribution: axial stretch increases spontaneous pacemaker activity in rabbit isolated sinoatrial node cells. *J Appl Physiol.* 2000;89: 2099–104.
6. Yasuma F, Hayano J. Respiratory sinus arrhythmia: why does the heartbeat synchronize with respiratory rhythm? *Chest.* 2004;125:683–90.
7. Bernardi L, Keller F, Sanders M, Reddy PS, Griffith B, Meno F, et al. Respiratory sinus arrhythmia in the denervated human heart. *J Appl Physiol.* 1989;67:1447–55.
8. Bernardi L, Salvucci F, Suardi R, Solda PL, Calciati A, Perlini S, et al. Evidence for an intrinsic mechanism regulating heart rate variability in the transplanted and the intact heart during submaximal dynamic exercise? *Cardiovasc Res.* 1990;24:969–81.
9. Casadei B, Moon J, Johnston J, Caiazza A, Sleight P. Is respiratory sinus arrhythmia a good index of cardiac vagal tone in exercise? *J Appl Physiol.* 1996;81:556–64.

10. Brooks CM, Lu HH, Lange G, Mangi R, Shaw RB, Geoly K. Effects of localized stretch of the sinoatrial node region of the dog heart. *Am J Physiol.* 1966;211:1197–202.
11. Wilson SJ, Bolter CP. Do cardiac neurons play a role in the intrinsic control of heart rate in the rat? *Exp Physiol.* 2002;87:675–82.
12. Hagiwara N, Masuda H, Shoda M, Irisawa H. Stretch-activated anion currents of rabbit cardiac myocytes. *J Physiol.* 1992;456:285–302.
13. Lei M, Kohl P. Swelling-induced decrease in spontaneous pacemaker activity of rabbit isolated sino-atrial node cells. *Acta Physiol Scand.* 1998;164:1–12.
14. Clemo HF, Stambler BS, Baumgarten CM. Persistent activation of a swelling-activated cation current in ventricular myocytes from dogs with tachycardia-induced congestive heart failure. *Circ Res.* 1998;83:147–57.
15. Le Guennec JY, Peineau N, Argibay JA, Mongo KG, Garnier D. A new method of attachment of isolated mammalian ventricular myocytes for tension recording: length dependence of passive and active tension. *J Mol Cell Cardiol.* 1990;22:1083–93.
16. Craelius W, Chen V, el-Sherif N. Stretch activated ion channels in ventricular myocytes. *Biosci Rep.* 1988;8:407–14.
17. Cooper PJ, Kohl P. Species- and preparation-dependence of stretch effects on sino-atrial node pacemaking. *Ann N Y Acad Sci.* 2005;1047:324–35.
18. Suchyna TM, Johnson JH, Hamer K, Leykam JF, Gage DA, Clemo HF, et al. Identification of a peptide toxin from Grammostola spatulata spider venom that blocks cation-selective stretch-activated channels. *J Gen Physiol.* 2000;115:583–98.
19. Stockbridge LL, French AS. Stretch-activated cation channels in human fibroblasts. *Biophys J.* 1988;54:187–90.
20. Camelliti P, Green CR, LeGrice I, Kohl P. Fibroblast network in rabbit sinoatrial node: structural and functional identification of homogeneous and heterogeneous cell coupling. *Circ Res.* 2004;94:828–35.
21. Kohl P, Kamkin AG, Kiseleva IS, Noble D. Mechanosensitive fibroblasts in the sino-atrial node region of rat heart: interaction with cardiomyocytes and possible role. *Exp Physiol.* 1994;79:943–56.
22. Bolter CP, Wilson SJ. Influence of right atrial pressure on the cardiac pacemaker response to vagal stimulation. *Am J Physiol.* 1999;276:R1112–7.
23. Kohl P. Cardiac stretch-activated channels and mechano-electric transduction. In: Zipes DP, Jalife J, editors. *Cardiac electrophysiology: from cell to bedside.* 5th ed. Philadelphia, Elsevier Saunders. 2009;115–26.
24. Lakatta EG, Maltsev VA, Vinogradova TM. A coupled SYSTEM of intracellular Ca^{2+} clocks and surface membrane voltage clocks controls the timekeeping mechanism of the heart's pacemaker. *Circ Res.* 2010;106:659–73.
25. Iribe G, Ward CW, Camelliti P, Bollensdorff C, Mason F, Burton RA, et al. Axial stretch of rat single ventricular cardiomyocytes causes an acute and transient increase in Ca^{2+} spark rate. *Circ Res.* 2009;104:787–95.
26. Nesbitt AD, Cooper PJ, Kohl P. Rediscovering commotio cordis. *Lancet.* 2001;357:1195–7.
27. Befeler B. Mechanical stimulation of the heart: its therapeutic value in tachyarrhythmias. *Chest.* 1978;73:832–8.
28. Kohl P, Hunter P, Noble D. Stretch-induced changes in heart rate and rhythm: clinical observations, experiments and mathematical models. *Prog Biophys Mol Biol.* 1999;71: 91–138.
29. Berdowski J, Tijssen JG, Koster RW. Chest compressions cause recurrence of ventricular fibrillation after the first successful conversion by defibrillation in out-of-hospital cardiac arrest. *Circ Arrhythm Electrophysiol.* 2010;3:72–8.
30. Levine JH, Guarneri T, Kadish AH, White RI, Calkins H, Kan JS. Changes in myocardial repolarization in patients undergoing balloon valvuloplasty for congenital pulmonary stenosis: evidence for contraction-excitation feedback in humans. *Circulation.* 1988;77:70–7.

31. Ninio DM, Saint DA. The role of stretch-activated channels in atrial fibrillation and the impact of intracellular acidosis. *Prog Biophys Mol Biol*. 2008;97:401–16.
32. Waxman MB, Wald RW, Finley JP, Bonet JF, Downar E, Sharma AD. Valsalva termination of ventricular tachycardia. *Circulation*. 1980;62:843–51.
33. Franz MR, Cima R, Wang D, Profitt D, Kurz R. Electrophysiological effects of myocardial stretch and mechanical determinants of stretch-activated arrhythmias. *Circulation*. 1992;86:968–78.
34. Hansen DE, Craig CS, Hondeghem LM. Stretch-induced arrhythmias in the isolated canine ventricle. Evidence for the importance of mechanoelectrical feedback. *Circulation*. 1990;81:1094–105.
35. Schlamka G, Hinrichs A. Experimentelle Untersuchungen über den Einfluß stumpfer Brustkorbverletzungen auf das Elektrokardiogramm. *Z Gesamte Exp Med*. 1932;81:43–61.
36. Schlamka G, Hinrichs A. Untersuchungen über den Einfluß stumpfer Brustkorbtraumen auf das Elektrokardiogramm (II. Mitteilung). *Z Gesamte Exp Med*. 1932;83:779–91.
37. Link MS, Wang PJ, Pandian NG, Bharati S, Udelson JE, Lee MY, et al. An experimental model of sudden death due to low-energy chest-wall impact (commotio cordis). *N Engl J Med*. 1998;338:1805–11.
38. Bode F, Franz M, Wilke I, Bonnemeier H, Schunkert H, Wiegand U. Ventricular fibrillation induced by stretch pulse: implications for sudden death due to commotio cordis. *J Cardiovasc Electrophysiol*. 2006;17:1011–7.
39. Sung D, Mills RW, Schettler J, Narayan SM, Omens JH, McCulloch AD. Ventricular filling slows epicardial conduction and increases action potential duration in an optical mapping study of the isolated rabbit heart. *J Cardiovasc Electrophysiol*. 2003;14:739–49.
40. Kaufmann R, Theophile U. Automatie-fördernde Dehnungseffekte an Purkinje-Fäden, Papillarmuskeln und Vorhoftrabekeln von Rhesus-Affen [Automaticity promoting extension effects in Purkinje fibers, papillary muscles and trabeculae carneae of rhesus monkeys]. *Pflugers Arch Gesamte Physiol Menschen Tiere*. 1967;297:174–89.
41. Dominguez G, Fozzard HA. Effect of stretch on conduction velocity and cable properties of cardiac Purkinje fibers. *Am J Physiol*. 1979;237:C119–24.
42. Chang SL, Chen YC, Chen YJ, Wangcharoen W, Lee SH, Lin CI, et al. Mechanoelectrical feedback regulates the arrhythmogenic activity of pulmonary veins. *Heart*. 2007;93:82–8.
43. Wang JH, Thampatty BP. Mechanobiology of adult and stem cells. *Int Rev Cell Mol Biol*. 2008;271:301–46.
44. Link MS, Maron BJ, Wang PJ, VanderBrink BA, Zhu W, Estes III NA. Upper and lower limits of vulnerability to sudden arrhythmic death with chest-wall impact (commotio cordis). *J Am Coll Cardiol*. 2003;41:99–104.
45. Alsheikh-Ali AA, Akelman C, Madias C, Link MS. Endocardial mapping of ventricular fibrillation in commotio cordis. *Heart Rhythm*. 2008;5:1355–6.
46. Cooper PJ, Epstein A, Macleod IA, Schaaf ST, Sheldon J, Boulin C, et al. Soft tissue impact characterisation kit (STICK) for ex situ investigation of heart rhythm responses to acute mechanical stimulation. *Prog Biophys Mol Biol*. 2006;90:444–68.
47. Quinn TA, Lee P, Bub G, Epstein A, Kohl P. Regional impact-induced arrhythmia in isolated rabbit heart visualised by optical mapping. *Heart Rhythm*. 2010;7:S353.
48. Garmy A, Kohl P. Mechanical induction of arrhythmias during ventricular repolarization: modeling cellular mechanisms and their interaction in two dimensions. *Ann N Y Acad Sci*. 2004;1015:133–43.
49. Seo K, Inagaki M, Nishimura S, Hidaka I, Sugimachi M, Hisada T, et al. Structural heterogeneity in the ventricular wall plays a significant role in the initiation of stretch-induced arrhythmias in perfused rabbit right ventricular tissues and whole heart preparations. *Circ Res*. 2010;106:176–84.
50. Parker KK, Lavelle JA, Taylor LK, Wang Z, Hansen DE. Stretch-induced ventricular arrhythmias during acute ischemia and reperfusion. *J Appl Physiol*. 2004;97:377–83.
51. Lu F, Jun-Xian C, Rong-Sheng X, Jia L, Ying H, Li-Qun Z, et al. The effect of streptomycin on stretch-induced electrophysiological changes of isolated acute myocardial infarcted hearts in rats. *Europace*. 2007;9:578–84.

52. Barrabes JA, Garcia-Dorado D, Padilla F, Agullo L, Trobo L, Carballo J, et al. Ventricular fibrillation during acute coronary occlusion is related to the dilation of the ischemic region. *Basic Res Cardiol.* 2002;97:445–51.
53. Chorro FJ, Trápero I, Guerrero J, Such LM, Canoves J, Mainar L, et al. Modification of ventricular fibrillation activation patterns induced by local stretching. *J Cardiovasc Electrophysiol.* 2005;16:1087–96.
54. Sachs F. Mechanical transduction by membrane ion channels: a mini review. *Mol Cell Biochem.* 1991;104:57–60.
55. Zabel M, Koller BS, Sachs F, Franz MR. Stretch-induced voltage changes in the isolated beating heart: importance of the timing of stretch. *Cardiovasc Res.* 1996;32:120–30.
56. Hansen DE, Borganelli M, Stacy GP, Taylor LK. Dose-dependent inhibition of stretch-induced arrhythmias by gadolinium in isolated canine ventricles. Evidence for a unique mode of antiarrhythmic action. *Circ Res.* 1991;69:820–31.
57. Craelius W. Stretch-activation of rat cardiac myocytes. *Exp Physiol.* 1993;78:411–23.
58. Bode F, Sachs F, Franz MR. Tarantula peptide inhibits atrial fibrillation. *Nature.* 2001;409:35–6.
59. Van Wagoner DR. Mechanosensitive gating of atrial ATP-sensitive potassium channels. *Circ Res.* 1993;72:973–83.
60. Link MS, Wang PJ, VanderBrink BA, Avelar E, Pandian NG, Maron BJ, et al. Selective activation of the K^+ _{ATP} channel is a mechanism by which sudden death is produced by low-energy chest-wall impact (Commotio cordis). *Circulation.* 1999;100:413–8.
61. Garan AR, Maron BJ, Wang PJ, Estes 3rd NA, Link MS. Role of streptomycin-sensitive stretch-activated channel in chest wall impact induced sudden death (commotio cordis). *J Cardiovasc Electrophysiol.* 2005;16:433–8.
62. Kohl P, Bollendorff C, Gurny A. Effects of mechanosensitive ion channels on ventricular electrophysiology: experimental and theoretical models. *Exp Physiol.* 2006;91:307–21.
63. Li W, Kohl P, Trayanova N. Induction of ventricular arrhythmias following mechanical impact: a simulation study in 3D. *J Mol Histol.* 2004;35:679–86.
64. Jie X, Gurev V, Trayanova N. Mechanisms of mechanically induced spontaneous arrhythmias in acute regional ischemia. *Circ Res.* 2010;106:185–92.
65. Morris CE, Juranka PF, Lin W, Morris TJ, Laitko U. Studying the mechanosensitivity of voltage-gated channels using oocyte patches. *Methods Mol Biol.* 2006;322:315–29.
66. Ter Keurs HE, Wakayama Y, Miura M, Shinozaki T, Stuyvers BD, Boyden PA, et al. Arrhythmogenic Ca^{2+} release from cardiac myofilaments. *Prog Biophys Mol Biol.* 2006;90:151–71.
67. Schott E. On ventricular standstill (Adam-Stokes attacks) together with other arrhythmias of temporary nature. *Dtsch Arch Klin Med.* 1920;131:211–29.
68. Hyman AS. Resuscitation of the stopped heart by intracardiac therapy. *Arch Intern Med.* 1930;46:553–68.
69. Lee HT, Cozine K. Incidental conversion to sinus rhythm from atrial fibrillation during external jugular venous catheterization. *J Clin Anesth.* 1997;9:664–7.
70. Scherf D, Bornemann C. Thumping of the precordium in ventricular standstill. *Am J Cardiol.* 1960;5:30–40.
71. Don Michael TA, Lond MB, Stanford RL. Precordial percussion in cardiac asystole. *Lancet.* 1963;1:699.
72. Pellis T, Kohl P. Antiarrhythmic effects of acute mechanical stimulation. In: Kohl P, Franz MR, Sachs F, editors. *Cardiac mechano-electric coupling and arrhythmias.* 2nd ed. Oxford, Oxford University Press. 2011; 361–8.
73. Criley JM, Blaufuss AH, Kissel GL. Cough-induced cardiac compression: self-administered form of cardiopulmonary resuscitation. *J Am Med Assoc.* 1976;236:1246–50.
74. Rajagopalan RS, Appu KS, Sultan SK, Jagannadhan TG, Nityanandan K, Sethuraman S. Precordial thump in ventricular tachycardia. *J Assoc Physicians India.* 1971;19:725–9.
75. Haman L, Parizek P, Vojacek J. Precordial thump efficacy in termination of induced ventricular arrhythmias. *Resuscitation.* 2009;80:14–6.

76. Pellis T, Kette F, Lovisa D, Franceschino E, Magagnin L, Mercante WP, et al. Utility of precordial thump for treatment of out of hospital cardiac arrest: a prospective study. *Resuscitation*. 2009;80:17–23.
77. Baderman H, Robertson NR. Thumping the precordium. *Lancet*. 1965;2:1293.
78. Yakkaitis RW, Redding JS. Precordial thumping during cardiac resuscitation. *Crit Care Med*. 1973;1:22–6.
79. Gertsch M, Hottinger S, Mettler D, Leupi F, Gurtner HP. Conversion of induced ventricular tachycardia by single and serial chest thumps: a study in domestic pigs 1 week after experimental myocardial infarction. *Am Heart J*. 1989;118:248–55.
80. Li W, Kohl P, Trayanova N. Myocardial ischemia lowers precordial thump efficacy: an inquiry into mechanisms using three-dimensional simulations. *Heart Rhythm*. 2006;3:179–86.
81. Van Wagoner DR, Lamorgese M. Ischemia potentiates the mechanosensitive modulation of atrial ATP-sensitive potassium channels. *Ann N Y Acad Sci*. 1994;723:392–5.
82. Kaufmann RL, Lab MJ, Hennekes R, Krause H. Feedback interaction of mechanical and electrical events in the isolated mammalian ventricular myocardium (cat papillary muscle). *Pflugers Arch*. 1971;324:100–23.
83. Cooper PJ, Kohl P. Mechanical modulation of sino-atrial node pacemaking. In: Kohl P, Franz MR, Sachs F, editors. *Cardiac mechano-electric feedback and arrhythmias: from pipette to patient*. 1st ed. Philadelphia, Elsevier Saunders. 2005;72–82.

Part II

Modeling

Chapter 8

A Historical Perspective on the Development of Models of Rhythm in the Heart

Penelope J. Noble and Denis Noble

8.1 Introduction

Models of cardiac rhythm have a long history, starting with the van der Pol equations in (1928) [1]. These equations were based on the idea of a relaxation oscillator, involving a threshold for activation of a rapid change to a different range of potentials, followed by a relatively slow relaxation towards a reverse threshold for return to the original range. Models of this type (including the Bonhoeffer modification in Bonhoeffer van der Pol (BVP) models) have their uses, particularly in mathematical analysis of rhythm, but they are not based on biophysically detailed experiments. Starting in the 1960s, 22 biophysically detailed models have been developed, of which 5 are Purkinje, 16 SA nodes and 1 AV node. Of the Purkinje models, three are mammalian, one canine and one human; seven of the SA node models are mammalian, eight are rabbit and one mouse and finally the AV Node model is of rabbit. In this chapter we simply explore the progress in model development, providing the reader with a comprehensive list of models and how they fit into the history of modelling of cardiac rhythm. In cases in which the authors own comments on the models seem to provide the best description we have quoted from the original paper as indicated.

The development of these models over time is illustrated in Table 8.1.

P.J. Noble and D. Noble (✉)

Department of Physiology, Anatomy and Genetics, Oxford University, Sherrington Building, Parks Rd, Oxford OX1 3PT, UK
e-mail: denis.noble@dpag.ox.ac.uk

Table 8.1 Historical development of cardiac models of rhythm

A. By model/species and cell type		1962	1975	1980	1984	1985	1989	1993	1994–2004	2006	2009
First cardiac mammalian Purkinje cell (model A)	Model A develop	First SAN model	SAN model B from model A	Model A develop	Model B develop	First network model atria and SAN	Eight (mostly rabbit) SAN	Mouse SAN model	Human and Canine Purkinje models	First AV Node model (rabbit)	
B. By model name (author)											
1962	1975	1980	1984	1985	1989	1993	1994–2004	2006	2009		
Noble	MNT	Yanagihara	Noble–Noble	DFN	Noble	Winslow	Demir et al. [2]	Mangoni	Stewart		
							Dokos [3]		Aslanidi		
							Endresen [4]				
							Demir et al. [5]				
							Zhang [6]				
							Sarai [7]				
							Garry [8]				
							Lovell [9]				
								Inada			

8.2 The Models and Their Key Features

8.2.1 Noble [10, 11]

The first model to be based on actual measurements of transmembrane ionic currents was that of Noble in 1962 [10], published in a preliminary form as a letter to *Nature* in 1960 [11].

Figure 8.1 shows the 1962 model run using COR. The top trace shows the cell voltage changes, while the bottom traces show the changes in ionic conductance in the sodium and potassium channels. The conductance scale has been chosen to

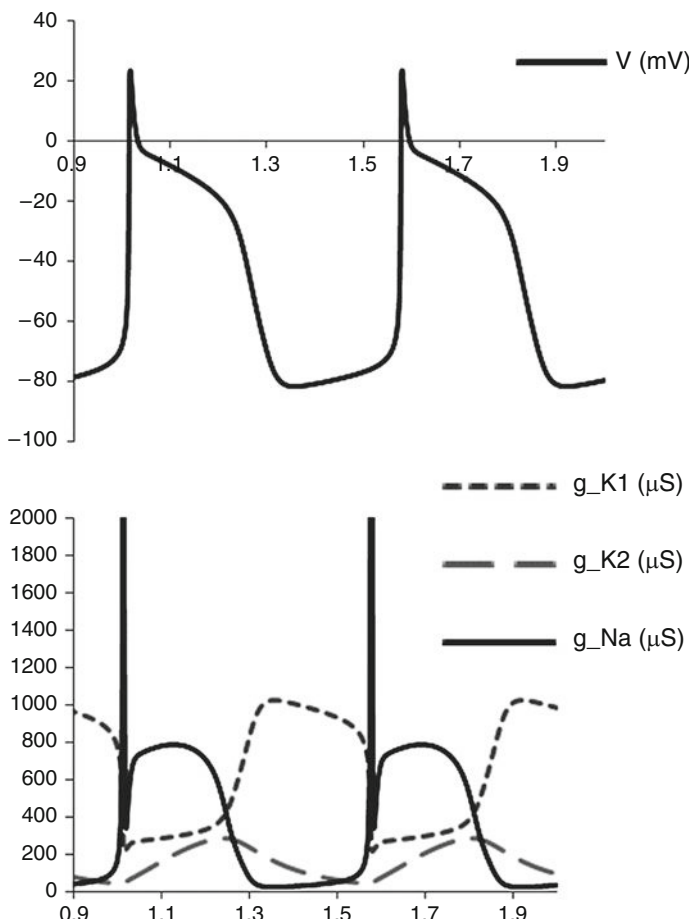


Fig. 8.1 The Noble 1962 model showing the role of the potassium conductances on the action potential profile. Note: g_{Na} peak up to around 12,000 μS

reveal the main changes during the plateau and pacemaker potential variations. The peak sodium conductance (at 12,000 μS) is way off the scale.

This model of a Purkinje fibre was developed using the Hodgkin–Huxley (1952) squid giant axon model [12] as a base. In fact, the sodium current equations were largely taken over from that model since Weidmann in 1956 [13] had shown great similarity between heart and nerve, while the potassium current equations were based on early membrane current measurements in sodium-deficient solutions. The classification of K current equations into inward and delayed rectifiers is still used today. The main success of the model was that it provided a counter-intuitive explanation of resistance changes during the action and pacemaker potentials, and in particular for the phenomenon of all-or-nothing repolarisation. This was inherent in the van de Pol equations, so this property is a very general one in the case of oscillators of the relaxation type. The existence of inward rectifier K current, I_{K1} , also provided a mechanism for energy conservation during the long plateau of the cardiac action potential.

Components: I_{Na} , I_K and I_{leak} .

8.2.2 McAllister–Noble–Tsien (MNT) [14]

This model was developed from Noble (1962) and is also a Purkinje fibre model. It was the first complete model to be based on the voltage clamp analyses of individual ionic current components performed over the 10 years leading up to the date of the model. The main advances in knowledge of ionic currents included the multiple components of the delayed rectifier K current. Noble and Tsien [15] were the first to identify the components I_{x1} and I_{x2} now referred to as I_{Kr} and I_{Ks} . It succeeded in reproducing slow action potentials in the absence of I_{Na} , so presaging the development of sinus node models, it established the independence of plateau and pacemaker mechanisms, and reproduced the notch separating spike and plateau phases of repolarisation. The main deficiency of the model was that the main contributor to the pacemaker depolarisation (I_{K2}) was interpreted as a pure potassium current. This is the current now known to be the hyperpolarising-activated current, I_f , carrying both sodium and potassium ions.

Components: I_{Na} , I_{si} , I_{K2} , I_{x1} , I_{x2} , I_{qr} , I_{K1} , I_{Nab} , I_{Clb} .

8.2.3 Yanagihara–Noma–Irisawa [16]

The first sinus node model was developed by Yanagihara, Noma and Irisawa in 1980. They were the first to succeed in difficult voltage clamp experiments in sinus node preparations (then multicellular), so this model based on their careful experimental measurements was a major step forward. In this model, the calcium current (called I_{si} in those days) is responsible for the upstroke and oscillation; changing the

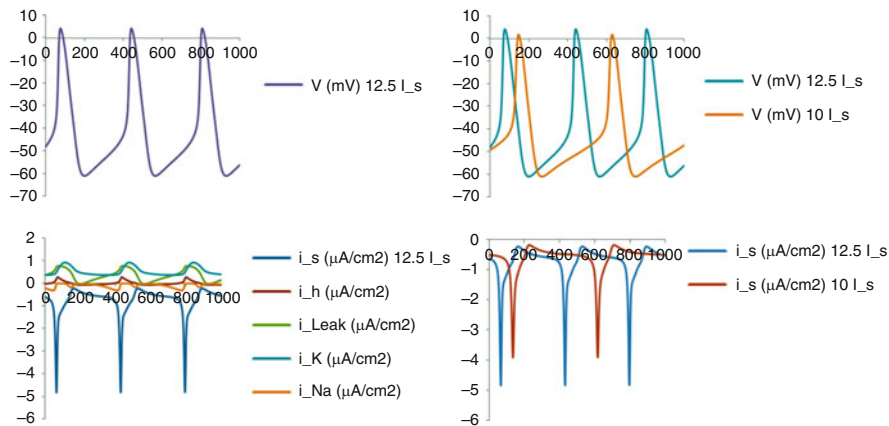


Fig. 8.2 The Yanagihara 1980 model showing the cell voltage (top left) and all underlying ionic currents in the model (bottom left). A lower maximum calcium current (I_s) reduces automaticity

maximum value for this current changes frequency of oscillation (see Fig. 8.2); an increase in frequency with increase in value of I_{\max} .

Components: I_{si} , I_K , I_f , I_{Na} , I_b .

8.2.4 Bristow–Clark [17]

This model is a modification of the MNT model to give SA node behaviour.

Components: I_{K1} , I_{K2} , I_{si} , I_K , I_{Na} , I_{bNa} , I_{bK} , I_{bsi} .

8.2.5 Noble–Noble [18]

8.2.5.1 Multicellular (100 Cells)

The first sinus node model to incorporate currents generated by Na–K and Na–Ca exchange processes and to reconstruct variations in intracellular and extracellular ion concentrations was that of Noble and Noble in 1984. It was developed from DFN even though DFN was actually published afterwards! This was simply attributable to the different time schedules of the two Royal Society journals involved. The method used was to change parameters from DFN to reflect data for the SA node, which had been obtained by Brown et al. [19, 20]. Both peripheral and central models were developed but these were speculative because of lack of data.

The really important development that this model established is that it was the first to highlight the role of Na–Ca exchange (NCX) and of Ca^{2+} oscillations in pacemaker activity. It can therefore be seen as a forerunner of models developed more recently by Lakatta's team [21]. Figure 8.3 shows the key result that NCX can

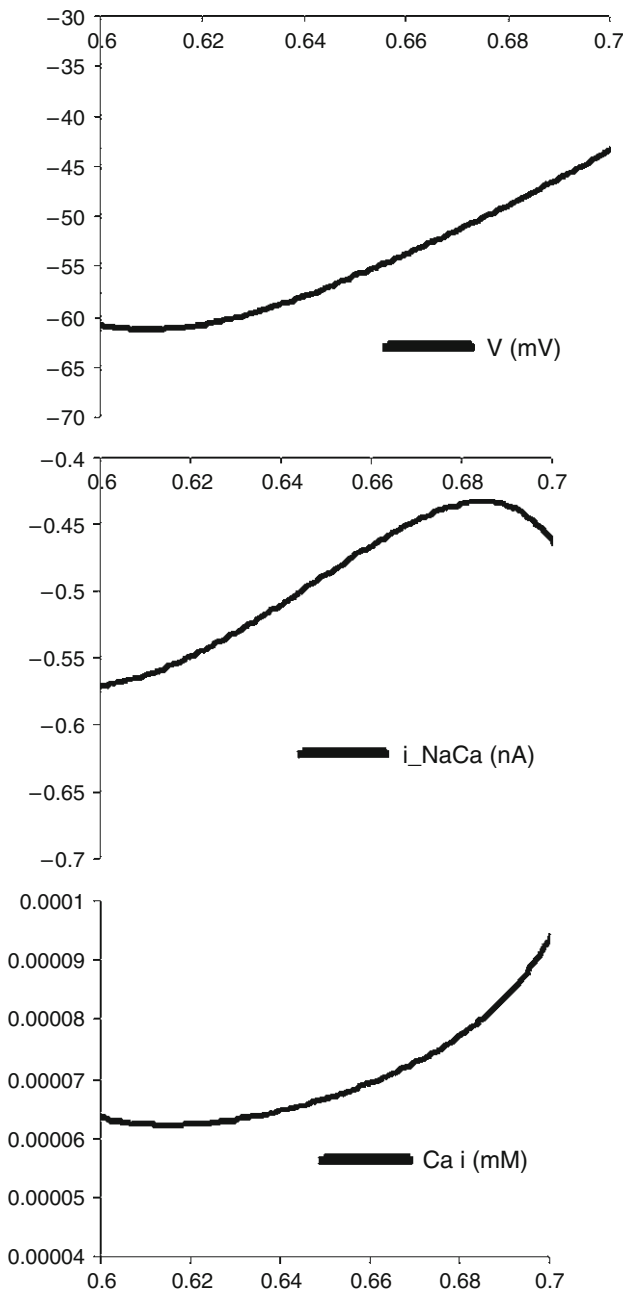


Fig. 8.3 *The Noble–Noble 1984 model. Role of calcium dynamics and NCX in depolarisation*

be activated towards the end of the pacemaker depolarisation by release of calcium from the sarcoplasmic reticulum occurring *before* the action potential upstroke. Only models reproducing variations in intracellular sodium and calcium can incorporate this property, as explained in the next section.

Components: I_f , I_K , I_{K1} , I_{Nab} , I_{Cab} , I_{NaK} , I_{NaCa} , I_{Na} , I_{si} , Na_i , Na_o , K_i , K_o , Ca_i , Ca_o .

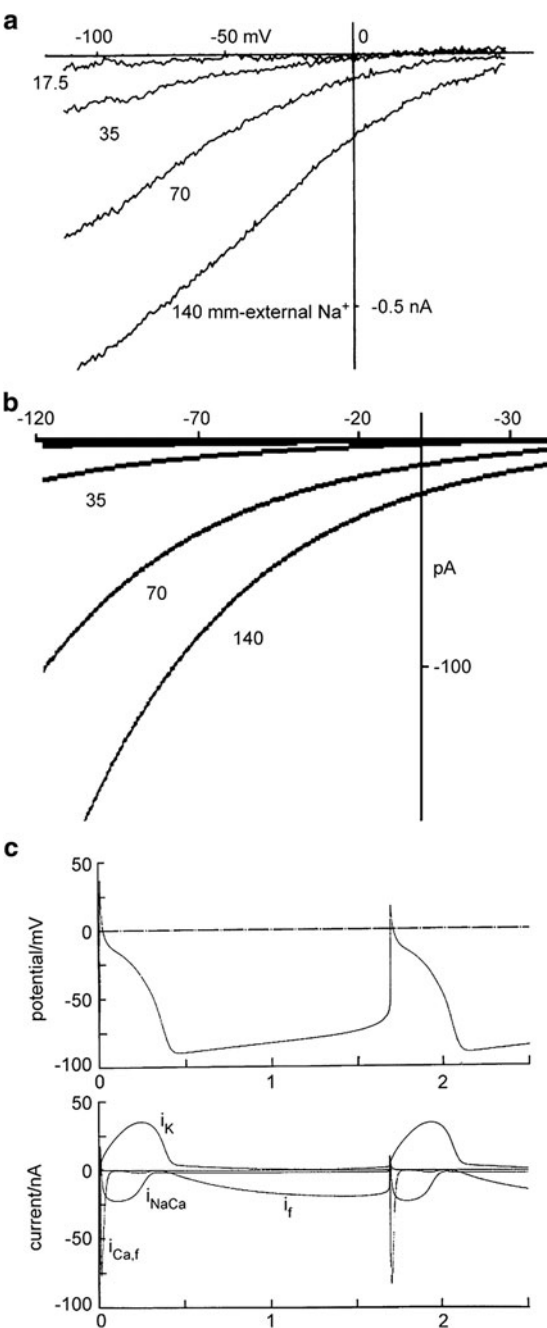
8.2.6 DiFrancesco–Noble (DFN) [22]

8.2.6.1 Multicellular (100 Cells)

This Purkinje fibre model was the first cardiac cell model to incorporate currents generated by Na–K and Na–Ca exchange processes and to reconstruct variations in intracellular and extracellular ion concentrations. As such, it is the generic model from which nearly all the subsequent models have been derived. It also incorporated the reinterpretation of I_{K2} (the pacemaker current in the MNT model) as I_f . Intracellular calcium sequestration and release by the sarcoplasmic reticulum were modelled, an aspect that was greatly improved in the Hilgemann–Noble [23] model of the atrial action potential by incorporating calcium buffers and the essential details of Fabiato's [24] work on calcium-induced calcium release. That model is not dealt with here since it does not concern pacemaker activity.

The incorporation of NCX into this model was originally quite controversial. Following its discovery in the heart by Reuter [25] in 1967, the exchanger had been thought to be electrically neutral, with a stoichiometry of two sodium ions for each calcium ion transported. But, with the known values for intracellular and extracellular sodium concentrations and external calcium concentration, this stoichiometry was found to be insufficient to drive resting calcium levels down to below those known to activate the contractile proteins. DiFrancesco and Noble therefore experimented with higher possible stoichiometries, including 4:1 (that favoured by Lorin Mullins [26], from whom the equations for sodium–calcium exchange were derived) and 3:1. The results were quite clear. Only 3:1 worked. The consequence, however, was the prediction that the exchanger must carry electric current during the action potential. The middle curves in Fig. 8.4 show the predicted current as a function of membrane potential at different levels of external sodium ion concentration. The lower figure shows a fairly large inward current predicted to occur during the plateau of the action potential. These results were mostly speculative until in 1986 and 1987 Kimura, Myamae and Noma [27] published their experimental results. The top curves in Fig. 8.4 show some of their results and how closely they correspond to the predicted curves (middle). The main difference is that the experimental results do not curve as strongly at very negative potentials, an effect that could be attributable to saturation of the carrier mechanism. It is not often that theoretical work leads to predictions as close as this to the experimental results! But it secured the main advance of the DiFrancesco–Noble model in incorporating not only successful representations of ion

Fig. 8.4 The DiFrancesco-Noble 1985 model. (a) Experimental results obtained by Kimura et al. [27]. (b) Current-voltage relations given by the equations for sodium-calcium exchange used in the DiFrancesco-Noble model. The curves show the relations at various external sodium concentrations. (c) Action and pacemaker potentials computed from the DiFrancesco-Noble modelling highlighting the roles played by activation of if during the pacemaker depolarisation and of i_{NaCa} during the action potential. Reproduced from Noble [28] with permission



concentration changes but also in making correct predictions of the consequences for ion current flow during normal rhythmic electrical activity.

Components: $I_f, I_K, I_{K1}, I_{to}, I_{Nab}, I_{Cab}, I_{NaK}, I_{NaCa}, I_{Na}, I_{si}, Na_i, Na_o, K_i, K_o, Ca_i, Ca_o$.

8.2.7 Reiner–Antzelevitch [29]

8.2.7.1 SA Node

This model is a modification of Bristow–Clark.

Components: $I_{K1}, I_f, I_{si}, I_K, I_{Na}, I_{bNa}, I_{bK}, I_{bsi}$.

8.2.8 Noble et al. [30]

8.2.8.1 SA Node

This model is based on Noble–Noble, modified to be appropriate to a single cell. The I_f and I_K equations were replaced by those from fits to more recent experimental data.

Components: $I_f, I_K, I_{K1}, I_{Nab}, I_{Cab}, I_{NaK}, I_{NaCa}, I_{Na}, I_{si}, Na_i, Na_o, K_i, K_o, Ca_i, Ca_o$.

8.2.9 Wilders [31]

8.2.9.1 SA Node

Wilders compared Bristow–Clark (1982), Irisawa–Noma (1980) and Noble–Noble (1984) models and found “drawbacks” which he aimed to correct in this model. In particular, he introduced I_{CaT} . Another major difference is that “in contrast to the other models only small amount of background current contributes to the overall electrical charge flow.”

Components: $I_{CaL}, I_{CaT}, I_f, I_K, I_{NaK}, I_{NaCa}, I_{bCa}, I_{bNa}, Na_i, Na_o, K_i, K_o, Ca_i, Ca_o$

8.2.10 Winslow et al. [32]

These were the first network models simulating atria and SA node together using Noble–Noble (1984) and Noble et al. (1989) models. They also represent the first use of massively parallel computers in cardiac electrophysiology. The computer used was the 64,000 processor Connection Machine at the University of Minnesota.

8.2.11 Demir et al. [2]

SA node; this was the first model specifically for rabbit. It used new equations for I_f , assessment of role of I_{CaT} during pacemaker depolarisation modifying pacemaker potential (whilst I_{CaL} important in upstroke and plateau). It incorporated I_{Na} based on recent experimental data and assessed the possible influence of pump, exchanger and background currents on pacemaker rate. The model incorporated the buffers troponin, calmodulin and calsequestrin and modified HN formulation for Ca dynamics.

Components: I_{Na} , I_{CaT} , I_{CaL} , I_K , I_f , I_B , I_{NaK} , I_{NaCa} , I_{CaP} , Na_i , Na_o , K_i , K_o , Ca_i , Ca_o .

8.2.12 Dokos et al. [3]

8.2.12.1 Rabbit SA Node

This chapter mentioned the Wilders et al. (1991) model. The authors provided a review and update of existing formulations – derived from a wide range of data from literature. The update included a significantly new formulation for NCX – not Mullins [26], but the E4 translocation model of Matsuoka and Hilgemann [33]. They found I_{bNa} to be the dominant mechanism underlying pacemaker depolarisation; I_K is insignificant in this phase in contrast to other models, if is not essential to pacemaker activity. A previous suggestion that net background current is outward during the pacemaker range of potentials was not found in this model. The AP overshoot is based on the reversal potential of I_{CaL} . The MDP is based on the reversal potential of I_K . The AP is sustained by incomplete deactivation of I_{CaL} and NCX. The model uses a square-root formula for inactivation of all K currents by $[K^+]_o$ – but is unable to reproduce correct response to elevated $[K^+]_o$.

Components: I_{CaL} , I_{CaT} , I_{Na} , I_K , I_f , I_{NaK} , I_{NaCa} , I_{bNa} , I_{bK} , Na_i , Na_o , K_i , K_o , Ca_i , Ca_o .

8.2.13 Endresen [4]

8.2.13.1 SA Node

This is a very simple model compared to previous models. It is modified from Morris and Lecar [34] barnacle giant muscle fibre model. The model is composed of two nonlinear first-order ODEs with ten constant parameters. Endresen stated that it perfectly reproduces experimentally recorded APs. A model of two coupled cells was developed. Vagal stimulation was simulated.

Components: I_s , I_K , I_{KACH} , I_j .

8.2.14 Demir et al. [5]

8.2.14.1 Rabbit SA Node

This model was an extension of the previous Demir et al. model to include responses to bath ACh and isoprenaline as well as neuronally released ACh; this was achieved via three types of muscarinic receptors. It was the first unified approach to modeling adrenergic and cholinergic effects on SAN pacemaker activity.

Components: I_{Na} , I_{CaT} , I_{CaL} , I_K , I_f , I_B , I_{NaK} , I_{NaCa} , I_{CaP} , I_{KACH} , Na_i , Na_o , K_i , K_o , Ca_i , Ca_o , cAMP.

8.2.15 Zhang et al. [6]

8.2.15.1 SA Node

This work included development of separate models of peripheral and central rabbit SA node cells based on experimental data. “The model-generated peripheral action potential has a more negative takeoff potential, faster upstroke, more positive peak value, prominent phase 1 repolarization, greater amplitude, shorter duration, and more negative maximum diastolic potential than the model-generated central action potential. In addition, the model peripheral cell shows faster pacemaking”. These results are consistent with experimental recordings. The model responds as in experiments to block of TTX- I_{Na} , I_{CaL} , I_{CaT} , I_{to} , I_{Kr} , I_{Ks} and I_f . “A one-dimensional model of a string of SA node tissue, incorporating regional heterogeneity, coupled to a string of atrial tissue has been constructed to simulate the behavior of the intact SA node”.

Components: I_{Na} , I_{CaL} , I_{CaT} , I_{to} , I_{sus} , I_{Kr} , I_{Ks} , I_f , I_{bNa} , I_{bCa} , I_{bK} , I_{NaCa} , I_{NaK} , I_{Cap} (concentrations constant).

8.2.16 Kurata et al. [35]

8.2.16.1 Rabbit SA Node

This is an “improved mathematical model for a single primary pacemaker cell of the rabbit sinoatrial node (SAN).” “Original features of our model include (1) incorporation of the sustained inward current (I_{st}) recently identified in primary pacemaker cells, (2) reformulation of voltage- and Ca^{2+} -dependent inactivation of the L-type Ca^{2+} channel current ($I_{\text{Ca,L}}$), (3) new expressions for activation kinetics of the rapidly activating delayed rectifier Kr channel current (I_{Kr}) and (4) incorporation of the subsarcolemmal space as a diffusion barrier for Ca^{2+} ”. This model was found to more accurately mimic effects of channel blockers and Ca^{2+} buffers on pacemaker activity than previous models.

Components: I_{CaL} , I_{CaT} , I_{Kr} , I_{Ks} , I_{to} , I_{sus} , I_{h} , I_{st} , I_{bNa} , I_{KACH} , I_{NaK} , I_{NaCa} , Na_i , Na_o , K_i , K_o , Ca_i , Ca_{sub} , Ca_o .

8.2.17 Sarai et al. [7, 36]

8.2.17.1 SA Node and Ventricular Cell

This model uses a common set of equations to describe SAN pacemaker [7] and ventricular [36] cells. The authors produced new kinetics for I_{K1} , I_K and I_{st} . Combined with NL contraction model it can reproduce the staircase phenomenon. They showed modulation by varying Ca_o and K_o to be well simulated and that the Ca gain agreed with experimental data. “Increasing the amplitude of L-type Ca^{2+} current (I_{CaL}) prolongs the duration of the action potential and thereby slightly decreases the spontaneous rate. On the other hand, a negative voltage shift of I_{CaL} gating by a few milliVolt markedly increases the spontaneous rate. When the amplitude of sustained inward current (I_{st}) is increased, the spontaneous rate is increased irrespective of the I_{CaL} amplitude. Increasing $[\text{Ca}^{2+}]_o$ shortens the action potential and increases the spontaneous rate. When the spontaneous activity is stopped by decreasing I_{CaL} amplitude, the resting potential is nearly constant (-35 mV) over 1–15 mM $[\text{K}^+]_o$ as observed in the experiment. This is because the conductance of the inward background nonselective cation current balances with the outward $[\text{K}^+]_{o-}$ dependent K^+ conductance. The unique role of individual voltage- and time-dependent ion channels is clearly demonstrated and distinguished from that of the background current by calculating an instantaneous zero current potential (‘lead potential’) during the course of the spontaneous activity.”

They included a comparison with other models: Wilders, Demir, “Oxsoft98”.

Components: I_{Na} , I_{CaL} , I_{CaT} , I_{K1} , I_{Kr} , I_i , I_{NaK} , I_{NaCa} , I_{st} , I_{ha} , I_{KACH} , I_{bNSC} , I_{Cab} , I_{Kpl} , I_{ICa} , I_{KATP} , Na_i , Na_o , K_i , K_o , Ca_i , Ca_o , ATP, NL contraction.

8.2.18 Garny et al. [8]

In 2002, Garny et al. [37] compared the Noble [30], Demir et al. [2], Dokos [3] and Zhang [6] SA node models, finding that according to current experimental data of that time, the Zhang (2000) model was the best model to use for incorporation into multicellular models of the atrium as it includes regional differences in SA node cells as well as responding correctly to interventions such as block of specific ionic currents.

This development was a “thorough overhaul” of Zhang. The authors “investigated the effects of intercellular coupling on SAN-atrial function. We reconfirm that removal of SAN to atrial connections causes a pacemaker shift from SAN center to its periphery, and show that (1) low dimensional multicellular models such as 1D SAN-atrial cell strands require larger, than experimentally established, coupling between individual cell pairs (to compensate for the lack in anatomic 3D spatial connectivity); (2) the increase in cell coupling from the center to the

periphery of the SAN is a crucial feature for rhythm entrainment and (3) the electrotonic effect of the atrium on SAN periphery is best described as opposing depolarization rather than hyperpolarizing".

"Thus, 1D models of the origin and spread of cardiac excitation, while limited by spatial parameter restrictions, can be a valuable tool for theoretical assessment of cardiac SAN atrial electrophysiology".

Figure 8.5 shows central and peripheral action potentials overlayed with the largest differences in currents: I_{sus} and I_{Kr} .

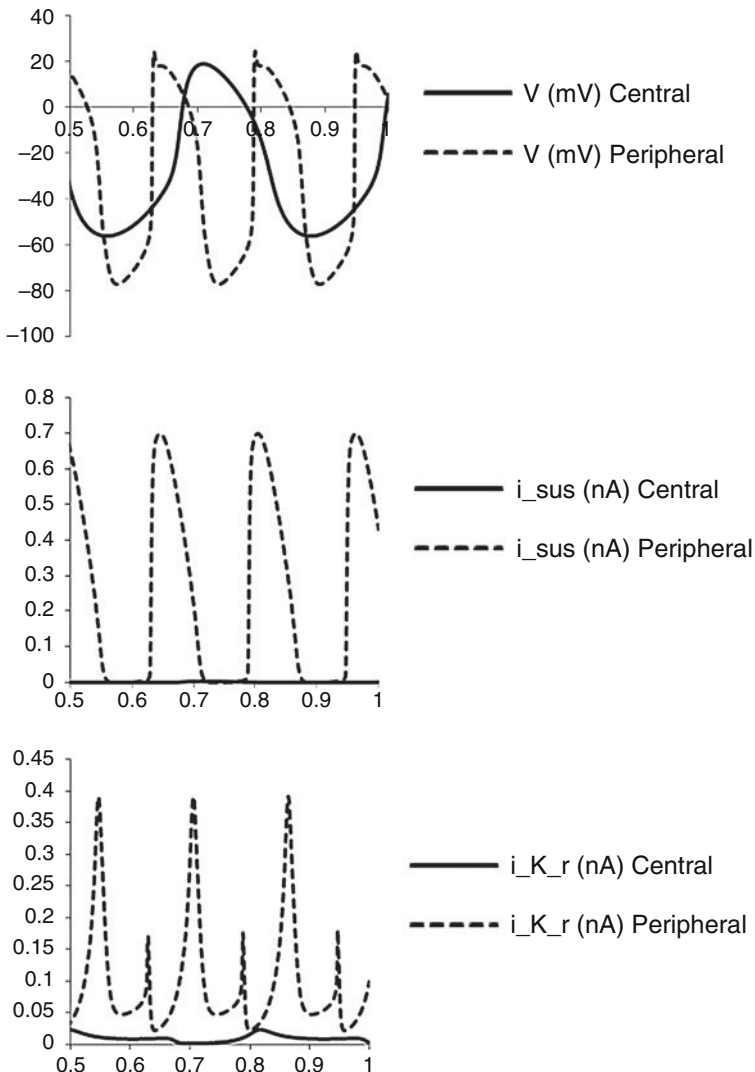


Fig. 8.5 The Gurny 2003 model showing central and peripheral versions. The conductances of many currents are higher in peripheral than central; most significantly ICaL and Ito are ~10 times, IKr 20 times and Isus 171 times

Components: I_{Na} , I_{CaL} , I_{CaT} , I_{to} , I_{sus} , I_{Kr} , I_{Ks} , I_{f} , I_{bNa} , I_{bCa} , I_{bK} , I_{NaCa} , I_{NaK} , I_{Cap} (concentrations constant).

8.2.19 Lovell et al. [9]

The authors said, “We have formulated a spatial-gradient model of action potential heterogeneity within the rabbit SAN, based on cell-specific ionic models of electrical activity from its central and peripheral regions. The ionic models are derived from a generic cell model, incorporating five background and exchange currents, and seven time-dependent currents based on three- or four-state Markov schemes. State transition rates are given by nonlinear sigmoid functions of membrane potential.”

“Using a custom least squares parameter optimisation routine, we have constructed a spatially-varying gradient model that exhibits a smooth transition in action potential characteristics from the central to the peripheral region, whilst ensuring individual membrane currents remain physiologically accurate. The gradient model is suitable for developing higher dimensional models of the right atrium, in which action potential heterogeneity within nodal tissue may be readily incorporated.”

Components: I_{f} , I_{Kr} , I_{Ks} , I_{bNa} , I_{Na} , I_{NaK} , I_{NaCa} , I_{to} , I_{CaL} , I_{CaT} , I_{bK} , I_{bCl} , Na_i , Na_o , K_i , K_o , Ca_i , Ca_o , Cl_i , Cl_o .

8.2.20 Mangoni et al. [38]

8.2.20.1 Mouse SA Node

This chapter emphasised the importance of calcium channels in pacemaking, because they substantially influence pacemaker rate. It dealt with knockout mice. This model is important as a mouse model and to illustrate different channel subtypes.

Cardiac and neuronal Na channels. Cardiac and pacemaker L-type Ca channels.

Components: I_{Na} , I_{Nas} , I_{CaD} , I_{CaL} , I_{CaT} , I_{to} , I_{sus} , I_{K1} , I_{Kr} , I_{Ks} , I_{f} , I_{bNa} , I_{bCa} , I_{bK} , I_{NaCa} , I_{NaK} , I_{st} .
(concentrations constant)

8.2.21 Stewart et al. [39]

It is interesting to note that, although the Purkinje fibre was the first cardiac tissue to be modelled, for two decades development of Purkinje fibre models had been neglected. This article introduced a human Purkinje fibre model and included validation against experimental data.

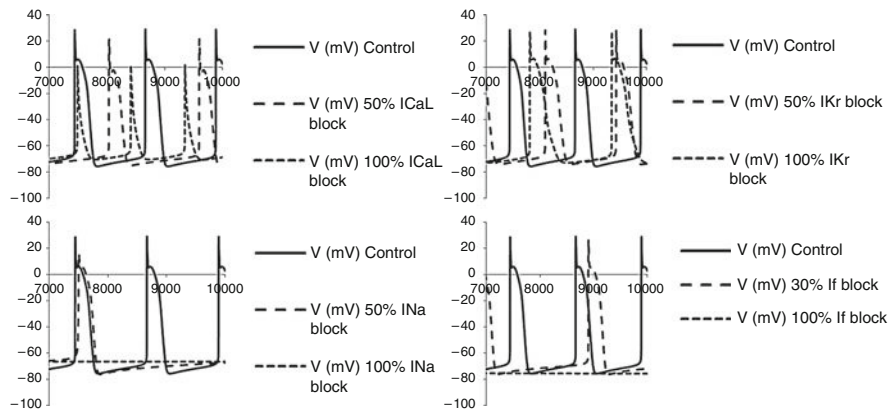


Fig. 8.6 The Stewart 2009 model showing the effects of block of ionic currents on autorythmicity. 100% block of ICaL increases automaticity whilst 50% block ICaL, INa or IKr and 30% block If slow the rate. Hundred percent block of INa or If abolish automaticity. IKs and Ito 50 and 100% blocks have minimal effects on rate (not shown)

Figure 8.6 illustrates the effects of blocked ionic currents on autorhythmic APs and suggests that I_{CaL} , I_{Na} and I_f have important roles in automaticity.

Components: I_{K1} , I_{to} , I_{sus} , I_{Kr} , I_{Ks} , I_{CaL} , I_{NaK} , I_{Na} , I_{bNa} , I_{NaCa} , I_{bCa} , I_{pK} , I_{pCa} , I_f , Na_i , Na_o , K_i , K_o , Ca_i , Ca_o .

8.2.22 Aslanidi et al. [40]

This work developed a structurally and electrophysiologically detailed model of the canine Purkinje-ventricular junction and varied heterogeneity parameters to determine the relationships between tissue structure, wave conduction velocity and safety through the nonuniform junction. The investigators note that slow and discontinuous wave conduction are considered to be proarrhythmogenic, hence their interest in investigating these features using their model.

Components: I_{Na} , I_{Nal} , I_{CaL} , I_{CaT} , I_{to1} , I_{to2} , I_{Kr} , I_{Ks} , I_{K1} , I_{NaCa} , I_{NaK} , I_{Nab} , I_{Kb} , I_{Cab} , I_{Clb} , I_{Cap} , I_{Kp} , Na_i , Na_o , K_i , K_o , Ca_i , Ca_o , Cl_i , Cl_o .

8.2.23 Inada et al. [41]

This is the first AV Node model. Separate action potential models were developed for single atrio-nodal, nodal and nodal-His cells. A 1D multicellular model including SAN and AVN was also created.

The models were found to show typical physiological and pathophysiological behaviour of the tissue.

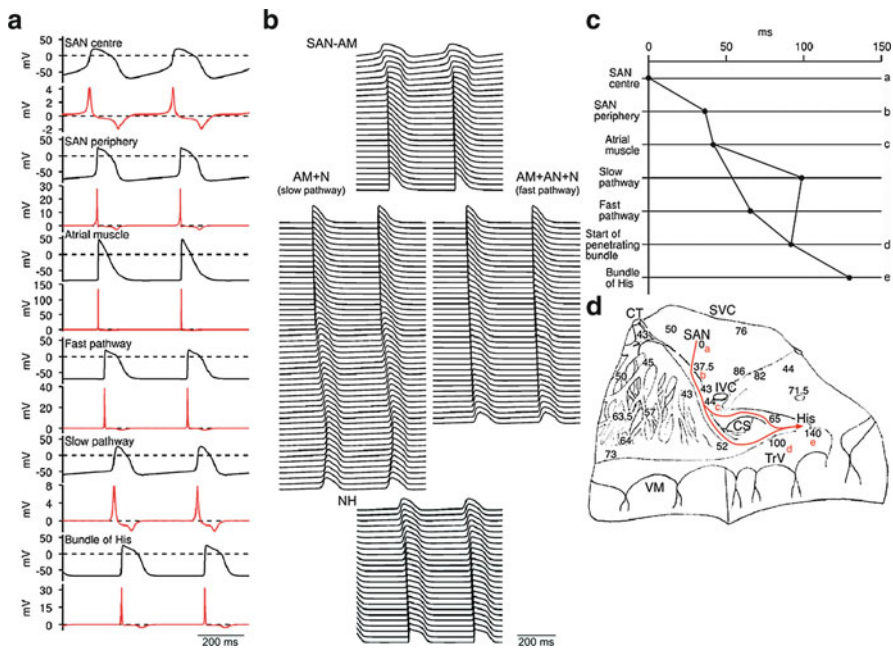


Fig. 8.7 The Inada 2009 model Action potential propagation from SAN to AVN. (A) Simulated action potentials and first derivative of membrane potential from centre and periphery of SAN, atrial muscle and AN, N and NH cells. (B) Action potentials from many cells along length of 1D multicellular model. Action potentials from consecutive cells are displaced downward. (C) Activation times at the centre and periphery of SAN, atrial muscle at start of fast and slow pathways into AVN, middle of fast and slow pathways, start of penetrating bundle and bundle of His (middle of penetrating bundle). (D) Activation times (in metrusecond) recorded experimentally in rabbit right atrial preparation including SAN and AVN during sinus rhythm (from DeCarvalho et al. [42]). Red or grey line is approximately equivalent to multicellular model. Letters a–e identify points along conduction pathway from SAN to AVN at which activation time was measured in simulation: a, centre of SAN; b, periphery of SAN; c, atrial muscle at start of fast and slow pathways into AVN; d, start of penetrating bundle; e, bundle of His. AM atrial muscle, CS coronary sinus, CT crista terminalis, His bundle of His, IVC inferior vena cava, SVC superior vena cava, TrV tricuspid valve, VM ventricular muscle. Reproduced from Inada et al. [37] with permission

Figure 8.7 illustrates the ability of the model to reproduce action potential propagation from sino-atrial node to atrio-ventricular node.

Components: I_{Na} , I_{CaL} , I_{to} , I_{Kr} , I_f , I_{st} , I_{K1} , I_{NaCa} , I_{NaK} , I_b , Ca_i , Ca_{sub} (Other concentrations constant).

8.3 Conclusions

In this chapter, we have given a systematic summary of all the known models of cardiac rhythm, while highlighting some of the most important milestones in the development of models in this field. It is clear that the range of species and types of

cardiac cell have greatly expanded in recent years. It is also clear to us that different models, even of the same cell type and species, concentrate on different applications. The idea that we could have a definitive set of models is elusive. Perhaps this is a reflection of the difficulty of dealing with the complexity of nature. A common experience in modelling is that when one aspect is improved in relation to fits to experimental data, other aspects of the model can “deteriorate” by this criterion. This is sometimes represented as a criticism of modelling. It seems to us rather to be an indication of the inevitably partial nature of all models. Models have ranges of application. Outside that range they can be misleading.

We hope that this chapter, through being systematic, will help researchers in this field to find their way through the large range of models available, to choose carefully those most appropriate to their applications. Used thoughtfully, and with good physiological insight, models can be a very helpful tool in physiology. After all, models are simply quantitative mathematical versions of what otherwise would be mere handwaving “ideas” on how cells work. It is better to be quantitative and precise than to hope to understand nature simply by reflecting on one’s experimental data in an armchair!

References

1. Van der Pol B, Van der Mark J. The heartbeat considered as a relaxation oscillation and an electrical model of the heart. *Philos Mag Suppl.* 1928;6:763–75.
2. Demir SS, Clark JW, Murphey CR, Giles WR. A mathematical model of a rabbit sinoatrial node cell. *Am J Physiol.* 1994;266:C832–52.
3. Dokos S, Celler B, Lovell N. Ion currents underlying sinoatrial node pacemaker activity: a new single cell mathematical model. *J Theor Biol.* 1996;181:245–72.
4. Endresen LP. Chaos in weakly-coupled pacemaker cells. *J Theor Biol.* 1997;184:41–50.
5. Demir SS, Clark JW, Giles WR. Parasympathetic modulation of sinoatrial node pacemaker activity in rabbit heart: a unifying model. *Am J Physiol.* 1999;276:H2221–44.
6. Zhang H, Holden AV, Kodama I, Honjo H, Lei M, Varghese T, et al. Mathematical models of action potentials in the periphery and center of the rabbit sinoatrial node. *Am J Physiol.* 2000;279:H397–421.
7. Sarai N, Matsuoka S, Kuratomi S, Ono K, Noma A. Role of individual ionic current systems in the SA node hypothesized by a model study. *Jpn J Physiol.* 2003;53:125–34.
8. Garny A, Kohl P, Hunter PJ, Boyett MR, Noble D. One-dimensional rabbit sinoatrial node models: benefits and limitations. *J Cardiovasc Electrophysiol.* 2003;14:S121–32.
9. Lovell NH, Cloherty SL, Celler BG, Dokos S. A gradient model of cardiac pacemaker myocytes. *Prog Biophys Mol Biol.* 2004;85:301–23.
10. Noble D. A modification of the Hodgkin–Huxley equations applicable to Purkinje fibre action and pace-maker potentials. *J Physiol.* 1962;160:317–52.
11. Noble D. Cardiac action and pacemaker potentials based on the Hodgkin–Huxley equations. *Nature.* 1960;188:495–7.
12. Hodgkin AL, Huxley AF. A quantitative description of membrane current and its application to conduction and excitation in nerve. *J Physiol.* 1952;117:500–44.
13. Weidmann S. *Elektrophysiologie der Herzmuselfaser.* Bern: Huber; 1956.
14. McAllister RE, Noble D, Tsien RW. Reconstruction of the electrical activity of cardiac Purkinje fibres. *J Physiol.* 1975;251:1–59.

15. Noble D, Tsien RW. Outward membrane currents activated in the plateau range of potentials in cardiac Purkinje fibres. *J Physiol.* 1969;200:205–31.
16. Yanagihara K, Noma A, Irisawa H. Reconstruction of the sino-atrial node pacemaker potential based on voltage clamp experiments. *Jpn J Physiol.* 1980;30:841–57.
17. Bristow DG, Clark JW. A mathematical model of primary pacemaking cell in SA node of the heart. *Am J Physiol.* 1982;243:H207–18.
18. Noble D, Noble SJ. A model of sino-atrial node electrical activity based on a modification of the DiFrancesco-Noble (1984) equations. *Proc R Soc Lond B.* 1984;222:295–305.
19. Brown HF, Kimura J, Noble D, Noble SJ, Taupignon A. The ionic currents underlying pacemaker activity in rabbit sino-atrial node: experimental results and computer simulations. *Proc R Soc Lond B.* 1984;222:329–47.
20. Brown HF, Kimura J, Noble D, Noble SJ, Taupignon A. 1984b Mechanisms underlying the slow inward current, i_{si} , in the rabbit sino-atrial node investigated by voltage clamp and computer simulation. *Proc R Soc Lond B.* 1984;222:305–28.
21. Maltsev VA, Lakatta EG. Synergism of coupled subsarcolemmal Ca^{2+} clocks and sarcolemmal voltage clocks confers robust and flexible pacemaker function in a novel pacemaker cell model. *Am J Physiol.* 2009;286:H594–615.
22. DiFrancesco D, Noble D. A model of cardiac electrical activity incorporating ionic pumps and concentration changes. *Philos Trans R Soc B.* 1985;307:353–98.
23. Hilgemann DW, Noble D. Excitation–contraction and extracellular calcium transients in rabbit atrium: reconstruction of basic cellular mechanisms. *Proc R Soc Lond B.* 1987;230:163–205.
24. Fabiato A. Calcium-induced release of calcium from the cardiac sarcoplasmic reticulum. *Am J Physiol.* 1983;243:C1–14.
25. Reuter H. The dependence of slow inward current in Purkinje fibres on the extracellular calcium-concentration. *J Physiol.* 1967;192:479–92.
26. Mullins LJ. Na/Ca exchange. In: *Ion transport in the Heart*. New York: Raven Press 1981; pp. 20–43.
27. Kimura J, Miyamae S, Noma A. Identification of sodium–calcium exchange current in single ventricular cells of guinea-pig. *J Physiol.* 1987;384:199–222.
28. Noble D. Hodgkin–Huxley–Katz prize lecture: From the Hodgkin–Huxley axon to the virtual heart. *J Physiol.* 2007;580:15–22.
29. Reiner VS, Antzelevitch C. Phase resetting and annihilation of a mathematical model of sinus node. *Am J Physiol.* 1985;249:H1143–53.
30. Noble D, DiFrancesco D, Denyer JC. Ionic mechanisms in normal and abnormal cardiac pacemaker activity. In: Jacklet J.W. *Cellular and neuronal oscillators*, 1989 59–85.
31. Wilders R, Jongasma HJ, van Ginneken ACG. Pacemaker activity of the rabbit sinoatrial node. A comparison of mathematical models. *Biophys J.* 1991;60:1202–16.
32. Winslow RL, Kimball AL, Varghese A, Noble D. Simulating cardiac sinus and atrial network dynamics on the connection machine. *Physica D.* 1993;64:281–98.
33. Matsuoka S, Hilgemann DW. Steady-state and dynamic properties of cardiac sodium–calcium exchange: ion and voltage dependencies of the transport cycle. *J Gen Physiol.* 1992; 100: 963–1001.
34. Morris C, Lecar H. Voltage oscillations in the barnacle giant muscle fiber. *Biophys J.* 1981; 35:193–213.
35. Kurata Y, Hisatome I, Imanishi S, Shibamoto T. Dynamical description of sinoatrial node pacemaking: improved mathematical model for primary pacemaker cell. *Am J Physiol.* 2002; 283:H2074–101.
36. Matsuoka S, Sarai N, Kuratomi S, Ono K, Noma A. Role of individual ionic current systems in ventricular cells hypothesized by a model study. *Jpn J Physiol.* 2003;53:105–23.
37. Garny A, Noble PJ, Kohl P, Noble D. Comparative study of rabbit sino-atrial node cell models. *Chaos Solitons Fractals.* 2002;13:1623–30.

38. Mangoni ME, Couette B, Marger L, Bourinet E, Striessnig J, Nargeot J. Voltage-dependent calcium channels and cardiac pacemaker activity: from ionic currents to genes. *Prog Biophys Mol Biol.* 2006;90:38–63.
39. Stewart P, Aslanidi OV, Noble D, Noble PJ, Boyett MR, Zhang H. Mathematical models of the electrical action potential of Purkinje fibre cells. *Philos Trans R Soc A.* 2009;367:2225–55.
40. Aslanidi OV, Stewart P, Boyett MR, Zhang H. Optimal velocity and safety of discontinuous conduction through the heterogeneous Purkinje-ventricular junction. *Biophys J.* 2009;97: 20–39.
41. Inada S, Hancox JC, Zhang H, Boyett MR. One-dimensional mathematical model of the atrioventricular node including atrio-nodal, nodal and nodal-His cells. *Biophys J.* 2009;97: 2117–27.
42. De Carvalho AP, Mello WC, Hoffman BF. Electrophysiological evidence for specialized fiber types in rabbit atrium. *Am J Physiol.* 1959;196:483–8.

Chapter 9

Simulation of Cardiac Action Potentials

Jonathan D. Moreno and Colleen E. Clancy

9.1 Introduction

The first simulation of action potentials traces its roots to Hodgkin and Huxley's mathematical formulations of the ionic currents in the squid giant axon in 1952 [1]. This seminal achievement helped usher in the era of simulation of cardiac action potentials with the Noble model of the cardiac Purkinje fiber [2, 3]. Computational modeling has proven useful in quantifying species-specific electrical behavior, gaining insight into diverse ionic mechanisms underlying normal and pathological action potential behavior, and making physiological predictions when experimental approaches are infeasible [4].

Action potential simulations are fundamentally a systems-based approach for understanding the biology that integrates data from the single channel and cellular levels to understand the effects of perturbations by mutations, pharmacology, and other aspects of cardiac dynamics. Cellular level predictions can then be readily extended into higher dimensions to study emergent dynamics in tissues and organs. In this chapter we describe how models of the isolated cardiac myocyte have evolved in the six decades since Hodgkin and Huxley, and highlight some applications of simulation-based approaches to understanding cardiac dynamics at the single-cell level.

J.D. Moreno

Tri-Institutional MD-PhD Program, Physiology, Biophysics and Systems Biology Graduate Program; Weill Cornell Medical College/The Rockefeller University/Sloan-Kettering Cancer Institute; Weill Medical College of Cornell University, 1300 York Avenue, New York, NY 10021, USA

C.E. Clancy (✉)

Department of Pharmacology, University of California, Genome Building Rm 3503, Davis, CA 95616-8636, USA
e-mail: ceclancy@ucdavis.edu

9.2 Brief Review of the Cardiac Action Potential Waveform

Action potentials can be divided into two categories: those that are self-oscillatory, such as pacemaker cells of the sinoatrial node, and those that require an external stimulus, such as atrial and ventricular cells [4]. This chapter focuses on the models of the ventricular myocyte, owing to the extensive literature base and because ventricular arrhythmias are believed to constitute the most reported fatal incidents of cardiac arrhythmias [5].

The ventricular myocardium displays many action potential morphologies owing to the wide variety of cell types including Purkinje cells, endocardial, midmyocardial, and epicardial cells found throughout the ventricular wall [4]. Although many action potential morphologies exist, depending on the location in the myocardium, the “classical” action potential generally has four phases. Phase 0 is the rapid depolarizing phase that results when Na^+ channels activate and an influx of Na^+ causes the membrane potential to depolarize. Phase 1 corresponds to inactivation of the Na^+ channels and also outward movement of K^+ ions through the I_{to} channels; this contributes to the notch found in some ventricular cell types. In phase 2, a low conductance plateau phase, inward and outward ion movements are balanced by Ca^{2+} channels (T-type and L-type) and delayed rectifier K^+ channels, respectively. Phase 3 marks the final repolarization phase of the action potential, allowing the cell to return to its resting potential (phase 4). Table 9.1 gives a brief summary of the ionic currents underlying a typical

Table 9.1 Major membrane currents underlying a typical ventricular action potential (reproduced from [4])

Membrane currents	Description	Protein (α -subunit)	Contribution to action potential
Inward ionic currents			
I_{Na}	Na^+ current	SCN5A	Initial depolarization of the action potential
$I_{\text{Ca,L}}$	L-type Ca^{2+} current	$\alpha_{\text{IC}}, \alpha_{\text{ID}}$	Maintains plateau phase of action potential
$I_{\text{Ca,T}}$	T-type Ca^{2+} current	$\alpha_{\text{IG}}, \alpha_{\text{IH}}$	Present in the late plateau phase
Outward ionic currents			
I_{to}	Ca^{2+} -independent transient outward K^+ current	Kv4.2, Kv4.3, Kv1.4	Responsible for early repolarization
$I_{\text{Kr}}, I_{\text{Ks}}$	Rapid and slow delayed K^+ rectifier currents	HERG, KvLQT1	Aids repolarization during plateau
$I_{\text{SS}}, I_{\text{Ks, Low}}$	Slow inactivating K^+ currents	Kv2.1, Kv1.5	Aids late repolarization
I_{K1}	Inward rectifier K^+ current	Kv2.1, Kir2.2	Late repolarization, helps establish V_{rest}
Other ionic currents			
I_{NaCa}	$\text{Na}^+-\text{Ca}^{2+}$ exchanger	NCX1, NCX2	Late depolarization
I_{NaK}	Na^+-K^+ pump	Na^+-K^+ ATPase	Late repolarization

ventricular action potential and their contribution to the cardiac action potential waveform.

Simulations allow for important characteristics of action potential shape, morphology and duration to be quantified. Common important parameters recorded for use in action potential simulations include [4]:

- The resting membrane potential, V_{rest}
- The maximum upstroke velocity, dV_m/dt , and the peak overshoot value during phase 0 depolarization
- Action potential duration at 50 and 90% repolarization, APD_{50} and APD_{90} , respectively

Parameters such as those listed above help to compare physiological and pathophysiological characteristics that the myocardium exhibits in response to disease, pharmacologic intervention, gender, and species differences.

9.3 First-Generation Models

As predicted by Hodgkin [6], the applicability of the HH formalism to other excitable cells gave way to first-generation models of the cardiac myocyte that were based largely on modification of the HH formalism. Broadly speaking, the evolution of cardiac models can be segmented into early first, and second-generation models. As compared to second-generation models, early cardiac myocyte models were based exclusively on the HH formalism and were relatively simple; they were formulated with a small number of equations, and were generic in species and cell type [7]. Mathematical representations for electrogenic ion pumps and exchangers did not exist, and thus ion concentrations were taken as constant [7]. While they were able to predict the general features of action potential morphology, there was no explicit link between the electrical activity and the underlying physiological processes such as openings and closings of specific ion channels [7]. Table 9.2 compares the first and second generation models.

Table 9.2 Comparison of first and second generation models

Model aspect	First generation	Second generation
Limited variables	Yes	No
Species-dependent	No	Yes
Cell-type specificity	No	Yes
Dynamic ion concentrations	No	Yes
Pumps and exchanger formulations	No	Yes
Hodgkin–Huxley formulations only	Yes	No
Markov formulations	No	Yes
Subspaces	No	Yes

9.4 Second Generation Models

Second generation models have now been developed that simulate cardiac action potentials from different species including canine [8, 9], guinea pig [10–15], human [16–19], frog [20], and rabbit [21]. Species specificity is important; for example, ventricular cells of some mammalian species (canine, human, guinea pig and rabbit) have action potentials characterized by a spike and dome morphology and a well-defined plateau phase [22]; in contrast, murine ventricular cells lack a well-defined plateau phase and have a much shorter APD₉₀ [4, 23–25]. Second-generation models also take into account the importance of gender [26] and specific cell-types (including endocardial, midmyocardial, and epicardial cells), which are important for transmural heterogeneity [27], and include numerous pumps, exchangers, and buffers that dynamically control the intracellular ion concentrations.

These models have allowed quantification of species-specific and cell type specific functional properties of action potential morphology, response to cardiac pharmacology, and general cardiac dynamics. For example, it is known that different drugs affect ionic currents to change action potential waveforms in a species, age, and gender-specific manner [4].

Tables 9.3 and 9.4 adapted from Professor Ronald Wilders [7] are by no means exhaustive, but list many seminal developments in first- and second-generation models with parent models and species type noted where appropriate.

9.5 The Noble Model of the Purkinje Fiber

Having just proven the existence of two kinds of K⁺ channels in Purkinje fibers of the heart, the inward and delayed rectifier, Denis Noble FRS showed in 1962 that with minor modification to the HH formulations, he could account for the widened plateau and the pace-making potential of Purkinje fibers [2]. The main elements of the model still included three currents, I_{Na} , I_K , and I_L , but this time included

Table 9.3 First generation, simplified models of the mammalian cardiac cell (reproduced from [7])

Cell type	Model	Parent model
Purkinje fiber models	Noble [2, 3]	—
	McAllister et al. [28]	Noble [2, 3]
Ventricular cell models	DiFrancesco and Noble [29]	McAllister et al. [28]
	Beeler and Reuter [30]	McAllister et al. [28]
Atrial cell models	Drouhard and Roberge [31]	Beeler and Reuter [30]
	Hilgemann and Noble [32]	DiFrancesco and Noble [29]
Sinoatrial cell models (rabbit)	Yanagihara et al. [33]	—
	Irisawa and Noma [34]	Yanagihara et al. [33]
	Bristow and Clark [35]	McAllister et al. [28]
	Noble and Noble [36]	DiFrancesco and Noble [29]

Table 9.4 Second-generation, detailed models of the mammalian cardiac cell (reproduced from [7])

Cell type	Model	Species	Parent model
Ventricular cell models	Noble et al. [37]	Guinea pig	Earm and Noble [38]
	Luo and Rudy [13]	Guinea pig	Beeler and Reuter [30]
	Nordin [10]	Guinea pig	–
	Luo and Rudy [11]	Guinea pig	Luo and Rudy [13]
	Jafri et al. [39]	Guinea pig	Luo and Rudy [11]
	Noble et al. [15]	Guinea pig	Noble et al. [37]
	Priebe and Beuckelmann [19]	Human	Luo and Rudy [11]
	Winslow et al. [8]	Canine	Jafri et al. [39]
	Pandit et al. [40]	Rat	Demir et al. [41]
	Puglisi and Bers [21]	Rabbit	Luo and Rudy [11]
	Bernus et al. [42]	Human	Priebe and Beuckelmann [19]
	Fox et al. [9]	Canine	Winslow et al. [8]
	Greenstein and Winslow [43]	Canine	Winslow et al. [8]
	Cabo and Boyden [44]	Canine	Luo and Rudy [11]
	Matsuoka et al. [45]	Guinea pig	–
	Bondarenko et al. [46] ^a	Mouse	–
	Shannon et al. [47] ^a	Rabbit	Puglisi and Bers [21]
	ten Tusscher et al. [18]	Human	–
Atrial cell models	Iyer et al. [48] ^a	Human	–
	Hund and Rudy	Canine	Luo and Rudy [11]
	ten Tusscher et al. [16]	Human	ten Tusscher et al. [18]
	Earm and Noble [38]	Rabbit	Hilgemann and Noble [32]
	Lindblad et al. [49]	Rabbit	–
	Courtemanche et al. [50]	Human	Luo and Rudy [11]
Sinoatrial cell models	Nygren et al. [51]	Human	Lindblad et al. [49]
	Ramirez et al. [52]	Canine	Courtemanche et al. [50]
	Noble et al. [53]	Rabbit	Noble and Noble [36]
	Wilders et al. [54]	Rabbit	Noble and Noble [36]
	Demir et al. [41]	Rabbit	–
	Dokos et al. [55]	Rabbit	Wilders et al. [54]
	Dokos et al. [56]	Rabbit	Dokos et al. [55]
	Demir et al. [57]	Rabbit	Demir et al. [41]
	Endresen et al. [58]	Rabbit	–
	Zhang et al. [59]	Rabbit	–
	Boyett et al. [60]	Rabbit	Zhang et al. [59]
	Zhang et al. [61]	Rabbit	Zhang et al. [59]
	Kurata et al. [62]	Rabbit	–
	Sarai et al. [63]	Rabbit	–
	Lovell et al. [64] ^a	Rabbit	–
	Mangoni et al. [65]	Mouse	Zhang et al. [59]

^aModel has Markov-type channel gating

nonlinear resistances in the K^+ current [2, 22]. Throughout the 1960s and 1970s, the model underwent significant revisions based on three discoveries, as outlined by Noble [66]. First, the discovery of Ca^{2+} current in the heart by Reuter in 1967 [67]; second, the multiple slow components of the K^+ current [68, 69]; and third, the

$\text{Na}^+/\text{Ca}^{2+}$ exchanger in cardiac muscle [70]. These discoveries formed the basis for the Beeler Reuter model of the first ventricular myocyte [30], and the Luo–Rudy models [11–13], as described below.

9.6 The Beeler Reuter Model of the Ventricular Myocardial Cell

In 1977, Beeler and Reuter [30] published the first mathematical reconstruction of the cardiac ventricular myocyte. This model was the first to link Ca^{2+} between electrical events at the membrane and the contractile response of the cell, and was bi-directional, allowing I_{Ca} to be a function of both the membrane potential as well as the dynamic ion concentration [22]. The model formulation contained I_{Na} , a slow inward current carried by Ca^{2+} , $I_S(I_{\text{Ca}})$, a time-independent outward potassium current, $I_{\text{K}1}$, and a time-dependent outward potassium current, $I_{\text{X}1}$. With only four currents, the BR model still adequately described slow recovery from inactivation of the Na^+ channel, frequency dependence of APD, all-or-nothing repolarization, and membrane oscillations [22, 30].

In 1985, the Di Francesco and Noble model [29] successfully incorporated ionic pumps, exchangers, dynamic ion concentrations, and multicompartment Ca^{2+} handling. Formulations for the Na^+/K^+ -ATPase, the $\text{Na}^+/\text{Ca}^{2+}$ exchanger and two formulations for the sarcoplasmic reticulum (uptake and release) were added. As outlined by Puglisi [22], this model allowed for intracellular Na^+ changes, the Na^+ dependence of the overshoot potential, APD shortening due to $[\text{K}^+]_o$, the increased automaticity at low $[\text{K}^+]_o$, and the depolarization to the plateau range with premature depolarizations, and low voltage oscillations at very low $[\text{K}^+]_o$. The Di Francesco and Noble model and the BR model set the stage for second-generation modeling, and in particular, the Luo–Rudy model, which has become classical in the field.

9.7 The Luo–Rudy Models of the Ventricular Myocyte

In 1991, Luo and Rudy published the first of three papers that substantially reformulated the Beeler Reuter model of the cardiac myocyte. The first Luo–Rudy model (LR1) [13], and the second, 1994 formulation [11] (LR2), have become a paradigm in the ventricular myocyte modeling field. These models were seminal works in the field for a few reasons; first, they were based mostly on guinea pig ventricular cell experiments, thus starting the transition to development of species-specific modeling (the so-called “second-generation” models). Second, the inclusion of intracellular ion dynamics, in particular Ca^{2+} , allowed for incorporation of feedback mechanisms between APD and $[\text{Ca}]_i$. It is known that APD influences the amplitude of $[\text{Ca}]_i$ [71], which in turn influences action potential waveform by Ca^{2+} -induced $-\text{Ca}^{2+}$ inactivation of I_{CaL} and by determining the

peak magnitude of I_{NaCa} [4, 72]. As can be seen from Table 9.4, the Luo–Rudy models have become the parent models for many ventricular and atrial myocyte models later published.

The 1991 Luo–Rudy model formulated four ionic currents: I_{Na} , the fast Na^+ current, which included fast and slow inactivation gating; I_K , the delayed rectifier current; I_{K1} , the inward rectifier K^+ current; and a plateau current, I_{Kp} [73]. The reformulation of I_{Na} with a much larger channel conductance, allowed the model to reproduce action potential upstroke velocity typically seen in single cardiac myocytes ($dV_m/dt_{\text{max}} \approx 400 \text{ V/s}$) [13]. LR1 was most significant for reproducing cardiac dynamics that were dependent on $[\text{K}^+]_o$ including APD and resting membrane potential. By incorporating $[\text{K}^+]_o$ as a dynamic variable, $[\text{K}^+]_o$ -dependent phenomena such as responses to premature stimuli and periodic stimulation reproduced monotonic Wenckebach patterns and alternans at normal $[\text{K}^+]_o$, and nonmonotonic Wenckebach periodicities, aperiodic patterns, and enhanced supernormal excitability at low $[\text{K}^+]_o$ [13]. These observations were consistent with experimental observations [74, 75], and suggested that intrinsic properties of single cardiac cells such as Wenckebach periodicities and aperiodic responses to periodic stimulation might be important in arrhythmogenesis [73].

The 1994 Luo–Rudy papers were published in two parts: “Simulations of ionic currents and concentration changes [11],” and “Afterdepolarizations, triggered activity, and potentiation [12].” Included were cell processes that regulated intracellular ion concentrations of Na^+ , K^+ , and Ca^{2+} . The first paper focused on Ca^{2+} -dependent processes and added formulations for an L-type Ca^{2+} channel, a $\text{Na}^+/\text{Ca}^{2+}$ exchanger, Na^+/K^+ pump, two compartment sarcoplasmic reticulum (SR) Ca^{2+} uptake and release, and a nonspecific Ca^{2+} -activated membrane current [11]. Release of Ca^{2+} from the SR could be triggered by both Ca^{2+} – induced – Ca^{2+} release and spontaneous release. Buffering of Ca^{2+} was implemented with both troponin and calmodulin for the cytoplasm and calsequestrin for the SR.

The inclusion of Ca^{2+} dynamics, in conjunction with dynamic calculations of $[\text{Na}^+]_i$ and $[\text{K}^+]_i$, allowed for simulations of triggered activity, EADs, and DADs in the accompanying article [12]. Two different mechanisms of EADs were proposed that depended on the phase of the action potential in which they occurred (phase 2, “plateau;” phase 3 EADs). For the first time, mechanisms of arrhythmogenesis could be studied at the single cell level, and would give way to higher dimensional simulations that have been effective in elucidating the spatiotemporal trends that allow for arrhythmia to propagate in higher dimensions.

9.8 Heterogeneity of Channel Expression: Cell-Type-Specific Modeling

It has been shown experimentally that the myocardium displays distinct cell types that are heterogeneous in ion channel expression across the ventricular wall. This heterogeneity plays a key role in the normal sequence of ventricular excitation and

in arrhythmogenesis [73, 76]. Potassium currents (I_{Kr} and I_{Ks}), in particular, which are essential in ventricular repolarization, show marked differences in expression between endocardial, midmyocardial, and epicardial cells [77]. By incorporating ion channel density heterogeneity into the Luo–Rudy (LR) model, Viswanathan et al. [78] have shown that M cells, which have reduced I_{Ks} density, display longer APD than other cell types, and these differences in multicellular models can give rise to transmural heterogeneity which may contribute to the arrhythmogenic potential in long-QT syndrome [79, 80].

9.9 Simulation of Human Cardiac Action Potentials

The use of experimental animals such as guinea pig, canine, rat, and mouse has helped to build species-specific models that allow comparison of simulation with experiment. However, to study phenomena such as arrhythmia, which are not necessarily the same in animal and human, requires models based on human data that recapitulate the specific characteristics of human cardiac electrodynamics. The relative paucity of human data, both because of invasive experimental techniques as well as insufficient methods to capture the 3D dynamics of arrhythmia initiation and propagation, makes quantitative modeling of the human heart a particularly useful tool in gaining insight into arrhythmia, mechanisms of heart disease, and physiological and pathophysiological responses to drugs and interventions.

In the past few years, models of the human cardiac ventricular myocyte have been developed from ten Tusscher [16, 18], Priebe and Beuckelmann [19], and Iyer [48] that rely mostly on human data. The first human ventricular myocyte model published was from Priebe and Bueckelmann [19] in 1998, and was based on the LR2 model in which formulations for the major ionic currents were adjusted to the limited dataset available for human ventricular cells [81]. The next substantial development in human modeling was the 2004 ten Tusscher–Noble–Noble–Panfilov model [18], which was based on a much larger dataset. Both models, however, still relied on human ventricular cell experiments as well as ion channel expression systems, each with their own strengths and weaknesses.

Human models (and others) have increased greatly in complexity and require sufficient computational power for higher dimension simulations [7]. Both the ten Tusscher and Priebe and Beuckelmann models are based on the HH formalism and have approximately 16 variables, while the Iyer model is Markov-based and has approximately 67 variables. These differences are important to consider; for example, ten Tusscher compared the efficiency of all three models and found that the Iyer model was as much as 1,000 times slower [7, 81].

Thus, the choice of a model must consider the application. For example, large-scale spatial simulations might require the use of less complex models such as the ten Tusscher or Priebe and Bueckelmann models that are computationally more efficient. Conversely, ion channel pharmacokinetic studies requiring the resolution of simulating single ion channel states might require the Markov formalism found

in the Iyer model. A detailed comparison of models for human ventricular cells and tissues can be found in [81].

9.10 Mutations in the Cardiac Sodium Channel: The Use of Simulations to Elucidate Mechanism

The wealth of information generated in the early 1990s has shown that the relationship between ion channel structure and function can be linked to aberrant kinetic gating in mutant ion channels leading to skeletal disease, nervous system disease, and cardiac arrhythmias [73, 82, 83]. Because most of these data were obtained in expression systems outside the milieu of the physiologic environment, interactions between ion channels and accessory proteins that dynamically influence the action potential have been lost. Simulation studies have been crucial in integrating this data into functional, virtual cardiac cells to relate molecular level interactions with whole cell and tissue-level function [73]. We will limit the focus to Na^+ channel mutations, but it should be noted that the computational methodology has been broadly applied to other ion channel mutations.

Since 1995 [84], more than 200 mutations have been linked to *SCN5A*, the gene encoding the cardiac Na^+ channel α subunit on chromosome 3p21 [85]. Initially segregated into distinct disease phenotypes such as long QT3 syndrome (LQT3), Brugada Syndrome (BrS), progressive cardiac conduction defect (PCCD), sick sinus syndrome (SSS), atrial fibrillation, and dilated cardiomyopathy (DCM), it is now known that multiple genetic defects can lead to overlapping syndromes with multiple clinical characteristics existing in one patient [86].

LQT3 is a subset of the congenital long QT syndrome and is characterized by a delay in cardiac cellular repolarization, leading to cardiac arrhythmias and sudden death, often in young people. It has been proposed that delayed ventricular repolarization promotes a substrate for triggered activity via early afterdepolarizations (EADs), which result from reactivation of L-type Ca^{2+} channels [80, 87, 88].

The first identified mutation in *SCN5A*, consequently shown to be a LQT3 variant, was ΔKPQ , a three amino acid deletion (lysine, proline, and glutamine at positions 1505–1507) in the linker region between domains III and IV [84]. ΔKPQ causes a transient failure of inactivation of the Na^+ channel, leading to a persistent inward Na^+ current that can cause syncope and sudden death [89]. Persistent Na^+ current causes an increase in the action potential duration that manifests as QT prolongation on the body surface ECG (see Fig. 9.1a, b). Numerous single channel recordings have shown that this persistent inward current during repolarization is due to channel fluctuations between a normal “dispersed” mode, and a “burst” mode of gating [84], which leads to the small (less than 5% of peak) persistent inward current shown in Fig. 9.1d.

The first use of state-specific Markov modeling to describe mutant Na^+ channels was done by Clancy and Rudy [92], who incorporated a formulation of ΔKPQ into the LRD model. The simulations showed that persistent Na^+ current caused by

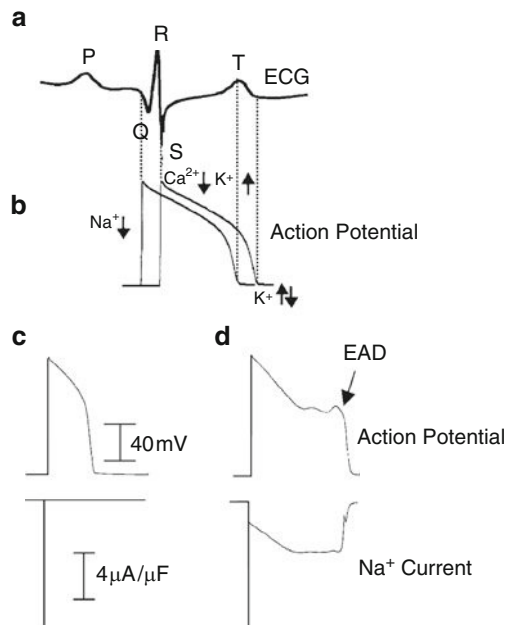


Fig. 9.1 Electrical gradients within the myocardium detected on the ECG, and action potential prolongation via mutation induced late I_{Na} . (a) and (b) relationship between an action potential and the ECG detected as spatial and temporal gradients for one complete cycle. The P wave represents atrial depolarization, the QRS complex represents ventricular activation, and the T wave represents the gradient of ventricular repolarization. (b) schematic of the cellular electrical activity underlying the ECG. (c) and (d) simulated action potential (top) and I_{Na} (bottom) for wild-type (c) and ΔKPQ (d). In the wild-type, Na^+ channels activate, followed quickly by inactivation; ΔKPQ mutant channels fail to inactivate and cause a small, persistent (<5% peak) Na^+ current [panel (d), bottom] that prolongs the action potential and can lead to arrhythmogenic early afterdepolarizations (EADs) shown in the top panel of (d). Note, in both (c) and (d) bottom panels, peak I_{Na} is off scale. Figure adapted from [90, 91]

mutant channel reopening from the inactivated state as well as channel bursting due to a transient failure of inactivation were sufficient to cause action potential prolongation and the development of EADs at bradycardic pacing frequencies. This is consistent with the clinical phenotype of arrhythmia initiation during sleep or relaxation in LQT3 patients [93].

Markov-derived models are state specific models based on the assumption that transitions between channels states depend on the present confirmation of the channel, but not on previous behavior; they represent specific, experimentally determined channel movements [94]. While Markov-derived models have the advantage of being closely related to the underlying mechanistic channel confirmations, the additional computation time necessary due to the large amount of additional differential equations and parameters added to the model must be taken into consideration [7].

9.11 In Silico Cardiac Dynamics: From DNA to Electrocardiogram

The integrative power of simulation is apparent from the ΔKPQ example. As can be seen in Fig. 9.2, after a train of 40 pulsed beats at BCL = 500 ms, a pause of 1,500 ms (clinical LQT arrhythmias often follow a pause) induces three plateau phase EADs, each preceded by a reactivation of the L-type Ca^{2+} channel. Note that in the prepause action potential, the action potential decreases monotonically, no reactivation of the L-type Ca^{2+} channel occurs, and no EAD is triggered.

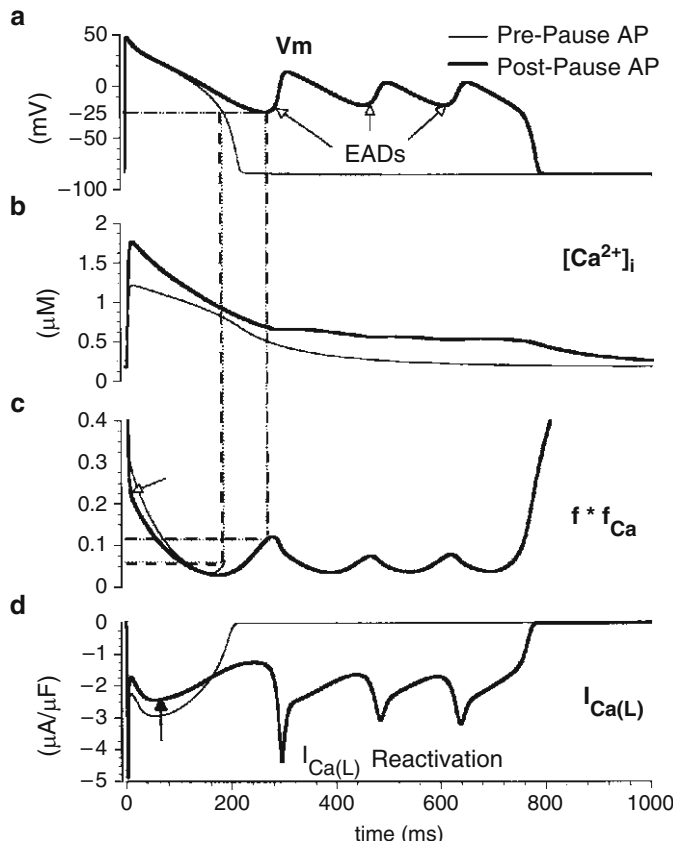


Fig. 9.2 Ionic mechanisms of pause induced EADs. (a) Action potential traces before (thin line) and after pause (thick line). Note the three EADs generated. (b) Intracellular Ca^{2+} concentration. (c) $I_{\text{Ca},L}$ inactivation, $f \times f_{\text{Ca}}$. (d) $I_{\text{Ca},L}$ current. The greater Ca^{2+} transient (b) induces greater inactivation of $I_{\text{Ca},L}$; however, prolongation of the plateau phase of the post-pause action potential allows greater recovery from inactivation of $I_{\text{Ca},L}$. The dotted lines correspond to the $f \times f_{\text{Ca}}$ value at the takeoff potential during the EAD. Greater recovery from inactivation ultimately leads to $I_{\text{Ca},L}$ reactivation [panel (d)] causing the arrhythmogenic EADs. Figure and legend adapted from [80]

Reactivation of the L-type Ca^{2+} channel immediately preceding the onset of EADs is a surprising result! While aberrant channel function is attributed to mutant Na^+ channels, the initiation of this type of EAD occurs due to reactivation of the normally functioning L-type Ca^{2+} channel, which carries the depolarizing charge. LQT3, characterized by a persistent Na^+ channel current, causes action potential prolongation that allows sufficient time for L-type Ca^{2+} channels to recover and reactivate [94]. This result was observed through simulation studies [80, 95], and highlights the importance of modeling and simulation in elucidating and predicting mechanisms of arrhythmogenesis.

Simulations have also shown, for example, that I1768V, another LQT3 mutation, may cause action potential prolongation through a novel mechanism of nonequilibrium gating [96]. By recovering faster from inactivation than wild-type channels, I1768V mutants can reopen during the repolarization phase of the action potential, tipping the delicate balance of repolarization and depolarization in the depolarizing phase, which ultimately leads to EADs [94, 96].

What this ultimately suggests is that mutations that have similar clinical presentation (i.e., prolongation of the QT interval on the body surface ECG) may respond differently to antiarrhythmic therapy and might require genetically defined therapeutic strategies that are based on ion channel mechanism leading to clinical phenotype. Such rational drug design strategies based on simulations will allow for more accurate prediction of treatment efficacy that is genotype and situation specific [97].

In some cases, mutations at the cellular level can be mapped to higher dimensions and a “pseudo” electrocardiogram can be computed [98]. These pseudo ECGs have resulted in a more complete understanding of arrhythmia in clinical observations (electrophysiology studies), genetics (positional cloning and genotyping), molecular biology (cloning), cellular physiology (electrophysiology), pharmacology, and theoretical modeling [99].

9.12 Modeling Calcium Dynamics and the Excitation Contraction (EC) Phenomenon

Accurate modeling of calcium dynamics is one of the most complex areas of cardiac action potential simulation. It is intrinsically complicated and highly integrated with multiple components including the L- and T-type Ca^{2+} current, ryanodine receptors, $\text{Na}^+/\text{Ca}^{2+}$ exchangers and SERCA pumps, Ca^{2+} binding proteins and buffering with calmodulin and troponin, and multiple sarcoplasmic reticulum (SR) subspaces [100]. Detailed formulations of Ca^{2+} dynamics serve as the link between electrical depolarization of the cellular membrane and activation of the contractile apparatus, so-called “EC coupling.” Part of the difficulty in building accurate models of the cardiac Ca^{2+} handling system stems from the seemingly paradoxical requirement of a high gain and graded response system that is under tight control of I_{Ca} [22], as well as incorporation of feedback and feedforward loops at multiple levels [22, 73].

EC coupling has a general mechanism as follows: Ca^{2+} influx into the sarcolemma induces a secondary Ca^{2+} release from the sarcoplasmic reticulum (so-called CICR, Ca^{2+} – induced – Ca^{2+} release) via ryanodine receptors. Ryanodine receptors sit in a restricted didactic space and sense local Ca^{2+} concentration. Ca^{2+} influx from the L-type Ca^{2+} channel (LTCC) and release from the SR form a negative feedback loop to induce inactivation of the LTCC and reduce further influx [100]. The released Ca^{2+} is then buffered by calmodulin and troponin, which generate force via myofilament activation. Most Ca^{2+} is resequestered via the SERCA pump, each heartbeat with the remainder extruded via the $\text{Na}^+/\text{Ca}^{2+}$ exchanger [100, 101].

In the early 1990s, it was realized that to fully capture the cyclical nature and essential features of EC coupling, modeling of Ca^{2+} dynamics needed to incorporate subcellular compartments. Nordin et al. [10] developed a three compartment model that relied on gradient diffusion laws and empirical adjustment [22]. More complex models have since been developed that incorporate subsarcolemmal microdomains for local Ca^{2+} sensing with three levels of organization: the cleft for LTCC and ryanodine receptor interactions; the subsarcolemmal space for interactions between transporters and their corresponding ions; and the cytosolic space where force is generated by interaction between Ca^{2+} and myofilaments [22].

These models have provided immense insight into EC coupling that is far more complex and integrated than intuition alone could predict. For example, the requirement of minute volume subspaces for Ca^{2+} -induced- Ca^{2+} release [47], and the interaction between ryanodine receptors and the LTCC [102], which includes the effects of surface charge and the electric field in the cardiac diad. The Soeller and Cannell model predicted that the surface charge has significant effects on the time course of calcium movements in the diad and causes local Ca^{2+} changes to occur more rapidly than predicted from models that consider sarcolemmal Ca^{2+} binding without field effects [102].

One persistent difficulty with the existing spatially complex models of Ca^{2+} dynamics is that they are computationally very expensive. This has made it difficult to integrate realistic models of the didactic space with larger-scale electrophysiology and contraction models. New research must focus on integrating multiple levels of control mechanisms and increased efficiency in computation, so that “third-generation” models can move away from the empiric modeling of Ca^{2+} dynamics that is still required due to current computational limitations.

9.13 Modeling Cell Signaling Pathways and Neurohumoral Regulation

Most models of the cardiac ventricular myocyte assume steady-state levels of neurohumoral response to adrenergic and other cell stimuli, and thus neglect cell-signaling pathways in action potential simulations. However, it is clear that cell signaling has profound effects on many cellular processes that regulate cardiac electrodynamics; for

example β -adrenergic modulation of I_{Ks} [103], indirect modulation of Ca^{2+} dynamics, and the L-type Ca^{2+} channel [94].

Briefly, the β -adrenergic signaling cascade relies on catecholamines to coordinate the control of contractility, metabolism, and gene regulation [104, 105]. β -Receptors couple with the GPCR subunit G_S to stimulate adenylyl cyclase, which synthesizes cAMP to act as a second messenger, promoting dissociation of PKA. PKA then phosphorylates and alters function of multiple target proteins and processes including the L-type Ca^{2+} channel, phospholamban [104], ryanodine receptors, I_{Na} , I_{Ks} , Na^+/K^+ -ATPase, sarcolemmal Ca^{2+} -ATPase, Troponin I, crossbridge cycling rates, and glycolysis [22, 72].

A problem arises with the assumption of either steady-state levels of neurohumoral response or bulk cytoplasmic concentrations of second messengers in signaling cascades. The need for models to incorporate microdomain-level processes is evidenced by the Iancu model of cAMP signaling in cardiac myocytes [106]. This model tested whether the effects of β_1 -adrenergic receptor and M_2 muscarinic activation involve compartmentation of cAMP. While the bulk cAMP concentration inside the myocyte is approximately 1 μM [106–108], the binding affinity for PKA is on the order of 100–300 nM [106, 109, 110]. By segregating cAMP within the cell into two submembrane microdomains (caveolar and extra-caveolar), and a bulk cytoplasmic domain, the model was able to show that while bulk basal cAMP levels are too high to appropriately regulate PKA, caveolar cAMP varies in a more appropriate range for regulation (~100 nM to ~2 μM) [106]. The same group later validated many of the hypotheses generated by the computational model in a subsequent experimental study [111].

With regard to disease processes, it has been recently shown that the β -adrenergic signaling cascade involves the association of PKA and PP1 with the C-terminal domain of KCNQ1 [103] (the α -subunit of I_{Ks}). β -Adrenergic modulation of I_{Ks} in LQT1 patients [112] upsets the delicate balance of repolarization and can lead to arrhythmia; this is the rationale for β -blockade pharmacotherapy for this subset of LQT patients. Interestingly, simulation studies have questioned the use of such therapy as a general treatment strategy for all LQT patients, and may actually be proarrhythmic in LQT3 patients [113]. Other diseases, such as catecholaminergic polymorphic ventricular tachycardia, are linked to abnormal Ca^{2+} cycling due to increased β -adrenergic tone [114, 115].

Saucerman et al. [104] have formulated a model linking β -adrenergic signaling with excitation contraction coupling in an in silico model of the rat ventricular myocyte. The model was notable for predicting that less than 40% of adenylyl cyclase molecules are required for maximal receptor activation, and that endogenous heat-stable PKI may enhance basal cAMP buffering by 68%, all suggesting validation through new experiments.

This model and others [21, 116, 117] highlight that the link between neurohumoral regulation, Ca^{2+} cycling, and cardiac electrodynamics is highly complex, with multiple levels of integration and subcellular localization. Most of these second messengers are not free to diffuse throughout the cell, but rather form compartmentalized networks, which allow for differential responses to multiple

stimuli, control cross-talk, and coordinate distinct phosphorylation targets [22, 118–120].

In sum, prediction of cellular responses to any of these cell components by disease, drugs and other interventions would be impossible without the use of predictive modeling [94]. “Third-generation” cardiac ventricular myocyte models will be notable for inclusion of complex signaling pathways and will most likely rely on a systems level prospective to understand how perturbations in any of these networks and components will affect cardiac dynamics.

9.14 Conclusions

Simulation of cardiac action potentials is important for understanding the effects of perturbations at the ion channel scale such as mutant channel aberrant gating and drug/channel interaction, but is also important as the foundation for higher dimensional simulations that integrate knowledge at different spatial scales into a framework for understanding physiology and pathophysiology of cardiac arrhythmia and heart disease.

Cardiac action potential modeling has been successful as an approach to understanding cardiac arrhythmia and other physiological mechanisms because it integrates multiple functional levels (protein, cell, tissue, organ, electrocardiogram) and the complex interplay between them, that allow for arrhythmia initiation. Traditional single-scale approaches typically fail to reveal how disruption in protein function due to mutations and/or drugs and, consequently, through complex interactions and behaviors of cells, lead to loss of synchronization and arrhythmic rhythms in tissue to cause failure of coordinated contraction [99]. Integration of different spatial scales allows the computational biologist to follow key parameters over multiple spatial scales and identify interacting components. The challenge ahead remains advancing computational power to be able to integrate sufficiently detailed models into 2D tissues, whole organs or even virtual torsos to study these phenomena. Integrated understanding from genes to electrocardiogram is slowly becoming a reality [73].

References

1. Hodgkin AL, Huxley AF. A quantitative description of membrane current and its application to conduction and excitation in nerve. *J Physiol.* 1952;117(4):500–44.
2. Noble D. A modification of the Hodgkin–Huxley equations applicable to Purkinje fibre action and pace-maker potentials. *J Physiol.* 1962;160:317–52.
3. Noble D. Cardiac action and pacemaker potentials based on the Hodgkin–Huxley equations. *Nature.* 1960;188:495–7.
4. Demir SS. Computational modeling of cardiac ventricular action potentials in rat and mouse: review. *Jpn J Physiol.* 2004;54:523–30.

5. Foundations of cardiac arrhythmias. P.a.R. Spooner, MR editor. 2000: Marcel Dekker.
6. Hodgkin AL. The ionic basis of electrical activity in nerve and muscle. *Biol Rev.* 1951;26: 339–409.
7. Wilders R. Computer modelling of the sinoatrial node. *Med Biol Eng Comput.* 2007;45: 189–207.
8. Winslow RL et al. Mechanisms of altered excitation–contraction coupling in canine tachycardia-induced heart failure II: model studies. *Circ Res.* 1999;84(5):571–86.
9. Fox JJ, McHarg JL, Gilmour Jr RF. Ionic mechanism of electrical alternans. *Am J Physiol Heart Circ Physiol.* 2002;282(2):H516–30.
10. Nordin C. Computer model of membrane current and intracellular Ca^{2+} flux in the isolated guinea pig ventricular myocyte. *Am J Physiol.* 1993;265(6 Pt 2):H2117–36.
11. Luo CH, Rudy Y. A dynamic model of the cardiac ventricular action potential I. Simulations of ionic currents and concentration changes. *Circ Res.* 1994;74(6):1071–96.
12. Luo CH, Rudy Y. A dynamic model of the cardiac ventricular action potential. II. After depolarizations, triggered activity, and potentiation. *Circ Res.* 1994;74(6):1097–113.
13. Luo CH, Rudy Y. A model of the ventricular cardiac action potential. Depolarization, repolarization, and their interaction. *Circ Res.* 1991;68(6):1501–26.
14. Zeng J et al. Two components of the delayed rectifier K^+ current in ventricular myocytes of the guinea pig type. Theoretical formulation and their role in repolarization. *Circ Res.* 1995;77(1):140–52.
15. Noble D et al. Improved guinea-pig ventricular cell model incorporating a diadic space, IKr and IKs, and length- and tension-dependent processes. *Can J Cardiol.* 1998;14(1):123–34.
16. ten Tusscher KH, Panfilov AV. Alternans and spiral breakup in a human ventricular tissue model. *Am J Physiol Heart Circ Physiol.* 2006;291:H1088–100.
17. ten Tusscher KH, Panfilov AV. Cell model for efficient simulation of wave propagation in human ventricular tissue under normal and pathological conditions. *Phys Med Biol.* 2006;51: 6141–56.
18. ten Tusscher KH et al. A model for human ventricular tissue. *Am J Physiol Heart Circ Physiol.* 2004;286(4):H1573–89.
19. Priebe L, Beuckelmann DJ. Simulation study of cellular electric properties in heart failure. *Circ Res.* 1998;82(11):1206–23.
20. Riemer TL, Sobie EA, Tung L. Stretch-induced changes in arrhythmogenesis and excitability in experimentally based heart cell models. *Am J Physiol.* 1998;275(2 Pt 2):H431–42.
21. Puglisi JL, Bers DM. LabHEART: an interactive computer model of rabbit ventricular myocyte ion channels and Ca transport. *Am J Physiol Cell Physiol.* 2001;281(6):C2049–60.
22. Puglisi JL, Wang F, and Bers DM. Modeling the isolated cardiac myocyte. *Prog Biophys Mol Biol.* 2004;85(2–3):163–78.
23. Fiset C et al. A rapidly activating sustained K^+ current modulates repolarization and excitation–contraction coupling in adult mouse ventricle. *J Physiol.* 1997;504(Pt 3):557–63.
24. Clark RB et al. Heterogeneity of action potential waveforms and potassium currents in rat ventricle. *Cardiovasc Res.* 1993;27(10):1795–9.
25. Watanabe T et al. Heterogeneity of the action potential in isolated rat ventricular myocytes and tissue. *Circ Res.* 1983;52(3):280–90.
26. Trepanier-Boulay V et al. Gender-based differences in cardiac repolarization in mouse ventricle. *Circ Res.* 2001;89(5):437–44.
27. Antzelevitch C et al. The M cell: its contribution to the ECG and to normal and abnormal electrical function of the heart. *J Cardiovasc Electrophysiol.* 1999;10(8):1124–52.
28. McAllister RE, Noble D, Tsien RW. Reconstruction of the electrical activity of cardiac Purkinje fibres. *J Physiol.* 1975;251(1):1–59.
29. DiFrancesco D, Noble D. A model of cardiac electrical activity incorporating ionic pumps and concentration changes. *Philos Trans R Soc Lond B Biol Sci.* 1985;307:353–98.
30. Beeler GW, Reuter H. Reconstruction of the action potential of ventricular myocardial fibres. *J Physiol (Lond).* 1977;268:177–210.

31. Drouhard JP, Roberge FA. Revised formulation of the Hodgkin–Huxley representation of the sodium current in cardiac cells. *Comput Biomed Res.* 1987;20(4):333–50.
32. Hilgemann DW, Noble D. Excitation–contraction coupling and extracellular calcium transients in rabbit atrium: reconstruction of basic cellular mechanisms. *Proc R Soc Lond B Biol Sci.* 1987;230(1259):163–205.
33. Yanagihara K, Noma A, Irisawa H. Reconstruction of sino-atrial node pacemaker potential based on the voltage clamp experiments. *Jpn J Physiol.* 1980;30(6):841–57.
34. Irisawa H.a.N. A, Pacemaker mechanisms of rabbit sinoatrial node cells. Cardiac rate and rhythm: physiological, morphological, and developmental aspects. L.a.J. Bouman, HJ. 1982 editors, London: Martinus Nijhoff.
35. Bristow DG, Clark JW. A mathematical model of primary pacemaking cell in SA node of the heart. *Am J Physiol.* 1982;243(2):H207–18.
36. Noble D, Noble SJ. A model of sino-atrial node electrical activity based on a modification of the DiFrancesco–Noble (1984) equations. *Proc R Soc Lond B Biol Sci.* 1984;222(1228):295–304.
37. Noble D et al. The role of sodium–calcium exchange during the cardiac action potential. *Ann N Y Acad Sci.* 1991;639:334–53.
38. Earm YE, Noble D. A model of the single atrial cell: relation between calcium current and calcium release. *Proc R Soc Lond B Biol Sci.* 1990;240(1297):83–96.
39. Jafri MS, Rice JJ, Winslow RL. Cardiac Ca²⁺ dynamics: the roles of ryanodine receptor adaptation and sarcoplasmic reticulum load. *Biophys J.* 1998;74(3):1149–68.
40. Pandit SV et al. A mathematical model of action potential heterogeneity in adult rat left ventricular myocytes. *Biophys J.* 2001;81(6):3029–51.
41. Demir SS et al. A mathematical model of a rabbit sinoatrial node cell. *Am J Physiol.* 1994;266(3 Pt 1):C832–52.
42. Bernus O et al. A computationally efficient electrophysiological model of human ventricular cells. *Am J Physiol Heart Circ Physiol.* 2002;282(6):H2296–308.
43. Greenstein JL, Winslow RL. An integrative model of the cardiac ventricular myocyte incorporating local control of Ca²⁺ release. *Biophys J.* 2002;83(6):2918–45.
44. Cabo C, Boyden PA. Electrical remodeling of the epicardial border zone in the canine infarcted heart: a computational analysis. *Am J Physiol Heart Circ Physiol.* 2003;284(1):H372–84.
45. Matsuoka S et al. Role of individual ionic current systems in ventricular cells hypothesized by a model study. *Jpn J Physiol.* 2003;53(2):105–23.
46. Bondarenko VE et al. Computer model of action potential of mouse ventricular myocytes. *Am J Physiol Heart Circ Physiol.* 2004;287:H1378–403.
47. Shannon TR et al. A mathematical treatment of integrated Ca dynamics within the ventricular myocyte. *Biophys J.* 2004;87(5):3351–71.
48. Iyer V, Mazhari R, Winslow RL. A computational model of the human left-ventricular epicardial myocyte. *Biophys J.* 2004;87(3):1507–25.
49. Lindblad DS et al. A model of the action potential and underlying membrane currents in a rabbit atrial cell. *Am J Physiol.* 1996;271(4 Pt 2):H1666–96.
50. Courtemanche M, Ramirez RJ, Nattel S. Ionic mechanisms underlying human atrial action potential properties: insights from a mathematical model. *Am J Physiol.* 1998;275(1 Pt 2):H301–21.
51. Nygren A et al. Mathematical model of an adult human atrial cell: the role of K⁺ currents in repolarization. *Circ Res.* 1998;82(1):63–81.
52. Ramirez RJ, Nattel S, Courtemanche M. Mathematical analysis of canine atrial action potentials: rate, regional factors, and electrical remodeling. *Am J Physiol Heart Circ Physiol.* 2000;279(4):H1767–85.
53. Noble D, DiFrancesco D, Denyer JC. Ionic mechanisms in normal and abnormal cardiac pacemaker activity. In: Jacklet J, editor. *Neuronal and cellular oscillators.* New York: Marcel Dekker; 1989.

54. Wilders R, Jongsma HJ, van Ginneken AC. Pacemaker activity of the rabbit sinoatrial node. A comparison of mathematical models. *Biophys J.* 1991;60(5):1202–16.
55. Dokos S, Celler B, Lovell N. Ion currents underlying sinoatrial node pacemaker activity: a new single cell mathematical model. *J Theor Biol.* 1996;181(3):245–72.
56. Dokos S, Celler BG, Lovell NH. Vagal control of sinoatrial rhythm: a mathematical model. *J Theor Biol.* 1996;182(1):21–44.
57. Demir SS, Clark JW, Giles WR. Parasympathetic modulation of sinoatrial node pacemaker activity in rabbit heart: a unifying model. *Am J Physiol.* 1999;276(6 Pt 2):H2221–44.
58. Endresen LP et al. A theory for the membrane potential of living cells. *Eur Biophys J.* 2000;29(2):90–103.
59. Zhang H et al. Mathematical models of action potentials in the periphery and center of the rabbit sinoatrial node. *Am J Physiol Heart Circ Physiol.* 2000;279(1):H397–421.
60. Boyett MR, Zhang H, Garney A, Holden AV. Control of the pacemaker activity of the sinoatrial node by intracellular Ca²⁺. Experiments and modeling. *Philos Trans R Soc Lond A Math Phys Eng Sci.* 2001;359:1091–110.
61. Zhang H et al. Analysis of the chronotropic effect of acetylcholine on sinoatrial node cells. *J Cardiovasc Electrophysiol.* 2002;13(5):465–74.
62. Kurata Y et al. Dynamical description of sinoatrial node pacemaking: improved mathematical model for primary pacemaker cell. *Am J Physiol Heart Circ Physiol.* 2002;283(5):H2074–101.
63. Sarai N et al. Role of individual ionic current systems in the SA node hypothesized by a model study. *Jpn J Physiol.* 2003;53(2):125–34.
64. Lovell NH et al. A gradient model of cardiac pacemaker myocytes. *Prog Biophys Mol Biol.* 2004;85(2–3):301–23.
65. Mangoni ME et al. Bradycardia and slowing of the atrioventricular conduction in mice lacking CaV3.1/alpha1G T-type calcium channels. *Circ Res.* 2006;98(11):1422–30.
66. Noble D. From the Hodgkin–Huxley axon to the virtual heart. *J Physiol (Lond).* 2007;580:15–22.
67. Reuter H. The dependence of slow inward current in Purkinje fibres on the extracellular calcium-concentration. *J Physiol.* 1967;192(2):479–92.
68. Noble D, Tsien RW. Outward membrane currents activated in the plateau range of potentials in cardiac Purkinje fibres. *J Physiol.* 1969;200(1):205–31.
69. Noble D, Tsien RW. The kinetics and rectifier properties of the slow potassium current in cardiac Purkinje fibres. *J Physiol.* 1968;195(1):185–214.
70. Reuter H, Seitz N. The dependence of calcium efflux from cardiac muscle on temperature and external ion composition. *J Physiol.* 1968;195(2):451–70.
71. Bouchard RA, Clark RB, Giles WR. Effects of action potential duration on excitation–contraction coupling in rat ventricular myocytes. Action potential voltage-clamp measurements. *Circ Res.* 1995;76(5):790–801.
72. Bers DM. Excitation–contraction coupling and cardiac contractile force. 2nd ed. The Netherlands: Kluwer Academic Publications; 2001.
73. Noble D, Rudy Y. Models of cardiac ventricular action potentials: interactive interaction between experiment and simulation. *Philos Trans R Soc Lond A.* 2001;359:1127–42.
74. Delmar M, Michaels DC, Jalife J. Slow recovery of excitability and the Wenckebach phenomenon in the single guinea pig ventricular myocyte. *Circ Res.* 1989;65(3):761–74.
75. Chialvo DR, Michaels DC, Jalife J. Supernormal excitability as a mechanism of chaotic dynamics of activation in cardiac Purkinje fibers. *Circ Res.* 1990;66(2):525–45.
76. Antzelevitch C, Yan G, Shimizu W, Burashnikov A. Electrical heterogeneity, the ECG, and cardiac arrhythmias, in Cardiac electrophysiology: from cell to bedside. Zipes DP, Jalife J, editor. 1999, Saunders: Philadelphia; pp. 222–38.
77. Liu DW, Antzelevitch C. Characteristics of the delayed rectifier current (IKr and IKs) in canine ventricular epicardial, midmyocardial, and endocardial myocytes. A weaker IKs contributes to the longer action potential of the M cell. *Circ Res.* 1995;76(3):351–65.

78. Viswanathan PC, Shaw RM, Rudy Y. Effects of IKr and IKs heterogeneity on action potential duration and its rate dependence: a simulation study. *Circulation*. 1999;99:2466–74.
79. Viswanathan PC, Rudy Y. Cellular arrhythmogenic effects of congenital and acquired long-QT syndrome in the heterogeneous myocardium. *Circulation*. 2000;102:1192–8.
80. Viswanathan PC, Rudy Y. Pause induced early after depolarizations in the long QT syndrome: a simulation study. *Cardiovasc Res*. 1999;42:530–42.
81. Ten Tusscher KH et al. Comparison of electrophysiological models for human ventricular cells and tissues. *Prog Biophys Mol Biol*. 2006;90(1–3):326–45.
82. Priori SG et al. Genetic and molecular basis of cardiac arrhythmias: impact on clinical management parts I and II. *Circulation*. 1999;99(4):518–28.
83. Priori SG et al. Genetic and molecular basis of cardiac arrhythmias: impact on clinical management part III. *Circulation*. 1999;99(5):674–81.
84. Bennett PB et al. Molecular mechanism for an inherited cardiac arrhythmia. *Nature*. 1995;376:683–5.
85. Wang Q et al. SCN5A mutations associated with an inherited cardiac arrhythmia, long QT syndrome. *Cell*. 1995;80:805–11.
86. Ruan Y, Liu N, Priori SG. Sodium channel mutations and arrhythmias. *Nat Rev Cardiol*. 2009;6(5):337–48.
87. Thomas G et al. Effects of L-type Ca²⁺ channel antagonism on ventricular arrhythmogenesis in murine hearts containing a modification in the Scn5a gene modelling human long QT syndrome 3. *J Physiol (Lond)*. 2007;578:85–97.
88. Lankipalli RS et al. Mechanisms underlying arrhythmogenesis in long QT syndrome. *J Electrocardiol*. 2005;38:69–73.
89. Nagatomo T, January C, Makielinski J. Preferential block of late sodium current in the LQT3 ΔKPQ mutant by the class IC antiarrhythmic flecainide. *Mol Pharmacol*. 2000;57:101–7.
90. Clancy CE, Kass RS. Defective cardiac ion channels: from mutations to clinical syndromes. *J Clin Invest*. 2002;110(8):1075–7.
91. Clancy CE, Kass R. Inherited and acquired vulnerability to ventricular arrhythmias: cardiac Na⁺ and K⁺ channels. *Physiol Rev*. 2005;85:33–47.
92. Clancy CE, Rudy Y. Linking a genetic defect to its cellular phenotype in a cardiac arrhythmia. *Nature*. 1999;400:566–9.
93. Schwartz PJ et al. Long QT syndrome patients with mutations of the SCN5A and HERG genes have differential responses to Na⁺ channel blockade and to increases in heart rate. Implications for gene-specific therapy. *Circulation*. 1995;92:3381–6.
94. Rudy Y, Silva JR. Computational biology in the study of cardiac ion channels and cell electrophysiology. *Q Rev Biophys*. 2006;39:57–116.
95. Zeng J, Rudy Y. Early after depolarizations in cardiac myocytes: mechanism and rate dependence. *Biophys J*. 1995;68(3):949–64.
96. Clancy CE et al. Non-equilibrium gating in cardiac Na⁺ channels: an original mechanism of arrhythmia. *Circulation*. 2003;107:2233–7.
97. Clancy CE, Zhu ZI, Rudy Y. Pharmacogenetics and anti-arrhythmic drug therapy: a theoretical investigation. *Am J Physiol Heart Circul*. 2007;292:H66–75.
98. Gima K, Rudy Y. Ionic current basis of electrocardiographic waveforms: a model study. *Circ Res*. 2002;90:889–96.
99. Clancy CE, Zhu ZI, Rudy Y. Pharmacogenetics and anti-arrhythmic drug therapy: a theoretical investigation. *Am J Physiol Heart Circ Physiol*. 2007;292:H66–75.
100. Rice J, Jafri MS. Modelling calcium handling in cardiac cells. *Philos Trans R Soc Lond A*. 2001;359:1143–57.
101. Bassani JW, Bassani RA, Bers DM. Relaxation in rabbit and rat cardiac cells: species-dependent differences in cellular mechanisms. *J Physiol*. 1994;476(2):279–93.
102. Soeller C, Cannell MB. Numerical simulation of local calcium movements during L-type calcium channel gating in the cardiac diad. *Biophys J*. 1997;73(1):97–111.

103. Marx SO et al. Requirement of a macromolecular signaling complex for beta adrenergic receptor modulation of the KCNQ1-KCNE1 potassium channel. *Science*. 2002;295(5554):496–9.
104. Saucerman JJ et al. Modeling beta-adrenergic control of cardiac myocyte contractility in silico. *J Biol Chem*. 2003;278(48):47997–8003.
105. Bers DM. Cardiac excitation–contraction coupling. *Nature*. 2002;415(6868):198–205.
106. Iancu RV, Jones SW, Harvey RD. Compartmentation of cAMP signaling in cardiac myocytes: a computational study. *Biophys J*. 2007;92(9):3317–31.
107. Kameyama M, Hofmann F, Trautwein W. On the mechanism of beta-adrenergic regulation of the Ca channel in the guinea-pig heart. *Pflugers Arch*. 1985;405(3):285–93.
108. Terasaki WL, Brooker G. Cardiac adenosine 3':5'-monophosphate. Free and bound forms in the isolated rat atrium. *J Biol Chem*. 1977;252(3):1041–50.
109. Mongillo M et al. Fluorescence resonance energy transfer-based analysis of cAMP dynamics in live neonatal rat cardiac myocytes reveals distinct functions of compartmentalized phosphodiesterases. *Circ Res*. 2004;95(1):67–75.
110. Adams SR et al. Fluorescence ratio imaging of cyclic AMP in single cells. *Nature*. 1991;349(6311):694–7.
111. Iancu RV et al. Cytoplasmic cAMP concentrations in intact cardiac myocytes. *Am J Physiol Cell Physiol*. 2008;295(2):C414–22.
112. Priori SG et al. Risk stratification in the long-QT syndrome. *N Engl J Med*. 2003;348(19):1866–74.
113. Ahrens-Nicklas RC, Clancy CE, Christini DJ. Re-evaluating the efficacy of beta-adrenergic agonists and antagonists in long QT-3 syndrome through computational modelling. *Cardiovasc Res*. 2009;82:439–47.
114. Lahat H, Pras E, Eldar M. RYR2 and CASQ2 mutations in patients suffering from catecholaminergic polymorphic ventricular tachycardia. *Circulation*. 2003;107(3):e29. author reply e29.
115. Francis J et al. Catecholaminergic polymorphic ventricular tachycardia. *Heart Rhythm*. 2005;2(5):550–4.
116. Saucerman JJ et al. Proarrhythmic consequences of a KCNQ1 AKAP-binding domain mutation: computational models of whole cells and heterogeneous tissue. *Circ Res*. 2004;95(12):1216–24.
117. Saucerman JJ, McCulloch AD. Mechanistic systems models of cell signaling networks: a case study of myocyte adrenergic regulation. *Prog Biophys Mol Biol*. 2004;85(2–3):261–78.
118. Michel JJ, Scott JD. AKAP mediated signal transduction. *Annu Rev Pharmacol Toxicol*. 2002;42:235–57.
119. Steinberg SF, Brunton LL. Compartmentation of G protein-coupled signaling pathways in cardiac myocytes. *Annu Rev Pharmacol Toxicol*. 2001;41:751–73.
120. Insel PA. Location, location, location. *Trends Endocrinol Metab*. 2003;14(3):100–2.

Part III

Cardiac Development and Anatomy

Chapter 10

Development of Pacemaker Activity in Embryonic and Embryonic Stem Cell-Derived Cardiomyocytes

Huamin Liang, Michael Reppel, Ming Tang, and Jürgen Hescheler

10.1 Introduction

The cyclical change in cardiac electrical activities, associated with spontaneous activity, is generated by the opening and closing of time- and voltage-dependent ion channels in the sarcolemmal membrane. In the adult mammalian heart, pacemaker, atrial, and ventricular cardiomyocytes are specialized cells with distinct morphology and specific physiological functions. The sino-atrial (SA) node is known as the pacemaker region of heart where primary pacemaker cardiomyocytes generate the dominant spontaneous electrical activity [1]. However, the differences among pacemaker, atrial, and ventricular cardiomyocytes are less pronounced in the early developmental stages (EDS) of the heart [2], and both atrial and ventricular cardiomyocytes are able to beat spontaneously although the ionic conductance responsible for pacemaking in adult hearts is either not or only partially expressed [3–8]. In the adult heart, generation of spontaneous electrical activity in SA node has been well described [1, 9], while the mechanisms underlying the electrical activity in fetal and embryonic stem cell (ESc)-derived cardiomyocytes are still under debate.

H. Liang

Institute of Neurophysiology, University of Cologne, Cologne, Germany
and

Department of Physiology, Tongji Medical College, Huazhong University of Science and Technology, Wuhan, Hubei, China

M. Reppel

Medizinische Klinik II, Medical University of Lübeck, Lübeck, Germany

M. Tang,

Department of Physiology, Tongji Medical College, Huazhong University of Science and Technology, Wuhan, Hubei, China

J. Hescheler (✉)

Institute of Neurophysiology, University of Cologne, Cologne, Germany

e-mail: j.hescheler@uni-koeln.de

For ESc-derived cardiomyocytes and native embryonic cardiomyocytes, early studies demonstrate that the functional role and gene expression of ion channels change dramatically during development [3–6]. The L-type and T-type Ca^{2+} channels, $\text{Na}^+/\text{Ca}^{2+}$ exchanger (NCX), and HCN pacemaker channel (funny current, I_f) appear to play a major role during early embryomyogenesis (Figs. 10.1 and 10.2).

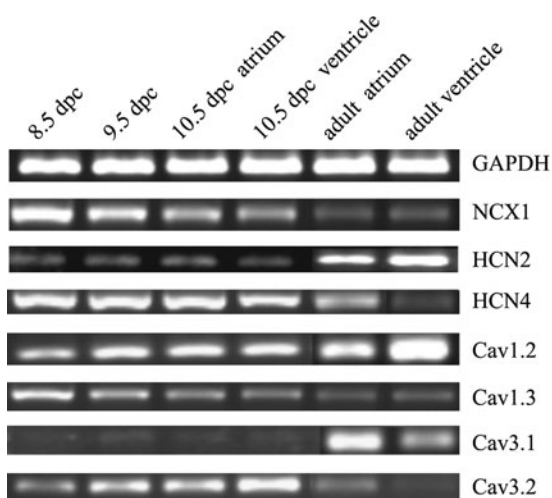


Fig. 10.1 Developmental changes in subtypes of ion channels in murine hearts. Using GAPDH as internal control, expressions of NCX1, Cav1.3, HCN4, and Cav3.2 at mRNA level are downregulated, while HCN2, Cav1.2, and Cav3.1 are upregulated

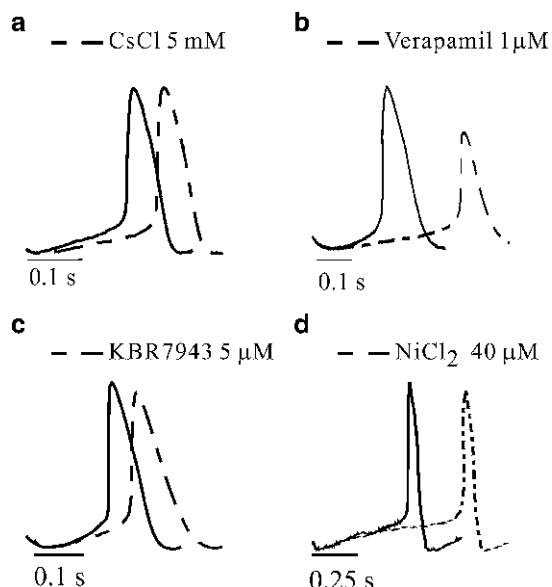


Fig. 10.2 Functional contribution of I_f , I_{CaL} , I_{NCX} , and I_{CaT} to action potentials in 10.5 dpc cardiomyocytes. Specific blockers of I_f [(a) CsCl 5 mM], I_{CaL} [(b) verapamil 1 μM], I_{NCX} [(c) KBR7943 5 μM], and I_{CaT} [(d) NiCl₂ 40 μM] slow down the diastolic depolarization phase

10.2 Development of Pacemaker Activity in Embryonic Cardiomyocytes

10.2.1 Electrophysiological Activity at Early Developmental Stage

It is not known when the first electrical activity occurs in the developing heart, although contractions are first observed at 8.5 days postcoitum (dpc), with regular beating at 9 dpc [10]. The earliest electrical activity appears as oscillations in membrane potential (Em), but not action potentials (APs) in native cardiomyocytes [11]. During development, Em oscillations develop into primitive APs, and then mature-like APs (Fig. 10.3). Em oscillations result from intracellular $[Ca^{2+}]_i$ oscillations because thapsigargin, a sarcoplasmic Ca^{2+} -ATPase inhibitor, leads to a rise in $[Ca^{2+}]_i$ and an abrupt halt of $[Ca^{2+}]_i$ oscillations. Thus, intracellular Ca^{2+} stores act as the primary rhythm generator in EDS cardiomyocytes. It is proposed that oscillations can activate a small depolarization of the Em that give rise to APs on reaching threshold potential. Other studies have shown that Ca^{2+} influx through T-type and L-type Ca^{2+} channels, and Na^+/Ca^{2+} exchanger can trigger transient Ca^{2+} release or Ca^{2+} sparks [12], and therefore might contribute to Em oscillations.

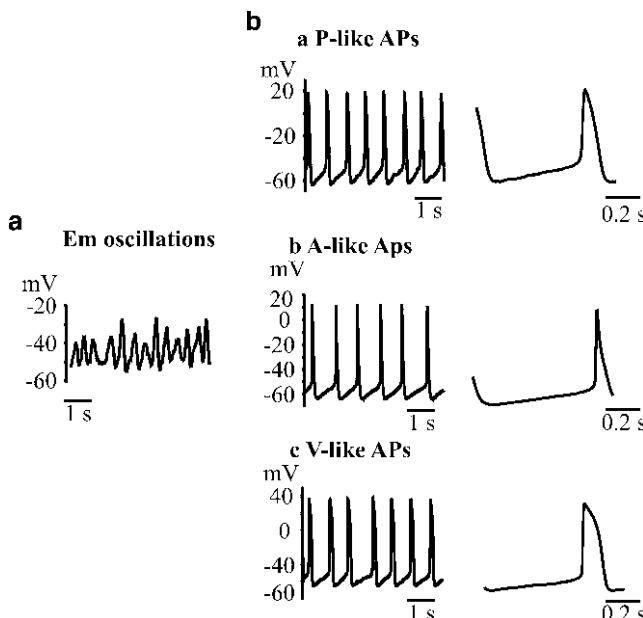


Fig. 10.3 Electrical activity of 8.5 dpc murine cardiomyocytes. Membrane potential (Em) oscillations (A) develop into mature like action potentials (B). P-like pacemaker like, V-like ventricular like, A-like atrial like

However, the mechanism underlying the transition from Em oscillations to APs is still unclear.

10.2.2 Hyperpolarization-Activated and Cyclic Nucleotide-Gated (HCN) Channel Current (I_f)

Although there is considerable debate over the exact role of I_f in pacemaker activity [1, 13, 14], the fact that cardiomyocytes without I_f do not beat spontaneously implies the important role of I_f in pacemaker activity in the SA node, especially with regard to the autonomic modulation of heart rate [13]. In the past decades, I_f has been well studied during fetal cardiac development, where it is downregulated over time [15, 16]. The expression of I_f is high in EDS (10.5 dpc) ventricular myocytes, low in intermediate developmental stage (IDS) (13.5 dpc) atrial or ventricular myocytes, and even lower in late developmental stage (LDS) (16.5 dpc) atrial or ventricular myocytes. The decrease in I_f is associated with a slight change in channel gating kinetics and a decrease in total mRNA expression of the genes encoding for I_f channel subunits [16].

Three pacemaker channel subtypes (HCN1, HCN2, and HCN4) are expressed in the mouse embryonic heart [16]. The most prevalent mRNA subtype switches from HCN4 to HCN2 during 9.5–18.5 dpc of embryonic development [16]. Major HCN gene subtypes detected at 9.5 dpc are HCN4 and HCN1 (HCN4 > HCN1 ≫ HCN2). At 18 dpc, the relative order of gene expression changes to HCN2 > HCN4 or HCN1, although the total amount is much less than that at 9.5 dpc. Thus, the predominant gene changes from HCN4 to HCN2 during embryonic development. The subtype shift of HCN channels during fetal development is in line with the studies on later development (from neonatal to adult) [17].

The HCN2 channels have a more negative voltage range for activation than the HCN1 or HCN4 channels [18], and their relative abundance determines the activation threshold in different regions of the heart or at different ages [17]. More interestingly, HCN2 expression in neonatal and adult ventricular myocytes in culture results in a comparable difference (18 mV) in $V_{1/2}$ of cultivated cells and that of native I_f (22 mV) [17], and I_f also activates at less negative voltages (−70 mV) in newborn rat ventricle [19, 20], indicating that the variations of HCN subtypes lead to the developmental changes in the electrical properties of I_f .

10.2.3 Long Lasting (L)-Type Ca^{2+} Channel Current (I_{CaL})

I_{CaL} is believed to be the most important pacemaker current because the generation of the diastolic depolarization (DD) phase of SA nodal cardiomyocytes is near the threshold potential for I_{CaL} . Moreover, L-type Ca^{2+} channel blockers easily suppress or prevent spontaneous APs. At low concentrations, Ca^{2+} channel blockers

suppress and slow the last part of the DD [21]. During fetal development, the I_{CaL} density and the opening and closing behavior of Ca^{2+} channels change significantly. In rat and mouse hearts, the density of Ca^{2+} current increases during fetal development and reaches its maximal level at about the day of birth [4, 22–25]. In chick embryonic heart, the density of peak Ca^{2+} current is already high at 3 dpc and decreases at 17 dpc [8]. I_{CaL} at 9.5 dpc activates and/or inactivates at more negative membrane potentials than at 18 dpc or in adult hearts. L-type Ca^{2+} channels at 9.5 dpc are less sensitive to inhibition by nisoldipine than at adult stage [26]. Nguemo et al. [25] also report that the fast phase of I_{CaL} inactivation (sf) is significantly enhanced by isoproterenol at LDS, whereas slow phase of inactivation (ss) is unaltered at both EDS and LDS. However, voltage-dependent inactivation is significantly reduced with isoproterenol in LDS and adult cardiomyocytes, implying that β -adrenergic modulation becomes of importance especially during fetal heart development.

Recent findings indicate that the subtype of I_{CaL} shifts from $\text{Cav}1.3$ to $\text{Cav}1.2$ in embryonic murine ventricle during development. At 9.5 dpc, the level of $\text{Cav}1.3$ mRNA is higher than that of $\text{Cav}1.2$ mRNA. With development, $\text{Cav}1.2$ mRNA increases and $\text{Cav}1.3$ mRNA decreases. $\text{Cav}1.3$ protein is detected only at 9.5 dpc, whereas $\text{Cav}1.2$ protein is expressed from 9.5 dpc onwards and its expression increases with development. $\text{Cav}1.1$ mRNA is detected slightly only at 9.5 dpc. Thus, the $\text{Cav}1.3$ Ca^{2+} channel is downregulated during the second half of embryonic development. Before birth, the $\text{Cav}1.2$ Ca^{2+} channel has already become the dominant type of I_{CaL} [26]. Two variants of $\text{Cav}1.2$, $\text{Cav}1.2\alpha$ and $\text{Cav}1.2\beta$, are expressed in murine embryos of 12.5 dpc [27], suggesting that embryonic cardiac cells may express the “cardiac” and the “smooth muscle” [28, 29] subtypes of $\text{Cav}1.2$ at 12.5 dpc. Two alternative amino termini of $\text{Cav}1.3$, termed $\text{Cav}1.3$ (1a) and $\text{Cav}1.3$ (1b), have also been identified. $\text{Cav}1.3$ (1b) mRNA is expressed at a higher density than $\text{Cav}1.3$ (1a) mRNA.

10.2.4 T-Type Ca^{2+} Channel Current (I_{CaT})

In the adult heart, I_{CaT} is most prevalent in the conduction system and is probably involved in automaticity [30] because selective inhibition of I_{CaT} produces a marked slowing of the pacemaker rhythm [31, 32]. I_{CaT} is observed at both 9.5 and 18 dpc [33], displaying similar electrophysiological properties in terms of current density, kinetics of activation/inactivation, voltage dependence of activation, steady-state inactivation, and kinetics of recovery from inactivation.

During development, $\text{Cav}3.2$ underlies functional I_{CaT} in the embryonic murine heart, and the subtype switches from $\text{Cav}3.2$ to $\text{Cav}3.1$ towards the perinatal period [34, 35]. $\text{Cav}3.2$ mRNA is downregulated by 50% during the second half of embryonic development, and $\text{Cav}3.1$ mRNA is upregulated by 300-fold. At 17.5 dpc, $\text{Cav}3.1$ became comparable to $\text{Cav}3.2$ mRNA level, as shown by Ferron et al. [33]. $\text{Cav}3.1$ and $\text{Cav}3.2$ channels can be distinguished based on their kinetics of recovery from inactivation: $\text{Cav}3.1$ recovers more rapidly than $\text{Cav}3.2$ [36, 37].

After birth $\text{Ca}_v3.2$ mRNA decreases rapidly and becomes undetectable at 5 weeks, whereas $\text{Ca}_v3.1$ mRNA level remains high in the postnatal periods [38]. Ferron et al. [33] reported that I_{Cat} is expressed in fetal rat ventricular myocytes, but decreases soon after birth to an undetectable level. They also show progressive decrease of Ni^{2+} sensitivity of I_{Cat} from the mid-embryonic stage ($\text{IC}_{50} = 49 \mu\text{M}$ at 16 dpc to the neonatal stage; $\text{IC}_{50} = 291 \mu\text{M}$ at 1 day after birth). The role of I_{Cat} in embryonic cardiomyocytes requires further study.

10.2.5 Sodium Calcium Exchanger Current (I_{NCX})

Early evidence for the role of I_{NCX} in pacemaker cardiomyocytes comes from measurement of two components of the inward current in response to depolarization [39]. These ideas are extended in studies of latent pacemaker cardiomyocytes in the cat atrium, which exhibit secondary slow inward currents and tail currents characteristic of I_{NCX} [40]. At the fetal stage, the I_{NCX} density is significantly decreased during development [16, 24, 41]. Both mRNA and protein expressions of NCX1 are significantly higher in early than in late developmental murine ventricles [16]. Both forward and reverse modes of NCX are activated by the Na^+ ionophore monensin at fetal stages [41]. An increase of NCX function is thought to potentially serve as an important compensating mechanism maintaining $[\text{Ca}^{2+}]_i$ homeostasis in the developing heart.

10.2.6 Delayed Rectifier K^+ Current

The delayed rectifier K^+ current (I_K) in SA nodal cardiomyocytes is comprised of both I_{Kr} and I_{Ks} [9, 42–44]. I_{Kr} is rapidly activated within 200 ms while I_{Ks} is slowly activated in 1–2 s. I_{Kr} inhibition may cause a more positive maximum diastolic potential (MDP) and a longer AP duration [45] and therefore contribute to the pacemaking activity by accelerating DD. I_{Kr} has been identified in mouse fetal [4, 46] and neonatal [9] ventricular myocytes and, at a much lower level of expression, in the ventricle of adult mice [47] and rats [48, 49].

10.2.7 Other Pacemaker Currents

Other currents also contribute in a minor way to DD of pacemaker cells and modulate MDP [1], especially in the diseased heart to contribute more significantly to DD.

The proportion of cardiomyocytes that have detectable I_{to} , I_{Kr} , and I_{Ks} is less at EDS than at LDS, although the current density does not change [4]. During development, the current density of I_{K1} increases in the rat, rabbit, chick, guinea

pig, and mouse hearts [50–54]. The subtype of I_{K1} switches from $K_{ir}2.1$ to $K_{ir}2.2$ during the development of fetal rat [55]. However, more details of the electrophysiological properties and the species differences need to be further elucidated.

Previous studies show that all the ATP-sensitive K^+ channel subunits ($K_{ir}6.1$, $K_{ir}6.2$, SUR1, SUR2A, and SUR2B) are expressed in the mouse heart during development [56]. However, the expression level of each subunit is low in the early developmental fetal heart and progressively increases with maturation. These subunits seem to be expressed in ventricular myocytes with a subcellular expression pattern matching that found in the adult [56]. I_{KACH} is expressed at similar densities in both early and late stages of development. At EDS, I_{KACH} is primarily formed by $K_{ir}3.1$, while in late embryonic and adult cardiomyocytes, $K_{ir}3.4$ is the predominant subunit. This change in subunit composition results in reduced rectification of I_{KACH} , allowing for marked K^+ currents over the whole physiological voltage range [5].

10.3 Pacemaker Activity in Murine ESc-Derived Cardiomyocytes

In mESc-derived cardiomyocytes (Fig. 10.4), the earliest detectable electrophysiological activity is Em oscillations that later develop into APs [57]. Studies on the importance of I_{CaL} for the generation of APs in EDS cardiomyocytes revealed that early APs in mES cells are mainly driven by L-type Ca^{2+} currents [2, 58]. Functional expression of the above-mentioned ion channel currents exhibits developmental changes similar to those observed in fetal cardiomyocytes. I_f is

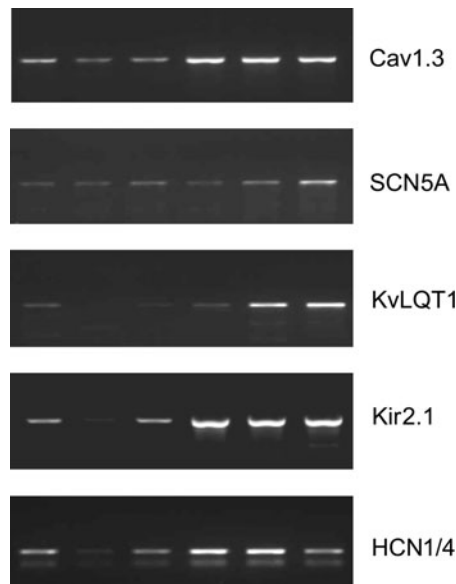


Fig. 10.4 Developmental changes in ion channels in murine embryonic stem cell-derived cardiomyocytes. Semiquantitative RT-PCR data [61] reveal the upregulation of I_{Na} subunit SCN5A, I_{CaL} subunit Ca $\sqrt{1.3}$, I_{Ks} subunit KvLQT1, I_{K1} subunit $K_{ir}2.1$, and downregulation of I_f subunit HCN1/4

detected in a large percentage (65%) of EDS cells at a current density of 11.4 ± 0.6 pA/pF. At LDS, the percentage of cells expressing I_f decreases (45%), but I_f density (15.5 ± 0.9 pA/pF) increases [59]. The density of Ca^{2+} current increases during cardiac development [58]. The expression of $\text{Ca}_v3.1$ subtypes that conduct I_{CaT} increases significantly by 7 + 10 days (10 days after plating at day 7 for further differentiation), peaks at 7 + 16 days, and declines significantly at 7 + 27 days [60]. Semiquantitative RT-PCR data (Fig. 10.4) [61] reveal the upregulation of the I_{Na} subunit SCN5A, I_{CaL} subunit $\text{Ca}_v1.3$, I_{Ks} subunit KvLQT1, I_{K1} subunit $\text{K}_{\text{ir}}2.1$, and downregulation of I_f subunits HCN1/4.

10.4 Pacemaker Activity in Human ESc-Derived Cardiomyocytes

Recently, there has been some progress in characterization of the pacemaker activity of immature human hearts, mostly from the study of human ESc (hES)-derived cardiomyocytes [62, 63]. The hES cells can differentiate into multiple types of cardiomyocytes displaying functional properties characteristic of embryonic human cardiac muscle. Currents that contribute to DD phase, I_f and I_{CaL} , undergo similar developmental changes to that in murine cardiomyocytes. HCN1, HCN2, and HCN4 are expressed throughout differentiation of cardiomyocytes but downregulated toward maturation. The expression of $\text{Ca}_v1.2$ increased along with the increase in whole cell I_{CaL} density. I_{to1} contributes more to repolarization at LDS [63]. I_{Kr} plays an important role in repolarization of the AP based on E-4031-induced prolongation of AP duration as anticipated for human cardiomyocytes, especially at EDS. I_{to1} contributes more to repolarization phase at LDS. I_{Kr} channel transcripts HERG1a and HERG1b are detected without developmental changes. Two isoforms of I_{to1} , Kv1.4 and Kv4.3, are upregulated with maturation. Accordingly, whole cell I_{to1} increases. Similarly to I_{to1} , I_{K1} seems to be a marker of cardiac differentiation and maturation, being expressed at a significantly higher density at LDS [63].

Current studies on pacemaker activity in hESc-derived cardiomyocytes are limited and inconclusive. For example, the mechanisms for the first AP during cardiogenesis are still unclear, although Satin et al. [64] report that 10- μM TTX causes cessation of spontaneous APs at mid-stage hESc-derived cardiomyocytes, indicating that Na^+ channel is important for initiating spontaneous excitability in mid-stage hESc-derived heart cells.

10.5 Conclusions

Taken together, all the important pacemaker currents found in working cardiomyocytes undergo developmental changes in fetal and ESc-derived cardiomyocytes (Table 10.1). A tremendous amount has been learned over the last 20 years

Table 10.1 Developmental changes of ion channels during cardiac differentiation

	Subtype	EDS	LDS
I_f	HCN1	++	+
	HCN2	+	++
	HCN4	+++	+
I_{CaL}	Cav1.2	++	++++
	Cav1.3	+++	+
I_{CaT}	Cav3.1	+	++
	Cav3.2	+++	+
I_{NCX}	NCX1	+++	+
I_{K1}	K _i r2.1	+	+++
I_{KACH}	K _i r3.1	++	+
	K _i r3.4	+	++
I_{Kr}	mERG/hERG	+	+

I_f Hyperpolarization-activated and cyclic nucleotide-gated (HCN) channel current, I_{CaL} long lasting (L)-type Ca^{2+} channel current, I_{CaT} transient (T)-type Ca^{2+} channel current, I_{NCX} Na^+/Ca^{2+} exchanger current, I_{K1} inward rectifier K^+ channel current, I_{Kr} rapidly activated delayed K^+ current, I_{KACH} acetylcholine-sensitive K^+ current

regarding the ionic and molecular basis of cardiac pacemaker activity of immature cardiomyocytes. Since the gene expression and functional expression of ion channel currents in the diseased heart resemble to some extent the early embryonic expression pattern [65–67], information about ion channel expression and their function in the immature cells may offer clues for a better understanding of pathophysiological processes in the heart. Moreover, fetal hearts or cardiomyocytes derived from ESc can serve as good tools for regenerative medicine because of similarity of pacemaker activities with diseased hearts.

Nevertheless, many aspects remain unexplained. The molecular biology of ion channel expression in pacemaker cardiomyocytes is largely unexplored. Species differences in ion channel expression of fetal cardiomyocytes are incompletely understood. Moreover, the functional contributions of individual ion channels to DD phase of APs in fetal cardiomyocytes need to be further demonstrated.

References

1. Satoh H. Sino-atrial nodal cells of mammalian hearts: ionic currents and gene expression of pacemaker ionic channels. *J Smooth Muscle Res.* 2003;39:175–93.
2. Maltsev VA, Wobus AM, Rohwedel J, Bader M, Hescheler J. Cardiomyocytes differentiated in vitro from embryonic stem cells developmentally express cardiac-specific genes and ionic currents. *Circ Res.* 1994;75:233–44.
3. Bony C, Roche S, Shuichi U, Sasaki T, Crackower MA, Penninger J, et al. A specific role of phosphatidylinositol 3-kinase gamma. A regulation of autonomic Ca^{2+} oscillations in cardiac cells. *J Cell Biol.* 2001;152:717–28.
4. Davies MP, An RH, Doevedans P, Kubalak S, Chien KR, Kass RS. Developmental changes in ionic channel activity in the embryonic murine heart. *Circ Res.* 1996;78:15–25.

5. Fleischmann BK, Duan Y, Fan Y, Schoneberg T, Ehlich A, Lenka N, et al. Differential subunit composition of the G protein-activated inward-rectifier potassium channel during cardiac development. *J Clin Invest.* 2004;114:994–1001.
6. Kolossov E, Fleischmann BK, Liu Q, Bloch W, Viatchenko-Karpinski S, Manzke O, et al. Functional characteristics of ES cell-derived cardiac precursor cells identified by tissue-specific expression of the green fluorescent protein. *J Cell Biol.* 1998;143:2045–56.
7. Kolossov E, Lu Z, Drobinskaya I, Gassanov N, Duan Y, Sauer H, et al. Identification and characterization of embryonic stem cell-derived pacemaker and atrial cardiomyocytes. *FASEB J.* 2005;19:577–9.
8. Tohse N, Meszaros J, Sperelakis N. Developmental changes in long-opening behavior of L-type Ca^{2+} channels in embryonic chick heart cells. *Circ Res.* 1992;71:376–84.
9. Ono K, Ito H. Role of rapidly activating delayed rectifier K^+ current in sinoatrial node pacemaker activity. *Am J Physiol.* 1995;269:H453–62.
10. Kaufman MH. The atlas of mouse development. London: Academic; 1995.
11. Sasse P, Zhang J, Cleemann L, Morad M, Hescheler J, Fleischmann BK. Intracellular Ca^{2+} oscillations, a potential pacemaking mechanism in early embryonic heart cells. *J Gen Physiol.* 2007;130:133–44.
12. Fabiato A. Two kinds of calcium-induced release of calcium from the sarcoplasmic reticulum of skinned cardiac cells. *Adv Exp Med Biol.* 1992;311:245–62.
13. DiFrancesco D. The pacemaker current (I_f) plays an important role in regulating SA node pacemaker activity. *Cardiovasc Res.* 1995;30:307–8.
14. Mangoni ME, Traboulsi A, Leoni AL, Couette B, Marger L, Le Quang K, et al. Bradycardia and slowing of the atrioventricular conduction in mice lacking $\text{Ca}_{v}3.1/\alpha 1\text{G}$ T-type calcium channels. *Circ Res.* 2006;98:1422–30.
15. Song GL, Tang M, Liu CJ, Luo HY, Liang HM, Hu XW, et al. Developmental changes in functional expression and beta-adrenergic regulation of I_f in the heart of mouse embryo. *Cell Res.* 2002;12:385–94.
16. Yasui K, Liu W, Ophof T, Kada K, Lee JK, Kamiya K, et al. I_f current and spontaneous activity in mouse embryonic ventricular myocytes. *Circ Res.* 2001;88:536–42.
17. Qu J, Barbuti A, Protas L, Santoro B, Cohen IS, Robinson RB. HCN2 overexpression in newborn and adult ventricular myocytes: distinct effects on gating and excitability. *Circ Res.* 2001;89:E8–14.
18. Proenza C, Tran N, Angoli D, Zahynacz K, Balcar P, Accili EA. Different roles for the cyclic nucleotide binding domain and amino terminus in assembly and expression of hyperpolarization-activated, cyclic nucleotide-gated channels. *J Biol Chem.* 2002;277:29634–42.
19. Robinson RB, Yu H, Chang F, Cohen IS. Developmental change in the voltage-dependence of the pacemaker current, if, in rat ventricle cells. *Pflugers Arch.* 1997;433:533–5.
20. Cerbai E, Pino R, Sartiani L, Mugelli A. Influence of postnatal development on I_f occurrence and properties in neonatal rat ventricular myocytes. *Cardiovasc Res.* 1999;42:416–23.
21. Verheijck EE, van Ginneken AC, Wilders R, Bouman LN. Contribution of L-type Ca^{2+} current to electrical activity in sinoatrial nodal myocytes of rabbits. *Am J Physiol.* 1999;276:H1064–77.
22. Cohen NM, Lederer WJ. Changes in the calcium current of rat heart ventricular myocytes during development. *J Physiol.* 1988;406:115–46.
23. Masuda H, Sumii K, Sperelakis N. Long openings of calcium channels in fetal rat ventricular cardiomyocytes. *Pflugers Arch.* 1995;429:595–7.
24. Liu W, Yasui K, Ophof T, Ishiki R, Lee JK, Kamiya K, et al. Developmental changes of Ca^{2+} handling in mouse ventricular cells from early embryo to adulthood. *Life Sci.* 2002;71:1279–92.
25. Nguemo F, Sasse P, Fleischmann BK, Kamanyi A, Schunkert H, Hescheler J, et al. Modulation of L-type Ca^{2+} channel current density and inactivation by beta-adrenergic stimulation during murine cardiac embryogenesis. *Basic Res Cardiol.* 2009;104:295–306.

26. Takemura H, Yasui K, Ophof T, Niwa N, Horiba M, Shimizu A, et al. Subtype switching of L-Type Ca^{2+} channel from $\text{Ca}_V1.3$ to $\text{Ca}_V1.2$ in embryonic murine ventricle. *Circ J.* 2005;69:1405–11.
27. Klugbauer N, Welling A, Specht V, Seisenberger C, Hofmann F. L-type Ca^{2+} channels of the embryonic mouse heart. *Eur J Pharmacol.* 2002;447:279–84.
28. Welling A, Ludwig A, Zimmer S, Klugbauer N, Flockerzi V, Hofmann F. Alternatively spliced IS6 segments of the $\alpha 1C$ gene determine the tissue-specific dihydropyridine sensitivity of cardiac and vascular smooth muscle L-type Ca^{2+} channels. *Circ Res.* 1997;81:526–32.
29. Hofmann F, Lacinova L, Klugbauer N. Voltage-dependent calcium channels: from structure to function. *Rev Physiol Biochem Pharmacol.* 1999;139:33–86.
30. Hagiwara N, Irisawa H, Kameyama M. Contribution of two types of calcium currents to the pacemaker potentials of rabbit sino-atrial node cells. *J Physiol.* 1988;395:233–53.
31. Masumiya H, Shijuku T, Tanaka H, Shigenobu K. Inhibition of myocardial L- and T-type Ca^{2+} currents by efonidipine: possible mechanism for its chronotropic effect. *Eur J Pharmacol.* 1998;349:351–7.
32. Protas L, Robinson RB. Mibepradil, an IC_A, T blocker, effectively blocks IC_A, L in rabbit sinus node cells. *Eur J Pharmacol.* 2000;401:27–30.
33. Ferron L, Capuano V, Deroubaix E, Coulombe A, Renaud JF. Functional and molecular characterization of a T-type Ca^{2+} channel during fetal and postnatal rat heart development. *J Mol Cell Cardiol.* 2002;34:533–46.
34. Niwa N, Yasui K, Ophof T, Takemura H, Shimizu A, Horiba M, et al. $\text{Ca}_V3.2$ subunit underlies the functional T-type Ca^{2+} channel in murine hearts during the embryonic period. *Am J Physiol Heart Circ Physiol.* 2004;286:H2257–63.
35. Mizuta E, Miake J, Yano S, Furuichi H, Manabe K, Sasaki N, et al. Subtype switching of T-type Ca^{2+} channels from $\text{Ca}_V3.2$ to $\text{Ca}_V3.1$ during differentiation of embryonic stem cells to cardiac cell lineage. *Circ J.* 2005;69:1284–9.
36. Klöckner U, Lee JH, Cribbs LL, Daud A, Hescheler J, Pereverzev A, et al. Comparison of the Ca^{2+} currents induced by expression of three cloned α subunits, $\alpha 1G$, $\alpha 1H$ and $\alpha 1I$, of low-voltage-activated T-type Ca^{2+} channels. *Eur J Neurosci.* 1999;11:4171–8.
37. McRory JE, Santi CM, Hamming KSC, Mezeyeva J, Sutton KG, Baillie DL, et al. Molecular and functional characterization of a family of rat brain T-type calcium channels. *J Biol Chem.* 2001;276:3999–4011.
38. Larsen JK, Mitchell JW, Best PM. Quantitative analysis of the expression and distribution of calcium channel $\alpha 1$ subunit mRNA in the atria and ventricles of the rat heart. *J Mol Cell Cardiol.* 2002;34:519–32.
39. Brown HF, Kimura J, Noble D, Noble SJ, Taupignon A. The ionic currents underlying pacemaker activity in rabbit sino-atrial node: experimental results and computer simulations. *Proc R Soc Lond B Biol Sci.* 1984;222:329–47.
40. Zhou Z, Lipsius SL. $\text{Na}^+-\text{Ca}^{2+}$ exchange current in latent pacemaker cells isolated from cat right atrium. *J Physiol.* 1993;466:263–85.
41. Reppel M, Fleischmann BK, Reuter H, Sasse P, Schunkert H, Hescheler J. Regulation of the $\text{Na}^+/\text{Ca}^{2+}$ exchanger (NCX) in the murine embryonic heart. *Cardiovasc Res.* 2007;75:99–108.
42. Sanguinetti MC, Jurkiewicz NK. Two components of cardiac delayed rectifier K^+ current. Differential sensitivity to block by class III antiarrhythmic agents. *J Gen Physiol.* 1990;96:195–215.
43. Matsuura H, Ehara T, Ding WG, Omatsu-Kanbe M, Isono T. Rapidly and slowly activating components of delayed rectifier K^+ current in guinea-pig sino-atrial node pacemaker cells. *J Physiol.* 2002;540:815–30.
44. Shinagawa Y, Satoh H, Noma A. The sustained inward current and inward rectifier K^+ current in pacemaker cells dissociated from rat sinoatrial node. *J Physiol.* 2000;523:593–605.
45. Clark RB, Mangoni ME, Lueger A, Couette B, Nargeot J, Giles WR. A rapidly activating delayed rectifier K^+ current regulates pacemaker activity in adult mouse sinoatrial node cells. *Am J Physiol Heart Circ Physiol.* 2004;286:H1757–66.

46. Wang L, Duff HJ. Identification and characteristics of delayed rectifier K⁺ current in fetal mouse ventricular myocytes. *Am J Physiol.* 1996;270:H2088–93.
47. Babij P, Askew GR, Nieuwenhuijsen B, Su CM, Bridal TR, Jow B, et al. Inhibition of cardiac delayed rectifier K⁺ current by overexpression of the long-QT syndrome HERG G628S mutation in transgenic mice. *Circ Res.* 1998;83:668–78.
48. Pond AL, Scheve BK, Benedict AT, Petrecca K, Van Wagoner DR, Shrier A, et al. Expression of distinct ERG proteins in rat, mouse, and human heart. Relation to functional IKr channels. *J Biol Chem.* 2000;275:5997–6006.
49. Wymore RS, Gintant GA, Wymore RT, Dixon JE, McKinnon D, Cohen IS. Tissue and species distribution of mRNA for the I_{Kr}-like K⁺ channel, erg. *Circ Res.* 1997;80:261–8.
50. Nuss HB, Marban E. Electrophysiological properties of neonatal mouse cardiac myocytes in primary culture. *J Physiol.* 1994;479:265–79.
51. Masuda H, Sperelakis N. Inwardly rectifying potassium current in rat fetal and neonatal ventricular cardiomyocytes. *Am J Physiol.* 1993;265:H1107–11.
52. Huynh TV, Chen F, Wetzel GT, Friedman WF, Klitzner TS. Developmental changes in membrane Ca²⁺ and K⁺ currents in fetal, neonatal, and adult rabbit ventricular myocytes. *Circ Res.* 1992;70:508–15.
53. Josephson IR, Sperelakis N. Developmental increases in the inwardly-rectifying K⁺ current of embryonic chick ventricular myocytes. *Biochim Biophys Acta.* 1990;1052:123–7.
54. Kato Y, Masumiya H, Agata N, Tanaka H, Shigenobu K. Developmental changes in action potential and membrane currents in fetal, neonatal and adult guinea-pig ventricular myocytes. *J Mol Cell Cardiol.* 1996;28:1515–22.
55. Nagashima M, Tohse N, Kimura K, Yamada Y, Fujii N, Yabu H. Alteration of inwardly rectifying background K⁺ channel during development of rat fetal cardiomyocytes. *J Mol Cell Cardiol.* 2001;33:533–43.
56. Morrissey A, Parachuru L, Leung M, Lopez G, Nakamura TY, et al. Expression of ATP-sensitive K⁺ channel subunits during perinatal maturation in the mouse heart. *Pediatr Res.* 2005;58:185–92.
57. Viatchenko-Karpinski S, Fleischmann BK, Liu Q, Sauer H, Gryshchenko O, Ji GJ, et al. Intracellular Ca²⁺ oscillations drive spontaneous contractions in cardiomyocytes during early development. *Proc Natl Acad Sci USA.* 1999;96:8259–64.
58. Maltsev VA, Rohwedel J, Hescheler J, Wobus AM. Embryonic stem cells differentiate in vitro into cardiomyocytes representing sinusnodal, atrial and ventricular cell types. *Mech Dev.* 1993;44:41–50.
59. Abi-Gerges N, Ji GJ, Lu ZJ, Fischmeister R, Hescheler J, Fleischmann BK. Functional expression and regulation of the hyperpolarization activated non-selective cation current in embryonic stem cell-derived cardiomyocytes. *J Physiol.* 2000;523:377–89.
60. Zhang Z, Xu Y, Song H, Rodriguez J, Tuteja D, Namkung Y, et al. Functional roles of Cav1.3 (alpha(1D)) calcium channel in sinoatrial nodes: insight gained using gene-targeted null mutant mice [see comment]. *Circ Res.* 2002;90:981–7.
61. van Kempen M, van Ginneken A, de Grijt I, Mutsaers N, Ophof T, Jongsma H, et al. Expression of the electrophysiological system during murine embryonic stem cell cardiac differentiation. *Cell Physiol Biochem.* 2003;13:263–70.
62. He JQ, Ma Y, Lee Y, Thomson JA, Kamp TJ. Human embryonic stem cells develop into multiple types of cardiac myocytes: action potential characterization. *Circ Res.* 2003;93:32–9.
63. Sartiani L, Bettoli E, Stillitano F, Mugelli A, Cerbai E, Jaconi ME. Developmental changes in cardiomyocytes differentiated from human embryonic stem cells: a molecular and electrophysiological approach. *Stem Cells.* 2007;25:1136–44.
64. Satin J, Kehat I, Caspi O, Huber I, Arbel G, Itzhaki I, et al. Mechanism of spontaneous excitability in human embryonic stem cell derived cardiomyocytes. *J Physiol.* 2004;559:479–96.
65. Bers DM. Altered cardiac myocyte Ca regulation in heart failure. *Physiology (Bethesda).* 2006;21:380–7.

66. Cohen O, Kanana H, Zoizner R, Gross C, Meiri U, Stern MD, et al. Altered Ca^{2+} handling and myofilament desensitization underlie cardiomyocyte performance in normothermic and hyperthermic heat-acclimated rat hearts. *J Appl Physiol.* 2007;103:266–75.
67. Martinez ML, Heredia MP, Delgado C. Expression of T-type Ca^{2+} channels in ventricular cells from hypertrophied rat hearts. *J Mol Cell Cardiol.* 1999;31:1617–25.

Chapter 11

Molecular Basis of the Electrical Activity of the Atrioventricular Junction and Purkinje Fibres

Halina Dobrzynski, Oliver Monfredi, Ian D. Greener, Andrew Atkinson, Shin Inada, Mary-Anne Taube, Joseph Yanni, Olga Fedorenko, Peter Molenaar, Robert H. Anderson, Igor R. Efimov, and Mark R. Boyett

11.1 Introduction

The atrioventricular junction and its associated Purkinje fibres are essential though complex components of the cardiac conduction system. The atrioventricular (AV) junction is enclosed within the triangle of Koch, and is made up of the transitional zone, inferior nodal extensions, the compact node and the penetrating bundle of His. Its function is to be the sole mechanism of transmission of the atrial action potential (AP) to the ventricular myocardium, and to delay the AP to allow atrial systole to complete so that the ventricles are optimally filled prior to their contraction. This delay also protects the ventricular myocardium from otherwise dangerous atrial arrhythmias. The molecular basis of this unique component of the conduction system that leads to these features is reviewed along with discussion of the consequences of malfunction of the AV junction. The Purkinje fibres are made up of specialised myocytes that form the terminal branches of the cardiac conduction system. They are adapted for rapid conduction and dissemination of the cardiac AP. The molecular basis of the above attributes is discussed. Armed with the knowledge of the molecular architecture of the cardiac conduction system discussed in this chapter, it is possible to generate mathematical models that can replicate the behaviour of the cardiac AP in the different cardiac regions. This may, in future, allow the generation of a 3-D working model of the cardiac conduction system upon which the effects of various states of disease and pharmacological agents may be tested.

H. Dobrzynski (✉), O. Monfredi, I.D. Greener, A. Atkinson, S. Inada, M.-A. Taube, J. Yanni, O. Fedorenko, R.H. Anderson, and M.R. Boyett
University of Manchester, Manchester, UK
e-mail: halina.dobrzynski@manchester.ac.uk

P. Molenaar
Queensland University of Technology and University of Queensland, The Prince Charles Hospital, Brisbane, QLD, Australia

I.R. Efimov
Washington University, St. Louis, MO, USA

11.2 Atrioventricular Node

11.2.1 Anatomical Location

We have studied the functional and molecular properties of the AV junction for over a decade, primarily in rabbit and human hearts. In this chapter, based on our work, we provide an account of the molecular basis of the electrical activity of the AV junction (this section) and Purkinje fibres (Sect. 11.3) mainly in these two species.

Figure 11.1 shows the AV node of the human heart. The AV node is located in the floor of the right atrium (Fig. 11.1a) and its anatomical landmarks are provided by the boundaries of the triangle of Koch (Fig. 11.1b) [1–4]. The apex of the triangle is formed by the membranous septum, which also forms an integral part of the aortic root. The membranous septum itself is divided by the hinge of the septal leaflet of the tricuspid valve into AV and interventricular components. The AV

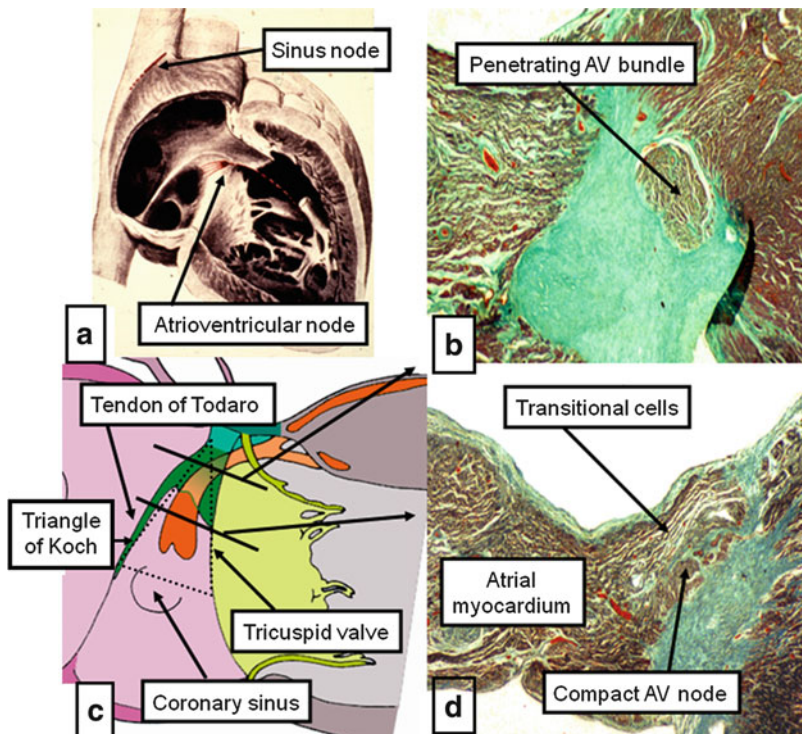


Fig. 11.1 Anatomy and histology of human atrioventricular junction. (a) Cut open view of the heart showing the atrioventricular node (in red) at the base of the right atrium. (c) Diagram of the atrioventricular conduction axis within the triangle of Koch. (b, d) Histological tissue sections cut at the levels shown in (c). From R.H. Anderson

component is continuous with the right fibrous trigone, the latter structure representing the rightward extent of the area of fibrous continuity between the leaflets of the mitral and aortic valves. The septum and trigone together form the central fibrous body. The AV node becomes the penetrating AV bundle, or the bundle of His, when it enters the central fibrous body (Fig. 11.1b, c) so as to provide the sole electrical communication in the normal heart between the atrial and ventricular muscle masses. The node is contained within the atrial myocardium in the floor of the triangle of Koch, with the posterior boundary of the triangle formed by the continuation of the fibrous commissure of the Eustachian and Thebesian valves, these structures guarding the entrances of the inferior caval vein and coronary sinus to the right atrium, through the atrial musculature to insert into the AV component of the membranous septum (Fig. 11.1b). This fibrous structure is the tendon of Todaro (Fig. 11.1b). The anterior boundary of the triangle is demarcated by the hinge of the septal leaflet of the tricuspid valve, and the base is formed by the mouth of the coronary sinus (Fig. 11.1b).

11.2.2 Histology

It was Tawara, in 1906 [5], who initially identified a histologically discrete group of cells at the proximal end of the bundle of His, which he termed the “Knoten”. The “Knoten” (compact node) in the human heart is shown in Fig. 11.1d and in the rabbit heart in Fig. 11.2b. Tawara [5] also depicted the two branches extending inferiorly from the node, which are now known as the inferior nodal extensions. The right inferior nodal extension in the rabbit is shown in Fig. 11.2b. The histologically specialised cells within the extensions gradually become less distinguishable as they extend into the vestibules of the tricuspid and mitral valves, but their specialised nature as AV ring tissues can be demonstrated using appropriate markers [8]. In the human heart, the right extension is more prominent than the left [9]. In order to describe the extent of the node, it is necessary to define its boundaries. In this respect, in 1910, at a meeting of the German Pathological Society, Aschoff and Mönckeberg established a set of criteria they deemed necessary to identify conducting tracts (e.g. [8, 10]). These criteria are, first, that the cells within the purported tracts must be histologically distinct from the surrounding tissues, second, that the cells should be traceable through serial sections of histologically prepared slides, and third that the cells should be separated from surrounding tissues by a fibrous sheath. The cells making up the AV node satisfy two of these three criteria, but do not qualify as tracts, since they are not insulated from the adjacent atrial myocardium. Instead, at the borders of the node, there are distinct areas of transition between the atrial myocytes and the specialised myocytes making up the “Knoten” (Fig. 11.2b). The transitional cells surround all parts of the compact node, running intramyocardially from the terminal crest, through the ridge between the orifices of the inferior caval vein and the coronary sinus, from the inferior rim of the oval fossa, and from the left side of the atrial septum [2, 4]. Overall, therefore,

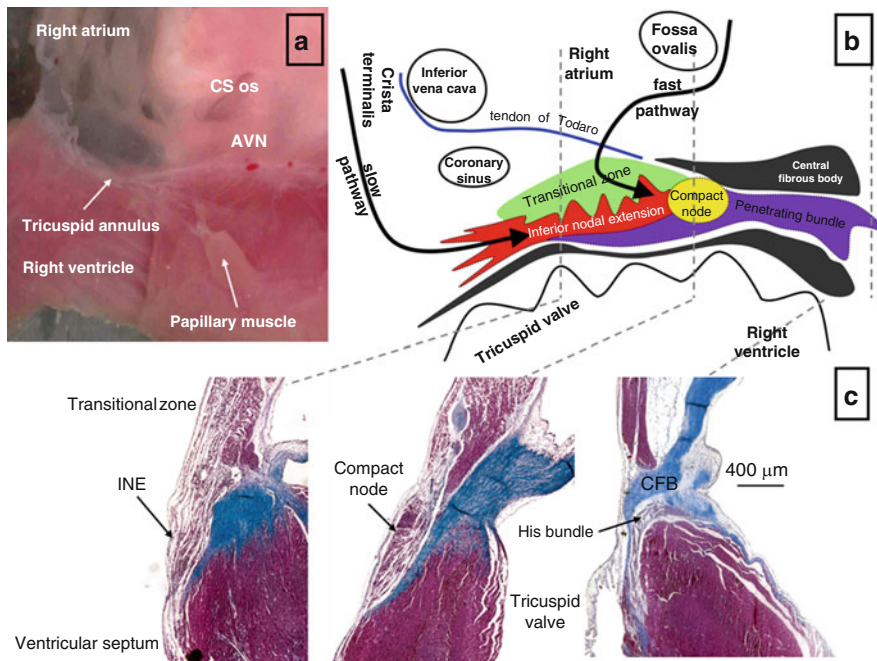


Fig. 11.2 Anatomy and histology of the rabbit atrioventricular junction. (a) Location of atrioventricular conduction axis at the atrioventricular junction of the rat heart. The endocardial surface of the preparation is shown. CS os coronary sinus ostium. (b) Schematic diagram of the different components of the atrioventricular conduction axis in the rabbit. (c) Masson's trichrome stained sections at the levels shown through the inferior nodal extension, compact node and bundle of His. CFB central fibrous body, INE inferior nodal extension. (b) is from [6] and (c) is from [7]

the AV junctional area has four distinct regions: the transitional zone, the compact node, the penetrating AV bundle, and the branching AV bundle (Fig. 11.2b). Debate continues regarding the cut-off point between the compact node and the penetrating AV bundle. It is pertinent, nonetheless, to remember the initial work of Tawara [5]. Recognising the indistinct nature of the histological boundary between the node and penetrating bundle in some species, he wrote “I set the boundary there, where the system breaks through the fibrous atrioventricular septum, because on the one hand this place is easy to determine anatomically and further, because in the sheep this system demonstrates the aforementioned remarkable histological change precisely at this point”. We believe this logical, simple, and accurate definition retains its currency. When considered relative to the rabbit heart, nonetheless, use of this definition means that the most histologically heterogeneous part of the conduction axis, previously considered as the “closed node” [11], should properly be defined as part of the penetrating AV bundle. The anatomic arrangement as found in the rabbit, and as shown in Fig. 11.2b, is markedly different from the pattern of the AV conduction axis in the human body. In the human body, the compact node is a half-oval of cells set against the central fibrous body and in contact with transitional

cells throughout its semi-circular atrial border (Fig. 11.1d). The transitional cells form inputs to the node from the right atrial myocardium via the septal isthmus, the Eustachian ridge, and the antero-superior rim of the oval fossa, and also from the left side of the atrial septum. In the human body, the origin of the bundle of His, as described by Tawara [5], is marked by the point at which the conduction axis enters the insulating tissues of the central fibrous body (Fig. 11.1b).

11.2.3 Function

The AV node is a part of the cardiac conduction system, and its functional properties have been extensively studied [12–17]. In the healthy heart, the action potential (AP) producing the heart beat is first generated by the sinus or sinoatrial (SA) node, the leading pacemaker of the heart (e.g. [18]). The SA node is considered in detail in other chapters. The AP from the SA node propagates through the atrial myocardium, and then into the AV node, where it is delayed to allow atrial systole to fill the ventricles during ventricular diastole. Subsequent to the AV delay, the AP travels through the penetrating bundle of His to the right and left bundle branches, and is then disseminated through the Purkinje fibres to initiate ventricular systole (e.g. [19]). The main purpose of the AV node, therefore, is to transmit the AP from the atria to the ventricles, while at the same time providing a sufficient delay to allow atrial contraction and ventricular filling. In the presence of abnormal rhythms, the AV node is also able to perform other vital functions, for example, preventing the transmission of atrial arrhythmias to the ventricles, thus protecting against potentially fatal conditions such as ventricular fibrillation. Moreover, should the SA node fail, then the AV node can assume the role of leading pacemaker [20].

Electrophysiologically, three AV regions have been identified: atrionodal (AN), compact nodal (N), and nodal-His (NH) [21]. In Fig. 11.3a, we show recordings of APs from these three distinct regions in the rabbit. N cells have a typical nodal AP with a slow upstroke and a relatively positive diastolic membrane potential. In N cells, the AP is followed by a diastolic depolarization (DD, pacemaker potential) and these cells are capable of pacemaking. In contrast, AN and NH cells are more transitional in nature. AN cells are thought to populate the transitional zone, N cells the inferior nodal extensions and compact node, and NH cells the penetrating bundle (Fig. 11.2b) [6].

11.2.3.1 Dual Pathway Electrophysiology

In an early investigation of rabbit hearts, Mendez and Moe, as long ago as 1966, suggested the existence of two pathways into the AV node, termed α and β , to explain AV nodal reentrant tachycardia (AVNRT) [24]. The β -pathway is the superior (anterior) pathway, proposed to arise from the superior nodal inputs of the atrial septum – it is thought to be formed by the transitional zone (Fig. 11.2b).

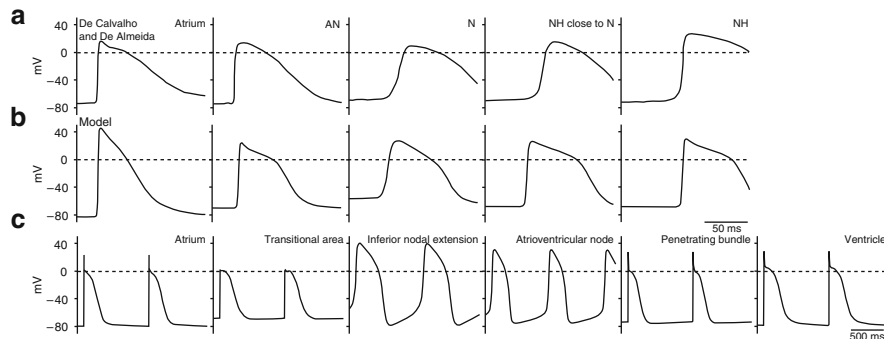


Fig. 11.3 Action potentials of the rabbit and human atrioventricular conduction axis. **(a, b)** APs of the rabbit atrioventricular conduction axis. **(a)** APs recorded experimentally by de Carvalho and de Almeida [22]. **(b)** APs calculated using the models of Inada [23]. **(c)** APs of the human atrioventricular conduction axis. The APs were calculated as described in the text

The α -pathway is inferior (posterior), and is thought to be formed by the right inferior nodal extension (Fig. 11.2b) [25]. The β -pathway is now designated the “fast” pathway, and the α -pathway the “slow” pathway (Fig. 11.2b). The fast pathway is said to have quicker conduction, but a longer effective refractory period (ERP), than the slow pathway [26]. Such dual pathways have been found not only in patients with AVNRT, but also in asymptomatic individuals, suggesting they may be a relatively normal feature of AV node electrophysiology [26]. Dual pathway electrophysiology was first demonstrated in humans by Schuilenberg and Durrer [27]. Early attempts to treat AVNRT by ablating the fast pathway carried a risk of AV nodal block [28], while ablation of the slow pathway proved highly successful [29]. This has led to the idea that normal sinus rhythm is carried over the fast pathway, with the slow pathway serving to carry the retrograde stimulus, contrary to the initial proposal of Mendez and Moe [24]. Stein and Lerman, nonetheless, concluded that both pathways are necessary for normal conduction, and that all inputs summate to stimulate the compact node [13]. However, recent mathematical simulations suggest that the fast pathway is responsible for normal conduction and the slow pathway is responsible for the conduction of the premature AP (because of its shorter ERP) [23].

11.2.3.2 AV Nodal Reentrant Tachycardia

AVNRT is a supraventricular tachycardia involving the AV node in a reentrant circuit (e.g. [30, 31]). The reentry is a manifestation of the dual pathway electrophysiology of the AV node. There are three types of AVNRT:

1. The commonest form, accounting for nine-tenths of cases, has a slow–fast character. Anterograde conduction (conduction in the normal direction) is thought to occur through the slow pathway, and retrograde conduction (conduction in the

opposite direction to normal) through the fast pathway. The ECG often produces an obscured P wave, and an RP interval shorter than the PR interval.

2. In the rarer fast–slow variant, conduction occurs anterogradely through the fast pathway, and retrogradely through the slow pathway. The P wave may be clearly visible, and the RP interval equals or is longer than the PR interval.
3. The third variant, a slow–slow form, is thought to arise through two slow pathways with differing functional properties, one conducting the impulse anterogradely, and the other returning retrogradely. The ECG trace in this variant is similar to that of the fast–slow AVNRT. This is apparent as a wide QRS complex with a P wave either before or after the QRS complex, or even an undetectable P wave. ST segment pseudo-depression is relatively common [28, 32].

Figure 11.4 shows an example of slow–fast AVNRT in the rabbit. An isolated rabbit AV node preparation was used – the preparation was stimulated at the top left (Fig. 11.4a). The first stimulus (S1) triggered an AP which propagated through the AV node to the bundle of His (Fig. 11.4b). The S1 stimulus was quickly followed by a premature stimulus (S2); the S2 AP propagated to the His bundle, but after

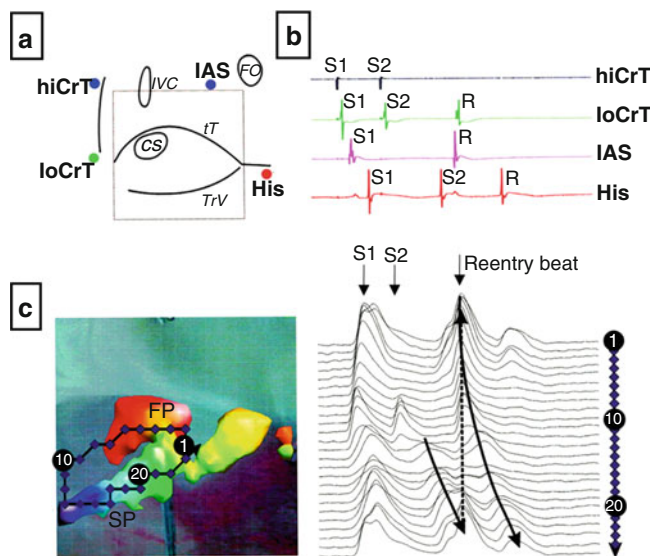


Fig. 11.4 Slow–fast AVNRT. (a) Schematic diagram of the preparation. *CS* coronary sinus, *FO* fossa ovalis, *hiCrT* high crista terminalis, *HIS* bundle of His, *IAS* interatrial septum, *IVC* inferior vena cava, *IoCrT* low crista terminalis, *TrV* tricuspid valve, *tT* tendon of Todaro. (b) Extracellular potential recordings from the sites shown by the corresponding coloured spots in (a). *S1*, AP in response to the regular *S1* stimulus; *S2*, AP in response to the premature *S2* stimulus; *R*, reentrant AP. (c) Reconstruction of the conduction pathway during slow–fast AVNRT by a three-dimensional stack plot of optical signal derivatives (see original paper for details). *FP* fast pathway, *SP* slow pathway. (d) Optical action potentials recorded at the 23 sites shown in (c). From [33].

a longer delay, and this AP was followed by a third – the reentrant beat (Fig. 11.4b). The reentrant circuit is shown in Fig. 11.4c. The S1 AP arrived at recording sites 1–10 at about the same time. It arrived at sites 10–20 in the slow pathway slightly later as a result of conduction along the slow pathway from the atrial muscle. The premature S2 AP failed to arrive at sites 1–9, presumably because of conduction block in the fast pathway as a result of its long ERP. However, the S2 AP did arrive at site 10 and it then propagated (albeit more slowly than normal) along the slow pathway (sites 10–20), presumably because its ERP is shorter. The S2 AP finally arrived at site 20 (but via the slow pathway rather than the atrial muscle as normal). From site 20 the AP must have retrogradely propagated along the fast pathway to re-excite the atrial muscle, because after a delay the AP reappeared at site 10 and then propagated along the slow pathway (sites 10–20). It is this re-entry beat that must have led to the third AP recorded in the bundle of His (Fig. 11.4b). We have simulated this form of re-entry [23].

11.2.4 Molecular Basis of Electrical Activity of the AV Node

For a review of ionic currents in the atrioventricular node see Hancox et al. [34]. In Table 11.1, we summarise our findings concerning the expression of ion channels in the different parts of the rabbit and human AV conduction axis ([6], and unpublished data from Greener and Dobrzynski).

Table 11.1 Expression of ion channels at the mRNA level in the inferior nodal extension, compact node and bundle of His (as compared to ventricular muscle) in the rabbit [6] and human (unpublished data from Greener and Dobrzynski)

Ion channel	Corresponding ionic current	Inferior nodal extension		Compact node		Bundle of His	
		Rabbit	Human	Rabbit	Human	Rabbit	Human
HCN1	I_f	↑	≈	↑	↑	↑	≈
HCN4	I_f	↑	↑	↑	↑	↑	↑
Na _v 1.1	I_{Na}	↑	≈	↑	≈	↑	≈
Na _v 1.5	I_{Na}	↓	↓	↓	↓	↓	≈
Ca _v 1.2	$I_{Ca,L}$	↓	≈	↓	≈	↓	≈
Ca _v 1.3	$I_{Ca,L}$	↑	↑	↑	↑	↑	↑
Ca _v 3.1	$I_{Ca,T}$?	↑	?	↑	?	↑
K _v 1.4	I_{to}	↓	≈	↓	↑	↓	↑
K _v 4.2	I_{to}	≈	≈	≈	↑	≈	↑
K _v 4.3	I_{to}	?	≈	?	≈	?	↑
K _v 1.5	$I_{K,ur}$?	≈	?	≈	?	≈
ERG	$I_{K,r}$	≈	≈	≈	≈	≈	≈
K _v LQT	$I_{K,s}$?	↓	?	≈	?	≈
K _i r2.1	$I_{K,i}$	↓	↓	↓	↓	↓	↓
K _i r3.1	$I_{K,ACh}$?	≈	?	↑	?	≈

↑, upregulated; ≈, unchanged; ↓, downregulated; ?, unknown

11.2.4.1 Pacemaker Channel

HCN1, 2 and 4 are responsible for the pacemaker current, I_f . In small mammals, this current is present in the cardiac pacemaker tissues, but absent for the most part from the working myocardium [35]. mRNA for HCN4 is more abundant in the rabbit and human inferior nodal extension, compact node, and bundle of His when compared to the ventricular muscle (Table 11.1). Only in the human, however, is this transcript found with the highest expression in the compact component of the AV conduction axis (Table 11.1). The higher expression of these channels explains the pacemaker activity of the AV node.

11.2.4.2 Na^+ Channel

mRNA for the cardiac Na^+ channel, $\text{Na}_v1.5$, which is primarily responsible for the Na^+ current, I_{Na} , is less abundant in all components of the conduction axis in both rabbit and human when compared to ventricular muscle (Table 11.1). The lower expression of this channel explains the slower upstroke of the AP in these regions.

11.2.4.3 Ca^{2+} Channels

Two separate Ca^{2+} currents have been recorded from cardiac myocytes, the L-type (I_{CaL}) and the T-type (I_{CaT}) [36]. I_{CaL} is carried by $\text{Ca}_v1.2$ and $\text{Ca}_v1.3$ channels, whereas $\text{Ca}_v3.1$ – $\text{Ca}_v3.3$ are responsible for I_{CaT} [37]. Expression of mRNA for $\text{Ca}_v1.2$ is lower in rabbit, but not in human, in the components of the conduction axis than in ventricular muscle (Table 11.1). Expression of mRNA for $\text{Ca}_v1.3$, however, is higher in the conduction axis of both rabbit and human when compared to the ventricular muscle (Table 11.1). $\text{Ca}_v1.3$ has been shown to have a role in pacemaking [36]. Furthermore, mice in which this gene has been knocked-out have been found to display a prolonged PR interval, i.e. slower conduction through the AV node [38]. Expression of mRNA for $\text{Ca}_v3.1$ is higher in the human AV conduction axis (Table 11.1) – I_{CaT} is also important for pacemaking [39].

11.2.4.4 K^+ Channels

There are two types of transient outward K^+ current (I_{to}) in the heart, fast and slow; the names relate to their kinetics of recovery from inactivation. The $\text{K}_v4.2$ and/or $\text{K}_v4.3$ channels underlie the fast current, whereas $\text{K}_v1.4$ is responsible for the slow current. There is complex expression of the mRNAs for all these channels within the AV conduction axis (Table 11.1). In the rabbit, for example, there is lower expression of the $\text{K}_v1.4$ mRNA compared to ventricular muscle, whereas in the human this transcript, along with $\text{K}_v4.2$ mRNA, is more abundant in the compact node and bundle of His compared to ventricular muscle (Table 11.1). This suggests

specific modulation of the K⁺ channels in the compartments of the AV conduction axis in different species.

There are three delayed rectifier K⁺ currents: ultra-rapid (I_{Kur}), rapid (I_{Kr}) and slow (I_{Ks}) currents. The ion channels responsible for these currents are Kv1.5, ERG, and KvLQT1, respectively. I_{Kur} is considered a major repolarizing current in the human atrium. Throughout the AV conduction axis in the human, mRNA underlying I_{Kur} is expressed at the same level as in ventricular muscle (Table 11.1). I_{Kr} and I_{Ks} are involved in repolarization in the heart in various species, including the human. Throughout the AV conduction axis in both rabbit and human, mRNA for ERG is expressed at the same level as in ventricular muscle (Table 11.1). In the compact node and bundle of His in the human, KvLQT1 mRNA is expressed at the same level as in ventricular muscle, but in the inferior nodal extension it is less abundant (Table 11.1).

The more positive diastolic membrane potential of the N cells in the inferior nodal extension and compact node is largely due to the reduced density of the inward rectifying K⁺ current, I_{K1} . In both species, we have found expression of mRNA for Kv2.1 (one of the channels responsible for I_{K1}) to be lower in all components of the AV conduction axis compared to ventricular muscle (Table 11.1).

Vagal (parasympathetic) nerve stimulation is known to slow conduction through the AV node (a negative dromotropic effect) by activating the ACh-activated K⁺ current, I_{KACH} . I_{KACH} is carried by a heteromultimer of Kv3.1 and Kv3.4 channel subunits. In the inferior nodal extension and bundle of His in the human, Kv3.1 mRNA is expressed at the same level as in ventricular muscle, but in the compact node it is more abundant (Table 11.1) and this is consistent with vagal control of AV nodal conduction.

11.2.4.5 Ca²⁺-Handling Proteins

In small mammals, intracellular Ca²⁺ handling is known to play an important role in SA node pacemaking [40]. Recent data suggests the “Ca²⁺-clock” mechanism to be also crucial for pacemaking in cells of the AV conduction axis in the rabbit [41]. We have measured the level of mRNAs for the Ca²⁺-handling proteins, RYR2, SERCA2A and NCX1. In the AV conduction axis of rabbit, but not of human, expression of mRNA for RYR2, responsible for release of Ca²⁺ from the sarcoplasmic reticulum (SR), is lower than in the ventricular muscle.

11.2.4.6 Changes in Ion Channels and Ca²⁺-Handling Proteins in the AV Conduction Axis of the Failing Heart

Heart failure can slow conduction through the AV node and prolong the PR interval in the ECG. In Table 11.2, we summarise the changes found thus far in our investigation of the expression of ion channels in the AV node of the failing human heart

Table 11.2 Changes in the expression of mRNAs for ion channels and Ca^{2+} -handling proteins in the AV node in the failing human heart (as compared to the normal heart; unpublished data from Taube and Dobrzynski)

Downregulated	Upregulated
$\text{Na}_v1.5 (I_{\text{Na}})$	$\text{HCN}1 (I_f)$
$\text{Ca}_v1.2 (I_{\text{Ca,L}})$	$\text{Ca}_v3.1 (I_{\text{Ca,T}})$
$\text{Ca}_v1.3 (I_{\text{Ca,I}})$	
$\text{K}_v1.5 (I_{\text{K,ur}})$	
$\text{ERG} (I_{\text{K,r}})$	
$\text{K}_{ir}3.1 (I_{\text{K,ACh}})$	
$\text{RYR}2 (\text{SR } \text{Ca}^{2+} \text{ release channel})$	
$\text{NCX}1 (\text{Na}^+-\text{Ca}^{2+} \text{ exchange})$	

Corresponding ionic currents are shown in parenthesis. SR sarcoplasmic reticulum

(unpublished data from Taube and Dobrzynski). HCN1 mRNA is upregulated in the AV node of the failing heart (Table 11.2) and that, by itself, is expected to increase pacemaker activity (but see below). $\text{Na}_v1.5$, $\text{Ca}_v1.2$ and $\text{Ca}_v1.3$ mRNAs are downregulated in the failing heart (Table 11.2). $\text{Ca}_v1.3$ has been shown to have a role in pacemaking [36], and mice with knock-out of this gene are reported to display a prolonged PR interval [38]. The downregulation of $\text{Ca}_v1.3$ mRNA in the failing heart is, therefore, expected to slow pacemaker activity, but it can help to explain the prolonged PR interval in heart failure. $\text{Ca}_v3.1$ mRNA is upregulated in the failing heart (Table 11.2) and is expected to increase pacemaker activity [42]. $\text{K}_v1.5$ and ERG mRNAs are downregulated in the failing heart (Table 11.2) and these changes are expected to result in a prolongation of the AP. $\text{K}_{ir}3.1$ mRNA is downregulated in the failing heart (Table 11.2) and this can explain the reduced vagal control of the AV node – in heart failure, a loss of vagal control of the SA node has been reported [43]. It is well known that Ca^{2+} -handling is remodelled in heart failure [44], and we observed a downregulation of RYR2 and NCX1 in the AV node (Table 11.2).

11.3 The Purkinje Network

The specialised myocytes within the Purkinje network provide the final pathways of the cardiac conduction system. The ventricular pathways are insulated from the underlying ventricular myocardium by sheaths of connective tissue, which are lost before the specialised myocytes form their terminal connections with the working myocardium.

11.3.1 Anatomy

The ramifications of the right and left bundle branches can be seen macroscopically, being lighter than the underlying ventricular myocytes, reflecting the fact that the

specialised myocytes possess fewer myofibrils than the working myocytes. The course of the Purkinje networks has been tracked in various species [4, 45, 46], showing complex sub-endocardial networks ramifying within the trabeculated apical ventricular components, along with free-running cords crossing the ventricular cavities (known as false tendons). Various studies show the marked asymmetry of the networks within the left and right ventricles. In Fig. 11.5, we show the complex arrangement as seen within the human (Fig. 11.5a) and rabbit (Fig. 11.5b) left ventricle. In both species, the overall pattern is comparable. The left bundle branch takes its origin as a fan from the branching component of the AV conduction axis as the axis itself is sandwiched between the membranous septum and the crest of the muscular ventricular septum. The left fascicle then divides into three interconnecting divisions, with the anterior and posterior divisions extending towards the bases of the paired papillary muscles of the mitral valve [5, 45]. The intermediate division extends down the smooth septal surface, interconnecting the other divisions. The specialised myocytes, no larger than ventricular myocytes in rabbit and human, then ramify within the apical trabeculations, losing their insulating sheath and gradually merging with the ventricular myocytes. Figure 11.6 shows long axis sections through the rat heart immunolabelled for the gap junction channel, Cx40 (marker of Purkinje tissue). The Purkinje tissue appears yellow and ramifies into the apical trabeculations. The right bundle branch, in contrast, originates as a narrow cord from the branching component of the AV conduction axis. It surfaces on the endocardial surface of the right ventricle in relation to the medial papillary muscle, and extends downwards on the surface of the septomarginal trabeculation, with a branch then crossing the cavity of the ventricle within the moderator band [5, 45, 50]. The right ventricular network then becomes extensive in the apical trabeculated part of the ventricle, with some specialised myocytes extending superiorly also to ramify within the free-standing subpulmonary infundibulum. There is then a gradual transition from specialised to working myocytes as the network loses its sheath of connective tissue.

11.3.2 Functional Properties

The myocytes within the Purkinje network are highly specialised to permit rapid AP conduction to all parts of the two ventricles – the conduction velocity of the Purkinje network is the fastest of all tissues in the heart to ensure that there is near synchronous activation of all ventricular muscle. Purkinje myocytes display distinct characteristics in terms of their AP having a rapid upstroke velocity, an increased duration, a prominent early phase of rapid repolarisation (phase 1), a negative plateau potential, and spontaneous DD (phase 4) [46, 51] (Fig. 11.5d). The faster upstroke velocity, in part, is responsible for the fast conduction velocity of the Purkinje network. Under normal conditions, the specialised myocytes do not exhibit automaticity when suppressed by overdrive in sinus rhythm. They are capable, nonetheless, of functioning as escape pacemakers [52]

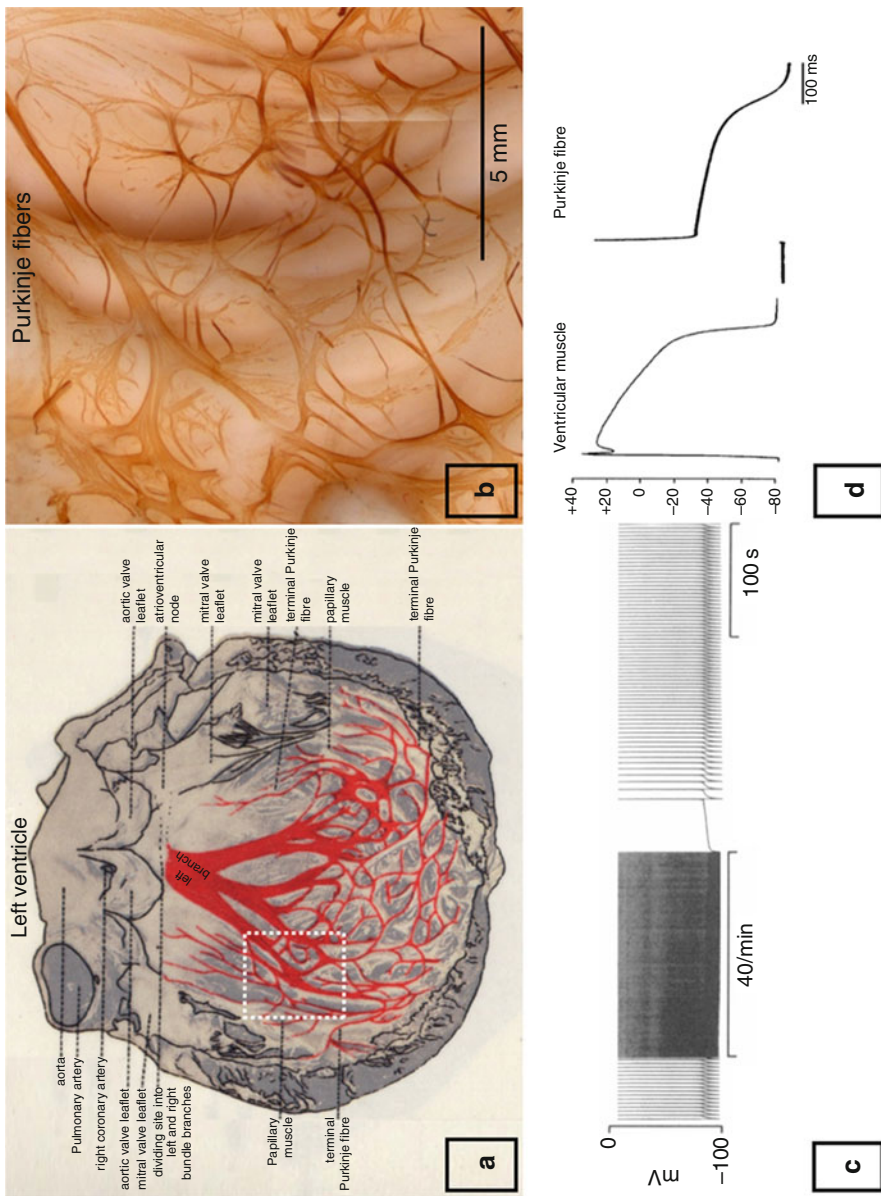


Fig. 11.5 Anatomy, histology and action potential of left ventricular Purkinje fibres. (a) Anatomy of human left ventricular Purkinje network. From Boyett [19]; modified from Tawara [5]. (b) Photograph of part of the Purkinje network in the left ventricle of the rabbit heart (unpublished data). The Purkinje tissue

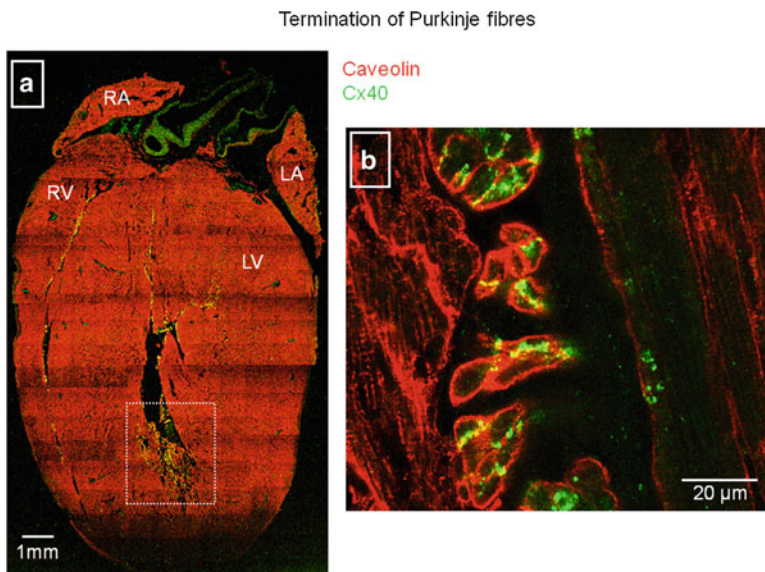


Fig. 11.6 Terminations of the Purkinje fibre network ramifying the apical trabeculations in the left ventricle of the rat heart. (a) Long axis sections through the rat heart double labelled using immunofluorescence for a general cardiac myocyte marker, caveolin (red signal), and a Purkinje tissue marker, Cx40 (green signal). The Purkinje tissue appears yellow as a result of the overlap of the two signals. Note the white box in highlights the terminations of the Purkinje fibre network ramifying the trabeculations at the apex of the left ventricle. (b) A closer view of termination of the Purkinje cells. LA left atrium, LV left ventricle, RA right atrium, RV right ventricle (unpublished data from Fedorenko and Dobrzynski)

(Fig. 11.5c), and can play a role in the generation and maintenance of arrhythmias. They have an increased resistance to ischaemia [53], and are thought to play a role in the maintenance of long duration ventricular fibrillation. The ablation of the Purkinje network leads to a shorter time to spontaneous termination of ventricular fibrillation [54]. The networks have been linked to a number of ventricular arrhythmias, including torsade de pointes associated with long QT syndrome. The long duration of the AP of the specialised myocytes makes them susceptible to the production of arrhythmogenic early and delayed afterdepolarizations [50, 55, 56].

Fig. 11.5 (continued) has been stained a darker brown colour by immunoenzyme labelling of a marker protein, neurofilament. Loose (darker) as well as subendocardial (lighter) Purkinje fibres can be seen. (c) Pacemaking in a dog Purkinje fibre (from [47]). (d) APs in ventricular muscle (from [48]) and a Purkinje fibre (from [49]) from sheep

11.3.3 Molecular Basis of the Electrical Activity of the Purkinje Network

The features of the characteristic AP reflect differences in ionic currents and the expression of ion channels between the specialised and working ventricular myocytes (Table 11.3). Differences in a number of ionic currents are recorded, e.g. prominent I_f , I_{Na} , I_{CaT} , I_{to} and I_{KACH} , but smaller I_{CaL} , I_{Kr} , $I_{K,s}$ and I_{K1} in the specialised myocytes [55, 56, 58]. Table 11.3 summarises the expression of various ion channels at the mRNA level in rabbit (unpublished data from Atkinson and Dobrzynski) and human [57] Purkinje fibres. In both species, there is higher expression of HCN1 and HCN4 mRNAs in the Purkinje fibres as compared to the ventricular muscle (Table 11.3) – this can explain the prominent I_f and the pacemaker activity of the Purkinje fibres [50, 52]. Surprisingly, there is a lower expression of $Na_v1.5$ mRNA in human Purkinje fibres compared to ventricular muscle (Table 11.3) – surprising, because $Na_v1.5$, responsible for I_{Na} , is expected to be elevated to explain the prominent I_{Na} and the fast upstroke and conduction velocities of Purkinje fibres. In rabbit Purkinje fibres, there is also no evidence of the expected higher expression of $Na_v1.5$ mRNA (Table 11.3). In both species, there is lower expression of $Ca_v1.2$ mRNA, but higher expression of $Ca_v1.3$ mRNA (Table 11.3). In the human, there is also a higher expression of $Ca_v3.1$ mRNA (Table 11.3). This pattern of expression of $Ca_v1.2$, $Ca_v1.3$ and $Ca_v3.1$ mRNAs appears to be a “hallmark” of the tissues of the cardiac conduction system – the SA [59] and the AV nodes tend to show a similar pattern (Table 11.1). This expression pattern presumably explains the smaller I_{CaL} and prominent I_{CaT} of Purkinje myocytes.

Table 11.3 Expression of ion channels at the mRNA level in rabbit (unpublished data from Atkinson and Dobrzynski) and human [57] Purkinje fibres as compared to ventricular muscle

Ion channel	Corresponding ionic current	Rabbit Purkinje fibres	Human Purkinje fibres
HCN1	I_f	↑	↑
HCN4	I_f	↑	↑
$Na_v1.1$	I_{Na}	↑	≈
$Na_v1.5$	I_{Na}	≈	↓
$Ca_v1.2$	$I_{Ca,L}$	↓	↓
$Ca_v1.3$	$I_{Ca,L}$	↑	↑
$Ca_v3.1$	$I_{Ca,T}$?	↑
$K_v1.4$	I_{to}	↓	≈
$K_v4.2$	I_{to}	≈	≈
$K_v4.3$	I_{to}	↑	↑
$K_v1.5$	$I_{K,ur}$	↓	≈
ERG	$I_{K,r}$	↓	≈
K_vLQT1	$I_{K,s}$	↓	≈
$K_{ir}2.1$	$I_{K,i}$	↓	↓
$K_{ir}3.1$	$I_{K,ACh}$	↑	↑

↑, upregulated; ≈, unchanged; ↓, downregulated; ?, unknown

The expression of K^+ channels is complex in the two species, with less expression of $K_v1.4$, $K_v1.5$, ERG and K_vLQT1 mRNAs (responsible for transient outward and delayed rectifier K^+ currents) in the rabbit (Table 11.3). In both species, there is similar expression of mRNA for the transient outward K^+ channel, $K_v4.2$, but higher expression of mRNA for another transient outward K^+ channel, $K_v4.3$ (Table 11.3). Such an expression of K^+ channels presumably explains the prominent I_{to} and smaller I_{Kr} and I_{Ks} of Purkinje myocytes. In both species, there is a lower expression of $K_{ir}2.1$ mRNA (Table 11.3). $K_{ir}2.1$, responsible for I_{K1} , and in turn for resting potential of the working myocardium helps explain the propensity for pacemaking in this tissue. In both species, there is a higher expression of $K_{ir}3.1$ mRNA (Table 11.3) explaining the prominent I_{KACh} in Purkinje myocytes.

Like the AV node, the Purkinje network is also affected in heart failure, e.g. bundle branch block is common in heart failure [60]. Ionic currents and ion channel expression in Purkinje fibres are also altered [61].

11.4 Mathematical Modelling of AV Node

Recently, we have developed mathematical models of the AP of the AN, N and NH cells in the rabbit based on published voltage clamp data from rabbit AV node cells [23]. The model APs of AN, N and NH cells are a reasonable fit to experimentally recorded data and they are different from the APs in the working myocardium (Fig. 11.3a). In the rabbit, the differences reflect differences in ionic currents (observed in experiments), which in turn reflect the differences in ion channel expression (reviewed above). In the case of the human AV node, there are no voltage clamp data. Instead, we have developed mathematical models of APs in different compartments of the human AV conduction axis (transitional zone, inferior nodal extension, compact node and penetrating bundle of His as well as ventricle) from the mRNA data reviewed above. The models were based on the model of Courtemanche et al. [62] for the human right atrial AP, based on extensive voltage clamp data. Along the AV conduction axis, it was assumed that the whole cell conductance for a particular ionic current is roughly proportional to the abundance of one or more mRNAs responsible for the relevant ion channel. Figure 11.3b shows calculated APs along the AV conduction axis as well as in the atrial muscle (unmodified from [62]) and ventricular muscle (calculated in the same way as the APs along the AV conduction axis). The computed APs have feasible characteristics and shapes (Fig. 11.3b). The transitional zone is predicted to have a transitional AP, the inferior nodal extension and compact node, a typical nodal AP, the penetrating bundle of His, and an AP with a fast upstroke velocity (Fig. 11.3b). The predicted ventricular AP has the roughly expected form (Fig. 11.3b). During diastole, in the atrium, there is a stable resting potential. It is predicted that in the ventricle there is also a stable resting potential, whereas in the transitional zone and penetrating bundle of His the membrane is more depolarized and less stable (Fig. 11.3b). In contrast, in the inferior nodal extension and compact

node, it is predicted that there is a slow DD (Fig. 11.3b). It is predicted that the inferior nodal extension and compact node are both capable of pacemaker activity. This is consistent with the finding that, in the human heart, the leading pacemaker site at the AV junction is in the compact node and its junction with the penetrating bundle of His. The maximum upstroke velocity of the AP is high in the atrium (124 V/s) and is predicted to be lower in the transitional zone (35 V/s), low in the inferior nodal extension and compact node (2–12 V/s), and high in the penetrating bundle of His and ventricle (>130 V/s) (Fig. 11.3b). The maximum upstroke velocity is known to be low along the AV conduction axis and this is one reason why conduction through the AV node is slow. We suggest that this technique of extrapolating from mRNA to function is a new form of bioinformatics to explore the consequences of a change in ion channel expression.

11.5 Conclusions

The AV junction and its associated Purkinje fibres are significantly more complex than can ever have been envisaged by Tawara when he first discovered the small group of innocent-looking cells at the proximal bundle of His at the beginning of the last century. Our knowledge has advanced significantly since this time. Accurate gross anatomical identification of the various components that demarcate these critical anatomical structures as described above is now routinely possible. However, the microscopic and molecular anatomy still holds significant mystique, and require further investigation, especially within human tissues. This will lead subsequently to a finer understanding of the complex physiology and pathophysiology of the AV junction and associated Purkinje fibres. Disease of these structures within the heart continues in 2010 to lead to a significant degree of morbidity and mortality, both in terms of AV conduction block and arrhythmogenesis, often as a component of extremely common conditions such as myocardial ischaemia and heart failure. Only through a more fundamental appreciation of the normal structure and function of these regions will the scientific and medical communities be able to place in context the rearrangements that occur at the macro- and microscopic levels as part of these disease states, so that ultimately more effective treatments or even cures may be developed to the benefit of all.

References

1. Anderson RH, Becker AE, Brechenmacher C, Davies MJ, Rossi L. The human atrioventricular junctional area. A morphological study of the A-V node and bundle. Eur J Cardiol. 1975;3:11–25.
2. Anderson RH, Ho SY. The atrial connections of the specialized axis responsible for AV conduction. In: Mazgalev TN, Tchou PJ, editors. Atrial-AV nodal electrophysiology: a view from the millennium. 1st ed. Armont, NY: Futura; 2000. p. 3–23.

3. Anderson RH, Ho SY. The morphology of the specialized atrioventricular junctional area: the evolution of understanding. *Pacing Clin Electrophysiol*. 2002;25:957–66.
4. Anderson RH, Yanni J, Boyett MR, Chandler NJ, Dobrzynski H. The anatomy of the cardiac conduction system. *Clin Anat*. 2009;22:99–113.
5. Tawara S. Das Reizleitungssystem des Säugetierherzens. Eine anatomisch histologische Studie über das Atrioventrikularbündel und die Purkinjeschen Fäden. Jena: Gustav Fischer; 1906.
6. Greener ID, Tellez JO, Dobrzynski H, Yamamoto M, Graham GM, Billeter R, et al. Ion channel transcript expression at the rabbit atrioventricular conduction axis. *Circ Arrhythm Electrophysiol*. 2009;2:305–15.
7. Li J, Greener ID, Inada S, Nikolski VP, Yamamoto M, Hancox JC, et al. Computer three-dimensional reconstruction of the atrioventricular node. *Circ Res*. 2008;102:975–85.
8. Yanni J, Boyett MR, Anderson RH, Dobrzynski H. The extent of the specialised atrioventricular ring tissue. *Heart Rhythm*. 2009;6:672–80.
9. Hucker WJ, McCain ML, Laughner JI, Iaizzo PA, Efimov IR. Connexin 43 expression delineates two discrete pathways in the human atrioventricular junction. *Anat Rec (Hoboken)*. 2008;291:204–15.
10. Cosio FC, Anderson RH. Living anatomy of the atrioventricular junctions. A guide to electrophysiological mapping. A consensus statement from the Cardiac Nomenclature Study Group, Working Group of Arrhythmias, European Society of Cardiology, and the Task Force on Cardiac Nomenclature from NASPE. *J Cardiovasc Electrophysiol*. 1999;10:1162–70.
11. Anderson RH. The disposition and innervation of atrioventricular ring specialized tissue in rats and rabbits. *J Anat*. 1972;113:197–211.
12. Paes de Carvalho A, de Almeida DF. Spread of activity through the atrioventricular node. *Circ Res*. 1960;8:801–9.
13. Stein KM, Lerman BB. Evidence for functionally distinct dual atrial inputs to the human AV node. *Am J Physiol*. 1994;267:H2333–41.
14. Mazgalev TN, Tchou PJ. Atrioventricular nodal conduction gap and dual pathway electrophysiology. *Circulation*. 1995;92:2705–14.
15. Efimov IR, Mazgalev TN. High-resolution three-dimensional fluorescent imaging reveals multilayer conduction pattern in the atrioventricular node. *Circulation*. 1998;98:54–7.
16. Hucker WJ, Sharma V, Nikolski VP, Efimov IR. Atrioventricular conduction with and without AV nodal delay: two pathways to the bundle of His in the rabbit heart. *Am J Physiol*. 2007;293:H1122–30.
17. Hucker WJ, Fedorov VV, Foyil KV, Moazami N, Efimov IR. Images in cardiovascular medicine. Optical mapping of the human atrioventricular junction. *Circulation*. 2008;117:1474–7.
18. Boyett MR, Honjo H, Kodama I. The sinoatrial node, a heterogeneous pacemaker structure. *Cardiovasc Res*. 2000;47:658–87.
19. Boyett MR. ‘And the beat goes on.’ The cardiac conduction system: the wiring system of the heart. *Exp Physiol*. 2009;94:1035–49.
20. Dobrzynski H, Nikolski VP, Sambelashvili AT, Greener ID, Yamamoto M, Boyett MR, et al. Site of origin and molecular substrate of atrioventricular junctional rhythm in the rabbit heart. *Circ Res*. 2003;93:1102–10.
21. Billette J. Atrioventricular nodal activation during periodic premature stimulation of the atrium. *Am J Physiol*. 1987;252:H163–77.
22. de Carvalho A, de Almeida D. Spread of activity through the atrioventricular node. *Circ Res*. 1960;8:801–9.
23. Inada S, Hancox JC, Zhang H, Boyett MR. One-dimensional mathematical model of the atrioventricular node including atrio-nodal, nodal, and nodal-his cells. *Biophys J*. 2009;97:2117–27.
24. Mendez C, Moe GK. Demonstration of a dual A-V nodal conduction system in the isolated rabbit heart. *Circ Res*. 1966;19:378–93.

25. Mazgalev TN, Tchou PJ. The AV nodal dual pathway electrophysiology: still a controversial concept, chapter 14. In: Mazgalev TN, Tchou PJ, editors. *Atrial-AV nodal electrophysiology: a view from the millennium*. 1st ed. Armonk, NY: Futura; 2000. p. 217–36.
26. Denes P, Wu D, Dhingra R, Amat-y-Leon F, Wyndham C, Rosen KM. Dual atrioventricular nodal pathways: a common electrophysiological response. *Br Heart J*. 1975;37:1069–76.
27. Schuilenburg RM, Durrer D. Atrial echo beats in the human heart elicited by induced atrial premature beats. *Circulation*. 1968;37:680–93.
28. Calkins H. Supraventricular tachycardia: AV-nodal reentry and Wolff-Parkinson-White syndrome, chapter 38. In: Fuster V, Hurst JW, O'Rourke RA, Walsh RA, Poole-Wilson P, editors. *Hurst's the heart*. 12th ed. New York: McGraw Hill; 2008. p. 984–5.
29. Kay GN, Epstein AE, Dailey SM, Plumb VJ. Role of radiofrequency ablation in the management of supraventricular arrhythmias: experience in 760 consecutive patients. *J Cardiovasc Electrophysiol*. 1993;4:371–89.
30. Ross DL, Johnson DC, Dennis AR, Cooper MJ, Richards DA, Uther JB. Curative surgery for atrioventricular junctional ‘a-v nodal’ nodal tachycardia. *J Am Coll Cardiol*. 1983;6: 1383–92.
31. Inoue S, Becker AE, Riccardi R, Gaita F. Interruption of the inferior extension of the compact atrioventricular node underlies successful radiofrequency ablation of atrioventricular nodal reentrant tachycardia. *J Interv Card Electrophysiol*. 1999;3:273–7.
32. Kumar P, Clark M. *Cardiovascular disease*. 6th ed. London: Elsevier-Saunders; 2005. p. 767–78. Chapter 13.
33. Nikolski VP, Jones SA, Lancaster MK, Boyett MR, Efimov IR. Cx43 and dual-pathway electrophysiology of the atrioventricular node and atrioventricular nodal reentry. *Circ Res*. 2003;92:469–75.
34. Hancox JC, Yuill KH, Mitcheson JS, Convery MK. Progress and gaps in understanding the electrophysiological properties of morphologically normal cells from the cardiac atrioventricular node. *Int J Bifurcat Chaos*. 2003;13:3675–91.
35. DiFrancesco D. Pacemaker mechanisms in cardiac tissue. *Annu Rev Physiol*. 1993;55: 455–72.
36. Mangoni ME, Couette B, Bourinet E, Platzer J, Reimer D, Striessnig J, et al. Functional role of L-type Cav1.3 Ca²⁺ channels in cardiac pacemaker activity. *Proc Natl Acad Sci USA*. 2003; 100:5543–8.
37. Mangoni ME, Nargeot J. Genesis and regulation of the heart automaticity. *Physiol Rev*. 2008; 88:919–82.
38. Matthes J, Yildirim L, Wietzorek G, Reimer D, Striessnig J, Herzig S. Disturbed atrioventricular conduction and normal contractile function in isolated hearts from Cav1.3-knockout mice. *Naunyn Schmiedebergs Arch Pharmacol*. 2004;369:554–62.
39. Hagiwara N, Irisawa H, Kameyama M. Contribution of two types of calcium currents to the pacemaker potentials of rabbit sino-atrial node cells. *J Physiol*. 1988;395:233–53.
40. Bogdanov KY, Vinogradova TM, Lakatta EG. Sinoatrial nodal cell ryanodine receptor and Na⁺-Ca²⁺ exchanger: molecular partners in pacemaker regulation. *Circ Res*. 2001;88: 1254–8.
41. Ridley JM, Cheng H, Harrison OJ, et al. Spontaneous frequency of rabbit atrioventricular node myocytes depends on SR function. *Cell Calcium*. 2008;44:580–91.
42. Irisawa H, Brown HF, Giles W. Cardiac pacemaking in the sinoatrial node. *Physiol Rev*. 1993;73:197–227.
43. Dunlap ME, Bibevski S, Rosenberry TL, Ernsberger P. Mechanisms of altered vagal control in heart failure: influence of muscarinic receptors and acetylcholinesterase activity. *Am J Physiol*. 2003;285:H1631–40.
44. Borlak J, Thum T. Hallmarks of ion channel gene expression in end-stage heart failure. *FASEB J*. 2003;17:1592–608.
45. Ansari A, Ho SY, Anderson RH. Distribution of the Purkinje fibres in the sheep heart. *Anat Rec*. 1999;254:92–7.

46. Anumonwo JM, Tallini YN, Vetter FJ, Jalife J. Action potential characteristics and arrhythmic properties of the cardiac conduction system of the murine heart. *Circ Res*. 2001;89:329–35.
47. Boyett MR, Fedida D. Changes in the electrical activity of dog cardiac Purkinje fibers at high heart rates. *J Physiol*. 1984;350:361–91.
48. Verkerk AO, Schumacher CA, van Ginneken AC, Veldkamp MW, Ravesloot JH. Role of Ca^{2+} - activated Cl^- current in ventricular action potentials of sheep during adrenoceptor stimulation. *Exp Physiol*. 2001;86:151–9.
49. Boyett MR. Effect of rate-dependent changes in the transient outward current on the action potential in sheep Purkinje fibers. *J Physiol*. 1981;319:23–41.
50. Miquerol L, Meysen S, Mangoni M, Bois P, van Rijen HV, Abran P, et al. Architectural and functional asymmetry of the His-Purkinje system of the murine heart. *Cardiovasc Res*. 2004; 63:77–86.
51. Schram G, Pourrier M, Melnyk P, Nattel S. Differential distribution of cardiac ion channel expression as a basis for regional specialization in electrical function. *Circ Res*. 2002;90: 939–50.
52. Callewaert G, Carmeliet E, Vereecke J. Single cardiac Purkinje cells: general electrophysiology and voltage-clamp analysis of the pace-maker current. *J Physiol*. 1984;349:643–61.
53. Friedman PL, Stewart JR, Fenoglio Jr JJ, Wit AL. Survival of subendocardial Purkinje fibers after extensive myocardial infarction in dogs. *Circ Res*. 1973;33:597–611.
54. Dosdall DJ, Tabereaux PB, Kim JJ, Walcott GP, Rogers JM, Killingsworth CR, et al. Chemical ablation of the Purkinje system causes early termination and activation rate slowing of long-duration ventricular fibrillation in dogs. *Am J Physiol*. 2008;295:H883–9.
55. Cordeiro JM, Bridge JH, Spitzer KW. Early and delayed afterdepolarizations in rabbit heart Purkinje cells viewed by confocal microscopy. *Cell Calcium*. 2001;29:289–97.
56. Dumaine R, Cordeiro JM. Comparison of K^+ currents in cardiac Purkinje cells isolated from rabbit and dog. *J Mol Cell Cardiol*. 2007;42:378–89.
57. Gaborit N, Le Bouter S, Szuts V, Varro A, Escande D, Nattel S, et al. Regional and tissue specific transcript signatures of ion channel genes in the non-diseased human heart. *J Physiol*. 2007;582:675–93.
58. Dun W, Boyden PA. The Purkinje cell; 2008 style. *J Mol Cell Cardiol*. 2008;45:617–24.
59. Chandler NJ, Greener ID, Tellez JO, Inada S, Musa H, Molenaar P, et al. Molecular architecture of the human sinus node: insights into the function of the cardiac pacemaker. *Circulation*. 2009; 119:1562–75.
60. Bristow MR, Saxson LA, Boehmer J, Krueger S, Kass D, De Marco T, et al. Cardiac-resynchronization therapy with or without an implantable defibrillator in advance chronic heart failure. *N Engl J Med*. 2004;350:2140–50.
61. Maguy A, Le Bouter S, Comtois P, Chartier D, Villeneuve L, Wakili K, et al. Ion channel subunit expression changes in cardiac Purkinje fibers. A potential role in conduction abnormalities associated with congestive heart failure. *Circ Res*. 2009;104:1113–22.
62. Courtemanche M, Ramirez RJ, Nattel S. Ionic mechanisms underlying human atrial action potential properties: insights from a mathematical model. *Am J Physiol*. 1998;275:H301–21.

Chapter 12

Molecular Basis and Genetic Aspects of the Development of the Cardiac Chambers and Conduction System: Relevance to Heart Rhythm

Martijn L. Bakker, Vincent M. Christoffels, and Antoon F.M. Moorman

12.1 Introduction

At the end of the nineteenth century, a famous English anatomist and physiologist, Walter Gaskell, studied the delay in the contraction wave in the atrioventricular (AV) canal of tortoises. He concluded that this delay was caused by “undifferentiated embryonic muscular tissue that was characterized by higher automaticity, but lower conductivity” [1]. More than a hundred years later, evidence from the fields of molecular and developmental biology has accumulated to support this view.

The heart tube consists of primitive embryonic myocardium that displays a high degree of automaticity (pacemaker activity) and low conductivity. Because of these characteristics, the heart beat in the embryonic heart tube is initiated spontaneously and the peristaltic wave of contraction is propagated slowly. With Doppler examination embryonic cardiac function can be observed from 3 weeks of human development onwards; it is the first organ to function. Initiation of the heart beat always occurs at the inflow of the heart tube. AV canal (AVC) myocardium is derived from primitive embryonic myocardium that, in contrast to the myocardium of the chambers, is inhibited in its further differentiation to working myocardium. It is the persistence of some important embryonic features in the AVC myocardium that causes the delay in impulse propagation in the “undifferentiated tissue” described by Gaskell. This chapter will focus on the molecular and developmental processes underlying development of the components of the cardiac conduction system. We will discuss in detail the origin of pacemaker and conduction system cells and the mechanism of heart beat generation in different stages of development. We will further explain how the above can help to understand the occurrence and source of arrhythmias and conduction disturbances.

M.L. Bakker, V.M. Christoffels, and A.F.M. Moorman (✉)
Heart Failure Research Center, Academic Medical Center, Meibergdreef 15, 1105 AZ Amsterdam,
The Netherlands
e-mail: a.f.moorman@amc.uva.nl

12.2 The Cardiac Pacemaker and Conduction System

In the adult heart, the pacemaker and conduction system is responsible for the initiation and propagation of the action potential to orchestrate simultaneous contractions of the atria, and after a short pause, the ventricles. The electrical impulse is initiated in the sinus node (SAN), spreads rapidly over the atria, is then directed through the AV node (AVN) to the specialized components of the ventricular conduction system (AV bundle (AVB), the bundle branches and the Purkinje fibers) that propagate the impulse rapidly to the working myocardium of the ventricles. During transit through the AVN, which is the only myocardial connection between the atria and the ventricles, the electrical impulse is decelerated to ensure sufficient time for the ventricles to fill during contraction of the atria. Some key characteristics of the cardiomyocytes within the subcomponents of the pacemaking and conduction system will be discussed first.

12.2.1 The Sinus Node

The sinus node is the primary pacemaker of the heart. It consists of a small group of myocytes that initiates and controls the heart beat. The most important feature of these pacemaker cells is automaticity, which is the result of interplay of multiple ion channels. Automaticity is caused by spontaneous depolarization of the resting membrane potential. When the membrane potential reaches a critical value, the “threshold,” the action potential is initiated. There is ongoing debate which mechanism is responsible for spontaneous diastolic depolarization, the funny current, the calcium clock, or both [2]. Hyperpolarization activated cyclic nucleotide gated (HCN) cation channels, responsible for the funny current I_f , have been regarded as the most important ion channels responsible for spontaneous depolarization. In the heart, expression of *HCN1*, *HCN2*, and *HCN4* has been reported, of which *HCN4* is highly enriched in the SAN [3–5]. Mouse embryos that do not express *Hcn4*, die early in development: between embryonic day (E) 9.5 and E11.5. Heart rates that were measured before embryos started to die were significantly reduced from 139 beats per minute in wild type embryos to 88 in *Hcn4*-null embryos [6]. Furthermore, blocking I_f resulted in a 30% reduction of the heart rate, but not in complete loss of automaticity, indicating that more mechanisms are involved in automaticity of pacemaker cells [7].

There is accumulating evidence that intracellular Ca^{2+} handling contributes significantly to automaticity, as reviewed elsewhere [8]. Because Ca^{2+} handling is a highly complex and vital process for each developing and mature cardiomyocyte, it is difficult to provide proof of necessity or requirement of proper Ca^{2+} handling, the Ca^{2+} clock, or Ca^{2+} releases for pacemaking.

A key feature of working myocardial cells is a high resting membrane potential, which is stabilized around -80 mV (versus -60 mV in pacemaker cardiomyocytes)

by the inwardly rectifying potassium current I_{K1} . In pacemaker cells, I_{K1} is virtually absent [9]. Indeed, if I_{K1} is blocked or absent in working myocardial cells, these cells become spontaneously active, suggesting that the absence of I_{K1} is a prerequisite for diastolic depolarization [10].

Initiation of the heart beat does not depend only on the highest intrinsic pacemaking rate. The ability of a small number of pacemaker cells to drive the surrounding myocardium depends on relative uncoupling of the pacemaker cells [11]. Electrical coupling of myocytes is mediated by gap junction (GJ) channels [12]. The conductive properties of the GJ channels are determined by subunits of the channels called connexins. Five major connexin subtypes have been identified in the myocardium, including Cx30, Cx30.2, Cx40, Cx43, and Cx45 [13–16]. Cx40 and Cx43 form high conductance (low resistance) GJ channels, resulting in fast intercellular conduction [17]. These two connexins are expressed in working cardiomyocytes and specifically absent from the sinus node [16, 18]. Instead, Cx30.2 and Cx45 are present in the SAN where they form low conductance (high resistance) GJ channels, causing relative uncoupling of pacemaker cells, which enables cells to depolarize spontaneously and initiate an action potential [14, 19].

12.2.2 *The Atrioventricular Node*

The AV node is a heterogeneous structure, which has a complex structure and physiology. It contains a fast and a slow conducting pathway [20] and paranodal areas consisting of transitional cells [16, 21]. It is, therefore, not surprising that the AVN can adopt different properties according to various (pathological) conditions. In essence, however, its main function is to delay propagation of the electrical impulse between atria and ventricles. Similar to SAN cells, this property could be established by the absence of connexins that form high conductance GJ channels (Cx40, Cx43) and the presence of connexins that form low conductance GJ channels (Cx30.2, Cx45). Cx40, however, is expressed at low levels in the AVN of several species [22, 23]. The debate has not been settled whether the observed Cx40 protein is truly within the AVN or in the surrounding tissues, as there is no generally accepted marker for AVN.

In pathological conditions, the AVN protects the ventricles from fast atrial arrhythmias, due to its prolonged refractory period. Furthermore, the AVN can act as the secondary pacemaker in case of SAN dysfunction. The mechanism of pacemaking in AVN cells is based on the same mechanisms as in SAN cells. The speed of spontaneous phase 4 depolarization in AVN cells, however, is lower. Therefore, the AVN will initiate the heart beat only when no faster (SAN) rhythm is present.

Cells within the AV junction, surrounding both the AV valves, have been shown to exhibit the same properties as AVN cells [24, 25]. This configuration resembles the embryonic heart in which the entire AVC functions as the embryonic AVN to delay impulse propagation in the embryonic heart.

12.2.3 The Ventricular Conduction System

The main function of the ventricular conduction system is to propagate the electrical impulse rapidly from AVN to the apex of the heart into the Purkinje fiber network. This rapid propagation depends on high conductance GJ channels that consist mainly of Cx40 [22, 26, 27]. Similar to the SAN and AV node, the AVB and ventricular conduction system display automaticity and can initiate the heart beat, although the frequency is low.

12.2.4 General Characteristics of Pacemaker Cells and Conduction System Cells

de Haan and Viragh and Challice were the first to describe in great detail the morphological development of the murine cardiac conduction system [28–30]. They observed that conduction system cells within the SAN, AVN, AVB, and bundle branches shared characteristic features. They are smaller and glycogen rich, they contain fewer T-tubules and mitochondria, and their sarcomeric apparatus and sarcoplasmic reticulum are less-well developed, resulting in poor contractility and a “pale” appearance. These morphological characteristics are also found in embryonic cardiomyocytes of the early heart tube. Interestingly, the embryonic cardiomyocytes of the early heart tube share more characteristics with the nodal myocardium (Table 12.1). They display automaticity and they are poorly coupled. This led to the hypothesis that pacemaker myocardium has an embryonic or primitive myocardium-like phenotype.

To understand the relation between embryonic myocardium and the cardiac conduction system components, we must first consider some general concepts of cardiac development.

Table 12.1 Comparison of key characteristics of embryonic (primary) myocardium with pacemaker myocardium and working myocardium

	Embryonic	Pacemaker	Working
Automaticity	Low	Low	High
Conduction velocity	Low	Low ^a	High
Contractility	Low	Low	High
SR activity	Low	Low	High
Cell size	Small	Small	Big
Mitochondria	Little	Little	Many
Proliferation (fetal)	Slow	Slow	Fast

^aHigh in ventricular conduction system

12.3 Development of the Heart

In early embryonic development, cardiogenic precursor cells form a myocardial layer around the endocardial heart tube. A rapidly proliferating pool of progenitor cells contributes cardiac cells to both poles of the heart tube. These newly added cells will form the atria, the right ventricle, and the outflow tract [31–33]. This implies that the early heart tube only contains the progenitors of the AVC and the left ventricle [34]. The cardiomyocytes within the embryonic heart tube are small, proliferate slowly, and are poorly coupled, which results in slow propagation of the electrical impulse [35, 36]. Although all cardiomyocytes can depolarize spontaneously, the leading pacemaker site is always at the inflow, resulting in a regular contraction wave from the inflow to the outflow.

Due to addition of cells, the heart tube becomes longer and while elongating, it loops (Fig. 12.1). During the process of looping, two regions within the heart tube start to proliferate rapidly and initiate expression of a set of working myocardial genes. These two regions are located at the outer curvatures and will become the ventricles and the atria (Fig. 12.1) [35, 37]. The regions in-between these highly proliferative, expanding cardiac chambers retain their “primary heart tube” characteristics.

Intriguingly, the simple configuration of alternating fast-conducting chamber-type and slow-conducting primary myocardium establishes cardiac function that resembles the function of a mature heart. The electrical impulse is initiated in the leading pacemaker site in the sinus venosus, propagated rapidly through the differentiated myocardial cells of the atria, after which the atria contract synchronously to pump blood through the AVC into the embryonic ventricle. Due to slow conduction in the AVC, the electrical impulse is delayed to allow complete filling of the ventricle. During subsequent activation and contraction of the ventricle, the AVC myocardium remains contracted as a result of slow relaxation, thus functioning as a sphincter valve. After ventricular and subsequent outflow tract contraction the outflow tract also functions as a sphincter valve through slow relaxation. Although the components of the mature conduction system cannot be recognized morphologically yet, an electrocardiogram (ECG) of the embryonic heart contains all components of a mature ECG [38, 39]. The ECG exhibits a P-wave, PQ-interval, and a narrow QRS-complex (Fig. 12.2).

In the adult heart, the PQ-interval represents the transfer time of the electrical impulse through the atria, AVN, and ventricular conduction system. Because there is no recognizable AVN and no fibrous insulation in the embryonic heart the electrical impulse can be propagated to the ventricle through the entire AVC [28–30]. The observation that the PQ-interval is normal indicates that the entire AVC functions as an AVN, delaying the electrical impulse without fibrous insulation.

The building plan of the heart with its alternating slow- and fast-conducting compartments is the same in vertebrates. This simple building plan is sufficient for

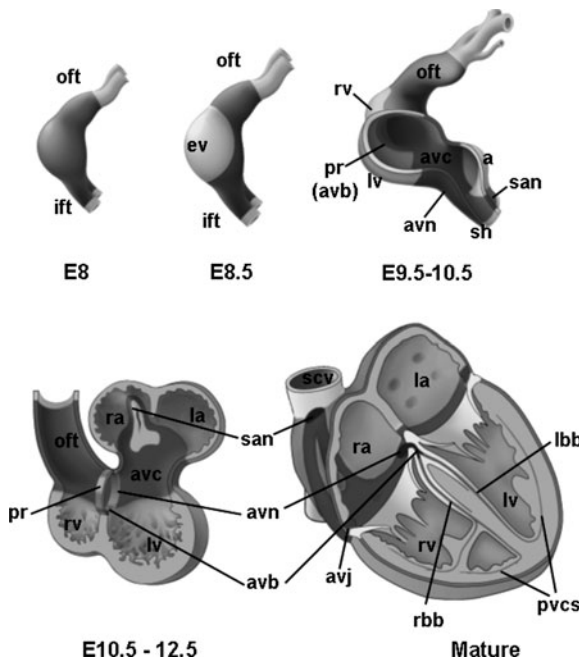


Fig. 12.1 Schematic overview of heart development in higher vertebrates. The early heart tube has a primitive phenotype (dark gray). Chamber myocardium (light gray) expands from the outer curvatures of the primary heart tube, whereas non-chamber myocardium (dark gray) of the inflow tract, sinus horns, AVC, outflow tract, and inner curvatures does not expand. Sinus horn myocardium gives rise to the sinus node; AVC myocardium to the AV node and AV junction. The part of the primary ring within the crest of the interventricular septum will form the AVB. First three panels show left-lateral views. AV atrioventricular, *avb* AV bundle, *avc* AV canal, *avj* AV junction, *avn* AV node, *ev* embryonic ventricle, *ift* inflow tract, *ivs* interventricular septum, *oft* outflow tract, *pr* primary ring, *pvc* peripheral ventricular conduction system, (*r/l*) *a* (right/left) atrium, (*r/l*) *v* right/left ventricle, (*r/l*) *bb* (right/left) bundle branch, *san* sinus node, *scv* superior caval vein, *sh* sinus horns

lower vertebrates, as the mono-atrium, AVC, mono-ventricle configuration of the fish heart demonstrates [40]. In cardiac development of higher vertebrates, additional developmental processes are required to separate the pulmonary and systemic circulatory systems and to form the morphological components of the conduction system. There is considerable species variation in the extent to which the conduction system components develop within higher vertebrates. In birds and hoofed animals the conduction system is very well-developed [41]; in rodents these structures are less well-developed, with human somewhere in between [37].

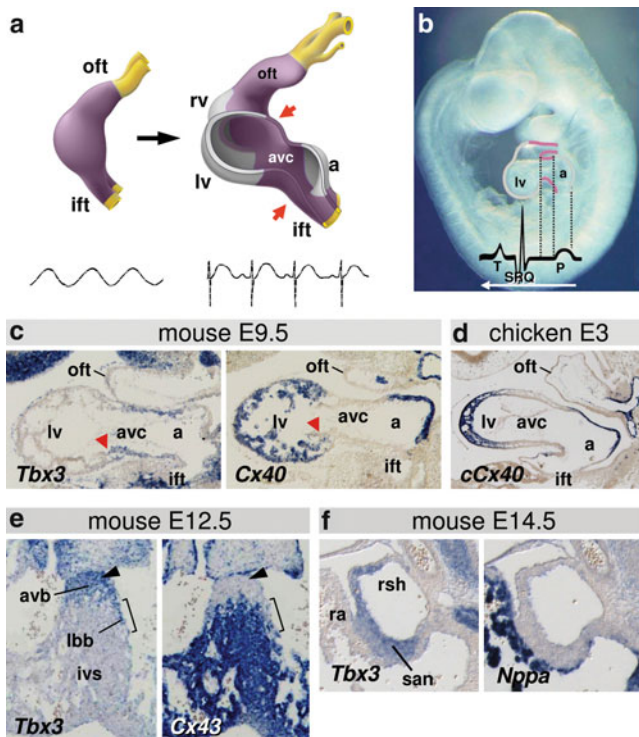


Fig. 12.2 (a, b) Development of chambers and ECG. (a) Left-sided view of embryonic hearts of embryonic day (E) 8–8.5 and E9.5–10.5, respectively. Formation of the chambers is in accordance with the development of an adult-like ECG. Red arrows demarcate the ventricular and atrial inner curvatures. (b) Schematic overview showing the different ECG segments correlating with the different components of the embryonic heart. The white arrow depicts the flow through and the sequential mode of activation. Note the PQ interval that represents the slow conducting AVC. (c–f) Strictly complementary expression of *Tbx3* and *Tbx3* target genes. *In situ* hybridization serial sections. Genes and developmental time points have been indicated in the panels. (c) *Cx40* is expressed in the developing chambers, whereas *Tbx3* demarcates the AVC (black arrow). (d) Expression of *Cx40* is conserved in the developing (E3) chicken heart. (e) *Cx43* is expressed in the working myocardium of the interventricular septum, whereas *Tbx3* is expressed in the crest of the septum, demarcating the developing AVB and bundle branches. (f) *Nppa* is expressed in the working myocardium of the right atrium, strictly complementary to the expression of *Tbx3* within the sinus node. For abbreviations see legends to Fig. 12.1

12.4 Cellular Origin of Conduction System Cardiomyocytes

The origin of the cardiac pacemaker and conduction system has been subject to debate. As the cardiac conduction system is the “electrical wiring” of the heart, it is hypothesized to be derived from the cardiac neural crest. Ablation of cardiac neural crest cells resulted in outflow tract malformation and defects in the AVB and the

Purkinje network [42, 43] indicating that the cardiac neural crest is important for development of the conduction system.

Convincing evidence that cardiomyocytes within all components of the conduction system are myocardial in origin was provided by the labs of Gourdie and Mikawa. Single myocardial cells were labeled through retroviral infection early in development. At mid fetal stages, clusters of daughter cells were demonstrated in the conduction system and in the adjacent working myocardium [44, 45] indicating that conduction system and working cardiomyocytes are derived from one common progenitor, present in the embryonic heart tube.

12.5 Transcriptional Regulation of Pacemaker and Conduction System Development

Recent progress in the fields of molecular and developmental biology has substantially increased the knowledge of the processes underlying the formation of the conduction system. A network of broadly expressed transcription factors has been identified that regulates formation of the subcomponents of the conduction system. Transgenic animal models have elucidated the role of key transcription factors in cardiac development, but many questions remain to be answered.

12.5.1 Development of the Sinus Node

In the embryonic heart, all cardiomyocytes possess pacemaker activity. Although cardiomyocytes are continuously added to the heart tube, the leading pacemaker site remains localized at the venous pole of the heart tube [39, 46]. This implies that cardiomyocytes that have most recently differentiated from cardiac precursors display the highest intrinsic beating rate. The mechanism of this “shift” may involve the expression pattern of pacemaker channel *Hcn4*, which is expressed at the caudal end of the *Nkx2-5⁺* heart tube. *Hcn4* is down-regulated in the *Nkx2-5* domain as soon as a new pool of *Tbx18⁺/Nkx2-5⁻/Hcn4⁺* cardiac precursor cells is added to the heart tube [47]. Thereby, *Hcn4* becomes restricted to these newly added cells that will form the sinus venosus. In vitro experiments revealed that cultured *Tbx18⁺* precursor cells differentiated into *Hcn4⁺* and *Nkx2-5⁻* cardiomyocytes with a higher intrinsic beating rate than age matched ventricular cardiomyocytes, indicating that the entire sinus venosus is derived from a separate progenitor pool with pacemaker potential [48, 49].

Genetic lineage analysis has revealed a strict border between the *Tbx18⁺* sinus venosus and the adjacent *Nkx2-5⁺* atrial working myocardium, suggesting key roles of these genes in the determination of the border between the sinus venosus and atrial myocardium. *Nkx2-5* is required to activate *Cx40*, *Nppa*, and other genes associated with atrial working myocardium. Analysis of *Nkx2-5* deficient hearts

revealed reduced expression levels of these genes in atrial working myocardium. Furthermore, these *Nkx2-5* deficient hearts ectopically expressed *Hcn4* in the atrium, indicating that *Nkx2-5* is a repressor of *Hcn4* [47, 50].

In a subdomain of the sinus venosus, transcriptional repressor *Tbx3* defines the area of the SAN primordium (Figs. 12.2f and 12.3a) [47, 51]. Initially, the entire

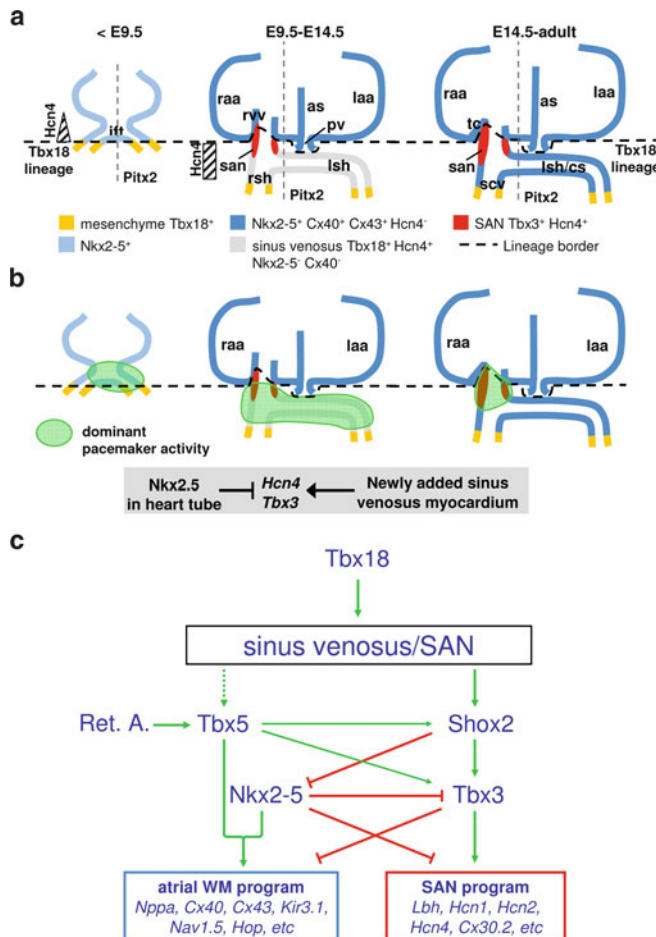


Fig. 12.3 Development of the sinus venosus and sinus node. (a) Schematic representation of the patterns of expression and lineages until E9.5 (left), between E9.5 and E14.5 (middle) and after E14.5 (right). Thin dotted line represents the border of the *Pitx2c* expression domain; heavy dotted line, the border of the *Tbx18*⁺ lineage. Except for the yellow-colored mesenchyme, only myocardium is depicted (see legend beneath illustrations). (b) Same as in (a), with the shown (left and right) and probable (middle) region where dominant pacemaker activity resides. Note the developmental shifts of activity. (c) Scheme depicting the roles and interactions of factors involved in sinus venosus and SAN formation. For abbreviations see legends to Fig. 12.1. In addition, *as* atrial septum, *cs* coronary sinus, *laa* left atrial appendage, *pv* pulmonary vein, *raa* right atrial appendage, *tc* terminal crest, *vv* venous valves

Tbx18⁺/Nkx2-5⁻ sinus venosus expresses *Hcn4*. During further maturation of sinus venosus, *Hcn4* becomes restricted to the SAN domain (Fig. 12.3b). Besides repression of *Hcn4* in the *Tbx3*-negative part of the sinus venosus, working myocardial genes are induced [49]. Additionally, low levels of *Nkx2-5* are detectable in the sinus venosus from E14.5 onwards [52].

As shown by knock-out and over-expression experiments, *Tbx3* is the molecular executor of the pacemaker gene program in the SAN region. In the absence of *Tbx3*, the expression domain of atrial working myocardial genes expanded into the SAN-domain and the expression of SAN-specific gene *Lbh* was reduced, indicating that *Tbx3* is necessary for the preservation of the pacemaker gene program [18]. The fact that a SAN primordium is formed, which expresses *Hcn4*, shows that *Tbx3* is not necessary for the early formation of the SAN. If *Tbx3* is conditionally over-expressed in developing atrial myocardium, working myocardial genes are repressed and SAN genes are induced. Moreover, functional pacemaker sites are formed in atrial myocardium, confirming that *Tbx3* is a key regulator in SAN development [18].

Recently, it has been shown that another homeobox transcription factor, *Shox2*, acts upstream of *Nkx2-5*, is expressed in the sinus venosus myocardium and is required for repression of *Nkx2-5* expression. In the absence of *Shox2* protein, the sinus venosus and SAN are hypoplastic and ectopically express *Nkx2-5*. Furthermore, *Cx43* and *Cx40* are up-regulated and *Tbx3* and *Hcn4* are down-regulated, revealing a critical role for *Shox2* in sinus venosus and SAN formation through regulation of *Nkx2-5* [53, 54].

Transcription factor *Pitx2c* is necessary to block SAN formation in the left side of the sinus venosus. Loss of *Pitx2c* results in two sinus nodes and complete right atrial isomerism, indicating that *Pitx2c* is crucial for left/right identity of the sinus venosus [52, 55].

12.5.2 Development of the Atrioventricular Node

Substantial evidence has been provided that the embryonic AVN contains most of the precursor cells of the AVN [31, 34, 56–58]. In addition, the adult AVN has been marked by several transgenes (cGata6-lacZ, CCS-lacZ, cTNI-promoter-lacZ, and BAC-Tbx3GFP), that mark the AVN myocardium in embryonic stages, indicating that the AVN is composed of cells that originate from the AVC [31, 59–62].

During early development, *Bmp2* is expressed specifically in the embryonic AVC. *Bmp2* is required to activate expression of *Tbx2* in the AVC, directly through Smad signaling [63, 64]. Cardiac specific *Bmp2* knock-out embryos die at E10.5 and fail to specify AVC myocardium [64]. Embryos were viable when the cGATA6-Cre cardiac-specific enhancer was used to abolish the expression of Bmp receptor *Bmpr1a*, which enabled investigation of the development of the AVC and AVN. These mice displayed mild to severe AV nodal defects, indicating that Bmp signaling is required for AVN formation [64–66].

Tbx20 is required to restrict *Tbx2* to the AVC by repression of *Tbx2* within the working myocardium. *Tbx20*-deficient embryos show ectopic expression of *Tbx2* in the entire heart tube [67–69]. Notch-Hey signaling further regulates the *Bmp2-Tbx2* pathway. In mouse, ventricular *Hey2* represses *Bmp2* and *Tbx2*, whereas atrial *Hey1* represses *Tbx2*, thereby confining the expression of *Tbx2* to the AVC [70, 71].

Nkx2-5 is involved in conduction system development and is one of the earliest transcription factors expressed in the myocardial lineage. Absence of *Nkx2-5* during development results in embryonic lethality with arrest of cardiac development at the looping heart tube stage [72, 73]. The AVN in *Nkx2-5* haplo-insufficient mouse hearts is hypoplastic [74]. Transgenic mice that lacked the expression of *Nkx2-5* specifically in the AVC and ventricles, using *Mlc2v-Cre* to delete a floxed *Nkx2-5* allele, suffered from several degrees of AV-block including complete AV-block [75].

Also reported in relation to conduction system development is transcription factor *Tbx5*. In human, mutations in *TBX5* cause Holt–Oram syndrome, which is an autosomal dominant disorder characterized by both structural cardiac disorders and rhythm disorders including sinus bradycardia, AV block, and atrial fibrillation (AF) [76]. Mice heterozygous for *Tbx5* mimicked the human phenotype. Electrophysiological analysis demonstrated first and second degree AV block and sinusatrial pauses [77]. In the heart tube, *Tbx5* is expressed in a gradient, with high expression at the inflow, tapering off towards the outflow tract. Later in development expression of *Tbx5* is restricted to the atria, AVC, and left ventricle [78, 79].

In case of proper specification of the AVC (Fig. 12.4), *Tbx2* and its family member *Tbx3*, are specifically expressed in the AVC (Fig. 12.2c). Like *Tbx3*, *Tbx2* is a direct repressor of working myocardial genes [80]. Due to presumed functional redundancy, AVN development appeared to be normal in *Tbx3* and *Tbx2* mutant embryos ([81] and our unpublished observations). Detailed examination of the

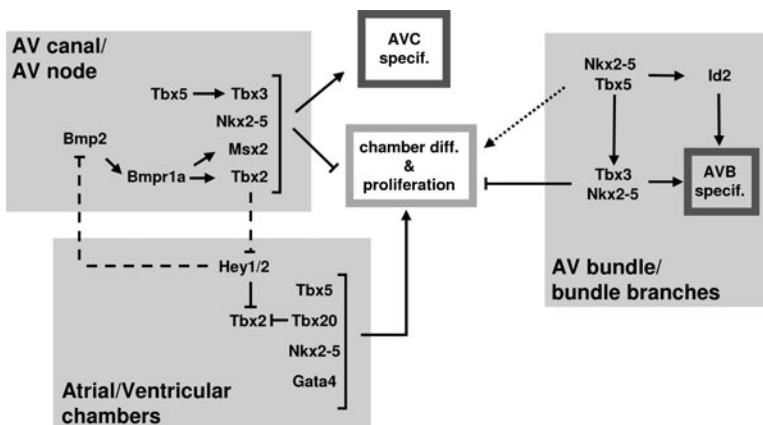


Fig. 12.4 Transcriptional regulation and genetic interactions within the developing AVC, AVB, and adjacent myocardium. Depicted factors control the specification, formation, and boundaries of these cardiac components

AVC of *Tbx2* null embryos, revealed that working myocardial genes were ectopically expressed in the absence of *Tbx2* at the left side of the AVC [34]. At the left side of the AVC there is only little expression of *Tbx3*, indicating that *Tbx2* is required for the repression of working myocardial genes and suggesting redundant effects of *Tbx2* and *Tbx3* in the remainder of the AVC, including the future AVN.

Throughout development, several genes demarcate the border between the AVC myocardium and the adjacent working myocardium. Nevertheless, there is no strict lineage segregation. Lineage analysis was performed by crossing transgenic mice that express *Cre* under control of the *Tbx2* locus with a reporter line, thereby identifying the fate of cells that once expressed *Tbx2*. This analysis revealed that a large proportion of the left ventricle once expressed *Tbx2* [34], indicating that a significant number of embryonic AVC cardiomyocytes can and will differentiate into working myocardial cells. This suggests a continuous process of *Tbx2*-expressing primitive AVC cardiomyocytes differentiating into working cardiomyocytes upon loss of *Tbx2/Tbx3* expression.

12.5.3 Development of the Atrioventricular Bundle (Bundle of His)

The AVB is the most rapidly conducting component of the cardiac conduction system. Essential for this fast conduction is *Cx40*, which is abundantly expressed in the AVB, bundle branches, and peripheral conduction system [82]. *Cx40* serves as an excellent marker to distinguish the fast conducting components of the ventricular conduction system from the AVN and the ventricular working myocardium [26]. The AVB is further characterized by absence of *Cx43* expression, which serves as a useful negative marker.

In the embryonic heart, the developing AVB does not express *Cx40* and the ventricular conduction system is not required for propagation of the cardiac impulse from the AVC to the ventricle. Instead, the cardiac impulse is propagated directly from the dorsal AVC into the primitive ventricle along the dorsal wall [83, 84], connecting the AVC with the *Cx40*-positive trabecules of the trabecular myocardium. These trabecules are probably responsible for rapid and coordinated propagation of the cardiac impulse in the absence of a functional His-Purkinje system in the ventricle.

Nkx2-5 and *Tbx5*, together with *Id2*, are necessary for proper AVB specification. *Nkx2-5* and *Tbx5* are transcriptional activators of working myocardial genes [77, 85]. Nevertheless, mice haplo-insufficient for both *Tbx5* and *Nkx2-5* fail to establish the AVB, as monitored by loss of *minK-lacZ* expression, and develop functional conduction block in postnatal animals. Inhibitor of differentiation *Id2*, which is expressed in the developing AVB, is not activated in *Tbx5-Nkx2-5* double heterozygous mice. This loss of expression may be responsible for the observed failure to repress ventricular differentiation of the AVB [86]. In *Nkx2-5* haplo-insufficient adult mice the AVB is hypoplastic [74].

The primordium of the AVB and bundle branches in the crest of the interventricular septum is first detected by the expression of *Tbx3*. Through (Tbx3^+) primary myocardium the developing AVB is in contact with the AVC in the dorsal wall of the heart tube [51, 57, 58, 81, 87]. Lineage analysis of *Tbx2*-expressing cells revealed that the AVC does not contribute any cells to the AVB [34], indicating that the AV-bundle is a distinct component of the conduction system, derived from separate progenitor cells.

Similar to the development of the SAN and AVN, *Tbx3* represses the differentiation into working myocardium within the developing AVB (Fig. 12.2e). In *Tbx3* knock-out embryos, which die between E12.5 and E15.5, the AVB identity is lost. Working myocardial genes are ectopically expressed and myocytes do not exit the cell cycle as they normally do [81], indicating that *Tbx3* imposes the conduction system phenotype on cells within the AVB domain.

Seemingly inconsistent with the notion that the AVB displays a nodal-like phenotype, *Cx40* expression increases dramatically in late fetal stages of development, although its repressor, *Tbx3*, is still present. In *Tbx3* knock-out embryos, *Cx40* is up-regulated in the AVB earlier in development. The homeodomain-only protein Hop, which is highly expressed in the conduction system, is also involved in the regulation of *Cx40* expression [88]. Hop knock-out mice display infra-nodal conduction slowing with down-regulation of *Cx40*, without gross anatomical alterations. Together, these findings suggest a mechanism that induces expression of *Cx40* in the presence of *Tbx3* in late fetal stages, when the mammalian embryo depends on a fast conducting ventricular conduction system. This mechanism could involve a shift in the balance of *Tbx5*, *Nkx2-5*, Hop, Id2, and *Tbx3* (Fig. 12.4).

12.5.4 Development of the Peripheral Ventricular Conduction System

The peripheral ventricular conduction system (PVCS), also referred to as the Purkinje-network, consists of a network of thin myocardial fibers located directly beneath the endocardium. The PVCS cells express *Cx40*, but otherwise resemble embryonic myocardium [22]. The embryonic hearts of mammalian embryos conduct the electrical impulse rapidly at developmental stages when trabeculations have just been formed [83, 89]. In the mature heart of lower vertebrates, which do not possess a PVCS, the ventricle is also activated from apex to base, indicating that the substrate for coordinated, rapid conduction is already present. The trabecular myocardium is remarkably similar in mammalian embryos and in adult lower vertebrates, suggesting that the trabeculations are responsible for the preferential conduction.

Initially, the entire embryonic ventricular wall expresses *Cx43*, *Cx40*, and other trabecular markers (*Kcnk3*, *Nppa*). Gradually, the expression of these genes becomes restricted to the trabecular myocardium. The $\text{Cx40}^-/\text{Kcnk3}^-/\text{Nppa}^-$ compact layer

at the epicardial side of the ventricular wall proliferates rapidly. The trabecular myocardium is further remodeled into the mature PVCS after birth, suggesting that the PVCS, which is also $Cx40^+/Kcnk3^+/Nppa^+$, is derived from the trabecular myocardium [26, 90, 91].

The endocardium has been shown to be important for further maturation of the trabecules into PVCS cells through endothelin signaling in chick and neuregulin-1 signaling in mouse [92, 93]. Neuregulin signaling has been shown to determine the relative contribution of trabecular and compact myocardium to the ventricular wall [84, 94], indicating a role in the formation of the trabecules and PVCS. In chicken, endothelin signaling regulates the formation of peri-arterial and sub-endocardial Purkinje cells [95, 96]. Endothelin-1 and endothelin converting enzyme are required for induction of the PVCS phenotype in ventricular cells in vitro and in vivo [93, 95]. In mammals, the role of endothelin signaling remains to be elucidated.

We conclude that localization, function, and expression of the same markers suggest that the trabecular myocardium contains the precursors of the mature PVCS. We hypothesize that the inner layer of the embryonic ventricular wall obtains a trabecular phenotype through signaling from the endocardium (through neuregulin). Next, again through signaling from the endocardium (through endothelin), the adjacent trabecular myocardium is reinforced to mature further into specialized PVCS cells. The outer layer of the embryonic ventricle differentiates into the rapidly proliferating compact layer of the ventricular wall, either due to the absence of cues from the endocardium or through signaling from the epicardium.

12.5.5 Model for Cardiac Conduction System Development

The formation of the components of the pacemaker and conduction system is summarized in Fig. 12.5. Most cardiomyocytes are derived from mesodermal cardiac progenitor cells that express cardiac transcription factor *Nkx2-5*. These cells will give rise to all components of the heart except the sinus venosus derived structures. The sinus venosus is formed by cells that are derived from a progenitor pool that expresses *Tbx18*, but not *Nkx2-5*. The sinus venosus will give rise to the SAN and the sinus horns, which will form the sinus venarum and the myocardium around the caval veins and the coronary sinus.

The *Nkx2-5⁺* myocardium of the embryonic heart tube can be divided into two populations. One population initiates a chamber myocardium gene expression program and one population retains the phenotype of primitive myocardium due to expression of transcriptional repressors (*Tbx2*, *Tbx3*, and *Id2*). Cells within the primitive myocardium that loose the expression of these repressors differentiate into chamber myocardium. Chamber myocardium will further mature into atrial working myocardium in the atria and into compact myocardium and trabecular myocardium in the ventricles. The trabecular layer of the ventricles is derived from

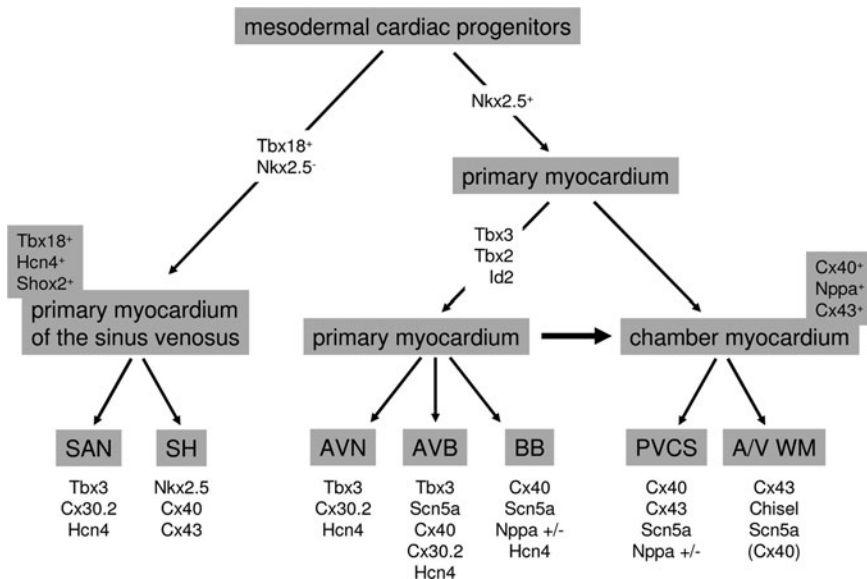


Fig. 12.5 Model for cardiomyocyte differentiation into all myocardial components of the heart. The thick black arrow between primary and chamber myocardium indicates continuous differentiation of primary cardiomyocytes into chamber myocardium. For abbreviations see legends to Fig. 12.1. In addition, A/V WM atrial/ventricular working myocardium

chamber myocardium and will give rise to the peripheral ventricular conduction system.

Due to the expression of transcriptional repressors, primary myocardium retains its initial phenotype. Its derivatives (AVN, AVB, and the proximal parts of bundle branches), which still express the transcriptional repressors, mature and differentiate significantly during further development.

12.6 Predilection Sites of Arrhythmogenesis

Atrial arrhythmias, of which AF is the most frequent form, occur frequently and contribute significantly to cardiac morbidity and mortality. The exact pathogenesis is not known, but contributing mechanisms to rapid arrhythmias are abnormal focal activity and re-entrant circuits, which depend on conduction velocity, refractoriness, and the anatomical composition of the tissue (for detailed review, see [97]). Interestingly, arrhythmias often originate from specific locations in the heart. The pulmonary vein myocardium is the most common source of AF. Other regions that are prone to arrhythmia are the entrances of the superior and inferior caval vein into the right atrium, the terminal crest, the ostium of the coronary sinus, the ligament of Marshall, and the AV junction (Table 12.2).

Table 12.2 Predilection sites of supraventricular arrhythmogenesis

Pulmonary vein
Superior caval vein
Inferior caval vein
Coronary sinus
AV junction
Marshall ligament
Terminal crest

Is there a developmental basis why these regions are more prone to arrhythmias than others? If certain cardiac regions do not sufficiently lose their embryonic properties (intrinsic pacemaker activity and slow conduction), this could be an explanation why these regions act as arrhythmia substrates under certain conditions such as disease, aging, or gene defects. How are these predilection sites related to embryonic myocardium?

The myocardium surrounding the superior and inferior caval vein, the terminal crest, the ostium of the coronary sinus, and the ligament of Marshall are all derived from the sinus venosus, and have all been reported in non-pulmonary vein paroxysmal AF [98–101]. In fetal development, the sinus venosus myocardium converts from pacemaker myocardium into myocardium with an atrial phenotype and gene expression profile. If this process of maturation does not occur completely, myocardium with pacemaker potential persists in the derivatives of the sinus venosus.

In between, the SAN and the AVN “internodal tracts” have been reported. Indeed, conduction system markers, such as HNK-1, CCS-lacZ, and *Tbx3*, are present in the dorsal wall of the atrium in the region of the terminal crest [51, 102, 103]. Whether these internodal tracts are functional is controversial. The fact that these cells express *Tbx3* implies that they are remnants of primary myocardium that connected the sinus venosus with the AVC. If these cells are nodal-like, they are slow-conducting and display a certain degree of automaticity. Interestingly, foci of arrhythmogenesis have been mapped to the terminal crest [98].

It has been suggested that the pulmonary vein myocardium is derived from the sinus venosus and, therefore, harbors pacemaker-like myocardium [104]. This conclusion was based on the observation that CCS-lacZ, which marks most of the conduction system components, is expressed in the left atrial working myocardium surrounding the pulmonary veins. CCS-lacZ does not precisely mark all the conduction system components and has been shown to be expressed in atrial working myocardium [105]. On the other hand, genetic labeling experiments have clearly demonstrated that the pulmonary myocardium is derived from a *Nkx2-5⁺*-precursor pool, whereas the sinus venosus is derived from a *Nkx2-5⁻*-precursor pool, indicating that the pulmonary venous return and the systemic venous return are derived from distinct precursor pools [47].

Although the myocardial sleeves surrounding the pulmonary veins resemble atrial working myocardium, these cells are reported to have distinctive electrophysiological properties, which might contribute to arrhythmogenesis [106]. Furthermore, experiments have revealed that pulmonary myocardium is relatively sensitive to changes in gene expression. When *Nkx2-5* levels were lowered in the pulmonary

myocardium in an animal model, the pulmonary myocardium switched to a *Cx40^{-/-}*/*Hcn4⁺* phenotype, resembling that of pacemaker myocardium [47].

Finally, pulmonary myocardium is more prone to fibrous remodeling, which further increases the risk of re-entrant circuits. These data suggest that pulmonary myocardium is more prone to develop into myocardium with arrhythmogenic properties due to mechanisms that we are beginning to understand, but are not based on persisting embryonic myocardium.

The embryonic AVC is a relatively large region consisting of nodal-like primitive myocardium. During late fetal development the expression domain of nodal markers, such as *Tbx3* and *minK-lacZ* become confined to the AV nodal area [51, 62], suggesting that the remainder of AVC myocardium disappears. If this process does not occur completely, pacemaker myocardium persists at the atrioventricular junction. Indeed, in AV junctional tissues of healthy dogs and pigs, cells were found that resembled nodal cells in their cellular electrophysiology [24]. These cells were located in close proximity to the base of both the mitral and tricuspid valves [107]. Clinically, arrhythmias originating from the mitral and tricuspid annulus region have been reported [108–110].

12.7 Conclusions

The components of the cardiac conduction system originate from embryonic myocardium that has maintained its primitive phenotype, while the adjacent myocardium differentiates into working myocardium. It is important to realize that a significant proportion of this primitive myocardium does not contribute to the conduction system, but differentiates into working myocardium at later stages of development. We think that these cells initiate the gene expression program of the working myocardium, due to loss of expression of transcriptional repressors. Abnormal regulation may result in ectopic persistence of pacemaker myocardium and/or increased susceptibility to arrhythmogenesis. The exact mechanism responsible for loss of transcriptional repressors remains to be elucidated.

Acknowledgments This work was supported by grants from the Netherlands Heart Foundation (2005B076 to V.M.C.) and the European Union, FP6 contract “Heart Repair” (LSHM-CT-2005-018630 to V.M.C., A.F.M.M.)

References

1. Gaskell WH. The contraction of cardiac muscle. In: Sharpey-Schafer EA, editor. Textbook of physiology. Edinburgh: Pentland; 1900. p. 169–227.
2. Lakatta EG, DiFrancesco D. What keeps us ticking: a funny current, a calcium clock, or both? J Mol Cell Cardiol. 2009;47:157–70.

3. Ishii TM, Takano M, Xie LH, Noma A, Ohmori H. Molecular characterization of the hyperpolarization-activated cation channel in rabbit heart sinoatrial node1. *J Biol Chem.* 1999; 274:12835–9.
4. Moosmang S, Stieber J, Zong X, Biel M, Hofmann F, Ludwig A. Cellular expression and functional characterization of four hyperpolarization-activated pacemaker channels in cardiac and neuronal tissues. *Eur J Biochem.* 2001;268:1646–52.
5. Garcia-Frigola C, Shi Y, Evans SM. Expression of the hyperpolarization-activated cyclic nucleotide-gated cation channel HCN4 during mouse heart development. *Gene Expr Patterns.* 2003;3:777–83.
6. Stieber J, Herrmann S, Feil S, Loster J, Feil R, Biel M, et al. The hyperpolarization-activated channel HCN4 is required for the generation of pacemaker action potentials in the embryonic heart. *Proc Natl Acad Sci USA.* 2003;100:15235–40.
7. Thollon C, Bedu S, Villeneuve N, Coge F, Piffard L, Guillaumin JP, et al. Use-dependent inhibition of hHCN4 by ivabradine and relationship with reduction in pacemaker activity. *Br J Pharmacol.* 2007;150:37–46.
8. Lakatta EG, Vinogradova TM, Maltsev VA. The missing link in the mystery of normal automaticity of cardiac pacemaker cells. *Ann N Y Acad Sci.* 2008;1123:41–57.
9. Chandler NJ, Greener ID, Tellez JO, Inada S, Musa H, Molenaar P, et al. Molecular architecture of the human sinus node: insights into the function of the cardiac pacemaker. *Circulation.* 2009;119:1562–75.
10. Miake J, Marban E, Nuss HB. Biological pacemaker created by gene transfer. *Nature.* 2002; 419:132–3.
11. Joyner RW, van Capelle FJL. Propagation through electrically coupled cells. How a small SA node drives a large atrium. *Biophys J.* 1986;50:1157–64.
12. Severs NJ. The cardiac gap junction and intercalated disc. *Int J Cardiol.* 1990;26:137–73.
13. Coppen SR, Dupont E, Rothery S, Severs NJ. Connexin45 expression is preferentially associated with the ventricular conduction system in mouse and rat heart. *Circ Res.* 1998; 82:232–43.
14. Kreuzberg MM, Willecke K, Bukauskas FF. Connexin-mediated cardiac impulse propagation: connexin 30.2 slows atrioventricular conduction in mouse heart. *Trends Cardiovasc Med.* 2006;16:266–72.
15. Gros D, Theveniau-Ruissy M, Bernard M, Calmels T, Kober F, Sohl G, et al. Connexin 30 is expressed in the mouse sino-atrial node, and modulates heart rate. *Cardiovasc Res.* 2010; 85(1):45–55.
16. van Kempen MJA, Ten Velde I, Wessels A, Oosthoek PW, Gros D, Jongsma HJ, et al. Differential connexin distribution accommodates cardiac function in different species. *Microsc Res Tech.* 1995;31:420–36.
17. Traub O, Eckert R, Lichtenberg-Fraté H, Elfgang C, Bastide B, Scheidtmann KH, et al. Immunochemical and electrophysiological characterization of murine connexin40 and 43 in mouse tissues and transfected human cells. *Eur J Cell Biol.* 1994;64:101–12.
18. Hoogaars WM, Engel A, Brons JF, Verkerk AO, de Lange FJ, Wong LY, et al. Tbx3 controls the sinoatrial node gene program and imposes pacemaker function on the atria. *Genes Dev.* 2007;21:1098–112.
19. Coppen SR, Kodama I, Boyett MR, Dobrzynski H, Takagishi Y, Honjo H, et al. Connexin45, a major connexin of the rabbit sinoatrial node, is co-expressed with connexin43 in a restricted zone at the nodal-crista terminalis border. *J Histochem Cytochem.* 1999;47:907–18.
20. Li J, Greener ID, Inada S, Nikolski VP, Yamamoto M, Hancox JC, et al. Computer three-dimensional reconstruction of the atrioventricular node. *Circ Res.* 2008;102:975–85.
21. Ko YS, Yeh HI, Ko YL, Hsu YC, Chen CF, Wu S, et al. Three-dimensional reconstruction of the rabbit atrioventricular conduction axis by combining histological, desmin, and connexin mapping data. *Circulation.* 2004;109:1172–9.
22. Miquerol L, Meysen S, Mangoni M, Bois P, Van Rijen HV, Abran P, et al. Architectural and functional asymmetry of the His-Purkinje system of the murine heart. *Cardiovasc Res.* 2004; 63:77–86.

23. Marionneau C, Couette B, Liu J, Li H, Mangoni ME, Nargeot J, et al. Specific pattern of ionic channel gene expression associated with pacemaker activity in the mouse heart. *J Physiol.* 2005;562:223–34.
24. McGuire MA, de Bakker JM, Vermeulen JT, Moorman AF, Loh P, Thibault B, et al. Atrioventricular junctional tissue. Discrepancy between histological and electrophysiological characteristics. *Circulation.* 1996;94:571–7.
25. Yanni J, Boyett MR, Anderson RH, Dobrzynski H. The extent of the specialized atrioventricular ring tissues. *Heart Rhythm.* 2009;6:672–80.
26. Delorme B, Dahl E, Jarry-Guichard T, Marics I, Briand JP, Willecke K, et al. Developmental regulation of connexin40 gene expression in mouse heart correlates with the differentiation of the conduction system. *Dev Dyn.* 1995;204:358–71.
27. Lo CW. Role of gap junctions in cardiac conduction and development. *Circ Res.* 2000; 87:346–8.
28. de Haan RL. Differentiation of the atrioventricular conducting system of the heart. *Circulation.* 1961;24:458–70.
29. Canale ED, Campbell GR, Smolich JJ, Campbell JH. Cardiac muscle. Berlin: Springer; 1986.
30. Virág S, Challice CE. The development of the conduction system in the mouse embryo heart. III. The development of sinus muscle and sinoatrial node. *Dev Biol.* 1980;80:28–45.
31. Davis DL, Edwards AV, Juraszek AL, Phelps A, Wessels A, Burch JB. A GATA-6 gene heart-region-specific enhancer provides a novel means to mark and probe a discrete component of the mouse cardiac conduction system. *Mech Dev.* 2001;108:105–19.
32. Buckingham M, Meilhac S, Zaffran S. Building the mammalian heart from two sources of myocardial cells. *Nat Rev Genet.* 2005;6:826–37.
33. van den Berg G, Abu-Issa R, de Boer BA, Hutson MR, de Boer PA, Soufan AT, et al. A caudal proliferating growth center contributes to both poles of the forming heart tube. *Circ Res.* 2009;104:179–88.
34. Aanhaanen WT, Brons JF, Dominguez JN, Rana MS, Norden J, Airik R, et al. The Tbx2+ primary myocardium of the atrioventricular canal forms the atrioventricular node and the base of the left ventricle. *Circ Res.* 2009;104:1267.
35. Soufan AT, van den Berg G, Ruijter JM, de Boer PAJ, van den Hoff MJB, Moorman AFM. Regionalized sequence of myocardial cell growth and proliferation characterizes early chamber formation. *Circ Res.* 2006;99:545–52.
36. de Jong F, Ophof T, Wilde AA, Janse MJ, Charles R, Lamers WH, et al. Persisting zones of slow impulse conduction in developing chicken hearts. *Circ Res.* 1992;71:240–50.
37. Moorman AFM, Christoffels VM. Cardiac chamber formation: development, genes and evolution. *Physiol Rev.* 2003;83:1223–67.
38. Paff GH, Boucek RJ, Harrell TC. Observations on the development of the electrocardiogram. *Anat Rec.* 1968;160:575–82.
39. van Mierop LHS. Localization of pacemaker in chick embryo heart at the time of initiation of heartbeat. *Am J Physiol.* 1967;212:407–15.
40. Randall DJ. The circulatory system. In: Hoar WS, Randall DJ, editors. *Fish physiology.* New York: Academic Press; 1970. p. 133–72.
41. Lu Y, James TN, Yamamoto S, Terasaki F. Cardiac conduction system in the chicken: gross anatomy plus light and electron microscopy. *Anat Rec.* 1993;236:493–510.
42. Gurjarpadhye A, Hewett KW, Justus C, Wen X, Stadt H, Kirby ML, et al. Cardiac neural crest ablation inhibits compaction and electrical function of conduction system bundles. *Am J Physiol Heart Circ Physiol.* 2007;292:H1291–300.
43. Hutson MR, Kirby ML. Model systems for the study of heart development and disease. Cardiac neural crest and conotruncal malformations. *Semin Cell Dev Biol.* 2007;18:101–10.
44. Gourdie RG, Mima T, Thompson RP, Mikawa T. Terminal diversification of the myocyte lineage generates Purkinje fibers of the cardiac conduction system. *Development.* 1995; 121:1423–31.

45. Cheng G, Litchenberg WH, Cole GJ, Mikawa T, Thompson RP, Gourdie RG. Development of the cardiac conduction system involves recruitment within a multipotent cardiomyogenic lineage. *Development*. 1999;126:5041–9.
46. DeHaan RL. Development of pacemaker tissue in the embryonic heart. *Ann N Y Acad Sci*. 1965;127:7–18.
47. Mommersteeg MTM, Brown NA, Prall OWJ, de Gier-de Vries C, Harvey RP, Moorman AFM, et al. Pitx2c and Nkx2-5 are required for the formation and identity of the pulmonary myocardium. *Circ Res*. 2007;101:902–9.
48. Wiese C, Grieskamp T, Airik R, Mommersteeg MT, Gardiwal A, de Gier-de VC, et al. Formation of the sinus node head and differentiation of sinus node myocardium are independently regulated by tbx18 and tbx3. *Circ Res*. 2009;104:388–97.
49. Mommersteeg MT, Dominguez JN, Wiese C, Norden J, de Gier-de VC, Burch JB, et al. The sinus venosus progenitors separate and diversify from the first and second heart fields early in development. *Cardiovasc Res*. 2010;87(1):92–101.
50. Dupays L, Jarry-Guichard T, Mazurais D, Calmels T, Izumo S, Gros D, et al. Dysregulation of connexins and inactivation of NFATc1 in the cardiovascular system of Nkx2-5 null mutants. *J Mol Cell Cardiol*. 2005;38:787–98.
51. Hoogaars WMH, Tessari A, Moorman AFM, de Boer PAJ, Hagoort J, Soufan AT, et al. The transcriptional repressor Tbx3 delineates the developing central conduction system of the heart. *Cardiovasc Res*. 2004;62:489–99.
52. Mommersteeg MTM, Hoogaars WMH, Prall OWJ, de Gier-de Vries C, Wiese C, Clout DEW, et al. Molecular pathway for the localized formation of the sinoatrial node. *Circ Res*. 2007;100:354–62.
53. Blaschke RJ, Hahurij ND, Kuijper S, Just S, Wisse LJ, Deissler K, et al. Targeted mutation reveals essential functions of the homeodomain transcription factor Shox2 in sinoatrial and pacemaking development. *Circulation*. 2007;115:1830–8.
54. Espinoza-Lewis RA, Yu L, He F, Liu H, Tang R, Shi J, et al. Shox2 is essential for the differentiation of cardiac pacemaker cells by repressing Nkx2-5. *Dev Biol*. 2009;327(2):376–85. doi:[10.1016/j.ydbio.2008.12.028](https://doi.org/10.1016/j.ydbio.2008.12.028).
55. Franco D, Campione M. The role of Pitx2 during cardiac development. Linking left-right signaling and congenital heart diseases. *Trends Cardiovasc Med*. 2003;13:157–63.
56. Wessels A, Vermeulen JLM, Virág S, Kálmán F, Lamers WH, Moorman AFM. Spatial distribution of “tissue specific” antigens in the developing human heart and skeletal muscle. II. An immunohistochemical analysis of myosin heavy chain isoform expression patterns in the embryonic heart. *Anat Rec*. 1991;229:355–68.
57. Virág S, Challice CE. The development of the conduction system in the mouse embryo heart. II. Histogenesis of the atrioventricular node and bundle. *Dev Biol*. 1977;56:397–411.
58. Virág S, Challice CE. The development of the conduction system in the mouse embryo heart. IV. Differentiation of the atrioventricular conduction system. *Dev Biol*. 1982;89:25–40.
59. Horsthuis T, Buermans HP, Brons JF, Verkerk AO, Bakker ML, Wakker V, et al. Gene expression profiling of the forming atrioventricular node using a novel Tbx3-based node-specific transgenic reporter. *Circ Res*. 2009;105:61–9.
60. Di Lisi R, Sandri C, Franco D, Ausoni S, Moorman AFM, Schiaffino S. An atrioventricular canal domain defined by cardiac troponin I transgene expression in the embryonic myocardium. *Anat Embryol (Berl)*. 2000;202:95–101.
61. Rentschler S, Vaidya DM, Tamaddon H, Degenhardt K, Sasseen D, Morley GE, et al. Visualization and functional characterization of the developing murine cardiac conduction system. *Development*. 2001;128:1785–92.
62. Kondo RP, Anderson RH, Kupershmidt S, Roden DM, Evans SM. Development of the cardiac conduction system as delineated by minK-lacZ. *J Cardiovasc Electrophysiol*. 2003;14:383–91.

63. Yamada M, Revelli JP, Eichele G, Barron M, Schwartz RJ. Expression of chick Tbx-2, Tbx-3, and Tbx-5 genes during early heart development: evidence for BMP2 induction of Tbx2. *Dev Biol.* 2000;228:95–105.
64. Ma L, Lu MF, Schwartz RJ, Martin JF. Bmp2 is essential for cardiac cushion epithelial–mesenchymal transition and myocardial patterning. *Development.* 2005;132:5601–11.
65. Gaussen V, Morley GE, Cox L, Zwijnen A, Vance KM, Emile L, et al. Alk3/Bmpr1a receptor is required for development of the atrioventricular canal into valves and annulus fibrosus. *Circ Res.* 2005;97:219–26.
66. Stroud DM, Gaussen V, Burch JB, Yu C, Mishina Y, Schneider MD, et al. Abnormal conduction and morphology in the atrioventricular node of mice with atrioventricular canal-targeted deletion of Alk3/Bmpr1a receptor. *Circulation.* 2007;116:2535–43.
67. Singh MK, Christoffels VM, Dias JM, Trowe MO, Petry M, Schuster-Gossler K, et al. *Tbx20* is essential for cardiac chamber differentiation and repression of *Tbx2*. *Development.* 2005;132:2697–707.
68. Cai CL, Zhou W, Yang L, Bu L, Qyang Y, Zhang X, et al. T-box genes coordinate regional rates of proliferation and regional specification during cardiogenesis. *Development.* 2005;132:2475–87.
69. Stennard FA, Costa MW, Lai D, Biben C, Furtado MB, Solloway MJ, et al. Murine T-box transcription factor Tbx20 acts as a repressor during heart development, and is essential for adult heart integrity, function and adaptation. *Development.* 2005;132:2451–62.
70. Rutenberg JB, Fischer A, Jia H, Gessler M, Zhong TP, Mercola M. Developmental patterning of the cardiac atrioventricular canal by Notch and Hairy-related transcription factors. *Development.* 2006;133:4381–90.
71. Kokubo H, Miyagawa-Tomita S, Nakazawa M, Saga Y, Johnson RL. Mouse *hesr1* and *hesr2* genes are redundantly required to mediate Notch signaling in the developing cardiovascular system. *Dev Biol.* 2005;278:301–9.
72. Lyons KM, Hogan BL, Robertson EJ. Colocalization of BMP 7 and BMP 2 RNAs suggests that these factors cooperatively mediate tissue interactions during murine development. *Mech Dev.* 1995;50:71–83.
73. Tanaka M, Chen Z, Bartunkova S, Yamasaki N, Izumo S. The cardiac homeobox gene *Csx/Nkx2.5* lies genetically upstream of multiple genes essential for heart development. *Development.* 1999;126:1269–80.
74. Jay PY, Harris BS, Maguire CT, Buerger A, Wakimoto H, Tanaka M, et al. Nkx2-5 mutation causes anatomic hypoplasia of the cardiac conduction system. *J Clin Invest.* 2004;113:1130–7.
75. Pashmforoush M, Lu JT, Chen H, Amand TS, Kondo R, Pradervand S, et al. Nkx2-5 pathways and congenital heart disease: loss of ventricular myocyte lineage specification leads to progressive cardiomyopathy and complete heart block. *Cell.* 2004;117:373–86.
76. Basson CT, Bachinsky DR, Lin RC, Levi T, Elkins JA, Soultz J, et al. Mutations in human TBX5 (corrected) cause limb and cardiac malformation in Holt–Oram syndrome. *Nat Genet.* 1997;15:30–5.
77. Bruneau BG, Nemer G, Schmitt JP, Charron F, Robitaille L, Caron S, et al. A murine model of Holt–Oram syndrome defines roles of the T-box transcription factor Tbx5 in cardiogenesis and disease. *Cell.* 2001;106:709–21.
78. Bruneau BG, Logan M, Davis N, Levi T, Tabin CJ, Seidman JG, et al. Chamber-specific cardiac expression of *Tbx5* and heart defects in Holt–Oram syndrome. *Dev Biol.* 1999;211:100–8.
79. Christoffels VM, Habets PEMH, Franco D, Campione M, de Jong F, Lamers WH, et al. Chamber formation and morphogenesis in the developing mammalian heart. *Dev Biol.* 2000;223:266–78.
80. Christoffels VM, Hoogaars WMH, Tessari A, Clout DEW, Moorman AFM, Campione M. T-box transcription factor Tbx2 represses differentiation and formation of the cardiac chambers. *Dev Dyn.* 2004;229:763–70.

81. Bakker ML, Boukens BJ, Mommersteeg MTM, Brons JF, Wakker V, Moorman AFM, et al. Transcription factor Tbx3 is required for the specification of the atrioventricular conduction system. *Circ Res*. 2008;102:1340–9.
82. Gourdie RG, Severs NJ, Green CR, Rothery S, Germroth P, Thompson RP. The spatial distribution and relative abundance of gap-junctional connexin40 and connexin43 correlate to functional properties of components of the cardiac atrioventricular conduction system. *J Cell Sci*. 1993;105:985–91.
83. Valderrabano M, Chen F, Dave AS, Lamp ST, Klitzner TS, Weiss JN. Atrioventricular ring reentry in embryonic mouse hearts. *Circulation*. 2006;114:543–9.
84. Rentschler S, Zander J, Meyers K, France D, Levine R, Porter G, et al. Neuregulin-1 promotes formation of the murine cardiac conduction system. *Proc Natl Acad Sci USA*. 2002;99:10464–9.
85. Harvey RP. Patterning the vertebrate heart. *Nat Rev Genet*. 2002;3:544–56.
86. Moskowitz IP, Kim JB, Moore ML, Wolf CM, Peterson MA, Shendure J, et al. A molecular pathway including id2, tbx5, and nkx2-5 required for cardiac conduction system development. *Cell*. 2007;129:1365–76.
87. Virág S, Challice CE. The development of the conduction system in the mouse embryo heart. I. The first embryonic A-V conduction pathway. *Dev Biol*. 1977;56:382–96.
88. Ismat FA, Zhang M, Kook H, Huang B, Zhou R, Ferrari VA, et al. Homeobox protein Hop functions in the adult cardiac conduction system. *Circ Res*. 2005;96:898–903.
89. Chuck ET, Freeman DM, Watanabe M, Rosenbaum DS. Changing activation sequence in the embryonic chick heart: implications for the development of the His-Purkinje system. *Circ Res*. 1997;81:470–6.
90. Gros D, van Kempen MJA, Théveniau M, Delorme B, Jarry-Guichard T, Ten Velde I, et al. Expression and distribution of connexin-40 in mammal heart. In: Kanno Y, Katoaka K, editors. *Progress in cell research*. New York: Elsevier; 1995. p. 181–6.
91. Graham V, Zhang H, Willis S, Creazzo TL. Expression of a two-pore domain K⁺ channel (TASK-1) in developing avian and mouse ventricular conduction systems. *Dev Dyn*. 2006;235:143–51.
92. Takebayashi-Suzuki K, Yanagisawa M, Gourdie RG, Kanzawa N, Mikawa T. In vivo induction of cardiac Purkinje fiber differentiation by coexpression of preproendothelin-1 and endothelin converting enzyme-1. *Development*. 2000;127:3523–32.
93. Hall CE, Hurtado R, Hewett KW, Shulimovich M, Poma CP, Reckova M, et al. Hemodynamic-dependent patterning of endothelin converting enzyme 1 expression and differentiation of impulse-conducting Purkinje fibers in the embryonic heart. *Development*. 2004;131:581–92.
94. Hertig CM, Kubalak SW, Wang Y, Chien KR. Synergistic roles of neuregulin-1 and insulin-like growth factor-I in activation of the phosphatidylinositol 3-kinase pathway and cardiac chamber morphogenesis. *J Biol Chem*. 1999;274:37362–9.
95. Pennisi DJ, Rentschler S, Gourdie RG, Fishman GI, Mikawa T. Induction and patterning of the cardiac conduction system. *Int J Dev Biol*. 2002;46:765–75.
96. Gourdie RG, Harris BS, Bond J, Edmonson AM, Cheng G, Sedmera D, et al. His-Purkinje lineages and development. In: Chadwick DJ, Goode J, editors. *Development of the cardiac conduction system*. Chichester: Wiley; 2003. p. 110–24.
97. Nattel S. Therapeutic implications of atrial fibrillation mechanisms: can mechanistic insights be used to improve AF management? *Cardiovasc Res*. 2002;54:347–60.
98. Kistler PM, Flynn SP, Haqqani H, Stevenson IH, Vohra JK, Morton JB, et al. Focal atrial tachycardia from the ostium of the coronary sinus: electrocardiographic and electrophysiological characterization and radiofrequency ablation. *J Am Coll Cardiol*. 2005;45:1488–93.
99. Tsai CF, Tai CT, Hsieh MH, Lin WS, Yu WC, Ueng KC, et al. Initiation of atrial fibrillation by ectopic beats originating from the superior vena cava: electrophysiological characteristics and results of radiofrequency ablation. *Circulation*. 2000;102:67–74.

100. Lin WS, Tai CT, Hsieh MH, Tsai CF, Lin YK, Tsao HM, et al. Catheter ablation of paroxysmal atrial fibrillation initiated by non-pulmonary vein ectopy. *Circulation*. 2003; 107:3176–83.
101. Doshi RN, Wu TJ, Yashima M, Kim YH, Ong JJ, Cao JM, et al. Relation between ligament of Marshall and adrenergic atrial tachyarrhythmia. *Circulation*. 1999;100:876–83.
102. Ikeda T, Iwasaki K, Shimokawa I, Sakai H, Ito H, Matsuo T. Leu-7 immunoreactivity in human and rat embryonic hearts, with special reference to the development of the conduction tissue. *Anat Embryol*. 1990;182:553–62.
103. Blom NA, Gittenberger-de Groot AC, deRuiter MC, Poelmann RE, Mentink MMT, Ottenkamp J. Development of the cardiac conduction tissue in human embryos using HNK-1 antigen expression: possible relevance for understanding of abnormal atrial automaticity. *Circulation*. 1999;99:800–6.
104. Jongbloed MR, Mahtab EA, Blom NA, Schalij MJ, Gittenberger-de Groot AC. Development of the cardiac conduction system and the possible relation to predilection sites of arrhythmogenesis. *ScientificWorldJournal*. 2008;8:239–69.
105. Viswanathan S, Burch JB, Fishman GI, Moskowitz IP, Benson DW. Characterization of sinoatrial node in four conduction system marker mice. *J Mol Cell Cardiol*. 2007;42:946–53.
106. Nattel S. Basic electrophysiology of the pulmonary veins and their role in atrial fibrillation: precipitators, perpetuators, and perplexers. *J Cardiovasc Electrophysiol*. 2003;14:1372–5.
107. Janse MJ, McGuire MA, Loh P, Thibault B, Hocini M, de Bakker JM. Electrical activity in Koch's triangle. *Can J Cardiol*. 1997;13:1065–8.
108. Gonzalez MD, Contreras LJ, Jongbloed MR, Rivera J, Donahue TP, Curtis AB, et al. Left atrial tachycardia originating from the mitral annulus-aorta junction. *Circulation*. 2004;110: 3187–92.
109. Kistler PM, Sanders P, Flynn SP, Stevenson IH, Hussin A, Vohra JK, et al. Electrophysiological and electrocardiographic characteristics of focal atrial tachycardia originating from the pulmonary veins: acute and long-term outcomes of radiofrequency ablation. *Circulation*. 2003;108:1968–75.
110. Otomo K, Azegami K, Sasaki T, Kawabata M, Hirao K, Isobe M. Successful catheter ablation of focal left atrial tachycardia originating from the mitral annulus aorta junction. *Int Heart J*. 2006;47:461–8.

Chapter 13

Role of the T-Tubules in the Response of Cardiac Ventricular Myocytes to Inotropic Interventions

C.H. Orchard, F. Brette, A. Chase, and M.R. Fowler

13.1 Introduction

During the cardiac action potential (AP), Ca influx across the cell membrane via L-type Ca channels (LTCCs) triggers the release of more Ca from the sarcoplasmic reticulum (SR) by activating ryanodine receptors (RyRs) in the adjacent SR membrane [1]. The rise of intracellular Ca that activates the contractile proteins – the systolic Ca transient – is the spatial and temporal sum of such local releases [2]; the fraction of the SR Ca content that is released depends on SR Ca content and the size of the Ca trigger [3].

Relaxation is brought about by removal of Ca from the cell cytoplasm by two main routes: the SR Ca ATPase (SERCA), which is regulated by phospholamban (PLB), pumps Ca back into the SR, while Na/Ca exchange (NCX) uses the inwardly directed electrochemical gradient for Na to extrude Ca from the cell [1]. The fraction of Ca removed from the cytoplasm by each of these pathways depends on their relative activities, although in the steady state the amount of Ca extruded from the cell must equal that entering during each beat [4]. Recent work suggests that in mammalian ventricular myocytes many of the proteins involved in excitation–contraction (EC) coupling are located predominantly at the transverse (t-) tubules [5, 6].

C.H. Orchard (✉) and A. Chase

School of Physiology and Pharmacology, Medical Sciences Building, University of Bristol, Bristol BS8 1TD, UK

e-mail: clive.orchard@bristol.ac.uk

F. Brette

Faculty of Life Sciences, University of Manchester, Manchester M13 9NT, UK

M.R. Fowler

Cardiovascular Physiology, University of Glasgow, Glasgow G12 8QQ, UK

13.2 Cardiac T-Tubules

The T-tubules of mammalian ventricular myocytes are invaginations of the cell membrane that occur at each Z-line [7]. These invaginations branch within the cell to form a complex network of tubules with diameters between 100 and 300 nm [8]. The T-tubule lumen is therefore continuous with the extracellular space, but forms a restricted diffusion space within the cell.

Immunohistochemical studies have shown that staining for many of the key membrane proteins involved in EC coupling, including LTCC, NCX, RyR and SERCA, occurs predominantly at the T-tubules [7]. However such studies do not enable the distribution of protein function between the surface and T-tubule membranes to be determined. We have therefore developed a technique to physically and functionally uncouple the T-tubules from the surface membrane of cardiac ventricular myocytes (detubulation) [9, 10]. Comparison of cell capacitance (a function of membrane area) and membrane currents before and after detubulation enables the distribution of currents between the surface and T-tubule membranes to be determined. Table 13.1 shows the distribution of some of the main currents involved in EC coupling, determined using this method, showing that many membrane currents, including L-type Ca current (I_{CaL}) and NCX current (I_{NCX}), flow predominantly across the T-tubule membrane (see Fig. 13.1). This ensures that Ca release occurs synchronously throughout the cell, and that Ca can be extruded rapidly, since no part of the cytoplasm is more than $\sim 1 \mu\text{m}$ from the nearest T-tubule and its Ca flux pathways. However, it also means that ion flux occurs in and out of a restricted diffusion space. In addition, it appears that proteins within the T-tubule membrane may be regulated differently from those at the surface membrane. These considerations may have important implications for the role of the T-tubules in the response of cardiac muscle to inotropic interventions; this chapter considers these implications.

Table 13.1 Fractional distribution of cell membrane and selected membrane currents between the cell surface and T-tubule membranes, determined using detubulation

Membrane	Percentage on cell surface	Percentage in T-tubules
I_{CaL}	60.1	39.9
I_{NCX}	5.7	94.3
$I_{\text{Na/K}}$	31.7	68.3 ^a
$I_{\text{Na,cardiac}}$	36.1	63.9 ^a
$I_{\text{Na,neuronal}}$	93.8	6.2
	6.6	93.4

^aExcludes apparently non-detubulated myocytes (by capacitance:volume ratio). All other values compensated for 13% non-detubulated myocytes, and all values corrected for 7.7% of T-tubule network remaining after detubulation

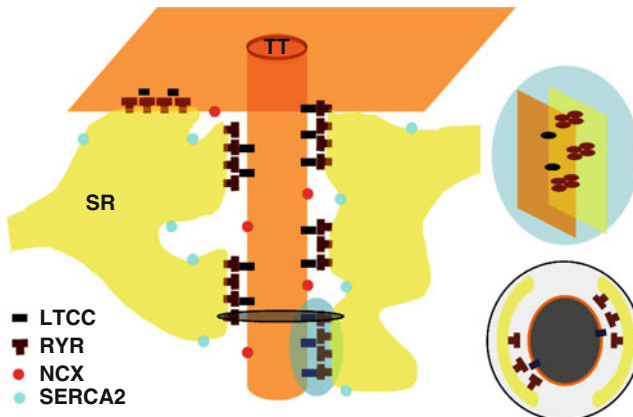


Fig. 13.1 Proteins involved in calcium signaling in mammalian ventricular myocytes. Junctional sarcoplasmic reticulum (SR) membrane in close proximity to the sarcolemma forms dyads, which are present mainly at the transverse tubules (TT) but also at the surface membrane. Dyads comprise a cluster of ryanodine receptors (RyRs) adjacent to, and under the functional control of, L-type Ca^{2+} channels; this forms a Ca^{2+} release unit (expanded view in the *blue panel*). Proteins involved in Ca^{2+} reuptake (SR Ca^{2+} -ATPase, SERCA2) and extrusion ($\text{Na}^{+}/\text{Ca}^{2+}$ exchanger, NCX) are preferentially located within or near the transverse tubules. A cross section of TT SR junction (~15 nm) is shown in the *light gray panel*

13.3 Autoregulation

Work from Eisner, Trafford and colleagues has demonstrated “autoregulation” of the Ca content of cardiac ventricular myocytes, so that Ca efflux is equal to Ca influx, thus maintaining the steady-state systolic Ca transient [4, 11]. In brief, an increase in Ca transient amplitude which is not due to a change in trans-sarcolemmal Ca influx or efflux, will decrease Ca influx (by enhancing Ca-dependent inactivation of I_{CaL}) and increase Ca efflux (by stimulating NCX) [12]. These changes will reduce intracellular Ca and hence Ca transient amplitude, and will continue until influx again equals efflux and a steady state is achieved [13].

Two lines of evidence suggest that the T-tubules may play an important role in autoregulation. First, inactivation of I_{CaL} at the T-tubules appears to be regulated differently from that at the surface membrane [14]: Ca-dependent inactivation due to Ca released from the SR appears to be more marked at the T-tubules than at the surface membrane, although voltage-dependent inactivation, and Ca-dependent inactivation due to Ca influx via I_{CaL} , appear to be the same at the two sites [14]. Thus inhibition of Ca influx due to increased SR Ca release will be more marked at the T-tubules than at the surface membrane; in addition a large fraction of I_{CaL} is located at the T-tubules (Table 13.1). This suggests that the T-tubules will play an important role in autoregulation via I_{CaL} . Secondly, NCX appears to have privileged access to Ca released from the SR [15]. Since RyR and NCX are also found predominantly at the T-tubules [16, 17], this will result in the T-tubules

playing an important role in the changes of Ca efflux via NCX in response to changes in SR Ca release.

13.4 Stimulation Frequency

Changing stimulation rate alters the amplitude of the systolic Ca transient, and hence contraction in ventricular myocytes, although the mechanisms are complex [18, 19]. For example, increasing stimulation rate causes (1) abbreviation of the AP but (2) increased I_{CaL} amplitude (facilitation); (3) increased time-averaged Ca influx via I_{CaL} as a result of more APs per unit time; (4) increased intracellular Na ion concentration (Na_i), due to an increase in time averaged Na influx via I_{Na} ; (5) increased SR Ca content as a direct consequence of (3) and an indirect consequence (via NCX) of (4); (6) decreased diastolic period, allowing less time for Ca efflux, which will also increase the cell's Ca load; (7) decreased SR restitution time. Some of these changes (e.g., 1, 7) will decrease Ca transient amplitude. The others, which will increase Ca transient amplitude, depend mainly on I_{CaL} and NCX, which are predominantly in the T-tubules. Previous work has shown that the increase in Ca transient amplitude that occurs on increasing stimulation rate depends principally on the increase of Na_i that, via NCX, increases intracellular Ca [18, 19].

Evidence that the T-tubules play an important role in shaping this response is provided by the observation that detubulation changes a flat or positive force–frequency relation into a markedly negative force–frequency relation (i.e., Ca transient amplitude and contraction decrease with increasing stimulation frequency; [20], see Fig. 13.2). However, the increase of Na_i accompanying the change of frequency is not significantly altered [20].

The T-tubules may play (at least) three roles in shaping the response of ventricular cells to a change of pacing rate, because: (1) NCX, which translates changes of Na_i to changes in cellular Ca load, is located predominantly in the T-tubules. Previous work has shown that the increase of Na_i that occurs when stimulation rate is increased plays an important role in the accompanying increase in Ca transient amplitude, by decreasing the electrochemical gradient for Na entry, thereby decreasing Ca extrusion by NCX, and increasing intracellular Ca load [21, 22]. Interventions that inhibit the rise of Na_i inhibit the positive inotropic response to increasing stimulation rate (e.g., TTX; [21, 22]). Thus, loss of NCX in detubulated cells, and therefore the inability to translate the increase of Na_i into an increase of intracellular Ca, may account for the appearance of a negative force–frequency relationship in detubulated cells, in which the response of the cell to changes in pacing frequency would be dominated by mechanisms that have a net negative inotropic effect, such as decreased restitution time between beats. (2) I_{CaL} is located predominantly in the T-tubules. Loss of the T-tubules will result in loss of I_{CaL} ; however the number of Ca currents per unit time would still increase with increasing stimulation rate. Thus although Ca transient and contraction amplitude might be expected to be smaller, Ca influx per unit time would still be expected to

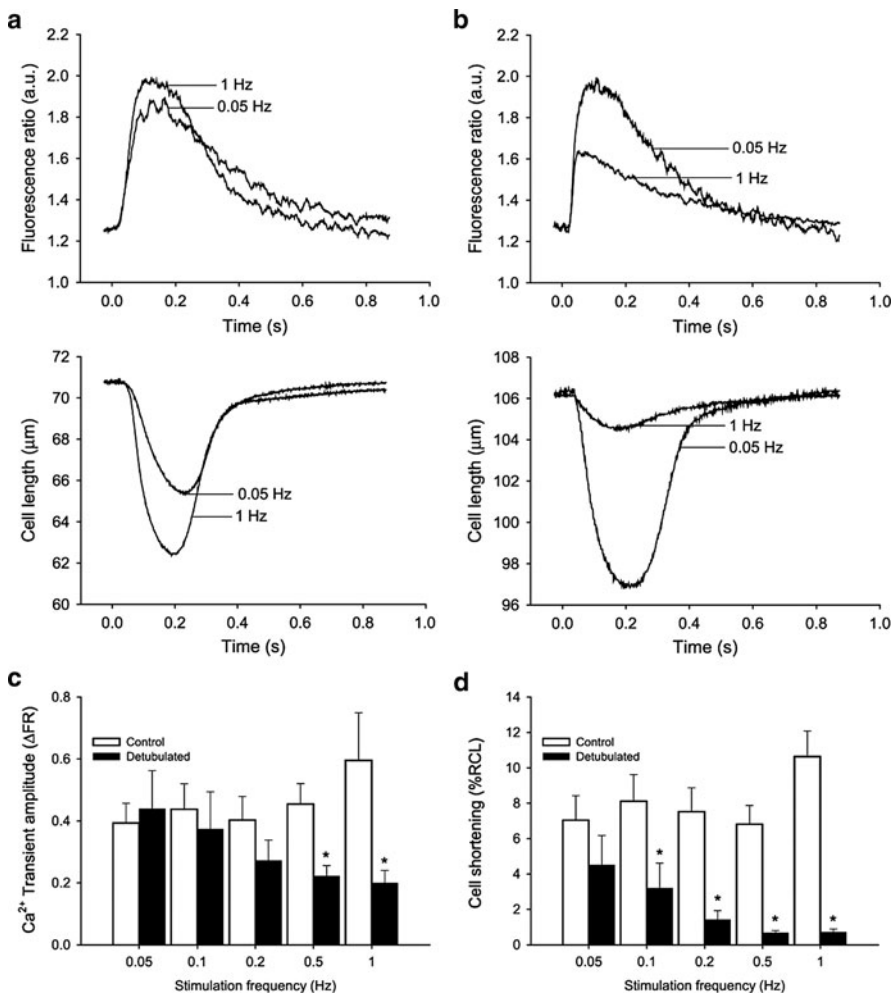


Fig. 13.2 Force–frequency relationship of normal and detubulated ventricular myocytes. Representative Ca^{2+} transients (top) and contractions (bottom) in control (a) and detubulated (b) cells at 0.05 and 1 Hz. Traces are an average of 10–20 consecutive records. (c) The effect of stimulation frequency on mean (\pm S.E.M.) Ca^{2+} transient amplitude in control ($n = 6$) and detubulated ($n = 10$) ventricular myocytes. (d) The effect of stimulation frequency on mean (\pm S.E.M.) contraction amplitude in control ($n = 6$) and detubulated ($n = 10$) ventricular myocytes. * $P < 0.05$, unpaired *t*-test between cell types at each stimulation frequency. Reproduced with permission from [20]

increase with stimulation rate. However, it has recently been shown that facilitation of I_{CaL} is absent in detubulated myocytes, whereas control myocytes show robust increase in Ca entry following increasing rate [23]. This could also account for the switch to negative force–frequency relation in detubulated myocytes. (3) Computer modeling suggests that Ca influx across the T-tubule membrane (predominantly via

I_{CaL}) is greater than Ca efflux (predominantly via NCX) [24]. Although the distribution of the sarcolemmal Ca ATPase is unknown (however recent work suggests that Ca extrusion via the sarcolemmal Ca ATPase occurs predominantly at the t-tubules [59]), and this imbalance will be decreased by the faster inactivation of I_{CaL} in the T-tubules (above), such modeling suggests that, due to restricted diffusion into and out of the T-tubules, Ca within the T-tubule lumen may decrease below that of the bulk extracellular solution at high stimulation rates [24, 25]. This will decrease I_{CaL} and become more marked as stimulation frequency is increased. This will decrease Ca transient amplitude, and reduce the positive inotropic effect of increasing stimulation rate. It may, however, help protect the cell from Ca overload, and the subsequent detrimental sequelae, such as spontaneous SR Ca release and arrhythmias.

13.5 Cardiac Glycosides

Cardiac glycosides, such as ouabain and strophanthidin, have been known to exert a positive inotropic effect on the heart since Withering first showed that foxglove extract could increase the strength of cardiac contraction at the end of eighteenth century (see [26] for review). This effect is due predominantly to the inhibitory action of these compounds on the sarcolemmal Na/K ATPase, which raises Na_i , slowing Ca extrusion via NCX and increasing cellular Ca load resulting in positive inotropy [27]. The resulting increase of Na_i , via NCX, increases intracellular Ca, and hence the amplitude of the systolic Ca transient and strength of contraction [26]. Interestingly, in detubulated cells the positive inotropic effect of strophanthidin is blunted; it appears likely that the T-tubules play two roles in the response to these agents [20]: first, the increase of Na_i produced by strophanthidin is similar, although slightly smaller, in detubulated cells than in control cells [20]; this presumably reflects the relative (approximately equal) loss of Na influx and efflux pathways [16], and the reduced activity of Na/K ATPase, which appears to be located predominantly in the T-tubules [16], following detubulation. Secondly, despite increases in Na_i , it is unlikely that this change will be translated functionally into an increase of intracellular Ca, because of loss of NCX in detubulated cells.

13.6 β -Adrenergic Stimulation

β -Adrenergic stimulation of ventricular muscle increases the amplitude, and abbreviates the time course, of the systolic Ca transient [1]. These changes are principally the result of protein kinase A (PKA) activity, which is stimulated directly by β -adrenergic stimulation, and Ca-calmodulin dependent protein kinase II (CaMKII), which is activated as a consequence of the PKA-induced rise of intracellular Ca. These kinases have been reported to regulate most of the major

Ca flux pathways: LTCC, RyR, SERCA and PLB have all been reported to be phosphorylated by PKA and CaMKII, and NCX by PKA. Phosphorylation has been reported to (1) increase I_{Ca} , although calmodulin (CaM) and CaMKII-induced phosphorylation also play a role in Ca dependent inactivation of I_{CaL} [28]; (2) increase the open probability of RyR and its sensitivity to trigger Ca release [29]; it has also been suggested that hyper-phosphorylation of RyR during heart failure increases Ca leak [30], although this has proved controversial [31]; (3) increase SERCA activity [32], although recent work has failed to find significant phosphorylation, and it currently seems unlikely that such phosphorylation plays a significant role in vivo [33]; (4) cause PLB to detach from SERCA, increasing the pump activity, and hence SR Ca content [34]; (5) increase NCX activity [35, 36], although some studies have shown little effect of phosphorylation on NCX [37, 38].

The most important factors in shaping the inotropic response appear to be the increase in I_{CaL} , which provides a larger trigger for SR Ca release, and increased Ca influx to load the SR with Ca; and accelerated SR Ca uptake, which abbreviates the Ca transient and increases SR Ca content, and thus the amplitude of the systolic Ca transient.

In 1985, Fabiato showed the I_{CaL} can be functionally divided into two parts: the initial fast Ca influx and the later, slowly inactivating phase [39]. The early (first 5–10 ms) component provides the trigger for Ca release from the SR, while the later component provides Ca that can be sequestered by the SR for release in a subsequent contraction. Interestingly, the large fraction of I_{CaL} in the T-tubules, and its rapid inactivation as a result of more effective Ca-dependent inactivation by Ca released from the SR (above), results in a large, rapidly inactivating I_{CaL} in the T-tubules, providing an I_{CaL} profile suited to triggering SR Ca release. Conversely, the smaller amplitude, but slowly inactivating, Ca influx across the surface membrane provides the I_{CaL} profile suited to loading the SR with Ca. Consistent with this suggestion, although detubulation slows SR Ca reloading following caffeine-induced depletion [16], this slowing is not as marked as would be predicted from the observed decrease in peak I_{CaL} : the slower inactivation of I_{CaL} in the surface membrane [14] means that Ca entry across the surface membrane is greater than might be expected from peak I_{CaL} (e.g., during an AP in a rat ventricular myocyte, 1.4 μM enters across the surface membrane vs. 3.0 μM across the T-tubule membrane); [40]. Normalizing to junctional area shows that Ca entry/ μm^2 of junction is actually higher in the surface membrane than at the T-tubules as a result of the slower inactivation (e.g., 1.4 nM in the surface membrane vs. 1.1 nM in the T-tubule membrane during a rat ventricular AP). Importantly, however, the extra Ca entry across the surface membrane occurs during the latter part of I_{CaL} , which appears to be important in loading the SR with Ca [39]. It is notable, however, that following caffeine-induced depletion of SR Ca in detubulated cells, SR Ca replenishment appears to be spatially uniform throughout the cell [41], in agreement with work suggesting rapid equilibration of Ca within the SR lumen [42]. The distribution of Ca entry, and of NCX (above; Table 13.1), may also explain why detubulation has little effect on SR Ca content [10, 16, 43].

β -Adrenergic stimulation has long been known to increase I_{CaL} [44]. However the β -adrenergic agonist isoprenaline causes a larger percentage increase in I_{CaL} in intact cells than in detubulated cells, suggesting that I_{CaL} is better coupled to β -receptor stimulation in the T-tubules than at the surface membrane [43]. This suggests that the effect of isoprenaline will be larger on the I_{CaL} “trigger” in the T-tubules than on the “loading” I_{CaL} at the surface membrane. This may lead to depletion of Ca in the T-tubule lumen (above), thus limiting the increase of I_{CaL} , particularly at the high heart rates that would be associated with β -adrenergic stimulation in the intact heart. In addition, isoprenaline increases the synchrony of Ca release in detubulated cells, as a result of the accompanying increase in SR Ca load, which will also help increase the amplitude of the Ca transient [43]. These effects may also be present under basal conditions, since it has been suggested that kinases may be tonically active [45]; such tonic activity, with better coupling to I_{CaL} at the T-tubules, may contribute to the high proportion of I_{CaL} that appears to flow across the T-tubule membrane (evidence to support this idea has recently been published [60]). The different coupling of β stimulation to I_{CaL} at the two sites may reflect molecular or ultrastructural differences, and could potentially contribute to other differences in LTCC function at the surface membrane and in the T-tubules.

The other main effect of β -adrenergic stimulation is phosphorylation of PLB, which increases the rate of Ca uptake into the SR (see [26] for review). Interestingly, phosphorylation of PLB is not altered by detubulation, suggesting that β -adrenergic signaling pathways are intact following detubulation and that PLB responds to global rather than local signaling [43]. Although not in the T-tubule membrane, recent immunohistochemical studies have shown SERCA and PLB close to the T-tubules and hence RyR [46]. This places SERCA in a region of the cell in which it can compete with sarcolemmal Ca extrusion mechanisms in the T-tubule membrane; thus sarcolemmal Ca efflux will decrease, and SR Ca content increase, until the systolic Ca transient increases sufficiently to stimulate NCX to extrude the same amount of Ca as enters the cell, achieving a new steady-state at a higher Ca transient amplitude.

13.7 Heart Failure

Myocytes from failing hearts exhibit reduced SR Ca content, and a systolic Ca transient that is smaller and slower than that in control myocytes [47]. Given the central role played by the T-tubules in EC coupling, and in synchronising Ca release throughout the cardiac myocyte, it has been speculated that T-tubule remodeling might contribute to the changes in EC coupling observed in the failing myocytes. It is notable that detubulation results in many of the functional changes observed in heart failure, including a smaller and slower Ca transient; less synchronized SR Ca release; a negative force–frequency relationship; a decreased response of I_{CaL} to β -adrenergic stimulation; and a decreased contractile response to cardiac glycosides.

Evidence to support this hypothesis is now emerging, with recent studies of T-tubule structure in myocytes from heart failure models and patients. A marked loss of T-tubules from ventricular myocytes has been described in pig, canine and rabbit models of heart failure [48–51]. In failing human ventricular myocytes, a prominent T-tubule network has been reported, although this study lacked control data [52]; more recently, it has been reported that there is an increase in the size of the T-tubules and in the number of longitudinal extensions, compared with control human heart [53]. More subtle changes in the structure of the T-tubules, including the appearance of gaps in the network, have been reported in mouse and rat models of heart failure [54, 55]. These gaps were associated with desynchronisation of Ca release, due to loss of triggered Ca release in regions of the cell lacking T-tubules. Loss of T-tubules may also result in altered spatial distribution of LTCCs, while RyR distribution remains normal, resulting in “orphaned” RyRs [55]. Such RyRs are likely to induce a delay in SR Ca release, as I_{CaL} -triggered Ca release is propagated to orphaned RyRs, thus contributing to desynchronised SR Ca release. The same subtle T-tubule reorganization has been observed in failing human heart [53]. Such desynchronisation will decrease the amplitude and slow the time course of the Ca transient, and hence contraction. Changes in T-tubule structure, and hence the proximity of any given region of cytoplasm to Ca extrusion pathways in the T-tubule membrane, might also be expected to slow Ca extrusion via NCX and thus alter the balance between SR and sarcolemmal Ca removal. In addition, an increase in Ca spark amplitude has been reported in heart failure models [56], attributed to alterations of T-tubule structure. This increased spark amplitude may increase the probability of Ca waves and arrhythmias, although the ability of a Ca spark to generate arrhythmias will depend on its access to NCX, which may be altered as a result of T-tubule reorganisation.

In addition to changes of T-tubule structure, changes in the expression of ion channels and transporters, and of their distribution between the surface and T-tubule membranes, may also occur; altered LTCC and NCX distribution could alter the efficacy of SR Ca release and Ca removal. Changes of LTCC expression, and isoform switching of the α_{1C} subunit of LTCC, have been reported in failing heart ([57]; see also the chapter by Dun, ter Keurs and Boyden); however the functional distribution of these proteins, which may be altered by changes of protein distribution or local regulation – for example by increased sympathetic stimulation – remains unknown. NCX expression and current density is increased in most hypertrophy and heart failure models [58], supporting the hypothesis that increased expression of NCX, which enhances Ca extrusion, coupled with reduced expression of SERCA, contributes to the reduction in SR Ca content observed in the failing myocardium [31]. However, whether NCX keeps its preferential localisation at the T-tubules remains to be determined. It seems likely, however, that changes in T-tubule structure and protein (co-) localisation contribute to the changes in function observed during heart failure.

Thus, although T-tubule remodeling cannot be responsible for all the changes of Ca handling that occur during heart failure, it seems possible that changes in T-tubule structure may contribute to the altered Ca handling and contraction. How these changes may interact with drug therapies used in failure is unknown.

13.8 Conclusions

The presence of key proteins involved in excitation–contraction coupling at the T-tubules, exposed to the restricted diffusion space in the T-tubule lumen, suggests that the T-tubules play an important role in determining the magnitude of the response of ventricular myocytes to inotropic interventions.

Acknowledgments The authors are grateful to the British Heart Foundation and the Wellcome Trust for financial support. We thank Dr Laurent Sallé for making a preliminary version of Fig. 13.1.

References

1. Bers DM. Cardiac excitation–contraction coupling. *Nature*. 2002;415:198–205.
2. Wier WG, Balke CW. Ca(2+) release mechanisms, Ca(2+) sparks, and local control of excitation–contraction coupling in normal heart muscle. *Circ Res*. 1999;85:770–6.
3. Bassani JW, Yuan W, Bers DM. Fractional SR Ca release is regulated by trigger Ca and SR Ca content in cardiac myocytes. *Am J Physiol*. 1995;268:C1313–9.
4. Eisner DA, Choi HS, Diaz ME, O’Neill SC, Trafford AW. Integrative analysis of calcium cycling in cardiac muscle. *Circ Res*. 2000;87:1087–94.
5. Brette F, Orchard C. Resurgence of cardiac t-tubule research. *Physiology (Bethesda)*. 2007; 22:167–73.
6. Orchard C, Brette F. t-Tubules and sarcoplasmic reticulum function in cardiac ventricular myocytes. *Cardiovasc Res*. 2008;77:237–44.
7. Brette F, Orchard C. T-tubule function in mammalian cardiac myocytes. *Circ Res*. 2003; 92:1182–92.
8. Soeller C, Cannell MB. Examination of the transverse tubular system in living cardiac rat myocytes by 2-photon microscopy and digital image-processing techniques. *Circ Res*. 1999; 84:266–75.
9. Brette F, Komukai K, Orchard CH. Validation of formamide as a detubulation agent in isolated rat cardiac cells. *Am J Physiol*. 2002;283:H1720–8.
10. Kawai M, Hussain M, Orchard CH. Excitation–contraction coupling in rat ventricular myocytes after formamide-induced detubulation. *Am J Physiol*. 1999;277:H603–9.
11. Eisner DA, Trafford AW, Diaz ME, Overend CL, O’Neill SC. The control of Ca release from the cardiac sarcoplasmic reticulum: regulation versus autoregulation. *Cardiovasc Res*. 1998;38:589–604.
12. Trafford AW, Diaz ME, Negretti N, Eisner DA. Enhanced Ca²⁺ current and decreased Ca²⁺ efflux restore sarcoplasmic reticulum Ca²⁺ content after depletion. *Circ Res*. 1997; 81:477–84.
13. Trafford AW, Diaz ME, Eisner DA. Coordinated control of cell Ca(2+) loading and triggered release from the sarcoplasmic reticulum underlies the rapid inotropic response to increased L-type Ca(2+) current. *Circ Res*. 2001;88:195–201.
14. Brette F, Salle L, Orchard CH. Differential modulation of L-type Ca²⁺ current by SR Ca²⁺ release at the T-tubules and surface membrane of rat ventricular myocytes. *Circ Res*. 2004; 95:e1–7.
15. Trafford AW, Diaz ME, O’Neill SC, Eisner DA. Comparison of subsarcolemmal and bulk calcium concentration during spontaneous calcium release in rat ventricular myocytes. *J Physiol*. 1995;488:577–86.
16. Despa S, Brette F, Orchard CH, Bers DM. Na/Ca exchange and Na/K-ATPase function are equally concentrated in transverse tubules of rat ventricular myocytes. *Biophys J*. 2003;85: 3388–96.

17. Yang Z, Pascarel C, Steele DS, Komukai K, Brette F, Orchard CH. Na⁺-Ca²⁺ exchange activity is localized in the T-tubules of rat ventricular myocytes. *Circ Res.* 2002;91:315–22.
18. Carmeliet E. Intracellular Ca²⁺ concentration and rate adaptation of the cardiac action potential. *Cell Calcium.* 2004;35:557–73.
19. Endoh M. Force-frequency relationship in intact mammalian ventricular myocardium: physiological and pathophysiological relevance. *Eur J Pharmacol.* 2004;500:73–86.
20. Fowler MR, Dobson RS, Orchard CH, Harrison SM. Functional consequences of detubulation of isolated rat ventricular myocytes. *Cardiovasc Res.* 2004;62:529–37.
21. Frampton JE, Harrison SM, Boyett MR, Orchard CH. Ca²⁺ and Na⁺ in rat myocytes showing different force-frequency relationships. *Am J Physiol.* 1991;261:C739–50.
22. Harrison SM, Boyett MR. The role of the Na⁽⁺⁾-Ca²⁺ exchanger in the rate-dependent increase in contraction in guinea-pig ventricular myocytes. *J Physiol.* 1995;482(Pt 3):555–66.
23. Salle L, Kharche S, Zhang H, Brette F. Mechanisms underlying adaptation of action potential duration by pacing rate in rat myocytes. *Prog Biophys Mol Biol.* 2008;96:305–20.
24. Pasek M, Simurda J, Christe G. The functional role of cardiac T-tubules explored in a model of rat ventricular myocytes. *Philos Transact A Math Phys Eng Sci.* 2006;364:1187–206.
25. Pasek M, Simurda J, Christe G, Orchard CH. Modelling the cardiac transverse-axial tubular system. *Prog Biophys Mol Biol.* 2008;96:226–43.
26. Bers DM. Excitation–contraction coupling and cardiac contractile force. 2nd ed. Dordrecht, Netherlands: Kluwer Academic; 2001.
27. Lee CO, Abete P, Pecker M, Sonn JK, Vassalle M. Strophanthidin inotropy: role of intracellular sodium ion activity and sodium-calcium exchange. *J Mol Cell Cardiol.* 1985;17:1043–53.
28. Brette F, Leroy J, Le Guennec JY, Salle L. Ca²⁺ currents in cardiac myocytes: old story, new insights. *Prog Biophys Mol Biol.* 2006;91:1–82.
29. Bers DM. Macromolecular complexes regulating cardiac ryanodine receptor function. *J Mol Cell Cardiol.* 2004;37:417–29.
30. Marx SO, Reiken S, Hisamatsu Y, Jayaraman T, Burkhoff D, Rosemblit N, et al. PKA phosphorylation dissociates FKBP12.6 from the calcium release channel (ryanodine receptor): defective regulation in failing hearts. *Cell.* 2000;101:365–76.
31. Bers DM, Eisner DA, Valdivia HH. Sarcoplasmic reticulum Ca²⁺ and heart failure: roles of diastolic leak and Ca²⁺ transport. *Circ Res.* 2003;93:487–90.
32. Hawkins C, Xu A, Narayanan N. Sarcoplasmic reticulum calcium pump in cardiac and slow twitch skeletal muscle but not fast twitch skeletal muscle undergoes phosphorylation by endogenous and exogenous Ca²⁺/calmodulin-dependent protein kinase. Characterization of optimal conditions for calcium pump phosphorylation. *J Biol Chem.* 1994;269:31198–206.
33. Rodriguez P, Jackson WA, Colyer J. Critical evaluation of cardiac Ca²⁺-ATPase phosphorylation on serine 38 using a phosphorylation site-specific antibody. *J Biol Chem.* 2004;279:17111–9.
34. Rodriguez P, Kranias EG. Phospholamban: a key determinant of cardiac function and dysfunction. *Arch Mal Coeur Vaiss.* 2005;98:1239–43.
35. Ruknudin A, He S, Lederer WJ, Schulze DH. Functional differences between cardiac and renal isoforms of the rat Na⁺-Ca²⁺ exchanger NCX1 expressed in Xenopus oocytes. *J Physiol.* 2000;529:599–610.
36. Schulze DH, Muqhal M, Lederer WJ, Ruknudin AM. Sodium/calcium exchanger (NCX1) macromolecular complex. *J Biol Chem.* 2003;278:28849–55.
37. Ginsburg KS, Bers DM. Isoproterenol does not enhance Ca-dependent Na/Ca exchange current in intact rabbit ventricular myocytes. *J Mol Cell Cardiol.* 2005;39:972–81.
38. Lin X, Jo H, Sakakibara Y, Tambara K, Kim B, Komeda M, et al. Beta-adrenergic stimulation does not activate Na⁺/Ca²⁺ exchange current in guinea pig, mouse, and rat ventricular myocytes. *Am J Physiol.* 2006;290:C601–8.
39. Fabiato A. Simulated calcium current can both cause calcium loading in and trigger calcium release from the sarcoplasmic reticulum of a skinned canine cardiac Purkinje cell. *J Gen Physiol.* 1985;85:291–320.
40. Brette F, Salle L, Orchard CH. Quantification of calcium entry at the T-tubules and surface membrane in rat ventricular myocytes. *Biophys J.* 2006;90:381–9.

41. Brette F, Despa S, Bers DM, Orchard CH. Spatiotemporal characteristics of SR Ca(2+) uptake and release in detubulated rat ventricular myocytes. *J Mol Cell Cardiol.* 2005;39:804–12.
42. Wu X, Bers DM. Sarcoplasmic reticulum and nuclear envelope are one highly interconnected Ca2+ store throughout cardiac myocyte. *Circ Res.* 2006;99:283–91.
43. Brette F, Rodriguez P, Komukai K, Colyer J, Orchard CH. Beta-adrenergic stimulation restores the Ca transient of ventricular myocytes lacking t-tubules. *J Mol Cell Cardiol.* 2004; 36:265–75.
44. Reuter H. The dependence of slow inward current in Purkinje fibres on the extracellular calcium-concentration. *J Physiol.* 1967;192:479–92.
45. duBell WH, Lederer WJ, Rogers TB. Dynamic modulation of excitation–contraction coupling by protein phosphatases in rat ventricular myocytes. *J Physiol.* 1996;493(Pt 3):793–800.
46. Greene AL, Lalli MJ, Ji Y, Babu GJ, Grupp I, Sussman M, et al. Overexpression of SERCA2b in the heart leads to an increase in sarcoplasmic reticulum calcium transport function and increased cardiac contractility. *J Biol Chem.* 2000;275:24722–7.
47. Bers DM. Altered cardiac myocyte Ca regulation in heart failure. *Physiology (Bethesda).* 2006;21:380–7.
48. Balijepalli RC, Lokuta AJ, Maertz NA, Buck JM, Haworth RA, Valdivia HH, et al. Depletion of T-tubules and specific subcellular changes in sarcolemmal proteins in tachycardia-induced heart failure. *Cardiovasc Res.* 2003;59:67–77.
49. He J, Conklin MW, Foell JD, Wolff MR, Haworth RA, Coronado R, et al. Reduction in density of transverse tubules and L-type Ca(2+) channels in canine tachycardia-induced heart failure. *Cardiovasc Res.* 2001;49:298–307.
50. Heinzel FR, Bito V, Biesmans L, Wu M, Detre E, von WF, et al. Remodeling of T-tubules and reduced synchrony of Ca2+ release in myocytes from chronically ischemic myocardium. *Circ Res.* 2008;102:338–46.
51. Quinn FR, Currie S, Duncan AM, Miller S, Sayeed R, Cobbe SM, et al. Myocardial infarction causes increased expression but decreased activity of the myocardial Na + –Ca2+ exchanger in the rabbit. *J Physiol.* 2003;553:229–42.
52. Louch WE, Bito V, Heinzel FR, Macianskiene R, Vanhaecke J, Flameng W, et al. Reduced synchrony of Ca2+ release with loss of T-tubules—a comparison to Ca2+ release in human failing cardiomyocytes. *Cardiovasc Res.* 2004;62:63–73.
53. Cannell MB, Crossman DJ, Soeller C. Effect of changes in action potential spike configuration, junctional sarcoplasmic reticulum micro-architecture and altered t-tubule structure in human heart failure. *J Muscle Res Cell Motil.* 2006;27:297–306.
54. Louch WE, Mork HK, Sexton J, Stromme TA, Laake P, Sjaastad I, et al. T-tubule disorganization and reduced synchrony of Ca2+ release in murine cardiomyocytes following myocardial infarction. *J Physiol.* 2006;574:519–33.
55. Song LS, Sobie EA, McCulle S, Lederer WJ, Balke CW, Cheng H. Orphaned ryanodine receptors in the failing heart. *Proc Natl Acad Sci U S A.* 2006;103:4305–10.
56. Shorofsky SR, Aggarwal R, Corretti M, Baffa JM, Strum JM, Al-Seikhan BA, et al. Cellular mechanisms of altered contractility in the hypertrophied heart: big hearts, big sparks. *Circ Res.* 1999;84:424–34.
57. Yang Y, Chen X, Margulies K, Jeevanandam V, Pollack P, Bailey BA, et al. L-type Ca2+ channel alpha 1c subunit isoform switching in failing human ventricular myocardium. *J Mol Cell Cardiol.* 2000;32:973–84.
58. Tomaselli GF, Marban E. Electrophysiological remodeling in hypertrophy and heart failure. *Cardiovasc Res.* 1999;42:270–83.
59. Chase A, Orchard CH. Ca efflux via the sarcolemmal Ca ATPase occurs only in the t-tubules of rat ventricular myocytes. *J Mol Cell Cardiol.* 2011;50:187–193.
60. Chase A, Colyer J, Orchard CH. Localised Ca channel phosphorylation modulates the distribution of L-type Ca current in cardiac myocytes. *J Mol Cell Cardiol.* 2010;49:121–131.

Part IV

Mechanisms of Acquired Arrhythmia

Chapter 14

An Overview of Spiral- and Scroll-Wave Dynamics in Mathematical Models for Cardiac Tissue

Rupamanjari Majumder, Alok Ranjan Nayak, and Rahul Pandit

14.1 Introduction

Mammalian hearts are among the most efficient electromechanical pumps in the biological world. They sustain pulmonary and systemic circulation by rhythmically pumping roughly 5 and 4.5 L/min of blood in normal adult human males and females, respectively. Aberrancy of normal cardiac rhythm is caused, *inter alia*, by abnormal rhythmicity of the pacemaker, unusual pathways of impulse propagation through the heart, interim blockages or the spontaneous generation of abnormal impulses in almost any part of the heart. These lead to conditions that are clinically identified as cardiac arrhythmias and often result in heart failure and sudden death. Cardiac arrhythmias contribute about 50% to the morbidity and mortality in patients with symptomatic heart failure. Approximately 450,000 people in the US, 90,000 in the UK [1], and 60,000 in France [2] die each year as a result of this fatal clinical disorder. It is generally believed that spiral or scroll waves of electrical activation in cardiac tissue play an important role in such arrhythmias. Thus the development of a detailed understanding of the propagation of waves of electrical activation through cardiac tissue is an interdisciplinary problem of central importance in the biological, physical and computational sciences.

This chapter provides a concise overview of the initiation, propagation and break-up of spiral and scroll waves in mathematical models of cardiac tissue. In Sect. 14.2 we begin with an introduction to the biological and experimental background required for our study of spiral- and scroll-wave dynamics in cardiac tissue; this is followed by brief descriptions of some mathematical models of cardiac tissue. Section 14.3 outlines numerical studies of models and presents representative results obtained from single-cell, two-dimensional (2D) sheet, and three-dimensional (3D) slab simulations of these models. In Sect. 14.4 we discuss

R. Majumder, A.R. Nayak, and R. Pandit (✉)

Centre for Condensed Matter Theory, Department of Physics, Indian Institute of Science, Bangalore, Karnataka 560012, India
e-mail: rahul@physics.iisc.ernet.in

the control of spiral- and scroll-wave turbulence by means of our mathematical analog of a defibrillating scheme. We end with concluding remarks in Sect. 14.5.

14.2 Experimental Background and Mathematical Models

In the clinic various forms of cardiac arrhythmias have been observed. Here we concentrate only on ventricular tachycardia (VT) and ventricular fibrillation (VF), which arise from disorders of impulse formation, impulse conduction, or both. Disorders of impulse formation relate to the abnormal discharge rate of the sino-atrial node (SAN) or premature contraction of the heart, resulting from the formation of ectopic foci. Disorders of impulse conduction include conduction delays and blocks that result in bradyarrhythmias and tachyarrhythmias. Tachyarrhythmias, such as VT and VF, occur when delays and blocks produce reentrant excitations.

To develop a mathematical model for cardiac tissue, several experimental inputs are required. Such inputs are obtained principally from patch-clamp experiments that are now capable of providing detailed information about parameters that govern the operation of ion channels in a cardiac cell. Each ion channel is modeled via Hodgkin–Huxley-type equations (Sect. 14.2.1). This requires parameters that include channel conductances and rate constants, which govern the behaviors of gating variables. To go from a single-cell model to a model for cardiac tissue we need, in addition, the cell’s membrane capacitance per unit area and diffusion coefficients along the various directions. These again can be obtained from patch-clamp experiments, and a realistic physiological model can then be developed by fitting these parameters in such a way that it can reproduce all the desired experimentally observed physiological properties at cell and tissue levels.

Excitability is an important property of cardiac tissue because it can support various spiral waves of electrical activation, such as a single spiral or multiple spirals that may annihilate or regenerate by random collision with each other; this has been known since the pioneering studies of Garrey [3, 4], Allessie et al. [5, 6], and Mines [7, 8]; these can arise because of anatomical or functional reentry. A single spiral wave, whose core is stationary, leads to monomorphic VT, whereas a drifting spiral is the cause of polymorphic tachycardia [9]. A drifting spiral or scroll wave occasionally gets attached to a small local inhomogeneity in its path, and this leads to a polymorphic-to-monomorphic tachycardia transition [9–13]. Furthermore, the tips of the spiral waves (spiral cores) or, in three dimensions, the lines connecting the spiral tips on all the layers of the scroll waves (scroll filaments) can drift towards the edges of the tissue and get terminated.

14.2.1 Mathematical Models of Cardiac Tissue

Cardiac tissue is excitable in the sense that sub-threshold perturbations decay, whereas super-threshold ones lead to an action potential (AP, Fig. 14.1a). Once

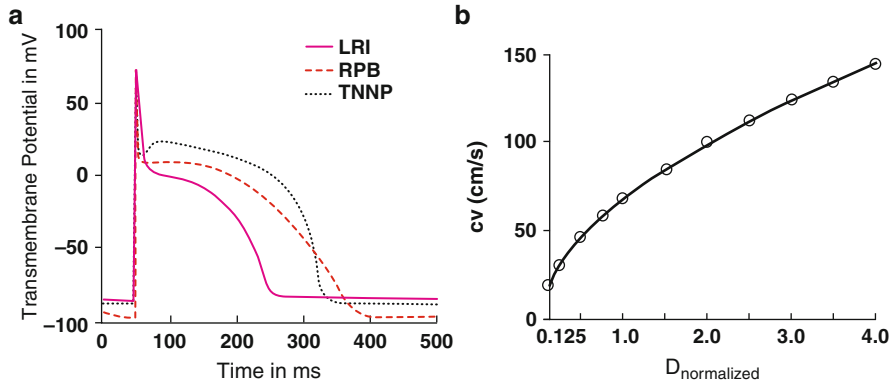


Fig. 14.1 (a) Action potentials for realistic ionic models: LRI (solid), RPB (dashed) and TNNP (dotted), obtained by applying a current pulse of amplitude $100 \mu\text{A}/\text{cm}^2$ for 1 ms. (b) A plot of conduction velocity CV versus the normalized diffusion coefficient $D_{\text{normalized}}$, i.e., the ratio of D and its maximal value $D_{\text{max}} = 0.00154 \text{ cm}^2/\text{ms}$; the solid line indicates a fit of the form $CV = AD^{\alpha}$; we find $A \cong 67.3$ and $\alpha \cong 0.5$, which is consistent with $CV \propto \sqrt{D}$

excited, the medium cannot be reexcited for a subsequent interval of time known as the refractory period. In general cardiac tissue is modeled by using a reaction-diffusion equation of the form

$$\frac{\partial V}{\partial t} = \nabla \cdot (D \nabla V) - \frac{I_{\text{ion}} + I_{\text{stimulus}}}{C_m}, \quad (14.1)$$

where V is the transmembrane potential, D is related to the conductivity of cardiac tissue, I_{ion} is the sum of the currents conducted by all the ion channels, I_{stimulus} is the excitation current, and C_m is the total cell-membrane capacitance per unit surface area. In general D should be a tensor, but at the simplest level of modeling it is assumed to be a scalar. Different models for cardiac tissue are distinguished by different forms for I_{ion} . Three common models are (a) the Luo–Rudy phase I (LRI) model, (b) the reduced Priebe–Beuckelmann (RPB) model, and (c) the model of ten Tusscher, Noble, Noble, and Panfilov (TNNP). The LRI model, based on guinea-pig data, includes ion pumps and has six ionic current components:

$$I_{\text{LR}} = I_{\text{Na}} + I_{\text{si}} + I_K + I_{K1} + I_{Kp} + I_b, \quad (14.2)$$

with current densities I_{Na} , I_{si} , I_K , I_{K1} , I_{Kp} , I_b for the fast inward Na^+ current, the L -type slow inward Ca^{2+} current, the slow outward time-dependent K^+ current, the time-independent K^+ current, the plateau K^+ current, and the total background current, respectively. Other model parameters and equations are given in [14].

The reduced PB model (RPB) [15] is the reduced version of the original Priebe–Beuckelmann (PB) [16] model. It aims at improving computational efficiency without losing any basic tissue properties such as the AP shape. The reformulated PB model reduces the total number of variables that have to be used. The model has a

single delayed rectifier K⁺ current, as opposed to individual rapid and slow components. It excludes the dynamics of intracellular ion concentrations by approximating the variables by suitable constants as described by Bernus et al. [15]. The total current is

$$I_{\text{RPB}} = I_{\text{Na}} + I_{\text{Ca}} + I_{\text{to}} + I_{\text{K}} + I_{\text{K1}} + I_{\text{NaCa}} + I_{\text{NaK}} + I_{\text{bNa}} + I_{\text{bCa}}, \quad (14.3)$$

with I_{Na} the fast inward Na⁺ current, I_{Ca} the slow inward Ca²⁺ current, I_{to} the transient outward current, I_{K} the delayed rectifier K⁺ current, I_{K1} the inward rectifier K⁺ current, I_{NaK} the Na⁺/K⁺ pump current, I_{NaCa} the Na⁺/Ca²⁺ exchanger current, and I_{bNa} and I_{bCa} the background Na⁺ and Ca²⁺ currents, respectively.

The TNNP model, by far the most explicit model available for computational studies, fits experimentally recorded APD properties of the human myocardium, is based on experimental data on most of the major ionic currents in human cardiac tissue, and includes simple calcium dynamics, which allows for realistic modeling of calcium transients, calcium current inactivation, and a positive contraction staircase. The total ionic current is

$$I_{\text{ion}} = I_{\text{Na}} + I_{\text{CaL}} + I_{\text{to}} + I_{\text{Ks}} + I_{\text{Kr}} + I_{\text{K1}} + I_{\text{NaCa}} + I_{\text{NaK}} + I_{\text{pCa}} + I_{\text{pK}} + I_{\text{bNa}} + I_{\text{bCa}}, \quad (14.4)$$

where I_{CaL} is the *L-type* slow inward Ca²⁺ current and I_{pCa} and I_{pK} are the plateau Ca²⁺ and K⁺ currents.

Each current, in the models above, is described by Hodgkin–Huxley-type equations, i.e., for ion channel i the current is

$$I_i(V_m, t) = (V_m - E_i)g_i, \quad (14.5)$$

where E_i is the reversal potential for the channel i and g_i its conductance. We must also include differential equations that govern the behaviors of voltage-gated ion channels; these are described in detail in [14].

It is often advantageous to use simple, two-variable models with a normalized transmembrane potential e and a slow recovery variable g , into which all the essential physics of ion channels is subsumed. One example of such a model is the Panfilov [17, 18] model:

$$\frac{\partial e}{\partial t} = \nabla^2 e - f(e) - g; \quad \frac{\partial g}{\partial t} = \varepsilon(e, g)(ke - g). \quad (14.6)$$

Here $f(e) = C_1e$ when $e < e_1$, $f(e) = -C_2e + a$ when $e_1 \leq e \leq e_2$ and $f(e) = C_3(e - 1)$ when $e > e_2$. $\varepsilon(e, g) = \varepsilon_1$ when $e < e_2$, $\varepsilon(e, g) = \varepsilon_2$ when $e > e_2$, $\varepsilon(e, g) = \varepsilon_3$ when $e < e_1$ and $g < g_1$, $e_1 = 0.0026$, $e_2 = 0.837$, $C_1 = 20$, $C_2 = 3$, $C_3 = 15$, $a = 0.06$ and $k = 3$. The dynamics of the recovery variable is specified by the function $\varepsilon(e, g)$. The recovery time constant for small e and g is specified by ε_3^{-1} . It approximately corresponds to the relative refractory period. The recovery

time constant for relatively large g and intermediate e is specified by ε_1^{-1} . Physiologically this corresponds to the wave-front, wave-back and to the absolute-refractory periods.

14.3 Numerical Studies and Representative Results

We have performed extensive numerical studies of these four models [14]. Here we give illustrative results from single-cell, 2D, and 3D simulations. For computing single-cell APs [(14.7) below] we use a time step $\delta t = 0.01$ ms for LRI, RPB and TNNP models. For studies in 2D and 3D, we use the forward-Euler method for time marching with time steps of 0.11 ms, 0.01 ms, 0.02 ms, and 0.02 ms for Panfilov, LRI, RPB, and TNNP models, respectively; and we integrate the Hodgkin–Huxley-type equations for the different gating variables (for LRI, RPB, and TNNP models) by using the Rush–Larsen scheme; furthermore, we use a finite-difference method with spatial steps of $\delta x = \delta y = 0.5$ for the Panfilov model, $\delta x = \delta y = 0.225$ mm for the LRI model, $\delta x = \delta y = 0.225$ mm for the 2D-TNNP model and $\delta x = \delta y = 0.225$ mm, $\delta z = 0.1$ mm for the 3D-TNNP. A five-point stencil is used for computing the Laplacian on a square simulation domain in 2D, whereas in 3D we use a seven-point stencil on a rectangular slab. For studies in 2D the domain contains 400×400 grid points for the Panfilov and LRI models and 600×600 grid points for the TNNP model. For studies in 3D we use $\delta z = \delta x$ for both Panfilov and LRI models, but $\delta z = 0.01$ cm for the TNNP model; we use $N_z = 20$ grid points along the z direction in 3D domains. We use Neumann (no-flux) boundary conditions (i.e., $\nabla V \cdot \hat{n} = 0$, where \hat{n} is the normal to the surface of the tissue drawn at the boundary) and test the accuracy of our numerical schemes by varying both the time and space steps [19].

14.3.1 Single Cell

At the single-cell level (14.1) becomes the ordinary differential equation (ODE):

$$\frac{dV}{dt} = \frac{I_{\text{ion}} + I_{\text{stim}}}{C_m} \quad (14.7)$$

with the ionic current given by (14.2), (14.3), or (14.4) for LRI, RPB, or TNNP models, respectively. Even though the Panfilov model is extremely simple, compared to the LRI, RPB, and TNNP models, it captures several essential properties of the spatiotemporal evolution of the transmembrane potential; e.g., the action potential of the Panfilov model contains both the absolute and relative refractory periods, predominantly seen in advanced models.

Table 14.1 Comparison between single-cell behaviors of four mathematical models of cardiac tissue

Model	APD (ms)	$V_{\text{threshold}}$ (mV)	V_{rest} (mV)	V_{plateau} (mV)	V_{notch} (mV)	CV_{\max} (cm/s)
Panfilov	330	–	-80	–	–	–
LRI	366	-60	-84	17.7	12.4	–
RPB	357.2	-60.2	-90.2	~13	~8.5	70.4
TNNP	286.8	-62.8	-86.2	22.6	13.6	68.8

The cardiac APs that follow from (14.7) for the LRI, RPB, and TNNP models are shown in Fig. 14.1a; to obtain these, we apply a current pulse of $100 \mu\text{A}/\text{cm}^2$ for 1 ms to a single cell of each type. From the plots in Fig. 14.1a we obtain the AP duration (APD), threshold potential $V_{\text{threshold}}$, resting membrane potential V_{rest} , maximum plateau potential V_{plateau} , potential at AP notch V_{notch} , and maximum conduction velocity CV_{\max} . We list these in Table 14.1 for all the four models above. The threshold potential is defined as the minimum voltage that is required for excitation of the cell. Its value is (as listed in Table 14.1) always much higher than the resting-state potential, so that the cells do not get excited because of slight ionic imbalances occurring within them. In other words, the relatively high value of $V_{\text{threshold}}$ indicates that proper excitation of a cardiac cell requires a large ionic-concentration drop across the cell wall. For a good review on cardiac propagation, we refer the reader to [20].

14.3.2 Homogeneous Two-Dimensional Sheet of Cells

A 2D sheet of cardiac cells is modeled by (14.1) in which the cells are coupled via the diffusive term [14]. Given this diffusive coupling, an AP generated from one cell can excite its neighboring cells and thus spread out as an expanding wave. The initial excitation is followed by a refractory period, so a second wave cannot follow the first one immediately. When two waves collide in such a medium, they cannot pass through each other because their wakes (i.e., the part of the medium that has passed into the refractory phase just behind the tail of the excitatory wave) are nonexcitable, so they annihilate [14]. It is known that the propagation velocity of a reaction-diffusion-type equation is directly proportional to the square root of the diffusion coefficient D [21]. To observe such a relation in the TNNP model of cardiac tissue, we measure CV by using different values of D and by injecting a plane wave into the homogeneous domain via a stimulation current of $150 \mu\text{A}/\text{cm}^2$ for 3 ms at the left boundary. The data in Fig. 14.1b are consistent with $CV \propto \sqrt{D}$. We also observe that CV and the wavelength λ , which is roughly the product of the refractory period and the CV , are 68.28 cm/s and 13.2 cm, respectively.

Generally, two methods are used to initiate spiral waves in simulations [9, 14, 15, 22] and experiments [9, 10], namely, (a) the S1–S2 cross-field protocol and (b) the S1–S2 parallel-field protocol. In the cross-field method, a super-threshold stimulus

S2 is applied at the boundary and perpendicular to the S1 stimulus. In the parallel-field method, S2 is applied parallel to the refractory tail of the S1 stimulus but not over the entire length of the domain. We use the parallel-field protocol.

To initiate a spiral wave in the TNNP model in a homogeneous domain, we inject a plane wave into the domain via an S1 stimulus of strength $100 \mu\text{A}/\text{cm}^2$ for 3 ms at the left boundary. We choose D to be $0.000385 \text{ cm}^2/\text{ms}$ (approximately 1/4th of its original value, 0.00154) in the beginning of our simulation to initiate a spiral wave. We then apply an S2 stimulus of strength $450 \mu\text{A}/\text{cm}^2$ for 3 ms after 560 ms and just behind the refractory tail of S1 ($x = 360, 1 \leq y \leq 550$). We then reset the conductivity to its original value after 880 ms. This procedure yields the fully developed spiral wave as shown in Fig. 14.2a at $t = 976$ ms; and this state is used as the initial condition for our subsequent studies. This procedure forms a stable spiral wave in a homogeneous domain [14]; its period of rotation is 263 ms as shown in Fig. 14.2b. However, it can also evolve to a state with spatiotemporal chaos. Whether it does so or not depends on the conductances of specific ion channels.

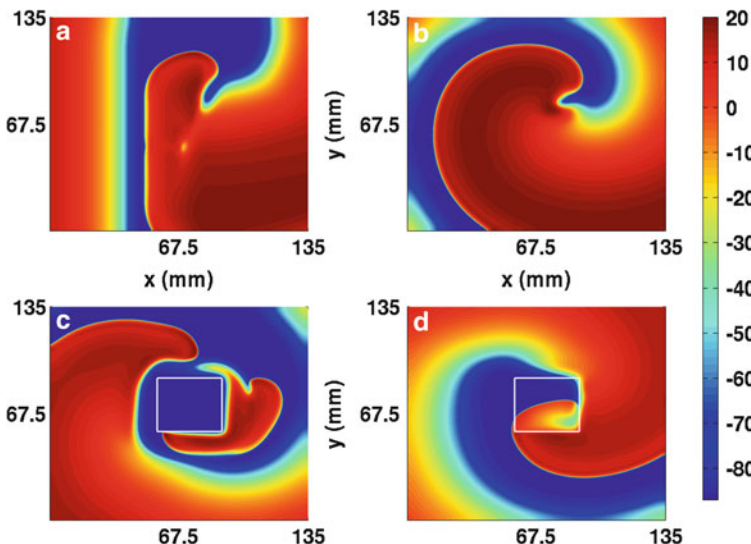


Fig. 14.2 Pseudocolor plots of the transmembrane potential V from 2D simulations of the TNNP model: (a) a fully developed spiral wave at time $t = 976$ ms that is used as an initial condition to study spiral-wave dynamics in this model; (b) stable rotating spiral state in a homogeneous domain at time $t = 2.4$ s; (c) spiral turbulence (ST) state with broken spirals at time $t = 2.4$ s, in the presence of a square conduction inhomogeneity (obstacle) of side length $l = 3.375$ cm, whose bottom-left corner is placed at (56.25 mm, 56.25 mm); (d) single-spiral state with complex periodic behavior in the same system at time $t = 2.4$ s, in the presence of a square ionic inhomogeneity of side length $l = 3.375$ cm, whose bottom-left corner is placed at (56.25 mm, 56.25 mm)

14.3.3 Two-Dimensional Sheet of Cells with Inhomogeneities

Cardiac tissue contains various types of heterogeneities [14] that can arise because of (a) genetic disorders, (b) scar tissue formed after a myocardial infarction, (c) major blood vessels, (d) connective tissue, (e) cells other than myocytes (e.g., fibroblasts), or (f) inter-cellular coupling. Therefore, it is important to understand the role of such heterogeneities on spiral- and scroll-wave dynamics in both experimental and numerical studies. We give illustrative studies for the TNCP model.

Conduction inhomogeneities, like scar tissues or major blood vessels, can affect spiral waves in several ways. In some cases such inhomogeneities can anchor a spiral wave or eliminate it completely [11, 13]; the larger the obstacle the more likely is the anchoring; however, even if the obstacle is large, the wave might not attach to it. Furthermore, an obstacle can convert multiple spirals to a single anchored spiral [12]. Such behavior has also been seen in numerical simulations of spiral-wave turbulence in models for cardiac tissue [14, 23, 24].

We introduce an obstacle in our 2D simulation domain by setting $D = 0$ at the location of the obstacle. The obstacles used in our study are square or circular in shape. Furthermore, we use Neumann (i.e., no-flux) boundary conditions on the boundaries of the obstacle.

Our systematic study of spiral-wave dynamics in the presence of an obstacle [14, 24] shows that the initial condition of Fig. 14.2a, which evolves to the stable rotating spiral of Fig. 14.2b in the absence of an obstacle, can give rise to one of the following results (a) the spiral wave can continue to rotate, without being anchored to the obstacle, and eventually break down to yield the state ST with spiral-wave turbulence; (b) the tip of the spiral wave can get anchored to the obstacle to give the state RS in which the anchored spiral rotates around the obstacle; (c) all spiral waves can be absorbed by the boundaries so that the system evolves into the quiescent state Q. A representative pseudocolor plot of V , for the ST case in the presence of a square obstacle, is shown in Fig. 14.2c. We also obtain similar results if the initial condition is a broken-spiral-wave state rather than one in which we have a single rotating spiral wave.

By changing the position of the obstacle, we find that spiral-wave dynamics depends sensitively on the position of an obstacle [14, 24]: small changes in the position of the obstacle can change the final state of the system from, say, ST to RS or Q. We have suggested [14, 24] that this arises because of an underlying fractal-type basin boundary between the domains of attraction of ST, RS, and Q states. We also observe similar sensitive dependence of spiral-wave dynamics on the position of an obstacle, if we use a circular obstacle; for details we refer the reader to [14, 24].

Cardiac tissue can contain other types of inhomogeneities that originate from changes in single-cell properties, which are caused in turn by changes in the chemical environment or metabolic modifications [25]. Collections of such cells are referred to as ionic inhomogeneities; some of their properties, like the conductances of ion channels, are slightly modified relative to those of normal cardiac cells.

We find that ionic inhomogeneities can also have dramatic effects on spiral-wave dynamics. In particular, they can eliminate spiral waves, or anchor a spiral wave, but with richer dynamics than that in the case of a conduction inhomogeneity. For example, our ionic-inhomogeneity studies in the Panfilov model [14, 24] show that such inhomogeneities can lead to the coexistence of the following types of behaviors: (a) ST outside the inhomogeneity and quasiperiodic behavior inside it; (b) an unbroken RS outside the inhomogeneity and broken spiral waves (ST) inside it; (c) a spiral anchored to the inhomogeneity with different quasiperiodic temporal evolution of V outside and inside the inhomogeneity. We have observed such complex behaviors in our numerical studies of ionic inhomogeneities in LRI, RPB and TNNP models [14]. Here we restrict ourselves to representative results for the TNNP model. We introduce square ionic inhomogeneities by changing the conductances G_{CaL} or G_{pCa} . We use the initial condition shown in Fig. 14.2a, which evolves to a stable rotating spiral (Fig. 14.2b) in the absence of an ionic inhomogeneity. Our numerical studies for the TNNP model show that this inhomogeneity can cause the elimination of spiral waves or give rise to complex periodic behaviors or have no significant effect on the spiral waves. Precisely which one of these behaviors is obtained depends on the position of the inhomogeneity. A representative case of the coexistence of spiral waves with different quasiperiodic behaviors inside and outside the inhomogeneity is shown in Fig. 14.2d. We also obtain similar results if the initial condition is a broken-spiral-wave state rather than a rotating spiral. Similar complex periodic oscillations and coexistence have also been reported in experiments [26]; however, it has been suggested that the oscillations observed in these experiments are caused by the interplay of conduction inhomogeneities and partial conduction blocks [14, 24]. For more information on studies in 2D, we refer the reader to [27, 28].

14.3.4 Homogeneous Three-Dimensional Slab of Tissue

In this section we compare 3D simulations of Panfilov, LRI, and TNNP models. In the 3D slab geometry, sheets of cells are stacked one on top of the other with an inter-layer coupling. Furthermore, D is taken to be a tensor with elements $D_{ij} \neq 0$ for any value of i, j . In the isotropic case, we have $D_{ij} = 0$ for $(i \neq j)$, $D_{xx} = D_{yy} = D_{\parallel}$ and $D_{zz} = D_{\perp}$. D_{\parallel} is the coefficient of diffusion along and perpendicular to, but in the plane of, the axis of cardiac muscle fibers; its value is the same as the value of D in the homogeneous 2D case. D_{\perp} is different from D_{\parallel} because of the difference in conduction velocities in the longitudinal and transmural directions in cardiac tissue. Typically we use the values $0.001 \text{ cm}^2/\text{s}$ and $0.0002 \text{ cm}^2/\text{s}$ for D_{\parallel} and D_{\perp} , respectively [25]. Representative isosurface and volume plots of V from our simulations for homogeneous 3D Panfilov and TNNP models are shown in Fig. 14.3a, c.

The effects of cardiac-muscle-fiber rotation in 3D have been studied for LRI and RPB models. We discuss briefly the effects of such fiber rotation on Panfilov, LRI,

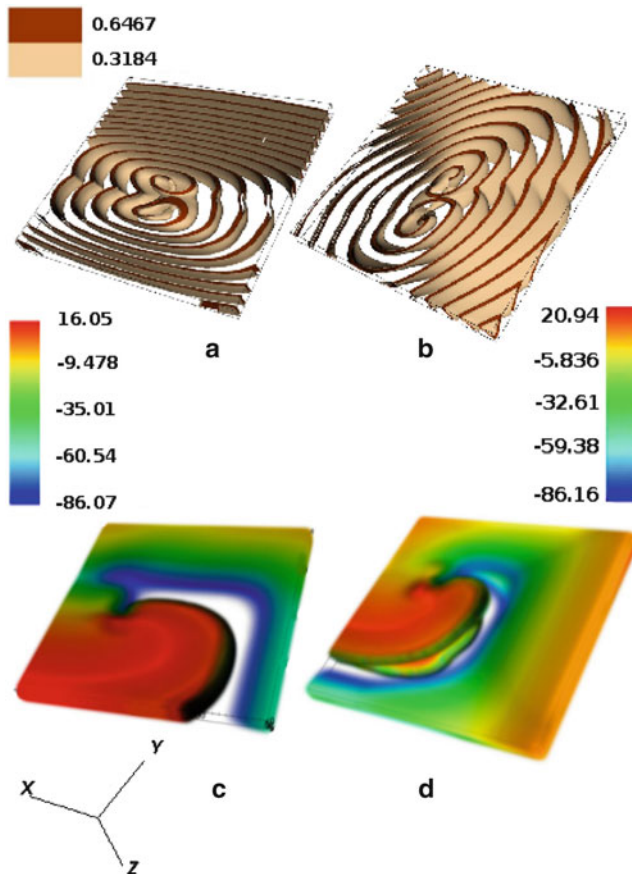


Fig. 14.3 (a) Isosurface plot of the transmembrane potential V in the homogeneous 3D Panfilov model at time $t = 1.6$ s; (b) the analog of (a) but for the 3D Panfilov model with fiber rotation and a rotation angle 40° ; (c) a volume plot of the transmembrane potential V in the homogeneous 3D TNRP model at time $t = 0.92$ s; (d) the analog of (c) but for the 3D TNRP model with fiber rotation and for a rotation angle 40°

and TNRP models; the diffusion tensor now has the form [29] $D_{11} = D_{||}\cos^2\theta(z) + D_{\perp 1}\sin^2\theta(z)$, $D_{22} = D_{||}\sin^2\theta(z) + D_{\perp 1}\cos^2\theta(z)$, $D_{33} = D_{\perp 2}$, $D_{13} = D_{31} = D_{23} = D_{32} = 0$, $D_{12} = D_{21} = (D_{||} - D_{\perp 1})\sin\theta(z)\cos\theta(z)$. $D_{||}$ is the diffusivity for propagation parallel to the fiber axis, $D_{\perp 1}$ the diffusivity perpendicular to this axis but in-plane, and $D_{\perp 2}$ the diffusivity perpendicular to the fiber axis in the transmural direction; $\theta(z)$ is the twist angle along the transmural direction. The total fiber rotation from the endocardium to the epicardium is $\theta(z) = \alpha L_z$, where α is the fiber-rotation rate. We assume that $\theta(z)$ changes continuously [29] from $-\theta_{\text{endocardial wall}}$ to $+\theta_{\text{epicardial wall}}$. For 3D studies on the Panfilov and TNRP models we use slabs of dimensions $20 \text{ cm} \times 20 \text{ cm} \times 4 \text{ mm}$ and $9 \text{ cm} \times 9 \text{ cm} \times 2 \text{ mm}$, respectively.

To study the effect of an initial filament twist on a scroll wave [25], we begin with a stack of 2D spiral waves; spirals in successive planes in the z direction are twisted with respect to each other; this is done by evolving a spiral wave in a 2D simulation and then using the spiral waves, separated by time intervals of, say, $50\delta t$, for successive planes. Thus the initial condition is a scroll wave that is twisted transmurally. For the homogeneous Panfilov and LRI models [25], with parameters belonging to the weak (stable) meander regimes of the corresponding spirals in 2D, the initially twisted scroll is seen to unwind and finally ends up with a straight filament. For the LRI model this phenomenon occurs for initial twist angles of over 300° , from the top of the filament to its bottom, in 9 mm thick slabs as well as for twist angles of 720° , i.e., two rotations [30]. We obtain analogous results for the Panfilov model.

The analogs of the calculations we have described in the previous paragraph can also be carried out with fiber rotation; we give illustrative results from our studies of the Panfilov and TNNP models in 3D. We begin with a straight scroll wave and observe that the mere introduction of fiber rotation stimulates bending and twisting of the scroll filament. For fixed tissue thickness we vary the rate of fiber rotation. The wave develops a complicated toroid-like structure as illustrated in Fig. 14.3b for the Panfilov model; this structure is unusually stable against both weak and strong perturbations [30]. A representative result from our simulations for the fiber-rotated 3D TNNP model is shown in Fig. 14.3d.

Scroll-wave break-up has been observed in the LRI model [25, 31–33]. With an initial twist in the scroll filament, a scroll wave in the strong-meander regime breaks up if the angle of twist is greater than a critical value; it then forms a small, less twisted filament along with a scroll ring whose radius shrinks as time increases. The scroll ring ultimately disappears and its counterpart exhibits behavior similar to its parent, depending on its initial twist. For details we refer the reader to [31–33]. For more information regarding the dynamics of scroll waves in 3D cardiac tissue, we refer the reader to [34].

14.4 The Control of Spiral-Wave Turbulence

Defibrillation is the application of electrical shocks to control the fibrillating heart and to restore its normal rhythm. The success rate of defibrillation is variable and sometimes it can also leave the heart damaged [1]. In external defibrillation, one applies electrical shocks (5 kV) across the patient's chest to depolarize all the cardiac cells simultaneously. This silences the ventricle electrically and forces all the cardiac cells, including the SAN and the atrio-ventricular node (AVN), to reset and resume normal electrophysiological activity [2].

The analog of defibrillation in mathematical models of cardiac tissue is the control of spiral-wave activity, preferably with low-amplitude voltage pulses. Several schemes have been suggested; here we discuss the control scheme proposed by Sinha et al. [35] for the Panfilov model. This uses very low-amplitude pulses

(of order mV) for a brief duration (of order 100 ms) and over a coarse mesh of lines on the model ventricle [35]. This scheme, if realized in an internal defibrillator, would constitute a significant advance in these devices, because it would lead to the development of low-amplitude defibrillation, which is a major challenge.

In the Panfilov model the analog of VF arises when the system evolves to a transient state in which large spirals break down [35]. The lifetime τ_L of this state increases rapidly with L , the linear size of the system. Qualitatively, this agrees with the experimental finding that hearts of small mammals are less prone to fibrillation than those of large mammals. For time scales longer than τ_L , a quiescent state is established with $e = g = 0$. In the 2D control scheme, the simulation domain (size $L \times L$) is divided into K^2 smaller blocks bounded by a mesh of lines. A super-threshold pulse is applied to the e -field on the selected mesh of lines. This pulse, applied for a short length of time τ_c , effectively simulates Neumann boundary conditions (for the block bounded by the mesh) because the region near the mesh lines becomes refractory. The mesh lines then absorb the spiral waves formed inside each block and spiral-wave turbulence is eliminated. For a generalization to the 3D case and for the details of the control protocol we refer the reader to [35]. We have extended this control scheme to the LRI, RPB, and TNNP models [14] both for homogeneous simulation domains and domains with inhomogeneities. We give representative results for this control scheme for the 2D TNNP model, both with and without inhomogeneities in Fig. 14.4a–d.

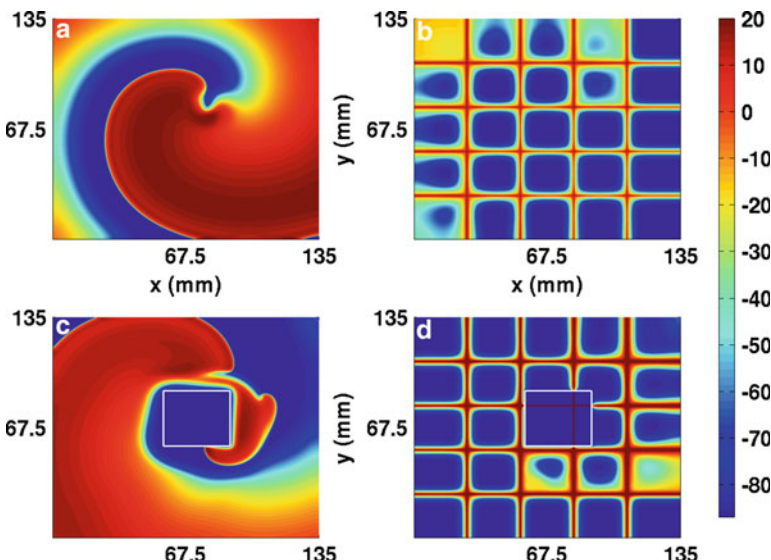


Fig. 14.4 Spiral-wave control in the 2D TNNP model by the application of a control pulse of amplitude $27.75 \mu\text{A}/\text{cm}^2$ for $t = 20$ ms over a square mesh with each block of size $L/K = 27$ mm, i.e., the simulation domain is divided into 5^2 square blocks. Panels (a) and (b) are pseudocolor plots of V for the homogeneous case at time $t = 0$ ms and $t = 280$ ms, respectively. Panels (c) and (d) are the analogs of (a) and (b) but in the presence of a square inhomogeneity of side length $l = 33.75$ mm, whose *bottom-left corner* is placed at (56.25 mm, 56.25 mm)

14.5 Conclusions

We have provided a brief overview of recent studies of spiral- and scroll-wave dynamics in mathematical models of cardiac tissue. These are believed to be important in developing an understanding of life-threatening cardiac arrhythmias like VT and VF. In addition to giving a summary of Panfilov, LRI, RPB, and TNNP models, we have described how spiral and scroll waves can be initiated in such models, how they evolve subsequently, how they interact with conduction and ionic inhomogeneities, how they are affected by the rotation of muscle fibers, and how they may be controlled. This sets the stage for systematic numerical studies of the analogs of low-amplitude defibrillation schemes in realistic mathematical models of cardiac tissue like the TNNP model in the presence of inhomogeneities. In future studies we plan to explore such schemes with even more features than we have discussed here. In particular, we expect to extend our studies to anatomically realistic simulation domains, to bidomain models, and to models that include the effects fibroblasts and their coupling to myocytes. Our eventual goal is to bring our *in silico* studies as close as possible to their *in vitro* and *in vivo* counterparts. We hope that our introduction to this challenging interdisciplinary field will stimulate further studies, especially ones that bring together techniques from physics, nonlinear dynamics, and biology.

Acknowledgments We thank T. K. Shajahan and P. Perlekar for discussions, DST, UGC, CSIR (India), and Microsoft Research for support and SERC (IISc) for computational resources.

References

1. Arrhythmia Awareness Week: [homepage on the Internet]. [cited 2009 June]; Available at <http://www.aaaw.org.uk/images/facts.swf>.
2. Zhou H, Hou KMN, Ponsonnaille J, Gineste L, De Vaulx C. A Real-Time Continuous Cardiac Arrhythmias Detection System: RECAD. Proceedings of the 27th IEEE Annual Conference on Engineering in Medicine and Biology; 2005.
3. Garrey WE. Auricular fibrillation. *Physiol Rev.* 1924;4:210.
4. Jalife J, Delmar M, Davidenko J, Anumonwo JMB. Basic cardiac electrophysiology for the clinician. Armonk, NY: Futura; 1999.
5. Allessie MA, Bonke FIM, Schopman FJC. Circus movement in rabbit atrial muscle as a mechanism of tachycardia. *Circ Res.* 1973;33:54.
6. Allessie MA, Bonke FIM, Schopman FJC. Circus movement in rabbit atrial muscle as a mechanism of tachycardia. III. The “leading circle” concept: a new model of circus movement in cardiac tissue without the involvement of an anatomical obstacle. *Circ Res.* 1977;41:9.
7. Mines GR. On dynamic equilibrium in the heart. *J Physiol.* 1913;46:349.
8. Mines GR. On circulating excitations in heart muscles and their possible relation to tachycardia and fibrillation. *Trans R Soc Can.* 1914;IV:43.
9. Pertsov AM, Davidenko JM, Salomonsz R, Baxter WT, Jalife J. Spiral waves of excitation underlie reentrant activity in isolated cardiac muscle. *Circ Res.* 1993;72:631.
10. Davidenko JM, Perstov AV, Salomonsz R, Baxter W, Jalife J. Stationary and drifting spiral waves of excitation in isolated cardiac muscle. *Nature.* 1992;355:349.
11. Ikeda T, Yashima M, Uchida T, Hough D, Fishbein MC, et al. Attachment of meandering reentrant wave fronts to anatomic obstacles in the atrium. *Circ Res.* 1997;81:753.

12. Valderrabano M, Kim YH, Yashima M, Wu TJ, Karagueuzian HS, et al. Obstacle-induced transition from ventricular fibrillation to tachycardia in isolated swine right ventricles. *J Am Coll Cardiol.* 2000;36:2000–8.
13. Lim ZY, Maskara B, Aguel F, Emokpae R, Tung L. Spiral wave attachment to millimeter-sized obstacles. *Circulation.* 2006;114:2113.
14. Shajahan TK, Nayak AR, Pandit R. Spiral-wave turbulence and its control in the presence of inhomogeneities in four mathematical models of cardiac tissue. *PLoS One.* 2009;4(3):e4738. [cited 2009, September] Available from <http://www.plosone.org/article>. doi:10.1371/journal.pone.0004738.
15. Bernus O, Wilders R, Zemlin CW, Verschelde H, Panfilov AV. A computationally efficient electrophysiological model of human ventricular cells. *Am J Physiol Heart Circ Physiol.* 2002;282:H2296.
16. Priebe L, Beuckelmann J. Simulation study of cellular electric properties in heart failure. *Circ Res.* 1998;82:1206.
17. Panfilov AV, Hogeweg P. Spiral breakup in a modified FitzHughNagumo model. *Phys Lett A.* 1993;176(5):295299.
18. Panfilov AV. Spiral breakup as a model of ventricular fibrillation. *Chaos.* 1998;8(1):57–64.
19. Clayton R, Panfilov A. A guide to modeling cardiac electrical activity in anatomically detailed ventricles. *Prog Biophys Mol Biol.* 2008;96:14.
20. Kleber AG, Rudy Y. Basic mechanisms of cardiac impulse propagation and associated arrhythmias. *Physiol Rev.* 2004;84:431–88.
21. Smith NP, Hunter PJ, Pullan AJ, Nash MP. An Anatomically Realistic Cardiac Model. Proceedings of the 11th Conference of the ESB, 1998, July 8–11; Toulouse: France.
22. ten Tusscher KHWJ, Noble D, Noble PJ, Panfilov AV. A model for human ventricular tissue. *Am J Physiol Heart Circ Physiol.* 2004;286:1073–89.
23. Xie F, Qu Z, Garfinkel A. Dynamics of reentry around a circular obstacle in cardiac tissue. *Phys Rev E.* 1998;58:6355.
24. Shajahan TK, Sinha S, Pandit R. Spiral-wave dynamics depends sensitively on inhomogeneities in mathematical models of ventricular tissue. *Phys Rev E.* 2007;75:011429.
25. Qu Z, Kil J, Xie F, Garfinkel A, Weiss JN. Scroll wave dynamics in a three-dimensional cardiac tissue model: roles of restitution, thickness, and fiber rotation. *Biophys J.* 2002;78: 2761–75.
26. Hwang SM, Kim TY, Lee KJ. Complex-periodic spiral waves in confluent cardiac cell cultures induced by localized inhomogeneities. *Proc Natl Acad Sci.* 2005;102:10363.
27. Panfilov AV. Theory of reentry. In: Zipes DP, Jalife J, editors. *Cardiac electrophysiology: from cell to bedside.* 5th ed. Amsterdam: Elsevier; 2009. p. 329–37.
28. Qu Z, Xie F, Garfinkel A, Weiss JN. Origins of spiral wave meander and breakup in a two-dimensional cardiac tissue model. *Ann Biomed Eng.* 2000;28:755–71.
29. Fenton F, Karma A. Vortex dynamics in three-dimensional continuous myocardium with fiber rotation: filament instability and fibrillation. *Chaos.* 1998;8(1):20–47.
30. Aranson IS, Bishop AR. Instability and stretching of vortex lines in the three-dimensional Complex Ginzburg-Landau Equation". *Phys Rev Lett.* 1997;79(21):4174–7.
31. Qu Z, Xie F, Garfinkel A. Diffusion-induced vortex filament instability in 3-dimensional excitable media. *Phys Rev Lett.* 1999;83(13):2668–71.
32. Ding M, Yang W. Stability of synchronous chaos and on-off intermittency in coupled map lattices. *Phys Rev E.* 1997;56(4):4009–16.
33. Yang P, Deng T, Zhao D, Feng P, Pine D, Chmelka BF, et al. Hierarchically ordered oxides. *Science.* 1998;282(5397):2244–6.
34. Clayton RH, Zhuchkova EA, Panfilov AV. Phase singularities and filaments: simplifying complexity in computational models of ventricular fibrillation. *Prog Biophys Mol Biol.* 2006;90:378–98.
35. Sinha S, Pande A, Pandit R. Defibrillation via the elimination of spiral turbulence in model for ventricular fibrillation. *Phys Rev Lett.* 2001;86:3678.

Chapter 15

Post-infarction Remodeling and Arrhythmogenesis: Molecular, Ionic, and Electrophysiological Substrates

Nabil El-Sherif

15.1 Introduction

Ventricular remodeling is the process by which ventricular size, shape, and function are regulated by mechanical, neurohormonal, and genetic factors [1, 2]. Remodeling may be physiological and adaptive during normal growth or pathological due to myocardial infarction (MI), cardiomyopathy, hypertension, or valvular heart disease. Following MI, the heart undergoes a complex time-dependent remodeling process that involves structural, biochemical, neurohormonal, and electrophysiological alterations. The acute loss of myocardium results in an abrupt increase in loading conditions that induces a unique pattern of remodeling involving the infarcted border zone and remote noninfarcted myocardium. Myocyte necrosis and the resultant increase in load trigger a cascade of biochemical intracellular signal processes (Fig. 15.1) [3] that initiates and subsequently modulates reparative changes, which include dilation, hypertrophy, and the formation of a discrete collagen scar. Ventricular remodeling may continue for weeks or months until the distending forces are counterbalanced by the tensile strength of the collagen scar [4].

Post-MI remodeling has been arbitrarily divided into an early phase (within 72 h) and a late phase (beyond 72 h) [3]. The early phase involves expansion of the infarct zone, which may result in early ventricular rupture or aneurysm formation. Late remodeling involves the left ventricle globally and is associated with time-dependent dilation, the distortion of ventricular shape, and hypertrophy of the noninfarcted myocardium. Following a variable period of compensatory hypertrophy, deterioration of contractile function may develop resulting in congestive heart failure (CHF).

N. El-Sherif

State University of New York, Downstate Medical Center, VA New York Harbor Healthcare System, Brooklyn, NY, USA
e-mail: nelsherif@aol.com

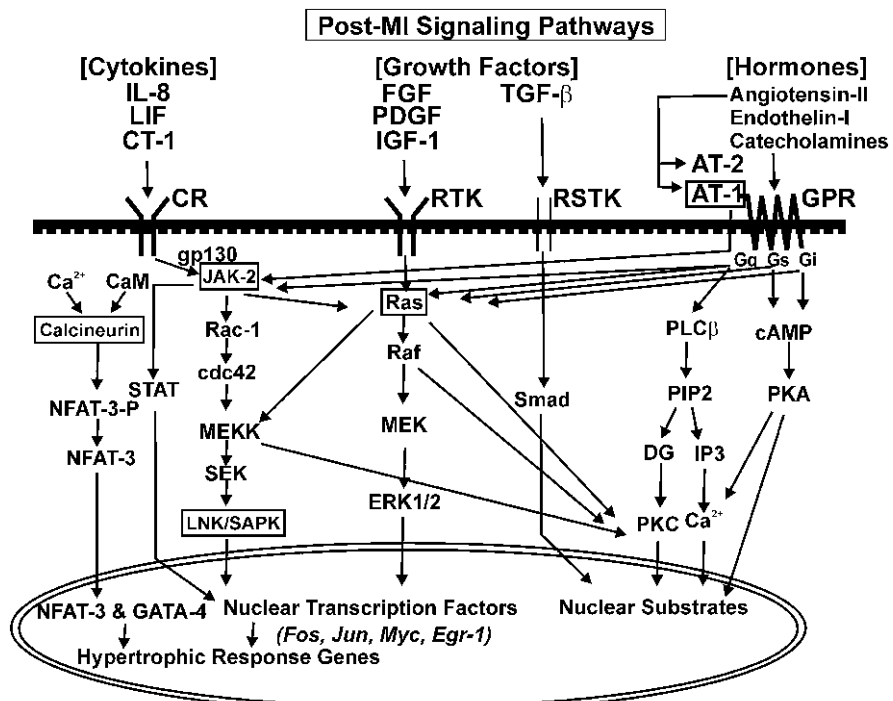


Fig. 15.1 Signaling pathways for post-infarction remodeling. With permission from [3]

15.2 Signal Transduction Pathways for Post-MI Remodeling

Hypertrophy of the noninfarcted myocardium is an adaptive response during post-MI remodeling, which offsets increased load, attenuates progressive dilation, and stabilizes contractile function. Myocyte hypertrophy is initiated by neurohormonal activation, myocardial stretch, the activation of local tissue rennin-angiotensin system, and paracrine/autocrine factors. Enhanced norepinephrine (NE) release contributes directly and indirectly to the hypertrophic response. Stimulation of α 1 adrenoceptors by NE leads to myocyte hypertrophy via the Gq-dependent signaling pathway. Angiotensin II (Ang II) and NE may augment endothelin (ET)-1 release, which is another stimulus for myocyte hypertrophy. The various biochemical and physical stimuli that induce cardiac hypertrophy are transduced through a common mechanism involving the activation of protein kinase cascades. The receptors for NE, ET-1, and Ang II are coupled to Gq proteins. The activation of Gq α stimulates phospholipase C β , which in turn leads to the production of 1,2 diacylglycerol and the activation of PKC [5]. Growth factors, including fibroblast growth factor, epidermal growth factor, platelet-derived growth factor, insulin, and insulin-like growth factor, activate receptor tyrosine kinase, p21 ras, and MAP kinase (extracellular regulated kinase of Jun N-terminal kinase). The activation of

MAP kinase is a prerequisite for the transcriptional and morphological changes of myocyte hypertrophy [6]. Ang II also activates p21 ras through the activation of the nonreceptor tyrosine kinase of the src family [7]. Intracellular Ca^{2+} seems critical for the activation of protein kinases in cardiomyocytes by Ang II and other hypertrophic stimuli before the fetal gene program can be switched on to increase protein synthesis.

Previous studies on left ventricular (LV) hypertrophy focused primarily on the effect of pressure overload [8] and spontaneous hypertension. [9]. In models of hemodynamic overload, hypertrophy was accompanied with the immediate activation of early response genes (proto-oncogene *c-fos*, *c-jun*, *c-myc*, *Hsp70*, *Erg-1*), followed by the induction of embryonic genes (ANF, β -MHC, skeletal α -actin) and an upregulation of constitutively expressed genes (cardiac α actin and myosin light chain-2). Chronic pressure and volume overload have been shown to result in morphologically and functionally distinct forms of hypertrophy [10]. The cellular and molecular mechanisms that contribute to cardiac hypertrophy after MI have features more consistent with those of volume overload.

An early study by Gidh-Jain et al. has emphasized the differences in cardiac gene expression in the post-MI heart compared with other overload hypertrophy models [11]. One striking difference is the continued expression of *c-fos*, which remains elevated up to 3 weeks post-MI, while its expression is generally rapid and quite short-lived in response to other cardiac stimuli causing hypertrophy [12]. The delayed activation of BNF and the return of β -MHC and α_2 Na-K ATPase to basal levels during the compensatory phase of hypertrophy are other noteworthy differences [10]. Table 15.1 compares changes in cardiac gene expression between post-MI remodeled hypertrophy in the rat model and other overload hypertrophy models.

Differences in fetal gene expression of cardiac ion channels between post-MI hypertrophy and other models of overload hypertrophy have also been reported. For example, in post-MI remodeled myocardium, there is a significant increase in the mRNA level of the fetal isoform of the L-type Ca^{2+} channel (LTCC), with reversion of the fetal/adult isoform ratio to fetal phenotype [13]. Similar changes were not

Table 15.1 Comparison of changes in cardiac gene expression between post-MI remodeled hypertrophy and other overload hypertrophy models in rat

	Post-MI remodeled hypertrophy		Other overload hypertrophy	
	3 days	3 weeks	Compensated	Onset
I_{CaL} (IVS3A isoform)	—	↑	—	—
<i>c-fos</i>	↑	↑	↑	↔
ANF	↑	↑	↑	↑
BNF	↔	↑	↑	↑
α_2 Na-K ATPase	↓	↔	↓	↓
α_3 Na-K ATPase	↔	↑	↑	↑
Cardiac α -actin	↔	↔	↑	↑
α MHC	↓	↔	↓	↓
β MHC	↑	↔	↑	↑
NaCh Ia	—	↑	—	—

reported in other overload hypertrophy models. The T-type Ca channel (TTCC), which is expressed only in fetal rat ventricular myocytes, is also reexpressed in the hypertrophied myocardium after MI [14] but not in other rat overload hypertrophy models [15]. Last but not least, there is differential expression of Na^+ channel subtypes in post-MI hypertrophied myocardium [16]. The electrophysiological significance of those changes will be discussed later.

MAPK pathways are activated in the post-MI heart and contribute to the remodeling process [17]. Table 15.2 shows that MAPKs changes vary in ischemic and nonischemic zones at different time intervals following MI. For example, p55 but not p46 isoform of JNK activity increased early in both nonischemic zone and ischemic zone, and continued to increase only in nonischemic zone; p38 MAPK activity increased early in both ischemic zone and nonischemic zone, peaked at 3 h and then decreased; p42 but not p44 isoform of MAPK activity was only increased in 1 day-old nonischemic zone. The data suggest that stretch but not ischemia caused early and continued stimulation of JNK while both stretch and ischemia caused transient increase of p38. Late stimulation of p42 MAPK may be a signal for remodeled hypertrophy in nonischemic zone.

Protein kinase C (PKC) is a key enzyme in the response of heart to stress and remodeled hypertrophy. Both induction and translocation of PKC isozymes have been reported in response to myocardial stretch and ischemia. Figure 15.2 shows that PKC- ϵ increased early in both ischemic and nonischemic zones but returned to normal after 1 day in nonischemic zone; PKC- η increased in ischemic zone but not

Table 15.2 Differential alterations of MAP Kinases in regional ischemia between ischemic and non ischemic zones

	Ischemic zone			Nonischemic zone			
	5 min	30 min	3 h	5 min	30 min	3 h	1 day
P42 MAPK	1.1	1.0	1.3	1.1	0.9	1.2	1.97*
P55 JNK	1.5*	1.3	1.0	1.74*	1.85*	2.02*	2.9*
P38 MAPK	2.1*	5.9*	10.3*	6.8*	7.8*	17.0*	1.1

$P<0.01$ compared to sham

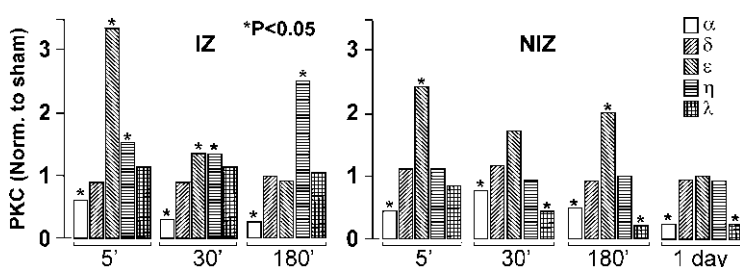


Fig. 15.2 Bar graph showing normalized PKC isoform immune-reactivities by measuring the signal for the proteins PKC- α , δ , ϵ , η , and λ by densitometry. Columns represent the mean, with error bars indicating SEM ($n = 6$). Regional ischemia was induced by ligation of left anterior descending artery in rat. Asterisks denote significance between groups

in nonischemic zone; On the one hand, PKC- α decreased in both ischemic and nonischemic zones. On the other hand, PKC- δ showed no significant change in both zones and PKC- λ showed no change in ischemic zone but persistently decreased in nonischemic zone up to 1 day. These data suggest that complex and different regulation of PKC isoforms occur in response to ischemia and stretch. The role of these changes in remodeled hypertrophy of nonischemic zone remains to be ascertained.

15.3 Remodeling of the Peri-Infarction Border Zone

15.3.1 Electrophysiological Changes

Key sources of post-infarction arrhythmias are situated in border-zone cells, including the often-spared epicardial rim, the lateral margins, and subendocardial Purkinje fibers nourished by LV cavity blood [18]. Alterations in border-zone tissues have been studied almost exclusively in large-animal models (dogs or cats). Surviving cardiomyocytes in the viable border zone adjacent to a prior infarction have signs of reduced excitability; reduced action potential (AP) amplitude and dV/dt_{max} [19] along with post-repolarization refractoriness [20] are suggestive of reduced I_{Na} . Increased APD in border zone cells, particularly in subendocardial Purkinje cells [21], causes early afterdepolarizations (EADs) and related arrhythmias [22, 23]. A variety of K^+ currents are down regulated in border-zone cells. Background K^+ conductance is reduced in surviving canine subendocardial Purkinje fibers [23] because of reduced I_{K1} and altered delayed-rectifier K^+ currents [24]. Border zone LV cardiomyocytes show reduced I_{to} [19]. I_{to} decreases are most prominent within days of acute infarction and tend to resolve over the subsequent 2 months [25]. Delayed-rectifier currents are also reduced in border-zone cardiomyocytes [26–28]. Amplitude of both I_{Kr} and I_{Ks} is decreased [27]. The expression of subunits encoding I_{Kr} (ERG) and I_{Ks} (KvLQT1 and minK) is down regulated in 2-day post-infarction border-zone cells. ERG and KvLQT1 expression normalizes by day five, whereas minK remains suppressed.

15.3.2 Changes in Connexin Function in the Post-infarction Border Zone

Cells in the surviving peri-infarct zone have prepotentials and notches on phase 0 upstrokes, reduced space constants, and discontinuous propagation due to abnormal cell-to-cell coupling [29–31]. Marked changes in gap junction organization and connexin43 distribution occur within healed MIs in humans [32], canine [32, 33], and rat models [34, 35]. Gap junction changes precede the formation of the infarct scar and are thus a primary phenomenon unrelated to physical cell separation by

scar tissue [32]. Post-infarction remodeling of gap junction distribution in rats is linked to desmosome and adherens junction alterations, with temporary intracellular junctional complexes formed as a component of complex remodeling or cell-to-cell and cell-to-extracellular matrix interactions [34]. In healed MIs from dogs, there are smaller and fewer gap junctions, with a decreased proportion of side-to-side vs. end-to-end connections [32]. Decreased side-to-side intercellular coupling contributes to transverse conduction block (perpendicular to fiber orientation) and anisotropic reentry [36]. Thus coupling abnormalities due to connexin changes are central to ventricular arrhythmogenesis post-MI. Recent studies suggest that the molecular mechanisms by which Cx43 is lost from the intercalated disk following MI includes an interaction of p-cSrc with ZO-1 and subsequent loss of scaffolding of Cx43 leaving Cx43 free to diffuse in myocyte membranes from areas of high Cx43, as at the intercalated disk, to regions of lower Cx43 content (the lateral myocyte membrane) [37].

15.4 Remodeling of the Remote Noninfarcted Myocardium

Three days post-MI in the rat, the area of infarction is well distinguished from the noninfarcted LV. However, there are no obvious changes in the thickness of the noninfarcted LV free wall compared with sham-operated rats at this time. By contrast, 3-weeks post-MI, the free wall of the infarcted area is very thin and the remaining LV wall is much thicker than the normal. Cells isolated from 3-day post-MI noninfarcted LV myocardium are not significantly different in size compared with cells from sham-operated rats. By 3 weeks, hypertrophy of noninfarcted LV myocytes is obvious [38].

Post-MI remodeling is also characterized by accumulation of collagen in both ventricles, mostly in the form of replacement and interstitial fibrosis, which exceeds the magnitude of scarring produced by MI and segmental fibrosis [39]. Although there is general agreement that myocyte loss is the etiological factor of replacement fibrosis in the ventricular wall, less clear is the mechanism responsible for activation of the cardiac interstitium, resulting in the accumulation of fibrillar collagen between myocytes. There is some evidence that hormonal/or hemodynamic overloads [40], or both, may trigger fibroblast proliferation and collagen neosynthesis in the myocardium independent of myocytolytic necrosis and myocyte loss.

The main consistent electrophysiological abnormality in post-MI remodeled hypertrophied myocytes is prolongation of APD (Fig. 15.3). However, our group [41] and others [42] have clearly demonstrated that electrical remodeling occurs before cellular hypertrophy and as early as 3 days post-MI [41]. Of the more than 20 ion-carrying systems in cardiac myocytes, at least 8 could be implicated in the prolongation of APD of hypertrophied myocytes, including post-MI remodeled myocytes. These are I_{CaL} , I_{to-f} , I_{to-s} , I_{Kr} , I_{Ks} , I_{K1} , the Na–Ca exchanger, and $I_{Na-slow}$. Several studies suggest that changes in I_{to} are a major factor in prolongation of APD of hypertrophied myocytes [38, 43, 44].

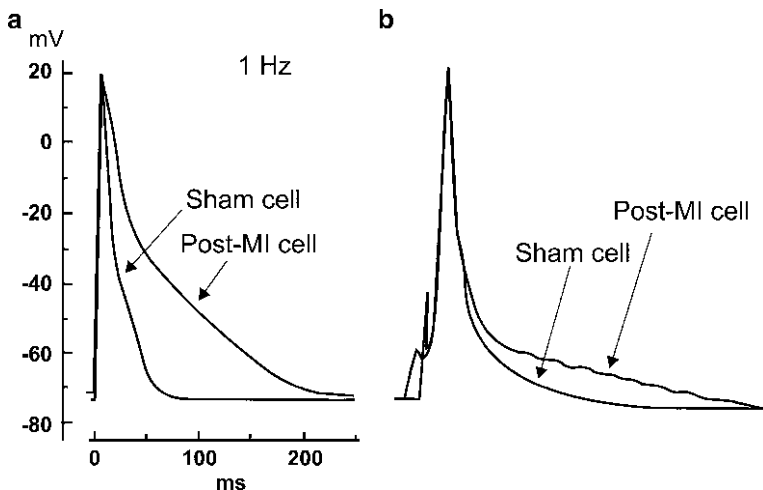


Fig. 15.3 Comparison of action potentials (APs) of sham and post-MI myocytes. APs were recorded with whole-cell patch-clamp configuration from two different sham myocytes and superimposed on APs recorded from two different post-MI remodeled LV myocytes. The AP duration of the two post-MI myocytes was significantly longer than that of sham myocytes. However, the time course of repolarization of the two posts-MI myocytes was markedly different. In the left panel, the APD₂₅, APD₅₀, and APD₉₀ of the post-MI myocytes were all prolonged compared with the sham myocyte, whereas in the right panel, only the APD₉₀ was significantly prolonged. With permission from [38]

15.4.1 LTCC Current (I_{CaL})

Because of its fundamental role in excitation–contraction (EC) coupling, I_{CaL} has been investigated more thoroughly than any other current. An increase in I_{CaL} density or slowing of current inactivation, or both, could potentially contribute to prolongation of APD in hypertrophied myocytes. The reports on I_{CaL} density in various models of hypertrophy are somewhat disconcerting. The discrepancies may reflect differences in etiology, species, nature of analyses, experimental conditions, and even more important, the stage of disease [43]. One study has shown that I_{CaL} increases at early stages of post-MI in the rat and returns to control values once cellular hypertrophy becomes established [42].

Our group has shown that the density and kinetics of I_{CaL} were not significantly different between 3-week old post-MI remodeled myocytes and sham myocytes [38]. Thus, alteration of I_{CaL} does not seem to contribute to prolongation of APD 3-weeks post-MI. The electrophysiological data are consistent with the observation that gene expression of LTCC is not changed compared with control in the remodeled LV 3 weeks post-MI [45]. In the post-MI remodeled rat myocardium, there is also a significant increase in mRNA level of the fetal isoform of I_{CaL} , with reversion of the fetal/adult isoform ratio to the fetal phenotype (Fig. 15.4) [13]. Similar changes were not reported in other overload hypertrophy models. The physiological significance of these findings remains to be determined. However,

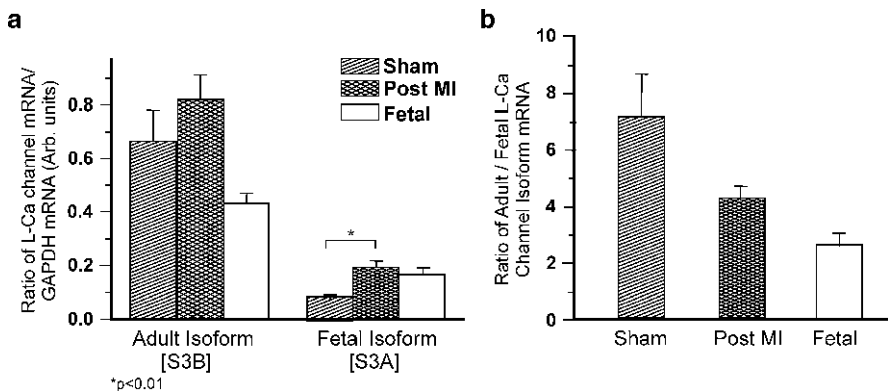


Fig. 15.4 **a**, Relative abundance of the α -1 subunit of the cardiac voltage-dependent L-type calcium channel (VDCC) S3A (fetal) and S3B (adult) transcripts in sham-operated rats ($n = 6$), 3-week old post-MI rats ($n = 6$) and fetal cardiac tissue pooled from six animals determined by the ratio of arbitrary densitometric units for S3A/GAPDH and S3B/GAPDH mRNA from RNase protection assay. **b**, Ratio of the VDCC S3A (fetal and S3B (adult) transcripts in sham-operated rats ($n = 6$), infarcted rats ($n = 6$) at 3 weeks after surgery and fetal cardiac tissue pooled from six rats normalized to internal control (GAPDH) mRNA. With permission from [13]

a novel DHP-resistant Ca^{2+} current that is otherwise similar to I_{CaL} has been described in the rat fetal myocyte, which disappears during development [46].

15.4.2 T -type Ca^{2+} Channel Current (I_{CaT})

The I_{CaT} , which in the rat is expressed only in fetal ventricular myocytes, is also reexpressed in the hypertrophied myocardium after MI (Fig. 15.5) [14], but not in other rat overload hypertrophy models [15]. Although the exact role of I_{CaT} is not clear, its appearance in post-MI remodeled hypertrophy may increase total Ca^{2+} influx, change the cell electrophysiological properties, and predispose for arrhythmias in the hypertrophied heart.

15.4.3 Na^+ Channel Current (I_{Na})

An early study by Huang et al. has shown increased Na^+ channel bursting activity during sustained depolarization in post-MI remodeled myocytes resulting in a large slow component of the I_{Na} decay (Fig. 15.6) [16]. A tetrodotoxin-sensitive current contributed 18% to the prolonged APD_{90} of isolated post-MI myocytes compared with 6% in control myocytes. Molecular studies revealed that in addition to the rat heart I (rH I) subtype, thought to be the predominant subtype that encodes a tetrodotoxin-resistant isoform, the brain subtypes NaCh I and NaCh Ia also are

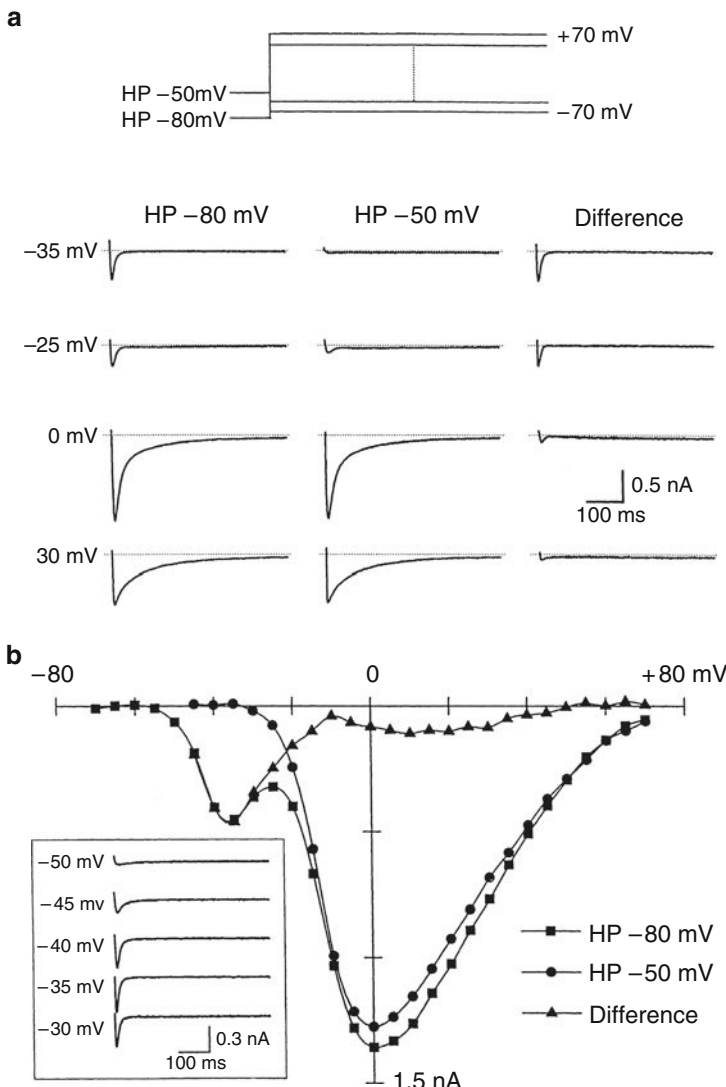
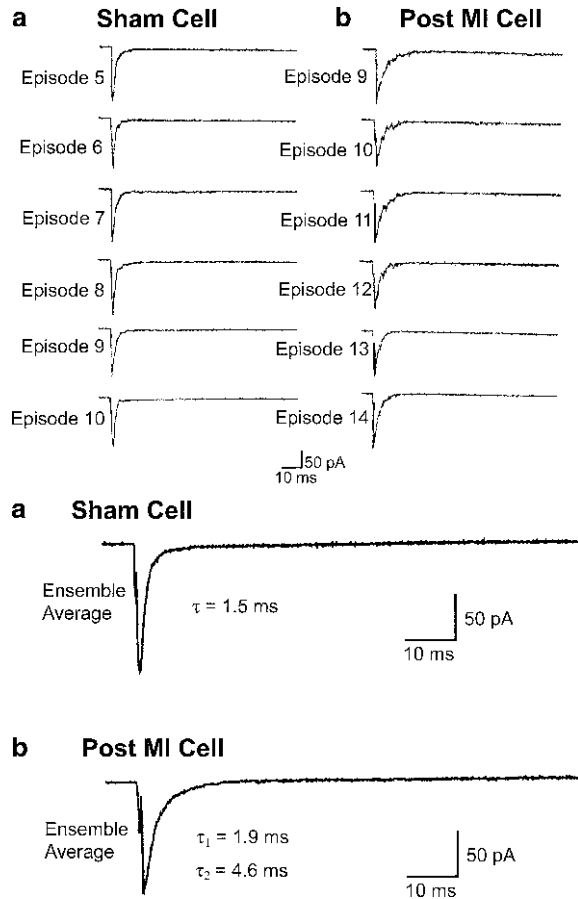


Fig. 15.5 I-V relationship of $L_{\text{Ca-L}}$ and $L_{\text{Ca-T}}$ in a post-MI remodeled ventricular myocyte obtained in Na^+ free solution. Depolarization protocol is illustrated at top. Panel **a** shows original recordings of Ca^{2+} currents at holding potential (HP) of -80 mV and -50 mV as well as current subtraction to isolate $L_{\text{Ca-T}}$. Lower panel show I-V curves obtained at HP of -80 and -50 mV and their subtraction. The inset on the lower left corner illustrates a family of $L_{\text{Ca-T}}$ currents below the threshold for $L_{\text{Ca-L}}$ between -50 and -30 mV . With permission from [14]

expressed in rat myocytes. Post-MI remodeled myocardium showed increased expression of NaCh I protein with reversion of the NaCh Ia/NaCh I isoform ratio toward the fetal phenotype. These findings raise the possibility that the increase in

Fig. 15.6 Top Panel: Recordings of Na^+ current in a macropatch for a sham cell (a) and postmyocardial infarction (post-MI) cell (b). Patches were held at -100 mV and depolarized once per second for 95 ms to -20 mV . Six consecutive sweeps are illustrated for both the sham and post-MI cells. Most of the sweeps in the sham cells showed openings clustered within 5 ms of the potential step. On the contrary, several sweeps in the post-MI cells showed delayed openings at multiple conductance that lasted between 20 and 30 ms.

Bottom Panel: Ensemble recording of Na^+ current from the two macropatches shown in top panel. Note that, on the one hand, the Na^+ current from sham cell had fast relaxation that was fitted with a single exponential of 1.5 ms. On the other hand, the Na^+ current in the postmyocardial infarction (post-MI) cell decayed with two exponentials with the slow relaxation of 4.6 ms. With permission from [16]



the slow component of I_{Na} in post-MI remodeled myocytes is secondary to the increased expression of NaCh I . Later studies of ventricular myocytes from failing canine and human hearts have described, in addition to decreased peak I_{Na} , an increased noninactivating late I_{Na} that may contribute to prolongation of APD [47].

15.4.4 Voltage-Gated Potassium Currents (K_v)

The K_v currents are major determinants of myocardial repolarization and are differently regulated in a variety of cardiovascular pathologies [48, 49]. In the rat post-MI remodeled myocardium, at least three K_v currents have been investigated $I_{\text{to,f}}$ (encoded by $K_v4.2$ and $K_v4.3$), $I_{\text{to-s}}$ ($K_v1.4$), and I_{Ks} ($K_v1.5$ and $K_v2.1$). In a study from our laboratory, there was down regulation of $K_v1.5$, $K_v2.1$, $K_v4.2$, and $K_v4.3$.

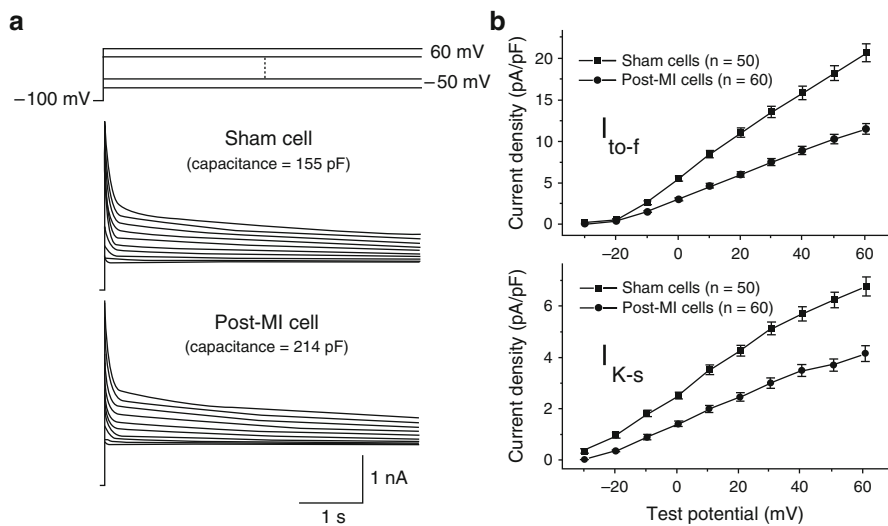


Fig. 15.7 Left Panel, Outward K^+ currents from a sham myocyte (top) and post-MI myocyte (bottom). The holding potential was -100 mV, and the membrane was depolarized for a duration of 5 s in the range of -50 to $+60$ mV in steps of 10 mV. Although the post-MI cell has larger membrane capacitance, the current amplitude was not significantly different between both cells. Right Panel: Comparison of I-V curves of both $I_{\text{to-f}}$ from sham and post-MI cells. Both currents gradually increased in amplitude at more positive potentials. The current density of both $I_{\text{to-f}}$ and $I_{\text{K-slow}}$ are decreased in post-MI cells. With permission from [38]

but no significant change in $K_v1.5$ in the 3-weeks post-MI myocardium [45]. This corresponded with reduced density of $I_{\text{to-f}}$ and $I_{\text{to-s}}$ [38], (Fig. 15.7). Besides, the post-MI remodeled myocardium, I_{to} density is also reduced in most cardiac hypertrophy models and is thought to play a major role in prolongation of APD [44]. There are also regional differences in the down regulation of K_v channel expression and density of K^+ currents in the post-MI remodeled heart [41]. This can be a significant determinant of spatial electrophysiological heterogeneity and may contribute to increased electrical instability in the post-MI heart.

15.4.5 Pacemaker (Funny) Current (I_f)

The hyperpolarization-activated cyclic nucleotide-gated (HCN) subunits HCN1-4 encode the relatively nonselective cation channel that conduct the pacemaker current I_f , which plays an important role in cardiac pacemaking [50, 51]. I_f channels are significantly overexpressed in ventricular myocytes isolated from the heart of post-MI rat and its amplitude is larger in myocytes from the area surrounding the scar in LV when compared with those isolated from areas remote from the scar [52]. I_f is significantly enhanced by β_1 adrenergic receptor activation while β_3 adrenergic

receptor modulation has the opposite effect. This probably reflects the increased activity of PTX-sensitive G_i proteins in post-MI cells [52].

15.4.6 ATP-Dependent Potassium (K_{ATP}) Channels

The Sarcolemmal K_{ATP} channels are important metabolic sensors regulating electrical activity of cardiomyocytes, and when activated, are capable of considerably shortening APD. The post-MI remodeled myocardium displays alterations of K_{ATP} expression and function with spatial heterogeneity matching that of the APD prolongation [53]. Drugs that selectively activate diazoxide-sensitive sarcolemmal K_{ATP} channels could theoretically be considered antiarrhythmic in post-MI heart failure [53].

15.5 Electrophysiological Mechanisms of Arrhythmia Generation in the Post-MI Remodeled Ventricular Myocardium

Three potential electrophysiological mechanisms for arrhythmia generation have been described in the post-MI remodeled hypertrophied ventricular myocardium: (1) EAD-triggered activity, (2) delayed afterdepolarization (DAD)-triggered activity, and (3) Reentrant excitation [44].

15.5.1 EAD-Triggered Activity

Prolongation of APD, the universal and consistent electrophysiological abnormality described in hypertrophied myocytes, is considered the priming step for development of EAD [54]. Several changes in ionic currents that have been described in different models of hypertrophy favor both the prolongation of APD and the generation of EADs. These include a decrease of I_{to} and I_K , shift of inactivation of I_{CaL} to more positive potentials, and prolongation of the current inactivation. Qin et al. has demonstrated the development of single and repetitive EADs in isolated post-MI remodeled myocytes (Fig. 15.8a) [38]. The in vivo representation of EAD-induced triggered activity is a prolonged QT interval associated with a polymorphic ventricular tachycardia, known as torsades de pointes [54].

15.5.2 DAD-Triggered Activity

DADs have been shown to be more easily induced in hypertrophied myocytes under the influence of increased $[Ca^{2+}]_i$ [55] or in the presence of β -adrenergic agonists (Fig. 15.8b), [38, 56]. Higher $[Ca^{2+}]_i$ through the Na^+-Ca^{2+} exchange

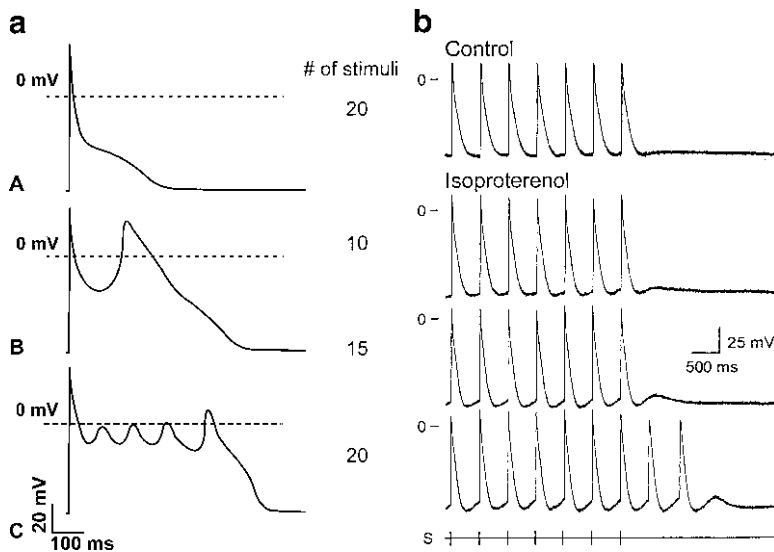


Fig. 15.8 **a**, AP recordings from an isolated post-MI remodeled myocyte using whole-cell patch-clamp configuration showing markedly prolonged APD during stimulation at 1 Hz (**a**) and spontaneous occurrence of single and multiple early after depolarizations (EADs) during stimulation at 2 and 5 Hz (**b** and **c**, respectively). **b**, Microelectrode recordings from an epicardial preparation from a post-MI remodeled left ventricle showing trains of stimulated action potentials (APs) at a cycle length of 500 ms during control and after isoproterenol superfusion (10 nmol). Note the development of a DAD on termination of the stimulating train. Increasing the length of stimulating train resulted in a graded increase in the slope and amplitude of the DAD, which eventually resulted in two triggered APs in the bottom trace. Note that only the last seven stimulated APs are shown in each panel. With permission from [38]

mechanism associated with the prolonged APD and impaired Ca^{2+} uptake by the SR in hypertrophied cells can favor the occurrence of DADs [57]. There is also evidence that I_f is increased in hypertrophied myocytes and post-MI heart [52], and may favor the occurrence of spontaneous action potentials [58]. Further, I_{CaT} was shown to be expressed in the post-MI remodeled myocardium [14]. The steady-state voltage relations for activation and inactivation of I_{CaT} are shifted by -35 mV compared with I_{CaL} , making I_{CaT} well suited for participating in pacemaker activity. I_{CaT} might be involved in several types of arrhythmias, including both DADs and EADs [15].

15.5.3 Reentrant Excitation

Reentrant excitation is an important electrophysiological mechanism of tachyarrhythmia in the post-MI remodeled myocardium. Changes in both active membrane properties [59] and passive resistivity [60] could create heterogeneity of

repolarization, slowed conduction, and functional conduction block, thus providing the necessary prerequisites for reentrant excitation. There is evidence that prolongation of APD in hypertrophied remodeled ventricle is not homogeneous [41], which provides a substrate for dispersion of refractoriness. Besides evidence for hypertrophy induced increase in interstitial tissue with possible impairment of intracellular coupling, there is evidence for quantitative changes in gap junctional proteins [61]. Regional differences in the expression of connexin in the remodeled post-MI myocardium can increase the anisotropic properties of the remodeled ventricle and predispose to reentrant excitation. Some studies suggest that changes in gap junctional distribution in the border zone of healing canine infarcts may define the locations of reentrant ventricular tachycardia in the surviving epicardial layer [33].

In 1977, El-Sherif and associates showed that in dogs studied 3–5 days post-MI, reentrant ventricular tachyarrhythmia (VT) occurred spontaneously, but were more commonly induced by programmed electrical stimulation [62]. The anatomic and electrophysiological substrates for the reentrant VT were later characterized in a series of reports [59, 63–65]. These studies have shown that reentrant excitation occurred around zones (arcs) of functional conduction block. The arcs were attributed to ischemia-induced spatially nonhomogeneous lengthening of refractoriness. Sustained reentrant tachycardia was found to have an activation pattern (Fig. 15.8), whereby clockwise and counter clockwise wavefronts were oriented around two separate arcs of functional conduction block. The two circulating wavefronts coalesced into a common wavefront that conducted slowly between the two arcs of block (Fig. 15.9). Using reversible cooling, reentrant excitation could be successfully terminated only from localized areas along the common reentrant wavefront. These original observations paved the way for therapeutic intervention of reentrant VT in post-MI patients by radiofrequency ablation of the reentrant pathway [66].

15.6 Pharmacological Agents That May Impact Arrhythmogenic Substrates of Post-MI Remodeling

Much less work has been done to study pharmacological interventions that can improve the negative aspects of post-MI remodeling, vis-à-vis arrhythmogenic susceptibility [67]. There is considerable evidence that electrophysiological changes associated with the hypertrophied noninfarcted myocardium play a key role in the arrhythmogenicity of the post-MI heart. For example, although β -blockers and angiotensin-converting enzyme (ACE) inhibitors have very different effects on ventricular dilatation, both agents have been shown to prevent the development of myocardial hypertrophy and may, thus, decrease the susceptibility to ventricular arrhythmias [68–70]. These two classes of pharmacological agents have also been shown to have direct effects on the arrhythmogenic substrate. ACE inhibitors were shown to attenuate increase in refractoriness heterogeneity and to prevent EAD

formation in the remote noninfarcted post-MI myocardium [71]. Furthermore, the combined α - and β -adrenoreceptor antagonist carvedilol was shown to suppress down regulation of both I_{Na} [72] and I_{CaL} [73].

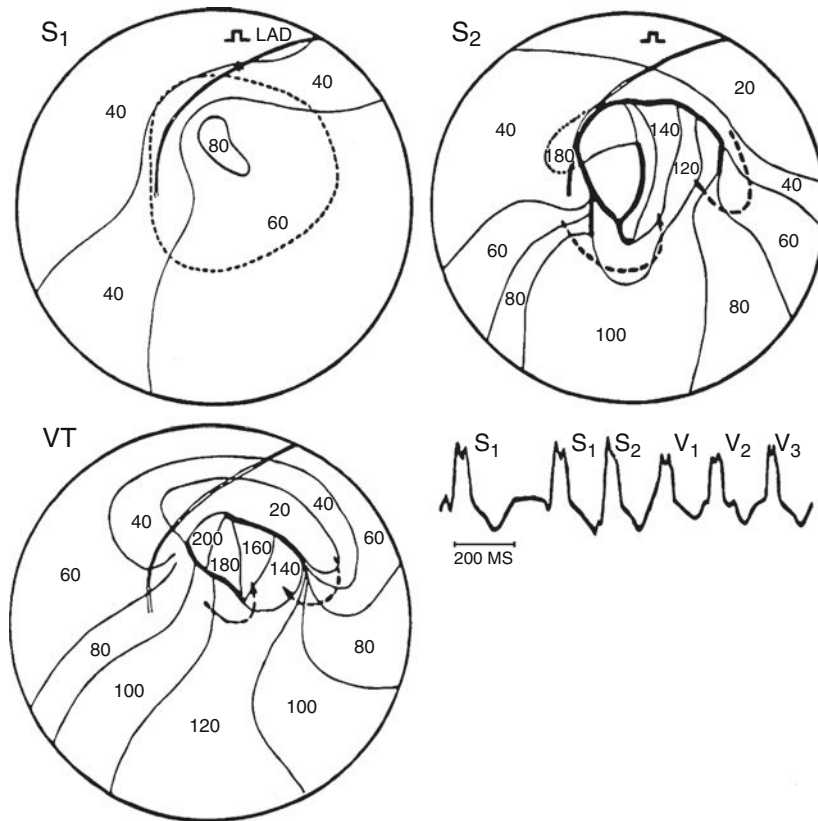


Fig. 15.9 Epicardial isochronal activation maps during a basic ventricular stimulated beat (S_1), initiation of reentry by a single premature stimulus (S_2), and sustained monomorphic reentrant ventricular tachycardia (VT). A representative electrocardiogram is shown in the lower right panel. The recordings were obtained from a dog 4-days post-ligation of the left anterior descending artery (LAD). Site of ligation is represented by a double bar. Epicardial activation is displayed as if the heart is viewed from the apex located at the center of the circular map. The perimeter of the circle represents the AV junction. The outline of the epicardial ischemic zone is represented by the dotted line. Activation isochrones are drawn at 20-ms intervals. Arcs of functional conduction block are represented by heavy solid lines and are depicted to separate contiguous areas that are activated at least 20 ms apart. During S_1 the epicardial surface was activated within 80 ms with the latest isochrones located in the center of the ischemic zone. S_2 resulted in a long continuous arc of conduction block within the border of the ischemic zone. The activation wavefront circulated around both ends of the arc of block and coalesced at the 100-ms isochrones. The common wavefront advanced within the arc of block before reactivating an area on the other side of the arc at the 180-ms isochrones to initiate the first reentrant cycle. During sustained VT, the reentrant circuit had a figure 8 activation pattern in the form of clockwise and counterclockwise wavefronts around two arcs of functional conduction block before coalescing into a slow common wavefront that conducted between the two arcs of block. With permission from [64]

15.6.1 Drugs That Modify Post-MI Downregulated K⁺ Currents

A key electrophysiological alteration in post-MI remodeled heart is downregulation of K⁺ channels gene expression and K⁺ currents resulting in spatially heterogenous prolongation of APD and increased dispersion of refractoriness [41]. It is, therefore, not surprising that the post-MI heart is more sensitive to hypokalemia and to the proarrhythmic effects of drugs that depress K⁺ currents, especially I_{Kr} blockers. On the other hand, some pharmacological interventions, such as magnesium and spironolactone have been shown in some studies to reduce the incidence of sudden death in post-MI patients. Further, the experimental thyroid hormone analog DITPA has been shown to restore Ito expression in post-MI heart.

15.6.2 Magnesium

The well-established link between Mg²⁺ and serum K⁺ leads one to expect that a correlation exists between hypomagnesemia and arrhythmias in infarcted patients. Mg²⁺ is also a cofactor for Na⁺, K⁺-ATPase, and Ca²⁺-ATPase, which are important in maintaining membrane stability. In spite of several large randomized trials on efficacy of Mg²⁺ in acute MI patients, its potential beneficial effects received a setback by the ISIS-4 study (International Study of Infarct Survival), in which no mortality benefit was obtained from the administration of magnesium [74].

15.6.3 Aldosterone-Receptor Antagonists

Aldosterone has an important role in the pathophysiology of heart failure. Aldosterone promotes the retention of sodium, the loss of magnesium and potassium, sympathetic activation, parasympathetic inhibition, myocardial and vascular fibrosis, baroreceptor dysfunction, vascular damage, and impairs arterial compliance [75]. A clinical multicenter study has shown that spironolactone, an aldosterone-receptor antagonist, when used in conjunction with an ACE inhibitor in patients with severe CHF and low LV ejection fraction, reduces the risk of death both from progressive failure and sudden death [76]. Although the exact cause of the reduction in the risk of death remains speculative, it is suggested that an aldosterone-receptor blocker can prevent progressive heart failure by averting sodium retention and myocardial fibrosis and prevent sudden death from cardiac causes by averting potassium loss and by increasing the myocardial uptake of norepinephrine [76]. Spironolactone may prevent myocardial fibrosis by blocking the effects of aldosterone on the formation of collagen, which in turn could play a part in reducing the risk of sudden death from cardiac causes, since myocardial fibrosis could predispose patients to heterogeneity of ventricular conduction and, hence, enhance the susceptibility to reentrant ventricular arrhythmias.

15.6.4 *Thyroid Hormone Analogs*

Down regulation of I_{to} is a key electrophysiological alteration of post-MI remodeled myocardium. Thyroid hormone has been shown to increase the expression of genes encoding for I_{to} [77], alter the biophysical properties of I_{to} , and hence, abbreviate APD. However, the effects of thyroid hormone are complicated by a plethora of noncardiac effects that may limit the beneficial effect of this agent. In a study in the post-MI rat model, chronic administration of the thyroid hormone analog 3,5-diiodothyropropionic acid (DITPA) has been shown to restore I_{to} expression, and improve the repolarization abnormalities associated with the post-MI heart, with only minor effects on heart rate and metabolism, compared with thyroid hormone [78]. The clinical validity of this therapeutic measure has not been tested.

15.6.5 *Calcium Channel Blockers*

On the one hand, the role of LTCC blockers in the post-MI heart is limited. On the other hand, the role of TTCC blockers remains unexplored [79]. The LTCC genes and current are reexpressed in rat post-MI remodeled LV myocytes [14]. Although the I_{CaT} density is smaller compared with that of I_{CaL} , it is possible that slight augmentation of $[\text{Ca}^{2+}]_i$ during certain phases of the AP can predispose to abnormal afterdepolarizations. However, an arrhythmogenic potential of reexpressed TTCC gene and current in the post-MI remodeled rat heart and possible antiarrhythmic effects of I_{CaT} blockers remain to be demonstrated.

15.7 Drugs That Modulate Post-MI Signaling Pathways

Although multiple signal transduction pathways may play a role in post-MI modeling, especially the hypertrophic response of the noninfarcted myocardium (see Fig. 15.1), the results of pharmacological modulation of at least three of these pathways have been reported. These three pathways are as follows: the calcineurin pathway, the JACK-STAT pathway, and the ras pathway.

15.7.1 *The Calcineurin Pathway*

Calcineurin participates in hypertrophic signal transduction in models of cardiac hypertrophy [80, 81]. Cyclosporine, a specific inhibitor of calcineurin, has been shown to ameliorate the hypertrophic process in a number of animal models.

Deng et al. have shown that calcineurin inhibition by cyclosporine A partially ameliorated post-MI remodeled hypertrophy, diastolic dysfunction, decrease in basal level of phosphorylated phospholamban, downregulation of key K⁺ genes expression, and decrease of K⁺ current, with no adverse effects on systolic function or mortality in the first 4 weeks after MI in the rat [82].

15.7.2 The JAK-STAT Pathway

The Janus kinase/signal transducer and activator of transcription (JAK-STAT) signaling pathway was found to be prominently associated with activation of the autocrine loop of the heart tissue-localized rennin angiotensin system (RAS) [83]. A study in the post-MI rat model compared the effects of in vivo blockade of RAS by the AT1 receptor blocker losartan with the in vivo blockade of the JAK-STAT pathway by the specific JAK2 blocker tyrphostin AG490 on certain aspects of early post-MI remodeling and suggested that drugs that inhibit JAK-STAT phosphorylation may provide a new approach to modify post-MI remodeling [84].

15.7.3 The Ras Pathway

Recently, a synthetic peptide designed to selectively block oncogenic ras was also found to counter the effects of norepinephrine-induced myocyte hypertrophy in vitro associated with over-expression of ras 21 by blocking JNK/jun and ERK activation [85]. These findings suggest a novel therapeutic approach to counteract the negative consequence of post-MI remodeling.

15.8 Conclusions

Coronary artery disease is a major public health concern. Prevention of coronary atherosclerosis as well as limiting myocardial damage once an acute ischemic syndrome develops should arguably be at the forefront of medical research. However, patients who survive an acute ischemic episode remain vulnerable to a negative cardiac remodeling process that can eventually result in terminal hemodynamic compromise or arrhythmogenic SCD. Better understanding of the molecular, ionic, and electrophysiological substrate of the arrhythmogenicity of the post-MI heart could lead to an optimal life saving management strategy.

References

- Pfeffer MA, Braunwald E. Ventricular remodeling after myocardial infarction: experimental observations and clinical implications. *Circulation*. 1990;81:1161–72.
- Rouleau JL, de Champlain J, Klein M, et al. Activation of neurohumoral systems in post-infarction left ventricular dysfunction. *J Am Coll Cardiol*. 1993;22:390–8.
- El-Sherif N, Turitto G. Risk stratification and management of sudden cardiac death: a new paradigm. *J Cardiovasc Electrophysiol*. 2003;14:1–7.
- Sutton MG St-J, Sharpe M. Left ventricular remodeling after myocardial infarction: pathophysiology and therapy. *Circulation*. 2000;101:2981–8.
- Ju H, Zhao S, Tappia PS, et al. Expression of Gq alpha and PLC-beta in scar and border tissue in heart failure due to myocardial infarction. *Circulation*. 1998;97:892–9.
- Glennon PE, Daddoura S, Sale EM, et al. Depletion of mitogen-activated protein kinase using an antisense oligodoxynucleotide approach downregulates the phenylephrine-induced hypertrophic response in rat cardiac myocytes. *Circ Res*. 1996;78:954–61.
- Sadoshima J, Izumo S. The heterotrimeric Gq protein-coupled angiotensin-II receptor activates p21 ras via the tyrosine kinase-Shc-Grb2-Sos pathway in cardiac myocytes. *EMBO J*. 1996;15:775–85.
- Izumo S, Nadal-Ginard B, Mahdavi V. Protooncogene induction and reprogramming of cardiac gene expression produced by pressure overload. *Proc Natl Acad Sci USA*. 1988;85:339–43.
- Kessler-Icekson G, Barhum Y, Schlesinger H, et al. Molecular manifestations of cardiac hypertrophy in the spontaneously hypertensive rat effects of antihypertensive treatments. In: Sideman S, Beyar R, editors. *Molecular and subcellular cardiology. Effects of structure and function*. New York: Plenum; 1995. p. 203–195.
- Oparil S. Pathogenesis of ventricular hypertrophy. *J Am Coll Cardiol*. 1985;5:57B–65.
- Gidh-Jain M, Huang B, Jain P, Gick G, El-Sherif N. Alterations in cardiac gene expression during ventricular remodeling following experimental myocardial infarction. *J Mol Cell Cardiol*. 1998;30:627–37.
- Brand T, Sharma HS, Schaper W. Expression of nuclear proto-oncogenes in isoproterenol-induced cardiac hypertrophy. *J Mol Cell Cardiol*. 1993;25:1325–37.
- Gidh-Jain M, Huang B, Jain P, et al. Reemergence of the fetal pattern of L-type calcium channel gene expression in non infarcted myocardium during left ventricular remodeling. *Biochem Biophys Res Commun*. 1995;216:892–7.
- Huang B, Qin D, Deng L, et al. Reexpression of T-type Ca⁺⁺ channel gene and current in the post-infarction remodeled rat left ventricle. *Cardiovasc Res*. 2000;46:442–9.
- Vassort G, Alvarez J. Cardiac T-type calcium current: pharmacology and role in cardiac tissues. *J Cardiovasc Electrophysiol*. 1994;5:376–93.
- Huang B, El-Sherif T, Gidh-Jain M, et al. Alterations of sodium channel kinetics and gene expression in the postinfarction remodeled myocardium. *J Cardiovasc Electrophysiol*. 2002;12:218–25.
- Shimizu N, Yoshiyama M, Omura T, et al. Activation of mitogen-activated protein kinases and activator protein-1 in myocardial infarction in rats. *Cardiovasc Res*. 1998;38(1):116–24.
- Janse MJ, Wit AL. Electrophysiological mechanisms of ventricular arrhythmias resulting from myocardial ischemia and infarction. *Physiol Rev*. 1998;69:1049–69.
- Lue WM, Boyden PA. Abnormal electrical properties of myocytes from chronically infarcted canine heart. Alterations in V_{max} and the transient outward current. *Circulation*. 1992;85:1175–88.
- Cabo C, Boyden PA. Electrical remodeling of the epicardial border zone in the canine infarcted heart: a computational analysis. *Am J Physiol Heart Circ Physiol*. 2003;284:H373–84.
- Friedman PL, Fenoglio JJ, Wit AL. Time course for reversal of electrophysiological and ultrastructural abnormalities in subendocardial Purkinje fibers surviving extensive myocardial infarction in dogs. *Circ Res*. 1975;36:127–44.

22. Gough WB, HU D, El-Sherif N. Effects of clofilium on ischemic subendocardial Purkinje fibers 1 day postinfarction. *J Am Coll Cardiol.* 1988;11:431–7.
23. Boyden PA, Albala A, Dresdner Jr KP. Electrophysiology and ultrastructure of canine subendocardial Purkinje cells isolated from control and 24-hour infarcted hearts. *Circ Res.* 1989;65:955–70.
24. Pinto JM, Boyden PA. Reduced inward rectifying and increased E-4031 sensitive K^+ current density in arrhythmogenic subendocardial Purkinje myocytes from the infarcted heart. *J Cardiovasc Electrophysiol.* 1988;9:299–311.
25. Dun W, Baba S, Yagi T, et al. Dynamic remodeling of K^+ and Ca^{2+} currents in cells that survived in the epicardial border zone of canine healed infarcted heart. *Am J Physiol Heart Circ Physiol.* 2004;287:H1046–54.
26. Dun W, Boyden PA. Diverse phenotypes of outward currents in cells that have survived in the 5-day infarcted heart. *Am J Physiol Heart Circ Physiol.* 2005;289:H667–73.
27. Jiang M, Cabo C, Yao J, et al. Delayed rectifier K currents have reduced amplitudes and altered kinetics in myocytes from infarcted canine ventricle. *Cardiovasc Res.* 2000;48:34–43.
28. Yuan F, Pinto JM, Li Q, et al. Characteristics of $I(K)$ and its response to quinidine in experimental healed myocardial infarction. *J Cardiovasc Electrophysiol.* 1999;10:844–54.
29. Gardner PI, Ursell PC, Genoglio Jr JJ, et al. Electrophysiologic and anatomic basis for fractionated electrograms recorded from healed myocardial infarcts. *Circulation.* 1985;72:596–611.
30. Spear JF, Michelson EL, Moore EN. Reduced space constant in slowly conducting regions of chronically infarcted canine myocardium. *Circ Res.* 1983;53:176–85.
31. Spear JF, Michelson EL, Moore EN. Cellular electrophysiologic characteristics of chronically infarcted myocardium in dogs susceptible to sustained ventricular tachyarrhythmias. *J Am Coll Cardiol.* 1983;1:1099–110.
32. Peters NS. Myocardial gap junction organization in ischemia and infarction. *Microsc Res Tech.* 1995;31:375–86.
33. Peters NS, Coromilas J, Severs NJ, et al. Disturbed connexin43 gap junction distribution correlates with the location of reentrant circuits in the epicardial border zone of healing canine infarcts that cause ventricular tachycardia. *Circulation.* 1997;95:988–96.
34. Matsushita T, Oyamada M, Fujimoto K. Remodeling of cell-cell and cell-extracellular matrix interactions at the border zone of rat myocardial infarcts. *Circ Res.* 1999;85:1046–55.
35. Matsushita T, Takamatsu T. Ischemia –induced temporal expression of connexin43 in rat heart. *Virchows Arch.* 1997;431:453–8.
36. Yao JA, Hussain W, Patel P, et al. Remodeling of gap junctional channel function in epicardial border zone of healing canine infarcts. *Circ Res.* 2003;92:437–43.
37. Kieken F, Mustsaers N, Dolmatova E, et al. Structural and molecular mechanisms of gap junction remodeling in the epicardial border zone myocytes following myocardial infarction. *Circ Res.* 2009;104:1103–12.
38. Qin D, Zang A-H, Caref EB, et al. Cellular and ionic basis of arrhythmias in postinfarction remodeled ventricular myocardium. *Circ Res.* 1996;79:461–73.
39. Anversa P, Kajstura J, Reiss K, et al. Ischemic cardiomyopathy: Myocyte cell loss, myocyte cellular hypertrophy, and myocyte cellular hyperplasia. *Ann N Y Acad Sci.* 1995;752:47–64.
40. Weber KT, Brilla CG. Pathological hypertrophy and cardiac interstitium: Fibrosis and renin-angiotension-aldosterone system. *Circulation.* 1991;83:1849–65.
41. Huang B, Qin D, El-Sherif N. Spatial alterations of K_v channels expression and K^+ currents in post-MI remodeled rat heart. *Cardiovasc Res.* 2001;52:246–54.
42. Perrier E, Kerfant B-G, Lalevee N, et al. Mineralocorticoid receptors antagonism prevents the electrical remodeling that precedes cellular hypertrophy after myocardial infarction. *Circulation.* 2004;110:776–83.
43. Hart G. Cellular electrophysiology in cardiac hypertrophy and failure. *Cardiovasc Res.* 1994; 28:933–46.

44. El-Sherif N, Huang B, Qin D. Cellular and molecular basis of arrhythmias in the postinfarction remodeled ventricular myocardium. In: Zipes DP, Jalife J, editors. Cardiac electrophysiology from cell to bedside. Philadelphia Cq: WB Saunders; 2000. p. 4045–414.
45. Gidh-Jain M, Huang B, Jain P, et al. Differential expression of voltage-gated K⁺ channel genes in left ventricular remodeled myocardium after experimental myocardial infarction. *Circ Res*. 1996;79:669–75.
46. Tohso N, Masuda H, Sperelakis N. Novel isoform of Ca²⁺ channel in rat fetal cardiomyocytes. *J Physiol (London)*. 1992;451:295–306.
47. Valdivia C, Chu WW, Pu J, et al. Increased late sodium current in myocytes from a canine heart failure model and from human heart. *J Mol Cell Cardiol*. 2005;38:475–83.
48. Nerbonne JM, Kass RS. Molecular physiology of cardiac repolarization. *Physiol Rev*. 2005; 85:1205–53.
49. Thomsen MB, Sosunov EA, Anyukhovsky EP, et al. Deleting the accessory subunit K Ch1P2 results in loss of I_{to, f} and increased I_K, slow that maintains normal action potential. *Heart Rhythm*. 2009;6(3):370–7.
50. DiFrancesco D, Ojeda C. Properties of the current i_r in the sino-atrial node of the rabbit compared with those of the current i_k, in Purkinje fibres. *J Physiol*. 1980;308:353–67.
51. Stieber J, Hoffmann F, Ludwig A. Pacemaker channels and sinus node arrhythmia. *Trends Cardiovasc Med*. 2004;14:23–8.
52. Sartiani L, De Paoli P, Stillitano F, et al. Functional remodeling in post-myocardial infarcted rats: focus on beta-adrenoreceptor subtypes. *J Mol Cell Cardiol*. 2005;40:258–66.
53. Tavares NI, Philip-Couderc P, Papageorgiou I, et al. Expression and function of ATP-dependent potassium channels in late post-infarction remodeling. *Mol Cell Cardiol*. 2007; 42:1016–25.
54. El-Sherif N, Craelius W, Boutjidir M, et al. Early afterdepolarizations and arrhythmogenesis. *J Cardiovasc Electrophysiol*. 1990;1:145–60.
55. Aronson RS. After potentials and triggered activity in hypertrophied myocardium from rats with renal hypertension. *Circ Res*. 1981;48:720–7.
56. Barbieri M, Varani K, Cerbai E, et al. Electrophysiological basis for the enhanced cardiac arrhythmogenic effect of isoprenaline in aged spontaneously hypertensive rats. *J Mol Cell Cardiol*. 1994;26:849–60.
57. Bing OHL, Brooks WW, Conrad CH, et al. Intracellular calcium transients in myocardium from spontaneously hypertensive rats during the transition to heart failure. *Circ Res*. 1991; 68:1390–400.
58. Cerbai E, Barbieri M, Mugelli A. Characterization of the hyperpolarization-activated current, I_f in ventricular myocytes isolated from hypertensive rats. *J Physiol*. 1994;481:585–91.
59. Restivo M, Gough WB, El-Sherif N. Ventricular arrhythmias in the subacute myocardial infarction period. High-resolution activation and refractory patterns of reentrant rhythms. *Circ Res*. 1990;66:1310–27.
60. Wit AL, Dillon SM, Coromilas J. Anisotropic reentry as a cause of ventricular tachyarrhythmias in myocardial infarction. In: Zipes DP, Jalife J, editors. Cardiac electrophysiology: from cell to bedside. 2nd ed. Philadelphia: WB Saunders; 1995. p. 511–26.
61. Peters NS, Green CR, Poole Wilson PA, et al. Reduced content of connexin43 gap junctions in ventricular myocardium from hypertrophied and ischemic human hearts. *Circulation*. 1993; 88:864–75.
62. El-Sherif N, Scherlag BJ, Lazzara R, et al. Reentrant ventricular arrhythmias in the late myocardial infarction period: conduction characteristics in the infarction zone. *Circulation*. 1977;55:686–702.
63. El-Sherif N, Smith RA, Evans K. Canine ventricular arrhythmias in the late myocardial infarction period: epicardial mapping of reentrant circuits. *Circ Res*. 1981;49:255–65.
64. El-Sherif N. Reentrant mechanism in ventricular arrhythmias. In: Zipes DP, Jalife J, editors. Cardiac electrophysiology and arrhythmias. Orlando, FL: Grune & Stratton; 1995. p. 365–78.

65. El-Sherif N, Mehra R, Gough WB, et al. Reentrant ventricular arrhythmias in the late myocardial infarction period: interruption of reentrant circuits by cryothermal techniques. *Circulation*. 1983;8:644–56.
66. Chillou C, Lacroix D, Klug D, et al. Isthmus characteristics of reentrant ventricular tachycardia after myocardial infarction. *Circulation*. 2002;105:726–31.
67. Nattel S, Maguy A, Le Bouter S, et al. Arrhythmogenic ion-channel remodeling in the heart: heart failure, myocardial infarction, and atrial fibrillation. *Physiol Rev*. 2007;87:425–56.
68. Michel JB, Lattion AL, Salzmann JL, et al. Hormonal and cardiac effects of converting enzyme inhibition in rat myocardial infarction. *Circ Res*. 1988;62:641–50.
69. Fishbein MC, Lei LQ, Rubin SA. Long-term propranolol administration alters myocyte and ventricular geometry in rat hearts with and without infarction. *Circulation*. 1988;78:369–75.
70. Belichard P, Savard P, Cardinal R, et al. Markedly different effects on ventricular remodeling result in a decrease in inducibility of ventricular arrhythmias. *Am Coll Cardiol*. 1994;23:505–13.
71. Li Y, Xue Q, Ma J, et al. Effects of imidapril on heterogeneity of action potential and calcium current of ventricular myocytes in infarcted rabbits. *Acta Pharmacol Sin*. 2004;25:1458–63.
72. Maltsev VA, Sabbab HN, Undrovinas AI. Down-regulation of sodium current in chronic heart failure: effect of long-term therapy with carvedilol. *Cell Mol Life Sci*. 2002;59:1561–8.
73. Li X, Huang CX, Jang H, et al. The beta-adrenergic blocker carvedilol restores L-type calcium current in a myocardial infarction model of rabbit. *Chin Med J*. 2005;118:377–82.
74. ISIS-4 (Fourth International Study of Infarct Survival) Collaborative Group. ISIS-4: a randomized factorial trial assessing early oral captopril, oral mononitrate and intravenous magnesium sulphate in 58050 patients with suspected acute myocardial infarction. *Lancet*. 1995;345:669–82.
75. Barr CS, Lang CC, Hanson J, et al. Effects of adding spironolactone to an angiotensin-converting enzyme inhibitor in chronic congestive heart failures secondary to coronary artery disease. *Am J Cardiol*. 1995;76:1259–65.
76. Pitt B, Zannad F, Remme WJ, et al. The effect of spironolactone on morbidity and mortality in patients with severe heart failure. *N Engl Med*. 1999;341:709–17.
77. Wickenden AD, Kaprielian R, Parker TG, et al. Effects of development and thyroid hormone on K⁺ currents and K⁺ channel gene expression in rat ventricle. *J Physiol (Lond)*. 1997;504:271–86.
78. Wickenden AD, Kaprielian R, You X-M, Backx PH. The thyroid hormone analog DITPA restore I_{to} in rats after myocardial infarction. *Am J Physiol*. 2000;278:H1105–16.
79. Mulder P, Richard V, Compagnon P, et al. Increased survival after long-term treatment with mibepradil, a selective T-channel calcium antagonist, in heart failure. *J Am Coll Cardiol*. 1997;29:416–21.
80. Sussman MA, Lim HW, Gude N, et al. Prevention of cardiac hypertrophy in mice by calcineurin inhibition. *Science*. 1998;281:1690–3.
81. Molkentin JD, Lu J-R, Antos CL, et al. A calcineurin-dependent transcriptional pathway for cardiac hypertrophy. *Cell*. 1998;93:215–28.
82. Deng L, Huang B, Qin D, et al. Calcineurin inhibition ameliorates structural, contractile, and electrophysiological consequences of post-infarction remodeling. *J Cardiovasc Electrophysiol*. 2001;12:1055–61.
83. Mascareno E, Dhar EM, Siddiqui MAQ. Signal transduction and activator of transcription (STAT) protein-dependent activation of ANG promoter. A cellular signal for hypertrophy in cardiac muscle. *Proc Natl Acad Sci USA*. 1998;95:5590–4.
84. El-Adawi H, Deng L, Tramontano A, et al. The functional role of the JAK-STAT pathway in post infarction remodeling. *Cardiovasc Res*. 2003;58:126–35.
85. Deng L, Boutjdir M, Tramontano A, et al. A peptide from a ras effector-domain blocks ras-dependent cardiac hypertrophy in myocytes. *Ann Clin Lab Sci*. 2009;39:351–60.

Chapter 16

The Role of Intracellular Ca^{2+} in Arrhythmias in the Postmyocardial Infarction Heart

Wen Dun, Henk ter Keurs, and Penelope A. Boyden

16.1 Introduction

16.1.1 Excitation–Contraction Coupling

During the action potential (AP), Ca^{2+} ions enter the cell through L-type Ca^{2+} channels. In ventricular cells, the number of Ca^{2+} channels is estimated to be 15 per μm^2 and yet only 3% are open at peak currents (for review see [1]). However, the amount of Ca^{2+} entering a cell per second depends on AP duration and the number of APs/min. L-type Ca^{2+} influx occurs at both T-tubular and cell surfaces, but in ventricular cells from normal hearts, more Ca^{2+} entry occurs per μm^2 at the cell surface than at T-tubules [2]. This Ca^{2+} influx begins ECC by triggering release of Ca^{2+} from the ryanodine (RyR) sensitive Ca^{2+} release channels located in the intracellular sarcoplasmic reticular (SR) membranes. In the rat [3], the ratio of RyR to L-type Ca^{2+} channels is 7:1 and would fit spatially with random coupling of the L-type Ca^{2+} channel to Ca^{2+} release via RyR [4]. Based on labeling studies, the ratio of cell surface L-type Ca^{2+} channels vs. T-tubular channels is 1:3 [5].

Intracellular Ca^{2+} -induced Ca^{2+} release (CICR) is proportional to the free intra-SR Ca^{2+} content and dictates the force of the cardiac contraction. Free Ca^{2+} in the SR has been spatially resolved [6] and these data show that intra-SR Ca^{2+} diffusion is rapid and local Ca^{2+} in SR in normal ventricular cells is only partially depleted with a contraction. Ca^{2+} -activated contraction of the sarcomere is short lived due to the rapid elimination of Ca^{2+} ions from the cytosol. About two thirds

W. Dun and P.A. Boyden (✉)

Department of Pharmacology, Center for Molecular Therapeutics, Columbia University, New York, NY, USA
e-mail: pab4@columbia.edu

H. ter Keurs

University of Calgary, Calgary, AB, Canada

of the Ca^{2+} is resequestered by the SR [7], while the remainder leaves the cell, mostly via the low affinity, high capacity, Na/Ca exchanger transport (NCX) protein. In the steady state, the sum of the Ca^{2+} efflux through the membrane balances the influx during the AP. It takes time for the RyR- Ca^{2+} release process to recover completely from the last release so that sequestered Ca^{2+} can again be released from the SR.

It is possible to load the SR excessively with Ca^{2+} ions. This may occur following damage of cardiac cells or after exposure to interventions that increase intracellular Ca^{2+} levels (digitalis, high $(\text{Ca}^{2+})_o$, high pacing rate). The SR membrane-associated channel proteins release Ca^{2+} spontaneously into the cytosol either by spontaneous activation of RyR due to luminal Ca^{2+} overload or to a local depolarization. Spontaneous uncoordinated Ca^{2+} release between paced beats can be observed as spontaneous contractions of small groups of sarcomeres in cells of the myocardium and gives rise to fluctuations of the light scattering properties of the muscle [8, 9]. Spontaneous Ca^{2+} release increases the diastolic force generated by the contractile filaments and in so doing, reduces Ca^{2+} release during the next heart beat [10, 11]. In turn, spontaneous release of Ca^{2+} ions can lead to cell depolarization as a result of activation of Ca^{2+} -modulated channels and/or by electrogenic NCX (the current generated has been called I_{ti} [12]).

16.1.2 ECC Coupling in Purkinje Cells from Normal Hearts

As a result of the different structure of the Purkinje cell (e.g., lacking T-tubuli) [13], coupling of excitation of the cell membrane with Ca^{2+} release in the core of these cells differs substantially from that of myocytes. Immunostaining experiments in rabbit Purkinje cells show that RyRs are subsarcolemmal (SSL) as well as within the cell (core) consistent with earlier reports [14–17]. In fact, canine Purkinje cells contain both RyR3 and RyR2 isoforms with the RyR3 protein being located predominantly in the SSL. The implication here is that the normal Purkinje cell contains both junctional and nonjunctional release channels. The AP of the Purkinje cell precedes rapid Ca^{2+} entry into the SSL space, which in turn induces Ca^{2+} release that in some species propagates into the core of the cell [18]. In rabbit Purkinje cells, experiments with ryanodine suggest that Ca^{2+} changes in the core of cells are best explained by simple buffered Ca^{2+} diffusion and not Ca^{2+} propagation [14]. However, in rabbit Purkinje cells, evoked Ca^{2+} transients are only seen to originate at peripheral cellular components, suggesting that RyRs in the cell center of this type of cell are “silent” [14]. However, in canine Purkinje cells, electrically evoked Ca^{2+} transients are multiphasic [18, 19]. In some Purkinje cells from normal hearts, if electrically evoked peripheral release is spatially and temporally inhomogeneous, a local Ca^{2+} wave is produced and can propagate as a traveling cell-wide Ca^{2+} wave along the length of the aggregate as well as towards the cell’s core [17, 18].

16.1.3 Reversal of Excitation–Contraction Coupling

In 2001 [20], Ter Keurs and Boyden defined the term reverse excitation–contraction coupling (RECC) to mean that in any cardiac cell, intracellular Ca^{2+} could feedback onto the cell surface membrane Ca^{2+} -dependent proteins to produce electrical signals. In this way, the released Ca^{2+} drives the membrane excitation. The RECC could occur in both ventricular and Purkinje cells and has gained recent attention as it underlies the mechanism of triggered beats in RyR and CASQ gene mutations arrhythmias [21, 22].

16.2 Ca^{2+} Homeostasis in Subendocardial Purkinje Cells During the Subacute Healing Phase Postmyocardial Infarction

Rapid ventricular arrhythmias after total coronary artery occlusion in the canine heart arise from ectopic foci (triggered or automatic) within the Purkinje fiber network located in the subendocardium of the infarct zone in the left ventricle [23]. These spontaneously occurring arrhythmias predictably occur between 24 and 48 h after occlusion. We have shown that density and function of several sarcolemmal ion channels are altered in the Purkinje cells dispersed from the subendocardium of the infarct zone (IZPCs) [24]. Further, we have shown that Ca^{2+} transients in cell aggregates from Purkinje tissues of normal LV subendocardium (NZPCs) consist of a membrane-linked Ca^{2+} transient that occurs in response to an AP. This initial Ca^{2+} transient usually leads to a Ca^{2+} transient that propagates to the cell core. Paced global Ca^{2+} transients of NZPCs are reasonably normal in amplitude with often a secondary plateau (asterisks in Fig. 16.1a) that occurs during the maintained AP plateau of the Purkinje cell [18]. In time as the cell completes repolarization, a slower decay of the global transient occurs. Cell-wide Ca^{2+} waves (CWW) that propagate along an aggregate occur spontaneously during the inter-stimulus interval and can give rise to nondriven electrical activity [18]. Because abnormal impulse initiation in the subendocardial Purkinje network is the cause of the infarction-related arrhythmias [23], we have gone on to determine whether electrically evoked Ca^{2+} transients and the incidence of spontaneous Ca^{2+} waves are altered in IZPCs.

16.2.1 Purkinje Cell Ca^{2+} Currents

Peak L-type Ca^{2+} channel current (I_{CaL}) density is significantly reduced in subendocardial Purkinje myocytes dispersed from the 48-h infarcted heart as compared to control and to those from the 24-h infarcted heart [25]. This current density

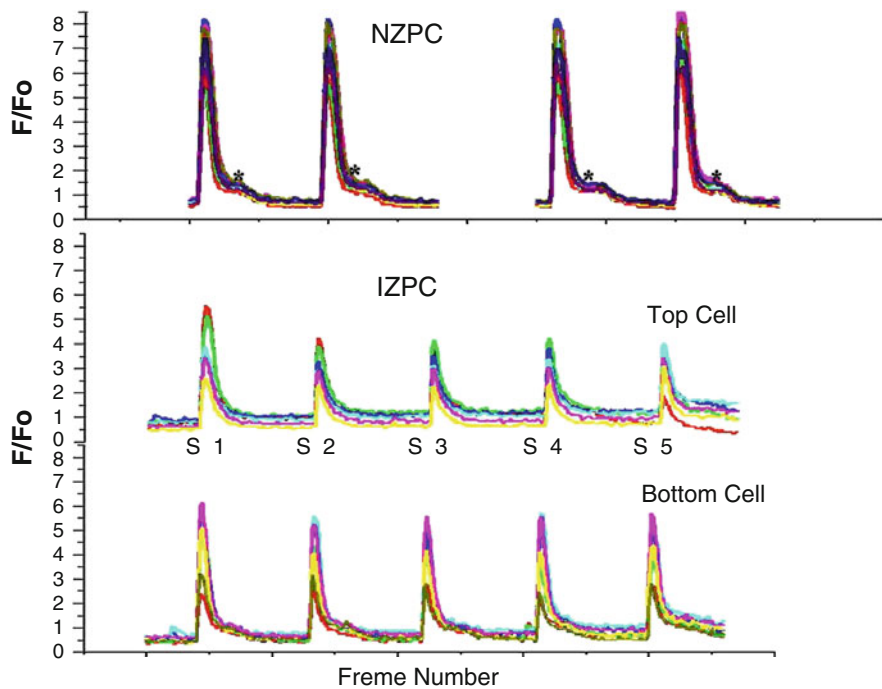


Fig. 16.1 Panel (a) Change in intensity (F/F_0) of fluorescence at various ROIs during pacing in an NZPC aggregate. Note action potential-evoked Ca^{2+} transients are robust and synchronous in the NZPC. Asterisk indicates a secondary plateau of Ca^{2+} which coincides with the terminal phase of repolarization. Panel (b) Change in intensity (F/F_0) of fluorescence at various ROIs during five paced beats (S1...S5) in two IZPCs (top and bottom). Note the action potential-evoked Ca^{2+} transients are nonuniform in IZPCs

reduction is not accompanied by a shift in the current–voltage relationship or a change in the time course of I_{CaL} decay, but by a hyperpolarizing shift in the steady-state availability of the channel. Peak T-type Ca^{2+} channel current (I_{CaT}) density is also decreased in subendocardial Purkinje myocytes that survive in the 24-h infarcted heart, and further reduction occurs by 48 h. The loss in Ca^{2+} channel function could contribute to the depressed and triangular plateau phase of the APs of these arrhythmogenic IZPCs [26].

16.2.2 Intracellular Ca^{2+} Cycling

One of the cellular mechanisms of triggered activity is the delayed after depolarization (DAD). We have shown that nonuniform Ca^{2+} transients in Purkinje cells that have survived the infarct underlie spontaneous membrane depolarizations, and both the *amplitude* of the Ca^{2+} waves that are present and their number and spatial

extent predict the membrane depolarization [19]. Further, electrically evoked Ca^{2+} transients in IZPCs arise faster than those in normal Purkinje cell aggregates, but show substantial spatiotemporal nonuniformity within an IZPC aggregate as well as between IZPC aggregates (Fig. 16.1b). Reduced Ca^{2+} influx via the I_{CaL} may be partially responsible for the abnormal AP-evoked global Ca^{2+} transients observed in IZPCs [19]. Importantly, IZPCs showed low amplitude, spontaneously occurring micro- Ca^{2+} (μCa^{2+}) transients at a fivefold higher incidence than in normal Purkinje aggregates. The μCa^{2+} transients meander over short distances and reduce the local Ca^{2+} transient of the next paced beat (Fig. 16.2). Finally, these spontaneous μCa^{2+} transients preceded cell-wide Ca^{2+} waves (Fig. 16.3). Cell-wide Ca^{2+} waves, in turn, clearly cause membrane depolarization and elicit spontaneous APs. Thus, the high incidence of μCa^{2+} transients in IZPCs is fundamental to the abnormal Ca^{2+} handling of the diseased Purkinje cells, underlying the arrhythmias originating in the subendocardial Purkinje network after a myocardial infarct.

Recently, we evaluated the reasons for increased incidence of μCa^{2+} transients in IZPCs. The μCa^{2+} transients are not affected by verapamil [27] and abnormal electrical rhythms in Purkinje cells that have survived in the infarcted heart are insensitive to the T-type Ca^{2+} channel blocker, mibepradil [28]. Finally, because Ca^{2+} waves and the resultant membrane depolarization in Purkinje cells are ryanodine sensitive [27], we sought to determine whether increased incidence of Ca^{2+} waves in IZPCs is due to *enhanced* spontaneous Ca^{2+} release secondary to altered activity of SR Ca^{2+} release channels.

Using 2D confocal microscopy, we found that the amplitude of Ca^{2+} release events, i.e., the Ca^{2+} sparks, was significantly increased in IZPCs compared to NZPCs. In addition, the event rate of Ca^{2+} release in cell regions just below the sarcolemma of IZPCs is also increased. Importantly, SR Ca^{2+} content did not differ between NZPCs and IZPCs in all cell regions, which suggested that there was an enhanced sensitivity of SR Ca^{2+} release channels in IZPCs. In fact, permeabilized IZPCs showed an increased Ca^{2+} release event rate in both SSL and core regions, confirming this idea [29]. Other Ca^{2+} release events such as wide, long-lasting Ca^{2+} release events [30], micro- Ca^{2+} transients, and cell-wide Ca^{2+} waves show an accelerated decay after Ca^{2+} release in IZPCs. These results indicate an enhanced extrusion of Ca^{2+} and suggest that there is an enhanced Ca^{2+} sequestration by SERCA2 and/or an enhanced efflux of Ca^{2+} by NCX in IZPCs. These properties would lower the threshold of Ca^{2+} release channels, setting the stage for the highly frequent arrhythmogenic cell-wide Ca^{2+} waves and DADs in Purkinje cells that survive in the infarcted heart.

16.2.3 Structural Remodeling in Purkinje Cells That Survive in the Infarcted Heart

Our functional data are consistent with the multiple Ca^{2+} release compartments in NZPCs, which we hypothesized to exist based on our immunocytochemistry data

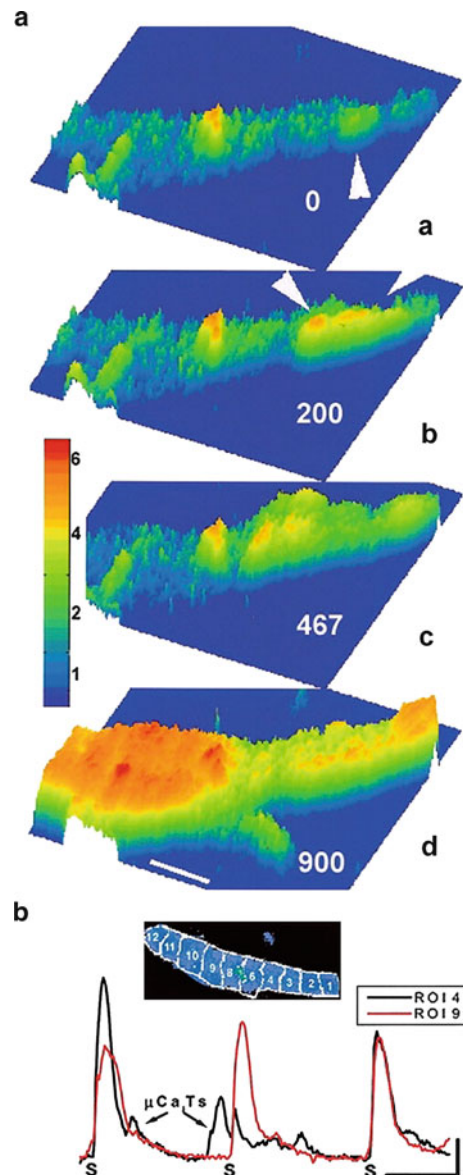


Fig. 16.2 Nonuniformly occurring micro- Ca^{2+} transients (arrowheads) cause nonuniformity of the action potential-evoked Ca^{2+} response in a canine IZPC aggregate. Panel (A) 3D surface plots of IZPC just preceding and during one electrically evoked Ca^{2+} transient [denoted by S in Panel (B)]. (Ca^{2+}) are denoted by both the color and height of the surface. White numbers indicate time of frame relative to $t = 0$ (Aa). The aggregate was stimulated just before $t = 900$ ms (Ad). Note the presence of micro- Ca^{2+} waves (arrowheads), which propagate over short distances ($t = 0$ to 467 ms) meandering from the right section of the aggregate toward the core. Subsequent stimulation causes a nonuniform electrically evoked local Ca^{2+} transients ($t = 900$ ms) particularly in regions where

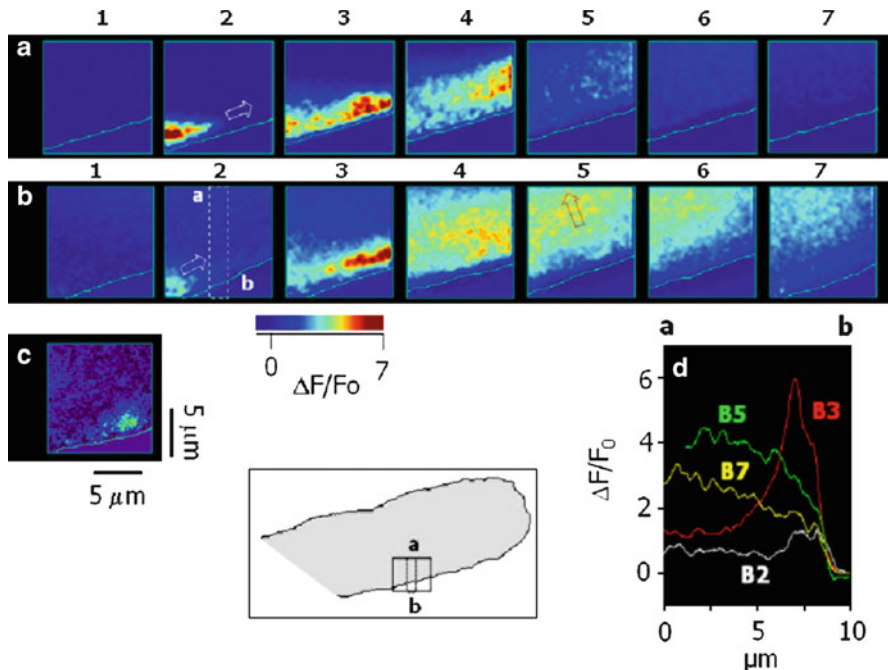


Fig. 16.3 Two-dimensional confocal Ca^{2+} images of the subsarcolemmal events in an NZPC. Panels (A) and (B) show two series of consecutive 2D frames constructed from x/y scanning (100 scan lines, 10 $\mu\text{m}/\text{line}$, 1.2 ms/line) of cell region covering sarcolemma (SL), Sub-SL, and a small region of the cell center (see bottom inset). (Ca^{2+})_i is expressed in relative variation of F/F_0 ($\Delta F/F_0 = (F - F_0)/F_0$). Panel (A) A wavelet propagates from the left to the right within a $\approx 6 \mu\text{m}$ wide region under the sarcolemma (Sub-SL). Panel (B) A similar wavelet in the same aggregate initiates (frame B4) a wave that propagates to the cell center (see arrow in B5). The green line, superimposed to the frames, underlines the position of the sarcolemma as the boundary between intracellular fluorescence and extracellular milieus. Panel (C) Sub-SL nonpropagating Ca^{2+} transient in the same aggregate. Panel (D) Spatiotemporal Ca^{2+} profiles (indicated by corresponding frame number: B2, B3, B5, B7) of wave generation shown in panel (B). From [17]

using specific RyR antibodies. Frequency analysis was then used to determine whether RyR2 staining was regularly organized in the two cell types (Fig. 16.4). We identified three different types of Purkinje cells. Type I cells showed regular periodicity of RyR2 staining [NZPCs 89% of total cells (31); IZPCs 38% of total

↔

Fig. 16.2 (continued) micro- Ca^{2+} transients had been. Horizontal bar indicates 50 μm . Color bar indicates ratio range. Panel (B) Changes in intensity of fluorescence (F/F_0) at two selected specific regions of interest (ROIs) in IZPC aggregate of panel (A). Stimuli are indicated (S). Each ROI is represented by a different color and location is noted in upper image. Note that when the micro- Ca^{2+} transients observed in ROI4 (see arrowheads of panel (A)) precede S, the subsequent Ca^{2+} transient of S is diminished compared to that of the previous S. Note that in ROIs where micro- Ca^{2+} transients were absent (e.g., ROI 9), response to stimulation was constant. Vertical and horizontal lines are 1 F/F_0 units and 1.58 s, respectively. From [19]

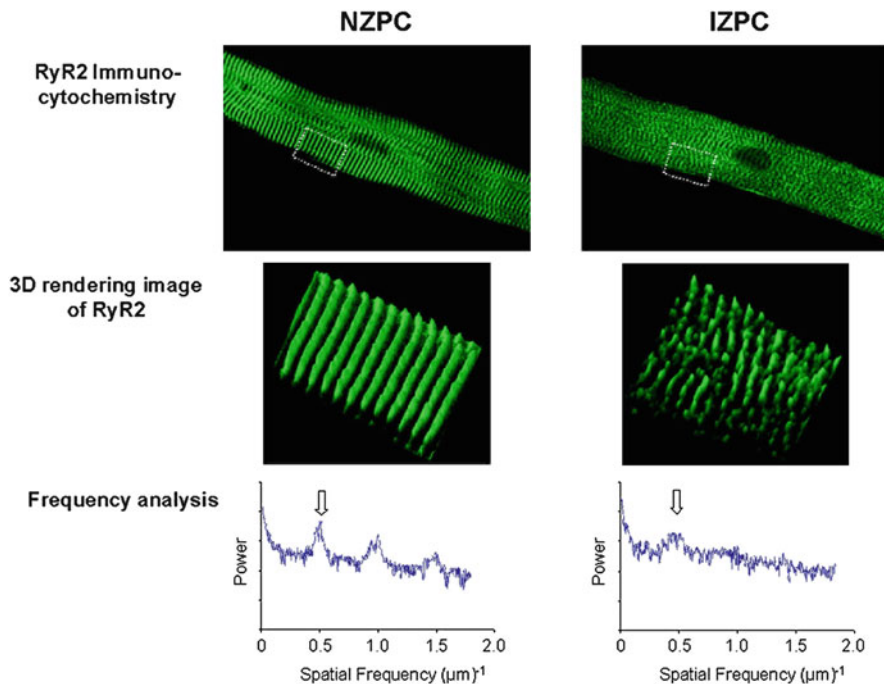


Fig. 16.4 A comparison of RyR2 staining in one NZPC and one IZPC. *Top panel* shows RyR2 staining in 2D representation in NZPC (left) and IZPC (right). *Middle panel* shows 3D rendering images of RyR2 in NZPC and IZPC. The image areas are marked as the white squares in the top panel. *Bottom panel* shows the frequency analysis of RyR2 staining in the NZPC and IZPC. Note that RyR2 staining was regularly organized in the NZPC while RyR2 staining was regionally disordered in the IZPC

((24), Fig. 16.4, left)]; type II cells lacked some periodicity {NZPCs (11%), IZPCs (42%)} while some IZPCs (21%) showed regions of disorder (Fig. 16.4, right) almost throughout the cell. In NZPCs, IP₃R1 staining was as before [17], showing sarcolemmal and not core, gap junctional and nuclear envelope but not intranuclear staining. In IZPCs (42% of total $n = 19$), we found that IP₃R1 signals appear to be shifted from discrete sarcolemma regions to the core, but they retain strong gap signals. IP₃R1s in the nuclear area were markedly changed in that most of the signal now appeared as ribbons within the nucleus.

16.3 Ca²⁺ Homeostasis in Epicardial Border Zone Cells of Healing Phase Post-MI (4–5 Days)

After several days postocclusion, spontaneous arrhythmias subside in this canine model until the 4–5th day postocclusion. At this time, long-lasting reentrant tachycardias are easily inducible. These arrhythmias arise from epicardial border

zone (EBZ) cells [32] and provide the substrate for these reentrant arrhythmias. The APs of these EBZ cells are triangular, having lost their plateau [33, 34]. Just a triangulation of the AP could cause abnormal global Ca^{2+} transients.

16.3.1 EBZ Ca^{2+} Currents

The peak I_{CaL} density of IZ cells dispersed from the 5-day EBZ of the infarcted heart (IZs) is significantly reduced by 36% compared to control [35]. Furthermore, this reduction is not due to a decrease in steady-state availability or a prolonged time course of recovery of I_{CaL} . However, the time course of decay of these currents is significantly faster than control cells. These findings may be related to a decrease in the number of functioning channels as well as an acceleration of inactivation of the remaining channels. Unlike the findings in the subendocardial Purkinje myocytes studies (see above), no significant differences were found between peak density and frequency of T-type Ca^{2+} currents in IZ myocytes vs. control epicardial myocytes from normal hearts (NZs). Our knowledge of altered sensitivity to transmitters of the autonomic system in diseased myocytes is derived from comparisons of the effects of adrenergic agonists on specific ionic currents. Commonly, adrenergic sensitivity is assessed by the effects of the adrenergic agonist, isoproterenol, on I_{CaL} . In NZs, isoproterenol depolarizes the resting membrane potential by inhibiting I_{K1} [36] and prolongs the AP by increasing I_{CaL} [37, 38]. Mimicry of isoproterenol effects using forskolin and cAMP has provided information regarding additional defects in the adrenergic complex.

Sympathetic stimulation produces minimal AP shortening in areas overlying the infarct and the border zone, whereas in areas remote from the arrhythmia substrate pronounced AP shortening occurs [39]. Furthermore, catecholamine-induced increase of the AP plateau phase is absent in the fibers of the EBZ of the 5- and 14-day infarcted heart [34]. Similar abbreviated responses to catecholamines have been documented in the ischemic human ventricle [40]. From voltage clamp data and in comparison with NZs, isoproterenol produces a smaller increase in I_{CaL} in cells from the 5-day- and 2-month-old infarct, independent of calcium-dependent inactivation [41, 42]. This is consistent with multiple defects in components of the adrenergic receptor complex in IZ cells of the 5-day old infarct, including, (1) decreases in adrenergic receptor density, (2) diminished basal, guanine nucleotide, isoproterenol, forskolin, and manganese-dependent adenylyl cyclase activities, (3) increases in the EC₅₀ for isoproterenol-dependent activation of adenylate cyclase, (4) diminished levels of the subunit of the Gs protein, and (5) elevated levels of the subunit of the Gi protein [43]. Therefore, an interesting question put forward is whether other signaling pathways are involved in the remodeled basal Ca^{2+} currents and isoproterenol-stimulated Ca^{2+} current function in IZs. Protein tyrosine kinases (PTKs) have been shown to modulate basal as well as β -adrenergic-stimulated Ca^{2+} current function in cardiac cells from normal hearts [44]. Our study showed that PKA activity contributes to I_{CaL} .

in both NZ and IZ cells, but dysregulation of PTK activity cannot account for the reduced basal Ca^{2+} currents or hyporesponsiveness of I_{CaL} to isoproterenol in the IZs [45].

Our new data point to a critical role for CaMKII in adverse Ca^{2+} remodeling after myocardial infarction [46]. First, the level of CaMKII autophosphorylation is increased in the EBZ. Second, results of computer simulations reveal that Ca^{2+} leak from the SR is due to CaMKII hyperphosphorylation. This then depletes SR Ca^{2+} content and contributes to depressed Ca^{2+} transients. Simulations (Fig. 16.5) also display the abnormal rate dependence of IZ Ca^{2+} transients seen experimentally [47].

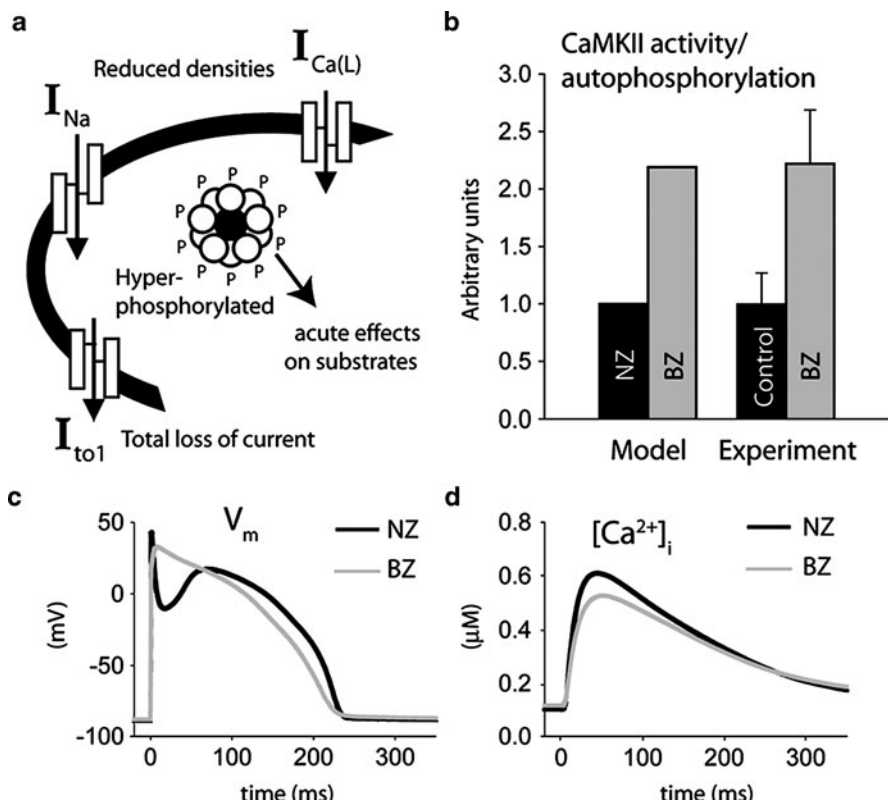


Fig. 16.5 Mathematical model of infarct border zone myocyte. Panel (a) Remodeling changes incorporated into the model include decreased $I_{\text{Ca(L)}}$, I_{Na} , and I_{to1} densities and acute effects of CaMKII hyperactivity on downstream substrates. Panel (b) Simulated basal CaMKII activity compared to experimentally measured autophosphorylation levels in NZ (black bars) and BZ (gray bars). Panel (c) Simulated action potentials (left panel) and calcium transients (right panel) in NZ (control HRd model, black line) and BZ (gray line) models for steady-state pacing at CL = 2,000 ms [46].

16.3.2 Remodeling of Ankyrin-B-Associated Proteins Following Myocardial Infarction

Ankyrin-B is an adapter protein required for targeting and stabilizing ion channels, exchangers, and pumps in excitable cells. While it is known that ankyrin-B gene mutations can give rise to LQTS type 4 in patients [48], little is known about ankyrin-B in common forms of acquired human disease. Mice lacking ankyrin-B phenocopy type 4 LQTS and ankyrin-B-deficient cardiomyocytes display abnormal calcium homeostasis due to abnormal targeting of key membrane proteins, resulting in cellular afterdepolarization. We were the first to present a report of ankyrin-B regulation in the EBZ post-MI [49] and showed that ankyrin-B protein levels are reduced in the EBZ (Fig. 16.6). We found no significant difference in expression levels of the IP₃R and NCX in EBZ at 5 or 14+ days postocclusion compared to normal. However, Na-K pump (NKA) protein expression was dramatically reduced in the EBZ 5 days postocclusion compared to normal, consistent with the reduction in ankyrin-B expression. Interestingly, NKA expression remained significantly reduced even at 14+ days, revealing a time course of recovery that follows recovery of ankyrin-B. Immunoblots indicated that, more specifically, NKA expression remains depressed at 14 days postocclusion but recovers to normal by 2 months.

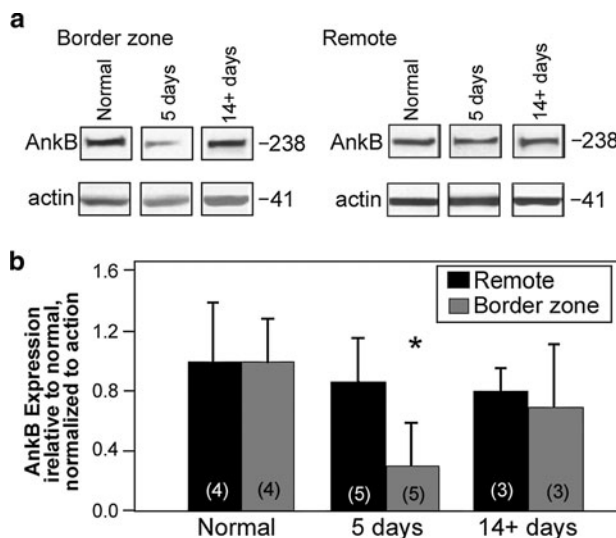


Fig. 16.6 Ankyrin-B protein levels decrease in the border zone 5 days postocclusion. Panel (a) Representative immunoblots and Panel (b) densitometry measurements (normalized to actin and expressed relative to normal levels) of AnkB from remote and BZ regions of normal and infarcted hearts. Error bars designate standard deviation (* $P < 0.01$ compared with normal BZ or remote, $n = 4$ for normal, $n = 5$ for 5-day, and $n = 3$ for 14+ day infarct). Densitometry measurements were made from all samples analyzed on same gel and normalized to the corresponding actin levels from the same blot. Equal protein loading was ensured by BCA assay and verified by analysis of Coomassie and Ponceau stains of gel and blots [49]

While we measured decreased expression of NKA by immunoblot in the EBZ, we detected no difference in protein levels of NCX or IP₃R [49]. As it is known that ankyrin helps to target ion channels to specific subcellular domains, we went on to determine whether subcellular redistribution of NCX and IP₃R occurred in 5-day postocclusion IZ myocytes. Immunofluorescence studies revealed cellular redistribution of both IP₃R and NCX in IZ myocytes 5 days postocclusion (Fig. 16.7). Specifically, while NCX and IP₃R show prominent localization at T-tubules in remote noninfarcted myocytes, their intracellular distribution is not uniform in IZs. Thus, cellular distribution but not total protein levels of NCX and IP₃R change in the cells from 5-day EBZ.

Recent studies have also demonstrated that ankyrin-B directly associates with the targeting subunit of the protein phosphatase PP2A. Therefore, we determined whether expression and/or distribution of PP2A was altered in the EBZ. Interestingly, by 5-days postocclusion, expression of the PP2A catalytic subunit (constituent of the core enzyme) increased to more than three times its normal level (Fig. 16.8). These changes in protein expression were paralleled by increased membrane expression of PP2A in IZ myocytes 5-days postocclusion. By 14+ days postocclusion, PP2A protein levels in the EBZ returned to normal levels following a time course similar to that of changes in ankyrin-B expression. Thus, ion channel transporter remodeling post-MI seems to be downstream from ankyrin-B remodeling.

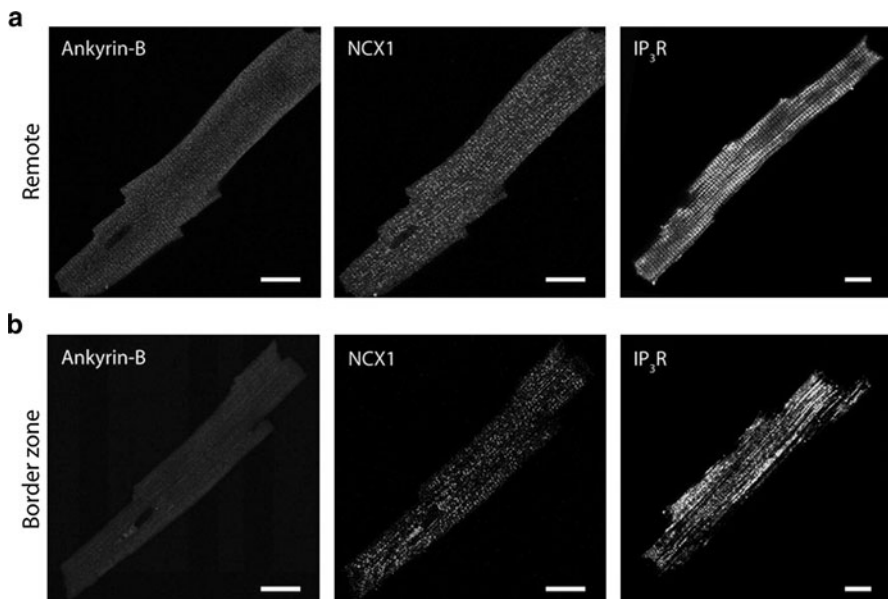


Fig. 16.7 Cellular redistribution of NCX and IP₃R in border zone myocytes. Isolated myocytes from remote and BZ regions of 5-day infarcted hearts were immunoassayed using antibodies against AnkB (left), NCX1 (middle), and IP₃R (right). Localization of NCX1 and IP₃R in BZ myocytes is less pronounced at T-tubules in BZ myocytes, where AnkB expression is reduced. Scale bars, 10 μ m [49]

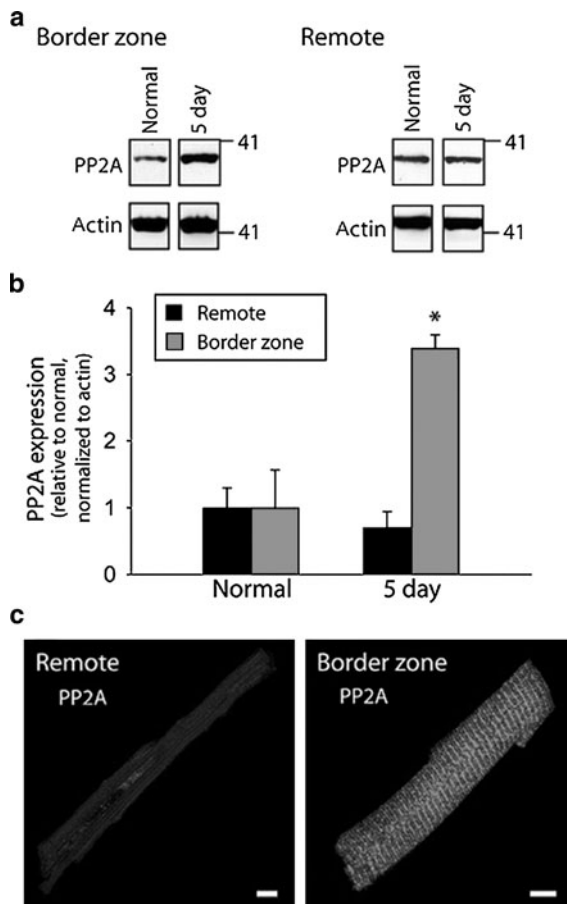


Fig. 16.8 Altered PP2A expression in the border zone 5 days postocclusion. Panel (a) Representative immunoblots and Panel (b) densitometry measurements (normalized to actin and expressed relative to normal levels) of PP2A catalytic subunit from remote and BZ regions of normal and 5-day infarcted hearts. Error bars designate standard deviation ($n = 4$ for each group). Panel (c) Isolated myocytes from remote and BZ regions of 5-day infarcted hearts were immunoassayed using antibody against the PP2A catalytic subunit. Scale bars, 10 μm [49]

16.3.3 Intracellular Ca^{2+} Cycling

In the pacing studies using fura2 AM loaded, nondialyzed cells, we found that the response of the amplitude of the global Ca^{2+} transient to a change with pacing rate in IZs is opposite to that which occurs in the normal epicardial cells [47]. In the NZs, an increase in rate is associated with an increase in Ca_i transient amplitude whereas in IZs, the rate causes a decrease in Ca^{2+} transient amplitude. In addition, the recovery of the amplitude of the AP-evoked Ca_i transient (restitution) is markedly

slowed in the IZ cells (Fig. 16.9A; [47]), yet there is marked rest potentiation of Ca_i transients in IZ cells vs. rest depression of the Ca_i transients in the normal cells. Presumably, the alteration in Ca^{2+} influx (see above) in IZ cells may alter ECC coupling in such a way that it results in less SR Ca^{2+} accumulation with the increase in pacing rate. While these fura2 experiments indicated an elevation of diastolic Ca^{2+} in IZ cells, precise determination of Ca^{2+} using fura2 in the patch pipette showed that at holding voltage of -50 mV, IZ cells have a 47% increase in resting ratio over NZ values [50].

Importantly, despite the reasonable, albeit smaller, amplitude Ca_i transients in the IZs, little or no cell shortening existed, which suggests that the lack of cell shortening in the IZs may be related to dramatic alterations in excitation–contraction coupling at the level of contractile element activation and/or to an altered

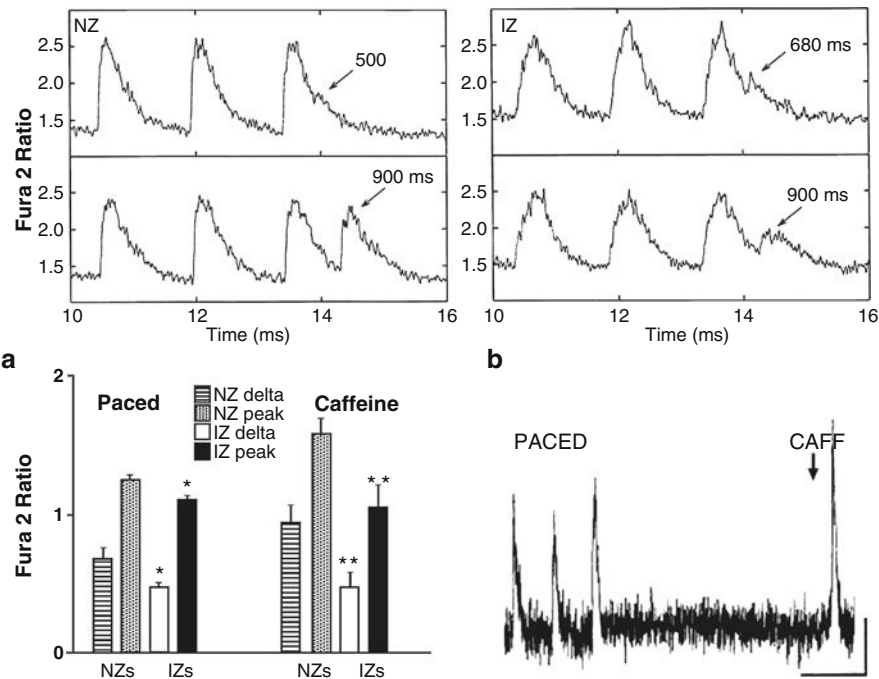


Fig. 16.9 Panel (A) Fura-2 tracings from NZ (left) and IZ (right) during restitution stimulation protocols. For each myocyte, both a short and long S1–S2 coupling interval are illustrated. Note that with a S1–S2 interval of 900 ms in the NZ, a large Ca_i transient is easily evoked while in the IZ a much smaller Ca_i transient is elicited. Panel (B) (a) Average Fura-2 ratio changes during six paced beats ($V_h = -70$ to $+10$ mV) and after exposure to caffeine (10 mM) in a subset of NZs and IZs. Height of bar indicates both peak ratio (solid bars) or delta ratio (grey bars) for each cell type during paced beats and caffeine. * $P < 0.05$ vs. NZ paced values, ** $P < 0.05$ vs. NZ caffeine. (b) Typical ratio changes in a cell during the last three paced clamp steps and caffeine exposure. Horizontal calibration bar equals 5 s while vertical bar equals 0.25 units. Holding voltage throughout protocol = -70 mV. From [47]

production of microtubules. In any case, the alteration in the Ca^{2+} transient in IZs would directly impact on the amplitude of several Ca^{2+} -dependent currents such as $I_{\text{to}2}$ [51]. Despite the relatively low Ca^{2+} sensitivity of this channel, they can conduct significant current transiently or in a sustained manner depending on Ca^{2+} and time course of the subplasmalemmal Ca^{2+} transient. Thus, IZ cells, which have highly remodeled I_{CaL} and Ca^{2+} transients, show $I_{\text{to}2}$ currents which vary in size [51].

When IZ cells were clamped with a transmembrane voltage similar to an AP profile, we found that abnormal Ca_i transients in the voltage-clamped IZ cells persisted [50]. In the NZs, Ca_i transients showed the expected voltage relationship to I_{CaL} while the IZ cells did not. Thus, the abnormalities in Ca_i handling in the IZ cells do not appear to arise secondary to changes in AP configuration nor do they appear to be due to disease-induced alterations in NCX function (see below). Interestingly, the abnormal Ca_i transients in IZ cells recover when cells are superfused with the L-type calcium channel agonist, Bay5959 [52]. This effect on the remodeled cells may underlie Bay5959 antiarrhythmic effect in this arrhythmia model [53]. When caffeine was used to compare amounts of SR Ca^{2+} in IZ vs. normal cells, we found that in IZ cells caffeine induced less Ca^{2+} release (Fig. 16.9B). Thus, while Ca^{2+} entry in normal epicardial NZs may not release all SR Ca^{2+} available for release, the smaller Ca^{2+} amplitudes of paced IZ cells appear to result from Ca^{2+} influx releasing most SR Ca^{2+} that is available for release.

16.3.4 *$\text{Na}-\text{Ca}$ Exchanger Currents*

In NZs with normal Ca_i cycling, it is well established that currents generated by NCX play an important role in the electrical activity of a myocyte [54]. The NCX current is either outward (normal mode) as the transporter protein exchanges Ca_i for external Na^+ ions or inward (reverse mode) as the transporter causes Ca^{2+} influx by exchanging external Ca^{2+} ions for Na_i . Therefore, the time course of the exchanger current is related to the time course of Ca_i cycling. There have been several reports of abnormal Ca_i cycling in cells that have survived in the infarcted heart [31, 55–57]. In myocytes dispersed from the EBZ of the 5-day infarcted heart, both nonclamp [47] and voltage clamp studies [50] show that the diminished globally assessed Ca_i transient of the IZ cell has a slow relaxation (decay) phase. Furthermore, these cells have an altered phase 3 of their APs. These changes are consistent with changes in the NCX current. However, when studied under strict conditions that isolate only Ca_i and ionic current changes secondary to NCX, both Ca^{2+} entry (via the reverse exchanger) and Ni^{2+} sensitive IZ currents as well as Ca^{2+} extrusion (via normal mode exchanger) in IZs are similar to those of NZs, no matter what the Na_i load [50]. Thus, in these cells where L-type Ca^{2+} channels are down-regulated (see above), the NCX has a reserve efficiency and continues to contribute current to the transmembrane AP.

16.4 Conclusions

Abnormalities in intracellular Ca^{2+} handling occur in both Purkinje and ventricular cells that have survived in the infarcted heart. Interestingly, these changes differ depending on the cell type (IZPC vs. IZ) and contribute differently to the arrhythmogenicity of the post-MI substrate. Thus, it is reasonable to assume that rational drug design could derive compounds against these intracellular Ca^{2+} changes that would be specific not only for the cell type but also for the type of arrhythmias occurring post-MI. For example, for Purkinje cells that survive in the infarcted heart, molecular targets may include Ca^{2+} -release channels, while targets in epicardial cells that survive in the EBZ may include Ca^{2+} channel agonists.

Acknowledgments This work was supported by grant HL58860 from the National Heart Lung and Blood Institute Bethesda, Maryland and AHFMR grant (20040163), Canada (HtK).

References

1. Ter Keurs HEDJ, Boyden PA. Calcium and arrhythmogenesis. *Physiol Rev.* 2007;87:457–506.
2. Brette F, Salle L, Orchard CH. Quantification of calcium entry at the T-tubules and surface membrane in rat ventricular myocytes. *Biophys J.* 2006;90:381–9.
3. Bers DM, Stiffel VM. Ratio of ryanodine to dihydropyridine receptors in cardiac and skeletal muscle and implications for EC coupling. *Am J Physiol.* 1993;264:C1587–93.
4. Cannell MB, Cheng H, Lederer WJ. Spatial nonuniformities in Ca^{2+} during excitation contraction coupling in cardiac myocytes. *Biophys J.* 1994;67:1942–56.
5. Wibo M, Bravo G, Godfraind T. Postnatal maturation of excitation contraction coupling in rat ventricle in relation to the subcellular localization and surface density of 1,4 dihydropyridine and ryanodine receptors. *Circ Res.* 1991;68:662–73.
6. Shannon TR, Guo T, Bers DM. Ca^{2+} scraps: local depletions of free Ca^{2+} in cardiac sarcoplasmic reticulum during contractions leave substantial Ca^{2+} reserve. *Circ Res.* 2003;93:40–5.
7. Bers DM. Excitation–contraction coupling and cardiac contractile force. 1st ed. Dordrecht: Kluwer; 1991.
8. Kort AA, Lakatta EG. Calcium-dependent mechanical oscillations occur spontaneously in unstimulated mammalian cardiac tissues. *Circ Res.* 1984;54:396–404.
9. Lakatta EG, Lappe DL. Diastolic scattered light fluctuation, resting force and twitch force in mammalian cardiac muscle. *J Physiol.* 1981;315:369–94.
10. Lakatta EG, Jewell BR. Length dependent activation. Its effect in the length tension relation in cat ventricular muscle. *Circ Res.* 1977;40:251–7.
11. Stern MD, Capogrossi MC, Lakatta EG. Spontaneous calcium release from the sarcoplasmic reticulum in myocardial cells: mechanisms and consequences. *Cell Calcium.* 1988;9(5–6):247–56.
12. Lederer WJ, Tsien RW. Transient inward current underlying arrhythmogenic effects of cardiotonic steroids in Purkinje fibers. *J Physiol.* 1976;263:73–100.
13. Di Maio A, Ter Keurs HEDJ, Franzini-Armstrong C. T-tubular profiles in Purkinje fibres of mammalian myocardium. *J Muscle Res Cell Motil.* 2007;28:115–21.
14. Cordeiro JM, Spitzer KW, Giles W, Ershler PR, Cannell MB, Bridge JHB. Location of the initiation of calcium transients and sparks in rabbit Purkinje cells. *J Physiol.* 2001;531:301–14.
15. Sommer JR, Johnson EA. Cardiac muscle. A comparative study of Purkinje fibers and ventricular fibers. *J Cell Biol.* 1968;36:497–526.

16. Jorgensen AO, Shen ACY, Arnold W, McPherson P, Campbell KP. The Ca^{2+} release channel/ryanodine receptor is localized in junctional and corbulular sarcoplasmic reticulum in cardiac muscle. *J Cell Biol.* 1993;120:969–80.
17. Stuyvers BD, Dun W, Matkovich SJ, Sorrentino V, Boyden PA, Ter Keurs HEDJ. Ca^{2+} sparks and Ca^{2+} waves in Purkinje Cells: a triple layered system of activation. *Circ Res.* 2005;97:35–43.
18. Boyden PA, Pu J, Pinto JMB, Ter Keurs HEDJ. Ca^{2+} Transients and Ca^{2+} waves in Purkinje Cells. Role in action potential initiation. *Circ Res.* 2000;86:448–55.
19. Boyden PA, Barhaiya C, Lee T, Ter Keurs HEDJ. Nonuniform Ca^{2+} transients in arrhythmic Purkinje Cells that survive in the infarcted canine heart. *Cardiovasc Res.* 2003;57:681–93.
20. Boyden PA, Ter Keurs HEDJ. Reverse excitation–contraction coupling: Ca^{2+} ions as initiators of arrhythmias. *J Cardiovasc Electrophysiol.* 2001;12:382–5.
21. Cerrone M, Noujaim SF, Tolkacheva EG, Talkachou A, O'Connell R, Berenfeld O, et al. Arrhythmogenic mechanisms in a mouse model of catecholaminergic polymorphic ventricular tachycardia. *Circ Res.* 2007;101:1039–48.
22. Viatchenko-Karpinski S, Terentyev D, Gyurke I, Terentyeva R, Volpe P, Priori SG, et al. Abnormal calcium signaling and sudden cardiac death associated with mutation of calsequestrin. *Circ Res.* 2004;94:471–7.
23. Janse MJ, Wit AL. Electrophysiological mechanisms of ventricular arrhythmias resulting from myocardial ischemia and infarction. *Physiol Rev.* 1989;69:1049–169.
24. Pinto JMB, Boyden PA. Electrophysiologic remodeling in ischemia and infarction. *Cardiovasc Res.* 1999;42:284–97.
25. Boyden PA, Pinto JMB. Reduced calcium currents in subendocardial Purkinje myocytes that survive in the 24 and 48 hour infarcted heart. *Circulation.* 1994;89:2747–59.
26. Friedman PL, Stewart JR, JJ Jr F, Wit AL. Survival of subendocardial Purkinje fibers after extensive myocardial infarction in dogs. *Circ Res.* 1973;33:597–611.
27. Boyden PA, Dun W, Barhaiya C, Ter Keurs HEDJ. 2APB- and JTV519(K201) sensitive micro Ca^{2+} waves in arrhythmogenic Purkinje cells that survive in infarcted canine heart. *Heart Rhythm.* 2004;1:218–26.
28. Pinto JMB, Sosunov EA, Gainullin RZ, Rosen MR, Boyden PA. The effects of mibepradil a T type calcium channel current antagonist on the electrophysiology of Purkinje fibers that have survived in the infarcted heart. *J Cardiovasc Electrophysiol.* 1999;10:1224–35.
29. Hirose M, Stuyvers BD, Dun W, Ter Keurs HED, Boyden PA. Function of Ca^{2+} release channels in Purkinje cells that survive in the infarcted canine heart; a mechanism for triggered Purkinje ectopy. *Circ Arrhythm Electrophysiol.* 2008;1:387–95.
30. Hirose M, Stuyvers BD, Dun W, Ter Keurs HEDJ, Boyden PA. Wide long lasting perinuclear Ca^{2+} release events generated by an interaction between ryanodine and IP₃ receptors in Canine Purkinje cell. *J Mol Cell Cardiol.* 2008;45:176–84.
31. Zhang X-Q, Moore RL, Tenhave T, Cheung JY. (Ca^{++})_i transients in hypertensive and postinfarction myocytes. *Am J Physiol.* 1995;269:C632–40.
32. Wit AL, Janse MJ. The ventricular arrhythmias of ischemia and infarction. Electrophysiological mechanisms. Mount Kisco, NY: Futura Publishing; 1993.
33. Ursell PC, Gardner PI, Albala A, JJ Jr F, Wit AL. Structural and electrophysiological changes in the epicardial border zone of canine myocardial infarcts during infarct healing. *Circ Res.* 1985;56:436–51.
34. Boyden PA, Gardner PI, Wit AL. Action potentials of cardiac muscle in healing infarcts: response to norepinephrine and caffeine. *J Mol Cell Cardiol.* 1988;20:525–37.
35. Aggarwal R, Boyden PA. Diminished calcium and barium currents in myocytes surviving in the epicardial border zone of the 5 day infarcted canine heart. *Circ Res.* 1995;77:1180–91.
36. Koumi SI, Backer CL, Arentzen CE, Sato R. Beta-adrenergic modulation of the inwardly rectifying potassium channel in isolated human ventricular myocytes. *J Clin Invest.* 1995;96:2870–81.
37. Kameyama M, Hofmann F, Trautwein W. On the mechanism of beta-adrenergic regulation of the Ca channel in the guinea-pig heart. *Pflugers Arch.* 1985;405:285–93.

38. Tsien RW, Bean BP, Hess P, Lansman JB, Nilius B, Nowycky MC. Mechanisms of calcium channel modulation by beta adrenergic agents and dihydropyridine calcium agonist. *J Mol Cell Cardiol*. 1986;18:691–710.
39. Gaide MS, Myerburg RJ, Kozlovskis PL, Bassett AL. Elevated sympathetic response of epicardial proximal to healed myocardial infarction. *Am J Physiol*. 1983;245:H646–52.
40. Mubagwa K, Flameng W, Carmeliet E. Resting and action potentials of nonischemic and chronically ischemic human ventricular muscle. *J Cardiovasc Electrophysiol*. 1994;5:659–71.
41. Pinto JMB, Yuan F, Wasserlauf BJ, Bassett AL, Myerburg RJ. Regional gradation of L-type calcium currents in the feline heart with a healed myocardial infarct. *J Cardiovasc Electrophysiol*. 1997;8:548–60.
42. Aggarwal R, Boyden PA. Altered pharmacologic responsiveness of reduced L-type calcium currents in myocytes surviving in the infarcted heart. *J Cardiovasc Electrophysiol*. 1996;7:20–35.
43. Steinberg SF, Zhang H, Pak E, Pagnotta G, Boyden PA. Characteristics of the beta-adrenergic receptor complex in the epicardial border zone of the 5-day infarcted canine heart. *Circulation*. 1995;91:2824–33.
44. Davis MJ, Wu X, Nurkiewicz TR, Kawasaki J, Gui P, Hill MA, et al. Regulation of ion channels by protein tyrosine phosphorylation. *Am J Physiol Heart Circ Physiol*. 2001;281:H1835–62.
45. Yagi T, Boyden PA. The function of protein tyrosine kinases and L type Ca^{2+} currents in cells that have survived in the canine infarcted heart. *J Cardiovasc Pharm*. 2002;40:669–77.
46. Hund TJ, Decker KF, Kanter E, Mohler PJ, Boyden PA, Schuessler RB, et al. Role of activated CaMKII in abnormal calcium homeostasis and INa remodeling after myocardial infarction: insights from mathematical modeling. *J Med Cell Cardiol*. 2008;45:420–8.
47. Licata A, Aggarwal R, Robinson RB, Boyden PA. Frequency dependent effects on Cai transients, cell shortening in myocytes that survive in the infarcted heart. *Cardiovasc Res*. 1997;33:341–50.
48. Mohler PJ, Schott JJ, Gramolini AO, Dilly K, Guatimosim S, DuBell WH, et al. AnkyrinB mutation causes type4 longQT cardiac arrhythmia and sudden cardiac death. *Nature*. 2003;421:634–9.
49. Hund TJ, Wright PJ, Dun W, Snyder JS, Boyden PA, Mohler PJ. Regulation of the ankyrin-B-based targeting pathway following myocardial infarction. *Cardiovasc Res*. 2009;81:742–9.
50. Pu J, Robinson RB, Boyden PA. Abnormalities in Cai handling in myocytes that survive in the infarcted heart are not just due to alterations in repolarization. *J Med Cell Cardiol*. 2000;32:1509–23.
51. Aggarwal R, Pu J, Boyden PA. Ca^{2+} dependent outward currents in myocytes from the epicardial border zone of the 5 day infarcted heart. *Am J Physiol*. 1997;273:H1386–94.
52. Pu J, Ruffy F, Boyden PA. Effects of Bay Y5959 on Ca^{2+} currents and intracellular Ca^{2+} in cells that have survived in the epicardial border zone of the infarcted canine heart. *J Cardiovasc Pharm*. 1999;33:929–37.
53. Cabo C, Schmitt H, Wit AL. New mechanism of antiarrhythmic drug action: Increasing inward L type calcium current prevents reentrant tachycardia in the infarcted canine heart. *Circulation*. 2000;102:2417–25.
54. Janvier NC, Boyett MR. The role of NaCa exchange current in the cardiac action potential. *Cardiovasc Res*. 1996;32:69–84.
55. Zhang X-Q, Tillotson DL, Moore RL, Cheung JY. Na/Ca exchange currents and SR Ca^{2+} contents in postinfarction myocytes. *Am J Physiol*. 1996;271:C1800–7.
56. Cheung JY, Musch TI, Misawa H, Semanchick A, Elensky M, Yelamarty RV, et al. Impaired cardiac function in rats with healed myocardial infarction: cellular vs. myocardial mechanisms. *Am J Physiol*. 1994;266:C29–36.
57. Litwin SE, Bridge JHB. Enhanced NaCa exchange in the infarcted heart. Implications for excitation contraction coupling. *Circ Res*. 1997;81:1083–93.

Chapter 17

Molecular and Biochemical Characteristics of the Intracellular Ca^{2+} Handling Proteins in the Heart

**Yasser Abdellatif, Vijayan Elimban, Delfin Rodriguez-Leyva,
and Naranjan S. Dhalla**

17.1 Introduction

Depolarization of cardiomyocytes causes Ca^{2+} influx through L-type channels (LTCCs) located in the sarcolemmal membrane (SL) and results in release of Ca^{2+} from the sarcoplasmic reticulum (SR). This release of Ca^{2+} from the SR stores occurs mainly by activation of Ca^{2+} release channels or ryanodine receptors (RyR) as well as, to some extent, by the inositol triphosphate receptors (InsP₃R). The increase in Ca^{2+} in the cytosol is rapidly dissipated via four complementary mechanisms in cardiomyocytes: (a) Ca^{2+} binding by proteins such as calmodulin (CaM) and troponin [1], (b) Ca^{2+} efflux through SL or plasma membrane Ca^{2+} -ATPase (PMCA) and SL Na^+ - Ca^{2+} exchanger (NCX), (c) storage in the SR by SR Ca^{2+} -ATPase (SERCA), and (d) Ca^{2+} buffering by intracellular organelles such as mitochondria and nucleus [2]. The mitochondria transport Ca^{2+} mainly via mitochondrial Ca^{2+} uniporter whereas the nucleus possesses a Ca^{2+} storing organelle, nucleoplasmic reticulum [3]. Fluctuation in the levels of cytoplasmic Ca^{2+} affects mitochondrial metabolism which may contribute to the pathogenesis of congestive heart failure (CHF) and ischemic heart disease (IHD) [4]. In addition, Ca^{2+} waves in the cytoplasm of cardiomyocytes trigger gene expression. In fact, the Ca^{2+} -dependent changes in cardiac gene expression have been implicated in the restructuring or remodeling of subcellular organelles during the development of ischemia-reperfusion injury, cardiac hypertrophy, and CHF [5, 6]. Accordingly, this chapter discusses the molecular and biochemical characteristics of the Ca^{2+} handling and regulatory proteins such as SR RyR, SR Ca^{2+} -ATPase, and InsP₃R. Furthermore, coupling of SR Ca^{2+} to cardiac contraction, as well as Ca^{2+} to mitochondrial metabolism and Ca^{2+} to nuclear transcription, are outlined for describing events

Y. Abdellatif, V. Elimban, D. Rodriguez-Leyva, and N.S. Dhalla (✉)

Institute of Cardiovascular Sciences, St. Boniface General Hospital Research Centre, Winnipeg, MB, Canada
and

Department of Physiology, Faculty of Medicine, University of Manitoba, Winnipeg, MB, Canada
e-mail: nsdhalla@sbsrc.ca

that follow excitation of cardiomyocytes. In addition, the involvement of SR, mitochondria, and nucleus in cardiac pathologies will be described. Finally, we will explore the potential of these organelles as pharmacological targets for the treatment of heart disease.

17.2 Excitation–Contraction Coupling

In view of the major role of SR in releasing Ca^{2+} for the occurrence of cardiac contraction upon excitation as well as in Ca^{2+} uptake for the occurrence of cardiac relaxation, we propose to describe the characteristics of SR Ca^{2+} release channel, SR Ca^{2+} -ATPase, and SR InsP_3R . All these three SR Ca^{2+} handling proteins are known to regulate the intracellular concentration of Ca^{2+} ($[\text{Ca}^{2+}]_i$) in cardiomyocytes.

17.2.1 SR Ca^{2+} Release Channels

Since SR Ca^{2+} release channels bind ryanodine, these channels are called RyR. RyR is a tetrameric protein having a molecular weight of 564 kDa and consists of at least four transmembrane segments as well as a large cytoplasmic domain. Three isoforms have been identified to date, RyR1 and RyR3 in skeletal muscle and RyR2 in cardiac muscle; these isoforms share up to 60% sequence homology. RyR in cardiac muscle is organized in groups of approximately 20 receptors each. It has been suggested that the close approximation of these receptors is required for orchestrated opening and closing of the Ca^{2+} release channels [7]. Ca^{2+} has a biphasic effect on RyR; submicromolar Ca^{2+} concentrations activate RyR whereas higher Ca^{2+} concentrations ($>1 \mu\text{M}$) inhibit the channel. RyR is inhibited by cytosolic Mg^{2+} but an increase in cytosolic Ca^{2+} relieves the Mg^{2+} inhibition [8]. RyR is also modulated by several cytosolic proteins; however, the most thoroughly studied modulators are CaM, Ca^{2+} -CaM dependent kinase (CaMK)II, protein kinase A (PKA), and protein phosphatases. CaM binding to RyR is Ca^{2+} dependent where Ca^{2+} binding increases the sensitivity of RyR to CaM. CaM binding inhibits the cardiac RyR in the presence of high concentration of Ca^{2+} ($10 \mu\text{M}$). Several kinases have been shown to affect the activity of cardiac RyR. These include protein kinases A, C, and G, in addition to the CaMKII [5, 8]. The RyR phosphorylation is of great importance in the pathogenesis of heart failure and arrhythmias [9]. Hyperphosphorylation of RyR in heart failure leads to the dissociation of “calstabin,” an accessory protein that stabilizes the closed conformation of the channel [10]. Phosphorylation of RyR cannot be interpreted in isolation from other SR proteins such as the SERCA and phospholamban (PLB). The PLB phosphorylation activates SERCA and increases the SR Ca^{2+} load, which then stimulates RyR [11]. While the overall effect of phosphorylation is stimulatory, protein phosphatases are inhibitory [8]. In addition to kinases and phosphatases,

several other cytoplasmic proteins modulate the activity of cardiac RyR. These include the transmembrane proteins, junctin and triadin, and the cytosolic proteins, S100, sorcin, glutathione transferase as well as intracellular chloride ion channels, glycolytic enzymes, and the accessory protein, calstabin [12].

Mutations in cardiac RyR have been linked to the development of premature heart beats. A “leaky” RyR will promote the buildup of Ca^{2+} in the cytosol, and subsequently trigger the SL NCX to remove the excess Ca^{2+} in exchange for Na^+ ; this then depolarizes the cell membrane leading to extrasystolic depolarizations and premature beats. On the other hand, adrenergic stimulation leading to the phosphorylation of RyR can cause fatal arrhythmias such as catecholaminergic polymorphic ventricular tachycardia (CPVT) in susceptible individuals. Susceptibility to CPVT was linked mainly to autosomal dominant mutations of RyR2; these mutations destabilize the channel or impair the binding to calstabin that stabilizes RyR [13, 14]. Recently, a mutation linked to the development of CPVT (R2474S) was found to produce “leaky” RyR in the hearts and to the development of CPVT in transgenic mice. It has been shown that these RyRs could be stabilized by a novel compound, S107, for averting fatal arrhythmias [15]. Interestingly, the expression of RyR is reduced in heart failure due to the development of myocardial infarction (MI); this change is believed to be mediated through angiotensin receptors because it is inhibited by angiotensin converting enzyme (ACE) inhibitors such as imidapril. Accordingly, a close involvement of the SR RyR in the cellular remodeling process has been suggested [16]. In addition to suppressing cardiac hypertrophy, ACE inhibitor therapy has been shown to decrease the hyperadrenergic state associated with heart failure, resulting in a reduction of PKA activity, which abolishes the phosphorylation of RyR. In fact, ACE inhibitors have been reported to promote the interaction of RyR with the accessory protein calstabin, which stabilizes the channel and reduces the RyR leak [16].

17.2.2 SR Ca^{2+} -ATPase

Most of the Ca^{2+} released from SR stores is rapidly accumulated by SR via SERCA while the rest is extruded from the cell by the PMCA and SL NCX. The SERCA transports two Ca^{2+} ions for the hydrolysis of a single ATP molecule [17]. The crystal structure of SERCA has revealed a protein that is organized into three interacting domains: the cytosolic nucleotide binding domain, the phosphorylation domain containing Asp351, and the transmembrane translocation domain. The cytosolic and transmembrane domains consist of ten transmembrane segments which are connected by the stalk domain [18]. At least six isoforms of SERCA have been identified as belonging to three different gene families, namely SERCA1, 2, and 3; cardiomyocytes express the SERCA2a isoform [19]. The SERCA activity is strictly regulated by phosphorylation of a SR-associated protein PLB, which is phosphorylated by PKA. The dephosphorylated PLB inhibits the pump by interacting with the enzyme phosphorylation site which is needed for ATP binding,

whereas phosphorylation of PLB by PKA or CaMK relieves this inhibition [20]. During adrenergic stimulation, PKA reduces the affinity of Ca^{2+} pump for Ca^{2+} and thus enhances cardiac muscle relaxation. The adrenergic stimulation of the heart enhances the SERCA activity and such a regulatory action has been suggested to be a compensatory mechanism to improve cardiac performance. In addition to PLB, sarcolipin is another modulator of SERCA [21]. Sarcolipin is a shorter homologue (31 amino acid) of PLB, which inhibits SERCA. However, unlike PLB, the level of expression of sarcolipin determines its interaction with SERCA rather than its phosphorylation level. It has been found that sarcolipin modulates SERCA in a Ca^{2+} -dependent manner; at low Ca^{2+} levels, sarcolipin reduces its affinity for Ca^{2+} and thus inhibits its activity, whereas at high Ca^{2+} levels, it increases its activity for Ca^{2+} by increasing the maximum turnover rate [22]. Sarcolipin and PLB both synergistically inhibit SERCA; coexpression of sarcolipin in HEK cells leads to a very strong inhibition of the SERCA activity whereas a sarcolipin knockout leads to enhanced SERCA activity [23]. On the other hand, the S100 protein, which is abundantly expressed in the heart and skeletal muscle, is believed to stimulate Ca^{2+} uptake by SERCA2a through a direct protein–protein interaction [24].

In cardiac hypertrophy and heart failure, the levels of SERCA expression as well as SERCA activity have been found to be reduced and cause inadequate function of the SR [25]. These findings have been suggested to explain some of the symptoms of these pathological states including reduced contractility. In fact, it was observed that an overexpression of SERCA can relieve such functional defects [26]. In heart failure, a reduction in the SERCA activity by about 50% was evident without any changes in the creatine kinase activity and mitochondrial functions [27]. While several studies have indicated a role for SERCA in heart function, heterozygous loss of function of the SERCA2 a and b isoforms in Darrier disease was not associated with any defects in cardiac performance [28, 29].

17.2.3 SR Inositol Trisphosphate Receptors

The InsP_3R plays a minor role in excitation–contraction (EC) coupling compared to the RyR in ventricular cardiomyocytes, where the ratio of RyR to InsP_3R is between 50:1 and 100:1 [30, 31]. However, the expression of InsP_3R in atrial myocytes is 3.5–10 times higher than in ventricular myocytes, suggesting a more prominent role in atrial contraction [32]. There are several isoforms of the InsP_3R in both excitable and non-excitable tissues; the heart expresses the $\text{InsP}_3\text{R}2$ isoform, which is a 300-kDa protein that coassembles to form a tetrameric channel. The channel is predicted to have six transmembrane segments and a large regulatory cytoplasmic domain [33]. $\text{InsP}_3\text{R}1$ is regulated by Ca^{2+} in a biphasic pattern similar to the RyR. In fact, it is activated by submicromolar concentration of Ca^{2+} ($<300 \text{ nM}$) and inhibited by micromolar concentrations of Ca^{2+} ($>1 \mu\text{M}$). The cardiac $\text{InsP}_3\text{R}2$ is resistant to high Ca^{2+} , remaining active in the presence of high Ca^{2+} concentration ($>100 \mu\text{M}$)

[34, 35]. The InsP_3R is modulated by cytosolic proteins such as calstabin, PKA, and CaM [36]. The most significant interaction of InsP_3R is with CaM, because Ca^{2+} -free CaM inhibits the cardiac $\text{InsP}_3\text{R}2$ in a Ca^{2+} -independent manner, indicating a permanent inhibition of these receptors by CaM in the absence of Ca^{2+} [37].

$\text{InsP}_3\text{R}2$ -dependent signaling has been shown to be involved in several disease states, such as the development and progression of cardiac hypertrophy, where an increase in the phospholipase C- InsP_3R expression increases the hypertrophic gene transcription. $\text{InsP}_3\text{R}2$ has been shown to be upregulated in heart failure in contrast to the reduction in RyR2 expression and activity [32]. In addition, the relative abundance of InsP_3R in Purkinje fibers suggests its potential participation in ventricular arrhythmias [38]. However, the precise role of InsP_3R in such pathological conditions requires further study.

17.3 Excitation–Metabolism Coupling

The process of EC coupling consumes a large amount of energy by involving the myosin ATPase, the SL Na^+-K^+ ATPase, and SERCA [5]. On the other hand, the mitochondria are the main source of energy production. Mitochondria take up to 30% of the myocyte volume and are present in close apposition to the contractile machinery where energy is most required [39]. Mitochondrial metabolism is regulated by Ca^{2+} levels because three main enzymes in the citric acid cycle, namely pyruvate dehydrogenase, isocitrate dehydrogenase, and α -ketoglutarate dehydrogenase, are activated by Ca^{2+} [40]; Ca^{2+} also activates the mitochondrial F_1/F_0 ATPase [41]. Ca^{2+} enters the mitochondrial membrane through the mitochondrial Ca^{2+} uniporter (mCUP), a low affinity (10–20 μM) and highly selective ion channel that accumulates Ca^{2+} in the mitochondria using the potential difference across the mitochondrial membrane; the mCUP is Ca^{2+} gated and requires CaM for its activation [42]. However, mitochondrial Ca^{2+} uptake is inhibited by high concentrations of cytosolic Ca^{2+} [43]. Ca^{2+} is extruded from mitochondria through the activity of mitochondrial $\text{Na}^+-\text{Ca}^{2+}$ exchanger (mNCX), which is believed to possess a stoichiometry similar to that of the SL NCX of 3 Na^+ to 1 Ca^{2+} [44]. Since the Ca^{2+} extrusion mechanism is slower relative to the rate of Ca^{2+} entry, this leads to accumulation of Ca^{2+} in the mitochondria [45].

Recent studies have shown that mitochondrial $[\text{Ca}^{2+}]$ synchronously rises with the rise of cytosolic $[\text{Ca}^{2+}]$ upon stimulation by an increase in cardiomyocyte pacing or β -adrenergic stimulation [46, 47]. The rise of mitochondrial $[\text{Ca}^{2+}]$ was shown to be dependent on the rise of cytosolic Ca^{2+} in the proximity of SR suggesting that mitochondria may act as a Ca^{2+} sink for some of the Ca^{2+} released by SR [48]. The ability of mitochondria to sense Ca^{2+} in a microdomain rather than the whole cytosol is predicted in modeling studies [49] and can explain the high threshold for Ca^{2+} uptake by the mCUP (1–3 μM), a threshold achievable probably through the close proximity to SR. Indeed, localized Ca^{2+} sparks (synchronous coordinated activity of 30–100 RyR) elicit miniature mitochondrial matrix Ca^{2+}

signals that last less than 500 ms [48]. The rapid buffering of cytosolic Ca^{2+} by mitochondria may not be only through the mCUP because there is evidence of a ryanodine sensitive channel that binds tritiated ryanodine in a bell-shaped Ca^{2+} -dependent manner similar to the SR RyRs [50].

The excitation–metabolism (EM) coupling process is modulated by two messengers, ADP and NADH. The ADP production activates the mitochondrial F_1/F_0 ATPase to generate more ATP, which consequently leads to the reduction of inner membrane potential. The drop in potential activates NADH production (the second messenger) to supply electrons to compensate the electron loss and maintain the inner mitochondrial membrane potential [51]. The second modulatory control of mitochondrial metabolism occurs through the mNCX which is needed to maintain the intramitochondrial Ca^{2+} concentration. A recent study has examined the influence of cytoplasmic Na^+ and mitochondrial potential on mNCX activity and has confirmed the role of mNCX as a Ca^{2+} extrusion mechanism for the mitochondria [52]. In addition, it was demonstrated that mNCX is electrogenic and that depolarization of the mitochondrial membrane activates the mNCX to shuffle Ca^{2+} into the mitochondria rather than eliminating Ca^{2+} ; this seems to be a potential protective mechanism against the loss of mitochondrial potential that follows ATP depletion [51]. A third potential mechanism of modulation of EM coupling process is mediated by ATP sensitive potassium (K_{ATP}) channels. These channels are activated by ADP and inhibited by ATP. It has been shown that K_{ATP} channels can be imported into the mitochondria and localize to the inner mitochondrial membrane following phosphorylation by protein kinase C. K_{ATP} are believed to have a protective effect against ischemia–reperfusion induced increase in cellular Ca^{2+} [53].

A rise in mitochondrial Ca^{2+} has been shown to be associated with an increase in metabolism [54]. Pathologies such as heart failure, ischemia–reperfusion, or potential arrhythmias lead to an increase in cytosolic Ca^{2+} and have a deleterious effect on mitochondrial metabolism [4]. In fact, a higher Na^+ concentration in the cytosol stimulates the mNCX leading to reduced Ca^{2+} accumulation and reduced activity of mitochondrial function [45]. In cardiomyopathies, the reduced cytoplasmic Ca^{2+} negatively affects the mitochondrial Ca^{2+} transient which is expected to inhibit mitochondrial function. Furthermore, a reduced rate of glycolysis, resulting in reduced availability of pyruvate, contributes to the energy starvation in cardiomyopathy [55]. Thus, the mitochondria appear to be a therapeutic target in ischemia–reperfusion injury and cardiomyopathies. It has been suggested that inhibition of the mNCX could be beneficial in cases of heart failure and during ischemia–reperfusion injury. In heart failure, the increase in cytosolic Na^+ activates the forward mode of mNCX to release mitochondrial Ca^{2+} . On the other hand, an increase in the cytosolic Ca^{2+} will trigger the reverse mode of mNCX and promote the accumulation of excess cytosolic Ca^{2+} in the mitochondria. As a consequence of its effect, the inhibition of mNCX has been shown to improve Ca^{2+} accumulation and mitochondrial energetics in isolated cardiomyocytes [55, 56]. In addition, various interventions such as trimetazidine, ranolazine, dichloroacetate, carnitine palmitoyl transferase, and coenzyme Q10 have been proposed to prevent ischemic injury via mitochondrial modulation [56].

17.4 Excitation–Transcription Coupling

The role of Ca^{2+} in controlling nuclear signaling has been established in some studies [57, 58]. In cardiomyocytes, nuclei are closely associated with SR; the nucleus of adult cardiomyocytes is reported to possess a nucleoplasmic reticulum, a nuclear Ca^{2+} store which is continuous with SR and the nuclear envelope [31]. The nucleoplasmic reticulum is loaded from cytosolic Ca^{2+} microdomains [59–62]. This organelle expresses functional InsP_3R and RyR. There is evidence that the nucleus contains key components of the phosphoinositide-PLC signaling cascade where the production of InsP_3 has been speculated. It is suggested that the nucleus is able to control the effect of Ca^{2+} on gene expression, allowing nuclear Ca^{2+} to regulate cellular functions independently of the cytosolic Ca^{2+} increase [63]. Likewise, InsP_3 can trigger release of Ca^{2+} directly into the nucleoplasm which may have an important impact on the excitation–transcription (ET) process [63]. An increase in nuclear Ca^{2+} concentration is reported to control the Ca^{2+} -activated gene expression mediated by cAMP response element [64]. Moreover, cytoplasmic and nuclear Ca^{2+} signals activate transcription through different pathways. Cytoplasmic Ca^{2+} signal activates transcription through the serum response element (SRE) transcription factor and does not require an increase in nuclear Ca^{2+} [65].

The effect of Ca^{2+} oscillations has been tackled in two elegant studies [66, 67], which show that the amplitude and duration of Ca^{2+} signals in B lymphocytes controls differential activation of the pro-inflammatory transcriptional regulators, NF- κ B, c-Jun N-terminal kinase (JNK), and nuclear factor of activated T cells (NFAT). It was pointed out that NF- κ B and JNK are selectively activated by a large transient $[\text{Ca}^{2+}]_i$ rise, whereas NFAT is activated by a low, sustained Ca^{2+} plateau. In addition, the specificity of response is encoded by the oscillation frequency; rapid oscillations stimulate all three transcription factors, whereas infrequent oscillations activate only NF- κ B [68]. Similar to SR, the nucleoplasmic reticulum seems to possess counter ion channels such as K^+ channels [68]; these channels would probably control the change in the potential across the nucleoplasm. This is especially important as the nucleoplasmic reticulum contains the voltage-gated R-type Ca^{2+} channels [68]. In addition, there is evidence that the nuclear membrane contains both NCX and Na^+-H^+ exchanger that may contribute to nuclear potential and cellular homeostasis.

The increase in nuclear Ca^{2+} signal has been closely associated with cardiac hypertrophy. The most well-characterized mechanism is via $\text{Ca}^{2+}\text{-CaM}$. This pathway acts through the influence of $\text{Ca}^{2+}\text{-CaM-CaMK}$ on histone deacetylase (HDAC) or the effect of $\text{Ca}^{2+}\text{-CaM}$ on the protein phosphatase calcineurin (CaN); the two ways may act in parallel contributing to cardiac hypertrophy [67, 69]. It has been shown that depolarization-mediated Ca^{2+} influx acts through CaMKII to inhibit the histone deacetylase (HDAC5), thereby sustaining high activity of the cerebellar granule neuron maintained under myocyte enhancer factor 2 (MEF2) depolarizing conditions. In adult rabbit and mouse cardiomyocytes, phenylephrine and endothelin-1 induced nuclear export of HDAC5 depends not only on CaMK II but also on protein kinase D (PKD) [69]. The nuclear export required

type II InsP₃R, Ca²⁺ release from stores, CaM, HDAC5 phosphorylation but was completely insensitive to Ca²⁺ transients associated with both nuclear and cytosolic Ca²⁺ and PKC inhibition [69, 70]. HDAC class II is expressed in heart and possesses a unique extension to bind MEF2 repressing its transcription activation, the relief of MEF2 repression by HDAC comes mainly through phosphorylation of HDAC by CaMK [71]. The latter argues for a local control of Ca²⁺ release in the nuclear region, where local activation of nuclear InsP₃R releases Ca²⁺ locally that activates CaMKII to phosphorylate HDAC and relieves transcription inhibition. MEF2 activation is strongly implicated in cardiac hypertrophy, and this has been shown in transgenic animals overexpressing CaMKII and IV [71]. The link between MEF2 and CaMK is through HDAC [72].

Other transcription factors that are regulated by CaMK include activating protein (AP-1), activating transcription factor (ATF-1), serum response factor (SRF), cyclic AMP response element (CREB), and the myocyte enhancing factor (MEF-2) [73]. While CREB can be phosphorylated by CaMKII, transgenic mice overexpressing CaMKII or CaMKIV that develop hypertrophy did not show an enhanced level of CREB phosphorylation [72, 74]. MEF2 activation is strongly implicated in hypertrophy, and this has been shown in transgenic animals that overexpress CaMKII and IV [75]. The other mechanism by which Ca²⁺-CaM controls transcription is through CaN, which is a Ca²⁺-CaM binding phosphatase, 500 times more sensitive to Ca²⁺ than CaM, allowing CaN to be more sensitive to small sustained Ca²⁺ transients [76]. CaN dephosphorylates NFAT, which leads to its translocation into the nucleus where it binds to the transcription factor GATA4 to activate hypertrophic gene transcription [77]. In some studies, a sustained global rise in Ca²⁺ is needed to activate NFAT [78] whereas in others, Ca²⁺ oscillations were more efficient NFAT activators [66]. In neurons, the C-terminal fragment of LTCCs was found to be proteolytically cleaved as it translocated into the nucleus; this is then bound to a transcriptional regulator, Ca²⁺ channel associated transcription (CCAT) factor, leading to an increase in the length of neurites [79, 80]. The latter leads to an increase in some genes such as connexins, regulators of G-protein and catenin, while other proteins such as K⁺ channel (Kcn3), NCX, myosin, NMDA receptor, serine threonine kinase, and glucokinase are downregulated. While the role of this catalytic fragment in cardiomyocytes remains to be examined, the potential in developing specific inhibitors of nuclear Ca²⁺ signaling is unlimited. The control of such mechanism could provide treatments for heart failure and cardiac hypertrophy as well as other conditions where Ca²⁺ oscillations affect gene expression and consequently the expression of signaling molecules that modulate Ca²⁺ cycling.

17.5 Conclusion

Following Ca²⁺ entry through the SL LTCCs and release of Ca²⁺ from SR due to stimulation of RyR in cardiomyocytes, the elevated cytosolic Ca²⁺ is rapidly reaccumulated in SR. Replenishing the SR Ca²⁺ stores is mediated by SERCA

and is essential for proper contraction of cardiomyocytes. RyR is considered to be a target for treating specific conditions such as CPVT and potentially other arrhythmias [14]. The critical role of SERCA in SR predicts an important role for heart function; however, partial loss of SERCA activity is not deleterious to cardiomyocytes. Ca^{2+} accumulation in mitochondria is usually beneficial as Ca^{2+} activates several of the citric acid cycle enzymes. However, excessive accumulation of Ca^{2+} in the mitochondria may induce the translocation of cytochrome C and other pro-apoptotic factors and cell death [81]. Maintaining this delicate balance rests on the activities of Ca^{2+} cycling proteins, mainly mCUP and mNCX, where the balance between Ca^{2+} uptake by mCUP and Ca^{2+} extrusion by mNCX directly affects mitochondrial metabolism [82]. Inhibition of mNCX is beneficial in preventing ischemia reperfusion injury and heart failure [4].

While the mitochondria are strictly dependent on cytosolic Ca^{2+} , the nucleus possesses a Ca^{2+} storage organelle, the nucleoplasmic reticulum [31]. We are beginning to explore the potential of the nucleus as a therapeutic target for the treatment of cardiovascular diseases [68]. Ca^{2+} oscillations seem to be essential for the disturbance mediating cardiovascular gene modulation of the heart size and rhythm. Future therapeutic interventions will continue to target classic mechanisms such as ion channels; however, emphasis will be on intracellular ion channels such as mitochondrial channels and exchangers to influence cellular metabolism, and nuclear ion channels to control cell proliferation and growth. Targeting intracellular ion channels is an attractive new area of cardiovascular research. It provides a lot of promise for the control of cardiovascular dysfunction as well as changes in metabolism and gene transcription, which may be valuable approaches to counteract the deleterious effect of myocardial ischemia and cardiac hypertrophy.

Acknowledgments The research in this article was supported by a grant from the Canadian Institutes of Health Research (CIHR). The infrastructural support for this study was furnished by the St. Boniface General Hospital Research Foundation.

References

1. Berlin JR, Bassani JW, Bers DM. Intrinsic cytosolic calcium buffering properties of single adult cardiac myocytes. *Biophys J.* 1994;67:1775–87.
2. Dhalla NS. Excitation-contraction coupling in heart. I. Comparison of calcium uptake by the sarcoplasmic reticulum and mitochondria of the rat heart. *Arch Int Physiol Biochim.* 1969;77:916–34.
3. Alonso MT, Villalobos C, Chamero P, Alvarez J, Garcia-Sancho J. Calcium microdomains in mitochondria and nucleus. *Cell Calcium.* 2006;40:513–25.
4. Dhalla NS, Saini-Chohan HK, Rodriguez-Leyva D, Elimban V, Dent MR, Tappia PS. Subcellular remodelling may induce cardiac dysfunction in congestive heart failure. *Cardiovasc Res.* 2009;81:429–38.
5. Bers DM. Calcium cycling and signaling in cardiac myocytes. *Annu Rev Physiol.* 2008;70: 23–49.

6. Dhalla NS, Saini HK, Tappia PS, Sethi R, Mengi SA, Gupta SK. Potential role and mechanisms of subcellular remodeling in cardiac dysfunction due to ischemic heart disease. *J Cardiovasc Med (Hagerstown)*. 2007;8:238–50.
7. Lukyanenko V, Ziman A, Lukyanenko A, Salnikov V, Lederer WJ. Functional groups of ryanodine receptors in rat ventricular cells. *J Physiol*. 2007;583:251–69.
8. Meissner G. Molecular regulation of cardiac ryanodine receptor ion channel. *Cell Calcium*. 2004;35:621–8.
9. Antos CL, Frey N, Marx SO, Reiken S, Gaburjatova M, Richardson JA, et al. Dilated cardiomyopathy and sudden death resulting from constitutive activation of protein kinase A. *Circ Res*. 2001;89:997–1004.
10. Marx SO, Reiken S, Hisamatsu Y, Jayaraman T, Burkhoff D, Rosemblit N, et al. PKA phosphorylation dissociates FKBP12.6 from the calcium release channel (ryanodine receptor): defective regulation in failing hearts. *Cell*. 2000;101:365–76.
11. Diaz ME, Graham HK, O'Neill SC, Trafford AW, Eisner DA. The control of sarcoplasmic reticulum Ca^{2+} content in cardiac muscle. *Cell Calcium*. 2005;38:391–6.
12. Zalk R, Lehnart SE, Marks AR. Modulation of the ryanodine receptor and intracellular calcium. *Annu Rev Biochem*. 2007;76:367–85.
13. Yamamoto T, Yano M, Xu X, Uchinoumi H, Tateishi H, Mochizuki M, et al. Identification of target domains of the cardiac ryanodine receptor to correct channel disorder in failing hearts. *Circulation*. 2008;117:762–72.
14. Yano M. Ryanodine receptor as a new therapeutic target of heart failure and lethal arrhythmia. *Circ J*. 2008;72:509–14.
15. Lehnart SE, Mongillo M, Bellinger A, Lindegger N, Chen BX, Hsueh W, et al. Leaky Ca^{2+} release channel/ryanodine receptor 2 causes seizures and sudden cardiac death in mice. *J Clin Invest*. 2008;118:2230–45.
16. Babick AP, Dhalla NS. Role of subcellular remodeling in cardiac dysfunction due to congestive heart failure. *Med Princ Pract*. 2007;16:81–9.
17. Tada M, Yamada M, Kadoma M, Inui M, Ohmori F. Calcium transport by cardiac sarcoplasmic reticulum and phosphorylation of phospholamban. *Mol Cell Biochem*. 1982;46:73–95.
18. Toyoshima C, Nakasako M, Nomura H, Ogawa H. Crystal structure of the calcium pump of sarcoplasmic reticulum at 2.6 Å resolution. *Nature*. 2000;405:647–55.
19. Tada M, Yamada M, Inui M, Ohmori F. Regulation of Ca^{2+} -dependent ATPase of cardiac sarcoplasmic reticulum by cAMP- and calmodulin-dependent phosphorylation of phospholamban. *Tanpakushitsu Kakusan Koso*. 1982;27:2350–64.
20. James P, Inui M, Tada M, Chiesi M, Carafoli E. Nature and site of phospholamban regulation of the Ca^{2+} pump of sarcoplasmic reticulum. *Nature*. 1989;342:90–2.
21. Asahi M, Nakayama H, Tada M, Otsu K. Regulation of sarco(endo)plasmic reticulum Ca^{2+} adenosine triphosphatase by phospholamban and sarcolipin: implication for cardiac hypertrophy and failure. *Trends Cardiovasc Med*. 2003;13:152–7.
22. Babu GJ, Bhupathy P, Timofeyev V, Petrashevskaya NN, Reiser PJ, Chiamvimonvat N, et al. Ablation of sarcolipin enhances sarcoplasmic reticulum calcium transport and atrial contractility. *Proc Natl Acad Sci USA*. 2007;104:17867–72.
23. Kiewitz R, Acklin C, Schafer BW, Maco B, Uhrig B, Wuytack F, et al. Ca^{2+} -dependent interaction of S100A1 with the sarcoplasmic reticulum Ca^{2+} -ATPase2a and phospholamban in the human heart. *Biochem Biophys Res Commun*. 2003;306:550–7.
24. Remppis A, Most P, Löffler E, Ehlermann P, Bernotat J, Pleger S, et al. The small EF-hand Ca^{2+} binding protein S100A1 increases contractility and Ca^{2+} cycling in rat cardiac myocytes. *Basic Res Cardiol*. 2002;97:156–62.
25. Mercadier JJ, Lompre AM, Duc P, Boheler KR, Fraysse JB, Wisnewsky C, et al. Altered sarcoplasmic reticulum Ca^{2+} -ATPase gene expression in the human ventricle during end-stage heart failure. *J Clin Invest*. 1990;85:305–9.

26. del Monte F, Williams E, Lebeche D, Schmidt U, Rosenzweig A, Gwathmey JK, et al. Improvement in survival and cardiac metabolism after gene transfer of sarcoplasmic reticulum Ca^{2+} -ATPase in a rat model of heart failure. *Circulation*. 2001;104:1424–9.
27. Joubert F, Wilding JR, Fortin D, Domergue-Dupont V, Novotova M, Ventura-Clapier R, et al. Local energetic regulation of sarcoplasmic and myosin ATPase is differently impaired in rats with heart failure. *J Physiol*. 2008;586:5181–92.
28. Prasad V, Okunade GW, Miller ML, Shull GE. Phenotypes of SERCA and PMCA knockout mice. *Biochem Biophys Res Commun*. 2004;322:1192–203.
29. Mayosi BM, Kardos A, Davies CH, Gumedze F, Hovnanian A, Burge S, et al. Heterozygous disruption of SERCA2a is not associated with impairment of cardiac performance in humans: implications for SERCA2a as a therapeutic target in heart failure. *Heart*. 2006;92:105–9.
30. Moschella MC, Marks AR. Inositol 1,4,5-trisphosphate receptor expression in cardiac myocytes. *J Cell Biol*. 1993;120:1137–46.
31. Kockskamper J, Zima AV, Roderick HL, Pieske B, Blatter LA, Bootman MD. Emerging roles of inositol 1,4,5-trisphosphate signaling in cardiac myocytes. *J Mol Cell Cardiol*. 2008;45:128–47.
32. Hund TJ, Ziman AP, Lederer WJ, Mohler PJ. The cardiac IP₃ receptor: uncovering the role of “the other” calcium-release channel. *J Mol Cell Cardiol*. 2008;45:159–61.
33. Lakatta EG, Vinogradova TM, Maltsev VA. The missing link in the mystery of normal automaticity of cardiac pacemaker cells. *Ann N Y Acad Sci*. 2008;1123:41–57.
34. Jiang QX, Thrower EC, Chester DW, Ehrlich BE, Sigworth FJ. Three-dimensional structure of the type 1 inositol 1,4,5-trisphosphate receptor at 24 Å resolution. *EMBO J*. 2002;21:3575–81.
35. Ramos-Franco J, Fill M, Mignery GA. Isoform-specific function of single inositol 1,4,5-trisphosphate receptor channels. *Biophys J*. 1998;75:834–9.
36. Swatton JE, Morris SA, Cardy TJ, Taylor CW. Type 3 inositol trisphosphate receptors in RINm5F cells are biphasically regulated by cytosolic Ca^{2+} and mediate quantal Ca^{2+} mobilization. *Biochem J*. 1999;344:55–60.
37. Adkins CE, Morris SA, De SH, Sienaert I, Torok K, Taylor CW. Ca^{2+} -calmodulin inhibits Ca^{2+} release mediated by type-1, 2 and 3 inositol trisphosphate receptors. *Biochem J*. 2000;345:357–63.
38. Bultynck G, Sienaert I, Parys JB, Callewaert G, De SH, Boens N, et al. Pharmacology of inositol trisphosphate receptors. *Pflugers Arch*. 2003;445:629–42.
39. Yoshikane H, Nihei T, Moriyama K. Three-dimensional observation of intracellular membranous structures in dog heart muscle cells by scanning electron microscopy. *J Submicrosc Cytol*. 1986;18:629–36.
40. Denton RM, McCormack JG. Ca^{2+} as a second messenger within mitochondria of the heart and other tissues. *Annu Rev Physiol*. 1990;52:451–66.
41. Territo PR, French SA, Dunleavy MC, Evans FJ, Balaban RS. Calcium activation of heart mitochondrial oxidative phosphorylation: rapid kinetics of mVO₂, NADH, AND light scattering. *J Biol Chem*. 2001;276:2586–99.
42. Kirichok Y, Krapivinsky G, Clapham DE. The mitochondrial calcium uniporter is a highly selective ion channel. *Nature*. 2004;427:360–4.
43. Moreau B, Nelson C, Parekh AB. Biphasic regulation of mitochondrial Ca^{2+} uptake by cytosolic Ca^{2+} concentration. *Curr Biol*. 2006;16:1672–7.
44. Gunter KK, Gunter TE. Transport of calcium by mitochondria. *J Bioenerg Biomembr*. 1994;26:471–85.
45. Maack C, Cortassa S, Aon MA, Ganesan AN, Liu T, O'Rourke B. Elevated cytosolic Na^+ decreases mitochondrial Ca^{2+} uptake during excitation-contraction coupling and impairs energetic adaptation in cardiac myocytes. *Circ Res*. 2006;99:172–82.
46. Maack C, O'Rourke B. Excitation-contraction coupling and mitochondrial energetics. *Basic Res Cardiol*. 2007;102:369–92.
47. Ohata H, Chacon E, Tesfai SA, Harper IS, Herman B, Lemasters JJ. Mitochondrial Ca^{2+} transients in cardiac myocytes during the excitation-contraction cycle: effects of pacing and hormonal stimulation. *J Bioenerg Biomembr*. 1998;30:207–22.

48. Pacher P, Csordas P, Schneider T, Hajnoczky G. Quantification of calcium signal transmission from sarco-endoplasmic reticulum to the mitochondria. *J Physiol*. 2000;529:553–64.
49. Cortassa S, Aon MA, Marbán E, Winslow RL, O'Rourke B. An integrated model of cardiac mitochondrial energy metabolism and calcium dynamics. *Biophys J*. 2003;84:2734–55.
50. Beutner G, Sharma VK, Lin L, Ryu SY, Dirksen RT, Sheu SS. Type 1 ryanodine receptor in cardiac mitochondria: transducer of excitation-metabolism coupling. *Biochim Biophys Acta*. 2005;1717:1–10.
51. Stanley WC, Chandler MP. Energy metabolism in the normal and failing heart: potential for therapeutic interventions. *Heart Fail Rev*. 2002;7:115–30.
52. Kim B, Matsuoka S. Cytoplasmic Na^+ -dependent modulation of mitochondrial Ca^{2+} via electrogenic mitochondrial $\text{Na}^+/\text{Ca}^{2+}$ exchange. *J Physiol*. 2008;586:1683–97.
53. Light PE, Kanji HD, Fox JE, French RJ. Distinct myoprotective roles of cardiac sarcolemmal and mitochondrial KATP channels during metabolic inhibition and recovery. *FASEB J*. 2001;15:2586–94.
54. Brandes R, Bers DM. Simultaneous measurements of mitochondrial NADH and Ca^{2+} during increased work in intact rat heart trabeculae. *Biophys J*. 2002;83:587–604.
55. Kuo TH, Zhu L, Golden K, Marsh JD, Bhattacharya SK, Liu BF. Altered Ca^{2+} homeostasis and impaired mitochondrial function in cardiomyopathy. *Mol Cell Biochem*. 2002;238:119–27.
56. O'Rourke B, Cortassa S, Akar F, Aon M. Mitochondrial ion channels in cardiac function and dysfunction. *Novartis Found Symp*. 2007;287:140–51.
57. Hamdan M, Urien S, Le LH, Tillement JP, Morin D. Inhibition of mitochondrial carnitine palmitoyltransferase-1 by a trimetazidine derivative, S-15176. *Pharmacol Res*. 2001;44:99–104.
58. Mellstrom B, Savignac M, Gomez-Villafuertes R, Naranjo JR. Ca^{2+} -operated transcriptional networks: molecular mechanisms and in vivo models. *Physiol Rev*. 2008;88:421–49.
59. Abrenica B, Gilchrist JS. Nucleoplasmic Ca^{2+} loading is regulated by mobilization of peri-nuclear Ca^{2+} . *Cell Calcium*. 2000;28:127–36.
60. Abrenica B, Pierce GN, Gilchrist JS. Nucleoplasmic calcium regulation in rabbit aortic vascular smooth muscle cells. *Can J Physiol Pharmacol*. 2003;81:301–10.
61. Echevarria W, Leite MF, Guerra MT, Zipfel WR, Nathanson MH. Regulation of calcium signals in the nucleus by a nucleoplasmic reticulum. *Nat Cell Biol*. 2003;5:440–6.
62. Chi TH, Crabtree GR. Perspectives: signal transduction. Inositol phosphates in the nucleus. *Science*. 2000;287:1937–9.
63. Zima AV, Bare DJ, Mignery GA, Blatter LA. IP₃-dependent nuclear Ca^{2+} signalling in the mammalian heart. *J Physiol*. 2007;584:601–11.
64. Hardingham GE, Chawla S, Johnson CM, Bading H. Distinct functions of nuclear and cytoplasmic calcium in the control of gene expression. *Nature*. 1997;385:260–5.
65. Dolmetsch RE, Xu K, Lewis RS. Calcium oscillations increase the efficiency and specificity of gene expression. *Nature*. 1998;392:933–6.
66. Dolmetsch RE, Lewis RS, Goodnow CC, Healy JI. Differential activation of transcription factors induced by Ca^{2+} response amplitude and duration. *Nature*. 1997;386:855–8.
67. Bkaily G, Nader M, Avedanian L, Choufani S, Jacques D, D'Orléans-Juste P. G-protein-coupled receptors, channels, and Na^+/H^+ exchanger in nuclear membranes of heart, hepatic, vascular endothelial, and smooth muscle cells. *Can J Physiol Pharmacol*. 2006;84:431–41.
68. Bkaily G, Avedanian L, Jacques D. Nuclear membrane receptors and channels as targets for drug development in cardiovascular diseases. *Can J Physiol Pharmacol*. 2009;87:108–19.
69. Bossuyt J, Helmstadter K, Wu X, Clements-Jewery H, Haworth RS, Avkiran M, et al. $\text{Ca}^{2+}/\text{calmodulin}$ -dependent protein kinase II delta and protein kinase D overexpression reinforce the histone deacetylase 5 redistribution in heart failure. *Circ Res*. 2008;102:695–702.
70. Wu X, Zhang T, Bossuyt J, Li X, McKinsey TA, Dedman JR, et al. Local InsP₃-dependent perinuclear Ca^{2+} signaling in cardiac myocyte excitation-transcription coupling. *J Clin Invest*. 2006;116:675–82.

71. Wu H, Naya FJ, McKinsey TA, Mercer B, Shelton JM, Chin ER, et al. MEF2 responds to multiple calcium-regulated signals in the control of skeletal muscle fiber type. *EMBO J.* 2000;19:1963–73.
72. Zhang T, Kohlhaas M, Backs J, Mishra S, Phillips W, Dybkova N, et al. CaMKIIdelta isoforms differentially affect calcium handling but similarly regulate HDAC/MEF2 transcriptional responses. *J Biol Chem.* 2007;282:35078–87.
73. Backs J, Song K, Bezprozvannaya S, Chang S, Olson EN. CaM kinase II selectively signals to histone deacetylase 4 during cardiomyocyte hypertrophy. *J Clin Invest.* 2006;116:1853–64.
74. McKinsey TA, Zhang CL, Olson EN. Activation of the myocyte enhancer factor-2 transcription factor by Ca²⁺/calmodulin-dependent protein kinase-stimulated binding of 14-3-3 to histone deacetylase 5. *Proc Natl Acad Sci USA.* 2000;97:14400–5.
75. Colella M, Grisan F, Robert V, Turner JD, Thomas AP, Pozzan T. Ca²⁺ oscillation frequency decoding in cardiac cell hypertrophy: role of calcineurin/NFAT as Ca²⁺ signal integrators. *Proc Natl Acad Sci U S A.* 2008;105:2859–64.
76. Molkentin JD. Calcineurin-NFAT signaling regulates the cardiac hypertrophic response in coordination with the MAPKs. *Cardiovasc Res.* 2004;63:467–75.
77. Timmerman LA, Clipstone NA, Ho SN, Northrop JP, Crabtree GR. Rapid shuttling of NF-AT in discrimination of Ca²⁺ signals and immunosuppression. *Nature.* 1996;383:837–40.
78. Hallhuber M, Burkard N, Wu R, Buch MH, Engelhardt S, Hein L, et al. Inhibition of nuclear import of calcineurin prevents myocardial hypertrophy. *Circ Res.* 2006;99:626–35.
79. Gomez-Ospina N, Tsuruta F, Barreto-Chang O, Hu L, Dolmetsch R. terminus of the L-type voltage-gated calcium channel Ca(V)1.2 encodes a transcription factor. *Cell.* 2006;127:591–606.
80. Chung HJ, Jan LY. Channeling to the nucleus. *Neuron.* 2006;52:937–40.
81. Gustafsson AB, Gottlieb RA. Heart mitochondria: gates of life and death. *Cardiovasc Res.* 2008;77:334–43.
82. Giacomello M, Drago I, Pizzo P, Pozzan T. Mitochondrial Ca²⁺ as a key regulator of cell life and death. *Cell Death Differ.* 2007;14:1267–74.

Chapter 18

Pharmacological Modulation and Clinical Implications of Sarcolemmal Ca^{2+} -Handling Proteins in Heart Function

Yasser Abdellatif, Adriana Adameova, and Naranjan S. Dhalla

18.1 Introduction

Since the discovery by Ringer in 1885 that Ca^{2+} is essential for cardiac contraction, the role of Ca^{2+} in the process of excitation–contraction coupling, myocardial metabolism, and maintenance of cardiac cell integrity has been examined extensively [1–5]. Depolarization activates the L-type Ca^{2+} channels, the sarcolemma (SL) membrane, leading to an influx of a small amount of Ca^{2+} . This Ca^{2+} then activates Ca^{2+} -release channels in the sarcoplasmic reticulum (SR) and results in a massive Ca^{2+} release to raise the cytosolic Ca^{2+} from nanomolar to micromolar levels. As a consequence, Ca^{2+} binds to troponin, relieves the inhibitory effect of the troponin complex on the actin and myosin filaments, and initiates the contraction of myofibrils. Most of the cytosolic Ca^{2+} is rapidly pumped into the SR by the ATP-dependent Ca^{2+} -pump ATPase, while the SL Ca^{2+} -pump ATPase and $\text{Na}^+–\text{Ca}^{2+}$ exchanger (NCX) remove the rest out of the cell. Various cation channels, pumps, and exchangers that are directly or indirectly involved in the excitation–contraction coupling process are shown in Fig. 18.1. This chapter describes the characteristics of SL Ca^{2+} channels, NCX, and Ca^{2+} -pump ATPase, which participate in the raising and lowering of the intracellular concentration of Ca^{2+} in cardiomyocytes. Some information regarding SL store-operated Ca^{2+} channels that participate in Ca^{2+} entry is provided. In addition, biochemical features of SL $\text{Na}^+–\text{K}^+$ ATPase and SL $\text{Na}^+–\text{H}^+$ exchanger (NHE), which regulate the intracellular concentration of Ca^{2+} , are discussed. Pharmacological modulation of SL Ca^{2+} -handling proteins for the regulation of intracellular Ca^{2+} in cardiomyocytes as well as SL Ca^{2+} -handling abnormalities during the development of cardiac dysfunction in heart disease is also discussed. The involvement of changes in the

Y. Abdellatif, A. Adameova, and N.S. Dhalla (✉)

Institute of Cardiovascular Sciences, St. Boniface General Hospital Research Centre, Winnipeg, MB, Canada
and

Department of Physiology, Faculty of Medicine, University of Manitoba, Winnipeg, MB, Canada
e-mail: nsdhalla@sbsrc.ca

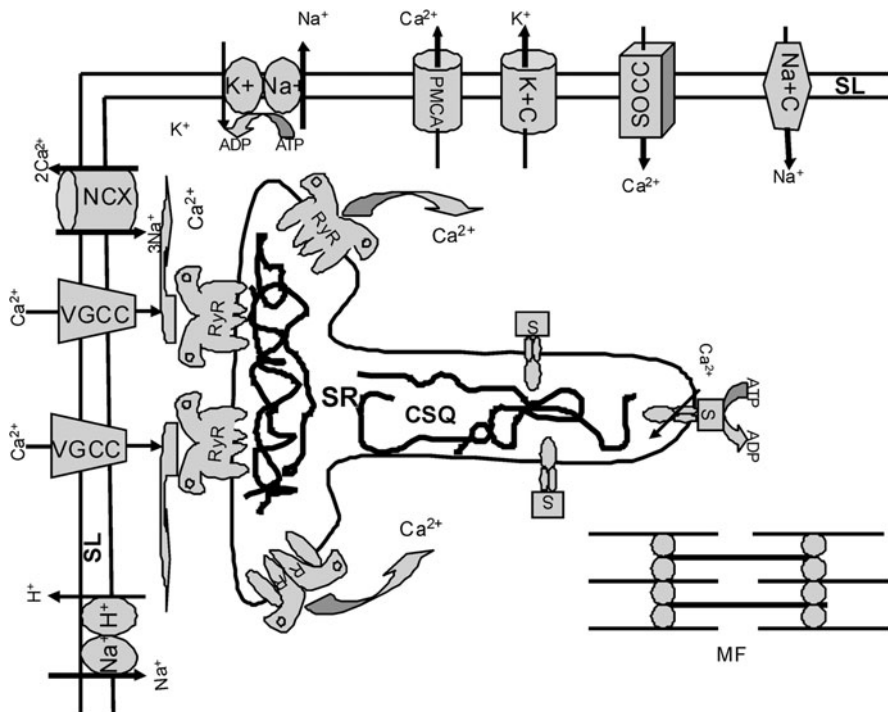


Fig. 18.1 Schematic representation of the cellular components in the excitation–contraction coupling process. In the cardiomyocyte, Na^+ entry through the voltage-gated Na^+ channels ($\text{Na}+\text{C}$) in the sarcolemma (SL) membrane leads to cellular depolarization, which then activates the voltage-gated Ca^{2+} channels (VGCC) causing a small amount of Ca^{2+} influx. This entry of Ca^{2+} activates the SR Ca^{2+} -release channels or ryanodine receptors (RyR) and results in the release of additional Ca^{2+} , which relieves the inhibitory effect of the troponin complex on the actin and myosin filaments in myofibrils (MF) and results in cardiac contraction. The high level of Ca^{2+} in the cytoplasm is taken up by the Ca^{2+} -pump ATPase (S) in the SR where it is stored by the Ca^{2+} -binding protein calsequestrin (CSQ). The cytosolic Ca^{2+} is also extruded through the $\text{Na}^+-\text{Ca}^{2+}$ exchanger (NCX) and the SL Ca^{2+} -pump ATPase (PMCA). Since both cardiac contraction and relaxation processes are intimately associated with hydrolysis of ATP and stimulation of metabolism, the resulting H^+ is removed by Na^+-H^+ exchanger (NHE). Thus, Na^+ entering into the cell through NHE, Na^+ channels, and NCX is extruded by the Na^+-K^+ ATPase. The store-operated Ca^{2+} channels (SOCC) are active only when the SR is depleted of Ca^{2+} , whereas K^+ is removed from the cell by K^+ channels (K+C)

activities of SL Ca^{2+} -handling proteins has been indicated in rate and rhythm disturbances under various pathological conditions.

18.2 Sarcolemmal L-type Ca^{2+} Channel

Voltage-gated Ca^{2+} channels, also referred to as long lasting or L-type Ca^{2+} channels, are embedded in the cardiac SL membrane and play a critical role in the process of excitation–contraction coupling. Following depolarization, L-type

Ca^{2+} channels are opened to allow the entry of a small amount of Ca^{2+} , which activates SR Ca^{2+} -release channels. Soon after the increase in cytoplasmic Ca^{2+} , L-type Ca^{2+} channels undergo rapid inactivation in order to terminate Ca^{2+} entry. There are several isoforms of L-type Ca^{2+} channels, but cardiomyocytes express the CaV 1.2 isoform. The L-type Ca^{2+} -channel pore forming unit (α -subunit) is composed of four homologous domains, each having six transmembrane segments [6]. The accessory subunits, β_2 and $\alpha_2\text{-}\delta$ subunits, of the L-type Ca^{2+} channel are also expressed in the heart [7]. There are several modulators of SL Ca^{2+} channels, of which the most important are calmodulin (CaM) and β -adrenergic stimulation. CaM has been found to be associated with the COOH terminal of the voltage-gated Ca^{2+} channels and can both activate and inactivate the channel in a Ca^{2+} -dependent manner. This mechanism prevents excessive channel activation when Ca^{2+} is high and facilitates channel inactivation when Ca^{2+} is low [8]. On the other hand, β -adrenergic stimulation increases channel current, thus increasing the contractile force development, which is mediated through phosphorylation of the channel via protein kinase A (PKA). L-type Ca^{2+} channels are actually associated with β -adrenergic receptor in a multimeric protein complex that may also include heterotrimeric G-proteins, adenylate cyclase, PKA, phosphatases, and PKA binding proteins; this conglomerate of proteins is called a signalosome [9].

Mutations in the gene encoding the cardiac L-type Ca^{2+} channels lead to a loss of their function and have been associated with short QT syndrome, which may result in atrial fibrillation, syncope, and sudden death [10]. SL L-type voltage-gated Ca^{2+} -channel blockers are used for the treatment of angina pectoris, high blood pressure, and arrhythmias. Voltage-gated Ca^{2+} -channel blockers belong to three chemical entities. The dihydropyridines such as amlodipine are used mainly for their effect on the vascular smooth muscle as vasodilator for the treatment of stable and vasospastic angina. Phenylalkylamines (verapamil), the second class, reduce cardiac oxygen demand and alleviate coronary vasospasm; these drugs are used for the treatment of angina pectoris. The third class, benzothiazepines (diltiazem), are intermediate in their selectivity between the myocardium and the vascular smooth muscles and reduce arterial pressure without depressing the heart muscle. Both verapamil and diltiazem are also used for the treatment of arrhythmias, mainly by acting on the Ca^{2+} channels in the heart pacemaker system [11].

18.3 Sarcolemmal $\text{Na}^+–\text{Ca}^{2+}$ Exchanger

The SL NCX is responsible for lowering the increased level of cytosolic Ca^{2+} due to activation of the voltage-gated Ca^{2+} channel [2, 3]. The cardiac SL NCX operates in either forward mode, where it removes cytosolic Ca^{2+} in exchange for extracellular Na^+ , or in reverse mode, in which excess Ca^{2+} is transported into the cytosol while Na^+ is extruded. The reverse exchange mechanism is relevant to conditions of ischemia-reperfusion where the rise in Na^+ ions is high enough to trigger the reverse activity of NCX [3]. The reverse mode of NCX can also be active in heart failure

where an increase in intracellular $[Na^+]$ leads to Ca^{2+} influx via the NCX [3]. Another important function of the NCX is related to the action of cardiac glycosides whereby inhibition of the plasma membrane Na^+-K^+ ATPase leads to Na^+ accumulation, which then triggers NCX reverse mode [2] leading to an increase in cytosolic Ca^{2+} and positive inotropic effect. At resting diastolic levels of 100 nM Ca^{2+} , the cardiac isoform NCX1 is completely activated. In addition, NCX1 is activated by phosphatidyl inositol biphosphate and ATP [12]. SL NCX is also modulated by a cytosolic protein phospholemman, whereas PKA and protein kinase C (PKC) phosphorylations inhibited this NCX1 activity [13].

The cardiac NCX plays a crucial role in ischemia–reperfusion injury. During ischemia, accumulation of H^+ in the cell leads to the activation of NHE that creates intracellular Na^+ overload. This change triggers the activation of NCX1 to extrude intracellular Na^+ in exchange for extracellular Ca^{2+} and results in the development of intracellular Ca^{2+} overload. As a consequence there occurs a depression in cardiac contractility as well as apoptotic cell death [14]. It has been documented that NCX is involved in β -adrenergic-stimulated Ca^{2+} entry in addition to SL L-type Ca^{2+} channels, because the catecholamine-induced increase in Ca^{2+} in cardiomyocyte was inhibited by both NCX and Ca^{2+} -channel antagonists [15]. An increase in the reverse mode activity of SL NCX due to β -adrenergic stimulation may contribute to arrhythmias in the failing heart [16]. On the other hand, NCX activity is also reduced in heart failure, and this effect is mitigated by angiotensin-converting enzyme inhibitors [17]. Several drugs have been developed to inhibit the reverse mode of NCX due to its involvement in ischemia–reperfusion injury [18]. SEA0400 is the most specific inhibitor for the cardiac NCX1, because it is less sensitive towards the brain and skeletal isoforms [19]. It has been shown to be protective against the ischemia–reperfusion induced injury in the heart [20].

18.4 Sarcolemmal Store-Operated Ca^{2+} Channel

The threshold of SR Ca^{2+} loading tightly controls Ca^{2+} release through RyR, which affects muscle contraction. Both excitable and non-excitable cells need Ca^{2+} in the endoplasmic reticulum for proper protein folding and, thus, emptying of the intracellular Ca^{2+} stores can be seen to have adverse effects. Measuring the Ca^{2+} current that enter the cell upon depletion of intracellular Ca^{2+} stores has helped to identify a group of cation channels that respond to intracellular stores Ca^{2+} depletion, and are called store-operated Ca^{2+} channels [21]. These cation channels belong to the large family of transient receptor potential (TRP) channels originally discovered in *Drosophila* and consist of six transmembrane (TM) spanning helices, and a pore region that exists between TM5 and TM6. The channels are gated by a variety of stimuli that include the binding of intracellular and extracellular messengers, changes in temperature as well as chemical and mechanical pressures [22]. Store-operated Ca^{2+} channels are activated either by agonists such as inositol triphosphate

(IP₃) and PKC or by internal Ca^{2+} store depletion [21]. Like other cation channels, the store-operated Ca^{2+} channels are modulated by phosphorylation. The phosphorylation of store-operated Ca^{2+} channels due to PKC inhibits Ca^{2+} entry in Jurkat cells and lymphocytes [23], whereas phosphorylation by PKA activates these channels. Inhibitors of serine/threonine phosphatase A (calyculin A and okadaic acid) have also been reported to reduce the activation of the store-operated Ca^{2+} channels [24]. In addition, thiol oxidation and cADP-ribose inhibition were found to reduce the channel activity in isolated pulmonary artery rings and human smooth muscle, respectively [25, 26].

Ca^{2+} influx through store-operated Ca^{2+} channels was implicated in protein kinase D and MAPK activation that may be a target of physiological agents such as decosahexanoic acid in Jurkat T-cells [27]. In addition to PKA and PKC, store-operated Ca^{2+} channels are modulated by CaMKII [28]. Acidic pH and hydrogen peroxide were also found to inhibit the store-operated Ca^{2+} channels in cultured human microglia [29, 30]. It should be pointed out that the activity of store-operated Ca^{2+} channels was increased in atrial cardiomyocytes as they progressed from a contractile to proliferative phenotype in tissue culture [31]. These channels were also shown to contribute to the increase of intracellular Ca^{2+} cardiomyocytes upon inhibition of the $\text{Na}^+–\text{K}^+$ ATPase [32]. In cardiomyocytes, Ca^{2+} entry through store-operated Ca^{2+} channels has been linked to the activation of calcineurin and the development of hypertrophy [33]. Thus, it is evident that the role of store-operated Ca^{2+} channels in cardiovascular biology is being explored, and the potential for development of therapy associated with store-operated Ca^{2+} channels in apoptosis, hypertrophy, and arrhythmias has been suggested [34, 35].

18.5 Sarcolemmal Ca^{2+} -Pump ATPase

The Ca^{2+} pump ATPase (PMCA) activity of the plasma membrane is critical for fine tuning the cytosolic Ca^{2+} . SL PMCA, a P-type ATPase [36] has more than 20 splice variants belonging to four isoforms. PMCA1 and 4 are expressed in most tissues, while the expression of PMCA2 and 3 is limited to brain and excitable tissues. The PMCA is believed to have ten transmembrane segments, with a large central loop, which contains the ATP binding site and a large C-terminal loop, which contains the CaM binding domain [37]. CaM is the main protein regulator of the pump [38] because in the absence of CaM, the pump is auto-inhibited by a mechanism that involves binding of the C-terminal tail to the two major intracellular loops. The activation of PMCA requires binding of Ca^{2+} with CaM to the C-terminal tail and conformational changes that displace the auto-inhibitory tail from the major catalytic domain. The release of the auto-inhibitory tail may be facilitated by acidic phospholipids as well as PKA- or PKC-mediated phosphorylations of specific (Ser/Thr) residues in the C-terminal. On the other hand, the activity of PMCA is depressed by partial proteolytic cleavage of the tail which is catalyzed by proteases such as calpain and caspases [39].

The cardiac PMCA is considered to play a minor role as a mechanism for lowering the intracellular concentration of Ca^{2+} compared to NCX and SERCA; however, there is growing evidence for the role of PMCA as a signaling center and housekeeping molecule [37]. The critical role of PMCA1 as a housekeeping gene has been demonstrated in a gene knockout study [40]. This study showed that complete knock out of PMCA1 led to embryonic lethality, while heterozygous animals did not show any defect. Interestingly, although PMCA4 is widely expressed, PMCA4 null mutants exhibited no embryonic lethality and appeared outwardly normal. PMCA4 null male mice were infertile but had normal spermatogenesis and mating behavior. In contrast to the minor effect obtained by ablating the PMCA4 gene, overexpression of PMCA4 in atrial smooth muscles had dramatic effects on cardiovascular function and provided evidence of its involvement in cellular signaling [41]. Cardiac overexpression of PMCA attenuates endothelin-1 stimulated early induction of cardiac gene expression, suggesting that PMCA may modulate myocardial growth responses. In fact, cardiomyocytes from rats over-expressing PMCA4b displayed a higher growth rate [42]. Likewise, blood pressure in these animals was increased, indicating a direct involvement of PMCA in Ca^{2+} cycling; however, no significant changes in Ca^{2+} content were found. The effect on blood pressure can be explained by the reduction of nNOS (neuronal nitric oxide synthetase), suggesting a role for PMCA in nNOS function. Another study showed that overexpression of PMCA4b leads to reduced inotropic effect in response to β -adrenergic stimulation, probably through an nNOS-mediated effect [40]. These mice also showed an increased hypertrophic response under continuous β -adrenergic stimulation. The PMCA downregulates the nNOS activity whereas its inhibition increased the nNOS activity. It seems that this regulation is beneficial for increasing cardiac contractility. Mouse hearts lacking nNOS have a reduced adrenergic and force frequency response [43].

18.6 Sarcolemmal $\text{Na}^+–\text{H}^+$ Exchanger

The maintenance of intracellular pH is critical for cardiac contractility and prevention of damage to cardiomyocytes. The NHE clears more than 50% of the cytosolic H^+ load produced by metabolism [14, 44]. The exchange of H^+ for Na^+ is electroneutral which indicates that NHE is not electrogenic. The human NHE consists of 12 transmembrane segments and an N terminal unstructured regulatory domain; cardiomyocytes express NHE1 [45]. The NHE as well as intracellular pH is regulated by several intracellular modulators such as phosphatidyl inositol 4,5-biphosphate (PIP_2) [46]. The phosphatase, calcineurin B homologous protein 3, was found to boost the production of mature NHE1 protein, as well as cell surface transport and longevity [47]. CaM has also been observed to modulate NHE1 activity; CaM and Ca^{2+} complex bind to NHE1 and activate the exchanger by interfering with its auto-inhibitory mechanism [48, 49]. Another important modulator of NHE1 is carbonic anhydrase, which increases its activity; the increase in activity is dependent on the phosphorylation of NHE upstream

of the carbonic anhydrase binding site [50]. This interaction may be useful for the removal of H^+ produced by carbonic anhydrase [51]. On the other hand, dephosphorylation inhibits the NHE1 activity [51, 52]. There are several extracellular activators of NHE such as thrombin, phorbol esters, and serum, which activate NHE through CaMKII, the mitogen-activated protein kinases (MAPK) and extracellular-regulated kinases 1 and 2 (ERK 1/2). Activation of NHE1 by insulin may be mediated via the ERK1/2/MAPK pathway and the PKC pathway [51]. In vascular smooth muscles, angiotensin II may lead to phosphorylation of NHE through a downstream target of ERK 1/2 and the ribosomal protein S6 kinase (P90RSK) [53, 54].

As indicated earlier, NHE is known to play a central role together with the NCX in ischemia–reperfusion injury. Activation of the NHE by the accumulation of H^+ under ischemic conditions leads to a massive influx of Na^+ that in turn activates the NCX [14]. NHE has also been implicated in cardiac hypertrophy because prohypertrophic factors, such as endothelin-1 and norepinephrine, stimulate a signaling cascade that leads to ERK1/2 and P90RSK activation and phosphorylation of NHE1 [55]. In fact, NHE1 overexpression has been shown to result in cardiac hypertrophy, contractile dysfunction, and heart failure [56]. Cariporide, a specific and effective NHE inhibitor was suggested as a potential drug for the prevention of ischemia–reperfusion injury [57]. Cariporide was mainly beneficial in patients undergoing coronary artery bypass when administered before the operation to avoid the consequences of ischemia–reperfusion injury [58]. Despite the fact that cariporide protected against ischemia–reperfusion injury in experimental animals, a paradoxical increase in death due to brain hemorrhage in phase III clinical trials discouraged the development of other NHE blockers [59].

18.7 Sarcolemmal Na^+-K^+ ATPase

The plasma membrane Na^+-K^+ ATPase was first described in 1957 by Skou [60]. The main function of the pump is the removal of intracellular Na^+ in exchange for extracellular K^+ to maintain the resting membrane potential by using ATP. This functional pump is composed of two major subunits; the α -subunit has approximately ten TM domains and three large intracellular loops. The loop between TM 4 and 5 contains the phosphorylation and the nucleotide binding domains [61]. The α -subunit also contains the binding site for Na^+ , K^+ , and cardiac glycosides [62]. The second subunit, the β -subunit, is essential for the maturation and targeting of the pump whereas a third subunit, the γ -subunit has no known function. Among the four α -isoforms, the $\alpha 1$ isoform is ubiquitously expressed, whereas the $\alpha 2$ isoform is specifically expressed in skeletal and cardiac muscles, brain, and adipose tissue [62]. Primate and canine myocardium express the $\alpha 1$ and $\alpha 3$ isoforms, whereas only the $\alpha 1$ isoform is found in sheep and guinea pig myocardium [63]. Prostaglandins (GE2, GF2, and GI2) have been shown to reduce the Na^+-K^+ ATPase activity [64]. On the other hand, insulin was found to stimulate Na^+-K^+ ATPase [65]. Interestingly, a cholesterol-enriched membrane showed high Na^+-K^+ pump activity [66], Caffeine

also appears to increase the efficiency of the pump [67]. Likewise, catecholamine-induced stimulation of PKA and PKC activities was shown to increase the $\text{Na}^+–\text{K}^+$ ATPase activity in cardiomyocytes [68].

The expression and activity of the $\text{Na}^+–\text{K}^+$ ATPase is significantly enhanced or reduced by a variety of disease states and physiological modulators. In heart failure, a characteristic change in the expression pattern of α -subunit has been observed where both the mRNA and protein levels of α -1, α -2, and β 1 isoforms were reduced, while α -3 isoform was increased in a rat model of congestive heart failure. These changes were prevented by treatment with imidapril and angiotensin-converting enzyme inhibitor [17, 69]. The reduction of the expression and activity of $\text{Na}^+–\text{K}^+$ ATPase in congestive heart failure was also shown to be due to the activation of the renin–angiotensin system [70]. The activity of $\text{Na}^+–\text{K}^+$ ATPase was also reduced due to ischemia–reperfusion; this change was found to be caused by reduction in the expression of the specific isoforms of the pump component, namely α 2, α 3, and β 1 subunits [71–73]. Antioxidants such as superoxide dismutase plus catalase or ischemic preconditioning have been reported to prevent these changes [74, 75]. The activity of the $\text{Na}^+–\text{K}^+$ ATPase was also depressed in diabetic and genetic cardiomyopathies [76–79].

Cardiac glycosides have been used to treat congestive heart failure and $\text{Na}^+–\text{K}^+$ ATPase is the classic receptor for these compounds. In human heart, all $\text{Na}^+–\text{K}^+$ ATPase α -subunits isoforms, namely α 1, α 2, and α 3, have shown a high affinity for cardiac glycosides [80]. The α 2– β subunit combination exhibits faster association and dissociation for the cardiac glycoside ouabain than the α 1– β subunit due to a difference in the specific amino acids in their extracellular domains. The beneficial effects of cardiac glycosides on cardiac function in chronic heart failure are believed to be twofold. First, the accumulation of Na^+ inside the cell triggers the reverse mode of NCX, leading to Ca^{2+} influx which causes a positive inotropic effect [81]. Second, due to signaling to the cell interior, particularly to the nucleus which affects membrane protein trafficking and protein kinase activity [82]. The human body has been reported to produce cardiac glycoside-like compounds [83]. Endogenous ouabain is produced by the adrenal cortex and medulla [84] and has been shown to be involved in the proliferation of smooth muscles, kidney cells, and endothelial cells [68]. There is also evidence for the existence of endogenous digoxin and the structurally related bufadienolides in human urine [85]. It should be pointed out that marked inhibition of SL $\text{Na}^+–\text{K}^+$ ATPase by high doses of cardiac glycosides is well known to be associated with cardiac arrhythmias; however, the mechanisms of this cardiotoxicity are not yet fully understood.

18.8 Conclusions

From the foregoing discussion, it is evident that Ca^{2+} movements across the SL membrane in cardiomyocytes involve L-type Ca^{2+} channels, NCX, NHE, PMCA, store-operated Ca^{2+} channels, and $\text{Na}^+–\text{K}^+$ ATPase. These cation channels and transporters participate in Ca^{2+} movements either directly or indirectly and are

highly regulated by the phosphorylation/dephosphorylation system [86]. Any defect in one or more of these Ca^{2+} -handling proteins, which may occur in congestive heart failure, [87] appears to result in loss of their coordinated function for the development of abnormalities in rate and rhythm of the heart. There seem to be three areas of investigation that are becoming the center of attention in cardiovascular research. First, as the classical view of the channels, transporters, and pumps with respect to cation conducting pathway has evolved, more emphasis is being placed on the role of the cation channels as signaling molecules, particularly the signaling mediated by SL $\text{Na}^+–\text{K}^+$ ATPase and Ca^{2+} -pump ATPase. The second is the challenging task of finding correlations between the activities of different Ca^{2+} -handling proteins. An example of the influence of one channel on another are the store-operated Ca^{2+} channels where emptying of the SR Ca^{2+} store activates the store-operated channel in the cell to permit the entry of more Ca^{2+} . Another example is the study of the interaction between the L-type Ca^{2+} channel and RyR. The mechanism of such an interaction in cardiac muscles has revealed that Ca^{2+} influx through the L-type Ca^{2+} channel activates RyR without any physical interaction of the SL and SR channels. Last but not least, developing novel therapeutic approaches to treat heart disease where a drug such as ranolazine specifically targets the late or persistent Na^+ current [88], or a specific current in a specific type of cell, such as targeting the ultra-rapid K^+ current in atrial myocytes for correction of arrhythmias [89]. In addition, the control of defective or mutated channels can be achieved before these are even translated. In a recent study, silencing micro-RNA was used to downregulate the expression of mutant K^+ channel, thus averting their arrhythmogenic action [90]. Although great progress on work related to the role of Ca^{2+} in heart function in health and disease has been carried out over 125 years, there is real challenge to undertake extensive research if we have to fully understand the role of different Ca^{2+} -handling proteins in cardiac function particularly with respect to rate and rhythm in health and disease.

Acknowledgments The research in this article was supported by a grant from the Canadian Institutes of Health Research (CIHR). The infrastructural support for this study was provided by the St. Boniface General Hospital Research Foundation.

References

1. Dhalla NS, Ziegelhoffer A, Harrow JA. Regulatory role of membrane systems in heart function. *Can J Physiol Pharmacol.* 1977;55:1211–34.
2. Dhalla NS, Pierce GN, Panagia V, Singal PK, Beamish RE. Calcium movements in relation to heart function. *Basic Res Cardiol.* 1982;77:117–39.
3. Dhalla NS, Saini HK, Tappia PS, Sethi R, Mengi SA, Gupta SK. Potential role and mechanisms of subcellular remodeling in cardiac dysfunction due to ischemic heart disease. *J Cardiovasc Med (Hagerstown).* 2007;8:238–50.
4. Gordon AM, Homsher E, Regnier M. Regulation of contraction in striated muscle. *Physiol Rev.* 2000;80:853–924.
5. Cheng H, Lederer WJ. Calcium sparks. *Physiol Rev.* 2008;88:1491–545.

6. Catterall WA, Perez-Reyes E, Snutch TP, Striessnig J. Nomenclature and structure-function relationships of voltage-gated calcium channels. *Pharmacol Rev.* 2005;57:411–25.
7. Colecraft HM, Alseikhan B, Takahashi SX, Chaudhuri D, Mittman S, Yegnasubramanian V, et al. Novel functional properties of Ca^{2+} channel beta subunits revealed by their expression in adult rat heart cells. *J Physiol.* 2002;541:435–52.
8. Halling DB, Racena-Parks P, Hamilton SL. Regulation of voltage-gated Ca^{2+} channels by calmodulin. *Sci STKE.* 2005;2005:re15.
9. Davare MA, Avdonin V, Hall DD, Peden EM, Burette A, Weinberg RJ, et al. A beta2 adrenergic receptor signaling complex assembled with the Ca^{2+} channel CaV1.2. *Science.* 2001; 293:98–101.
10. Splawski I, Timothy KW, Sharpe LM, Decher N, Kumar P, Bloise R, et al. Ca(V)1.2 calcium channel dysfunction causes a multisystem disorder including arrhythmia and autism. *Cell.* 2004;119:19–31.
11. Hockerman GH, Peterson BZ, Johnson BD, Catterall WA. Molecular determinants of drug binding and action on L-type calcium channels. *Annu Rev Pharmacol Toxicol.* 1997;37:361–96.
12. Hilgemann DW, Yaradanakul A, Wang Y, Fuster D. Molecular control of cardiac sodium homeostasis in health and disease. *J Cardiovasc Electrophysiol.* 2006;17:S47–56.
13. Cheung JY, Rothblum LI, Moorman JR, Tucker AL, Song J, Ahlers BA, et al. Regulation of cardiac $\text{Na}^+/\text{Ca}^{2+}$ exchanger by phospholemmann. *Ann N Y Acad Sci.* 2007;1099:119–34.
14. Karmazyn M, Gan XT, Humphreys RA, Yoshida H, Kusumoto K. The myocardial Na^+/H^+ exchange: structure, regulation, and its role in heart disease. *Circ Res.* 1999;85:777–86.
15. Saini HK, Tripathi ON, Zhang S, Elimban V, Dhalla NS. Involvement of $\text{Na}^+/\text{Ca}^{2+}$ exchanger in catecholamine-induced increase in intracellular calcium in cardiomyocytes. *Am J Physiol Heart Circ Physiol.* 2006;290:H373–80.
16. Wei SK, Ruknudin AM, Shou M, McCurley JM, Hanlon SU, Elgin E, et al. Muscarinic modulation of the sodium-calcium exchanger in heart failure. *Circulation.* 2007;115:1225–33.
17. Shao Q, Ren B, Elimban V, Tappia PS, Takeda N, Dhalla NS. Modification of sarcolemmal Na^+/K^+ -ATPase and $\text{Na}^+/\text{Ca}^{2+}$ exchanger expression in heart failure by blockade of renin-angiotensin system. *Am J Physiol Heart Circ Physiol.* 2005;288:H2637–46.
18. Iwamoto T. Forefront of $\text{Na}^+/\text{Ca}^{2+}$ exchanger studies: Molecular pharmacology of $\text{Na}^+/\text{Ca}^{2+}$ exchange inhibitors. *J Pharmacol Sci.* 2004;96:27–32.
19. Iwamoto T, Kita S, Uehara A, Imanaga I, Matsuda T, Baba A, et al. Molecular determinants of $\text{Na}^+/\text{Ca}^{2+}$ exchange (NCX1) inhibition by SEA0400. *J Biol Chem.* 2004;279:7544–53.
20. Namekata I, Nakamura H, Shimada H, Tanaka H, Shigenobu K. Cardioprotection without cardio suppression by SEA0400, a novel inhibitor of $\text{Na}^+/\text{Ca}^{2+}$ exchanger, during ischemia and reperfusion in guinea-pig myocardium. *Life Sci.* 2005;77:312–24.
21. Parekh AB, Putney Jr JW. Store-operated calcium channels. *Physiol Rev.* 2005;85:757–810.
22. Montell C, Birnbaumer L, Flockerzi V. The TRP channels, a remarkably functional family. *Cell.* 2002;108:595–8.
23. Parekh AB, Penner R. Depletion-activated calcium current is inhibited by protein kinase in RBL-2H3 cells. *Proc Natl Acad Sci USA.* 1995;92:7907–11.
24. Evans NE, Forth MK, Simpson AK, Mason MJ. Inhibition by calyculin A and okadaic acid of the Ca^{2+} release-activated Ca^{2+} entry pathway in rat basophilic leukemia cells: evidence for regulation by type 1/2A serine/threonine phosphatase activity. *Biochim Biophys Acta.* 2005; 1718:32–43.
25. Schach C, Xu M, Platoshyn O, Keller SH, Yuan JX. Thiol oxidation causes pulmonary vasodilation by activating K^+ channels and inhibiting store-operated Ca^{2+} channels. *Am J Physiol Lung Cell Mol Physiol.* 2007;292:L685–98.
26. Thompson M, White T, Chini EN. Modulation of store-operated Ca^{2+} entry by cyclic-ADP-ribose. *Braz J Med Biol Res.* 2006;39:739–48.
27. Denys A, Aires V, Hichami A, Khan NA. Thapsigargin-stimulated MAP kinase phosphorylation via CRAC channels and PLD activation: inhibitory action of docosahexaenoic acid. *FEBS Lett.* 2004;564:177–82.

28. Machaca K. Ca^{2+} -calmodulin-dependent protein kinase II potentiates store-operated Ca^{2+} current. *J Biol Chem.* 2003;278:33730–7.
29. Khoo C, Helm J, Choi HB, Kim SU, McLarnon JG. Inhibition of store-operated Ca^{2+} influx by acidic extracellular pH in cultured human microglia. *Glia.* 2001;36:22–30.
30. Tornquist K, Vainio PJ, Bjorklund S, Titievsky A, Dugue B, Tuominen RK. Hydrogen peroxide attenuates store-operated calcium entry and enhances calcium extrusion in thyroid FRTL-5 cells. *Biochem J.* 2000;351(Pt 1):47–56.
31. Berra-Romani R, Mazzocco-Spezia A, Pulina MV, Golovina VA. Ca^{2+} handling is altered when arterial myocytes progress from a contractile to a proliferative phenotype in culture. *Am J Physiol Cell Physiol.* 2008;295:C779–90.
32. Saini HK, Dhalla NS. Sarcolemmal cation channels and exchangers modify the increase in intracellular calcium in cardiomyocytes on inhibiting Na^+ - K^+ ATPase. *Am J Physiol Heart Circ Physiol.* 2007;293:H169–81.
33. Onohara N, Nishida M, Inoue R, Kobayashi H, Sumimoto H, Sato Y, et al. TRPC3 and TRPC6 are essential for angiotensin II-induced cardiac hypertrophy. *EMBO J.* 2006;25:5305–16.
34. Inoue R, Jensen LJ, Shi J, Morita H, Nishida M, Honda A, et al. Transient receptor potential channels in cardiovascular function and disease. *Circ Res.* 2006;99:119–31.
35. Watanabe H, Murakami M, Ohba T, Takahashi Y, Ito H. TRP channel and cardiovascular disease. *Pharmacol Ther.* 2008;118:337–51.
36. Axelsen KB, Palmgren MG. Evolution of substrate specificities in the P-type ATPase superfamily. *J Mol Evol.* 1998;46:84–101.
37. Strehler EE, Filoteo AG, Penniston JT, Caride AJ. Plasma-membrane Ca^{2+} pumps: structural diversity as the basis for functional versatility. *Biochem Soc Trans.* 2007;35:919–22.
38. Strehler EE, Caride AJ, Filoteo AG, Xiong Y, Penniston JT, Enyedi A. Plasma membrane Ca^{2+} ATPases as dynamic regulators of cellular calcium handling. *Ann N Y Acad Sci.* 2007;1099:226–36.
39. Carafoli E, Stauffer T. The plasma membrane calcium pump: functional domains, regulation of the activity, and tissue specificity of isoform expression. *J Neurobiol.* 1994;25:312–24.
40. Okunade GW, Miller ML, Pyne GJ, Sutliff RL, O'Connor KT, Neumann JC, et al. Targeted ablation of plasma membrane Ca^{2+} -ATPase (PMCA) 1 and 4 indicates a major housekeeping function for PMCA1 and a critical role in hyperactivated sperm motility and male fertility for PMCA4. *J Biol Chem.* 2004;279:33742–50.
41. Gros R, Afroze T, You XM, Kabir G, Van WR, Kalair W, et al. Plasma membrane calcium ATPase overexpression in arterial smooth muscle increases vasomotor responsiveness and blood pressure. *Circ Res.* 2003;93:614–21.
42. Pihula J, Hammes A, Schuh K, Neyses L, Vuolteenaho O, Ruskoaho H. Overexpression of sarcolemmal calcium pump attenuates induction of cardiac gene expression in response to ET-1. *Am J Physiol Regul Integr Comp Physiol.* 2001;281:R699–705.
43. Oceandy D, Buch MH, Cartwright EJ, Neyses L. The emergence of plasma membrane calcium pump as a novel therapeutic target for heart disease. *Mini Rev Med Chem.* 2006;6:583–8.
44. Fliegel L. Regulation of myocardial Na^+/H^+ exchanger activity. *Basic Res Cardiol.* 2001;96:301–5.
45. Slepkov ER, Rainey JK, Sykes BD, Fliegel L. Structural and functional analysis of the Na^+/H^+ exchanger. *Biochem J.* 2007;401:623–33.
46. Aharonovitz O, Zaun HC, Balla T, York JD, Orlowski J, Grinstein S. Intracellular pH regulation by Na^+/H^+ exchange requires phosphatidylinositol 4,5-bisphosphate. *J Cell Biol.* 2000;150:213–24.
47. Zaun HC, Shrier A, Orlowski J. Calcineurin B homologous protein 3 promotes the biosynthetic maturation, cell surface stability, and optimal transport of the Na^+/H^+ exchanger NHE1 isoform. *J Biol Chem.* 2008;283:12456–67.
48. Bertrand B, Wakabayashi S, Ikeda T, Pouyssegur J, Shigekawa M. The Na^+/H^+ exchanger isoform 1 (NHE1) is a novel member of the calmodulin-binding proteins. Identification and characterization of calmodulin-binding sites. *J Biol Chem.* 1994;269:13703–9.

49. Wakabayashi S, Bertrand B, Ikeda T, Pouyssegur J, Shigekawa M. Mutation of calmodulin-binding site renders the Na^+/H^+ exchanger (NHE1) highly H^+ -sensitive and Ca^{2+} regulation-defective. *J Biol Chem*. 1994;269:13710–5.
50. Li X, Alvarez B, Casey JR, Reithmeier RA, Fliegel L. Carbonic anhydrase II binds to and enhances activity of the Na^+/H^+ exchanger. *J Biol Chem*. 2002;277:36085–91.
51. Malo ME, Fliegel L. Physiological role and regulation of the Na^+/H^+ exchanger. *Can J Physiol Pharmacol*. 2006;84:1081–95.
52. Sardet C, Counillon L, Franchi A, Pouyssegur J. Growth factors induce phosphorylation of the Na^+/H^+ antiporter, glycoprotein of 110 kD. *Science*. 1990;247:723–6.
53. Phan VN, Kusuvara M, Lucchesi PA, Berk BC. A 90-kD Na^+/H^+ exchanger kinase has increased activity in spontaneously hypertensive rat vascular smooth muscle cells. *Hypertension*. 1997;29:1265–72.
54. Takahashi E, Abe J, Berk BC. Stimulates p90rsk in vascular smooth muscle cells. A potential Na^+/H^+ exchanger kinase. *Circ Res*. 1997;81:268–73.
55. Fliegel L. Molecular biology of the myocardial Na^+/H^+ exchanger. *J Mol Cell Cardiol*. 2008; 44:228–37.
56. Nakamura TY, Iwata Y, Arai Y, Komamura K, Wakabayashi S. Activation of Na^+/H^+ exchanger 1 is sufficient to generate Ca^{2+} signals that induce cardiac hypertrophy and heart failure. *Circ Res*. 2008;103:891–9.
57. Scholz W, Albus U, Counillon L, Gogelein H, Lang HJ, Linz W, et al. Protective effects of HOE642, a selective sodium-hydrogen exchange subtype 1 inhibitor, on cardiac ischaemia and reperfusion. *Cardiovasc Res*. 1995;29:260–8.
58. Chaitman BR. A review of the GUARDIAN trial results: clinical implications and the significance of elevated perioperative CK-MB on 6-month survival. *J Card Surg*. 2003;18 Suppl 1:13–20.
59. Mentzer J, Lasley RD, Jessel A, Karmazyn M. Intracellular sodium hydrogen exchange inhibition and clinical myocardial protection. *Ann Thorac Surg*. 2003;75:S700–8.
60. Skou JC. The influence of some cations on an adenosine triphosphatase from peripheral nerves. *Biochim Biophys Acta*. 1957;23:394–401.
61. Takeyasu K, Okamura H, Yasuhara JC, Ogita Y, Yoshimura SH. P-type ATPase diversity and evolution: the origins of ouabain sensitivity and subunit assembly. *Cell Mol Biol* (Noisy-le-grand). 2001;47:325–33.
62. Blanco G, Mercer RW. Isozymes of the Na^+/K^+ -ATPase: heterogeneity in structure, diversity in function. *Am J Physiol*. 1998;275:F633–50.
63. Sweedner KJ, Herrera VL, Amato S, Moellmann A, Gibbons DK, Repke KR. Immunologic identification of Na^+/K^+ -ATPase isoforms in myocardium. Isoform change in deoxycorticosterone acetate-salt hypertension. *Circ Res*. 1994;74:669–78.
64. Karmazyn M, Tuana BS, Dhalla NS. Effect of prostaglandins on rat heart sarcolemmal ATPases. *Can J Physiol Pharmacol*. 1981;59:1122–7.
65. Pierce GN, Ganguly PK, Dzurba A, Dhalla NS. Modification of the function of cardiac subcellular organelles by insulin. *Adv Myocardiol*. 1985;6:113–25.
66. Moffat MP, Dhalla NS. Heart sarcolemmal ATPase and calcium binding activities in rats fed a high cholesterol diet. *Can J Cardiol*. 1985;1:194–200.
67. Gupta MP, Makino N, Takeo S, Kaneko M, Dhalla NS. Cardiac sarcolemma as a possible site of action of caffeine in rat heart. *J Pharmacol Exp Ther*. 1990;255:1188–94.
68. Tian J, Xie ZL. The $\text{Na}-\text{K}$ -ATPase and calcium-signaling microdomains. *Physiology (Bethesda)*. 2008;23:205–11.
69. Dixon IM, Hata T, Dhalla NS. Sarcolemmal calcium transport in congestive heart failure due to myocardial infarction in rats. *Am J Physiol Heart Circ Physiol*. 1992;262:H1387–94.
70. Guo X, Wang J, Elimban V, Dhalla NS. Both enalapril and losartan attenuate sarcolemmal Na^+/K^+ -ATPase remodeling in failing rat heart due to myocardial infarction. *Can J Physiol Pharmacol*. 2008;86:139–47.

71. Dhalla NS, Panagia V, Singal PK, Makino N, Dixon IM, Eyolfson DA. Alterations in heart membrane calcium transport during the development of ischemia-reperfusion injury. *J Mol Cell Cardiol.* 1988;20 Suppl 2:3–13.
72. Ostadal P, Elmoselhi AB, Zdobnicka I, Lukas A, Chapman D, Dhalla NS. Ischemia-reperfusion alters gene expression of Na^+ - K^+ -ATPase isoforms in rat heart. *Biochem Biophys Res Commun.* 2003;306:457–62.
73. Ostadal P, Elmoselhi AB, Zdobnicka I, Lukas A, Elimban V, Dhalla NS. Role of oxidative stress in ischemia-reperfusion-induced changes in Na^+ - K^+ -ATPase isoform expression in rat heart. *Antioxid Redox Signal.* 2004;6:914–23.
74. Elmoselhi AB, Lukas A, Ostadal P, Dhalla NS. Preconditioning attenuates ischemia-reperfusion-induced remodeling of Na^+ - K^+ -ATPase in hearts. *Am J Physiol Heart Circ Physiol.* 2003;285:H1055–63.
75. Shao Q, Matsubara T, Bhatt SK, Dhalla NS. Inhibition of cardiac sarcolemma Na^+ - K^+ -ATPase by oxyradical generating systems. *Mol Cell Biochem.* 1995;147:139–44.
76. Golzman L, Dixon IM, Takeda N, Lukas A, Dakshinamurti K, Dhalla NS. Cardiac sarcolemmal Na^+ - Ca^{2+} exchange and Na^+ - K^+ ATPase activities and gene expression in alloxan-induced diabetes in rats. *Mol Cell Biochem.* 1998;188:91–101.
77. Kato K, Chapman DC, Rupp H, Lukas A, Dhalla NS. Alterations of heart function and Na^+ - K^+ -ATPase activity by etomoxir in diabetic rats. *J Appl Physiol.* 1999;86:812–8.
78. Kato K, Lukas A, Chapman DC, Dhalla NS. Changes in the expression of cardiac Na^+ - K^+ -ATPase subunits in the UM-X7.1 cardiomyopathic hamster. *Life Sci.* 2000;67:1175–83.
79. Kato K, Lukas A, Chapman DC, Rupp H, Dhalla NS. Differential effects of etomoxir treatment on cardiac Na^+ - K^+ ATPase subunits in diabetic rats. *Mol Cell Biochem.* 2002;232:57–62.
80. Crambert G, Hasler U, Beggah AT, Yu C, Modyanov NN, Horisberger JD, et al. Transport and pharmacological properties of nine different human Na, K-ATPase isozymes. *J Biol Chem.* 2000;275:1976–86.
81. Hilgemann DW, Ball R. Regulation of cardiac Na^+ , Ca^{2+} exchange and KATP potassium channels by PIP2. *Science.* 1996;273:956–9.
82. Schoner W, Scheiner-Bobis G. Endogenous and exogenous cardiac glycosides and their mechanisms of action. *Am J Cardiovasc Drugs.* 2007;7:173–89.
83. Hamlyn JM, Ringel R, Schaeffer J, Levinson PD, Hamilton BP, Kowarski AA, et al. A circulating inhibitor of (Na^+ - K^+) ATPase associated with essential hypertension. *Nature.* 1982;300:650–2.
84. Hamlyn JM, Lu ZR, Manunta P, Ludens JH, Kimura K, Shah JR, et al. Observations on the nature, biosynthesis, secretion and significance of endogenous ouabain. *Clin Exp Hypertens.* 1998;20:523–33.
85. Qazaz HM, Cao Z, Bolanowski DD, Clark BJ, Valdes Jr R. De novo biosynthesis and radiolabeling of mammalian digitalis-like factors. *Clin Chem.* 2004;50:612–20.
86. Lakatta EG, Vinogradova TM, Maltsev VA. The missing link in the mystery of normal automaticity of cardiac pacemaker cells. *Ann N Y Acad Sci.* 2008;1123:41–57.
87. Dhalla NS, Saini-Chohan HK, Rodriguez-Leyva D, Elimban V, Dent MR, Tappia PS. Subcellular remodelling may induce cardiac dysfunction in congestive heart failure. *Cardiovasc Res.* 2008;81(3):429–38.
88. Undrovinas A, Maltsev VA. Late sodium current is a new therapeutic target to improve contractility and rhythm in failing heart. *Cardiovasc Hematol Agents Med Chem.* 2008;6:348–59.
89. Sanguineti MC, Bennett PB. Antiarrhythmic drug target choices and screening. *Circ Res.* 2003;93:491–9.
90. Yang B, Lin H, Xiao J, Lu Y, Luo X, Li B, et al. The muscle-specific microRNA miR-1 regulates cardiac arrhythmogenic potential by targeting GJA1 and KCNJ2. *Nat Med.* 2007;13:486–91.

Chapter 19

Calmodulin Kinase II Regulation of Heart Rhythm and Disease

Thomas J. Hund

19.1 Introduction

Calmodulin kinase II (CaMKII) is a broadly expressed serine/threonine kinase that regulates critical cell functions including synaptic transmission in neurons, solute adsorption and secretion in the epithelium, and excitation–contraction coupling in cardiac myocytes [1]. Central to the multifunctional nature of CaMKII is its ability to detect elevations in intracellular Ca^{2+} . In heart, CaMKII coordinates the activities of a host of intracellular substrates to regulate Ca^{2+} homeostasis, cell excitability, and gene transcription. Over the past decade, CaMKII has emerged as an important determinant of the heart’s response to injury.

Up to 30 CaMKII isoforms are encoded by four genes (α , β , δ , γ) with CaMKII α and CaMKII β being expressed predominantly in neurons, and CaMKII δ and CaMKII γ showing a broader tissue distribution [2]. The main isoform in the heart is CaMKII δ [3]. In vitro studies have shown that each isoform has a unique dynamic response to Ca^{2+} /calmodulin [4]. This functional variability combined with the heteromultimeric nature of CaMKII allows for tissue specific tuning of CaMKII dynamic response to changes in Ca^{2+} . In neurons, CaMKII is highly enriched in postsynaptic densities, wherein it composes ~3% of total protein [5]. In vitro studies have shown that CaMKII is able to detect the frequency, amplitude, and duration of Ca^{2+} spikes in neurons [6], which allows the kinase to mediate the dependence of synaptic transmission on stimulus frequency (long-term potentiation) important for some forms of learning and memory [7].

CaMKII is a multimeric kinase composed of 12 monomers [4, 8]. Each kinase monomer has an *N*-terminal catalytic domain, autoregulatory domain, and *C*-terminal association domain (Fig. 19.1). In its inactive state, the autoregulatory subunit binds

T.J. Hund

Department of Internal Medicine, University of Iowa Carver College of Medicine, 285 Newton Rd. 2269 CBRB, Iowa City, IA 52242, USA
e-mail: thomas-hund@uiowa.edu

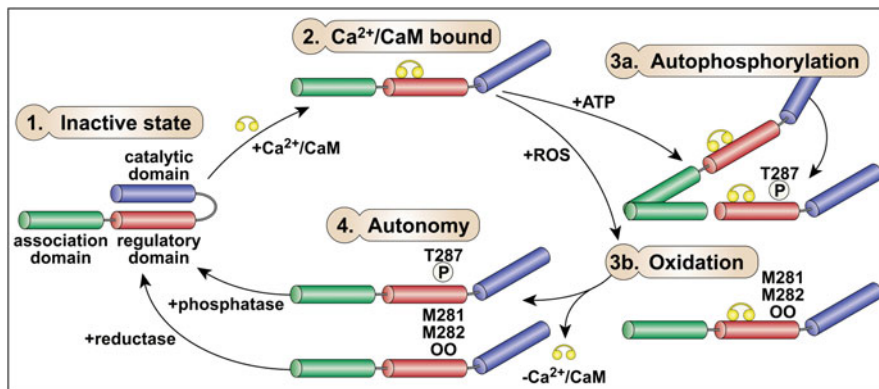


Fig. 19.1 Regulation of CaMKII activity by Ca²⁺/calmodulin, autophosphorylation, and oxidation. In its inactive form, the autoregulatory domain of CaMKII inhibits the catalytic domain. Binding of Ca²⁺/calmodulin displaces the autoregulatory domain resulting in an active kinase and exposing critical residues for autophosphorylation (T287) or oxidation (M281/282). Autophosphorylation at the exposed T287 site by a neighboring active subunit produces a maximally active subunit that retains activity even upon dissociation of Ca²⁺/calmodulin (autonomy). Similar autonomy is observed with oxidation at exposed M281 or M282. The kinase is tightly regulated by phosphatase and reductase activities

to and inhibits the kinase catalytic domain. Binding of Ca²⁺/calmodulin to the autoregulatory domain relieves auto-inhibition and exposes the catalytic subunit enabling the kinase to phosphorylate its substrates (Fig. 19.1). Among the many known CaMKII substrates is the kinase itself. A specific threonine residue in the autoregulatory domain (T286/287) that is exposed with binding of Ca²⁺/calmodulin may be phosphorylated by a neighboring active subunit (“autophosphorylation”) to produce a maximally active kinase [9, 10]. Autophosphorylation also increases the affinity of the kinase for calmodulin (“trapping”) and enables the kinase to remain active even upon the dissociation of Ca²⁺/calmodulin (“autonomy”) [11]. There is also a negative regulatory site (T306) in the regulatory domain that reduces CaMKII activity (“capping”) thereby providing negative feedback for control of enzyme activity [12]. Recently, a novel pathway for kinase activation was discovered involving oxidation at specific methionine residues (M281 and M282) in proximity to the autophosphorylation site in the autoregulatory domain [13]. Similar to autophosphorylation, binding of Ca²⁺/CaM exposes critical residues in the autoregulatory domain and therefore must precede the oxidation step [13]. Although an oxidized subunit retains activity once Ca²⁺/calmodulin dissociates, unlike autophosphorylation, oxidation does not alter the affinity for calmodulin. Analogous to regulation of autophosphorylation by local kinase/phosphatase activity and local concentrations of Ca²⁺/calmodulin, oxidative activation is likely controlled by a delicate balance of oxidase/reductase activity, mitochondrial function, and local calcium signaling.

19.2 CaMKII Subcellular Localization

CaMKII is preferentially localized to the cardiomyocyte Z-line where it colocalizes with L-type Ca^{2+} channels and type 2 ryanodine receptors (RyR2) [14, 15]. However, CaMKII regulates proteins at multiple subcellular domains, including the intercalated disc, t-tubules, mitochondria, and nucleus [16–20] (Fig. 19.2). Thus, localization of the kinase and local regulation by Ca^{2+} and phosphatase activities are critical determinants of downstream CaMKII effects. For example, while it is known that cAMP signaling in cardiomyocytes depends on subcellular compartmentalization maintained by A-kinase anchoring proteins (AKAPs) [21], an analogous family of anchoring proteins for CaMKII has not been identified. Rather, CaMKII targeting sequences appear to be embedded in target proteins themselves. For example, CaMKII directly binds to the β_{2a} subunit of L-type Ca^{2+} channels [22]. Furthermore, CaMKII regulation of L-type Ca^{2+} channels is mediated by phosphorylation of β_{2a} at Thr498. Thus, the β_{2a} subunit serves not only as a target

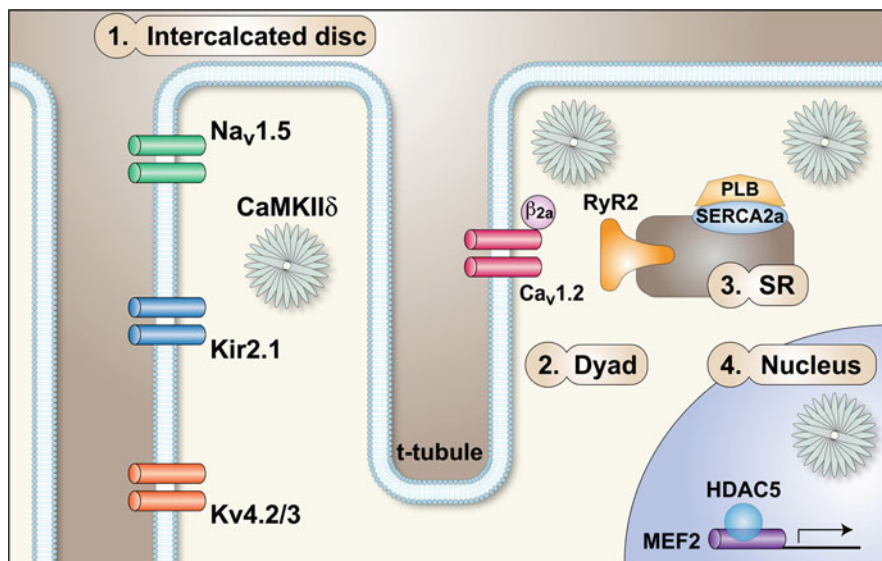


Fig. 19.2 CaMKII subcellular domains and key substrates. CaMKII targets many intracellular substrates localized to distinct subcellular domains. The cardiomyocyte intercalated disc is a specialized membrane domain important for maintaining mechanical integrity and electrical coupling between cells. CaMKII targets voltage-gated Na^+ channel, $\text{Na}_v1.5$ at the cardiomyocyte intercalated disc to regulate electrical propagation, as well as $\text{Kv}4.3$ (transient outward K^+ current, I_{to}) and Kir2.1 (inwardly rectifying K^+ current, $I_{\text{K}1}$) (also found at t-tubules). CaMKII regulates L-type Ca^{2+} channels (composed of $\text{Ca}_v1.2$, $\alpha 2\delta$ and β -subunits) and RyR2 SR Ca^{2+} release channels located in proximity in the cardiac dyadic space created by apposition of t-tubular and SR membranes. CaMKII regulates activity of the SR Ca^{2+} ATPase SERCA2a through direct phosphorylation of the associated inhibitory protein phospholamban (PLB). In the nucleus, CaMKII targets HDAC5, a repressor of MEF2, to regulate transcription of hypertrophic gene program

for CaMKII phosphorylation, but also as a CaMKII anchoring protein (CaMKAP) that exerts spatial control over CaMKII signaling. In neurons, CaMKII directly binds the NR2B subunit of the NMDA receptor forming a complex at postsynaptic densities to mediate long-term potentiation [23, 24]. Interestingly, both the β_{2a} and NR2B subunits contain CaMKII binding domains with high homology to a portion of the CaMKII association domain [22]. It will be important for future studies to address the mechanism for CaMKII targeting to its many other substrates.

19.3 CaMKII Regulation of Excitation–Contraction Coupling

Mechanical action of the heart depends on coordinated release of Ca^{2+} from intracellular stores. Calcium entry through sarcolemmal voltage-gated Ca^{2+} channels triggers Ca^{2+} release from RyR2 Ca^{2+} release channels located nearby ($\sim 10 \text{ nm}$) in the cisternal sarcoplasmic reticulum (SR) membrane. Close apposition of voltage-gated Ca^{2+} channels and RyR SR Ca^{2+} release channels creates a dyadic space that is important for local control of Ca^{2+} -induced Ca^{2+} release in ventricular myocytes. After Ca^{2+} release, some Ca^{2+} ions are extruded from the cell by the $\text{Na}^+/\text{Ca}^{2+}$ exchanger but most of them are sequestered back into the SR by the SR Ca^{2+} ATPase (SERCA2a). SR Ca^{2+} ATPase activity is tightly regulated by the SERCA2a associated protein, phospholamban (PLB). CaMKII regulates several key members involved in excitation–contraction coupling. CaMKII directly phosphorylates the $\text{Ca}_{v1.2}$ channel complex to produce an alternative channel gating mode characterized by long open times (mode 2) and current facilitation [25]. CaMKII colocalizes with and phosphorylates RyR2 to regulate channel activity, although studies have produced conflicting data as to the functional effects (increased or decreased channel activity) [26–32]. In fact, CaMKII may regulate Ca^{2+} entry and Ca^{2+} release via phosphorylation of L-type Ca^{2+} channels: Ca^{2+} release via phosphorylation of RyR2 Ca^{2+} release channels, and Ca^{2+} reuptake via phosphorylation of SERCA2a and/or PLB. Furthermore, CaMKII is localized to the dyadic space through direct binding of α - and β -subunits of the L-type Ca^{2+} channel [22, 33]. Thus, CaMKII is uniquely positioned to simultaneously regulate several aspects of excitation–contraction coupling.

19.4 CaMKII Regulation of Cardiac Pacemaking and Conduction

The heartbeat begins as a spontaneous action potential generated from a central location in the sinoatrial node (SAN), a compact collection of specialized excitable cardiomyocytes in the right atrium [34]. The electrical signal then passes through the atria to the atrioventricular node and into the His-Purkinje system and then

rapidly through the ventricles. CaMKII is able to regulate heart rate and rhythm by affecting cell excitability at multiple loci in this electrical activation sequence.

SAN cells possess unique structural and electrophysiological properties that facilitate spontaneous cell membrane depolarization. In fact, SAN pacemaking results from the complex coordination at the level of the single cell of both depolarizing and repolarizing currents [34, 35]. Furthermore, the SAN has evolved an elaborate system for storing and cycling intracellular Ca^{2+} . SR Ca^{2+} load in SAN cells is comparable to that of ventricular myocytes [36]. Intracellular Ca^{2+} cycling is an important pathway through which SAN cells regulate spontaneous electrical activity [37]. Specifically, Ca^{2+} release hastens phase 4 depolarization of the SAN cell membrane by increasing depolarizing current via forward-mode $\text{Na}^+-\text{Ca}^{2+}$ exchange [38, 39].

CaMKII coordinates the activities of multiple sarcolemmal and SR proteins (Cav1.2, RyR2, and SERCA2a/PLB) to regulate Ca^{2+} cycling in SAN cells. Recent studies indicate that CaMKII mediates the fight-or-flight response of SAN activity and heart rate to β -adrenergic stimulation [36]. Specifically, transgenic mice expressing a peptide inhibitor of CaMKII (AC3-I) show a blunted response of heart rate to isoproterenol both in vivo and ex vivo [36]. Basal heart rate is unaffected in AC3-I mice or CaMKII δ -KO mice [40], suggesting that the role of CaMKII is restricted to the fight-or-flight response. However, AV node conduction is altered in AC3-I mice even under basal conditions [41].

In the ventricle, CaMKII regulates cell excitability and electrical conduction via phosphorylation of voltage-gated Na^+ channels ($\text{Na}_v1.5$) [18] [42–44]. Voltage-gated Na^+ channels (Na_v) generate the rapid upstroke of the cardiac action potential and are critical for normal electrical conduction through the heart. Na_v dysfunction caused by mutations in *SCN5A*, the gene encoding the primary cardiac Na_v α -subunit, $\text{Na}_v1.5$, have been associated with several life-threatening cardiac arrhythmia syndromes including type 3 long QT syndrome (LQT3), Brugada syndrome, and cardiac conduction disease, as well as dilated cardiomyopathy [45, 46]. Abnormalities in $\text{Na}_v1.5$ expression and function have also been identified in common forms of acquired heart disease (e.g., heart failure and myocardial infarction) [47] where slow conduction plays an important role in arrhythmia and sudden death [48–50]. CaMKII alters Na_v channel gating in a manner consistent with Na_v channel mutations that produce combined loss-of-function/gain-of-function phenotypes (e.g., 1795insD producing combined LQT/Brugada Syndrome) [18, 51]. Specifically, CaMKII overexpression has been shown to decrease channel availability and increase the persistent current in ventricular myocytes [18, 43, 44].

Several studies have identified a role for CaMKII in regulating the activities of K^+ currents important for maintaining the resting membrane potential and action potential repolarization. Transgenic mice expressing the CaMKII inhibitory peptide AC3-I show decreased action potential durations, and increased transient outward K^+ current, $I_{\text{to},\text{fast}}$ (encoded by Kv4.2/3), and inward rectifier K^+ current, I_{K1} . In contrast, transgenic mice overexpressing CaMKII show prolonged action potentials consistent with decreased $I_{\text{to},\text{fast}}$ and I_{K1} [19, 20]. The mechanism for CaMKII

regulation of these K^+ currents is unclear, but likely involves regulation of expression, trafficking, and/or inactivation of these channels [19, 20, 52].

19.5 CaMKII Role in Disease and Arrhythmias

Mounting experimental evidence demonstrates an important role for CaMKII in heart disease and arrhythmias (Fig. 19.3). Specifically, CaMKII overexpression occurs in human heart failure [53, 54] and transgenic mice overexpressing

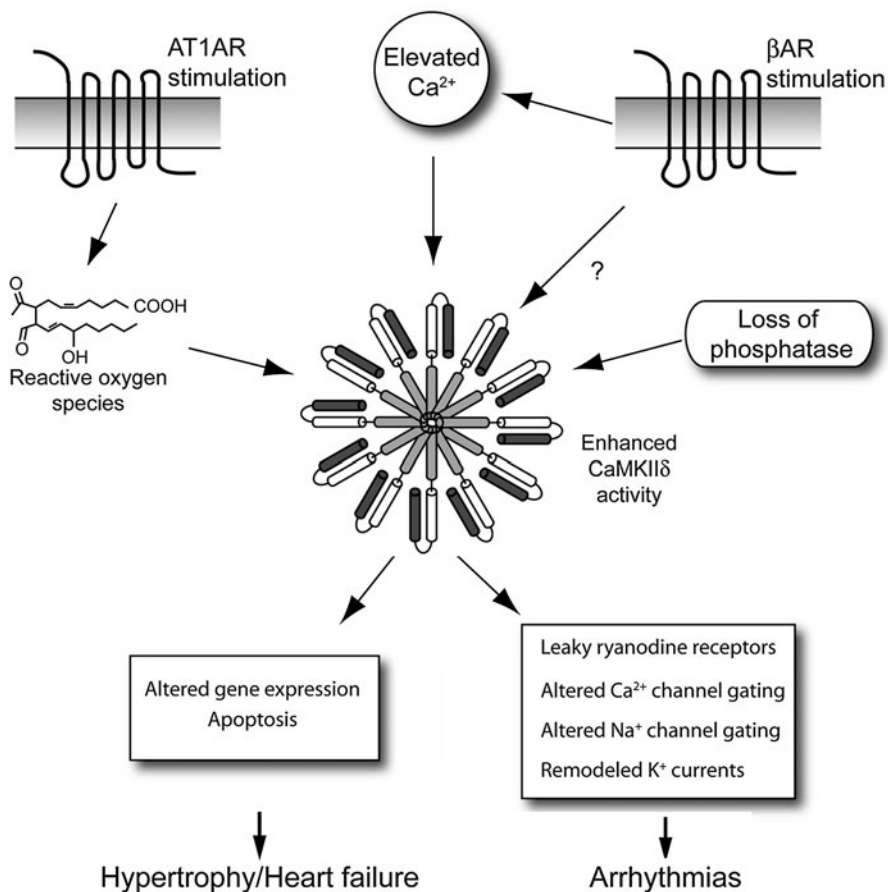


Fig. 19.3 CaMKII dysfunction in heart disease and arrhythmias. CaMKII is a potential mediator of multiple upstream pathological stimuli including oxidative stress, stimulation of β -adrenergic (β -AR) and angiotensin receptors (AT1AR), and decreased phosphatase activity. Excess CaMKII activity has been linked to hypertrophy and heart failure through alterations in gene transcription and/or apoptosis as well as arrhythmias through its effects on ion channels. Thus, CaMKII is ideally suited as a critical mediator of cardiac pathogenesis

CaMKII δ develop dilated cardiomyopathy [55, 56]. Increased CaMKII activity has been linked to Ca²⁺ leak from the SR, altered gene expression, and ventricular arrhythmias in a rabbit model of heart failure [57, 58]. Several studies have provided compelling evidence that CaMKII hyperphosphorylation of RyR2 in the setting of heart failure leads to inappropriately active channels that promote diastolic Ca²⁺ leak from the SR, reduced SR Ca²⁺ content and contractile dysfunction [55].

Cardiac hypertrophy is the heart's adaptive response to an increase in demand imposed by multiple stress stimuli [59]. At the level of the individual cell, the hypertrophic response involves the assembly of additional sarcomeres and/or loss of normal sarcomeric arrangement [59]. Importantly, hypertrophy is associated with the activation of alternative gene expression profiles [60]. While Ca²⁺ activates multiple signal transduction pathways that regulate expression of genes important for cardiac growth [60], it is clear that CaMKII is a critical regulator of this hypertrophic response [61–64]. CaMKII has been shown to regulate MEF2-dependent gene transcription via phosphorylation of HDAC5 [17, 58], NFAT-dependent transcription via calcineurin [65], and postnatal remodeling through regulation of splicing [66]. Moreover, deletion of CaMKII δ (CaMK2d $^{-/-}$) in mice has been shown to prevent the development of cardiac hypertrophy after 3 weeks of aortic constriction [64], while another study using a different CaMKII δ -deficient mouse showed that CaMKII δ deletion prevented the transition from hypertrophy to overt heart failure [40]. Several groups have identified a role for CaMKII in the development of heart failure [40, 53, 55, 56]. Thus, it is clear that CaMKII activation is an important step in the heart's hypertrophic response and/or progression of disease.

A role for CaMKII has also been implicated in remodeling (structural and electrical) and arrhythmias during myocardial ischemia and infarction [42, 67–72]. Calcium overload, β -adrenergic stimulation, acidosis, and oxidative stress are all possible upstream activators of CaMKII in ischemia and infarction [67, 68, 73]. The heart undergoes dramatic structural and electrical remodeling following myocardial infarction [74–76]. These changes not only help create a substrate favorable to the initiation of life-threatening arrhythmias, but also may promote progression of more advanced heart disease. At the cellular level, a dramatic remodeling of ion channels has been documented along with alterations in Ca²⁺ cycling and the action potential [74, 75]. Alterations in CaMKII activity and/or expression have been identified following myocardial infarction in several animal models of this disease [42, 67, 69–72]. Studies in a large animal model of arrhythmias following myocardial infarction have shown that the levels of both autophosphorylated and oxidized CaMKII are dramatically increased in a highly localized region (infarct border zone) corresponding to the location of reentrant arrhythmias [42, 69]. Recent studies indicate that CaMKII also plays a role in altered expression of inflammatory genes following myocardial infarction [70]. Consistent with a maladaptive role for CaMKII following myocardial infarction, transgenic mice expressing the CaMKII inhibitory peptide AC3-I show less structural remodeling and improved heart function following myocardial infarction compared with mice expressing the control peptide [67].

A specific role for CaMKII in promoting potentially lethal arrhythmias has been identified in several animal models of heart disease [77–81]. CaMKII inhibition prevents arrhythmias in transgenic mice models of hypertrophy and heart failure [77, 78, 81]. CaMKII has also been implicated in abnormal Ca^{2+} cycling and atrial arrhythmias in a transgenic model of atrial fibrillation (AF) [79] as well as in a dog model of congestive heart failure [80]. The mechanism for CaMKII-dependent arrhythmias is unclear, although CaMKII activity regulates intracellular Ca^{2+} cycling and ion channels involved in generation of the cardiac action potential (e.g., $\text{Ca}_v1.2$, $\text{K}_v4.3$, $\text{Na}_v1.5$), providing for a number of links between CaMKII activity and arrhythmia. One likely mechanism involves secondary depolarization of the action potential during the action potential repolarization phase or diastole (afterdepolarization) [82, 83]. CaMKII activity has been implicated in the formation of afterdepolarizations in response to H_2O_2 treatment [84], aging [85], as well as acquired and congenital arrhythmia syndromes [86, 87]. It is likely that CaMKII promotes afterdepolarizations, in part, by increasing mode 2 gating of the L-type Ca^{2+} channel [25, 88] characterized by long channel open times conducive to reactivation of the channel during action potential repolarization. CaMKII hyperphosphorylation of RyR2 channels in the cardiac SR [57, 79] may also play a role by increasing the likelihood of spontaneous Ca^{2+} release.

19.5.1 Pathways for Increased Calmodulin Kinase Activation in Disease

Calmodulin kinase is activated by both Ca^{2+} /calmodulin and reactive oxygen species, which are tightly regulated second messengers important for normal physiology of heart (Fig. 19.3). However, elevations in both intracellular Ca^{2+} and ROS levels have been linked to maladaptive remodeling and arrhythmias in heart disease (e.g., heart failure). Thus, CaMKII, with both Ca^{2+} - and ROS-dependent activation pathways, is ideally suited to regulate the heart's response to insult. Increased β -adrenergic stimulation, commonly observed following myocardial infarction and in heart failure, has been shown to activate the kinase both *in vitro* and *in vivo* through elevations in Ca^{2+} [67, 89, 90]. Importantly, CaMKII has been shown to mediate apoptosis in response to isoproterenol treatment *in vitro* and *in vivo* [16, 89, 91–93]. Neurohumoral agents such as angiotensin II play important roles in the progression of heart failure and have been shown to activate the kinase via oxidative stress [13, 91, 94]. It is also important to note that CaMKII regulation is the result of a delicate balance between kinase and phosphatase activities. Thus, dysfunction in kinase signaling may occur through increased kinase activity or decreased phosphatase activity [95, 96]. For example, reduced expression of the regulatory subunit of the serine/threonine protein phosphatase 2A, PP2A, has been shown to cause CaMKII-dependent hyperphosphorylation of RyR2 and afterdepolarizations in rat cardiomyocytes [97]. Since phosphatase levels are known to

change in heart disease, this may be a critical pathway for dysfunction in kinase signaling in disease. Furthermore, considering that changes in upstream CaMKII activators and phosphatases are associated with disease, it is likely that multiple pathways are involved in CaMKII dysregulation in disease.

19.6 Conclusions

Over the past decade, numerous studies have established a critical role for CaMKII in regulating the heart's response to injury. Central to this role is the activation of the kinase by intracellular second messengers Ca^{2+} /calmodulin and reactive oxygen species and its regulation of key proteins involved in Ca^{2+} cycling, gene transcription, and apoptosis. Thus, CaMKII is ideally suited to respond to multiple pathological stimuli and coordinate the activities of downstream effectors to alter cell function. CaMKII signaling pathway represents a logical and highly promising therapeutic target for treatment of heart disease and prevention of sudden death.

Acknowledgments This work was supported by the National Institutes of Health (HL096805 to TJH).

References

1. Braun AP, Schulman H. The multifunctional calcium/calmodulin-dependent protein kinase: from form to function. *Annu Rev Physiol.* 1995;57:417–45.
2. Tobimatsu T, Fujisawa H. Tissue-specific expression of four types of rat calmodulin-dependent protein kinase II mRNAs. *J Biol Chem.* 1989;264(30):17907–12.
3. Edman CF, Schulman H. Identification and characterization of δ_B -CaM kinase and δ_C -CaM kinase from rat heart, two new multifunctional Ca^{2+} /calmodulin-dependent protein kinase isoforms. *Biochim Biophys Acta.* 1994;1221(1):89–101.
4. Gaertner TR, Kolodziej SJ, Wang D, Kobayashi R, Koomen JM, Stoops JK, et al. Comparative analyses of the three-dimensional structures and enzymatic properties of α , β , γ and δ isoforms of Ca^{2+} -calmodulin-dependent protein kinase II. *J Biol Chem.* 2004;279(13):12484–94.
5. Schulman H. Activity-dependent regulation of calcium/calmodulin-dependent protein kinase II localization. *J Neurosci.* 2004;24(39):8399–403.
6. De Koninck P, Schulman H. Sensitivity of CaM kinase II to the frequency of Ca^{2+} oscillations. *Science.* 1998;279(5348):227–30.
7. Lisman J, Schulman H, Cline H. The molecular basis of CaMKII function in synaptic and behavioural memory. *Nat Rev Neurosci.* 2002;3(3):175–90.
8. Kolodziej SJ, Hudmon A, Waxham MN, Stoops JK. Three-dimensional reconstructions of calcium/calmodulin-dependent (CaM) kinase II α and truncated CaM kinase II α reveal a unique organization for its structural core and functional domains. *J Biol Chem.* 2000;275(19):14354–9.
9. Hanson PI, Meyer T, Stryer L, Schulman H. Dual role of calmodulin in autophosphorylation of multifunctional CaM kinase may underlie decoding of calcium signals. *Neuron.* 1994;12(5):943–56.

10. Kuret J, Schulman H. Mechanism of autophosphorylation of the multifunctional Ca^{2+} /calmodulin-dependent protein kinase. *J Biol Chem.* 1985;260(10):6427–33.
11. Meyer T, Hanson PI, Stryer L, Schulman H. Calmodulin trapping by calcium-calmodulin-dependent protein kinase. *Science.* 1992;256(5060):1199–202.
12. Colbran RJ. Inactivation of Ca^{2+} /calmodulin-dependent protein kinase II by basal autophosphorylation. *J Biol Chem.* 1993;268(10):7163–70.
13. Erickson JR, Joiner ML, Guan X, Kutschke W, Yang J, Oddis CV, et al. A dynamic pathway for calcium-independent activation of CaMKII by methionine oxidation. *Cell.* 2008;133(3):462–74.
14. O-Uchi J, Komukai K, Kusakari Y, Obata T, Hongo K, Sasaki H, et al. Alpha1-adrenoceptor stimulation potentiates L-type Ca^{2+} current through Ca^{2+} /calmodulin-dependent PK II (CaMKII) activation in rat ventricular myocytes. *Proc Natl Acad Sci USA.* 2005;102(26):9400–5.
15. Wu Y, MacMillan LB, McNeill RB, Colbran RJ, Anderson ME. CaM kinase augments cardiac L-type Ca^{2+} current: a cellular mechanism for long Q-T arrhythmias. *Am J Physiol Heart Circ Physiol.* 1999;276(6 Pt 2):H2168–78.
16. Timmins JM, Ozcan L, Seimon TA, Li G, Malagelada C, Backs J, et al. Calcium/calmodulin-dependent protein kinase II links ER stress with Fas and mitochondrial apoptosis pathways. *J Clin Invest.* 2009;119(10):2925–41.
17. Wu X, Zhang T, Bossuyt J, Li X, McKinsey TA, Dedman JR, et al. Local InsP₃-dependent perinuclear Ca^{2+} signaling in cardiac myocyte excitation–transcription coupling. *J Clin Invest.* 2006;116(3):675–82.
18. Wagner S, Dybkova N, Rasenack EC, Jacobshagen C, Fabritz L, Kirchhof P, et al. Ca/calmodulin-dependent protein kinase II regulates cardiac Na channels. *J Clin Invest.* 2006;116(12):3127–38.
19. Li J, Marionneau C, Zhang R, Shah V, Hell JW, Nerbonne JM, et al. Calmodulin kinase II inhibition shortens action potential duration by upregulation of K^+ currents. *Circ Res.* 2006;99(10):1092–9.
20. Wagner S, Hacker E, Grandi E, Weber SL, Dybkova N, Sossalla S, et al. Ca/calmodulin kinase II differentially modulates potassium currents. *Circ Arrhythm Electrophysiol.* 2009;2(3):285–94.
21. McConnachie G, Langeberg LK, Scott JD. AKAP signaling complexes: getting to the heart of the matter. *Trends Mol Med.* 2006;12(7):317–23.
22. Grueter CE, Abiria SA, Dzhura I, Wu Y, Ham AJ, Mohler PJ, et al. L-type Ca^{2+} channel facilitation mediated by phosphorylation of the beta subunit by CaMKII. *Mol Cell.* 2006;23(5):641–50.
23. Bayer KU, De Koninck P, Leonard AS, Hell JW, Schulman H. Interaction with the NMDA receptor locks CaMKII in an active conformation. *Nature.* 2001;411(6839):801–5.
24. Strack S, Colbran RJ. Autophosphorylation-dependent targeting of calcium/ calmodulin-dependent protein kinase II by the NR2B subunit of the N-methyl-D-aspartate receptor. *J Biol Chem.* 1998;273(33):20689–92.
25. Dzhura I, Wu Y, Colbran RJ, Balser JR, Anderson ME. Calmodulin kinase determines calcium-dependent facilitation of L-type calcium channels. *Nat Cell Biol.* 2000;2(3):173–7.
26. Wehrens XH, Lehnart SE, Reiken SR, Marks AR. Ca^{2+} /calmodulin-dependent protein kinase II phosphorylation regulates the cardiac ryanodine receptor. *Circ Res.* 2004;94(6):e61–70.
27. Witcher DR, Kovacs RJ, Schulman H, Cefali DC, Jones LR. Unique phosphorylation site on the cardiac ryanodine receptor regulates calcium channel activity. *J Biol Chem.* 1991;266(17):11144–52.
28. Yang D, Zhu WZ, Xiao B, Brochet DX, Chen SR, Lakatta EG, et al. Ca^{2+} /calmodulin kinase II-dependent phosphorylation of ryanodine receptors suppresses Ca^{2+} sparks and Ca^{2+} waves in cardiac myocytes. *Circ Res.* 2007;100(3):399–407.
29. Hain J, Onoue H, Mayrleitner M, Fleischer S, Schindler H. Phosphorylation modulates the function of the calcium release channel of sarcoplasmic reticulum from cardiac muscle. *J Biol Chem.* 1995;270(5):2074–81.

30. Kohlhaas M, Zhang T, Seidler T, Zibrova D, Dybkova N, Steen A, et al. Increased sarcoplasmic reticulum calcium leak but unaltered contractility by acute CaMKII overexpression in isolated rabbit cardiac myocytes. *Circ Res.* 2006;98(2):235–44.
31. Maier LS, Zhang T, Chen L, DeSantiago J, Brown JH, Bers DM. Transgenic CaMKIIC overexpression uniquely alters cardiac myocyte Ca^{2+} handling: reduced SR Ca^{2+} load and activated SR Ca^{2+} release. *Circ Res.* 2003;92(8):904–11.
32. Wu Y, Colbran RJ, Anderson ME. Calmodulin kinase is a molecular switch for cardiac excitation–contraction coupling. *Proc Natl Acad Sci USA.* 2001;98(5):2877–81.
33. Hudmon A, Schulman H, Kim J, Maltez JM, Tsien RW, Pitt GS. CaMKII tethers to L-type Ca^{2+} channels, establishing a local and dedicated integrator of Ca^{2+} signals for facilitation. *J Cell Biol.* 2005;171(3):537–47.
34. Dobrzynski H, Boyett MR, Anderson RH. New insights into pacemaker activity: promoting understanding of sick sinus syndrome. *Circulation.* 2007;115(14):1921–32.
35. Mangoni ME, Nargeot J. Genesis and regulation of the heart automaticity. *Physiol Rev.* 2008;88(3):919–82.
36. Wu Y, Gao Z, Chen B, Koval OM, Singh MV, Guan X, et al. Calmodulin kinase II is required for fight or flight sinoatrial node physiology. *Proc Natl Acad Sci USA.* 2009;106(14):5972–7.
37. Eisner DA, Cerbai E. Beating to time: calcium clocks, voltage clocks, and cardiac pacemaker activity. *Am J Physiol Heart Circ Physiol.* 2009;296(3):H561–2.
38. Bogdanov KY, Vinogradova TM, Lakatta EG. Sinoatrial nodal cell ryanodine receptor and $\text{Na}^+–\text{Ca}^{2+}$ exchanger: molecular partners in pacemaker regulation. *Circ Res.* 2001;88(12):1254–8.
39. Huser J, Blatter LA, Lipsius SL. Intracellular Ca^{2+} release contributes to automaticity in cat atrial pacemaker cells. *J Physiol.* 2000;524(Pt 2):415–22.
40. Ling H, Zhang T, Pereira L, Means CK, Cheng H, Gu Y, et al. Requirement for $\text{Ca}^{2+}/$ calmodulin-dependent kinase II in the transition from pressure overload-induced cardiac hypertrophy to heart failure in mice. *J Clin Invest.* 2009;119(5):1230–40.
41. Khoo M, Kannankeril P, Li J, Zhang R, Kupershmidt S, Zhang W, et al. Calmodulin kinase activity is required for normal atrioventricular nodal conduction. *Heart Rhythm.* 2005;2:634–40.
42. Christensen MD, Dun W, Boyden PA, Anderson ME, Mohler PJ, Hund TJ. Oxidized calmodulin kinase II regulates conduction following myocardial infarction: a computational analysis. *PLoS Comput Biol.* 2009;5(12):e1000583.
43. Aiba T, Hesketh GG, Liu T, Carlisle R, Villa-Abrille MC, O'Rourke B, et al. Na^+ channel regulation by Ca^{2+} /calmodulin and Ca^{2+} /calmodulin-dependent protein kinase II in guinea-pig ventricular myocytes. *Cardiovasc Res.* 2009;85:454–63.
44. Maltsev VA, Reznikov V, Undrovinas NA, Sabbah HN, Undrovinas A. Modulation of late sodium current by Ca^{2+} , calmodulin, and CaMKII in normal and failing dog cardiomyocytes: similarities and differences. *Am J Physiol Heart Circ Physiol.* 2008;294(4):H1597–608.
45. Lehnart SE, Ackerman MJ, Benson Jr DW, Brugada R, Clancy CE, Donahue JK, et al. Inherited arrhythmias: a National Heart, Lung, and Blood Institute and Office of Rare Diseases workshop consensus report about the diagnosis, phenotyping, molecular mechanisms, and therapeutic approaches for primary cardiomyopathies of gene mutations affecting ion channel function. *Circulation.* 2007;116(20):2325–45.
46. Remme CA, Wilde AA, Bezzina CR. Cardiac sodium channel overlap syndromes: different faces of SCN5A mutations. *Trends Cardiovasc Med.* 2008;18(3):78–87.
47. Nattel S, Maguy A, Le Bouter S, Yeh YH. Arrhythmogenic ion-channel remodeling in the heart: heart failure, myocardial infarction, and atrial fibrillation. *Physiol Rev.* 2007;87(2):425–56.
48. Saumarez RC, Chojnowska L, Derkens R, Pytkowski M, Sterlinski M, Huang CL, et al. Sudden death in noncoronary heart disease is associated with delayed paced ventricular activation. *Circulation.* 2003;107(20):2595–600.
49. Wang Y, Cheng J, Joyner RW, Wagner MB, Hill JA. Remodeling of early-phase repolarization: a mechanism of abnormal impulse conduction in heart failure. *Circulation.* 2006;113(15):1849–56.

50. Janse MJ, Wit AL. Electrophysiological mechanisms of ventricular arrhythmias resulting from myocardial ischemia and infarction. *Physiol Rev.* 1989;69(4):1049–169.
51. Grandi E, Puglisi JL, Wagner S, Maier LS, Severi S, Bers DM. Simulation of Ca-calmodulin-dependent protein kinase II on rabbit ventricular myocyte ion currents and action potentials. *Biophys J.* 2007;93(11):3835–47.
52. El-Haou S, Balse E, Neyroud N, Dilanian G, Gavillet B, Abriel H, et al. Kv4 potassium channels form a tripartite complex with the anchoring protein SAP97 and CaMKII in cardiac myocytes. *Circ Res.* 2009;104(6):758–69.
53. Hoch B, Meyer R, Hetzer R, Krause EG, Karczewski P. Identification and expression of delta-isoforms of the multifunctional Ca^{2+} /calmodulin-dependent protein kinase in failing and nonfailing human myocardium. *Circ Res.* 1999;84(6):713–21.
54. Kirchhefer U, Schmitz W, Scholz H, Neumann J. Activity of cAMP-dependent protein kinase and Ca^{2+} /calmodulin-dependent protein kinase in failing and nonfailing human hearts. *Cardiovasc Res.* 1999;42(1):254–61.
55. Zhang T, Maier LS, Dalton ND, Miyamoto S, Ross Jr J, Bers DM, et al. The delta_C isoform of CaMKII is activated in cardiac hypertrophy and induces dilated cardiomyopathy and heart failure. *Circ Res.* 2003;92:912–9.
56. Zhang T, Johnson EN, Gu Y, Morissette MR, Sah VP, Gigena MS, et al. The cardiac-specific nuclear δ_B isoform of Ca^{2+} /calmodulin-dependent protein kinase II induces hypertrophy and dilated cardiomyopathy associated with increased protein phosphatase 2A activity. *J Biol Chem.* 2002;277(2):1261–7.
57. Ai X, Curran JW, Shannon TR, Bers DM, Pogwizd SM. Ca^{2+} /calmodulin-dependent protein kinase modulates cardiac ryanodine receptor phosphorylation and sarcoplasmic reticulum Ca^{2+} leak in heart failure. *Circ Res.* 2005;97(12):1314–22.
58. Bossuyt J, Helmstadter K, Wu X, Clements-Jewery H, Haworth RS, Avkiran M, et al. Ca^{2+} /calmodulin-dependent protein kinase II δ and protein kinase D overexpression reinforce the histone deacetylase 5 redistribution in heart failure. *Circ Res.* 2008;102(6):695–702.
59. Hunter JJ, Chien KR. Signaling pathways for cardiac hypertrophy and failure. *N Engl J Med.* 1999;341(17):1276–83.
60. Frey N, McKinsey TA, Olson EN. Decoding calcium signals involved in cardiac growth and function. *Nat Med.* 2000;6(11):1221–7.
61. Ramirez MT, Zhao XL, Schulman H, Brown JH. The nuclear δ_B isoform of Ca^{2+} /calmodulin-dependent protein kinase II regulates atrial natriuretic factor gene expression in ventricular myocytes. *J Biol Chem.* 1997;272(49):31203–8.
62. Zhu W, Zou Y, Shiojima I, Kudoh S, Aikawa R, Hayashi D, et al. Ca^{2+} /calmodulin-dependent kinase II and calcineurin play critical roles in endothelin-1-induced cardiomyocyte hypertrophy. *J Biol Chem.* 2000;275(20):15239–45.
63. Zhang T, Brown JH. Role of Ca^{2+} /calmodulin-dependent protein kinase II in cardiac hypertrophy and heart failure. *Cardiovasc Res.* 2004;63(3):476–86.
64. Backs J, Backs T, Neef S, Kreusser MM, Lehmann LH, Patrick DM, et al. The delta isoform of CaM kinase II is required for pathological cardiac hypertrophy and remodeling after pressure overload. *Proc Natl Acad Sci U S A.* 2009;106(7):2342–7.
65. MacDonnell SM, Weisser-Thomas J, Kubo H, Hanscome M, Liu Q, Jaleel N, et al. CaMKII negatively regulates calcineurin-NFAT signaling in cardiac myocytes. *Circ Res.* 2009;105(4):316–25.
66. Xu X, Yang D, Ding JH, Wang W, Chu PH, Dalton ND, et al. ASF/SF2-regulated CaMKII delta alternative splicing temporally reprograms excitation–contraction coupling in cardiac muscle. *Cell.* 2005;120(1):59–72.
67. Zhang R, Khoo MS, Wu Y, Yang Y, Grueter CE, Ni G, et al. Calmodulin kinase II inhibition protects against structural heart disease. *Nat Med.* 2005;11:409–17.
68. Said M, Becerra R, Palomeque J, Rinaldi G, Kaetzel MA, Diaz-Sylvester PL, et al. Increased intracellular Ca^{2+} and SR Ca^{2+} load contribute to arrhythmias after acidosis in rat heart. Role of Ca^{2+} /calmodulin-dependent protein kinase II. *Am J Physiol Heart Circ Physiol.* 2008;295(4):H1669–83.

69. Hund TJ, Decker KF, Kanter E, Mohler PJ, Boyden PA, Schuessler RB, et al. Role of activated CaMKII in abnormal calcium homeostasis and I_{Na} remodeling after myocardial infarction: insights from mathematical modeling. *J Mol Cell Cardiol.* 2008;45:420–8.
70. Singh MV, Kapoun A, Higgins L, Kutschke W, Thurman JM, Zhang R, et al. Ca^{2+} /calmodulin-dependent kinase II triggers cell membrane injury by inducing complement factor B gene expression in the mouse heart. *J Clin Invest.* 2009;119(4):986–96.
71. Netticadan T, Temsah RM, Kawabata K, Dhalla NS. Sarcoplasmic reticulum Ca^{2+} /calmodulin-dependent protein kinase is altered in heart failure. *Circ Res.* 2000;86(5):596–605.
72. Currie S, Smith GL. Calcium/calmodulin-dependent protein kinase II activity is increased in sarcoplasmic reticulum from coronary artery ligated rabbit hearts. *FEBS Lett.* 1999;459(2):244–8.
73. Kinugawa S, Tsutsui H, Hayashidani S, Ide T, Suematsu N, Satoh S, et al. Treatment with dimethylthiourea prevents left ventricular remodeling and failure after experimental myocardial infarction in mice: role of oxidative stress. *Circ Res.* 2000;87(5):392–8.
74. Pinto JM, Boyden PA. Electrical remodeling in ischemia and infarction. *Cardiovasc Res.* 1999;42(2):284–97.
75. Ursell PC, Gardner PI, Albala A, Fenoglio Jr JJ, Wit AL. Structural and electrophysiological changes in the epicardial border zone of canine myocardial infarcts during infarct healing. *Circ Res.* 1985;56(3):436–51.
76. Wit AL, Janse MJ. The ventricular arrhythmias of ischemia and infarction: electrophysiological mechanisms. Mount Kisco, NY: Futura Publishing Company, Inc; 1992.
77. Wu Y, Temple J, Zhang R, Dzhura I, Zhang W, Trimble R, et al. Calmodulin kinase II and arrhythmias in a mouse model of cardiac hypertrophy. *Circulation.* 2002;106(10):1288–93.
78. Khoo MS, Li J, Singh MV, Yang Y, Kannankeril P, Wu Y, et al. Death, cardiac dysfunction, and arrhythmias are increased by calmodulin kinase II in calcineurin cardiomyopathy. *Circulation.* 2006;114(13):1352–9.
79. Chelu MG, Sarma S, Sood S, Wang S, van Oort RJ, Skapura DG, et al. Calmodulin kinase II-mediated sarcoplasmic reticulum Ca^{2+} leak promotes atrial fibrillation in mice. *J Clin Invest.* 2009;119(7):1940–51.
80. Yeh YH, Wakili R, Qi XY, Chartier D, Boknik P, Kaab S, et al. Calcium-handling abnormalities underlying atrial arrhythmogenesis and contractile dysfunction in dogs with congestive heart failure. *Circ Arrhythm Electrophysiol.* 2008;1(2):93–102.
81. Sag CM, Wadsack DP, Khabbazzadeh S, Abesser M, Grefe C, Neumann K, et al. Calcium/calmodulin-dependent protein kinase II contributes to cardiac arrhythmogenesis in heart failure. *Circ Heart Fail.* 2009;2(6):664–75.
82. Anderson ME, Braun AP, Wu Y, Lu T, Schulman H, Sung RJ. KN-93, an inhibitor of multifunctional Ca^{2+} /calmodulin-dependent protein kinase, decreases early afterdepolarizations in rabbit heart. *J Pharmacol Exp Ther.* 1998;287(3):996–1006.
83. Wu Y, Roden DM, Anderson ME. Calmodulin kinase inhibition prevents development of the arrhythmogenic transient inward current. *Circ Res.* 1999;84(8):906–12.
84. Xie LH, Chen F, Karagueuzian HS, Weiss JN. Oxidative-stress-induced afterdepolarizations and calmodulin kinase II signaling. *Circ Res.* 2009;104(1):79–86.
85. Morita N, Sovari AA, Xie Y, Fishbein MC, Mandel WJ, Garfinkel A, et al. Increased susceptibility of aged hearts to ventricular fibrillation during oxidative stress. *Am J Physiol Heart Circ Physiol.* 2009;297:H1594–605.
86. Thiel WH, Chen B, Hund TJ, Koval OM, Purohit A, Song LS, et al. Proarrhythmic defects in Timothy syndrome require calmodulin kinase II. *Circulation.* 2008;118(22):2225–34.
87. Qi X, Yeh YH, Chartier D, Xiao L, Tsuji Y, Brundel BJ, et al. The calcium/calmodulin/kinase system and arrhythmogenic afterdepolarizations in bradycardia-related acquired long-QT syndrome. *Circ Arrhythm Electrophysiol.* 2009;2(3):295–304.
88. Tanskanen AJ, Greenstein JL, O'Rourke B, Winslow RL. The role of stochastic and modal gating of cardiac L-type Ca^{2+} channels on early after-depolarizations. *Biophys J.* 2005;88(1):85–95.

89. Zhu WZ, Wang SQ, Chakir K, Yang D, Zhang T, Brown JH, et al. Linkage of β 1-adrenergic stimulation to apoptotic heart cell death through protein kinase A-independent activation of Ca^{2+} /calmodulin kinase II. *J Clin Invest.* 2003;111(5):617–25.
90. Wang W, Zhu W, Wang S, Yang D, Crow MT, Xiao RP, et al. Sustained betal-adrenergic stimulation modulates cardiac contractility by Ca^{2+} /calmodulin kinase signaling pathway. *Circ Res.* 2004;95(8):798–806.
91. Zhu W, Woo AY, Yang D, Cheng H, Crow MT, Xiao RP. Activation of CaMKII-delta C is a common intermediate of diverse death stimuli-induced heart muscle cell apoptosis. *J Biol Chem.* 2007;282(14):10833–9.
92. Yang Y, Zhu WZ, Joiner ML, Zhang R, Oddis CV, Hou Y, et al. Calmodulin kinase II inhibition protects against myocardial cell apoptosis in vivo. *Am J Physiol Heart Circ Physiol.* 2006;291(6):H3065–75.
93. Little GH, Saw A, Bai Y, Dow J, Marjoram P, Simkovich B, et al. Critical role of nuclear calcium/calmodulin-dependent protein kinase II δ B in cardiomyocyte survival in cardiomyopathy. *J Biol Chem.* 2009;284(37):24857–68.
94. Howe CJ, Lahair MM, McCubrey JA, Franklin RA. Redox regulation of the calcium/calmodulin-dependent protein kinases. *J Biol Chem.* 2004;279(43):44573–81.
95. Saucerman JJ, Bers DM. Calmodulin mediates differential sensitivity of CaMKII and calcineurin to local Ca^{2+} in cardiac myocytes. *Biophys J.* 2008;95(10):4597–612.
96. Chiba H, Schneider NS, Matsuoka S, Noma A. A simulation study on the activation of cardiac CaMKII delta-isoform and its regulation by phosphatases. *Biophys J.* 2008;95(5):2139–49.
97. Terentyev D, Belevych AE, Terentyeva R, Martin MM, Malana GE, Kuhn DE, et al. miR-1 overexpression enhances Ca^{2+} release and promotes cardiac arrhythmogenesis by targeting PP2A regulatory subunit B56alpha and causing CaMKII-dependent hyperphosphorylation of RyR2. *Circ Res.* 2009;104(4):514–21.

Chapter 20

MicroRNA and Pluripotent Stem Cell-Based Heart Therapies: The Electrophysiological Perspective

Ellen Poon, Deborah K. Lieu, and Ronald A. Li

20.1 Introduction

Cardiomyocytes (CMs) originate from the mesodermal germ layer. During the course of gastrulation, cardiac progenitors migrate through the node region and primitive streak to form the cardiac crescent [1–3]. At this stage, CMs become specified, along with the expression of various cardiac transcription factors (reviewed in [4]). Fetal CMs continue to proliferate until they terminally exit the cell cycle a few days after birth; further growth is accomplished via physiological hypertrophy by increasing the size rather than the number of CMs [5, 6]. Subsequent development of CMs also involves the structural and functional maturation of their electrophysiological, Ca^{2+} -handling, and contractile properties. Taken collectively, the formation of the adult heart is a complex developmental event, which involves the orchestrated interplay of numerous biological factors and processes.

E. Poon

Stem Cell and Regenerative Medicine Consortium, University of Hong Kong, Hong Kong, China

D.K. Lieu

Center of Cardiovascular Research, Mount Sinai School of Medicine, Atran Berg Laboratory Building Floor 3 Room 3-22, 1428 Madison Avenue, New York, NY 10029, USA

R.A. Li (✉)

Stem Cell and Regenerative Medicine Consortium, University of Hong Kong, Hong Kong, China
and

Heart, Brain, Hormone and Healthy Ageing Research Center, University of Hong Kong, Hong Kong, China
and

Departments of Medicine and Physiology, University of Hong Kong, Hong Kong, China
and

Center of Cardiovascular Research, Mount Sinai School of Medicine, Atran Berg Laboratory Building Floor 3 Room 3-22, 1428 Madison Avenue, New York, NY 10029, USA
e-mail: ronald.li@mssm.edu

20.2 MicroRNAs as Negative Transcriptional Regulators

MicroRNAs (miRs) are nonencoding RNAs of ~22 nucleotides that function as negative transcriptional regulators via degradation or inhibition by RNA interference [7, 8]. They have been suggested to regulate ~30% of human genes [9]. To date, 706 human miRs have been identified, of which approximately 50% of pre-miR sequences are located within introns, according to the Sanger Database. Figure 20.1 summarizes the biogenesis of miRs. MiRs are transcribed by RNA polymerase II or III in the nucleus to form primary miR (pri-miR) transcripts and are capped and polyadenylated [10, 11]. The miR encoding portion of the pri-miR forms a hairpin structure that is recognized and cleaved in the nucleus by a microprocessing complex. This complex consists of the double-stranded RNA-specific nuclease, Drosha, and its cofactor, DiGeorge syndrome critical region 8 (DGCR8), also known as Pasha [12]. Pre-miR is transported by RanGTP and exportin 5 into the cytoplasm [13], where it is processed by RNase III enzyme Dicer to generate a transient 18–24 nucleotide duplex. The duplex is loaded into the miR-associated miRISC (multiprotein RNA-induced silencing complex) [14]. One strand of the miR is preferentially retained in this complex and becomes the mature miR; the opposite strand, known as the passenger strand or miR*, is removed. In addition to this pathway for miR biogenesis, some intronic miR precursors can

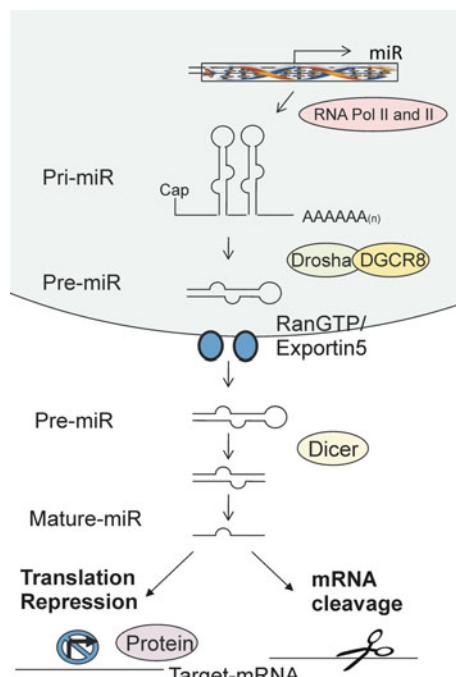


Fig. 20.1 Schematic of miR biogenesis

bypass Drosha processing to produce miRs [15, 16]. For biological action, a mature miR binds to the complementary site(s) in the mRNA target to negatively regulate gene expression via translational silencing or by inducing mRNA cleavage [17–19].

20.3 Role of miR in Heart Development

The expression of miRs is highly regulated and dependent on tissue, cell type, metabolic status and diseases states. In coronary arterial smooth muscle cells, the most abundantly expressed miRs are miR-145, let-7, miR-125b, miR-125a, miR-23, and miR-143, although miR-1 and miR-133 are also expressed in coronary arterial smooth muscles [20]. Other miRs, such as the let-7 family, miR-126, miR-221, and miR-222, are highly expressed in human endothelial cells [21]. In the heart, some of the most abundant miRs include miR-1, let-7, miR-133, miR-126-3p, miR-30c, and miR-26a [22]. In particular, miR-1, miR-133 [23], and miR-208 are specific to cardiac and skeletal muscles.

Functionally, in transgenic mouse models, the biogenesis of miR has been demonstrated to be essential for cardiogenesis and cardiac development. Targeted deletion of Dicer, the miR processing enzyme, in heart leads to rapidly progressive dilated cardiomyopathy, heart failure, and postnatal lethality [24]. Similarly, CM-specific deletion of DGCR8, a gene required for miR biogenesis, reveals a fully penetrant phenotype that begins with left ventricular (LV) malfunction progressing to a dilated cardiomyopathy and premature lethality. This indicates the global requirement of miRs in the mouse heart [25]. Gain- and loss-of-function experiments further show that individual miRs can regulate many aspects of cardiovascular development via the inhibition of a large number of target genes. For instance, miR-1, -18b, -20b, -21, -106a, -126, -133, -138, and -208 have been implicated in normal cardiovascular development [26–31]. Several specific miRs are further discussed below. Various recent profiling efforts have revealed profound alterations of miR expression in the pathogenesis of human heart failure [32–34]. Despite the knowledge gained from these studies, the functional roles of miRs in human cardiogenesis remain elusive because of the paucity of cause-and-effect data in human heart cells. Given the significant species differences (e.g., miRs that regulate pluripotency genes were discovered in mouse but four of five have no known human homologs) [35], further studies of miRs in human heart cells are warranted.

20.3.1 MiR-1

The miR-1 family consists of the miR-1 subfamily and miR-206 [36]. The mature forms of miR-1-1 and miR-1-2 have identical sequence but are encoded by distinct genes located on chromosomes 2 and 18, respectively. Targeted deletion of miR-1-2 in mice leads to embryonic death attributable to ventricular septal defects and cardiac

dysfunction [30]. By contrast, transgenic overexpression of miR-1 results in developmental arrest at E13.5, secondary to thin-walled ventricles and heart failure [31]. This lethality is attributed to premature differentiation and early withdrawal of myocytes from the cell cycle. Interestingly, miR-1 over-expression in adult murine ventricular CMs (VCM) promotes arrhythmogenesis by slowing conduction and depolarizing the sarcolemmal membrane via post-transcriptional repression of the Kir2.1-encoded inwardly rectifying current (I_{K1}) and connexin (Cx) 43-mediated gap junction [37]. In hypertrophic adult rat VCMs, down-regulation of miR-1/miR-133 levels promotes automaticity via up-regulation of HCN2/HCN4, but this defect can be reversed by forced expression of miR-1/miR-133 [23, 38]. Collectively, these results suggest that the effects of miR-1 are context- as well as dose-dependent. Mechanistically, the phenotype from the gain and loss of miR-1 is likely related to the dysregulation of Hand2. Hand2 is a cardiac transcription factor whose precise dosage is critical for normal cardiac development and morphogenesis [39–41]. Hand2 null embryos display right ventricular hypoplasia and vascular abnormalities, causing severe growth retardation by E9.5 and death by E10.5 [42]. Bioinformatic analyses and in vitro assay show that Hand2 is a direct target of miR-1 repression [31].

MiR-1 null adult mice show an increased heart-to-body weight ratio due to hyperplasia [30]. This is associated with an increase in the number of mitotic nuclei at P10 and karyokinesis that persist into adulthood. Conversely, miR-1 overexpression leads to early withdrawal of myocytes from the cell cycle [31]. These experiments are suggestive of a negative regulatory role of miR-1 in the cell cycle of CMs.

Additionally, miR-1 plays a prominent role in the apoptosis of CMs. In response to oxidative stress and high glucose, the miR-1 level in rat VMCs increases significantly [43–45]. Overexpression of miR-1 facilitates apoptosis in CMs under normal culture conditions and when induced by H_2O_2 . In stark contrast, miR-1 inhibition confers resistance to H_2O_2 [44]. Anti-apoptotic members of the mitochondrial death pathway, including Bcl-2, heat shock protein (HSP) 60, and HSP 70 were identified as targets of miR-1 repression [44, 45]. MiR-1 may also reduce the expression of prosurvival proteins.

20.3.2 *MiR-133*

The miR-133 family comprises miR-133a-1, miR-133a-2, and miR-133b and is expressed from bicistronic units together with the miR-1 subfamily [46, 47]. MiR-133a-1 and miR-133a-2 share identical mature sequences, with miR-133b differing by a single nucleotide at the 3' end [36, 47]. Similar to miR-1, miR-133 has been shown to regulate many aspects of cardiac biology (reviewed in [46]). Both miR-1 and miR-133 levels are decreased in cardiac hypertrophy models [23]. The same pattern has been observed in human patients. Adenovirus-mediated overexpression of miR-133 in neonatal and adult CMs inhibits such hallmark parameters of hypertrophy as increased cell size, enhanced protein synthesis, up-regulation of

fetal genes, acto-myosin chain rearrangement, and subsequent cytoskeletal reorganization as well as perinuclear localization of atrial natriuretic factor protein [23]. By contrast, suppression of miR-133 exerts the opposite effect. Antagomir-induced inhibition of miR-133 by 70% leads to increased diastolic LV posterior wall and diastolic interventricular septum thickness, LV mass index, and the LV weight to body weight ratio, indicating hypertrophy. RhoA, Cdc42, and Whsc2 (human gene: NELFA) have been identified as direct targets of miR-133. RhoA and Cdc42 are members of the Rho subfamily of small GTP-binding proteins and are associated with cytoskeletal and myofibrillar rearrangements during hypertrophy [48, 49]. NELF-A/Whsc2, a negative regulator of RNA polymerase II, is linked to Wolf-Hirschhorn syndrome, which is characterized by cardiac dysgenesis as well as several other abnormalities [50]. Taken collectively, dysregulation of miR-133 appears to play a role in the establishment and progression of hypertrophy. Modulation of miR-133 expression may lead to effective therapies for hypertrophy.

MiR-133 has also been demonstrated to function as a negative regulator of the mitochondrial apoptosis pathway via the repression of caspase-9 [45]. Caspase-9, a critical regulator of mitochondria-mediated apoptosis, forms a multimeric complex with cytochrome c and Apaf-1 to activate downstream caspases (e.g., caspase-3) for apoptotic cell death [51–53]. By down-regulating caspase-9, miR-133 imposes a protective effect on CMs.

20.3.3 Other miRs

Other than cardiac muscle-specific miRs, several miRs have also been shown to affect cardiac function. For instance, miR-23a, miR-23b, miR-24, miR-195, miR-199a, and miR-214 are up-regulated in cardiac hypertrophy [54]. Overexpression of miR-23a, miR-23b, miR-24, miR-195, or miR-214 via adenovirus-mediated gene transfer induces hypertrophic growth of cultured rat CMs [54]. On the one hand, MiR-24, miR-125b, miR-195, miR-199a, and miR-214 are up-regulated in the tissue of patients with end-stage failing human hearts [54]. On the other hand, miR-150 and miR-181b are down-regulated in murine models of cardiac hypertrophy and their overexpression leads to a decrease in CM size [54]. Alterations of miR-208a and miR-208b, members of the miR-208 family, can lead to electrical disturbances by affecting gap junction-mediated conduction [55]. The expression of miR-18b, miR-21, miR-23a, and miR-125b is increased in hypertrophic CMs and inhibition of endogenous miR-21 or miR-18b augments hypertrophic growth [56].

20.4 MiR and Arrhythmias

Circulation requires the highly coordinated efforts of atrial, ventricular, and pacemaker cells. Pacemaker cells of the sino-atrial (SA) node *spontaneously* depolarize upon repolarization to generate rhythmic action potentials (AP) (pacemaking or

automaticity) that subsequently propagate to induce the contractions of atrial and ventricular muscles. Arrhythmias, a major cause for death in myocardial infarction and heart failure [57], occur as a consequence of abnormal electrical activities in automaticity, conduction, depolarization, repolarization, etc. In brief, the electrical and subsequent contractile activities of the heart are largely orchestrated by ion channels and pumps. When the fine balance of their activities is disrupted, arrhythmias result. The inter-relationships of several miRs with some of these crucial signaling proteins in the heart and the biological processes involved are discussed later.

20.4.1 Automaticity

Defects in automaticity underlie several forms of arrhythmias. I_f , the funny current, is a diastolic depolarizing current activated by hyperpolarization, is a key player in cardiac pacing. In VCMs, I_f is expressed during fetal and neonatal life and its level decreases toward adulthood. Altered I_f expression in the atria and ventricles may contribute to arrhythmias [58]. I_f is encoded by the hyperpolarization-activated cyclic-nucleotide-gated (HCN1-4) gene family. HCN1, HCN2, and HCN4 are found in the heart but are differentially expressed among the SA node, AV node, Purkinje fibers, and the myocardium. Dysregulation of HCN isoforms is associated with cardiac diseases. For instance, in human VCMs isolated from failing hearts of patients with ischemic cardiomyopathy, I_f is increased by approximately twofold [59]. In agreement with these observations, both the transcript and protein levels of HCN2 and HCN4 are upregulated in atria and VCMs of failing hearts explanted from patients with end-stage ischemic cardiomyopathy [60]. MiR-1 and miR-133 are significantly down-regulated in hypertrophic and failing hearts [23, 54, 61]. Interestingly, forced expression of miR-1/miR-133 prevents overexpression of HCN2/HCN4 in rat hypertrophic CMs [38]. Further analyses establish HCN2 as a downstream target of miR-1 and miR-133 while HCN4 is a target for miR-1 only [38]. Dysregulation of miR-1 and miR-133 is therefore anticipated to result in aberrant I_f expression and play a causative role in the development of arrhythmias. Modulations of miR-1 and miR-133 may lead to novel therapeutic approaches for HCN-related arrhythmias.

20.4.2 Excitation–Contraction Coupling

During AP of adult CMs, Ca^{2+} entry into the cytosol through sarcolemmal L-type Ca^{2+} ($I_{\text{Ca,L}}$) channels triggers the release of Ca^{2+} from the intracellular Ca^{2+} storage structures (a.k.a. sarcoplasmic reticulum, SR) via the ryanodine receptors (RyR). This process, the so-called Ca^{2+} -induced Ca^{2+} -release (CICR)[62], elevates the cytosolic free Ca^{2+} concentration ($[\text{Ca}^{2+}]_i$) to activate the contractile apparatus for

contraction. For relaxation, Ca^{2+} gets pumped back into the SR by the sarco/endoplasmic reticulum Ca^{2+} -ATPase (SERCA) and extruded by the $\text{Na}^+–\text{Ca}^{2+}$ exchanger (NCX) to return $[\text{Ca}^{2+}]_i$ to the resting level. Such a rise and decay of $[\text{Ca}^{2+}]_i$ can be recorded as a Ca^{2+} transient and its amplitude and kinetic properties determine both the contractile force (inotropic) and frequency (chronotropic) of CMs. Given the central importance of CICR in cardiac excitation–contraction (EC) coupling, proper electrophysiological and Ca^{2+} handling properties are crucial for CMs to function. Indeed, abnormal electrophysiology/ Ca^{2+} handling, as in the case of heart failure, is arrhythmogenic [62].

Ca^{2+} cycling is mediated by phosphorylation of a range of proteins including RyR, Ca^{2+} /calmodulin-dependent protein kinase II (CaMKII), and phosphatases PP1 and PP2A. MiR-1 has been reported to modulate cardiac contractility by regulating Ca^{2+} release [63]. Adenovirus-mediated overexpression of miR-1 in cultured adult rat VCMs results in a marked increase in the amplitude of $I_{\text{Ca,L}}$, flattening of voltage dependence of Ca^{2+} transients, and augmented spontaneous Ca^{2+} sparks while reducing the SR Ca^{2+} content [63]. These effects are attributable to the translational inhibition of the B56-regulatory subunit of PP2A by miR-1. The PP2A catalytic subunit complexes with RyR2 [64] and is critical to dephosphorylation of these proteins following their phosphorylation by protein kinase A and/or CaMKII [64, 65]. MiR-1-mediated repression of B56 results in hyperphosphorylation of RyR by CaMKII, and CaMKII inhibitor abolishes these effects.

20.4.3 Conduction and Gap Junctions

Gap junctions, encoded by the Cx multi-gene family, couple adjacent cells and underlie cell–cell communications. In the heart, gap junctions are important for effective propagation of electrical signals to induce coordinated contraction. Gap junctions consist of two connexons that are each composed of six Cx. To date, over 20 Cx genes have been identified (reviewed in [66]). Cx40, Cx43, and Cx45 are expressed in CMs.

Cx40 is normally expressed in fast-conducting cardiac tissues and in the atria [67]. Mice lacking Cx40 have cardiac conduction abnormalities characteristic of AV block and bundle branch block [68, 69]. Cx40 has been demonstrated to be an indirect target of miR-208a [55]. MiR-208a and miR-208b are encoded within the introns of the α -cardiac muscle myosin heavy chain (α MHC) gene and the β MHC gene, respectively [55]. They are differentially expressed during heart development and heart pathology, mirroring the expression of their respective host genes, α MHC and β MHC [55]. Overexpression of miR-208a under the control of the α MHC promoter induces cardiac arrhythmias, while its targeted deletion results in abnormal atrial conduction. These effects are accompanied by a corresponding reduction or increase in the level of Cx40. By examining genes that are known to be involved in the activation of Cx40 gene, GATA4 and homeodomain-only protein (Hop) are

found to be up and down-regulated, respectively, in miR208a $-/-$ hearts; GATA4 and Hop are direct and indirect targets of miR-208a.

Cx43 is the most abundant Cx isoform in the mammalian heart [70–72]. Although homozygous Cx43 knockout mice die at birth due to pulmonary outflow tract obstruction and conotruncal heart malformation [73], heart defects associated with malformations in the conotruncus have also been observed in transgenic mice that globally overexpress Cx43 [74]. Thus, the precise temporal expression level of Cx43 plays an important role in the mammalian heart development. Using a murine model, miR-1 has been shown to directly repress Cx43 expression [37]. MiR-1 is also significantly up-regulated in ischemic human hearts with coronary heart disease [37]. A similar increase is likewise detected in a rat model of MI [37]. Injection of miR-1 promotes ischemic arrhythmias in healthy as well as infarcted rat myocardium by slowing conduction and membrane depolarization [37]. Conversely, inhibition of miR-1 by an antisense suppresses arrhythmias. Thus, repression of Cx43 is likely to contribute significantly to the pro-arrhythmic effect of miR-1.

20.4.4 Membrane Repolarization

Cardiac repolarization is determined by a balance between inward and outward ionic currents. Voltage-gated K $^{+}$ channels play an important role in regulating cardiac muscle excitability by controlling AP duration (APD) and frequency. Both gain and loss of the K $^{+}$ channel function can lead to arrhythmias. An increase in K $^{+}$ currents abbreviates APD and thereby functions as a trigger to facilitate re-entry; diminished K $^{+}$ currents cause APD prolongation (e.g., in heart failure), predisposing to cellular triggers (early after depolarizations, EADs) and arrhythmias such as torsades de pointes reviewed in [57, 75].

20.4.4.1 I_{Ks}

In cardiac myocytes, the KCNQ1 pore-forming α -subunit assembles with the KCNE1 β -subunit to underlie the slow component of the delayed rectifier K $^{+}$ current or I_{Ks} [76, 77]. Mutations in KCNQ1 or KCNE1 can result in dysfunction of I_{Ks} and abnormality of cardiac repolarization as in long QT syndrome type 1 (LQT1) [78, 79]. Luo et al. reported that KCNQ1 and KCNE1 are direct targets of miR133 and miR-1, respectively [80]. A spatial correlation between the distribution of KCNQ1 and KCNE1 proteins, and those of miR133 and miR-1, has been observed. Specifically, miR-133 level and the regional distribution of KCNQ1 protein display a reciprocal pattern. Together with Stimulating Protein 1, miR133 and miR-1 likely contribute to the establishment of the expression gradient of I_{Ks} in heart. As a determinant of the spatial dispersion of electrical activities [81], which maintain the sequential excitation of cardiac muscles, any disruptions of such regional heterogeneity via dysregulated miR expression can lead to arrhythmia.

20.4.4.2 I_{Kr}

The human ether-a-go-go-related gene (*hERG*) encodes the channel responsible for rapid component of the delayed rectifier K⁺ current or I_{Kr} that provides the major source of outward current for ventricular repolarization. I_{Kr} is significantly down-regulated in diabetic hearts and this contributes critically to repolarization slowing and QT prolongation [82, 83]. Xiao et al. showed that the miR-133 and miR-1 expression levels are up-regulated in the ventricular samples from diabetic patients [84]. However, miR-133, but not miR-1, targets rabbit *ERG*. Delivery of miR-133 into rabbit CMs results in the reduction of *ERG* protein level and a significantly depressed I_{Kr} current without altering the transcript level. MiR-133 antisense inhibitor abrogates this effect. Functional inhibition of serum response factor, a known activator of miR-133, downregulates miR-133 and increases the I_{Kr} density.

20.4.4.3 I_{to}

The transient outward K⁺ current I_{to} is responsible for the initial phase of repolarization and is regulated by miR-1-2. Disruption of miR-1-2 by gene knockout results in cardiac electrophysiological defects [30]. The heart rate of miR-1-2 knockout mice was significantly lower than that of wild-type littermates, and the normal delay between atrial and ventricular depolarization (the PR interval) was shortened. In addition, ventricular depolarization, manifested by the QRS complex, was significantly prolonged in the mutant hearts. Synchronous depolarization of VCMs is coordinated by rapid conduction through the atrioventricular bundle, bundle branches, and Purkinje fibers. The increased width and the morphology of the QRS complex in the mutants were typical of abnormal conduction along one of the bundle branches (bundle branch block), a finding that in humans can be associated with an increased risk of sudden death. These results showed that miR-1-2 is required for propagation of cardiac electrical activity. Bioinformatic searches of miR-1-2 binding sites and subsequent in vitro assays confirmed Irx5 as a direct target of miR-1-2. Both Irx5 mRNA and protein were upregulated in the heart of miR-1-2 knockout mice, and this was accompanied by the downregulation of Irx5 target gene *Kcnd2* (encoding K_v4.2). Irx5 functions as a transcription factor to repress *Kcnd2* by recruiting mBop [30]. K_v4.2 is a K⁺ channel subunit responsible for I_{to} in rodents and perturbations of its activity has been associated with increased susceptibility to arrhythmias and the induction of polymorphic ventricular tachycardia [85, 86].

20.5 MiR and Human Cardiovascular Biology

The dysregulation of many individual miRs has been linked to the development and progression of cardiac diseases in humans [87, 88]. Profound alterations of miR expression have been identified in failing hearts [33, 34, 54, 89–91]. Different types

of heart diseases, such as ischemic cardiomyopathy, dilated cardiomyopathy, and aortic stenosis, are associated with distinct changes in miR expression, and 43 out of 87 tested miRs are differentially expressed in at least one of these disease groups [89]. A subsequent study also demonstrated differences and commonalities in the expression of 33 miRs in ischemic cardiomyopathy and idiopathic dilated cardiomyopathy [90]. Bioinformatic analysis demonstrated a concordance between regulated mRNA expression in heart failure and the presence of miR binding sites in the respective 3' untranslated regions, suggesting that some of the transcriptional changes associated with heart failure may be regulated by changes in miR levels [34]. The functional significance of miR expression was explored by van Rooij et al. [54], who identified a group of miRs upregulated in the tissue of patients with end-stage failing hearts and showed that adenoviral overexpression of these miRs could induce hypertrophic growth of cultured rat CMs [54].

20.6 Pluripotent hESCs and iPSCs as a Potential Source of CMs

Terminally differentiated adult CMs lack the ability to regenerate. Cell-based therapies offer a promising option for myocardial repair. Human embryonic stem cells (hESCs), isolated from the inner cell mass of blastocysts, can self-renew while maintaining their pluripotency to differentiate into all cell types [92], including CMs [93–97]. Although hESC-derived CMs (hESC-CMs) have been reported to improve cardiac function in several animal MI models [98, 99], numerous hurdles need to be overcome before their clinical applications. For instance, generation of patient-specific cells for autologous transplantation has been pursued to avoid immune rejection of the transplanted grafts. Direct reprogramming of adult somatic cells to become pluripotent hES-like cells (a.k.a. induced pluripotent stem cells or iPSCs) has been accomplished, eliminating potential ethical concerns and making hES/iPS cell-based therapies one step closer to reality. Forced expression of four pluripotency genes (*Oct3/4*, *Sox2*, *c-Myc*, and *Klf4* [100, 101] or *Oct3/4*, *Sox2*, *Nanog*, and *Lin28* [102]) suffices to reprogram mouse and human fibroblasts into iPSCs. hiPSCs have morphology, proliferation, feeder dependence, surface markers, gene expression, epigenetic status, formation of embryoid bodies in vitro, promoter activities, telomerase activities, and in vivo teratoma formation similar to hESCs.

20.6.1 MiR Profile of hiPSC and hESC

Genome-wide analysis has been done to compare the miR profiles of hiPSC, hESC, and fibroblasts [103, 104]. Both pluripotent cell types have miR profiles vastly different from fibroblasts. The most dramatic difference is the miR-302 cluster whose expression is significantly increased in hiPSC and hESC. The miR-17-92

cluster is also up-regulated in hiPSC and hESC and has been implicated in cell cycle control and apoptosis [105, 106]. Overall, miR expression is similar among hiPSC and hESC, consistent with their similarities in phenotypes and transcriptomic profiles [104]. Nevertheless, a number of differences do exist and a group of miRs, including miR-886-5p, miR372, and miR-373, are expressed more highly in hESCs than in hiPSCs [104]. Interestingly, all of the miRs that exhibit higher expression in hESCs relative to hiPSC, except miR-629 and miR-96, are located together within a 130-kb intergenic region of chromosome 19. This region of clustered miRs includes the miR-371/372/373 cluster, shown previously to be up-regulated in hESCs [107, 108], as well as a larger 54-miR cluster spanning 96 kb [109], much of which is highly expressed in hESCs. It is still unclear whether this difference in expression has any biological significance.

20.6.2 Pluripotent Stem Cell-Derived CMs

The functional properties of hESC–CMs have also been investigated by us and several laboratories. Functional SR proteins (i.e., RyR and SERCA2a) are expressed in hESC–CMs [110]. In spite of this, hESC–CMs exhibit immature Ca^{2+} dynamics such as I_{CaL} with lower amplitude and slower kinetics relative to those of the adult. Ca^{2+} transients are unsynchronized and this has been attributed to the absence of t-tubules [111]. hESC–CM can integrate with recipient CMs and are capable of actively pacing quiescent, recipient VCMs in vitro and ventricular myocardium in vivo [96]. Although present observations suggest that hESC resembles fetal rather than adult CM, our laboratory has shown that adenovirus-mediated expression of calsequestrin can facilitate maturation of Ca^{2+} handling properties [112], as reflected by an increased SR load, an elevated basal cytosolic Ca^{2+} , augmented Ca^{2+} -transient amplitude, and accelerated kinetics.

Recent reports show that human iPSCs can likewise differentiate into CMs [113]. The derived CMs expressed cardiac-specific transcription factors and structural proteins [114]. Functional CMs with nodal-, atrial-, or ventricular-like electrophysiological phenotypes have also been derived using methods based on those effective for hESC [113]. Multielectrode array recordings established the development of a functional syncytium with stable pacemaker activity and AP propagation. Positive and negative chronotropic responses were induced by application of isoproterenol and carbamylcholine, respectively [114].

20.6.3 miR-1 and miR-499 Play Differential Roles in Cardiac Differentiation of hESC

There have been few studies on the role of miR in CMs derived from hESCs or hiPSCs. Ivey et al. showed that miR-1 promotes differentiation of mouse and human ESCs into the cardiac lineage, as evidenced by an increased expression

of *nkx2.5* and percentage of spontaneously contracting EB outgrowths [26]. MiR-133 is normally co-expressed with miR-1 in developing muscle, and blocks differentiation of myogenic precursors. The effect of miR-1 in murine ESC is mediated by the translational repression of the Notch ligand δ -like 1. Despite the significant knowledge gained from these studies, the functional roles of miRs in human cardiogenesis remain elusive due to paucity of cause-and-effect data in human heart cells.

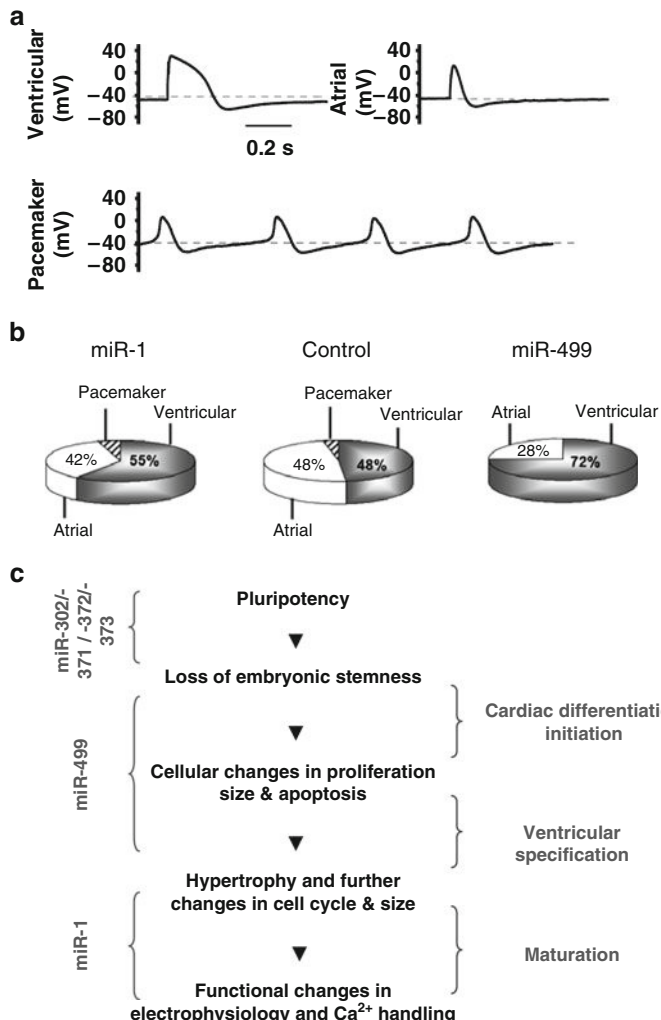


Fig. 20.2 (a) Representative tracings of ventricular, atrial, and pacemaker APs of control hESC-CMs. (b) The percentage distribution of ventricular, atrial, and pacemaker phenotypes before and after LV-miR-1 or -miR-499 transduction. (c) The role of miR in cardiomyocyte differentiation, specification, and maturation

Our group recently mapped and compared the miR profiles of hESC, hESC derived VCMs (hESC–VCM), human fetal and adult VCMs (Fig. 20.2). Sixty-three mRNAs were differentially expressed in hESC–VCMs compared with hESCs, of which 23 were also expressed highly in human fetal and adult VCMs. miR-1 and miR-499 displayed the biggest differences, and thus were chosen for further characterization. Overexpression of miR-499 by lentiviral transduction significantly enhanced the differentiation of cardiac progenitors into VCMs and augmented the expression of contractile proteins (Fig. 20.2a–b). By contrast, miR-1 overexpression did not affect the yield of VCMs from hESC differentiation, but decreased ADP and hyperpolarized RMP/MDP in hESC–VCM due to increased I_{to} , I_{Ks} , and I_{Kr} , and decreased I_f , indicating maturation. Also, overexpression of miR-1 but not miR-499 augmented the immature Ca^{2+} transient amplitude and kinetics. Therefore, miR-499 seems to promote ventricular specification of hESCs, while miR-1 serves to facilitate electrophysiological maturation (Fig. 20.2c).

20.7 Conclusions

Profound alterations of miR expression have been identified in cardiovascular diseases. A better understanding of the underlying biology may lead to novel miR-based therapies for the heart. Additionally, miRs can be utilized for directed differentiation and maturation of hESC/iPSC-derived CMs with improved safety and efficacy for clinical and other applications (such as cardiotoxicity screening and human heart disease model).

References

1. Abu-Issa R, Kirby ML. Heart field: from mesoderm to heart tube. *Annu Rev Cell Dev Biol.* 2007;23:45–68.
2. Buckingham M, Meilhac S, Zaffran S. Building the mammalian heart from two sources of myocardial cells. *Nat Rev Genet.* 2005;6(11):826–35.
3. Garry DJ, Olson EN. A common progenitor at the heart of development. *Cell.* 2006;127(6):1101–4.
4. Harvey RP, Meilhac SM, Buckingham ME. Landmarks and lineages in the developing heart. *Circ Res.* 2009;104(11):1235–7.
5. Ahuja P, Sdeka P, MacLellan WR. Cardiac myocyte cell cycle control in development, disease, and regeneration. *Physiol Rev.* 2007;87(2):521–44.
6. McGill CJ, Brooks G. Cell cycle control mechanisms and their role in cardiac growth. *Cardiovasc Res.* 1995;30(4):557–69.
7. Ambros V. The functions of animal microRNAs. *Nature.* 2004;431(7006):350–5.
8. Bartel DP. MicroRNAs: genomics, biogenesis, mechanism, and function. *Cell.* 2004;116(2):281–97.
9. Lewis BP, Burge CB, Bartel DP. Conserved seed pairing, often flanked by adenosines, indicates that thousands of human genes are microRNA targets. *Cell.* 2005;120(1):15–20.

10. Borchert GM, Lanier W, Davidson BL. RNA polymerase III transcribes human microRNAs. *Nat Struct Mol Biol*. 2006;13(12):1097–101.
11. Kim VN. MicroRNA biogenesis: coordinated cropping and dicing. *Nat Rev Mol Cell Biol*. 2005;6(5):376–85.
12. Landthaler M, Yalcin A, Tuschl T. The human DiGeorge syndrome critical region gene 8 and Its D. melanogaster homolog are required for miRNA biogenesis. *Curr Biol*. 2004; 14(23):2162–7.
13. Bohnsack MT, Czaplinski K, Gorlich D. Exportin 5 is a RanGTP-dependent dsRNA-binding protein that mediates nuclear export of pre-miRNAs. *RNA*. 2004;10(2):185–91.
14. Hutvagner G, Simard MJ. Argonaute proteins: key players in RNA silencing. *Nat Rev Mol Cell Biol*. 2008;9(1):22–32.
15. Kim YK, Kim VN. Processing of intronic microRNAs. *EMBO J*. 2007;26(3):775–83.
16. Ruby JG, Jan CH, Bartel DP. Intronic microRNA precursors that bypass Drosha processing. *Nature*. 2007;448(7149):83–6.
17. Hutvagner G, Zamore PD. A microRNA in a multiple-turnover RNAi enzyme complex. *Science*. 2002;297(5589):2056–60.
18. Zeng Y, Cullen BR. Sequence requirements for micro RNA processing and function in human cells. *RNA*. 2003;9(1):112–23.
19. Zeng Y, Yi R, Cullen BR. MicroRNAs and small interfering RNAs can inhibit mRNA expression by similar mechanisms. *Proc Natl Acad Sci U S A*. 2003;100(17):9779–84.
20. Ji R, Cheng Y, Yue J, Yang J, Liu X, Chen H, et al. MicroRNA expression signature and antisense-mediated depletion reveal an essential role of MicroRNA in vascular neointimal lesion formation. *Circ Res*. 2007;100(11):1579–88.
21. Kuehbacher A, Urbich C, Zeiher AM, Dimmeler S. Role of Dicer and Drosha for endothelial microRNA expression and angiogenesis. *Circ Res*. 2007;101(1):59–68.
22. Lagos-Quintana M, Rauhut R, Yalcin A, Meyer J, Lendeckel W, Tuschl T. Identification of tissue-specific microRNAs from mouse. *Curr Biol*. 2002;12(9):735–9.
23. Care A, Catalucci D, Felicetti F, Bonci D, Addario A, Gallo P, et al. MicroRNA-133 controls cardiac hypertrophy. *Nat Med*. 2007;13(5):613–8.
24. Chen JF, Murchison EP, Tang R, Callis TE, Tatsuguchi M, Deng Z, et al. Targeted deletion of Dicer in the heart leads to dilated cardiomyopathy and heart failure. *Proc Natl Acad Sci USA*. 2008;105(6):2111–6.
25. Rao PK, Toyama Y, Chiang HR, Gupta S, Bauer M, Medvid R, et al. Loss of cardiac microRNA-mediated regulation leads to dilated cardiomyopathy and heart failure. *Circ Res*. 2009;105(6):585–94.
26. Ivey KN, Muth A, Arnold J, King FW, Yeh RF, Fish JE, et al. MicroRNA regulation of cell lineages in mouse and human embryonic stem cells. *Cell Stem Cell*. 2008;2(3):219–29.
27. Morton SU, Scherz PJ, Cordes KR, Ivey KN, Stainier DY, Srivastava D. microRNA-138 modulates cardiac patterning during embryonic development. *Proc Natl Acad Sci USA*. 2008; 105(46):17830–5.
28. Sayed D, Rane S, Lypowy J, He M, Chen IY, Vashistha H, et al. MicroRNA-21 targets Sprouty2 and promotes cellular outgrowths. *Mol Biol Cell*. 2008;19(8):3272–82.
29. van Rooij E, Sutherland LB, Qi X, Richardson JA, Hill J, Olson EN. Control of stress-dependent cardiac growth and gene expression by a microRNA. *Science*. 2007;316(5824): 575–9.
30. Zhao Y, Ransom JF, Li A, Vedantham V, von Drehle M, Muth AN, et al. Dysregulation of cardiogenesis, cardiac conduction, and cell cycle in mice lacking miRNA-1-2. *Cell*. 2007; 129(2):303–17.
31. Zhao Y, Samal E, Srivastava D. Serum response factor regulates a muscle-specific microRNA that targets Hand2 during cardiogenesis. *Nature*. 2005;436(7048):214–20.
32. Cheng Y, Ji R, Yue J, Yang J, Liu X, Chen H, et al. MicroRNAs are aberrantly expressed in hypertrophic heart: do they play a role in cardiac hypertrophy? *Am J Pathol*. 2007;170(6): 1831–40.

33. Matkovich SJ, Van Booven DJ, Youker KA, Torre-Amione G, Diwan A, Eschenbacher WH, et al. Reciprocal regulation of myocardial microRNAs and messenger RNA in human cardiomyopathy and reversal of the microRNA signature by biomechanical support. *Circulation.* 2009;119(9):1263–71.
34. Thum T, Galuppo P, Wolf C, Fiedler J, Kneitz S, van Laake LW, et al. MicroRNAs in the human heart: a clue to fetal gene reprogramming in heart failure. *Circulation.* 2007;116(3):258–67.
35. Tay Y, Zhang J, Thomson AM, Lim B, Rigoutsos I. MicroRNAs to Nanog, Oct4 and Sox2 coding regions modulate embryonic stem cell differentiation. *Nature.* 2008;455(7216):1124–8.
36. Chen JF, Mandel EM, Thomson JM, Wu Q, Callis TE, Hammond SM, et al. The role of microRNA-1 and microRNA-133 in skeletal muscle proliferation and differentiation. *Nat Genet.* 2006;38(2):228–33.
37. Yang B, Lin H, Xiao J, Lu Y, Luo X, Li B, et al. The muscle-specific microRNA miR-1 regulates cardiac arrhythmogenic potential by targeting GJA1 and KCNJ2. *Nat Med.* 2007;13(4):486–91.
38. Luo X, Lin H, Pan Z, Xiao J, Zhang Y, Lu Y, et al. Down-regulation of miR-1/miR-133 contributes to re-expression of pacemaker channel genes HCN2 and HCN4 in hypertrophic heart. *J Biol Chem.* 2008;283(29):20045–52.
39. McFadden DG, Barbosa AC, Richardson JA, Schneider MD, Srivastava D, Olson EN. The Hand1 and Hand2 transcription factors regulate expansion of the embryonic cardiac ventricles in a gene dosage-dependent manner. *Development.* 2005;132(1):189–201.
40. Yamagishi H, Yamagishi C, Nakagawa O, Harvey RP, Olson EN, Srivastava D. The combinatorial activities of Nkx2.5 and dHAND are essential for cardiac ventricle formation. *Dev Biol.* 2001;239(2):190–203.
41. Liu N, Barbosa AC, Chapman SL, Bezprozvannaya S, Qi X, Richardson JA, et al. DNA binding-dependent and -independent functions of the Hand2 transcription factor during mouse embryogenesis. *Development.* 2009;136(6):933–42.
42. Srivastava D, Thomas T, Lin Q, Kirby ML, Brown D, Olson EN. Regulation of cardiac mesodermal and neural crest development by the bHLH transcription factor, dHAND. *Nat Genet.* 1997;16(2):154–60.
43. Yu XY, Song YH, Geng YJ, Lin QX, Shan ZX, Lin SG, et al. Glucose induces apoptosis of cardiomyocytes via microRNA-1 and IGF-1. *Biochem Biophys Res Commun.* 2008;376(3):548–52.
44. Tang Y, Zheng J, Sun Y, Wu Z, Liu Z, Huang G. MicroRNA-1 regulates cardiomyocyte apoptosis by targeting Bcl-2. *Int Heart J.* 2009;50(3):377–87.
45. Xu C, Lu Y, Pan Z, Chu W, Luo X, Lin H, et al. The muscle-specific microRNAs miR-1 and miR-133 produce opposing effects on apoptosis by targeting HSP60, HSP70 and caspase-9 in cardiomyocytes. *J Cell Sci.* 2007;120(Pt 17):3045–52.
46. Meder B, Katus HA, Rottbauer W. Right into the heart of microRNA-133a. *Genes Dev.* 2008;22(23):3227–31.
47. Rao PK, Kumar RM, Farkhondeh M, Baskerville S, Lodish HF. Myogenic factors that regulate expression of muscle-specific microRNAs. *Proc Natl Acad Sci U S A.* 2006;103(23):8721–6.
48. Brown JH, Del Re DP, Sussman MA. The Rac and Rho hall of fame: a decade of hypertrophic signaling hits. *Circ Res.* 2006;98(6):730–42.
49. Nagai T, Tanaka-Ishikawa M, Aikawa R, Ishihara H, Zhu W, Yazaki Y, et al. Cdc42 plays a critical role in assembly of sarcomere units in series of cardiac myocytes. *Biochem Biophys Res Commun.* 2003;305(4):806–10.
50. Bergemann AD, Cole F, Hirschhorn K. The etiology of Wolf–Hirschhorn syndrome. *Trends Genet.* 2005;21(3):188–95.
51. Han Y, Chen YS, Liu Z, Bodyak N, Rigor D, Bisping E, et al. Overexpression of HAX-1 protects cardiac myocytes from apoptosis through caspase-9 inhibition. *Circ Res.* 2006;99(4):415–23.

52. Bialik S, Cryns VL, Drincic A, Miyata S, Wollowick AL, Srinivasan A, et al. The mitochondrial apoptotic pathway is activated by serum and glucose deprivation in cardiac myocytes. *Circ Res*. 1999;85(5):403–14.
53. Kannan K, Jain SK. Oxidative stress and apoptosis. *Pathophysiology*. 2000;7(3):153–63.
54. van Rooij E, Sutherland LB, Liu N, Williams AH, McAnally J, Gerard RD, et al. A signature pattern of stress-responsive microRNAs that can evoke cardiac hypertrophy and heart failure. *Proc Natl Acad Sci USA*. 2006;103(48):18255–60.
55. Callis TE, Pandya K, Seok HY, Tang RH, Tatsuguchi M, Huang ZP, et al. MicroRNA-208a is a regulator of cardiac hypertrophy and conduction in mice. *J Clin Invest*. 2009;119(9):2772–86.
56. Tatsuguchi M, Seok HY, Callis TE, Thomson JM, Chen JF, Newman M, et al. Expression of microRNAs is dynamically regulated during cardiomyocyte hypertrophy. *J Mol Cell Cardiol*. 2007;42(6):1137–41.
57. Akar FG, Tomaselli GF. Ion channels as novel therapeutic targets in heart failure. *Ann Med*. 2005;37(1):44–54.
58. Stilli D, Sgoifo A, Macchi E, Zaniboni M, De Iasio S, Cerbai E, et al. Myocardial remodeling and arrhythmogenesis in moderate cardiac hypertrophy in rats. *Am J Physiol Heart Circ Physiol*. 2001;280(1):H142–50.
59. Cerbai E, Sartiani L, DePaoli P, Pino R, Maccherini M, Bizzarri F, et al. The properties of the pacemaker current I(F) in human ventricular myocytes are modulated by cardiac disease. *J Mol Cell Cardiol*. 2001;33(3):441–8.
60. Stillitano F, Lonardo G, Zicha S, Varro A, Cerbai E, Mugelli A, et al. Molecular basis of funny current (If) in normal and failing human heart. *J Mol Cell Cardiol*. 2008;45(2):289–99.
61. Sayed D, Hong C, Chen IY, Lypowy J, Abdellatif M. MicroRNAs play an essential role in the development of cardiac hypertrophy. *Circ Res*. 2007;100(3):416–24.
62. Bers DM. Cardiac excitation–contraction coupling. *Nature*. 2002;415(6868):198–205.
63. Terentyev D, Belevych AE, Terentyeva R, Martin MM, Malana GE, Kuhn DE, et al. miR-1 overexpression enhances Ca(2+) release and promotes cardiac arrhythmogenesis by targeting PP2A regulatory subunit B56alpha and causing CaMKII-dependent hyperphosphorylation of RyR2. *Circ Res*. 2009;104(4):514–21.
64. Marx SO, Reiken S, Hisamatsu Y, Jayaraman T, Burkhoff D, Rosemblit N, et al. PKA phosphorylation dissociates FKBP12.6 from the calcium release channel (ryanodine receptor): defective regulation in failing hearts. *Cell*. 2000;101(4):365–76.
65. Davare MA, Horne MC, Hell JW. Protein phosphatase 2A is associated with class CL-type calcium channels (Cav1.2) and antagonizes channel phosphorylation by cAMP-dependent protein kinase. *J Biol Chem*. 2000;275(50):39710–7.
66. Sohl G, Willecke K. Gap junctions and the connexin protein family. *Cardiovasc Res*. 2004; 62(2):228–32.
67. Delorme B, Dahl E, Jarry-Guichard T, Marics I, Briand JP, Willecke K, et al. Developmental regulation of connexin 40 gene expression in mouse heart correlates with the differentiation of the conduction system. *Dev Dyn*. 1995;204(4):358–71.
68. Simon AM, Goodenough DA, Paul DL. Mice lacking connexin40 have cardiac conduction abnormalities characteristic of atrioventricular block and bundle branch block. *Curr Biol*. 1998;8(5):295–8.
69. Kirchhoff S, Nelles E, Hagendorff A, Kruger O, Traub O, Willecke K. Reduced cardiac conduction velocity and predisposition to arrhythmias in connexin40-deficient mice. *Curr Biol*. 1998;8(5):299–302.
70. Severs NJ. Gap junction remodeling and cardiac arrhythmogenesis: cause or coincidence? *J Cell Mol Med*. 2001;5(4):355–66.
71. Vozzi C, Dupont E, Coppen SR, Yeh HI, Severs NJ. Chamber-related differences in connexin expression in the human heart. *J Mol Cell Cardiol*. 1999;31(5):991–1003.
72. Miquerol L, Dupays L, Theveniau-Ruissy M, Alcolea S, Jarry-Guichard T, Abran P, et al. Gap junctional connexins in the developing mouse cardiac conduction system. *Novartis Found Symp*. 2003;250:80–98. discussion-109, 276–9.

73. Reaume AG, de Sousa PA, Kulkarni S, Langille BL, Zhu D, Davies TC, et al. Cardiac malformation in neonatal mice lacking connexin43. *Science*. 1995;267(5205):1831–4.
74. Ewart JL, Cohen MF, Meyer RA, Huang GY, Wessels A, Gourdie RG, et al. Heart and neural tube defects in transgenic mice overexpressing the Cx43 gap junction gene. *Development*. 1997;124(7):1281–92.
75. Shah M, Akar FG, Tomaselli GF. Molecular basis of arrhythmias. *Circulation*. 2005; 112(16):2517–29.
76. Barhanin J, Lesage F, Guillemaire E, Fink M, Lazdunski M, Romey G. K(V)LQT1 and IsK (minK) proteins associate to form the I(Ks) cardiac potassium current. *Nature*. 1996;384(6604):78–80.
77. Sanguineti MC, Curran ME, Zou A, Shen J, Spector PS, Atkinson DL, et al. Coassembly of K(V)LQT1 and minK (IsK) proteins to form cardiac I(Ks) potassium channel. *Nature*. 1996; 384(6604):80–3.
78. Jost N, Virag L, Bitay M, Takacs J, Lengyel C, Biliczki P, et al. Restricting excessive cardiac action potential and QT prolongation: a vital role for IKs in human ventricular muscle. *Circulation*. 2005;112(10):1392–9.
79. Roden DM, Viswanathan PC. Genetics of acquired long QT syndrome. *J Clin Invest*. 2005; 115(8):2025–32.
80. Luo X, Xiao J, Lin H, Li B, Lu Y, Yang B, et al. Transcriptional activation by stimulating protein 1 and post-transcriptional repression by muscle-specific microRNAs of IKs-encoding genes and potential implications in regional heterogeneity of their expressions. *J Cell Physiol*. 2007;212(2):358–67.
81. Liu DW, Antzelevitch C. Characteristics of the delayed rectifier current (IKr and IKs) in canine ventricular epicardial, midmyocardial, and endocardial myocytes. A weaker IKs contributes to the longer action potential of the M cell. *Circ Res*. 1995;76(3):351–65.
82. Zhang Y, Xiao J, Lin H, Luo X, Wang H, Bai Y, et al. Ionic mechanisms underlying abnormal QT prolongation and the associated arrhythmias in diabetic rabbits: a role of rapid delayed rectifier K⁺ current. *Cell Physiol Biochem*. 2007;19(5–6):225–38.
83. Zhang Y, Xiao J, Wang H, Luo X, Wang J, Villeneuve LR, et al. Restoring depressed HERG K⁺ channel function as a mechanism for insulin treatment of abnormal QT prolongation and associated arrhythmias in diabetic rabbits. *Am J Physiol Heart Circ Physiol*. 2006;291(3): H1446–55.
84. Xiao J, Luo X, Lin H, Zhang Y, Lu Y, Wang N, et al. MicroRNA miR-133 represses HERG K⁺ channel expression contributing to QT prolongation in diabetic hearts. *J Biol Chem*. 2007;282(17):12363–7.
85. Costantini DL, Arruda EP, Agarwal P, Kim KH, Zhu Y, Zhu W, et al. The homeodomain transcription factor Irx5 establishes the mouse cardiac ventricular repolarization gradient. *Cell*. 2005;123(2):347–58.
86. Barry DM, Xu H, Schuessler RB, Nerbonne JM. Functional knockout of the transient outward current, long-QT syndrome, and cardiac remodeling in mice expressing a dominant-negative Kv4 alpha subunit. *Circ Res*. 1998;83(5):560–7.
87. Latronico MV, Condorelli G. MicroRNAs and cardiac pathology. *Nat Rev Cardiol*. 2009; 6(6):419–29.
88. Zhang C. MicroRNAs: role in cardiovascular biology and disease. *Clin Sci (Lond)*. 2008; 114(12):699–706.
89. Ikeda S, Kong SW, Lu J, Bisping E, Zhang H, Allen PD, et al. Altered microRNA expression in human heart disease. *Physiol Genomics*. 2007;31(3):367–73.
90. Sucharov C, Bristow MR, Port JD. miRNA expression in the failing human heart: functional correlates. *J Mol Cell Cardiol*. 2008;45(2):185–92.
91. Naga Prasad SV, Duan ZH, Gupta MK, Surampudi VS, Volinia S, Calin GA, et al. Unique microRNA profile in end-stage heart failure indicates alterations in specific cardiovascular signaling networks. *J Biol Chem*. 2009;284(40):27487–99.

92. Thomson JA, Itskovitz-Eldor J, Shapiro SS, Waknitz MA, Swiergiel JJ, Marshall VS, et al. Embryonic stem cell lines derived from human blastocysts. *Science*. 1998;282(5391):1145–7.
93. He JQ, Ma Y, Lee Y, Thomson JA, Kamp TJ. Human embryonic stem cells develop into multiple types of cardiac myocytes: action potential characterization. *Circ Res*. 2003;93(1):32–9.
94. Mummery C, Ward-van Oostwaard D, Doevedans P, Spijker R, van den Brink S, Hassink R, et al. Differentiation of human embryonic stem cells to cardiomyocytes: role of coculture with visceral endoderm-like cells. *Circulation*. 2003;107(21):2733–40.
95. Xu C, Police S, Rao N, Carpenter MK. Characterization and enrichment of cardiomyocytes derived from human embryonic stem cells. *Circ Res*. 2002;91(6):501–8.
96. Xue T, Cho HC, Akar FG, Tsang SY, Jones SP, Marban E, et al. Functional integration of electrically active cardiac derivatives from genetically engineered human embryonic stem cells with quiescent recipient ventricular cardiomyocytes: insights into the development of cell-based pacemakers. *Circulation*. 2005;111(1):11–20.
97. Kehat I, Kenyagin-Karsenti D, Snir M, Segev H, Amit M, Gepstein A, et al. Human embryonic stem cells can differentiate into myocytes with structural and functional properties of cardiomyocytes. *J Clin Invest*. 2001;108(3):407–14.
98. Laflamme MA, Chen KY, Naumova AV, Muskheli V, Fugate JA, Dupras SK, et al. Cardiomyocytes derived from human embryonic stem cells in pro-survival factors enhance function of infarcted rat hearts. *Nat Biotechnol*. 2007;25(9):1015–24.
99. Caspi O, Huber I, Kehat I, Habib M, Arbel G, Gepstein A, et al. Transplantation of human embryonic stem cell-derived cardiomyocytes improves myocardial performance in infarcted rat hearts. *J Am Coll Cardiol*. 2007;50(19):1884–93.
100. Takahashi K, Yamanaka S. Induction of pluripotent stem cells from mouse embryonic and adult fibroblast cultures by defined factors. *Cell*. 2006;126(4):663–76.
101. Meissner A, Wernig M, Jaenisch R. Direct reprogramming of genetically unmodified fibroblasts into pluripotent stem cells. *Nat Biotechnol*. 2007;25(10):1177–81.
102. Yu J, Vodyanik MA, Smuga-Otto K, Antosiewicz-Bourget J, Frane JL, Tian S, et al. Induced pluripotent stem cell lines derived from human somatic cells. *Science*. 2007;318(5858):1917–20.
103. Chin MH, Mason MJ, Xie W, Volinia S, Singer M, Peterson C, et al. Induced pluripotent stem cells and embryonic stem cells are distinguished by gene expression signatures. *Cell Stem Cell*. 2009;5(1):111–23.
104. Wilson KD, Venkatasubrahmanyam S, Jia F, Sun N, Butte AJ, Wu JC. MicroRNA profiling of human-induced pluripotent stem cells. *Stem Cells Dev*. 2009;18(5):749–58.
105. Diabdado B, van de Wiel MA, Terhaar Sive Droste JS, Mongera S, Postma C, Meijerink WJ, et al. MiR-17-92 cluster is associated with 13q gain and c-myc expression during colorectal adenoma to adenocarcinoma progression. *Br J Cancer*. 2009;101(4):707–14.
106. Yan HL, Xue G, Mei Q, Wang YZ, Ding FX, Liu MF, et al. Repression of the miR-17-92 cluster by p53 has an important function in hypoxia-induced apoptosis. *EMBO J*. 2009;28(18):2719–32.
107. Lakshmipathy U, Love B, Goff LA, Jornsten R, Graichen R, Hart RP, et al. MicroRNA expression pattern of undifferentiated and differentiated human embryonic stem cells. *Stem Cells Dev*. 2007;16(6):1003–16.
108. Suh MR, Lee Y, Kim JY, Kim SK, Moon SH, Lee JY, et al. Human embryonic stem cells express a unique set of microRNAs. *Dev Biol*. 2004;270(2):488–98.
109. Bentwich I, Avniel A, Karov Y, Aharonov R, Gilad S, Barad O, et al. Identification of hundreds of conserved and nonconserved human microRNAs. *Nat Genet*. 2005;37(7):766–70.
110. Liu J, Fu JD, Siu CW, Li RA. Functional sarcoplasmic reticulum for calcium handling of human embryonic stem cell-derived cardiomyocytes: insights for driven maturation. *Stem Cells*. 2007;25(12):3038–44.

111. Lieu DK, Liu J, Siu CW, McNerney GP, Tse HF, Abu-Khalil A, et al. Absence of transverse tubules contributes to non-uniform Ca(2+) wavefronts in mouse and human embryonic stem cell-derived cardiomyocytes. *Stem Cells Dev.* 2009;18(10):1493–500.
112. Liu J, Lieu DK, Siu CW, Fu JD, Tse HF, Li RA. Facilitated maturation of Ca2+ handling properties of human embryonic stem cell-derived cardiomyocytes by calsequestrin expression. *Am J Physiol Cell Physiol.* 2009;297(1):C152–9.
113. Zhang J, Wilson GF, Soerens AG, Koonce CH, Yu J, Palecek SP, et al. Functional cardiomyocytes derived from human induced pluripotent stem cells. *Circ Res.* 2009;104(4):e30–41.
114. Zwi L, Caspi O, Arbel G, Huber I, Gepstein A, Park IH, et al. Cardiomyocyte differentiation of human induced pluripotent stem cells. *Circulation.* 2009;120(15):1513–23.

Part V

Mechanisms of Inherited Arrhythmia

Chapter 21

Intracellular Calcium Handling and Inherited Arrhythmogenic Diseases

Nicola Monteforte, Carlo Napolitano, Raffaella Bloise, and Silvia G. Priori

21.1 Introduction

Diseases caused by a single genetic defect are referred to as monogenic disorders. These disorders are inherited as dominant or recessive traits with different inheritance patterns (autosomal dominant, autosomal recessive, X-linked dominant, X-linked recessive, matrilineal transmission).

In cardiology, there are two major clusters of monogenic disorders: (a) the cardiomyopathies due to alterations in sarcomeric and in cytoskeletal proteins, and (b) the arrhythmogenic diseases that are caused by mutations in ion channels and ion channel-controlling proteins such as the long QT syndromes (LQTS), the Brugada syndromes, the short QT syndromes (SQTS), and the catecholaminergic polymorphic ventricular tachycardia (CPVT).

N. Monteforte and R. Bloise

Molecular Cardiology, Fondazione S. Maugeri IRCCS, Via Salvatore Maugeri 10/10A, 27100 Pavia, Italy

C. Napolitano

Molecular Cardiology, Fondazione S. Maugeri IRCCS, Via Salvatore Maugeri 10/10A, 27100 Pavia, Italy

and

Cardiovascular Genetics Program; Leon H. Charney Division of Cardiology, New York University, New York, NY, USA

S.G. Priori (✉)

Molecular Cardiology, Fondazione S. Maugeri IRCCS, Via Salvatore Maugeri 10/10A, 27100 Pavia, Italy

and

Cardiovascular Genetics Program; Leon H. Charney Division of Cardiology, New York University, New York, NY, USA

and

Department of Cardiology, Università degli Studi di Pavia, Pavia, Italy

e-mail: silvia.priori@fsm.it

Inherited arrhythmogenic diseases are associated with an increased risk for ventricular arrhythmias. These diseases are often asymptomatic for many years and are not detected until the first clinical presentation such as syncope or sudden cardiac death. In approximately 10–20% of all sudden deaths, no structural cardiac abnormalities can be identified [1]. These diseases often affect young, otherwise healthy individuals, and the conventional electrocardiogram (ECG) is important for diagnosing established diseases or detecting novel entities associated with sudden cardiac death [2–4]. The β-blockers are effective in some instances (e.g., LQTS, catecholaminergic ventricular tachycardia) but often an implantable cardioverter defibrillator (ICD) is the only option for high risk patients.

It is important to consider that the clinical manifestations of these diseases may significantly vary from one patient to the other even in the presence of the same genetic defect. In technical terms, this phenomenon is attributed to the “variable expressivity” (nonuniform clinical severity of carriers of the same genetic defect) and the incomplete penetrance (i.e., the ratio between carriers of a given gene defect and the number of clinically affected individuals is lower than 1). The identification of the genes underlying the inherited arrhythmogenic syndromes has greatly contributed to the understanding of the substrate for the arrhythmia development, but more importantly, it has provided major practical information that is helpful when managing affected individuals.

In this chapter, we focus on the genetic basis, the clinical features, and the main therapeutic strategies of the most important channelopathies caused by a genetically determined impairment of intracellular calcium handling such as CPVT, Timothy syndrome [(TS), a variant of long QT syndrome (LQT8)], and two genetic variants of Brugada syndrome (BrS3 and BrS4).

21.2 Catecholaminergic Polymorphic Ventricular Tachycardia

CPVT is a severe disorder, with a high incidence of sudden cardiac death among affected individuals. The first report of a patient with this disease was published in 1975 [5], but the first systematic description came in 1978 with the work of Coumel et al. [6] and was further refined by the same group in 1995 [7]. In 2001, molecular genetic studies unveiled that CPVT results from inherited defects of intracellular calcium handling that cause abnormal Ca^{2+} release from the sarcoplasmic reticulum (SR). We reported for the first time that the autosomal dominant form of the disease was caused by mutations in the gene encoding for the cardiac ryanodine receptor (*RyR2*) [8]. Shortly after, the gene for the autosomal recessive form of CPVT was identified as the gene encoding cardiac calsequestrin (*CASQ2*) [9]. After identification of the underlying genetic causes, basic science studies in cell systems and animal models brought a major advancement to the understanding of arrhythmogenic mechanisms in this disease.

21.2.1 Calcium Handling and Arrhythmogenesis in CPVT

The discovery that genetic defects in Ca^{2+} regulatory proteins such as the ryanodine receptor (RyR2) [10, 11] and calsequestrin (CASQ2) [12], result in CPVT, has stimulated many fundamental studies that provided new and compelling evidence to link abnormal intracellular Ca^{2+} signaling and arrhythmia. Calcium that enters the cell during the plateau phase of the action potential (AP) triggers the release of Ca^{2+} from SR through ryanodine receptors [13] (Fig. 21.1). This process, known as Ca^{2+} -induced Ca^{2+} release (CICR), amplifies the initial Ca^{2+} entry signal to produce an elevation of cytosolic Ca^{2+} [Ca^{2+}]_i, triggering the cascade of conformational changes leading to contraction of the sarcomere. During relaxation, most of the Ca^{2+} in the cytosol is recycled into the SR by cardiac SR calcium adenosine triphosphatase (SERCA2), the activity of which is controlled by phospholamban

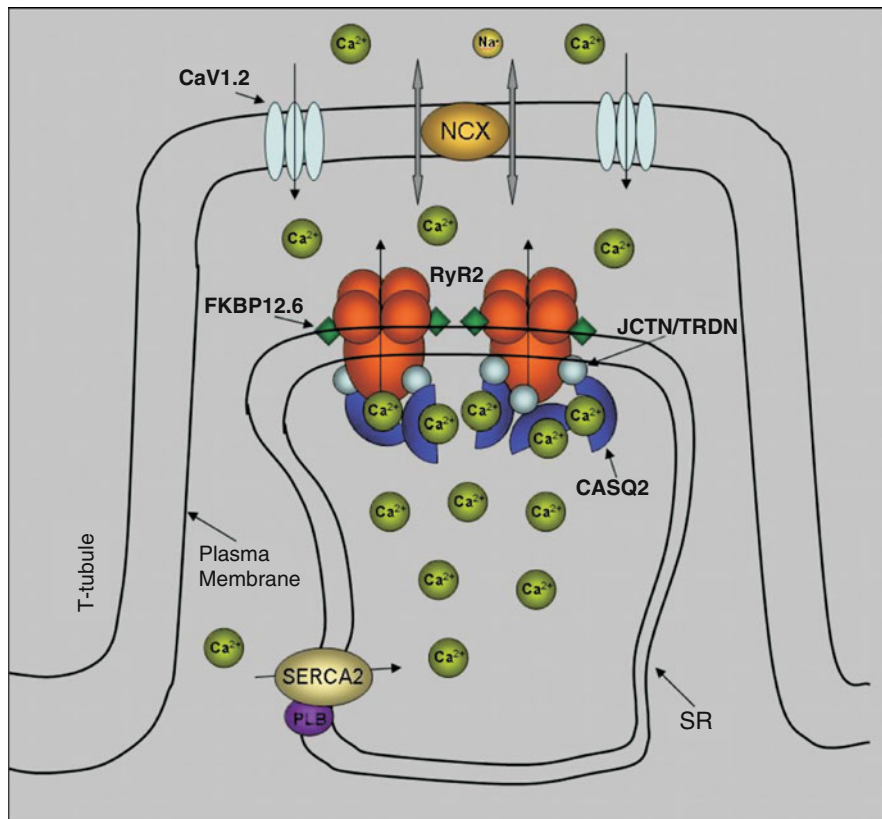


Fig. 21.1 Diagram showing the localization of the proteins involved in the pathogenesis of Ca^{2+} handling. *SR* sarcoplasmic reticulum, *NCX* sodium–calcium exchanger, *JCTN* junctin, *TRDN* triadin *SERCA* SR calcium adenosine triphosphatase, *PLB* phospholamban

(PLB). Additionally, some of the Ca^{2+} is extruded from the cell by the $\text{Na}^+/\text{Ca}^{2+}$ exchange (NCX) to balance the Ca^{2+} entry.

Spontaneous Ca^{2+} release occurs in the form of self-propagating waves of CICR that originate locally as spontaneous release events, known as Ca^{2+} sparks [14]. During diastole, individual sparks can lead to local increase in Ca^{2+} current. In the presence of calcium overload, the diastolic Ca^{2+} spark rate and SR channel sensitivity to cytosolic Ca^{2+} increase. Spontaneous Ca^{2+} waves are arrhythmogenic and induce Ca^{2+} -dependent depolarizing currents, thereby causing oscillations of the membrane potential known as delayed afterdepolarizations (DAD) [15]. When sufficiently large, DADs evoke extrasystolic APs, thereby causing triggered arrhythmias.

Substantial evidence supports the concept that changes in luminal Ca^{2+} contribute to termination of CICR and facilitate RyR2 to enter in a refractory state that suppresses diastolic Ca^{2+} release. Alterations in luminal Ca^{2+} control of Ca^{2+} release are, therefore, expected to lead to serious disruptions of the cellular Ca^{2+} cycling.

Alternative hypotheses have been advanced to explain the functional consequences of *RyR2* mutations. CPVT-associated mutations may lead to abnormal dissociation (reduced binding affinity) of the auxiliary protein FKBP12.6 from RyR2 [16]. Less RyR2-FKBP12.6 binding in turn influences channel gating causing increased diastolic Ca^{2+} leak from the sarcoplasmic reticulum (SR), a phenomenon known to favor the onset of DADs and arrhythmias. Alternatively, mutations may change RyR2 sensitivity to luminal Ca^{2+} , thus reducing the Ca^{2+} threshold required for generation of spontaneous Ca^{2+} release [17]. *CASQ2* mutations in the autosomal recessive form of CPVT also result in deregulated SR Ca^{2+} release and arrhythmogenic DADs [18–22]. This effect is due to reduced Ca^{2+} buffering properties of CASQ2 and/or by loss of CASQ2-mediated RyR2 regulation. Irrespective of which of these mechanisms is involved, the final effect is the generation of arrhythmogenic spontaneous Ca^{2+} release from the SR and generation of DADs.

21.2.2 Genetic Bases of CPVT

Most familial CPVTs show autosomal dominant pattern of inheritance. In 1999, Swan et al. [23] identified a significant linkage between the CPVT phenotype and microsatellite markers at locus 1q42-q43. Based on this information, we performed molecular screening and identified cardiac *RyR2* as the mutant CPVT gene [8]. Involvement of RyR2 in the genesis of CPVT was subsequently confirmed by several other investigators (<http://www.fsm.it/cardmoc>). A recent analysis of published *RyR2* mutations shows that they tend to cluster in 25 exons encoding 4 discrete domains of RyR2 protein: domain I (amino acid (AA) 77–466), II (AA 2246–2534), III (AA 3778–4201), and IV (AA 4497–4959) (DI-DIV). These clusters are composed of amino acid sequences highly conserved through species and among RyR isoforms [24] and are thought to be functionally important.

Soon after identification of the *RyR2* mutations in the autosomal dominant form of CPVT, Lahat et al. [9] mapped the recessive variant on chromosome 1p23-21 and subsequently identified one mutation on the *CASQ2* gene, encoding for cardiac calsequestrin. *CASQ2* mutations represent only 1–2% of all genotyped CPVTs.

More recently, based on the evidence that the patients with Andersen–Tawil syndrome may develop bidirectional ventricular tachycardia [25, 26], i.e., the typical arrhythmia observed in CPVT, it has been suggested that some CPVT cases can be explained by *KCNJ2* mutations (phenocopy). In 2007, a new autosomal recessive form of CPVT mapping on the chromosomal locus 7p14-22 was reported by Bhuiyan et al. [27], but the responsible gene has not yet been discovered.

So far, more than 70 different mutations have been associated with CPVT, and these are all single-base pair substitutions causing the substitution of an amino acid. As expected for autosomal recessive disorders, the number of families with CPVT linked to *CASQ2* mutations is fairly small. At present, only seven mutations have been discovered, and they can be inherited in homozygous or compound heterozygous form. A recent analysis from our group [28] has demonstrated that genetic screening on the *RyR2* gene is able to identify at least 60–65% of patients with the clinical phenotype; therefore, genetic screening should be recommended since it is able to identify most of the affected subjects and could then be extended to family members.

21.2.3 Mechanisms of Arrhythmias in Autosomal Dominant CPVT

The *RyR2* is a tetrameric channel that regulates the release of Ca^{2+} from SR to the cytosol during the plateau phase of the cardiac AP. When *RyR2* activity is modified/ altered leading to an increase or reduction of the amount of Ca^{2+} released, both the SR and the cytosolic Ca^{2+} concentration may be affected. This induces compensatory phenomena that tend to restore the cellular calcium balance, such as the activation of the cardiac NCX. Unfortunately, such compensatory mechanisms may be arrhythmogenic. *RyR2* function (SR Ca^{2+} release) is regulated by several accessory proteins, such as *CASQ2*, triadin, junctin, and *FKBP12.6* (Fig. 21.1). Furthermore, the adrenergic tone controls the *RyR2* channel through phosphorylation, which is a crucial step determining the amount of Ca^{2+} released from SR. Catecholamines activate protein kinase-A (PKA) and calcium-calmodulin dependent kinase II (CaMKII) that phosphorylates *RyR2* at different sites and acts as a throttle on the Ca^{2+} release process [29].

21.2.3.1 RyR2 Mutations and CPVT

The effects of *RyR2* mutations have been studied in vitro and in vivo using different experimental models. *RyR2* mutations can affect both the activation

and the inactivation of the channel in several ways. It is noteworthy that, when viewed independently from the subcellular mechanisms, the final common effect of CPVT mutations (both *RyR2* and *CASQ2*) appears similar to that of digitalis intoxication, viz. Ca^{2+} overload, activation of NCX in the forward mode, generation of transient inward NCX current (I_{ti}), and delayed after-depolarizations (DADs).

The proposed “primum movens” leading to Ca^{2+} overload is the uncontrolled Ca^{2+} release (leakage) during diastole, which is mainly detectable upon adrenergic activation [30] (phosphorylation); but according to different authors, it may already be present in the unstimulated conditions [31, 32]. Given the complexity of the SR Ca^{2+} release process, the leakage could in principle be due to several mechanisms [16, 30, 31].

21.2.3.2 RyR2–CPVT Mouse Models

Knock-in mouse models have been pivotal to the understanding of the cellular and whole-heart pathophysiology of CPVT [33–35]. Based on the assumption that by engineering RyR2–CPVT mutation in the mouse genome, it is possible to reproduce the phenotype observed in the clinical setting, the initial evidence was provided by our group in 2005. By homologous recombination, we created a conditional knock-in mouse harboring the R4496C mutation. This is the first mutation that we identified in CPVT patients and it is present in several unrelated CPVT families [34]. R4496C mice develop typical CPVT bidirectional VT in the absence of structural abnormalities [34]. This model has been instrumental to demonstrate adrenergic-dependent DADs, increased NCX-transient inward current (I_{ti}), and triggered activity as the cellular mechanisms for CPVT [36] (Fig. 21.2). In a subsequent study [37], we observed the onset of abnormal Ca^{2+} waves during diastole, which paralleled the occurrence of DAD development both at baseline and during isoproterenol superfusion. Increased propensity to DAD development in RyR2-R4496C mice was also demonstrated in isolated Purkinje

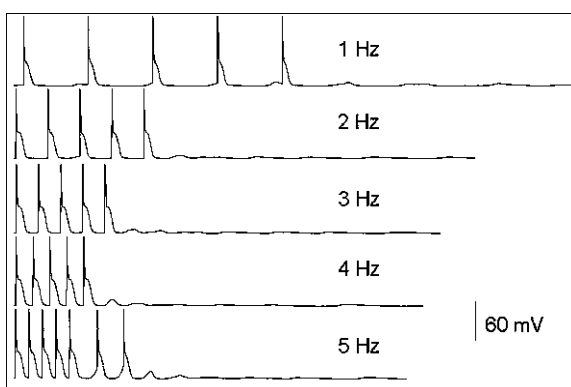


Fig. 21.2 DADs recorded from an isolated *RyR2^{R4496C+/-}* myocyte stimulated at 1–5 Hz. Note that DAD amplitude increases and DAD coupling interval decreases at faster pacing frequencies (modified from [36])

cells by Cerrone et al. [38]. Finally, additional data supporting the concept that DAD-mediated triggered activity is the arrhythmogenic mechanism for CPVT were provided by Paavola et al. [39], who recorded DADs using monophasic APs in CPVT patients.

In an optical mapping study in collaboration with Dr. Jalife and his coworkers, we showed that both polymorphic and bidirectional VT have a focal origin [38]. Epicardial optical mapping was used to demonstrate that during bidirectional VT, the ventricular beats alternatively originate from the right and from the left ventricle and arise from an area coincident with the anatomic insertion of the major bundle branches of the conduction system. Interestingly, administration of Lugol's solution that ablates the Purkinje network is able to convert bidirectional VT to monomorphic left-sided VT. In the same study, endocardial optical maps also showed that during polymorphic VT the site of origin of the beats mapped on the endocardial right ventricular wall correspond to free running Purkinje fibers. Overall these experiments support the relevant role of Purkinje network in the pathogenesis of arrhythmias in CPVT.

21.2.4 Mechanisms of Arrhythmias in Autosomal Recessive CPVT

CASQ2 has been initially described as a Ca^{2+} buffering protein resident in the SR lumen and exists in monomeric and polymeric forms. When luminal $[\text{Ca}^{2+}]$ is low, CASQ2 binds to junctin and triadin and inhibits SR calcium release from RyR2. Conversely, in the presence of a rise in luminal SR $[\text{Ca}^{2+}]$, the binding between CASQ2, triadin, and junctin is weakened and the open probability for RyR2 increases [40]. Overall evidence concurs to attribute to CASQ2 the roles of a Ca^{2+} buffer molecule and a RyR2 modulator.

21.2.4.1 CASQ2 Mutations and CPVT

Mutations in *CASQ2* that cause the autosomal recessive CPVT are rather uncommon, and so far no phenotypical differences have been identified between *CASQ2*- and RyR2-CPVT. The few *CASQ2* mutations reported so far have been extensively studied in in-vitro and in transgenic animal MODELS. In vitro studies have highlighted that the mutations may lead to major alterations in CASQ2 functions as they may impair CASQ2 polymerization, alter its buffering properties, and modify CASQ2-RyR2 interaction. Terentyev et al. [17] suggested that a reduction or absence of CASQ2, as it happens with the truncation mutants, leads to a decrease of the time necessary to reestablish Ca^{2+} storage, thus facilitating a premature activation of RyR2 and, as a consequence, diastolic Ca^{2+} leakage.

21.2.4.2 CASQ2–CPVT Mouse Models

As in the case of RyR2–CPVT, mouse models reproducing the autosomal recessive CASQ2–CPVT have provided important pathophysiological information but have also been of great value for the unraveling of some molecular mechanisms of cardiac Ca^{2+} regulation. Knollmann et al. [21] created a *CASQ2* knock-out mouse model, in which VT and ventricular fibrillation (VF) could be induced by β -adrenergic stimulation (isoproterenol) or even acute stressors such as auditory stimuli. In isolated *CASQ2* null myocytes, the authors observed increased diastolic Ca^{2+} leakage leading to DADs and triggered activity, thus proving that DADs are the common final arrhythmogenic mechanisms in RyR2- and *CASQ2*–CPVT.

More recently, we developed the *CASQ2*–R33Q/R33Q knock-in mouse model that reproduces the typical CPVT phenotype [41]. At variance with the *RyR2*–R449C model, arrhythmias in these mice occur in the presence of mild stressors (Fig. 21.3). *CASQ2*–R33Q/R33Q cardiomyocytes showed DADs and triggered activity not only during β -adrenergic stimulation but also in resting conditions [41]. Interestingly, we observed a prominent reduction of *CASQ2* in our mice with the R33Q mutation and we were able to show that mutant calsquestrin is prone to increased trypsin degradation. On the basis of these observations, it is possible to speculate that the key mechanism for autosomal recessive CPVT is the reduction in the

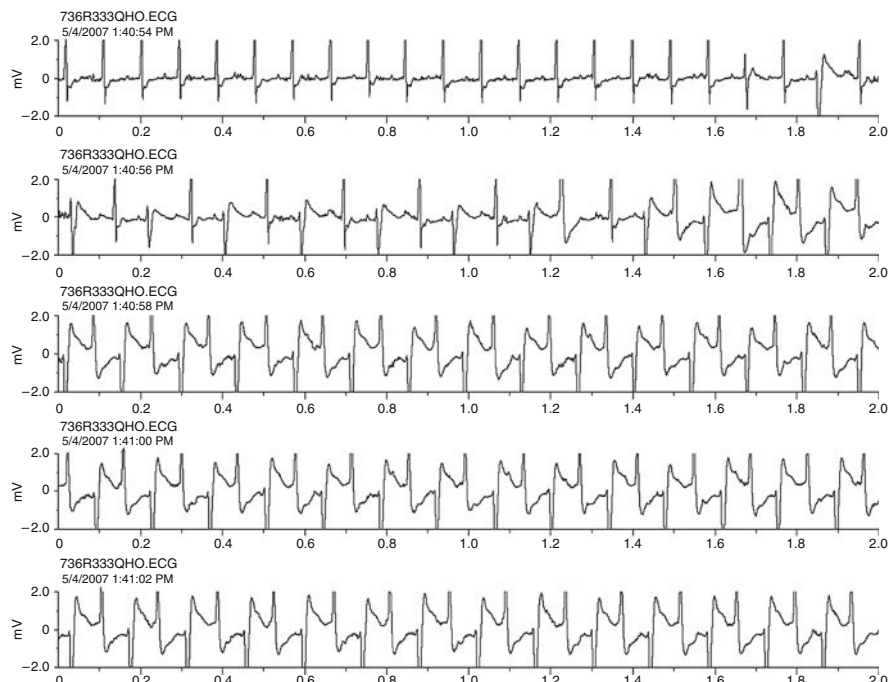


Fig. 21.3 ECG recording showing the onset of bidirectional ventricular tachycardia in a mouse model (modified from [41])

cellular content of caslequestrin that leads to an increased propensity for diastolic Ca^{2+} leak.

21.2.5 Clinical Presentation and Diagnosis

Patients with CPVT typically present with stress-induced syncope and/or sudden cardiac death [7, 8]. Symptoms can occur in early childhood [42] and the mean age of onset of the first syncope in our large cohort of CPVT [43], and recently confirmed in an additional series [44], is 12 years. In the absence of treatment, the disease is highly lethal, with an estimated incidence of sudden death of 30% before age 40 [45]. Growing evidence shows that sudden death may be the first manifestation of the disease, making prevention of lethal events a difficult task.

Individuals with CPVT show an unremarkable ECG, which also makes the diagnosis difficult. Frequently, CPVT patients seek medical attention for the evaluation of unexplained syncope; in this setting, very often they are misdiagnosed as being affected by vasovagal syncope or epilepsy since resting ECG is normal. Minor, nondiagnostic features at rest are sinus bradycardia and prominent U waves [46] (Fig. 21.4). Some authors also reported sinus bradycardia in some

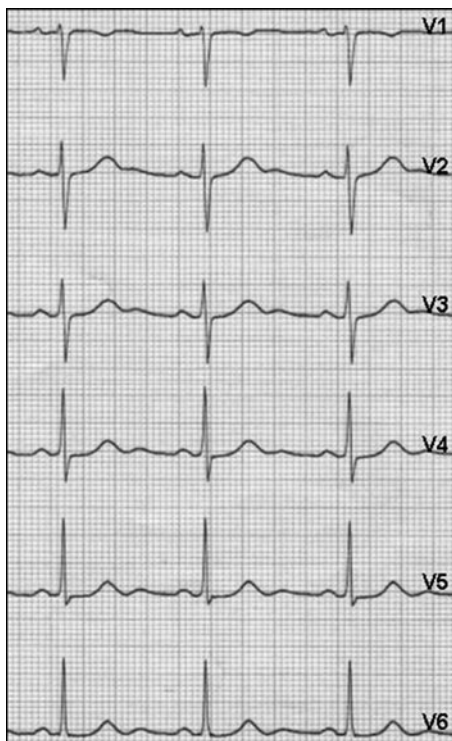


Fig. 21.4 Resting ECG in a CPVT patient showing a low heart rate and prominent U wave

CPVT patients [7, 47] and Postma et al. [47] hypothesized that bradycardia may result from impaired Ca^{2+} handling by mutant RyR2 channels in sinoatrial nodal cells. The presence of prominent U waves has also been reported, but its diagnostic value has never been systematically evaluated or demonstrated. Furthermore, a mild QT prolongation in some CPVT cases was reported [6, 7]; thus CPVT differential diagnosis should include LQTS. LQTS patients with a mild phenotype (borderline QT interval and no symptoms) do exist, but their prognosis is completely different from that of CPVT, which presents a higher incidence of sudden death and a limited response to β -blocker therapy [42, 48].

Independently from the clinical presentation (syncope or aborted sudden death), the most important clinical test to diagnose CPVT is the exercise stress test. Indeed, in clinically overt CPVT (penetrant cases), there is a highly reproducible pattern of arrhythmias evoked during exercise stress test or isoproterenol infusion [42, 49]. These observations enforce the concept that an exercise stress test should be performed in the routine evaluation of unexplained syncope, especially if adrenergic trigger is evident. The typical behavior of CPVT arrhythmias is that of a progressive worsening upon increase in workload: isolated premature beats or couplets initially appear between 90 and 110 bpm followed by runs of nonsustained or sustained VT when heart rate further increases [50] (Fig. 21.5). Supraventricular arrhythmias are also a common finding and often precede the onset of ventricular

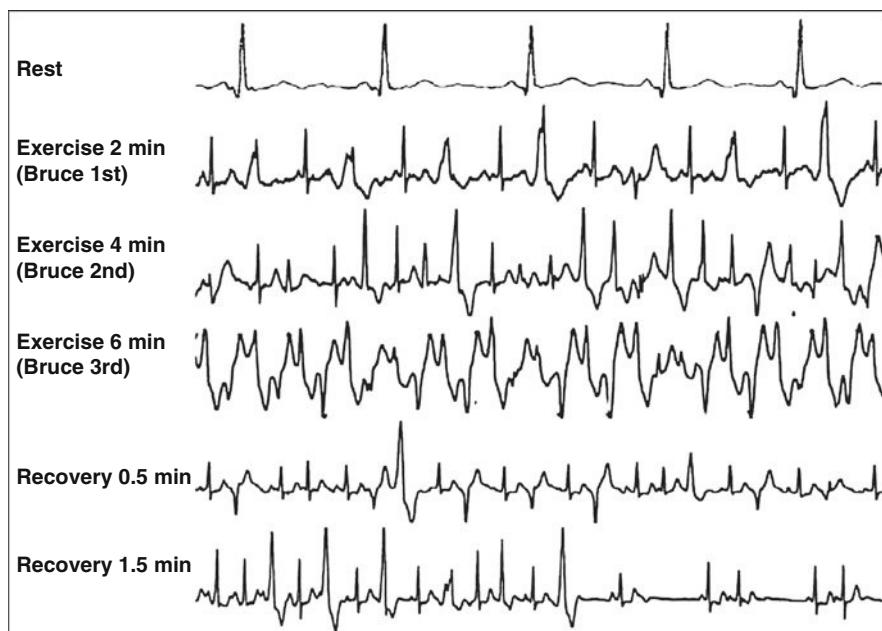


Fig. 21.5 ECG during an exercise stress test in a CPVT patient showing the onset of ventricular extrasystoles and the increase of ventricular arrhythmias before the onset of typical bidirectional ventricular tachycardia

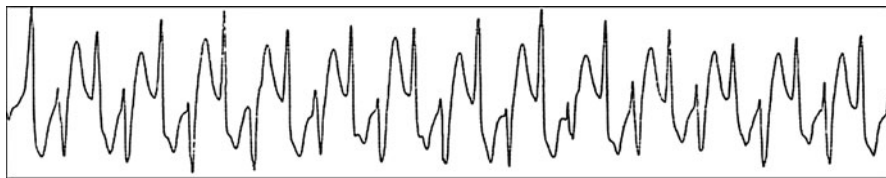


Fig. 21.6 Typical bidirectional ventricular tachycardia in a CPVT patient

arrhythmias [51]. The morphology of VT is often the hallmark of the disease: the so-called bidirectional VT [8, 42] which is characterized by a 180° beat-to-beat rotation of the axis of the QRS complexes on the frontal plane (Fig. 21.6). Although this pattern is recognizable in the majority of patients, it is important to be aware that some patients also present irregular polymorphic VT. Furthermore, the initial presentation of the disease may also be that of a VF triggered by sudden adrenergic activation [42] that may be interpreted as idiopathic VF in the absence of documentation of typical CPVT arrhythmias. Holter monitoring and implantable loop recorders may be helpful for diagnosis in such instances and especially for those patients in whom emotional triggers (alone or in combination with exercise) is more arrhythmogenic than exercise alone [52, 53].

Programmed electrical stimulation (PES) does not contribute to the clinical evaluation of CPVT patients since ventricular arrhythmias are rarely inducible in CPVT; conversely epinephrine infusion may often induce the typical pattern of VT, although its diagnostic sensitivity does not appear to be higher than that of exercise stress test.

In 2002, we reported data showing that exercise/emotion-induced syncope occurs in 67% of patients, while in 33% of families juvenile SCD was detectable [42]. These data were substantially confirmed by a Japanese group in 2003 [51], by another European study in 2005 [47], and by a follow-up reanalysis of our database on 119 patients (which showed that close to 80% of patients experience cardiac events before 40 years of age) [45]. Overall, approximately 30% of the patients have a first syncope or cardiac arrest before 10 years of age, and death or aborted cardiac arrest occurring with an incidence close to 20% up to 20 years of age.

An additional hallmark of severity is the low percentage (20%) of asymptomatic carriers of mutations in the *CPVT* genes (high penetrance) [42, 47]. Therefore, on the basis of current data, CPVT should be regarded as one of the most severe among the inherited arrhythmogenic disorders.

21.2.6 Current Therapy and Future Directions

21.2.6.1 CPVT Therapy in the Clinical Setting

Based on the evidence of the critical role of adrenergic stimulation as a trigger for arrhythmias, β -blockers were proposed as the mainstay of CPVT therapy since the

earlier reports [6, 7] and are indeed indicated both for chronic treatment as well as acute therapy of sustained ventricular tachycardia. β -blockers should be started immediately when CPVT is diagnosed; agreement in the scientific community seems to indicate nadolol as the first choice among the available options – for its once daily dosing and nonselective inhibition of adrenergic stimuli. Asymptomatic bradycardia in these patients should not be considered as a reason to reduce the dosage of β -blocker therapy. In fact, the demonstration that DADs induce triggered activity and that DAD-induced arrhythmias are facilitated by faster heart rates, provides a rationale to consider the bradycardic effect of β -blockers, an additional antiarrhythmic benefit, along with the inhibition of sympathetic drive [54].

There are conflicting evidences on the long-term effectiveness of β -blockers in the published reports. Although Leenhardt [7] and Postma [47] have reported an almost complete prevention from the recurrence of cardiac events with the exception of noncompliant patients, we [42] and others [44, 49] observed recurrences of cardiac events or incomplete protection from exercise-induced arrhythmias in CPVT patients treated with the maximally tolerated dose. In the Italian CPVT Registry, the incidence of recurrent arrhythmia while on therapy is as high as 30% [42]. In case of recurrences of syncopal episodes or VT while on therapy, the implant of an ICD should be considered. Obviously, after ICD implant β -blocker treatment should be maintained to minimize the risk of device interventions. Furthermore, in our series, 50% of implanted patients received an appropriate device intervention in a 2-year follow-up [45]. The incomplete protection afforded by β -blockers calls for the need to identify adjunctive affective therapies.

Calcium channel blockers (CCB), in particular verapamil, have been studied by different groups in a limited patient series as a possible alternative to β -blocker therapy by Swan et al. [55] and Sumitomo et al. [49]. The study of Rosso et al. [56] evaluated the efficacy of a combined association between β -blockers and verapamil: in their series, the combination of therapies reduced or even suppressed the recurrences of exercise-induced arrhythmias and/or ICD shocks. More recently, Watanabe et al. [57] reported a previously unrecognized inhibitory action of flecainide on RyR2 channels, which, together with flecainide's inhibition of Na^+ channels, was able to prevent CPVT in two individuals that had remained highly symptomatic on conventional drug therapy. Wilde et al. [58] provided preliminary evidence for a long-term effectiveness of left cardiac sympathetic denervation (LCSD) in three CPVT patients, and Scott et al. [59] reported a case of successful bilateral thorascopic sympathectomy, but patients with recurrences of sustained VT and syncope on β -blockers and LCSD are present in our cohort of CPVT patients.

21.2.6.2 Experimental Therapies for CPVT

Experiments in cell systems and CPVT animal models have been carried out to explore new therapeutic possibilities. The attempt to use FKBP12.6 stabilizing drugs [S107 [33] or K201 [60]] yielded conflicting results. Another interesting approach is that of inhibiting the effects of β -adrenergic stimulation by acting on

the downstream targets of RyR2 phosphorylation. The pharmacological inhibition of CAMKII (that phosphorylates RyR2 during adrenergic activation) is a promising approach. CAMKII phosphorylates RyR2 at different sites. Moreover, it is known that CAMKII inhibition reduces diastolic Ca^{2+} leakage and NCX- I_{ti} [61] that generates DADs. Preliminary observations from our group in the *RyR2*-R4496C/WT mouse model suggest that a specific CAMKII inhibitor, KN93 [62], could prevent arrhythmias both in vitro and in vivo, thus providing encouraging data toward novel therapeutic strategies involving this pathway.

21.3 Timothy Syndrome

Timothy syndrome (TS) is a recently described variant of long QT syndrome (LQT8) that results from mutations present in the gene encoding for the L-type calcium channel ($\text{Ca}_v1.2$). It is considered a very rare and malignant form of LQTS, with very high lethality. The high lethality in some cases is not related to the cardiac phenotype, but to extracardiac problems. Indeed, in addition to excessive prolongation of QT interval, patients affected by TS have multi-organ disorders including lethal arrhythmias, congenital heart diseases, syndactyly, development delay, metabolic disturbance, immunodeficiency, and autism.

21.3.1 L-Type Calcium Channel

The pore forming $\alpha 1$ protein responsible for L-type Ca^{2+} channel (LTCC) in heart is identified as $\text{Ca}_v1.2$ [63]. This channel is made up of $\alpha 1$, $\alpha 2/\delta$, and β subunits. The $\alpha 1$ subunit forms the ion-selective pore, the voltage sensor, the gating machinery, and the binding sites for channel-modulating drugs. β , $\alpha 2$, and δ subunits appear to have a regulatory effect [64, 65] (Fig. 21.7). $\text{Ca}_v1.2$ is the major Ca^{2+} channel

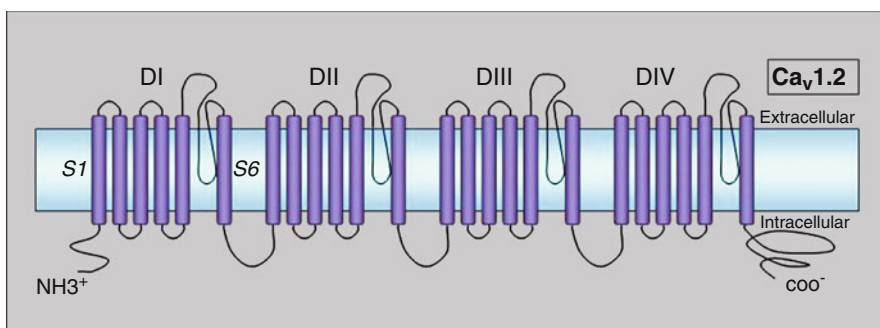


Fig. 21.7 Diagram showing predicting topology of L-type Ca^{2+} channel

expressed in ventricular myocytes. It produces a voltage-dependent inward Ca^{2+} current (I_{CaL}) that activates upon depolarization and it is a crucial player in the maintenance of the plateau of cardiac AP. Ca^{2+} ions play an important role in excitation–contraction coupling, and I_{Ca} is the critical trigger for the release of Ca^{2+} ions from the sarcoplasmic reticulum to initiate contraction. Therefore, any perturbation of LTCC is likely to induce arrhythmias. Protein kinase A (PKA), protein kinase C (PKC), and Ca^{2+} -binding protein calmodulin constitute key mechanisms that control Ca^{2+} influx. Furthermore, $\text{Ca}_v1.2$ channel activity is also enhanced by Ca^{2+} , catecholamines, and CaMKII [66].

21.3.2 Genetic Basis of Timothy Syndrome

In 2004, we identified the G1216A transition in exon 8A (an alternatively spliced exon) in *CACNA1C*, which caused the G406R amino acid replacement in DI/S6 in TS patients [67]. In 2005, Splawski et al. reported two individuals with a severe variant of TS but without syndactyly; they named this form of the disease as Timothy Syndrome type 2 (TS2) [68]. Genetic analyses showed two mutations G1216A and G1204A in exon 8, which caused G406R and G402S amino acid transitions, respectively. Exons 8 and 8A are mutually exclusive as they encode the same structural domain (DI/S6), but one of the two must be present to encode a functional channel. Familial recurrence of TS phenotype is rare. Functional in vitro characterization of G406R mutation suggested that the mutation leads to an increase of inward I_{Ca} due to loss of voltage-dependent inactivation. APs are likely to be significantly prolonged as a consequence of this TS mutation and DADs and, therefore, triggered activities are likely to be the electrophysiological mechanisms for arrhythmias in this disease.

21.3.3 Clinical Presentation and Diagnosis

The most apparent features of this syndrome are the extreme prolongation of QT interval (Fig. 21.8) associated with lethal arrhythmias and syndactyly, which may provide clues for preliminary diagnosis [69, 70]. However, other cardiac or noncardiac manifestations, including congenital heart disease, facial dysmorphisms, neuropsychiatric disorders, metabolic disturbances, immunodeficiency, and recurrent infection are also common, but may not simultaneously occur in the same TS patient. Arrhythmic events (TdP, VT, VF, or SCD) represent the most relevant cause of death in TS patients, but several other features contribute to the TS phenotype: congenital heart disease (PDA, PFO, ToF); hypertrophic cardiomyopathy and ventricular systolic dysfunction; hand/feet syndactyly; facial dysmorphisms; predisposition to sepsis; metabolic (severe hypoglycemia) and immunologic

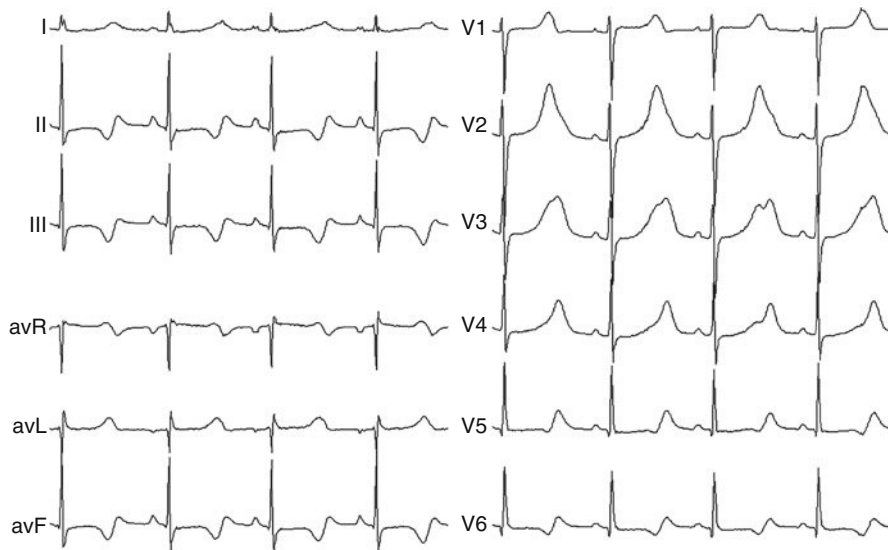


Fig. 21.8 Resting ECG in a patient with Timothy syndrome showing an important QT prolongation (recurrent infections) disturbances; neuropsychiatric involvement (autism, seizures, psychological developmental delays).

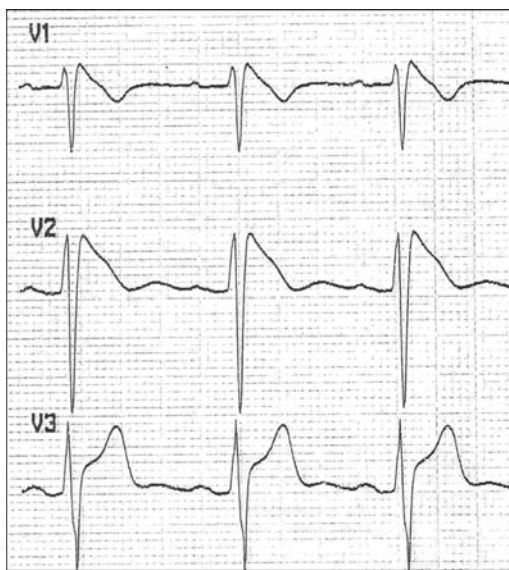
CACNA1C is highly expressed in adult heart and its mRNA is also widely expressed in multiple adult and fetal tissues, including brain, gastrointestinal system, lung, immune system, smooth muscle and testis. This may explain why a TS patient has both cardiac and extracardiac disorders even at birth. At present, most of the TS patients have been treated with β -blockers as it is considered a generally effective therapy in patients with congenital LQTS. Additional pharmacological therapies (mexiletine, CCBs) have been proposed in an attempt to shorten ventricular repolarization, restore 1:1 conduction, and reduce the risk of arrhythmias but their use has to be considered to be still in an experimental evaluation phase. The implantable defibrillator is an alternative for patients who remain at risk for cardiac arrest despite pharmacological therapy.

Finally, it is important to note that due to extensive multiorgan involvement in TS, the patients may also die due to other causes such as severe infections probably related to an altered immune response and intractable hypoglycemia.

21.4 Brugada Syndrome

Brugada syndrome (BrS) is an inherited cardiac arrhythmogenic disorder that was described as a clinical entity in 1992 [71]. It is considered a “primary electrical disease,” occurring mostly in the absence of overt structural abnormalities. The electrocardiographic diagnostic feature of the disease is the presence of an ST

Fig. 21.9 Resting ECG in a patient with Brugada syndrome showing “coved” ST segment elevation



segment elevation ≥ 2 mm in, at least, two of the three right precordial leads (V1–V3) [72], with a “coved morphology” and with incomplete or complete right bundle branch block (Fig. 21.9). The syndrome is associated with an increased risk of SCD among affected patients. The age of onset of clinical manifestations is the third to fourth decade of life, and male gender is associated with a more malignant form of the disease.

At the present time, no pharmacological therapy has proven effective in improving survival in BrS patients. Therefore, clinicians should risk stratify patients to decide whether an implantable defibrillator is needed. At present, the accuracy of risk stratification is rather poor. Conflicting evidence exists on the prognostic value of PES and no other predictors of adverse outcome are available. A consensus exists on the indication of an ICD in cardiac arrest survivors. Patients with a spontaneous pattern and history of syncope are at higher risk of cardiac arrest, and they should be regarded as candidates for an ICD. Patients with a spontaneous ST segment elevation without history of syncope present an intermediate risk of sudden cardiac death. Finally, patients with a negative phenotype or who have a diagnostic ECG only after receiving a pharmacological challenge, consisting of intravenous administration of Na^+ channel blocking agents, are at lower risk of cardiac events [73]. In symptomatic patients, the treatment of choice is the ICD.

The initial identification of mutations in cardiac Na^+ channel, *SCN5A*, was published in 1998 [74] and several *SCN5A* mutations in BrS have now been reported (<http://www.fsm.it/cardmoc>). However, *SCN5A* mutations account for no more than 20% of clinically diagnosed BrS cases. Another gene, *GPD1-L*, encoding for the glycerol-3-phosphate-dehydrogenase 1-like protein, has also been linked with the BrS. Recently, mutations in genes encoding the cardiac LTCC $\alpha 1$ subunit

(*CACNA1C*) and the $\beta 2b$ subunit (*CACNB2*) have been associated with a clinical entity encompassing a BrS phenotype combined with short QT intervals [2]. Antzelevitch et al. [2] demonstrated an association between loss-of-function mutations in the α_1 and β_{2b} subunits of LTCC and the BrS phenotype (defined as BrS types 3 and 4, respectively).

Defective Na^+ channels amplify the heterogeneity in electrical characteristics among different transmural cell types and result in voltage gradients between epicardium and endocardium that drive an electrotonic current causing ST segment elevations and arrhythmias based on transmural phase 2 reentry. By analogy, it has been suggested that a loss-of-function in LTCC activity, secondary to mutations in *CACNA1C* and *CACNB2*, may create arrhythmogenic transmural dispersion due to the preferential abbreviation of right ventricular epicardial APs. Little is known about outcome of patients affected by this new type of BrS, and further studies are needed to characterize the clinical features of these patients.

21.5 Conclusions

Although mutations only in the genes encoding for Na^+ and K^+ channels had been implicated in the genesis of inherited arrhythmogenic syndromes for several years, there is now evidence that proteins controlling intracellular Ca^{2+} abnormalities play a major role in determining genetically determined arrhythmogenic substrates. Of particular impact in the field has been the discovery of mutations in *RyR2*. This discovery has opened the field of what we could call the “sarcoplasmic reticulum diseases.” Besides *RyR2*, *CASQ2* has also been implicated in arrhythmogenesis, and it is likely that other proteins of the *RyR2* macromolecular complex and/or additional sarcoplasmic proteins that concur to regulate intracellular Ca^{2+} will be added to the list of proteins that cause inherited arrhythmias.

Finally, we now know that mutations in genes encoding different subunits of the L-type Ca^{2+} channel may cause different arrhythmogenic diseases. The paradigm of opposite phenotypes associated with loss-of-function vs. gain-of-function mutations, identified in cardiac channelopathies, holds true for mutations affecting LTCCs. Interestingly, both gain-of-function mutations that cause Timothy syndrome and loss-of-function mutations that cause an overlapping syndrome combining Brugada syndrome and Short QT syndrome seem to be very rare, suggesting that the vital role of the Ca^{2+} channel may tolerate few mutations and be otherwise noncompatible with life.

One fascinating aspect of mutations that alter cardiac cellular Ca^{2+} homeostasis is that they open the scope for very interesting investigations about possible methods to counteract these dysfunctions by acting on several molecular targets. The effort to devise novel therapeutic strategies for severe phenotypes associated with intracellular calcium handling abnormalities is the next challenge for clinicians and basic scientists in this field.

References

1. Wever EF, de Medina EO Robles. Sudden death in patients without structural heart disease. *J Am Coll Cardiol.* 2004;43:1137–44.
2. Antzelevitch C, Pollevick GD, Cordeiro JM, Casis O, Sanguinetti MC, Aizawa Y, et al. Loss-of-function mutations in the cardiac calcium channel underlie a new clinical entity characterized by ST-segment elevation, short QT intervals, and sudden cardiac death. *Circulation.* 2007; 115:442–9.
3. Gussak I, Brugada P, Brugada J, Wright RS, Kopecky SL, Chaitman BR, et al. Idiopathic short QT interval: a new clinical syndrome? *Cardiology.* 2000;94:99–102.
4. Haissaguerre M, Sacher F, Derval N, Jesel L, Deisenhofer I, de Roy L, et al. Early repolarization in the inferolateral leads: a new syndrome associated with sudden cardiac death. *J Interv Card Electrophysiol.* 2007;18:281.
5. Reid DS, Tynan M, Braidwood L, Fitzgerald GR. Bidirectional tachycardia in a child. A study using His bundle electrography. *Br Heart J.* 1975;37:339–44.
6. Coumel P, Fidelle J, Lucet V, Attuel P, Bouvrain Y. Catecholamine-induced severe ventricular arrhythmias with Adam-Stokes in children: report of four cases. *Br Heart J.* 1978; 40(Suppl):28–37.
7. Leenhardt A, Lucet V, Denjoy I, Grau F, Ngoc DD, Coumel P. Catecholaminergic polymorphic ventricular tachycardia in children. A 7-year follow-up of 21 patients. *Circulation.* 1995; 91:1512–9.
8. Priori SG, Napolitano C, Tiso N, Memmi M, Vignati G, Bloise R, et al. Mutations in the cardiac ryanodine receptor gene (*RyR2*) underlie catecholaminergic polymorphic ventricular tachycardia. *Circulation.* 2001;103:196–200.
9. Lahat H, Pras E, Olender T, Avidan N, Ben-Asher E, Man O, et al. A missense mutation in a highly conserved region of *CASQ2* is associated with autosomal recessive catecholamine-induced polymorphic ventricular tachycardia in Bedouin families from Israel. *Am J Human Genet.* 2001;69:1378–84.
10. Napolitano C, Priori SG. Diagnosis and treatment of catecholaminergic polymorphic ventricular tachycardia. *Heart Rhythm.* 2007;4:675–8.
11. Laitinen PJ, Swan H, Piippo K, Viitasalo M, Toivonen L, Kontula K. Genes, exercise and sudden death: molecular basis of familial catecholaminergic polymorphic ventricular tachycardia. *Ann Med.* 2004;36 Suppl 1:81–6.
12. Eldar M, Pras E, Lahat H. A missense mutation in the *CASQ2* gene is associated with autosomal-recessive catecholamine-induced polymorphic ventricular tachycardia. *Trends Cardiovasc Med.* 2003;13:148–51.
13. Bers DM. Cardiac excitation–contraction coupling. *Nature.* 2002;415:198–205.
14. Venetucci LA, Trafford AW, O'Neill SC, Eisner DA. The sarcoplasmic reticulum and arrhythmogenic calcium release. *Cardiovasc Res.* 2008;77:285–92.
15. Pogwizd SM, Bers DM. Cellular basis of triggered arrhythmias in heart failure. *Trends Cardiovasc Med.* 2004;14:61–6.
16. Wehrens XH, Lehnart SE, Huang F, Vest JA, Reiken SR, Mohler PJ, et al. FKBP12.6 deficiency and defective calcium release channel (ryanodine receptor) function linked to exercise-induced sudden cardiac death. *Cell.* 2003;113:829–40.
17. Jiang D, Wang R, Xiao B, Kong H, Hunt DJ, Choi P, et al. Enhanced store overload-induced Ca²⁺ release and channel sensitivity to luminal Ca²⁺ activation are common defects of *RyR2* mutations linked to ventricular tachycardia and sudden death. *Circ Res.* 2005;97: 1173–81.
18. Terentyev D, Viatchenko-Karpinski S, Györke I, Volpe P, Williams SC, Györke S. Calsequestrin determines the functional size and stability of cardiac intracellular calcium stores: mechanism for hereditary arrhythmia. *Proc Natl Acad Sci USA.* 2003;100:11759–64.

19. Terentyev D, Nori A, Santoro M, Viatchenko-Karpinski S, Kubalova Z, Gyorke I, et al. Abnormal interactions of calsequestrin with the ryanodine receptor calcium release channel complex linked to exercise induced sudden cardiac death. *Circ Res.* 2006;98:1151–8.
20. di Barletta MR, Viatchenko-Karpinski S, Nori A, Memmi M, Terentyev D, Turcato F, et al. Clinical phenotype and functional characterization of *CASQ2* mutations associated with catecholaminergic polymorphic ventricular tachycardia. *Circulation.* 2006;114:1012–9.
21. Knollmann BC, Chopra N, Hlaing T, Akin B, Yang T, Effensohn K, et al. *CASQ2* deletion causes sarcoplasmic reticulum volume increase, premature Ca^{2+} -release, and catecholaminergic polymorphic ventricular tachycardia. *J Clin Invest.* 2006;116:2510–20.
22. Dirksen WP, Lacombe VA, Chi M, Kalyanasundaram A, Viatchenko-Karpinski S, Terentyev D, et al. A mutation in calsequestrin, *CASQ2* D307H, impairs sarcoplasmic reticulum Ca^{2+} -handling and causes complex ventricular arrhythmias in mice. *Cardiovasc Res.* 2007;75:69–78.
23. Swan H, Piippo K, Viitasalo M, Heikkilä P, Paavonen T, Kainulainen K, et al. Arrhythmic disorder mapped to chromosome 1q42-q43 causes malignant polymorphic ventricular tachycardia in structurally normal hearts. *J Am Coll Cardiol.* 1999;34:2035–42.
24. George CH, Jundi H, Thomas NL, Fry DL, Lai FA. Ryanodine receptors and ventricular arrhythmias: emerging trends in mutations, mechanisms and therapies. *J Mol Cell Cardiol.* 2007;42(1):34–50.
25. Plaster NM, Tawil R, Tristani-Firouzi M, Canún S, Bendahhou S, Tsunoda A, et al. Mutations in *Kir2.1* cause the developmental and episodic electrical phenotypes of Andersen's syndrome. *Cell.* 2001;105:511–9.
26. Tristani-Firouzi M, Jensen JL, Donaldson MR, Sansone V, Meola G, Hahn A, et al. Functional and clinical characterization of *KCNJ2* mutations associated with LQT7 (Andersen syndrome). *J Clin Invest.* 2002;110:381–8.
27. Bhuiyan ZA, Hamdan MA, Shamsi ET, Postma AV, Mannens MM, Wilde AA, et al. A novel early onset lethal form of catecholaminergic polymorphic ventricular tachycardia maps to chromosome 7p14-p22. *J Cardiovasc Electrophysiol.* 2007;18:1060–6.
28. Bai R, Napolitano C, Bloise R, Monteforte N, Priori S. Yield of genetic screening in inherited cardiac channelopathies: how to prioritize access to genetic testing. *Circ Arrhythmia Electrophysiol.* 2009;2:6–15.
29. Stern MD, Cheng H. Putting out the fire: what terminates calcium-induced calcium release in cardiac muscle? *Cell Calcium.* 2004;35:591–601.
30. George CH, Higgs GV, Lai FA. Ryanodine receptor mutations associated with stress-induced ventricular tachycardia mediate increased calcium release in stimulated cardiomyocytes. *Circ Res.* 2003;93:531–40.
31. Jiang D, Xiao B, Zhang L, Chen SR. Enhanced basal activity of a cardiac Ca^{2+} release channel (ryanodine receptor) mutant associated with ventricular tachycardia and sudden death. *Circ Res.* 2002;91:218–25.
32. Jiang D, Xiao B, Yang D, Wang R, Choi P, Zhang L, et al. *RyR2* mutations linked to ventricular tachycardia and sudden death reduce the threshold for store-overload-induced Ca^{2+} release (SOICR). *Proc Natl Acad Sci USA.* 2004;101:13062–7.
33. Lehnart SE, Mongillo M, Bellinger A, Lindegger N, Chen BX, Hsueh W, et al. Leaky Ca^{2+} release channel/ryanodine receptor 2 causes seizures and sudden cardiac death in mice. *J Clin Invest.* 2008;118:2230–45.
34. Cerrone M, Colombi B, Santoro M, di Barletta MR, Scelsi M, Villani L, et al. Bidirectional ventricular tachycardia and fibrillation elicited in a knock-in mouse model carrier of a mutation in the cardiac ryanodine receptor. *Circ Res.* 2005;96:e77–82.
35. Kannankeril PJ, Mitchell BM, Goonasekera SA, Chelu MG, Zhang W, Sood S, et al. Mice with the R176Q cardiac ryanodine receptor mutation exhibit catecholamine-induced ventricular tachycardia and cardiomyopathy. *Proc Natl Acad Sci USA.* 2006;103:12179–84.

36. Liu N, Colombi B, Memmi M, Zissimopoulos S, Rizzi N, Negri S, et al. Arrhythmogenesis in catecholaminergic polymorphic ventricular tachycardia: insights from a *RyR2* R4496C knock-in mouse model. *Circ Res*. 2006;99:292–8.
37. Fernandez-Velasco M, Rueda A, Rizzi N, Benitah JP, Colombi B, Napolitano C, et al. Increased Ca²⁺ sensitivity of the ryanodine receptor mutant *RyR2*-R4496C underlies catecholaminergic polymorphic ventricular tachycardia. *Circ Res*. 2009;104:201–9.
38. Cerrone M, Noujaim SF, Tolkacheva EG, Talkachou A, O'Connell R, Berenfeld O, et al. Arrhythmogenic mechanisms in a mouse model of catecholaminergic polymorphic ventricular tachycardia. *Circ Res*. 2007;101:1039–48.
39. Paavola J, Viitasalo M, Laitinen-Forsblom PJ, Pasternack M, Swan H, Tikkanen I, et al. Mutant ryanodine receptors in catecholaminergic polymorphic ventricular tachycardia generate delayed afterdepolarizations due to increased propensity to Ca²⁺ waves. *Eur Heart J*. 2007; 28:1135–42.
40. Bers DM. Macromolecular complexes regulating cardiac ryanodine receptor function. *J Mol Cell Cardiol*. 2004;37:417–29.
41. Rizzi N, Liu N, Napolitano C, Nori A, Turcato F, Colombi B, et al. Unexpected structural and functional consequences of the R33Q homozygous mutation in cardiac calsequestrin: a complex arrhythmogenic cascade in a knock in mouse model. *Circ Res*. 2008;103:298–306.
42. Priori SG, Napolitano C, Memmi M, Colombi B, Drago F, Gasparini M, et al. Clinical and molecular characterization of patients with catecholaminergic polymorphic ventricular tachycardia. *Circulation*. 2002;106:69–74.
43. Rossenbacher T, Bloise R, De Giuli L, Raytcheva-Buono EV, Theilade J, Keegan R, et al. Catecholaminergic polymorphic ventricular tachycardia: genetics, natural history and response to therapy. *Circulation*. 2007;116(Suppl II):179.
44. Hayashi M, Denjoy I, Extramiana F, Maltret A, Buisson NR, Lupoglazoff JM, et al. Incidence and risk factors of arrhythmic events in catecholaminergic polymorphic ventricular tachycardia. *Circulation*. 2009;119:2426–34.
45. Cerrone M, Colombi B, Bloise R, Memmi M, Moncalvo C, Potenza D, et al. Clinical and molecular characterization of a large cohort of patients affected with catecholaminergic polymorphic ventricular tachycardia. *Circulation*. 2004;110(Suppl):552.
46. Aizawa Y, Komura S, Okada S, Chinushi M, Aizawa Y, Morita H, et al. Distinct U wave changes in patients with catecholaminergic polymorphic ventricular tachycardia (CPVT). *Int Heart J*. 2006;47(3):381–9.
47. Postma AV, Denjoy I, Kambllock J, Alders M, Lupoglazoff JM, Vaksmann G, et al. Catecholaminergic polymorphic ventricular tachycardia: *RyR2* mutations, bradycardia, and follow up of the patients. *J Med Genet*. 2005;42:863–70.
48. Priori SG, Napolitano C, Schwartz PJ, Grillo M, Bloise R, Ronchetti E, et al. Association of long QT syndrome loci and cardiac events among patients treated with beta-blockers. *J Am Med Assoc*. 2004;292:1341–4.
49. Sumitomo N, Harada K, Nagashima M, Yasuda T, Nakamura Y, Aragaki Y, et al. Catecholaminergic polymorphic ventricular tachycardia: electrocardiographic characteristics and optimal therapeutic strategies to prevent sudden death. *Heart*. 2003;89:66–70.
50. Liu N, Ruan Y, Priori SG. Catecholaminergic polymorphic ventricular tachycardia. *Prog Cardiovasc Dis*. 2008;51:23–30.
51. Monteforte N, Raytcheva-Buono E, Bloise R, Shakibi J, Correia MJ, Gasparini M, et al. Electrocardiographic analysis of arrhythmias developing during exercise in patients with catecholaminergic polymorphic ventricular tachycardia. *Circulation*. 2007;116(II):492.
52. Ormaetxe JM, Saez R, Arkotxa MF, Martinez-Alday JD. Catecholaminergic polymorphic ventricular tachycardia detected by an insertable loop recorder in a pediatric patient with exercise syncopal episodes. *Pediatr Cardiol*. 2004;25:693–5.
53. Hasdemir C, Priori SG, Overholt E, Lazzara R. Catecholaminergic polymorphic ventricular tachycardia, recurrent syncope, and implantable loop recorder. *J Cardiovasc Electrophysiol*. 2004;15:729.

54. Rosen MR, Danilo Jr P. Effects of tetrodotoxin, lidocaine, verapamil, and AHR-2666 on Ouabain-induced delayed afterdepolarizations in canine Purkinje fibers. *Circ Res.* 1980;46: 117–24.
55. Swan H, Laitinen P, Kontula K, Toivonen L. Calcium channel antagonism reduces exercise-induced ventricular arrhythmias in catecholaminergic polymorphic ventricular tachycardia patients with *RyR2* mutations. *J Cardiovasc Electrophysiol.* 2005;16:162–6.
56. Rosso R, Kalman JM, Rogowski O, Diamant S, Birger A, Biner S, et al. Calcium channel blockers and beta-blockers versus beta-blockers alone for preventing exercise-induced arrhythmias in catecholaminergic polymorphic ventricular tachycardia. *Heart Rhythm.* 2007; 4:1149–54.
57. Watanabe H, Chopra N, Laver D, Hwang HS, Davies SS, Roach DE, et al. Flecainide prevents catecholaminergic polymorphic ventricular tachycardia in mice and humans. *Nat Med.* 2009; 15(4):380–3.
58. Wilde AA, Bhuiyan ZA, Crotti L, Facchini M, De Ferrari GM, Paul T, et al. Left cardiac sympathetic denervation for catecholaminergic polymorphic ventricular tachycardia. *N Engl J Med.* 2008;358:2024–9.
59. Scott PA, Sandilands AJ, Morris GE, Morgan JM. Successful treatment of catecholaminergic polymorphic ventricular tachycardia with bilateral thoracoscopic sympathectomy. *Heart Rhythm.* 2008;5:1461–3.
60. Wehrens XH, Lehnart SE, Reiken SR, Deng SX, Vest JA, Cervantes D, et al. Protection from cardiac arrhythmia through ryanodine receptor-stabilizing protein calstabin2. *Science.* 2004; 304:292–6.
61. Wu Y, Roden DM, Anderson ME. Calmodulin kinase inhibition prevents development of the arrhythmogenic transient inward current. *Circ Res.* 1999;84:906–12.
62. Liu N, Colombi B, Napolitano C, Priori S. Ca^{2+} /calmodulin kinase II inhibitor abolishes and prevents triggered activity in myocytes from *RyR2*^{R4496C+/-} knock-in mice. *Heart Rhythm.* 2007;4(Suppl):S107–8.
63. Catterall WA. Structure and regulation of voltage-gated Ca^{2+} channels. *Annu Rev Cell Dev Biol.* 2000;16:521–55.
64. Hanlon MR, Wallace BA. Structure and function of voltage-dependent ion channel regulatory β subunits. *Biochemistry.* 2002;41:2886–94.
65. Klugbauer N, Marais E, Hofmann F. Calcium channel $\alpha 2\delta$ subunits: differential expression, function, and drug binding. *J Bioenerg Biomembr.* 2003;35:639–47.
66. Gurney AM, Charnet P, Pye JM, Nargeot J. Augmentation of cardiac calcium current by flash photolysis of intracellular caged- Ca^{2+} molecules. *Nature.* 1989;341:65–8.
67. Splawski I, Timothy KW, Sharpe LM, Decher N, Kumar P, Bloise R, et al. Ca(V)1.2 calcium channel dysfunction causes a multisystem disorder including arrhythmia and autism. *Cell.* 2004; 119:19–31.
68. Splawski I, Timothy KW, Decher N, Kumar P, Sachse FB, Beggs AH, et al. Severe arrhythmia disorder caused by cardiac L-type calcium channel mutations. *Proc Natl Acad Sci USA.* 2005;102:8089–96.
69. Reichenbach H, Meister EM, Theile H. The heart–hand syndrome. A new variant of disorders of heart conduction and syndactylia including osseous changes in hands and feet. *Kinderarztl Prax.* 1992;60:54–6.
70. Marks ML, Whisler SL, Clericuzio C, Keating M. A new form of long QT syndrome associated with syndactyly. *J Am Coll Cardiol.* 1995;25:59–64.
71. Brugada P, Brugada J. Right bundle branch block, persistent ST segment elevation and sudden cardiac death: a distinct clinical and electrocardiographic syndrome. A multicenter report. *J Am Coll Cardiol.* 1992;20:1391–6.
72. Antzelevitch C, Brugada P, Borggrefe M, Brugada J, Brugada R, Corrado D, et al. Brugada syndrome: report of the second consensus conference: endorsed by the Heart Rhythm Society and the European Heart Rhythm Association. *Circulation.* 2005;111:659–70.

73. Priori SG, Napolitano C, Gasparini M, Pappone C, Della Bella P, Giordano U, et al. Natural history of Brugada syndrome: insights for risk stratification and management. *Circulation*. 2002;105:1342–7.
74. Chen Q, Kirsch GE, Zhang D, Brugada R, Brugada J, Brugada P, et al. Genetic basis and molecular mechanism for idiopathic ventricular fibrillation. *Nature*. 1998;392:293–6.

Chapter 22

Molecular Mechanisms of Voltage-Gated Na⁺ Channel Dysfunction in LQT3 Syndrome

Thomas Zimmer and Klaus Benndorf

22.1 Introduction

Voltage-gated sodium channels (VGNC) mediate the fast upstroke of action potentials (APs) in electrically excitable cells by rapidly increasing the Na⁺ permeability [1]. These channels are heteromultimeric proteins consisting of a large pore-forming α subunit and small accessory β subunits. Ten different α and four β subunit isoforms have been cloned from different mammalian tissues [2]. The α subunit is composed of four homologous domains (DI–DIV) that are connected by intracellular linkers (Fig. 22.1a). Each domain contains six transmembrane spanning segments (S1–S6). The S4 regions are essential structural elements of the voltage sensor. They carry regularly arranged positive charges that respond to a depolarizing voltage pulse by a transient outward movement, thereby initiating the opening of the pore. The pore is formed by S5 and S6 segments, and the connecting extracellular loops, the so-called P loops. These P loops contain key residues for ion selectivity and tetrodotoxin binding [1]. Images derived from cryo-electron microscopy provided fascinating insight into the 3-D structure of a VGNC [3]. The channel is bell-shaped and forms a central pore that is connected to the intra- and extracellular sides by four separate branches.

The Na⁺ channel isoform Na_v1.5, encoded by the *SCN5A* gene, is the predominant α subunit in the heart and plays a key role for excitability of atrial and ventricular cardiomyocytes and for rapid impulse propagation through the conduction system [4, 5]. Electrophysiological and biochemical studies provided strong evidence in support of the expression of neuronal and skeletal muscle Na⁺ channels in the heart [6]. However, the functional significance of these isoforms for the human heart is still a matter of debate. Mutations in neuronal and skeletal muscle isoforms have not yet been linked to cardiac diseases. In contrast, mutations in *SCN5A* can cause a broad variety of pathophysiological phenotypes (Table 22.2).

T. Zimmer (✉) and K. Benndorf

Institute of Physiology II, University Hospital Jena, Friedrich Schiller University Jena, Kollegien-gasse 9, Jena 07743, Germany

e-mail: thomas.zimmer@mti.uni-jena.de

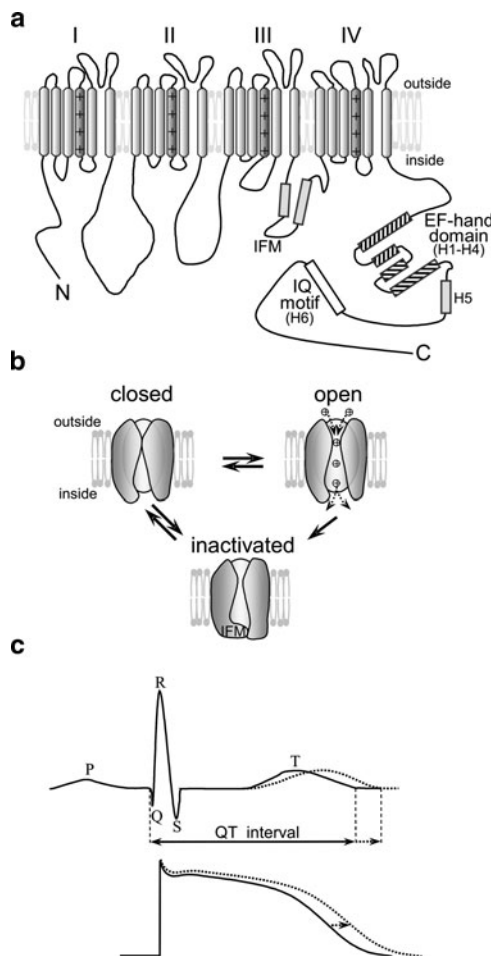


Fig. 22.1 Structure and function of the cardiac voltage-gated Na^+ channel. (a) Proposed membrane topology of $\text{Na}_v 1.5$ and important structural elements controlling channel gating. Each of the four domains (DI–IV) is composed of six transmembrane helices. The fourth segment (S4) contains regularly arranged positive charges that are essential elements of the voltage sensor. The intracellular loop between DIII and DIV forms the inactivation gate with the key residues isoleucine, phenylalanine, and methionine (IFM motif) [1]. The proximal C terminus is composed of six helices (H1–H6) [18, 19]. H1–H4 form an EF-hand domain involved in the binding of Ca^{++} , CaM and the downstream CaM binding motif (IQ motif or H6) [16, 19, 40, 41]. The linker between DIVS6 and H1 is very flexible, but highly conserved among Na^+ channels, implicating an essential role for proper interaction of the C terminus with other intracellular channel regions during inactivation [19]. (b) Functional states of voltage-gated Na^+ channels. (c) Schematic time relationship between ECG and ventricular action potential in normal (solid line) and LQT3 hearts (dotted line). The control QT interval corrected for heart rate (QTc) is <460 ms. The mean QTc in the LQT3 cases listed in Table 22.2 is 542.5 ± 82 ms (s.d.; $n = 26$ mutations)

Table 22.1 Electrophysiological properties of known LQT3 mutant channels

Mutant	QTc (ms)	$I_{\text{Na, persistent}}$	Shift of steady-state			I_{window}	$\Delta[\Delta V]$ (mV)	Current decay	Recovery	$I_{\text{Na, peak}}$	References
			Inactivation	Activation	ΔV_m (mV)						
S216L ^{a, ##}	7.8-fold	+4.7	=	+4.7		Faster	=	=	=	=	[30]
N406K	=	=	=	=		=	=	↓	=	=	[72, 73]
A572D ^{a, ##}	6.5-fold/delQ1077	=	=	=		Faster	=	=	=	=	[45, 74]
G615E ^b	=	≈	=	≈		Faster	=	↑	=	=	[30]
L618F ^{a, ##}	3.0-fold	+5.8	=	+5.8		Faster	=	=	=	=	[45, 74, 75]
L619F	R680H [#]	2.3-fold/acidosis	=	=		Faster	≈	=	=	=	[75]
S941N [#]	586	2.8-fold/delQ1077	=	=		Slower	=	=	=	=	[76]
A997S ^{a, ##}	2.6-fold	-6.0	=	-6.0		Slower	=	=	=	=	[77]
R1193Q ^{a, ##}	3.1-fold	+3.9	=	+3.9		Faster	=	=	=	=	[78]
	4.2-fold	-5.0	=	-5.0		Faster	=	=	=	=	[79]
		-5.2	=	-5.2		=	=	=	=	=	[80]
F1250L ^b	=	=	=	=		=	=	=	=	=	[75]
E1295K	480	+5.2	+3.4	+1.8		Slower					[35]
T1304M [#]	462	7.2-fold	+11.2	+6.7	+4.5	Faster					[30, 49]
N1325S	460	>9-fold	=	-6.4	+6.4	Slower					[12, 25, 81]
A1330P [#]	600	=	+8.3	=	+8.3	Slower					[36]
A1330T	500	=	+6.9	=	+6.9	Faster					[37]
P1332L	605	=	-6.4	-5.0	-1.4	Slower					[28, 82]
S1333Y [#]	=	4.3-fold	+7.0	-8.5	+15.5	Slower					[83]
F1473C	808	6.3-fold	+8.8	=	+8.8	Faster					[84, 85]
F1486L [#]	720	5.2-fold	+14.3	+3.7	+10.6	Slower					[30, 86]
delIK1500**	481	3.8-fold	-13.4	+3.0	-16.4	Slower ^d					[68]
delKPQ1505–1507	528	~10-fold	=	+6.0	-6.0	Slower ^d					[25, 87, 88]
	~10-fold	-5.8	=	=		Faster	≈	≈	≈	≈	[24]
		=	=	=		Slower ^d					[89]

(continued)

Table 22.1 (continued)

Mutant	QTC (ms)	$I_{Na, \text{persistent}}$	Shift of steady-state		I_{Window}	Current decay	Recovery	$I_{Na, \text{peak}}$	References
			Inactivation ΔV_{in} (mV)	Activation ΔV_{in} (mV)					
delOKP1507-1509	586	~7-fold ↑ at +40 mV	= -11.4 -6.6	+11.6 =	-11.6 -11.4 -6.6	Faster Slower Slower ^d	Faster Slower ↓	[90] [58] [91]	
delF1617*		↑ at -60 mV	=	-4.1	-5.8 +1.7	Slower ^d Slower Slower	Faster =	[71] [26, 92, 93]	
T1620K**	488			=	=	Slower Slower Slower	=	[27]	
R1623Q	572			= ~10-fold 4.0-fold ~4-fold	= -7.1 =	= -7.1 =	=	[94]	
R1626P	480			=	=	Slower Slower Slower	=	[28]	
R1644H				=	= +8.5	=	[25]		
R1644C				=	= +7.6 +12.0 +11.0	+7.6 +12.0 +11.0	Faster Faster Faster	[29]	
M1652R	607	2.7-fold	+7.6	=	+7.6	Slower	Faster	[28]	
V1763M	596	~3-fold	+12.0	=	+12.0	Slower	Faster	[95]	
M1766L	513	~10-fold	+11.0	=	+11.0	Slower	Faster	[96]	
II768V	497	=	+7.6	=	+7.6	=	Faster	[38, 39]	
V1777M	526	~12-fold	-12.4	= -9.0	-3.4	=	Faster	[97]	
E1784K*	485	↑ (2-4%) ↑ (1.5%)	-5.2 -14.4	+8.8 +12.5	-23.2 -27.5	=	Faster Faster	[31] [98] [99]	
D1790G	517	5.8-fold	-15.0	= -16.3 ^f	-16.3 -21.0	=	Faster Faster	[70] [100, 101] [102]	
		=	-15.0 -14.6	+6.0 +5.4	-20.0	=	≈	[103]	
		3.2-fold (+cAMP)	-14.6	=	=			[104]	
1795insD*	489		-12.4 -7.3 -9.7 -19.2	= +8.1 =	-12.4 -15.4 -9.7 -28.3	= =	Slower Slower Slower Slower	[20] [69] [105] [103]	
		↑ (6%)	=	=	=		↓	[106]	

	Y1795C ^{##}	515	4.5-fold	=	=	=	Slower	=
			4.6-fold					[107]
	L1825P ^b		8.0-fold	-11.0	+8.9	-19.9	Slower	[104]
			↑	-7.3	≈	-7.3	Slower	[108]
	R1826H [#]	46	3.0-fold	-4.9	=	-4.9	Slower	[109]
	S1904L		4.8-fold	=	=	Faster	=	[53]
	V1951L *, #, ##		2.6-fold/delQ1077	+4.7	=	+4.7	Slower	[110]
	F2004L *, #, ##		3.9-fold	+4.7	=	+4.7	Faster	[30]
	P2006A #		2.4-fold			=	Faster	[30]

The size of the persistent current was either indicated as the fraction of the sustained current relative to the peak current (in%) or as the λ -fold increase of this fraction when the control values for the wild-type h Na_v 1.5 channel were available from the original studies. Because relative shifts of steady-state activation and inactivation curves are most likely key determinants for the size of the window current (I_{window}), we attempted to quantify changes in I_{window} as $\Delta[\Delta V] = (\Delta V_h) - (\Delta V_m)$, where ΔV_h and ΔV_m are the shifts of the mid-inactivation and mid-activation potentials, respectively. Depolarizing and hyperpolarizing shifts are indicated as positive and negative values (in millivolt), respectively. Positive or negative values for $\Delta[\Delta V]$ indicate an increased or decreased I_{window} , respectively. Please note that slope alterations, which may influence I_{window} , are not considered. QTc values are from single patients, or when available, the mean QTc calculated from several mutation carriers of the same family or from different families. Overlapping phenotypes are marked as follows: * LQT3+BS, ** LQT3+CCD, *** LQT3+BS+CCD; ↓ – reduced; ↑ – increased; =, ≈ – no change or similar to wild-type Na_v 1.5; # – SIDS cases; ## – also related to AF; dark grey – gain-of-function properties; light grey – loss-of-function properties

^aThe LQTS patient also carried KCNQ1 mutation V254M [111]

^bDrug-induced LQT syndrome

^cEffects were observed in the Q1077, but not in the delQ1077 background

^dVoltage dependency of inactivation was reduced resulting in faster inactivation at less depolarized potentials, but significantly or slightly slower inactivation at more depolarized potentials

^eChannel expression was rescued by $\beta 1$ subunit, lower temperature, and mexiletine [96]. The H558R polymorphism also restored surface expression [112]

^fCoexpression with the $\beta 1$ subunit did not shift steady-state inactivation toward depolarized potentials, as observed in case of wild-type channels, resulting in reduced availability of D1790G/ $\beta 1$ channels [100]

^gThe mutation has been identified in a patient with drug-induced torsades de pointes. Cisapride restored surface expression thereby exposing the inactivation deficient mutant channel [109]

Table 22.2 Gain- and loss-of-function *SCN5A* mutations related to distinct cardiac excitation disorders

Mutant channel property	Disease phenotype	References
Gain-of-function	Long QT syndrome subtype 3 (LQT3)	[23–25]
	Sudden infant death syndrome (SIDS)	[28, 44, 52, 53]
	Atrial fibrillation (AF)	[32–34, 54]
Loss-of-function	Brugada syndrome (BrS)	[23, 55]
	Cardiac conduction disease (CCD)	[23, 56, 57]
	Sick sinus syndrome (SSS)	[58, 59]
	Atrioventricular block (AV block)	[60]
	Atrial standstill (AS)	[61]
	Atrial fibrillation (AF)	[54, 62, 63]
	Sudden infant death syndrome (SIDS)	[8]
	Dilated cardiomyopathy (DCM)	[62, 64]
	“ <i>SCN5A</i> overlap syndromes”	[23, 65, 66]
Gain- and loss-of-function	–BrS + CCD + SSS	[67]
	“ <i>SCN5A</i> overlap syndromes”	[23, 65, 66]
	–LQT3 + BrS + CCD	[68]
	–LQT3 + BrS	[69, 70]
	–LQT3 + CCD	[71]

Mutations can either result in gain-of-function or loss-of-function defects, depending on whether Na^+ entry into the cell is enhanced or reduced, respectively. Both gain-of-function and loss-of-function can be caused by an alteration of several distinct channel properties. Consequently, a single point mutation can also lead to a combination of both types of gating defects (Table 22.2), although such mutations are rare.

The most important *SCN5A* channelopathies are long QT syndrome type 3 (LQT3) and Brugada syndrome (BrS). LQT3 is caused exclusively by *SCN5A* mutations, whereas BrS has been associated with *SCN5A* mutations in less than 20% of the patients [7]. The other cardiac excitation abnormalities, listed in Table 22.2, are anything but rare. However, point mutations in *SCN5A* as the primary cause of these diseases are more the exception than the rule. For example, sudden infant death syndrome (SIDS) is a fatal event that can result from various origins, like position in crib, location of pillow, passive smoking, nonbreast feeding, or mutations in several genes including the cardiac K^+ channels *KCNQ1* and *KCNH2* [8]. *SCN5A* mutations detected in SIDS victims were investigated upon heterologous expression, and both LQT3- and BrS-type mutant channels were observed (Table 22.2). However, the situation becomes more complicated when taking into account that $\text{Na}_v1.5$ is regulated by more than ten interacting proteins [9]. In the last 3 years already nine distinct cardiac disease phenotypes have been attributed to mutations in genes coding for $\text{Na}_v1.5$ regulatory proteins. One can expect the discovery of a growing number of such mutations by future genetic screenings in cardiac cases. Defects in interacting proteins resulted in gain- or loss-of-function of wild-type $\text{Na}_v1.5$, i.e., in defects similar to those observed in mutant $\text{Na}_v1.5$ channels [9].

This chapter outlines the currently known *SCN5A* mutations linked to LQT3. We summarize the results on mutant channel function, and we discuss these functional data in terms of Na⁺ channel structure–function relationships and in terms of the impact on QTc intervals. The mutations considered herein cannot make up a complete list as considerably more mutations may have been identified by genetic screenings but not studied electrophysiologically, published, or included in online databases.

22.2 Gating Mechanism

The gating mechanism in VGNCs can be described by a simple three-state model (Fig. 22.1b). At the resting membrane potential, channels are in the closed state. Depolarization of the cell initiates the transition to the open, i.e., the conducting state. Initially, three of the four S4 segments (DI–DIII) respond to the change of membrane voltage by a fast transient outward movement across the membrane [1]. It is very likely that these charged S4 helices move along a spiral path through four distinct gating pores, visible as peripherally located transmembrane pores in images from cryo-electron microscopy [1, 3]. The transition to the inactivated state normally occurs within a few milliseconds of opening. Notably, this open-state inactivation is coupled to activation and is initiated by the S4 in domain IV [10, 11]. This positively charged segment displays a delayed response to an external voltage stimulus. It moves when the channel already conducts Na⁺. This decelerated response finally generates the signal for a movement of intracellularly located channel structures, occluding the pore and terminating Na⁺ influx. A tight channel closure is essential for an efficient AP repolarization and termination. In wild-type channels, the fraction of the Na⁺ current, that persists throughout the AP, is less than 0.3% of the transient current [12].

Three Na⁺ channel structures are essentially involved in this fast open-state inactivation. The most important structure is the inactivation gate which is formed by the DIII–DIV linker. This linker contains a cluster of the hydrophobic residues isoleucine, phenylalanine, and methionine (IFM motif) that are flanked by two α helices (Fig. 22.1a) [13]. The IFM motif in the inactivation gate serves as a lid and neighboring glycine and proline residues function as molecular hinges (“hinged-lid model”) [1]. Inactivation initiates when the inactivation gate moves toward its receptor formed by amino acid residues in DIVS6 and in intracellular loops DIIIS4/S5 and DIVS4/S5, and located within and near the intracellular mouth of the pore [1]. The third structure involved in channel inactivation is the C terminus [14]. Evidence has accumulated that the proximal half of the C terminus functionally interacts with the DIII–DIV linker, which stabilizes the inactivation gate-occluded channel and minimizes channel reopening [13]. This interaction involves calmodulin (CaM) [15–17], which can bind to a C terminal CaM binding motif (IQ motif or helix H6 in Fig. 22.1a) [16]. Interestingly, CaM is not the only Ca²⁺ sensor regulating Na_v1.5 inactivation. The channel also contains an EF-hand

domain, i.e., an intrinsic Ca^{2+} sensor (helices H1–H4 in Fig. 22.1a) [17–19]. This EF-hand domain provides structural elements not only for Ca^{2+} but also for CaM/IQ motif binding [16, 19]. Together these data indicate that channel inactivation is a complex process, involving excitation-mediated fluctuations in intracellular $[\text{Ca}^{2+}]_i$, CaM action on different $\text{Na}_v1.5$ intracellular structures, as well as Ca^{2+} sensing and IQ motif binding by an EF-hand domain. The detailed sequence of cellular events and intramolecular rearrangements in $\text{Na}_v1.5$ resulting in correct channel inactivation remains an interesting and challenging field of ongoing research.

The recovery from the inactivated state, i.e., the transition back to the closed state (Fig. 22.1b), depends on both time and membrane potential. In the closed state, the inactivation gate has returned to its initial conformation and the channel is occluded by pore residues. Upon membrane depolarization, Na^+ channels may open again, or alternatively, they may inactivate without opening (“closed-state inactivation”). The membrane potential at which half of the cardiac Na^+ channels are available for activation is a few millivolt negative to -80 mV [2]. A rise in intracellular calcium ion concentration ($[\text{Ca}^{2+}]_i$) destabilizes the inactivated state, i.e., it shifts the steady-state availability toward depolarized potentials [17, 20]. The opposite effect is seen when antiarrhythmic drugs, like lidocaine, are applied [21, 22].

Rapid opening, fast transition to the inactivated state, tight channel closure during the AP plateau and during the early phase of repolarization are essential prerequisites for the generation of proper cardiac APs and, consequently, also for normal QT intervals in the ECG. The inherited LQT syndrome is characterized by prolonged ventricular repolarization and increased QT intervals (Fig. 22.1c), predisposing to torsades de pointes (TdP), ventricular tachyarrhythmias, recurrent syncope, or even sudden cardiac death (SCD). In LQT3, mutant $\text{Na}_v1.5$ channels interfere with ventricular repolarization by antagonizing the repolarizing K^+ current, i.e., they conduct Na^+ ions when wild-type channels are normally closed. Different mutations and mechanisms leading to such a depolarizing effect are described below.

22.3 LQT3 Mutations

To our knowledge, 87 *SCN5A* mutations are known to be related to LQT3 (Fig. 22.2a). Eighty of them are missense mutations. In seven cases, nucleotide deletions ($n = 6$) or insertions ($n = 1$) caused in-frame modifications of the protein. Nonsense mutations have not yet been discovered in LQT3 patients, in contrast to many BrS mutations leading to loss-of-function. Figure 22.2a illustrates that most of the LQT3 mutations cluster in intracellular regions and that transmembrane segments as well as extracellular S1/S2 and S3/S4 regions are less frequently affected. This conclusion is true in terms of the absolute numbers of mutations (Fig. 22.2b). However, it ignores that intracellular regions form more than half of the channel protein (1,080 amino acids) [4], whereas transmembrane segments and extracellular S1/S2 plus S3/S4 regions constitute smaller protein parts (totally 551 and 68 amino acids, respectively). Figure 22.2b suggests that these three

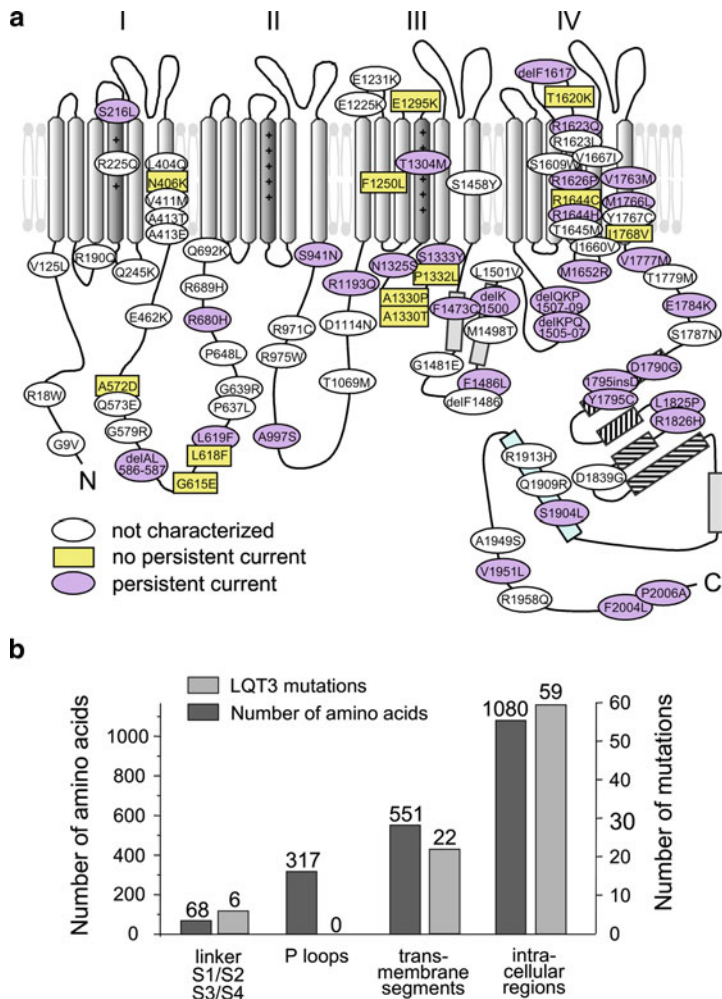


Fig. 22.2 *SCN5A* mutations associated with LQT3 (a) and their incidence in extracellular, transmembrane, and intracellular regions (b). Note that persistent currents are frequently detected in combination with other gain-of-function features (for details see Table 22.1). Q692K was associated with the *KCNQ1* mutation R562M [42]. Other references for mutations not yet characterized and thus not listed in Table 22.1 are: [43] for G9V, R225Q, G639R, S1609W; [44] for R975W; [45] for R18W, V125L, Q245K, L404Q, N406K, V411M, E462K, P637L, P648L, R971C, T1069M, E1225K, E1231K, S1458Y, G1481E, R1623L, V1667I, T1779M, Q1909R, A1949S, R1958Q; [46] for D1114N, L1501V, R1623L, S1787N; [47] for R190Q; [48] for A413T, A413E, Q573E, G579R, R689H, M1498T, I1660V, Y1767C, R1913H; [49] for T1645M; [50] for D1839G; [51] for delF1486

Na_v1.5 regions are similarly important for channel gating and inactivation (Fig. 22.2b). In contrast, LQT3 mutations were not detected in the P loops connecting S5 and S6 (totally 317 amino acids), in S1 segments (totally 93 amino

acids), or in the transmembrane part of domain 2 (228 amino acids). Consequently, gating defects leading to a clinically relevant gain-of-function can either not be achieved by mutations in these regions or generate lethality during embryonic development. In contrast to LQT3 mutations, the P loops are a preferred target for BrS and cardiac conduction disease (CCD) mutations [23].

Only 45 of the 87 mutant channels have been characterized so far by heterologous expression and electrophysiological measurements. Most of them (33 mutations) developed an increased persistent Na^+ current compared to wild-type $\text{Na}_v1.5$ (see Sect. 22.4; Fig. 22.2a and Table 22.1). For the other 12 mutants, only alternative gain-of-function mechanisms were observed (see Sect. 22.5; Fig. 22.2a and Table 22.1).

22.4 Persistent Na^+ Current: A Characteristic Feature of Most LQT3 Mutant Channels

A persistent Na^+ current is caused by a continuous flow of Na^+ through the inactivation-deficient channel during the AP plateau and repolarization phase. Such a sustained current component, schematically illustrated in Fig. 22.3a, can be expected to prolong the ventricular AP by directly counteracting repolarizing K^+ currents. This mechanism is considered as the primary cause of the disease, because most LQT3 mutations characterized so far resulted in this inactivation defect (Fig. 22.2a). The persistent inward current is still small compared to the transient inward current, indicating that even minor inactivation defects result in serious clinical consequences. For instance, in ΔKPQ channels that generate some of the largest mutation-associated persistent currents, the sustained current component is still smaller than 5% of the transient current [12, 24, 25].

Because a persistent current results from defective open-state inactivation, LQT3 mutations should indicate amino acid positions that are essential for the transition to and stabilization of the inactivated state. Those mutations indeed cluster in regions known to be involved in open-state inactivation (Fig. 22.3a). An increased persistent current was detected in all LQT3 mutations in the inactivation gate (DIII–IV linker) and in the proximal part of the C terminus, as well as in five out of nine mutations in known inactivation gate receptor regions (DIIIS4/S5, DIVS4/S5, and DIVS6). Due to the essential role of DIVS4 in coupling Na^+ channel activation to fast inactivation, it is conceivable that mutations in this S4 helix also destabilize the inactivated state. Moreover, onset of inactivation should be also delayed when gating charges are removed. Both features, i.e., decelerated current decay and a sustained inward current, are indeed intrinsic to R1623Q, R1626P, and R1644H [12, 25–28]. However, R1644C was also associated with BrS [29], and increased persistent currents through mutant R1644C channels were not reported (Table 22.1).

A persistent current caused by mutations in DI–DII and DII–DIII linkers indicates that these regions are also involved in open-state inactivation. The function of these

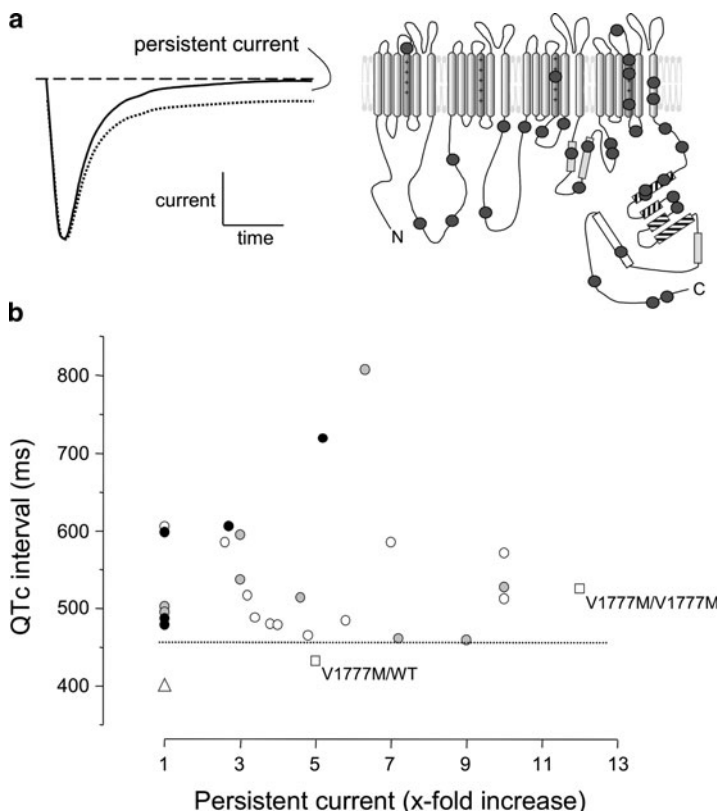


Fig. 22.3 Summary on LQT3 mutations showing enlarged persistent currents. **(a)** Schematic current traces from normally inactivating (solid line) and partially noninactivating (dotted line) channels, and distribution of corresponding mutations over the proposed $\text{Na}_v 1.5$ structure. The size of the persistent current relative to the transient current is typically between 1 and 3% in LQT3 mutants, and 0.3% in wild-type $\text{Na}_v 1.5$. **(b)** Plot of QTc intervals in LQT3 patients versus the relative persistent current in corresponding mutant channels. There is no proportional relation between both parameters. QTc values and electrophysiological properties of the mutant channels are given in Table 22.1. White dots – one additional gain-of-function mechanism, grey dots – two other gain-of-function mechanisms, black dots – three other gain-of-function mechanisms. No other gain-of-function properties were reported for V1777M [31]. The horizontal dotted line represents the borderline QTc value of 460 ms; the triangle indicates the average QTc of healthy controls. WT wild-type allele

linkers in channel inactivation is not yet clear. The distal portion of the C terminus may act in a similar way. However, deletion of this region (del1922–2016) did not result in an elevated persistent current [18], suggesting that it is not necessary for tight channel closure. Mutation S216L, located three amino acid positions upstream of the first positively charged arginine in DIS4, is the only known LQT3 mutation in an extracellular region that resulted in a robust persistent Na^+ current [30].

Published QTc values as a function of the persistent current in corresponding mutant channels are plotted in Fig. 22.3b. Remarkably, there is no obvious correlation

between the size of this noninactivating current fraction and QTc intervals in patients. QTc can be prolonged even in the absence of a persistent current, while on the other hand, relatively large persistent currents can be linked to borderline QTc values. There are several reasons for this apparent inconsistency. Firstly, several cellular, genetic, and environmental factors may considerably influence the activity of mutant channels in the intact heart [23]. Interacting proteins, *SCN5A* polymorphisms, xenobiotics, or body core temperature are examples for such modulatory factors that are often not considered when expressing mutant channels in a heterologous host. Consequently, severe electrophysiological defects, which could be expected from a life-threatening clinical phenotype, might not be detected. Such parameters may even cause variability of the QTc interval among mutant gene carriers of the same family. Second and most importantly, LQT3 is caused by multiple gain-of-function mechanisms in $\text{Na}_v1.5$ (see Sect. 22.5 below; Table 22.1). Mutant channels can be characterized by one, two, or even three additional gain-of-function mechanisms (white, grey, and black symbols in Fig. 22.3b, respectively). Figure 22.3b illustrates that most symbols for those mutant channels showing no or small persistent currents, or for those causing the most extreme QTc prolongations, are either black or grey. Furthermore, it is obvious that all data points above the dotted line, indicating the borderline QTc value of 460 ms, represent mutants with at least one alternative gain-of-function feature, suggesting that a persistent current alone is not sufficient to generate a clinically relevant LQT3 phenotype. It is intriguing to speculate that the cardiac AP can tolerate even a robust persistent current, as long as no other gain-of-function features additively counteract repolarization. This interpretation finds further support from the data of Lupoglazoff and co-workers on V1777M [31]. Only the homozygous mutation caused a serious QT prolongation (526 ms), whereas the heterozygous mutation in the parents and siblings of the index patient resulted in normal or borderline QTc intervals (415–442 ms). Heterologously expressed V1777M channels, however, generated a large persistent current (3%) that was reduced by 50% when co-expressing simultaneously wild-type and mutant channels. Alternative gain-of-function mechanisms were not reported for this mutation. Taken together these findings support the intriguing idea that an increased persistent current is one of the QTc-prolonging factors, but does not induce the LQT3 syndrome in the absence of additional gating defects.

22.5 Alternative Gain-of-Function Defects in $\text{Na}_v1.5$ Mutant Channels

Four alternative mechanisms have been suggested in LQT3 syndrome: (a) increased window current, (b) delayed onset of open-state inactivation resulting in decelerated current decay, (c) faster recovery from inactivation, and (d) a higher peak current density. As mentioned above, combinations of two or more gain-of-function features are the rule rather than the exception (Table 22.1). We would like to

emphasize that several of those alternative gain-of-function defects were also observed in Na_v1.5 mutant channels related to atrial fibrillation (AF) (K1493R, Y1795C, and M1875T in [32–34], respectively). However, patients showed normal QTc intervals (K1493R, M1875T).

A window current results from the overlap of the steady-state inactivation and steady-state activation curves (Fig. 22.4a). A small percentage of channels are not inactivated within this voltage range; they are available for activation and the depolarized membrane potential is sufficient to open them. This window current flows during the repolarization phase of the AP when the membrane slowly re-enters this voltage range. In wild-type channels, this voltage range is very narrow and the effect should be minimal (Fig. 22.4a). However, LQT3 mutations often result in relative shifts of the steady-state inactivation and activation curves or in increased slope factors of these curves (i.e., less steep curves). Such alterations in gating can increase both the critical voltage range and the magnitude of the resulting window current (Table 22.1). In many LQT3 mutants, the steady-state inactivation curve is shifted toward depolarized potentials (Fig. 22.4a), but steady-state activation is unchanged or shifted to a lesser extent into the same direction. Some of those LQT3 mutations cause critically prolonged QT intervals even in the absence of a persistent current (e.g., E1295K, A1330P, A1330T, and I1768V) [35–38]. It is interesting to note that most of those mutations cluster in structural elements known to be involved in fast channel closure, except for those located in the proximal half of the C terminus (Fig. 22.4a). Those mutations collectively reduced steady-state availability, thus creating a substrate for a loss-of-function disease finally resulting in a “SCN5A overlap syndrome” (E1784K, 1795insD; Tables 22.1 and 22.2).

A delayed onset of fast inactivation resulting in a decelerated decay of macroscopic currents is often observed not only in combination with a persistent current, but occurs also in the absence of a persistent current (Table 22.1, Fig. 22.4b). A slower current decay alone does not necessarily directly prolong the AP, but may affect voltage-dependent activity of other outward or inward currents that are crucial for AP duration. Interestingly, several of the LQT3 mutant channels show a partial loss of the voltage dependency of fast inactivation (current decay), resulting not only in accelerated inactivation kinetics at less depolarized potentials, but also in slowing of current decay at more depolarized potentials (Table 22.1). Channels showing faster current decay kinetics (Fig. 22.4b) are characterized by other gain-of-function features.

A faster recovery from inactivation, the third alternative arrhythmia mechanism, is found in most LQT3 mutant channels (Fig. 22.4c). As shown for I1768V [39], faster recovery from inactivation results in channel re-opening and thus in an increased Na⁺ current component during cardiac repolarization, which in turn prolongs the AP. A theoretical approach confirmed that a twofold increase in the recovery rate results in nearly a doubling of this inward current [39].

Larger current amplitudes could also prolong the cardiac AP, via an indirect effect on other ionic currents, or alternatively, via proportionally increased persistent currents. Currently, it is not clear whether higher current densities are specific

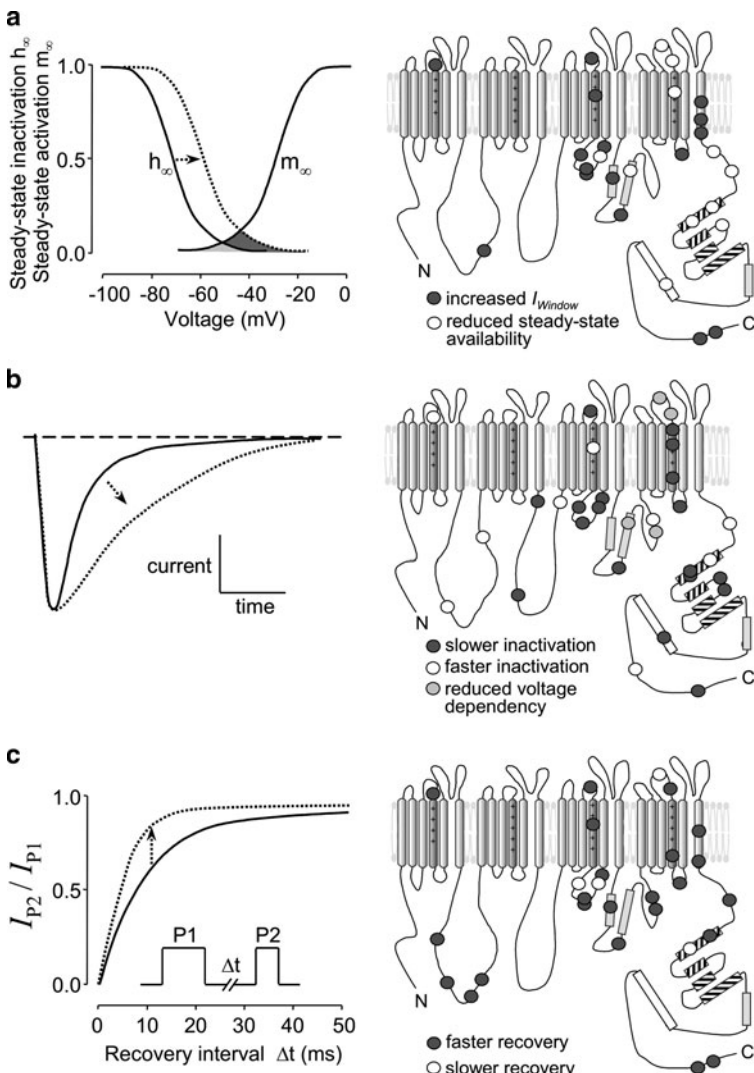


Fig. 22.4 Alternative gain-of-function mechanisms in LQT3 mutant channels. (a) An increased window or overlap current is caused by relative shifts of the steady-state inactivation and activation curves (dark grey area), as seen in 16 out of the 45 characterized LQT3 mutant channels. In most cases, only a depolarizing shift of steady-state inactivation was observed (see Table 22.1). Alterations of the steepness of both curves may also affect the window current, but were not considered in this report. (b) Slower current decay resulting from decelerated open-state inactivation was reported in 18 different LQT3 mutant channels. Interestingly, preferred targets were the S4/S5 linkers in DIII and DIV, which are part of the inactivation gate receptor. A reduced voltage dependency of inactivation, i.e., a faster inactivation at less depolarized potentials and a slower inactivation at more depolarized potentials, was preferentially seen when the inactivation gate and the extracellular S3/S4 linker in DIV were mutated. (c) Accelerated recovery from inactivation was frequently observed in LQT3 mutant channels (23 out of 45). In 4, 7, and 11 cases, recovery was decelerated, not investigated, or unchanged compared to wild-type $\text{Na}_v1.5$ (Table 22.1), respectively

for the heterologous host and whether they are indeed relevant for the patients' phenotype. The mutant channels that produced larger current densities also displayed at least one of the other gain-of-function features (Table 22.1).

22.6 Conclusions

We conclude that it is difficult to assess the contribution of an individual gain-of-function defect for a QTc prolongation, and for the severity of the clinical phenotype. Definitely, LQT3 is caused by multiple gain-of-function gating defects in Na_v1.5 mutant channels, and an increased persistent current is only one of the key QTc prolonging factors. However, this inactivation defect seems not to be sufficient, suggesting that ventricular cells can somehow tolerate such a late current, at least in heterozygous mutant gene carriers. Moreover, as shown in Table 22.1 and Fig. 22.4, some LQT3 mutant channels showed also loss-of-function properties, like faster open-state inactivation or reduced steady-state availability. These properties may counteract QT prolongation. They may even lead to a diagnosed combination of a gain-of-function and loss-of-function disease, resulting in a "SCN5A overlap syndrome".

References

1. Catterall WA. From ionic currents to molecular mechanisms: the structure and function of voltage-gated sodium channels. *Neuron*. 2000;26:13–25.
2. Catterall WA, Goldin AL, Waxman SG. International Union of Pharmacology. XLVII. Nomenclature and structure–function relationships of voltage-gated sodium channels. *Pharmacol Rev*. 2005;57:397–409.
3. Sato C, Ueno Y, Asai K, Takahashi K, Sato M, Engel A, et al. The voltage-sensitive sodium channel is a bell-shaped molecule with several cavities. *Nature*. 2001;409:1047–51.
4. Gellens ME, George Jr AL, Chen LQ, Chahine M, Horn R, Barchi RL, et al. Primary structure and functional expression of the human cardiac tetrodotoxin-insensitive voltage-dependent sodium channel. *Proc Natl Acad Sci USA*. 1992;89:554–8.
5. Blechschmidt S, Haufe V, Benndorf K, Zimmer T. Voltage-gated Na⁺ channel transcript patterns in the mammalian heart are species-dependent. *Prog Biophys Mol Biol*. 2008;98:309–18.
6. Haufe V, Chamberland C, Dumaine R. The promiscuous nature of the cardiac sodium current. *J Mol Cell Cardiol*. 2007;42:469–77.
7. Schulze-Bahr E, Eckardt L, Breithardt G, Seidl K, Wichter T, Wolpert C, et al. Sodium channel gene (*SCN5A*) mutations in 44 index patients with Brugada syndrome: different incidences in familial and sporadic disease. *Hum Mutat*. 2003;21:651–2.
8. Otagiri T, Kijima K, Osawa M, Ishii K, Makita N, Matoba R, et al. Cardiac ion channel gene mutations in sudden infant death syndrome. *Pediatr Res*. 2008;64:482–7.
9. Abriel H. Cardiac sodium channel Na_v1.5 and interacting proteins: Physiology and pathophysiology. *J Mol Cell Cardiol*. 2010;48:2–11.

10. Sheets MF, Kyle JW, Kallen RG, Hanck DA. The Na channel voltage sensor associated with inactivation is localized to the external charged residues of domain IV, S4. *Biophys J.* 1999;77:747–57.
11. Chanda B, Bezanilla F. Tracking voltage-dependent conformational changes in skeletal muscle sodium channel during activation. *J Gen Physiol.* 2002;120:629–45.
12. Dumaine R, Wang Q, Keating MT, Hartmann HA, Schwartz PJ, Brown AM, et al. Multiple mechanisms of Na^+ channel-linked long-QT syndrome. *Circ Res.* 1996;78:916–24.
13. Motoike HK, Liu H, Glaaser IW, Yang AS, Tateyama M, Kass RS. The Na^+ channel inactivation gate is a molecular complex: a novel role of the COOH-terminal domain. *J Gen Physiol.* 2004;123:155–65.
14. Mantegazza M, Yu FH, Catterall WA, Scheuer T. Role of the C-terminal domain in inactivation of brain and cardiac sodium channels. *Proc Natl Acad Sci USA.* 2001;98:15348–53.
15. Kim J, Ghosh S, Liu H, Tateyama M, Kass RS, Pitt GS. Calmodulin mediates Ca^{2+} sensitivity of sodium channels. *J Biol Chem.* 2004;279:45004–12.
16. Shah VN, Wingo TL, Weiss KL, Williams CK, Balser JR, Chazin WJ. Calcium-dependent regulation of the voltage-gated sodium channel hH1: intrinsic and extrinsic sensors use a common molecular switch. *Proc Natl Acad Sci USA.* 2006;103:3592–7.
17. Potet F, Chagot B, Anghelescu M, Viswanathan PC, Stepanovic SZ, Kupershmidt S, et al. Functional interactions between distinct sodium channel cytoplasmic domains through the action of calmodulin. *J Biol Chem.* 2009;284:8846–54.
18. Cormier JW, Rivolta I, Tateyama M, Yang AS, Kass RS. Secondary structure of the human cardiac Na^+ channel C terminus: evidence for a role of helical structures in modulation of channel inactivation. *J Biol Chem.* 2002;277:9233–41.
19. Chagot B, Potet F, Balser JR, Chazin WJ. Structure of the C-terminal EF-hand domain of human cardiac sodium channel $\text{Na}_v1.5$. *J Biol Chem.* 2009;284:6436–45.
20. Biswas S, DiSilvestre D, Tian Y, Halperin VL, Tomaselli GF. Calcium-mediated dual-mode regulation of cardiac sodium channel gating. *Circ Res.* 2009;104:870–8.
21. Nuss HB, Kambouris NG, Marbán E, Tomaselli GF, Balser JR. Isoform-specific lidocaine block of sodium channels explained by differences in gating. *Biophys J.* 2000;78:200–10.
22. Hanck DA, Nikitina E, McNulty MM, Fozzard HA, Lipkind GM, Sheets MF. Using lidocaine and benzocaine to link sodium channel molecular conformations to state-dependent antiarrhythmic drug affinity. *Circ Res.* 2009;105:492–9.
23. Zimmer T, Surber R. *SCN5A* channelopathies – an update on mutations and mechanisms. *Prog Biophys Mol Biol.* 2008;98:120–36.
24. Bennett PB, Yazawa K, Makita N, George Jr AL. Molecular mechanism for an inherited cardiac arrhythmia. *Nature.* 1995;376:683–5.
25. Wang DW, Yazawa K, George Jr AL, Bennett PB. Characterization of human cardiac Na^+ channel mutations in the congenital long QT syndrome. *Proc Natl Acad Sci USA.* 1996;93:13200–5.
26. Kambouris NG, Nuss HB, Johns DC, Tomaselli GF, Marban E, Balser JR. Phenotypic characterization of a novel long-QT syndrome mutation (R1623Q) in the cardiac sodium channel. *Circulation.* 1998;97:640–4.
27. Makita N, Shirai N, Nagashima M, Matsuoka R, Yamada Y, Tohse N, et al. A de novo missense mutation of human cardiac Na^+ channel exhibiting novel molecular mechanisms of long QT syndrome. *FEBS Lett.* 1998;423:5–9.
28. Ruan Y, Liu N, Bloise R, Napolitano C, Priori SG. Gating properties of *SCN5A* mutations and the response to mexiletine in long-QT syndrome type 3 patients. *Circulation.* 2007;116:1137–44.
29. Frustaci A, Priori SG, Pieroni M, Chimenti C, Napolitano C, Rivolta I, et al. Cardiac histological substrate in patients with clinical phenotype of Brugada syndrome. *Circulation.* 2005;112:3680–7.
30. Wang DW, Desai RR, Crotti L, Arnestad M, Insolia R, Pedrazzini M, et al. Cardiac sodium channel dysfunction in sudden infant death syndrome. *Circulation.* 2007;115:368–76.

31. Lupoglazoff JM, Cheav T, Baroudi G, Berthet M, Denjoy I, Cauchemez B, et al. Homozygous *SCN5A* mutation in long-QT syndrome with functional two-to-one atrioventricular block. *Circ Res.* 2001;89:E16–21.
32. Li Q, Huang H, Liu G, Lam K, Rutberg J, Green MS, et al. Gain-of-function mutation of Na_v1.5 in atrial fibrillation enhances cellular excitability and lowers the threshold for action potential firing. *Biochem Biophys Res Commun.* 2009;380:132–7.
33. Benito B, Brugada R, Perich RM, Lizotte E, Cinca J, Mont L, et al. A mutation in the sodium channel is responsible for the association of long QT syndrome and familial atrial fibrillation. *Heart Rhythm.* 2008;5:1434–40.
34. Makiyama T, Akao M, Shizuta S, Doi T, Nishiyama K, Oka Y, et al. A novel *SCN5A* gain-of-function mutation M1875T associated with familial atrial fibrillation. *J Am Coll Cardiol.* 2008;52:1326–34.
35. Abriel H, Cabo C, Wehrens XH, Rivolta I, Motoike HK, Memmi M, et al. Novel arrhythmic mechanism revealed by a long-QT syndrome mutation in the cardiac Na⁺ channel. *Circ Res.* 2001;88:740–5.
36. Wedekind H, Smits JP, Schulze-Bahr E, Arnold R, Veldkamp MW, Bajanowski T, et al. De novo mutation in the *SCN5A* gene associated with early onset of sudden infant death. *Circulation.* 2001;104:1158–64.
37. Smits JP, Veldkamp MW, Bezzina CR, Bhuiyan ZA, Wedekind H, Schulze-Bahr E, et al. Substitution of a conserved alanine in the domain III S4–S5 linker of the cardiac sodium channel causes long QT syndrome. *Cardiovasc Res.* 2005;67:459–66.
38. Rivolta I, Clancy CE, Tateyama M, Liu H, Priori SG, Kass RS. A novel *SCN5A* mutation associated with long QT-3: altered inactivation kinetics and channel dysfunction. *Physiol Genomics.* 2002;10:191–7.
39. Clancy CE, Tateyama M, Liu H, Wehrens XH, Kass RS. Non-equilibrium gating in cardiac Na⁺ channels: an original mechanism of arrhythmia. *Circulation.* 2003;107:2233–7.
40. Wingo TL, Shah VN, Anderson ME, Lybrand TP, Chazin WJ, Balser JR. An EF-hand in the sodium channel couples intracellular calcium to cardiac excitability. *Nat Struct Mol Biol.* 2004;11:219–25.
41. Miloushev VZ, Levine JA, Arbing MA, Hunt JF, Pitt GS, Palmer 3rd AG. Solution structure of the Na_v1.2 C-terminal EF-hand domain. *J Biol Chem.* 2009;284:6446–54.
42. Van Langen IM, Birnie E, Alders M, Jongbloed RJ, Le Marec H, Wilde AA. The use of genotype-phenotype correlations in mutation analysis for the long QT syndrome. *J Med Genet.* 2003;40:141–5.
43. Millat G, Chevalier P, Restier-Miron L, Da Costa A, Bouvagnet P, Kugener B, et al. Spectrum of pathogenic mutations and associated polymorphisms in a cohort of 44 unrelated patients with long QT syndrome. *Clin Genet.* 2006;70:214–27.
44. Millat G, Kugener B, Chevalier P, Chahine M, Huang H, Malicier D, et al. Contribution of long-QT syndrome genetic variants in sudden infant death syndrome. *Pediatr Cardiol.* 2009;30:502–9.
45. Tester DJ, Will ML, Haglund CM, Ackerman MJ. Compendium of cardiac channel mutations in 541 consecutive unrelated patients referred for long QT syndrome genetic testing. *Heart Rhythm.* 2005;2:507–17.
46. Splawski I, Shen J, Timothy KW, Lehmann MH, Priori S, Robinson JL, et al. Spectrum of mutations in long-QT syndrome genes. *KVLQT1, HERG, SCN5A, KCNE1, and KCNE2.* *Circulation.* 2000;102:1178–85.
47. Chung SK, MacCormick JM, McCullery CH, Crawford J, Eddy CA, Mitchell EA, et al. Long QT and Brugada syndrome gene mutations in New Zealand. *Heart Rhythm.* 2007;4:1306–14.
48. Napolitano C, Priori SG, Schwartz PJ, Bloise R, Ronchetti E, Nastoli J, et al. Genetic testing in the long QT syndrome: development and validation of an efficient approach to genotyping in clinical practice. *J Am Med Assoc.* 2005;294:2975–80.

49. Wattanasirichaigoon D, Vesely MR, Duggal P, Levine JC, Blume ED, Wolff GS, et al. Sodium channel abnormalities are infrequent in patients with long QT syndrome: identification of two novel *SCN5A* mutations. *Am J Med Genet.* 1999;86:470–6.
50. Benhorin J, Goldmit M, MacCluer JW, Blangero J, Goffen R, Leibovitch A, et al. Identification of a new *SCN5A* mutation, D1840G, associated with the long QT syndrome. *Mutations in brief no. 153. Online. Hum Mutat.* 1998;12:72.
51. Yamamura K, Muneuchi J, Uike K, Ikeda K, Inoue H, Takahata Y, Shiokawa Y, Yoshikane Y, Makiyama T, Horie M, Hara T. A novel *SCN5A* mutation associated with the linker between III and IV domains of Na_v1.5 in a neonate with fatal long QT syndrome. *Int J Cardiol.* 2010;145:61–4.
52. Schwartz PJ, Priori SG, Dumaine R, Napolitano C, Antzelevitch C, Stramba-Badiale M, et al. A molecular link between the sudden infant death syndrome and the long-QT syndrome. *N Engl J Med.* 2000;343:262–7.
53. Ackerman MJ, Siu BL, Sturner WQ, Tester DJ, Valdivia CR, Makielski JC, et al. Postmortem molecular analysis of *SCN5A* defects in sudden infant death syndrome. *J Am Med Assoc.* 2001;286:2264–9.
54. Darbar D, Kannankeril PJ, Donahue BS, Kucera G, Stubblefield T, Haines JL, et al. Cardiac sodium channel (*SCN5A*) variants associated with atrial fibrillation. *Circulation.* 2008;117:1927–35.
55. Chen Q, Kirsch GE, Zhang D, Brugada R, Brugada J, Brugada P, et al. Genetic basis and molecular mechanism for idiopathic ventricular fibrillation. *Nature.* 1998;392:293–6.
56. Tan HL, Bink-Boelkens MT, Bezzina CR, Viswanathan PC, Beaufort-Krol GC, van Tintelen PJ, et al. A sodium-channel mutation causes isolated cardiac conduction disease. *Nature.* 2001;409:1043–7.
57. Schott JJ, Alshinawi C, Kyndt F, Probst V, Hoornje TM, Hulsbeek M, et al. Cardiac conduction defects associate with mutations in *SCN5A*. *Nat Genet.* 1999;23:20–1.
58. Benson DW, Wang DW, Dyment M, Knilans TK, Fish FA, Strieper MJ, et al. Congenital sick sinus syndrome caused by recessive mutations in the cardiac sodium channel gene (*SCN5A*). *J Clin Invest.* 2003;112:1019–28.
59. Lei M, Huang CL, Zhang Y. Genetic Na⁺ channelopathies and sinus node dysfunction. *Prog Biophys Mol Biol.* 2008;98:171–8.
60. Wang DW, Viswanathan PC, Balser JR, George Jr AL, Benson DW. Clinical, genetic, and biophysical characterization of *SCN5A* mutations associated with atrioventricular conduction block. *Circulation.* 2002;105:341–6.
61. Groenewegen WA, Firouzi M, Bezzina CR, Vliex S, van Langen IM, Sandkuyl L, et al. A cardiac sodium channel mutation cosegregates with a rare connexin40 genotype in familial atrial standstill. *Circ Res.* 2003;92:14–22.
62. Olson TM, Michels VV, Ballew JD, Reyna SP, Karst ML, Herron KJ, et al. Sodium channel mutations and susceptibility to heart failure and atrial fibrillation. *J Am Med Assoc.* 2005;293:447–54.
63. Ellinor PT, Nam EG, Shea MA, Milan DJ, Ruskin JN, MacRae CA. Cardiac sodium channel mutation in atrial fibrillation. *Heart Rhythm.* 2008;5:99–105.
64. Bezzina CR, Remme CA. Dilated cardiomyopathy due to sodium channel dysfunction: what is the connection? *Circ Arrhythmia Electrophysiol.* 2008;1:80–2.
65. Remme CA, Wilde AAM, Bezzina CR. Cardiac sodium channel overlap syndromes: different faces of *SCN5A* mutations. *Trends Cardiovasc Med.* 2008;18:78–87.
66. Makita N. Phenotypic overlap of cardiac sodium channelopathies: individual-specific or mutation-specific? *Circ J.* 2009;73:810–7.
67. Smits JP, Koopmann TT, Wilders R, Veldkamp MW, Ophof T, Bhuiyan ZA, et al. A mutation in the human cardiac sodium channel (E161K) contributes to sick sinus syndrome, conduction disease and Brugada syndrome in two families. *J Mol Cell Cardiol.* 2005;38:969–81.

68. Grant AO, Carboni MP, Neplioueva V, Starmer CF, Memmi M, Napolitano C, et al. Long QT syndrome, Brugada syndrome, and conduction system disease are linked to a single sodium channel mutation. *J Clin Invest.* 2002;110:1201–9.
69. Bezzina C, Veldkamp MW, van Den Berg MP, Postma AV, Rook MB, Viersma JW, et al. A single Na⁺ channel mutation causing both long-QT and Brugada syndromes. *Circ Res.* 1999;85:1206–13.
70. Makita N, Behr E, Shimizu W, Horie M, Sunami A, Crotti L, et al. The E1784K mutation in *SCN5A* is associated with mixed clinical phenotype of type 3 long QT syndrome. *J Clin Invest.* 2008;118:2219–29.
71. Surber R, Hensellek S, Prochnau D, Werner GS, Benndorf K, Figulla HR, et al. Combination of cardiac conduction disease and long QT syndrome caused by mutation T1620K in the cardiac sodium channel. *Cardiovasc Res.* 2008;77:740–8.
72. Xiao YF, Ke Q, Wang SY, Yang Y, Wang GK, Morgan JP, et al. Point mutations in alpha-subunit of human cardiac Na⁺ channels alter Na⁺ current kinetics. *Biochem Biophys Res Commun.* 2001;281:45–52.
73. Xiao YF, Ke Q, Wang SY, Auktor K, Yang Y, Wang GK, et al. Single point mutations affect fatty acid block of human myocardial sodium channel alpha subunit Na⁺ channels. *Proc Natl Acad Sci USA.* 2001;98:3606–11.
74. Albert CM, Nam EG, Rimm EB, Jin HW, Hajjar RJ, Hunter DJ, et al. Cardiac sodium channel gene variants and sudden cardiac death in women. *Circulation.* 2008;117:16–23.
75. Yang P, Kanki H, Drolet B, Yang T, Wei J, Viswanathan PC, et al. Allelic variants in long-QT disease genes in patients with drug-associated torsades de pointes. *Circulation.* 2002;105:1943–8.
76. Wehrens XH, Rossenbacker T, Jongbloed RJ, Gewillig M, Heidbüchel H, Doevedans PA, et al. A novel mutation L619F in the cardiac Na⁺ channel *SCN5A* associated with long-QT syndrome (LQT3): a role for the I-II linker in inactivation gating. *Hum Mutat.* 2003;21:552.
77. Wang Q, Chen S, Chen Q, Wan X, Shen J, Hoeltge GA, et al. The common *SCN5A* mutation R1193Q causes LQTS-type electrophysiological alterations of the cardiac sodium channel. *J Med Genet.* 2004;41:e66.
78. Vatta M, Dumaine R, Varghese G, Richard TA, Shimizu W, Aihara N, et al. Genetic and biophysical basis of sudden unexplained nocturnal death syndrome (SUNDS), a disease allelic to Brugada syndrome. *Hum Mol Genet.* 2002;11:337–45.
79. Tan BH, Valdivia CR, Rok BA, Ye B, Ruwaldt KM, Tester DJ, et al. Common human *SCN5A* polymorphisms have altered electrophysiology when expressed in Q1077 splice variants. *Heart Rhythm.* 2005;2:741–7.
80. Huang H, Zhao J, Barrane FZ, Champagne J, Chahine M, Na,1.5/R1193Q polymorphism is associated with both long QT and Brugada syndromes. *Can J Cardiol.* 2006;22:309–13.
81. Yong SL, Ni Y, Zhang T, Tester DJ, Ackerman MJ, Wang QK. Characterization of the cardiac sodium channel *SCN5A* mutation, N1325S, in single murine ventricular myocytes. *Biochem Biophys Res Commun.* 2007;352:378–83.
82. Kehl HG, Haverkamp W, Rellensmann G, Yelbuz TM, Krasemann T, Vogt J, et al. Images in cardiovascular medicine. Life-threatening neonatal arrhythmia: successful treatment and confirmation of clinically suspected extreme long QT-syndrome-3. *Circulation.* 2004;109: e205–6.
83. Huang H, Millat G, Rodriguez-Lafrasse C, Rousson R, Kugener B, Chevalier P, et al. Biophysical characterization of a new *SCN5A* mutation S1333Y in a SIDS infant linked to long QT syndrome. *FEBS Lett.* 2009;583:890–6.
84. Bankston JR, Yue M, Chung W, Spyres M, Pass RH, Silver E, et al. A novel and lethal de novo LQT-3 mutation in a newborn with distinct molecular pharmacology and therapeutic response. *PLoS One.* 2007;2:e1258.
85. Silver ES, Liberman L, Chung WK, Spotnitz HM, Chen JM, Ackerman MJ, et al. Long QT syndrome due to a novel mutation in *SCN5A*: treatment with ICD placement at 1 month and

- left cardiac sympathetic denervation at 3 months of age. *J Interv Card Electrophysiol.* 2009;26:41–5.
86. Arnestad M, Crotti L, Rognum TO, Insolia R, Pedrazzini M, Ferrandi C, et al. Prevalence of long-QT syndrome gene variants in sudden infant death syndrome. *Circulation.* 2007;115:361–7.
 87. Schwartz PJ, Priori SG, Locati EH, Napolitano C, Cantù F, Towbin JA, et al. Long QT syndrome patients with mutations of the *SCN5A* and *HERG* genes have differential responses to Na^+ channel blockade and to increases in heart rate. Implications for gene-specific therapy. *Circulation.* 1995;92:3381–6.
 88. Zareba W, Sattari MN, Rosero S, Couderc JP, Moss AJ. Altered atrial, atrioventricular, and ventricular conduction in patients with the long QT syndrome caused by the DeltaKPQ *SCN5A* sodium channel gene mutation. *Am J Cardiol.* 2001;88:1311–4.
 89. Chandra R, Starmer CF, Grant AO. Multiple effects of KPQ deletion mutation on gating of human cardiac Na^+ channels expressed in mammalian cells. *Am J Physiol.* 1998;274:H1643–54.
 90. Keller DI, Acharfi S, Delacréz E, Benamar N, Rotter M, Pfammatter JP, et al. A novel mutation in *SCN5A*, delQKP 1507–1509, causing long QT syndrome: role of Q1507 residue in sodium channel inactivation. *J Mol Cell Cardiol.* 2003;35:1513–21.
 91. Chen T, Inoue M, Sheets MF. Reduced voltage dependence of inactivation in the *SCN5A* sodium channel mutation delF1617. *Am J Physiol Heart Circ Physiol.* 2005;288:H2666–76.
 92. Miller TE, Estrella E, Myerburg RJ, Garcia de Viera J, Moreno N, Rusconi P, et al. Recurrent third-trimester fetal loss and maternal mosaicism for long-QT syndrome. *Circulation.* 2004;109:3029–34.
 93. Ten Harkel AD, Witsenburg M, de Jong PL, Jordaeens L, Wijman M, Wilde AA. Efficacy of an implantable cardioverter-defibrillator in a neonate with LQT3 associated arrhythmias. *Europace.* 2005;7:77–84.
 94. Tsurugi T, Nagatomo T, Abe H, Oginosawa Y, Takemasa H, Kohno R, et al. Differential modulation of late sodium current by protein kinase A in R1623Q mutant of LQT3. *Life Sci.* 2009;84:380–7.
 95. Chang CC, Acharfi S, Wu MH, Chiang FT, Wang JK, Sung TC, et al. A novel *SCN5A* mutation manifests as a malignant form of long QT syndrome with perinatal onset of tachycardia/bradycardia. *Cardiovasc Res.* 2004;64:268–78.
 96. Valdivia CR, Ackerman MJ, Tester DJ, Wada T, McCormack J, Ye B, et al. A novel *SCN5A* arrhythmia mutation, M1766L, with expression defect rescued by mexiletine. *Cardiovasc Res.* 2002;55:279–89.
 97. Groenewegen WA, Bezzina CR, van Tintelen JP, Hoornje TM, Mannens MM, Wilde AA, et al. A novel LQT3 mutation implicates the human cardiac sodium channel domain IVS6 in inactivation kinetics. *Cardiovasc Res.* 2003;57:1072–8.
 98. Wei J, Wang DW, Alings M, Fish F, Wathen M, Roden DM, et al. Congenital long-QT syndrome caused by a novel mutation in a conserved acidic domain of the cardiac Na^+ channel. *Circulation.* 1999;99:3165–71.
 99. Deschênes I, Baroudi G, Berthet M, Barde I, Chalvidan T, Denjoy I, et al. Electrophysiological characterization of *SCN5A* mutations causing long QT (E1784K) and Brugada (R1512W and R1432G) syndromes. *Cardiovasc Res.* 2000;46:55–65.
 100. An RH, Wang XL, Kerem B, Benhorin J, Medina A, Goldmit M, et al. Novel LQT-3 mutation affects Na^+ channel activity through interactions between alpha- and beta1-subunits. *Circ Res.* 1998;83:141–6.
 101. Benhorin J, Taub R, Goldmit M, Kerem B, Kass RS, Windman I, et al. Effects of flecainide in patients with new *SCN5A* mutation: mutation-specific therapy for long-QT syndrome? *Circulation.* 2000;101:1698–706.
 102. Wehrens XH, Abriel H, Cabo C, Benhorin J, Kass RS. Arrhythmogenic mechanism of an LQT-3 mutation of the human heart Na^+ channel alpha-subunit: A computational analysis. *Circulation.* 2000;102:584–90.

103. Baroudi G, Chahine M. Biophysical phenotypes of *SCN5A* mutations causing long QT and Brugada syndromes. *FEBS Lett.* 2000;487:224–8.
104. Tateyama M, Rivolta I, Clancy CE, Kass RS. Modulation of cardiac sodium channel gating by protein kinase A can be altered by disease-linked mutation. *J Biol Chem.* 2003;278: 46718–26.
105. Veldkamp MW, Viswanathan PC, Bezzina C, Baartscheer A, Wilde AA, Balser JR. Two distinct congenital arrhythmias evoked by a multidysfunctional Na⁺ channel. *Circ Res.* 2000;86:E91–7.
106. Remme CA, Verkerk AO, Nuyens D, van Ginneken AC, van Brunschot S, Belterman CN, et al. Overlap syndrome of cardiac sodium channel disease in mice carrying the equivalent mutation of human *SCN5A*-1795insD. *Circulation.* 2006;114:2584–94.
107. Rivolta I, Abriel H, Tateyama M, Liu H, Memmi M, Vardas P, et al. Inherited Brugada and long QT-3 syndrome mutations of a single residue of the cardiac sodium channel confer distinct channel and clinical phenotypes. *J Biol Chem.* 2001;276:30623–30.
108. Makita N, Horie M, Nakamura T, Ai T, Sasaki K, Yokoi H, et al. Drug-induced long-QT syndrome associated with a subclinical *SCN5A* mutation. *Circulation.* 2002;106:1269–74.
109. Liu K, Yang T, Viswanathan PC, Roden DM. New mechanism contributing to drug-induced arrhythmia: rescue of a misprocessed LQT3 mutant. *Circulation.* 2005;112:3239–46.
110. Bankston JR, Sampson KJ, Kateriya S, Glaaser IW, Malito DL, Chung WK, et al. A novel LQT-3 mutation disrupts an inactivation gate complex with distinct rate-dependent phenotypic consequences. *Channels (Austin).* 2007;1:273–80.
111. Paulussen A, Matthijs G, Gewillig M, Verhasselt P, Cohen N, Aerssens J. Mutation analysis in congenital Long QT Syndrome-a case with missense mutations in KCNQ1 and *SCN5A*. *Genet Test.* 2003;7:57–61.
112. Ye B, Valdivia CR, Ackerman MJ, Makielis JC. A common human *SCN5A* polymorphism modifies expression of an arrhythmia causing mutation. *Physiol Genomics.* 2003;12:187–93.

Chapter 23

The Short QT Syndrome

Jules C. Hancox, Mark J. McPate, Aziza El Harchi, Rona S. Duncan,
Chris E. Dempsey, Harry J. Witchel, Ismail Adeniran, and Henggui Zhang

23.1 Introduction: The Genetic Short QT Syndrome as a Distinct Clinical Entity

The relationship between abnormally long QT intervals and increased arrhythmia risk is well-established. Rate corrected QT (QT_C) intervals of $>440\text{--}460$ ms (in males and females, respectively) are considered to be prolonged, with values of 500 ms or greater being particularly associated with arrhythmias, particularly the polymorphic ventricular tachycardia *torsades de pointes* (TdP; [1]). Pathological QT_C interval prolongation (the ‘long QT syndrome’; LQTS) can be due to genetic ‘channelopathies’ or be ‘acquired’ as a result of ion channel remodelling in a disease state, such as heart failure, or caused by ion channel-blocking effects of clinically used cardiac and non-cardiac drugs. Preceding Chaps. 21 and 22 consider in detail molecular and pharmacological aspects of the LQTS.

A number of factors unrelated to ion channel gene mutations can lead to QT interval shortening; these include catecholamines, acetylcholine, hypercalcemia, and hyperthermia [2]. Anabolic steroid use is also associated with shortened QT

J.C. Hancox (✉), M.J. McPate, A. El Harchi, and R.S. Duncan
Department of Physiology and Pharmacology, School of Medical Sciences, University Walk,
Bristol BS8 1TD, UK
e-mail: Jules.Hancox@bristol.ac.uk

C.E. Dempsey
Department of Biochemistry, School of Medical Sciences, University Walk, Bristol BS8 1TD, UK

H.J. Witchel
Department of Physiology and Pharmacology, School of Medical Sciences, University Walk,
Bristol BS8 1TD, UK
and
Medical Research Building, Brighton and Sussex Medical School, University of Sussex, Falmer,
Brighton BN1 9PS, UK

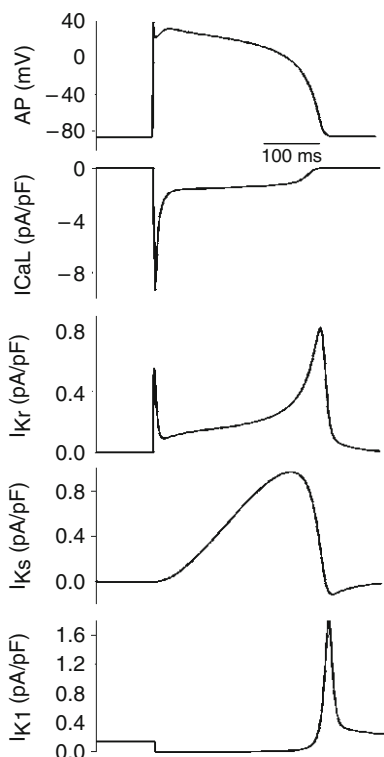
I. Adeniran and H. Zhang
Biological Physics Group, School of Physics and Astronomy, University of Manchester, Manchester
M13 9PL, UK

intervals [3–5], to the extent that it has been suggested that QT_c interval shortening may be a reliable marker of steroid abuse in bodybuilders and strength-athletes [5, 6]. QT interval shortening can be seen on patient ECGs following digitalis administration [7–9]. Cardiac glycosides shorten ventricular repolarisation, at least in part because the combined rise in intracellular Na and Ca following glycoside exposure can promote outward Na–Ca exchange current during the AP plateau [10]; they can also lead to augmented K conductance [11]. Although glycoside-related arrhythmogenesis is strongly associated with after-depolarisations linked to sodium/calcium overload [12], ventricular refractory period shortening has also been reported [13], which could predispose to re-entrant arrhythmia and, thereby, influence ventricular arrhythmia risk [2].

By comparison with the LQTS, short QT syndrome (SQTS) as a *genetic* cardiac channelopathy is a comparatively young clinical entity. The SQTS is typically characterised by abnormally short QT intervals on the electrocardiogram, together with changes to T-wave morphology (tall, peaked T-waves), poor rate-adaptation of the QT interval, and an increased risk of atrial and ventricular arrhythmias and of sudden death [14–18]. The first published description of SQTS with a familial link as a distinct clinical syndrome was by Gussak and colleagues in 2000 [19]. Three members of the same family had QT intervals of <300 ms over the resting heart rate range, the youngest of whom presented with episodes of syncope and paroxysmal atrial fibrillation (AF), whilst similar ECG changes were noted for an unrelated individual who underwent sudden death [19]. A distinction was made between the idiopathic form of SQT, in which QT interval shortening was independent of heart rate and a deceleration-dependent form likely to result from excessive vagal stimulation [19–21]. Subsequently, six members of two different families (members of whom had been referred due to syncope, palpitations, and resuscitated cardiac arrest) were identified as exhibiting QT_C intervals of 300 ms or less [14]; short atrial and ventricular refractory periods and sensitivity to induced ventricular arrhythmia were observed [14]. A year later, a further independent study noted shortened QT intervals as characteristic of children with a familial history of sudden death [22]. The first gene to be implicated in the SQTS was *KCNH2* in 2004 [23, 24], mutations to which are considered to be responsible for the ‘SQT1’ form of the syndrome. Mutations to *KCNQ1* were implicated in a second (SQT2) variant [25, 26], and in *KCNJ2*, for the third, SQT3 variant [27]. More recently, mutations to *CACNB2b* and *CACNA1C* have been linked to a mixed short QT/Brugada phenotype, in which QT interval abbreviation is accompanied by ST-segment elevation [28]. Figure 23.1 shows in schematic form the normal profiles during the ventricular action potential of the ionic currents carried by channels involving *KCNH2*-, *KCNQ1*-, *KCNJ2*- and *CACNA1C* + *CACNB2b*-encoded subunits.

The principal aim of this chapter is to review the experimental evidence that links specific gene mutations to altered ion channel function that leads to accelerated repolarisation and, thereby, the SQTS. Mechanisms of arrhythmogenesis and treatment will also be considered.

Fig. 23.1 Schematic diagram showing the normal profiles during the ventricular AP of repolarising and depolarising currents that have been implicated in the SQTS. The depolarising current shown is L-type Ca current ($I_{Ca,L}$), whilst in terms of repolarising currents, both rapid and slow sub-types of delayed rectifier K⁺ current (I_{Kr} and I_{Ks} , respectively) and the inwardly rectifying K⁺ current I_{K1} are shown. *CACNA1C* and *CACNB2b* encode $I_{Ca,L}$ subunits, whilst *KCNH2*, *KCNQ1* and *KCNJ2* respectively encode I_{Kr} , I_{Ks} and I_{K1} pore-forming subunits



23.2 SQT1 and KCNH2

The first clear genetic cause for SQTS was identified through candidate gene screening of three families, two of which had affected members who exhibited mutations to *KCNH2* [23] (alternative nomenclature *hERG*: human *ether-à-go-go-related gene* [29]). Members of both families exhibited QT_C intervals of <300 ms, episodes of both atrial and ventricular arrhythmias, and there were incidences of sudden death in patients without cardiac structural abnormalities [23]. One family showed cases of severe arrhythmia and sudden death in the first year of life [23]. On genetic screening, members of the two families exhibited distinct mutations at the same nucleotide position (1764) of *KCNH2*. Thus, in one family, there was a C → G substitution, and in the second, there was a C → A substitution; however, these led to a common amino-acid substitution in the *KCNH2* product, the ‘*hERG*’ K channel (Kv11.1), with an asparagine → lysine switch at residue 588 (N588K) [23]. A subsequent independent study identified another family with the C1764G nucleotide and N588K amino-acid substitution [24]. Affected individuals exhibited short QT intervals (between 225 and 240 ms over the normal heart rate range),

paroxysmal AF, short atrial and ventricular refractory periods and AF and ventricular fibrillation (VF) that was inducible on programmed electrical stimulation [24].

hERG mediates the α -subunit of the I_{Kr} channel [30, 31], which plays a critical role in ventricular AP repolarisation (Fig. 23.1) and setting the QT interval of the electrocardiogram [32–35]. Loss-of-function mutations of I_{Kr} are responsible for the LQT2 form of the long QT syndrome, whilst unique structural features of the *KCNH2*-encoded subunit render the channel uniquely susceptible to pharmacological blockade, underlying the acquired form of the LQTS [32–36].

One feature of hERG current (I_{hERG})/ I_{Kr} kinetics that is of key importance to the channel's contribution to ventricular repolarisation is the presence of fast, voltage-dependent inactivation that limits current flow at positive voltages and leads to an area of negative slope in the current–voltage (I–V) relation [30, 31, 37, 38]; this normally limits the channel's contribution to repolarisation immediately after the peak of the AP [39–41]. Conformational changes at the outer mouth of the channel underlie this rapid inactivation [34, 35, 37, 42]. The N588 residue identified in SQT1 patients resides in the S5-Pore (S5-P) linker region of the channel, and this region has also been implicated in hERG's rapid inactivation process (e.g. [43–45]). In the original study identifying the basis of SQT1, N588K-hERG was expressed both with and without the putative hERG accessory subunit KCNE2 (MiRP1; [46]) and, when compared with WT-hERG at ambient temperature, N588K-hERG appeared not to rectify at positive voltages [23]. Measurements of hERG current (I_{hERG}) using the 'AP clamp' technique showed that this mutation led to increased current early during the ventricular AP plateau. Collectively, the cellular electrophysiological data from this study led to the suggestion that the N588K mutation results in a loss of hERG channel inactivation [23]. Subsequent detailed kinetic studies conducted at both ambient [47] and physiological [48] temperatures showed that inactivation of I_{hERG} was in fact not eliminated by the N588K mutation, but rather was positive shifted (by ~+60 to +90 mV); this was accompanied by a modest increase in the Na/K permeability ratio [47, 48]. These alterations to function occur both when the major hERG '1a' isoform is studied alone [47, 48] and when hERG 1a is co-expressed together with the shorter hERG 1b isoform [49] (heteromeric hERG 1a/1b has recently been proposed to recapitulate native I_{Kr} more closely than hERG1a alone; [50, 51]). Interestingly, although hERG 1a and 1b differ only in that the latter has a truncated N-terminus, and this might not be anticipated to influence the effect on channel function of a mutation in the S5-Pore linker, in our hands, the inactivation-attenuating effect of the N588K mutation actually appeared to be greater for hERG 1a/1b heteromeric channels than for hERG1a alone [49]. AP clamp measurements at 37°C showed augmented I_{hERG} during both atrial and ventricular AP waveforms, with peak repolarising current occurring earlier during the AP [52]. This is consistent with SQT1 leading to abbreviation of atrial as well as ventricular repolarisation, and with reports of shortened atrial effective refractory period (ERP) and incidence of AF in SQT1 patients [23, 24]. Potential mechanisms of arrhythmogenesis and the treatment of SQT1 are considered in Sects. 23.6 and 23.7.

Recently, additional *KCNH2* mutations have been implicated in QT interval shortening. An arginine → histidine mutation (R1135H) was recently identified in a 34-year-old male with a QT_C interval of 329 ms and Brugada-type features on his ECG [53]. His brother had a non-documented arrhythmia and moderately shortened QT interval (QT_C of 377 ms), whilst his mother had not reported episodes of arrhythmia, but had bradycardia and a QT_C interval of 379 ms. All three were heterozygous for the R1135H mutation [53]. In vitro investigation of R1135H-hERG identified a slowing of I_{hERG} deactivation [53]. This is a distinct kinetic change from the inactivation modification of N588K-hERG but has been shown in simulations to be able to lead both to shortened repolarisation and, potentially, also to Brugada-like ECG changes [54]. Thus far, heterozygous expression-studies (to mimic the status of the proband) have not yet been reported. In another recent study, a further novel *KCNH2* mutation has been identified in a young male who had experienced syncope whilst driving [55]. His minimal QT_C interval was 366 ms, and his QT-interval showed poor rate adaptation during exercise-testing [55]. Genetic screening identified an N-terminal glutamate to aspartate mutation (D50E) in hERG [55]. As yet, there are no in vitro data regarding the functional consequences of this mutation.

23.3 SQT2 and *KCNQ1*

SQT2 is associated with *KCNQ1* mutations [25, 26]. The *KCNQ1* product (also called KCNQ1 or Kv7.1; previous nomenclature KvLQT1) combines with KCNE1 (minK) to produce the cardiac I_{Ks} channel [56, 57]. I_{Ks} contributes to ventricular repolarisation over the AP plateau phase (Fig. 23.1) and constitutes an important ‘repolarisation reserve’ when I_{Kr} is reduced [33, 58, 59]. The importance of KCNQ1 to ventricular function is illustrated by the fact that loss-of-function KCNQ1 mutations give rise to the LQT1 form of long QT syndrome [33, 36, 58]. The SQT2 variant of SQTS was first reported for a 70-year-old male resuscitated from VF [25], with no evident abnormalities on physical examination but with a short QT_C interval of 302 ms. Genetic analysis showed no abnormalities in *KCNH2*, *KCNE1* or *KCNE2* but revealed a G → C substitution at nucleotide 919 of *KCNQ1*. This led to a single amino-acid substitution (V307L) in the pore helix of the KCNQ1 channel protein [25]. In vitro electrophysiological analysis revealed that the V307L mutation resulted in a negative-shift in the voltage-dependence of activation of recombinant ' I_{Ks} ' channels incorporating mutant KCNQ1 subunits. The time-course of current activation was also faster for mutant than for WT channels [25]. Incorporation of these changes to I_{Ks} into a human ventricular AP model led to AP shortening [25] and QT interval shortening [27]. Subsequent detailed modelling at cell and tissue levels indicates significant effects of the V307L mutation under both homozygotic and heterozygotic conditions on APD across the ventricular wall and to marked shortening of ventricular ERP [60].

The second SQT2 KCNQ1 mutation was found in a baby girl delivered at 38 weeks following bradycardia and irregular rhythm in utero [26]. Once born, her heart rate (in the sixties) was markedly bradycardic for a neonate, whilst her ECG exhibited a QT interval of 280 ms and irregular rhythm with no P or F waves [26]. Genetic analysis revealed a G → A substitution at nucleotide 421, which resulted in a valine to methionine substitution at position 141 (V141M) in the S1 domain of the KCNQ1 channel protein; the mutation was absent in the girl's parents and therefore it represented a *de novo* mutation in the infant [26]. When expressed with KCNE1, the V141M-KCNQ1 mutation led to an instantaneous current component that was absent for WT-KCNQ1 [26]. Incorporation of the changes to KCNQ1 + KCNE1 with the V141M mutation into a human ventricular cell model led to AP shortening, whilst its incorporation into a rabbit SAN cell model (which may approximate though not necessarily recapitulate precisely human pacemaking) arrested spontaneous activity [26]. Interestingly, the affected residue in this form of SQT2 lies immediately adjacent to a residue (S140) mutation to which (S140G) is implicated in one form of familial AF [61]. A recent study has suggested that both of these KCNQ1 mutations lead to a marked negative shift in the voltage dependence of I_{Ks} and to a profound slowing of current deactivation [62].

23.4 SQT3 and KCNJ2

The SQT3 variant of the SQTS was reported in 2005 for a 5-year-old child who exhibited an abnormal ECG during a routine clinical examination [27]. Although asymptomatic, her QT_C interval was 315 ms and showed a narrow and peaked T-wave. Her mother's ECG did not exhibit abnormalities, but that of her father had a QT_C interval of 320 ms and he had a history of palpitations and pre-syncopal events [27]. On genetic analysis, no mutations were found in *KCNH2* or *KCNQ1*, but both father and daughter exhibited a single base pair substitution (G514A) in *KCNJ2* [27]. This resulted in an aspartate → asparagine (D → N) amino-acid substitution at position 172 of the Kir2.1 K channel protein.

Kir2.1 is a member of the family of inward rectifiers (Kir2.1, 2.2 and 2.3) responsible for the inwardly rectifying K channel current I_{K1} [33]. I_{K1} contributes to maintaining the negative resting potential of atrial and ventricular myocytes, and outward I_{K1} is important for the AP terminal repolarisation phase (Fig. 23.1) [33, 63, 64]. Kir2.1 is expressed in both human atrial and ventricular tissue [65]. Its importance to ventricular repolarisation is illustrated by the fact that loss-of-function Kir2.1 mutations underlie Andersen's syndrome [66, 67], whilst familial AF has been associated with the V93I gain-of-function Kir2.1 mutation [68]. The D172 residue is located in the ion conduction pathway of the channel and had previously been implicated in the binding of polyamines and Mg²⁺ ions that gives rise to the inward rectification of Kir2.1 current [69]. The D172N mutation, presumably by impairing this process, leads to an increase in outward Kir2.1 current accompanied by a modest rightward voltage-shift of peak outward current [27, 69, 70]. Co-expression

of WT and D172N channels, to mimic the heterozygous state of the SQT3 proband, results in an increase in outward Kir2.1 current that is intermediate between WT and D172N-Kir2.1 when expressed alone [27, 70]. Incorporation of the kinetic changes to I_{K1} predicted from Kir2.1-D172N data into a ventricular AP model led to AP shortening and steeper restitution of AP duration, whilst incorporation into a 1D tissue strand could replicate the changes to T-wave morphology seen in the SQT3 proband [27]. The subsequent use of the AP clamp technique in *in vitro* experiments on heterozygous WT-D172N Kir2.1 channels has provided direct evidence for increased I_{K1} during the terminal repolarisation phase of ventricular APs [70] and has also shown the potential for the mutation to affect the contribution of I_{K1} to atrial repolarisation [70].

23.5 SQT4 and SQT5

SQT4 and SQT5 can be distinguished from the primary mutations identified for the SQT1-3 variants of SQTS in that (1) they involve loss-of-functions to channel subunits of an ion channel involved in membrane potential depolarisation (L-type calcium current; see Fig. 23.1) rather than repolarisation (to *CACNA1C* for SQT4 and *CACNB2b* for SQT5); (2) a mixed Brugada-SQT phenotype is present, which is unsurprising, given that the mutations came to light from genetic screening of patients with Brugada syndrome [28]. When the clinical phenotype and underlying mutations were first published, this was in the context of presenting a novel clinical entity [28]. However, given that QT interval abbreviation was a marked feature of the ECG, it is appropriate to include some consideration of the identified genotypes in the context of the SQTS. Of the 82 probands with Brugada syndrome, 7 were found to have mutations in the genes responsible for the α and β_{2b} subunits of the L-type Ca channel, three of whom exhibited moderately shortened QT_C intervals (≤ 360 ms). The first patient, a 2-year-old male with a QT_C interval of 330 ms and ajmaline-inducible ST segment elevation, presented with aborted sudden cardiac death (SCD) and had a brother who was also symptomatic and other relatives (in all, a total of 6 from 10) with ECG abnormalities, including tall peaked T-waves. On genetic analysis, the proband exhibited a heterozygous C1442T change in *CACNB2b* that led to a serine → leucine substitution (S481L) in the β_{2b} subunit [28]. The second patient, a 41-year-old male, had a QT_C interval of 300 ms and presented with AF. His brother had died suddenly at 45. Programmed electrical stimulation was able to elicit monomorphic ventricular tachycardia. An A → G substitution (A1468G) led to a glycine → arginine substitution (G490R) in the *CACNA1C* product, which was also present in his two daughters [28]. The third patient, a 44-year-old male, had prominent ST segment elevation and a QT_C interval of 360 ms; his mother had undergone SCD at 48 years of age, while his father had no known medical problems. He had a heterozygous C → T transition at position 116 of *CACNA1C*, leading to an alanine → valine amino-acid substitution (A39V) in the gene product [28]. Co-expression of the relevant mutant α/β subunit with its WT partner led to marked current suppression for each of the observed mutations [28]. Confocal microscopy showed that the A39V-Ca_v1.2 mutation

Table 23.1 Summary of known ion channel gene mutations linked to the SQTS and their functional consequences

SQT Variant	Gene/gene product	Channel (subunit)	Mutation (amino-acid change)	Principal alterations to channel function/activity
SQT1	<i>KCNH2</i> (hERG)	I_{Kr} (α [pore-forming] sub-unit)	N588K R1135H D50E	Reduced inactivation Delayed deactivation Not known
SQT2	<i>KCNQ1</i> (KCNQ1/ KvLQT1)	I_{Ks} (α sub-unit)	V307L	Enhanced/ accelerated activation
			V141M	Constitutively open/ shifted activation and delayed deactivation
SQT3	<i>KCNJ2</i> (Kir2.1)	I_{K1}	D172N	Preferential \uparrow in outward current
SQT4	<i>CACNA1C</i> ($Ca_v1.2$)	L-type I_{Ca} (α sub-unit)	A39V G490R	\downarrow trafficking/current
SQT5	<i>CACNB2b</i> (β_{2b} subunit)	L-type I_{Ca} (β_{2b} sub-unit)	S481L	\downarrow current

was associated with marked perinuclear as opposed to membrane staining, suggestive of impaired trafficking, whilst the G490R $Ca_v1.2$ and S481L $Ca_v\beta_{2b}$ mutations did not appear to impair channel trafficking.

Currently identified ion channel mutations associated with the SQTS and their functional consequences are summarised in Table 23.1.

23.6 Mechanisms of Arrhythmogenesis

Given the evidence for dangerous ventricular arrhythmia and sudden death in SQT families [16, 71], it is of some importance that mechanisms of arrhythmogenesis in the syndrome are understood. Whilst shortened atrial and ventricular refractory periods of SQTS patients [16, 71] might be anticipated to increase the risk of re-entrant arrhythmia, it is difficult to investigate in detail the mechanisms underlying SQT-linked arrhythmogenesis in humans. At present, there is no animal model that mimics accurately the identified gene mutations in human SQTS. Perhaps the closest model in genetic terms is the *reggae* zebrafish mutant, which exhibits a gain-of-function zERG (zebrafish-erg) mutation to the zERG channel voltage sensor region that can be linked causally to abbreviated repolarisation and cardiac fibrillation [72]. However, there is at present no mammalian genetic model of SQTS. Instead, insight into the mechanisms of arrhythmogenesis has been provided by (1) pharmacological models of abbreviated repolarisation and (2) the combination of *in vitro* experimental data and computer modelling. Insight into the effect of

ventricular AP shortening in facilitating an arrhythmogenic substrate has come from experiments using the K_{ATP} channel activator pinacidil on canine ventricular wedge preparations. Although this model does not correspond precisely to SQTS channel gene mutations, it reproduces QT interval shortening and demonstrates increased maximal transmural dispersion of repolarisation (TDR) and susceptibility to polymorphic ventricular tachycardia [73]. Subsequent use of an I_{Kr} -activating compound (PD-118057) in experiments with the ventricular wedge preparation has shown QT interval shortening, increased TDR and ERP abbreviation and susceptibility to evoked arrhythmia [74].

Computer simulations that mimic the major kinetic changes to I_{Kr} , I_{Ks} and I_{K1} of the major SQT1-3 mutations have shown accelerated repolarisation convincingly at cell and tissue levels [26, 27, 60, 75–77], though with changes to T-wave morphology more accurately reproduced for SQT2 [60] and SQT3 [27] variants than for SQT1 [75, 76]. At the single cell level, AP shortening in simulated SQT1 and SQT2 is heterogeneous, with mid-myocardial AP repolarisation more greatly affected than that in epicardial or endocardial cells [60, 75, 76]. Simulated AP shortening has been shown to be accompanied by altered AP restitution (e.g., [27, 75]). AP voltage-clamp experiments and simulations have shown that, in the case of SQT1, there is a markedly smaller effect of the N588K-hERG mutation on I_{hERG} during Purkinje fibre APs than during ventricular APs [47, 49, 52]. This is attributable to differences in AP morphology between the two cell types and may lead to increased heterogeneity between ventricular and Purkinje fibre repolarisation in SQT1, which could feasibly contribute to prominent U-waves seen in some SQTS patients [47, 49, 52]. One simulation study has suggested that hERG gating defects due to the N588K mutation might facilitate early after-depolarisations in SQT1 [77], with reduced hERG ‘tail currents’ [78] and altered response to ‘premature’ stimuli *in vitro* [52]. Our most detailed simulation work to-date has been for V307L-KCNQ1-linked SQT2. Using a combination of cellular, 1D and 2D tissue simulations, we were able to reproduce QT interval shortening and altered T-wave amplitude (Fig. 23.2a, b), by incorporating kinetic changes to I_{Ks} to match those observed for V307L-KCNQ1 + KCNE1 [25, 60]. Maximal transmural voltage heterogeneity during APs was augmented, associated with augmented heterogeneity of AP duration (Fig. 23.2c,d) and ERP. In ventricular tissue models, the vulnerable window for unidirectional conduction block was increased and re-entrant arrhythmias facilitated in simulations of the V307L mutant [60].

23.7 Treatment

Due to the risk of fatal ventricular arrhythmia, the primary treatment for SQTS patients is the use of implantable cardioverter defibrillator devices (ICDs; [16, 71, 79, 80]). However, the marked changes to T-wave morphology present in many patients means that there is an inherent risk in ICD use of inappropriate shock delivery, due to T-wave over-sensing [16, 17, 71, 79]. Although this risk can be

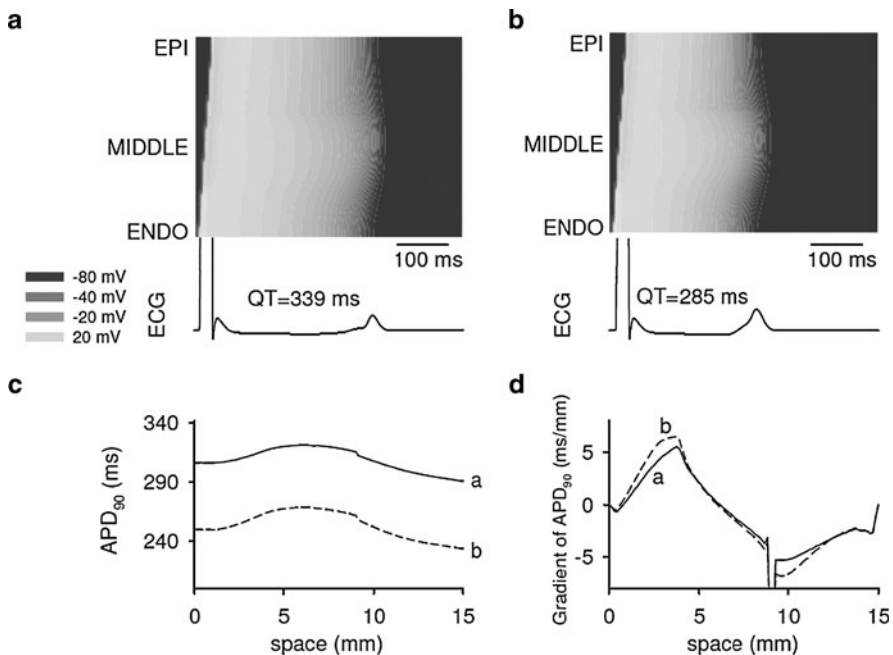


Fig. 23.2 (a) and (b): Space–time plot of computed AP propagation and the pseudo-ECG and reconstructed QT-intervals for WT (a) and heterozygous V307L-KCNQ1 mutant (b) conditions in I_{Ks} -linked SQT2. The membrane potential of cells along the 1D strand is mapped into grey spectrum ranging from black for -100 mV to bright for $+50$ mV (see grey-scale key). Space runs vertically from the ENDO end at the bottom to the EPI end at the top. Time runs horizontally (left to right). (c): Spatial distribution of action potential duration at 90% repolarisation (APD_{90}) on 1D transmural strand in WT (marked by a) and heterozygous V307L KCNQ1 mutant (marked by b) conditions; (d): Spatial gradient of APD_{90} on 1D transmural strand in WT (marked by a) and heterozygous mutant (marked by b) conditions. For further information on simulated SQT2, see [60]

mitigated by ICD reprogramming [79], ICD use does not *per se* restore normal QT interval duration or rate dependence; also some patients (e.g., very young infants) may not be suitable for ICD implantation. Consequently, (adjunct) pharmacotherapeutic options that can restore QT intervals towards normal and protect against arrhythmia generation may be desirable [16, 71, 81, 82].

In the initial study that identified SQT1, pharmacological treatment with the class III anti-arrhythmic drug sotalol was attempted, but this failed to restore a normal QT interval [23]. In vitro experiments in the same study showed that N588K-hERG was less sensitive to inhibition by D-sotalol than was WT-hERG. A subsequent study tested a number of drugs on a sample of six SQTS patients; the drugs investigated included the class Ic anti-arrhythmic drug flecainide, the class Ia agent hydroquinidine and the class III agents sotalol and ibutilide [83]. Of these agents, only hydroquinidine produced substantial QT interval lengthening and also prolonged ventricular ERP and protected against induced VF [83]. A subsequent

comparison of quinidine and sotalol showed that, at ambient temperature, the IC_{50} for I_{hERG} current by sotalol was increased 20-fold by the N588K mutation, whereas that for quinidine was only increased by 5.8-fold [84]. Quinidine also restored towards normal the heart rate adaptation of the QT interval of SQT1 patients [84].

High potency hERG inhibition appears to depend, directly or indirectly, on hERG channel inactivation [35, 85–87]. The greater effectiveness of quinidine than of sotalol against SQT1 and N588K-hERG channels was suggested to reflect the fact that quinidine's ability to inhibit hERG is comparatively insensitive to inactivation of the channel [23, 84, 88]. We investigated another class Ia anti-arrhythmic agent, disopyramide, finding that the I_{hERG} blocking potency of this agent was also little-affected by the N588K-hERG mutation (an IC_{50} 1.5-fold that of WT-hERG compared to 3.5-fold that for quinidine [88] see also Fig. 23.3a). In direct comparison, the high affinity Class III inhibitor E-4031 showed a >11-fold change in IC_{50} [88]. Disopyramide was subsequently tested in a pilot study on two SQT1 patients and was found to exert beneficial effects on QT interval, rate dependence and ventricular ERP [89]. Moreover, disopyramide has also been reported to be beneficial in a patient with SQTS of unknown genotype [90]. By comparing the potency of a series of agents against WT-hERG, N588K-hERG, another attenuated-inactivation mutant S631A and a N588K-S631A double mutant, we recently demonstrated a strong correlation between the extent of attenuation of inactivation and the reduction in drug inhibitory potency [91], with an independent study providing evidence that

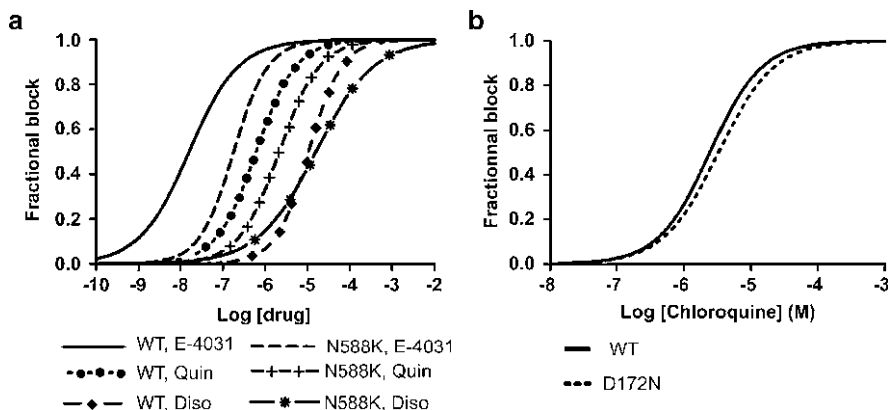


Fig. 23.3 In vitro pharmacology of SQT1 and SQT3. (a) Comparative pharmacology of WT and N588K hERG. Figure shows concentration–response relations for inhibition by three drugs of WT and N588K (SQT1) hERG currents recorded from hERG-expressing Chinese Hamster Ovary cells. Half-maximal inhibitory (IC_{50}) values for inhibition by E-4031, quinidine and disopyramide are as follows, E-4031: WT 16 nM, SQT1 183 nM; Quinidine: WT 0.62 μ M, SQT1 2.2 μ M; Disopyramide: WT 10.7 μ M, SQT1 15.8 μ M. Note that symbols do not denote plotted data-points; rather the concentration–response relations have been plotted as continuous lines, and some line types incorporate symbols to help differentiate between the different plots. For further information, see [88]. (b) Comparative responses of WT and D172N Kir2.1 to chloroquine. Observed IC_{50} values were WT: 2.45 μ M and 3.3 μ M for D172N. For further information, see [70]

inactivation is necessary but not sufficient for high affinity drug-block of the channel [92]. Our study identified (in addition to disopyramide and quinidine) both amiodarone and propafenone as effective inhibitors of N588K-hERG [91]. Effectiveness in vivo of amiodarone against SQT1 remains to be established, though it has been found effective in SQT of unknown genotype [93]. Propafenone has been found to be effective in preventing AF in SQT1, but without normalising the QT interval [24], despite comparatively little effect of the N588K-hERG mutation on hERG-blocking potency of the drug [91]. This likely reflects the fact that propafenone is also an effective inhibitor of L-type calcium channels [94, 95], an effect that is known to offset repolarisation-prolonging effects of hERG channel inhibitors [35]. Synthetic S5-Pore linker peptides have been shown to be able to interact with hERG in electrophysiological experiments [96]. We have investigated the effect of exogenous wild-type S5-Pore linker peptide on N588K-hERG channels; however, whilst a modest inhibitory effect on I_{hERG} amplitude was observed, the peptide was less effective in this regard than classical anti-arrhythmic agents and did not normalise the mutant channel's current profile during AP waveforms (McPate et al. unpublished). It seems likely that, at least in the short term, future developments in respect of SQT1 pharmacology will involve conventional pharmacological approaches.

Although the notion of genotype-specific pharmacology for the SQTS is attractive [81], there is at present comparatively little information available on the in vitro pharmacology of other SQT phenotypes than SQT1. The V307L-KCNQ1 SQT mutation has been shown to attenuate the blocking potency of the I_{Ks} -inhibitor chromanol 293B [97], but there is otherwise little published information on this SQT variant. Recently, the quinolone agent chloroquine has been reported to be effective against SQT3 D172N-Kir2.1 channels in vitro [70, 98]. Using AP clamp, we have demonstrated that chloroquine exhibits similar inhibitory potency against WT, D172N and (heterozygous) WT-D172N channels [70] (Fig. 23.3b shows a comparison between WT and D172N). Independent confirmation of this observation, together with an *in silico* prediction that chloroquine is likely to prolong both ventricular AP duration and refractoriness [98], raises the possibility that chloroquine or an allied chemical structure may be effective against SQT3. Calcium-channel-related SQTS/Brugada syndrome has been reported to be responsive to quinidine [28]. Quinidine has also been shown to prolong AP duration, refractoriness, post-repolarisation refractoriness and to reduce dispersion of repolarisation in the pinacidil- K_{ATP} model of the SQTS [99]. It is possible, therefore, that Class Ia anti-arrhythmics, and quinidine in particular, might offer generic (or at least first line) pharmacological treatments in the SQTS, although this remains to be verified in further patient studies.

23.8 Conclusions

At the time of writing, mutations to five ion channel subunit genes have been discovered in SQTS patients (discussed in Sects. 23.2–23.5). However, it has been noted that a number of SQTS cases are not linked to identified mutations and

therefore that the condition seems to exhibit marked genetic heterogeneity [71]. Case reports highlight patients in whom gene mutations have not been identified (e.g. [90, 93, 100]), and a recent review reported no (identified) mutations in six of eight families and two sporadic cases [15]. It seems highly likely, therefore, that in time, additional genes/gene mutations will be identified in patients/families with the SQTS. The poor rate adaptation of the QT interval in genetic forms of SQTS means that abbreviated QT intervals of SQTS patients are likely more readily to be detected at lower than at faster heart rates [71, 101].

Another area in which future developments might be anticipated is that of further insight into the prevalence of the condition. The probands identified in each of the original SQT1–3 reports all had QT_C intervals <320 ms [23, 25–27], and QT_C values of 320–340 ms have been proposed to denote short QT intervals [15, 16]. Recent epidemiological analyses suggest that the incidence of markedly short QT intervals may be low. Thus, an analysis of a large middle-aged Finnish cohort (of 10,822 randomly chosen individuals) showed that 0.1% exhibited QT_C intervals of <320 ms and 0.4% showed QT_C intervals of <340 ms [102]. Analysis of ECGs from a large sample (12,012) of subjects who had undergone medical examination for occupational reasons revealed that the shortest QT_c interval found was 335 ms [103]. A third study reported that careful (including manual in addition to automated) analysis of 106,432 hospital patients found no QT_C interval <300 ms [104]. A recent analysis of Swiss army male conscripts also found no QT_C intervals <300 ms and 0.02% of <320 ms [105]. Thus, it seems reasonable to conclude that highly abbreviated QT_C intervals are likely to be rare in the normal population. On the other hand, it is notable that the recently reported QT_C intervals of the short QT patient with the D50E hERG mutation [55] and that the QT_C interval associated with the short-QT Brugada A39V CACNA1C mutation [28] exceeded 340 ms. Just as the prolongation of the QT interval is not a perfect indicator of risk in LQTS patients (some of whom can show little QT interval prolongation [106]), the shortness of the QT interval may be an imperfect surrogate of SQTS, whereas its risks may be linked to cellular and transmural mechanisms related to repolarisation. In its favour, the occurrence of moderately shortened QT_C intervals has been reported to be greater amongst male patients with idiopathic VF (though no such correlation was seen for women) [107]. Ultimately, the progressive emergence of case reports of SQTS patients raises the possibilities both that, in time, a clearer picture will emerge of the boundary between safe and dangerously shortened QT_C intervals and that increasing number of SQTS cases will be recognised as general awareness of the condition increases.

A final issue worth highlighting relates to a growing interest in whether or not acquired QT interval shortening (as for drug induced long QT syndrome) could be associated with increased risk of arrhythmia [108, 109]. At present, there are probably insufficient data to reach a clear view on this and there are no current consensus regulatory guidelines regarding drug candidates that result in QT interval shortening. Now that the issue is one that is being discussed in the literature, it is likely that this will be the subject of further investigation out of which a clearer picture will emerge over the next few years.

Acknowledgement The authors' work on the short QT syndrome has been funded by the British Heart Foundation (PG 04/090, PG 06/139, PG 06/147, FS 08/021).

References

1. Yap YG, Camm AJ. Drug induced QT prolongation and torsades de pointes. *Heart*. 2003;89:1363–72.
2. Garberoglio L, Giustetto C, Wolpert C, Gaita F. Is acquired short QT due to digitalis intoxication responsible for malignant ventricular arrhythmias? *J Electrocardiol*. 2007;40:43–6.
3. Bidoggia H, Maciel JP, Capalozza N, Mosca S, Blaksley EJ, Valverde E, et al. Sex differences on the electrocardiographic pattern of cardiac repolarization: possible role of testosterone. *Am Heart J*. 2000;140:678–83.
4. Charbit B, Christin-Maitre S, Demolis JL, Soustre E, Young J, Funck-Brentano C. Effects of testosterone on ventricular repolarization in hypogonadic men. *Am J Cardiol*. 2009;103:887–90.
5. Bigi MA, Aslani A, Aslani A. Short QT interval: a novel predictor of androgen abuse in strength trained athletes. *Ann Noninvasive Electrocardiol*. 2009;14:35–9.
6. Hancox JC, Choisy SC, James AF. Short QT interval linked to androgen misuse: wider significance and possible basis. *Ann Noninvasive Electrocardiol*. 2009;14:31–2.
7. Cheng TO. Digitalis administration: an underappreciated but common cause of short QT interval. *Circulation*. 2004;109:e152.
8. Hachimi-Idrissi S, Corne L, Maes V, Ramet J. Gitaloxin poisoning in a child. *Intensive Care Med*. 1996;22:1442–4.
9. Jowett NI. Foxglove poisoning. *Hosp Med*. 2002;63:758–9.
10. Levi AJ. A role for Na/Ca exchange in the action potential shortening caused by strophanthidin in guinea-pig ventricular myocytes. *Cardiovasc Res*. 1993;27:471–81.
11. Bassingthwaite JB, Fry CH, McGuigan JA. Relationship between internal calcium and outward current in mammalian ventricular muscle; a mechanism for the control of the action potential duration? *J Physiol*. 1976;262:15–37.
12. Levi AJ, Dalton GR, Hancox JC, Mitcheson JS, Issberner J, Bates JA, et al. Role of intracellular sodium overload in the genesis of cardiac arrhythmias. *J Cardiovasc Electrophys*. 1997;8:700–21.
13. Gomes JA, Dhatt MS, Akhtar M, Carambas CR, Rubenson DS, Damato AN. Effects of digitalis on ventricular myocardial and His-Purkinje refractoriness and reentry in man. *Am J Cardiol*. 1978;42:931–8.
14. Gaita F, Giustetto C, Bianchi F, Wolpert C, Schimpf R, Riccardi R, et al. Short QT syndrome: a familial cause of sudden death. *Circulation*. 2003;108:965–70.
15. Giustetto C, Di Monte F, Wolpert C, Borggrefe M, Schimpf R, Sbragia P, et al. Short QT syndrome: clinical findings and diagnostic-therapeutic implications. *Eur Heart J*. 2006;27:2440–7.
16. Schimpf R, Wolpert C, Gaita F, Giustetto C, Borggrefe M. Short QT syndrome. *Cardiovasc Res*. 2005;67:357–66.
17. Anttonen O, Junttila J, Giustetto C, Gaita F, Linna E, Karsikas M, et al. T-Wave morphology in short QT syndrome. *Ann Noninvasive Electrocardiol*. 2009;14:262–7.
18. McPate MJ, Witchel HJ, Hancox JC. Short QT Syndrome. *Future Cardiol*. 2006;2:293–301.
19. Gussak I, Brugada P, Brugada J, Wright RS, Kopecky SI, Chaitman BR, et al. Idiopathic short QT interval: a new clinical syndrome? *Cardiology*. 2000;94:99–102.
20. Gussak I, Brugada P, Brugada J, Antzelevitch C, Osbakken M, Bjerregaard P. ECG phenomenon of idiopathic and paradoxical short QT intervals. *Cardiac Electrophysiol Rev*. 2002;6:49–53.
21. Gussak I, Liebl N, Nouri S, Bjerregaard P, Zimmerman F, Chaitman BR. Deceleration-dependent shortening of the QT interval: a new electrocardiographic phenomenon? *Clin Cardiol*. 1999;22:124–6.
22. Makarov LM, Chuprova SN, Kiseleva II. QT interval shortening in families with history of sudden death at young age. *Kardiologiiia*. 2004;44:51–6.

23. Brugada R, Hong K, Dumaine R, Cordeiro J, Gaita F, Borggrefe M, et al. Sudden death associated with short-QT syndrome linked to mutations in HERG. *Circulation*. 2004;109:30–5.
24. Hong K, Bjerregaard P, Gussak I, Brugada R. Short QT syndrome and atrial fibrillation caused by mutation in KCNH2. *J Cardiovasc Electrophysiol*. 2005;16:394–6.
25. Bellocq C, van Ginneken AC, Bezzina CR, Alders M, Escande D, Mannens MM, et al. Mutation in the KCNQ1 gene leading to the short QT-interval syndrome. *Circulation*. 2004;109:2394–7.
26. Hong K, Piper DR, Diaz-Valdecantos A, Brugada J, Oliva A, Burashnikov E, et al. De novo KCNQ1 mutation responsible for atrial fibrillation and short QT syndrome in utero. *Cardiovasc Res*. 2005;68:433–40.
27. Priori SG, Pandit SV, Rivolta I, Berenfeld O, Ronchetti E, Dhamoon A, et al. A novel form of short QT syndrome (SQT3) is caused by a mutation in the KCNJ2 gene. *Circ Res*. 2005;96:800–7.
28. Antzelevitch C, Pollevick GD, Cordeiro JM, Casis O, Sanguinetti MC, Aizawa Y, et al. Loss-of-function mutations in the cardiac calcium channel underlie a new clinical entity characterized by ST-segment elevation, short QT intervals, and sudden cardiac death. *Circulation*. 2007;115:442–9.
29. Warmke JW, Ganetzky B. A family of potassium channel genes related to *eag* in *Drosophila* and mammals. *Proc Natl Acad Sci USA*. 1994;91:3438–42.
30. Sanguinetti MC, Jiang C, Curran ME, Keating MT. A mechanistic link between an inherited and an acquired cardiac arrhythmia: HERG encodes the I_{Kr} potassium channel. *Cell*. 1995;81:299–307.
31. Trudeau MC, Warmke JW, Ganetzky B, Robertson GA. HERG, an inward rectifier in the voltage-gated potassium channel family. *Science*. 1995;269:92–5.
32. Witchel HJ, Hancox JC. Familial and acquired long QT syndrome and the cardiac rapid delayed rectifier potassium channel. *Clin Exp Pharmacol Physiol*. 2000;27:753–66.
33. Tamargo J, Caballero R, Gómez R, Valenzuela C, Delpón E. Pharmacology of cardiac potassium channels. *Cardiovasc Res*. 2004;62:9–33.
34. Sanguinetti MC, Tristani-Firouzi M. hERG potassium channels and cardiac arrhythmia. *Nature*. 2006;440:463–9.
35. Hancox JC, McPate MJ, El Harchi A, Zhang YH. The hERG potassium channel and hERG screening for drug-induced torsades de pointes. *Pharmacol Ther*. 2008;119(118):118–32.
36. Modell SM, Lehmann MH. The long QT syndrome family of cardiac ion channelopathies: a HuGE review. *Genet Med*. 2006;8:143–55.
37. Smith PL, Baukowitz T, Yellen G. The inward rectification mechanism of the HERG cardiac potassium channel. *Nature*. 1996;379:833–6.
38. Spector PS, Curran ME, Zou A, Keating MT, Sanguinetti MC. Fast inactivation causes rectification of the I_{Kr} channel. *J Gen Physiol*. 1996;107:611–9.
39. Hancox JC, Levi AJ, Witchel HJ. Time course and voltage dependence of expressed HERG current compared with native ‘rapid’ delayed rectifier K current during the cardiac ventricular action potential. *Pflugers Arch*. 1998;436:843–53.
40. Hancox JC, Witchel HJ, Varghese A. Alteration of HERG current profile during the cardiac ventricular action potential, following a pore mutation. *Biochem Biophys Res Commun*. 1998;253:719–24.
41. Zhou Z, Gong Q, Ye B, Fan Z, Makielinski JC, Robertson GA, et al. Properties of HERG channels stably expressed in HEK 293 cells studied at physiological temperature. *Biophys J*. 1998;74:230–41.
42. Schönherz R, Heinemann SH. Molecular determinants for activation and inactivation of HERG, a human inward rectifier potassium channel. *J Physiol*. 1996;493:635–42.
43. Liu J, Zhang M, Jiang M, Tseng GN. Structural and functional role of the extracellular S5-P linker in the HERG potassium channel. *J Gen Physiol*. 2002;120:723–37.

44. Jiang M, Zhang M, Maslennikov IV, Liu J, Wu DM, Korolkova YV, et al. Dynamic conformational changes of extracellular S5-P linkers in the hERG channel. *J Physiol.* 2005;569:75–89.
45. Clarke CE, Hill AP, Zhao J, Kondo M, Subbiah RN, Campbell TJ, et al. Effect of S5P alpha-helixcharge mutants on inactivation of hERG K⁺ channels. *J Physiol.* 2006;573:291–304.
46. Abbott GW, Sesti F, Splawski I, Buck M, Lehmann MH, Timothy KW, et al. MiRP1 forms I_{Kr} potassium channels with HERG and is associated with cardiac arrhythmia. *Cell.* 1999;97:175–87.
47. Cordeiro JM, Brugada R, Wu YS, Hong K, Dumaine R. Modulation of I_{Kr} inactivation by mutation N588K in KCNH2: a link to arrhythmogenesis in short QT syndrome. *Cardiovasc Res.* 2005;67:498–509.
48. McPate MJ, Duncan RS, Milnes JT, Witchel HJ, Hancox JC. The N588K-HERG K⁺ channel mutation in the ‘short QT syndrome’: mechanism of gain-in-function determined at 37°C. *Biochem Biophys Res Commun.* 2005;334:441–9.
49. McPate MJ, Zhang H, Cordeiro JM, Dempsey CE, Witchel HJ, Hancox JC. hERG1a/1b heteromeric currents exhibit amplified attenuation of inactivation in variant 1 short QT syndrome. *Biochem Biophys Res Commun.* 2009;386:111–7.
50. Jones EM, Roti Roti EC, Wang J, Robertson GA. Cardiac I_{Kr} channels minimally comprise hERG 1a and 1b subunits. *J Biol Chem.* 2004;279:44690–4.
51. Sale H, Wang J, O’Hara TJ, Tester DJ, Phartiyal P, He JQ, et al. Physiological properties of hERG 1a/1b heteromeric currents and a hERG 1b-specific mutation associated with Long-QT syndrome. *Circ Res.* 2008;103:e81–95.
52. McPate MJ, Zhang H, Ideniran I, Cordeiro JM, Witchel HJ, Hancox JC. Comparative effects of the short QT N588K mutation at 37°C on hERG K⁺ channel current during ventricular, Purkinje fibre and atrial action potentials: an action potential clamp study. *J Physiol Pharmacol.* 2009;60:23–41.
53. Itoh H, Sakaguchi T, Ashihara T, Ding WG, Nagaoka I, Oka Y, et al. A novel KCNH2 mutation as a modifier for short QT interval. *Int J Cardiol.* 2009;137:83–5.
54. Wilders R, Verkerk AO. Role of the R1135H KCNH2 mutation in Brugada syndrome. *Int J Cardiol.* 2010;144:149–51.
55. Redpath CJ, Green MS, Birnie DH, Gollob MH. Rapid genetic testing facilitating the diagnosis of short QT syndrome. *Can J Cardiol.* 2009;25:e133–5.
56. Barhanin J, Lesage F, Guillemare E, Fink M, Lazdunski M, Romey G. KvLQT1 and IsK (minK) proteins associate to form the I_{Ks} cardiac potassium current. *Nature.* 1996;384:78–80.
57. Sanguinetti MC, Curran ME, Zou A, Shen J, Spector PS, Atkinson DL, et al. Coassembly of KvLQT1 and minK (IsK) proteins to form cardiac I_{Ks} potassium channel. *Nature.* 1996;384:80–3.
58. Roden DM, Lazzara R, Rosen MR, Schwartz PJ, Towbin JA, Vincent M, et al. Multiple mechanisms in the Long-QT syndrome. Current knowledge, gaps and future directions. The SADS foundation task force on LQTS. *Circulation.* 1996;94:1996–2012.
59. Jost N, Virág L, Bitay M, Takács J, Lengyel C, Biliczki P, et al. Restricting excessive cardiac action potential and QT prolongation: a vital role for I_{Ks} in human ventricular muscle. *Circulation.* 2005;112:1392–9.
60. Zhang H, Kharche S, Holden AV, Hancox JC. Repolarisation and vulnerability to re-entry in the human heart with short QT syndrome arising from KCNQ1 mutation-a simulation study. *Prog Biophys Mol Biol.* 2008;96:112–31.
61. Chen YH, Xu SJ, Bendahhou S, Wang XL, Wang Y, Xu WY, et al. KCNQ1 gain-of-function mutation in familial atrial fibrillation. *Science.* 2003;299:251–4.
62. Restier L, Cheng L, Sanguinetti MC. Mechanisms by which atrial fibrillation-associated mutations in the S1 domain of KCNQ1 slow deactivation of I_{Ks} channels. *J Physiol.* 2008;586:4179–91.
63. Shimoni Y, Clark RB, Giles WR. Role of an inwardly rectifying potassium current in rabbit ventricular action potential. *J Physiol.* 1992;448:709–27.

64. Mitcheson JS, Hancox JC. An investigation of the role played by the E-4031-sensitive (rapid delayed rectifier) potassium current in isolated rabbit atrioventricular nodal and ventricular myocytes. *Pflugers Arch.* 1999;438:843–50.
65. Gaborit N, Le Bouter S, Szuts V, Varro A, Escande D, Nattel S, et al. Regional and tissue specific transcript signatures of ion channel genes in the non-diseased human heart. *J Physiol.* 2007;582:675–93.
66. Plaster NM, Tawil R, Tristani-Firouzi M, Canún S, Bendahhou S, Tsunoda A, et al. Mutations in Kir2.1 cause the developmental and episodic electrical phenotypes of Andersen's syndrome. *Cell.* 2001;105:511–9.
67. Tristani-Firouzi M, Jensen JL, Donaldson MR, Sansone V, Meola G, Hahn A, et al. Functional and clinical characterization of KCNJ2 mutations associated with LQT7 (Andersen syndrome). *J Clin Invest.* 2002;110:381–8.
68. Xia M, Jin Q, Bendahhou S, He Y, Larroque MM, Chen Y, et al. A Kir2.1 gain-of-function mutation underlies familial atrial fibrillation. *Biochem Biophys Res Commun.* 2005;332:1012–9.
69. Abrams CJ, Davies NW, Shelton PA, Stanfield PR. The role of a single aspartate residue in ionic selectivity and block of a murine inward rectifier K⁺ channel Kir2.1. *J Physiol.* 1996;493:643–9.
70. El Harchi A, McPate MJ, Zhang YH, Zhang H, Hancox JC. Action potential clamp and chloroquine sensitivity of mutant Kir2.1 channels responsible for variant 3 short QT syndrome. *J Mol Cell Cardiol.* 2009;47:743–7.
71. Maury P, Extramiana F, Sbragia P, Giustetto C, Schimpf R, Duparc A, et al. Short QT syndrome. Update on a recent entity. *Arch Cardiovasc Dis.* 2008;101:779–86.
72. Hassel D, Scholz EP, Trano N, Friedrich O, Just S, Meder B, et al. Deficient zebrafish ether- α -go-go-related gene channel gating causes short-QT syndrome in zebrafish reggae mutants. *Circulation.* 2008;117:866–75.
73. Extramiana F, Antzelevitch C. Amplified transmural dispersion of repolarization as the basis for arrhythmogenesis in a canine ventricular-wedge model of short-QT syndrome. *Circulation.* 2004;110:3661–6.
74. Patel C, Antzelevitch C. Cellular basis for arrhythmogenesis in an experimental model of the SQT1 form of the short QT syndrome. *Heart Rhythm.* 2008;5:585–90.
75. Zhang H, Hancox JC. In silico study of action potential and QT interval shortening due to loss of inactivation of the cardiac rapid delayed rectifier potassium current. *Biochem Biophys Res Commun.* 2004;322:693–9.
76. Weiss DL, Seemann G, Sachse FB, Dössel O. Modelling of short QT syndrome in a heterogeneous model of the human ventricular wall. *Europace.* 2005;7 Suppl 2:105–17.
77. Itoh H, Horie M, Ito M, Imoto K. Arrhythmogenesis in the short-QT syndrome associated with combined HERG channel gating defects: a simulation study. *Circ J.* 2006;70:502–8.
78. Grunnet M, Diness TG, Hansen RS, Olesen SP. Biophysical characterization of the short QT mutation hERG-N588K reveals a mixed gain-and loss-of-function. *Cell Physiol Biochem.* 2008;22:611–24.
79. Schimpf R, Wolpert C, Bianchi F, Giustetto C, Gaita F, Bauersfeld U, et al. Congenital short QT syndrome and implantable cardioverter defibrillator treatment: inherent risk for inappropriate shock delivery. *J Cardiovasc Electrophysiol.* 2003;14:1273–7.
80. Schimpf R, Bauersfeld U, Gaita F, Wolpert C. Short QT syndrome: successful prevention of sudden cardiac death in an adolescent by implantable cardioverter-defibrillator treatment for primary prophylaxis. *Heart Rhythm.* 2005;2:416–7.
81. Bjerregaard P, Jahangir A, Gussak I. Targeted therapy for short QT syndrome. *Expert Opin Ther Targets.* 2006;10:393–400.
82. Duncan RS, McPate MJ, Ridley JM, Gao Z, James AF, Leishman DJ, et al. Inhibition of the HERG potassium channel by the tricyclic antidepressant doxepin. *Biochem Pharmacol.* 2007;74:425–37.

83. Gaita F, Giustetto C, Bianchi F, Schimpf R, Haissaguerre M, Calò L, et al. Short QT syndrome: pharmacological treatment. *J Am Coll Cardiol.* 2004;43:1494–9.
84. Wolpert C, Schimpf R, Giustetto C, Antzelevitch C, Cordeiro JM, Dumaine R, et al. Further insights into the effect of quinidine in short QT syndrome caused by a mutation in HERG. *J Cardiovasc Electrophysiol.* 2005;16:54–8.
85. Weerapura M, Hebert TE, Nattel S. Dofetilide block involves interactions with open and inactivated states of HERG channels. *Pflugers Arch.* 2002;443:520–31.
86. Chen J, Seeböhm G, Sanguinetti MC. Position of aromatic residues in the S6 domain, not inactivation, dictates cisapride sensitivity of HERG and eag potassium channels. *Proc Natl Acad Sci USA.* 2002;99:12461–6.
87. Witchel HJ. The hERG potassium channel as a therapeutic target. *Expert Opin Ther Targets.* 2007;11:321–36.
88. McPate MJ, Duncan RS, Witchel HJ, Hancox JC. Disopyramide is an effective inhibitor of mutant HERG K⁺ channels involved in variant 1 short QT syndrome. *J Mol Cell Cardiol.* 2006;41:563–6.
89. Schimpf R, Veltmann C, Giustetto C, Gaita F, Borggreffe M, Wolpert C. In vivo effects of mutant HERG K⁺ channel inhibition by disopyramide in patients with a short QT-1 syndrome: a pilot study. *J Cardiovasc Electrophysiol.* 2007;18:1157–60.
90. Mizobuchi M, Enjoji Y, Yamamoto R, Ono T, Funatsu A, Kambayashi D, et al. Nifekalant and disopyramide in a patient with short QT syndrome: evaluation of pharmacological effects and electrophysiological properties. *Pacing Clin Electrophysiol.* 2008;31:1229–32.
91. McPate MJ, Duncan RS, Hancox JC, Witchel HJ. Pharmacology of the short QT syndrome N588K-hERG K⁺ channel mutation: differential impact on selected class I and class III antiarrhythmic drugs. *Br J Pharmacol.* 2008;155:957–66.
92. Perrin MJ, Kuchel PW, Campbell TJ, Vandenberg JI. Drug binding to the inactivated state is necessary but not sufficient for high-affinity binding to human ether-à-go-go-related gene channels. *Mol Pharmacol.* 2008;74:1443–52.
93. Lu LX, Zhou W, Zhang X, Cao Q, Yu K, Zhu C. Short QT syndrome: a case report and review of literature. *Resuscitation.* 2006;71:115–21.
94. Fei L, Gill JS, McKenna WJ, Camm AJ. Effects of propafenone on calcium currents in single ventricular myocytes of guinea-pig. *Br J Pharmacol.* 1993;109:178–82.
95. Mitcheson JS, Hancox JC. Inhibition of L-type calcium current by propafenone in single myocytes isolated from the rabbit atrioventricular node. *Br J Pharmacol.* 1997;121:7–14.
96. Torres AM, Bansal PS, Sunde M, Clarke CE, Bursill JA, Smith DJ, et al. Structure of the HERG K⁺ channel S5P extracellular linker: role of an amphipathic alpha-helix in C-type inactivation. *J Biol Chem.* 2003;278:42136–48.
97. Lerche C, Bruhova I, Lerche H, Steinmeyer K, Wei AD, Strutz-Seeböhm N, et al. Chromanol 293B binding in KCNQ1 (Kv7.1) channels involves electrostatic interactions with a potassium ion in the selectivity filter. *Mol Pharmacol.* 2007;71:1503–11.
98. Lopez-Izquierdo A, Ponce-Balbuena D, Ferret T, Sachse FB, Tristani-Firouzi M, Sanchez-Chapula JA. Chloroquine blocks a mutant Kir2.1 channel responsible for short QT syndrome and normalizes repolarization properties in silico. *Cell Physiol Biochem.* 2009;24:153–60.
99. Milberg P, Tegelkamp R, Osada N, Schimpf R, Wolpert C, Breithardt G, et al. Reduction of dispersion of repolarization and prolongation of postrepolarization refractoriness explain the antiarrhythmic effects of quinidine in a model of short QT syndrome. *J Cardiovasc Electrophysiol.* 2007;18:658–64.
100. Villafane J, Young ML, Maury P, Wolpert C, Anttonen O, Hamilton R, et al. Short QT syndrome in a pediatric patient. *Pediatr Cardiol.* 2009;30:846–50.
101. Wolpert C, Schimpf R, Veltmann C, Giustetto C, Gaita F, Borggreffe M. Clinical characteristics and treatment of short QT syndrome. *Expert Rev Cardiovasc Ther.* 2005;3:611–7.
102. Anttonen O, Junnila MJ, Rissanen H, Reunanan A, Viitasalo M, Huikuri HV. Prevalence and prognostic significance of short QT interval in a middle-aged Finnish population. *Circulation.* 2007;116:714–20.

103. Gallagher MM, Magliano G, Yap YG, Padula M, Morgia V, Postorino C, et al. Distribution and prognostic significance of QT intervals in the lowest half centile in 12, 012 apparently healthy persons. *Am J Cardiol.* 2006;98:933–5.
104. Reinig MG, Engel TR. The shortage of short QT intervals. *Chest.* 2007;132:246–9.
105. Kobza R, Roos M, Niggli B, Abächerli R, Lupi GA, Frey F, et al. Prevalence of long and short QT in a young population of 41, 767 predominantly male Swiss conscripts. *Heart Rhythm.* 2009;6:652–7.
106. Johnson JN, Ackerman MJ. QT_c: how long is too long? *Br J Sports Med.* 2009;43:657–62.
107. Viskin S, Zeltser D, Ish-Shalom M, Katz A, Glikson M, Jutso D, et al. Is idiopathic ventricular fibrillation a short QT syndrome? Comparison of QT intervals of patients with idiopathic ventricular fibrillation and healthy controls? *Heart Rhythm.* 2004;1:587–91.
108. Pugsley MK, Curtis MJ. Safety pharmacology methods: anticipating the transition from long QT (LQTS) to short QT syndromes (SQTS)? *J Pharmacol Toxicol Methods.* 2007;56:87–90.
109. Shah RR. Drug-induced QT interval shortening: potential harbinger of proarrhythmia and regulatory perspectives. *Br J Pharmacol.* 2010;159:58–69.

Chapter 24

Adrenergic Regulation and Heritable Arrhythmias: Key Roles of the Slowly Activating Heart I_{Ks} Potassium Channel

David Y. Chung, Kevin J. Sampson, and Robert S. Kass

24.1 Introduction

In cardiac myocytes, repolarization of the cellular action potential is achieved largely by activation of two delayed rectifier K^+ currents. Of these two, the slowly activating delayed rectifier I_{Ks} channel plays a critical role in normal cardiac physiology as it responds robustly to β -adrenergic receptor (β -AR) stimulation in order to shorten the action potential duration (APD) and ensure adequate repolarization in the setting of an increased heart rate. Furthermore, the interrelationship between the regulation of I_{Ks} and the L-type calcium channel current (I_{CaL}) is essential for maintenance of normal cardiac function in the face of sympathetic stimulation [1] where the interbeat interval is drastically reduced with increased heart rate. Perhaps not surprisingly, because of its critical role in repolarization, mutations in the genes encoding the I_{Ks} channel and its associated AKAP have been shown to lead to heritable cardiac arrhythmia including the Long QT (LQTS) and short QT syndromes (SQTS) as well as familial atrial fibrillation (FAF) with strong association to arrhythmia susceptibility related to increased adrenergic activity.

24.2 Early Studies

The regulation of the delayed rectifier was observed as early as 1972 when Tsien et al. observed that treatment of calf Purkinje fibers with cell-permeable cAMP, a key β -adrenergic mediator, or reagents that increase intracellular cAMP could cause the slow outward current, then called I_X , to have faster activation kinetics and conduct greater steady state current [2]. Subsequent studies of I_{Ks} showed that the increase in current that occurs as a result of β -adrenergic stimulation was a result of cAMP-dependent protein kinase A phosphorylation of I_{Ks} , or as yet

D.Y. Chung, K.J. Sampson, and R.S. Kass (✉)

Department of Pharmacology, College of Physicians and Surgeons of Columbia University,
630 W. 168th St., New York, NY 10032, USA
e-mail: rsk20@columbia.edu

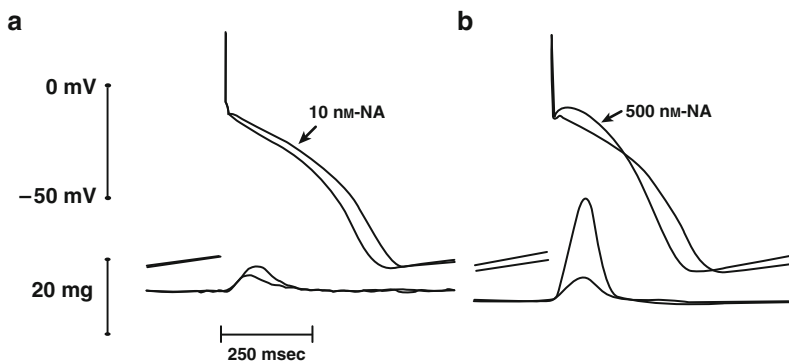


Fig. 24.1 Concentration-dependent control of electrical and mechanical activity by norepinephrine in the cardiac Purkinje fiber. Action potentials (upper) and contractile responses (lower panel) recorded in an isolated calf Purkinje fiber before and after 10 nM (a) and 500 nM (b) norepinephrine was applied. Note concentration-dependent effects on APD and twitch. From Kass and Weigers [1]

unidentified target proteins [3–6]; however, the molecular basis for this regulation remained poorly understood before the revelation of the two key I_{K_s} subunits (KCNQ1, KCNE1) through LQTS studies. The increased outward I_{K_s} during β -adrenergic stimulation shortens the APD while an increased inward I_{CaL} triggers greater muscle contraction (Fig. 24.1). Together these β -adrenergic-mediated effects ensure an adequate diastolic refilling time and response despite the decreasing interpulse interval.

24.3 Molecular Identity of the I_{K_s} Channel

In 1996, the molecular determinants of I_{K_s} were determined and the connection to LQTS was made. A positional cloning study carried out in the search for the causative gene for the LQT1 variant of the congenital Long QT syndrome linked the clinical phenotype of LQT1 to the then novel and uncharacterized KCNQ1 protein [7]. KCNQ1 is a prototypical 6 transmembrane domain K^+ channel that forms a conducting pore; however, this protein by itself cannot reconstitute the slowly activating current observed in cardiac myocytes. Two groups of investigators independently showed that KCNE1, cloned 8 years earlier [8], and KCNQ1 comprised the I_{K_s} channel [9, 10] thereby defining the molecular determinants of the channel. When KCNQ1 and KCNE1 are coassembled the kinetics slow, the $V_{1/2}$ of activation is shifted in the depolarizing direction, and there is a roughly fivefold increase in current (Fig. 24.2) [9]. Later studies showed that the increase in current is due, at least in part, to an increase in single channel conductance [11, 12].

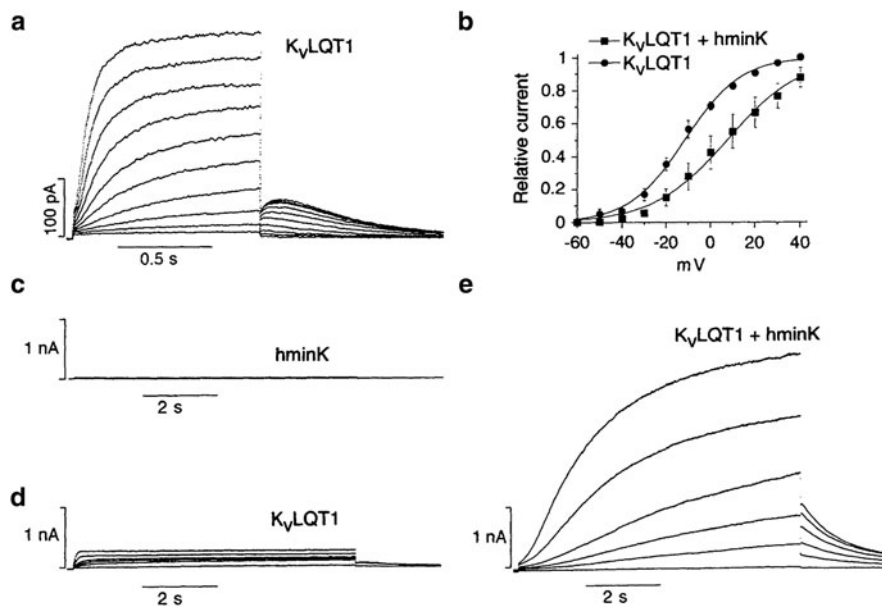


Fig. 24.2 Expression of I_{K_s} depends on the presence of both KCNQ1 (K_v LQT1) and KCNE1 (minK) message. Expression of KCNQ1 channels shows rapidly activating and inactivating current (a). Coexpression of KCNQ1 with KCNE1 encodes channels that do not inactivate but activated very slowly. This activity is very similar to native I_{K_s} . From Sanguinetti et al. [9]

Despite KCNQ1/KCNE1 coexpression recapitulating the basic voltage dependence and kinetics of I_{K_s} , cAMP regulation was not reproducible in recombinant systems. Further experiments revealed that the KCNQ1/KCNE1 channel is part of a more complicated macromolecular signaling complex in human heart [13]. The channel was shown to complex with an adaptor protein, Yotiao (AKAP9), coexpression of which was essential to restore the functional response of I_{K_s} channels to elevated cAMP. When coexpressed with AKAP9, KCNQ1/KCNE1 channels exhibited the characteristic hyperpolarizing shift in activation, slowing of deactivation, and increase in peak current, hallmarks of adrenergic regulation of I_{K_s} in mammalian cardiac myocytes (Fig. 24.3 [14, 15]). Furthermore, this investigation revealed that phosphorylation of a single serine in the amino terminus of KCNQ1 (S27) was necessary for the characteristic functional response to cAMP. A subsequent study found that AKAP9 itself is phosphorylated and that phosphorylation is required for the functional response [14, 15]. In recent years, the role of AKAPs has been studied in depth and AKAP9 has been shown to directly bind key enzymes in the β -AR signaling cascade (e.g., kinases, phosphatase, adenylate cyclase, and phosphodiesterases, see Fig. 24.4) in order to recruit them to the channel complex and form a local signaling environment to control the phosphorylation state of local proteins [16–19]. Thus, the most recent picture of the micro-signaling environment of the I_{K_s} channel shows an ensemble of critical signaling molecules brought together by AKAP9 which controls not only the phosphorylation/dephosphorylation state of

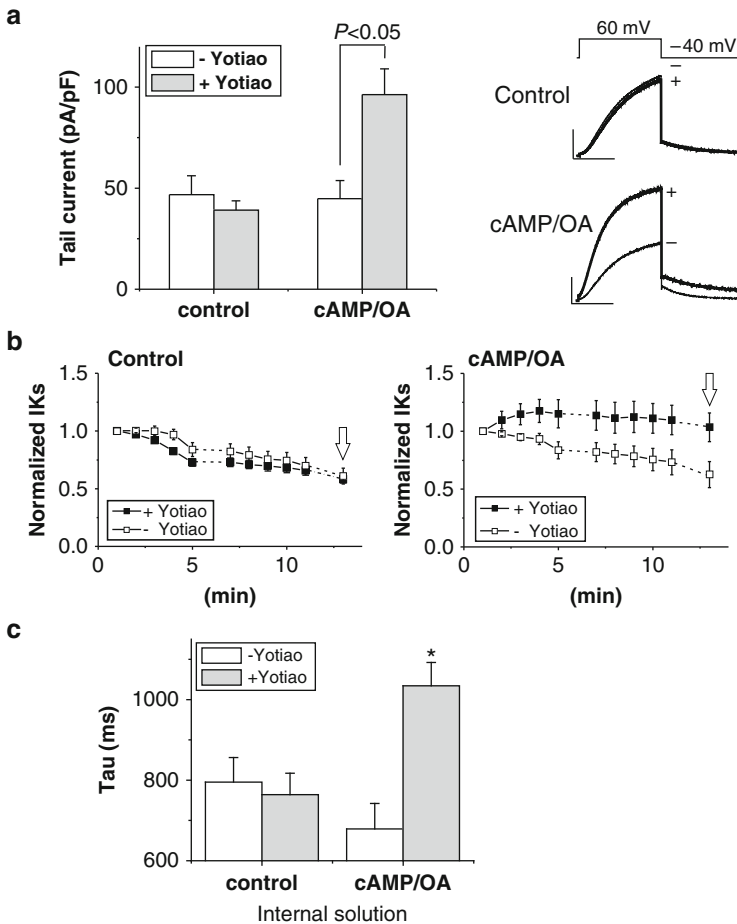


Fig. 24.3 Yotiao is required for functional response of I_{Ks} channels to cAMP. (a) Yotiao coexpression increases KCNQ1/KCNE1 channel currents with (cAMP/OA) but not without (control) cAMP (0.2 mM) and OA (0.2 μ M) dialysis. Shown are records and analysis obtained 12 min after membrane rupture. (Left) The bar graphs plot mean tail-current amplitude minus (open bars) or plus (filled bars) Yotiao coexpression (control: -Yotiao, $n = 10$, and +Yotiao, $n = 20$; cAMP/OA: -Yotiao, $n = 8$, and +Yotiao, $n = 12$). (Right) Mean current traces elicited by test pulses (+60 mV, -40 mV return) are superimposed without (- or with (+) Yotiao coexpression for control (Upper) and with cAMP/OA (Lower). (Scale: 100 pA/pF, 1 s.) (b) Mean \pm SEM tail-current amplitude (normalized to amplitude recorded 1 min after membrane rupture) is plotted versus time after membrane rupture. Data in a were obtained at times indicated by open arrows. (c) Time constants of I_{Ks} deactivation are slowed by Yotiao expression (+Yotiao) in the presence (cAMP/OA) but not in the absence (control) of cAMP. From Kurokawa et al. [15]

KCNQ1 (Ser 27), but also the cAMP concentration in the immediate vicinity of the channel. This local collection of signaling molecules ensures rapid and reversible control of the I_{Ks} channel in the face of physiologically essential changes in sympathetic nerve activity in the heart.

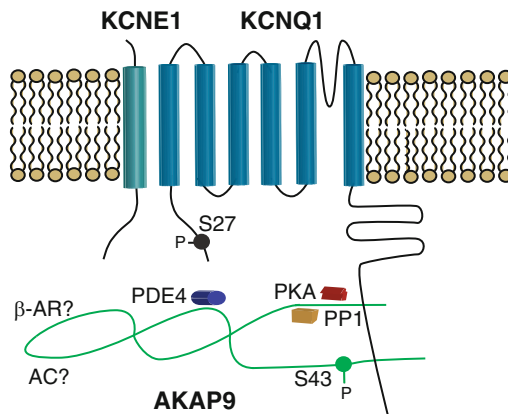


Fig. 24.4 Schematic of the I_{K_s} macromolecular complex. I_{K_s} channels are comprised of a-(KCNQ1) and b-(KCNE1) subunits with a PKA phosphorylation site on the N-terminus of KCNQ1 at position 27. The AKAP Yotiao (AKAP9) has a functionally important phosphorylation site at position 43 and interacts with the C-terminus of KCNQ1 to recruit several key enzymes, including PKA, PP1, and PDE4, to the channel complex. From Sampson and Kass [19]

24.4 I_{K_s} and Heritable Arrhythmia

The long QT syndrome (LQTS) is a relatively uncommon (1 in 2,500) genetic disorder associated with life-threatening arrhythmias and represents a channelopathy that has provided a wealth of information into the role of I_{K_s} in the human cardiac action potential. The LQTS (Romano–Ward syndrome, RWS) is a heterogeneous, autosomal dominant, congenital disease that is caused by mutations in genes coding for ion channel subunits or accessory proteins that are expressed in the heart [20, 21]. These channelopathies are associated with delayed repolarization of the ventricular chambers and are clinically manifested by syncope and sudden death from ventricular arrhythmias, notably torsade de pointes (TdP) [22]. Clinically, LQTS is identified by abnormal QT interval prolongation on the electrocardiogram (ECG). The QT prolongation may arise from either a decrease in repolarizing cardiac membrane currents (potassium channel currents) or an increase in excitatory membrane currents (sodium and/or calcium channel currents) during the plateau phase of the cardiac ventricular action potential.

Patients with LQTS are usually identified by QT prolongation on the ECG during clinical evaluation of unexplained syncope, as part of a family study when one family member has been identified with the syndrome, or in the investigation of patients with congenital neural deafness. The first family with LQTS was reported in 1957 and was thought to be an autosomal recessive disorder [23], but in 1997 it was shown to result from a dominant, homozygous mutation involving the KvLQT1 gene [24], now called the KCNQ1 gene. The more common autosomal dominant RWS was described in 1963–1964, and hundreds of different mutations involving 12 different genes (LQT1–12) have now been reported [25].

Amongst the genes responsible for LQTS, three of them encode for proteins that are part of the I_{K_s} channel complex: KCNQ1 (LQT1), KCNE1 (LQT5), and AKAP9 (LQT11). All of these mutations have a common pathway to the long QT seen clinically: decreased I_{K_s} current during an action potential. This can come as a result of any one of or a combination of the following: an expression or trafficking defect, alteration of the voltage dependence and kinetics of the channel, or blunting of the channels' ability to respond to cAMP.

Using a computational model of a human ventricular myocyte [26, 27], the effect of a reduced I_{K_s} current can be seen (Fig. 24.5). The most common and best studied long QT variant relating to I_{K_s} , LQT1 (KCNQ1), has a unique clinical phenotype compared to other common LQT variants wherein patients are particularly vulnerable to arrhythmia in the face of physical or emotional stressors [28]. That arrhythmia risk is elevated during exercise for LQT1 patients stimulated investigations into the molecular basis of this risk factor based on the hypothesis that molecular links between the I_{K_s} channel and β -adrenergic receptors were necessary and sufficient for normal physiological responses to increased sympathetic nervous system (SNS) activity that occurs during exercise.

This hypothesis was supported by demonstrations that mutations in KCNQ1 [13], KCNE1 [29], or Yotiao [30] can disrupt this SNS regulation and create heterogeneity in the cellular response to β -AR stimulation, a novel mechanism that may contribute to the triggering of some arrhythmias in LQT1, LQT5, and LQT11 [31]. The I_{K_s} channel, like most other ion channels, is a collection of assembled proteins that provides direct and rapid local control of ion movement through its central pore-conducting pathway. Several properties of the regulatory machinery for this pathway appear to be quite distinct: the functional consequences of channel phosphorylation require the presence of the regulatory subunit KCNE1 [29] as well as the presence of the adaptor protein in the channel complex [15]; furthermore, the adaptor protein itself is a substrate for PKA phosphorylation [14] adding yet another degree both of complexity and flexibility in the regulatory machinery necessary to regulate this physiologically essential channel.

More recently, the role of I_{K_s} in FAF and the short QT syndrome has been of great interest. These mutations all share the opposite characteristic of the LQTS mutants; an increase in I_{K_s} current during the cardiac action potential leading to premature repolarization (Fig. 24.5). This is achieved either through changes in the voltage dependence of the channels opening or simply through defects in channel deactivation that can allow the channel to accumulate in the open state after repetitive stimulation [32]. Although very rare amongst the population of atrial fibrillation patients [33], multiple mutations in KCNQ1 have been identified and linked with atrial fibrillation [34–36]. Interestingly, while atrial fibrillation is typically thought of as a disease of older age, usually affecting individuals greater than 65 years old, in patients harboring FAF mutations, the onset of arrhythmia occurs often at an early age. For example, in the first identified family, harboring KCNQ1 S140G, the average age of onset of atrial fibrillation was 24 years old [34]. Further characterization of two KCNQ1 mutants responsible for AF has shown that the primary mode of increased current is due to a defect in deactivation leading to accumulation of channels in the open state. As I_{K_s} has a hyperpolarized shift in activation and slowed deactivation in its phosphorylated state, it raises the question

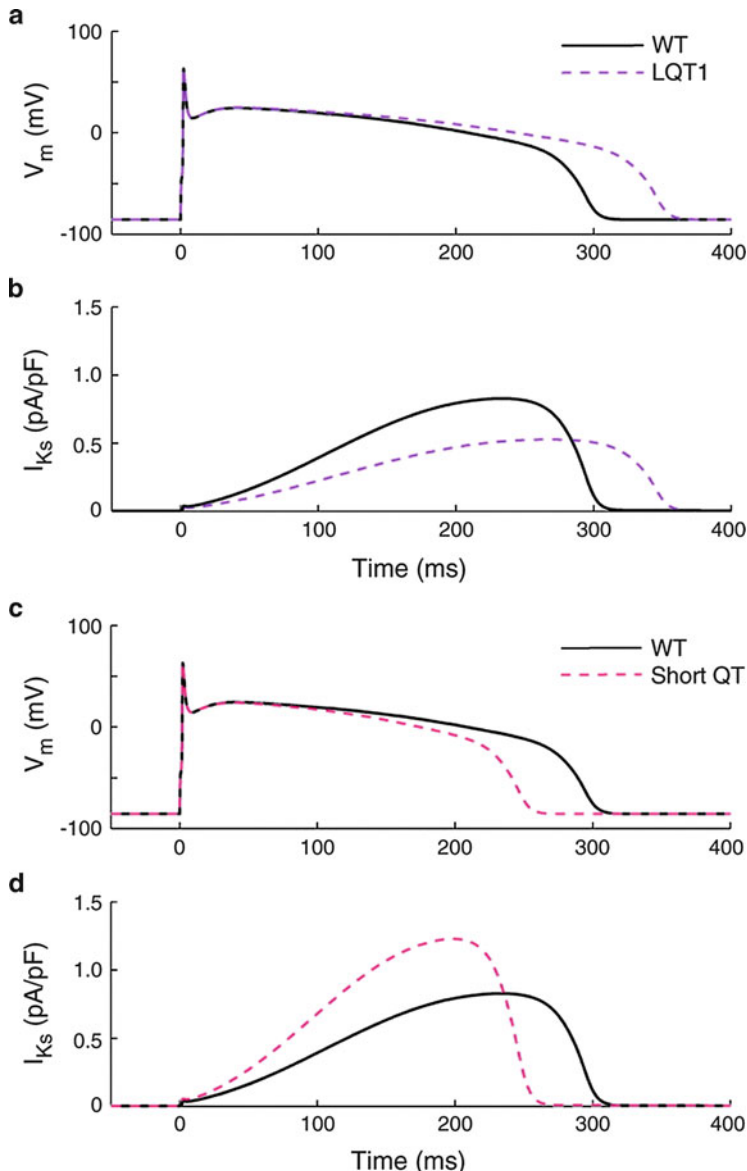


Fig. 24.5 Simulations reveal the effects of loss of function (LQT1) and gain of function (short QT) mutations in $KCNQ1$. Steady-state action potential waveforms (a and c) and outward I_{Ks} currents (b and d) were simulated (103,105). Control action potential and current waveforms simulated for wild-type $KCNQ1$ -encoded I_{Ks} currents are depicted as the solid black lines in a–d. The corresponding simulated voltage and current waveforms depicting the effects of $KCNQ1$ mutations are illustrated by the dashed purple (LQT1) and red (short QT) lines in a–d. “Loss of function” LQT1 mutations (Fig. 24.3c), resulting in a decrease in the maximum amplitude and a slowing of the time to peak of I_{Ks} (b), lead to marked action potential prolongation (a). In contrast, “gain of function” short QT mutations in $KCNQ1$ increase the maximal amplitude of I_{Ks} (d) and shorten action potential durations. From Nerbonne and Kass [27]

of whether the channel may play a role in other forms of atrial fibrillation. One such scenario is heart failure where several proteins in the heart have been shown to be hyperphosphorylated [37]. A transgenic mouse model confirmed the possibility that phosphorylated I_{K_s} can contribute to stabilizing atrial arrhythmias [38].

24.5 Conclusions

The mammalian cardiac ventricular action potential is distinguished by the long-lasting period of sustained depolarization that separates excitation and repolarization of the ventricular cell and hence establishes a measurable QT duration in the EKG. It has been well known since the classic experiments of Silvio Weidmann in [39] that this “plateau phase” of the action potential is a period in which the cellular input resistance is highest. Consequently, small changes in net membrane current that flow during the action potential plateau were predicted to have marked consequences on the timing of ventricular repolarization. Clearly this hypothesis and Weidmann’s fundamental insights into cardiac electrophysiology have been confirmed by the essential role played by the I_{K_s} channel and its regulation by SNS in human physiology and pathophysiology. Changes in the expression, regulation, and biophysical activity of this channel can perturb human cardiac electrophysiology and contribute to the broad range of human diseases summarized above. Too little I_{K_s} activity induced by heritable mutations place mutation carriers at risk of Torsades de Pointes and sudden cardiac death (SCD); too much I_{K_s} activity can contribute to atrial arrhythmias and re-entrant ventricular arrhythmias that too can place mutation carriers at risk of SCD.

The collaborative efforts starting from systematic evaluation of disease phenotype, arrhythmia risk, and patient genotype were the driving factors in the work summarized in this chapter. Through this partnership, not only has the critical role of the I_{K_s} channel in human physiology been unraveled and confirmed, the identification of channel-associated signaling molecules has been revealed. There is no doubt that continued efforts combining clinical data, molecular genetic data, and more detailed investigations probing both the temporal and “micro” spatial control not only of protein phosphorylation but of local cAMP will underlie the next level of understanding of regulation of this critical cardiac potassium channel as well as lead to potential novel targets to control the I_{K_s} macromolecular complex in the face of multiple human diseases.

References

1. Kass RS, Wiegers SE. The ionic basis of concentration-related effects of noradrenaline on the action potential of calf cardiac Purkinje fibres. *J Physiol.* 1982;322:541–58.
2. Tsien RW, Giles W, Greengard P. Cyclic AMP mediates the effects of adrenaline on cardiac Purkinje fibres. *Nat New Biol.* 1972;240(101):181–3.

3. Walsh KB, Kass RS. Distinct voltage-dependent regulation of a heart-delayed IK by protein kinases A and C. *Am J Physiol.* 1991;261(6 Pt 1):C1081–90.
4. Walsh KB, Kass RS. Regulation of a heart potassium channel by protein kinase A and C. *Science.* 1988;242(4875):67–9.
5. Yang WP, Levesque PC, Little WA, Conder ML, Shalaby FY, Blanar MA. KvLQT1, a voltage-gated potassium channel responsible for human cardiac arrhythmias. *Proc Natl Acad Sci USA.* 1997;94(8):4017–21.
6. Zhang ZJ, Jurkiewicz NK, Folander K, Lazarides E, Salata JJ, Swanson R. K^+ currents expressed from the guinea pig cardiac IsK protein are enhanced by activators of protein kinase C. *Proc Natl Acad Sci USA.* 1994;91:1766–70.
7. Wang Q, Curran ME, Splawski I, Burn TC, Millholland JM, VanRaay TJ, et al. Positional cloning of a novel potassium channel gene: KVLQT1 mutations cause cardiac arrhythmias. *Nat Genet.* 1996;12(1):17–23.
8. Takumi T, Ohkubo H, Nakanishi S. Cloning of a membrane protein that induces a slow voltage-gated potassium current. *Science.* 1988;242:1042–5.
9. Sanguinetti MC, Curran ME, Zou A, Shen J, Spector PS, Atkinson DL, et al. Coassembly of K(V)LQT1 and minK (IsK) proteins to form cardiac I(Ks) potassium channel. *Nature.* 1996;384(6604):80–3.
10. Barhanin J, Lesage F, Guillemaire E, Fink M, Lazdunski M, Romeo G. K(V)LQT1 and IsK (minK) proteins associate to form the I(Ks) cardiac potassium current. *Nature.* 1996;384(6604):78–80.
11. Yang Y, Sigworth FJ. Single-channel properties of I_{Ks} potassium channels. *J Gen Physiol.* 1998;112(6):665–78.
12. Sesti F, Goldstein SA. Single-channel characteristics of wild-type I_{Ks} channels and channels formed with two minK mutants that cause long QT syndrome. *J Gen Physiol.* 1998;112(6):651–63.
13. Marx SO, Kurokawa J, Reiken S, Motoike H, D'Armiento J, Marks AR, et al. Requirement of a macromolecular signaling complex for beta adrenergic receptor modulation of the KCNQ1-KCNE1 potassium channel. *Science.* 2002;295(5554):496–9.
14. Chen L, Kurokawa J, Kass RS. Phosphorylation of the A-kinase-anchoring protein Yotiao contributes to protein kinase A regulation of a heart potassium channel. *J Biol Chem.* 2005;280(36):31347–52.
15. Kurokawa J, Motoike HK, Rao J, Kass RS. Regulatory actions of the A-kinase anchoring protein Yotiao on a heart potassium channel downstream of PKA phosphorylation. *Proc Natl Acad Sci U S A.* 2004;101(46):16374–8.
16. Terrenoire C, Houslay MD, Baillie GS, Kass RS. The cardiac I_{Ks} potassium channel macromolecular complex includes the phosphodiesterase PDE4D3. *J Biol Chem.* 2009;284(14):9140–6.
17. Dessauer CW. Adenylyl cyclase-A-kinase anchoring protein complexes: the next dimension in cAMP signaling. *Mol Pharmacol.* 2009;76(5):935–41.
18. Piggott LA, Bauman AL, Scott JD, Dessauer CW. The A-kinase anchoring protein Yotiao binds and regulates adenylyl cyclase in brain. *Proc Natl Acad Sci USA.* 2008;105(37):13835–40.
19. Sampson KJ, Kass RS. Molecular mechanisms of adrenergic stimulation in the heart. *Heart Rhythm.* 2010;7(8):1151–31.
20. Moss AJ, Kass RS. Long QT syndrome: from channels to cardiac arrhythmias. *J Clin Invest.* 2005;115(8):2018–24.
21. Kass RS, Moss AJ. Mutation-specific pharmacology of the long QT syndrome. *Handb Exp Pharmacol.* 2006;171:287–304.
22. Moss AJ, Schwartz PJ, Crampton RS, Tzivoni D, Locati EH, MacCluer J, et al. The long QT syndrome: prospective longitudinal study of 328 families. *Circulation.* 1991;84:1136–44.
23. Jervell A, Lange-Nielsen F. Congenital deaf-mutism, functional heart disease with prolongation of the Q-T interval and sudden death. *Am Heart J.* 1957;54(1):59–68.

24. Splawski I, Timothy KW, Vincent GM, Atkinson DL, Keating MT. Molecular basis of the long-QT syndrome associated with deafness. *N Engl J Med.* 1997;336(22):1562–7.
25. Splawski I, Shen J, Timothy KW, Lehmann MH, Priori S, Robinson JL, et al. Spectrum of mutations in long-QT syndrome genes. *KVLQT1, HERG, SCN5A, KCNE1, and KCNE2.* *Circulation.* 2000;102(10):1178–85.
26. ten Tusscher KH, Noble D, Noble PJ, Panfilov AV. A model for human ventricular tissue. *Am J Physiol Heart Circ Physiol.* 2004;286(4):H1573–89.
27. Nerbonne JM, Kass RS. Molecular physiology of cardiac repolarization. *Physiol Rev.* 2005;85(4):1205–53.
28. Schwartz PJ, Priori SG, Spazzolini C, Moss AJ, Vincent GM, Napolitano C, et al. Genotype–phenotype correlation in the long-QT syndrome: gene-specific triggers for life-threatening arrhythmias. *Circulation.* 2001;103(1):89–95.
29. Kurokawa J, Chen L, Kass RS. Requirement of subunit expression for cAMP-mediated regulation of a heart potassium channel. *Proc Natl Acad Sci USA.* 2003;100(4):2122–7.
30. Chen L, Marquardt ML, Tester DJ, Sampson KJ, Ackerman MJ, Kass RS. Mutation of an A-kinase-anchoring protein causes long-QT syndrome. *Proc Natl Acad Sci USA.* 2007;104(52):20990–5.
31. Kass RS, Moss AJ. Long QT syndrome: novel insights into the mechanisms of cardiac arrhythmias. *J Clin Invest.* 2003;112(6):810–5.
32. Restier L, Cheng L, Sanguinetti MC. Mechanisms by which atrial fibrillation-associated mutations in the S1 domain of KCNQ1 slow deactivation of IKs channels. *J Physiol.* 2008;586(Pt 17):4179–91.
33. Ellinor PT, Moore RK, Patton KK, Ruskin JN, Pollak MR, Macrae CA. Mutations in the long QT gene, KCNQ1, are an uncommon cause of atrial fibrillation. *Heart.* 2004;90(12):1487–8.
34. Chen YH, Xu SJ, Bendahhou S, Wang XL, Wang Y, Xu WY, et al. KCNQ1 gain-of-function mutation in familial atrial fibrillation. *Science.* 2003;299(5604):251–4.
35. Hong K, Piper DR, Diaz-Valdecantos A, Brugada J, Oliva A, Burashnikov E, et al. De novo KCNQ1 mutation responsible for atrial fibrillation and short QT syndrome in utero. *Cardiovasc Res.* 2005;68(3):433–40.
36. Lundby A, Ravn LS, Svendsen JH, Olesen SP, Schmitt N. KCNQ1 mutation Q147R is associated with atrial fibrillation and prolonged QT interval. *Heart Rhythm.* 2007;4(12):1532–41.
37. Lehmart SE, Maier LS, Hasenfuss G. Abnormalities of calcium metabolism and myocardial contractility depression in the failing heart. *Heart Fail Rev.* 2009;14(4):213–24.
38. Sampson KJ, Terrenoire C, Cervantes DO, Kaba RA, Peters NS, Kass RS. Adrenergic regulation of a key cardiac potassium channel can contribute to atrial fibrillation: evidence from an I_{Ks} transgenic mouse. *J Physiol.* 2008;586(2):627–37.
39. Weidmann S. Effect of current flow on the membrane potential of cardiac muscle. *J Physiol.* 1951;115(2):227–36.

Chapter 25

Defects in Ankyrin-Based Protein Targeting Pathways in Human Arrhythmia

Hjalti Gudmundsson, Francis Jareczek, and Peter J. Mohler

25.1 Introduction

Ankyrins are a family of proteins responsible for the organization of membrane-associated, cytoskeletal, and signaling proteins at specialized membrane domains [1–4]. Ankyrins were first identified in the 1970s as a key structural component of the erythrocyte membrane cytoskeleton [5]. Nearly a decade later, ankyrin defects were linked with human hereditary spherocytosis [6, 7]. Over the past 20 years, ankyrin proteins have been shown to coordinate the physiological roles of a host of cell types including Purkinje neurons, renal epithelial cells, and pancreatic beta cells [8–12]. In the past 10 years, ankyrin function in excitable cardiomyocytes has been widely explored [13–15].

Ankyrin polypeptides are derived from three human genes. Ankyrin-R polypeptides, encoded by *ANK1* on human chromosome 8p11, are the prototypic ankyrins first characterized from the erythrocyte cytoskeleton [16]. *ANK1* gene products are also expressed in neurons and muscle [1, 17]. Ankyrin-B, encoded by *ANK2* on human chromosome 4q25-27, is expressed in most cell types including brain and heart [18, 19]. Ankyrin-G is encoded by *ANK3* on human chromosome 10q21. Similar to ankyrin-B, *ANK3* gene products are expressed in most vertebrate cells [3, 20–23].

Splicing of ankyrin genes results in a spectrum of structurally- and functionally-diverse polypeptides ranging in size from 26 to 480 kDa [3]. Canonical ankyrins (190–220 kDa) are composed of four distinct structural domains including a

H. Gudmundsson and F. Jareczek

Department of Internal Medicine, Division of Cardiovascular Medicine, University of Iowa, Iowa City, IA, USA

P.J. Mohler (✉)

Department of Internal Medicine, Division of Cardiovascular Medicine, University of Iowa, Iowa City, IA, USA

and

Department of Molecular Physiology and Biophysics, University of Iowa, Iowa City, IA, USA

e-mail: peter-mohler@uiowa.edu

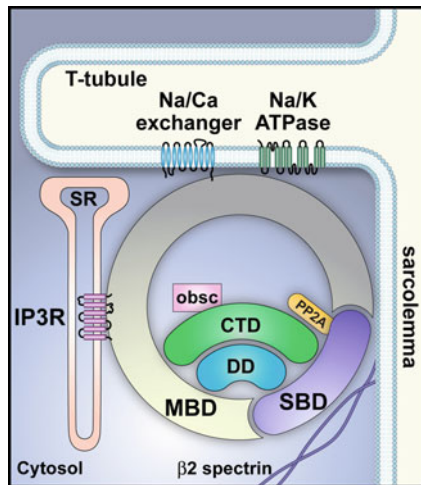
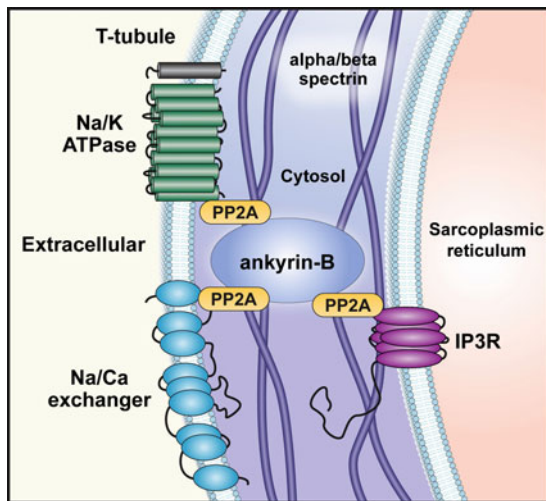


Fig. 25.1 Ankyrin-B-associated membrane protein complex. Ankyrins are comprised of four major structural domains including the membrane-binding domain (MBD), the spectrin-binding domain (SBD), the C-terminal domain (CTD), and the death domain (DD). Together, the CTD and DD comprise the regulatory domain. Ankyrin-B targets cardiac ion channels and transporters including Na^+/K^+ -ATPase, $\text{Na}^+/\text{Ca}^{2+}$ exchanger, IP₃ receptor, and targets protein phosphatase 2A (PP2A) through obscurin (obsc)

membrane-binding domain (MBD) of 24 ANK repeats, a spectrin-binding domain (SBD), a death domain (DD), and a C-terminal domain (CTD) (Fig. 25.1). Giant ankyrin isoforms that have specialized functions in neurons and in targeting voltage-gated Na_v channels to axon initial segments may also result from an insertion of a 220 kDa random coil between the SBD and DD [24]. Small ankyrin isoforms lacking large regions of a canonical ankyrin may be localized to specialized membrane sites including the Golgi apparatus, lysosomes, and sarcoplasmic reticulum (SR) [3]. In heart, ventricular cardiomyocytes express one major isoform of ankyrin-B (220 kDa ankyrin-B) and ankyrin-G (190 kDa ankyrin-G) [25, 26]. 220 kDa ankyrin-B is primarily localized to M-line and transverse (T) tubule/Z-line membranes and is hypothesized to function as a cellular chaperone for targeting specific ion channels/transporters to T-tubule/sarcoplasmic reticulum membrane domains [15]. In fact, as discussed below, a single ankyrin-B polypeptide may target a large membrane protein complex of Na^+/K^+ -ATPase, inositol 1,4,5 trisphosphate (IP₃) receptor, and $\text{Na}^+/\text{Ca}^{2+}$ exchanger to specific membrane sites (Fig. 25.2) [27]. 190 kDa ankyrin-G is localized at both ventricular cardiomyocyte intercalated disc and transverse-tubule membrane domains. Ankyrin-G is required for the specific targeting of the cardiac voltage-gated sodium channel ($\text{Na}_{v1.5}$) [25, 28].

The ankyrin MBD interacts with a host of diverse membrane proteins including ion channels, transporters, pumps, and cell adhesion molecules including the Na^+/K^+ -ATPase, voltage-gated Na^+ and K^+ channels, the $\text{Na}^+/\text{Ca}^{2+}$ exchanger, the IP₃

Fig. 25.2 Ankyrin-B protein complexes in the cardiomyocyte. Ankyrin-B links structurally unrelated proteins, including cardiac ion channels and transporters (Na^+/K^+ -ATPase, $\text{Na}^+/\text{Ca}^{2+}$ exchanger, IP3 receptor) with key structural (beta-spectrin, obscurin) and signaling (PP2A) molecules



receptor, the anion exchanger, CD44, and E-cadherin [27, 29–35]. In fact, ankyrin molecules may form large homomeric and heteromeric protein complexes to orchestrate large structural and signaling complexes [36, 37]. While the ankyrin SBD has been shown to have critical roles in linking ankyrin-associated membrane proteins with the spectrin- and actin-based cytoskeleton [38], recent evidence suggests that this large domain may also interact with key signaling proteins. For example, the SBD of ankyrin-B was recently demonstrated to interact with the targeting subunit (B56 alpha) of the protein phosphatase 2A (PP2A) protein complex [39]. In fact, loss of ankyrin-B impairs PP2A targeting to specific membrane domains in ventricular cardiomyocytes which may alter local signaling in the myocyte [39]. Finally, as described below, the ankyrin SBD is the site of select human ANK2 loss-of-function variants associated with arrhythmia [14, 15, 40]. Currently, the molecular basis for ankyrin-B loss-of-function of each variant is unknown. Nonetheless, these data strongly support a role of the SBD for normal ankyrin function.

The ankyrin DD and CTD comprise the ankyrin regulatory domain (RD) that mediates ankyrin interactions with proteins including obscurin, Hdj1, and Fas [41–50]. In fact, Cunha et al. recently reported that interaction of ankyrin-B with the large Rho-GEF obscurin is critical for the subcellular localization of PP2A in cardiomyocytes [48]. In addition to mediating intermolecular interactions, the ankyrin RD modulates intramolecular interactions (Fig. 25.1). Specifically, Bennett and colleagues recently demonstrated direct intramolecular interaction between the ankyrin-B MBD and CTD [51]. While the cellular role of intramolecular interactions for ankyrin-B functions is currently unknown, it is possible that intramolecular binding modulates (inhibits) the association of MBD with ankyrin membrane protein binding partners [27]. Finally, the association of multiple human ANK2 loss-of-function arrhythmia variants in the ankyrin-B DD and CTD further supports an important role of this region of the ankyrin in normal cardiac function [14].

25.2 Ankyrin Dysfunction in Human Arrhythmia

Over the past decade, the importance of ankyrin polypeptides for cardiac function has been unexpectedly supported by the link between ankyrin dysfunction and human cardiac disease. The next sections will review the association of human cardiac disease and ankyrin-based cellular pathways.

25.2.1 *Ankyrin-B Dysfunction in Human Ventricular Arrhythmia*

Long QT syndrome (LQTS) is a heterogenous group of inherited arrhythmias characterized by prolonged QT_c intervals on the electrocardiogram (ECG) and increased likelihood for sudden death [52]. Variants in the three genes (*KCNQ1*, *KCNH2*, and *SCN5A*) account for the majority of clinical LQT cases [53]. In fact, most inherited LQT syndromes are associated with variants in potassium or sodium channel gene products that delay repolarization and result in a prolonged rate-corrected QT interval [53]. The atypical type 4 long QT syndrome (type 4 LQTS) was described first by Schott et al. in 1995 in a large French kindred with a complex cardiac phenotype including sinus bradycardia, abnormal heart rate variability, atrial fibrillation, and long QT interval [54]. This French family also had two cases of sudden death. Linkage analysis revealed a new LQTS locus on chromosome 4 [54]. Nearly 8 years later, *ANK2* gene mis-sense variants were identified in affected individuals of the large kindred [15]. Specifically, the implicated gene variant resulted in the substitution of glycine for a highly conserved glutamic acid at residue 1425 (E1425G) near the C-terminus of the SBD [15]. This mutation was not present in unaffected family members or in a control population with normal ECGs [15]. Thus, the linkage of the *ANK2* gene with type 4 LQTS was the first example of a LQTS gene that encoded a protein other than an ion channel or an ion channel subunit.

To date, nine *ANK2* variants have been identified that demonstrate loss-of-function activity for ankyrin-B in cardiomyocytes [14, 15, 40]. The clinical phenotypes associated with these variants range from no obvious symptoms to sudden death [14]. In fact, different variants result in different degrees of ankyrin-B loss-of-function in vitro that correlate with the clinical severity [14]. Importantly, three variants represent severe ankyrin-B loss-of-function mutations when introduced into cardiomyocytes [14]. The clinical phenotypes in individuals heterozygous for *ANK2* variants include severe bradycardia, idiopathic ventricular fibrillation, atrial fibrillation, and polyphasic T waves on the ECG [14]. Interestingly, prolongation of the QT interval is not a consistent finding in individuals heterozygous for ankyrin-B loss-of-function, giving rise to the new name “ankyrin-B syndrome” instead of LQT4 syndrome. However, despite inconsistencies in QTc, individuals heterozygous for ankyrin-B loss-of-function variants are clearly at risk for these fatal arrhythmias [14, 15, 40].

25.2.2 *Ankyrin-B Dysfunction in Human Sinus Node Disease*

Recent data suggest that in addition to its association with severe ventricular arrhythmias, ankyrin-B plays an unexpected, but important role in the regulation of sinoatrial node (SAN) automaticity [13]. Sinus node dysfunction (SND) is a highly prevalent condition affecting individuals of all ages but is more common with increasing age [55]. This common clinical entity leads to bradycardia and syncope and accounts for approximately half of pacemaker implantations in the United States [56]. SND has been thought to be mostly caused by fibrous tissue replacing the nodal tissue although the etiology of the disease is far from being fully understood [57]. Work on familial forms of this disease has elucidated single gene defects associated with ion channels [58–60]. Two families with severe and highly penetrant SND were mapped to the *ANK2* locus. In one family, affected individuals carried the E1425G *ANK2* mutation. In a second family, affected individuals were carriers of a mutual haplotype at the *ANK2* locus although to date no mutation has been identified [13]. The molecular mechanisms underlying SND due to ankyrin-B dysfunction are unknown. Based on the spectrum of cardiac phenotypes displayed by carriers of different polymorphisms, the molecular phenotype is likely to be complex involving multiple protein partners in the sinus node cell. In summary, the ankyrin-B syndrome represents a new class of arrhythmias distinct from the classic long QT syndrome, representing sick sinus syndrome with bradycardia, ventricular arrhythmias, and risk of sudden death.

25.2.3 *Physiological and Cellular Roles of Ankyrin-B in the Ventricle*

Ankyrin-B^{+/−} mice have served as a robust tool for elucidating the role of ankyrin-B in human arrhythmia. Ankyrin-deficient mice die shortly after birth [19]. However, ankyrin-B^{+/−} mice are viable and display a number of cardiac phenotypes similar to individuals heterozygous for the ankyrin-B E1425G variant. Specifically, ankyrin-B^{+/−} mice display significant bradycardia and exhibit a high degree of heart rate variability compared to wild-type mice. Similar to many patients with ankyrin-B syndrome, ankyrin-B^{+/−} mice display significant QT_c prolongation and episodes of intermittent isorhythmic atrioventricular dissociation compared to wild-type littermates [13, 15]. Select individuals harboring the ankyrin-B E1425G loss-of-function mutation have experienced sudden death following physical exertion [15]. Likewise, ankyrin-B^{+/−} mice but not wild-type littermates subjected to exercise followed by epinephrine injection are predisposed to sudden death [15]. In summary, ankyrin-B^{+/−} mice, similar to patients with human ankyrin-B syndrome, display severe bradycardia, prolonged QT interval, heart rate variability, syncope, polymorphic ventricular arrhythmia, and sudden cardiac death in response to catecholaminergic stimulation [15].

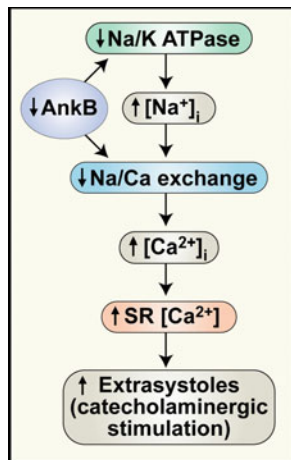


Fig. 25.3 Putative mechanism for ANK2-based catecholamine-induced arrhythmias. Decreased ankyrin-B activity results in reduced expression of the Na^+/K^+ -ATPase. Reduced Na^+/K^+ -ATPase activity increases cytosolic Na^+ concentration, which inhibits cytosolic calcium extrusion via the $\text{Na}^+/\text{Ca}^{2+}$ exchanger. Reduced ankyrin-B function also alters the expression and localization of the $\text{Na}^+/\text{Ca}^{2+}$ exchanger. Loss of I_{NCX} further reduces cytosolic calcium extrusion, resulting in elevated SR calcium stores (calcium taken up to SR via SERCA2). Subsequent and/or excessive catecholaminergic stimulation may result in cellular afterdepolarizations and extrasystoles

Studies in isolated ankyrin-B $^{+/-}$ cardiomyocytes have provided important information regarding the underlying ionic mechanism for arrhythmias in ankyrin-B-deficient mice and human patients with ankyrin-B mutations. Reduced expression of ankyrin-B in ankyrin-B $^{+/-}$ ventricular cardiomyocytes results in reduced expression and abnormal localization of ankyrin-B-associated proteins including Na^+/K^+ -ATPase, $\text{Na}^+/\text{Ca}^{2+}$ exchanger, and IP_3 receptor [15]. Decreased ankyrin-B function results in a reduced $\text{Na}^+/\text{Ca}^{2+}$ exchange activity through direct and indirect mechanisms (Fig. 25.3) [15]. Reduced Na^+/K^+ -ATPase activity increases cytosolic Na^+ concentration, which inhibits the activity of Ca^{2+} export via the $\text{Na}^+/\text{Ca}^{2+}$ exchanger, similar to the activity of digitalis [61]. In addition, reduced ankyrin-B function directly alters the membrane expression and localization of the $\text{Na}^+/\text{Ca}^{2+}$ exchanger [15]. This likely further reduces extracellular Ca^{2+} export via the $\text{Na}^+/\text{Ca}^{2+}$ exchanger, resulting in elevated SR Ca^{2+} stores and increased propensity for spontaneous Ca^{2+} release. At a single-cell level, ankyrin-B $^{+/-}$ cells display elevated SR Ca^{2+} stores and catecholamine-induced afterdepolarizations [4] that may result in extrasystoles and even arrhythmia at the level of the whole heart [15].

25.2.4 Physiological and Cellular Roles of Ankyrin-B in the Sinus Node

In addition to the ventricle, dysfunction in ankyrin-B protein targeting leads to loss of cytosolic Ca^{2+} regulation in the sinoatrial node [13]. Precise handling of cytosolic

Ca^{2+} is essential for normal SAN function and thus electrical automaticity of the SAN [62]. Ankyrin-B is expressed in SAN cells and is necessary for the localization and membrane expression of the voltage-gated Ca^{2+} channel, $\text{Ca}_v1.3$, in addition to the $\text{Na}^+/\text{Ca}^{2+}$ exchanger, Na^+/K^+ -ATPase, and IP_3 receptor [13]. Le Scouarnec et al. observed action potential rate reduction and increased rate variability in ankyrin-B^{+/−} SAN cells compared to wild type (WT) cells [13]. Previous studies have reported a similar cellular phenotype and spontaneous SAN arrhythmias in mice lacking $\text{Ca}_v1.3$ [63]. I_{NCX} has also been shown to be important for SAN automaticity. Specifically, $\text{Na}^+/\text{Ca}^{2+}$ exchanger knockout mice die before birth with significant heart rate defects [64, 65]. These data suggest that defects in ankyrin-B^{+/−} mouse SAN automaticity may be in large part due to loss of ankyrin-B targeting of $\text{Ca}_v1.3$ and $\text{Na}^+/\text{Ca}^{2+}$ exchanger.

Finally, in addition to sinus node disease and ventricular arrhythmias, individuals carrying *ANK2* variants may display atrial fibrillation [13, 15]. The molecular basis for atrial fibrillation associated with ankyrin dysfunction is currently unknown. However, based on findings in other cardiac excitable cell types, it is logical to postulate that loss of ankyrin targeting of key membrane and signaling proteins may represent the underlying cause. The link between ankyrin dysfunction and human atrial fibrillation is an exciting and obvious future direction for the field.

25.2.5 Ankyrin-G Dysfunction and Human Brugada Syndrome

Ankyrin-G is required for the targeting of voltage-gated Na_v channels in excitable cells. Experiments from cerebellar-specific ankyrin-G knockout mice reveal that ankyrin-G deficiency results in abnormal expression and localization of neuronal Na_v channels [66]. Moreover, recordings from neurons isolated from ankyrin-G null mice displayed deficiencies in action potential initiation and inability of the neurons to support rapid, repetitive discharges [66]. Biochemical experiments demonstrate that, through direct binding, ankyrin-G and $\text{Na}_v1.5$ co-localize at the intercalated disc and T-tubule membranes of ventricular cardiomyocytes [25, 28]. Moreover, ankyrin-G-, but not ankyrin-B-deficient cardiomyocytes display significant loss of $\text{Na}_v1.5$ expression (other ion channels show normal expression). As a result of deficient targeting, Na^+ current was either reduced or non-existent in ankyrin-G null myocytes [28]. In the context of the whole heart, decreased Na^+ current may reduce membrane excitability, resulting in slow and discontinuous conduction favorable to the initiation and maintenance of arrhythmias [67].

The Brugada syndrome, first described in 1992, is an autosomal-dominant potentially fatal cardiac arrhythmia characterized by ST segment elevation in the right precordial leads, right bundle branch block, and T wave inversions on the ECG [68]. Affected individuals are at high risk of death as a result of ventricular tachycardia or fibrillation despite having structurally normal hearts [68]. Typically, the syndrome manifests itself in adulthood, though cases have been reported in

children and in the elderly [69]. Variants in the *SCN5A* gene that encodes for Na_v1.5 are associated with a host of Brugada syndrome cases [70]. Specifically, *SCN5A*-associated variants are hypothesized to affect the biophysical properties of the sodium channel resulting in reduced or inconsistent inward I_{Na} . Recent work demonstrates a link between ankyrin-G, Na_v1.5, and the Brugada syndrome. Specifically, *SCN5A* variants that block association of Na_v1.5 with ankyrin-G have been associated with human Brugada syndrome probands [25]. In fact, Na_v1.5 E1053K that blocks ankyrin-G association is ineffectively targeted to the cardiomyocyte intercalated disc, consistent with reduced I_{Na} and the Brugada syndrome phenotype associated with this mutation [25]. Together, these findings illustrate a key role for ankyrin-G in myocyte ion channel targeting to the intercalated disc. Moreover, these studies demonstrate that dysfunction of the ankyrin-G-based protein targeting pathway may result in defects in normal physiology and human disease.

In addition to its role as a targeting protein, ankyrin-G serves as a structural component in various cell types. In epithelial cells, ankyrin-G directly interacts with a cell adhesion protein, E-cadherin, and is required for its localization to the lateral membrane [9, 71–73]. This interaction is critical for maintaining cell–cell adhesion. N-cadherin, found in both neural and cardiac tissues, may also interact with ankyrin-G in vivo [9, 71]. Inappropriate N-cadherin expression at the intercalated disc in cardiomyocytes may disrupt mechanical adhesion and electrical communication between cells and predispose the heart to arrhythmias [72, 73]. These observations further suggest the critical importance of ankyrin-G as a component of cell adhesion assemblies as well as in channel and transporter targeting. The potential role of ankyrin-G for protein organization at the myocyte intercalated disc is an important future direction for the field.

25.3 Conclusion

The last decade has been fruitful in identifying new cellular pathways associated with arrhythmias. Cardiac ankyrin polypeptides have been recognized as key components in targeting transporters and ion channels in the cardiomyocyte. Ankyrin-B-based targeting pathways are essential for handling cytosolic calcium and thus play a major role in the normal physiology of excitable cells. Dysfunction in cardiac ankyrins may result in several clinically-relevant arrhythmias. Ankyrin-B syndrome represents a new class of arrhythmia distinct from the classic long QT syndrome, representing sick sinus syndrome with bradycardia, atrial fibrillation, ventricular arrhythmias, and risk of sudden death. Similarly, defects in ankyrin-G-based pathways in cardiomyocytes result in a Brugada syndrome-like phenotype, an autosomal-dominant disease associated with sudden death. These points further underline the importance of ankyrins in normal cardiovascular function. However, while these findings illustrate the importance of cardiac ankyrins, there is a great deal still unknown. In fact, as ankyrins organize a host of key signaling, ion

transport, and structural components of the myocyte, these molecules may ultimately represent an unexpected, but potentially powerful therapeutic target for modulation of cellular excitability in cardiac rhythm disorders.

References

1. Mohler PJ, Gramolini AO, Bennett V. Ankyrins. *J Cell Sci.* 2002;115:1565–6.
2. Mohler PJ, Bennett V. Ankyrin-based cardiac arrhythmias: a new class of channelopathies due to loss of cellular targeting. *Curr Opin Cardiol.* 2005;20:189–93.
3. Cunha SR, Mohler PJ. Cardiac ankyrins: essential components for development and maintenance of excitable membrane domains in heart. *Cardiovasc Res.* 2006;71:22–9.
4. Mohler PJ. Ankyrins and human disease: what the electrophysiologist should know. *J Cardiovasc Electrophysiol.* 2006;17:1153–9.
5. Bennett V. Purification of an active proteolytic fragment of the membrane attachment site for human erythrocyte spectrin. *J Biol Chem.* 1978;253:2292–9.
6. Eber SW, Gonzalez JM, Lux ML, Scarpa AL, Tse WT, Dormwell M, et al. Ankyrin-1 mutations are a major cause of dominant and recessive hereditary spherocytosis. *Nat Genet.* 1996;13:214–8.
7. Palek J. Hereditary elliptocytosis, spherocytosis and related disorders: consequences of a deficiency or a mutation of membrane skeletal proteins. *Blood Rev.* 1987;1:147–68.
8. Bennett V, Baines AJ. Spectrin and ankyrin-based pathways: metazoan inventions for integrating cells into tissues. *Physiol Rev.* 2001;81:1353–92.
9. Kizhatil K, Bennett V. Lateral membrane biogenesis in human bronchial epithelial cells requires 190-kDa ankyrin-G. *J Biol Chem.* 2004;279:16706–14.
10. Kizhatil K, Sandhu NK, Peachey NS, Bennett V. Ankyrin-B is required for coordinated expression of beta-2-spectrin, the Na/K-ATPase and the Na/Ca exchanger in the inner segment of rod photoreceptors. *Exp Eye Res.* 2009;88:57–64.
11. Kizhatil K, Yoon W, Mohler PJ, Davis LH, Hoffman JA, Bennett V. Ankyrin-G and beta2-spectrin collaborate in biogenesis of lateral membrane of human bronchial epithelial cells. *J Biol Chem.* 2007;282:2029–37.
12. Mohler PJ, Healy JA, Xue H, Puca AA, Kline CF, Allingham RR, et al. Ankyrin-B syndrome: enhanced cardiac function balanced by risk of cardiac death and premature senescence. *PLoS One.* 2007;2:e1051.
13. Le Scouarnec S, Bhasin N, Vieyres C, Hund TJ, Cunha SR, Koval O, et al. Dysfunction in ankyrin-B-dependent ion channel and transporter targeting causes human sinus node disease. *Proc Natl Acad Sci USA.* 2008;105:15617–22.
14. Mohler PJ, Le Scouarnec S, Denjoy I, Lowe JS, Guicheney P, Caron L, et al. Defining the cellular phenotype of “ankyrin-B syndrome” variants: human ANK2 variants associated with clinical phenotypes display a spectrum of activities in cardiomyocytes. *Circulation.* 2007;115:432–41.
15. Mohler PJ, Schott JJ, Gramolini AO, Dilly KW, Guatimosim S, duBell WH, et al. Ankyrin-B mutation causes type 4 long-QT cardiac arrhythmia and sudden cardiac death. *Nature.* 2003;421:634–9.
16. Lambert S, Yu H, Prchal JT, Lawler J, Ruff P, Speicher D, et al. cDNA sequence for human erythrocyte ankyrin. *Proc Natl Acad Sci USA.* 1990;87:1730–4.
17. Lambert S, Bennett V. Postmitotic expression of ankyrinR and beta R-spectrin in discrete neuronal populations of the rat brain. *J Neurosci.* 1993;13:3725–35.
18. Otto E, Kunimoto M, McLaughlin T, Bennett V. Isolation and characterization of cDNAs encoding human brain ankyrins reveal a family of alternatively spliced genes. *J Cell Biol.* 1991;114:241–53.

19. Scotland P, Zhou D, Benveniste H, Bennett V. Nervous system defects of AnkyrinB (-/-) mice suggest functional overlap between the cell adhesion molecule L1 and 440-kD AnkyrinB in premyelinated axons. *J Cell Biol.* 1998;143:1305–15.
20. Kordeli E, Bennett V. Distinct ankyrin isoforms at neuron cell bodies and nodes of Ranvier resolved using erythrocyte ankyrin-deficient mice. *J Cell Biol.* 1991;114:1243–59.
21. Kordeli E, Davis J, Trapp B, Bennett V. An isoform of ankyrin is localized at nodes of Ranvier in myelinated axons of central and peripheral nerves. *J Cell Biol.* 1990;110:1341–52.
22. Kordeli E, Lambert S, Bennett V. AnkyrinG. A new ankyrin gene with neural-specific isoforms localized at the axonal initial segment and node of Ranvier. *J Biol Chem.* 1995;270:2352–9.
23. Kordeli E, Ludosky MA, Deprette C, Frappier T, Cartaud J. AnkyrinG is associated with the postsynaptic membrane and the sarcoplasmic reticulum in the skeletal muscle fiber. *J Cell Sci.* 1998;111:2197–207.
24. Zhang X, Bennett V. Restriction of 480/270-kD ankyrin G to axon proximal segments requires multiple ankyrin G-specific domains. *J Cell Biol.* 1998;142:1571–81.
25. Mohler PJ, Rivolta I, Napolitano C, Lemaitre G, Lambert S, Priori SG, et al. Nav1.5 E1053K mutation causing Brugada syndrome blocks binding to ankyrin-G and expression of Nav1.5 on the surface of cardiomyocytes. *Proc Natl Acad Sci USA.* 2004;101:17533–8.
26. Tuvia S, Buhusi M, Davis L, Reedy M, Bennett V. Ankyrin-B is required for intracellular sorting of structurally diverse Ca²⁺ homeostasis proteins. *J Cell Biol.* 1999;147:995–1008.
27. Mohler PJ, Davis JQ, Bennett V. Ankyrin-B coordinates the Na/K ATPase, Na/Ca exchanger, and InsP(3) receptor in a cardiac T-tubule/SR microdomain. *PLoS Biol.* 2005;3:e423.
28. Lowe JS, Palygin O, Bhasin N, Hund TJ, Boyden PA, Shibata E, et al. Voltage-gated Nav channel targeting in the heart requires an ankyrin-G dependent cellular pathway. *J Cell Biol.* 2008;180:173–86.
29. Cunha SR, Bhasin N, Mohler PJ. Targeting and stability of na/ca exchanger 1 in cardiomyocytes requires direct interaction with the membrane adaptor ankyrin-B. *J Biol Chem.* 2007;282:4875–83.
30. Li ZP, Burke EP, Frank JS, Bennett V, Philipson KD. The cardiac Na⁺-Ca²⁺ exchanger binds to the cytoskeletal protein ankyrin. *J Biol Chem.* 1993;268:11489–91.
31. Malhotra JD, Kazen-Gillespie K, Hortsch M, Isom LL. Sodium channel beta subunits mediate homophilic cell adhesion and recruit ankyrin to points of cell–cell contact. *J Biol Chem.* 2000;275:11383–8.
32. Pan Z, Kao T, Horvath Z, Lemos J, Sul JY, Cranstoun SD, et al. A common ankyrin-G-based mechanism retains KCNQ and NaV channels at electrically active domains of the axon. *J Neurosci.* 2006;26:2599–613.
33. Morrow JS, Cianci CD, Ardito T, Mann AS, Kashgarian M. Ankyrin links fodrin to the alpha subunit of Na⁺, K⁺-ATPase in Madin-Darby canine kidney cells and in intact renal tubule cells. *J Cell Biol.* 1989;108:455–65.
34. Bourguignon LY, Iida N, Jin H. The involvement of the cytoskeleton in regulating IP3 receptor-mediated internal Ca²⁺ release in human blood platelets. *Cell Biol Int.* 1993;17:751–8.
35. Lokeshwar VB, Fregien N, Bourguignon LY. Ankyrin-binding domain of CD44(GP85) is required for the expression of hyaluronic acid-mediated adhesion function. *J Cell Biol.* 1994;126:1099–109.
36. Jenkins SM, Bennett V. Ankyrin-G coordinates assembly of the spectrin-based membrane skeleton, voltage-gated sodium channels, and L1 CAMs at Purkinje neuron initial segments. *J Cell Biol.* 2001;155:739–46.
37. Michael P, Bennett V. The ANK repeats of erythrocyte ankyrin form two distinct but cooperative binding sites for the erythrocyte anion exchanger. *J Biol Chem.* 1995;270:22050–7.
38. Bennett V, Stenbuck PJ. Identification and partial purification of ankyrin, the high affinity membrane attachment site for human erythrocyte spectrin. *J Biol Chem.* 1979;254:2533–41.

39. Bhasin N, Cunha SR, Mudannayake M, Gigena MS, Rogers TB, Mohler PJ. Molecular basis for PP2A regulatory subunit B56{alpha} targeting in cardiomyocytes. *Am J Physiol Heart Circ Physiol.* 2007;293:H109–19.
40. Mohler PJ, Splawski I, Napolitano C, Bottelli G, Sharpe L, Timothy K, et al. A cardiac arrhythmia syndrome caused by loss of ankyrin-B function. *Proc Natl Acad Sci USA.* 2004;101:9137–42.
41. Kontogianni-Konstantopoulos A, Jones EM, Van Rossum DB, Bloch RJ. Obscurin is a ligand for small ankyrin 1 in skeletal muscle. *Mol Biol Cell.* 2003;14:1138–48.
42. Bagnato P, Barone V, Giacomello E, Rossi D, Sorrentino V. Binding of an ankyrin-1 isoform to obscurin suggests a molecular link between the sarcoplasmic reticulum and myofibrils in striated muscles. *J Cell Biol.* 2003;160:245–53.
43. Hopitzan AA, Baines AJ, Kordeli E. Molecular evolution of ankyrin: gain of function in vertebrates by acquisition of an obscurin/titin-binding-related domain. *Mol Biol Evol.* 2006;23:46–55.
44. Kontogianni-Konstantopoulos A, Catino DH, Strong JC, Sutter S, Borisov AB, Pumplin DW, et al. Obscurin modulates the assembly and organization of sarcomeres and the sarcoplasmic reticulum. *FASEB J.* 2006;20:2102–11.
45. Raeker MO, Su F, Geisler SB, Borisov AB, Kontogianni-Konstantopoulos A, Lyons SE, et al. Obscurin is required for the lateral alignment of striated myofibrils in zebrafish. *Dev Dyn.* 2006;235:2018–29.
46. Armani A, Galli S, Giacomello E, Bagnato P, Barone V, Rossi D, et al. Molecular interactions with obscurin are involved in the localization of muscle-specific small ankyrin1 isoforms to subcompartments of the sarcoplasmic reticulum. *Exp Cell Res.* 2006;312:3546–58.
47. Borzok MA, Catino DH, Nicholson JD, Kontogianni-Konstantopoulos A, Bloch RJ. Mapping the binding site on small ankyrin 1 for obscurin. *J Biol Chem.* 2007;282:32384–96.
48. Cunha SR, Mohler PJ. Obscurin targets ankyrin-B and protein phosphatase 2A to the cardiac M-line. *J Biol Chem.* 2008;283:31968–80.
49. Del Rio M, Imam A, DeLeon M, Gomez G, Mishra J, Ma Q, et al. The death domain of kidney ankyrin interacts with Fas and promotes Fas-mediated cell death in renal epithelia. *J Am Soc Nephrol.* 2004;15:41–51.
50. Mohler PJ, Hoffman JA, Davis JQ, Abdi KM, Kim CR, Jones SK, et al. Isoform specificity among ankyrins: an amphipathic alpha-helix in the divergent regulatory domain of ankyrin-B interacts with the molecular co-chaperone Hdj1/Hsp40. *J Biol Chem.* 2004;279:25798–804.
51. Abdi KM, Mohler PJ, Davis JQ, Bennett V. Isoform specificity of ankyrin-B: a site in the divergent C-terminal domain is required for intramolecular association. *J Biol Chem.* 2006;281:5741–9.
52. Moss AJ, Schwartz PJ, Crampton RS, Locati E, Carleen E. The long QT syndrome: a prospective international study. *Circulation.* 1985;71:17–21.
53. Splawski I, Shen J, Timothy KW, Lehmann MH, Priori S, Robinson JL, et al. Spectrum of mutations in long-QT syndrome genes. *KVLQT1, HERG, SCN5A, KCNE1, and KCNE2.* *Circulation.* 2000;102:1178–85.
54. Schott JJ, Charpentier F, Peltier S, Foley P, Drouin E, Bouhour JB, et al. Mapping of a gene for long QT syndrome to chromosome 4q25-27. *Am J Hum Genet.* 1995;57:1114–22.
55. Rubenstein JJ, Schulman CL, Yurchak PM, DeSanctis RW. Clinical spectrum of the sick sinus syndrome. *Circulation.* 1972;46:5–13.
56. Adan V, Crown LA. Diagnosis and treatment of sick sinus syndrome. *Am Fam Physician.* 2003;67:1725–32.
57. Demoulin JC, Kulbertus HE. Histopathological correlates of sinoatrial disease. *Br Heart J.* 1978;40:1384–9.
58. Benson DW, Wang DW, Dymment M, Knilans TK, Fish FA, Strieper MJ, et al. Congenital sick sinus syndrome caused by recessive mutations in the cardiac sodium channel gene (SCN5A). *J Clin Invest.* 2003;112:1019–28.
59. Smits JP, Koopmann TT, Wilders R, Veldkamp MW, Ophof T, Bhuiyan ZA, et al. A mutation in the human cardiac sodium channel (E161K) contributes to sick sinus syndrome,

- conduction disease and Brugada syndrome in two families. *J Mol Cell Cardiol.* 2005;38:969–81.
60. Ueda K, Nakamura K, Hayashi T, Inagaki N, Takahashi M, Arimura T, et al. Functional characterization of a trafficking-defective HCN4 mutation, D553N, associated with cardiac arrhythmia. *J Biol Chem.* 2004;279:27194–8.
 61. Akera T, Brody TM. The role of Na^+ , K^+ -ATPase in the inotropic action of digitalis. *Pharmacol Rev.* 1977;29:187–220.
 62. Kodama I, Nikmaram MR, Boyett MR, Suzuki R, Honjo H, Owen JM. Regional differences in the role of the Ca^{2+} and Na^+ currents in pacemaker activity in the sinoatrial node. *Am J Physiol.* 1997;272:H2793–806.
 63. Mangoni ME, Couette B, Bourinet E, Platzer J, Reimer D, Striessnig J, et al. Functional role of L-type Cav1.3 Ca^{2+} channels in cardiac pacemaker activity. *Proc Natl Acad Sci USA.* 2003;100:5543–8.
 64. Bogdanov KY, Maltsev VA, Vinogradova TM, Lyashkov AE, Spurgeon HA, Stern MD, et al. Membrane potential fluctuations resulting from submembrane Ca^{2+} releases in rabbit sino-atrial nodal cells impart an exponential phase to the late diastolic depolarization that controls their chronotropic state. *Circ Res.* 2006;99:979–87.
 65. Wakimoto K, Kobayashi K, Kuro OM, Yao A, Iwamoto T, Yanaka N, et al. Targeted disruption of $\text{Na}^+/\text{Ca}^{2+}$ exchanger gene leads to cardiomyocyte apoptosis and defects in heartbeat. *J Biol Chem.* 2000;275:36991–8.
 66. Zhou D, Lambert S, Malen PL, Carpenter S, Boland LM, Bennett V. AnkyrinG is required for clustering of voltage-gated Na channels at axon initial segments and for normal action potential firing. *J Cell Biol.* 1998;143:1295–304.
 67. Shaw RM, Rudy Y. Ionic mechanisms of propagation in cardiac tissue. Roles of the sodium and L-type calcium currents during reduced excitability and decreased gap junction coupling. *Circ Res.* 1997;81:727–41.
 68. Brugada P, Brugada J. Right bundle branch block, persistent ST segment elevation and sudden cardiac death: a distinct clinical and electrocardiographic syndrome. A multicenter report. *J Am Coll Cardiol.* 1992;20:1391–6.
 69. Antzelevitch C, Brugada P, Borggrefe M, Brugada J, Brugada R, Corrado D, et al. Brugada syndrome: report of the second consensus conference. *Heart Rhythm.* 2005;2: 429–40.
 70. Smits JP, Eckardt L, Probst V, Bezzina CR, Schott JJ, Remme CA, et al. Genotype–phenotype relationship in Brugada syndrome: electrocardiographic features differentiate SCN5A-related patients from non-SCN5A-related patients. *J Am Coll Cardiol.* 2002;40:350–6.
 71. Kizhatil K, Davis JQ, Davis L, Hoffman J, Hogan BL, Bennett V. Ankyrin-G is a molecular partner of E-cadherin in epithelial cells and early embryos. *J Biol Chem.* 2007;282:26552–61.
 72. Li J, Levin MD, Xiong Y, Petrenko N, Patel VV, Radice GL. N-cadherin haploinsufficiency affects cardiac gap junctions and arrhythmic susceptibility. *J Mol Cell Cardiol.* 2008;44:597–606.
 73. Li J, Patel VV, Kostetskii I, Xiong Y, Chu AF, Jacobson JT, et al. Cardiac-specific loss of N-cadherin leads to alteration in connexins with conduction slowing and arrhythmogenesis. *Circ Res.* 2005;97:474–81.

Chapter 26

Genetically Modified Mice: Useful Models to Study Cause and Effect of Cardiac Arrhythmias?

Gregor Sachse, Martin Kruse, and Olaf Pongs

26.1 Introduction

A powerful approach to understanding cardiac disease mechanisms is to characterize mutations in respective genes, followed by a study of their physiological impact with molecular biological methods. Frequently, this involves the generation of transgenic mice, where the gene of interest is either deleted (knockout), mutated (knockin) or overexpressed. The importance of genetically modified mice lies in the ability to address specific physiological questions *in vitro* as well as *in vivo*. These types of studies have made significant contributions to our current understanding, for example, of cardiac channelopathies and strategies to treat them. However, since the physiology of human and mouse cardiac systems inevitably exhibits substantial differences, it is not a straightforward and easy matter to recapitulate in the mouse a specific mutational effect on human cardiac function. Furthermore, influences of genetic background, environmental factors, life style, emotional status, etc. on human cardiac phenotype are difficult to assess in genetically modified mice. From the molecular biological and physiological results in mice, extracting a conclusive picture about the mechanistic impact of a mutation on cardiac phenotype is a demanding task. In this context, we refer the reader to a recent review on currently available techniques for screening cardiovascular phenotypes in intact, conscious mice [1]. Our aim in the present chapter is to discuss possibilities and potentials which studies with genetically modified mice offer for characterizing cardiophysiological phenotypes. We place particular emphasis on methodological limitations that one may encounter when using genetically modified mice for studying the molecular biological and physiological basis of human cardiac channelopathies.

G. Sachse, M. Kruse, and O. Pongs (✉)

Institut für Neurale Signalverarbeitung, ZMNH, University Hospital Hamburg-Eppendorf, Martinistr.
52, 20246 Hamburg, Germany
e-mail: morin@zmnh.uni-hamburg.de

26.2 Comparison of Human and Mouse Heart Rate

The electrical impulse of each heartbeat is propagated through the heart by direct cell-cell coupling of cardiac muscle cells and through the cardiac conduction system, composed of the sinoatrial node (the natural pacemaker), ill-defined atrial tracks, and the atrioventricular node, and thereafter the ventricular conduction system, formed by the bundle of His, the left and right bundle branches, and Purkinje fibers. The final read-out of electrical impulse propagation consists in a contraction of ventricular muscle [2]. In general, the mechanisms in human and mouse heart which regulate the propagation of cardiac electrical impulse display common features. In detail, however, there are important differences to be seen. For example, the frequency of beats in a non-diseased human heart may vary between 60 and 180 bpm depending on the state of activity. This corresponds to a heart beat frequency of 1–3 Hz [3, 4]. A mouse heart, on the other hand, beats significantly faster (400–750 bpm), thus exhibiting an about five- to tenfold increase in heart beat frequency [5, 6]. The increase is associated with a significant shortening of P-wave, PR-interval and QT-interval in a mouse electrocardiogram (ECG) as compared to a human ECG [7] (Fig. 26.1a, b; Table 26.1). Furthermore, the mouse ECG almost completely lacks a visible T-wave (Fig. 26.1a, b) [5–9]. Thus, human and mouse

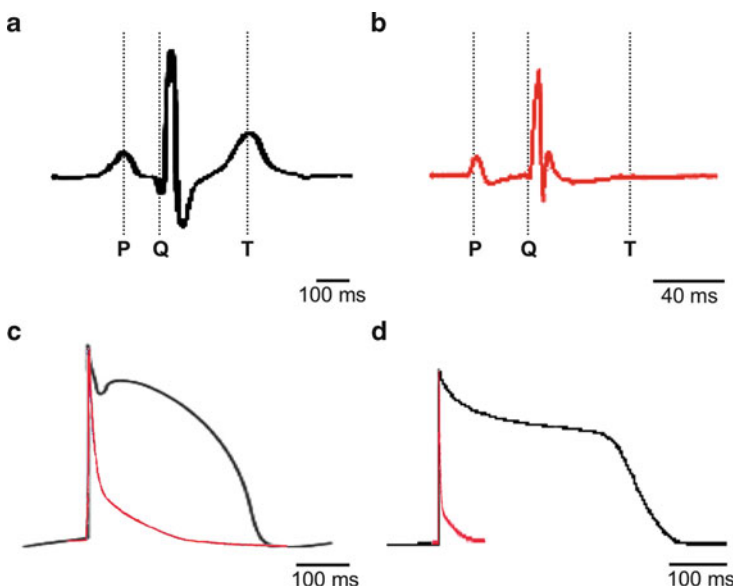


Fig. 26.1 Electocardiograms and ventricular action potentials of human and mouse. (a) Electrocardiogram of a healthy human [8]. (b) Electrocardiogram of a wild-type mouse [9]. (c) Action potential recorded on a human (black) and a mouse (red) atrial myocyte [5]. (d) Action potential recorded on a human (black) and an adult ventricular mouse (red) myocyte [5]

Table 26.1 Comparison of ECG parameters in mouse and human

	Mouse	Human
PQ interval (ms)	40	120–200
QRS interval (ms)	10–15	<100
QT interval (ms)	80	<430
HR (min^{-1})	500–700	60–70

PQ interval, time for atrioventricular conduction; QRS interval, time for ventricular depolarization; QT interval, time for ventricular depolarization and repolarization; HR, heart rate. Data are from [1]

ECGs exhibit important differences in shape and duration, most likely reflecting some differences in electrical impulse propagation throughout the heart.

It is still quite difficult to break down the contribution of single tissue and, in particular, single cardiac cells to the complex pattern of propagation of cardiac electrical impulse. Although advanced technologies for measuring electrical pulse propagation in Langendorff heart preparations are available [10], the future availability of acute cardiac tissue slice preparations for electrophysiological experiments represents a major development to carry out informative (electro) physiological studies on cardiac activity in genetically modified mice. Complementary electrophysiological studies are usually carried out on freshly isolated, primary cardiac cells. As a last resort, if genetically modified mice are unavailable for the specific mutation, the effect of the mutation is studied with cloned ion channels in *in vitro* expression systems. The ventricular cardiomyocyte represents the most popular primary cardiac cell for molecular biological and electrophysiological studies. One can easily evoke action potential (AP) firing under current clamp conditions and dissect the contributions of specific ion channels to shape and frequency of AP firing in the voltage-clamp configuration of the patch-clamp method. Electrophysiological studies on primary atrial cardiomyocytes (Fig. 26.1c) and on sino-atrial node cells have also been published, albeit not as extensively as on primary ventricular cardiomyocytes. We concentrate our discussion on the data on ventricular cardiomyocytes (Fig. 26.1d). The data show that human and mouse ventricular cardiomyocytes have similar depolarizing current properties mediated by voltage-gated Na^+ and Ca^{2+} channels [5]. Thus, depolarization phases (time rise to peak) of APs recorded on adult human or mouse ventricular myocytes are very similar. The repolarization phases, however, display characteristic differences between both species (Fig. 26.1d). After a first brief repolarization phase, the human ventricular AP enters a plateau phase, which lasts 200–300 ms, and the membrane potential remains relatively constant during this phase. Subsequently, a relatively rapid repolarization ensues bringing the membrane potential back to rest. In contrast, APs recorded from atrial and ventricular myocytes of adult mice lack the plateau phase, and repolarization takes place very rapidly within 30–50 ms (Fig. 26.1d) [5, 7].

26.3 Different Expression Patterns of Voltage-Gated K⁺ Channels in Human and Mouse Ventricular Myocytes

Apparently, human and mouse ventricular myocytes have comparable sets of (depolarizing) voltage-gated Na⁺ and Ca²⁺ channels, but they differ with respect to the number and kind of (repolarizing) voltage-gated K⁺ (K_V) channels (Table 26.2) [5]. Note that little information is available on cardiac Cl⁻ channels and, therefore, they are not considered here. The differing K_V channel “outfits” can nicely explain the differences observed between human and mouse ventricular AP shape and duration (see Fig. 26.1). For example, human ventricular myocytes prominently express KCNH2 (HERG, K_V11.1) and KCNQ1 (K_V7.1)/KCNE1 K⁺ channels. The two K_V channels are responsible for two major repolarizing K⁺ currents I_{K_r} and I_{K_s} , respectively [13, 14]. By contrast, adult mouse ventricular myocytes predominantly express $I_{to,f}$, $I_{to,s}$, and I_{K_ur} , whereas I_{K_s} plays a subordinate role and I_{K_r} is absent [5, 15]. In fact, mouse adult ventricular myocytes express neither K_V11.1 (mouse ERG) channels nor KCNE1 subunits. As a result, KCNQ1 channels in mouse cardiomyocytes have very different gating characteristics in comparison with KCNQ1/KCNE1 channels in human cardiomyocytes [15]. Thus, mouse cardiomyocytes may be very useful tools for investigating specific characteristics of electrical impulse propagation and contributions of specific ion channel activities. However, one should be aware that mouse data may be neither informative for studying pharmacological effects in relation to the diseased human heart nor useful for characterizing human cardiac phenotypes associated with altered HERG and KCNQ1/KCNE1 channel activity. Similar concerns may also hold for published studies on the role of specific ion channels such as hyperpolarization-activated cyclic nucleotide gated ion channels (HCN) or T-type voltage-gated Ca²⁺ channel [16, 17].

Note that mouse embryos and newborn mice display heart rates (~2 Hz) which are more comparable to human heart rates, and the developing mouse heart expresses I_{K_r} and I_{K_s} as major ventricular repolarizing K⁺ currents [15]. The molecular correlates are like those in the human heart, viz., HERG and KCNQ1/KCNE1 channels, respectively. Mice lacking a functional KCNH2 gene die during

Table 26.2 Contribution of voltage-gated potassium channels to the repolarization of adult human and mouse ventricular action potentials

Contribution	Human AP	Mouse AP
Major	KCNQ1/KCNE1	K _V 4.2/KChIP2
	HERG	K _V 4.3/KChIP2
	K _V 4.3/KChIP2	K _V 2.1
Minor	K _V 1.2	K _V 1.1
	K _V 1.5	K _V 1.5
	K _V 2.1	KCNQ1

K_V, voltage-gated K⁺ channel; AP, action potential; HERG, human *ether-à-go-go* related K_V channel; KCNE1 and KChIP2 (K-channel interacting protein 2) are ancillary K_V channel subunits. Data were taken from [5, 11, 12]

embryonic development due to heart failure [18]. After birth, KCNE1 as well as mouse ERG ($K_v11.1$) expression is down regulated. The developmental switch in the expression of K^+ channel genes correlates well with the observed acceleration in AP repolarization in the adult mouse heart. Potentially, the embryonic mouse heart may be more useful in some comparative studies than that of the adult mouse. In conclusion, mouse and human electrocardiograms show significant differences in shape and duration which are associated with different K_v channel expression patterns and probably also with that of other proteins involved in the propagation of cardiac electrical impulse.

26.4 What Is Wrong with My Mouse?

The advent of techniques to genetically modify the mouse genome and to produce directed mutations in both a conditional and tissue-specific manner represents a dramatic advance for specifically addressing questions in cardiophysiological research. Over the recent years, many different genetically modified mice have been generated for studying disease-related cardiac phenotypes, for example, to study the effect of mutations on voltage-gated ion channels in relation to channelopathies (Table 26.3). The data resulting from the studies with genetically modified mice have provided valuable and important information to further our understanding of cardiac electrical impulse propagation and the role of particular ion channels in this process. However, the wealth of studies with genetically modified mice has also unveiled certain limitations that may be encountered when studying disease-related cardiac phenotypes resulting from an altered genotype. In this context, it cannot be overemphasized that the significance of phenotype–genotype correlations is limited as long as in-depth studies of the underlying mechanisms were not performed. Potentially, a genetically modified mouse exhibits some unexpected functional characteristics (see below), requiring a critical re-evaluation of the hypothesized genotype–phenotype relation.

26.4.1 Methodologies to Genetically Modified Mice

There are two principally different methods available for obtaining genetically modified mice. The first method relies on pronucleus injection of recombinant DNA of interest to generate transgenic mice. This method entails many pitfalls. In general, several copies of the injected DNA become integrated into the genome leading to ectopic expression as well as overexpression of the gene product of interest. Position effects may alter both strength and pattern of expression – potentially to such an extent that from over 20 transgenic mouse lines, no two show the same pattern of expression [34]. Furthermore, the integrated gene may interact with other genes close to the integration site producing unexpected results,

Table 26.3 Selected genetically modified mice related to cardiac function

Genetic modification	Phenotype	Reference
<i>cacna1d</i> ^{-/-}	Bradyarrhythmias, conduction slowing, AV block	[19]
<i>cacna1g</i> ^{-/-}	Bradycardia, conduction slowing	[20]
<i>hcn2</i> ^{-/-}	Sinus dysrhythmia	[17]
<i>hcn4</i> ^{-/-} and cardiac specific <i>hcn4</i> ^{-/-}	Embryonic lethal, embryonic bradycardia	[16]
Cardiac specific TG: Kv1.5 α DN	QT prolongation	[21]
Cardiac specific TG: Kv2.1DN	QT prolongation	[22]
<i>kcdn2</i> ^{-/-}	Electrical and molecular remodeling, loss of $I_{to,f}$	[23]
<i>kcn1</i> ^{-/-}	Arrhythmogenic atrial and ventricular phenotypes of varying severity	[24–26]
<i>kcn2</i> ^{-/-}	Hypothyroidism; cardiac hypertrophy, ventricular fibrosis; hypernatremia	[10, 27]
<i>kcnh2</i> ^{-/-}	Embryonic lethal	[18]
<i>kcnh2</i> ^{-/-} (splice variant B specific)	Episodic sinus bradycardia	[28]
<i>kcnip2</i> ^{-/-}	Highly susceptible to arrhythmias, otherwise normal structure and function of the heart	[29]
<i>kcnj2</i> ^{-/-}	Lowered heart rate in neonates, postnatal lethal	[30]
<i>kcnj5</i> ^{-/-}	Abnormal heart rate regulation	[31]
<i>kcnq1</i> ^{-/-}	Jervell and Lange-Nielsen syndrome	[32]
TG: Kv7.1DN	Bradyarrhythmias, AV block	[7]
KI: <i>Scn5a</i> ^{Δ/+}	Spontaneous and inducible tachyarrhythmias	[33]

^{-/-} homozygous for knockout, *TG* ectopic transgene, *DN* dominant negative mutant, *KI* knockin, ^{Δ/+} heterozygous for deletion mutant

confounding the phenotype [35] or causing a disease unrelated to the transgene [36]. The second method involves genetic targeting by homologous recombination in ES cell lines followed by subsequent blastocyst injection to generate knockout (usually a deletion) or knockin (usually a muantation) heterozygous and homozygous mouse lines, respectively. The methodology has become increasingly more refined, most notably by the introduction of conditional gene-targeting methods using the CRE/lox^P system, followed by inducible genetic modifications [37] and response elements for reversible gene activation [38]. Homologous recombination in ES cells circumvents many of the problems that one may encounter with transgenic animals because it leads to a specific integration at the site of the gene of interest. The methodology provides for the powerful option to specifically manipulate the existing genotype instead of adding an ectopic gene.

26.4.2 Influence of Genetic Background on Phenotype

For generating recombinant ES cells, ES cells derived from inbred mouse 129 strain are commonly used; these are injected into the blastocysts of the inbred mouse strain C57BL/6J for establishing a genetically modified mouse line. The subsequent

breeding is usually performed with the C57BL/6J strain, because the C57BL/6J mice are more easily maintained than 129X1/SvJ mice in the laboratory. C57BL/6J may be regarded as the common laboratory mouse. In addition, the C57BL/6J genome has been sequenced to near completeness [39]. The drawback of this procedure is that many (>10) generations of backcrossing are required to generate a congenic strain. Because this is both time-consuming and costly, it is not done frequently. The breeding may be greatly accelerated using a marker-assisted breeding scheme including SNP analysis [40]. It is quite a common practice to keep an inbred strain having a hybrid (129X1/SvJ/C57BL/6J) genetic background. Mice heterozygous for the introduced mutation are then used for breeding, and littermates with or without the mutation are used for experimental studies. Littermate controls eliminate some environmental variability. Also, studying mixed backgrounds may increase the chance of discovering a phenotype [41]. But the inherent problem of this approach is that variations in genetic background and comparison of “wild-type” and mutant mice of different genetic background potentially confound the data. ES-cell methodology is far from foolproof. Genetic background variability has been shown to greatly influence cardiovascular parameters in mice and, for example, can generate blood pressure differences of as much as ~40 mmHg [42]. Progressive loss of heterozygosity results in genetic drift for such colonies. Hybrid background composition is random and may impede reproducibility of results between genetic mouse models. Measurements of physiological parameters under these circumstances typically exhibit a high variance. For instance, tenfold differences in mean plasma aldosterone levels were seen in littermate controls from two hybrid colonies that had been generated from the same original background strains [43]. It is noteworthy that a side effect of elevated plasma aldosterone levels is an increased sensitivity of cardiac tissue to arrhythmia [44]. If one can take advantage of available high-throughput screens to analyze a specific cardiac phenotype, one may be able to circumvent these problems [45].

26.4.3 Influence of Flanking Genes on Phenotypic Outcome

An additional difficulty in studies with genetically altered mice arises from the “flanking gene” problem. This is an often overlooked potential source of artifact. Alleles in the vicinity of the modified locus will belong to the strain background in which the modification was generated (usually 129X1/SvJ) and alleles of controls will belong to the other (e.g., C57BL/6J). Because chromosomal crossover events are rare, flanking allele inequality will persist even after extensive backcrossing, effectively linking a modified gene to its flanking regions [40]. The flanking regions can contain modifier genes or small RNAs that differ between the two strains and play a significant role in the manifestation of the phenotype. This situation can potentially create a phenotype that is unconnected to the modified gene. Several approaches to this problem have been proposed. One approach that the Branbury Conference on Genetic Background has recommended [46] is to backcross to both

original backgrounds (e.g., 129X1/SvJ and C57BL/6J). Subsequently the phenotype of F1 hybrids is analyzed, which allows for control of flanking gene effects (see [41] and [47] for review).

26.4.4 Complications in Phenotypic Analysis

Several transgenic as well as knockout mouse lines have been generated to address the role of specific ion channel subunits in cardiac function (Table 26.3). In quite a few of these studies, a pleiotropic effect was observed. Furthermore, an increasing number of studies show that a loss of one ion channel subunit can alter the expression of existing subunits or even stipulate de novo expression of ion channel subunits [48]. The phenotypic analysis of *kcne2*^{-/-} mice is a case in point. Analysis of ventricular myocytes of *kcne2*^{-/-} mice showed a ~50% reduction in the $I_{K,\text{slow}}$ mediated by Kv1.5, and a ~25% reduction in the $I_{\text{to},f}$ current, mediated by Kv4.2 [10]. The data were supported by co-immunoprecipitation experiments indicating an association of KCNE2 with native Kv1.5 and Kv4.2 ion channel subunits. Consistent with a reduced ventricular K⁺ current was the cardiac *kcne2*^{-/-} phenotype. Isolated, perfused intact hearts of *kcne2*^{-/-} mice exhibited prolonged ventricular action potential duration (APD). The data appear clear-cut as long as one ignores the fact that *kcne2*^{-/-} mice have not only an “electrical” cardiac phenotype, but also other symptoms that may have an important influence on the apparent cardiac phenotype. The *kcne2*^{-/-} mice have clear symptoms of hypothyroidism, including impaired thyroid iodide accumulation, cardiac hypertrophy, alopecia, dwarfism, and goiter. KCNQ1/KCNE2 K⁺ channels play an important role in thyroid tri- and tetraiodothyronine (T₃, T₄) biosynthesis [27]. Hypothyroidism is associated with dilated and hypertrophic cardiomyopathies, reduced fractional shortening, and heart failure [49]. Remarkably, administration of T₃ and T₄ to *kcne2*^{-/-} pups dramatically alleviates the hypothyroidism and also the abnormal electrophysiological phenotype observed with *kcne2*^{-/-} cardiomyocytes [27]. These remarkable data indicate an unexpected pathway as a major source of the observed cardiac phenotype implicating an endocrine component for known KCNE2- and KCNQ1-linked human cardiac arrhythmias [27]. Another important implication of the data is that structural heart disease and cardiac arrhythmia may have a common denominator, for example, being linked to thyroid dysfunction as a result of a defective ion channel in the thyroid.

26.4.5 Effects of Ion Channel Mislocation on Cardiac Phenotype

Mutations which lead to altered ion channel trafficking to and from the membrane or to mislocalization of the ion channel to the plasma membrane also lead to ion channel dysfunction and to cardiac arrhythmia. Obviously, a misplaced ion channel

may have a similar effect on arrhythmia than a non-functional ion channel, which cannot gate properly. Interestingly, various cardiac ion channels, especially the nodal HCN4 pacemaker channel, the voltage-gated SCN5A Na⁺ channel and the L-type CACNA1C Ca²⁺ channel, necessary for excitation–contraction coupling in ventricular muscle, and the adrenergic receptors are closely associated with caveolin-3 (CAV3) and caveolae. Mutations in *CAV3* as well as in *CAVIN* lead to a cardiac phenotype with features of arrhythmias and long QT syndromes, most probably because the mutations interfere with caveolae formation, which has an important influence on cardiac ion channel activity [50, 51]. It shows that in-depth characterizations of ion channel mutations can yield new and exciting insights into the regulation of ion channel function. In this context, genetically modified mice are invaluable tools to significantly further our understanding on how a mutation in an ion channel gene may lead to cardiac dysfunction.

26.5 Conclusions

Genetically modified mice represent a powerful tool for cardiophysiological research, which has dramatically enhanced our ability to answer physiological questions. Careful experimental design including the use of conditional, inducible, and multiple genetic modifications, or rescue experiments is essential to exploit the potential that a genetically modified mouse line has to offer. Elucidating genotype–phenotype relations is a formidable task, and the results may be confounded by genetic background variations or be misled by a strictly hypothesis-driven approach missing out an unexpected physiological or molecular biological mechanism as the cause of the phenotype.

Acknowledgments We gratefully acknowledge financial support of the Deutsche Forschungsgemeinschaft and the Fonds der Chemischen Industrie for the cardiovascular research in our laboratory.

References

1. Fitzgerald SM, Gan L, Wickman A, Bergstrom G. Cardiovascular and renal phenotyping of genetically modified mice: a challenge for traditional physiology. *Clin Exp Pharmacol Physiol*. 2003;30:207–16.
2. Josephson ME, Zimetbaum P, Buxton AE, Marchlinski FE. The tachyarrhythmias. In: Fauci AS, Braunwald E, Isselbacher KJ, Wilson JD, Martin JB, Kasper DL, Hauser SL, Longo DL, editors. *Harrison's principles of internal medicine*. New York: McGraw-Hill; 1998.
3. Fuster V. *Hurst's the heart*. 10th ed. New York: McGraw-Hill Health Professions Division; 2001.
4. Chiang CE, Roden DM. The long QT syndromes: genetic basis and clinical implications. *J Am Coll Cardiol*. 2000;36:1–12.

5. Nerbonne JM. Studying cardiac arrhythmias in the mouse – a reasonable model for probing mechanisms? *Trends Cardiovasc Med.* 2004;14:83–93.
6. London B. Cardiac arrhythmias: from (transgenic) mice to men. *J Cardiovasc Electrophysiol.* 2001;12:1089–91.
7. Demolombe S, Lande G, Charpentier F, van Roon MA, van den Hoff MJ, Toumaniantz G, et al. Transgenic mice overexpressing human KvLQT1 dominant-negative isoform. Part I: phenotypic characterisation. *Cardiovasc Res.* 2001;50:314–27.
8. Technische Universität CAROLO-WILHELMINA zu Braunschweig. 2010. http://www.emg.tu-bs.de/bilder/forschung/eegekg/ekg_kurve.jpg.
9. Knollmann BC, Blatt SA, Horton K, de Freitas F, Miller T, Bell M, et al. Inotropic stimulation induces cardiac dysfunction in transgenic mice expressing a troponin T (I79N) mutation linked to familial hypertrophic cardiomyopathy. *J Biol Chem.* 2001;276:10039–48.
10. Roepke TK, Kontogeorgis A, Ovanez C, Xu X, Young JB, Purtell K, et al. Targeted deletion of *Kcnex2* impairs ventricular repolarization via disruption of *I(K,slow1)* and *I(to,f)*. *FASEB J.* 2008;22:3648–60.
11. Nerbonne JM, Kass RS. Molecular physiology of cardiac repolarization. *Physiol Rev.* 2005; 85:1205–53.
12. Pongs O, Schwarz J. Ancillary subunits associated with voltage-dependent K^+ channels. *Physiol Rev.* 2010;90:755–96.
13. Kurokawa J, Abriel H, Kass RS. Molecular basis of the delayed rectifier current *I(ks)* in heart. *J Mol Cell Cardiol.* 2001;33:873–82.
14. Sanguinetti MC. Dysfunction of delayed rectifier potassium channels in an inherited cardiac arrhythmia. *Ann N Y Acad Sci.* 1999;868:406–13.
15. Knollmann BC, Casimiro MC, Katchman AN, Sirenko SG, Schober T, Rong Q, et al. Isoproterenol exacerbates a long QT phenotype in *Kcnq1*-deficient neonatal mice: possible roles for human-like *Kcnq1* isoform 1 and slow delayed rectifier K^+ current. *J Pharmacol Exp Ther.* 2004;310:311–8.
16. Stieber J, Herrmann S, Feil S, Loster J, Feil R, Biel M, et al. The hyperpolarization-activated channel HCN4 is required for the generation of pacemaker action potentials in the embryonic heart. *Proc Natl Acad Sci USA.* 2003;100:15235–40.
17. Ludwig A, Budde T, Stieber J, Moosmang S, Wahl C, Holthoff K, et al. Absence epilepsy and sinus dysrhythmia in mice lacking the pacemaker channel HCN2. *EMBO J.* 2003;22:216–24.
18. London B, Pan X. QT interval prolongation and arrhythmias in heterozygous MERG1-targeted mice. *Circulation.* 1998;98:279.
19. Platzer J, Engel J, Schrott-Fischer A, Stephan K, Bova S, Chen H, et al. Congenital deafness and sinoatrial node dysfunction in mice lacking class D L-type Ca^{2+} channels. *Cell.* 2000; 102:89–97.
20. Mangoni ME, Traboulsi A, Leoni AL, Couette B, Marger L, Le Quang K, et al. Bradycardia and slowing of the atrioventricular conduction in mice lacking $CaV3.1/\alpha 1G$ T-type calcium channels. *Circ Res.* 2006;98:1422–30.
21. Li H, Guo W, Yamada KA, Nerbonne JM. Selective elimination of *I(K,slow1)* in mouse ventricular myocytes expressing a dominant negative Kv1.5alpha subunit. *Am J Physiol Heart Circ Physiol.* 2004;286:H319–28.
22. Xu H, Barry DM, Li H, Brunet S, Guo W, Nerbonne JM. Attenuation of the slow component of delayed rectification, action potential prolongation, and triggered activity in mice expressing a dominant-negative Kv2 alpha subunit. *Circ Res.* 1999;85:623–33.
23. Guo W, Jung WE, Marionneau C, Aimond F, Xu H, Yamada KA, et al. Targeted deletion of Kv4.2 eliminates *I(to, f)* and results in electrical and molecular remodeling, with no evidence of ventricular hypertrophy or myocardial dysfunction. *Circ Res.* 2005;97:1342–50.
24. Charpentier F, Merot J, Riochet D, Le Marec H, Escande D. Adult KCNE1-knockout mice exhibit a mild cardiac cellular phenotype. *Biochem Biophys Res Commun.* 1998;251: 806–10.

25. Drici MD, Arrighi I, Chouabe C, Mann JR, Lazdunski M, Romey G, et al. Involvement of IsK-associated K⁺ channel in heart rate control of repolarization in a murine engineered model of Jervell and Lange-Nielsen syndrome. *Circ Res.* 1998;83:95–102.
26. Temple J, Frias P, Rottman J, Yang T, Wu Y, Verheijck EE, et al. Atrial fibrillation in KCNE1-null mice. *Circ Res.* 2005;97:62–9.
27. Roepke TK, King EC, Reyna-Neyra A, Paroder M, Purtell K, Koba W, et al. Kcne2 deletion uncovers its crucial role in thyroid hormone biosynthesis. *Nat Med.* 2009;15:1186–94.
28. Lees-Miller JP, Guo J, Somers JR, Roach DE, Sheldon RS, Rancourt DE, et al. Selective knockout of mouse ERG1 B potassium channel eliminates I(Kr) in adult ventricular myocytes and elicits episodes of abrupt sinus bradycardia. *Mol Cell Biol.* 2003;23:1856–62.
29. Kuo HC, Cheng CF, Clark RB, Lin JJ, Lin JL, Hoshijima M, et al. A defect in the Kv channel-interacting protein 2 (KChIP2) gene leads to a complete loss of I(to) and confers susceptibility to ventricular tachycardia. *Cell.* 2001;107:801–13.
30. Zaritsky JJ, Redell JB, Tempel BL, Schwarz TL. The consequences of disrupting cardiac inwardly rectifying K(+) current (I(K1)) as revealed by the targeted deletion of the murine Kir2.1 and Kir2.2 genes. *J Physiol.* 2001;533:697–710.
31. Wickman K, Nemec J, Gendler SJ, Clapham DE. Abnormal heart rate regulation in GIRK4 knockout mice. *Neuron.* 1998;20:103–14.
32. Casimiro MC, Knollmann BC, Ebert SN, Vary Jr JC, Greene AE, Franz MR, et al. Targeted disruption of the Kcnq1 gene produces a mouse model of Jervell and Lange-Nielsen Syndrome. *Proc Natl Acad Sci USA.* 2001;98:2526–31.
33. Nuyens D, Stengl M, Dugarmaa S, Rossenbacher T, Compernolle V, Rudy Y, et al. Abrupt rate accelerations or premature beats cause life-threatening arrhythmias in mice with long-QT3 syndrome. *Nat Med.* 2001;7:1021–7.
34. Feng G, Mellor RH, Bernstein M, Keller-Peck C, Nguyen QT, Wallace M, et al. Imaging neuronal subsets in transgenic mice expressing multiple spectral variants of GFP. *Neuron.* 2000;28:41–51.
35. Assarsson E, Chambers BJ, Hogstrand K, Berntman E, Lundmark C, Fedorova L, et al. Severe defect in thymic development in an insertional mutant mouse model. *J Immunol.* 2007;178:5018–27.
36. Vogler C, Galvin N, Levy B, Grubb J, Jiang J, Zhou XY, et al. Transgene produces massive overexpression of human beta -glucuronidase in mice, lysosomal storage of enzyme, and strain-dependent tumors. *Proc Natl Acad Sci USA.* 2003;100:2669–73.
37. Kuhn R, Schwenk F, Aguet M, Rajewsky K. Inducible gene targeting in mice. *Science.* 1995;269:1427–9.
38. Gossen M, Bujard H. Tight control of gene expression in mammalian cells by tetracycline-responsive promoters. *Proc Natl Acad Sci USA.* 1992;89:5547–51.
39. Ensembl. 2010. http://www.ensembl.org/Mus_musculus/info/Index.
40. Markel P, Shu P, Ebeling C, Carlson GA, Nagle DL, Smutko JS, et al. Theoretical and empirical issues for marker-assisted breeding of congenic mouse strains. *Nat Genet.* 1997;17:280–4.
41. Doetschman T. Influence of genetic background on genetically engineered mouse phenotypes. *Methods Mol Biol.* 2009;530:423–33.
42. SchLAGER G. Selection for blood pressure levels in mice. *Genetics.* 1974;76:537–49.
43. Merillat AM, Charles RP, Porret A, Maillard M, Rossier B, Beermann F, et al. Conditional gene targeting of the ENaC subunit genes Scnn1b and Scnn1g. *Am J Physiol Renal Physiol.* 2009;296:F249–56.
44. Struthers AD. The clinical implications of aldosterone escape in congestive heart failure. *Eur J Heart Fail.* 2004;6:539–45.
45. Svenson KL, Bogue MA, Peters LL. Invited review: Identifying new mouse models of cardiovascular disease: a review of high-throughput screens of mutagenized and inbred strains. *J Appl Physiol.* 2003;94:1650–9. Discussion 1673.

46. Mutant mice and neuroscience: recommendations concerning genetic background. Banbury Conference on genetic background in mice. *Neuron* 1997;19:755–9.
47. Wolfer DP, Crusio WE, Lipp HP. Knockout mice: simple solutions to the problems of genetic background and flanking genes. *Trends Neurosci.* 2002;25:336–40.
48. Nerbonne JM, Gerber BR, Norris A, Burkhalter A. Electrical remodelling maintains firing properties in cortical pyramidal neurons lacking KCND2-encoded A-type K⁺ currents. *J Physiol.* 2008;586:1565–79.
49. Tang YD, Kuzman JA, Said S, Anderson BE, Wang X, Gerdes AM. Low thyroid function leads to cardiac atrophy with chamber dilatation, impaired myocardial blood flow, loss of arterioles, and severe systolic dysfunction. *Circulation*. 2005;112:3122–30.
50. Rajab A, Straub V, McCann LJ, Seelow D, Varon R, Barresi R, et al. Fatal cardiac arrhythmia and long-QT syndrome in a new form of congenital generalized lipodystrophy with muscle rippling (CGL4) due to PTRF-CAVIN mutations. *PLoS Genet.* 2010;6:e1000874.
51. Gazzero E, Sotgia F, Bruno C, Lisanti MP, Minetti C. Caveolinopathies: from the biology of caveolin-3 to human diseases. *Eur J Hum Genet.* 2010;18:137–45.

Chapter 27

Genetics of Atrial Fibrillation

**Saagar Mahida, Michiel Rienstra, Moritz F. Sinner, Steven A. Lubitz,
Patrick T. Ellinor, and Stefan Kääb**

27.1 Introduction

Inherited forms of atrial fibrillation (AF), characterized by Mendelian segregation of the trait, have been recognized since the 1940s [1]. Most of the early research in AF genetics focused on Mendelian AF families. In the last decade, investigators have identified mutations in ion channel coding genes as well as non-ion channel

Patrick T. Ellinor and Stefan Kääb have contributed equally to this manuscript.

S. Mahida

Cardiovascular Research Center, Massachusetts General Hospital, Charlestown, MA, USA

M. Rienstra

Cardiovascular Research Center, Massachusetts General Hospital, Charlestown, MA, USA
and

University Medical Center Groningen, University of Groningen, Groningen, The Netherlands

M.F. Sinner

Cardiovascular Research Center, Massachusetts General Hospital, Charlestown, MA, USA
and

Department of Medicine I, Ludwig-Maximilians-University Munich, Klinikum Grosshadern,
Marchioninistr. 15, Munich 81377, Germany

and

The NHLBI's Framingham Heart Study, Framingham, MA, USA

S.A. Lubitz and P.T. Ellinor

Cardiovascular Research Center, Massachusetts General Hospital, Charlestown, MA, USA
and

Cardiac Arrhythmia Service, Massachusetts General Hospital, Boston, MA, USA

S. Kääb (✉)

Department of Medicine I, Ludwig-Maximilians-University Munich, Klinikum Grosshadern,
Marchioninistr. 15, Munich 81377, Germany

e-mail: stefan.kaab@med.uni-muenchen.de

coding genes [2–10]. However these mutations have only been identified in isolated AF families and overall, monogenic forms of AF represent a rare disease subtype [11].

More recently, evidence has emerged to suggest that the heritability of AF is more widespread. A number of population based studies have demonstrated that AF in the general population is not simply an acquired disease but in fact has a significant heritable component [12–15]. The elucidation of the genetic substrate underlying the common AF phenotype is more challenging. As is the case with most complex traits, AF risk is likely to be determined by an interaction between environmental influences and multiple genetic variants that individually exert modest effects.

A number of candidate gene association studies in AF cohorts have attempted to identify genetic polymorphisms that increase the risk of developing AF [16–23]. However, these results have been confounded by limitations in study design. In recent years, the advent of genome-wide association studies (GWAS) has fundamentally accelerated our understanding of the genetic basis of complex traits. GWAS in AF cohorts have led to the identification of novel loci that confer increased susceptibility to the arrhythmia [24–28]. However, the mechanisms by which these variants lead to AF are presently unclear.

In this chapter, we describe current molecular genetic approaches to the investigation of AF and outline the evidence for the involvement of susceptibility genes in the pathogenesis of AF.

27.2 Heritability of AF

A number of population-based studies have demonstrated that the heritability of AF extends beyond rare monogenic subtypes. Investigators from the Framingham Heart Study reported that a parental history of AF independently predicts risk of future disease in offspring. Specifically, having a parent with AF almost doubles the 4-year risk of developing the arrhythmia, even after adjustment for risk factors such as hypertension, diabetes mellitus, and preexisting heart disease [12]. Similar findings regarding genetic predisposition to AF were reported in an Icelandic study [13]. In both studies, if the parent developed AF before the age of 60 years, the risk for the offspring increased further, to nearly 5-fold.

The evidence from studies involving patients with lone AF, or AF in the absence of established risk factors, is even more compelling. Investigators at Mayo Clinic and Massachusetts General Hospital have reported that between 15% and 40% of probands with lone AF have a family history of the arrhythmia [14, 15]. Interesting results have also emerged from a Danish Twin Study which demonstrated that amongst monozygotic twins in whom one sibling has AF, the risk of the other sibling developing AF was higher as compared to dizygotic twins in the same situation [29]. The authors reported a heritability estimate of 62%.

27.3 Monogenic Forms of AF

Once it has been established that a condition is heritable, a number of techniques can be used to identify the underlying genetic substrate. Two approaches have dominated genetic analysis of monogenic forms of AF: linkage analysis and candidate gene resequencing.

27.3.1 Linkage Analysis

Linkage analysis is a technique for mapping the chromosomal location of genetic mutations that underlie simple monogenic disorders with Mendelian inheritance patterns. The principle of linkage analysis is based on the observation that genes that lie close together on the same chromosome are inherited together. Linkage studies involve an analysis of the cosegregation of a disease gene relative to genetic markers whose positions have previously been mapped. Linked segregation of a disease gene and a specific marker suggests close physical proximity on a chromosome. Therefore, if a given Mendelian trait is transmitted to offspring along with a specific marker, then one can conclude that the disease gene is located on the chromosome in close proximity to that marker.

The LOD score (logarithm of the odds) is a statistical test that is widely used to assess linkage between a disease locus and a marker locus. The LOD score compares the likelihood of marker and disease locus cosegregating due to true linkage, to the likelihood of cosegregation purely by chance. A positive LOD score of 3 or more is conventionally considered as statistical evidence of linkage. Once significant linkage has been detected, re-examining the region of interest with more closely spaced markers can further narrow the search for the causative gene. Potential candidate genes at the refined locus can then be identified using online genome databases and pathophysiological considerations. Ultimately, the identification of a causative genetic mutation requires systematic analysis of putative genes at the locus by mutation screening and sequencing.

Since 1997, a number of susceptibility loci have been identified in families with AF using linkage analysis. In the majority of cases, the causative genetic mutations at these loci have been identified although some mutations remain elusive [2, 30, 31]. The majority of the mutations are located in genes encoding ion channels. The first reported ion channel mutation was located in the *KCNQ1* gene, which encodes the pore-forming α -subunit of the cardiac I_{Ks} channel [2]. Two further mutations in *KCNQ1* have since been reported [32, 33]. A sodium channel gene mutation has also been reported in a large family in which affected individuals variably presented with AF, dilated cardiomyopathy and abnormalities of conduction and automaticity [34]. *SCN5A* encodes the major pore-forming α -subunit of the sodium channel.

Linkage studies have also identified non-ion channel gene mutations in two AF kindreds. One of the mutations was located in the nucleoporin gene (*NUP155*) [9]. *NUP155* encodes a nucleoporin which is an important component of the nuclear

pore complex (NPC) [35]. In a more recent study, a heterozygous frameshift mutation in *NPPA*, the gene encoding atrial natriuretic peptide (ANP) has been reported. The mutation is associated with elevated levels of mutant ANP in the affected family members [10].

27.3.2 Candidate Gene Studies

When assumptions can be made regarding a mechanistic role of a gene in the pathogenesis of a disease, a candidate gene approach can be applied to screen for causative mutations. Following on from early linkage studies in monogenic AF kindred, investigators broadened their studies to screen cohorts of AF patients for mutations using a candidate gene approach.

Based on the results from linkage studies, a majority of the candidate gene studies have screened for mutations in ion channel coding genes. However, these studies have either failed to identify mutations or have only identified isolated, non-segregating mutations. Potassium channel mutations have been identified in *KCNQ1*, *KCNE2*, *KCNE5*, *KCNJ2*, and *KCNA5* [3, 5–7, 36]. *KCNQ1* encodes the α subunit of the cardiac I_{K_s} channel, while *KCNE2* and *KCNE5* encode β -subunits. *KCNJ2* encodes the Kir2.1 channel, which contributes to the inward rectifier potassium current (I_{K1}) [37, 38]. *KCNA5* encodes for Kv1.5, which underlies the ultrarapid delayed rectifier I_{Kur} current [39–41]. Sodium channel mutations have been identified in *SCN5A*, *SCN1B*, and *SCN2B*. *SCN5A* encodes the major pore-forming α -subunit of the sodium channel, while *SCN1B* and *SCN2B* encode the function-modifying β subunits.

To date, one candidate gene study has reported a non-ion channel mutation. In a small cohort of unrelated AF patients, four novel missense mutations were identified in the *GJA5* gene [8]. *GJA5* encodes connexin-40, a gap-junction protein which mediates coordinated conduction of the action potential through cell-to-cell electrical coupling [42]. Interestingly, three patients had somatic mutations while only one patient had a germ-line sequence variant.

In sum, linkage studies and candidate gene resequencing have led to the identification of a variety of genetic mutations, most of which are located in ion channel coding genes (summarized in Table 27.1). However, while these mutations are an important cause of rare familial forms of AF, they provide little explanation for the genetic basis of AF occurring in the general population.

Despite their limited prevalence, monogenic mutations have provided valuable insights into the pathogenesis of AF. The majority of potassium channel gene mutations are associated with a gain-of-function effect and increased repolarizing currents [2, 3, 5, 32, 33, 36]. These effects shorten the atrial effective refractory period and facilitate reentry, thereby creating a profibrillatory substrate [46, 47]. Conversely, loss-of-function potassium channel gene mutations cause prolongation of the atrial action potential and early afterdepolarizations, effects that would also promote arrhythmias [48].

Table 27.1 Summary of monogenic mutations associated with AF

Gene	Technique used to identify mutation	Gene product	Functional assay performed, yes/no	Functional effect of mutations	Ref
<i>KCNQ1</i>	Linkage analysis	α subunit of I_{Ks} channel	Yes	Gain-of-function effect with increased I_{Ks}	[2]
<i>KCNQ1</i>	Linkage analysis	α subunit of I_{Ks} channel	Yes	Gain-of-function effect with increased I_{Ks}	[33]
<i>KCNQ1</i>	Linkage analysis	α subunit of I_{Ks} channel	Yes	Gain-of-function effect with increased I_{Ks}	[32]
<i>KCNE2</i>	Candidate gene study	β subunit of I_{Ks} channel	Yes	Gain-of-function effect with increased I_{Ks}	[3]
<i>KCNE5</i>	Candidate gene study	β subunit of I_{Ks} channel	Yes	Gain-of-function effect with increased I_{Ks}	[36]
<i>KCNJ2</i>	Candidate gene study	K_{ir} 2.1 channel	Yes	Gain-of-function effect with increased I_{K1}	[5]
<i>KCNA5</i>	Candidate gene study	K_v 1.5 channel	Yes	Loss-of-function effect with reduced I_{kur}	[6]
<i>SCN5A</i>	Linkage analysis	Sodium channel α subunit	No	Predicted to have a loss-of-function effect with reduced sodium current density	[34]
<i>SCN5A</i>	Candidate gene study	Sodium channel α subunit	Yes	Loss-of-function effect with hyperpolarizing shift in channel steady-state inactivation	[43]
<i>SCN5A</i>	Candidate gene study	Sodium channel α subunit	Yes	Gain-of-function effect with depolarized shift of voltage dependence of steady-state inactivation	[44]
<i>SCN1B</i>	Candidate gene study	Sodium channel β subunit	Yes	Loss-of-function effect with reduced sodium current and altered channel gating	[45]
<i>SCN2B</i>	Candidate gene study	Sodium channel β subunit	Yes	Loss-of-function effect with reduced sodium current and altered channel gating	[45]
<i>NUP155</i>	Linkage analysis	Nucleoporin	Yes	Reduction in nuclear membrane permeability	[9]
<i>GJA5</i>	Candidate gene study	Connexin-40	Yes	Impaired intracellular transport and intercellular electrical coupling	[8]
<i>NPPA</i>	Linkage analysis	Mutant atrial natriuretic peptide	Yes	Elevated levels of mutant ANP	[10]

Both gain- and loss-of-function mutations have also been described in sodium channel genes. Gain-of-function mutations can potentially induce triggered activities through a mechanism similar to that observed with loss-of-function potassium

channel mutations. Loss-of-function mutations in sodium channels can decrease conduction velocity in the atria, effectively lengthening the atrial re-entry wavelength and promoting atrial re-entry circuits [49].

The mechanisms by which non-ion channel genes promote AF are less clear. Mutations in the *GJA5* gene impair cell–cell electrical coupling and it has been proposed that this may give rise to conduction heterogeneity which in turn may increase the risk of AF [8]. *NPPA* mutations are associated with pathophysiological levels of ANP. Interestingly, in an isolated whole-heart animal model, elevated levels of ANP have been reported to shorten atrial monophasic action potentials [10]. These effects may provide a proarrhythmogenic substrate. *NUP155* encodes a nucleoporin which is one of the main components of the nuclear pore complex [35]. The link between nuclear pore complexes and AF is presently unclear.

27.4 AF in the General Population (Community-Based AF)

In contrast to rare monogenic forms of AF, the common form of AF encountered in the general population is likely to have multifactorial or complex inheritance. In other words, disease risk is influenced by multiple common genetic variants which interact with environmental factors. Individually, the genetic variants or polymorphisms that underlie complex traits exert a relatively subtle effect. Therefore, dissecting the genetic basis of common forms of AF is more challenging.

As discussed in the previous section, linkage studies have traditionally been used to investigate monogenic forms of AF. Classic linkage studies require the assumption of a precise genetic model and are therefore generally not appropriate for investigation of complex traits. Association studies are considered more effective in this situation as they have greater statistical power to detect common genetic variants with more modest effects.

By convention, genetic variants are considered common when they occur with an allele frequency of $\geq 1\%$ in the population. Several types of genetic variations exist across the genome at this frequency. By far the most common forms are single nucleotide polymorphisms (SNPs). SNPs are characterized by single DNA-base substitutions, leading to a sequence alteration compared to the wild type. SNPs maybe intergenic or intragenic. Rarely, intragenic SNPs can alter the structure of an encoded protein.

27.4.1 Association Studies

Two subtypes of association studies are commonly used to investigate complex genetic traits such as AF: candidate gene association studies and GWAS. Both types of association studies use a case–control design to compare genotype frequencies between a diseased population and a population of healthy controls.

Candidate gene association studies involve an assessment of the association between a particular allele, which is selected based on its potential to play a mechanistic role in the pathogenesis of a disease, and the disease itself. One of the major limitations of candidate gene association studies is that they depend on pre-existing knowledge about disease pathophysiology.

GWAS are a more powerful tool to investigate how common genetic variants influence disease susceptibility. The basic approach in GWAS involves the use of high-throughput genotyping technologies to assay SNPs distributed across the entire genome. These SNPs are then related to the condition of interest.

The correlation of SNPs in the genome to one another is referred to as linkage disequilibrium. Linkage disequilibrium is defined as a non-random association of two or more alleles, which in simple terms means that by knowing the genotype at one locus, one can predict the genotype at a second locus. Linkage disequilibrium between millions of genomic SNPs has been investigated by international consortia such as the HapMap project [50]. The results of such studies have allowed researchers to make predictions about SNP behavior and facilitated the selection of a minimal set of markers that can act as surrogates for untyped markers in GWAS.

In contrast to candidate gene association studies, GWAS is an unbiased genetic mapping approach that does not rely on assumptions about biological pathways underlying a given disease. GWAS therefore have the potential to identify novel disease susceptibility loci. However, refinement of an association signal following a GWAS is essential to identify causal variants involved in disease pathogenesis [51].

While the methodological approach in association studies is fairly straightforward, there are several potential pitfalls that should be taken into consideration when interpreting results. Most importantly, the size of effect conferred by an individual SNP is generally small. Thus large sample sizes are needed to reliably identify true associations. A second hurdle is that there is a high risk for false-positive associations because there are millions of SNPs in the genome, and often, as is the case in GWAS, numerous SNPs are tested simultaneously. When multiple analyses are conducted at the same time, the probability of detecting a significant association by chance alone is high. Two approaches have been established to overcome these problems. The first is to raise the threshold of significance in order to identify associations that are truly present. The most common way to do this is to perform a Bonferroni correction, although other statistical methods are also available. The second means is to perform independent replication analyses to reproduce significant findings. Ideally, both approaches should be combined [52].

27.4.2 Candidate Gene Association Studies in AF

Over the past decade, a number of candidate gene association studies in AF cohorts have implicated polymorphisms that may influence susceptibility to the arrhythmia. Examples include polymorphisms in potassium channel genes [17–20], sodium

channel genes [16], genes that encode ion channel regulating proteins [21, 53], genes encoding connexins [22], genes encoding circulating hormones [54–56] and genes encoding inflammatory mediators [57, 58]. The results from association studies are summarized in Table 27.2.

Unfortunately, these studies have been hampered by a number of important limitations. Given that there are millions of polymorphisms in the human genome, one of the inherent limitations of a candidate gene approach is a low pretest probability that a selected variant is actually involved in the pathogenesis of AF. Further, the majority of studies have been limited by modest sample sizes and inconsistent replication. In fact, only one of these studies provided an independent replication analysis, and suggested evidence for an association between AF and the K897T variant in *KCNH2* [18].

As discussed in the previous section, mutations in ion channel subunit genes have previously been identified in monogenic forms of AF [2–10]. The results of the association studies are therefore interesting as they suggest that both mutations and polymorphisms in ion channel coding genes may increase susceptibility to AF and by implication, familial and non-familial forms of AF may share a common mechanism [80].

27.4.3 *Genome Wide Association Studies in AF*

In 2007, the first GWAS in AF reported a susceptibility locus on the long arm of chromosome 4 (4q25). Two polymorphisms at the locus (rs2200733 and rs10033464) were associated with AF [24]. rs2200733 was the most significantly associated polymorphism. The association between rs2200733 and AF has since been replicated in GWAS involving cohorts of Asian patients as well as patients of European ancestry [25, 26, 60, 61]. Neither variant at the 4q25 locus has been correlated with AF risk factors such as obesity, hypertension, or myocardial infarction.

Figure 27.1 summarizes the results of studies demonstrating the association between SNP rs2200733 at the chromosome 4q25 locus and AF, illustrating the robustness of this association signal. Each copy of the T allele of SNP rs2200733 carries an estimated 1.68-fold increase in the relative risk of AF (95% CI, 1.50–1.87). The magnitude of risk conferred by variants at this locus is comparable to other commonly accepted risk factors for AF, and appears independent of such risk factors.

How the 4q25 locus influences susceptibility to AF has yet to be established. The association signal observed at the locus lies within a region that has not been reported to encode any genes or transcripts. The closest gene, *PITX2* (paired-like homeodomain transcription factor 2), is located approximately 150,000 bases away, but it is an intriguing candidate gene for AF. *PITX2* encodes a transcription factor which has been reported to be involved in embryonic cardiac development [63]. Specifically, *PITX2* is involved in determination of right–left asymmetry, suppresses

Table 27.2 Summary of results from association studies in AF cohorts

Gene	Polymorphism	Cases	Controls	Ethnicity	Comment	P-value	Odds ratio	Ref
<i>KCNE1 minK</i>	38G	331	441	Caucasian		0.004	1.73	[17]
<i>KCNE1 minK</i>	38G	108	108	Asian		0.024	1.80	[19]
<i>KCNES5</i>	9TT	158	96	Caucasian		0.007	0.52	[20]
<i>KCNH2</i>	K897T	1,207	2,475	Caucasian		0.00033	1.25	[18]
<i>GNB3</i>	C825T	291	292	Caucasian		0.02	0.46	[21]
<i>eNOS</i>	2786C	331	441	Caucasian		0.01	1.50	[17]
<i>eNOS</i>	G894T	51	289	Caucasian	HF patients	0.001	3.2	[54]
<i>SCN5A</i>	H558R	157	314	Caucasian		0.002	1.6	[16]
<i>GJA5</i>	-44AA/+71GG	173	232	Asian		< 0.006	1.514	[22]
<i>AGT</i>	M235T	250	250	Asian		< 0.001	2.5	[59]
<i>AGT</i>	G-6A	250	250	Asian		0.005	3.3	[59]
<i>AGT</i>	G-217A	250	250	Asian		0.002	2.0	[59]
<i>AGT</i>	T174M	968	8,267	Caucasian		0.05	1.2	[55]
<i>AGT</i>	20C/C	968	8,267	Caucasian		0.01	1.5	[55]
<i>ACE</i>	D/D	51	289	Caucasian	HF patients	0.016	1.5	[54]
<i>ACE</i>	D/D	404	520	Caucasian		< 0.001	1.89	[56]
<i>MMP2</i>	Cl.306T	196	873	Asian		1.26×10^{-2}	8.1	[57]
<i>IL10</i>	A-592C	196	873	Asian		3.7×10^{-3}	0.32	[57]
<i>IL6</i>	G-174C	26	84	Caucasian	Post-operative AF (after CABG)	< 0.001	3.25	[58]
<i>SLN</i>	C-65G	147	92	Caucasian		0.011	1.98	[53]

ACE angiotensin-converting enzyme, AGT angiotensinogen, CABG coronary artery bypass graft surgery, eNOS endothelial nitric oxide synthase 3, GNB3 guanine nucleotide binding protein, GJA5 connexin 40, HF heart failure, IL6 interleukin 6, IL10 interleukin 10, MMP matrix metalloproteinase, SLN sarcolipin gene

Relation between rs2200733 and AF

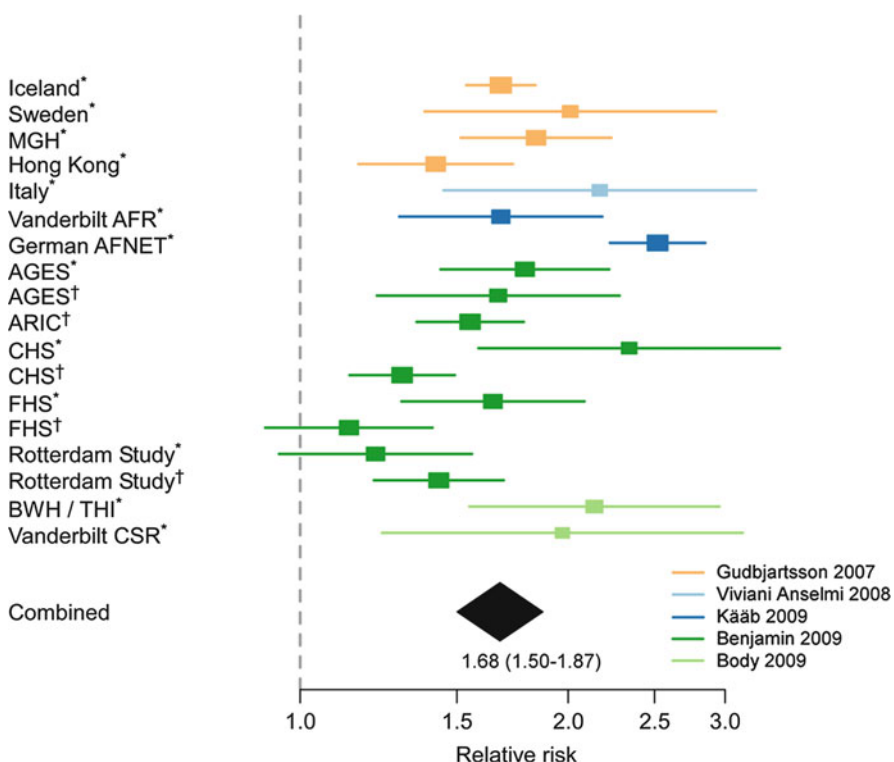


Fig. 27.1 The AF susceptibility locus on chromosome 4q25 has been widely replicated. The association between AF and the T-allele of rs2200733, which tags an AF susceptibility locus on chromosome 4q25, is displayed across independent samples from published studies (total $n = 10,115$ affected, 65,229 unaffected). Adapted with permission of Lubitz et al. [62]. Colors indicate the different studies from which the samples were reported. *Case-control study sample. †Prospective cohort study. AFR, Atrial Fibrillation Registry; BWH, Brigham and Women's Hospital; CSR, Cardiac Surgery Registry; ARIC, Atherosclerosis Risk in Communities Study; AGES, Age, Gene/Environment Susceptibility Reykjavik Study; CHS, Cardiovascular Health Study; FHS, Framingham Heart Study; MGH, Massachusetts General Hospital; THI, Texas Heart Institute

the default formation of a sinoatrial node in the left atrium and is necessary for the development of pulmonary venous myocardium [63, 64]. The latter is a particularly interesting observation considering the fact that ectopic foci from the pulmonary veins commonly trigger AF [65]. Nonetheless, resequencing of *PITX2* has not revealed any mutations directly associated with AF in a sample of 96 patients with AF [66].

Two additional AF susceptibility loci have been identified using GWAS. Two independent consortia have reported a susceptibility locus on chromosome 16q22 in

the gene zinc finger homeobox 3 (*ZFHX3*) [25, 26]. Each copy of the T allele of SNP rs2106261 carries a modest estimated 1.19-fold increase in the relative risk of AF. This was consistent in both prevalent and incident AF cases [26]. *ZFHX3* encodes a transcription factor that has been reported to regulate expression of 1 α -fetoprotein [60]. The mechanisms by which *ZFHX3* predisposes to AF are unclear.

A third locus on chromosome 1q21 has been identified in a GWAS of lone AF patients [27]. Additional analysis found this locus is also associated with more typical forms of AF observed in the community, although the effect was weaker. The top SNP at this locus, rs13376333, is located within a calcium-activated potassium channel gene, *KCNN3* (also known as KCa2.3 or SK3). *KCNN3* channels are expressed in the brain and the heart. In the brain, these channels respond to elevated calcium levels and are responsible for the inward potassium current and after hyperdepolarization. In the heart, the role of these channels is less clear. In a rabbit burst pacing model, pharmacological inhibition of the *KCNN* channels has been demonstrated to alter action potential properties [68, 69].

27.4.4 PR Interval as Intermediate Phenotype for AF

AF is likely to be the terminal manifestation of a number of intermediate phenotypes. The genetic variance associated with AF may encode proteins and regulatory factors that have key roles in multiple intermediate pathways. By using intermediate and quantitative phenotypes, it is possible to detect variants responsible for even subtle variances. In this regard, the PR interval has been studied as an intermediate quantitative phenotype because observations in the community-based cohorts found that PR-interval prolongation is associated with AF [70]. Furthermore, multiple studies have reported that PR-interval prolongation and increased P-wave duration or dispersion are associated with an increased risk of AF [71].

Previous twin studies have supported the heritability of PR-interval duration [72]. Two GWAS of the PR interval have found additional loci, which were associated with the PR interval that may also be associated with AF [73]. However, the SNPs related to both the PR interval and AF did not show a robust pattern. Both SNPs related to a prolonged or shortened PR interval were associated with a decreased risk of AF. This emphasizes that the association between PR interval and AF is complex, and the genetic variance of the PR interval cannot be directly translated to AF risk.

The variants related to both PR interval and AF are located close to multiple different genes: *CAV1*, *CAV2*, *SCN5A*, *SCN10A*, *NKX2-5*, and *SOX5*. In the other GWAS, variants in *TBX5* were also associated with both PR interval and AF [73]. *CAV1* and *CAV2* are located on chromosome 7q31.2 and encode for caveolins, signal transduction proteins that localise to small invaginations in cell membranes [74]. Interestingly, in a mouse model, caveolin deficiency has been reported to cause cardiac hypertrophy, dilated cardiomyopathy and pulmonary hypertension [75]. *SCN5A* and *SCN10A* are two adjacent voltage-gated sodium channels. Mutations

in *SCN5A* are related to numerous arrhythmias, including the sick sinus syndrome, long QT syndrome, the Brugada syndrome, and AF [76]. So far, *SCN10A* has not been related to cardiac arrhythmias.

27.5 Conclusion and Future Perspectives

In the past decade, significant advances have been made in uncovering the genetic basis of AF. The identification of monogenic mutations in familial forms of AF has provided valuable insights into the molecular mechanisms of the disease [52]. More recently, GWAS have led to the identification of interesting though as yet poorly defined susceptibility loci. Future research in this area will focus on identification further susceptibility loci as well as identifying the molecular pathways linking genetic variants to disease pathophysiology.

The ultimate goal is individualized, genetic-variation-based management of patients with AF. In terms of risk stratification, genotype-based scores are promising predictive and prognostic tools. However, so far the clinical use of individual variants identified in GWAS as predictors of disease risk has been limited [77]. This is not surprising given that the risk conferred by each variant is relatively small. In future, the development of genotype-based risk scores that incorporate multiple genetic variants is likely to allow for more accurate prediction of risk [78, 79]. From a therapeutic perspective, the application of pharmacogenomics is likely to lead to the development of novel, more targeted therapies for the management of patients with AF. Much work remains however, before knowledge gained from molecular genetic research can be translated into genotype-guided patient management.

Disclosures The authors declare no conflict of interest.

Acknowledgments This work was funded by grants from the Netherlands Organization for Scientific Research (Rubicon Grant 825.09.020) to Dr. Rienstra, the LMU Research Grant FöFoLe 577/569 to Dr. Sinner, German Competence Network on AF (AF-Net) 01 GI 0204/N, Leducq Foundation 07-CVD 03 and LMU Excellence Initiative to Dr. Käab, from the German National Genome Research Network NGFN 01GR0803 and by grants to Dr. Ellinor from the Deane Institute for Integrative Research in Atrial Fibrillation and Stroke and from the NIH (R01HL092577, R01HL104156, R21DA027021).

References

1. Wolff L. Familial auricular fibrillation. N Engl J Med. 1943;229:396–7.
2. Chen YH et al. KCNQ1 gain-of-function mutation in familial atrial fibrillation. Science. 2003; 299(5604):251–4.
3. Yang Y et al. Identification of a KCNE2 gain-of-function mutation in patients with familial atrial fibrillation. Am J Hum Genet. 2004;75(5):899–905.

4. Hong K et al. Short QT syndrome and atrial fibrillation caused by mutation in KCNH2. *J Cardiovasc Electrophysiol.* 2005;16(4):394–6.
5. Xia M et al. A Kir2.1 gain-of-function mutation underlies familial atrial fibrillation. *Biochem Biophys Res Commun.* 2005;332(4):1012–9.
6. Olson TM et al. Kv1.5 channelopathy due to KCNA5 loss-of-function mutation causes human atrial fibrillation. *Hum Mol Genet.* 2006;15(14):2185–91.
7. Otway R et al. Stretch-sensitive KCNQ1 mutation A link between genetic and environmental factors in the pathogenesis of atrial fibrillation? *J Am Coll Cardiol.* 2007;49(5):578–86.
8. Gollobo MH et al. Somatic mutations in the connexin 40 gene (GJA5) in atrial fibrillation. *N Engl J Med.* 2006;354(25):2677–88.
9. Zhang X et al. Mutation in nuclear pore component NUP155 leads to atrial fibrillation and early sudden cardiac death. *Cell.* 2008;135(6):1017–27.
10. Hodgson-Zingman DM et al. Atrial natriuretic peptide frameshift mutation in familial atrial fibrillation. *N Engl J Med.* 2008;359(2):158–65.
11. Ellinor PT et al. Potassium channel gene mutations rarely cause atrial fibrillation. *BMC Med Genet.* 2006;7:70.
12. Fox CS et al. Parental atrial fibrillation as a risk factor for atrial fibrillation in offspring. *JAMA.* 2004;291(23):2851–5.
13. Arnar DO et al. Familial aggregation of atrial fibrillation in Iceland. *Eur Heart J.* 2006;27(6):708–12.
14. Ellinor PT et al. Familial aggregation in lone atrial fibrillation. *Hum Genet.* 2005;118(2):179–84.
15. Darbar D et al. Familial atrial fibrillation is a genetically heterogeneous disorder. *J Am Coll Cardiol.* 2003;41(12):2185–92.
16. Chen LY et al. A common polymorphism in SCN5A is associated with lone atrial fibrillation. *Clin Pharmacol Ther.* 2007;81(1):35–41.
17. Fatini C et al. Analysis of minK and eNOS genes as candidate loci for predisposition to non-valvular atrial fibrillation. *Eur Heart J.* 2006;27(14):1712–8.
18. Sinner MF et al. The non-synonymous coding IKr-channel variant KCNH2-K897T is associated with atrial fibrillation: results from a systematic candidate gene-based analysis of KCNH2 (HERG). *Eur Heart J.* 2008;29(7):907–14.
19. Lai LP et al. Association of the human minK gene 38G allele with atrial fibrillation: evidence of possible genetic control on the pathogenesis of atrial fibrillation. *Am Heart J.* 2002;144(3):485–90.
20. Ravn LS et al. Relation of 97T polymorphism in KCNE5 to risk of atrial fibrillation. *Am J Cardiol.* 2005;96(3):405–7.
21. Schreieck J et al. C825T polymorphism of the G-protein beta3 subunit gene and atrial fibrillation: association of the TT genotype with a reduced risk for atrial fibrillation. *Am Heart J.* 2004;148(3):545–50.
22. Juang JM et al. The association of human connexin 40 genetic polymorphisms with atrial fibrillation. *Int J Cardiol.* 2007;116(1):107–12.
23. Firouzi M et al. Association of human connexin40 gene polymorphisms with atrial vulnerability as a risk factor for idiopathic atrial fibrillation. *Circ Res.* 2004;95(4):e29–33.
24. Gudbjartsson DF et al. Variants conferring risk of atrial fibrillation on chromosome 4q25. *Nature.* 2007;448(7151):353–7.
25. Gudbjartsson DF et al. A sequence variant in ZFHX3 on 16q22 associates with atrial fibrillation and ischemic stroke. *Nat Genet.* 2009;41(8):876–8.
26. Benjamin EJ et al. Variants in ZFHX3 are associated with atrial fibrillation in individuals of European ancestry. *Nat Genet.* 2009;41(8):879–81.
27. Ellinor PT et al. Common variants in KCNN3 are associated with lone atrial fibrillation. *Nat Genet.* 2010;42(3):240–4.
28. Pfeufer A et al. Genome-wide association study of PR interval. *Nat Genet.* 2010;42(2):153–9.

29. Christoffersen IE et al. Familial aggregation of atrial fibrillation: a study in Danish twins. *Circ Arrhythm Electrophysiol*. 2009;2(4):378–83.
30. Brugada R et al. Identification of a genetic locus for familial atrial fibrillation. *N Engl J Med*. 1997;336(13):905–11.
31. Ellinor PT et al. Locus for atrial fibrillation maps to chromosome 6q14–16. *Circulation*. 2003;107(23):2880–3.
32. Das S et al. Mutation in the S3 segment of KCNQ1 results in familial lone atrial fibrillation. *Heart Rhythm*. 2009;6(8):1146–53.
33. Hong K et al. De novo KCNQ1 mutation responsible for atrial fibrillation and short QT syndrome in utero. *Cardiovasc Res*. 2005;68(3):433–40.
34. Olson TM et al. Sodium channel mutations and susceptibility to heart failure and atrial fibrillation. *J Am Med Assoc*. 2005;293(4):447–54.
35. Zhang X et al. Localization of a human nucleoporin 155 gene (NUP155) to the 5p13 region and cloning of its cDNA. *Genomics*. 1999;57(1):144–51.
36. Ravn LS et al. Gain of function in IKs secondary to a mutation in KCNE5 associated with atrial fibrillation. *Heart Rhythm*. 2008;5(3):427–35.
37. Zobel C et al. Molecular dissection of the inward rectifier potassium current (IK1) in rabbit cardiomyocytes: evidence for heteromeric co-assembly of Kir2.1 and Kir2.2. *J Physiol*. 2003;550(Pt 2):365–72.
38. Lopatin AN et al. Inward rectifiers in the heart: an update on I(K1). *J Mol Cell Cardiol*. 2001;33(4):625–38.
39. Tamkun MM et al. Molecular cloning and characterization of two voltage-gated K⁺ channel cDNAs from human ventricle. *FASEB J*. 1991;5(3):331–7.
40. Wang Z et al. Delayed rectifier outward current and repolarization in human atrial myocytes. *Circ Res*. 1993;73(2):276–85.
41. Simard C et al. Polymorphism screening in the cardiac K⁺ channel gene KCNA5. *Clin Pharmacol Ther*. 2005;77(3):138–44.
42. Kanno S et al. The role of myocardial gap junctions in electrical conduction and arrhythmogenesis. *Cardiovasc Pathol*. 2001;10(4):169–77.
43. Ellinor PT et al. Cardiac sodium channel mutation in atrial fibrillation. *Heart Rhythm*. 2008;5(1):99–105.
44. Makiyama T et al. A novel SCN5A gain-of-function mutation M1875T associated with familial atrial fibrillation. *J Am Coll Cardiol*. 2008;52(16):1326–34.
45. Watanabe H et al. Mutations in sodium channel beta1- and beta2-subunits associated with atrial fibrillation. *Circ Arrhythm Electrophysiol*. 2009;2(3):268–75.
46. Moe GK. Evidence for reentry as a mechanism of cardiac arrhythmias. *Rev Physiol Biochem Pharmacol*. 1975;72:55–81.
47. Nattel S. New ideas about atrial fibrillation 50 years on. *Nature*. 2002;415(6868):219–26.
48. Ehrlich JR et al. Atrial fibrillation-associated minK38G/S polymorphism modulates delayed rectifier current and membrane localization. *Cardiovasc Res*. 2005;67(3):520–8.
49. Allessie MA. Is atrial fibrillation sometimes a genetic disease? *N Engl J Med*. 1997;336(13):950–2.
50. International HapMap Consortium. A haplotype map of the human genome. *Nature*. 2005;437(7063):1299–320.
51. Milan DJ et al. Genome-wide association studies in cardiac electrophysiology: recent discoveries and implications for clinical practice. *Heart Rhythm*. 2010;7(8):1141–8.
52. Roberts JD et al. Impact of genetic discoveries on the classification of lone atrial fibrillation. *J Am Coll Cardiol*. 2010;55(8):705–12.
53. Nyberg MT et al. The variation of the sarcolipin gene (SLN) in atrial fibrillation, long QT syndrome and sudden arrhythmic death syndrome. *Clin Chim Acta*. 2007;375(1–2):87–91.
54. Bedi M et al. Genetic susceptibility to atrial fibrillation in patients with congestive heart failure. *Heart Rhythm*. 2006;3(7):808–12.
55. Ravn LS et al. Angiotensinogen and ACE gene polymorphisms and risk of atrial fibrillation in the general population. *Pharmacogenet Genomics*. 2008;18(6):525–33.

56. Fatini C et al. Lone and secondary nonvalvular atrial fibrillation: role of a genetic susceptibility. *Int J Cardiol.* 2007;120(1):59–65.
57. Kato K et al. Genetic factors for lone atrial fibrillation. *Int J Mol Med.* 2007;19(6):933–9.
58. Gaudino M et al. The -174G/C interleukin-6 polymorphism influences postoperative interleukin-6 levels and postoperative atrial fibrillation. Is atrial fibrillation an inflammatory complication? *Circulation.* 2003;108 Suppl 1:II195–9.
59. Tsai CT et al. Renin-angiotensin system gene polymorphisms and atrial fibrillation. *Circulation.* 2004;109(13):1640–6.
60. Kaab S et al. Large scale replication and meta-analysis of variants on chromosome 4q25 associated with atrial fibrillation. *Eur Heart J.* 2009;30(7):813–9.
61. Shi L et al. Assessment of association of rs2200733 on chromosome 4q25 with atrial fibrillation and ischemic stroke in a Chinese Han population. *Hum Genet.* 2009;126(6):843–9.
62. Lubitz SA et al. Genetics of atrial fibrillation: implications for future research directions and personalized medicine. *Circ Arrhythm Electrophysiol.* 2010;3(3):291–9.
63. Logan M et al. The transcription factor Pitx2 mediates situs-specific morphogenesis in response to left-right asymmetric signals. *Cell.* 1998;94(3):307–17.
64. Mommersteeg MT et al. Molecular pathway for the localized formation of the sinoatrial node. *Circ Res.* 2007;100(3):354–62.
65. Haissaguerre M et al. Spontaneous initiation of atrial fibrillation by ectopic beats originating in the pulmonary veins. *N Engl J Med.* 1998;339(10):659–66.
66. Boldt LH, Posch MG, Perrot A, Polotzki M, Rolf S, Parwani AS, Huemer M, Wutzler A, Ozcelik C, Haverkamp W. Mutational analysis of the *PITX2* and *NKX2-5* genes in patients with idiopathic atrial fibrillation. *Int J Cardiol.* 2010 Nov 19;145(2):316–7.
67. Morinaga T et al. A human alpha-fetoprotein enhancer-binding protein, ATBF1, contains four homeodomains and seventeen zinc fingers. *Mol Cell Biol.* 1991;11(12):6041–9.
68. Tuteja D et al. Differential expression of small-conductance Ca²⁺-activated K⁺ channels SK1, SK2, and SK3 in mouse atrial and ventricular myocytes. *Am J Physiol Heart Circ Physiol.* 2005;289(6):H2714–23.
69. Ozgen N et al. Early electrical remodeling in rabbit pulmonary vein results from trafficking of intracellular SK2 channels to membrane sites. *Cardiovasc Res.* 2007;75(4):758–69.
70. Cheng S et al. Long-term outcomes in individuals with prolonged PR interval or first-degree atrioventricular block. *J Am Med Assoc.* 2009;301(24):2571–7.
71. Darbar D et al. P wave signal-averaged electrocardiography to identify risk for atrial fibrillation. *Pacing Clin Electrophysiol.* 2002;25(10):1447–53.
72. Hanson B et al. Genetic factors in the electrocardiogram and heart rate of twins reared apart and together. *Am J Cardiol.* 1989;63(9):606–9.
73. Holm H et al. Several common variants modulate heart rate, PR interval and QRS duration. *Nat Genet.* 2010;42(2):117–22.
74. Razani B et al. Caveolae: from cell biology to animal physiology. *Pharmacol Rev.* 2002;54(3): 431–67.
75. Zhao YY et al. Defects in caveolin-1 cause dilated cardiomyopathy and pulmonary hypertension in knockout mice. *Proc Natl Acad Sci USA.* 2002;99(17):11375–80.
76. Ruan Y et al. Sodium channel mutations and arrhythmias. *Nat Rev Cardiol.* 2009;6(5): 337–48.
77. Pereira NL et al. Cardiovascular pharmacogenomics and individualized drug therapy. *Nat Rev Cardiol.* 2009;6(10):632–8.
78. Wei Z et al. From disease association to risk assessment: an optimistic view from genome-wide association studies on type 1 diabetes. *PLoS Genet.* 2009;5(10):e1000678.
79. Purcell SM et al. Common polygenic variation contributes to risk of schizophrenia and bipolar disorder. *Nature.* 2009;460(7256):748–52.
80. Tsai CT, Lai LP, Hwang JJ, Lin JL, Chiang FT. Molecular genetics of atrial fibrillation. *J Am Coll Cardiol.* 2008 Jul 22;52(4):241–50.

Part VI

**Role of Specific Channels and
Transporters in Arrhythmia**

Chapter 28

The Role of Gap Junctions in Impulse Propagation in the Heart: New Aspects of Arrhythmogenesis and New Antiarrhythmic Agents Targeting Gap Junctions

Stefan Dhein, Joanna Jozwiak, Anja Hagen, Thomas Seidel, Anna Dietze, Aida Salameh, Martin Kostelka, and Friedrich Wilhelm Mohr

28.1 Introduction

The heart is a rhythmically beating organ serving as a pump. The basic feature of this organ is to maintain a regular rhythm and to adapt the frequency of beating to the actual demands of the organism. The contraction of this pump needs to be coordinated, i.e. it should start in the lower parts of the heart, at the apex cordis, and should proceed to the free walls towards the valves, with a small delay of a few milliseconds between the right and the left ventricle. This is necessary to allow the directed propulsion of the blood. If this coordination is disturbed, e.g. in dys-synchrony, the efficacy of the pump will be lowered.

To maintain this feature, electrical activation of the myocardium is coupled to the contraction (electro-mechanical coupling), so that contraction starts after reaching the plateau phase of the action potential, and the working myocardium is activated by the specific conduction system, which ends up in the tree of the Purkinje fibres. From the endings of the Purkinje fibres, in the lower parts of the heart near the apex cordis, the activation wave propagates through the working myocardium from cell to cell.

The working myocardium is organized as a syncytium, thus enabling a coordinated response. This feature is realized via intercellular communication channels, which are called gap junction channels. These gap junction channels form intercellular low resistance contacts enabling the transfer of electrical current (for action potential transfer) and the exchange of small molecules (maximum size: about 1,000 Da) such as cAMP [1]. These channels function as ohmic resistors for voltage differences of ± 50 mV with <200 ms duration [2–5].

S. Dhein (✉), J. Jozwiak, A. Hagen, T. Seidel, A. Dietze, A. Salameh, M. Kostelka, and F.W. Mohr
Heart Centre Leipzig, Clinic for Cardiac Surgery, University of Leipzig, Struempellstr. 39, 04289 Leipzig, Germany
e-mail: dhes@medizin.uni-leipzig.de

The gap junction coupling is highly regulated: the conductance is regulated by a number of factors either enhancing (e.g. PKC α , in certain cases: PKA) or reducing (e.g. H $^+$, Ca $^{++}$, Na $^+$, loss of ATP, PKC ϵ , acylcarnitine) coupling (see below; for review see [6, 7]); moreover, the synthesis of gap junction channel proteins is regulated as well as their insertion into the membrane and their degradation via proteasomal or lysosomal pathways, thus regulating channel density [8]. Interestingly, gap junction proteins possess a relatively short half life time (about 90 min for Cx43) [9–11], which means a rapid turnover of the channels when compared with other integral membrane proteins. The gap junction channels are preferentially situated at the poles of the cells, and only a small part is inserted at the lateral side of the cardiomyocytes [12, 13]. However, in cardiac diseases such as cardiomyopathy, hypertrophy, postinfarction or atrial fibrillation (AF), the amount of lateral gap junction protein often is up-regulated, and it has been speculated that this may change the biophysics of the tissue [14, 15]. However, this is still a matter of debate. It seems that certain pathways regulate the trafficking of gap junction proteins and the location of their membrane insertion. However, this process and its regulation is – at present – not well understood. It can be assumed that a permanent adaption of the communication features to the actual situation and actual needs seems to be very important for the cell.

Gap junction coupling is a prerequisite for propagation of the activation. Although the propagation velocity along the cell depends on the availability of Na channels for activation [16], the spread from one cell to another – from the present point of view – depends on gap junction coupling [17]. The sum of both processes gives the final macroscopic conduction velocity resulting in longitudinal velocities of 0.4–0.7 m/s and transverse velocities of approximately 0.1–0.2 m/s [18–20].

Another function related to gap junction coupling is that small differences in the endogenous action potential duration of each cell will be smoothed since each difference in action potential duration results in a voltage gradient between the cells, which will cause a gap junction current between these cells, leading to assimilation of the potential durations. Thus, local dispersion or inhomogeneity is kept at a minimum by gap junction coupling.

From the considerations above, it follows that decoupling can lead to slowing of conduction, which will probably affect transverse conduction to a greater extend than longitudinal conduction [19, 20], as well as to enhanced local dispersion of action potential duration. Thereby, gap junction decoupling can contribute, facilitate or even may cause (in certain situations) cardiac arrhythmia.

28.2 Structure, Function and Regulation of Cardiac Gap Junctions

Cardiac gap junctions are found in clusters located in the intercalated disks. The gap between the two neighbouring membranes is narrowed to about 4 nm, which are bridged by the intercellular communicating gap junction channels (outside the

intercalated disk, the normal distance between the membranes is about 20 nm) [21]. These gap junction channels are formed by two neighbouring cells with each cell contributing a hemichannel. These hemichannels dock to each other via their extracellular loops and thus form the intercellular communication channel. A gap junction channel consists of 12 protein subunits, the connexins. Six connexins constitute a connexon or hemichannel.

At present the connexins represent a protein family with 21 isoforms in humans and 20 isoforms in mice [22, 23] (Table 28.1). A connexin protein has an intracellular C- and N-terminus, four transmembrane domains and two extracellular loops, the latter being stabilized by intramolecular disulfide bonds. The most variable region of these proteins is the C-terminal domain. Its length and molecular weight varies among the isoforms. The connexins are named Cx followed by a number indicating the molecular weight in kDa, i.e. Cx43, the most abundant connexin, has a molecular weight of 43 kDa. Often the name is preceded by a suffix indicating the species, i.e. hCx43 means human connexin43, and rCx40 means the rat connexin40. Two connexons of two neighbouring cells dock to each other via H-bonds (Fig. 28.1). It is possible that the complete dodecameric channel consists of only 1 isoform, and thus is homomeric and homotypic. However, it is also possible that a connexon is formed of two isoforms and thus is heteromeric. Moreover, it is possible that two connexons of different composition form the channel, which is then heterotypic. Since each isoform has specific biophysical properties with regard to conductance and voltage-dependent inactivation, a broad range of channels can be composed.

Gap junction channels resemble low resistance pathways behaving as ohmic resistors between the cells and enabling the transfer of current and the propagation

Table 28.1 Cardiovascular connexin isoforms. $t_{1/2}$ is indicated for those connexins where known [33]. For the last four connexins, there is no murine counterpart [23]

Murine connexin	Human ortholog (if different)	Organs	Cardiac (Y/N)
Cx 30.2	Human: Cx31.9	Heart	Conduction system low levels
Cx37		Endothelium	
Cx40		Heart, vasculature (endothelium and smooth muscle)	Atrium, conduction system
Cx43		Ubiquitous in heart and vessels many other organs	Working myocardium, atrium, and partially in the conduction system; $t_{1/2} = \text{ca. } 1.5 \text{ h}$
Cx45		Heart	Conduction system and early developmental states $t_{1/2} = \text{ca. } 3\text{--}4 \text{ h}$
hCx30.2		Heart	Unknown function
hCx31.9		Heart	Unknown function
hCx40.1		Heart	Unknown function
hCx62		Heart	Unknown function

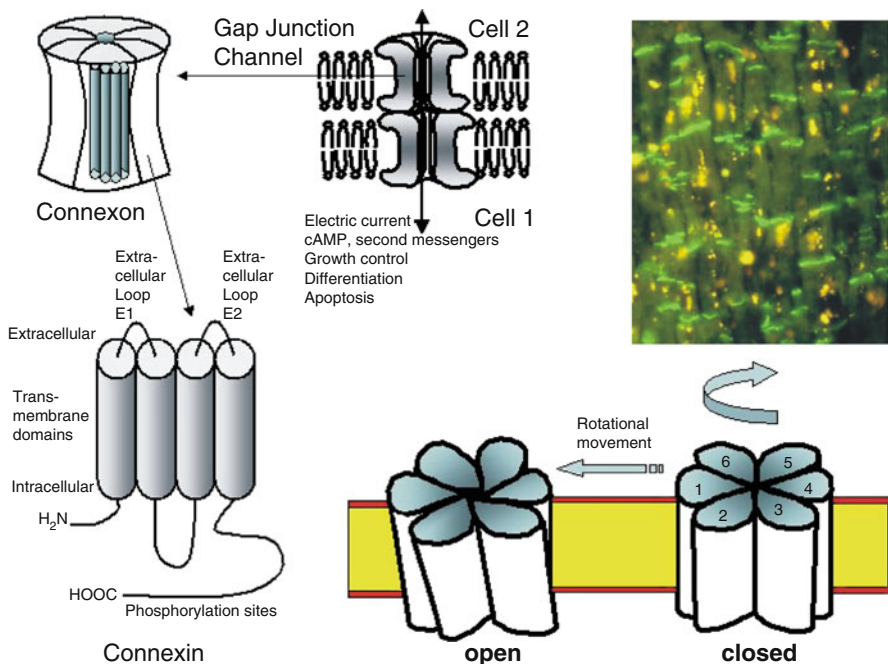


Fig. 28.1 Cx43 (green) distribution in the human atrium (*upper right*). Note the location at the cell poles. Gap junction channel (*upper middle*) made from 2 connexons (*upper left*), each of which consists of six connexins (*lower left*). Opening and closure is thought to be realized via a rotational movement (*lower right*)

of the action potential (electrical coupling). In addition, they can transfer small molecules of up to 1,000 Da such as cAMP between the cells (metabolic coupling). The most common view is that they open and close by a twisting motion. The single channel conductance can vary between several states, a closed state, a residual state and several conducting states. The preference for a certain state can be regulated by phosphorylation of the C-terminal [24].

Gap junctions connect neighbouring cells as low resistance pathways and allow the spread of the action potential from cell to cell. They have a slight preference for cations, and thus Na^+ , H^+ and Ca^{++} can pass the channels. Since, in the heart, the gap junctions are located mainly in the intercalated disks and as cardiomyocytes possess an elongated shape (long axis \gg transverse axis), a predominant propagation of the action potential in longitudinal direction results from this structure. Moreover, the longitudinal conduction velocity is mainly dependent on the I_{Na} availability [16], while the transverse conduction velocity predominantly depends on the gap junction conductance [19, 20].

However, according to Jongsma and Wilders [25], a 90% reduction in the number of gap junction channels would cause only a 25% drop in conduction velocity. This is, however, still a matter of debate and might be different in hypoxic

or partially depolarised cells within areas of uneven or inhomogeneous current source/sink relationships.

The macroscopic gap junction (GJ) conductance (g) follows the equation:

$$g(\text{GJ}) = N \times \gamma \times P_o,$$

where N is the number of channels; γ is the single channel conductance; P_o is the open probability. Single channel conductance is regulated by phosphorylation processes via PKC (various isoforms have different effects), PKA, PKG and MAPKs [24, 26], or by ions such as Na^+ , H^+ and Ca^{2+} [2]. Whether P_o also might be regulated is under discussion [27]. As a result, macroscopic gap junction conductance can be acutely regulated by a number of stimuli (see Table 28.2).

Among these regulators, acidosis (H^+), Na^+ and Ca^{2+} -overload, loss of ATP and acylcarnitines among other factors play a particular role in ischemia and contribute to ischemic closure of gap junctions, which occurs after about 20 min of ischemia [28]. On the one hand, this isolates the ischemic area electrically thereby reducing oxygen consumption, and on the other hand, it leads to changed geometry of the spread of activation, which can initiate or facilitate arrhythmia.

Another possibility to regulate gap junction communication is to affect the number of channels (see Table 28.3). Connexins are synthesized in the SR, then folded and transported to the trans-Golgi network, where they are oligomerized to form connexons and thereafter are transported to the membrane [29–31], where they move probably on lipid rafts in cholesterol-rich domains until they dock to the hemichannel of neighbouring cells, typically in regions with N-cadherin and ZO-1 protein [32]. With a short half-life time of around 90 min, they are degraded via phosphorylation, ubiquitylation and proteasomal degradation, or in some cases via lysosomal degradation [8, 33].

Table 28.2 Stimuli affecting acute macroscopic gap junction conductance

Stimulus	Opening	Closure	Comment
H^+ ; CO_2	X		Takes 7–10 min
Na^+ , Ca^{2+}	X		
Acylcarnitine, lysophosphoglycerides	X		In ischemia/ reperfusion injury
ATP loss	X		In ischemia
Arachidonic acid, oleic acid, palmitoleic acid, heptanol, octanol, narcotics (halothane)	X		Via incorporation? or via altered phosphorylation?
PKC stimulation (e.g. phorbol esters)		X	Depends on PKC isoform
cAMP or cAMP enhancing drugs (isoprenaline, forskolin)	X		Via PKA, in Cx40 or Cx45 coupled cells
PKA	X		In Cx40 or Cx45 coupled cells
Antiarrhythmic peptides, AAP10, rotigaptide	X		Via PKC α

Table 28.3 Stimuli regulating the number of cardiovascular gap junction channels

Stimulus	Enhanced number	Enhanced degradation	Comment
Phenylephrine (α -adrenergic stimulator)	Cx43		Via PKC, MAPKs (cardiomyocytes)
Isoprenaline (β -adrenergic stimulator)	Cx43		Via PKA, MAPKs (cardiomyocytes)
Angiotensin-II	Cx43		Via AT ₁ receptors (cardiomyocytes)
Endothelin	Cx43		Via ET _A -receptors (cardiomyocytes)
Thyroid hormone	Cx40, Cx43		Mechanism unclear
VEGF	Cx43		Via TGF β
bFGF		Cx43	Via PKC ϵ
EGF		Cx43	Enhanced internalization
Nicotin		Cx37, Cx43	Via nACh-R (endothelium)

28.3 Propagation of the Cardiac Impulse

28.3.1 Cable Theory

The passive electrical properties of a muscle bundle in a first approximation are similar to passive cable properties: cables formed by cells coupled in series via ohmic resistors with each cell representing a resistor with a parallel capacitor (see Fig. 28.2; for review see [34]). The change in voltage is a function of distance (x) according to $V_x = V_{x0}(\exp - x/\lambda)$ with the length constant $\lambda = \sqrt{(r_m/r_i)}$ (r_m = membrane resistance; r_i = internal longitudinal resistance); the input resistance at $x = 0$ can be described as $r_{\text{input}} = V_{x0}/I = r_i\lambda$. Because of the fibre geometry, the specific membrane resistance R_m equals $2\pi ar_m$ [Ωcm^2] and specific internal resistance $R_i = \pi a^2 r_i$ [Ωcm]. The specific membrane capacitance can be described as $C_m = \tau/R_m$ with τ being the time constant. In a multicellular preparation with parallel running fibres, the longitudinal resistance of the extracellular space r_o also has to be considered. For these conditions $\lambda = \sqrt{(r_m/(r_i + r_o))}$ and the conduction velocity, $\theta = \sqrt{(1/(T_{\text{foot}}C_m(r_i + r_o)))}$. However, this cable theory, originally formulated for nerve axons [35] and later on for Purkinje fibres [36], holds true for a continuous cable.

In the heart, the situation is more complex, and there are discontinuities between the fibres at the cell–cell contact zones, where two membranes are closely neighbouring, connected via extracellular fluid and the two cytoplasmata are connected via a low resistance gap junction channel (Fig. 28.2, lower part). The electrical situation is very complex at the cell–cell border, in particular because Na channels are probably clustered at these cell–cell contact zones [37, 38].

extracellular

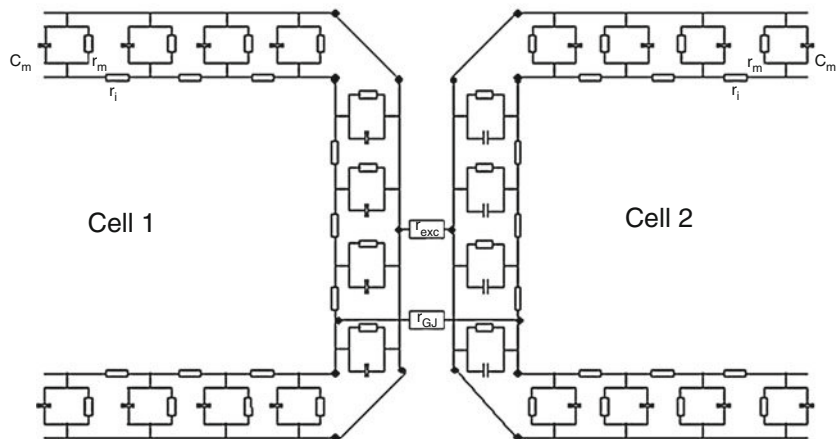
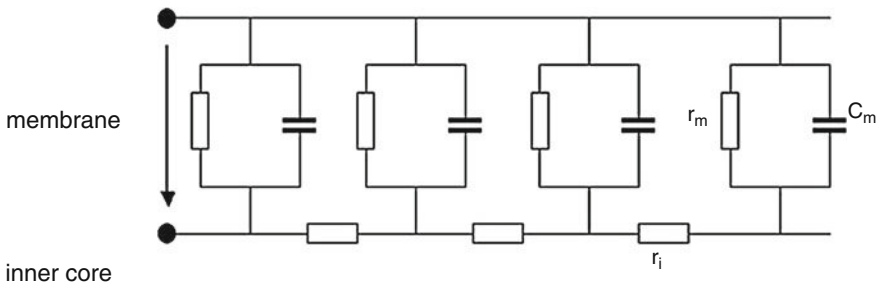


Fig. 28.2 Continuous cable (*upper part*) and discontinuous cable (*lower panel*), where the two cells are interconnected via (a) an extracellular resistance (extracellular fluid) (r_{exc}) and (b) the cores via gap junction resistances (r_{GJ})

28.3.2 Ephaptic Coupling

Prior to the understanding that gap junctions act as low resistance pathways between cells, the theory of ephaptic coupling was formulated [39] under the assumption that the two neighbouring cells can be considered similar to two closely packed capacitors.

Capacitive coupling and electrical field coupling have been proposed as alternative mechanisms of electrical transmission. For several physical reasons [(a) junctional capacitive coupling would be decreased by a factor 2 since the junction resembles two capacitors in series; (b) if only a small portion of the intercalated disk is involved, the total capacitance would be accordingly smaller; (c) there may

be a shunt to ground if the two membranes are not close enough to each other], capacitive coupling may not be operative in normal cardiac tissue [39]. Electrical field coupling [40] means the induction of an action potential in the post-cell by the electrical field arising from the action potential at the intercalated disk of the pre-cell. An accumulation of K^+ in the cleft of the intercalated disk is an important factor allowing the membrane of the pre-cell at the intercalated disk to fire a fraction of a millisecond earlier than the surface membrane, which is necessary for effective coupling. At present it is uncertain what the contribution of electrical field coupling to electrical transmission is in normal tissue. However, computer simulation studies indicate that in certain situations ephaptic coupling by electro-diffusion may play a role [41].

28.3.3 *Gap Junction Coupling*

If two cells are manipulated into intimate side-to-side contact, initially there is no transmission of electrotonic potentials or action potentials from one cell to the other [17]. After the cells establish new gap junctions, action potential transfer is possible [17]. This experimental result is contrary to the theory of ephaptic impulse transmission or of electrical field coupling [39] as non-gap junctional mechanism of intercellular action potential spreading. The time delay at gap junctions has been determined with 0.21–0.27 ms [42]. Taken together, the most important mechanism for transmission of excitation is coupling via the gap junction channels.

28.3.4 *Anisotropy and Non-uniformity (Inhomogeneity)*

Basic features of cardiac tissue are anisotropy, i.e. longitudinal resistance is lower than transverse resistance, discontinuity, i.e. fibres are separated by intercalated disks (in contrast to continuous cable), and non-uniformity, i.e. the degree of anisotropy varies from area to area because of variability in the morphology and to the deposition of connective tissue or other non-conducting structures (fat, vessels, etc.). The difference between uniform and non-uniform anisotropy has many consequences for the pathophysiology of arrhythmia [43]. In diseased myocardium, the expression of gap junction proteins is often changed. For example, Cx43 levels are decreased in chronic infarction or in heart failure, or enhanced in cardiac hypertrophy and in certain forms of atrial fibrillation [12–15, 44, 45]. Moreover, in some of these situations, the ratio Cx43/Cx40 was shifted and, probably most importantly, much of the gap junction protein was not found at the cell poles but at the lateral sides of the cells (lateralization) [14, 15]. These factors probably enhance non-uniformity in cardiac disease. In non-uniform anisotropic tissue, fractionated extracellular waveforms are typically encountered. Such complex waveforms with multi-phasic shape can be interpreted as the reflection of discontinuous propagation, and each of the

multiple negative peaks represent the activation of a small group of fibres. With increasing age, there is a general change in the biophysical properties of the cardiac tissue from uniform to non-uniform anisotropy because of the predominant uncoupling of side-to-side connections [43, 46, 47].

28.3.5 Source–Sink Problem

It has been observed that the action potential upstroke velocity and amplitude were greater during transverse propagation, accompanied by a faster foot potential, which led to the hypothesis that longitudinal propagation, although faster, is more vulnerable to block because of its lower upstroke velocity and amplitude. This behaviour can be explained on a theoretical basis: the upstroke velocity increases as a result of reduced coupling [20] since current cannot pass to the neighbouring cells.

Transfer of an action potential principally means that current has to flow from a current source to a sink. This current flow is highly dependent on gap junction conduction; however, the relationship is not trivial, since the dimensions of source and sink have to be taken into account: if a small source, represented by a tiny strand of activated cardiomyocytes meets a large sink (large area of non-activated cardiomyocytes), current will flow radially to many sites so that the current is divided among many neighbours, and in each of these neighbouring cells this current may be too low to allow propagation, resulting in conduction failure [48, 49]. Moreover, this behaviour is critically modulated by gap junction conductance: if in this situation of source–sink mismatch gap junction conductance is low, this may preserve conduction by limiting fast current loss to many sites. In contrast, if there is high coupling this might enable conduction failure by current loss.

These phenomena can be mathematically described by the safety factor SF of propagation as $SF = Q_c + Q_{out}/Q_{in}$ (=charge produced/charge consumed) [50, 51]. If coupling is reduced gradually the safety factor first is enhanced, but if very low levels of coupling are reached, SF will be reduced until conduction failure occurs at $SF < 1$. In contrast, if I_{Na} is reduced this will result in a progressive reduction of SF. However, propagation velocity will be reduced in both situations [50, 51].

Situations related to these source–sink problems may be found at the end of a Purkinje fibre or at the border between normal cardiac tissue and an ischemic (electrically silent, depolarised and uncoupled) region.

28.4 Role of Gap Junctions in Arrhythmogenesis

From the considerations above, one can imagine that disturbances of GJIC may result in altered conduction thereby finally leading or contributing to cardiac arrhythmia. There are several arrhythmias which are (at least in parts-related to changes in gap junction coupling) as follows: acute ischemia, digitalis intoxication,

aconitine intoxication, acidosis, remodelling (chronic ischemia; atrial fibrillation, heart failure, cardiac hypertrophy).

28.4.1 Acute Ischemia

During ischemia, Cx43 becomes de-phosphorylated within 30 min [18, 52–54] due to the shortage in ATP [55], and the reduced thermodynamic driving force for phosphorylation [52]. This de-phosphorylation together with Ca^{2+} -overload [28, 56, 57], intracellular acidosis [56–58] and accumulation of lipid metabolites such as lysophospholipids and arachidonic acid metabolites [59, 60] contribute to acute ischemic gap junction uncoupling. Increase in intracellular Na^+ might also promote uncoupling, since it was shown that H^+ , Ca^{2+} and Na^+ can uncouple gap junctions [2, 56, 61–64]. The consequences are an acute closure of gap junctions and – via de phosphorylation – a reduced presence in the membrane probably by removal of gap junctions. This reduction at the membrane can be seen within 30 min of ischemia in the ischemic centre and border [18] and was described as a translocation of Cx43 from membrane to cytosol [54, 65]. In consequence, the ischemic area becomes uncoupled and thereby activation spreading is slowed or ceased so that the ischemic centre becomes electrically isolated, because of gap junction uncoupling and depolarisation (which results in lower I_{Na} availability). Additionally, since the low resistance shortcuts between the cells are closed, local inhomogeneities in action potential duration cannot be equalized, so that the dispersion is enhanced [18]. These inhomogeneities together with the conduction slowing can lead to a close neighbourhood of still activated cells and already inactivated (excitable) cells, thereby enabling the occurrence of re-entrant arrhythmia. There are two peaks of ventricular fibrillation (VF) in acute ischemia: first, within the first 10 min (type IA VF), which has been ascribed to depolarisation, mechanical factors and catecholamine release; second, after ca. 20 min (type IB VF), which has been shown to be dependent on gap junction uncoupling [28, 66, 67].

Against the hypothesis of a role for uncoupling, Jongsma and Wilders [25] showed that under normoxic conditions, a 90% decrease in the number of gap junctions is required for a 25% reduction in conduction velocity. It is unclear whether this also holds true for hypoxic conditions. However, heterozygous Cx43 knock out mice under standard conditions also exhibited only 25% reduction in conduction velocity [68–70]. In simulated ischemia, gap junction coupling of cell pairs remained large enough to equilibrate action potential duration between the coupled cells until inexcitability occurred [71].

In contrast, there are studies in favour of a role of gap junctions in acute ischemia. For example, the number of hearts exhibiting pacing-induced ventricular tachycardia was significantly higher in Cx43 $+/-$ mice than in Cx43 $/+$ mice [69]. Moreover, we could demonstrate that the antiarrhythmic peptide AAP10 ($\text{H}_2\text{N}\text{-Gly-Ala-Gly-Pro-[4-OH-Pro]-Tyr-CONH}_2$), which enhanced macroscopic gap junction conductance [72–74] in human cardiomyocytes [75] without affecting the action

potential, could prevent from type IB VF in isolated rabbit hearts [76]. Similar antiarrhythmic effects could also be shown by another group using a chemical derivative of AAP10 (ZP123, now called rotigaptide) [77]. These latter results indicate that gap junction uncoupling probably contributes to type IB ischemic VF. For a detailed review and discussion see [78].

28.4.2 *Intoxications (Digitalis)*

Ventricular arrhythmia is the most serious complication of digitalis intoxication. While certainly depolarization caused by Na^+/K^+ -ATPase inhibition and enhanced automaticity plays a role, the Na^+/K^+ -ATPase inhibition results in increased intracellular $[\text{Na}^+]$ and $[\text{Ca}^{2+}]$ via altered dynamics of the $\text{Na}^+/\text{Ca}^{++}$ -exchanger. It is known that both intracellular $[\text{Na}^+]$ and $[\text{Ca}^{2+}]$ can promote cellular uncoupling [5] and that ouabain leads to gap junction uncoupling at $0.68 \mu\text{M}$ [64], a concentration that is typically reached or exceeded with intoxication. Thus, gap junction uncoupling may play a contributory role in digitalis intoxication.

28.4.3 *Acidosis*

Gap junctions uncouple in acidotic areas. According to our own experience, pH has to be reduced to values below 6.5 to provoke uncoupling, which develops slowly after a latency of about 7–10 min [75], while gap junction conductance (g_j) is nearly constant in a pH range from 7.4 to 6.5 [2]. The pH– g_j relationship is principally not affected by intracellular pCa. In neonatal rat heart cells, Firek and Weingart [79] found a pK_H of 5.85. One H^+ binding site could be identified as histidine-95 in cardiac connexin 43 by Ek et al. [80]. Hermans and colleagues [81] investigated the effects of site-directed mutations in Cx43 transfected SKHep1 cells by exchange of His-126 and His-142 and found an uncoupling effect of acidification related to the position of histidines in the cytoplasmic loop rather than to the total number of histidines. They reported that a fall in pH_i caused a reduction in channel open probability but not in channel conductance. Using a transfection system, it was found that Cx45 channels are more sensitive to pH than Cx43 channels [81]. Regarding the pH sensor, the carboxy tail length has been demonstrated to be a determinant of pH sensitivity [63, 82] and is thought to occlude (close) the channel, comparable to the ball-and-chain model for N-type inactivation of potassium channels.

28.4.4 *Chronic Infarction*

After myocardial ischemia the tissue is submitted to complex remodelling processes starting with increased fibrosis. Among these changes, gap junctions are also

remodelled with a decrease in Cx43 and altered distribution of Cx43 and Cx40 [13]. Local contractility is reduced and the necrosis zone is replaced by connective tissue. Fibroblast growth factor FGF-2, which can be released from cardiomyocytes during contraction and after stimulation with catecholamines, is up-regulated in response to myocardial damage, and can decrease intercellular dye coupling in cardiomyocytes whereas in fibroblasts coupling may be enhanced [83, 84]. It is unclear whether this result from neonatal cardiomyocytes also holds true for adult cardiomyocytes. These changes might be somehow linked to arrhythmias observed after myocardial infarction originating from abnormal conduction of activation in the vicinity of scar areas [85] and slowed anisotropic conduction [86].

The effects seen in the *chronic* phase of ischemia after infarction are as follows: (a) loss of the common ordered (polarized) distribution of the gap junctions, which was found predominantly in the border zone adjacent to infarct scars and (b) reduction in the quantity of connexin 43 gap junctions in areas distant from the infarct zone [12, 13], which may lead to heterogeneous anisotropic conduction with locally slowed conduction despite nearly normal active properties of cells [86–88]. Gap junctions belong to the most important determinants of these passive conduction properties [85, 89]. In the border zone of healed infarcts (some 100 µm from the infarct scar), the distribution of gap junctions is significantly altered and connexins are scattered over the whole membrane and no longer confined to the cell poles (intercalated disks), although some of the cells show the normal type of distribution, while in the non-ischemic-normal areas, there is a regular distribution [12]. In addition, fibroblast/myocyte coupling probably plays an additional pathophysiological role [90]. Interestingly, successful conduction can be established between cardiomyocytes separated by (non-excitatory) fibroblasts over a distance of up to 300 µm [49].

Decrease in Cx43, altered Cx43/Cx40 ratio, lateralization in the subcellular gap junction distribution, decrease in gap junction number and alterations in gap junction size, remodelling processes and fibroblast/myocyte coupling all together initiate a complete change in the biophysical architecture of the tissue with a high degree in heterogeneity and non-uniform anisotropy forming an arrhythmogenic substrate.

28.4.5 Atrial Fibrillation

In the atrium, Cx43 and Cx40 mediated GJIC. The most common finding in AF is an increased heterogeneity in the regional distribution of gap junctions, in the amounts of Cx43 and Cx40 [14, 91, 92] (with various findings, probably depending on the accompanying diseases (coronary heart disease, heart failure, mitral valve disease, hyperthyreosis) or on the disease model or the tissue under investigation (right atrium or left atrium)), and an alteration in the subcellular distribution with enhanced expression of connexins at the lateral side of the cells (lateralization) [14, 15]. What is the specific role of gap junctions in AF?

Regarding initiation, AF mostly originates from left atrial sleeves, which protrude from the atrium into the pulmonary veins and form circumferential structures, which are coupled by Cx43 and to a lower extend by Cx40 [93]. Among many other factors, this circumferential structure of conducting tissue around the pulmonary veins seems to be necessary for the initiation of a first re-entrant circuit from which AF develops. Obviously, other factors (stretch, heterogeneity, fibrosis, ANF, amyloid, ischemia, age, vagal tone, angiotensin, Ca^{2+}) may also contribute to the initiation of AF. Thus, gap junctions do not seem to be directly/causally involved in AF initiation.

Regarding maintenance of AF (chronification, remodelling), there is evidence that gap junction remodelling is an important factor leading to the formation of an arrhythmogenic substrate. In lone AF, we found an up-regulation of Cx40, while Cx43 was little affected [14, 94]. Cx up-regulation was also found in patients suffering from postoperative AF [44]. Moreover, we found that connexins were localized to the lateral sides of the cardiomyocytes (lateralization) [14], which was later verified [15]. Others found also an up-regulation of Cx43 in right atrium [95]. An additional factor found by Kostin and colleagues [15] is increased heterogeneity in the presence of connexins with the free right atrial wall showing elevated Cx40, but reduced Cx43 expression and the appendage with both connexins being reduced. In another patient population (AF with underlying mitral valve disease), we found Cx43 being up-regulated in the left, but not in the right atrium. This up-regulation was accompanied by an elevated expression of AT1-receptors in the left but not right atrium [45]. Since we have also shown that angiotensin-II can up-regulate Cx43 via AT1-receptors [96], and since it is now known clinically that the maintenance of SR after cardioversion is improved if ACE-inhibitors are applied, one may suppose that angiotensin-II might be involved in the gap junction remodelling process.

The findings in humans differ from animal disease models with regard to the expression level of certain connexins [92, 97–99], but a common phenomenon seems to be regional heterogeneity of connexin expression and lateralization. These latter effects will probably change the biophysics of the tissue and may lead to local conduction slowing and to irregular spread of activation, which together with the other factors enable AF to persist. By gap junction remodelling, AF becomes structurally fixed. For a detailed review and discussion see [100].

28.5 Heart Failure and Cardiac Hypertrophy

If the muscular force of the heart is chronically reduced, compensatory mechanisms lead to cardiac hypertrophy and remodelling processes. A basic mechanism is the activation of the sympathetic nervous system and of the renin-angiotensin-aldosteron cascade and probably of endothelin with stimulation of α_1 - and β -adrenergic receptors as well as AT₁-receptors and ET_A-receptors, which all are known to enhance Cx43 expression [96, 101]. In addition, fibrosis is increased in most types of

cardiomyopathy. These changes affect the conducting properties as well. Because of the altered morphology, the cells are larger, which affects both longitudinal and transverse velocity. Fibrotic strands, mostly parallel to the fibres, lead to a transverse separation of the fibres and can reduce transverse propagation. Because of the inhomogeneous nature of fibrosis and the changes in tissue architecture, it is reasonable to assume that the resulting changes in conduction will also be heterogeneous. In addition, it has been shown that gap junction distribution becomes heterogeneous in de-compensated hypertrophy with areas of tissue with normal or a very low (or no) expression of gap junction [102]. In dilated cardiomyopathy and myocarditis, focal disarrays of gap junctions were found [103]. In compensated hypertrophy, Kostin et al. [102] observed lateralization of Cx43. Thus, heart failure and hypertrophy seem to be associated with a dis-organization (heterogeneity, lateralization) of gap junctions (=structural remodelling). Lateralization of connexin43 was also seen in patients suffering from hypertrophic obstructive cardiomyopathy (HOCM) [104]. Regarding the level of connexin expression, it was found that Cx43 expression was diminished in patients suffering from congestive or ischemic heart failure [89, 105], or such that there was a heterogeneous loss in non-ischemic dilated cardiomyopathy with ventricular tachycardia [106]. In HOCM, however, the Cx43 expression was enhanced [104], as it was in guinea pig hearts with renovascular hypertension [107]. It has been hypothesized that the decline in Cx43 expression in manifest heart failure is preceded by an increased expression during the phases of compensated hypertrophy [102]. The up-regulation in hypertrophy was also seen in cell culture models of cardiac hypertrophy and, thus, has been suggested to be possibly related to adrenergic or angiotensinergic stimulation [96, 101]. Interestingly, Yamada et al. [108] reported that Cx45 was up-regulated in heart failure in parallel to decreased Cx43 expression. Cx40 does not seem to be elevated in idiopathic dilated cardiomyopathy, but was found to be elevated in ischemic heart failure [105].

Nevertheless, while the level of connexin expression seems to depend on the phase of the disease [13, 102, 109], a common phenomenon seems to be the changes in the network architecture with lateralization of gap junctions, heterogeneous expression of connexins, and with transverse separation of the fibres by strands of connective tissue. Regarding the functional consequences, there is still an ongoing debate about the contribution of cardiomyopathic gap junction remodelling to ventricular arrhythmia. Although ventricular arrhythmia and conduction disturbances in cardiomyopathy are clearly present, there is a plethora of factors, which may be involved, and which is out of scope of the present article. However, the changes described earlier may lead to local conduction slowing in areas without gap junctions or with very low levels. As stated earlier, it was argued that reductions below 50% are necessary to affect conduction significantly [25]. However, these considerations did not take fibrotic strands, enlarged cells, heterogeneity, together with altered electrophysiology in heart failure into account. Taken together, these factors may lead to altered source–sink ratios, so that it might be imagined that even lower reductions in connexin level could affect conduction in diseased myocardium (see above). It has been speculated that lateralized gap junctions may enable transverse conduction or may facilitate re-entrant circuit, although this has not

been clearly shown in the diseased ventricle until now. It would be a prerequisite, that these lateralized gap junctions are functional, and that in that area the cells are not separated by fibrotic strands. It will be difficult to prove, whether these lateralized gap junctions are functional or not. However, large reduction in Cx43 expression levels will probably slow conduction, and an up-regulation of Cx45 might result in heteromeric channels with altered electrophysiology. Thus, it is reasonable to assume that the changes seen in connexin expression and localisation may lead to an altered electrical architecture and may contribute to the formation of an arrhythmogenic substrate.

It is necessary to state that there are many other factors contributing to cardiac remodelling in heart failure and to the pathophysiology of this disease, which cannot be mentioned here due to the limitation of space, so that we focus here on a brief description of those processes affecting gap junctions.

28.6 Antiarrhythmic Peptides Targeting Gap Junctions

Regarding therapeutical or pharmacological consequences, in 1994 we developed synthetic antiarrhythmic peptides, among which AAP10 ($\text{H}_2\text{N-Gly-Ala-Gly-HYP-Pro-Tyr-CONH}_2$) was found to be the most effective [72]. This peptide was found to reduce dispersion with an EC_{50} of 1 nM, to enhance gap junction electrical conductance, to maintain conduction under hypoxic conditions in papillary muscles [72, 74] and to prevent type IB VF [76]. AAP10 was also effective in suppression of VF in rabbits with healed myocardial infarction [110].

The peptide exhibits a semicyclic horse-shoe like spatial structure as evaluated in 2D mass spectroscopy studies ([111]; see Figs. 28.3 and 28.4), so that it was possible to construct an equally effective cyclopeptide cAAP10RG [76, 111], which served as basis for the development of rotigaptide, a recent AAP10 derivative with certain D-amino acids in reverse order (so that the functional groups are at the same positions as in AAP10), which has been recently tested in clinical trials. Rotigaptide has been shown also to prevent spontaneous ventricular extrasystoles and ventricular tachycardia during myocardial ischemia/reperfusion [77, 112].

AAP10 acts via activation of $\text{PKC}\alpha$ and phosphorylation of Cx43, probably via a G-protein coupled membrane receptor [113]. In ischemic rabbit hearts, AAP10 exhibits its inhibitory effect on Cx43-de-phosphorylation preferentially in the ischemic region, as it prevents from Cx43 loss from the cell poles in the ischemic centre and border without affecting the non-ischemic zone [18]. According to these results, Ser368 on the C-terminal of Cx43 is one (but probably not the only) of the phosphorylation sites targeted by AAP10 [18]. Typically, a loss of Cx43 from the cells is observed during ischemia [114]. Recently, we showed that AAP10 enhances both electric and metabolic coupling, and that it acts on Cx43 and Cx45, but not on Cx40 [75]. Moreover, we showed that AAP10 prevents acidosis-induced uncoupling (pre-treatment), such that its effects are significantly larger if cells are partially uncoupled in good accordance to our findings in ischemic hearts (see above) and that

Fig. 28.3 AAP10 and its putative receptor pouch as deduced from Grover and Dhein [76, 111]

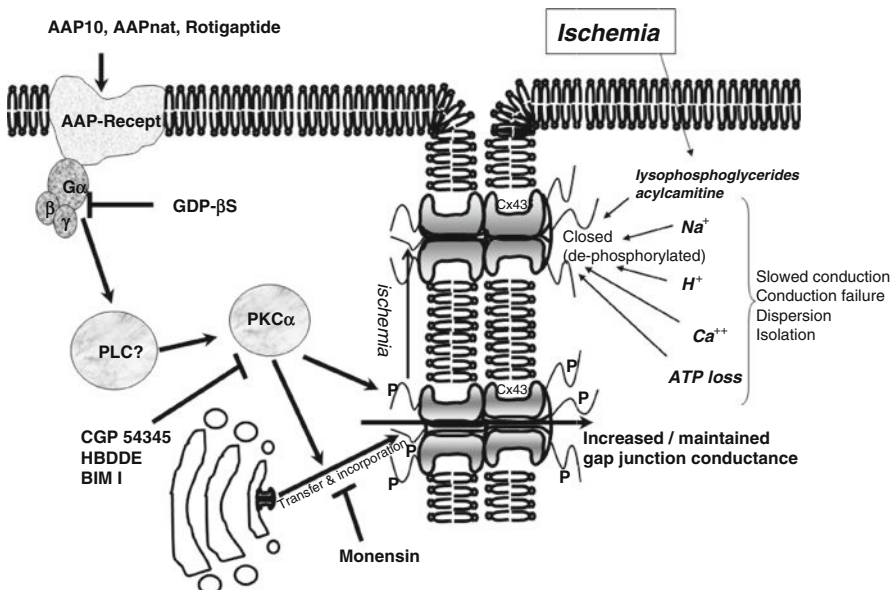
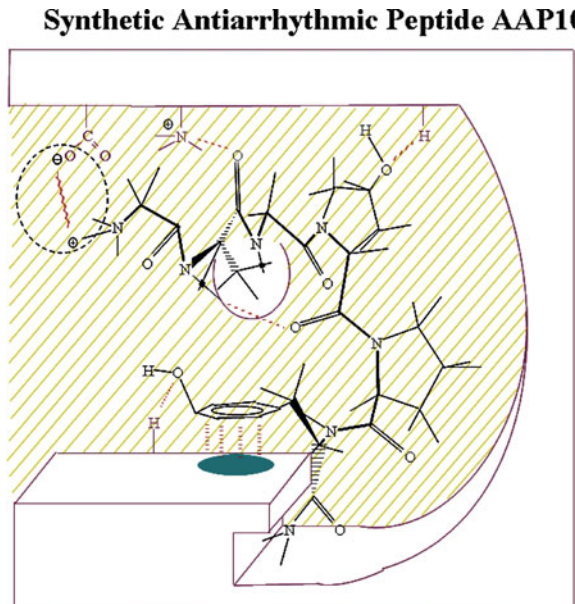


Fig. 28.4 Present view of the mechanism of action of AAP10 in acute ischemia

it also can reverse acidosis-induced uncoupling (treatment) [75]. Finally, we found that AAP10 acts on human cardiac myocytes [75].

In 1995, we formulated the theory of improvement in gap junction conductance as an antiarrhythmic principle for certain arrhythmia [115].

28.7 Conclusions

Gap junctions play an important role in the conduction properties of cardiac tissues and in arrhythmogenesis. Acute closure of gap junctions is a typical phenomenon in ischemia and acidosis, which is thought to be related to late ischemic ventricular fibrillation. Changes in the expression of connexins, in the subcellular location (cell pole vs. lateral side of the cells) or in the regional expression level (heterogeneity) have been found in cardiac disease (heart failure, hypertrophy, infarction, atrial fibrillation). The new group of antiarrhythmic peptides that open gap junctions provides a new approach to antiarrhythmic treatment.

Acknowledgments This study was generously supported by the Deutsche Forschungsgemeinschaft DFG, Bonn, Germany, with a grant to Stefan Dhein.

References

1. Bedner P, Niessen H, Odermatt B, Willecke K, Harz H. A method to determine the relative cAMP permeability of connexin channels. *Exp Cell Res.* 2003;291:25–35.
2. Noma A, Tsuboi N. Dependence of junctional conductance on proton, calcium and magnesium ions in cardiac paired cells of guinea pig. *J Physiol (Lond).* 1987;382:193–211.
3. Spray DC, Harris AL, Bennett MVL. Equilibrium properties of a voltage dependent junctional conductance. *J Gen Physiol.* 1981;77:77–93.
4. Spray DC, White RL, Mazet F, Bennett MVL. Regulation of gap junction conductance. *Am J Physiol.* 1985;248:H753–64.
5. Weingart R, Maurer P. Cell-to-cell coupling studied in isolated ventricular cell pairs. *Experientia.* 1987;43:1091–4.
6. Dhein S. Pharmacology of gap junctions in the cardiovascular system. *Cardiovasc Res.* 2004;62:287–98.
7. Salameh A, Dhein S. Pharmacology of gap junctions. New pharmacological targets for treatment of arrhythmia, seizure and cancer? *Biochim Biophys Acta.* 2005;1719(1–2):36–58.
8. Salameh A. Life cycle of connexins: regulation of connexin synthesis and degradation. *Adv Cardiol.* 2006;42:57–70.
9. Fallon RF, Goodenough DA. Five hour half-life of mouse liver gap junction protein. *J Cell Biol.* 1981;127:343–55.
10. Darrow BJ, Laing JG, Lampe PD, Saffitz JE, Beyer EC. Expression of multiple connexins in cultured neonatal rat ventricular myocytes. *Circ Res.* 1995;76:381–7.
11. Beardslee AMA, Laing JG, Beyer EC, Saffitz JE. Rapid turnover of connexin43 in the adult rat heart. *Circ Res.* 1998;83:629–35.

12. Severs NJ. Pathophysiology of gap junctions in heart disease. *J Cardiovasc Electrophysiol*. 1994;5:462–75.
13. Severs NJ, Dupont E, Thomas N, Kaba R, Rothery S, Jain R, et al. Alterations in cardiac connexin expression in cardiomyopathies. *Adv Cardiol*. 2006;42:228–42.
14. Polontchouk L, Haefliger J-A, Ebelt B, Schaefer T, Stuhlmann D, Mehlhorn U, et al. Effects of chronic atrial fibrillation on gap junction distribution in human and rat atria. *J Am Coll Cardiol*. 2001;38:883–91.
15. Kostin S, Klein G, Szalay Z, Hein S, Bauer EP, Schaper J. Structural correlate of atrial fibrillation in human patients. *Cardiovasc Res*. 2002;54:361–79.
16. Buchanan JW, Saito T, Gettes LS. The effect of antiarrhythmic drugs, stimulation frequency and potassium induced resting membrane potential changes on conduction velocity and dV/dt_{max} in guinea pig myocardium. *Circ Res*. 1985;56:696–703.
17. Weingart R, Maurer P. Action potential transfer in cell pairs isolated from adult rat and guinea pig ventricles. *Circ Res*. 1988;63:72–80.
18. Jozwiak J, Dhein S. Local effects and mechanisms of antiarrhythmic peptide AAP10 in acute regional myocardial ischemia: electrophysiological and molecular findings. *Naunyn Schmiedebergs Arch Pharmacol*. 2008;378:459–70.
19. Dhein S, Krüsemann K, Schaefer T. Effects of the gap junction uncoupler palmitoleic acid on activation and repolarization pattern in isolated rabbit hearts. A mapping study. *Br J Pharmacol*. 1999;128:1375–84.
20. Delmar M, Michaels DC, Johnson T, Jalife J. Effects of increasing intercellular resistance on transverse and longitudinal propagation in sheep epicardial muscle. *Circ Res*. 1987;60:780–5.
21. Unger VM, Kumar NM, Gilula NB, Yeager M. Three-dimensional structure of a recombinant gap junction membrane channel. *Science*. 1999;283(5405):1176–80.
22. Cruciani V, Mikalsen SO. Evolutionary selection pressure and family relationships among connexin genes. *Biol Chem*. 2007;388:253–64.
23. Söhl G, Willecke K. Gap junctions and the connexion protein family. *Cardiovasc Res*. 2004;62:228–32.
24. Kwak BR, Jongsma HJ. Regulation of cardiac gap junction channel permeability and conductance by several phosphorylating conditions. *Mol Cell Biochem*. 1996;157:93–9.
25. Jongsma HJ, Wilders R. Gap junctions in cardiovascular disease. *Circ Res*. 2000;86:1193–7.
26. Kwak BR, Hermanns MMP, De Jonge HR, Lohmann SM, Jongsma HJ, Chanson M. Differential regulation of distinct types of gap junction channels by similar phosphorylating conditions. *Mol Biol Cell*. 1995;6:1707–19.
27. Christ GJ, Brink PR. Analysis of the presence and physiological relevance of subconducting states of connxin43-derived gap junction channels in cultured human corporal vascular smooth muscle cells. *Circ Res*. 1999;85:797–803.
28. Dekker LRC, Fiolet JWT, VanBavel E, Coronel R, Ophof T, Spaan JAE, et al. Intracellular Ca²⁺, intercellular electrical coupling and mechanical activity in ischemic rabbit papillary muscle. Effects of preconditioning and metabolic blockade. *Circ Res*. 1996;79:237–46.
29. Musil LS, Goodenough DA. Multisubunit assembly of an integral plasma membrane channel protein, gap junction connexin43, occurs after exit from the ER. *Cell*. 1993;74:1065–77.
30. Musil LS, Goodenough DA. Biochemical analysis of connexon assembly. In: Kanno Y, Kataoka K, Shiba Y, Shibata Y, Shimazu T, editors. *Intercellular communication through gap junctions. Progress in cell research*, vol. 4. Amsterdam: Elsevier Science Publications; 1995. p. 327–30.
31. Falk MM. Connexin-specific distribution within gap junctions revealed in living cells. *J Cell Sci*. 2000;113:4109–20.
32. Giepmans BN. Gap junctions and connexin-interacting proteins. *Cardiovasc Res*. 2004;62:233–45.
33. Berthoud VM, Minogue PJ, Laing JG, Beyer EC. Pathways for degradation of connexins and gap junctions. *Cardiovasc Res*. 2004;62:256–67.

34. Weidmann S. Passive properties of cardiac fibers. In: Rosen MR, Janse MJ, Wit AL, editors. *Cardiac electrophysiology. A textbook*. Mount Kisco, New York: Futura Publishing Company Inc.; 1990. p. 29–35.
35. Hodgkin AL, Rushton WAH. The electrical constants of a crustacean nerve fibre. *Proc R Soc Lond Ser B*. 1946;133:444–79.
36. Weidmann S. The electrical constants of Purkinje fibers. *J Physiol (Lond)*. 1952;118:348–60.
37. Kucera J, Rohr S, Rudy Y. Localization of sodium channels in intercalated disks modulates cardiac conduction. *Circulation*. 2002;91:1176–82.
38. Maier SKG, Westenbroek RE, McCormick KA, Curtis R, Scheuer T, Catterall WA. Distinct subcellular localization of different sodium channel α and β subunits in single ventricular myocytes from mouse heart. *Circulation*. 2004;109:1421–7.
39. Sperelakis N. Propagation mechanisms in the heart. *Annu Rev Physiol*. 1979;41:441–57.
40. Sperelakis N, Mann JE. Evaluation of electric field changes in the cleft between excitable cells. *J Theor Biol*. 1977;64:71–96.
41. Mori Y, Fishman GI, Peskin CS. Ephaptic conductin in a cardiac strand model with 3D electrodiffusion. *Proc Natl Acad Sci U S A*. 2008;105:6463–8.
42. Hubbard ML, Ying W, Henriquez CS. Effect of gap junction distribution on impulse propagation in a monolayer of myocytes: a model study. *Europace*. 2007;9 Suppl 6:vi20–8.
43. Spach MS, Dolber PC. Discontinuous anisotropic propagation. In: Rosen MR, Janse MJ, editors. *Wit AL: cardiac electrophysiology: a textbook*. Mount Kisco, New York: Futura Publishing Company Inc; 1990. p. 517–34.
44. Dupont E, Ko Y-S, Rothery S, Coppen SR, Baghai M, Haw M, et al. The gap junctional protein connexin40 is elevated in patients susceptible to postoperative atrial fibrillation. *Circulation*. 2001;103:842–9.
45. Boldt A, Wetzel U, Weigl J, Garbade J, Lauschke J, Hindricks G, et al. Expression of angiotensin II receptors in human left and right atrial tissue in atrial fibrillation with and without underlying mitral valve disease. *J Am Coll Cardiol*. 2003;42:1785–92.
46. Spach MS, Dolber PC. Relating extracellular potentials and their derivatives to anisotropic propagation at a microscopic level in human cardiac muscle. Evidence for electrical uncoupling of side-to-side fiber connections with increasing age. *Circ Res*. 1986;58:356–71.
47. Dhein S, Hammerrath SB. Aspects of the intercellular communication in aged hearts. Effects of the gap junction uncoupler palmitoleic acid. *Naunyn Schmiedebergs Arch Pharmacol*. 2001;364:397–408.
48. Rohr S, Kucera JP, Fast VG, Kleber AG. Paradoxical improvement of impulse conduction in cardiac tissue by partial cellular uncoupling. *Science*. 1997;275(5301):841–4.
49. Rohr S. Role of gap junctions in the propagation of the cardiac action potential. *Cardiovasc Res*. 2004;62:309–22.
50. Shaw RM, Rudy Y. Electrophysiologic effects of acute myocardial ischemia. A mechanistic investigation of action potential conduction and conduction failure. *Circ Res*. 1997;80:124–38.
51. Shaw RM, Rudy Y. Ionic mechanisms of propagation in cardiac tissue: roles of the sodium and L-type calcium currents during reduced excitability and decreased gap-junction coupling. *Circ Res*. 1997;81:727–41.
52. Beardslee MA, Lerner DL, Tadros PN, Laing JG, Beyer EC, Yamada KA, et al. Dephosphorylation and intracellular redistribution of ventricular connexin43 during electrical uncoupling induced by ischemia. *Circ Res*. 2000;87:656–62.
53. Schulz R, Gres P, Syschally A, et al. Ischemic preconditioning preserves connexin43 phosphorylation during sustained ischemia in pig hearts *in vivo*. *FASEB J*. 2003;17:1355–7.
54. Jain SK, Schuessler RB, Saffitz JE. Mechanisms of delayed electrical uncoupling induced ischemic preconditioning. *Circ Res*. 2003;92:1138–44.
55. Verecchia F, Duthe F, Duval S, Duchatelle I, Sarrouilhe D, Hervé JC. ATP counteracts the rundown of gap junctional channels of rat ventricular myocytes by promoting protein phosphorylation. *J Physiol (Lond)*. 1999;516:447–59.

56. Burt JM. Block of intercellular communication: interaction of intracellular H⁺ and Ca²⁺. *Am J Physiol.* 1987;253:C607–9.
57. White RL, Doeller JE, Verselis VK, Wittenberg BA. Gap junctional conductance between pairs of ventricular myocytes is modulated synergistically by H⁺ and Ca²⁺. *J Gen Physiol.* 1990;95:1061–75.
58. Yan GX, Kléber AG. Changes in extracellular and intracellular pH in ischemic rabbit papillary muscle. *Circ Res.* 1992;71:460–70.
59. Massey KD, Minnich BN, Burt JM. Arachidonic acid and lipoxygenase metabolites uncouple neonatal rat cardiac myocyte pairs. *Am J Physiol.* 1992;263:C494–501.
60. Wu J, McHowat J, Saffitz JE, Yamada KA, Corr PB. Inhibition of gap junctional conductance by long-chain acylcarnitines and their preferential accumulation in junctional sarcolemma during hypoxia. *Circ Res.* 1993;72:879–89.
61. Maurer P, Weingart R. Cell pairs isolated from guinea pig and rat hearts: effects of [Ca²⁺]_i on nexal membrane resistance. *Pflügers Arch.* 1987;409:394–402.
62. Reber WR, Weingart R. Ungulate cardiac Purkinje fibers: the influence of intracellular pH on the electrical cell-to-cell coupling. *J Physiol (Lond).* 1982;328:87–104.
63. Morley GE, Taffet SM, Delmar M. Intramolecular interactions mediate pH regulation of connexin 43 channels. *Biophys J.* 1996;70:1294–302.
64. De Mello WC. Influence of the sodium pump on intercellular communication in heart fibers: effect of intracellular injection of sodium ion on electrical coupling. *J Physiol (Lond).* 1976;263:171–97.
65. Hatanaka K, Kawata H, Toyofuku T, Yoshida K. Down-regulation of connexin43 in early myocardial ischemia and protective effect by ischemic preconditioning in rat heart *in vivo*. *Jpn Heart J.* 2004;45:1007–19.
66. Smith IV WT, Fleet WF, Johnson TA, Engle CL, Cascio WE. The Ib phase of ventricular arrhythmias in ischemic *in situ* porcine heart is related to changes in cell-to-cell electrical coupling. Experimental Cardiology Group, University of North Carolina. *Circulation.* 1995;92:3051–60.
67. de Groot JR, Wilms-Schopman FJ, Ophof T, Remme CA, Coronel R. Late ventricular arrhythmias during acute regional ischemia in the isolated blood perfused pig heart. Role of electrical cellular coupling. *Cardiovasc Res.* 2001;50:362–72.
68. Morley GE, Vaidya D, Samie FH, Lo C, Delmar M, Jalife J. Characterization of conduction in the ventricles of normal and heterozygous Cx43 knockout mice using optical mapping. *J Cardiovasc Electrophysiol.* 1999;10:1361–75.
69. Lerner DL, Yamada KA, Schuessler RB, Saffitz JE. Accelerated onset and increased incidence of ventricular arrhythmias induced by ischemia in Cx43-deficient mice. *Circulation.* 2000;101:547–52.
70. Thomas SP, Kucera JP, Bircher-Lehmann L, Rudy Y, Saffitz JE, Kleber AG. Impulse propagation in synthetic strands of neonatal cardiac myocytes with genetically reduced levels of connexin43. *Circ Res.* 2003;92:1209–16.
71. De Groot JR, Schumacher CA, Verkerk AO, Baartscheer A, Fiolet JWT, Coronel R. Intrinsic heterogeneity in repolarization is increased in isolated failing rabbit cardiomyocytes during simulated ischemia. *Cardiovasc Res.* 2003;59:705–14.
72. Dhein S, Manicone N, Müller A, Gerwin R, Ziskoven U, Irankhahi A, et al. A new synthetic antiarrhythmic peptide reduces dispersion of epicardial activation recovery interval and enhances cellular communication. Antiarrhythmic properties in regional ischemia. *Naunyn Schmiedebergs Arch Pharmacol.* 1994;350:174–84.
73. Dhein S, Weng S, Grover R, Tudyka T, Gottwald M, Schaefer T, et al. Protein kinase C α mediates the effect of antiarrhythmic peptide on gap junction conductance. *Cell Adhes Commun.* 2001;8:257–64.
74. Müller A, Gottwald M, Tudyka T, Linke W, Klaus W, Dhein S. Increase in gap junction conductance by an antiarrhythmic peptide. *Eur J Pharmacol.* 1997;327:65–72.

75. Hagen A, Dietze A, Dhein S. Human cardiac gap junction coupling: effects of antiarrhythmic peptide AAP10. *Cardiovasc Res.* 2009;83:405–15.
76. Grover R, Dhein S. Structure–activity relationships of novel peptides related to the antiarrhythmic peptide AAP10 which reduce the dispersion of epicardial action potential duration. *Peptides.* 2001;22:1011–21.
77. Xing D, Kjolbye AL, Nielsen MS, Petersen JS, Harlow KW, Holstein-Rathlou N-H, et al. ZP123 increases gap junctional conductance and prevents reentrant ventricular tachycardia during myocardial ischemia in open chest dogs. *J Cardiovasc Electrophysiol.* 2003;14:510–20.
78. Dhein S. Cardiac ischemia and uncoupling: gap junctions in ischemia and infarction. *Adv Cardiol.* 2006;42:198–212.
79. Firek L, Weingart R. Modification of gap junction conductance by divalent cations and protons in neonatal rat heart cells. *J Mol Cell Cardiol.* 1995;27:1633–43.
80. Ek JF, Delmar M, Perzova R, Taffet SM. Role of histidine 95 on pH gating of the cardiac gap junction protein connexin43. *Circ Res.* 1994;74:1058–64.
81. Hermans MMP, Kortekaas P, Jongsma HJ, Rook MB. pH sensitivity of the cardiac gap junction proteins, connexin 45 and 43. *Pflügers Arch.* 1995;431:138–40.
82. Liu S, Taffet S, Stoner L, Delmar M, Vallano ML, Jalife J. A structural basis for the unequal sensitivity of the major cardiac and liver gap junctions to intracellular acidification: the carboxy tail length. *Biophys J.* 1993;64:1422–33.
83. Doble BW, Kardami E. Basic fibroblast growth factor stimulates connexin-43 expression and intercellular communication of cardiac fibroblasts. *Mol Cell Biochem.* 1995;143:81–7.
84. Doble BW, Chen Y, Bosc DG, Litchfield DW, Kardami E. Fibroblast growth factor-2 decreases metabolic coupling and stimulates phosphorylation as well as masking of connexin43 epitopes in cardiac myocytes. *Circ Res.* 1996;79:647–58.
85. Saffitz JE, Hoyt RH, Luke RA, Kanter HL, Beyer EC. Cardiac myocyte interconnections at gap junctions: role in normal and abnormal electrical conduction. *Trends Cardiovasc Med.* 1992;2:56–60.
86. Dillon SM, Allessie MA, Ursell PC, Wit AL. Influences of anisotropic tissue structure on reentrant circuits in the epicardial border zone of subacute canine infarcts. *Circ Res.* 1988;63:182–206.
87. Spach MS, Dolber PC, Heidlage JF. Influence of the passive anisotropic properties on directional differences in propagation following modification of the sodium conductance in human atrial muscle. A model of reentry based on anisotropic discontinuous propagation. *Circ Res.* 1988;62:811–32.
88. Ursell PC, Gardner PI, Albala A, Fenoglio JJ, Wit AL. Structural and electrophysiological changes in the epicardial border zone of canine myocardial infarcts during infarct healing. *Circ Res.* 1985;56:436–51.
89. Peters NS, Green CR, Poole-Wilson PA, Severs NJ. Reduced content of connexin43 gap junctions in ventricular myocardium from hypertrophied and ischaemic human hearts. *Circulation.* 1993;88:864–75.
90. Camelliti P, Green CR, Kohl P. Structural and functional coupling of cardiac myocytes and fibroblasts. *Adv Cardiol.* 2006;42:132–49.
91. Van der Velden HMW, Ausma J, Rook MB, Hellemons AJCGM, Van Veen TAAB, Allessie MA, et al. Gap junctional remodeling in relation to stabilization of atrial fibrillation in the goat. *Cardiovasc Res.* 2000;46:476–86.
92. Van der Velden HMW, van Kempen MJA, Wijffels MCEF, van Zijverden M, Groenewegen WA, Allessie MA, et al. Altered pattern of connexin40 distribution in persistent atrial fibrillation in the goat. *J Cardiovasc Electrophysiol.* 1998;9:596–607.
93. Verheule S, Wilson EE, Arora R, Engle SK, Scott LR, Ogin JE. Tissue structure and connexion expression of canine pulmonary veins. *Cardiovasc Res.* 2002;55:727–38.
94. Wetzel U, Boldt A, Lauschke J, Weigl J, Schirdehahn P, Dorszewski A, et al. Expression of connexins40 and 43 in human left atrium in atrial fibrillation of different aetiologies. *Heart.* 2005;91:166–70.

95. Yan H, Chen JZ, Zhu JH, Ni YM, Yu GW, Hu SJ, et al. Expression of connexin in atrium of patients with atrial fibrillation and its signal transduction pathway. *Zhonghua Yi Xue Za Zhi*. 2004;84:209–13.
96. Polontchouk L, Ebelt B, Jackels M, Dhein S. MAP kinases mediate the effects of endothelin-1 and angiotensin-II on the cardiac connexin expression. *FASEB J*. 2002;16:87–9.
97. Schotten U, Blaauw Y, Allessie MA. In-vivo models of atrial fibrillation. In: Dhein S, Mohr FW, Delmar M, editors. Practical methods in cardiovascular research. Heidelberg: Springer; 2005. p. 129–49.
98. Ausma J, Van der Velden HMW, Lenders M-H, van Ankeren EP, Jongsma HJ, Ramaekers FCS, et al. Reverse structural and gap-junctional remodeling after prolonged atrial fibrillation in the goat. *Circulation*. 2003;107:2051–8.
99. Elvan A, Huang X-D, Pressler ML, Zipes DP. Radiofrequency catheter ablation of the atria eliminates pacing-induced sustained atrial fibrillation and reduces connexin 43 in dogs. *Circulation*. 1997;96:1675–85.
100. Dhein S. Role of connexins in atrial fibrillation. *Adv Cardiol*. 2006;42:161–74.
101. Salameh A, Frenzel C, Boldt A, Rassler B, Glawe I, Schulte J, et al. Subchronic alpha- and beta-adrenergic regulation of cardiac gap junction protein expression. *FASEB J*. 2006;20(2):365–7.
102. Kostin S, Dammer S, Hein S, Klövekorn WP, Bauer EP, Schaper J. Connexin 43 expression and distribution in compensated and decompensated cardiac hypertrophy in patients with aortic stenosis. *Cardiovasc Res*. 2004;62:426–36.
103. Kostin S, Rieger M, Dammer S, Hein S, Richter M, Klövekorn WP, et al. Gap junction remodeling and altered connexin43 expression in the failing human heart. *Mol Cell Biochem*. 2003;242:135–44.
104. Salameh A, Mühlberg K, Rahmel A, Dhein S, Pfeiffer D. Änderungen der connexin expression bei humanen dilatativen und hypertrophen kardiomyopathien. *Z Kardiol*. 2005;94 Suppl 1:V1186.
105. Dupont E, Matsushita T, Kaba RA, et al. Altered connexin expression in human congestive heart failure. *J Mol Cell Cardiol*. 2001;33:359–71.
106. Kitamura H, Ohnishi Y, Yoshida A, Okajima K, Azumi H, Ishida A, et al. Heterogeneous loss of connexin43 protein in nonischemic dilated cardiomyopathy with ventricular tachycardia. *J Cardiovasc Electrophysiol*. 2002;13:865–70.
107. Peters NS. New insights into myocardial arrhythmogenesis: distribution of gap junctional coupling in normal, ischaemic and hypertrophied hearts. *Clin Sci*. 1996;90:447–52.
108. Yamada KA, Rogers JG, Sundset R, Steinberg TH, Saffitz JE. Up-regulation of connexin45 in heart failure. *J Cardiovasc Electrophysiol*. 2003;14:1205–12.
109. Severs NJ, Coppen SR, Dupont E, Yeh H-I, Ko Y-S, Matsushita T. Gap junction alterations in human cardiac disease. *Cardiovasc Res*. 2004;62:368–77.
110. Ren Y, Zhang CT, Wu J, Ruan YF, Pu J, He L, et al. The effects of antiarrhythmic peptide AAP10 on ventricular arrhythmias in rabbits with healed myocardial infarction. *Zhonghua Xin Xue Guan Bing Za Zhi*. 2006;34:825–8.
111. Grover R, Dhein S. Spatial structure determination of antiarrhythmic peptide using nuclear magnetic resonance spectroscopy. *Peptides*. 1998;19:1725–9.
112. Hennan JK, Swillo RE, Morgan GA, Keith Jr JC, Schaub RG, Smith RP, et al. Rotigaptide (ZP123) prevents spontaneous ventricular arrhythmias and reduces infarct size during myocardial ischemia/reperfusion injury in open-chest dogs. *J Pharmacol Exp Ther*. 2006;317:236–43.
113. Weng S, Lauven M, Schaefer T, Polontchouk L, Grover R, Dhein S. Pharmacological modulation of gap Junction coupling by an antiarrhythmic peptide via protein kinase C activation. *FASEB J*. 2002;16:1114–6.
114. Kaprielian RR, Gunning M, Dupont E, Sheppard MN, Rothery SM, Underwood R, et al. Down-regulation of immunodetectable connexin43 and decreased gap junction size in the pathogenesis of chronic hibernation in the human left ventricle. *Circulation*. 1998;97:651–60.
115. Dhein S, Tudyka T. The therapeutic potential of antiarrhythmic peptides. Cellular coupling as a new antiarrhythmic target. *Drugs*. 1995;49:851–5.

Chapter 29

Possible Mechanisms of the Acute Ischemia-Induced Ventricular Arrhythmias: The Involvement of Gap Junctions

Ágnes Végh and Rita Papp

29.1 Introduction

The problem of sudden cardiac death (SCD) from ventricular fibrillation (VF) during coronary artery occlusion or reperfusion, outside the hospital setting, is still the biggest challenge that clinical cardiology faces. More than half of SCDs can be attributed to sudden VF. As drug therapy has proved to be largely ineffective except in the hospital setting, understanding the underlying mechanisms that lead to these life-threatening ventricular arrhythmias is crucial for developing novel therapeutic strategies.

Several experimental models – from cells to *in situ* animal models – are available for exploring the dynamic changes during the acute phase of myocardial ischemia that are responsible for the occurrence of the accompanying severe, often fatal, ventricular arrhythmias. The dynamic nature of ischemia development can be discussed by considering its several aspects. With respect to associated arrhythmias, four phases of the ischemic events are distinguished within the first hour. The sequence of these changes is time-dependent. Studies in large animals showed that after commencement of occlusion, the rapidly developing and progressing ischemic changes give rise to an early phase of arrhythmias (phase 1A) which, in anesthetized dogs, is apparent between 3 and 8 min of start of ischemia [1]. This is followed by a restoration of normal rhythm (compensatory phase) during which the ionic changes become balanced, and electrophysiological parameters seem to return to normal [2]. This phase might be of particular importance as changes during this short (5 min) period directly contribute to the next event (phase 1B) of arrhythmias. Phase 1B lasts from 15 to 30 min of ischemia and is more severe than phase 1A arrhythmias, often terminating in sudden VF [3, 4]. After this period, if ischemia is maintained, a “healing over” process starts during which the dying cells are sharply demarcated from the viable ones by interrupting the electrical and metabolic

Á. Végh (✉) and R. Papp

Department of Pharmacology and Pharmacotherapy, University of Szeged, 6720 Szeged, Dóm tér 12, Szeged, Hungary
e-mail: vegh@phcol.szote.u-szeged.hu

cell-to-cell communication. Complete uncoupling of cells limits arrhythmia generation [4–6], and indeed, the arrhythmias remain suppressed during the next few hours of ischemia.

An account of the current understanding of events that underlie acute ischemia-induced ventricular arrhythmias, with particular emphasis on the role of GJs in the generation of these arrhythmias, is presented below. It also includes evidence derived from our studies on dogs that the modulation of GJ function, either by preconditioning or by pharmacological means, modifies the severity of arrhythmias during the acute phase of myocardial ischemia.

29.2 Early Metabolic, Ionic, and Electrophysiological Alterations Occurring After Coronary Artery Occlusion and Their Role in the Genesis of Phase 1A Arrhythmias

As the myocardium has only limited energy stored as glycogen and high-energy phosphate, normal metabolism depends on the continuous fatty acid and glucose supply provided by coronary circulation [7]. Abrupt occlusion of coronary artery causes reduction in blood flow and deprivation in oxygen flow leading to an inhibition of oxidative phosphorylation within the affected myocardial region. Metabolism switches from aerobic to anaerobic to produce high-energy phosphates [8]. Despite this, high-energy phosphate concentrations in cytosol fall, as ATP gained by anaerobic glycolysis is not sufficient to keep up with the ATP utilizing processes. As a result of anaerobic metabolism, a rapid fall in intracellular pH occurs, as lactate accumulates in cytosol [9] further inhibiting the rate-limiting enzymes of glycolysis. These rapid metabolic changes, apparent within seconds or minutes after onset of ischemia, directly affect the function of ion channels and exchangers leading to dramatic alterations in impulse generation and conduction (Fig. 29.1). Movement of protons from cytosol to extracellular compartment, by Na^+/H^+ exchanger, causes a decrease in extracellular pH and increase in intracellular Na^+ level ($[\text{Na}^+]_i$) [9, 10]. The fall in ATP/ADP ratio triggers the opening of sarcolemmal K_{ATP} channels leading to enhanced K^+ efflux into extracellular space [11]. This rise in extracellular K^+ together with the inactivation of Na^+ channels results in a decrease in resting membrane potential, and reduced amplitude, duration and maximum upstroke velocity (dV/dt_{max}) of AP [12, 13]. The changes in resting membrane potential and loss of K^+ are manifested in TQ depression and ST-segment alterations in ECG [14] considered as clinical markers of acute ischemia [15]. As the depolarizing current decreases, it will not be sufficient to depolarize the neighboring cells; consequently, an inhomogeneous slowing of conduction or even block may develop. These conditions favor reentry, which is thought to be the main mechanism underlying phase 1A arrhythmias [13, 16].

Ventricular arrhythmias occurring during the early phase of ischemia are many and varied, e.g., single ectopic beats, couplets, salvos, tachycardia, and fibrillation.

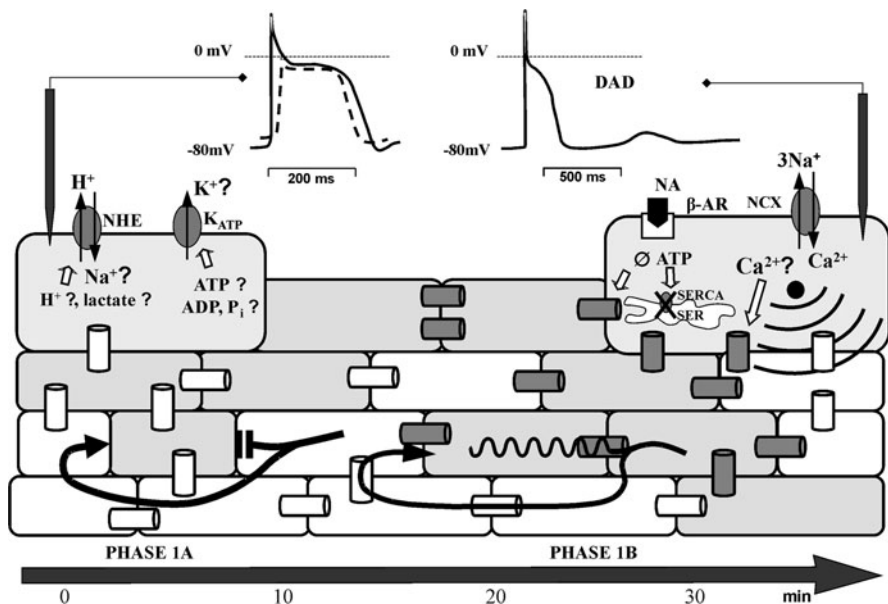


Fig. 29.1 Possible mechanisms involved in phase 1A and phase 1B arrhythmias resulting from acute myocardial ischemia. The primary mechanism of arrhythmias occurring during phase 1A is the reentry which is associated with the ischemia-induced rapid metabolic and ionic alterations that evoke slowing of impulse conduction and eventually block impulse propagation. With the progression of ischemia, the further loss of ATP, the increased intracellular calcium levels, and the acidosis uncouple gap junctions (GJ), which also cause a delay in impulse propagation and lead to the formation of reentry circuits. The calcium overload favors the appearance of delayed afterdepolarizations and triggered activity

These arrhythmias are most likely generated in the border zone where interaction of various factors implicated in arrhythmogenesis is apparent [17]. The boundary between ischemic and nonischemic tissue, with steep gradients of metabolic, ionic, and neurologic changes, results in heterogeneities of tissue activation, refractoriness [18], and impulse conduction. Within the ventricular myocardium such a boundary exists not only laterally but also vertically, as the epicardium and the endocardium have different susceptibilities for ischemia [6, 19]. Although reentry is considered to be the main mechanism underlying phase 1A arrhythmias, mapping studies reveal that 24% of ectopic beats occurring during this phase originate from a nonreentrant mechanism [20].

By around 10 min of ischemia, the number and severity of arrhythmias decrease despite maintained occlusion. Although the mechanism of this relatively arrhythmia-free interval is not fully understood, it is suggested that the electrophysiological changes occurring immediately after occlusion return to almost normal during this period [2, 21]. For example, the initial increase in extracellular [K⁺] stops and remains constant [22], and the dispersion of refractoriness decreases and conduction improves [1]. The local release of catecholamines from nerve endings during

this phase [23] and the subsequent activation of Na^+/K^+ pump might be responsible for these electrophysiological improvements [24]. It is also likely that endogenous myocardial protective substances, generated and released soon after the onset of coronary occlusion [25, 26], may contribute to attenuation of the early consequences of acute ischemia. Some of these substances, such as bradykinin [27] and nitric oxide [28], markedly reduce arrhythmias resulting from coronary occlusion. Nevertheless, if ischemia is maintained, these compensatory attempts are attenuated or even exhausted, and in the absence of washout, accumulation of harmful metabolites, ions, catecholamines etc. would lead to phase 1B arrhythmias.

29.3 Mechanisms of Generation of Phase 1B Arrhythmias: Role of Gap Junctions

The processes underlying generation of phase 1B arrhythmias are less well understood in contrast to the phase 1A arrhythmias. In the last two decades several in vitro and in vivo studies revealed that uncoupling of GJs plays a pivotal role in the occurrence of phase 1B arrhythmias [3, 4, 29, 30]. The findings of these studies substantiate the early notion of Theodor Engelmann that “Die Zellen leben zusammen, aber sterben einzeln” (cells live together but die alone [31]). And, indeed, we now know that adjacent myocardial cells are tightly connected through GJs which provide fast electrical and metabolic communication between them, enabling homogeneous impulse conduction and synchronous working of heart, despite its electrical and structural heterogeneity [32, 33]. Discontinuation of this cell-to-cell coupling, for example, during myocardial ischemia, not only causes disturbances in impulse propagation and rhythm but also creates a milieu in which the severely injured cells seal themselves off from their still viable neighbors [34].

Extensive studies on the role of GJs in normal impulse propagation have established that conduction in the uniformly anisotropic heart is largely dependent upon the resistance of GJs which is lower in longitudinal than transversal direction (see Chap. 28; [35–37]). Such an arrangement gives longitudinal conduction preference over transversal conduction [35, 38, 39], thus providing an important safety factor for normal impulse propagation [40]. It has been proposed recently that in the presence of normal intercellular coupling the architectural and electrophysiological heterogeneity of myocardium serves as an intrinsic protective mechanism against arrhythmia generation [41]. However, under ischemic conditions, this myocardial heterogeneity would play an important role in arrhythmogenesis. With the progression of ischemia, uncoupling of GJs increases, resulting in nonuniform changes in tissue resistance (Fig. 29.1; [29, 42]) and inhomogeneous impulse conduction [4, 43]. This asynchronous conduction may initiate and maintain reentry during phase 1B [44]. On the other hand, the increased resistance resulting from interruption of cell-to-cell connections decreases the injury current, although at moderate levels of uncoupling this current would still be sufficient to induce DAD and trigger focal activity [45].

Although there appears to be no doubt that GJs are involved in the functions of both normal and diseased heart, their exact role in arrhythmia generation under *in situ* conditions is difficult to assess. One reason for this is that besides GJs several other factors may also influence excitability and conduction, the role of which in the generation of phase 1B arrhythmias is difficult to separate from that of GJs. One of these factors that inevitably influences arrhythmogenesis is the local release of catecholamines (noradrenaline in particular) from the ischemic nerve endings [46]. The time course of catecholamine accumulation and GJ uncoupling is similar, both starting at around 12 min of ischemia [42, 46]. This local accumulation of catecholamines in ischemic myocardium [2, 46–48] as well as acidification [49, 50] and intracellular calcium overload [51], which have also established by this time, either by themselves or via the closure of GJs [52], contribute to generation of phase 1B arrhythmias (Fig. 29.1).

The other problem with assessment of the role of GJs in arrhythmogenesis is rather methodological. Most of the currently used methods provide only indirect evidence on the coupling status of GJs. For example, conduction velocity, which depends on GJ coupling, is measured with activation-mapping techniques both in *in vivo* and *in vitro* settings [53, 54]. Measurement of GJ permeability is performed using small molecular weight dyes, which penetrate into the tissue only through GJs [55]. Determination of connexin (Cx) phosphorylation [56] is used to assess GJ coupling. Dephosphorylation of Cx43, the most abundant GJ forming protein in left ventricle [57], is suggested to indicate closure of GJs during ischemia [58, 59]. These methods, however, allow evaluation of coupling status of GJs only at a certain time point.

Measurement of tissue impedance represents another methodological approach in the assessment of GJ function. The seminal work of Kléber and colleagues [29] provided the first convincing evidence for the relationship between increased intracellular resistance and uncoupling of GJs by showing that tissue resistivity increases in rabbit isolated papillary muscle during myocardial ischemia in a biphasic manner. The first rise that occurs immediately after the onset of ischemia is associated with cell swelling and edema resulting from collapse of the vasculature. The second, steeper rise of resistivity starts around 15 min of ischemia and is thought to relate to the uncoupling of GJs [29]. Although tissue impedance represents another indirect measure of GJ function, continuous recording of this parameter *in vivo* allows one to relate changes in GJ coupling to arrhythmia. Evidence for such a relationship resulted from two studies in anesthetized pigs. First study showed that appearance of phase 1B arrhythmias was preceded by a steep rise in resistivity [3], and second one [30] reported that ischemic preconditioning delayed uncoupling of GJs and delayed occurrence of phase 1B arrhythmias.

Our own studies on dogs subjected to 60-min occlusion of the anterior descending branch of left coronary artery (LAD), gave somewhat different results [60]. Tissue impedance changes assessed in parallel with arrhythmia distribution (Fig. 29.2a) showed an immediate rise in tissue resistivity and a decline in phase angle (reflects closure of GJs more accurately than resistivity [61]). This phase lasted for about 5 min. A second, steeper impedance change then started around

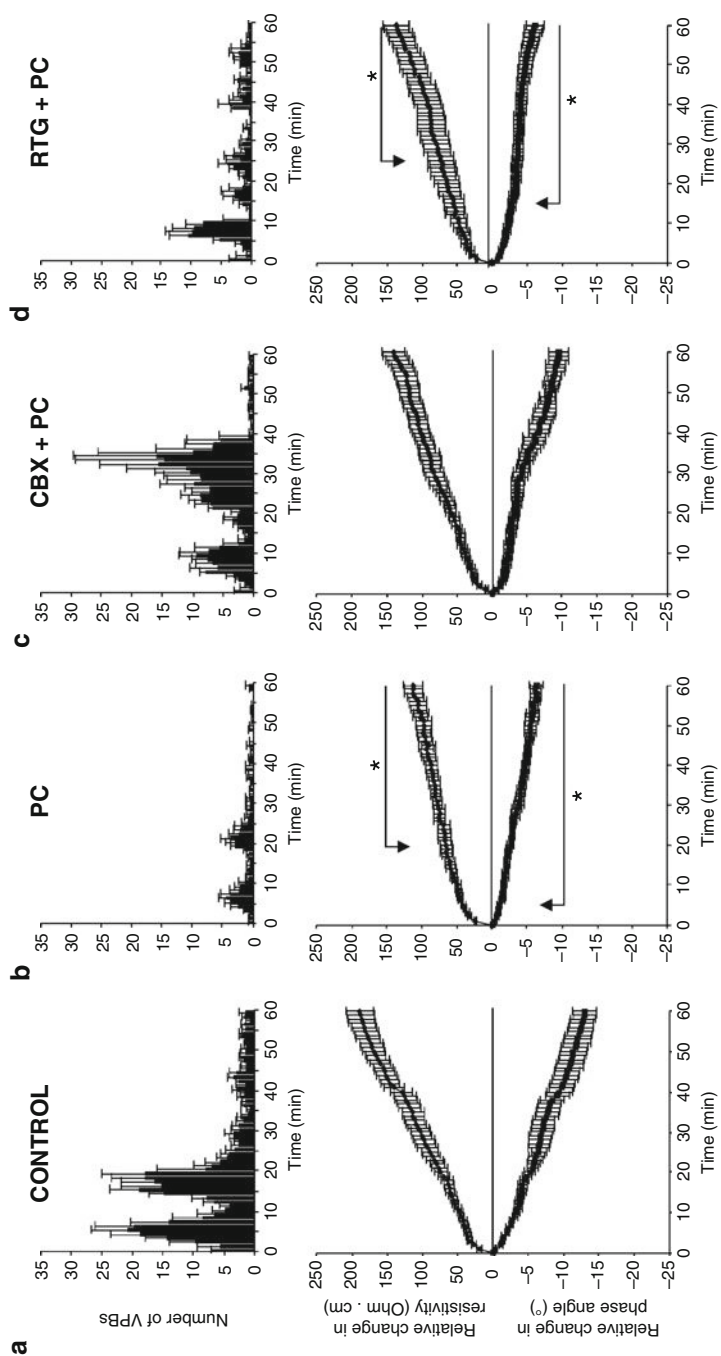


Fig. 29.2 Relationship between arrhythmia distribution and changes in tissue impedance (resistivity and phase angle) during a 60-min coronary artery occlusion in control dogs (**a**), in preconditioned dogs (**b**), and in dogs preconditioned in the presence of the intracoronary infusion of carbenoxolone (CBX; 50 μ M; **c**) and rotigapide (RTG; 2 μ g kg^{-1} min $^{-1}$; **d**). The infusions were commenced 15 min prior to and maintained during the 5-min preconditioning occlusion. Values are means \pm s.e.m. * $P < 0.05$ cp. control group

15 min of ischemia, and although not as marked as in pigs [3] or in isolated heart preparations [29], preceded the occurrence of phase 1B arrhythmias. The distribution of arrhythmias during such a period of occlusion in dogs is also different from that in pigs. In pigs, a third of arrhythmia peak occurs around 40 min of ischemia [3], whereas in dogs after the cessation of phase 1B, arrhythmias almost completely disappear, only a few ectopic beats appearing during the rest of 1-h occlusion. However, the main difference between these two species lies in their response to ischemic preconditioning. As mentioned above, whereas in pigs preconditioning delays both GJ uncoupling and occurrence of phase 1B arrhythmias [30], in dogs it results in an absolute reduction in the number and severity of arrhythmias, i.e., there is no shift in their distribution to a later period of occlusion [62]. Furthermore, in these preconditioned dogs impedance changes are less marked compared to the controls over the entire occlusion period (Fig. 29.2b). This indicates that in dogs preconditioning not only delays but indeed reduces the closure of GJs. This finding is also supported by the results of in vitro measurements. In preconditioned dogs, both GJ permeability and Cx43 phosphorylation were substantially preserved even at the end of the 60-min occlusion period (Fig. 29.3).

These species differences can be associated with the extent of functionally effective preexisting collaterals which influence the time of appearance and severity of arrhythmias following sudden coronary artery occlusion [63]. Meesmann and colleagues [64] showed in 1970s that in dogs the rate of mortality within 1 h after

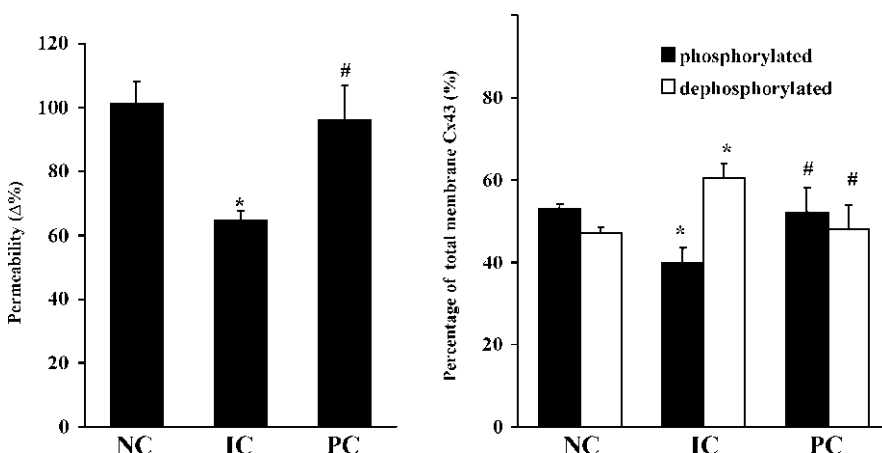


Fig. 29.3 Changes in gap junction permeability and in connexin 43 (Cx43) phosphorylation, determined at the end of a 60-min coronary artery occlusion in the nonischemic control (NC), in the ischemic control (IC) and in the preconditioned (PC) heart samples. Following a 60-min occlusion, GJ permeability was significantly reduced within the ischemic area, but it was largely preserved when the dogs had been preconditioned. In tissue samples taken from the nonischemic area the phosphorylated and the dephosphorylated forms of Cx43 were almost equally distributed. In the ischemic control hearts, the phospho/dephospho ratio shifted toward dephosphorylation. This marked dephosphorylation was prevented by PC. Values are means \pm s.e.m. * $P < 0.05$ cp. nonischemic control, # $P < 0.05$ cp. ischaemic control

the occlusion of a main coronary artery may vary between 0 and 100% depending upon the preexisting collateralization. They also pointed out that although the preexisting collaterals are not able to prevent myocardial ischemia in dogs, collateral flow attenuates rapid development of inhomogeneity and electrical instability of heart [64]. In contrast, in pigs which have a poor collateral system, more than 50% of the animals develop VF during phase 1A and about one-third during phase 1B [65]. Interestingly, in sheep, total absence of collaterals [65] promotes development of complete cessation of excitability and leads to a rapid demarcation of excitable from nonexcitable tissue. Therefore, the danger of fatal arrhythmias following coronary artery occlusion is minimal in this species [65].

The apparent discrepancy that both absence (sheep) and presence (dogs) of adequate collateral perfusion may protect against arrhythmias could be explained by the rate of development of inhomogeneity within the myocardium. It is likely that the inhomogeneous flow distribution and thus the rate and the extent of development of electrical inhomogeneity between ischemic and nonischemic areas are important for arrhythmia generation and not the absolute values of perfusion. Although cells in the border area are metabolically separated to ischemic or normal [66], the boundary between the ischemic and nonischemic area is irregular, with varying depths of interdigititation dependent on collateralization. As an important ionic and electrical cross-talk takes place between these interdigitating areas, the preexisting collateralization influences arrhythmogenesis through the extent of this border. Consequently, in a species with no collaterals (sheep), the sharply demarcated boundary rapidly develops, inhibiting the cross-talk between the excitable viable and the nonexcitable ischemic cells. On the other hand, a well-developed preexisting collateral system, which allows broader interdigititation into the ischemic area, is able to provide a better blood supply and ultimately a smaller ischemic area. Consequently, the rate of development of electrical inhomogeneity in dogs, depending partially on GJ uncoupling [53, 67], is more gradual. This may partly explain why in dogs many ventricular premature beats (VPB), couplets, and salvos occur during phase 1B with a variable incidence of VF, but in pigs with little collateral supply [65], VF may suddenly appear without previous ectopics. This “in-between situation” is highly dangerous because the interdigitating surface is large enough to create electrical inhomogeneities but is not sufficient to provide adequate blood supply to reduce infarct size.

Although the severity of arrhythmias occurring during ischemia seems to be influenced by the existence of collaterals, the cardioprotective (antiarrhythmic) effect of preconditioning is independent of preexisting collateral system [68, 69]. Although we do not know the mechanism(s) by which preconditioning attenuates GJ uncoupling, it is likely that this can somehow be connected to preserved Cx43 phosphorylation [60]. We presume that preconditioning activates a cascade of events which eventually inhibit or attenuate ischemia-induced dephosphorylation of connexins, thereby providing a better cell-to-cell coupling. This hypothesis is supported by the observations that (1) during the early period of ischemia (preconditioning occlusion), endogenous substances are released from the myocardium, [25] some of which influence arrhythmogenesis [26], and (2) these endogenous

substances, through the activation of protein kinases, cGMP, and cAMP, may regulate connexin phosphorylation and thus modulate GJ function [52, 70]. Our recent study shows that nitric oxide (NO), which plays an important trigger and mediator preconditioning-induced antiarrhythmic protection [71], may modulate GJs [72]. This is evident from the observation that NO donor sodium nitroprusside, administered by intracoronary infusion prior to and during a 60-min occlusion, attenuates ischemia-induced impedance changes and preserves GJ permeability and phosphorylated form of Cx43, in parallel with suppression of arrhythmia severity. This effect of NO may be mediated through regulation of autonomic nervous system [73], as NO inhibits noradrenaline release [74] and facilitates release of acetylcholine from nerve endings [75]. More recently, two studies reported that stimulation of cardiac sympathetic nerve reduced [76], whereas the vagal nerve stimulation preserved [56], the phosphorylated form of Cx43.

The role of endogenous substances released during preconditioning in arrhythmogenesis, through regulation of Cx43 phosphorylation and subsequent modification of GJ function, is also supported by studies in which carbenoxolone (CBX), a relatively selective GJ uncoupler [77], was infused into a small branch of LAD both prior to and during preconditioning occlusion. CBX markedly attenuated the antiarrhythmic effect of preconditioning and impedance changes during prolonged ischemia. We suggested that closing of GJs during preconditioning with CBX may inhibit transfer of the protective substances released during preconditioning and serve as triggers and/or mediators in antiarrhythmic protection [60]. It is interesting, but perhaps not surprising, that opening of GJs with rotigaptide (RTG) during preconditioning did not influence the antiarrhythmic protection associated with preconditioning (Fig. 29.2d).

29.4 Pharmacological Modification of Gap Junction Function and Arrhythmias

The fact that preconditioning markedly attenuates the impedance changes just preceding the occurrence of phase 1B arrhythmias raises the possibility that this period of ischemia might be of particular importance in the generation of these arrhythmias. This “critical” ischemia period coincides with the end of the intermediate interval during which the previous metabolic and electrophysiological alterations transiently normalize [2]. But, as ischemia progresses, accumulation of catecholamines, increased $[Ca^{2+}]_i$, and further decrease of ATP and pH create a milieu for enhanced closure of GJs [19, 43, 78]. The resultant electrophysiological alterations are then manifested in a second arrhythmia burst. There is increasing evidence that ventricular arrhythmias, particularly VF, occur at a “moderate degree of gap junctional uncoupling” [4, 5] which may happen during this critical ischemia phase – when the rate of uncoupling speeds up. A more advanced degree of uncoupling suppresses arrhythmogenesis, because the substrate for arrhythmias diminishes if the cells have already uncoupled [43].

These facts prompted us to examine (1) whether the pharmacological modification of GJ uncoupling during this “critical” period of ischemia would modify phase 1B arrhythmias and (2) whether opening or closing of GJs is necessary for arrhythmia suppression. The GJ uncoupler CBX [77] and the GJ opener RTG [79] were used to test these possibilities. The intracoronary infusion of CBX, 20 min prior to a 60-min coronary artery occlusion resulted in a preconditioning-like protection as the number of VPBs was markedly reduced and impedance changes were substantially attenuated during the occlusion (Fig. 29.4b). In contrast, the GJ opener RTG, given also by intracoronary infusion over 20 min, did not influence the severity of arrhythmias during occlusion 20 min later. Further, ischemia-induced impedance changes in the RTG-treated dogs were as marked as in the controls (Fig. 29.4c).

Mechanism of similarity between the antiarrhythmic effects of CBX and preconditioning is not known. We suggest that some GJs are closed following CBX administration, as evident from the moderate impedance changes [60] acting as a trigger for inducing protection, perhaps through modification of Cx43. This protein, besides having pore-forming and gating properties, may indeed play a role in signal transduction as it colocalizes with MAP kinases or translocates to mitochondria, nucleus etc. [80]. Involvement of Cx43 in CBX-induced protection is also supported by the fact that CBX, similar to preconditioning, preserved the phosphorylated form of Cx43 even after a 60-min occlusion period [60].

Failure of RTG to protect against arrhythmias could be explained by presuming that keeping GJs opened prior to occlusion does not induce any mechanism which could prevent closure of GJs during subsequent ischemia. It may be pointed out that the antiarrhythmic effect of endogenous and synthetic antiarrhythmic peptides is controversial (see Chap. 28). A decrease in inhomogeneity of refractoriness and prevention of conduction delay is suggested by *in vitro* studies on these peptides [81–83]. RTG increases GJ conductance, reverses conduction block, and reduces inducibility of reentrant, but not the focal arrhythmias in dogs [84, 85]. In contrast, these peptides failed to reduce the ischemia and reperfusion-induced ventricular arrhythmias in rabbit hearts [81, 86]. In our own studies RTG was only able to effectively reduce the ischemia-induced ventricular arrhythmias when the intracoronary infusion was started 15 min prior to and maintained throughout the occlusion period (Fig. 29.5c). Under these conditions RTG significantly reduced phase 1B arrhythmias and attenuated the steep impedance changes seen in controls around 15 min of the occlusion (Fig. 29.5e).

It is interesting that CBX infused, 15 min prior to and over the entire occlusion period, showed antiarrhythmic effects (Fig. 29.5b). As both ischemia and CBX uncouple GJs, one expects that closing of GJs during ischemia with CBX would enhance arrhythmias. Indeed, the decline in phase angle, immediately after occlusion, was more marked with CBX infusion than in the controls (Fig. 29.5d), indicating an early uncoupling of GJs. However, the impedance changes became slower thereafter and remained constant until 30 min of occlusion. Moreover, the increase in resistivity and decline in phase angle during the “critical” phase of ischemia were absent. The distribution of ventricular arrhythmias was also unusual with CBX infusion and the total number of VPBs was significantly reduced

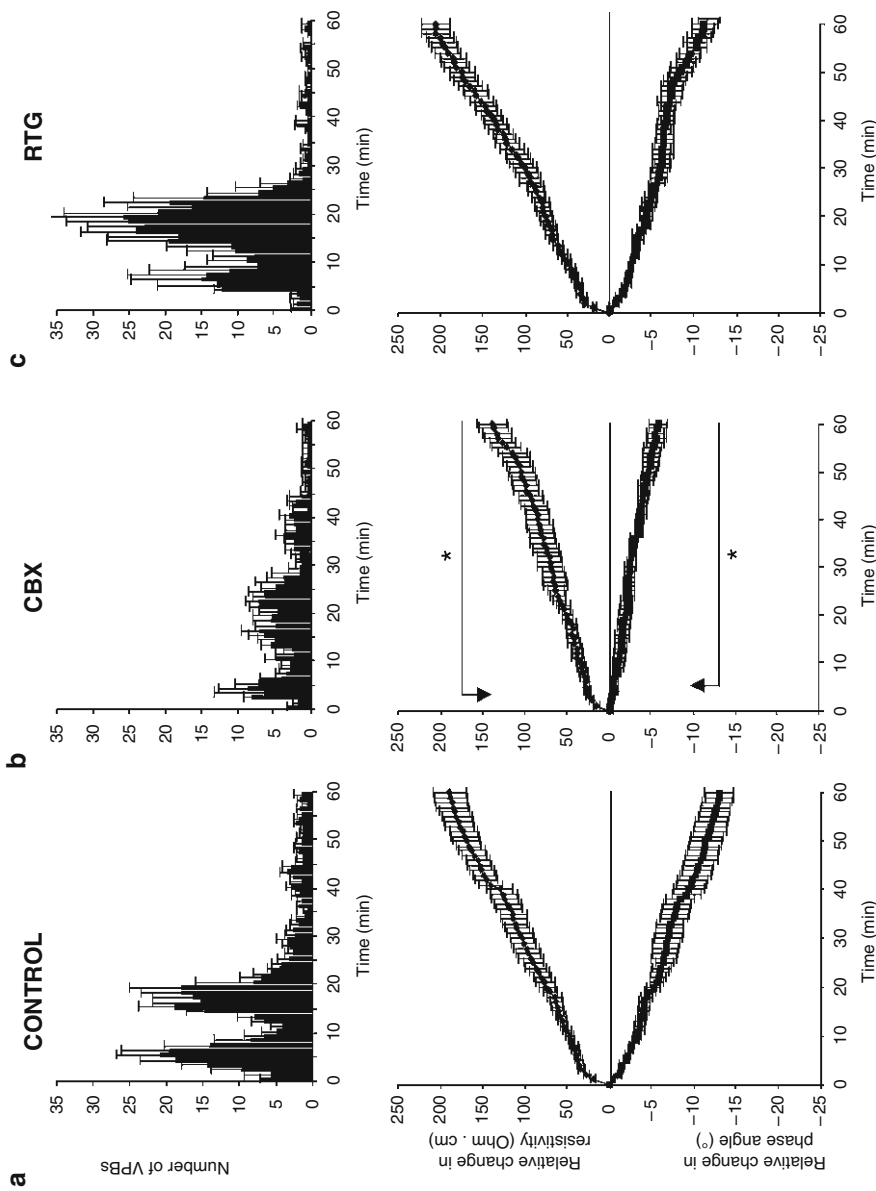


Fig. 29.4 Relationship between arrhythmia distribution and changes in tissue impedance (resistivity and phase angle) during a 60-min occlusion of the LAD in control dogs (a), and in dogs infused for 20 min with CBX (b) and RTG (c), 20 min prior to the occlusion. CBX resulted in a PC-like protection against arrhythmias and impedance changes (b), whereas RTG was without effect on these ischemia-induced changes. Values are means \pm s.e.m. * $P < 0.05$ cp. control group

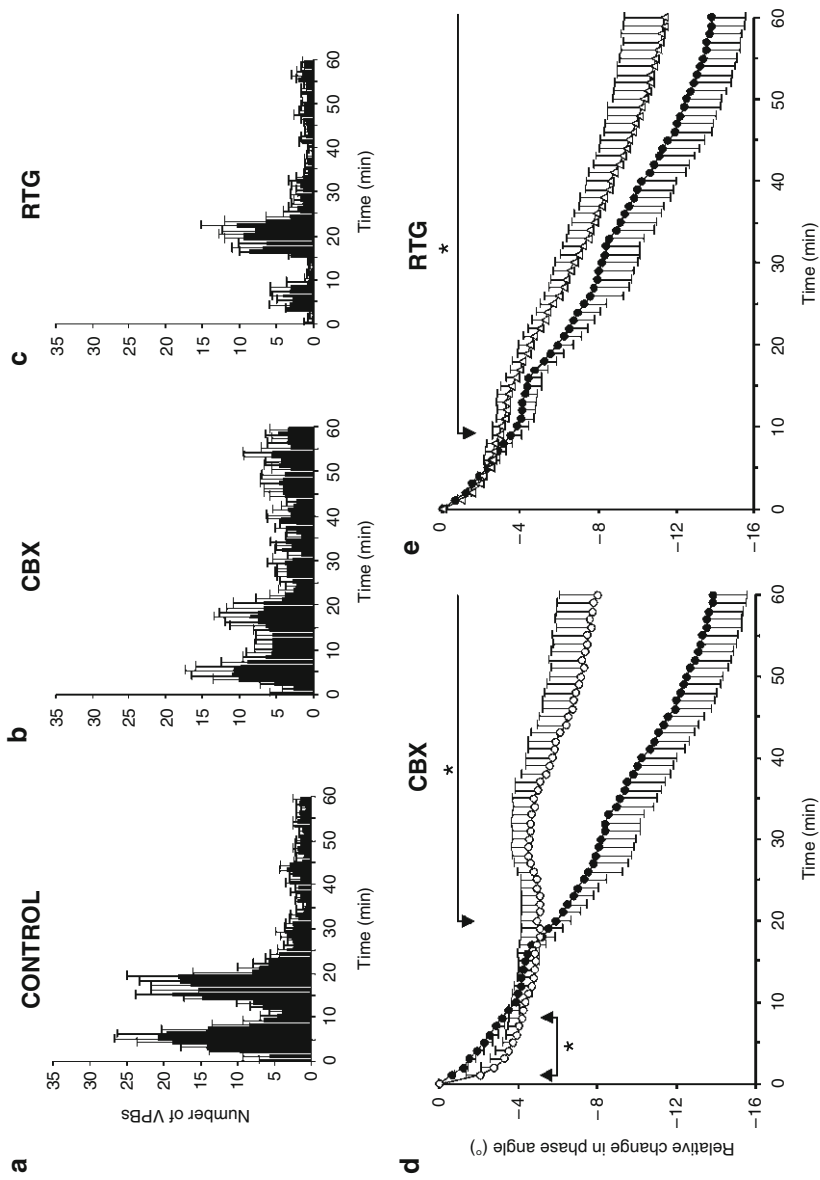


Fig. 29.5 The effect of CBX (**B**) and RTG (**C**) in comparison with saline-treated controls (**A**) on changes in phase angle and on the distribution of ventricular premature beats (VPBs) during a 60-min occlusion of the LAD. CBX and RTG were administered by intracoronary infusion, commenced 15 min prior to and maintained throughout the entire occlusion period. Under these conditions both drugs proved to be antiarrhythmic, and they attenuated the marked impedance changes that were apparent in the controls (filled diamonds) just prior to the occurrence of phase 1B arrhythmias. This figure also shows that CBX (open circles) shifted uncoupling to an earlier ischemia period, whereas RTG (open triangles) maintained the coupling of GJs during this critical ischemia phase. Values are means \pm s.e.m. * $P < 0.05$ cp. control group

(226 ± 43 vs. 452 ± 72). The two characteristic arrhythmia phases disappeared and a continuous ectopic activity was observed over the entire occlusion period. Despite the ongoing debate whether GJ uncoupling occurs during early course of ischemia [87], evidence suggests that the early impedance changes are not attributable to closure of GJs [29]. Nevertheless, possible existence of cells, severely injured and uncoupled during early stage of ischemia, within the ischemic area cannot be ruled out [32, 88, 89]. However, this possibility is difficult to prove because a substantial portion of GJs needs to be closed to detect changes in tissue impedance [90]. Nevertheless, the marked impedance changes around 15 min of ischemia are not seen, and phase 1B arrhythmias are markedly suppressed by CBX. This finding could perhaps be associated with the phenomenon termed “paradoxical restoration of conduction” [91]. There is convincing evidence to suggest that, in the border zone, the viable cells are electrically depressed through electrical interactions from their neighboring ischemic cells resulting in slowing of conduction [19, 92]. However, with the progression of uncoupling, this electrotonic interaction decreases, resulting in an improvement in conduction and, consequently, a reduction in arrhythmia severity [19]. In contrast, RTG, which is supposed to keep GJs open, attenuates impedance changes during the “critical” phase of ischemia, and consequently reduces phase 1B arrhythmias, this protection being not as marked as with preconditioning or CBX.

The hypothesis that both an uncoupler and an opener may result in an antiarrhythmic effect raises the possibility that “local, specific modulation of GJ uncoupling, either by reducing or by increasing it, may suppress severe, often lethal arrhythmias during phase 1B of myocardial ischemia” [19]. This is based on the assumption that a moderate degree of uncoupling is associated with arrhythmias, whereas a more advanced uncoupling is antiarrhythmic [4, 19]. Therefore, theoretically an uncoupler, selective to the ischemic tissue, would preferentially uncouple the already poorly coupled cells causing a further reduction in conduction velocity. On the other hand, keeping GJs coupled during ischemia would result in antiarrhythmic effect by maintaining conduction velocity [19].

29.5 Conclusions

Our studies, using two pharmacological modulators of gap junctions, provide good *in vivo* evidence that, paradoxically, both increasing and decreasing gap junctional uncoupling during the acute phase of ischemia may result in antiarrhythmic protection. We propose that the main principle is the rate and/or the degree of uncoupling during that “critical” period of ischemia when other factors, implicated in arrhythmogenesis, are also present. Thus, shifting GJ uncoupling to an earlier or to a later ischemia phase using uncouplers or openers may attenuate the interaction of arrhythmogenic factors. A better understanding of the role of GJs in arrhythmogenesis and of the consequences of their pharmacological modulation, would allow of the development of novel therapeutic strategies in the treatment of

arrhythmias. The currently available antiarrhythmic drugs act primarily on ion channels and, through modification of the action potential, influence impulse conduction and ultimately arrhythmia severity, but a potential danger lies in their proarrhythmogenic properties, which might limit their use in patients with ischemic syndromes. This necessitates the finding of new possibilities for the development of novel compounds targeting different arrhythmogenic mechanisms.

Acknowledgments This work was supported by the Hungarian Scientific Research Foundation (OTKA; Project number K75281 and NI61092) and by BIO-37-49. We are grateful to Dr. Zoltán Gingl (Department of Experimental Physics, University of Szeged) for constructing the impedance-measuring system and recording software. We thank Dr. Antal Nógrádi and his laboratory (Clinics of Ophthalmology, University of Szeged) for their help in the histological examinations and Dr. Ernő Zádor (Department of Biochemistry, University of Szeged) for his expert advice on the protein work.

References

1. Kaplinsky E, Ogawa S, Balke CW, Dreifus LS. Two periods of early ventricular arrhythmias in the canine acute infarction model. *Circulation*. 1979;60:397–403.
2. Penny WJ. The deleterious effects of myocardial catecholamines on cellular electrophysiology and arrhythmias during ischemia and reperfusion. *Eur Heart J*. 1984;5:960–73.
3. Smith WT, Fleet WF, Johnson TA, Engle CL, Cascio WE. The 1b phase of ventricular arrhythmias in ischemic *in situ* porcine heart is related to changes in cell-to-cell electrical coupling. *Circulation*. 1995;92:3051–60.
4. DeGroot JR, Wihns-Schopman FJG, Ophtof T, Remme CA, Coronel R. Late ventricular arrhythmias during acute regional ischemia in the isolated blood perfused pig heart. Role of electrical cellular coupling. *Cardiovasc Res*. 2001;50:362–72.
5. Pollard AE, Cascio WE, Fast VG, Knisley SB. Modulation of triggered activity by uncoupling in the ischemic border. A model study with phase 1b-like conditions. *Cardiovasc Res*. 2002;56:381–92.
6. Jie X, Rodriguez B, De Groot JR, Coronel R, Trayanova N. Reentry in survived subepicardium coupled to depolarized and inexcitable midmyocardium: insights into arrhythmogenesis in ischemia phase 1B. *Heart Rhythm*. 2008;5:1036–44.
7. Sun KT, Yeatman LA, Buxton DB, Chen K, Johnson JA, Huang SC, et al. Simultaneous measurement of myocardial oxygen consumption and blood flow using [^{11}C] acetate. *J Nucl Med*. 1998;39:272–80.
8. Jennings RB, Reimer KA, Steenbergen Jr C. Myocardial ischemia revisited. The osmolar load, membrane damage, and reperfusion. (Editorial). *J Mol Cell Cardiol*. 1986;18:769–80.
9. Fleet WF, Johnson TA, Graebner CA, Gettes JS. Effect of serial brief ischemic episodes on extracellular K^+ , pH, and activation in the pig. *Circulation*. 1985;72:922–32.
10. Fiolet JWT, Baartscheer A, Schumacher CA, Coronel R, terVelle HF. The change of the free energy of ATP hydrolysis during global ischemia and anoxia in the rat heart. Its possible role in the regulation of transsarcolemmal sodium and potassium gradients. *J Mol Cell Cardiol*. 1984;16:1023–36.
11. Noma A. ATP-regulated K^+ channels in cardiac muscle. *Nature*. 1983;305:147–8.
12. Kléber AG. Resting membrane potential, extracellular potassium activity, and intracellular sodium activity during acute global ischemia in isolated perfused guinea pig hearts. *Circ Res*. 1983;52:442–50.
13. Janse MJ, Kléber AG, Capucci A, Coronel R, Wilms-Schopman F. Electrophysiological basis for arrhythmias caused by acute ischemia. *J Mol Cell Cardiol*. 1986;18:339–55.

14. Kléber AG, Janse MJ, van Capelle FJ, Durrer D. Mechanism and time course of S-T and T-Q segment changes during acute regional myocardial ischemia in the pig heart determined by extracellular and intracellular recordings. *Circ Res.* 1978;42:603–13.
15. Kléber AG. ST-segment elevation in the electrocardiogram: a sign of myocardial ischemia. *Cardiovasc Res.* 2000;45:111–8.
16. Janse MJ, Kléber AG. Electrophysiological changes and ventricular arrhythmias in the early phase of regional myocardial ischemia. *Circ Res.* 1981;49:1069–81.
17. Cascio WE. Myocardial ischemia: what factors determine arrhythmogenesis? *J Cardiovasc Electrophysiol.* 2001;12:726–9.
18. Ophof T, Coronel R, Vermeulen JT, Verberne HJ, vanCapelle FJL, Janse MJ. Dispersion of refractoriness in normal and ischemic canine ventricle: effects of sympathetic stimulation. *Cardiovasc Res.* 1993;27:1954–60.
19. deGroot JR, Coronel R. Acute ischemia-induced gap junctional uncoupling and arrhythmogenesis. *Cardiovasc Res.* 2004;62:323–34.
20. Pogwizd SM, Corr PB. Reentrant and nonreentrant mechanisms contribute to arrhythmogenesis during early myocardial ischemia: Results using three dimensional mapping. *Circ Res.* 1987;61:352–71.
21. Cascio WE, Yan GX, Kléber AG. Passive electrical properties, mechanical activity, and extracellular potassium in arterially perfused and ischemic rabbit ventricular muscle. Effects of calcium entry blockade or hypocalcemia. *Circ Res.* 1990;66:1461–73.
22. Hill JL, Gettes LS. Effects of acute coronary artery occlusion on local myocardial extracellular K⁺ activity in swine. *Circulation.* 1980;61:768–78.
23. Carlsson L. Mechanisms of local noradrenaline release in acute myocardial ischemia. *Acta Physiol Scand.* 1987;129 Suppl 559:7–85.
24. Désilets M, Baumgarten CM. Isoproterenol directly stimulates the Na⁺-K⁺ pump in isolated cardiac myocytes. *Am J Physiol.* 1986;251:H218–25.
25. Parratt JR. Endogenous myocardial protective (antiarrhythmic) substances. *Cardiovasc Res.* 1993;27:693–702.
26. Curtis MJ, Pugsley MK, Walker MJA. Endogenous chemical mediators of ventricular arrhythmias in ischemic heart disease. *Cardiovasc Res.* 1993;27:703–19.
27. Végh Á, Szekeres L, Parratt JR. Local intracoronary infusions of bradykinin profoundly reduce the severity of ischemia induced arrhythmias in anesthetized dogs. *Br J Pharmacol.* 1991;104:294–5.
28. György K, Végh Á, Rastegar MA. Isosorbide-2-mononitrate reduces the consequences of myocardial ischemia, including arrhythmia severity: implications for preconditioning. *Cardiovasc Drugs Ther.* 2000;14:481–8.
29. Kléber AG, Rieger CB, Janse MJ. Electrical uncoupling and increase in extracellular resistance after induction of ischemia in isolated, arterially perfused rabbit papillary muscle. *Circ Res.* 1987;61:271–9.
30. Cinca J, Warren M, Careno A, Tresanchez M, Armadans L, Gomez P, et al. Changes in myocardial electrical impedance induced by coronary artery occlusion in pigs with and without preconditioning. *Circulation.* 1997;96:3079–86.
31. Engelmann TW. Über die Leitung der Erregung in Herzmuskel. *Pflügers Arch.* 1875;11:465–80.
32. Wolk R, Cobbe SM, Hicks MN, Kane KA. Functional, structural and dynamic basis of electrical heterogeneity in healthy and diseased cardiac muscle: implications for arrhythmogenesis and anti-arrhythmic drug therapy. *Pharmacol Ther.* 1999;84:207–31.
33. Boukens BJD, Christoffels VM, Coronel R, Moorman AFM. Developmental basis for electrophysiological heterogeneity in the ventricular and outflow tract myocardium as a substrate for life-threatening ventricular arrhythmias. *Circ Res.* 2009;104:19–31.
34. DeMello WC. Effect of intracellular injection of calcium and strontium on cell communication in heart. *J Physiol.* 1975;250:231–45.

35. Spach MS, Miller WT, Geselowitz DB, Barr RC, Kootsey JM, Johnson EA. The discontinuous nature of propagation in normal canine cardiac muscle. Evidence for recurrent discontinuities of intracellular resistance that affect the membrane currents. *Circ Res.* 1981;48:39–54.
36. Rudy Y, Quan WL. A model study of the effects of the discrete cellular structure on electrical propagation in cardiac tissue. *Circ Res.* 1987;61:815–23.
37. Rohr S. Role of gap junctions in propagation of the cardiac action potential. *Cardiovasc Res.* 2004;62:309–12.
38. Peters NS, Wit AL. Myocardial architecture and ventricular arrhythmogenesis. *Circulation.* 1998;97:1746–54.
39. Spear JF, Kleval RS, Moore EN. The role of myocardial anisotropy in arrhythmogenesis associated with myocardial ischemia and infarction. *J Cardiovasc Electrophysiol.* 1992;3:579–88.
40. Shaw RM, Rudy Y. Ionic mechanisms of propagation in cardiac tissue. Roles of sodium and L-type calcium currents during reduced excitability and decreased gap junction coupling. *Circ Res.* 1997;81:727–41.
41. Spach MS, Heidlage JF. The stochastic nature of cardiac propagation at a microscopic level. Electrical description of myocardial architecture and its application to conduction. *Circ Res.* 1995;76:366–80.
42. Wojtczak J. Contractures and increase in internal longitudinal resistance of cow ventricular muscle induced by hypoxia. *Circ Res.* 1979;44:88–95.
43. Cascio WE, Yang H, Muller-Borer BJ, Johnson TA. Ischemia-induced arrhythmia: the role of connexins, gap junctions, and attendant changes in impulse propagation. *J Electrocardiol.* 2005;38:55–9.
44. Spach MS, Dolbert PC, Heidlage JF. Influence of the passive anisotropic properties on directional differences in propagation following modification of the sodium conductance in human atrial muscle. A model of reentry based anisotropic discontinuous propagation. *Circ Res.* 1988;62:811–32.
45. Janse MJ, vanCapelle FJL. Electrotonic interactions across an inexcitable region as a cause of ectopic activity in acute regional ischemia. A study in intact porcine and canine hearts and computer models. *Circ Res.* 1982;50:527–37.
46. Schömig A, Dart AM, Dietz R, Mayer R, Kübler W. Release of endogenous catecholamines in the ischemic myocardium of the rat. Part A. Locally mediated release. *Circ Res.* 1984;55:689–701.
47. Wilde AAM, Peters RJG, Janse MJ. Catecholamine release and potassium accumulation in the isolated globally ischemic rabbit heart. *J Mol Cell Cardiol.* 1988;20:887–96.
48. Lameris TW, DeZeuw S, Alberts G, Boomsma F, Duncker DJ, Verdouw P, et al. Time course and mechanism of myocardial catecholamine release during transient ischemia in vivo. *Circulation.* 2000;101:2645–50.
49. Yan G-X, Kléber AG. Changes in extracellular and intracellular pH in ischemic rabbit papillary muscle. *Circ Res.* 1992;71:460–70.
50. Reber WR, Weingart R. Ungulate cardiac Purkinje fibers. The influence of intracellular pH on the electrical cell-to-cell coupling. *J Physiol.* 1982;328:87–104.
51. Steenbergen CE, Murphy E, Levy L, London RE. Elevation in cytosolic free calcium concentration early in myocardial ischemia in perfused rat heart. *Circ Res.* 1987;60:700–7.
52. Dhein S. Gap junction channels in the cardiovascular system: pharmacological and physiological modulation. *TIPS.* 1998;19:229–41.
53. Rohr S, Kucera JP, Kléber AG. Slow conduction in cardiac tissue. I. Effects of a reduction of excitability versus a reduction of electrical coupling on microconduction. *Circ Res.* 1998;83:781–94.
54. Henriquez AP, Vogel R, Muller-Borer BJ, Henriquez CS, Weingart R, Cascio WE. Influence of dynamic gap junction resistance on impulse propagation in ventricular myocardium: a computer stimulation study. *Biophys J.* 2001;81:2112–21.

55. Ruiz-Meana M, Garcia-Dorado D, Lane S, Pina P, Inserte J, Mirabet M, et al. Persistence of gap junction communication during myocardial ischemia. *Am J Physiol Heart Circ Physiol.* 2001;280:H2563–71.
56. Ando M, Katare RG, Kakinuma Y, Zhang D, Yamasaki F, Muramoto K, et al. Efferent vagal nerve stimulation protects heart against ischemia-induced arrhythmias by preserving connexin43 protein. *Circulation.* 2005;112:164–70.
57. VanKampen MJ, Fromaget C, Gross D, Moorman AF, Lamers WH. Spatial distribution of connexin43, the major cardiac gap junction protein, in the developing and adult rat heart. *Circ Res.* 1991;68:1638–51.
58. Huang XD, Sandusky GF, Zipes DP. Heterogenous loss of connexin43 protein in ischemic dog hearts. *J Cardiovasc Electrophysiol.* 1999;10:79–91.
59. Beardslee MA, Lerner DL, Tardos PN, Lang JG, Beyer EC, Yamada KA, et al. Dephosphorylation and intracellular redistribution of ventricular connexin43 during electrical uncoupling induced by ischemia. *Circ Res.* 2000;87:656–62.
60. Papp R, Gönczi M, Kovács M, Seprényi Gy, Végh A. Gap junctional uncoupling plays a trigger role in the antiarrhythmic effect of ischemic preconditioning. *Cardiovasc Res.* 2007;74:396–405.
61. Padilla F, Garcia-Dorado D, Rodriguez-Sinovas A, Ruiz-Meana M, Inserte J, Soler-Soler J. Protection afforded by ischemic preconditioning is not mediated by effects on cell-to-cell electrical coupling during myocardial ischemia-reperfusion. *Am J Physiol.* 2003;285:H1909–16.
62. Végh Á, Komori S, Szekeres L, Parratt JR. Antiarrhythmic effects of preconditioning in anesthetized dogs and rats. *Cardiovasc Res.* 1992;26:487–95.
63. Meesmann W. Early arrhythmias and primary ventricular fibrillation after acute myocardial ischemia in relation to preexisting coronary collaterals. In: Parratt JR, editor. *Early arrhythmias resulting from myocardial ischemia.* New York: Oxford University Press; 1982. p. 93–112.
64. Meesmann W, Schulz FW, Schley G, Adolphsen P. Überlebensquote nach akutem experimentellem Coronarverschluss in Abhängigkeit von Spontankollateralen des Herzens. *Z Ges Exp Med.* 1970;153:246–64.
65. Schaper W. Collateral anatomy and blood flow: its potential role in sudden coronary death. In: Greenberg HM, Dwyer EM, editors. *Sudden coronary death, Annals of the New York Academy of Sciences.* The New York Academy of Sciences 1982;382:69–90.
66. Hearse DJ, Yellon DM. Therapeutic approaches to myocardial infarct size limitation. New York: Raven; 1984.
67. Kléber AG. Conduction of the impulse in the ischemic myocardium: implications for malignant ventricular arrhythmias. *Experimentia.* 1987;43:1056–61.
68. Murry CE, Jennings RB, Reimer KA. Preconditioning with ischemia: a delay of lethal cell injury in ischemic myocardium. *Circulation.* 1986;74:1124–36.
69. Babai L, Szigeti Zs, Parrat JR. Delayed cardioprotective effects of exercise in dogs are aminoguanidine sensitive: possible involvement of nitric oxide. *Clin Sci.* 2002;102:435–45.
70. Saez JC, Nairn AC, Czernik AJ, Fishman GI, Spray DC, Hertzberg EL. Phosphorylation of connexin43 and the regulation of neonatal rat cardiac myocyte gap junctions. *J Mol Cell Cardiol.* 1997;29:2131–45.
71. Végh Á, Szekeres L, Parratt JR. Preconditioning of the ischemic myocardium; involvement of the L-arginine – nitric oxide pathway. *Br J Pharmacol.* 1992;107:648–52.
72. Gönczi M, Papp R, Kovács M, Seprényi Gy. Modulation of gap junctions by nitric oxide contributes to the antiarrhythmic effect of sodium nitroprusside. *Br J Pharmacol.* 2009;156:786–93.
73. Végh Á, Parratt JR. Noradrenaline, infused locally, reduces arrhythmia severity during coronary artery occlusion in anaesthetised dogs. *Cardiovasc Res.* 2002;55:53–63.
74. Schwartz PJ, Diem R, Dun NJ, Forstermann U. Endogenous and exogenous nitric oxide inhibits norepinephrine release from rat heart sympathetic nerves. *Circ Res.* 1995;77:841–8.

75. Sears CE, Choate JK, Patterson DJ. NO-cGMP pathway accentuates the decrease in heart rate caused by cardiac vagal nerve stimulation. *J Appl Physiol.* 1999;86:510–6.
76. Jiang H, Hu X, Lu Z, Wen H, Zhao D, Tang Q, et al. Effects of sympathetic nerve stimulation in ischemia-induced ventricular arrhythmias by modulating connexin43 in rats. *Arch Med Res.* 2008;39:647–54.
77. deGroot J, Veenstra T, Verkerk AO, Wilders R, Smits JPP, Wilms-Schopman FJG, et al. Conduction slowing by the gap junction uncoupler carbenoxolone. *Cardiovasc Res.* 2003;60:288–97.
78. Ehlert FA, Goldberger JJ. Cellular and pathophysiological mechanisms of ventricular arrhythmias in acute ischemia and infarction. *PACE.* 1997;20:966–75.
79. Haugan K, Olsen KB, Hartvig L, Petersen JS, Holstein-Rathlou NH, Hennan JK, et al. The antiarrhythmic peptide analog ZP123 prevents atrial conduction slowing during metabolic stress. *J Cardiovasc Electrophysiol.* 2005;16:537–45.
80. Plotkin LI, Manolagas SC, Bellido T. Transduction of cell survival signals by connexin-43 hemichannels. *J Biol Chem.* 2002;277:8648–57.
81. Burt JM, Spray DC. Inotropic agents modulate gap junctional conductance between cardiac myocytes. *Am J Physiol.* 1988;254:H1206–10.
82. Dhein S, Manicone N, Müller A, Gerwin R, Ziskoven U, Irankhahi A, et al. A new synthetic antiarrhythmic peptide reduces dispersion of epicardial activation recovery intervals and diminishes alterations of epicardial activation patterns induced by regional ischemia. *N-S Arch Pharmacol.* 1994;350:174–84.
83. Müller A, Gottwald M, Tudyka T, Linke W, Klaus W, Dhein S. Increase in gap junction conductance by an antiarrhythmic peptide. *Eur J Pharmacol.* 1997;327:65–72.
84. Xing D, Kjolby AL, Nielsen MS, Petersen JS, Harlow KW, Holstein-Rathlou NH, et al. ZP123 increases gap junctional conductance and prevents reentrant ventricular tachycardia during myocardial ischemia in open chest dogs. *J Cardiovasc Electrophysiol.* 2003;14: 510–20.
85. Xing D, Kjolby AL, Petersen JS, Martins JB. Pharmacological stimulation of cardiac gap junction coupling does not affect ischemia-induced focal ventricular tachycardia or triggered activity in dogs. *Am J Physiol Heart Circ Physiol.* 2005;288:H511–6.
86. Kjolby AL, Holstein-Rathlou NH, Petersen JE. Anti-arrhythmic peptide *N*-3-(4-hydroxyphenyl)propynyl Pro-Hyp-Gly-Ala-Gly-OH reduces dispersion of action potential duration during ischemia/reperfusion in rabbit hearts. *J Cardiovasc Pharmacol.* 2002;40:770–9.
87. Janse MJ, Kléber AG. Propagation of electrical activity in ischemic and infarcted myocardium as the basis of ventricular arrhythmias. *J Cardiovasc Electrophysiolog.* 1992;3:77–87.
88. Daleau P, Boudriau S, Michaud M, Jolicoeur C, Kingma JG. Preconditioning in the absence or presence of sustained ischemia modulates myocardial Cx43 protein levels and gap junction distribution. *Can J Physiol Pharmacol.* 2001;79:371–8.
89. Vetterlein F, Mühlfeld C, Cetegen C, Volkmann R, Schrader C, Hellige G. Redistribution of connexin43 in regional acute ischemic myocardium: influence of ischemic preconditioning. *Am J Physiol.* 2006;291:H813–9.
90. Jongsma HJ, Wilders R. Gap junctions in cardiovascular disease. *Circ Res.* 2000;86:1193–7.
91. Rohr S, Kucera JP, Fast VG, Kléber AG. Paradoxical improvement of impulse conduction in cardiac tissue by partial cellular uncoupling. *Science.* 1997;275:841–4.
92. Wit AL, Janse MJ. The ventricular arrhythmias of ischemia and infarction. *Electrophysiological mechanisms.* Mount Kisco, New York: Futura; 1993.

Chapter 30

Role of NCX1 and NHE1 in Ventricular Arrhythmia

András Tóth and András Varró

30.1 Introduction: The Origin and Diversity of Cardiac Arrhythmias

Sudden cardiac death (SCD) is presumed to be related to abnormal generation and/or propagation of electrical impulse causing lethal cardiac arrhythmias. It may occur in a wide variety of pathophysiological situations such as IHD, major forms of heart failure, atrial fibrillation (AF), and congenital ion channel abnormalities.

The cellular mechanism of cardiac arrhythmias includes (1) enhanced automaticity, (2) reentry, (3) triggered activity, and (4) the combinations of these factors. Enhanced normal automaticity can be due to changes in electrophysiological properties of either the SA or the AV nodal cells or the Purkinje fibers under certain conditions, such as largely increased sympathetic tone, ischemia/reperfusion, cardiac hypertrophy, and atrial or ventricular remodeling. Reentry is due to abnormal impulse conduction or changes in refractoriness and often the combination of both. Triggered arrhythmias have been shown to have rather complex background involving several ion channels, pumps, and exchangers and are manifested as early and/or delayed afterdepolarizations (EADs, DADs). In this chapter, we focus on the relationship between triggered cardiac activity and the upregulation of sarcolemmal ion exchangers, NCX1 and NHE1, clarifying its basic mechanisms at the cellular level.

A. Tóth

Department of Pharmacology and Pharmacotherapy, University of Szeged, 6720 Szeged, Dóm tér 12, Szeged, Hungary

A. Varró (✉)

Department of Pharmacology and Pharmacotherapy, University of Szeged, 6720 Szeged, Dóm tér 12, Szeged, Hungary

and

Division of Cardiovascular Pharmacology, Hungarian Academy of Sciences, Szeged, Hungary
e-mail: a.varro@phcol.szote.u-szeged.hu

30.2 NCX1: A Major Regulator of $[Ca^{2+}]_i$ Balance in Cardiac Cells

The cardiac NCX1 plays a pivotal role in maintaining both the beat-to-beat and the long term Ca^{2+} balance in cardiomyocytes. The energy used for exchange is normally provided by the sarcolemmal Na^+/K^+ -ATPase (NKA). The molecular properties and physiological functions of NCX have been well explored [1–6]. The primary physiological role of the NCX1 is the regulation of $[Ca^{2+}]_i$ content by beat-to-beat removal of the trigger Ca^{2+} entering the cell during the action potential (AP) via L-type Ca^{2+} channels (LTCC) and the NCX1 itself. However, by doing this – especially when Ca_i^{2+} homeostasis is severely disturbed – it may result in an arrhythmogenic inward current (I_{ti}), primarily responsible for triggered arrhythmias and nonreentrant ventricular tachyarrhythmia [7–12]. Furthermore, since the direction of the Ca^{2+} transport by the NCX1 is fully reversible, beyond its primary (*forward mode*) action of extruding Ca^{2+} from the cells, under certain conditions, Ca^{2+} influx into the cells from the extracellular space by the exchanger (*reverse mode transport*) may substantially contribute to cytoplasmic Ca^{2+} overload – also widely recognized as major inductor of triggered arrhythmogenic activity.

30.2.1 The Significance of NCX1 in Maintaining Intracellular Ca^{2+} Balance

During depolarization, a relatively small, but essential Ca^{2+} flux enters the cell mainly via sarcolemmal LTCCs as the first step in excitation–contraction (EC) coupling. A minor Ca^{2+} influx (<10% of total) via “*reverse*” mode transport of the NCX1 contributes to the influx. The localized $[Ca^{2+}]$ increase in the submembrane “fuzzy space” is essential in triggering the release of a larger Ca^{2+} flux via the ryanodine sensitive Ca^{2+} channels (RyRs) of SR (calcium induced calcium release, CICR). Integrated Ca^{2+} flux (Ca^{2+} transient) in turn activates myofilaments and generates contractile force. The contribution of the extracellular Ca^{2+} influx to total Ca_i^{2+} elevation is species dependent (~7% to ~30%). In pathological conditions (e.g., heart failure), it may reach a much higher (50–60%) proportion. For steady activity of the heart, maintaining the balance between transsarcolemmal and intracellular Ca^{2+} transport systems is critical. In functional steady state, the exact amount of Ca^{2+} entering the cell during AP should be extruded. Any major and/or chronic imbalance exceeding functional physiological shifts may result in gradual Ca^{2+} overload, leading to increased arrhythmia propensity, cell injury and apoptosis, or gradual cellular Ca^{2+} loss compromising cardiac pump function. For normal cardiac relaxation, fast dissociation of the activator calcium from the myofilaments and its fast removal from the cytosol is likewise essential. Reduced Ca^{2+} decay rate might lead to incomplete relaxation, subsequently limiting ventricular refilling.

Cellular Ca^{2+} removal mechanisms permanently compete for Ca_i^{2+} , and their relative contribution dynamically change throughout the cardiac cycle.

The single transporter mechanism to pump back Ca^{2+} to the SR is the sarcoplasmic Ca^{2+} -ATPase (SERCA2). Its activity is essential to maintain the Ca^{2+} content of the SR for consequent Ca^{2+} release. The major transport mechanism extruding the surplus Ca^{2+} from cardiac cells is the *forward mode* activity of the low affinity but high capacity NCX1. Depending on species, 3–47% of the total removed cytosolic Ca^{2+} is extruded from the cell by the NCX1. The plasma membrane Ca^{2+} -ATPase (PMCA) was shown to contribute less than 5% to cytoplasmic Ca^{2+} removal. Nonetheless, PMCA may be more involved in fine-tuning the end-diastolic $[\text{Ca}^{2+}]_i$ and also in intracellular Ca^{2+} signaling. A fourth, but physiologically insignificant alternative mechanism for cytoplasmic Ca^{2+} removal is uptake into the mitochondria via their Ca^{2+} uniporter. This uptake only occurs when cytoplasmic Ca^{2+} levels are largely elevated ($>500 \text{ nM}$) and may represent a safety mechanism that can transiently reduce cellular Ca^{2+} overload. A recently described, but practically unexplored alternative of Ca^{2+} removal is into the nuclear envelope. Surprisingly, while NCX function was expected to be essential for normal contraction–relaxation cycling, cardiac-specific (NCX1) KO mice were not only able to survive to adulthood, but also with relatively minor cardiac dysfunction. In these animals, the absence of NCX1 was nearly fully compensated by secondary shifts in their Ca^{2+} handling [13, 14].

30.2.2 Physiological Regulation of NCX1 Activity: $[\text{Ca}^{2+}]_i$, $[\text{Na}^+]_i$, and pH_i Dependence

A unique feature of NCX is that its transport substrates also exert important regulatory effects on its transport activity. Indeed, crucial physiological regulation of the direction and rate of the transport is accomplished by Na_i^+ (Na^+ -dependent inactivation, I1) and Ca_i^{2+} (Ca_i^{2+} -dependent activation, I2). Ca_i^{2+} -dependent activation is an essential mechanism to activate Ca^{2+} extrusion (and subsequent inward current) in forward mode operation. Elevated $[\text{Na}^+]_i$ typically activates reverse mode transport, while, in contrast, highly increased $[\text{Na}^+]_i$ may completely inactivate $I_{\text{Na}/\text{Ca}}$. This Na^+ -dependent inactivation, however, is abolished by highly elevated $[\text{Ca}^{2+}]_i$. These basic NCX1 regulatory mechanisms depend on the practically unknown local Ca^{2+} and Na^+ concentrations in the vicinity of the NCX1 proteins. Indirect estimation of the peak $[\text{Ca}^{2+}]$ in the fuzzy space ($[\text{Ca}^{2+}]_{\text{sm}}$) yielded $3.5 \mu\text{M}$, a value substantially higher than any measured $[\text{Ca}^{2+}]_i$ [15]. On the other hand, Na^+ -dependent inactivation could be observed only at dramatically elevated ($>30 \text{ mM}$) $[\text{Na}^+]_i$, thus normally is not likely to be active.

Lowering pH_i inhibits and elevation of pH_i stimulates NCX1 [16]. Moderate decrease in pH_i (0.4 units) may induce its ~90% inhibition. ATP increases the affinity of the exchanger to $[\text{Ca}^{2+}]_i$, and $[\text{Na}^+]_o$ may inhibit Na^+ -dependent

inactivation and stimulate PIP₂ synthesis. The principal action for negatively charged phospholipids is to inhibit Na⁺-dependent inactivation. Several regulatory proteins may also have important roles in physiological NCX1 modulation. Phospholemman is an endogenous inhibitor of NCX1, and also has a role in controlling activity of the NKA. Stimulatory actions by AT-II and ET-1 may be mediated by PKC. NCX1 activity is also modulated by local factors, such as phosphorylation state or subcellular location. The phosphorylation state of the NCX1 is probably regulated by a large macromolecular complex [17].

30.2.3 The Contribution of NCX1 Currents to AP and the I_{ti}

The net ion transport by NCX1 is not electroneutral. An exchange stoichiometry of $3\text{Na}^+ \leftrightarrow 1\text{Ca}^{2+}$ is widely accepted, though higher exchange ratios were also proposed [18]. Uneven charge exchange results in a transmembrane current ($I_{\text{Na/Ca}}$) of at least one net charge per transport cycle. The direction of the $I_{\text{Na/Ca}}$ is determined by the magnitudes of the membrane potential (E_m) and NCX1 equilibrium potential (E_{NCX}). The latter is defined by local transmembrane gradients of Na⁺ and Ca²⁺ ($E_{\text{NCX}} = 3E_{\text{Na}} - 2E_{\text{Ca}}$). Whenever the difference ($E_m - E_{\text{NCX}}$) is positive, Ca²⁺ entry and Na⁺ loss should occur, generating *outward* current. If ($E_m - E_{\text{NCX}}$) is negative, Ca²⁺ extrusion and Na⁺ gain leading to *inward* current is energetically favored. Consequently, both *depolarizing and repolarizing* contribution of $I_{\text{Na/Ca}}$ to AP is possible. Depolarization by $I_{\text{Na/Ca}}$ may facilitate *arrhythmogenesis* by increasing short term variability of AP duration (APD). Increased $I_{\text{Na/Ca}}$ may have particular importance in *heart failure* when NCX1 expression/function is enhanced.

The direction of the $I_{\text{Na/Ca}}$ during the different phases of AP is not properly clarified. In the guinea pig, it was found predominantly outward during the plateau phase, while in rat cardiomyocytes, inward $I_{\text{Na/Ca}}$ prolonged the APD. Results from rabbit studies suggested that $I_{\text{Na/Ca}}$ is mostly inward during AP. In a study based on measurements with buffered $[\text{Ca}^{2+}]_i$, elevated $I_{\text{Na/Ca}}$ led to APD prolongation [19]. In a complex model [20, 21], NCX1 current was found inward during the plateau phase if $[\text{Na}^+]_i$ was normal. In a study based on an integrative model of the canine ventricular myocyte [22], and supposing colocalization between NCX1 and RyR2, a multiinflection model has been developed [23]. In nodal pacemaker cells, $I_{\text{Na/Ca}}$ may significantly contribute to depolarization [24].

30.3 NHE1: The Major Regulator of H_i⁺ (pH_i) and Na_i⁺ in Cardiomyocytes and an Important Promoter of Cardiac Hypertrophy

The NHE is an integral membrane transport protein playing an essential role in a wide range of cell types in the regulation of intracellular acid–base balance and cellular electrolyte and volume homeostasis by translocating one intracellular H⁺ in

exchange for one extracellular Na^+ . For its exchange activity, it uses the energy provided by the *trans*-sarcolemmal Na^+ gradient.

In the mammalian heart, its type 1 isoform (NHE1) is predominant and is expressed in large quantity. Its molecular properties and physiological functions have been well explored [25–28]. Shifts in normal NHE1 activity may also contribute to pathological changes. At physiological pH_i , its activity is low; however, even moderate decrease in pH_i substantially activates proton extrusion, leading to subsequent Na_i^+ accumulation and Ca_i^{2+} overload. Increased NHE1 activity was reported to promote cellular growth, leading to cardiac hypertrophy [29, 30]. It also plays a crucial role in induction of necrotic and/or apoptotic tissue damage and is a major cause of increased arrhythmia generation during/following myocardial infarct (MI) and also in HF. Its activation in *sympathetic nerve endings* leads to significantly increased NE release and decreased reuptake, leading to increased arrhythmia propensity of the heart [31].

There are some important differences between the NCX and NHE. The NCX is electrogenic, whereas the NHE is electroneutral. However, since their activity is tightly coupled, increased proton extrusion still would induce depolarizing current through coactivation of the NCX1. Another major difference is that in contrast to the NCX1, the Na^+ transport by NHE1 is practically always unidirectional (inward).

30.3.1 The Essential Role of NHE1 in pH_i and Na_i^+ Regulation and Cellular Growth

The NHE is responsible for pH_i regulation [32]. By removing excess protons, it protects the cells from intracellular acidosis. In hypoxia or acidosis, when excess protons are generated in large quantities (lactacidosis), NHE is several times more effective than other transporters involved in pH_i regulation. By modulating Na^+ uptake, it also participates in regulation of the transmembrane Na^+ flux and contributes to osmotic cell volume control. In addition, it can be activated by growth factors and normal NHE activity is essential for cell growth and proliferation. NHE also plays an important role in promoting or inhibiting apoptosis. In cardiomyocytes, NHE1 is restricted to specialized membrane microdomains and its regulatory function is tightly coupled to the modulation of pH-sensitive membrane proteins. In the transverse tubulus, it is localized in close proximity to the RyRs (consequently in the vicinity the NCX1) and exerts modulatory action on EC coupling. At the intercalated disks, it is localized in close proximity to connexin 43 and was shown to modulate cell-to-cell coupling. NHE1 is also present in the caveolae and substantially influences the rate of cAMP-synthesis by its modulatory effect on adenylcyclase. It is also involved in regulating cytoskeletal organization and act as plasma membrane scaffold assembling regulatory proteins and signaling molecules for enhanced functional interaction [33].

30.3.2 Physiological Regulation of NHE1

In cardiomyocytes, NHE1 activity is regulated by multiple mechanisms [34]. Its primary stimulus is intracellular acidosis. Under normal physiological conditions (i.e., oxidative energy metabolism), its basal activity is practically negligible but is rapidly activated as pH_i decreases [28]. To explain this steep pH_i dependence, NHE1 has been suggested to contain an extra proton-binding site for its allosteric regulation.

NHE1 is also regulated through phosphorylation–dephosphorylation, accomplished by cellular signaling protein kinases in response to hormone or growth-factor stimulation or sustained acidosis. Acidosis- or ischemia-activated protein kinases are implicated in myocardial NHE1 regulation. Phosphorylation stimulates (by moving its setpoint) the exchanger to be more active at more alkaline pH values. NHE1 activity in response to angiotensin II may be inhibited through its phosphorylation by the p38 MAPK. This kinase inhibits the NHE1 via inhibition of the ERK pathway, but it may also induce alkalization and stimulate NHE1 in a separate, apoptotic pathway. Its modulation by protein kinases C and D is probably indirect. Protein phosphatases 1 and 2A inhibit NHE1 through dephosphorylation, while calmodulin blocks its autoinhibitory region. Further regulatory factors shown to bind to NHE1 are carbonic anhydrase II, PIP2, HSP70, and CHP (calcineurin homologous protein), but their role is not yet fully clarified. NHE1 expression is also regulated at the transcriptional level [35]. NHE1 expression was induced and its activity was elevated in isolated cardiomyocytes subjected to chronic external acidosis. In isolated perfused hearts and also in coronary ligated rats, ischemic insult resulted in increased NHE1 mRNA levels [36]. It is important, however, to emphasize that while *acute activation* of the NHE1 usually contributes to physiological maintenance of functional integrity of the myocytes, its *sustained activation* and/or highly *increased* expression results in myocardial injury and structural remodeling, leading to arrhythmogenesis and mechanical dysfunction.

30.4 Role of Altered Exchanger Activities in Cardiac Arrhythmia and Heart Disease

Marked alterations in trans- and/or intracellular Na^+ and Ca^{2+} transport rates leading to impairment of cellular Na^+ and Ca^{2+} regulation are characteristic to several life-threatening cardiac diseases. Irregular AP morphology commonly caused by cellular Ca^{2+} overload and increased SR Ca^{2+} leakage may result in abnormal EC coupling and increased arrhythmia propensity. In congestive heart failure (CHF), leaky SR initiates depolarizing currents and may trigger extrasystoles during diastole via the upregulated NCX1, thus substantially increasing the risk of SCD. In sustained ischemia, gradual but substantial Ca_i^{2+} and Na_i^+ overload

deteriorates normal electrical activity. If acute or chronic focal ischemia is generalized, it may lead to high probability of SCD.

30.4.1 NCX1-Induced $[Ca^{2+}]_i$ Overload and Its Role in Triggered Arrhythmia

Ca^{2+} -dependent arrhythmias are usually triggered by abnormal membrane potential changes induced by Ca_i^{2+} overload, generated either by increased Ca^{2+} influx (caused by enhanced open probability of LTCCs) or by decreased Ca^{2+} efflux (induced by the elevated $[Na^+]_i$). Sustained rise in $[Ca^{2+}]_i$ raises the SR Ca^{2+} content and subsequently increases the normally low probability of Ca^{2+} spark generation. If the spark rate is above a threshold, spontaneous Ca^{2+} waves are likely to be induced.

The principal cellular mechanisms leading to triggered focal arrhythmias are EADs and DADs. *Early* EADs arise during the plateau phase of AP due to maintained late Na^+ current [37], increased NCX1 activity, or reactivation of a fraction of LTCCs. *Late* EADs are most likely induced by activation of Ca^{2+} -dependent inward currents during the end phase of the cardiac repolarization. DADs are initiated by spontaneous, generalized SR Ca^{2+} release (multiple Ca^{2+} sparks, Ca^{2+} waves) during diastole through a current carried by the NCX1. EADs are more probable at low heart rates when APs are prolonged. DADs are more likely at high heart rates due to enhanced Ca^{2+} entry in spite of the shortened APs.

Altered NCX1 activity may play a crucial role in EAD initiation [38], especially in cardiac Purkinje fibers. Inward NCX1 current, generated by the extrusion of the spontaneously released Ca^{2+} , promotes membrane depolarization through enabling window Ca^{2+} currents. Enhanced NCX1 function may also be important in DAD generation through its contribution to elevated cytosolic and highly increased SR Ca^{2+} content [39]. Since SERCA2 is depressed by the high SR Ca^{2+} content, the sudden large elevation in $[Ca^{2+}]_i$ caused by spontaneous Ca^{2+} waves is ultimately removed by the exchanger. Though, during diastole, the membrane potential is at or close to its resting level, sudden release of a large amount of Ca^{2+} – when extruded by the NCX1 – may induce sufficiently large depolarizing inward current (I_{ti}) to shift the membrane potential to the threshold of I_{Na} , thus eliciting *propagating* extrasystoles. This is the proposed mechanism in a rare, often lethal genetical disorder, catecholaminergic polymorphic ventricular tachycardia (CPVT), where RyR mutations cause intermittent abnormal release of Ca^{2+} in response to catecholamine challenge [40].

Thus, cardiac arrhythmia propensity may be attributed to irregular micro- and macroheterogeneities in generation or propagation of APs, caused by focal, cellular level disturbances in intracellular Ca^{2+} handling. Abnormally high $[Ca^{2+}]_i$ in a particular cardiomyocyte may easily spread over to the surrounding cells either via membrane depolarization or by direct cell-to-cell diffusion through gap junctions, triggering subsequent secondary intracellular Ca^{2+} release [41].

30.4.2 NHE1-Induced $[Na^+]$ _i Overload, a Generator of Ischemia-Induced $[Ca^{2+}]$ _i Overload, and Cardiac Hypertrophy

Under physiological conditions, NHE1 removes excess intracellular protons in exchange for extracellular Na^+ . Surplus intracellular Na^+ is then removed by the high capacity NKA and to a limited extent the reverse mode activity of NCX1. In hypoxic or ischemic cardiomyocytes – due to the anaerobic shift and largely enhanced glycolysis – proton production is highly elevated. The subsequent acidosis activates NHE1 and intracellular protons are rapidly exchanged for external Na^+ . Therefore, a crucial consequence of hypoxic NHE1 activation is increased Na^+ influx. Since, due to the increasing energy deficit NKA is gradually inhibited, surplus Na^+ content may only be removed by the NCX1 resulting in intracellular Ca^{2+} accumulation. Ca^{2+} overload may trigger various pathways, leading to mechanical dysfunction, arrhythmia generation, and eventually cellular death. The crucial role of NHE1 activation in induction of ischemia–reperfusion injury is further underlined by the fact that in mice, genetic ablation of NHE1 protects the heart from ischemia-induced injury [42].

NHE1 is also an important factor in inducing cardiac hypertrophy and its inhibition limits hypertrophy [30, 34]. The hypertrophic effect of norepinephrine, aldosterone, or stretch can, indeed, be prevented by NHE1 inhibition. The details of this mechanism are not fully clarified. Since intracellular alkalosis is *not induced* by NHE1 activation, the actions of NHE1 inhibition are probably *not mediated* through pH_i modulation. Since NHE1 inhibition also limits Na_i^+ accumulation, the latter may provide a feasible mechanism by which NHE1 modulates hypertrophy [29]. Elevation of $[Na^+]$ _i could act through several alternative mechanisms: increased reverse mode activity of NCX1, increased reactive oxygen species (ROS) generation, or activation of intracellular signaling or phosphorylation pathways. All these pathways were studied in detail, but no final agreement on the role of NHE1 in induction of hypertrophy has been reached. Enhanced NHE1 expression was also found in hypertrophy, but the significance of this apparently positive feedback mechanism is not fully understood.

30.4.3 NCX1 and Ventricular Arrhythmias in Congestive Heart Failure

Perturbations in intracellular Ca^{2+} handling leading to mechanical dysfunction and/or arrhythmia propensity in HF are summarized in Fig. 30.1. NCX1 mRNA and protein expression and activity are markedly elevated, while SERCA2 activity is depressed, though its expression levels are not always decreased. Decreased SERCA2 activity causes slower and decreased Ca^{2+} reuptake and slower and reduced decay in systolic $[Ca^{2+}]$ _i. Consequently, during relaxation, Ca^{2+} extrusion by NCX1 is increased relative to Ca^{2+} reuptake via SERCA2. Furthermore, in HF,

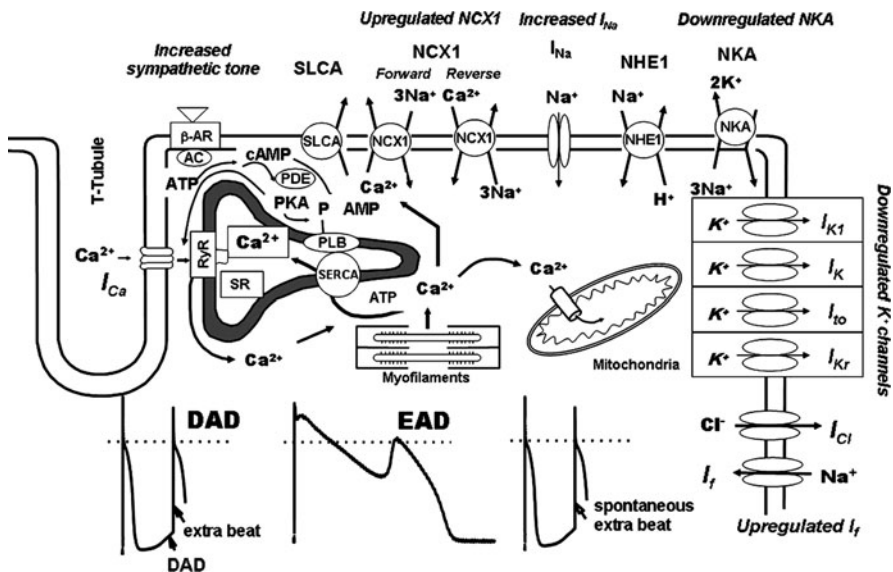


Fig. 30.1 Schematics summarizing the principal mechanisms leading to arrhythmogenesis (EAD, DAD, and Ca²⁺ wave generation) in the failing heart (see details in the text)

the increased open probability of RyRs leads to marked diastolic Ca²⁺ leak from SR [43]. Phospholamban expression is not necessarily changed, but its phosphorylation level is often lowered. The primary consequences of the inverse shift in NCX1 and SERCA2 activities are (1) decreased SR Ca²⁺ content and subsequently depressed [Ca²⁺]_i transients causing systolic dysfunction, and (2) largely elevated diastolic [Na⁺]_i and [Ca²⁺]_i, leading to diastolic dysfunction.

Increased [Na⁺]_i due to decreased Na⁺ extrusion by NKA, or increased Na⁺ influx through slowly inactivating Na⁺ channels is a typical perturbation in HF. Since [Ca²⁺]_i and [Na⁺]_i are tightly coupled, elevated [Na⁺]_i should have important implications for intracellular Ca²⁺ handling. Elevated [Na⁺]_i in the fuzzy space shifts the NCX1 reversal potential towards more negative values, leading to larger, prolonged Ca²⁺ influx during systole and shorter, smaller efflux during diastole. Elevated diastolic [Ca²⁺]_i, reduced SR Ca²⁺ content, and subsequently compromised relaxation are the major consequences of downregulated SERCA2, upregulated NCX1 expression, and elevated diastolic [Na⁺]_i. Since depressed and leaky SERCA2 is the primary cause behind compromised relaxation and subsequent diastolic dysfunction, the enhanced NCX1 expression may be considered a compensatory mechanism. Indeed, in failing hearts, increased Ca²⁺ influx through the NCX1 during systole may partially compensate for decreased SR Ca²⁺ content by increasing SR Ca²⁺ load, elevating Ca²⁺ transients, and enhancing contractile force.

Increased arrhythmia propensity in the failing heart is a consequence of a number of changes in the electrophysiological state of the heart. The results are often diverse and conflicting, depending on the nature of disease (hypertrophic vs.

dilatative), the model applied (pacing vs. valve dysfunction), and the species (rat, rabbit, dog). Reduced SA node pacemaker activity is usually accompanied by enhanced automaticity of the AV node and/or the Purkinje fibers and ventricles (trigger). It may be caused by corresponding shifts in I_f distribution and often lead to enhanced ectopic beat formation (trigger). Furthermore, elevation of the mRNA and protein expression and the current density of I_f channels were also reported in HF [44].

Since in the failing heart Ca^{2+} -dependent NCX1-mediated depolarizing activity is usually increased and repolarizing K^+ currents (I_{K1} , I_{Ks} , I_{to}) are downregulated, while late Na^+ plateau current (I_{NaL}) is enhanced, APD prolongation and dispersion occurs (substrate), subsequently favoring EAD formation (trigger). Indeed, increased inward exchanger current density during the plateau phase is suggested as a major contributor to electrical instability and delaying of the repolarization [45–47]. The probability of EAD initiation and incidence of EADs (trigger) was demonstrated to be increased as a consequence of reduced repolarization reserve due to K^+ channel downregulation and increased inward $I_{\text{Na}/\text{Ca}}$ generated by the upregulated NCX1. The proarrhythmic effect of the enhanced inward NCX1 current would further be amplified by a reduction in I_{K1} , a current known to stabilize cardiac membrane potential.

Elevated exchanger activity and increased Ca^{2+} leakage from the hyperphosphorylated RyRs promotes DAD formation (trigger). While in healthy myocytes increased SR Ca^{2+} content is a prerequisite for DAD generation, in HF, as a consequence of the decreased K^+ channel expression, the subsequently depressed I_{K1} cannot carry enough repolarizing current to oppose DADs, which may even be generated at lowered SR Ca^{2+} content. The probability of DAD generation may further be increased by cardiac glycosides and β -agonists, commonly used to improve contractile force in the failing heart. HF may also be associated with chronic AF, since in the atria, the enhanced NCX1 has greater contribution to maintaining AP plateau and duration [48]. Finally, as a consequence of the reduced impulse conduction velocity (substrate), caused by the downregulated connexin 43 density, decreased I_{Na} , and increased APD variability, reentrant activity is substantially increased. Enhanced dispersion of repolarization and cellular refractoriness is a further important factor (substrate) in increasing the probability of reentrant arrhythmias and has been demonstrated in both cardiac hypertrophy and HF.

30.4.4 NHE1–NCX1 Interaction and Ventricular Arrhythmia Generation During Acute Ischemia–Reperfusion Injury and Chronic IHD

Sustained cardiac ischemia is characterized by deprived energy metabolism, acidosis, hypoxia, and elevated $[K^+]_o$. Decreased pH_i (acidosis) exerts severe negative inotropic effects on myocardial contractility (reduced developed force and maximal

tension) and depresses Ca^{2+} transport proteins (SERCA2, RyR2, NCX1), while, surprisingly, the amplitude of the Ca_i^{2+} transient increases [49, 50]. This contrast suggests that the negative inotropic effect of acidosis is a consequence of the decreased myofilament Ca^{2+} sensitivity and turnover rate and not the depressed Ca^{2+} transport. In acidosis, both $[\text{Ca}^{2+}]_i$ and $[\text{Na}^+]_i$ are elevated. The latter is caused by increased proton extrusion by NHE1 and depressed NKA activity. In sustained, severe acidosis, the substantial pH_o decrease suppresses Na^+/H^+ exchange, and since $\text{Na}^+/\text{Ca}^{2+}$ exchange is also inhibited, elevated $[\text{Na}^+]_i$ is accompanied by elevated $[\text{Ca}^{2+}]_i$. In contrast to acidosis-induced reduction in Ca^{2+} uptake, the SR Ca^{2+} content is usually elevated.

Perturbations in pH_i and Ca^{2+} handling leading to arrhythmia propensity in the ischemic heart are summarized in Fig. 30.2. In acute hypoxia, reactivation of the late Na^+ channels leads to increased Na^+ influx. Na^+ efflux is substantially reduced due to the energy deficit of the NKA. NHE1 activity is significantly enhanced as a consequence of the increased $[\text{Na}^+]_i$. During sustained hypoxia, $[\text{Na}^+]_i$ may rise to very high levels ($>40 \text{ mM}$). Subsequent activation of the *reverse mode* transport by NCX1 leads to enhanced Ca^{2+} influx and increased $[\text{Ca}^{2+}]_i$. Due to the increased K^+ efflux transmembrane, K^+ gradient also gradually decreases. The decreased K^+ gradient in combination with a direct effect of hypoxia on K^+ channels induces depolarization. This further boosts arrhythmogenic reverse mode NCX1 current. Permanent elevation of $[\text{Ca}^{2+}]_i$ during *lasting* hypoxia inevitably leads to *massive*

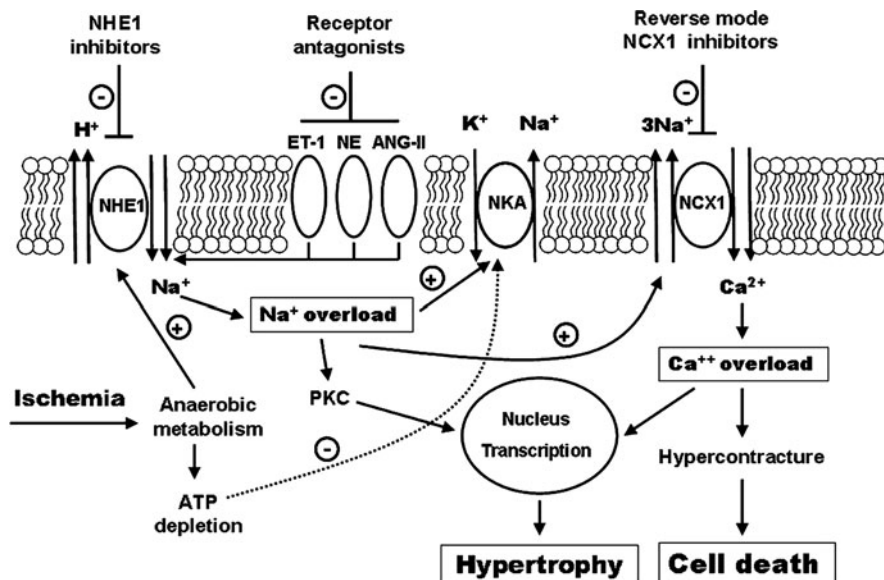


Fig. 30.2 Central role of NHE-1 in mediating acute and chronic responses to myocardial ischemia–reperfusion and the three principal preventive strategies to limit ischemia–reperfusion-induced tissue injury (see details in the text)

Ca^{2+} overload of both the sarcoplasma and the SR, substantial membrane depolarization, and may initiate triggered arrhythmias.

In acute ischemia, intracellular acidosis activates NHE-1, resulting in elevated $[\text{Na}^+]_i$. Increased $[\text{Na}^+]_i$ in turn activates *reverse mode* transport of NCX1, leading to increased $[\text{Ca}^{2+}]_i$. Na^+ overload is also facilitated by intracellular acidosis, leading to further Na^+ entry through the NHE1. LTCCs are partially inactivated due to gradual membrane depolarization. Therefore, their contribution to enhanced Ca^{2+} influx during late ischemia and early reperfusion is limited. In *prolonged, severe ischemia*, unbalanced Ca_i^{2+} accumulation leads to gradual Ca_i^{2+} overload. When $[\text{Ca}^{2+}]_i$ reaches a threshold (~ 500 nM), mitochondria begin to accumulate Ca^{2+} . This safety mechanism may transiently decrease the rate of $[\text{Ca}^{2+}]_i$ rise [51], but *permanently* increased Ca^{2+} entry during *sustained* ischemia would inevitably lead to high probability of triggered arrhythmias and *permanent* mitochondrial and subsequent cellular damage. Interestingly, during the early phase of ischemia, the primary source of Ca_i^{2+} increase is the SR, for two important reasons. First, the open probability of RyR2s is increasing when $[\text{Ca}^{2+}]_i$ reaches micromolar levels [52]. Second, SERCA2 activity is depressed if ATP delivery is compromised. The initial elevation in $[\text{Ca}^{2+}]_i$ further increases open probability of RyRs, leading to additional Ca^{2+} release from SR. In contrast, during the late phase of ischemia, and especially during reperfusion, Ca_i^{2+} accumulation is further accelerated by uptake of *extracellular* Ca^{2+} through the *reverse mode* transport of NCX enhanced both by membrane depolarization and increased $[\text{Na}^+]_i$.

Upon reperfusion, $[\text{Ca}^{2+}]_i$ may either further increase due to the sustained entry of extracellular Ca^{2+} , invariably leading to cell death, or – if the level of ischemia was moderate – progressively normalize, leading to survival of the cell. During sustained ischemia, $[\text{Na}^+]_i$ gradually increases; however, as NHE1 is temporarily inactivated due to low pH_o , its increase via NCX1 is limited. During the initial phase of reperfusion, pH_o rapidly recovers, while pH_i still remains relatively low. The large pH gradient fully activates NHE1, inducing a second, very rapid increase in $[\text{Na}^+]_i$. Since $[\text{Ca}^{2+}]_i$ is also high, Na^+ -dependent inactivation of NCX1 is not feasible. Indeed, largely elevated $[\text{Na}^+]_i$ further accelerates the reverse mode activity of NCX1. The rapid and dramatic gain in $[\text{Ca}^{2+}]_i$ may facilitate extreme Ca_i^{2+} overload (calcium paradox), often leading to reperfusion-induced cellular injury. The subsequent depolarization enhances arrhythmia propensity.

Another major problem during reperfusion is the rapid induction of a burst of free oxygen radicals. The reason for this is the substantially decreased amount of free radical scavengers combined with markedly elevated ROS production. Oxygen free radicals were shown to significantly participate in the induction of the cellular Ca^{2+} overload, increased I_{ti} and triggered arrhythmias, and were reported to harmfully modulate the activity of all major Ca^{2+} transporters, including NCX1 [53, 54]. Ca^{2+} leak and window Na^+ current may be enhanced during reperfusion, leading to further aggravation of Ca^{2+} overload and substantial depolarization.

Under chronic ischemic conditions (postinfarction myocardial remodeling, IHD), overactivation of endothelin-1 (ET-1), angiotensin II (Ang II), and norepinephrine (NE) signaling pathways promote NHE1 expression and synthesis. Permanent NHE1

activation leads to increased intracellular Ca^{2+} and Na^+ levels. In acute responses, these shifts result in sustained Ca_i^{2+} overload, increased arrhythmia propensity, and activation of intracellular necrotic/apoptotic pathways, while chronic overactivation of these signaling pathways lead to transcriptional level changes induced via multiple Ca^{2+} , and Na^+ -dependent mechanisms promoting ventricular remodeling, hypertrophy, and finally heart failure.

30.5 Inhibition of the NCX1 and NHE1 as Possible Pharmacological Strategy in Ventricular Arrhythmias

30.5.1 *The Effects of Acute NCX1 Inhibition in Ventricular Arrhythmia Models*

Antiarrhythmic effects of NCX1 inhibition are controversial, primarily due to the lack of specific inhibitors. Amran et al. [55] compared antiarrhythmic efficacy of KB-R7943 and SEA0400 in guinea pigs on aconitine-induced triggered arrhythmias. KB-R7943 suppressed ventricular tachycardia, but SEA0400 was found ineffective. They concluded that the less specific KB-R7943, in addition to suppressing NCX1, also decreases Na_i^+ and Ca_i^{2+} overload through inhibiting Na^+ and Ca^{2+} channels. NCX1 was proposed not to be involved in aconitine-induced triggered activity and the protective effect of KB-R7943 has been related to a different inhibitory mechanism.

In isolated cardiomyocytes treated with 50 $\mu\text{M/L}$ strophanthidine, KB-R7943 reduced diastolic $[\text{Ca}^{2+}]_i$ and abolished spontaneous Ca^{2+} oscillations, without preventing the inotropic action of strophanthidin [56]. In guinea pig, papillary muscles 10 μM KB-R7943 decreased the incidence and shortened the duration of reoxygenation-induced arrhythmias [57]. In an in vivo rat model, KB-R7943 suppressed ischemia–reperfusion-induced ventricular fibrillation [58], while in a similar study, it failed to significantly affect coronary ligation- and reperfusion-induced arrhythmias [59]. In a guinea pig, arrhythmia model pretreatment with 3 mg/kg KB-R7943 increased the ouabain dose required to induce ventricular arrhythmias and delayed the onset of arrhythmias and cardiac arrest following ouabain infusion [60]. Other studies in the rat, rabbit, and dog also reported controversial results, leaving open the questions of dose-related problems of KB-R 7943 specificity on NCX1.

Postischemic administration of SEA0400 effectively suppressed the incidence of ventricular fibrillation and mortality induced by coronary ligation and reperfusion in an in vivo rat model [61]. The novel NCX inhibitor, YM-244769, was also effective in prevention of ischemia–reperfusion-induced ventricular tachycardia and fibrillation in rats [62]. In contrast, neither preischemic nor postischemic administration of SEA0400 could influence the incidence of ischemia–reperfusion-induced arrhythmias in dogs, while the drug was shown to exert a suppressive effect

on digitalis induced tachyarrhythmias [63]. In canine papillary muscles, APD prolongation induced EADs, and in isolated Purkinje fibers, the strophanthin-induced DADs were substantially decreased (Fig. 30.3) following the application of SEA0400

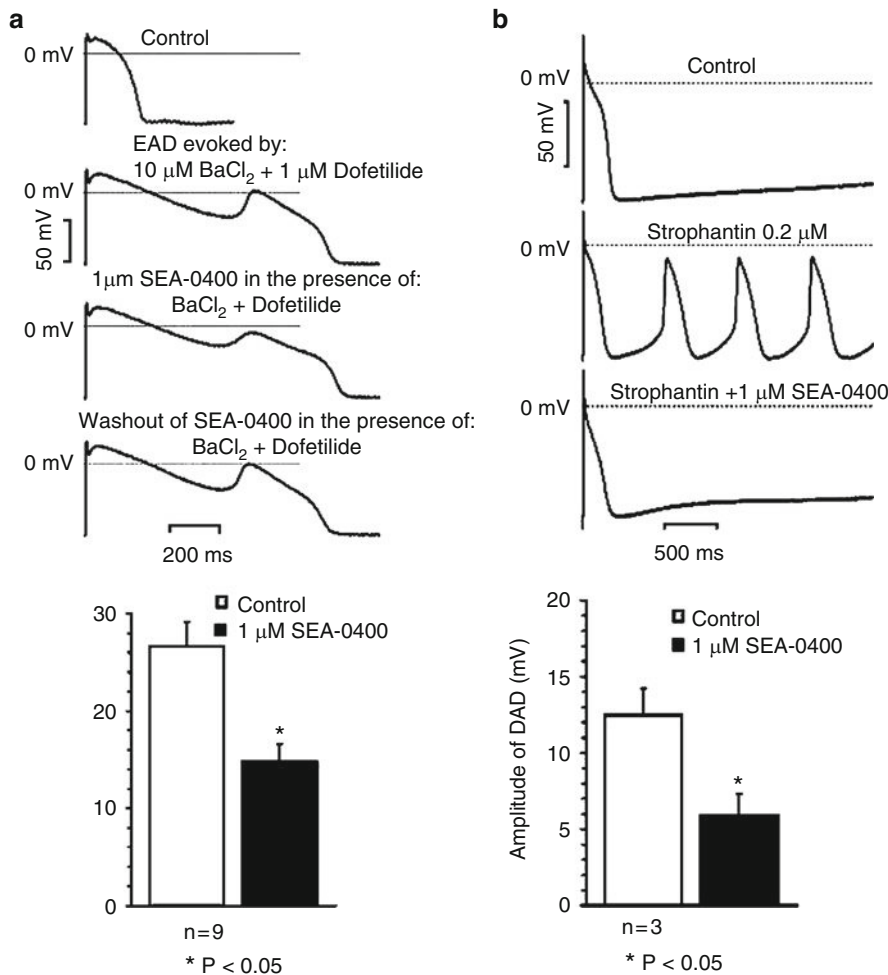


Fig. 30.3 Blocking effect of SEA-0400 on EADs and DADs in canine myocardium. (a) The effect of 1 μM SEA-0400 on EADs in right ventricular papillary muscles, stimulated at slow cycle lengths (1,500–3,000 ms) in the presence of 1 μM dofetilide plus 10 μM BaCl_2 . On the left, the results of a representative experiment are shown, and on the right, the average values of the amplitude of EADs are presented before (open bars) and after (filled bars) the administration of SEA-0400. (b) The effect of SEA-0400 on the delayed afterdepolarization (DAD) in canine cardiac Purkinje fibers, superfused with 0.2 μM strophanthine. A train of 40 stimuli was applied at a cycle length of 400 ms, followed by a 20-s long stimulation-free period that generated DADs. On the left, results of a representative experiment are shown, and on the right, average values of the amplitude of DADs are given before (open bars) and after (filled bars) the application of 1 μM SEA-0400. (Reproduced from [64])

(1 μ M), which fairly selectively inhibits NCX1 [64]. These data argue for possible antiarrhythmic effect of NCX1 inhibition in triggered arrhythmias.

30.5.2 *The Effects of Acute NHE1 Inhibition in Ventricular Arrhythmia Models*

Both ischemia and reperfusion can increase the incidence of fatal cardiac arrhythmias. It was suggested long ago that inhibiting NHE1 during ischemia and/or reperfusion may have beneficial effects on myocardium. Numerous investigators have reported that NHE1 inhibitors can abolish ischemia–reperfusion-induced arrhythmias. Even low concentration of amiloride, a nonselective NHE inhibitor, suppressed sustained ventricular tachyarrhythmia in experimental MI in dogs, *in vivo*. It was also effective to suppress symptomatic ventricular tachycardia in humans, but not to the high degree observed in the dog model [65]. In subsequent clinical studies, amiloride suppressed spontaneous ventricular premature beats. If administered before ischemia *and* during reperfusion, EIPA and HOE 694 also afforded substantial protection against reperfusion-induced ventricular fibrillation [66–68]. However, the clinical studies with cariporide derivatives are still controversial and have not fulfilled the expectations [69–72].

30.6 Conclusions

There is a plethora of experimental evidence that both NCX1 and NHE1 play vital roles not only in the regulation of the myocardial Ca^{2+} homeostasis, but also in arrhythmogenesis. Nonetheless, our understanding on how these transporters function and how they are regulated is far from being satisfactory. Therefore, further intensive research is needed in these directions. Though clinical data with NHE1 inhibition are not yet satisfactory, combination of NHE1 blockade with other cardioprotective mechanisms may have improved beneficial effects. For example, proper combination of NCX1 *and* NHE1 inhibition may be an interesting and important new approach, but to our knowledge, no such experimental work has been done, so far. Another promising approach could be enhancing NCX1 activity in the forward mode during the systole in acute Ca^{2+} overload, but subsequent diastolic depolarization and arrhythmia can be a potential risk.

A special potential implication of the NCX1 inhibition is the prevention of triggered arrhythmias in heart failure. Partial blockade of the upregulated NCX1 may decrease the magnitude of EADs and DADs in HF, preventing propagating extrasystoles and enhanced dispersion of repolarization without marked interference with systolic and diastolic Ca^{2+} levels. If the NCX1 block is incomplete and other cardiac Ca^{2+} extrusion mechanisms are functioning, Ca^{2+} overload probably can be avoided. Future work with more specific NCX1 inhibitors is necessary to address this possibility.

References

1. Bers DM. Excitation-contraction coupling and cardiac contractile force. Dordrecht: Kluwer Academic; 2001.
2. Hryshko LV. Tissue-specific modes of Na/Ca exchanger regulation. *Ann NY Acad Sci.* 2002;976:166–75.
3. Blaustein MP, Lederer WJ. Sodium/calcium exchange: its physiological implications. *Physiol Rev.* 1999;79(3):763–854.
4. Egger M, Niggli E. Regulatory function of Na-Ca exchange in the heart: milestones and outlook. *J Membr Biol.* 1999;168(2):107–30.
5. Philipson KD, Nicoll DA. Sodium-calcium exchange: a molecular perspective. *Annu Rev Physiol.* 2000;62:111–33.
6. Lytton J. Na+/Ca₂₊ exchangers: three mammalian gene families control Ca₂₊ transport. *Biochem J.* 2007;406(3):365–82.
7. Pogwizd SM, Bers DM. Cellular basis of triggered arrhythmias in heart failure. *Trends Cardiovasc Med.* 2004;14(2):61–6.
8. Scoote M, Williams AJ. Myocardial calcium signalling and arrhythmia pathogenesis. *Biochem Biophys Res Commun.* 2004;322(4):1286–309.
9. Sipido KR. Calcium overload, spontaneous calcium release, and ventricular arrhythmias. *Heart Rhythm.* 2006;3(8):977–9.
10. Homma N, Amran MS, Nagasawa Y, Hashimoto K. Topics on the Na+/Ca₂₊ exchanger: involvement of Na+/Ca₂₊ exchange system in cardiac triggered activity. *J Pharmacol Sci.* 2006;102(1):17–21.
11. Ter Keurs HE, Boyden PA. Calcium and arrhythmogenesis. *Physiol Rev.* 2007;87(2):457–506.
12. Nattel S, Maguy A, Le Bouter S, Yeh YH. Arrhythmogenic ion-channel remodeling in the heart: heart failure, myocardial infarction, and atrial fibrillation. *Physiol Rev.* 2007;87(2):425–56.
13. Henderson SA, Goldhaber JI, So JM, Han T, Motter C, Ngo A, et al. Functional adult myocardium in the absence of Na+-Ca₂₊ exchange: cardiac-specific knockout of NCX1. *Circ Res.* 2004;95(6):604–11.
14. Pott C, Philipson KD, Goldhaber JI. Excitation-contraction coupling in Na+-Ca₂₊ exchanger knockout mice: reduced transsarcolemmal Ca₂₊ flux. *Circ Res.* 2005;97(12):1288–95.
15. Weber CR, Piacentino 3rd V, Ginsburg KS, Houser SR, Bers DM. Na(+)-Ca(2+) exchange current and submembrane [Ca(2+)] during the cardiac action potential. *Circ Res.* 2002;90(2):182–9.
16. Doering AE, Lederer WJ. The mechanism by which cytoplasmic protons inhibit the sodium-calcium exchanger in guinea-pig heart cells. *J Physiol.* 1993;466:481–99.
17. Schulze DH, Muqhal M, Lederer WJ, Ruknudin AM. Sodium/calcium exchanger (NCX1) macromolecular complex. *J Biol Chem.* 2003;278(31):28849–55.
18. Fujioka Y, Komeda M, Matsuoka S. Stoichiometry of Na+-Ca₂₊ exchange in inside-out patches excised from guinea-pig ventricular myocytes. *J Physiol.* 2000;523(Pt 2):339–51.
19. Janvier NC, Harrison SM, Boyett MR. The role of inward Na(+)-Ca₂₊ exchange current in the ferret ventricular action potential. *J Physiol.* 1997;498(Pt 3):611–25.
20. Weber CR, Ginsburg KS, Bers DM. Cardiac submembrane [Na+] transients sensed by Na+-Ca₂₊ exchange current. *Circ Res.* 2003;92(9):950–2.
21. Shannon TR, Bers DM. Integrated Ca₂₊ management in cardiac myocytes. *Ann NY Acad Sci.* 2004;1015:28–38.
22. Greenstein JL, Hinch R, Winslow RL. Mechanisms of excitation-contraction coupling in an integrative model of the cardiac ventricular myocyte. *Biophys J.* 2006;90(1):77–91.
23. Sher AA, Noble PJ, Hinch R, Gavaghan DJ, Noble D. The role of the Na+/Ca₂₊ exchangers in Ca₂₊ dynamics in ventricular myocytes. *Prog Biophys Mol Biol.* 2008;96(1–3):377–98.

24. Sanders L, Rakovic S, Lowe M, Mattick PA, Terrar DA. Fundamental importance of Na⁺-Ca²⁺ exchange for the pacemaking mechanism in guinea-pig sino-atrial node. *J Physiol.* 2006;571(Pt 3):639–49.
25. Karmazyn M, Gan XT, Humphreys RA, Yoshida H, Kusumoto K. The myocardial Na(+)–H(+) exchange: structure, regulation, and its role in heart disease. *Circ Res.* 1999;85(9):777–86.
26. Avkiran M. Basic biology and pharmacology of the cardiac sarcolemmal sodium/hydrogen exchanger. *J Card Surg.* 2003;18 Suppl 1:3–12.
27. Fliegel L. Molecular biology of the myocardial Na⁺/H⁺ exchanger. *J Mol Cell Cardiol.* 2008;44(2):228–37.
28. Slepkov ER, Rainey JK, Sykes BD, Fliegel L. Structural and functional analysis of the Na⁺/H⁺ exchanger. *Biochem J.* 2007;401(3):623–33.
29. Cingolani HE, Ennis IL. Sodium-hydrogen exchanger, cardiac overload, and myocardial hypertrophy. *Circulation.* 2007;115(9):1090–100.
30. Karmazyn M, Kilic A, Javadov S. The role of NHE-1 in myocardial hypertrophy and remodelling. *J Mol Cell Cardiol.* 2008;44(4):647–53.
31. Dampney RA, Coleman MJ, Fontes MA, Hirooka Y, Horiuchi J, Li YW, et al. Central mechanisms underlying short- and long-term regulation of the cardiovascular system. *Clin Exp Pharmacol Physiol.* 2002;29(4):261–8.
32. Vaughan-Jones RD, Spitzer KW, Swietach P. Intracellular pH regulation in heart. *J Mol Cell Cardiol.* 2009;46(3):318–31.
33. Baumgartner M, Patel H, Barber DL. Na(+)/H(+) exchanger NHE1 as plasma membrane scaffold in the assembly of signaling complexes. *Am J Physiol Cell Physiol.* 2004;287(4):C844–50.
34. Avkiran M, Cook AR, Cuello F. Targeting Na⁺/H⁺ exchanger regulation for cardiac protection: a RSKy approach? *Curr Opin Pharmacol.* 2008;8(2):133–40.
35. Yang W, Wang H, Fliegel L. Regulation of Na⁺/H⁺ exchanger gene expression. Role of a novel poly(dA.dT) element in regulation of the NHE1 promoter. *J Biol Chem.* 1996;271(34):20444–9.
36. Gan XT, Chakrabarti S, Karmazyn M. Modulation of Na⁺/H⁺ exchange isoform 1 mRNA expression in isolated rat hearts. *Am J Physiol.* 1999;277(3 Pt 2):H993–8.
37. Boutjdir M, Restivo M, Wei Y, Stergiopoulos K, el-Sherif N. Early afterdepolarization formation in cardiac myocytes: analysis of phase plane patterns, action potential, and membrane currents. *J Cardiovasc Electrophysiol.* 1994;5(7):609.
38. Volders PG, Vos MA, Szabo B, Sipido KR, de Groot SH, Gorgels AP, et al. Progress in the understanding of cardiac early afterdepolarizations and torsades de pointes: time to revise current concepts. *Cardiovasc Res.* 2000;46(3):376–92.
39. Fedida D, Noble D, Rankin AC, Spindler AJ. The arrhythmogenic transient inward current iTI and related contraction in isolated guinea-pig ventricular myocytes. *J Physiol.* 1987;392:523–42.
40. Marks AR, Priori S, Memmi M, Kontula K, Laitinen PJ. Involvement of the cardiac ryanodine receptor/calcium release channel in catecholaminergic polymorphic ventricular tachycardia. *J Cell Physiol.* 2002;190(1):1–6.
41. Miura M, Boyden PA, ter Keurs HE. Ca²⁺ waves during triggered propagated contractions in intact trabeculae. *Am J Physiol.* 1998;274(1 Pt 2):H266–76.
42. Wang Y, Meyer JW, Ashraf M, Shull GE. Mice with a null mutation in the NHE1 Na⁺-H⁺ exchanger are resistant to cardiac ischemia-reperfusion injury. *Circ Res.* 2003;93(8):776–82.
43. Marx SO, Reiken S, Hisamatsu Y, Jayaraman T, Burkhoff D, Rosemblit N, et al. PKA phosphorylation dissociates FKBP12.6 from the calcium release channel (ryanodine receptor): defective regulation in failing hearts. *Cell.* 2000;101(4):365–76.
44. Stillitano F, Lonardo G, Zicha S, Varro A, Cerbai E, Mugelli A, et al. Molecular basis of funny current (If) in normal and failing human heart. *J Mol Cell Cardiol.* 2008;45(2):289–99.

45. Sipido KR, Volders PG, de Groot SH, Verdonck F, Van de Werf F, Wellens HJ, et al. Enhanced Ca(2+) release and Na/Ca exchange activity in hypertrophied canine ventricular myocytes: potential link between contractile adaptation and arrhythmogenesis. *Circulation*. 2000;102(17):2137–44.
46. Sipido KR, Volders PG, Vos MA, Verdonck F. Altered Na/Ca exchange activity in cardiac hypertrophy and heart failure: a new target for therapy? *Cardiovasc Res*. 2002;53(4):782–805.
47. Veldkamp MW, Verkerk AO, van Ginneken AC, Baartscheer A, Schumacher C, de Jonge N, et al. Norepinephrine induces action potential prolongation and early afterdepolarizations in ventricular myocytes isolated from human end-stage failing hearts. *Eur Heart J*. 2001;22(11):955–63.
48. Benardeau A, Hatem SN, Rucker-Martin C, Le Grand B, Mace L, Dervanian P, et al. Contribution of Na+/Ca2+ exchange to action potential of human atrial myocytes. *Am J Physiol*. 1996;271(3 Pt 2):H1151–61.
49. Allen DG, Orchard CH. The effects of changes of pH on intracellular calcium transients in mammalian cardiac muscle. *J Physiol*. 1983;335:555–67.
50. Hulme JT, Orchard CH. Effect of acidosis on Ca2+ uptake and release by sarcoplasmic reticulum of intact rat ventricular myocytes. *Am J Physiol*. 1998;275(3 Pt 2):H977–87.
51. Duchen MR. Mitochondria and Ca(2+)in cell physiology and pathophysiology. *Cell Calcium*. 2000;28(5–6):339–48.
52. Meissner G. Molecular regulation of cardiac ryanodine receptor ion channel. *Cell Calcium*. 2004;35(6):621–8.
53. Reeves JP, Bailey CA, Hale CC. Redox modification of sodium-calcium exchange activity in cardiac sarcolemmal vesicles. *J Biol Chem*. 1986;261(11):4948.
54. Goldhaber JI. Free radicals enhance Na+/Ca2+ exchange in ventricular myocytes. *Am J Physiol*. 1996;271(3 Pt 2):H823–33.
55. Amran MS, Hashimoto K, Homma N. Effects of sodium-calcium exchange inhibitors, KB-R7943 and SEA0400, on aconitine-induced arrhythmias in guinea pigs *in vivo*, *in vitro*, and in computer simulation studies. *J Pharmacol Exp Ther*. 2004;310(1):83–9.
56. Satoh H, Ginsburg KS, Qing K, Terada H, Hayashi H, Bers DM. KB-R7943 block of Ca(2+) influx via Na(+)/Ca(2+) exchange does not alter twitches or glycoside inotropy but prevents Ca(2+) overload in rat ventricular myocytes. *Circulation*. 2000;101(12):1441–6.
57. Mukai M, Terada H, Sugiyama S, Satoh H, Hayashi H. Effects of a selective inhibitor of Na+/Ca2+ exchange, KB-R7943, on reoxygenation-induced injuries in guinea pig papillary muscles. *J Cardiovasc Pharmacol*. 2000;35(1):121–8.
58. Nakamura A, Harada K, Sugimoto H, Nakajima F, Nishimura N. Effects of KB-R7943, a novel Na+/Ca2+ exchange inhibitor, on myocardial ischemia/reperfusion injury. *Nippon Yakurigaku Zasshi*. 1998;111(2):105–15.
59. Lu HR, Yang P, Remeyen P, Saels A, Dai DZ, De Clerck F. Ischemia/reperfusion-induced arrhythmias in anaesthetized rats: a role of Na+ and Ca2+ influx. *Eur J Pharmacol*. 1999;365(2–3):233–9.
60. Watano T, Harada Y, Harada K, Nishimura N. Effect of Na+/Ca2+ exchange inhibitor, KB-R7943 on ouabain-induced arrhythmias in guinea-pigs. *Br J Pharmacol*. 1999;127(8):1846–50.
61. Takahashi K, Takahashi T, Suzuki T, Onishi M, Tanaka Y, Hamano-Takahashi A, et al. Protective effects of SEA0400, a novel and selective inhibitor of the Na+/Ca2+ exchanger, on myocardial ischemia-reperfusion injuries. *Eur J Pharmacol*. 2003;458(1–2):155–62.
62. Kuramochi T, Kakefuda A, Yamada H, Tsukamoto I, Taguchi T, Sakamoto S. Discovery of an N-(2-aminopyridin-4-ylmethyl)nicotinamide derivative: a potent and orally bioavailable NCX inhibitor. *Bioorg Med Chem*. 2005;13(12):4022–36.
63. Nagasawa Y, Zhu BM, Chen J, Kamiya K, Miyamoto S, Hashimoto K. Effects of SEA0400, a Na+/Ca2+ exchange inhibitor, on ventricular arrhythmias in the *in vivo* dogs. *Eur J Pharmacol*. 2005;506(3):249–55.

64. Nagy ZA, Virág L, Toth A, Biliczki P, Acsai K, Banyasz T, et al. Selective inhibition of sodium-calcium exchanger by SEA-0400 decreases early and delayed after depolarization in canine heart. *Br J Pharmacol.* 2004;143(7):827–31.
65. Duff HJ, Mitchell LB, Kavanagh KM, Manyari DE, Gillis AM, Wyse DG. Amiloride. Antiarrhythmic and electrophysiologic actions in patients with inducible sustained ventricular tachycardia. *Circulation.* 1989;79(6):1257–63.
66. du Toit EF, Opie LH. Role for the Na⁺/H⁺ exchanger in reperfusion stunning in isolated perfused rat heart. *J Cardiovasc Pharmacol.* 1993;22(6):877–83.
67. Scholz W, Albus U, Lang HJ, Linz W, Martorana PA, Englert HC, et al. Hoe 694, a new Na⁺/H⁺ exchange inhibitor and its effects in cardiac ischaemia. *Br J Pharmacol.* 1993;109(2):562–8.
68. Sack S, Mohri M, Schwarz ER, Arras M, Schaper J, Ballagi-Pordány G, et al. Effects of a new Na⁺/H⁺ antiporter inhibitor on postischemic reperfusion in pig heart. *J Cardiovasc Pharmacol.* 1994;23(1):72–8.
69. Theroux P, Chaitman BR, Danchin N, Erhardt L, Meinertz T, Schroeder JS, et al. Inhibition of the sodium-hydrogen exchanger with cariporide to prevent myocardial infarction in high-risk ischemic situations. Main results of the GUARDIAN trial. Guard during ischemia against necrosis (GUARDIAN) Investigators. *Circulation.* 2000;102(25):3032–8.
70. Zeymer U, Suryapranata H, Monassier JP, Opolski G, Davies J, Rasmanis G, et al. The Na(+) / H(+) exchange inhibitor eniporide as an adjunct to early reperfusion therapy for acute myocardial infarction. Results of the evaluation of the safety and cardioprotective effects of eniporide in acute myocardial infarction (ESCAMI) trial. *J Am Coll Cardiol.* 2001;38(6):1644–50.
71. Rupprecht HJ, Vom Dahl J, Terres W, Seyfarth KM, Richardt G, Schultheibeta HP, et al. Cardioprotective effects of the Na(+)/H(+) exchange inhibitor cariporide in patients with acute anterior myocardial infarction undergoing direct PTCA. *Circulation.* 2000;101(25):2902–8.
72. Mentzer Jr RM, Lasley RD, Jessel A, Karmazyn M. Intracellular sodium hydrogen exchange inhibition and clinical myocardial protection. *Ann Thorac Surg.* 2003;75(2):S700–8.

Chapter 31

TRP Channels in Cardiac Arrhythmia: Their Role During Purinergic Activation Induced by Ischemia

Guy Vassort and Julio Alvarez

Abbreviations

[Ca ²⁺] _i	Intracellular Ca ²⁺ concentration
Ang II	Angiotensin II
ATP	Adenosine 5'-triphosphate
CNRS	Nonspecific cationic current
DAG	Diacylglycerol
IP ₃	Inositol-1,4,5-triphosphate
PIP2	Phosphatidylinositol 4,5-bisphosphate
PKC	Protein kinase C
PLC	Phospholipase C
SAC	Stretch-activated channels
SERCA	Sarcoplasmic/endoplasmic reticulum Ca ²⁺ -ATPase
SHR	Spontaneously hypertensive rats
SiRNA	Small interfering RNA
SOC	Store-operated channel
SR	Sarcoplasmic reticulum
TRPA	Transient receptor potential “Ankyrin”
TRPC	Transient receptor potential “Canonical”
TRPM	Transient receptor potential “Melastatin”
TRPML	Transient receptor potential “Mucolipin”
TRPN	Transient receptor potential “NOMP”
TRPP	Transient receptor potential “Polycystin”
TRPV	Transient receptor potential “Vanilloid”
UTP	Uridine 5'-triphosphate

G. Vassort (✉)

INSERM U-1046 Physiopathologie cardiovasculaire, CHU Arnaud de Villeneuve, Montpellier,
France

e-mail: guy.vassort@inserm.fr

J. Alvarez

Laboratorio de Electrofisiología, Instituto de Cardiología, La Habana, Cuba

31.1 Introduction

Very recently a new large family of cationic channels expressed in most cell types in mammals has been described. The founding protein member was discovered in *Drosophila melanogaster* in which it contributes to phototransduction by conducting calcium ions; however, a mutation induces a transitory response despite sustained lightening [1]. The corresponding *trp* gene was cloned in 1989 [2] that led to identification of a cationic channel permeable to Ca^{2+} ions. Each single TRP subunit is made of six transmembrane domains with a pore between the fifth and sixth transmembranous segments, a structure very similar to voltage-dependent K^+ (Kv) channels. Like Kv channels, TRP subunits coassemble in homo- or heterotetramers to form a nonselective cation channel [3–5]. According to their amino acids sequences, TRP channels comprise seven families: TRPC (canonical), TRPM (melanostatin), TRPV, TRPA (ankyrin), TRPP (polycystin), TRPML (mucolipin), and TRPN (NO mechanopotential, NOMP). Besides the 13 members initially reported in *Drosophila*, up to 28 members are described in mammals, although TRPN are not found in mammals. Detailed reviews of TRP channels [5–9] and databases such as <http://www.ensembl.org> are available.

The TRP channels are permeant to cations. Most carry Ca^{2+} with a $P_{\text{Ca}}/P_{\text{Na}}$ permeability ratio varying from 0.3 to 10. The pore structure plays a major role in permeability and selectivity of a given channel. The functional significance of pore-structure alterations on the properties of TRP channels has been recently reviewed [10]. The TRP channels can be activated by direct binding of ligands, following activation of G-protein coupled receptors or tyrosine kinase receptors modulating PLC activity and IP_3 and DAG production, or directly by physical factors including temperature, hypo-osmotic shock, and mechanical stimuli [8, 11]. They are weakly sensitive to membrane potential that clearly distinguish them from voltage-dependent channels whose study has been so successful using the patch-clamp technique.

The TRP channels play a major role in the integration of most information arising from the external medium or the detection of the physical properties of the cellular surrounding. The physiological processes involved are more and more numerous. They are key players in photosensory, thermosensory, chemosensory, and mechanosensory activities [12]. Some channels are constitutively open while others are activated according to the Ca^{2+} load of the intracellular stores. Indeed, some channels are located in the intracellular membranes. Remarkably, the biophysical properties of TRP channels were first described following their overexpression in heterologous systems, even if some properties are quite specific to the overexpressing cell type, the level of expression, or their cellular environment. The demonstration of their physiological and pathological roles in a given cell type is made difficult by the lack of natural or synthetic modulators. Moreover, some TRP channels are heterotetramers that have functions that differ significantly from the corresponding homotetrameric channels. The use of dominant-negative variants, siRNA or antisense technologies, can alter both homo- and heterotetramers, in addition to the experimental artifacts related to cell culturing and compensatory

mechanisms in knockdown studies. Finally, most of these channels have a very slow turnover such that their effective knockdown may require several days. Various transgenic mice are becoming available; however, the functional redundancy of TRP channels can complicate interpretation of their phenotypes.

As these channels act as multifunctional cellular sensors and are involved in several fundamental cell functions such as contraction, proliferation, and cell death, investigation of their roles in the control of cardiovascular activities and various cardiovascular diseases is very important. Our present knowledge of TRP channel expression in heart is summarized in Table 31.1. Evidence suggest that up-regulation of TRPC channels is involved in the development of cardiac hypertrophy and heart failure. Also, an increased expression of TRPC channels is associated with vascular remodeling and pulmonary hypertension [33]. Recent investigations

Table 31.1 Transient receptor potential channels expressed in heart and their main activators

TRP	Main activators	Expression in species and tissues				
		Human heart	Mouse heart	Mouse node	Neonatal rat heart	Adult rat heart
C1	DAG, stretch, store depletion			[13]	[14] ^a	
C3	DAG, stretch,		[15, 16]	[13]	[13, 14, 17]	[18] ^b , [19] ^c , [20]
C4	DAG, stretch,			[13]		
C5	DAG, Stretch, Ca ²⁺ [14]	[19] ^c ,			[21] ^d	
C6	DAG, stretch, hypoxia	[22] ^e	[15, 16]	[13]	[14, 17]	
C7	DAG, stretch, store depletion					[18] ^b
V1	Capsaicin, heat >43°C, acidic pH		[23] ^f			
V2	Stretch, heat >52°C		[15]			
V4	Anandamide, arachidonic acid, 4aPDD, stretch		[15]			
V6	Low Ca _i ²⁺ , hyperpolarization		[15]			
M4	Increased Ca _i ²⁺ , heat, decananate,	[24] ^b	[15]	[25]		[26] ^g
M5	Increased Ca _i ²⁺ , heat PIP ₂ ,					[26] ^g
M7	Shear stress, decreased ATP _i and Mg _i ²⁺ ,		[15]			
P1 PKD1		[27, 28]	[27]			
P2 PKD2	Store depletion, increased Ca _i ²⁺ , mechanical stress	[28, 29]	[29]			[30]
P3 PKD2L1	Increased Ca ²⁺	[31, 32]				

^aUp-regulation during hypertrophy

^bAdult rat ventricular cardiomyocytes

^cInduced during failure

^dInduced during SERCA2 silencing

^eUp-regulation during pressure overload in rat and in failing human heart

^fIn cardiac sensory neurons, decreased under diabetes

^gUnder hypertension

have revealed that at least ten mammalian TRPs exhibit mechanosensitivity. In the cardiovascular system in which hemodynamic forces constantly operate, the impact of mechanical stress may be particularly significant [34]. This chapter presents a short overview of our current knowledge about the general properties and the physiological and pathological roles of TRP channels. More specifically, this chapter highlights that several TRPC and TRPM4 participate in some features of cardiac arrhythmias. Ultimately, TRP channels will become important novel pharmacological targets for the treatment of human cardiovascular diseases including arrhythmia.

31.2 General Properties of TRP Channels

31.2.1 Canonical TRP, TRPC

This family characterized by the common sequence, EWFAR, and lacking the voltage sensors in the 4th transmembrane domain, involves TRPC1, TRPC2, TRPC3/6/7, and TRPC4/5. A comprehensive review of these channels has recently appeared [35]. All these channels are activated following stimulation of receptors known to activate various phospholipase C isoforms, PLC, and are modulated by calmodulin and several proteins that bind Ca^{2+} [36]. Notably, TRPC3/6/7 are activated more specifically by diacylglycerol (DAG), while the cascade leading to TRPC4/5 activation is still controversial. Furthermore Ca^{2+} -store depletion was suggested to activate all the canonical channels [37]. TRPC6 was the first protein of this family reported to be essential during the activation of nonselective cationic channels by α_1 -adrenergic stimulation in smooth muscle of the rabbit portal vein [38].

In cardiac tissues, the presence of mRNA and protein for all TRPC, except TRPC4 and TRPC5, has been reported, although expression may vary with species and age. It was recently suggested that TRPC7 acts as a G protein-activated Ca^{2+} channel mediating angiotensin II-induced myocardial apoptosis [39].

Exhibiting weak cation selectivity, TRPCs also allow for Na^+ entry. Alterations in the Na^+ gradient will interfere with Ca^{2+} distribution via the $\text{Na}^+/\text{Ca}^{2+}$ exchanger. Thus, a limited increase in Na^+ together with a weak depolarization might be sufficient to trigger Ca^{2+} entry. Moreover, TRPC3 and $\text{Na}^+/\text{Ca}^{2+}$ exchanger participate in a protein complex that is activated by PLC in rat cardiomyocytes [40]. A larger complex including also the Na^+ pump has been detected in the transverse–axial-tubular system [20]. Similarly, the simultaneous overexpression in HEK cells of TRPC7 with SERCA induced a local control of $[\text{Ca}^{2+}]_i$ that prevents the inhibition of the TRP channel by Ca^{2+} entry. Indeed, TRPC3 colocalizes with the $\text{Na}^+/\text{Ca}^{2+}$ exchanger and the Na^+ ATPase in the transverse tubular system in rat ventricular cardiomyocytes [41].

31.3 Vanilloid Channels, TRPV

The six members of this family, TRPV1/TRPV2, TRPV3, TRPV4, and TRPV5/TRPV6, form tetrameric complexes that contain 3–5 ankyrin residues in their NH₂ domain. TRPV1–4 channels are all activated by heat and are chemosensory for a large number of endogenous or synthetic ligands. These channels are also important as stretch sensors throughout the animal kingdom [42]. Like TRPC, TRPV1–4 have a permeability ratio P_{Ca}/P_{Na} that varies between 1 and 10 while TRPV5/TRPV6 are 100-fold more permeant to Ca²⁺ ions. Both TRPV5 and TRPV6 channels are regulated by a Ca²⁺-dependent inactivation (half-inactivation ≈100 nM) and demonstrate voltage-dependent block by Mg²⁺ [10].

31.4 Melastatin Channels, TRPM

Eight TRPM channels, TRPM1/TRPM3, TRPM2/TRPM8, TRPM4/TRPM5, and TRPM6/TRPM7, have been described. The first, TRPM1 was so named because of its expression in melanoma cells. A negative correlation exists between TRPM1 expression and melanoma development. All other members of the family are also associated with human tumors [43] and are involved in tumorigenesis, cell proliferation and differentiation. Their permeability to Ca²⁺ and Mg²⁺ varies considerably. TRPM4 and TRPM5 are not permeable to Ca²⁺ whereas TRPM6, TRPM7, as well as some TRPM3 variants have a large permeability to both ions.

TRPM2, TRPM6, and TRPM7 channels are coupled to an enzyme to form “chanzymes” such that the enzymatic domain could modulate the channel activity or vice versa [44]. Thus, TRPM2 exhibits an ADP-ribose hydrolase activity associated with the NUDT9 motif (*human nucleoside diphosphate linked moiety X-type motif 9*) of its C-terminal. Also TRPM2 might be a sensor of the cellular redox status [45]. TRPM6 and TRPM7 contribute to Mg²⁺ homeostasis. Both channels show a high permeability towards this ion while being modulated by its intracellular concentration. Their long C-terminal tail is linked to a domain demonstrating an α-kinase activity such that these proteins are bifunctional [46].

TRPM4 and TRPM5 are both nonpermeant to Ca²⁺ but conduct monovalent ions with a 20–25 pS conductance. Both are good candidates to be the endogenous nonselective cationic channel activated by Ca²⁺. TRPM4 is expressed in sino-atrial node cells and is involved in controlling cardiac rhythmic activity [25]. PIP₂ is a strong TRPM4 modulator. PIP₂ shifted the voltage dependence of TRPM4 activation towards negative potentials and increased the channel Ca²⁺ sensitivity 100-fold. Conversely, its degradation during PLC activation by various mediators (α-adrenergic, muscarinic, angiotensin, etc.) is a remarkable break to TRPM4 activity [10].

31.5 Mucolipin Channels, TRPML

The three subunits expressed in animals, TRPML1–3 are relatively short, with less than 600 amino acids. TRPML1 also has a lipase domain. These channels are all constitutively active, and their activity is increased by Ca^{2+} , decreased by acidosis, and inhibited by amiloride.

31.6 Polycystin Channels, TRPP

This family subsumes the polycystins divided in two structurally quite different groups. The polycystin 1 proteins or PKD1 (polycystic kidney disease 1)-like, and TRPP1-like, including TRPP1, TKDREJ, PKD1L1, PKD1L2, and PKD1L3, are mostly involved in cellular junctions and are coupled to G-proteins. The polycystin 2 proteins or PKD2 (polycystic kidney disease 2)-like, and TRPP2-like including PKD2, PKD2L1, and PKD2L2 today known as TRPP2, TRPP3, and TRPP5, respectively, form a Ca^{2+} channel. Mutations in TRPP1 and TRPP2 cause autosomal dominant polycystic kidney disease. Proteins of the two groups physically heterodimerize to form a multimeric receptor-ion channel complex. Polycystine proteins are involved in multiple functions. TRPP2 is required for cilia movement and in the development of skeletal muscle, kidney, and the heart, particularly its left-right axis. It was also suggested to play a role in fertility. TRPP3 is found abundantly in heart muscle [31] as well as polycystin 1L2 [27].

31.7 Ankyrin Channels, TRPA

The only mammalian member is TRPA1 activated by harmful cold and pungent substances, including isothiocyanates and as shown recently by nicotine [47]. It is insensitive to menthol and capsaicin.

31.8 NO-Mechano-Potential Sensitive Channels, TRPN

These channels, not found in mammals, are characterized by the presence of 29-ankyrin sequence repeats in their C-terminal domain.

One further very important property of TRP proteins is the possibility to form heterotetramers that exhibit characteristics different from the homotetramers [5]. Heteromerization occurs between members of the same group, but also between members of different groups such as the formation of a receptor-operated channel by heteromeric assembly of TRPP2 and TRPC1 or TRPV4 subunits. The TRPC1–TRPP2 channel has several unique properties compared to homomeric

channels, including activation in response to G-protein coupled receptor, specific single channel conductance, and ionic permeability [48].

31.9 TRP Channels and Arrhythmia

The TRP channels are reported to be involved in several cardiovascular diseases including cardiac arrhythmia as reviewed elsewhere [33–35, 38, 49].

31.9.1 *Mechanosensitive TRP Channels*

Mechanical stimulation such as stretch or dilation of the heart is known to modulate the electrical activity of myocytes which suggests that there is a feedback system in the heart, in addition to excitation–contraction coupling, whereby mechanical stimuli modulates electrical activity. This feedback system, often referred to as mechano-electric feedback, has been known for a long time in an extreme example named *commotio cordis* where the heart can be stopped by an external impact applied to the chest without causing tissue damage [50]. More generally, the stretch-induced modulation of electrical activity includes after-depolarization, depolarization of the resting potential, and alteration of the action potential duration. In severe cases, these changes are found to be arrhythmogenic as recognized 20 years ago [51]. It has been suggested that major events of mechano-electric feedback are mediated by the activation of stretch-activated channels, SACs [52–54]. These channels conduct Na^+ but not Ca^{2+} , and most of these channels are sensitive to block by Gd^{3+} . Recent investigations have revealed that at least ten mammalian TRP channels exhibit mechanosensitivity (TRPC1, 5, 6; TRPV1, 2, 4; TRPM3, 7; TRPA1; TRPP2), although the mechanisms underlying the mechanosensitivity appear quite divergent and complex. These include lipid bilayer mechanics, specialized force-transducing structures, biochemical reactions, membrane trafficking, and transcriptional regulation [34]. It can be anticipated that TRPM4 contributes largely to these SACs since overexpression of hTRPM4B in HEK293 cells resulted in the appearance of cation channels that are activated by both negative pressure and Ca^{2+} [55]. Moreover, myocytes isolated from human failing hearts exhibited enhanced stretch sensitivity with increased density of Gd^{3+} -sensitive currents and arrhythmic electrophysiological features [53]. In a recent study, the same group demonstrated that mechanical deformation of murine ventricular myocytes activates TRPC6 channels, together with reducing Kir2.3 channel activity, on the basis that the tarantula peptide GsMTx-4 and the antibody Ab-TRPC6 prevented current activation [56]. Furthermore, the authors proposed that the signaling cascade involves activation by integrins of the AT1 receptors, which trigger the production of nitric oxide and superoxide via NOS3 and NAD(P)H oxidase, respectively, to form peroxynitrite that stimulates the activity of phospholipases [57]. Compelling

evidence have been provided to show that AT1 receptors demonstrate a conformational switch upon mechanical activation while the tight binding of candesartan to the AT1 receptors stabilizes them in their inactive conformation [58].

Pace-making activity in the heart is primarily thought to result from time-dependent decay of the delayed rectifier K⁺ current together with the activation of various inward currents (I_f , “funny” current, T-type, and L-type Ca²⁺ current) and to be facilitated by an elusive inward background current. In Ca²⁺-overloaded Purkinje cells, spontaneous Ca²⁺ release occurs from the SR that could activate the inward Na⁺/Ca²⁺ exchange current (and potentially to the TRPM4 channel, see below). The SOC channels also contribute, as was recently reported in mouse sino-atrial node on the basis that the SOC blocker, SKF96365, slows pace making while blocking the L-type Ca²⁺ channel (by nifedipine) or the Na⁺/Ca²⁺ exchange (by KBR7943) has little or no effect [13, 59]. Furthermore, the authors suggest a complex interaction between SOC, SR, and Na⁺/Ca²⁺ exchange.

31.9.1.1 The Ca²⁺-Activated Nonselective Cation Channel, TRPM4

Cardiac arrhythmia might occur in a variety of conditions that includes activation of an inward current when [Ca²⁺]_i is elevated. Since the first measurements of single-channel openings in cardiomyocytes revealed a Ca²⁺-activated nonselective cation channel, the so-called CNRS channel [60], considerable effort has been devoted to identify its molecular basis. Functional characterization of a Ca²⁺-activated nonselective cationic current in human atrial cardiomyocytes showed that the channel is equally permeable to Na⁺ and K⁺ but not permeable to Ca²⁺ and exhibits a 25-pS conductance. These properties match those of TRPM4 [24] and marked this channel as a serious candidate for sustaining the delayed after-depolarizations (DADs) observed under conditions of Ca²⁺ overload. TRPM4 is more expressed in atrial than in ventricular myocardium [10]. TRPM4 is much higher in spontaneously hypertensive rats (SHR) than in Wistar-Kyoto rats. TRPM4 is also expressed in mouse sino-atrial node cells [25]. TRPM4 is inhibited by flufenamic acid, a nonsteroidal anti-inflammatory drug and by glibenclamide, a hypoglycemic agent [24]. TRPM4 is sensitive to PIP₂ such that the activation of PLC could reduce channel activity [10]. Agonists could favor TRPM4 activation by increasing Ca²⁺ release from the sarcoplasmic reticulum (SR) following inositol-1,4,5-triphosphate (IP₃) production. It was reported that the Ca²⁺-activated nonselective cationic channel could be activated by external ATP or its poorly degradable homolog in cultured rat ventricular myocytes [61]. It has also been proposed that during ATP application, the transient early surge of nonselective cationic current could be carried by TRPM4 channel as the consequence of its activation by free Ca²⁺ following subsarcolemmal acidification induced by activation of the CO₃H⁻/Cl⁻ exchanger and Ca²⁺ release after its displacement by H⁺ from binding sites [62]. In support of this assumption, both acidosis and transient current activation require the presence of Mg²⁺. Thus, TRPM4 could be a key player in the generation and/or perturbation of cardiac rhythm in any condition implying Ca²⁺ overload.

31.9.2 Purinergic Receptor-Mediated Activation of TRPC Channels

Cardiac automaticity might also result from the activation, following receptor stimulation, of nonselective cationic current that would appear inward and depolarizing. Such appears to be the case during the application of ATP to isolated cardiomyocytes [62, 63]. In fact, ATP and UTP are known to be released during various pathophysiological conditions, including hypoxia during which they appeared to be associated with arrhythmia in animal models and humans [64, 65]. The diverse range of physiological actions of ATP was early recognized by Drury and Szent-Györgyi [66]. Moreover, the role of ATP as a “nonadrenergic, noncholinergic neurotransmitter” rather than an energy supplier was reported in 1970 by Burnstock [67]. Today, ionotropic P2X(1–7) receptors and metabotropic P2Y(1–14) receptors have been cloned and their mRNA found in cardiomyocytes [68–71]. P2X receptors, first described in 1994 [72, 73], are ligand-gated ion channels opened by micromolar extracellular ATP. Although mRNA of P2X(1–7) are found in heart, the precise role of these receptors is unknown. The first cloning of a P2Y receptor was reported in 1993 from chick brain [74]. Subsequently, most P2Y were shown to have a wide tissue distribution. All members of the P2Y family couple to heteromeric G-proteins that, in turn, activate intracellular second messengers to modulate the physiological functions of the cells. In the cardiomyocytes, ATP was demonstrated to modulate most cellular activities including ionic currents, Ca^{2+} transients, pH, as well as kinases and lipases and many secondary messengers to control contractile force [71]. Particularly several electrophysiological studies have, since the late 1980s, reported that ATP activates transient nonspecific cationic currents in frog, rat, and guinea pig heart [62, 75, 76].

More recently, a more detailed analysis in ventricular cardiomyocytes isolated from various species including human revealed that ATP and UTP, in their free form, ATP^{4-} and UTP^{4-} , activate two nonspecific cationic currents (Fig. 31.1). Thus, besides the fast transient nonspecific cationic current that we reported earlier

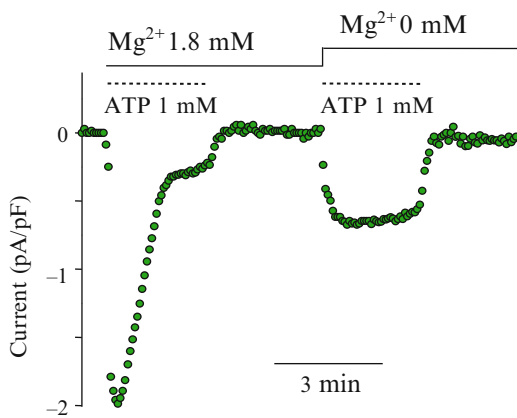


Fig. 31.1 Purinergic activation of ionic currents at resting potential. ATP (1 mM) elicits two inward currents in a rat cardiomyocyte held at -80 mV . The fast transient current requires the presence of Mg^{2+} in the external solution. Reproduced from [18] with permission

[62], a sustained current with lower amplitude is also activated [18]. However, while the activation of the fast transient current requires the presence of Mg^{2+} , suggesting that MgATP is the probable agonist, the sustained current could be elicited by ATP and UTP, in their free form, ATP^{4-} and UTP^{4-} . At a constant 300 μM free external Ca^{2+} concentration, the EC_{50} of the ATP^{4-} effect determined in various ATP-containing (Mg^{2+} -free) solutions was $\approx 58 \mu M$ (about 0.5 mM ATP added). The ATP-induced current reversed near 0 mV, exhibited a weak inward rectification, and was inhibited by increasing external Ca^{2+} concentrations (Fig. 31.2). Surprisingly, flufenamic acid,

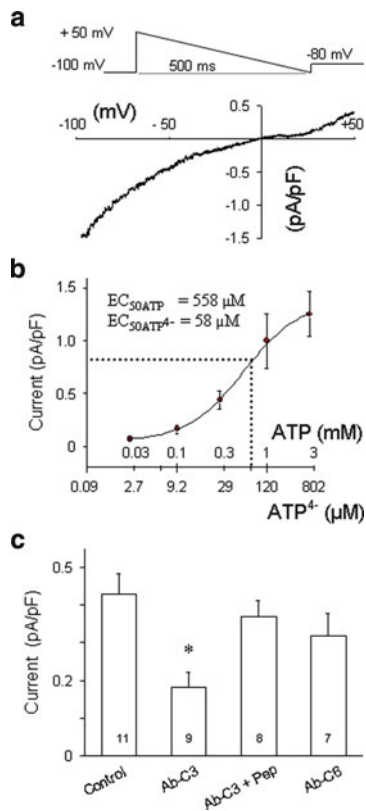


Fig. 31.2 Characterization of the sustained current elicited by ATP in rat ventricular cardiomyocytes under whole-cell patch-clamp. (a) Current–voltage relationship established during a ramp potential after the application of 300 μM ATP in the absence of Mg^{2+} . (b) Dose–response curve of I_{ATP} amplitude elicited by various ATP concentrations at $HP = -80$ mV in a Mg^{2+} -free, 300- μM Ca^{2+} solution ($n = 6$). The apparent half-efficient ATP concentration, EC_{50} was 558 μM corresponding to a calculated $EC_{50-ATP^{4-}}$ of 58 μM . (c) An anti-TRPC3 antibody (Ab-C3) added to the pipette solution (1:200 dilution) significantly reduced I_{ATP} recorded within 5 min after the giga-seal formation. Antibody-induced inhibition was prevented by further adding the TRPC3-antigenic peptide (Ab-C3+ Pep, 1:200) to the pipette solution. Adding the anti-TRPC6 antibody (Ab-C6) to the pipette solution did not significantly affect the ATP-induced current. Number of cells in bars, * $P < 0.05$. Reproduced from [18] with permission

known to inhibit TRPC6, significantly enhanced current amplitude. Using fluorescence experiments, it was verified that channel activity was negligible both in control conditions and in Ca^{2+} -free media since there was no significant Ba^{2+} and Mn^{2+} influx while ATP, applied at 10 μM , triggered marked changes in fluorescence in the presence of one or the other cation. The nonselective cationic channel is a heterotetramer composed of TRPC3 and TRPC7 as evidenced by coimmunoprecipitation. The channel allows cationic flux only in the presence of agonists and exhibits two main conductance levels of 14 and 23 pS. The intracellular application of an anti-TRPC3 antibody markedly inhibits the current [18]. Furthermore, it was shown that this sustained current results from the activation of the metabotropic P2Y2 receptor that leads to DAG formation and the activation of the phospholipase C β . Of note, P2X4-KO mice (as well as P2X1- and P2X1- and P2X4-KO) always exhibited one and the other of the ATP-induced transitory and sustained cationic currents recorded in control [18].

As noted above, Ca^{2+} release from the SR after purine application [71] could also contribute to activation of various TRP channels including TRPM4. The signal transduction cascades activated by ATP/UTP and leading to TRP activation are shown in Fig. 31.3. Thus after purinergic activation, the sustained inward current conducted by the TRP channels together with Ca^{2+} overload and the subsequent activation of the $\text{Na}^+/\text{Ca}^{2+}$ exchanger in the reverse mode could trigger electrical abnormalities (Fig. 31.4).

A major role of TRPC has also been demonstrated in the control of rhythmic activity in the toad pacemaker node [13, 59]. The authors suggested that ATP, by activating P2Y1 receptors, leads to Ca^{2+} depletion and the activation of SOC. Immunochemistry using anti-TRPC1, 3, 4, and 6 antibodies revealed positive labeling in the sinus node or single pacemaker cells. However, no TRPC subtype was yet related to SOC activation. The involvement of SOC in pacemaker activity

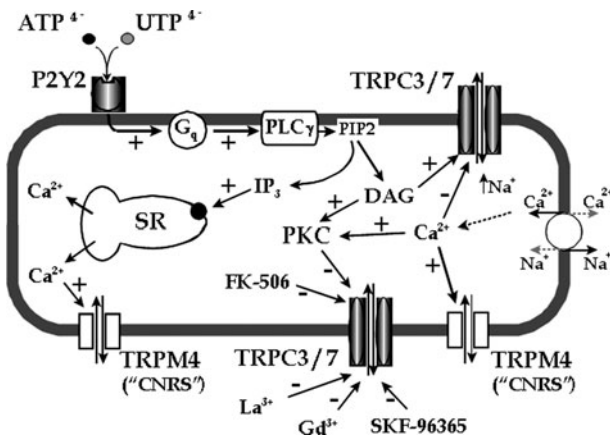


Fig. 31.3 Schematic representation of the biochemical pathways involved after ATP or UTP application, after their free form binds to the P2Y2 purinoceptors on a cardiomyocyte, leading to activation of TRPC3/7 and TRPM4 channels. See text for abbreviations

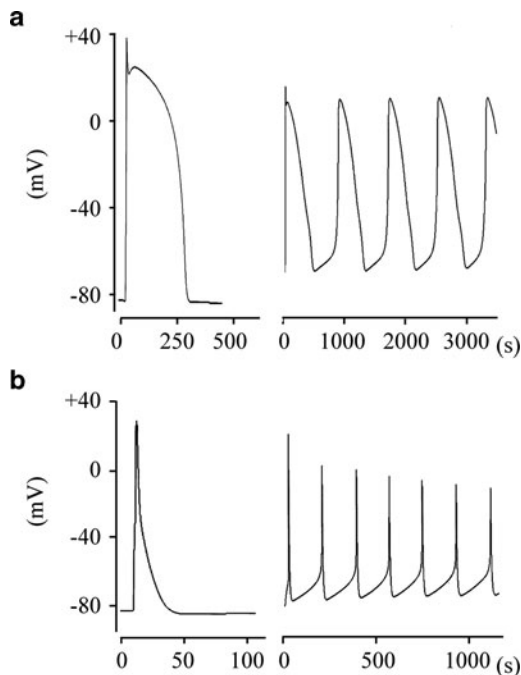


Fig. 31.4 Simulated human and mouse action potentials under control conditions, and repetitive activity elicited by adding a time-independent, voltage-independent, nonspecific cationic channel representative of the TRPC3/7 activated by ATP. **(a)** Repetitive activity observed using the TenTusscher et al. model for human ventricular tissue [77] after adding a nonspecific cationic channel with a conductance of 30 pS/pF to be compared with a G_{CaL} of 173 pS/pF. All other parameters unchanged. **(b)** Repetitive activity observed when using the Bondarenko et al.'s model of mouse ventricular myocytes [78] after increasing G_{CaL} and each K^+ conductance by 30% (including adding a $G_{K-tos} = 1/3 G_{K-tof}$) and adding a nonspecific cationic channel with a conductance of 20 μ S/ μ F to be compared with a G_{CaL} of 250 μ S/ μ F. Note that in both models the addition of a nonspecific conductance of similar amplitude induces cell automaticity in the absence of any initial stimulation

could be a key parameter in the modulation of cardiac rhythm by neuromodulators following alterations in intracellular Ca^{2+} content.

31.10 Conclusions

In the cardiovascular system, the specific physiological and pathological roles of each TRP channel are barely known. This is consequent to the multiplicity of the TRP expressed in a single cell, to the fact that they can form heterotetramers with specific properties different from both homotetramers, and to the lack of specific pharmacological tools. TRP expression is highly tissue dependent. Moreover, there

are large variations in their expression pattern according to species and even strain, age, and pathological status. This emphasizes the necessity to analyze TRP expression in isolated myocytes, rather than the whole heart in order to establish some correlation with their specific physiological or pathological function. Despite the present limitations, the discovery of TRP 20 years ago is probably a milestone of similar importance to the discovery of voltage-dependent channels in the 1950s considering the diversity of their physiological and pathological functions presently reported. In the heart, by generating a background inward current at diastolic potential, the TRP channels whether constitutively opened, or activated under specific conditions by various neuromodulators under control and pathological conditions, are relevant modulators of cardiac rhythm. It is noteworthy that in addition to the depolarizing current resulting from TRP activation, the influx of cations might contribute via the electrogenic $\text{Na}^+/\text{Ca}^{2+}$ exchanger and Na^+/K^+ -ATPase to further inward currents. Despite the very weak amplitudes of these sustained currents, relative to the voltage-dependent currents controlling the action potential, their occurrence in a range of membrane potentials at which the membrane resistance is high modulates membrane potential sufficient to markedly affect cardiac rhythm. Furthermore, nothing is presently known about the role of other groups of TRPs that are present in cardiac and vascular tissues, i.e., the TRPP, namely the PKD1L2a transcript that is highly expressed together with PKD2L (TRPP3). A comparison with the regulation occurring in kidney by related TRPs suggests that a pharmacological coupling might control Ca^{2+} release from the SR, in addition to the classical electrophysiological Ca^{2+} -induced Ca^{2+} release. Thus, various compounds and neurotransmitters that activate the polycystin 1 receptor might also modulate intracellular Ca^{2+} level and indirectly, cardiac rhythm on top of the presently reported involvement of TRPCs and TRPM4, particularly.

Under the sudden release of ATP and UTP expected to occur during early ischemia, several currents conducted by several TRPC, and TRPM4 channels after Ca^{2+} overload, could contribute to cell automaticity and ectopic foci to trigger ventricular arrhythmia. Finally, it could be anticipated that, to some extent, other agonists such as angiotensin II, norepinephrine, and endothelin [79] that activate the DAG pathway and thus TRPC, could favor or induce arrhythmic activities.

Acknowledgments The authors wish to thank Dr S. Richard for continuous support and Pierre Fontanau for help with computation of the cardiac action potential.

References

1. Cosens DJ, Manning A. Abnormal electroretinogram from a Drosophila mutant. *Nature*. 1969;224(5216):285–7.
2. Montell C, Rubin GM. Molecular characterization of the Drosophila trp locus: a putative integral membrane protein required for phototransduction. *Neuron*. 1989;2(4):1313–23.
3. Clapham DE. TRP channels as cellular sensors. *Nature*. 2003;426(6966):517–24.

4. Schaefer M. Homo- and heteromeric assembly of TRP channel subunits. *Pflugers Arch.* 2005;451(1):35–42.
5. Venkatachalam K, Montell C. TRP Channels. *Annu Rev Biochem.* 2007;76:387–417.
6. Kiselyov K, Sojombo A, Mualem S. TRPpathies. *J Physiol.* 2007;578(Pt 3):641–53.
7. Nilius B, Owsianik G, Voets T, Peters JA. Transient receptor potential cation channels in disease. *Physiol Rev.* 2007;87(1):165–217.
8. Nilius B, Voets T. TRP channels: a TR(I)P through a world of multifunctional cation channels. *Pflugers Arch.* 2005;451(1):1–10.
9. Ramsey IS, Delling M, Clapham DE. An introduction to TRP channels. *Annu Rev Physiol.* 2006;68:619–47.
10. Owsianik G, D'Hoedt D, Voets T, Nilius B. Structure-function relationship of the TRP channel superfamily. *Rev Physiol Biochem Pharmacol.* 2006;156:61–90.
11. Pedersen SF, Owsianik G, Nilius B. TRP channels: an overview. *Cell Calcium.* 2005;38 (3–4):233–52.
12. Damann N, Voets T, Nilius B. TRPs in our senses. *Curr Biol.* 2008;18(18):R880–9.
13. Ju YK, Chu Y, Chaulet H, Lai D, Gervasio OL, Graham RM, et al. Store-operated Ca²⁺ influx and expression of TRPC genes in mouse sinoatrial node. *Circ Res.* 2007;100(11):1605–14.
14. Ohba T, Watanabe H, Murakami M, Takahashi Y, Iino K, Kuromitsu S, et al. Upregulation of TRPC1 in the development of cardiac hypertrophy. *J Mol Cell Cardiol.* 2007;42(3):498–507.
15. Kunert-Keil C, Bisping F, Kruger J, Brinkmeier H. Tissue-specific expression of TRP channel genes in the mouse and its variation in three different mouse strains. *BMC Genomics.* 2006;7:159.
16. Fauconnier J, Lanner JT, Sultan A, Zhang SJ, Katz A, Bruton JD, et al. Insulin potentiates TRPC3-mediated cation currents in normal but not in insulin-resistant mouse cardiomyocytes. *Cardiovasc Res.* 2007;73(2):376–85.
17. Onohara N, Nishida M, Inoue R, Kobayashi H, Sumimoto H, Sato Y, et al. TRPC3 and TRPC6 are essential for angiotensin II-induced cardiac hypertrophy. *EMBO J.* 2006;25(22):5305–16.
18. Alvarez J, Coulombe A, Cazorla O, Ugur M, Rauzier JM, Magyar J, et al. ATP/UTP activate cation-permeable channels with TRPC3/7 properties in rat cardiomyocytes. *Am J Physiol Heart Circ Physiol.* 2008;295(1):H21–8.
19. Bush EW, Hood DB, Papst PJ, Chapo JA, Minobe W, Bristow MR, et al. Canonical transient receptor potential channels promote cardiomyocyte hypertrophy through activation of calcineurin signaling. *J Biol Chem.* 2006;281(44):33487–96.
20. Goel M, Zuo CD, Sinkins WG, Schilling WP. TRPC3 channels colocalize with Na⁺/Ca²⁺ exchanger and Na⁺ pump in axial component of transverse-axial tubular system of rat ventricle. *Am J Physiol Heart Circ Physiol.* 2007;292(2):H874–83.
21. Seth M, Sumbilla C, Mullen SP, Lewis D, Klein MG, Hussain A, et al. Sarco(endo)plasmic reticulum Ca²⁺ ATPase (SERCA) gene silencing and remodeling of the Ca²⁺ signaling mechanism in cardiac myocytes. *Proc Natl Acad Sci USA.* 2004;101(47):16683–8.
22. Kuwahara K, Wang Y, McAnally J, Richardson JA, Bassel-Duby R, Hill JA, et al. TRPC6 fulfills a calcineurin signaling circuit during pathologic cardiac remodeling. *J Clin Invest.* 2006;116(12):3114–26.
23. Song JX, Wang LH, Yao L, Xu C, Wei ZH, Zheng LR. Impaired transient receptor potential vanilloid 1 in streptozotocin-induced diabetic hearts. *Int J Cardiol.* 2009;134(2):290–2.
24. Guinamard R, Chatelier A, Demion M, Potreau D, Patri S, Rahmati M, et al. Functional characterization of a Ca(2+)-activated non-selective cation channel in human atrial cardiomyocytes. *J Physiol.* 2004;558(Pt 1):75–83.
25. Demion M, Bois P, Launay P, Guinamard R. TRPM4, a Ca²⁺-activated nonselective cation channel in mouse sino-atrial node cells. *Cardiovasc Res.* 2007;73(3):531–8.
26. Guinamard R, Demion M, Magaud C, Potreau D, Bois P. Functional expression of the TRPM4 cationic current in ventricular cardiomyocytes from spontaneously hypertensive rats. *Hypertension.* 2006;48(4):587–94.

27. Li A, Tian X, Sung SW, Somlo S. Identification of two novel polycystic kidney disease-1-like genes in human and mouse genomes. *Genomics*. 2003;81(6):596–608.
28. Chauvet V, Qian F, Boute N, Cai Y, Phakdeekitacharoen B, Onuchic LF, et al. Expression of PKD1 and PKD2 transcripts and proteins in human embryo and during normal kidney development. *Am J Pathol*. 2002;160(3):973–83.
29. Guo L, Schreiber TH, Weremowicz S, Morton CC, Lee C, Zhou J. Identification and characterization of a novel polycystin family member, polycystin-L2, in mouse and human: sequence, expression, alternative splicing, and chromosomal localization. *Genomics*. 2000;64(3):241–51.
30. Volk T, Schwoerer AP, Thiessen S, Schultz JH, Ehmke H. A polycystin-2-like large conductance cation channel in rat left ventricular myocytes. *Cardiovasc Res*. 2003;58(1):76–88.
31. Wu G, Hayashi T, Park JH, Dixit M, Reynolds DM, Li L, et al. Identification of PKD2L, a human PKD2-related gene: tissue-specific expression and mapping to chromosome 10q25. *Genomics*. 1998;54(3):564–8.
32. Dai XQ, Ramji A, Liu Y, Li Q, Karpinski E, Chen XZ. Inhibition of TRPP3 channel by amiloride and analogs. *Mol Pharmacol*. 2007;72(6):1576–85.
33. Watanabe H, Murakami M, Ohba T, Takahashi Y, Ito H. TRP channel and cardiovascular disease. *Pharmacol Ther*. 2008;118(3):337–51.
34. Inoue R, Jian Z, Kawarabayashi Y. Mechanosensitive TRP channels in cardiovascular pathophysiology. *Pharmacol Ther*. 2009;123(3):371–85.
35. Abramowitz J, Birnbaumer L. Physiology and pathophysiology of canonical transient receptor potential channels. *FASEB J*. 2009;23(2):297–328.
36. Zhu MX. Multiple roles of calmodulin and other Ca(2+)-binding proteins in the functional regulation of TRP channels. *Pflugers Arch*. 2005;451(1):105–15.
37. Vazquez G, Wedel BJ, Aziz O, Trebak M, Putney Jr JW. The mammalian TRPC cation channels. *Biochim Biophys Acta*. 2004;1742(1–3):21–36.
38. Inoue R, Jensen LJ, Shi J, Morita H, Nishida M, Honda A, et al. Transient receptor potential channels in cardiovascular function and disease. *Circ Res*. 2006;99(2):119–31.
39. Satoh S, Tanaka H, Ueda Y, Oyama J, Sugano M, Sumimoto H, et al. Transient receptor potential (TRP) protein 7 acts as a G protein-activated Ca²⁺ channel mediating angiotensin II-induced myocardial apoptosis. *Mol Cell Biochem*. 2007;294(1–2):205–15.
40. Eder P, Poteser M, Groschner K. TRPC3: a multifunctional, pore-forming signalling molecule. *Handb Exp Pharmacol*. 2007;179:77–92.
41. Lemonnier L, Trebak M, Lievremont JP, Bird GS, Putney Jr JW. Protection of TRPC7 cation channels from calcium inhibition by closely associated SERCA pumps. *FASEB J*. 2006;20(3):503–5.
42. O’Neil RG, Heller S. The mechanosensitive nature of TRPV channels. *Pflugers Arch*. 2005;451(1):193–203.
43. Kraft R, Harteneck C. The mammalian melastatin-related transient receptor potential cation channels: an overview. *Pflugers Arch*. 2005;451(1):204–11.
44. Scharenberg AM. TRPM2 and TRPM7: channel/enzyme fusions to generate novel intracellular sensors. *Pflugers Arch*. 2005;451(1):220–7.
45. Yang KT, Chang WL, Yang PC, Chien CL, Lai MS, Su MJ, et al. Activation of the transient receptor potential M2 channel and poly(ADP-ribose) polymerase is involved in oxidative stress-induced cardiomyocyte death. *Cell Death Differ*. 2006;13(10):1815–26.
46. Levitan IB, Cibulsky SM. Biochemistry. TRP ion channels—two proteins in one. *Science*. 2001;293(5533):1270–1.
47. Talavera K, Gees M, Karashima Y, Meseguer VM, Vanoorbeek JA, Damann N, et al. Nicotine activates the chemosensory cation channel TRPA1. *Nat Neurosci*. 2009;12(10):1293–9.
48. Bai CX, Giampieri A, Rodat-Despoix L, Padilla F, Downs T, Tsikas L, et al. Formation of a new receptor-operated channel by heteromeric assembly of TRPP2 and TRPC1 subunits. *EMBO Rep*. 2008;9(5):472–9.

49. Guinamard R, Demion M, Chatelier A, Bois P. Calcium-activated nonselective cation channels in mammalian cardiomyocytes. *Trends Cardiovasc Med.* 2006;16(7):245–50.
50. Link MS, Estes 3rd NA. Mechanically induced ventricular fibrillation (commotio cordis). *Heart Rhythm.* 2007;4(4):529–32.
51. Dean JW, Lab MJ. Arrhythmia in heart failure: role of mechanically induced changes in electrophysiology. *Lancet.* 1989;1(8650):1309–12.
52. Franz MR, Bode F. Mechano-electrical feedback underlying arrhythmias: the atrial fibrillation case. *Prog Biophys Mol Biol.* 2003;82(1–3):163–74.
53. Kamkin A, Kiseleva I, Isenberg G. Stretch-activated currents in ventricular myocytes: amplitude and arrhythmogenic effects increase with hypertrophy. *Cardiovasc Res.* 2000;48 (3):409–20.
54. Zhang YH, Youm JB, Sung HK, Lee SH, Ryu SY, Ho WK, et al. Stretch-activated and background non-selective cation channels in rat atrial myocytes. *J Physiol.* 2000;523(Pt 3):607–19.
55. Morita H, Honda A, Inoue R, Ito Y, Abe K, Nelson MT, et al. Membrane stretch-induced activation of a TRPM4-like nonselective cation channel in cerebral artery myocytes. *J Pharmacol Sci.* 2007;103(4):417–26.
56. Dyachenko V, Husse B, Rueckschloss U, Isenberg G. Mechanical deformation of ventricular myocytes modulates both TRPC6 and Kir2.3 channels. *Cell Calcium.* 2009;45(1):38–54.
57. Dyachenko V, Rueckschloss U, Isenberg G. Modulation of cardiac mechanosensitive ion channels involves superoxide, nitric oxide and peroxynitrite. *Cell Calcium.* 2009;45(1):55–64.
58. Yasuda N, Miura S, Akazawa H, Tanaka T, Qin Y, Kiya Y, et al. Conformational switch of angiotensin II type 1 receptor underlying mechanical stress-induced activation. *EMBO Rep.* 2008;9(2):179–86.
59. Ju YK, Allen DG. Store-operated Ca²⁺ entry and TRPC expression; possible roles in cardiac pacemaker tissue. *Heart Lung Circ.* 2007;16(5):349–55.
60. Colquhoun D, Neher E, Reuter H, Stevens CF. Inward current channels activated by intracellular Ca in cultured cardiac cells. *Nature.* 1981;294(5843):752–4.
61. Guinamard R, Rahmati M, Lenfant J, Bois P. Characterization of a Ca²⁺-activated nonselective cation channel during dedifferentiation of cultured rat ventricular cardiomyocytes. *J Membr Biol.* 2002;188(2):127–35.
62. Scamps F, Vassort G. Mechanism of extracellular ATP-induced depolarization in rat isolated ventricular cardiomyocytes. *Pflugers Arch.* 1990;417(3):309–16.
63. Shoda M, Hagiwara N, Kasanuki H, Hosoda S. ATP-activated cationic current in rabbit sinoatrial node cells. *J Mol Cell Cardiol.* 1997;29(2):689–95.
64. Kuzmin AI, Lakomkin VL, Kapelko VI, Vassort G. Interstitial ATP level and degradation in control and postmyocardial infarcted rats. *Am J Physiol.* 1998;275(3 Pt 1):C766–71.
65. Wihlborg AK, Balogh J, Wang L, Borna C, Dou Y, Joshi BV, et al. Positive inotropic effects by uridine triphosphate (UTP) and uridine diphosphate (UDP) via P2Y2 and P2Y6 receptors on cardiomyocytes and release of UTP in man during myocardial infarction. *Circ Res.* 2006;98(7):970–6.
66. Drury AN, Szent-Gyorgyi A. The physiological activity of adenine compounds with especial reference to their action upon the mammalian heart. *J Physiol.* 1929;68(3):213–37.
67. Burnstock G, Campbell G, Satchell D, Smythe A. Evidence that adenosine triphosphate or a related nucleotide is the transmitter substance released by non-adrenergic inhibitory nerves in the gut. *Br J Pharmacol.* 1970;40(4):668–88.
68. Burnstock G. Historical review: ATP as a neurotransmitter. *Trends Pharmacol Sci.* 2006;27 (3):166–76.
69. Burnstock G, Knight GE. Cellular distribution and functions of P2 receptor subtypes in different systems. *Int Rev Cytol.* 2004;240:31–304.
70. Ralevic V, Burnstock G. Receptors for purines and pyrimidines. *Pharmacol Rev.* 1998;50 (3):413–92.
71. Vassort G. Adenosine 5'-triphosphate: a P2-purinergic agonist in the myocardium. *Physiol Rev.* 2001;81(2):767–806.

72. Brake AJ, Wagenbach MJ, Julius D. New structural motif for ligand-gated ion channels defined by an ionotropic ATP receptor. *Nature*. 1994;371(6497):519–23.
73. Valera S, Hussy N, Evans RJ, Adami N, North RA, Surprenant A, et al. A new class of ligand-gated ion channel defined by P2x receptor for extracellular ATP. *Nature*. 1994;371(6497):516–9.
74. Webb TE, Simon J, Krishek BJ, Bateson AN, Smart TG, King BF, et al. Cloning and functional expression of a brain G-protein-coupled ATP receptor. *FEBS Lett*. 1993;324(2):219–25.
75. Friel DD, Bean BP. Two ATP-activated conductances in bullfrog atrial cells. *J Gen Physiol*. 1988;91(1):1–27.
76. Matsuura H, Ehara T. Activation of chloride current by purinergic stimulation in guinea pig heart cells. *Circ Res*. 1992;70(4):851–5.
77. ten Tusscher KH, Noble D, Noble PJ, Panfilov AV. A model for human ventricular tissue. *Am J Physiol Heart Circ Physiol*. 2004;286(4):H1573–89.
78. Bondarenko VE, Szigeti GP, Bett GC, Kim SJ, Rasmusson RL. Computer model of action potential of mouse ventricular myocytes. *Am J Physiol Heart Circ Physiol*. 2004;287(3):H1378–403.
79. Ren AJ, Yuan X, Lin L, Xu J, Chen T, Wang WZ, et al. Arrhythmogenic action of endothelin-1(1-31) through conversion to endothelin-1(1-21). *Exp Biol Med (Maywood)*. 2006;231(6):937–41.

Chapter 32

Cardiac Aquaporins: Significance in Health and Disease

Tanya L. Butler and David S. Winlaw

32.1 Introduction

Discovery of the identity of the first aquaporin (AQP) by Dr. Peter Agre and his team was recognised by the 2003 Nobel Prize in Chemistry. The AQPs are a family of proteins that form transmembrane pores to facilitate bidirectional flow of water or other small molecules. Movement of permitted molecules through the pore is gradient driven. To date, 13 family members have been shown in mammals (AQP0–12). Broad expression, from plants through to man, together with a high level of sequence conservation and tissue-specific distribution of individual AQPs suggests this is an ancient protein family with essential function.

AQP pores are made up of six transmembrane α -helices separated by five linking loops and with intracellular N- and C-terminal tails (Fig. 32.1a). Loops B and E contain the conserved amino acid sequence Asn-Pro-Ala (NPA). These residues interact at the centre of the pore to form a constricted passage, with an hourglass appearance (Fig. 32.1b,c), and are key to the specificity of AQPs for water and the ability to exclude protons. At the membrane, AQPs are seen as homo-tetramers, although each monomer functions as an independent water pore (Fig. 32.1d).

32.1.1 Water and Non-water Transporting Roles

Although first known for facilitation of water movement across cellular membranes, the AQPs actually fall into three classes based on sequence and functional homology: the AQPs, aquaglyceroporins and superaquaporins. The AQPs are high capacity water carriers and include AQP0, 1, 2, 4, 5, 6 and 8. Aquaglyceroporins are so named for their ability to transport glycerol in addition to other small molecules.

T.L. Butler (✉) and D.S. Winlaw

Kids Heart Research, The Children's Hospital at Westmead, Locked Bag 4001, Westmead NSW 2145 Sydney, Australia

e-mail: TanyaB@chw.edu.au, DavidW@chw.edu.au

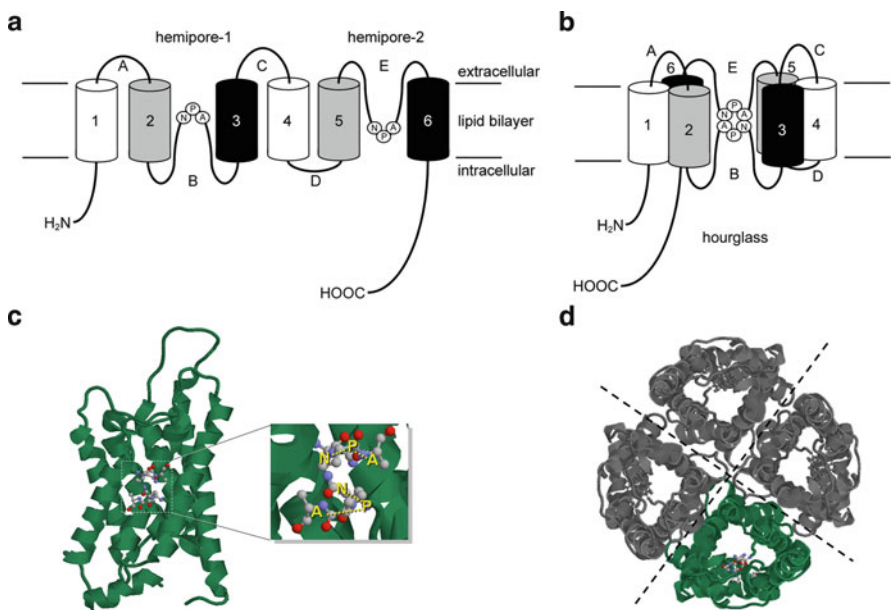


Fig. 32.1 Each aquaporin monomer is formed from six transmembrane segments and two hydrophobic loops (a) that fold to create a pore with the highly conserved NPA motifs at the centre (b, c). A ribbon representation of the side view of AQP1 is shown with the location of the NPA residues (c). The pore resembles an hourglass, narrowing near the centre. This physical constriction and the NPA motifs provide specificity for water or other transported solutes and the ability to exclude protons. When assembled into the membrane, aquaporins are seen as tetramers with each monomer independently functional. Shown is a view of an AQP1 tetramer from above with one monomer in green (d). Images reproduced with permission from [95, 96]

This subgroup includes AQP3, 7, 9 and 10. Two of the most recently identified AQPs, AQP11 [1] and AQP12 [2] are less conserved than the other family members, found in intracellular membranes and their transport function is still to be determined. Although grouped with the AQPs due to close sequence homology with AQP2 and AQP5, AQP6 differs from other family members. It is found in intracellular vesicles in the kidney and is suggested to play a role in acid secretion [3].

High rates of active fluid absorption and secretion are achieved by AQPs in a number of settings. Examples include water transport via AQP1 in the choroid plexus to produce cerebrospinal fluid. Normal saliva production relies on the expression of AQP5 in serous acini. Many AQPs are expressed in kidney and AQP1 is critical amongst these for water reabsorption in the proximal tubule to concentrate urine. In the absence of AQPs, cell membranes remain permeable to water. The volume of sweat produced following pilocarpine stimulation is unaffected in AQP5-null mice despite this protein being expressed in the luminal membranes of the gland epithelium [4]. Fluid clearance by lung alveoli is the same in wild-type, AQP1-null and AQP5-null mice. The rate of water movement in salivary glands has been calculated

to be over $0.5 \mu\text{L}/\text{min}/\mu\text{m}^2$ of the epithelial surface while in the lung this figure is less than $0.02 \mu\text{L}$. Thus, it has been suggested that AQP_s may not be required for fluid transport at low rates [5]. Choice of methodology may be critical for demonstrating function. For example, evidence against a requirement for AQP5 in sweat production [4] is balanced by support for fewer functional sweat glands when AQP5 is absent [6]. Slow water transport through AQP0 may also be a requirement for maintaining optical transparency of the lens [7].

The highly ordered distribution of AQP_s within organs, cells and subcellular regions may facilitate water transport to distant sites rather than simply across a single membrane. In astrocytes of the brain, AQP4 is highly enriched in endfeet membranes that are in contact with capillaries and pia mater. Non-endfeet membranes within the neuropil also contain a low density of AQP4. This subcellular compartmentalisation facilitates redistribution of water between the extracellular space and vascular or ventricular compartments [8].

It is becoming increasingly apparent that water transport is functionally coupled to various cellular processes. Examples include cell motility, K⁺ handling and cytoskeletal structure. Direct and indirect interaction of AQP_s with other proteins, participation in macromolecular complexes, and cellular signalling facilitate these complex functions. AQP1, AQP3 and AQP4 have each independently been shown to contribute to cell migration, although they are not absolutely required [9]. Water transport is also required for normal neural signal transduction. Disruption of the functional coupling between AQP_s and the K⁺ channel Kir4.1 alters seizure susceptibility and intensity [10, 11].

32.1.2 Signalling and Regulation

Most AQP_s are thought to be constitutively active, with the bulk of evidence suggesting regulation at the transcriptional level rather than acutely. The expression is sensitive to osmolarity, hormones, metabolic disturbance and tissue injury [12–15]. Ischaemia has been a particular focus following a striking demonstration of functionally relevant involvement of AQP4 in the ischaemic response in brain [5].

Activity of these integral membrane proteins may also be sensitive to phosphorylation, pH, osmolarity and hormones depending on the setting [15, 16]. The atypical AQP6 appears to play a role in acid/base regulation, with the pore being activated in response to acidic pH [3]. pH sensitivity has also been demonstrated for other AQP family members [17]. Gating of AQP4 involves phosphorylation in *in vitro* models [18] and is thought to also occur *in vivo*.

The AQP4 water pore is a specialised member of the AQP family. It has the highest water transporting capacity of all members, is insensitive to mercurial inhibition, and uniquely forms orthogonal arrays of particles (OAPs) when viewed in freeze-fractured membranes via scanning electron microscopy (Fig. 32.2). Both size and permeability of this specialised configuration in membranes is dependent

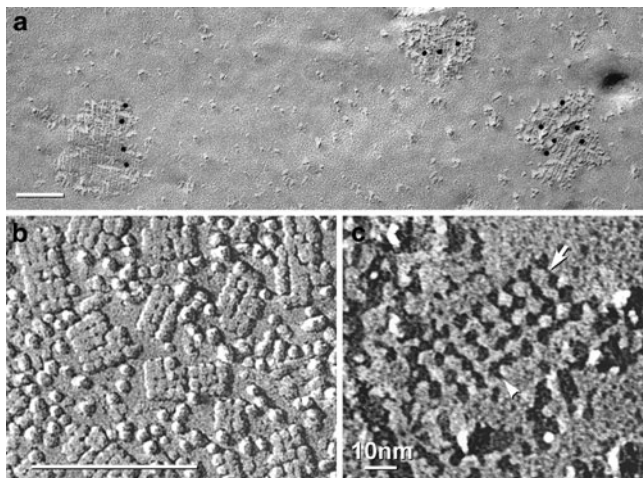


Fig. 32.2 The short form of AQP4 (AQP4-M23) assembles into structured arrays in the membrane. (a) Formaldehyde-fixed CHO cell membranes expressing AQP4-M23 were immunogold labelled for AQP4. Specific labelling only of the orthogonal arrays of particles (OAP) is seen. (b) The array structure is seen more clearly at higher magnification with conventional preparation. (c) A preparation modified to reduce water vapour contamination shows additional structure, with particles linked by grooves or furrows (arrow) and furrows at the edge of the array suggesting attachment sites for additional particles (arrowhead). Calibration bars in a and b: 100 nm. Image reproduced with permission from [20]

on the M1:M23 ratio [19] and it has been hypothesised that altered membrane organisation may contribute to functional regulation [20]. OAP formation in the kidney is responsive to chronic vasopressin administration in Battleboro rats [19]. Phosphorylation of AQP4-M23 may further influence OAP formation and subsequent water permeability [19] to allow acute regulation.

32.1.3 Protein Partners

The characteristic AQP structure includes six membrane-spanning segments with cytoplasmic N- and C-terminal tails [21], providing broad opportunity for interaction with other proteins both inside and outside the cell. While the number of confirmed functional protein partners is limited, a range of proteins that appear in linked regulatory pathways exist. Several AQP-containing molecular complexes have been described in red blood cells [22], brain, muscle [23], eye [24] and kidney [25]. Cardiac tissue has not been similarly investigated. Proteins with which AQPs interact include signalling molecules, membrane pumps and channels, as well as cytoskeletal proteins.

Interaction with other proteins diversifies the already broad family of water pores into a range of cellular processes outside strict water transport. Co-localisation of AQP4 and the Kir4.1 has been demonstrated in retinal Muller cells by EM immunogold labelling [26] and co-immunoprecipitation [27]. The partnership facilitates K⁺ siphoning within the central nervous system to clear excess potassium around active neurones [8]. Water transport in this setting controls neural signal transduction. A macromolecular complex is also formed in astrocytes that contain AQP4, metabotropic glutamate receptor 5 and Na,K-ATPase [28]. Functions include maintenance of the electrochemical gradient across the membrane, extracellular K⁺ homeostasis and control of brain metabolism [28].

The dystrophin-associated protein complex (DAPC) participates in cross-talk between the intracellular and extracellular environment. Interaction of several proteins with the DAPC supports appropriate membrane targeting or anchorage. Association between AQP4 and DAPC has been demonstrated in brain, eye and muscle. Diseases of muscle related to altered or absent DAPs are increasingly well characterised and there is significant central nervous system involvement in many of these [29]. Recruitment of AQP4 to DAPC is thought to involve interaction with α -syntrophin [30], however direct binding of AQP4 and α -syntrophin has not been demonstrated. Nevertheless, polarisation of a major pool of AQP4 is lost in the brain of Dp71-null, *mdx*- β geo and syntrophin-deficient mice [29].

Several different AQPs are able to contribute to cell migration [9]. Their involvement relies on relocation to the leading edge of the cell membrane to enhance filopodia formation and forward movement. Molecular partners are still to be determined, and may differ given the sequence diversity in the AQP family members known to participate in cell migration, but in the case of AQP4, association with the actin cytoskeleton and the dystrophin-associated protein α -syntrophin may target expression to appropriate membrane regions [31, 32].

Both AQP0 and AQP4 interact via the extracellular loops in opposing membranes to promote cell adhesion [33]. Formation of highly ordered OAP structures by AQP4 is mediated by residues in the N-terminal cytoplasmic tail [34]. It has been hypothesised that the size of arrays, producing junctions of different strength, facilitates osmo-sensing [34]. Targeting and anchorage of water pores to relevant membrane domains is also likely to involve interactions with the extracellular matrix [35].

32.1.4 Involvement in Health and Disease

There are a variety of excellent reviews describing the involvement of AQPs in human health and disease [21, 36–38]. The loss-of-function mutations in AQPs have been linked to a small number of disorders, including a rare form of nephrogenic diabetes insipidus for AQP2 [39], and congenital cataracts for AQP0 [40]. However, research utilising knockout mice predicts more broad disease involvement.

Altered function resulting from polymorphic variation in AQP genes has significantly expanded their disease association [41]. Polymorphism in the AQP1 gene is seen as Colton blood group variants Co^a and Co^b. This facilitated identification of a small number of Colton-null individuals in whom an AQP1 mutation abolishes expression. Sequence differences in AQP4 are associated with outcome following stroke [42, 43]. Obesity and type 2 diabetes have been linked to a polymorphism in the promoter of AQP7 that impairs transcription [44].

Altered expression of AQPs is seen in diverse pathologies. In several of these, the AQPs appear to be downstream from the primary disease-causing event, although may still be involved in disease progression. Skeletal muscle expression and localisation of AQP1 and AQP4 are influenced in myopathy and muscular dystrophy [45, 46]. Targeted deletion of Dp71, the retinal dystrophin isoform, leads to reduced AQP4, mislocalized Kir4.1 and renders the retina susceptible to transient ischaemic injury [47]. Transcript for both AQP4 and Kir4.1 is down-regulated in patients with proliferative vitreoretinopathy [48] and severe cerebral amyloid angiopathy [49]. In fact, brain tissue exhibiting a range of pathologies shows functional disconnection between AQP4 and Kir4.1 [50]. Increased AQP4 expression is a common finding, seen in contused brain, bacterial meningitis and tumour growth, and is associated with oedema.

The AQPs are also a target in autoimmunity. Neuromyelitis optica is characterised by the production of auto-antibodies to AQP4 [51]. Susceptibility of the optic nerves and spinal cord may result from specificity of the antibodies for AQP4 assembled into large OAPs [52].

32.2 Aquaporins in the Heart

Transcript is detectable for several AQPs in mammalian cardiac tissue although protein expression is restricted to a smaller number of family members [53]. Expression of AQP1, AQP7 and possibly also AQP11 is common to the hearts of all species. AQP1 is seen in the capillary endothelium of all species examined and the cardiomyocytes of rats [54] and humans [55]. Some groups report AQP7 expression exclusively in endothelia [56] while others provide evidence for cardiomyocyte expression of this protein [57]. Non-quantitative RT-PCR reveals AQP11 transcript in the heart of various species [53] while Northern analysis showed levels to be much lower in the heart than other expressing tissues [1]. A lack of available antibodies for AQP11 precludes investigation of protein expression and localisation at this time.

Endothelial water transport is slower in AQP1-null humans [58], but for the small number of people without AQP1 who have been investigated no overt cardiac phenotype has been noted [21]. AQP1 expressed in cardiomyocytes may benefit gaseous transport in the metabolically active heart [59]. If this is the case, it might be expected that loss of AQP1 may increase susceptibility to ischaemic injury. One report provides evidence for internalisation of AQP1-containing caveolae in

cardiomyocytes subjected to hypertonic exposure [54], although this is yet to be independently validated.

AQP4 has been demonstrated in mouse cardiomyocyte sarcolemma by immunohistochemistry [53] and freeze fracture preparations that reveal OAP structure [60]. Rat and human heart, in contrast, do not contain detectable levels of AQP4 protein [53]. The reason for this species difference remains unknown. Skeletal muscle is thought to require AQP4 in the equilibration of osmotic gradients resulting from the production of metabolites in working muscle [61]. Thus, the high basal heart rate of the mouse may necessitate the presence of a high-capacity AQP. Alternatively, water may be conveyed by other cardiac water pores in the absence of AQP4. We have presented evidence for the expression of AQP1 in human cardiomyocytes [55] and a mercury-sensitive form of water transport in rat cardiomyocytes may similarly be explained by the presence of AQP1 [62], also shown by immunofluorescent microscopy [54]. Neither knockout [63] nor overexpression [64] of AQP4 results in altered gross morphology of the mouse heart.

Using knockout mice as controls, the expression of aquaglyceroporin AQP7 has been demonstrated in cardiac capillaries [56]. Transcript is readily detectable in mouse, rat and human heart [53]. Cardiac morphology of AQP7-null mice is normal [57]. However, ATP levels are lower and impaired glycerol consumption results in the inability of some hearts to continue contracting ex vivo when glycerol is the only energy substrate supplied [57]. The effect of AQP7 knockout is seen in vivo as a decompensated response to isoproterenol challenge. Null hearts display prominent hypertrophy, together with increased fibrosis and a reduction in fractional shortening [57]. These findings reveal glycerol to be an important metabolic substrate of the heart and show aquaglyceroporins to be necessary for glycerol transport in cardiac tissue.

AQP8 appears to show species-specific expression similar to that of AQP4. Transcript is seen in mouse heart [53, 65] but not human [66] or rat [67]. While knockout mice have been produced [68], this AQP family member has not been actively studied in the context of its cardiac function. Transport of ammonia by AQP8 is seen when expressed in oocytes and on this basis it has been suggested that the importance of AQP8 may be in acid–base regulation [69].

Absence of the other known AQP family members in the heart has been demonstrated largely by Northern assays and occasionally via Western when antibodies were available. No expression of AQP2 [70], AQP3 [53, 71], AQP5 [53], AQP6 [72], AQP9 [73, 74], AQP10 [75] and AQP12 [2] is evident.

32.2.1 Physiological and Pathological Conditions

Evidence for association of AQPs, physically or functionally, with other protein partners, together with restricted localisation in plasma membrane domains suggests the importance of regional control of water flux in the heart. As discussed previously, there are several organ systems in which coordinated water movement

is controlled by the expression of AQPs in different cells and compartments. A comprehensive model of cardiac water handling has been described in paired publications by Kellen and Bassingthwaite [76, 77]. This considers the movement of water between tissue compartments; namely the vascular, interstitial and intracellular compartments. The model predicts a primary role for AQP-dependent removal of water from the extracellular space into blood vessels. Resolution of cardiac oedema, therefore, may rely on vascular AQP expression [78] somewhat akin to resolution of vasogenic oedema in the brain. In other organs, the expression of AQP1 is seen in the lymphatics [79] and may also facilitate cardiac fluid movement.

The cardiac and skeletal muscles, both being striated in nature, have dual involvement in a range of pathologies. AQP4 is altered in several muscular dystrophies and myopathies and some argue that loss of AQP4 contributes to the pathophysiology of disease progression. Cardiomyopathy is prominent in Duchenne and Becker muscular dystrophy, X-linked cardiomyopathy and Limb girdle muscular dystrophy type 2B, 2E and 2F [80]. While cardiac AQP expression and localisation has not been characterised, AQP4 is severely reduced in diseased skeletal muscle [45, 46, 81].

Ischaemic injury is associated with the development of oedema. Transcriptional regulation of AQPs is seen in the heart [53, 82, 83] and it is tempting to speculate that cardiac AQPs could be a therapeutic target to improve the outcome of ischaemic injury. Cardiac AQP4 expression has been reported to increase following focal ischaemia in the mouse [84]. The response appears to be associated with irreversible ischaemic damage and also occurs in rat and human heart, in which AQP4 is not normally detectable (Butler and Winlaw, unpublished data). Swelling develops during the ischaemic event [85, 86] before AQP protein levels change. As such, a delayed change in AQP expression is unlikely to contribute meaningfully to ischaemic swelling or protection. Late modulation of expression may contribute to a delayed functional impact following an ischaemic event, although this is yet to be assessed.

The availability of extracellular glycerol modifies energy utilisation by the heart [57, 87]. Usage of glycerol in states of high energy demand may be cardioprotective by reducing the oxygen-consuming contribution of fatty acid oxidation to energy production [87]. In addition, glycerol usage enhances the incorporation of fatty acids into the membrane to enhance its maintenance. Mice that lack AQP7 develop excessive cardiac hypertrophy and higher mortality rates in response to pressure overload [57]. This has relevance to metabolic disorders affecting the heart, including diabetes and ischaemic heart disease. Investigation of the functional effect of ischaemia in Langendorff models that includes glycerol as a substrate will be a useful addition to the area. Extension of the phenotypic investigation of AQP7 polymorphism in human subjects to include the heart may also prove fruitful.

Peripheral organ systems must also be considered in water handling that affects the heart. Severe congestive heart failure is associated with abnormal kidney function leading to Na^+ and water retention. The cause is altered vasopressin release and dysregulation of expression and localisation of AQP2 in the kidney [16].

Ca^{2+} signalling is also involved in regulation of AQP2 through the calcineurin-NFATc pathway [88] and the raised intracellular Ca^+ that results from ischaemic injury may later lead to dysregulation of water handling.

32.2.2 Heart Rate and Rhythm

In this young field, the contribution of AQPs to the control of heart rate and rhythm is largely unknown. The emerging picture within the field of AQP research is that function is often seen within a complex system in which phenotype is highlighted only in response to strain. Information gathered from other organs places the AQPs in roles that may have significant functional impact in the heart and control of rhythm. These include potential involvement in ion handling, cell-cell communication and anchorage, metabolic regulation, plasticity, and regional water movement.

Little detail exists on the expression of AQPs in specialised cardiac cells, such as those of SA node, AV node and Purkinje fibres. Similarly, the localisation of water pores within plasma membrane sub-domains requires further clarification. Human cardiac AQP1 is found in association with the t-tubules and caveolae [55]. The t-tubular system is a functionally important specialisation of ventricular cardiac myocytes that facilitates co-ordination of ion handling in the control of cardiac myocyte contraction [89]. Ion transport is thought to involve obligatory water movement, which is likely to exert micro-regional control of ion concentration. While untested at this time, it may be argued that any water movement in partnership with the ion fluxes during contraction will require participation of AQPs as high capacity pores. Analogous to this would be the coordinated function of AQPs and ion channels in the regulation of neural activity.

Cardiac involvement is common in skeletal muscle myopathies and in some cases the heart is the primary organ affected. Manifestation can include impaired impulse generation and conduction [90]. Electrocardiographic (ECG) abnormalities are variable and point to complex pathologic mechanisms. Loss of AQP4 is a feature in the skeletal muscle of many of these pathologies, but whether and how this translates to the heart is not known. Anchorage of AQP4 in the muscle involves interaction with the proteins of DAPC. Na^+ and K^+ channels interact with DAPC in similar ways. Disruption of dystrophin in the mdx^{5cv} model alters cardiac conduction via an effect on Na^+ channel $\text{Na}_v1.5$ [91], but AQP involvement remains untested. Importantly, cardiac and skeletal muscles of humans differ in their AQP expression; AQP4 is prominent in the skeletal muscle sarcolemma but is absent in the human heart. This is in contrast to the mouse, in which AQP4 is expressed in both cardiac and skeletal muscles.

Preliminary work conducted by our group, utilising AQP1- and AQP4-null mice, suggests that basal heart rate and response to exercise is normal (Butler, Verkman and Winlaw, unpublished data). Surface ECG of wild-type, AQP1-null and AQP4-null mice was measured via telemetry (EA-F20, Data Science International) in freely moving animals over a 24-h period and average heart rate was calculated.

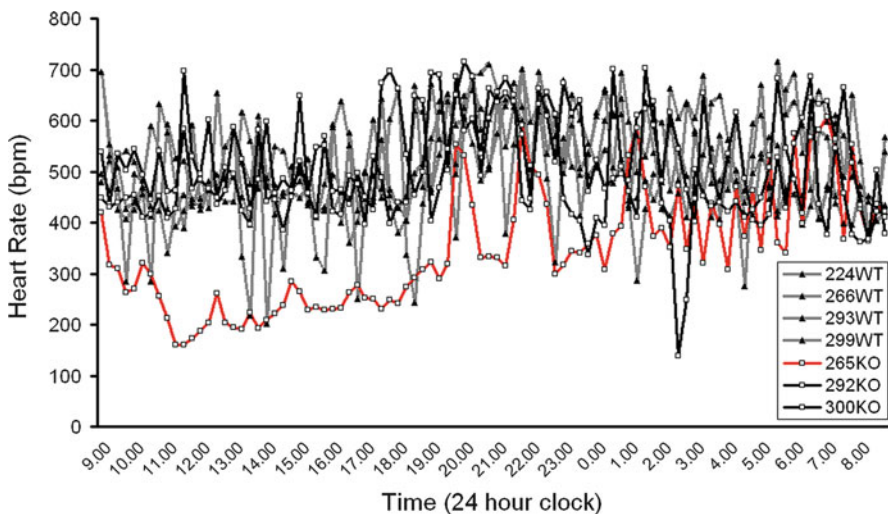


Fig. 32.3 Heart rate was recorded in freely moving mice for 24 h and charted at 15-min intervals. The first 12 h incorporates the *light* (sleep) portion of the cycle and the second 12 h is the *dark* (wake) portion. Wild-type C57BL/6 mice and two of the three analysed AQP4-knockout mice showed a similar variation in the heart rate during the recording period. The AQP4-null mouse 265 displayed a sustained bradycardia over several hours

No significant difference was found in association with knockout of AQP1 or AQP4. A single AQP4-null mouse on a BL/6 background demonstrated prolonged bradycardia during the day (sleep) period of a 24-h cycle of monitoring (Fig. 32.3). However, the group sizes were small and this animal may be an anomaly. Mice subjected to swim-based exercise were able to achieve comparable peak heart rates regardless of genotype.

A single report links up-regulation of AQP expression with reduced dysrhythmia following pharmacological treatment of rats subjected to ischaemia/reperfusion injury [92]. The focus was on AQP4 expression visualized by immunohistochemistry. However, others have reported that AQP4 is absent in the heart of rats [53, 93]. Clarification of this will require the use of knockout mice.

32.3 Conclusion

Understanding the role of cardiac AQPs, including their potential involvement in the control of heart rate and rhythm, is an open and exciting field that invites exploration. Expanding evidence for participation of AQP family members in multiprotein complexes and coordinated cell function is likely to reveal physiologically relevant roles for these proteins in the heart. Various functions are suggested

that include modulation of ion handling, cell communication and adhesion, metabolic regulation and control of regional water movement. Interest in AQP expression and activity as a pharmacotherapeutic target is expanding [94] and future developments in this field may provide new tools for the treatment of cardiac disease.

References

1. Morishita Y, Matsuzaki T, Hara-chikuma M, Andoo A, Shimono M, Matsuki A, et al. Disruption of aquaporin-11 produces polycystic kidneys following vacuolization of the proximal tubule. *Mol Cell Biol*. 2005;25(17):7770–9.
2. Itoh T, Rai T, Kuwahara M, Ko SB, Uchida S, Sasaki S, et al. Identification of a novel aquaporin, AQP12, expressed in pancreatic acinar cells. *Biochem Biophys Res Commun*. 2005;330(3):832–8.
3. Yasui M, Hazama A, Kwon T, Nielsen S, Guggino WB, Agre P. Rapid gating and anion permeability of an intracellular aquaporin. *Nature*. 1999;402(6758):184–7.
4. Song Y, Sonawane N, Verkman AS. Localization of aquaporin-5 in sweat glands and functional analysis using knockout mice. *J Physiol*. 2002;541(Pt 2):561–8.
5. Verkman AS. Novel roles of aquaporins revealed by phenotype analysis of knockout mice. *Rev Physiol Biochem Pharmacol*. 2005;155:31–55.
6. Nejsum LN, Kwon TH, Jensen UB, Fumagalli O, Frokiaer J, Krane CM, et al. Functional requirement of aquaporin-5 in plasma membranes of sweat glands. *Proc Natl Acad Sci U S A*. 2002;99(1):511–6.
7. Jensen MO, Dror RO, Xu H, Borhani DW, Arkin IT, Eastwood MP, et al. Dynamic control of slow water transport by aquaporin 0: implications for hydration and junction stability in the eye lens. *Proc Natl Acad Sci U S A*. 2008;105(38):14430–5.
8. Roberta A, Rossella B. Aquaporins and Glia. *Curr Neuropharmacol*. 2010;8:84–91.
9. Papadopoulos MC, Saadoun S, Verkman AS. Aquaporins and cell migration. *Pflugers Arch*. 2008;456(4):693–700.
10. Amiry-Moghaddam M, Ottersen OP. The molecular basis of water transport in the brain. *Nat Rev Neurosci*. 2003;4(12):991–1001.
11. Binder DK, Papadopoulos MC, Haggie PM, Verkman AS. *In vivo* measurement of brain extracellular space diffusion by cortical surface photobleaching. *J Neurosci*. 2004;24(37):8049–56.
12. Taniguchi M, Yamashita T, Kumura E, Tamatani M, Kobayashi A, Yokawa T, et al. Induction of aquaporin-4 water channel mRNA after focal cerebral ischemia in rat. *Brain Res Mol Brain Res*. 2000;78(1–2):131–7.
13. Yamamoto N, Yoneda K, Asai K, Sobue K, Tada T, Fujita Y, et al. Alterations in the expression of the AQP family in cultured rat astrocytes during hypoxia and reoxygenation. *Brain Res Mol Brain Res*. 2001;90(1):26–38.
14. Kuriyama H, Shimomura I, Kishida K, Kondo H, Furuyama N, Nishizawa H, et al. Coordinated regulation of fat-specific and liver-specific glycerol channels, aquaporin adipose and aquaporin 9. *Diabetes*. 2002;51(10):2915–21.
15. Arima H, Yamamoto N, Sobue K, Umenishi F, Tada T, Katsuya H, et al. Hyperosmolar mannitol stimulates expression of aquaporins 4 and 9 through a p38 mitogen-activated protein kinase-dependent pathway in rat astrocytes. *J Biol Chem*. 2003;278(45):44525–34.
16. Nielsen S, Frokiaer J, Marples D, Kwon TH, Agre P, Knepper MA. Aquaporins in the kidney: from molecules to medicine. *Physiol Rev*. 2002;82(1):205–44.
17. Nemeth-Cahalan KL, Kalman K, Hall JE. Molecular basis of pH and Ca²⁺ regulation of aquaporin water permeability. *J Gen Physiol*. 2004;123(5):573–80.

18. Yukutake Y, Yasui M. Regulation of water permeability through aquaporin-4. *Neuroscience*. 2010;168(4):885–91.
19. Silberstein C, Bouley R, Huang Y, Fang P, Pastor-Soler N, Brown D, et al. Membrane organization and function of M1 and M23 isoforms of aquaporin-4 in epithelial cells. *Am J Physiol Renal Physiol*. 2004;287(3):F501–11.
20. Rash JE, Davidson KG, Yasumura T, Furman CS. Freeze-fracture and immunogold analysis of aquaporin-4 (AQP4) square arrays, with models of AQP4 lattice assembly. *Neuroscience*. 2004;129(4):915–34.
21. Agre P, King LS, Yasui M, Guggino WB, Ottersen OP, Fujiyoshi Y, et al. Aquaporin water channels – from atomic structure to clinical medicine. *J Physiol (Lond)*. 2002;542(1):3–16.
22. Bruce LJ, Beckmann R, Ribeiro ML, Peters LL, Chasis JA, Delaunay J, et al. A band 3-based macromplex of integral and peripheral proteins in the RBC membrane. *Blood*. 2003;101(10):4180–8.
23. Nicchia GP, Cogotzi L, Rossi A, Basco D, Brancaccio A, Svelto M, et al. Expression of multiple AQP4 pools in the plasma membrane and their association with the dystrophin complex. *J Neurochem*. 2008;105(6):2156–65.
24. Lindsey Rose KM, Gourdie RG, Prescott AR, Quinlan RA, Crouch RK, Schey KL. The C terminus of lens aquaporin 0 interacts with the cytoskeletal proteins filensin and CP49. *Invest Ophthalmol Vis Sci*. 2006;47(4):1562–70.
25. Noda Y, Horikawa S, Katayama Y, Sasaki S. Identification of a multiprotein “motor” complex binding to water channel aquaporin-2. *Biochem Biophys Res Commun*. 2005;330(4):1041–7.
26. Nagelhus EA, Horio Y, Inanobe A, Fujita A, Haug FM, Nielsen S, et al. Immunogold evidence suggests that coupling of K⁺ siphoning and water transport in rat retinal Muller cells is mediated by a coenrichment of Kir4.1 and AQP4 in specific membrane domains. *Glia*. 1999;26(1):47–54.
27. Connors NC, Kofuji P. Potassium channel Kir4.1 macromolecular complex in retinal glial cells. *Glia*. 2006;53(2):124–31.
28. Illarionova N, Gunnarson E, Li Y, Brismar H, Bondar A, Zelenin S, et al. Functional and molecular interactions between aquaporins and Na⁺, K⁺-ATPase. *Neuroscience*. 2009;164(4):915–25.
29. Waite A, Tinsley CL, Locke M, Blake DJ. The neurobiology of the dystrophin-associated glycoprotein complex. *Ann Med*. 2009;41(5):344–59.
30. Amiry-Moghaddam M, Frydenlund DS, Ottersen OP. Anchoring of aquaporin-4 in brain: molecular mechanisms and implications for the physiology and pathophysiology of water transport. *Neuroscience*. 2004;129(4):997–1008.
31. Saadoun S, Papadopoulos MC, Watanabe H, Yan D, Manley GT, Verkman AS. Involvement of aquaporin-4 in astroglial cell migration and glial scar formation. *J Cell Sci*. 2005;118(Pt 24):5691–8.
32. Nicchia GP, Rossi A, Mola MG, Procino G, Frigeri A, Svelto M. Actin cytoskeleton remodeling governs aquaporin-4 localization in astrocytes. *Glia*. 2008;56(16):1755–66.
33. Engel A, Fujiyoshi Y, Gonon T, Walz T. Junction-forming aquaporins. *Curr Opin Struct Biol*. 2008;18(2):229–35.
34. Hiroaki Y, Tani K, Kamegawa A, Gyobu N, Nishikawa K, Suzuki H, et al. Implications of the aquaporin-4 structure on array formation and cell adhesion. *J Mol Biol*. 2006;355(4):628–39.
35. Guadagno E, Moukhles H. Laminin-induced aggregation of the inwardly rectifying potassium channel, Kir4.1, and the water-permeable channel, AQP4, via a dystroglycan-containing complex in astrocytes. *Glia*. 2004;47(2):138–49.
36. King LS, Kozono D, Agre P. From structure to disease: the evolving tale of aquaporin biology. *Nat Rev Mol Cell Biol*. 2004;5(9):687–98.
37. Ishibashi K, Hara S, Kondo S. Aquaporin water channels in mammals. *Clin Exp Nephrol*. 2009;13(2):107–17.
38. Verkman AS. Aquaporins: translating bench research to human disease. *J Exp Biol*. 2009;212(Pt 11):1707–15.

39. Bichet DG. Nephrogenic diabetes insipidus. *Adv Chronic Kidney Dis.* 2006;13(2):96–104.
40. Francis P, Chung JJ, Yasui M, Berry V, Moore A, Wyatt MK, et al. Functional impairment of lens aquaporin in two families with dominantly inherited cataracts. *Hum Mol Genet.* 2000;9(15):2329–34.
41. Sorani MD, Manley GT, Giacomini KM. Genetic variation in human aquaporins and effects on phenotypes of water homeostasis. *Hum Mutat.* 2008;29(9):1108–17.
42. Kleffner I, Bungeroth M, Schifflauer H, Schabitz WR, Ringelstein EB, Kuhlenbaumer G. The role of aquaporin-4 polymorphisms in the development of brain edema after middle cerebral artery occlusion. *Stroke.* 2008;39(4):1333–5.
43. Sorani MD, Zador Z, Hurowitz E, Yan D, Giacomini KM, Manley GT. Novel variants in human Aquaporin-4 reduce cellular water permeability. *Hum Mol Genet.* 2008;17(15):2379–89.
44. Prudente S, Flex E, Morini E, Turchi F, Capponi D, De Cosmo S, et al. A functional variant of the adipocyte glycerol channel aquaporin 7 gene is associated with obesity and related metabolic abnormalities. *Diabetes.* 2007;56(5):1468–74.
45. Asereto S, Mastrototaro M, Stringara S, Gazzero E, Broda P, Nicchia GP, et al. Aquaporin-4 expression is severely reduced in human sarcoglycanopathies and dysferlinopathies. *Cell Cycle.* 2008;7(14):2199–207.
46. Au CG, Butler TL, Egan JR, Cooper ST, Lo HP, Compton AG, et al. Changes in skeletal muscle expression of AQP1 and AQP4 in dystrophinopathy and dysferlinopathy patients. *Acta Neuropathol.* 2008;116(3):235–46.
47. Dalloz C, Sarig R, Fort P, Yaffe D, Bordais A, Pannicke T, et al. Targeted inactivation of dystrophin gene product Dp71: phenotypic impact in mouse retina. *Hum Mol Genet.* 2003;12(13):1543–54.
48. Tenckhoff S, Hollborn M, Kohen L, Wolf S, Wiedemann P, Bringmann A. Diversity of aquaporin mRNA expressed by rat and human retinas. *Neuroreport.* 2005;16(1):53–6.
49. Wilcock DM, Vitek MP, Colton CA. Vascular amyloid alters astrocytic water and potassium channels in mouse models and humans with Alzheimer's disease. *Neuroscience.* 2009;159(3):1055–69.
50. Saadoun S, Papadopoulos MC, Krishna S. Water transport becomes uncoupled from K⁺ siphoning in brain contusion, bacterial meningitis, and brain tumours: immunohistochemical case review. *J Clin Pathol.* 2003;56(12):972–5.
51. Lennon VA, Kryzer TJ, Pittock SJ, Verkman AS, Hinson SR. IgG marker of optic-spinal multiple sclerosis binds to the aquaporin-4 water channel. *J Exp Med.* 2005;202(4):473–7.
52. Nicchia GP, Mastrototaro M, Rossi A, Pisani F, Tortorella C, Ruggieri M, et al. Aquaporin-4 orthogonal arrays of particles are the target for neuromyelitis optica autoantibodies. *Glia.* 2009;57(13):1363–73.
53. Butler TL, Au CG, Yang B, Egan JR, Tan YM, Hardeman EC, et al. Cardiac aquaporin expression in humans, rats, and mice. *Am J Physiol Heart Circ Physiol.* 2006;291(2):H705–13.
54. Page E, Winterfield J, Goings G, Bastawrous A, Upshaw-Earley J, Doyle D. Water channel proteins in rat cardiac myocyte caveolae: osmolarity-dependent reversible internalization. *Am J Physiol.* 1998;274(6 Pt 2):H1988–2000.
55. Au CG, Cooper ST, Lo HP, Compton AG, Yang N, Wintour EM, et al. Expression of aquaporin 1 in human cardiac and skeletal muscle. *J Mol Cell Cardiol.* 2004;36(5):655–62.
56. Skowronski MT, Lebeck J, Rojek A, Praetorius J, Fuchtbauer EM, Frokiaer J, et al. AQP7 is localized in capillaries of adipose tissue, cardiac and striated muscle: implications in glycerol metabolism. *Am J Physiol Renal Physiol.* 2007;292(3):F956–65.
57. Hibuse T, Maeda N, Nakatsuji H, Tochino Y, Fujita K, Kihara S, et al. The heart requires glycerol as an energy substrate through aquaporin 7, a glycerol facilitator. *Cardiovasc Res.* 2009;83(1):34–41.
58. King LS, Nielsen S, Agre P, Brown RH. Decreased pulmonary vascular permeability in aquaporin-1-null humans. *Proc Natl Acad Sci U S A.* 2002;99(2):1059–63.

59. Miller RT. Aquaporin in the heart – only for water? *J Mol Cell Cardiol.* 2004;36(5):653–4.
60. McNutt NS. Ultrastructure of the myocardial sarcolemma. *Circ Res.* 1975;37(1):1–13.
61. Frigeri A, Nicchia GP, Balena R, Nico B, Svelto M. Aquaporins in skeletal muscle: reassessment of the functional role of aquaporin-4. *FASEB J.* 2004;18(7):905–7.
62. Ogura T, Matsuda H, Imanishi S, Shibamoto T. Sarcolemmal hydraulic conductivity of guinea-pig and rat ventricular myocytes. *Cardiovasc Res.* 2002;54(3):590–600.
63. Ma T, Yang B, Gillespie A, Carlson EJ, Epstein CJ, Verkman AS. Generation and phenotype of a transgenic knockout mouse lacking the mercurial-insensitive water channel aquaporin-4. *J Clin Invest.* 1997;100(5):957–62.
64. Wakayama Y, Takahashi J, Shibuya S, Inoue M, Kojima H, Oniki H, et al. Generation of muscle aquaporin 4 overexpressing transgenic mouse: Its characterization at RNA and protein levels including freeze-fracture study. *Micron.* 2006;38(3):257–67.
65. Ma T, Yang B, Verkman AS. Cloning of a novel water and urea-permeable aquaporin from mouse expressed strongly in colon, placenta, liver, and heart. *Biochem Biophys Res Commun.* 1997;240(2):324–8.
66. Koyama N, Ishibashi K, Kuwahara M, Inase N, Ichioka M, Sasaki S, et al. Cloning and functional expression of human aquaporin8 cDNA and analysis of its gene. *Genomics.* 1998;54(1):169–72.
67. Ishibashi K, Kuwahara M, Kageyama Y, Tohsaka A, Marumo F, Sasaki S. Cloning and functional expression of a second new aquaporin abundantly expressed in testis. *Biochem Biophys Res Commun.* 1997;237(3):714–8.
68. Yang B, Song Y, Zhao D, Verkman AS. Phenotype analysis of Aquaporin-8 null mice. *Am J Physiol Cell Physiol.* 2005;288(5):C1161–70.
69. Liu K, Nagase H, Huang CG, Calamita G, Agre P. Purification and functional characterization of Aquaporin-8. *Biol Cell.* 2005;98(3):153–61.
70. Yang B, Ma T, Xu Z, Verkman AS. cDNA and genomic cloning of mouse aquaporin-2: functional analysis of an orthologous mutant causing nephrogenic diabetes insipidus. *Genomics.* 1999;57(1):79–83.
71. Ishibashi K, Sasaki S, Fushimi K, Uchida S, Kuwahara M, Saito H, et al. Molecular cloning and expression of a member of the aquaporin family with permeability to glycerol and urea in addition to water expressed at the basolateral membrane of kidney collecting duct cells. *Proc Natl Acad Sci U S A.* 1994;91(14):6269–73.
72. Ma T, Yang B, Kuo WL, Verkman AS. cDNA cloning and gene structure of a novel water channel expressed exclusively in human kidney: evidence for a gene cluster of aquaporins at chromosome locus 12q13. *Genomics.* 1996;35(3):543–50.
73. Ishibashi K, Kuwahara M, Gu Y, Tanaka Y, Marumo F, Sasaki S. Cloning and functional expression of a new aquaporin (AQP9) abundantly expressed in the peripheral leukocytes permeable to water and urea, but not to glycerol. *Biochem Biophys Res Commun.* 1998;244(1):268–74.
74. Hibuse T, Maeda N, Nagasawa A, Funahashi T. Aquaporins and glycerol metabolism. *Biochim Biophys Acta.* 2006;1758(8):1004–11.
75. Hatakeyama S, Yoshida Y, Tani T, Koyama Y, Nihei K, Ohshiro K, et al. Cloning of a new aquaporin (AQP10) abundantly expressed in duodenum and jejunum. *Biochem Biophys Res Commun.* 2001;287(4):814–9.
76. Kellen MR, Bassingthwaite JB. An integrative model of coupled water and solute exchange in the heart. *Am J Physiol Heart Circ Physiol.* 2003;285(3):H1303–16.
77. Kellen MR, Bassingthwaite JB. Transient transcapillary exchange of water driven by osmotic forces in the heart. *Am J Physiol Heart Circ Physiol.* 2003;285(3):H1317–31.
78. Egan JR, Butler TL, Au CG, Tan Y-M, North KN, Winlaw DS. Myocardial water handling and the role of aquaporins. *Biochim Biophys Acta.* 2006;1758(8):1043–52.
79. Gannon BJ, Carati CJ. Endothelial distribution of the membrane water channel molecule aquaporin-1: implications for tissue and lymph fluid physiology? *Lymphat Res Biol.* 2003;1(1):55–66.

80. Goodwin FC, Muntoni F. Cardiac involvement in muscular dystrophies: molecular mechanisms. *Muscle Nerve*. 2005;32(5):577–88.
81. Frigeri A, Nicchia GP, Repetto S, Bado M, Minetti C, Svelto M. Altered aquaporin-4 expression in human muscular dystrophies: a common feature? *FASEB J*. 2002;16(9):1120–2.
82. Egan JR, Butler TL, Cole AD, Aharonyan A, Baines D, Street N, et al. Myocardial ischemia is more important than the effects of cardiopulmonary bypass on myocardial water handling and postoperative dysfunction: a pediatric animal model. *J Thorac Cardiovasc Surg*. 2008;136(5):1265–73.
83. Egan JR, Butler TL, Cole AD, Abraham S, Murala JS, Baines D, et al. Myocardial membrane injury in pediatric cardiac surgery: An animal model. *J Thorac Cardiovasc Surg*. 2009;137(5):1154–62.
84. Warth A, Eckle T, Kohler D, Faigle M, Zug S, Klingel K, et al. Upregulation of the water channel aquaporin-4 as a potential cause of postschematic cell swelling in a murine model of myocardial infarction. *Cardiology*. 2007;107(4):402–10.
85. Askenasy N. Is cytotoxic cellular edema real? The effect of calcium ion on water homeostasis in the rat heart. *Cardiovasc Toxicol*. 2001;1(1):21–34.
86. Butler TL, Egan JR, Graf FG, Au CG, McMahon AC, North KN, et al. Dysfunction induced by ischemia versus edema: does edema matter? *J Thorac Cardiovasc Surg*. 2009;138(1):141–7. 7 e1.
87. Gambert S, Helies-Toussaint C, Grynberg A. Extracellular glycerol regulates the cardiac energy balance in a working rat heart model. *Am J Physiol Heart Circ Physiol*. 2007;292(3):H1600–6.
88. Li SZ, McDill BW, Kovach PA, Ding L, Go WY, Ho SN, et al. Calcineurin-NFATc signaling pathway regulates AQP2 expression in response to calcium signals and osmotic stress. *Am J Physiol Cell Physiol*. 2007;292(5):C1606–16.
89. Brette F, Orchard C. T-tubule function in mammalian cardiac myocytes. *Circ Res*. 2003;92(11):1182–92.
90. Finsterer J, Stollberger C. Primary myopathies and the heart. *Scand Cardiovasc J*. 2008;42(1):9–24.
91. Gavillet B, Rougier JS, Domenighetti AA, Behar R, Boixel C, Ruchat P, et al. Cardiac sodium channel Nav1.5 is regulated by a multiprotein complex composed of syntrophins and dystrophin. *Circ Res*. 2006;99(4):407–14.
92. He XP, Chen DF, Zheng JH, Du S, Deng B, Zhang S. Effect of jianxin pinglu pill on arrhythmia and aquaporin 4 expression in rats with myocardial ischemia/reperfusion injury. *Zhongguo Zhong Xi Yi Jie He Za Zhi*. 2004;24(9):823–6.
93. Frigeri A, Gropper MA, Umenishi F, Kawashima M, Brown D, Verkman AS. Localization of MIWC and GLIP water channel homologs in neuromuscular, epithelial and glandular tissues. *J Cell Sci*. 1995;108:2993–3002.
94. Frigeri A, Nicchia GP, Svelto M. Aquaporins as targets for drug discovery. *Curr Pharm Des*. 2007;13(23):2421–7.
95. Jung JS, Preston GM, Smith BL, Guggino WB, Agre P. Molecular structure of the water channel through aquaporin CHIP. The hourglass model. *J Biol Chem*. 1994;269(20):14648–54.
96. Castle NA. Aquaporins as targets for drug discovery. *Drug Discov Today*. 2005;10(7):485–93.

Part VII

Drugs and Cardiac Arrhythmia

Chapter 33

Ion Channels as New Drug Targets in Atrial Fibrillation

Ursula Ravens

33.1 Introduction

Atrial fibrillation (AF) is initiated when abnormal focal electrical activity encounters a suitable substrate that allows re-entry propagation. AF is often associated with cardiac disease, especially heart failure, and old age is a risk factor. Nevertheless, about one-third of the patients have so-called “lone” AF without underlying heart disease. Current pharmacological therapy is often ineffective and has many side effects, so new drugs are highly desired. A brief outline of the atrial action potential, the electrophysiological mechanisms of AF, and the accompanying remodelling processes provide the conceptual framework that has led to new drug development for treatment of AF.

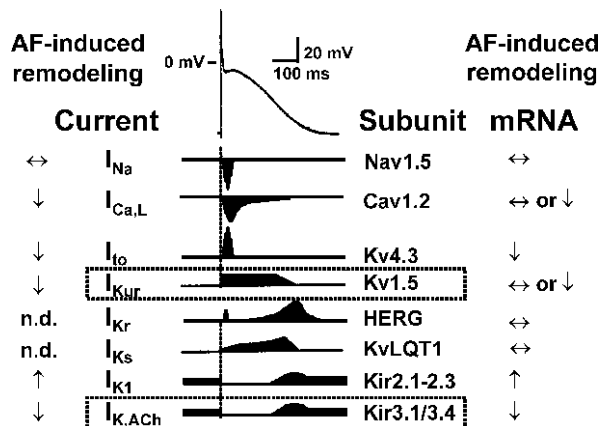
33.2 The Atrial Action Potential

During the cardiac action potential (AP), distinct ion channels open and close in a voltage- and time-dependent manner, producing depolarizing (inward) and repolarizing (outward) current (see Fig. 33.1). The resting membrane potential is mainly determined by the inward K^+ rectifier currents, I_{K1} , $I_{K,ACh}$, and $I_{K,ATP}$, in combination with electrogenic ion transporters and exchangers. The upstroke of the action potential is initiated by the rapidly activating and inactivating Na^+ current I_{Na} . The plateau phase is maintained by a delicate balance of depolarizing Ca^{2+} influx (L-type Ca^{2+} current $I_{Ca,L}$) and repolarizing K^+ currents. The latter include the transient outward current I_{to} , the ultrarapidly activating, outwardly rectifying current I_{Kur} , the rapidly and the slowly activating delayed rectifier currents, I_{Kr} and I_{Ks} , the background inward rectifier, I_{K1} , and the acetylcholine-activated inward

U. Ravens

Department of Pharmacology and Toxicology, Medical Faculty Carl Gustav Carus, Dresden University of Technology, Fetscherstrasse 74, 01307 Dresden, Germany
e-mail: ravens@rcs.urz.tu-dresden.de

Fig. 33.1 Typical shape of an atrial action potential from a patient in sinus rhythm, and scheme of the underlying currents and ion channels. The changes due to electrical remodelling are indicated by the arrows, *n.d.*, not determined. The dotted frames emphasize “atrial-selective” outward currents not found in ventricles. Modified from The Sicilian gambit [71]



rectifier, $I_{K,ACh}$. Among these potassium channels, I_{Kur} and $I_{K,ACh}$ are confined to the atria with almost no expression in the ventricles and are, therefore, considered as atrial-selective.

33.3 Electrophysiological Background of AF

Ectopic pacemaker activity, often originating in the orifices of the pulmonary veins, or individual extrasystoles developing at any site within the atria are typical triggers for AF, which must meet a substrate that will support re-entrant activity. Re-entry occurs when an excitation wavefront returns to its origin and encounters tissue that is no longer refractory. The circulating wavefront can initiate further excitatory waves to the surrounding tissue at its own high frequency thereby maintaining AF (“leading circle theory” [1]). Short refractoriness and slow conduction increase the likelihood of re-entry. Conversely, prolonged refractoriness and enhanced conduction terminate re-entry because the wavefront is extinguished when reaching tissue that is still in the refractory state. Re-entry can also be conceived as a spiral wave where the wavefront is rotating around a central core (rotor) [2]. The rotor turns faster and in a more stable position when the excitability is higher and the refractory period shorter (stabilization of rotor). Reduction of excitability and prolongation of refractoriness slow down and enlarge the rotor, so it is more likely to collapse.

Instabilities of the membrane potential either at the AP plateau or resting level are referred to as early and delayed after depolarizations (EADs, DADs), respectively, which can serve as triggers for ectopic activity. During critical prolongation of the AP plateau phase, inactivated Na^+ and/or Ca^{2+} channels may reopen, providing the extradepolarizing current for EADs (see Chap. 9). In the atria EADs may provide a trigger for initiating AF, and in the ventricles, EADs lead to

torsades de pointes arrhythmia or even fibrillation; DADs are typically observed under conditions of sarcoplasmic reticulum (SR) Ca^{2+} overload [3] or abnormal SR Ca^{2+} release [4, 5]. Physiologically, cellular excitation-induced Ca^{2+} influx through L-type Ca^{2+} channels triggers Ca^{2+} release from the SR via Ca^{2+} release channels. This Ca^{2+} is pumped back into the SR during diastole. High Ca^{2+} load of the SR causes spontaneous Ca^{2+} release without prior excitation. The resulting cytosolic Ca^{2+} increase activates the plasmalemmal Na^+ , Ca^{2+} exchanger that produces the transient inward current underlying DADs (see Chap. 30).

The autonomic nervous system regulates heart rate and rhythm and malfunction of either sympathetic or vagal tone can generate and maintain arrhythmia. In particular AF is promoted by adrenergic as well as cholinergic mechanisms [6–8]. Adrenergic stimulation is an effective trigger of arrhythmias via enhancing EADs and DADs with little effect on arrhythmia maintenance. Conversely, cholinergic mechanisms are important both as triggers and contributors to the maintenance of AF [9].

33.4 Electrical and Structural Remodelling in AF

Patients with lone AF have been studied for genetic causes of the arrhythmia. Most known mutations in genes encoding for K^+ channel proteins associated with familial atrial fibrillation suggest that gain of function of K^+ currents (I_{Kr} , I_{Ks} , I_{K1}) increases arrhythmogenic risk, but also loss of function mutations have been reported [10]. Several gene polymorphisms enhance susceptibility to AF without causing the arrhythmia (see Chap. 27).

Atrial fibrillation has a strong tendency to become persistent the longer the arrhythmia lasts [11]. This characteristic property of AF is thought to be due to profound structural and electrical alterations (remodelling) caused by a plethora of malfunctions, including disturbed intracellular Ca^{2+} handling [12, 13]. Electrical remodelling is characterized by shortening of the atrial refractory period and the inability of the cardiac action potential to adapt to increased frequency [14]. Reduced refractoriness supports multiple wavelet re-entry and periodic activity of sustained, high-frequency functional re-entry sources known as “rotors,” which are thought to contribute to sustained AF [15]. The high rate of electrical activity during AF imposes an enormous Ca^{2+} load on the myocardial cells, compromising cellular Ca^{2+} homeostasis [16]. As a consequence, multiple cellular functions are altered including stability of membrane potential, regulation of proteins by phosphorylation or nitrosylation, or changes in gene expression of ion channels.

Remodeled action potentials in chronic AF have a short triangular shape, [14] and the underlying cellular mechanisms for atrial electrical remodelling have been reviewed in depth [17]. Briefly, $I_{\text{Ca,L}}$ is reduced [72] probably due to altered channel phosphorylation [18], although some authors also found decreased expression of mRNA [73]. I_{to} and $I_{\text{K,ACh}}$ are also diminished in amplitude and this is associated with a decline in mRNA for the ion conducting α -subunits $\text{K}_{\text{v}}4.3$ and $\text{K}_{\text{ir}}3.1/\text{K}_{\text{ir}}3.4$,

respectively (compare Fig. 33.1). Delayed rectifier K⁺ currents I_{Kr} is extremely small [76] and I_{Ks} measured as current sensitive to the selective I_{Ks} blocker HMR-1556 is increased [76, 77]. The findings on I_{Kur} are conflicting, with reports of no change or down-regulation of current, mRNA and protein of the pore forming α -subunit Kv1.5. Current amplitude of background inward rectifier I_{K1} and mRNA for Kv2.1/Kv2.3 were up-regulated [19, 20]. These findings raise the question whether atrial remodelling will leave the two atria-selective channels I_{Kur} and I_{K_ACh} in a sufficiently intact state of function for them to serve as useful drug targets.

Atrial fibrillation also induces structural and ultrastructural changes in atrial tissue, for which the term “structural remodelling” has been coined [21]. High-frequency, uncoordinated atrial activation during AF leads to an increase in local angiotensin synthesis, oxidative injury to atrial myocytes, inflammation, altered cell metabolism, restructuring of extracellular matrix, uncoupling of gap junctions, hypertrophy and fibrosis, all of which provide a “morphologic substrate” for maintenance of atrial fibrillation [22–24]. Therefore, drugs that interfere with these mechanisms may prevent structural remodelling.

33.5 Current Drug Treatment of AF

Unlike ventricular fibrillation, AF is not immediately life-threatening although mortality is increased largely due to associated stroke [25]. By intuition, rhythm control would be the optimal therapeutic goal in AF; however, rate control was shown to be equivalent with respect to mortality [26]. Suppression of atrial triggers and prolongation of atrial refractory period should terminate AF and hence support rhythm control, whereas rate control involves prolongation of atrioventricular nodal refractoriness and slowing of atrioventricular nodal conduction by different classes of drugs like β -blockers, Ca²⁺ channel blockers or amiodarone.

Currently available antiarrhythmic drugs for treatment of AF – perhaps with the exception of amiodarone – are not sufficiently effective and are burdened by cardiac and extracardiac side effects that may offset their therapeutic benefits. Treatment of AF with class I agents is limited by negative inotropic effects and by ventricular proarrhythmic effects particularly in patients with ischemic heart disease and severe left ventricular dysfunction [27]. Interestingly, the two theories of re-entry will result in opposite consequences of drug-induced Na⁺ channel block on re-entry. According to the leading circle theory, reduced conduction velocity due to block of Na⁺ channels facilitates re-entry. Re-entrant rotors, on the other hand, are destabilized by reduced excitability due to Na⁺ channel block. This antiarrhythmic effect is therapeutically exploited when using class I antiarrhythmic drugs (flecainide, propafenone) for conversion of AF to sinus rhythm.

Class III drugs (sotalol, dofetilide) suppress re-entry by prolongation of action potential duration and refractoriness, but may induce EADs and torsades de pointes arrhythmias in the atria and the ventricles. The risk for torsades de pointes and sudden cardiac death may be particularly high with agents directed towards selective block

of individual K^+ channels, e.g., hERG channels [28]. In fact, it is not clear whether targeting an individual ion channel may be a good idea in the first place given the antiarrhythmic efficacy of the multiple ion channel blocker amiodarone, although this drug is discriminated by serious extracardiac side effects.

The concept of “upstream therapy” comprises angiotensin-converting enzyme inhibitors, angiotensin-receptor blockers, aldosterone antagonists, statins, and omega-3 polyunsaturated fatty acids, although the effectiveness of some of these agents remains controversial [29].

33.6 Novel Approaches

Given the chronic character of AF, new drugs must meet high standards regarding efficacy and safety. As outlined above, combination of block of different ion channels may produce the most favorable electrophysiological profile. The newly registered antiarrhythmic drug dronedarone does in fact block I_{Na} , $I_{Ca,L}$, I_{to} , I_{Kr} , I_{Ks} , $I_{K,ACh}$, and β_1 -adrenoceptors, but lacks the iodine moiety that may be responsible for the pulmonary, thyroid, hepatic, and ocular toxicity of amiodarone. Dronedarone is supposed to have less side effects, but also less efficacy [30]. Another strategy is to develop drugs with high selectivity for atrial versus ventricular myocardium (see below).

33.6.1 Atrial-Selective Drugs

Sodium channel blockers will exhibit selectivity for atrial over ventricular tissue when a number of prerequisites are met: The drugs must bind preferentially to inactivated rather than open or closed channels and have rapid dissociation kinetics during rest. Ranolazine and amiodarone fulfill these conditions and are considered to be “atrial-selective” Na^+ channel blockers [31]. Atrial selectivity is also due to the differences in electrophysiological properties between atria and ventricles. In atria, the resting membrane potential is more depolarized than in ventricle and the potential for half-maximum inactivation of I_{Na} is about -10 mV more negative. Therefore, in atria fewer channels fully recover during diastole but remain in the inactivated, drug-binding state. Since drug affinity is lower for resting than inactivated channels, drug is preferentially released from channels in the resting state. This condition is met in the ventricles where a larger fraction of Na^+ channels recovers from inactivation during diastole and hence allows drug to dissociate. In addition, there is a disease-specific component of atrial selectivity due to the high atrial rate in AF, which further enhances block of Na^+ channels [32]. In the case of vernakalant, which also blocks inactivated Na^+ channels and has rapid dissociation kinetics [74], atrial selectivity is further supported by block of atrial-selective $I_{K,ACh}$ [75] and I_{Kur} [33] (see below). Vernakalant has been approved in Europe

by the EU for intravenous conversion of AF to sinus rhythm by the end of 2010 (Merck personal information).

The cardiac Na^+ current consists of two components, a rapidly activating and inactivating “peak” current $I_{\text{Na},\text{P}}$ and a “late” current $I_{\text{Na},\text{L}}$. In ventricular cardiomyocytes of normal donor and explanted failing human hearts this $I_{\text{Na},\text{L}}$ has been characterized by an ultraslow, voltage-independent inactivation and reactivation [34]. $I_{\text{Na},\text{L}}$ is increased in ischemia, hypertrophy, and heart failure [35] and is likely to contribute to heart failure-associated AP prolongation and beat-to-beat variability, since block of $I_{\text{Na},\text{L}}$ with ranolazine shortens action potential duration in heart failure myocytes and eliminates EADs [36]. Amiodarone also blocks $I_{\text{Na},\text{L}}$ in heart failure [37]. Notably, several drugs that display atrial selectivity as outlined above also block $I_{\text{Na},\text{L}}$ [38], which may counteract the block of I_{Kr} and hence provide protection against excessive ventricular action potential prolongation when these drugs are used in AF. $I_{\text{Na},\text{L}}$ has been observed in rabbit [38], but so far not in human atrial tissue.

In humans, the ultrarapidly activating K^+ current, I_{Kur} , is detected only in the atria but not in the ventricle, allowing atrial-selective drug targeting. Indeed, many drug companies are developing selective I_{Kur} blockers which prolong atrial APD and hence ERP, without producing ventricular AP prolongation that may deteriorate into torsades de pointes arrhythmias [39]. However, AF-induced remodelling decreases I_{Kur} amplitude and may alter its sensitivity towards block [40], casting some doubt on the usefulness of this principle.

Block of another atrial-selective current, the acetylcholine-activated inwardly rectifying K^+ current, $I_{\text{K},\text{ACh}}$, could be useful in vagally induced AF. However, selective $I_{\text{K},\text{ACh}}$ blockers could produce undue sinus bradycardia. Interestingly, the new multichannel blocker dronedarone is 100 times more potent in blocking $I_{\text{K},\text{ACh}}$ than its precursor compound amiodarone [30, 41]. We and others have recently reported that $I_{\text{K},\text{ACh}}$ develops constitutive activity during AF-induced remodelling [42–44]. In cell-attached single channel recordings, current flow through $I_{\text{K}1}$ and $I_{\text{K},\text{ACh}}$ channels can be distinguished by their distinct gating behavior and single channel conductance (Fig. 33.2). Constitutive activity of $I_{\text{K},\text{ACh}}$ provides not only an atrial selective, but also a pathology-selective drug target. In dogs, a corresponding

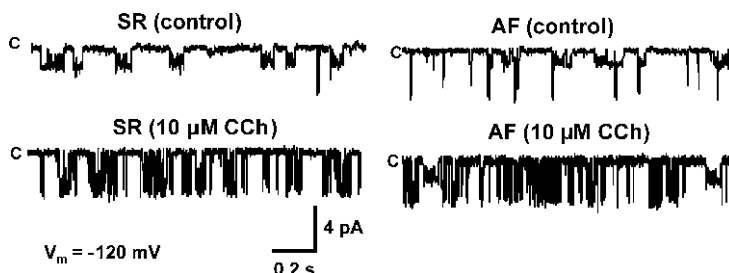


Fig. 33.2 Cell-attached single channel recording of inward rectifier $I_{\text{K}1}$ and constitutively active $I_{\text{K},\text{ACh}}$ in atrial myocytes isolated from a patient in sinus rhythm (left) and in chronic atrial fibrillation (right). Data from [19], with kind permission of the publisher

constitutively active $I_{K,ACh}$ -like current is upregulated in response to atrial tachypacing and blockade of this current by the highly selective $I_{K,ACh}$ blocker tertiapin-Q resulted in prolongation of the APD and suppression of inducible AF episodes [42].

Many antiarrhythmic drugs block ligand-activated $I_{K,ACh}$ in a concentration-dependent manner with no difference in potency between atrial cardiomyocytes from sinus rhythm or AF. However, in a recent study only flecainide and the investigative compound AVE0118 also reduced AF-related constitutively active $I_{K,ACh}$ while dofetilide and propafenone did not [45]. It is presently not known, whether block of constitutively active $I_{K,ACh}$ contributes to clinical therapeutic efficacy in converting atrial fibrillation and maintaining sinus rhythm.

33.6.2 *Ion Channels with Unknown Potential as Drug Targets*

Besides conventional ion channels that are accepted to determine the shape of the atrial AP (Fig. 33.1), multiple additional families of ion channels have been suggested to contribute. Two-pore-domain potassium (K2P) channels belong to a large family of background leak channels that are highly regulated and control excitability, stabilize membrane potential below firing threshold and shorten ERP [46]. They are robustly expressed in the cardiovascular system and are involved in multiple physiological functions, including cardioprotection, regulation of cardiac rhythm and mechanical stress [47]. Block of these K^+ background channels prolongs APD in mouse ventricle [48] and could contribute to arrhythmogenesis via initiation of EAD leading to torsades de pointes and fibrillation. However, it is not known whether K2P channels could be promising antiarrhythmic drug targets in AF. Human cardiac K2P3.1 (TASK-1) potassium leak channels heterologously expressed in *Xenopus* oocytes were blocked by amiodarone in therapeutically relevant concentrations [49].

The transient receptor potential (TRP) channels of the canonical family (TRPC) have been recognized to contribute to abnormal Ca^{2+} influx under pathophysiological conditions such as hypertrophy (for recent review see, [50]). TRPC1 and TRPC3 are expressed in human atrial myocytes from patients with diseased hearts, and protein expression of TRPC3 is increased in AF patients [51]. Further details on TRPC channels are summarized in Chap. 31.

The transient inward current underlying DADs is carried by the Na^+ , Ca^{2+} exchanger, but in addition, a Ca^{2+} -activated nonselective cation current may also contribute to DADs in human atrial myocytes [52]. However, contribution of a Ca^{2+} -activated Cl^- current seems unlikely because these currents are absent in human atria [53]. Detailed electrophysiological analysis of Ca^{2+} -activated nonselective cation channels in freshly isolated human atrial myocytes revealed striking resemblance to the properties of TRP channels of the melastatin family TRPM4b and TRPM5 [52], suggesting that these channels might indeed be involved in Ca^{2+} overload induced arrhythmogenesis [54].

Mechanical stretch is a cause of spontaneous electrical activity [55] and arrhythmia. Stretch-activated channels were shown to be involved in AF, because arrhythmia

induction by acute atrial dilation can be suppressed with the selective stretch-activated channel blocker GsMTx4, a peptide isolated from tarantula venom [56]. Interestingly, in ventricular myocytes TRPC6 channel activity is modulated by mechanical strain [57]. Modulation of stretch-activated channels as an antiarrhythmic target is worthy of investigation, although effective model drugs are not known. For further details of the role of TRP channels in cardiac arrhythmia the reader is referred to recent reviews [58, 59].

Recent evidence suggests that Ca^{2+} -activated K^+ channels with small conductance (SK), long known for limiting excessive Ca^{2+} entry in vascular smooth muscle [60], are also expressed in mouse and human hearts, and of the three channel subunits SK1-3, SK2 is selectively distributed in atria [61]. In genetically engineered mice, increase in SK2 abbreviated APD [62], while loss of SK2 function prolonged APD and induced EAD [63]. This ion channel has been proposed to be a novel contributor in AF associated electrical remodelling of atria [64].

33.6.3 Other Mechanisms

Facilitating conduction via gap junctions is an important new antiarrhythmic principle in both ventricular and atrial arrhythmias [65]. The antiarrhythmic peptide AAP10 [66, 67] and the stable analog rotigaptide (ZIP123) [68] improved intercellular coupling and prevented ischemia-induced slowing of conduction. Though rotigaptide enhanced conduction in various AF models, the arrhythmia was only suppressed in the ischemic substrate model [69].

Enhancing instead of blocking K^+ channel activity in order to stabilize the resting membrane potential, especially in patients with long QT syndrome, could be a useful antiarrhythmic principle. Indeed, several drug companies are at present investigating HERG channel openers for their antiarrhythmic potential [70].

33.7 Conclusions

Increased knowledge of the pathophysiology of AF-induced remodelling has led to the development of atrial- and pathology-selective drugs. Exploration of new putative antiarrhythmic concepts directed at previously neglected ion channels (K2P, TRP), gap junctions, proteins involved in Ca^{2+} homeostasis, neurohormones, and receptor systems may lead to new drugs with the expected level of efficacy and safety for treatment of AF.

Acknowledgments The author acknowledges financial support from Fondation Leducq (07 CVD 03, “Leducq European-North American Atrial Fibrillation Research Alliance”) and the German Federal Ministry of Education and Research (Atrial Fibrillation Competence Network, member of the steering committee; New Antiarrhythmic Drugs, Research project 03FPB00226).

References

1. Allessie MA, Bonke FI, Schopman FJ. Circus movement in rabbit atrial muscle as a mechanism of tachycardia. III. The “leading circle” concept: a new model of circus movement in cardiac tissue without the involvement of an anatomical obstacle. *Circ Res*. 1977;41(1):9–18.
2. Vaquero M, Calvo D, Jalife J. Cardiac fibrillation: from ion channels to rotors in the human heart. *Heart Rhythm*. 2008;5(6):872–9.
3. Bers DM. Cardiac excitation–contraction coupling. *Nature*. 2002;415(6868):198–205.
4. Dobrev D, Nattel S. Calcium handling abnormalities in atrial fibrillation as a target for innovative therapeutics. *J Cardiovasc Pharmacol*. 2008;52(4):293–9.
5. Vest JA, Wehrens XH, Reiken SR, Lehnart SE, Dobrev D, Chandra P, et al. Defective cardiac ryanodine receptor regulation during atrial fibrillation. *Circulation*. 2005;111(16):2025–32.
6. Betttoni M, Zimmermann M. Autonomic tone variations before the onset of paroxysmal atrial fibrillation. *Circulation*. 2002;105(23):2753–9.
7. Jordae L, Tavernier R, Gorgov N, Kindt H, Dimmer C, Clement DL. Signal-averaged P wave: predictor of atrial fibrillation. *J Cardiovasc Electrophysiol*. 1998;9(8 Suppl):S30–4.
8. Workman AJ. Cardiac adrenergic control and atrial fibrillation. *Naunyn Schmiedebergs Arch Pharmacol*. 2010;381(3):235–249.
9. Liu L, Nattel S. Differing sympathetic and vagal effects on atrial fibrillation in dogs: role of refractoriness heterogeneity. *Am J Physiol*. 1997;273(2 Pt 2):H805–16.
10. Olson TM, Alekseev AE, Liu XK, Park S, Zingman LV, Bienengraeber M, et al. Kv1.5 channelopathy due to KCNA5 loss-of-function mutation causes human atrial fibrillation. *Hum Mol Genet*. 2006;15(14):2185–91.
11. Wijffels MC, Kirchhof CJ, Dorland R, Allessie MA. Atrial fibrillation begets atrial fibrillation. A study in awake chronically instrumented goats. *Circulation*. 1995;92(7):1954–68.
12. Lenaerts I, Bito V, Heinzel FR, Driesen RB, Holemans P, D’hooge J, et al. Ultrastructural and functional remodeling of the coupling between Ca^{2+} influx and sarcoplasmic reticulum Ca^{2+} release in right atrial myocytes from experimental persistent atrial fibrillation. *Circ Res*. 2009;105(9):876–85.
13. Nattel S, Maguy A, Le Bouter S, Yeh YH. Arrhythmogenic ion-channel remodeling in the heart: heart failure, myocardial infarction, and atrial fibrillation. *Physiol Rev*. 2007;87(2):425–56.
14. Dobrev D, Ravens U. Remodeling of cardiomyocyte ion channels in human atrial fibrillation. *Basic Res Cardiol*. 2003;98(3):137–48.
15. Pandit SV, Berenfeld O, Anumonwo JM, Zaritski RM, Kneller J, Nattel S, et al. Ionic determinants of functional reentry in a 2-D model of human atrial cells during simulated chronic atrial fibrillation. *Biophys J*. 2005;88(6):3806–21.
16. Dobrev D. Atrial Ca^{2+} signaling in atrial fibrillation as an antiarrhythmic drug target. *Naunyn Schmiedebergs Arch Pharmacol*. 2010;381(3):195–206.
17. Nattel S, Burstein B, Dobrev D. Atrial remodeling and atrial fibrillation: mechanisms and implications. *Circ Arrhythm Electrophysiol*. 2008;1(1):62–73.
18. Christ T, Boknik P, Wohrl S, Wettwer E, Graf EM, Bosch RF, et al. L-type Ca^{2+} current downregulation in chronic human atrial fibrillation is associated with increased activity of protein phosphatases. *Circulation*. 2004;110(17):2651–7.
19. Dobrev D, Graf E, Wettwer E, Himmel HM, Hala O, Doerfel C, et al. Molecular basis of downregulation of G-protein-coupled inward rectifying K(+) current ($I_{\text{K}, \text{ACh}}$) in chronic human atrial fibrillation: decrease in GIRK4 mRNA correlates with reduced $I_{\text{K}, \text{ACh}}$ and muscarinic receptor-mediated shortening of action potentials. *Circulation*. 2001;104(21):2551–7.
20. Voigt N, Trausch A, Knaut M, Matschke K, Varro A, Van Wagoner DR, et al. Left-to-right atrial inward rectifier potassium current gradients in patients with paroxysmal versus chronic atrial fibrillation. *Cir Arrhythm Electrophysiol*. 2010;3(5):472–480.

21. Ausma J, Wijffels M, Thone F, Wouters L, Allessie M, Borgers M. Structural changes of atrial myocardium due to sustained atrial fibrillation in the goat. *Circulation*. 1997;96(9):3157–63.
22. Goette A, Lendeckel U. Nonchannel drug targets in atrial fibrillation. *Pharmacol Ther*. 2004;102(1):17–36.
23. Li D, Fareh S, Leung TK, Nattel S. Promotion of atrial fibrillation by heart failure in dogs: atrial remodeling of a different sort. *Circulation*. 1999;100(1):87–95.
24. Nattel S. New ideas about atrial fibrillation 50 years on. *Nature*. 2002;415(6868):219–26.
25. Tsang TS, Miyasaka Y, Barnes ME, Gersh BJ. Epidemiological profile of atrial fibrillation: a contemporary perspective. *Prog Cardiovasc Dis*. 2005;48(1):1–8.
26. Wyse DG, Waldo AL, DiMarco JP, Domanski MJ, Rosenberg Y, Schron EB, et al. A comparison of rate control and rhythm control in patients with atrial fibrillation. *N Engl J Med*. 2002;347(23):1825–33.
27. Echt DS, Liebson PR, Mitchell LB, Peters RW, Obias-Manno D, Barker AH, et al. Mortality and morbidity in patients receiving encainide, flecainide, or placebo. The cardiac arrhythmia suppression trial. *N Engl J Med*. 1991;324(12):781–8.
28. Sanguinetti MC, Tristani-Firouzi M. hERG potassium channels and cardiac arrhythmia. *Nature*. 2006;440(7083):463–9.
29. Savelieva I, Kourliouros A, Camm J. Primary and secondary prevention of atrial fibrillation with statins and polyunsaturated fatty acids: review of evidence and clinical relevance. *Naunyn Schmiedebergs Arch Pharmacol*. 2010;381(3):1–13.
30. Patel C, Yan GX, Kowey PR. Dronedarone. *Circulation*. 2009;120(7):636–44.
31. Antzelevitch C, Burashnikov A. Atrial-selective sodium channel block as a novel strategy for the management of atrial fibrillation. *J Electrocardiol*. 2009;42(6):543–8.
32. Burashnikov A, Di Diego JM, Zygmunt AC, Belardinelli L, Antzelevitch C. Atrium-selective sodium channel block as a strategy for suppression of atrial fibrillation: differences in sodium channel inactivation between atria and ventricles and the role of ranolazine. *Circulation*. 2007;116(13):1449–57.
33. Kozlowski D, Budrejko S, Lip GY, Mikhailidis DP, Rysz J, Raczk G, et al. Vernakalant hydrochloride for the treatment of atrial fibrillation. *Expert Opin Investig Drugs*. 2009;18(12):1929–37.
34. Maltsev VA, Sabbah HN, Higgins RS, Silverman N, Lesch M, Undrovinas AI. Novel, ultraslow inactivating sodium current in human ventricular cardiomyocytes. *Circulation*. 1998;98(23):2545–52.
35. Valdivia CR, Chu WW, Pu J, Foell JD, Haworth RA, Wolff MR, et al. Increased late sodium current in myocytes from a canine heart failure model and from failing human heart. *J Mol Cell Cardiol*. 2005;38(3):475–83.
36. Undrovinas AI, Belardinelli L, Undrovinas NA, Sabbah HN. Ranolazine improves abnormal repolarization and contraction in left ventricular myocytes of dogs with heart failure by inhibiting late sodium current. *J Cardiovasc Electrophysiol*. 2006;17 Suppl 1:S169–77.
37. Maltsev VA, Sabbah HN, Undrovinas AI. Late sodium current is a novel target for amiodarone: studies in failing human myocardium. *J Mol Cell Cardiol*. 2001;33(5):923–32.
38. Persson F, Andersson B, Duker G, Jacobson I, Carlsson L. Functional effects of the late sodium current inhibition by AZD7009 and lidocaine in rabbit isolated atrial and ventricular tissue and Purkinje fibre. *Eur J Pharmacol*. 2007;558(1–3):133–43.
39. Ford JW, Milnes JT. New drugs targeting the cardiac ultra-rapid delayed-rectifier current (I_{Kur}): rationale, pharmacology and evidence for potential therapeutic value. *J Cardiovasc Pharmacol*. 2008;52(2):105–20.
40. Christ T, Wetzweller E, Voigt N, Hala O, Radicke S, Matschke K, et al. Pathology-specific effects of the $I_{Kur}/I_{to}/I_K$, ACh blocker AVE0118 on ion channels in human chronic atrial fibrillation. *Br J Pharmacol*. 2008;154(8):1619–30.
41. Guillemaire E, Marion A, Nisato D, Gautier P. Inhibitory effects of dronedarone on muscarinic K^+ current in guinea pig atrial cells. *J Cardiovasc Pharmacol*. 2000;36(6):802–5.

42. Cha TJ, Ehrlich JR, Chartier D, Qi XY, Xiao L, Nattel S. Kir3-based inward rectifier potassium current: potential role in atrial tachycardia remodeling effects on atrial repolarization and arrhythmias. *Circulation*. 2006;113(14):1730–7.
43. Dobrev D, Friedrich A, Voigt N, Jost N, Wettwer E, Christ T, et al. The G protein-gated potassium current I(K, ACh) is constitutively active in patients with chronic atrial fibrillation. *Circulation*. 2005;112(24):3697–706.
44. Voigt N, Friedrich A, Bock M, Wettwer E, Christ T, Knaut M, et al. Differential phosphorylation-dependent regulation of constitutively active and muscarinic receptor-activated IK, ACh channels in patients with chronic atrial fibrillation. *Cardiovasc Res*. 2007;74(3):426–37.
45. Voigt N, Rozmaritsa N, Trausch A, Zimniak T, Christ T, Wettwer E, et al. Inhibition of $I_{K,ACh}$ current may contribute to clinical efficacy of class I and class III antiarrhythmic drugs in patients with atrial fibrillation. *Naunyn Schmiedebergs Arch Pharmacol*. 2010;381(3):251–259.
46. Goldstein SA, Bockenhauer D, O'Kelly I, Zilberman N. Potassium leak channels and the KCNK family of two-P-domain subunits. *Nat Rev Neurosci*. 2001;2(3):175–84.
47. Gerten J, Ficker E, Bloehs R, Schlomer K, Kathofer S, Scholz E, et al. Regulation of two-pore-domain (K2P) potassium leak channels by the tyrosine kinase inhibitor genistein. *Br J Pharmacol*. 2008;154(8):1680–90.
48. Putzke C, Wemhoner K, Sachse FB, Rinne S, Schlichthorl G, Li XT, et al. The acid-sensitive potassium channel TASK-1 in rat cardiac muscle. *Cardiovasc Res*. 2007;75(1):59–68.
49. Gerten J, Ficker E, Bloehs R, Schweizer PA, Zitron E, Scholz E, et al. The human cardiac K2P3.1 (TASK-1) potassium leak channel is a molecular target for the class III antiarrhythmic drug amiodarone. *Naunyn Schmiedebergs Arch Pharmacol*. 2010;381(3):261–270.
50. Nishida M, Kurose H. Roles of TRP channels in the development of cardiac hypertrophy. *Naunyn Schmiedebergs Arch Pharmacol*. 2008;378(4):395–406.
51. Van Wagoner DR, Voigt N, Bunnell B, Barnard J, Schotten U, Nattel S, et al. Transient receptor potential canonical (TRPC) channel subunit remodeling in clinical and experimental AF. *Heart Rhythm*. Abstract 2009;PO06-77.
52. Guinamard R, Chatelier A, Demion M, Potreau D, Patri S, Rahmati M, et al. Functional characterization of a Ca(2+)-activated non-selective cation channel in human atrial cardiomyocytes. *J Physiol*. 2004;558(Pt 1):75–83.
53. Koster OF, Szigeti GP, Beuckelmann DJ. Characterization of a $[Ca^{2+}]_i$ -dependent current in human atrial and ventricular cardiomyocytes in the absence of Na^+ and K^+ . *Cardiovasc Res*. 1999;41(1):175–87.
54. Guinamard R, Demion M, Chatelier A, Bois P. Calcium-activated nonselective cation channels in mammalian cardiomyocytes. *Trends Cardiovasc Med*. 2006;16(7):245–50.
55. Kaufmann R, Theophile U. Autonomously promoted extension effect in Purkinje fibers, papillary muscles and trabeculae carneae of rhesus monkeys. *Pflugers Arch Gesamte Physiol Menschen Tiere*. 1967;297(3):174–89.
56. Bode F, Sachs F, Franz MR. Tarantula peptide inhibits atrial fibrillation. *Nature*. 2001;409(6816):35–6.
57. Dyachenko V, Husse B, Rueckschloss U, Isenberg G. Mechanical deformation of ventricular myocytes modulates both TRPC6 and Kir2.3 channels. *Cell Calcium*. 2009;45(1):38–54.
58. Vassort G, Alvarez J. Transient receptor potential: a large family of new channels of which several are involved in cardiac arrhythmia. *Can J Physiol Pharmacol*. 2009;87(2):100–7.
59. Watanabe H, Murakami M, Ohba T, Ono K, Ito H. The pathological role of transient receptor potential channels in heart disease. *Circ J*. 2009;73(3):419–27.
60. Ledoux J, Werner ME, Brayden JE, Nelson MT. Calcium-activated potassium channels and the regulation of vascular tone. *Physiology (Bethesda)*. 2006;21:69–78.
61. Xu Y, Tuteja D, Zhang Z, Xu D, Zhang Y, Rodriguez J, et al. Molecular identification and functional roles of a Ca(2+)-activated K^+ channel in human and mouse hearts. *J Biol Chem*. 2003;278(49):49085–94.

62. Ozgen N, Dun W, Sosunov EA, Anyukhovsky EP, Hirose M, Duffy HS, et al. Early electrical remodeling in rabbit pulmonary vein results from trafficking of intracellular SK2 channels to membrane sites. *Cardiovasc Res.* 2007;75(4):758–69.
63. Li N, Timofeyev V, Tuteja D, Xu D, Lu L, Zhang Q, et al. Ablation of a Ca^{2+} -activated K^+ channel (SK2 channel) results in action potential prolongation in atrial myocytes and atrial fibrillation. *J Physiol.* 2009;587(Pt 5):1087–100.
64. Nattel S. Calcium-activated potassium current: a novel ion channel candidate in atrial fibrillation. *J Physiol.* 2009;587(Pt 7):1385–6.
65. Dhein S, Hagen A, Jozwiak J, Dietze A, Garbade J, Barten M, et al. Improving cardiac gap junction communication as a new antiarrhythmic mechanism: the action of antiarrhythmic peptides. *Naunyn Schmiedebergs Arch Pharmacol.* 2010;381(3):221–34.
66. Easton JA, Petersen JS, Martin PE. The anti-arrhythmic peptide AAP10 remodels Cx43 and Cx40 expression and function. *Naunyn Schmiedebergs Arch Pharmacol.* 2009;380(1):11–24.
67. Jozwiak J, Dhein S. Local effects and mechanisms of antiarrhythmic peptide AAP10 in acute regional myocardial ischemia: electrophysiological and molecular findings. *Naunyn Schmiedebergs Arch Pharmacol.* 2008;378(5):459–70.
68. Clarke TC, Thomas D, Petersen JS, Evans WH, Martin PE. The antiarrhythmic peptide rotigaptide (ZP123) increases gap junction intercellular communication in cardiac myocytes and HeLa cells expressing connexin 43. *Br J Pharmacol.* 2006;147(5):486–95.
69. Shiroshita-Takeshita A, Sakabe M, Haugan K, Hennan JK, Nattel S. Model-dependent effects of the gap junction conduction-enhancing antiarrhythmic peptide rotigaptide (ZP123) on experimental atrial fibrillation in dogs. *Circulation.* 2007;115(3):310–8.
70. Seeho姆 G. Activators of cation channels: potential in treatment of channelopathies. *Mol Pharmacol.* 2005;67(3):585–8.
71. The Sicilian Gambit. A new approach to the classification of antiarrhythmic drugs based on their actions on arrhythmogenic mechanisms. Task Force of the Working Group on Arrhythmias of the European Society of Cardiology. *Circulation.* 1991;84(4):1831–51.
72. Van Wagoner DR, Pond AL, Lamorgese M, Rossie SS, McCarthy PM, Nerbonne JM. Atrial L-type Ca^{2+} currents and human atrial fibrillation. *Circ Res.* 1999;85(5):428–436.
73. Lai LP, Su MJ, Lin JL, Lin FY, Tsai CH, Chen YS, et al. Changes in the mRNA levels of delayed rectifier potassium channels in human atrial fibrillation. *Cardiology.* 1999;92(4):248–255.
74. Fedida D. Vernakalant (RSD1235): a novel, atrial-selective antifibrillatory agent. *Expert Opin Investig Drugs.* 2007;16(4):519–532.
75. Fedida D, Orth PM, Chen JY, Lin S, Plouvier B, Jung G, et al. The mechanism of atrial antiarrhythmic action of RSD1235. *J Cardiovasc Electrophysiol.* 2005;16(11):1227–1238.
76. Caballero R, de la Fuente MG, Gomez R, Barana A, Amoros I, Dolz-Gaiton P, et al. In humans, chronic atrial fibrillation decreases the transient outward current and ultrarapid component of the delayed rectifier current differentially on each atria and increases the slow component of the delayed rectifier current in both. *J Am Coll Cardiol.* 2010;55(21):2346–2354.
77. Christ T, Wettwer E, Hála O, Dobrev D, Goldack S, Varro A, et al. The slowly activating outward rectifier I_{Ks} is increased in human atrial fibrillation. *J Molec Cell Cardiol.* 2004;36:721 (Abstr.)

Chapter 34

hERG1 Channel Blockers and Cardiac Arrhythmia

Michael C. Sanguinetti and Matthew Perry

34.1 Introduction

Cardiac myocytes express many different types of K^+ channels which conduct currents (Fig. 34.1) that either maintain the resting potential (I_{K1}) or mediate repolarization of the action potential (e.g., I_{to} , I_{Kur} , I_{Kr} , I_{Ks}). I_{to} and I_{Kr} activate and inactivate in response to membrane depolarization, whereas I_{Kur} and I_{Ks} activate but do not inactivate. I_{to} inactivates by an N-type mechanism involving occlusion of the inner vestibule with a ball peptide attached to the N-terminal domain of the α -subunit, whereas I_{Kr} inactivates by a C-type mechanism involving the selectivity filter of the α -subunits. A reduction in any of these currents can slow the rate of ventricular repolarization and prolong the QT interval measured on the body surface ECG. QT lengthening alone is not a problem, but when combined with other risk factors such as hypokalemia or bradycardia, it increases the risk of torsades de pointes, a ventricular arrhythmia that usually reverts to normal sinus rhythm, but that sometimes degenerates into ventricular fibrillation and causes sudden death.

A common cause of drug-induced QT interval prolongation (Fig. 34.2) is the treatment with class III antiarrhythmic agents such as quinidine or dofetilide. These drugs block I_{Kr} and thereby prolong action potential duration of ventricular cardiomyocytes and lengthen QT interval measured on the body surface (Fig. 34.2). Noncardiac medications can also block I_{Kr} and prolong the QT interval as an unintended side effect. Some antihistaminic and antibacterial drugs that are known to block I_{Kr} are only rarely associated with arrhythmia, but are considered dangerous because their intended use is for nonlife-threatening ailments and alternative medications are available that do not share this risk.

M.C. Sanguinetti (✉) and M. Perry

Department of Physiology, Nora Eccles Harrison Cardiovascular Research and Training Institute, University of Utah, 95 South 2000 East, Salt Lake City, UT 84112, USA
e-mail: sanguinetti@cvti.utah.edu

Fig. 34.1 Model of action potential and ionic currents for a human ventricular myocyte

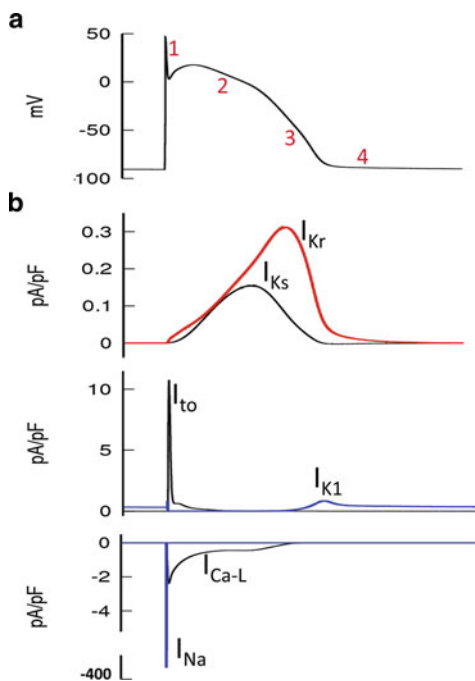
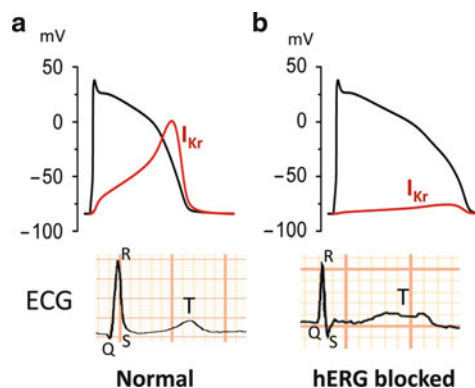


Fig. 34.2 Reduction of I_{Kr} causes prolongation of action potential in cardiac myocytes and lengthening of QT interval measured on body surface ECG. I_{Kr} reduction can result from block of hERG1 channels by drugs or by loss-of-function mutation in the *HERG* gene



In humans, I_{Kr} is conducted by human *ether-a-go-go-related gene* type 1 (hERG1) K^+ channels. With few exceptions, drug-induced QT prolongation in humans is caused by block of hERG1 channels, and not by block of the channels that conduct I_{Ks} , I_{to} or I_{K1} . In this chapter a brief description of the biophysical properties and physiological roles of ERG channels is provided, and the molecular features of hERG1 that explain why these channels are so readily blocked by structurally diverse drugs are considered.

34.2 Molecular and Biophysical Properties of ERG1 Channels

The ERG1 subunit was originally cloned from a human hippocampus cDNA library [1]. In humans, the ERG1 gene is *KCNH2* and it encodes a protein with a predicted molecular mass of 127 kDa. The full-length hERG1 protein is now called hERG1a and alternative splicing produces an N-terminal truncated protein called hERG1b [2, 3]. Two related genes (*KCNH6* and *KCNH7* in humans) encode related channel proteins called hERG2 and hERG3 that are expressed in the nervous system, but not in the heart [4]. Like other Kv channels, functional hERG1 channels are formed by co-assembly of four α -subunits into a tetramer. Channels formed from hERG1b alone are largely retained in the endoplasmic reticulum because of an “RXR” ER retention signal specific to its N terminus and are thus poorly expressed at the cell surface membrane [5]. However, when hERG1b is associated with hERG1a subunits, the heteromultimeric channels readily traffic to the plasma membrane. In addition, the biophysical properties of heterologously expressed hERG1 channels can be altered when co-expressed with β -subunits such as MinK or MiRP1 [6–8], but the physiological relevance of this modulation has been disputed [9]. Moreover, although there is disagreement regarding the expression pattern of MiRP1 in the heart, the subunit appears to be most highly expressed in Purkinje cells of the conduction system with little expression in ventricular muscle [10].

Although hERG1 channels are structurally related to classical delayed rectifier voltage-gated K⁺ (Kv) channels (e.g., *Shaker*), their biophysical properties are intermediate between a typical Kv channel and an inward rectifier K⁺ (Kir) channel. Like Kv channels, the kinetics and open probability of hERG1 are highly voltage-dependent. However, similar to Kir channels, hERG1 currents exhibit significant inward rectification, defined by the negative slope conductance of the fully activated current–voltage (*I*–*V*) relationship at potentials positive to E_K , the equilibrium potential for K⁺. The biophysical basis for the rectification properties of hERG1 is explained by the results of voltage clamp experiments as shown in Fig. 34.3. In these experiments, the cell was bathed in a solution containing a high [K⁺]. Whole-cell current at a positive test potential (+40 mV) is small, whereas, by comparison, tail currents measured at a negative potential (−120 mV) are quite large (Fig. 34.3a). Currents are small at the positive potentials because most channels are inactivated. This can be seen most easily with single-channel recordings (Fig. 34.3b) where, at +40 mV, channel opening is rare if compared to channel activity recorded when the membrane potential is subsequently pulsed to −120 mV. An example of whole-cell currents elicited at physiologically relevant test potentials (−70 to +40 mV) while using the normal level of extracellular [K⁺] (4 mM) is shown in Fig. 34.4a. At most of the negative potentials examined, the currents activate slowly and do not reach a steady-state value during the 2-s pulse. The current magnitude peaks at about −10 mV and at pulses to more positive potentials the rate of current activation increases as the magnitude is decreased. At the end of each 2-s pulse, the membrane potential is returned to −70 mV and the current is transiently increased in magnitude as channels recover from inactivation into the open state. The decay of current that

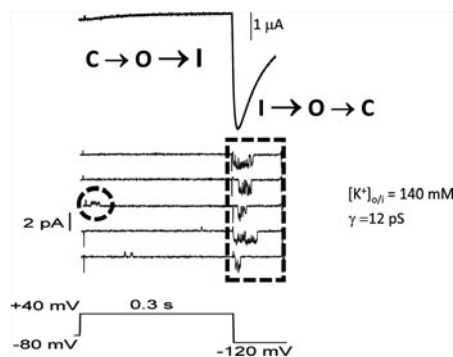


Fig. 34.3 Whole-cell and single-channel hERG1a currents measured in voltage-clamped *Xenopus* oocytes. Lower panel shows voltage pulse protocol used to elicit a whole-cell current (top panel) or a single-channel activity in a patch of oocyte membrane during four separate test pulses (middle panel). Channel openings are rare at +40 mV (example of opening is *circled*) because channels are mostly inactivated. Repolarization of the membrane to −120 mV allows channels to recover from inactivation to an open state (*boxed*). Channels are only open for a short time because deactivation is rapid at −120 mV. Whole-cell currents were recorded with two-microelectrode voltage clamp technique, and extracellular $[K^+]$ was 4 mM. Single-channel currents were measured in a cell-attached patch using a solution containing a high $[K^+]$ of 140 mM

ensues during the 2-s pulse to −70 mV represents channel deactivation. The I–V relationship for peak outward currents, measured at the end of each 2-s test pulse, is bell-shaped and peaks near −10 mV (Fig. 34.4b). The shape of this I–V relationship is determined by the overlap of voltage dependence of slow activation (Fig. 34.4c) and rapid inactivation (Fig. 34.4d).

The molecular basis of slow activation and extremely fast inactivation is not well understood. Gating of hERG1 channels exhibits a fast and slow component when measured either with fluorescent probes attached to the extracellular end of S4 [11] or by gating currents [12, 13]. The fast component is not specifically associated with inactivation and likely represents rapid transitions between multiple closed states. Inactivation of hERG1 is slowed by extracellular tetraethylammonium or high $[K^+]$ and altered by point mutations in regions of the pore near the selectivity filter [11, 14–16]. These features are typical for C-type inactivation of other Kv channels, but it is also clear that the mechanism and kinetics of C-type inactivation are diverse. The structural basis of C-type inactivation is believed to involve a poorly defined conformational change in the selectivity filter that reduces K^+ conductance.

34.3 Physiological Roles of ERG Channels

ERG channels have diverse physiological functions in neurons and neuroendocrine cells. In hippocampal astrocytes, ERG channels maintain K^+ homeostasis by facilitating K^+ release [17]. In glomus cells of the carotid body, a reduction in

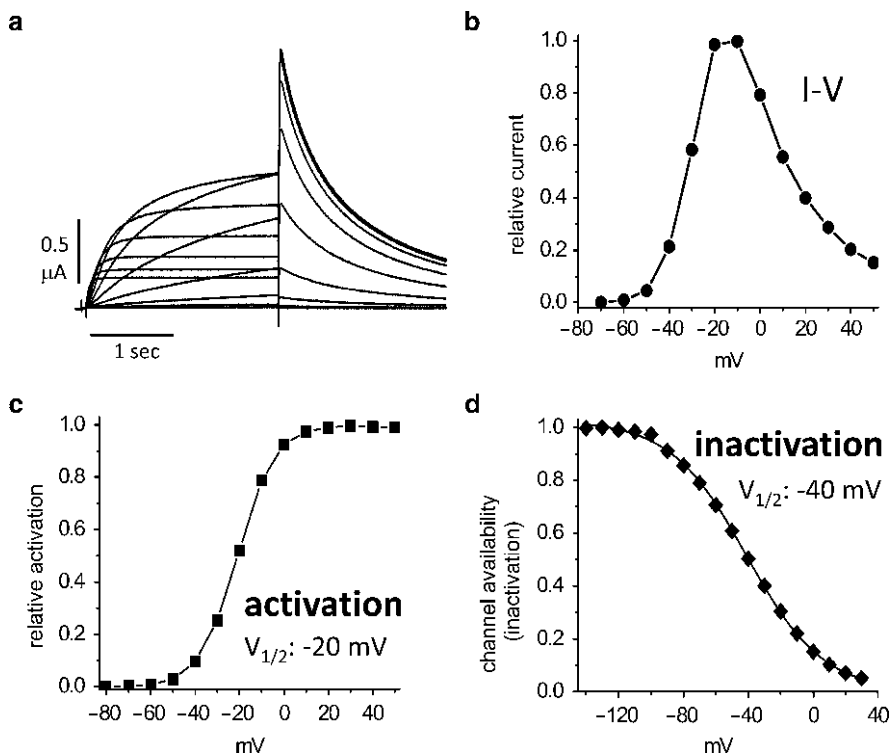


Fig. 34.4 Whole-cell hERG1a channel currents recorded in a *Xenopus* oocyte. **a**, Currents recorded at test potentials applied in 10-mV increments and ranging from -70 to +40 mV. The second half of the traces are tail currents that result from deactivation of channels after the membrane potential was returned to -70 mV. **b**, Current-voltage (*I*-*V*) relationship for hERG1a currents measured at the end of the 2-s test pulse. **c**, Voltage dependence of hERG current activation determined by plotting relative value of tail current amplitude as a function of test potential. The $V_{1/2}$ for activation is -20 mV. **d**, Voltage dependence of hERG1a current inactivation. The $V_{1/2}$ for inactivation is -40 mV

ERG current causes an increase in spike frequency of afferent nerve fibers, mimicking the effect of hypoxia [18]. In anterior pituitary lactotrophs, thyrotropin-releasing hormone reduces ERG current and increases prolactin secretion [19, 20]. ERG channels also regulate firing frequency and insulin secretion in pancreatic β -cells [21], and in neuroblastoma cells they regulate cell cycle [22] and neurogenesis [23]. These channels also control neuronal excitability during the early period of spinal network development [24] and play a role in firing frequency adaptation and neuronal discharge pattern in cerebellar Purkinje neurons, activities that may contribute to motor control [25]. ERG channels also maintain the resting membrane potential of smooth muscle cells in the gastrointestinal tract [26–28].

In the human heart, hERG1 channels contribute toward repolarization during phase 2 (plateau) and phase 3 (terminal repolarization) of the action potential. During the plateau phase, most hERG1 channels are inactivated, but they recover

from inactivation to an open state as the myocyte repolarizes, resulting in an enhanced outward current during phase 3 (Fig. 34.1a, b). Inherited loss-of-function mutations in the hERG1 gene *KCNH2* cause long QT syndrome [29], a disorder of ventricular repolarization that increases the risk of lethal ventricular fibrillation. Loss-of-function mutations in several other K⁺ channel genes (*KCNQ1*, *KCNE1*, *KCNE2*, *KCNJ1*) or gain of function in genes that encode cardiac Na⁺ (*SCN5A*) or L-type Ca²⁺ (*CACNA1C*) channels can cause long QT syndrome [30, 31]. As of July 2008, 291 mutations in *KCNH2* had been reported (Gene Connection for the Heart website; <http://www.fsm.it/cardmoc/>).

34.4 Drug-Induced QT Prolongation and Torsades de Pointes Arrhythmia

Class III antiarrhythmic drugs prolong the cardiac refractory period and can suppress arrhythmias by providing protection against premature excitation. However, these drugs can also induce arrhythmias, especially after a sinus pause and in the presence of hypokalemia. The class III drug quinidine was reported to induce torsades de pointes (TdP) in 2–9% of treated patients [32]. These drugs were developed specifically because of their ability to prolong cardiac refractoriness and provide protection against premature excitation. However, because drug-induced changes in refractory period are not uniform throughout the heart, these drugs can also be proarrhythmic. Noncardiac medications can also reduce I_{Kr} and prolong the QT interval as an unintended side effect. These compounds are diverse in structure and include several therapeutic drug classes, including psychiatric, antimicrobial, and antihistaminic compounds. Drug-induced TdP by these compounds is relatively rare. For example, TdP associated with terfenadine or cisapride treatment is estimated to have occurred in ~1 of 100,000 patients [33]. Of course, this incidence is unacceptable for drugs such as these that are prescribed for treatment of nonlife-threatening disorders (e.g., allergies for terfenadine). Cisapride, sertindole, grepafloxacin, terfenadine, and astemizole were removed from the US market or their use severely restricted by drug enforcement agencies once a clear association was confirmed between their use and inappropriate QT prolongation or arrhythmia.

34.5 Structural Basis for Sensitivity of hERG1 Channels to Block by Structurally Diverse Drugs

Voltage clamp studies have provided unequivocal evidence that most drugs can only block hERG1 after the channel has opened. A simple voltage clamp protocol can be used to show that drugs such as MK-499 do not block closed hERG1

channels [34]. Cells are exposed to a high concentration of MK-499 (10 μM) while clamped at a negative membrane potential to ensure that all channels are in the closed state. After prolonged incubation with the drug, the cell is depolarized to a positive potential to activate channels. The initial current magnitude is identical to control (pre-drug) current, and block develops slowly over a few seconds. Thus, MK-499 blocks only activated hERG1 channels, implying that a binding site within a region of the pore (the central cavity) is made accessible only after the activation gate is opened. Slow recovery from block appears to be caused by a trapping of drug inside the central cavity behind the activation gate that closes when the channel deactivates [35, 36]. Recovery from block by terfenadine can be strikingly accelerated when hERG1 channels contain a specific mutation (D540K) that allows the activation gate to reopen in response to membrane hyperpolarization [37]. These characteristics of block are very similar to several other well studied and potent blockers of hERG1, including MK-499, dofetilide, E-4031, and bepridil [37, 38]. Stork et al. [37] compared the rates of onset and recovery from hERG1 block by several drugs. Cisapride has a fast onset of, and recovery from block, whereas the kinetics for onset and recovery from block by terfenadine or E-4031 were very slow. The differences in blocking kinetics cannot be predicted based on simple measures of physicochemical properties of the drugs. Many studies have demonstrated that hERG1 blockers preferentially block inactivated channels [39–41], but it is also clear that noninactivating channels are readily blocked by some hERG1 blockers such as halofantrine [42].

On the basis of the results of binding studies using radio-labeled dofetilide or astemizole [43–45], a wide spectrum of structurally diverse drugs bind to a common site on the hERG1 channel. The most important amino acid residues that form this site were identified by using a site-directed mutagenesis approach and the Class III antiarrhythmic drug MK-499, a methanesulfonanilide [46]. Mutation of three residues near the pore helix (T623, S624, V625) and three residues in the S6 domain (G648, Y652, F656) reduced channel sensitivity to block (Fig. 34.5a). In addition, mutation of V659 slightly reduced block by MK-499. The structurally related drugs E4031 and dofetilide have a nearly identical pattern of residue interactions [38]. V625 is located just inside the narrow selectivity filter and is therefore not expected to be capable of direct interaction with a drug located in the central cavity. It seems likely that the V625A mutation affects drug block by an indirect mechanism, perhaps by altering the position of its nearest neighbor, S624, a residue identified as important for potent block by many drugs. V659A slows deactivation of hERG1 and could therefore lessen drug potency by reducing drug trapping.

The side chains of T623, S624, Y652, and F656 are orientated toward the large central cavity of the channel (Fig. 34.5a), consistent with open channel block. The two pore helix residues (T623 and S624) are highly conserved in Kv channels and thus cannot easily explain the promiscuous blocking of hERG1 by drugs. In contrast, the two S6 residues (Y652 and F656) are not conserved and most Kv channels have an Ile and a Val at these positions (Fig. 34.5b). Potent hERG1 block by MK-499 requires an aromatic residue in position 652 (Fig. 34.6a), suggesting a

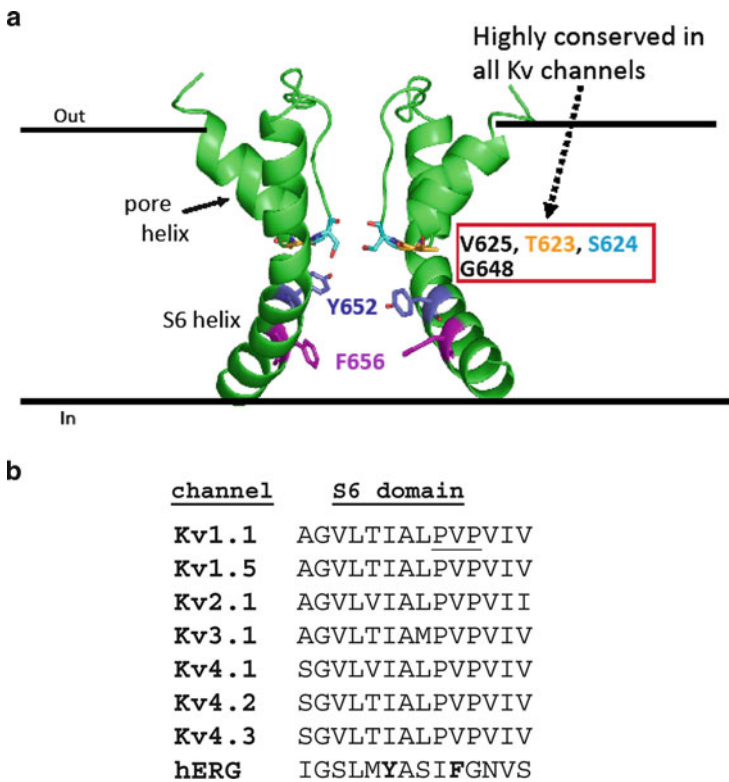


Fig. 34.5 Residues of hERG1 that are important for drug binding. **a**, hERG1 homology model of the pore domain (pore helix and S6 domain) based on MthK bacterial K⁺ channel [72]. Two hERG1 subunits are shown, and the most important residues for interaction with drugs (e.g., dofetilide or MK-499) are highlighted. **b**, Sequence alignment of a portion of the S6 domain of several Kv channels. The two most important S6 residues for drug binding in hERG1 (Y652 and F656) are colored blue and purple; these residues are Ile and Val in most other Kv channels. Note also that hERG1 does not have the Pro-Val-Pro motif common to these other Kv channels

cation–π interaction between the positively charged N of the drug and the π-electrons of Y652. Mutation of F656 to another aromatic or a highly hydrophobic residue maintains potency that is inversely related to the hydrophobicity of this residue (Fig. 34.6b). Modeling of drug interaction with the pore of the hERG1 channel largely corroborates the mutagenesis studies [46, 47]. An induced fit model predicts that the piperidine N and the two hydroxyl groups of terfenadine are located nearest the hydrophilic space formed by the intracellular base of the pore helix and selectivity filter of hERG1 [48]. This docking model also predicts π–π interactions with two Y652 and two F656 residues, and two additional hydrophobic interactions with Y652.

F656 was first reported as a critical residue for the binding of dofetilide and quinidine [49]. Later studies demonstrated the importance of Y652 and F656 for

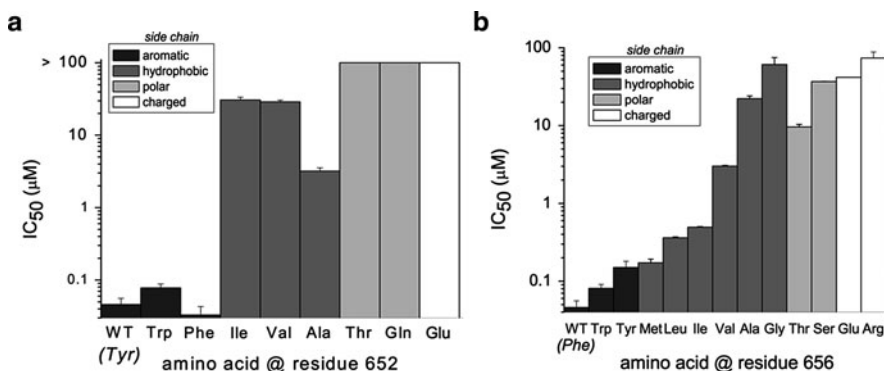


Fig. 34.6 Substitution of Tyr652 and Phe656 with other amino acids alters the sensitivity of hERG1 channels to block by the antiarrhythmic drug MK-499. **a**, Mutation of Tyr652 to other aromatic residues (Trp or Phe) did not appreciably alter drug sensitivity. **b**, Altered drug sensitivity of Phe656 mutant hERG1 channels varies as a function of hydrophobicity of the substituted residue

many other drugs, including chloroquine [50], quinidine [51], halofantrine [42], terfenadine and cisapride [47], lidoflazine [52], clofilium and ibutilide [53], and cocaine [54]. However, not all hERG1 blockers interact with all of the residues identified by using the methanesulfonanilides. Bepridil does not interact with G648, Y652 or V659 [38] and mutation of F656 and/or Y652 only slightly reduced hERG block by fluvoxamine and dronedarone [55, 56]. For terfenadine and cisapride, T623, S624, Y652, and F656 were critical for normal block, but mutation of V625, G648, and V659 was without effect [57]. Perhaps the multiple aromatic side chains (eight per channel), arranged in two concentric rings, can accommodate multiple and compound-specific interactions, partially explaining the surprising chemical diversity of hERG1 blockers. The main interactions that mediate drug binding to the pore of hERG1 channels are summarized in Fig. 34.7.

34.6 Drug-Induced Alteration of hERG1 Trafficking

Drug-induced QT prolongation and TdP are most often caused by block of hERG1 channels. However, some drugs interfere with hERG1-channel trafficking to the cell surface. This was first reported by Ficker et al. for arsenic trioxide, a compound used to treat acute promyelocytic leukemia [58]. It was subsequently reported that other drugs, including the antiprotozoal pentamidine [59], the antidepressant fluoxetine [60], and cardiac glycosides [61] also reduced I_{Kr} by disrupting the trafficking of hERG1 channels. Arsenic trioxide and fluoxetine directly block and inhibit trafficking of hERG1 channels at similar concentrations; however, pentamidine [62] and celastrol [63] only block current at much higher concentrations. The exact mechanisms that underlie the drug-induced trafficking defects are unknown,

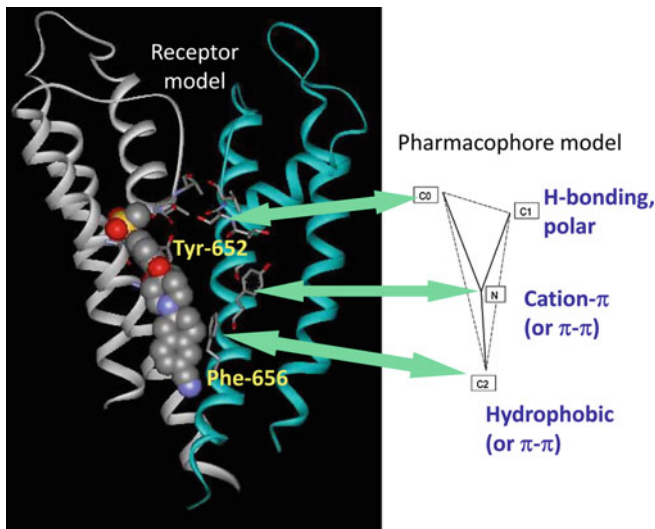


Fig. 34.7 Model of MK-499 docked to the inner cavity of hERG1 channel in the closed state. Homology model is based on KcsA bacterial K⁺ channel structure [73]. The pore region (S5–S6) of two hERG1 subunits is shown

but at least for fluoxetine, it does not appear to be mediated by binding to the site responsible for pore block. Trafficking of F656A hERG1 is inhibited by fluoxetine even though these channels are resistant to pore block [60]. The recent realization that hERG1 channel function can be reduced by mechanisms other than pore block prompted the development of simple assays (e.g., HERG-Lite^R) to test for drug-induced effects on hERG1 channel trafficking [64, 65].

34.7 hERG1 Channel Activators as Therapy for Long QT Syndrome?

β-Adrenergic receptor blockers are the only drugs used commonly to treat LQTS [66]. However, because reduced hERG1 channel activity is a common cause of inherited and acquired LQTS, the newly discovered ERG channel activators may eventually provide an alternative and more specific pharmacological treatment for this disorder.

Several compounds have been identified that activate hERG1 channels and shorten cardiac action potentials. Two compounds, NS1643 [67, 68] and PD-118057 [69], increase the magnitude of outward hERG1 current, but have little or no effect on the rate of channel deactivation. RPR260243 (RPR) primarily slows the rate of hERG1 deactivation [70], but this compound also slows activation and enhances current

magnitude by attenuation of P-type inactivation [71]. It remains to be determined whether an increase in hERG1 current magnitude with or without slowed deactivation will provide a safe and effective treatment for LQTS.

To identify the putative binding site for RPR, we examined the effect of the drug on channels with point mutations in the pore and S4–S5 linker domains of hERG1 [71]. Single mutations of residues located in the S5 (L553, F557) and an adjacent region of S6 (N658, V659) attenuated both the deactivation and inactivation effects of RPR. These residues likely form the binding site for RPR. Point mutations in another region located in adjacent regions of the S4–S5 linker (V549, L550) and cytoplasmic end of S6 (I662, L666, Y667) only prevented the slowing of deactivation. These residues are likely the key components of coupling voltage sensor movement to channel opening.

34.8 Conclusions

hERG1 channels conduct a repolarizing K⁺ current that is the major determinant of cardiac repolarization in humans. In clinical practice, drug-induced QT prolongation is most often caused by block of hERG1 channels. The most important molecular determinants of hERG1 block have been elucidated in recent years. The molecular insights provided by these studies, combined with a growing database of structure–activity relationships for diverse pharmacophores, have greatly facilitated the rational design of new noncardiac medications that are devoid of the potentially life-threatening side effect caused by hERG1 channel block and QT prolongation.

References

1. Warmke JW, Ganetzky B. A family of potassium channel genes related to *eag* in *Drosophila* and mammals. Proc Natl Acad Sci U S A. 1994;91:3438–42.
2. London B, Trudeau MC, Newton KP, Beyer AK, Copeland NG, Gilbert DJ, et al. Two isoforms of the mouse *ether-a-go-go*-related gene coassemble to form channels with properties similar to the rapidly activating component of the cardiac delayed rectifier K⁺ current. Circ Res. 1997;81:870–8.
3. Lees-Miller JP, Kondo C, Wang L, Duff HJ. Electrophysiological characterization of an alternatively processed ERG K⁺ channel in mouse and human hearts. Circ Res. 1997;81:719–26.
4. Shi W, Wymore RS, Wang H-S, Pan Z, Cohen IS, McKinnon D, et al. Identification of two nervous system-specific members of the *erg* potassium channel gene family. J Neurosci. 1997;17:9423–32.
5. Phartiyal P, Sale H, Jones EM, Robertson GA. Endoplasmic reticulum retention and rescue by heteromeric assembly regulate human ERG 1a/1b surface channel composition. J Biol Chem. 2008;283:3702–7.

6. McDonald TV, Yu Z, Ming Z, Palma E, Meyers MB, Wang K-W, et al. A minK-HERG complex regulates the cardiac potassium current I_{Kr} . *Nature*. 1997;388:289–92.
7. Bianchi L, Shen Z, Dennis AT, Priori SG, Napolitano C, Ronchetti E, et al. Cellular dysfunction of LQT5-minK mutants: abnormalities of I_{Ks} , I_{Kr} and trafficking in long QT syndrome. *Hum Mol Genet*. 1999;8:1499–507.
8. Abbott GW, Sesti F, Splawski I, Buck ME, Lehmann MH, Timothy KW, et al. MiRP1 forms IKr potassium channels with HERG and is associated with cardiac arrhythmia. *Cell*. 1999;97:175–87.
9. Weerapura M, Nattel S, Chartier D, Caballero R, Hebert TE. A comparison of currents carried by HERG, with and without coexpression of MiRP1, and the native rapid delayed rectifier current. Is MiRP1 the missing link? *J Physiol*. 2002;540:15–27.
10. Pourrier M, Zicha S, Ehrlich J, Han W, Nattel S. Canine ventricular KCNE2 expression resides predominantly in Purkinje fibers. *Circ Res*. 2003;93:189–91.
11. Smith PL, Baukrowitz T, Yellen G. The inward rectification mechanism of the HERG cardiac potassium channel. *Nature*. 1996;379:833–6.
12. Smith PL, Yellen G. Fast and slow voltage sensor movements in HERG potassium channels. *J Gen Physiol*. 2002;119:275–93.
13. Piper DR, Varghese A, Sanguinetti MC, Tristani-Firouzi M. Gating currents associated with intramembrane charge displacement in HERG potassium channels. *Proc Natl Acad Sci USA*. 2003;100:10534–9.
14. Schonherr R, Heinemann SH. Molecular determinants for activation and inactivation of HERG, a human inward rectifier potassium channel. *J Physiol*. 1996;493(3):635–42.
15. Ficker E, Jarolimek W, Kiehn J, Baumann A, Brown AM. Molecular determinants of dofetilide block of HERG K^+ channels. *Circ Res*. 1998;82:386–95.
16. Wang S, Morales MJ, Liu S, Strauss HC, Rasmussen RL. Time, voltage and ionic concentration dependence of rectification of h-erg expressed in *Xenopus* oocytes. *FEBS Lett*. 1996;389:167–73.
17. Emmi A, Wenzel HJ, Schwartzkroin PA, Tagliafata M, Castaldo P, Bianchi L, et al. Do glia have heart? Expression and functional role for ether-a-go-go currents in hippocampal astrocytes. *J Neurosci*. 2000;20:3915–25.
18. Overholt JL, Ficker E, Yang T, Shams H, Bright GR, Prabhakar NR. HERG-Like potassium current regulates the resting membrane potential in glomus cells of the rabbit carotid body. *J Neurophysiol*. 2000;83:1150–7.
19. Kirchberger NM, Wulfsen I, Schwarz JR, Bauer CK. Effects of TRH on heteromeric rat erg1a/1b K^+ channels are dominated by the rerg1b subunit. *J Physiol*. 2006;571:27–42.
20. Schleidermann W, Wulfsen I, Schwarz JR, Bauer CK. Modulation of rat erg1, erg2, erg3 and HERG K^+ currents by thyrotropin-releasing hormone in anterior pituitary cells via the native signal cascade. *J Physiol*. 2001;532:143–63.
21. Rosati B, Marchetti P, Crociani O, Lecchi M, Lupi R, Arcangeli A, et al. Glucose- and arginine-induced insulin secretion by human pancreatic beta-cells: the role of HERG $K(+)$ channels in firing and release. *FASEB J*. 2000;14:2601–10.
22. Arcangeli A, Bianchi L, Beccetti A, Faravelli L, Coronello M, Mini E, et al. A novel inward-rectifying K^+ current with a cell-cycle dependence governs the resting potential of mammalian neuroblastoma cells. *J Physiol*. 1995;489:455–71.
23. Arcangeli A, Beccetti A, Mannini A, Mugnai G, DeFilippi P, Tarone G, et al. Integrin-mediated neurite outgrowth in neuroblastoma cells depends on the activation of potassium channels. *J Cell Biol*. 1993;122:1131–43.
24. Furlan F, Guasti L, Avossa D, Beccetti A, Cilia E, Ballerini L, et al. Interneurons transiently express the ERG K^+ channels during development of mouse spinal networks in vitro. *Neuroscience*. 2005;135:1179–92.
25. Sacco T, Bruno A, Wanke E, Tempia F. Functional roles of an ERG current isolated in cerebellar Purkinje neurons. *J Neurophysiol*. 2003;90:1817–28.

26. Akbarali HI, Thatte H, He XD, Giles WR, Goyal RK. Role of HERG-like K⁽⁺⁾ currents in opossum esophageal circular smooth muscle. *Am J Physiol.* 1999;277:C1284–90.
27. Farrelly AM, Ro S, Callaghan BP, Khoyi MA, Fleming N, Horowitz B, et al. Expression and function of KCNH2 (HERG) in the human jejunum. *Am J Physiol.* 2003;284:G883–95.
28. Shoeb F, Malykhina AP, Akbarali HI. Cloning and functional characterization of the smooth muscle ether-a-go-go-related gene K⁺ channel. Potential role of a conserved amino acid substitution in the S4 region. *J Biol Chem.* 2003;278:2503–14.
29. Curran ME, Splawski I, Timothy KW, Vincent GM, Green ED, Keating MT. A molecular basis for cardiac arrhythmia: HERG mutations cause long QT syndrome. *Cell.* 1995;80:795–803.
30. Keating MT, Sanguinetti MC. Molecular and cellular mechanisms of cardiac arrhythmias. *Cell.* 2001;104:569–80.
31. Splawski I, Timothy KW, Sharpe LM, Decher N, Kumar P, Bloise R, et al. CaV1.2 calcium channel dysfunction causes a multisystem disorder including arrhythmia and autism. *Cell.* 2004;119:19–31.
32. Haverkamp W, Breithardt G, Camm AJ, Janse MJ, Rosen MR, Antzelevitch C, et al. The potential for QT prolongation and proarrhythmia by non-antiarrhythmic drugs: clinical and regulatory implications. Report on a policy conference of the European Society of Cardiology. *Eur Heart J.* 2000;21:1216–31.
33. Vitola J, Vukanovic J, Roden DM. Cisapride-induced torsades de pointes. *J Cardiovasc Electrophysiol.* 1998;9:1109–13.
34. Spector PS, Curran ME, Keating MT, Sanguinetti MC. Class III antiarrhythmic drugs block HERG, a human cardiac delayed rectifier K⁺ channel; open channel block by methanesulfonanilides. *Circ Res.* 1996;78:499–503.
35. Armstrong CM. Interaction of tetraethylammonium ion derivatives with the potassium channels of giant axons. *J Gen Physiol.* 1971;58:413–37.
36. Mitcheson JS, Chen J, Sanguinetti MC. Trapping of a methanesulfonanilide by closure of the HERG potassium channel activation gate. *J Gen Physiol.* 2000;115:229–40.
37. Stork D, Timin EN, Berjukow S, Huber C, Hohaus A, Auer M, et al. State dependent dissociation of HERG channel inhibitors. *Br J Pharmacol.* 2007;151:1368–76.
38. Kamiya K, Niwa R, Mitcheson JS, Sanguinetti MC. Molecular determinants of HERG channel block. *Mol Pharmacol.* 2006;69:1709–16.
39. Numaguchi H, Mullins FM, Johnson Jr JP, Johns DC, Po SS, Yang IC, et al. Probing the interaction between inactivation gating and Dd-sotalol block of HERG. *Circ Res.* 2000;87:1012–8.
40. Tie H, Walker BD, Singleton CB, Valenzuela SM, Bursill JA, Wyse KR, et al. Inhibition of HERG potassium channels by the antimalarial agent halofantrine. *Br J Pharmacol.* 2000;130:1967–75.
41. Ficker E, Jarolimek W, Brown AM. Molecular determinants of inactivation and dofetilide block in ether a-go-go (EAG) channels and EAG-related K⁺ channels. *Mol Pharmacol.* 2001;60:1343–8.
42. Sanchez-Chapula JA, Navarro-Polanco RA, Sanguinetti MC. Block of wild-type and inactivation-deficient human ether-a-go-go-related gene K⁺ channels by halofantrine. *Naunyn Schmiedebergs Arch Pharmacol.* 2004;370:484–91.
43. Finlayson K, Turnbull L, January CT, Sharkey J, Kelly JS. [3 H]dofetilide binding to HERG transfected membranes: a potential high throughput preclinical screen. *Eur J Pharmacol.* 2001;430:147–8.
44. Diaz GJ, Daniell K, Leitza ST, Martin RL, Su Z, McDermott JS, et al. The [3 H]dofetilide binding assay is a predictive screening tool for hERG blockade and proarrhythmia: Comparison of intact cell and membrane preparations and effects of altering [K⁺]o. *J Pharmacol Toxicol Methods.* 2004;50:187–99.

45. Chiu PJ, Marcoe KF, Bounds SE, Lin CH, Feng JJ, Lin A, et al. Validation of a [3 H] astemizole binding assay in HEK293 cells expressing HERG K⁺ channels. *J Pharmacol Sci.* 2004;95:311–9.
46. Mitcheson JS, Chen J, Lin M, Culberson C, Sanguinetti MC. A structural basis for drug-induced long QT syndrome. *Proc Natl Acad Sci USA.* 2000;97:12329–33.
47. Fernandez D, Ghanta A, Kauffman GW, Sanguinetti MC. Physicochemical features of the hERG channel drug binding site. *J Biol Chem.* 2004;279:10120–7.
48. Farid R, Day T, Friesner RA, Pearlstein RA. New insights about HERG blockade obtained from protein modeling, potential energy mapping, and docking studies. *Bioorg Med Chem.* 2006;14:3160–73.
49. Lees-Miller JP, Duan Y, Teng GQ, Duff HJ. Molecular determinant of high-affinity dofetilide binding to HERG1 expressed in Xenopus oocytes: involvement of S6 sites. *Mol Pharmacol.* 2000;57:367–74.
50. Sanchez-Chapula JA, Navarro-Polanco RA, Culberson C, Chen J, Sanguinetti MC. Molecular determinants of voltage dependent HERG K⁺ channel block. *J Biol Chem.* 2002;277: 23587–95.
51. Sanchez-Chapula JA, Ferrer T, Navarro-Polanco RA, Sanguinetti MC. Voltage-dependent profile of human ether-a-go-go-related gene channel block is influenced by a single residue in the S6 transmembrane domain. *Mol Pharmacol.* 2003;63:1051–8.
52. Ridley JM, Dooley PC, Milnes JT, Witchel HJ, Hancox JC. Lidoflazine is a high affinity blocker of the HERG K(+)channel. *J Mol Cell Cardiol.* 2004;36:701–5.
53. Perry M, de Groot MJ, Helliwell R, Leishman D, Tristani-Firouzi M, Sanguinetti MC, et al. Structural determinants of HERG channel block by clofilium and ibutilide. *Mol Pharmacol.* 2004;66:240–9.
54. Guo J, Gang H, Zhang S. Molecular determinants of cocaine block of human ether-a-go-go-related gene potassium channels. *J Pharmacol Exp Ther.* 2006;317:865–74.
55. Milnes JT, Crociani O, Arcangeli A, Hancox JC, Witchel HJ. Blockade of HERG potassium currents by fluvoxamine: incomplete attenuation by S6 mutations at F656 or Y652. *Br J Pharmacol.* 2003;139:887–98.
56. Ridley JM, Milnes JT, Witchel HJ, Hancox JC. High affinity HERG K⁺ channel blockade by the antiarrhythmic agent dronedarone: resistance to mutations of the S6 residues Y652 and F656. *Biochem Biophys Res Commun.* 2004;325:883–91.
57. Kamiya K, Niwa R, Morishima M, Honjo H, Sanguinetti MC. Molecular determinants of hERG channel block by terfenadine and cisapride. *J Pharmacol Sci.* 2008;108:301–7.
58. Ficker E, Kuryshev YA, Dennis AT, Obejero-Paz C, Wang L, Hawryluk P, et al. Mechanisms of arsenic-induced prolongation of cardiac repolarization. *Mol Pharmacol.* 2004;66:33–44.
59. Kuryshev YA, Ficker E, Wang L, Hawryluk P, Dennis AT, Wible BA, et al. Pentamidine-induced long QT syndrome and block of hERG trafficking. *J Pharmacol Exp Ther.* 2005;312:316–23.
60. Rajamani S, Eckhardt LL, Valdivia CR, Klemens CA, Gillman BM, Anderson CL, et al. Drug-induced long QT syndrome: hERG K⁺ channel block and disruption of protein trafficking by fluoxetine and norfluoxetine. *Br J Pharmacol.* 2006;149:481–9.
61. Wang L, Wible BA, Wan X, Ficker E. Cardiac glycosides as novel inhibitors of human ether-a-go-go-related gene channel trafficking. *J Pharmacol Exp Ther.* 2007;320:525–34.
62. Cordes JS, Sun Z, Lloyd DB, Bradley JA, Opsahl AC, Tengowski MW, et al. Pentamidine reduces hERG expression to prolong the QT interval. *Br J Pharmacol.* 2005;145:15–23.
63. Sun H, Liu X, Xiong Q, Shikano S, Li M. Chronic inhibition of cardiac Kir2.1 and HERG potassium channels by celastrol with dual effects on both ion conductivity and protein trafficking. *J Biol Chem.* 2006;281:5877–84.
64. Dennis A, Wang L, Wan X, Ficker E. hERG channel trafficking: novel targets in drug-induced long QT syndrome. *Biochem Soc Trans.* 2007;35:1060–3.

65. Wible BA, Hawryluk P, Ficker E, Kuryshov YA, Kirsch G, Brown AM. HERG-Lite: a novel comprehensive high-throughput screen for drug-induced hERG risk. *J Pharmacol Toxicol Methods*. 2005;52:136–45.
66. Schwartz PJ. The congenital long QT syndromes from genotype to phenotype: clinical implications. *J Intern Med*. 2006;259:39–47.
67. Casis O, Olesen SP, Sanguinetti MC. Mechanism of action of a novel human ether-a-go-go-related gene channel activator. *Mol Pharmacol*. 2006;69:658–65.
68. Hansen RS, Diness TG, Christ T, Demnitz J, Ravens U, Olesen S-P, et al. Activation of hERG potassium channels by the diphenylurea NS1643. *Mol Pharmacol*. 2005;69:266–77.
69. Zhou J, Augelli-Szafran CE, Bradley JA, Chen X, Koci BJ, Volberg WA, et al. Novel potent human ether-a-go-go-related gene (hERG) potassium channel enhancers and their in vitro antiarrhythmic activity. *Mol Pharmacol*. 2005;68:876–84.
70. Kang J, Chen XL, Wang H, Ji J, Cheng H, Incardona J, et al. Discovery of a small molecule activator of the Human Ether-a-go-go-Related Gene (HERG) cardiac K⁺ channel. *Mol Pharmacol*. 2005;67:827–36.
71. Perry M, Sachse FB, Sanguinetti MC. Structural basis of action for a human ether-a-go-go-related gene 1 potassium channel activator. *Proc Natl Acad Sci USA*. 2007;104:13827–32.
72. Jiang Y, Lee A, Chen J, Cadene M, Chait BT, MacKinnon R. Crystal structure and mechanism of a calcium-gated potassium channel. *Nature*. 2002;417:515–22.
73. Doyle DA, Morais Cabral J, Pfuetzner RA, Kuo A, Gulbis JM, Cohen SL, et al. The structure of the potassium channel: molecular basis of K⁺ conduction and selectivity. *Science*. 1998;280:69–77.

Chapter 35

Preclinical Drug Safety and Cardiac Ion Channel Screening

Zhi Su and Gary Gintant

35.1 Introduction

A new chemical entity must demonstrate efficacy and safety in order to be considered a successful therapeutic agent. Towards that goal, it is best to discover drugs demonstrating a wide concentration range between (lower) preclinical efficacious plasma concentrations and (higher) plasma concentrations eliciting preclinical off-target adverse effects. Drugs possessing such characteristics provide greater flexibility in clinical trials and explorations into alternative indications. Thus, preclinical studies related to both efficacy and safety must be considered equally important during drug discovery efforts. Cardiac safety plays a key role in defining the safety of novel therapeutics, and defining a drug's therapeutic window/safety margin.

Much emphasis has been placed in the past decade on detecting (and avoiding) the ability of non-cardiovascular drugs to delay or alter ventricular repolarization (acquired long QT syndrome [1]). This focus arises in part from the association of delayed repolarization to the rare but potentially life-threatening arrhythmia torsades de pointes. As torsades is a rare event, surrogate markers are employed to detect and avoid this potential proarrhythmic risk. Preclinically, the most recognized *in vitro* marker for delayed repolarization is drug block of I_{Kr} (an outward repolarizing current that initiates and defines terminal ventricular repolarization). In humans, the α -subunit of the I_{Kr} channel is encoded by the human ether-a-go-go related gene (hERG) gene. Block of hERG/ I_{Kr} along with prolongation of the QT interval (an interval on the ECG that generally represents the onset of ventricular depolarization and the termination of ventricular repolarization) form the present-day cornerstone for cardiac electrophysiologic safety testing. Due to the importance of testing hERG current as a surrogate marker of proarrhythmia, great strides have been made in developing and streamlining testing protocols/procedures to evaluate

Z. Su and G. Gintant (✉)

Department of Integrative Pharmacology, Global Pharmaceutical Research and Development, Abbott Laboratories, 100 Abbott Park Road, Abbott Park, IL 60064, USA
e-mail: gary.gintant@abbott.com

effects of drugs on cardiac ion channels. The goal of this chapter is to provide an overview of efforts directed towards preclinical cardiac ion channel screening as related to the preclinical evaluation of drug safety. Towards this goal, we use experiences with hERG channel testing as an example of various approaches towards cardiac ion channel screening efforts.

35.2 In Vitro Cardiac Ion Channel Screening Techniques

Numerous techniques have been developed for screening drug effects on cardiac ion channels for the purposes of both therapeutics and safety. In the last decade, significant experience has been gained while developing assays to screen out drug effects on hERG/ I_{Kr} channels early in drug discovery. These approaches have been fueled by the application of cloning techniques developed from molecular biology along with evolving automated patch-clamp techniques that are rapidly outpacing manual patch operations.

35.2.1 *Electrophysiological Screens for Drug Effects on hERG/ I_{Kr} Channels*

Most cardiac ion channels are voltage-dependent; that is, their conductance changes in response to changes in transmembrane potential. Thus, the effects of drugs on these channels are best studied using voltage-clamp techniques that provide for control of membrane potential while monitoring changes in membrane current. In conventional voltage-clamp techniques, an investigator must gain electrical access to the interior of a cell (typically using a patch pipette) allowing for the application of voltage-clamp protocols to elicit transmembrane currents. In this way, drug-effects are defined based on changes in membrane currents affected in response to imposed voltage-clamp protocols.

Conventional (or so-called manual patch-clamp (MPC)) techniques are considered as the “gold standard” electrophysiological assay for evaluating drug effects on voltage-gated channels [2–5]. MPC technique can be applied to many electrically excitable cells, including cells either transiently or stably expressing the hERG channel and native cardiac myocytes. When studying cells expressing predominantly one channel type (for example, hERG expressed in HEK-293 cells, a popular model), the recorded membrane current reflects predominantly one ionic current, making analysis of current changes relatively simple. While hERG current can be recorded in voltage-clamped cardiac myocytes from larger mammals, it is relatively small (and hence difficult to measure) compared to multiple other (contaminating) ionic currents that are active in the voltage range over which hERG current is active. Finally, while most drugs studied either have no effect or block hERG current, some drugs enhance hERG current [6–9].

35.2.1.1 Traditional Approaches to Measuring Drug Effects on hERG

Traditionally, hERG current has been evaluated based on square-shaped voltage-clamp pulses with depolarization eliciting channel opening (activation current) and repolarization leading to decline in current (so-called “tail current,” see Fig. 35.1). Some investigators use a repolarizing ramp pulse to affect repolarization, as the ramp resembles (in a very general sense) the time course of ventricular repolarization, and is a compromise between a ventricular action potential waveform and step-clamp waveform. Conventional step-step and step-ramp protocols have both been used to determine IC_{50} values for hERG block (or in the case of current enhancement, EC_{50} for hERG activation) [9–13]. Figure 35.1a shows hERG current blockade by the withdrawn antipsychotic drug mesoridazine using a step-step protocol and Fig. 35.1b illustrates the hERG current enhancement by an experimental compound A-935142 using a step-ramp protocol.

Drug potency is usually characterized by providing an IC_{50} value for hERG blockers (or an EC_{50} value for hERG activators). This allows for comparison with *in vivo* effects of drugs and calculation of therapeutic margins [3, 14]. The IC_{50} value for hERG blockade is the concentration at which hERG current (usually peak tail) is inhibited by 50% and is obtained by fitting the concentration-response relationship to the Hill equation: typically 3–4 concentrations should be tested that encompass a reasonable concentration range. The EC_{50} value for hERG enhancement is the concentration at which 50% of the maximal enhancement of hERG current is achieved and this is also obtained by fitting the concentration-response relationship to the Hill equation.

For a few drugs, the applied voltage-clamp protocol influences drug potency, yielding different IC_{50} values with different protocols [12, 13]. Pulsing rate (frequency

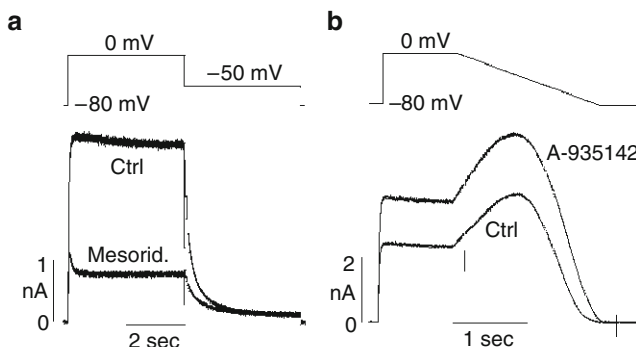


Fig. 35.1 Conventional whole cell manual patch-clamp protocols used to quantify drug effects on hERG current. (a) hERG currents elicited by a two-step protocol at 37°C from an hERG-expressing HEK-293 cell in the absence (Ctrl) and presence of mesoridazine (1.8 μ M, Mesorid.). (b) hERG currents elicited by a step-ramp protocol at 37°C from an hERG-expressing HEK-293 cell in the absence (Ctrl) and presence of A-935142 (60 μ M). Panels a and b reproduced from [10] and [9], respectively

of application of the voltage-clamp protocol) also affects the quantification of drug-mediated hERG channel block, with different frequencies generating different IC₅₀ values [15]. In addition, temperature is another important factor influencing drug potency [12, 13]. It has been suggested that use of a step-ramp protocol at physiological temperature produces conservative IC₅₀ values for hERG inhibition. More importantly, measured bath concentrations should be used when determining drug potency (IC₅₀ or EC₅₀ values) in order to enhance the accuracy of estimation of drug effects on hERG channels [16–18]. A significant advantage of MPC assay in the study of drug effects on hERG current is that drug concentrations in the perfusion bath can be verified.

35.2.1.2 Automated Planar Patch-Clamp Methods

An obvious disadvantage for the conventional MPC method is its low assay throughput. Consequently, automated, planar patch-clamp (APC) methods have emerged [4, 5, 19]. Several APC platforms, including IonWorks HT, IonWorks Quattro, PatchXpress, QPatch, and Patchliner, have been evaluated and subsequently validated for hERG channel studies. For APC techniques, there are two patch-clamp configurations: the population patch-clamp (PPC) configuration and the non-PPC configuration. PPC is performed by modifying the existing planar substrate (plates or chips) such that each recording well contains multiple recording sites or apertures. The PPC technique makes an ensemble measurement of the currents in cells sealed to an array of n measurement apertures (1 cell per aperture) in each well of a planar plate using a single voltage-clamp amplifier per well. The PPC technique allows success rates to exceed 95% and frequently reach 100%. Currently, only IonWorks Quattro can perform PPC measurements with 64 apertures per well [20]. All other APC platforms presently available can only perform non-PPC measurement in which current is obtained from one individual cell sealed to a single aperture per well. Reported success rates for non-PPC planar patch techniques range from 30% to 80% (success defined as obtaining one data point from an individual well or cell).

Using CHO cells that stably express hERG channels, IonWorks allows for assessment of approximately 200 data points per Patch plate and about 80 concentration-response curves per day [21–24]. A good pharmacological correlation with conventional MPC data was observed in terms of rank-order of compounds with hERG activity although the concentration-response curves were shifted to the right (within 3- to 5-fold). PatchXpress, QPatch, and Patchliner allow stable recordings of high-quality hERG current from giga-ohm seals for 20–30 min, allow the complete concentration-response experiment to be performed on a single cell, and exhibit good pharmacological data correlation with conventional MPC experiments, although potency shift has also been reported for one of the automated patch-clamp systems [25–29]. In comparison to the MPC technique, the most significant advantage of the APC technique is high throughput, which facilitates analysis of structure–activity relationships across compounds. The availability of

automated electrophysiology technologies has reenergized drug discovery efforts targeting ion channels and made it possible to screen cardiac liabilities early in drug discovery. The APC technologies are evolving at an amazingly fast pace, focusing on higher quality of seal, success rate, and throughput. For example, SyncroPatch 96, the third generation of the APC platform from Nanion, offers 10-times higher throughput than the second generation of the Nanion APC workstation, Patchliner (5,000 data points vs. 500 data points per day). In addition, future generations of APC platforms are expected to provide higher level of automation and analysis of more complex data sets.

Despite advantages cited above for APC methods, there is room for further improvement. First, recording at physiological temperatures is not presently possible in most APC platforms presently available. Second, test drug concentrations cannot be verified. Third, only mammalian cell lines can be used in the automated patch-clamp platforms and it is still challenging to use native cells, in particular, even more difficult to use native cardiac myocytes. Fourth, it is seldom the case that a well-behaved MPC assay with mammalian cells transitions easily to an automated platform. More typically, significant effort and resources are required to optimize conditions for both cell performance and assay reproducibility.

Overall, the MCP method provides the most accurate and precise measurements of drug effects on hERG channel activity when the assay is performed at physiological temperature and bath drug concentrations are verified. When characterizing the electrophysiologic effects of your test compound, it is always advantageous to include an evaluation test of a recognized positive standard (for example, cisapride when evaluating hERG current), thus providing a reference standard to calibrate assay sensitivity. Therefore, the APC technologies and other alternative methods (see below) designed for detecting drug-hERG channel interactions are all validated against the data obtained using the “gold standard,” the MPC method. An individual APC platform validated for hERG screen can often be employed (with modifications in experimental conditions) in assays for other cardiac ion channels for the purposes of drug safety and efficacy studies [5].

35.2.2 Non-electrophysiological Approaches for Determining hERG Channel–Drug Interactions

Before high-throughput electrophysiological techniques became available, alternative experimental methods with higher throughput (including radioligand binding approaches, ion flux assays, and fluorometric methods) were employed for screening compounds for hERG liability. These methods are still used today to screen larger chemical libraries and complement electrophysiologic approaches described above. Radioligand binding assays measure displacement by compounds of interest of radiolabeled high affinity blockers such as dofetilide [30, 31], astemizole [32], and MK-499 [33]. The binding assay can use native myocytes, mammalian cell lines (HEK-293 cells) expressing hERG channels, or cell membranes (for example,

HEK-293 cell membranes [31, 34]). Evaluation of [³H]-dofetilide displacement as a high-throughput screen has reported generally good correlation between binding K_i values and IC₅₀ values for hERG current block [31, 34]. Therefore, radioligand binding assays provide a useful initial screen for potential interactions of new chemical entities. It should be noted that binding assays provide no information on the agonist or inhibitory action of a compound (as they do not directly examine hERG channel function) and are likely to miss drug–channel interactions at sites distinct from the radioligand binding site [14]. Therefore, the binding assay cannot be substituted for functional electrophysiologic cardiac safety testing.

Rubidium (Rb⁺) efflux assays involve loading hERG-expressing cells with Rb⁺ ions, and then measuring drug effects on Rb⁺ efflux in response to a depolarizing challenge (typically an increase in extracellular [K⁺]). Although reasonable correlation between this assay and patch-clamp electrophysiology has been reported [34], the assay tends to lack sensitivity and underestimate drug affinity [35]. Rb⁺ itself appears to be at least partly responsible for the low sensitivity of the assay, as Rb⁺ reduces hERG channel inactivation at potentials relevant to the efflux assay [35]. Therefore, the utility of Rb⁺ efflux assay is limited by a tendency to underestimate blocking potency and the fact that measurement of Rb⁺ flux does not constitute a direct measurement of hERG channel current per se.

Fluorescence-based assay using voltage-sensitive dyes has also been described. This assay measures drug-induced membrane depolarization of hERG channel-expressing cells in which hERG channel is the primary potassium current responsible for setting the resting membrane potential [36]. The utility of this assay is also limited by its low sensitivity with a false negative rate of ~12%, the inability to efficiently rank compounds based on IC₅₀ values [37], and the fact that changes in membrane potential are an indirect measure of hERG channel activity.

Recently, a fluorescence-based thallium (Tl⁺) flux assay has been developed to detect drug effects on voltage- and ligand-gated K⁺ channels (including hERG channels) expressed in mammalian cells [38, 39]. This assay involves loading a Tl⁺-sensitive fluorescent dye into cells expressing K⁺ channels [39]. The drug effects on K⁺ channel activity are reflected as changes in the Tl⁺-sensitive fluorescence. The Tl⁺ flux assay uses instruments such as fluorescent imaging plate reader (FLIPR), equipment considered standard in most high-throughput screening laboratories. This assay proved to be quite robust and amenable to both workstation and fully automated screening approaches, with throughput suitable for screening larger chemical libraries [38, 39].

Novel non-electrophysiological assays are still being developed. For example, a homogeneous, fluorescence polarization-based assay to characterize the affinity of small molecules for the hERG channel was recently reported [40]. This assay has demonstrated tight correlation with data obtained from patch-clamp assays. The key to the development of this assay was creation of a cell line that expressed highly elevated levels of hERG protein.

All the non-electrophysiological methods provide only indirect measurements of the hERG channel activity and, therefore, cannot fully characterize the drug effects on the hERG channel function (i.e., it is formidable for these assays to

provide an accurate IC_{50} value for hERG block, which is essential in the estimation of the safety margin for later-stage discovery compounds). However, the non-electrophysiological assays may be useful in rank-ordering a large number of compounds and avoiding chemical series or structures early in drug discovery.

35.3 Safety Screenings of Non-hERG Cardiac Ion Channel Currents

It is relatively straightforward to consider the examples with hERG/ I_{Kr} current mentioned above and apply the lessons learned to screening of other cardiac channels. Indeed, pharmaceutical companies as well as various vendors routinely screen numerous cardiac ion channels in either manual or automated patch modes as part of either safety or screening efforts (the latter, for example, screening drugs to prevent atrial fibrillation). A representative list of cardiac ion channels that have been cloned and are available for screening is shown in Table 35.1. However, few would advocate characterizing multiple compounds across the entire list of ion channels available, in part due to resource considerations. While significant effects on individual ionic currents may not be manifest in the overall electrophysiologic response, they are useful in planning studies to gauge potential proarrhythmic risk.

At a minimum, the ICH-S7B guidelines [The Non-Clinical Evaluation of the Potential for Delayed Ventricular Repolarization (QT Interval Prolongation) by Human Pharmaceuticals] suggest that a functional hERG current assay be conducted as part of the preclinical assessment of cardiac safety (ICH S7B). Due to advances in techniques employed to evaluate drug effects on ECGs in clinical thorough QT studies, drug effects on the PR and QRS intervals are also evaluated now (along with the QT interval). In general, changes in the PR and QRS intervals reflect drug effects on cardiac L-type Ca^{2+} and fast inward Na^+ current,

Table 35.1 Various cardiac ion channels available for in vitro electrophysiologic assays

Channel	Corresponding current	Action
$Na_v1.5$	I_{Na}	Inward, depolarizing
$Ca_v1.2$	I_{CaL}	Inward, depolarizing
$Ca_v3.2$	I_{CaT}	Inward, depolarizing
$K_v4.3$	I_{to}	Outward, repolarizing
$K_v11.1$ (hERG)	I_{Kr}	Outward, repolarizing
$K_vLQT1/mink$	I_{Ks}	Outward, repolarizing
$K_v1.5$	I_{Kur}	Outward, repolarizing
$Kir2.1$	I_{K1}	Outward, repolarizing
$Kir6.2/SUR$	I_{KATP}	Outward, repolarizing
$NCX1$	$I_{Na/Ca}$	Inward/outward
$HCN2$	I_f , pacemaker current	Inward, depolarizing
$HCN4$	I_f , pacemaker current	Inward, depolarizing
$Kir3.1/3.4$	I_{KACH}	Outward, repolarizing

The upper section lists channels generally present in ventricular myocardium, while those in the lower section are largely active in atrial myocardium, SA node and AV node

respectively. Thus, it might seem prudent to determine drug effects on the L-type Ca^{2+} current ($\text{Ca}_{v1.2}$) and fast inward Na^+ current ($\text{Na}_{v1.5}$) earlier in drug discovery to further understand potential cardiac liabilities. While not an essential focus of the S7B guidelines (the purpose of which is to identify risk associated with delayed ventricular repolarization), such studies do fall within the purview of the ICH S7A guidelines (ICH S7A. Safety Pharmacology Studies for Human Pharmaceuticals) that call for a determination of the effects of test substances on the cardiovascular system, with specific mention of electrocardiograms. Results from cardiac ion channel screening assays could be considered as part of the “integrated risk assessment” mentioned within the S7B guidance document. More recently, Towart and colleagues have called for screening for block of the slowly activating cardiac delayed rectifier current I_{Ks} for new medical entities before testing in humans, recognizing this as a gap in the testing for delayed repolarization liability [41].

35.4 Timing of Cardiac Ion Channel Screening in Drug Discovery: hERG and Non-hERG Channels

Given the association between hERG block and the risk of delayed repolarization, in vitro ion channel assays to detect hERG liabilities are being conducted earlier in drug discovery. Indeed, some companies will quickly follow-up on in silico studies with synthesis and testing of novel drug targets in automated patch-clamp systems even prior to efficacy testing for therapeutic targets. The term “frontloading” has been used to describe safety studies conducted during lead optimization of compounds before selection of candidates for drug development and before regulatory studies are performed [42]. According to this study, approximately 70% of companies responding reported testing for hERG liabilities prior to candidate selection, and approximately 65% of companies reported testing for “other ion channels” prior to lead selection. Cavero has used the phrase “Exploratory Safety Pharmacology” to describe an emerging branch of Safety Pharmacology studies that addresses identification of safety liabilities by application of multiple in silico and non-GLP in vitro assays in parallel with early candidate selection [43]. Such studies differ in scope from “frontloaded” studies in that the later are conducted during lead optimization in order to identify drug candidates with (oftentimes) specific liabilities. Independent of the stage of drug discovery, cardiac ion channel screening studies have the potential to derisk compounds early, provide mechanistic information to assist in designing subsequent pharmacodynamic investigations, and guide future risk management strategies.

Perhaps it is best to consider the utility of cardiac ion channel screening on the basis of the stage of discovery/development of a compound. For example, in the situation where multiple compounds have been selected in early lead optimization, it might be prudent to compare the effects of these compounds on multiple cardiac ion channels in an effort to discharge risk early in the compound selection process. If, however, only one or two compounds have been identified that demonstrate efficacy in preclinical studies, extensive screening against multiple cardiac ion channels

might be supplanted by studies using more “integrative” electrophysiological preparations, such as in vitro repolarization assays or ECG studies (the latter being conducted either in vitro e.g., Langendorff hearts) or in vivo (anesthetized or conscious animal studies). In the latter situation, the goal is not to avoid risk, but rather to detect and manage risk. This could be accomplished by comparing concentration-response curves for the ion channel signal in vitro versus concentration-response curves on the pharmacologic target. By understanding the preclinical effects of an evolving drug or drug series, it may be possible to guide the focus of early clinical trials, providing for an early clinical “go-no-go” decision (fail fast, fail early concept). For example, for a drug with an IC_{50} value for hERG block within 10-fold the estimated clinical C_{max} value, an earlier clinical exploration of the potential for QT prolongation might be considered during first in human studies conducted early in development. Indeed, such determinations are well suited for multiple-ascending dose tolerability studies conducted during phase 1 studies, which often-times evaluate the highest exposures achieved during clinical development.

The in vitro ion channel studies, when conducted appropriately and with proper additional support (analysis of bath concentrations, physiologic temperatures), can precisely characterize the effects of evolving drug candidates on one type of channel (such as may be expressed in heterologous expression system). However, it must be realized that the effect of a drug on cardiac electrical activity reflects potential interactions with multiple ionic channels, pumps, and exchangers, and that even the most exacting of IC_{50} values may not provide the full account of a drug’s overall cardiac effect. For example, it is well recognized that not all drugs that block hERG elicit delayed repolarization: verapamil is an often-cited example. Verapamil is not associated with either QT prolongation or torsades de pointes clinically despite blocking hERG at concentrations comparable to therapeutic (total) plasma concentrations [44]. This result is most easily explained by the fact that verapamil also blocks the L-type (inward) cardiac Ca^{2+} current, likely offsetting the reduced outward K^+ current due to hERG block. The simultaneous effects of a drug on multiple ion channels (termed multichannel block) are best appreciated when comparing ion channel assay results with in vitro repolarization studies [3, 45, 46]. Indeed, one may consider the cardiac action potential as a collection of simultaneous (and possibly interdependent) ion channel assays with different sensitivities to block different channels. Indeed, prolongation of the action potential (simple extension of the final repolarization phase) vs. triangulation of the action potential (a change in the overall repolarization configuration of an action potential, rendering the action potential more “triangular”) leads to very different initial interpretations (the former consistent with hERG block, the latter consistent with either augmentation of an early outward plateau current or reduction of an inwardly directed plateau current). Some studies have also suggested that proarrhythmia is better predicted based on drug-induced changes in the action potential configuration [47, 48]. Alternatively, one could argue that a rational strategy for drug discovery might include initial repolarization studies to detect changes in the action potential configuration, followed by specific cardiac ion channel assays to determine which ion channels are responsible for the repolarization changes.

35.5 Conclusion and Future Directions

With continuing technologic developments advancing the capabilities of automated patch-clamp platforms, it is expected that cardiac ion channel safety screening efforts will become as commonplace in the future as radiolabeled displacement binding studies for receptors were a decade ago. The future challenge for cardiac ion channel screening will not be related to either assay technologies or automation, but rather to interpreting and understanding the volumes of data generated. This must include an assessment of the limitations of the approach, which will be accomplished by comparing in vitro results with feedback provided from preclinical in vivo and clinical data sets. Such feedback from more integrated physiologic systems (including humans) will allow for the evaluation of the sensitivity and specificity of individual ion channel assays. A systems biology approach to integrate the multiple assay results to predict clinical responses could be beneficial for placing cardiac ion channel screening results in context. Such efforts are essential to provide confidence in optimally positioning cardiac ion channel assays in future drug discovery efforts.

References

1. Roden DM. Long QT syndrome: reduced repolarization reserve and the genetic link. *J Int Med.* 2006;259(1):59–69.
2. Redfern WS, Carlsson L, Davis AS, Lynch WG, Mackenzie I, Palethorpe S, et al. Relationships between preclinical cardiac electrophysiology, clinical QT interval prolongation and Torsade de pointes for a broad range of drugs: evidence for a provisional safety margin in drug development. *Cardiovasc Res.* 2003;58(1):32–45.
3. Gintant GA, Su Z, Martin RL, Cox BF. Utility of hERG assays as surrogate markers of delayed cardiac repolarization and QT study. *Toxicol Pathol.* 2006;34:81–90.
4. Dunlop J, Bowlby M, Peri R, Vasilyev D, Arias R. High-throughput electrophysiology: an emerging paradigm for ion-channel screening and physiology. *Nat Rev Drug Discov.* 2008; 7:358–68.
5. Brown AM. High throughput functional screening of an ion channel library for drug safety and efficacy. *Eur Biophys J.* 2009;38:273–8.
6. Kang J, Chen XL, Wang H, Ji J, Cheng H, Incardona J, et al. Discovery of a small molecule activator of the human ether-a-go-go-related gene (HERG) cardiac K⁺ channel. *Mol Pharmacol.* 2005;67:827–36.
7. Casis O, Olesen SP, Sanguinetti MC. Mechanism of action of a novel human ether-a-go-go-related gene channel activator. *Mol Pharmacol.* 2006;69:658–65.
8. Polak S, Wiśniewska B, Brandys J. Collation, assessment and analysis of literature in vitro data on hERG receptor blocking potency for subsequent modeling of drugs' cardiotoxic properties. *J Appl Toxicol.* 2009;29(3):183–206.
9. Su Z, Limbers J, Souers A, Kym P, Mikhail A, Houseman K, et al. Electrophysiologic characterization of a novel hERG channel activator. *Biochem Pharmacol.* 2009;77:1383–90.
10. Su Z, Marin R, Cox BF, Gintant GA. Mesoridazine: an open-channel blocker of human ether-a-go-go-related gene K⁺ channel. *J Mol Cell Cardiol.* 2004;36:151–60.
11. Roy M, Dumaine R, Brown AM. HERG, a primary human ventricular target of the nonsedating antihistamine terfenadine. *Circulation.* 1996;94(4):817–23.

12. Kirsch GE, Trepakova ES, Brimecombe JC, Sidach SS, Erickson HD, Kochan MC, et al. Variability in the measurement of hERG potassium channel inhibition: effects of temperature and stimulus pattern. *J Pharmacol Toxicol Methods*. 2004;50:93–101.
13. Yao J, Du X, Lu D, Baker RL, Daharesh E, Atterson P. Estimation of potency of hERG channel blockers: impact of voltage protocol and temperature. *J Pharmacol Toxicol Methods*. 2005;52:146–53.
14. Hancox JC, McPate MJ, Harchi AE, Zhang YH. The hERG potassium channel and hERG screening for drug-induced torsades de pointes. *Pharmacol Ther*. 2008;119:118–32.
15. Stork D, Timmin EN, Berjukow S, Huber C, Hohaus A, Suer M, et al. State dependent dissociation of hERG channel inhibitors. *Br J Pharmacol*. 2007;151:1368–76.
16. Herron W, Towers C, Templeton A. Experiences in method development for the analysis of *in vitro* study solutions for content. *J Pharmacol Toxicol Methods*. 2004;49(3):211–6.
17. Hanson LA, Bass AS, Gintant G, Mittelstadt S, Rampe D, Thomas K. ILSI-HESI cardiovascular safety subcommittee initiative: Evaluation of three non-clinical models of QT prolongation. *J Pharmacol Toxicol Methods*. 2006;54:116–29.
18. Brimecombe JC, Kirsch GE, Brown AM. Test article concentrations in the hERG assay: losses through the perfusion, solubility and stability. *J Pharmacol Toxicol Methods*. 2009;59(1):29–34.
19. Milligan CJ, Li J, Sukumar P, Majeed Y, Dallas ML, English A, et al. Robotic multiwall planar patch-clamp for native and primary mammalian cells. *Nat Protocol*. 2009;4:244–55.
20. Finkel A, Wittel A, Yang N, Handran S, Hughes J, Costantin J. Population patch clamp improves data consistency and success rates in the measurement of ionic current. *J Biomol Screen*. 2006;11:488–96.
21. Schroeder K et al. IonWorks HT: a new high-throughput electrophysiology measurement platform. *J Biomol Screen*. 2003;8:50–64.
22. Sorota S, Zhang XS, Margulis M, Tucker K, Priestley T. Characterization of a hERG screen using the IonWorks HT: comparison to a hERG rubidium efflux screen. *Assay Drug Dev Technol*. 2005;3:47–57.
23. Bridgland-Taylor MH, Hargreaves AC, Easter A, Orme A, Henthorn DC, Ding M, et al. Optimisation and validation of a medium-throughput electrophysiology-based hERG assay using IonWorks HT. *J Pharmacol Toxicol Methods*. 2006;54:189–99.
24. Guthrie H, Livingston FS, Gubler U, Garippa R. A place for high-throughput electrophysiology in cardiac safety: screening hERG cell lines and novel compounds with the ion works HTTM system. *J Biomol Screen*. 2005;10:832–40.
25. Tao H, Santa Ana D, Guia A, Huang M, Ligutti J, Walker G, et al. Automated tight seal electrophysiology for assessing the potential hERG liability of pharmaceutical compounds. *Assay Drug Dev Technol*. 2004;2(5):497–506.
26. Kutchinsky J et al. Characterization of potassium channel modulators with QPatch automated patch-clamp technology: system characteristics and performance. *Assay Drug Dev Technol*. 2003;1:685–93.
27. Mathes C. QPatch: the past, present and future of automated patch clamp. *Expert Opin Ther Targets*. 2006;10:319–27.
28. Dubin AE, Nasser N, Rohrbacher J, Hermans AN, Marrannes R, Grantham C, et al. Identifying modulators of hERG channel activity using the PatchXpress planar patch clamp. *J Biomol Screen*. 2005;10:168–81.
29. Guo L, Guthrie H. Automated electrophysiology in the preclinical evaluation of drugs for potential QT prolongation. *J Pharmacol Toxicol Methods*. 2005;52:123–35.
30. Chadwick CC, Ezrin AM, Oconnor B, Volberg WA, Smith DI, Wedge KJ, et al. Identification of a specific radioligand for the cardiac rapidly activating delayed rectifier K⁺ channel. *Circ Res*. 1993;72:707–14.
31. Diaz GJ, Daniel K, Leitza ST, Martin RL, Su Z, McDermott JS, et al. The [³H] dofetilide binding assay is a predictive screening tool for hERG blockade and proarrhythmia:

- comparison of intact cell and membrane preparations and effects of altering $[K^+]$ _o. *J Pharmacol Toxicol Methods*. 2004;50:187–99.
- 32. Chiu PJ, Marcoe KF, Bounds SE, Lin CH, Feng JJ, Lin A, et al. Validation of a [³H]-astemizole binding assay in HEK293 cells expressing HERG K⁺ channels. *J Pharmacol Sci*. 2004;95:311–9.
 - 33. Raab CE, Butcher JW, Connolly TM, Karczewski J, Yu NX, Staskiewicz SJ, et al. Synthesis of the first sulfuer-35-labeled hERG radioligand. *Bioorg Med Chem Lett*. 2006;16:1692–5.
 - 34. Murphy SM, Palmer M, Poole MF, Padegimas L, Hunady K, Danzig J, et al. Evaluation of functional and binding assays in cells expressing either recombinant or endogenous hERG channel. *J Pharmacol Toxicol Methods*. 2006;54:42–55.
 - 35. Rezazadeh S, Hesketh JC, Fedida D. Rb⁺ flux through hERG channels affects the potency of channel blocking drugs: correlation with data obtained using a high-throughput Rb⁺ efflux assay. *J Biomol Screen*. 2004;9:588–97.
 - 36. Netzer R, Bischoff U, Ebneth A. HTS techniques to investigate the potential effects of compounds on cardiac ion channel at early-stages of drug discovery. *Curr Opin Drug Discov Dev*. 2003;6:462–9.
 - 37. Dorn A, Hermann F, Ebneth A, Bothmann H, Trube G, Christensen K, et al. Evaluation of a high-throughput fluorescence assay method for HERG potassium channel inhibition. *J Biomol Screen*. 2005;10:339–47.
 - 38. Weaver CD, Harden D, Dworetzky SI, Robertson B, Knox RJ. A thallium-sensitive, fluorescence-based assay for detecting and characterizing potassium channel modulators in mammalian cells. *J Biomol Screen*. 2004;9:671–7.
 - 39. Titus SA, Beacham D, Shahane SA, Southall N, Xia M, Huang R, et al. A new homogeneous high-throughput screening assay for profiling compound activity on the human ether-a-go-go-related gene channel. *Anal Biochem*. 2009;394:30–8.
 - 40. Piper DR, Duff SR, Eliason HC, Frazee WJ, Frey EA, Fuerstenau-Sharp M, et al. Development of the predictor HERG fluorescence polarization assay using a membrane protein enrichment approach. *Assay Drug Dev Technol*. 2008;6:213–23.
 - 41. Towart R, Linders JT, Hermans AN, Rohrbacher J, van der Linde HJ, Ercken M, et al. Blockade of the I_{Ks} potassium channel: an overlooked cardiovascular liability in drug safety screening? *J Pharmacol Toxicol Methods*. 2009;60(1):1–10.
 - 42. Lindgren S, Bass AS, Briscoe R, Bruse K, Friedrichs GS, Kallman MJ, et al. Benchmarking safety pharmacology regulatory packages and best practice. *J Pharmacol Toxicol Methods*. 2008;58(2):99–109.
 - 43. Cavero I. Exploratory safety pharmacology: a new safety paradigm to de-risk drug candidates prior to selection for regulatory science investigations. *Expert Opin Drug Saf*. 2009;8(6): 627–47.
 - 44. Zhang S, Zhou Z, Gong Q, Makielski JC, January CT. Mechanism of block and identification of the verapamil binding domain to HERG potassium channels. *Circ Res*. 1999;84(9):989–98.
 - 45. Bril A, Gout B, Bonhomme M, Landais L, Faivre JF, Linee P, et al. Combined potassium and calcium channel blocking activities as a basis for antiarrhythmic efficacy with low proarrhythmic risk: experimental profile of BRL-32872. *J Pharmacol Exp Ther*. 1996;276(2): 637–46.
 - 46. Martin RL, McDermott JS, Salmen HJ, Palmatier J, Cox BF, Gintant GA. The utility of hERG and repolarization assays in evaluating delayed cardiac repolarization: influence of multi-channel block. *J Cardiovasc Pharmacol*. 2004;43(3):369–79.
 - 47. Hondeghem LM. TRIaD: foundation for proarrhythmia (triangulation, reverse use dependence and instability). *Novartis Found Symp*. 2005;266:235–44.
 - 48. Grant AO, Tranquillo J. Action potential and QT prolongation not sufficient to cause Torsade de Pointes: role of action potential triangulation. *J Cardiovasc Electrophysiol*. 2007;18(2): 204–5.

Chapter 36

QT Prolongation Is a Poor Predictor of Proarrhythmia Liability: Beyond QT Prolongation!

Luc M. Hondeghem

36.1 Introduction: QT Paradox

Prolongation of the APD, as reflected by QT prolongation in the ECG, was introduced as a major antiarrhythmic mechanism [1, 2], but soon QT prolongation became instead a liability [3, 4]. QT prolongation even graduated to a surrogate [5] for *Torsade de Pointes* (TdP): what a paradox! It is then not surprising that QT prolonging drugs range from potently torsadogenic to antiarrhythmic agents [6]. Thus, QT interval alone can clearly not satisfactorily identify anti- and proarrhythmic actions.

In this chapter, cardiac wavelength (λ) and TRIaD (Triangulation, Reverse use dependence, Instability and Dispersion) are described with respect to proarrhythmia. The QT paradox is resolved: it is emphasized that QT prolongation by itself (i.e., in the absence of disturbances of λ -TRIaD) can be antiarrhythmic. In contrast, QT prolongation alone (i.e., without consideration of λ -TRIaD) yields false positives (depriving patients from valuable drugs) and false negatives (exposing patients to preventable risks).

36.2 Proarrhythmia

Arrhythmias can result from disturbances in automaticity, disturbances of conduction, disturbances of repolarization and mechanical disturbances. The present chapter will be limited to disturbances of conduction and repolarization (which does not mean that the others cannot also contribute) and focus upon TdP and VF.

L.M. Hondeghem

Pharmacology, Catholic University Leuven, Westlaan 85, 8400 Oostende, Belgium
e-mail: Luc.Hondeghem@screenQT.com

36.2.1 Cardiac Wavelength

In Fig. 36.1a, 11 cardiac strands are represented. At time 0 (top trace), the strand is fully rested (green). Upon application of a stimulus at the right end, the impulse propagates towards the left at 1 block/100 ms so that by 100 ms (second trace), the rightmost rectangle is depolarized (red). By 600 ms, the head of the wave reaches the left end of the strand. The action potential duration (APD) is assumed to be 400 ms: 300 ms in the plateau (red) plus 100 ms repolarization (red to yellow). During the plateau, the tissue is absolutely refractory, but as repolarization progresses the tissue regains excitability and eventually can conduct again (yellow): end of effective refractory period (ERP). The repolarization tail of the wave follows

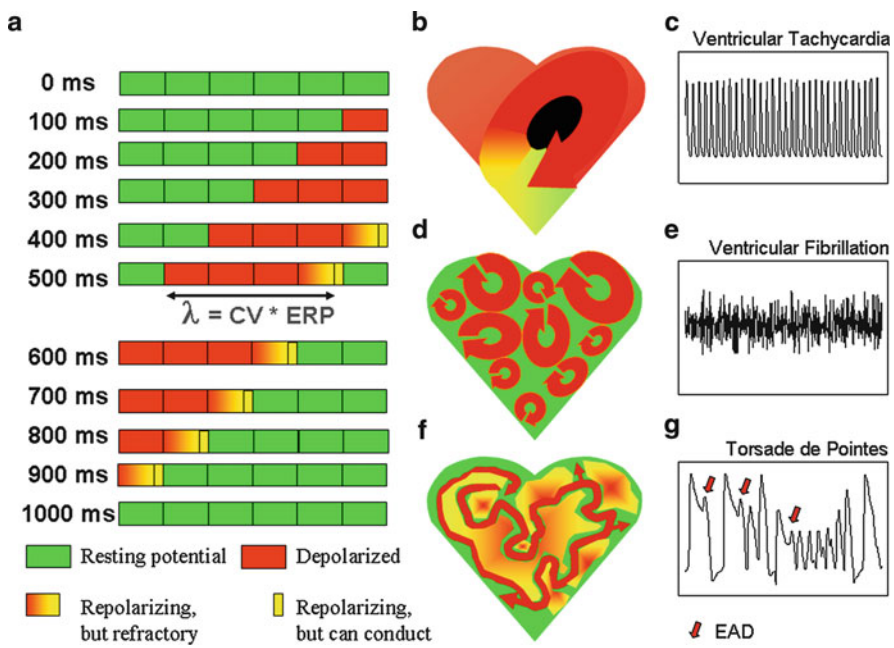


Fig. 36.1 Cardiac Wavelength, VT, VF and TdP. For a detailed description of the important concepts in this figure see Sect. 36.2.2. Panel (a) illustrates linear propagation in a strand of cardiac tissue. Throughout the figure, green color indicates the tissue that is at more negative potentials and fully excitable; red indicates that the tissue is at more positive potentials and inexcitable; during repolarization as tissue becomes partly excitable the color goes from red to yellow and finally back to green. Panel (b) shows a wave rotating around an unexcitable lesion (black) and creating a VT [resulting monophasic action potential recording shown in panel (c)]. In panel (d), λ has become so short that numerous wavelets can coexist in the heart and result in VF [recording shown in panel (e)]. Panel (f) illustrates grossly simplified two-dimensional snapshot of a three-dimensional mosaic of waves traveling through excitable tissue strings running between refractory islands. In such a complex ever changing three-dimensional progress, the wave keeps on twisting through ever changing paths: TdP [panel (g)]. The arrows highlight the presence of EADs

the head (also at 1 block/100 ms) until the strand becomes again fully repolarized (bottom trace).

Figure 36.1a clearly illustrates that the wavelength (λ) is proportional to conduction velocity (CV) and the duration of the ERP:

$$\lambda = CV \times \text{ERP}.$$

If shortening of λ facilitates reentry, then from the above equation it follows that slowed CV and/or shortening of ERP must be important proarrhythmic parameters.

36.2.2 Reentry

36.2.2.1 Ectopics and Ventricular Tachycardia

Cardiac waves can also circulate (Fig. 36.1b) around an obstacle (e.g., an old infarct) and under appropriate conditions (e.g., λ shorter than available path), an impulse may then chase its own repolarization tail: reentry [1, 7]. This can result in ectopics and if repetitive, in ventricular tachycardia (VT; Fig. 36.1c). Clearly shortening λ by slowing conduction and/or shortening ERP facilitates reentry. Conversely, as λ prolongs, the available excitable gap (yellow-green) decreases...until this gap closes and conduction must fail. Thus, prolongation of λ can be antiarrhythmic.

36.2.2.2 Ventricular Fibrillation

As CV slows and/or ERP declines, λ may shorten so much that multiple wavelets may fit into the heart (Fig. 36.1d) and produce a chaotic activation of the heart: ventricular fibrillation (VF; Fig. 36.1e) [8]. Drugs that shorten λ (slow conduction and/or shorten ERP) facilitate VF. Conversely, agents that lengthen λ until insufficient wavelets can persist have antifibrillatory properties. Effective antifibrillatory agents must thus minimize opportunities for slowed conduction and short ERP. (Optimal antifibrillatory action, where the drugs also exhibit time- and voltage-dependent actions [9], is very complex and beyond the scope of this chapter.)

36.2.2.3 Torsade de Pointes

Sometimes the cardiac action potential can become unstable with respect to its upstroke, duration of the plateau and/or duration of repolarization. This results not only in instability of λ , but because it can be poorly synchronized, [10] it may also yield temporal [11] dispersion in addition to spatial [12] dispersion. This in turn creates ever changing three-dimensional pockets of refractoriness intermixed

with three-dimensional paths for conduction (Fig. 36.1f is an oversimplified two-dimensional representation of only one such instance). As a result, the wavefront(s) must then twist through ever changing available paths for activation around ever changing refractory obstacles: *TdP* [13] (Fig. 36.1g). TdP is most frequently initiated by early afterdepolarizations or EAD (see arrows in Fig. 36.1g), or other rhythm disturbances in tissue that exhibits instability of conduction and/or APD [14–16]. When these disturbances are relatively minor, the required excitable paths may fail to persist for long times, so only short runs of TdP can persist. As the disturbances get worse, the runs may become longer. Finally, as more and more paths and obstacles coexist and the wave(s) become more easily accommodated (e.g., shorter λ), deterioration into VF becomes likely.

36.2.3 Disturbances of Depolarization

Slowing and destabilization of CV are primary proarrhythmic factors. The most important causes of slowed conductions are (1) depolarization of the membrane potential (e.g., ischemia), which not only reduces the steady state availability of sodium channels, but also slows the restitution of their availability; (2) intercellular uncoupling (e.g., closing gap junctions by intracellular calcium overload, acidosis); and (3) chemicals that block sodium channels (e.g., class I antiarrhythmic agents). Slowed conduction reduces λ and facilitates reentry.

Even when a reentry encroaches on its own tail, a negative feedback mechanism may facilitate its persistence. Indeed, when the reentry wave travels too fast, it climbs up the repolarization tail where sodium channel availability declines and hence CV slows (Fig. 36.2). This reduces the probability that the wave will have to invade fully refractory tissue, which would terminate the reentry. Thus slow repolarization (see triangulation below) will widen the period during which such proarrhythmic feedback can operate (prolongation of vulnerable period (VP) in Fig. 36.2c) and facilitate persistence of reentry. Conversely, agents which delay restitution of the sodium channels till more complete repolarization without much slowing of restitution at full repolarization, can seriously shorten this period and thus hinder reentry (Fig. 36.2b), e.g., ultra fast sodium channel blockers like ω 3-fatty acids [17]. Other relatively fast sodium channel blockers may also have net antiarrhythmic benefits (e.g., like amiodarone, lidocaine).

Unfortunately, when the sodium channel has intermediate kinetics of restitution (e.g., mexiletine [18]), small variation in restitution time can yield large variation in available sodium current over a relatively long interval. Slight variations in diastolic recovery interval can then provide substantial changes of sodium current and render λ unstable and contribute to TdP [16]. It is then not surprising that mexiletine (an agent that does not prolong the APD) has nevertheless been described to rarely cause TdP [19].

Finally, as the restitution time lengthens, the problem to be solved may become substituted by a larger one and instead result in *predictable* proarrhythmia [20, 21].

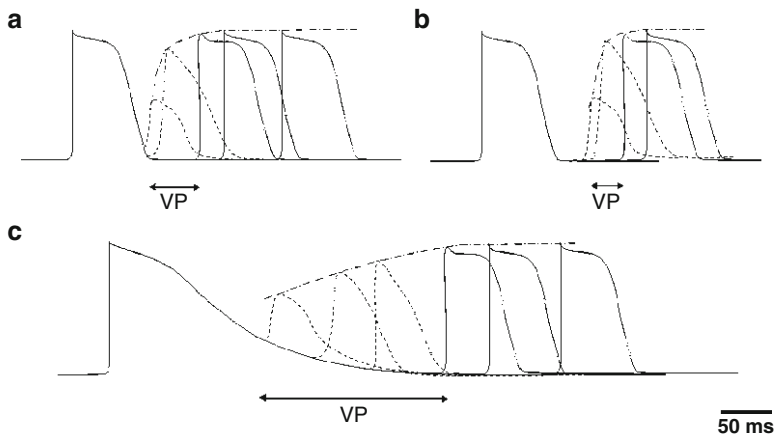


Fig. 36.2 Vulnerable period (VP). The solid traces show action potentials that can propagate at near normal speed, the dashed lines indicate that only slowly propagating responses can be obtained. At shorter coupling intervals, only local responses that cannot yet propagate can be obtained (not shown). The dot-dashed line illustrates the rate of recovery of the action potential (both its conduction and duration). Under normal conditions [panel (a)], recovery begins during the tail of the action potential and is fully recovered in about 50 ms. In panel (b), recovery is delayed till full repolarization (e.g., ω_3 fish oil) where it occurs faster, so that the slowest recovery part of the vulnerable period may actually be shortened, which may shorten the vulnerable period. Panel (c) illustrates how triangulation of the action potential markedly prolongs the restitution at depolarized potentials (where it proceeds much more slowly). As a result, the vulnerable period is markedly extended

Indeed, if enough block is present to interfere with reentry early in diastole, then the slow restitution mandates that the sinus beat will also be slowed (more vulnerable to reentry); conversely, if the concentration is low enough so that conduction of the sinus beat is not slowed, then the early diastolic reentry can also not be suppressed.

36.2.4 Disturbances of Repolarization: TRIaD

36.2.4.1 Reverse Use Dependence

Prolongation of the APD normally prolongs the ERP, and thus also λ . As λ increases, the possibility for reentry is reduced, which is expected to be antiarrhythmic. Unfortunately, most class III [2] antiarrhythmic agents primarily prolong the APD at slow heart rates, while losing this desired effect as the cardiac cycle length shortens: *reverse use dependence* [22]. Such agents have thus least effect upon λ when most needed and were consequently predicted to be less efficacious. In addition, following long cycle lengths, reverse use dependence can yield excessive APD prolongation, which can lead to *predictable proarrhythmia* [22, 23].

36.2.4.2 Instability

Instability was detected in my laboratory by Bruno Hespel in 1995 (unpublished observation): he observed that when successive APDs became unstable, serious arrhythmias like TdP or VF were imminent. In a blinded test, instability of APD appeared so predictive that it was applied to a large study of hERG blockers [11]. Actually, instability of T waves was described in patients as commonly preceding the development of TdP [15], and was recently elegantly described to also precede VT and VF [24]. Instability of the action potential can be latent so that during a regular train, successive action potentials appear completely alike. However, a disturbance of the diastolic interval (e.g., ectopic, EAD) may uncover the latent instability (see figure 3 of reference [11]). It is then not surprising that in patients TdP is frequently initiated upon variation of ventricular cycle [15].

Instability may in part be a direct consequence of reverse use dependence. Indeed, an ectopic is followed by a shorter or longer (compensatory pause) cycle length. Reverse use dependence renders the APD following a short diastole shorter (and vice versa); but at any basic cycle length, a shorter APD is followed by a longer diastole; the longer diastole results in a longer APD...this vicious cycle yields instability of APD.

36.2.4.3 Triangulation

When in a study of over 700 chemicals (mostly hERG blockers [11]), all drugs that induced reverse use dependence or instability were removed, a substantial fraction of the remaining compounds continued to be proarrhythmic. However, the ten most proarrhythmic agents all induced triangular action potentials, while the action potential of the ten least proarrhythmic agents showed a more rectangular appearance. The time from APD_{30} to APD_{90} was therefore defined as a measure for triangulation [11].

When, in this drug series, all agents that exhibited triangulation, reverse use dependence or instability were removed, the antiarrhythmic action for the remaining agents increased as the APD prolonged (and vice versa). Furthermore, in all subgroups with either triangulation, reverse use dependence, instability or any combination thereof, shortening of APD worsened the proarrhythmia while prolongation of APD reduced proarrhythmia. Unfortunately, the antiarrhythmic action of APD prolongation was not large enough to overcome the proarrhythmia induced by triangulation, reverse use dependence and/or instability.

36.2.4.4 TRIaD

Since the above three disturbances develop neither uniformly nor in synchrony, they necessarily induce dispersion of APD and therefore triangulation, reverse use dependence, instability and dispersion became abbreviated to TRIaD [6].

It is important to stress that the above disturbances of depolarization and repolarization frequently concur and interact in complex ways. For example,

triangulation prolongs the period for restitution of the action potential (compare Fig. 36.2a, c). Thus, CV remains slower and APD shorter for a longer period of time. This combination can markedly shorten λ and facilitate reentry, resulting in facilitation of VT, VF and TdP: vulnerable period (VP in Fig. 36.2). As the magnitude and the number of the depolarization and repolarization disturbances increase, their interactions may become more complex and the probability of serious proarrhythmia can increase sharply.

36.3 VT, VF and TdP

36.3.1 Two Proarrhythmic Axes

From the above it is clear that λ and TRIaD define two proarrhythmic axes (Fig. 36.3). Shortening of λ and induction of TRIaD yield a proarrhythmic pole,

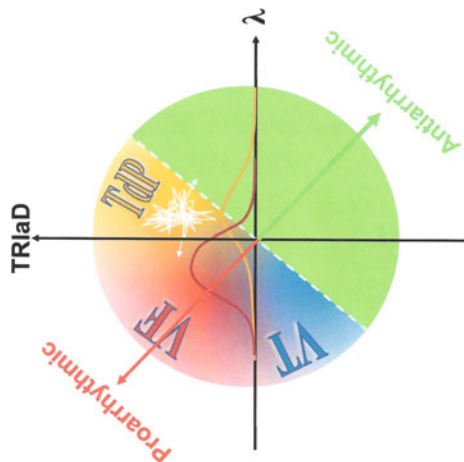


Fig. 36.3 Pro- and antiarrhythmic vectors. Concurrence of shortening of λ and induction of TRIaD defines the most proarrhythmic pole, while the converse defines the antiarrhythmic pole. The proarrhythmic hemisphere consists of preferential but overlapping regions of TdP, VF and VT. The curves illustrate the relative incidences of VF and TdP as a function of λ . With shortening of λ , initiation of VF initially sharply increases, until no new VF can develop because all hearts already fibrillate before such short λ is reached. Importantly, in isolated rabbit hearts drug-induced VF is about 50% more frequent than TdP (*high* vs. *plain* curve). As λ prolongs, the incidence of VF declines to zero (the wavelength becomes too long to allow simultaneous presence of multiple reentry waves). While TdP (*plain* curve) can occur with shortened λ , its incidence initially increases with prolongation of λ . However, beyond some critical prolongation of λ , TdP sharply declines (λ too long and TdP can no longer fit in the heart). The white vectors show that during TdP, λ and the amount of TRIaD change beat-by-beat (instability). This can continue as long as λ does not become too short (and terminate in VF as shown by *left white arrow*, in about 15% of cases) or too long (no longer fits in the available path and hence must stop as indicated by *right white arrow*, in about 85% of cases)

while prolongation of λ with reduction of TRIaD forms an antiarrhythmic pole. In the proarrhythmic hemisphere arrhythmias are not distributed uniformly: as λ shortens reentry is facilitated; in the absence of TRIaD the arrhythmia is expected to be more stable (e.g., VT) but when combined with TRIaD the proarrhythmic may be less stable (e.g., VF).

In contrast, as λ prolongs, reentry is rendered more difficult. Actually, when λ exceeds the available path, it must normally stop. However, as temporal instability leads to out of phase oscillations [10], the heart can become a three-dimensional mosaic of ever changing patterns of refractory and excitable tissues. It then can become possible to fold wavelength(s) exceeding the cardiac circumference into the heart (Fig. 36.1g). This wave must then three-dimensionally fold and meander around ever changing obstacles in ever changing directions (twisting of the pointes of the QRS or TdP; Dessertenne [13]). If reverse use dependence is marked, then as λ shortens and reentry is facilitated, the likelihood for VF increases (~15% of TdP terminate into VF [6], see left white arrow Fig. 36.3). Fortunately, 85% of TdPs run out of excitable tissue and thus simply terminate into sinus rhythm (right white arrow in Fig. 36.3).

Disturbances of conduction and repolarization precede VF and TdP in a concentration-dependent fashion. Actually at 1/100th the actual proarrhythmic concentration, ~15% of hearts already exhibit λ -TRIaD disturbances. By 1/10th the proarrhythmic concentration, λ -TRIaD disturbances become detectable in ~50% and by 1/3rd that concentration, in ~80%. TdPs always show λ -TRIaD disturbances *before* the actual arrhythmia strikes. Unfortunately, VF can sometime occur without generating any obvious λ -TRIaD disturbance. Thus, additional or more sensitive parameters will need to be found to fully detect VF liability.

36.3.2 QT Prolongation: A TdP Surrogate?

It has been proposed that QT prolongation is such an essential part of TdP [3, 4] that drug-induced prolongation of the QT interval has become a surrogate liability [5]. It is essential to test the validity of the above two declarations against factual observations.

1. To begin with, TdP was first described by Dessertenne [13] as: “*La tachycardia alternante...complexes qui ont tantôt la pointe en haut et tantôt la pointe en bas*” (translation: The alternating tachycardia...with complexes that have the points at times upwards then downwards). The “pointe” here refers to the QRS complex, which reflects ever changing conduction and has nothing to do with APD/QT. Actually, QT is not even mentioned in Dessertenne’s paper (neither QT duration nor QT prolongation). It was later (correctly) noted that TdP is frequently associated with QT prolongation, but that does neither mean that TdP can *only* occur with QT prolongation nor that the QT prolongation *causes* TdP.

2. In fact, in 2005 [6], at least 18 clinical studies showed that TdP frequently occurs in the absence of QT prolongation or even can occur with QT shortening (*false negatives*).
3. In addition, there exist many drugs that prolong the QT but *never* have been reported to cause TdP (*false positives*) [25].
4. In contrast, *all* torsadogenic drugs induce disturbances of repolarization and/or conduction. I have asked at numerous meetings (including at the FDA) for examples of torsadogenic drugs that neither augment TRIaD nor shorten λ . So far nobody has been able to produce even a single one.
5. Even for drugs that are torsadogenic and can prolong the APD, TdP can develop *before* the QT is prolonged [6].
6. Drugs that prolong the APD with little or no TRIaD have even been documented to have antiarrhythmic efficacy and can even be used to treat TdP (e.g., amiodarone).

Thus, TdP cannot be dissociated from disturbances of λ -TRIaD, but can occur with prolongation, no change or shortening of the APD. More importantly, drugs devoid of λ -TRIaD disturbances are never torsadogenic. Since QT prolongation as a surrogate for TdP produces false positives and false negatives, this surrogate cannot satisfactorily prevent exposure of patients to TdP but can deprive patients from valuable medications.

36.3.3 *TdP: Only the Tip of the Iceberg*

In rabbits, the incidence of drug-induced VF (red line in Fig. 36.3) is about 50% greater than that of TdP (orange line), at least with the set of compounds we tested. This may partly reflect preselection of compounds for absence of hERG block using, for instance, high-throughput binding before testing in rabbit hearts. While TdP is only ~15% lethal (when it deteriorates into VF), VF is nearly always lethal. Thus, if the distribution in humans were similar to that in rabbits, then the expected mortality for drug-induced VF may be an order of magnitude greater than that for TdP. When I first presented this calculation (ICH, London 2004), Dr. Shah confirmed that on his regulatory desk there were more drug-induced fatalities related to VF than TdP [6]. This is far more remarkable than might appear: 85% of patients survive TdP and can provide records documenting TdP...most VF patients do not get an opportunity to provide a record. Hence the ratio of drug-induced mortality by VF/TdP is likely much underestimated.

36.4 Cardiac Safety Evaluation

Optimal patient safety in drug development requires sound strategies. Many powerful preclinical tools exist, but their optimal path for establishing cardiac safety is highly complex and subject to much debate. In my opinion, a standard optimal path

cannot exist as no chemical has a single target or a single action and thus a single tool or standard recipe cannot be the most effective for all conditions (just as even the best compass cannot alone detect the upcoming iceberg).

There can be no doubt that TdP appears most frequently associated with QT prolongation and VF most frequently with QT shortening. Drug safety based upon *casual* association will then ban both, drugs that prolong QT as well as those that shorten QT (rendering drug development all but impossible). Clearly, such nonsense follows from a simplistic and noncausal but casual relation.

Would it then not be more logical to concentrate safety studies on detection of proven proarrhythmic factors (disturbances of λ -TRIaD), rather than concentrating on QT prolongation, which in the absence of λ -TRIaD disturbances can factually be antiarrhythmic?

36.4.1 Proarrhythmic Safety Index

The therapeutic index (dose 50% toxic to dose 50% therapeutic) is not optimal when toxicity and therapeutic concentration curves are not widely separated and their slopes not parallel (dot-dashed curves in Fig. 36.4): (1) proarrhythmic incidences may then overlap with the therapeutic range (dot-dashed line in Fig. 36.4).

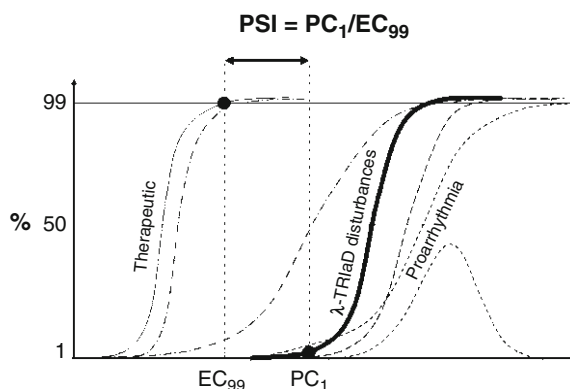


Fig. 36.4 Proarrhythmic safety index (PSI). The PSI is defined as the ratio of the concentration that starts to show λ -TRIaD disturbances (PC_1 at bottom of thick solid line) to that concentration which is usually therapeutically effective (EC_{99} at top of thin solid line). Rarely, proarrhythmia—concentration curves (dot-dashed curves) can overlap with the therapeutic concentration curve and result in a $PSI < 1$. For most useful drugs the PC_1 exceeds the EC_{99} (dashed lines). λ -TRIaD disturbances (thick solid line) always precede TdP, while rarely VF can develop before overt λ -TRIaD disturbances are detected. This problem is acknowledged by the fact that some dashed lines slightly cross the base of the λ -TRIaD response curve. Note that proarrhythmia curves need not be parallel to the λ -TRIaD curve and may not even be monotonic (e.g., the proarrhythmic action may become attenuated by an additional superimposed antiarrhythmic action as illustrated by the right most curve)

(2) Proarrhythmia may only occur over a limited range (3) or may not even reach the 50% level (e.g., rightmost dashed curve in Fig. 36.4), making a 50% level immeasurable. (4) Peak proarrhythmic incidence may even be so low (e.g., terfenadine) that it may not be (reliably) detectable. However, even then the agents cannot hide their λ -TRIaD disturbances, i.e., remain readily detectable. Therefore, it is more prudent to determine the concentration where disturbances of λ -TRIaD (thick line in Fig. 36.4) become detectable (PC_1), relative to the concentration that is usually effective (EC_{99}):

$$PSI = PC_1/EC_{99}.$$

36.4.2 Overt Proarrhythmia (PSI < 10)

For small proarrhythmic safety index (PSI) values, the proarrhythmic and therapeutic curves can slightly overlap or leave little margin for error when metabolic or disease conditions vary. As a result, actual proarrhythmia becomes expected in a few patients. Such narrow safety margins are common for “antiarrhythmic” agents, and it is then not surprising that these can also become proarrhythmic [21, 23]. A low PSI does not necessarily render an agent useless, but normally there should then be medical evidence that expected benefits outweigh the risks.

36.4.3 Absence of Proarrhythmia (PSI > 100)

For 110 therapeutic agents in 394 blinded tests (unpublished observation), when the $PC_1/EC_{99} > 100$, no proarrhythmic agent could be found (and vice versa). This 100-fold safety margin is only an initial approximation (needing additional validation). Indeed, only a small fraction of pharmaceutical agents have been tested, so that the estimate may not be representative for agents at large. These experiments were mostly done under “screening” conditions, where the short exposure times may be too short to reach steady state; underestimation of the full drug effect could overestimate their safe level [25].

36.4.4 Gray Zone (10 < PSI < 100)

Agents in the gray zone varied from a few proarrhythmic incidences to undetectable. Such agents should therefore probably be avoided, especially where other safer agents are available. At least, they should be used only extra carefully (detailed follow-up) and limited to situations where evidence of benefit appear to exceed the potential risk.

In summary, the safety margin of 100 is at this time only a rough bearing, which must be evaluated with respect to the therapeutic application. For example, a low safety margin (expected to have some proarrhythmic liability) may be quite acceptable under life threatening conditions. At the other extreme, a safety margin only just 100 may be less than optimal for a minor potential therapeutic benefit and may become unacceptable where safer agents are already available.

36.5 Preclinical Detection of Disturbances of λ -TRIaD

Detection of proarrhythmia is a continuous endeavor, starting from the time a chemical is first synthesized and continuing long after the drug approval. The endeavor must be optimized for cost effectiveness while at the same time aspire to be fail-safe.

Cellular, tissue and organ tests done in screening mode usually cost only a few thousands of dollars. When done in larger series under GLP conditions, the costs may increase to tens of thousands of dollars. Whole animal studies can easily climb into the hundreds of thousands of dollars. Finally, clinical safety tests commonly run into (many) millions of dollars. Clearly, it is of paramount importance to weed out proarrhythmic agents as early as possible, and definitely before patients may have been harmed. Below I will briefly focus on some common preclinical tests, their optimal use and their potential short-comings.

36.5.1 Cellular

Voltage clamp to characterize interactions of drugs with specific channels can now be done very quickly and at relatively little cost. Therefore, such tests deserve to be done early on. At the very least it should include the main candidates for serious proarrhythmia: I_{Na} , I_{Ca} , I_{Kr} , I_{K1} and I_{Ks} . Interaction of drugs with ion channels are best studied under physiologically appropriate conditions: membrane potential, pulse patterns and temperature can markedly alter the resulting PC₁ for these channels. In addition, pathological conditions should be considered (e.g., long vs. short conditioning pulses, long and short cycle lengths, depolarization, etc.).

Lack of interaction with cardiac channels is clearly desirable (at least for agents not intended for cardiac applications). Conversely, detection of interaction with cardiac ionic channels definitely raises a warning flag, which requires more careful and detailed follow-up analysis. Nevertheless, this does not necessarily mean that all such agents should be rejected from further development as some may be important and safe therapeutic agents (not all hERG blockers are necessarily proarrhythmic).

The main disadvantage of intracellular voltage clamping is that breaking into the cell results in run down of the preparation, which shortens the useful time of study.

In addition, no matter how detailed and how many channels are evaluated, it must be remembered that their distribution, function, voltage- and time-dependent kinetics throughout the heart are highly variable. Therefore, it is never possible to estimate the full electrophysiological symphony that these interacting channels will create, i.e., study of tissues, organs and animals cannot be ruled out.

36.5.2 Isolated Cardiac Tissues

If a test item does not have any electrophysiological effects on any part of the cardiac action potentials at up to 100-fold the therapeutic concentration, then the chances that major surprises will appear in later tests become greatly reduced. Indeed, the two primary proarrhythmic offenders, block of sodium channels and hERG will, respectively, slow the upstroke (phase 0) and fast repolarization (phase 3) of the action potential (thick lines in Fig. 36.5a). This does not mean that diastole and plateau (dashed lines in Fig. 36.5a) are unimportant: a less negative or spontaneous depolarizing diastolic potential can yield a slower and smaller upstroke (Fig. 36.5b). Likewise, a less positive and sloping plateau will usually yield a slow repolarization (triangulation). Thus, as drugs make the upstroke/repolarization less steep and diastole/plateau less flat, their proarrhythmic liability is expected to increase.

The main shortcoming of isolated tissues can be that contact with superfusate may be inadequate, so that only the superficial tissue may be in adequate condition

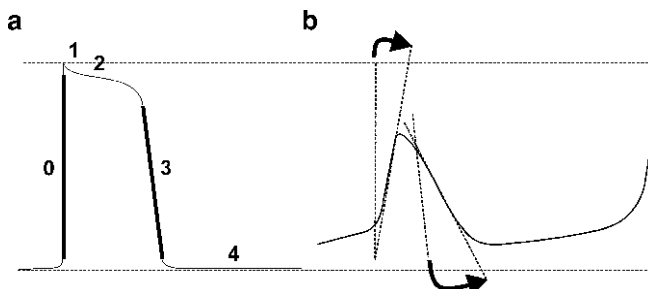


Fig. 36.5 Primary proarrhythmic changes of the action potential. A baseline action potential is shown in panel (a). The upstroke (thick line labeled phase 0) is primarily generated by inward sodium current, and fast repolarization (thick line labeled phase 3) by outward potassium current. Block of sodium channels and potassium channels can generate primary proarrhythmic liabilities which can be detected as a slowing of the upstroke [top arrow in panel (b)] and slowing of repolarization [bottom arrow in panel (b)]. This does not imply that the thin lines of the action potential in panel (a) are not important. Indeed, an upstroke starting from a less negative potential can have a greatly reduced upstroke (both in slope and amplitude), which reduces conduction velocity. Similarly, a repolarization following a less positive plateau is usually also slowed (triangulation) and less robust or stable (instability). As drugs render the upstroke and repolarization of the action potential less robust, their proarrhythmic liability usually sharply increases

and sufficiently equilibrated with the test item. This problem may be partly remedied in the “perfused” wedge slice. However, it is highly unlikely such perfusion will be uniform: at any coronary cut perfusate will leak away from the slice, while coronaries beyond a cut may not be (adequately) perfused. In addition, a transmural slice necessarily will damage numerous cells in the preparation. Nevertheless, this preparation has been highly useful for elucidation of drug effects upon various layers of the myocardium.

36.5.3 Perfusion Isolated Heart

The main advantage of the Langendorff perfused heart is that the coronary circulation is intact and when perfused with buffers enriched with pyruvate and creatine, stable electrophysiology and contraction can be maintained for many hours. At the same time, measurements can be obtained from most cardiac cells as well as from many cells simultaneously. Measurements can include intracellular recordings, monophasic action potentials, unipolar and bipolar extracellular recordings and cardiac electrocardiograms.

Unfortunately, perfused hearts require somewhat larger quantities of test substance which early in development is sometimes a problem. At the same time, absence of hormonal, sympathetic and metabolic influences can obscure drug effects.

36.5.4 Animal

Use of animals usually requires still larger amounts of chemical, but this is largely offset by the fact that now the perfusate is blood and the heart remains controlled by autonomic and hormonal influences. In addition, drug metabolism, pharmacokinetics and effects upon other organs can now be evaluated in acute and chronic administration. In addition to healthy animals, drug effects can also be evaluated in models of disease (e.g., heart failure, ischemia), some of which are known to greatly enhance the vulnerability to proarrhythmia.

Preclinical studies range widely in price and thus it is important to weed out agents with proarrhythmic liabilities as early as possible. It is not possible to give an absolutely optimal generalized flow chart for how this is best done, so that the above is only a general guideline which will need to be adapted to specific situations.

36.6 Conclusions

1. Change of QT duration is important: shortening is proarrhythmic, prolongation can be antiarrhythmic.
2. But, prolongation can become proarrhythmic when contaminated by disturbances of λ -TRIaD, where it will then preferentially result in TdP.

3. Relying on QT prolongation by itself is simplistic and can be wrong: it can generate false positives as well as false negatives.
4. Screening for disturbances of automaticity, conduction and repolarization (λ -TRIaD) must be comprehensive.
5. Any chemical has undesirable effects at some concentration, but as the PSI increases, concerns for proarrhythmia sharply decline.

Acknowledgments This work was supported by a grant from HPC. I wish to thank Drs. De Clerck, Duker and Dumotier for their helpful comments and suggestions during the preparation of the manuscript.

References

1. Lewis T, Drury AN. Revised views of refractory period in relation to drugs reputed to prolong it and in relation to circus movement. *Heart*. 1926;13:95–100.
2. Vaughan Williams EM. Classification of antiarrhythmic agents. In: Vaughan Williams EM, editor. *Antiarrhythmic drugs, Handbook of Experimental Pharmacology Series*, vol. 89. Berlin: Springer; 1989. p. 45–67.
3. Roden DM. Current status of class III antiarrhythmic drug therapy. *Am J Cardiol*. 1993;72:50B–2.
4. Lipicky RJ. A viewpoint on drugs that prolong the QTc interval. *Am J Cardiol*. 1993;72:53B–4.
5. Roden DM. Drug-induced prolongation of the QT interval. *N Engl J Med*. 2004;350:1013–22.
6. Shah RR, Hondeghem LM. Refining detection of drug-induced proarrhythmia: QT interval and TRIaD. *Heart Rhythm*. 2005;2:758–72.
7. Moe GK, Abildskov JA. Atrial fibrillation as a self-sustaining arrhythmia independent of focal discharge. *Am Heart J*. 1959;58:59–70.
8. Konings KT, Kirchhof CJ, Smeets JR, Wellens HJ, Penn OC, Allessie MA. High-density mapping of electrically induced atrial fibrillation in humans. *Circulation*. 1994;89:1665–80.
9. Hondeghem LM, Katzung BG. Time and voltage dependent interactions of antiarrhythmic drugs with cardiac sodium channels. *Biochim Biophys Acta*. 1977;472:373–98.
10. Qian YW, Qian YW, Sung RJ, Lin SF, Province R, Clusin WT. Spatial heterogeneity of action potential alternans during global ischemia in the rabbit heart. *Am J Physiol Heart Circ Physiol*. 2003;285:H2722–33.
11. Hondeghem L, Carlsson L, Duker G. Instability and triangulation of the action potential predict serious proarrhythmia, but APD prolongation is antiarrhythmic. *Circulation*. 2001;103:2004–13.
12. Antzelevitch C. Heterogeneity and cardiac arrhythmias: an overview. *Heart Rhythm*. 2007;4:967–72.
13. Dessertenne F. La tachycardie ventriculaire à deux foyers oppose variables. *Arch Mal Coeur*. 1966;59:263–72.
14. January CT, Chau V, Makielinski JC. Triggered activity in the heart: cellular mechanisms of early after-depolarizations. *Eur Heart J* 1991;12 Suppl F:4–9.
15. Kay GN, Plumb VJ, Arciniegas JG, Henthorn RW, Waldo AL. Torsade de pointes: the long-short initiating sequence and other clinical features: observations in 32 patients. *J Am Coll Cardiol*. 1983;2:806–17.
16. Hondeghem LM, Dumotier B, Traebert M. Oscillations of cardiac wave length and proarrhythmia. *Naunyn Schmiedebergs Archives of Pharmacology*. 2010;382:367–376

17. Dujardin KS, Dumotier B, David M, Guizy M, Valenzuela C, Hondeghem LM. Ultrafast sodium channel block by dietary fish oil prevents dofetilide-induced ventricular arrhythmias in rabbit hearts. *Am J Physiol Heart Circ Physiol.* 2008;295:1414–21.
18. Homma N, Tsujimoto G, Hashimoto K. Electrophysiologic effects of an antiarrhythmic agent, bidisomide, on sodium current in isolated rat ventricular myocytes: comparison with mexiletine and disopyramide. *Jpn J Pharmacol.* 2001;86:23–31.
19. Morganroth J. Comparative efficacy and safety of oral mexiletine and quinidine in benign or potentially lethal ventricular arrhythmias. *Am J Cardiol.* 1987;60:1276–81.
20. Hondeghem LM. Antiarrhythmic agents: modulated receptor applications. *Circulation.* 1987;75:514–20.
21. Echt DS, Liebson PR, Mitchell LB, Peters RW, Obias-Manno D, Barker AH, et al. Mortality and morbidity in patients receiving encainide, flecainide, or placebo. The Cardiac Arrhythmia Suppression Trial. *N Engl J Med.* 1991;324:781–8.
22. Hondeghem LM, Snyders DJ. Class III antiarrhythmic agents have a lot of potential but a long way to go: reduced effectiveness and dangers of reverse use-dependence. *Circulation.* 1990;81:686–90.
23. Waldo AL, Camm AJ, deRuyter H, Friedman PL, MacNeil DJ, Pauls JF, et al. Effect of d-sotalol on mortality in patients with left ventricular dysfunction after recent and remote myocardial infarction. The SWORD Investigators. *Survival with Oral d-Sotalol.* *Lancet.* 1996;348:7–12.
24. Swerdlow CD, Zhou X, Voroshilovsky O, Abeyratne A, Gillberg J. High amplitude T-wave alternans precedes spontaneous ventricular tachycardia or fibrillation in ICD electrograms. *Heart Rhythm.* 2008;5:670–6.
25. Hondeghem LM. QT prolongation is an unreliable predictor of ventricular arrhythmia. *Heart Rhythm.* 2008;5:1210–2.

Chapter 37

K Channel Openers as New Anti-arrhythmic Agents

Nathalie Strutz-Seebohm and Guiscard Seebohm

37.1 Introduction

Ion channels are membrane integral proteins that allow controlled passage of ions through cellular membranes. Cation-selective channels play key roles in physiological processes such as control of ion homeostasis and cell volume, vesicle trafficking, neurotransmitter and hormone secretion, and electrical control of excitable tissues. Many therapeutic drugs mediate their effects by targeting cation channel proteins. Potassium-selective channels are the most genetically and functionally diverse family of cation channels. After the cloning of the first potassium-selective ion channel, Shaker from *Drosophila*, several hundred potassium channel genes have been identified in the human genome. The number of functionally distinct channels in native tissues is further increased by heteromultimeric coassembly of potassium channel α -subunits with other α - and β -subunits and by posttranscriptional or post-translational modifications such as alternative splicing of mRNAs, glycosylation, sumoylation, and phosphorylation. In light of the broad range of physiological roles of K channels it is not surprising that channel impairment results in a variety of pathophysiological conditions.

The following text will give an overview of molecular details and availability of potassium channel modulators and try to address their potential as anti-arrhythmic drugs.

N. Strutz-Seebohm and G. Seebohm (✉)

Lehrstuhl für Biochemie I, Cation Channel Group, Ruhr University Bochum, Room NC6/132, Universitätstr. 150, 44780 Bochum, Germany
e-mail: guiscard.seebohm@rub.de

37.2 Acquired and Inherited Alterations of the ECG Morphology

Channels might lose or gain function as a result of mutations in the promoter or coding region of a gene. Much less understood are effects by genetic variations and chemical modifications (e.g., DNA methylation) in the noncoding region of ion channel loci. Further, alteration of channel function might be caused by regulatory derangements or by autoantibodies. The diseases based on altered K⁺ channel function are called channelopathies and include Bartter's syndrome type 2 (KCNJ1, Kir1.1 or RomK) [1], persistent hyperinsulinaemic hypoglycaemia of infancy (Kir 6.2 and SUR 1, [2, 3]), and episodic ataxia type 1 (KCNA1 or Kv1.1, [4]). Cardiac arrhythmia can result from structural alterations of the heart as a result of aging and/or viral infection (e.g., the picorna-virus Coxsackie virus B3). In these contexts age-related or cardiomyopathic dilatative responses lead to altered cardiac geometry, increase in fibroblasts, and altered gene expression and function of ion channels. The changes in cardiac geometry and increase in fibroblasts are very difficult to address pharmacologically, leaving ion channels as preferential targets for clinically relevant drug development.

Less common but still clinically relevant are genetics-based ion channel defects. The inherited long QT syndrome (iLQTS) is a disorder that can occur by mutations in the coding region of the cardiac Na⁺-channel (SCN5A, LQT 3) [5] or ankyrin-B (LQT4) [6]. However, in most cases of LQTS, the K channel α -subunits KCNQ1 (LQT1) and hERG (*human ether-a-go-go-related gene*, LQT2) or their β -subunits (KCNE1, 2; LQT5, LQT6) are affected. A second group of patients develops LQTS as response to clinically used drugs. This type of LQTS is called acquired LQTS (aLQTS) or drug-induced LQTS and is far more common than the inherited forms. Drugs associated with increased risk of aLQTS include anti-arrhythmics (dofetilide, ibutilide, procainamide, quinidine, sotalol, amiodarone, disopyramide), psychoactive drugs (chlorpromazine, droperidol, haloperidol, risperidone, levomethadyl, mesoridazine, methadone, pimozide, thioridazine), anti-malaria drugs (halofantrine, chloroquine), antibiotics (clarithromycin, erythromycin, sparfloxacin), and others. A more complete list of drugs with risk of prolonging the QT interval inducing *torsade-de-pointes* arrhythmias (QT drug list by Risk Groups) is available by the Arizona Center for Education and Research on Therapeutics at <http://www.cert.org/medical-pros/drug-lists/browse-drug-list.cfm>. Most of the listed drugs are highly potent hERG channel blockers. However, some are KCNQ1/KCNE1-blockers as well. The iLQTS-associated KCNQ1/KCNE1 and hERG/KCNE2 channel mutations cause a decrease in net ventricular repolarizing current I_K by reducing K currents through "loss of function" mechanisms, whereas the aLQTS is the result of I_K blockade. Thus, the reduced repolarizing I_K in both cases results in prolonged action potentials, reduced repolarization reserve, increased Ca²⁺ influx, increased likelihood of early after depolarizations, and prolongation of the QT interval in the electrocardiogram (ECG), predisposing affected individuals to syncope, seizures, aborted cardiac arrests, and sometimes sudden cardiac death. Treatment for iLQTS includes invasive

and cost-intensive therapies like high thoracic left sympathectomy and implantation of a cardioverter-defibrillator [7]. These invasive treatments are not favored by patients and are especially problematic in children. The primary drug therapy of LQTS is the blockade of β -adrenergic receptors which was shown to be beneficial in symptomatic LQTS patients [8, 9]. However, about 20–35% of LQTS patients presented as resistant to β -blocker therapy [10, 11]. These high-risk patients still have breakthrough cardiac events like aborted cardiac arrest, syncope, and sudden death even with ongoing β -blocker therapy. The failure rate of β -blocker therapy might be higher in patients carrying mutations in the potassium channel gene *hERG* than in the sodium channel gene *SCN5A*, as indicated by a patient study by Chatrath et al. [12]. In iLQTS the standard therapies have considerably reduced mortality. The aLQTS forces the discontinuation of drug treatment and prevents the use of certain drugs in predisposed patients. This can be highly problematic if the drug causing aLQTS is vital to the patient in a different clinical context. Thus, there is a well-recognized need for improved treatments of both iLQTS and aLQTS.

37.3 Pharmacological Inhibition of Cardiac Potassium Channels

Selective block of the ventricular repolarizing I_{Kr} or I_{Ks} channels could be beneficial under special conditions, and several companies developed selective blockers [13, 14]. Indeed, some of the most effective anti-arrhythmic drugs, amiodarone and its newly released (possibly less potent) analog dronedarone, have several ion channel targets including I_{Kr} channels. The block of I_{Kr} channels is regarded as a severe problem for pharmaceutical compounds intended for clinical use, and testing for I_{Kr} blockade has become an integral part of drug development and safety pharmacology. In the future, I_{Ks} blockade may be tested as well, since inhibition of I_{Ks} has recently been identified as another potential side effect of drugs.

hERG channels somehow act as “black hole-like super-absorber” for many drugs on the market: Many small hydrophobic drugs with aromatic rings inhibit I_{Kr} channels. For some time it remained elusive why so many drugs bind to and block the *hERG* channel as an unintended and unwanted side effect. Then, roughly a decade ago Mitcheson et al. [15] determined the putative binding site of the highly potent I_{Kr} inhibitors MK-499, cisapride and terfenadine. The main determinants of the “sticky” binding site for highly potent blockers are aromatic residues pointing toward the central cavity. These aromatic residues allow hydrophobic and/or pi-stacking interactions with lipophilic and aromatic constituents of the respective drug molecules [16]. Thus, the fact that many clinically relevant drugs contain aromatic ring systems and are lipophilic to favor membrane passage explains the high incidence of interactions of the drugs with the I_{Kr} channels. A more detailed overview of the molecular nature of *hERG*-inhibitor interactions is given in Chap. 34.

Currently, especially the pharmaceutic industry is trying to develop in silico tools for the prediction of potential I_{Kr} inhibitors by combining pharmacophore modeling of I_{Kr} inhibitors with structural constraints for the I_{Kr} channel pore derived from homology to the known potassium channel structures [17] with the goal to generate in silico tools for the prediction of potential I_{Kr} inhibitors. In any case, for acute aLQTS, a drug counteracting the I_{Kr} block would be highly desirable.

37.4 Impaired Channel Function Can Cause Cardiac Arrhythmia

Cardiac arrhythmia results from altered electrical substrate. These alterations include the heterogeneity of functional tissue as a result of ischemia/infarction or the substitution of injured cardiomyocytes by fibroblasts as age- or infection-associated event. Further, the breakdown of ion channel functional gradients (e.g., the transient outward current, I_{to}), impaired cell–cell contacts with altered Connexin 43 function, or dysbalances of ion fluxes within cardiomyocytes may lead to changes in the electrical properties of cardiac tissue which facilitate the generation of ectopic foci and subsequent potentially lethal cardiac arrhythmias. Key in understanding arrhythmias is the concerted function of ion channels in the myocyte. Arrhythmia can be regarded as primary (altered function of ion channel protein by mutation) or secondary (altered functions of ion channels as a secondary event) channelopathy.

Channelopathies are mainly caused by impaired channel function resulting in disrupted balance of ion fluxes in the affected tissue. In cardiac tissue the concerted action of cation channels generates the typical action potential and the tightly controlled calcium influx necessary for a regular heart rhythm. Loss- as well as gain-of-function mutations in cardiac K channels cause a dissonance in the ion channel concert leading to altered action potential shape and changed timing and amplitude of ion fluxes, often resulting in cardiac arrhythmias. For example, loss of function in delayed rectifier potassium channels causes the aforementioned lengthened ventricular action potential with prolonged QT interval and *torsade de pointes* arrhythmia. Therefore, an attractive approach of treating channelopathies is the activation of the impaired ion channels to restore their function and thus the balance of ion fluxes.

37.5 Activation of Potassium Channels

To activate ion channels, several different parameters in their mechanism of action can be targeted. The ionic current I conducted by a homogeneous population of ion channels is defined by three main parameters expressed in the equation:

$$I = i \times P_{\text{o}} \times N_{\text{f}}.$$

i is the unitary current through a single open channel, P_o the open probability, and N_f the number of functional channels. P_o can be influenced by gating modifiers, which alter activation, deactivation, or voltage dependence of the channel. N_f is defined by the total number of channels in the membrane and their ability to open. Channel trafficking is another target mechanism for the development of activators. Recent studies raised the possibility that pharmacological compounds facilitating I_{Kr} channel exocytosis and thus increasing the number of functional ion channels in the membrane may become available in the future. Determining a compound's mechanism of action can be difficult and usually requires detailed single-channel analysis combined with whole cell current recording and analysis of surface expression. Further complicating the characterization of candidate compounds is the fact that some are not pure agonists, activating the channel under all conditions, but partial agonists, which can act as either agonists or antagonists in a state- or concentration-dependent manner.

To test the potential clinical benefit of K channel activation in treatment of cardiac arrhythmias, specific agonists are needed. Yet, only a few K channel agonists are available to date, and some of them are either nonspecific or have a low potency [18]. In general, K channel agonists are relatively small, hydrophobic compounds with numerous aromatic ring/aryl groups (Fig. 37.1). Examples of such compounds are:

- A variety of K_{ATP} channel agonists (BMS-180448, cromakalim, celikalim, diazoxide, JTV-506, KR-30450, lemakalim, levosimendan, minoxidil sulfate, nicorandil, P1075, pinacidil, rilmakalim, SKP-450, WAY-133537, Y 26763, ZD6169, ZM-244085)
- Nine examples of Ca^{2+} -activated K^+ channel (BK and SK) activators (BMS-204352, chlorzoxazone, zoxazolamine, DHS-I, 1-EBIO/DC-EBIO, maxiKdiol, NS304/analogs, BRL-55834, NS11021)
- More than 11 KCNQ activator classes (BMS-204352/MaxiPost, retigabine, meclofenamic acid and other fenamates, R-L3, stilbenes, ICA-27243, benzo(d) isoxazole, salicylate analogs, 3-aminoquinazolin-one, 2-acrylthiazol)
- Several I_{Kr} agonists (RPR260243, RD-307243, A-935142, NS1643, PD118057 and NS3623)
- The KCNK agonist riluzol
- The GIRK1.4 channel agonist flupirtine
- The Kv4.3 channel agonist NS5806

Some K channel agonists are already clinically used or have the potential to serve as potent drugs in the treatment of various channel-related diseases. The KCNQ channel (M channel) agonists retigabine, R-L3 and BMS-204352, may be useful for treatment of hypertension, cardiac arrhythmia, epilepsy, and incontinence, while BK channel activators might be used to treat hypertension, stroke, and overactive bladder disorder [19]. The KCNK channel activator riluzole has anti-seizure effects in the treatment of epilepsy [20] and may be useful as an anti-arrhythmic agent as well. Furthermore, specific channel agonists might be of use in treating several other disorders caused by ion channel dysfunctions, e.g., migraine,

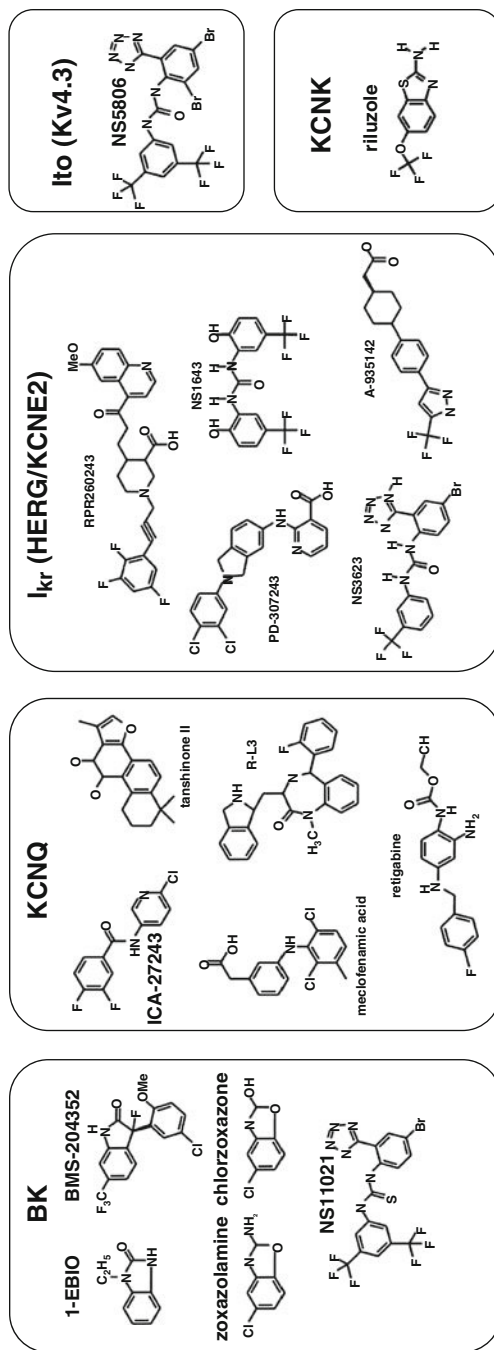


Fig. 37.1 Structure of potassium channel agonists

episodic ataxia, autosomal dominant deafness, hypokalemic periodic paralysis, and erectile dysfunction [21, 22]. Thus, although relatively rare in use presently, K channel agonists have a high potential for the treatment of various diseases including cardiac arrhythmia.

37.6 In Vitro and In Vivo Effects of Potassium Channel Activators

In 1998 the first highly potent selective KCNQ1/KCNE1 (I_{K_s}) activator R-L3 was published [23]. R-L3 acts as a gating modifier by mildly slowing channel activation but dramatically decreasing the rate of channel deactivation. In addition, it increases macroscopic current amplitudes by a mechanism independent of its effects on kinetics [24]. R-L3 shortens action potential duration, and suppresses early afterdepolarizations in ventricular myocytes isolated from hypertrophied rabbit hearts. In addition, R-L3 reverses action potential lengthening and thereby suppresses early afterdepolarizations in myocytes treated with the I_{K_r} blocker dofetilide [25] (Fig. 37.2). Since the I_{K_r} inhibition by dofetilide mimicks LQTS, these experiments suggest that R-L3 may be beneficial in iLQTS and aLQTS. In 2004 Kang et al. [26] provided the first characterization of an I_{K_r} channel activator, RPR260243. This compound markedly slows I_{K_r} channel deactivation, thereby enhancing net I_{K_r} currents. RPR260243 increases the energy barrier for open state to closed state transitions.

The two compounds NS1643 and NS3623 increase current by strongly affecting inactivation and in case of NS1643 by mildly affecting activation properties of hERG1 channels [27, 28]. However, both compounds shift the inactivation curve

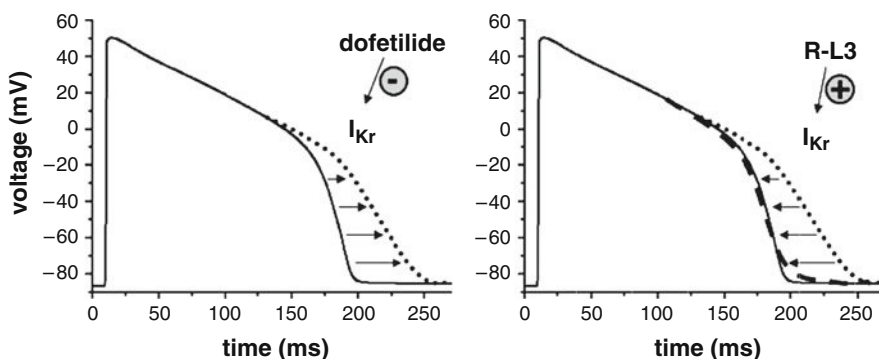


Fig. 37.2 Dofetilide inhibition of I_{K_r} channels induces action potential lengthening, which can be reversed by activation of I_{K_s} by R-L3

to the right. The naturally occurring hERG1 channel agonist mallotoxin activates hERG1 channels by a left-ward shift of the activation curve and slowing of deactivation [29]. The compound PD-307243 showed hERG1 channel agonism by slowing of both, deactivation and inactivation [30]. The manifold modulation of basic kinetic parameters identifies these compound as a gating modifiers similar to R-L3.

Recordings from acutely isolated guinea pig myocytes clearly demonstrated action potential shortening after application of NS3623 and to a lesser extend RPR260243 shortened the action potential in acutely isolated guinea pig myocytes, proving that increased I_{Kr} increases the cardiac repolarization capacity [31, 32]. Action potentials preprolonged by application of dofetilide could be shortened by both compounds [32, 33]. Effects in ex vivo preparations could be shown: RPR260243 functionally counteracts blockade by dofetilide in retrograde perfused hearts (Langendorff heart model). NS3623 shortened action potentials in papillary muscle from guinea pigs and NS3623 exerted anti-arrhythmic properties when tested in intact guinea pig hearts [32, 34]. PD-118057 has been tested in wedge preparations from rabbit. There it shortened action potential length, reduced dispersion and showed anti-arrhythmic effects [35, 36].

In vivo effect of potassium channel activators was reported: NS1643 has demonstrated anti-arrhythmic properties in rabbit models favoring *Torsades de Pointes* arrhythmias [37]. NS1643 significantly reduced the amount of ectopic activity and *torsades de pointes* [32]. Drug-induced QT prolongation was reverted by application of NS3623 in guinea pigs [37]. These results point to in vivo anti-arrhythmic properties of hERG1 channel activation under certain settings. These experiments suggest that activation of cardiac I_{Kr} and/or I_{Ks} may shorten QT interval in iLQTS and aLQTS in in vitro and in vivo situation.

The I_{to} agonist NS5806 [27] recapitulated the electrocardiographic and proarrhythmic manifestations of Brugada syndrome in isolated canine ventricular myocytes. In canine ventricular wedge preparations, NS5806 increased epicardial phase 1 and notch amplitude of the action potential and led to the development of phase 2 reentry and polymorphic ventricular tachycardia. These data suggest that I_{to} activation is not suited for the development of an anti-arrhythmic agent. Rather, these data might strengthen the arguments for a pharmacological I_{to} inhibition as an anti-arrhythmic approach. Indeed, pharmaceutical companies aim to identify and test compounds like amiodarone/dronedarone analogs which include I_{to} inhibition as one of their effects.

R-L3 has the potential to activate most of the LQT1-associated mutant channels. However, one mutation disrupted the activating effect probably by disrupting the R-L3 binding site [24]. These data provided proof of principle of the concept that the combined knowledge of an inherited gene variant in an ion channel gene and the binding site of a drug in the respective channel could be used to predict a possible drug resistance by mutational disruption of the molecular binding site in the ion channel protein. The specific activation of cardiac potassium channels may therefore represent a novel anti-arrhythmic principle [37].

37.7 The Structural Basis of Channel Activation

The pharmaceutical industry searches for ion channel modulators using high throughput screening methods and huge compound libraries. Robust assays can easily screen 10,000–100,000 compounds per day on a single target. However, only a limited set of K channel activator lead scaffolds have been reported so far. Why was it so difficult to discover activators in the past? A glimpse of an idea arises when studying data on interactions of K channel agonists with their specific binding site(s) on the respective channel. The variety of K_{ATP} -channel activators might arise from the fact that all of them bind to one of the two binding sites in the sulfonylurea subunit of the channel and that this subunit provides a relatively easily accessible drug target. Thus, these compounds do not bind to the pore-forming subunit of Kir6.1 and Kir6.2. Some BK channel agonists bind to calmodulin in the BK channel protein complex to increase the Ca^{2+} sensitivity of the channels. Thus, these agonists do not bind to the channel-forming subunit either. However, as calmodulin is an integral part in several multiprotein complexes, drugs acting like the BK agonists could be expected to exert pharmacological side effects when systemically administered. Therefore, compounds binding to the channel-forming subunit promise greater selectivity. (S)-(-)Bay K 8644 is believed to interact with the S5–S6 pore module and probably with the III/IV interface of L-type Ca^{2+} channels [28, 29]. However, the experimental data are still vague and further experimental data like from a systematic alanine scan to identify the (S)-(-)Bay K 8644 binding site would be helpful.

The identification of the binding site of an agonist for a cardiac voltage-dependent potassium channel with relatively high resolution was a pioneering step into understanding agonist-pore interactions. Alanine-scanning methods combined with 3D-modeling techniques were used to determine the putative binding site of the benzodiazepine R-L3 that activates KCNQ1 channels [24]. The binding site is located deep in the K channel protein among the pore helix, S5, S6, and possibly S4 segments. Theoretically, this position and the small size of the binding pocket might allow only closely related chemicals to enter and bind to this position. This may be a desired prerequisite for the generation of selective drug candidates. If substances have to bind to binding sites deep inside channel proteins, as suggested for BAY K 8644 and R-L3, then even minor structural changes in the agonist scaffold could disrupt correct binding and the chemical optimization process might be challenging. However, chemical optimization should generate sufficient selectivity toward closely related ion channel proteins. In line with this idea, retigabine, a first-generation drug candidate as an anti-epileptic, does not target cardiac I_{Ks} channels (KCNQ1) but their closely related neuronal homologues (KCNQ2–5) [30–35]. On the other hand R-L3 activates the cardiac I_{Ks} channels (KCNQ1) but not the neuronal KCNQ2 and KCNQ3 channels [23]. Recently, the putative binding site of retigabine could be localized to the lower S5–S6 region below the pore helix and adjacent to the neighboring channel subunit [30, 33, 35], demonstrating that there are two binding sites for KCNQ channel agonists (Fig. 37.3). These putative

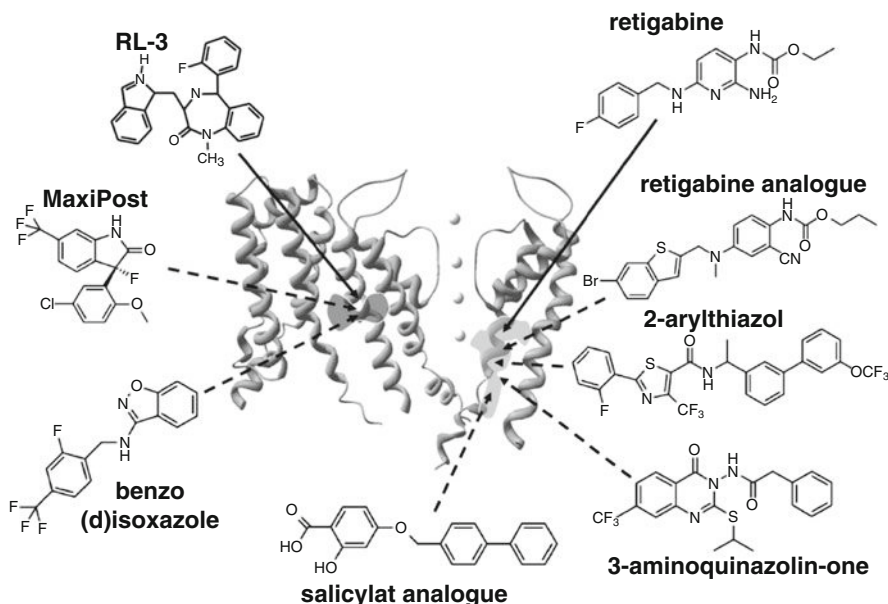


Fig. 37.3 Structure and putative discrete binding sites of two classes of KCNQ channel agonists. The binding sites of R-L3 and retigabine have been shown experimentally

binding sites suggest very strict molecular requirements for the compounds to be ligands for the specific agonist binding pocket. These molecular constraints determine size (volume), geometry, and chemical nature (hydrophobicity, aromaticity) of the compound. Meanwhile, several additional KCNQ channel agonists have been reported. Based on the knowledge on R-L3 and retigabine binding sites, the binding sites of these new compounds can be predicted. The size and chemical nature of the agonists suggest a scheme, in which MaxiPost and benzo(d)isoxazole may bind to the R-L3 site and retigabine analogs, 2-aryltiazole, and 3-aminoquinazoline-one may target the retigabine binding site (Fig. 37.3). However, these predictions have not yet been experimentally tested.

37.8 The Quest for Potassium Channel Activators

Often agonists are found by accident when screening for compounds intended for other targets. Possibly there is a technical problem unaddressed by modern screening techniques: Pharmaceutical companies screen for lead structures. Then they modify these leads to explore the structure in detail to find the molecule with the best combination of EC₅₀, bioavailability, selectivity, and drug stability. This concept works well for binding sites on the surface or in relatively large cavities. An example is the search for small molecule K channel blockers, for which the

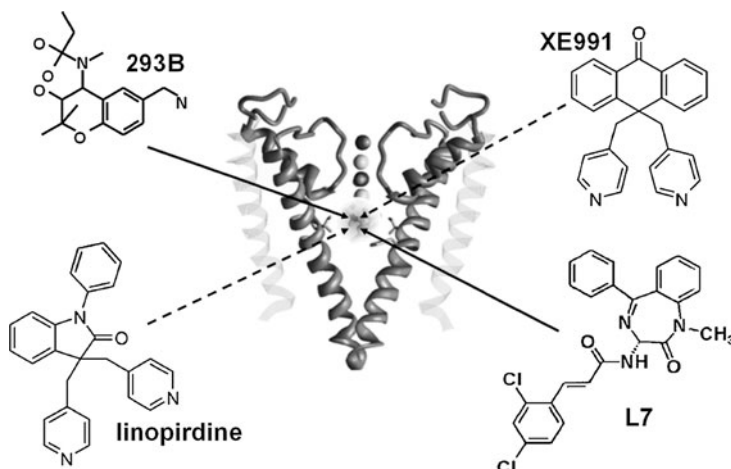


Fig. 37.4 Structure and putative binding site in the central cavity of I_{Ks} (KCNQ1/KCNE1) channel inhibitors. The binding sites of 293B and L7 have been shown experimentally

preferential binding site is the large central cavity of K channels (Fig. 37.4). Thus, in the conventional screen, lead structures and analogs binding to surface-accessible binding sites are preferentially identified. Therefore, it is not surprising that agonists are often found randomly when working with compounds intended for distinct targets but not by systematic screens for channel activators. For example, an I_{Ks} antagonist with a lead benzodiazepine scaffold was found to lengthen the QT interval by MSD. Testing this compound discovered that it was a potent I_{Ks} blocker. Screens for further I_{Ks} antagonists with the benzodiazepine scaffold were performed. By accident the I_{Ks} agonist R-L3 was identified. The classical screening methods of the last years used to identify channel blockers are possibly not well suited for the identification of activators. Most commonly voltage-dependent fluorescence in cell-based assays is used to identify channel blockers. These assays might identify blockers of K^+ permeation relatively well. However, it is questionable whether they are sensitive enough to identify the effects of agonists. Thus, the classical fluorescence-based screening methods might not be very effective for the discovery of activators. Alternative screening methods such as automated patch clamp or automated two electrode voltage clamp (TEVC) helped to overcome the insensitivity of fluorescence-based screens. These electrophysiological methods used to be relatively slow [36], but very recent technical advances in automated patch clamp in 386-well format increased the throughput considerably. The analysis of functional data and 3D-modeling of channel activator interactions could allow us to use computer-aided approaches to design putative K channel agonists. Such in silico approaches could be combined with the electrophysiological screening methods to aid the identification and development of K channel agonists.

37.9 Conclusions

Activators of K channels are promising candidates to restore channel function in acquired or inherited cardiac channelopathies. However, a shortage in K channel activators prevents testing the efficacy and/or safety of this approach. This shortage might have resulted from the relative incapability of drug screening methods in the past but may be overcome by current direct electrophysiological ion channel screening. An increased knowledge about K channel activator binding and mechanisms of action might enable in silico-guided drug design of K channel agonists. New potent K channel activators will enable us to test the concept of ion channel activation as a clinically relevant principle in the treatment of cardiac arrhythmias.

References

1. Derst C, Konrad M, Kockerling A, Karolyi L, Deschenes G, Daut J, et al. Mutations in the ROMK gene in antenatal Bartter syndrome are associated with impaired K⁺ channel function. *Biochem Biophys Res Commun.* 1997;230:641–5.
2. Nestorowicz A, Wilson BA, Schoor KP, Inoue H, Glaser B, Landau H, et al. Mutations in the sulfonylurea receptor gene are associated with familial hyperinsulinism in Ashkenazi Jews. *Hum Mol Genet.* 1996;5:1813–22.
3. Thomas PM, Cote GJ, Wohllk N, Haddad B, Mathew PM, Rabl W, et al. Mutations in the sulfonylurea receptor gene in familial persistent hyperinsulinemic hypoglycemia of infancy. *Science.* 1995;268:426–9.
4. Adelman JP, Bond CT, Pessia M, Maylie J. Episodic ataxia results from voltage-dependent potassium channels with altered functions. *Neuron.* 1995;15:1449–54.
5. Wang Q, Shen J, Splawski I, Atkinson D, Li Z, Robinson JL, et al. SCN5A mutations associated with an inherited cardiac arrhythmia, long QT syndrome. *Cell.* 1995;80:805–11.
6. Mohler PJ, Schott JJ, Gramolini AO, Dilly KW, Guatimosim S, duBell WH, et al. Ankyrin-B mutation causes type 4 long-QT cardiac arrhythmia and sudden cardiac death. *Nature.* 2003;421:634–9.
7. Schwartz PJ, Priori SG, Dumaine R, Napolitano C, Antzelevitch C, Stramba-Badiale M, et al. A molecular link between the sudden infant death syndrome and the long-QT syndrome. *N Engl J Med.* 2000;343:262–7.
8. Schwartz PJ, Periti M, Malliani A. The long Q-T syndrome. *Am Heart J.* 1975;89:378–90.
9. Ward OC. A new cardiac syndrome in children. *J Irish Med Assoc.* 1964;54:103–6.
10. Ackerman MJ. The long QT syndrome: ion channel diseases of the heart. *Mayo Clin Proc.* 1998;73:250–69.
11. Moss AJ, Zareba W, Hall WJ, Schwartz PJ, Crampton RS, Benhorin J, et al. Effectiveness and limitations of beta-blocker therapy in congenital long-QT syndrome. *Circulation.* 2000;101:616–23.
12. Chatrath R, Bell CM, Ackerman MJ. Beta-blocker therapy failures in symptomatic probands with genotyped long-QT syndrome. *Pediatr Cardiol.* 2004;25:459–65.
13. Gerlach U. Blockers of the slowly delayed rectifier potassium IKs channel: potential antiarrhythmic agents. *Curr Med Chem Cardiovasc Hematol Agents.* 2003;1:243–52.
14. Lee K, Park JY, Ryu PD, Kwon LS, Kim HY. IKr channel blockers: novel antiarrhythmic agents. *Curr Med Chem Cardiovasc Hematol Agents.* 2003;1:203–23.
15. Mitcheson JS, Chen J, Lin M, Culberson C, Sanguinetti MC. A structural basis for drug-induced long QT syndrome. *Proc Natl Acad Sci USA.* 2000;97:12329–33.

16. Chen J, Seeböhm G, Sanguinetti MC. Position of aromatic residues in the S6 domain, not inactivation, dictates cisapride sensitivity of HERG and eag potassium channels. *Proc Natl Acad Sci USA.* 2002;99:12461–6.
17. Bains W, Basman A, White C. HERG binding specificity and binding site structure: evidence from a fragment-based evolutionary computing SAR study. *Prog Biophys Mol Biol.* 2004;86:205–33.
18. Seeböhm G. Activators of cation channels: potential in treatment of channelopathies. *Mol Pharmacol.* 2005;67(3):585–8.
19. Malysz J, Buckner SA, Daza AV, Milicic I, Perez-Medrano A, Gopalakrishnan M. Functional characterization of large conductance calcium-activated K⁺ channel openers in bladder and vascular smooth muscle. *Naunyn Schmiedebergs Arch Pharmacol.* 2004;369:481–9.
20. Borowicz KK, Rwiader M, Drelewski E, Czuczwar SJ. Interactions between riluzole and conventional antiepileptic drugs – a comparison of results obtained in the subthreshold method and isobolographic analysis. *J Neural Transm.* 2004;111:1511–22.
21. Cooper EC, Jan LY. Ion channel genes and human neurological disease: recent progress, prospects, and challenges. *Proc Natl Acad Sci USA.* 1999;96:4759–66.
22. Lawson K, Dunne MJ. Peripheral channelopathies as targets for potassium channel openers. *Expert Opin Invest Drugs.* 2001;10:1345–59.
23. Salata JJ, Jurkiewicz NK, Wang J, Evans BE, Orme HT, Sanguinetti MC. A novel benzodiazepine that activates cardiac slow delayed rectifier K⁺ currents. *Mol Pharmacol.* 1998;54:220–30.
24. Seeböhm G, Pusch M, Chen J, Sanguinetti MC. Pharmacological activation of normal and arrhythmia-associated mutant KCNQ1 potassium channels. *Circ Res.* 2003;93:941–7.
25. Xu X, Salata JJ, Wang J, Wu Y, Yan GX, Liu T, et al. Increasing I(Ks) corrects abnormal repolarization in rabbit models of acquired LQT2 and ventricular hypertrophy. *Am J Physiol Heart Circ Physiol.* 2002;283:H664–70.
26. Kang J, Chen XL, Wang H, Ji J, Cheng H, Incardona J, et al. Discovery of a small molecule activator of the human ether-a-go-go-related gene (HERG) cardiac K⁺ channel. *Mol Pharmacol.* 2004;67(3):827–36.
27. Calloe K, Soltyssinska E, Jespersen T, Lundby A, Antzelevitch C, Olesen SP, et al. Differential effects of the transient outward K(+) current activator NS5806 in the canine left ventricle. *J Mol Cell Cardiol.* 2010;48(1):191–200.
28. Yamaguchi S, Zhorov BS, Yoshioka K, Nagao T, Ichijo H, Adachi-Akahane S. Key roles of Phe1112 and Ser1115 in the pore-forming IIIS5-S6 linker of L-type Ca²⁺ channel alpha1C subunit (CaV 1.2) in binding of dihydropyridines and action of Ca²⁺ channel agonists. *Mol Pharmacol.* 2003;64:235–48.
29. Zhorov BS, Folkman EV, Ananthanarayanan VS. Homology model of dihydropyridine receptor: implications for L-type Ca(2+) channel modulation by agonists and antagonists. *Arch Biochem Biophys.* 2001;393:22–41.
30. Lange W, Geissendorfer J, Schenzer A, Grötzingher J, Seeböhm G, Friedrich T, et al. Refinement of the binding site and mode of action of the anticonvulsant Retigabine on KCNQ K⁺ channels. *Mol Pharmacol.* 2008;75(2):272–80.
31. Main MJ, Cryan JE, Dupere JR, Cox B, Clare JJ, Burbidge SA. Modulation of KCNQ2/3 potassium channels by the novel anticonvulsant retigabine. *Mol Pharmacol.* 2000;58:253–62.
32. Rundfeldt C, Netzer R. The novel anticonvulsant retigabine activates M-currents in Chinese hamster ovary-cells transfected with human KCNQ2/3 subunits. *Neurosci Lett.* 2000;282:73–6.
33. Schenzer A, Friedrich T, Pusch M, Saftig P, Jentsch TJ, Grötzingher J, et al. Molecular determinants of KCNQ (Kv7) K⁺ channel sensitivity to the anticonvulsant retigabine. *J Neurosci.* 2005;25(20):5051–60.
34. Wickenden AD, Yu W, Zou A, Jegla T, Waggoner PK. Retigabine, a novel anti-convulsant, enhances activation of KCNQ2/Q3 potassium channels. *Mol Pharmacol.* 2000;58:591–600.

35. Wuttke TV, Seebohm G, Bail S, Maljevic S, Lerche H. The new anticonvulsant retigabine favors voltage-dependent opening of the Kv7.2 (KCNQ2) channel by binding to its activation gate. *Mol Pharmacol.* 2005;67(4):1009–17.
36. Xu J, Wang X, Ensign B, Li M, Wu L, Guia A, et al. Ion-channel assay technologies: quo vadis? *Drug Discov Today.* 2001;6:1278–87.
37. Grunnet M. Repolarization of the cardiac action potential. Does an increase in repolarization capacity constitute a new anti-arrhythmic principle? *Acta Physiol (Oxf).* 2010;198:1–48.

Index

A

AAP10, 507, 512, 513, 517–519
Acetylcholine (ACh), 15, 16, 73, 95, 101, 127, 128, 165, 203, 220, 226, 431, 533, 599, 604, 605
Acidosis, 18, 358, 507, 512, 513, 517, 519, 547, 548, 552–554, 568, 570, 642
Aconitine, 512
Actin, 463
Action potential (AP), 3, 5–8, 10, 12, 14, 18, 22, 474–477
AN cells, 215, 226
clamp technique, 434, 437, 442
diastolic depolarisation, 5, 16, 215
model, 435–437
morphology, 439
N cells, 215
NH cells, 215, 226
optical AP, 217
pacemaker potential, 5, 10, 33, 215
plateau, 5, 9, 12, 147, 161, 178, 274, 389, 392, 400, 416, 432, 434, 435, 455, 475, 546, 600, 616, 641
prolongation, 409
propagation, 440
Purkinje fibres, 211, 215–219, 221, 222, 224–227
repolarisation, see Repolarization
resting potential, 5, 6, 11, 14, 18, 109, 176, 226, 569, 611
shape, 271, 276
shortening, 435–437, 439
space–time plot, 440
upstroke velocity, 177, 181, 222, 226, 227, 511, 526
ventricular, 211, 215, 216, 219, 221, 222, 224–226
waveforms, 176–178, 180, 434, 442

Action potential-clamp, 105–107
Activation curve, 38, 53, 60–63, 65–67, 74
Adrenergic
cascade, 50, 51
signaling, 50, 51
stimulation, 48, 50–55, 57
 β -adrenergic receptor (β -AR), 94–95
 β -adrenergic stimulation, 260–262, 339, 340, 342, 355, 357, 358
 α_2 adrenoceptor, 126, 128
 β adrenoceptor, 126
Afterdepolarization, 358
Agonist
binding site, 663
effects, 659
examples, 659
Akap10, 128
A-kinase anchoring proteins (AKAPs), 353
Aldosterone, 479
Alinidine, 69
Andersen syndrome, 14, 15
Angina, 70, 129, 339
Angiotensin-II, 508, 515
Anisotropy, 510–511, 514
AnkB, 128
ANK2 variant, 127
Ankyrin-B syndrome, 461–468
Ankyrin-G, 461, 462, 467–468
Ankyrin-R, 461
Ankyrins, 461–469
Antiarrhythmic, 8, 20, 22, 71, 144, 299, 319, 416, 512, 517, 533–535, 555, 602–606, 616, 617, 639, 641–649, 652
APD, 180–182
APD, QT and ERP
prolongation, 639–653
shortening, 641, 644, 647, 648, 652

- Apoptosis, 368, 369, 375, 376
 Aquaporins, 581–589
 Arrhythmia, 9–12, 18, 61, 125–127, 139–146, 176, 183–185, 224, 245–247, 263, 270, 294–296, 307–319, 324, 325, 339–341, 344, 345, 356–359, 369–373, 388–403, 431–435, 451–456, 463–468, 477–481, 485–496, 511, 526–537, 544–556, 569–575, 601, 616, 646, 658–661
 DAD, 18, 19, 181, 294–295, 309, 390–394, 549–556, 570, 601–605
 EAD, 18, 181–186, 287, 294, 549, 552, 556, 600–602, 642
 reentry, See Reentry
 Arrhythmogenesis, 9, 18, 21, 141, 181, 246, 288, 368, 438, 503–519, 527–529, 532, 533, 546, 548, 605
 mechanisms, 432, 434, 438–439, 443
 treatment, 432, 434
 Arrhythmogenesis predilection sites, 245
 arrhythmia substrates, 246
 atrial arrhythmias, 245
 embryonic AVC, 240, 242, 247
 genetic labeling, 246
 internodal tracts, 247
 pulmonary vein myocardium, 245, 246
 ATP, 504, 507, 513, 518
 ATP-dependent potassium channel (K_{ATP}), 15, 21, 143, 146, 166, 203, 294, 328, 439, 526, 599, 659, 663
 AT1-receptor, 515
 Atrial fibrillation (AF), 11–16, 19–21, 183, 241–246, 358, 421, 432, 434, 456, 464, 467, 468, 485–496, 504, 514–515, 599–606
 familial (FAF), 451, 456
 Atrioventricular (AV) junction
 atrial myocardium, 213, 215
 branching AV bundle, 214
 bundle development, 242–243
 central fibrous body (CFB), 213–215
 compact atrioventricular (AV) node, 211, 213–216, 218–220, 226, 227
 conduction axis, 212, 214–216, 218–221, 226, 227
 coronary sinus (CS), 213, 214, 217
 crista terminalis, 217
 Eustachian valve, 213
 fossa ovalis, 217
 inferior nodal extensions (INE), 211, 213–215, 218–220, 226, 227
 inferior vena cava, 217
 node, 233
 penetrating (AV)/ His bundle, 213–215, 226, 227
 tendon of Todaro, 213, 217
 Thebesian valves, 213
 transitional cells/zone, 211, 213–215, 226, 227
 triangle of Koch, 211–213
 tricuspid valve, 212, 213, 217
 ventricular myocardium, 211
 Automated planar patch clamp (APC), 630–631
 Automaticity, 231, 232, 234, 246, 368, 370
 Autoregulation, 257–258
 AVC myocardium, 231, 236, 240, 247
 AVN development, 241
 AV nodal re-entrant tachycardia (AVNRT)
 dual pathway, 215–216
 fast-slow, 217
 slow-fast, 216, 217
 slow-slow, 217
 AV node, 155, 156, 169, 233
- B**
- Bainbridge response, 134
 B56 alpha, 463
 $\beta_2\alpha$ subunit, 353
 Binding assays, 631, 632
 Bio-pacemaker, 109, 111
Bmp2, 240, 241
 Border zone, 283, 287, 296, 313, 315–317, 514, 527
 Bradycardia, 68, 72–73
 Bradykinin, 528
 Brugada syndrome (BrS), 8, 14, 183, 387, 388, 401–403, 467–468
 Bundle of His, 242–243
- C**
- Ca ATPase, 255, 260
 Cable theory, 508, 509
 Ca^{2+} /calmodulin, 351, 352, 358, 359
 Ca-calmodulin dependent protein kinase II, 260, 261
 Ca channels, 8–10
 activators, CCA, 9–10
 blockers, CCB, 9–10
 L-type, 9
 R-type, 10, 21
 T-type, 10
 Ca^{2+} clock, 83, 93
 CACNA1C, 9, 400–403, 432, 437, 444, 481, 616

- Ca^{2+} handling proteins, 337, 338, 345
 NCX1, 220–221
 RYR2, 220, 221
 SERCA2A, 220
- Calcineurin, 357
- Calcium, 313–315, 319, 387–403
 dynamics, 160, 164, 186–187
 NCX, 159–161, 164
- Calmodulin kinase II (CAMKII), 92–96,
 351–359
- cAMP, 60–63, 65, 72, 74, 84, 92,
 95, 188
- Carbenoxolone, 530, 533
- Cardiac action potential, 158, 176–189, 355,
 358, 455, 599, 620, 641, 651
- Cardiac conduction system, 474
 AV node, 211, 215, 221, 225
 branching AV bundle, 214
 development, 244–245
 left bundle branch, 215, 221
 penetrating (AV)/ His bundle, 211,
 213–215, 226, 227
 Purkinje fibres, 211, 215, 221, 225
 right bundle branch, 222
 sinus/sinoatrial (SA) node, 215
- Cardiac cycle, 3, 4, 19, 22
- Cardiac glycosides, 260, 262, 432
- Cardiac hypertrophy, See Hypertrophy
- Cardiac ion channel, 3–21, 175–183, 285,
 462, 463, 481, 628–636
- Cardiac T-tubules, 256–257
- Cardiac wave length, 639–641
- Cardiomyocyte differentiation, 245
- Cardiomyocytes, 323–326, 328–331
- Cardiomyopathy, 12, 15, 19, 20
 hypertrophic obstructive (HOCM), 516
 PKC α , 504, 517
- Ca release channels, 20
 InsP₃ receptor, 20, 21, 323, 326–330
 Ryanodine receptor, 20–21, 324
- Catecholaminergic polymorphic ventricular
 tachycardia (CPVT), 20, 21, 325,
 331, 387–399, 549
- Catecholamines, 50–56, 527–529, 533
- Ca transient, 255, 257, 258, 260–263
- Ca²⁺ transient, 46, 48, 53–55, 57
- Cav1.2, 9, 20, 198, 201, 204, 205, 219, 225,
 226, 354, 399, 437, 633
- Cav1.3, 9, 10, 201, 219, 221, 467
- Cav3.2, 10, 198, 201, 202, 205, 633
- Caveolae, 5, 62, 65–66, 481, 547, 586, 589
- Caveolin 3, 65–66, 481
- CAVIN, 481
- Cell cycle, 365, 368, 376
- Cell signalling pathway, 187–189
- Channel-blocking effects, 431
- Channelopathies, 7, 22, 388, 403, 414, 432,
 455, 473, 656, 658
- CICR, 86, 93, 187
- Cilobradine, 69, 71
- Cl channels, 17, 18
- C-linker, 62, 65
- Clonidine, 69
- Closed state, 415, 416
- Closed-state inactivation, 416
- Collateralization, 532
- Commotio cordis* (CC), 139–141, 143, 145
- Conduction, 368–373
 failure, 511
 system cells, 234
 velocity, 504, 506, 512
- Conduction system cardiomyocytes
 cardiac neural crest, 237–238
 cellular origin, 237–238
 Purkinje network, 238
- Congestive heart failure (CHF), 12, 20,
 140, 323, 344, 345, 358,
 548–551, 588
- Connexin (Cx), 19, 20, 233, 287–288, 296,
 368, 371, 372, 505–507, 513–517,
 519
 half-life time, 19, 507
- Constant field approximation, 40
- Contraction, 337, 338, 340
- Control, defibrillation, 279–280
- Coronary artery disease (CAD), 71
- Coupled system, 96
- Coupling, 103, 107, 108, 113–115
 capacitive, 509, 510
 ephaptic, 509–510
 gap junction, 504, 510–512
- Coupling-clamp, 107–109, 114
- Current-clamp, 102–105, 107, 108, 111, 112
- Current decay, 411, 412, 418, 421, 422
- Cx37, 505, 508
- Cx40, 19, 371, 505, 507, 508, 510,
 514–517
- Cx40, 233, 234, 237, 238, 240, 242–244,
 247
- Cx43, 19, 233, 288, 371, 372, 503–506, 508,
 510, 512–517, 532–533
 phosphorylation, 531–533
- Cx45, 19, 233, 371, 505, 507, 513, 516, 517
- Cyclic nucleotide binding domain (CNBD),
 16, 62, 72–73
- Cyclopiazonic acid (CPA), 88, 90, 91, 93

D

Delayed afterdepolarization (DAD), 18, 19, 37, 181, 295, 308, 390–394, 400, 549–552, 570, 601, 605

Delayed rectifier

 current, 634
 K⁺ current, 202, 372, 373

Delayed repolarization, 627, 634, 635**Development**, 230–247

Diastolic depolarization (DD), 5, 16, 34–38, 44, 45, 47, 49, 54, 55, 59, 61, 62, 68–70, 73, 84–87, 101, 105–107, 110–113, 115, 136, 138, 140, 200, 215, 232, 557

Diffusion, 270, 271, 274, 277, 278**Digitalis**, 511, 513**Dilated cardiomyopathy (DCM)**, 183

Dispersion, 504, 512, 517, 518, 639, 641, 644

Disturbances of repolarization, 639, 643–645, 647

Drug potency, 617, 629, 630

Dynamic AP-clamp, 107, 108, 111, 112, 115

Dynamic-clamp, 101–115

E

Early afterdepolarization (EAD), 18, 181, 185, 186, 294, 372, 549, 552, 600, 604, 642

Early, first and second-generation model, 177

E-cadherin, 463, 468

Electrical cycle, 3, 5

Electrical inhomogeneity, 532

Electrocardiogram (ECG), 3, 4, 19, 22, 72, 120, 134, 184–185, 217, 220, 235, 295, 388, 402, 416, 432, 435–437, 455, 464, 467, 474–475, 477, 589, 611–612, 627, 632, 639, 652, 656

Embryonic cardiomyocytes, 197–205, 234

Embryonic heart, 231, 233, 235, 237, 238, 242–244

Embryonic stem cell (ESC), 68, 69, 74

Em oscillations, 199, 200, 203

Entrainment, 83–92, 96

Epicardial border zone (EBZ), 313–316, 319, 320

Exchangers

 Na-Ca, 159, 161, 162
 Na-k, 159

Excitation contraction coupling (ECC), 3, 8, 9, 20, 133, 146, 186, 187, 255, 256, 262, 264, 324–327, 351, 354

Excitation-metabolism coupling, 7, 327–328

Excitation-transcription coupling, 7, 21,

329–330

Exploratory safety pharmacology, 634

F

Falipamil, 69

Fendiline, 9

Fiber rotation, 277–279

Fibrillation

 atrial (AF), 11, 12, 14, 16, 19, 20, 72, 140, 183, 241, 245, 339, 358, 414, 421, 432–451, 456–464, 467, 485–496, 504, 514–515, 543, 599–606
 ventricular (VF), 140, 215, 224, 270, 394, 464, 512, 519, 525, 532, 555, 557, 611, 616, 641

Fibroblast, 138, 141

Fibroblast growth factor (FGF), 514

Force-frequency relation, 258, 259, 262

Frontloading, 634

Funny current (I_f), 16, 38, 53, 59–74, 80, 87, 101–113, 158, 163–165, 168–170, 198, 200, 203–205, 225, 232, 293, 370, 552, 633

G

Gain-of-function, 413, 414, 417, 419–423

Gap junction (GJ), 233, 503–519, 525–538
 remodelling, 515, 516

Gap junction channels, 5, 19–20, 114, 503–506

 connexins, 19–20, see also Cx

Gating, 410, 414–418, 420–423

Gene mutations, 431, 432, 438, 439, 443

Genetically modified mice, 473–481

Genetic mutation, 485

Genetic polymorphisms, 124, 126, 486

Genetics, 71, 231–247, 344, 374, 387–403, 414, 415, 431–443, 455, 473, 485–496, 550, 601, 655

GIRK1/GIRK4, 15, 127, 659

GJ uncoupling, 529, 531, 532, 534, 537

Glycoside-related arrhythmogenesis, 432

Goldman-Hodgkin-Katz (GHK) current equation, 40–41

G protein-coupled receptor (GPCR), 94–96

H

HCN4, 16, 63–75, 103–107, 112, 113, 115, 200, 204, 218–219, 232, 238–240, 370, 481

HCN channels, 15, 16, 62–75, 109–111, 200, 222, 232, 293, 370

- cyclic nucleotide binding domain (CNBD), 16, 62, 72, 73
 ivabradine, 16, 68–71
HDAC5, 353, 357
Heart
 development, 72, 201, 236, 367, 372
 disease, 182, 323, 355–359, 374, 399–401, 480, 514, 548, 588
Heart failure (HF), 10–12, 15, 16, 18, 21, 262–263, 355–358, 510, 512, 514–517, 519
 AV node, 220, 221, 226, 227
 Ca^{2+} handling proteins, 220–221
 ion channels, 220, 221, 226
 PR interval, 220, 221
 Purkinje fibres, 220, 221, 226, 227
Heart rate (HR), 4, 16, 19, 56, 61, 69, 71, 127, 133–147, 232, 262, 299, 355, 398, 432, 443, 474–476, 549, 589–590, 601, 643
Heart rate variability (HRV), 119–129
hERG, 12, 66, 204, 373, 433–444, 476, 606, 611–621, 627–635, 644–645, 650–651, 656, 667
 activator, 629
 blocker, 629
 current, 434, 441
Hodgkin-Huxley, 158, 177, 270, 272, 273
Holt-Oram syndrome, 241
HRV
 effect of
 ambient temperature, 123
 circadian autonomic rhythm, 124
 physical training, 124
 postprandial hypotension, 123
 posture, 123, 124
 frequency domain methods, 121
 frequency domain parameters, 122, 124
 nonlinear methods, 120, 121
 nonlinear parameters (Poincare' plot), 123
 parameters, 122, 127
 time domain methods, 119, 120
 time domain parameters, 122, 124
Human embryonic stem cells, 374
Human ESc-derived cardiomyocytes, 204
Hyperpolarization-activated Cyclic Nucleotide-gated (HCN), See HCN channels
Hypertrophy, 10, 11, 14, 17, 18, 21, 61, 136, 263, 284–300, 323, 325–330, 341, 343, 357–358, 368, 369, 480, 495, 510, 515–516, 546–547, 550, 565, 587–588
I
 I_{CaL} , 9, 10, 34, 37, 45–46, 52, 86–88, 101, 109, 163–165, 185, 198, 200–201, 203–205, 219, 225, 256–263, 272, 290, 307–309, 313, 375, 400, 433, 452, 633
 I_{CaT} , 10, 38, 46, 163–168, 190, 198, 201–202, 204, 205, 218, 225, 290, 295, 299, 308, 633
ICH S7A, 634
ICH S7B, 633
 I_f , See Funny current
IFM motif, 410, 415
Ignition, 86, 87
 I_K
 components, 159, 161, 163–166, 169
 sinus, 158, 159, 170
 $I_{\text{KACH}}/I_{\text{K,ACH}}$, 15, 95, 101, 127, 128, 164–166, 203, 220, 225, 599–605
Inactivation gate, 410, 415, 416, 418, 422
 I_{NCX} , 198, 202, 205
Induced pluripotent stem cells, 374
Inhibitor, 657, 658, 665
Inhomogeneities
 conduction, 275–277
 ionic, 275–277
Inositol 1,4,5 trisphosphate (InsP3/IP3) receptor, 20, 21, 312, 316, 324, 326–327, 329–330, 462–463, 466, 467
Instability, 639, 641, 642, 644–646, 651
Intercalated disc, 8, 19, 353, 462, 467, 468
Intracellular Ca^{2+} handling, 323–331
Inward rectifier K⁺ current, I_{K_1} , 14–15, 41, 111, 158, 181, 220, 272, 353, 355, 368, 436, 488, 599, 602
Ion channels, 5–22, 36, 40, 67, 84, 105, 144, 166, 177, 181–183, 186, 189, 205, 218, 220–221, 226, 232, 263, 270, 285, 307, 316, 325, 331, 357, 370, 387, 430, 438, 455, 462, 464, 475–476, 480–481, 485, 487, 488, 492, 543, 571, 589, 599–606, 628–636, 655–660
 density heterogeneity, 182
 gene mutations, 431, 438
 I_{CaL} , See ICaL
 I_{CaT} , See ICaT
 I_f , See Funny current
 I_{Na} , 7–8, 158, 176, 184, 204, 219, 225, 258, 287, 288, 290–292, 410–412, 468, 549, 552, 604, 650
K_{ATP}, See ATP-dependent K channel (KATP)

- I**
- Ion channels (*cont.*)
 - K_v, 10–12, 74, 176, 218–221, 292–293, 476, 564, 613, 618
 - mislocation, 480–481
 - mutation, 487, 490
 - Ion channels/Ionic currents
 - Ca_v1.2 , Ca_v1.3 (I_{CaL}), 9–10, 218, 219, 221, 225
 - Ca_v3.1, Ca_v3.2, Ca_v3.3 (I_{CaT}), 10, 219
 - ERG (I_{Kr}), 12, 218, 220, 221, 225, 226
 - HCN1, HCN2, HNC4 (I_f), 16, 219
 - K_{ir}2.1 (I_{K1}), 14, 41, 111, 218, 220, 225, 226
 - K_{ir}3.1, K_{ir}3.4 (I_{KACH}), 15, 203, 220, 601
 - K_v1.5 (I_{Kur}), 11, 218, 220, 221, 225, 226, 292, 480, 488, 602
 - K_v1.4, K_v4.2, K_v4.3 (I_{to}), 11–12, 104, 218, 219, 225
 - K_vLQT (I_{KS}), 12, 204, 218, 220, 225, 226, 287, 435, 455
 - Na_v1.1, Na_v1.5 (I_{Na}), 7–8, 218, 225, 355, 409–422, 462, 467–468, 589
 - Ischemia, 507, 511–515, 517–519, 525–538
 - acute, 511–513, 518
 - chronic, 512–514
 - Ischemia-reperfusion, 15, 20–21, 328, 339, 340, 343, 344, 517, 552–555
 - Ischemic heart disease (IHD), 69, 323, 343, 552–555
 - Ischemic preconditioning, 344, 529, 531
 - Isoprenaline (ISO), 50–52, 55, 56, 256–263
 - Ivabradine, 16, 68–71
- K**
- K (potassium) channels, 10–15, 143, 294, 455, 488, 657
 - Ca-activated (K_{Ca}), 10, 12–13, 21, 495, 606
 - inwardly rectifying (K_{ir}), 10, 14–15, 176, 203–205, 218, 221, 225–226, 351, 368, 436–438, 488, 569, 583, 586, 601, 602, 613, 633, 656, 663
 - K_v channels, See under Ion channels
 - Na-activated (K_{Na}), 10, 12–13
 - two pore (K_{2P}), 13–14, 19, 605
 - KCNE1, 452–456, 476–477, 480
 - KCNE2, 480. *See also* MiRP1
 - KCNH2, 464
 - KCNQ1, 12, 51, 188, 414, 422, 435–436, 452–457, 464, 476, 478, 480, 487–489, 616, 656, 661, 663
 - KCR1, 65–67
 - Knockout
 - conditional, 72
 - inducible, 72
- L**
- ΔKPQ, 183–185
 - K_v1.5, 11, 476, 478, 480
 - K_v4.2, 12, 476, 480
- M**
- Late diastolic Ca²⁺ elevation (LDCAE), 85, 86, 88, 92, 95
 - Lateralization, 510, 514–516
 - Lead potential (V_L), 33–57
 - Leptin receptor, 128
 - Lipid rafts, 65
 - Local Ca²⁺ releases (LCR), 85–88, 91–95
 - Long QT syndrome (LQT), 4, 8, 9, 12, 14, 183, 186, 188, 315, 355, 388, 399, 409–423, 434–435, 455, 464, 465, 656–658, 619–621, 661–662 variant, 452
 - Looping, heart tube, 235–241
 - L-type Ca channels (LTCC), 9, 30, 86, 91, 92, 127, 165, 185–188, 200–201, 255–257, 261–263, 285, 307, 329, 337–340, 345, 353–354, 358, 399–400, 437, 544, 570, 601, 616, 633, 663
 - L-type Ca current (I_{CaL}/I_{Ca,L}), 9, 34, 52–54, 86–87, 109, 163, 165–166, 176, 200–201, 207, 218, 224–225, 256, 263, 289–290, 307–308, 313, 370, 375, 400, 433, 451, 601, 633
 - Luo–Rudy models, 180–181
 - Luo–Rudy phase I, LRI, 271, 273, 274, 277, 279–281
- M**
- Magnesium, 298
 - Manual patch clamp (MPC), 628–631
 - MAP kinase, 341, 343
 - Mathematical modelling, 211, 226–227
 - Mechano-electric feedback (MEF), 17, 133–147
 - MEF2-dependent gene transcription, 357
 - Membrane clock (M clock), 83, 94
 - Mesenchymal stem cell (MSC), 74
 - Microdomains, 62, 65, 67
 - MicroRNA, 365–377
 - miR-1, 367–368, 371–373, 375–377
 - miR-133, 367–370, 372, 373, 376
 - miR-499, 376–377
 - MiRP1, 65–67
 - Mitochondria, 323, 324, 326–328, 331
 - Mitochondrial channels, 7, 18, 21, 22
 - Mode 2 gating, 358
 - Model
 - AV node, 155, 156, 169

- cardiac rhythm, 155, 170
experiment, 155, 158, 161, 162,
164–166, 168, 170
historical development, 156
NCX, 159–161, 164
relaxation oscillator, 155, 158
Model-clamp, 107–111, 114
M₂R, 15, 94, 95
Multichannel block, 635
Murine ESc-derived cardiomyocytes, 203–204
Mutant ion channel, 183
Mutation, 485–490, 492, 494–496
missense, 72, 73
point, 73
Myocardial infarction (MI), 11, 18, 119, 125,
126, 314–317
Myocardial ischemia and infarction, 355,
357, 358
- N**
Na-Ca exchange (NCX), 86–89, 93, 159–161,
164, 255–258, 260–263, 432
Na⁺/Ca²⁺ exchanger, 337–340, 354, 462,
463, 466, 467
Na channels, 7–8, 135, 176, 182, 409–423, 462,
468, 487–489, 508, 604, 642, 657
Na⁺-H⁺ exchanger (NHE), 337, 338, 342–343
Na⁺/K⁺-ATPase, 159, 337, 338, 340, 341,
343–345, 462, 463, 466, 467
Na_v1.5, 8, 219, 225, 353, 355, 358, 409–423,
467–468, 589, 634
N-cadherin, 468
NCX1, 198, 202, 205
Nernst equation, 35
Network, 156, 163
Nifedipine, 9, 570
Nitric oxide, 528, 533
N588K
amino-acid mutation, 433, 434, 438,
439, 441
hERG mutation, 434, 435, 438–442
Nkx2-5
NMDA receptor, NR2B subunit, 354
Nonequilibrium gating, 186
Non-ion channel, 485, 487, 488, 490
Non-uniformity, 510–511
Nuclear ion channels, 21, 331
Nucleus, 323, 324, 329–331
Numerical modeling, 83, 86, 96
- O**
Obscurin, 462, 463
Occlusion, coronary artery, 307, 525–537
- Ohm's law, 40
Open-state inactivation, 418, 420, 423
Oscillations, calcium, 158, 159
- P**
Pacemaker
biological, 73–74
cells, 3, 6, 17, 33, 48, 50, 87, 114, 134–136,
165, 176, 202, 232–234, 369, 546,
573
electronic, 73
gene program, 240
myocardium, 234, 246, 247
potential, 5, 9, 33, 158, 215, 238, 246
system cells, 234
Pacemaker activity, 7, 16, 19, 20, 33–56,
67–71, 101–115, 159–166, 197–205,
219, 221, 227, 375, 552, 573
adrenergic, 165
cholinergic effects, 165
PDE, 92, 94, 95
Peptide, antiarrhythmic, 507, 512,
517–519
Peripheral ventricular conduction system,
236, 243
development, 243–244
endothelin, 244
neuregulin signaling, 244
Purkinje network, 243
signaling, 244
trabecular myocardium, 243–244
Persistent current, 413, 417–421, 423
Phase 1A arrhythmias, 525–528
Phase 1B arrhythmias, 527–534, 536, 537
Phosphatidylinositol 4,5-bisphosphate
(PI(4,5)P₂), 65
Phospholamban (PLB), 255, 261, 262,
353–355
Phosphorylation, 84, 91–96, 261, 262
Pitx2c, 239, 240
PKC, 504, 507, 508, 517
Plasma membrane Ca²⁺ ATPase, 341
Pluripotent stem cell derived cardiomyocytes,
375
Polymorphisms, 486, 491–493
Population patch clamp (PPC), 630
Positive chronotropy, 50–56
PR interval, 3, 4, 217, 219–221, 373, 474,
495, 633
Precordial thump (PT), 144–146
Primary ventricular cardiomyocytes, 475
Primitive myocardium, 234, 244, 247
Proarrhythmia, 639–653

- Progressive cardiac conduction defect (PCCD), 183
- Propagation, 3, 73, 182, 232–235, 242, 274, 278, 287, 353, 371, 375, 409, 474–477, 503–519, 528, 550
SA to AV nodes, 169–170
- Protein kinase, 260–261
- Protein kinase A (PKA), 50–53, 55, 57, 91–96, 339
- Protein kinase C (PKC), 340
- Protein phosphatase 2A (PP2A), 358, 462, 463
- Purkinje, 155, 156, 158, 161, 168, 169
human, 156, 168
Markov, 168
ventricle junction, canine, 169
- Purkinje cells, 176, 244, 287, 306–312, 320, 392, 570, 613
- Purkinje fibres, 3, 6, 8, 10–12, 14, 16–18, 20–21, 60, 69, 109, 140, 155, 168, 178–211, 221–227, 232, 238, 242, 287, 327, 370, 373, 439, 451–452, 474, 503, 549, 556, 589
- Cx40, 222, 224
left bundle branch, 215, 221, 222
network, 234, 238, 307, 393
right bundle branch, 222
terminal, 211, 213, 221
- Q**
QRS, 3, 184, 217, 235, 373, 397, 475, 633, 646
- QT interval, 4, 186, 294, 396, 399, 403, 410, 416, 421, 431–443, 455, 464–465, 474, 611, 616, 633, 639, 646, 656–658, 663
- QT variability (QTV), 125–127
- R**
Reactive oxygen species, 358, 359
- Receptors
β-adrenergic (β -AR), 61, 73
muscinic, 61, 65
- Reduced Priebe-Beuckelmann (RBP) model, 271, 277
- Reentry (re-entry), 143, 216, 270, 288, 403, 488, 526–528, 543, 641–643, 646
- Relative contribution (rc), 43, 45
- Remodeling, 357, 358
- Respiratory sinus arrhythmia (RSA), 119, 134, 135, 138
- Reverse use dependence, 643, 644, 646
- R1135H mutation, 435
- Rotigaptide, 507, 513, 517, 530, 533
- R-type Ca channels, 10, 21
- Rubidium flux, 632
- Ryanodine, 20, 88–91, 95, 306, 328
- Ryanodine receptors (RyRs), 20, 21, 46, 84–86, 88, 90, 92–95, 186–188, 220, 255, 257, 261–263, 305–307, 312, 324–325, 353–355, 357, 370, 388, 389, 391–394, 399, 544, 546, 551–554
- S**
Safety factor, 511
- Safety index, 648–649
- SAP97, 65–67
- Sarcolemma (SL), 5, 7, 8, 13–16, 18–22, 337–345
- Sarcoplasmic reticulum (SR), 5, 7, 20–22, 46, 48, 51, 55, 255, 257, 258, 260–263, 323–331, 337–340, 345
 Ca^{2+} ATPase, 337
InsP₃/IP₃ receptor, 20, 21, 316, 323–324, 326–327, 462–463, 466, 467
- Ryanodine receptor, See Ryanodine receptor (RyRs)
- SCN5A, 8, 176, 183, 204, 355, 402, 409, 414–417, 420, 421, 464, 468, 478, 481, 488–489, 495, 616, 656, 657
- SERCA, 84, 86, 91–93, 323–327, 330, 331.
See SR Ca ATPase
- Short QT syndrome (SQTS), 12, 451, 456
long, 431, 432, 434, 435, 443
shortened interval, 431, 432, 435, 437, 439, 443
treatment, 439–442
- Shox2, 240
- Sick sinus syndrome (SSS), 8, 16, 95, 183, 414, 465, 468, 496
- Signaling
calcineurin, 299–300
JAK-STAT, 300
MAP kinases, 286
PKC isoforms, 287
Ras, 300
- Simulations, 46, 88–91, 93–95, 107, 112, 170, 175–189, 216, 273–280, 314, 439, 457, 510
- Sinoatrial node (SAN), 3, 6–12, 15–17, 19, 20, 57, 59, 64, 83, 104, 109–115, 127, 134–139, 146, 155, 159, 163–166, 168, 176, 232–234, 240, 354, 355, 465–467, 474, 494

- cell (SANC), 33–36, 38, 42, 46, 48, 50, 55, 57, 83–96
 central, 19, 69, 159, 165, 167, 168
 contraction model, 51, 166
 development, 232, 240
 formation, 239, 240
 heterogeneity, 165, 168, 169
 I_f , See Funny Current
 I_K , 159, 163–166
 I_{Kr} , 165–170
 I_{st} , 165, 166, 168, 170
 I_{sus} , 165–169
 model, 33, 38, 45, 50, 51
 pacemaker activity, 16, 19–21, 35–56, 67–69, 71, 101–115, 159, 238–239, 552
 peripheral, 19, 159, 165, 167, 168
 potential, 33, 34, 36, 38
 primordium, 239, 240
 rhythm, 20, 70, 170, 216, 222, 600, 602, 604–605, 611, 646
- Sinus**
 node, 232–233, 236–240
 node development, 238–240
 pauses, 72, 616
 venous, 67, 85, 235, 238–240, 244, 246
- Sinus node dysfunction (SND)**, 72, 128, 465, 467
- Sodium channel (Na^+ channel/NaV)**, 7–8, 157, 183, 218–219, 225, 353–355, 409–423, 462, 468, 487–490, 580, 633, 642, 651
- Source-sink-problem**, 511
- Spectrin**, 463
- SQT1 and KCNH2**, 433–435
- SQT3 and KCNJ2**, 436–438
- SQT2 and KCNQ1**, 435–436, 438, 442
- SQT4 and SQT5**, 437–438
- SQTS**, treatment, 439–442
- SR Ca ATPase**, 255, 256, 261–263
- SR Ca^{2+} ATPase (SERCA2a)**, 353, 354
- SR Ca^{2+} release channels**, 323–325
- Sterol regulatory element binding protein-1 (SREBP-1)**, 127
- Store operated Ca^{2+} channel (SOCC)**, 17, 337, 338, 340–341, 344, 345
- Stretch-activated channels (SAC)**, 18–19, 133, 136–147, 569
- cation non-selective (SAC_{NS}), 136–138, 142, 143, 146
 - potassium-selective (SAC_K), 142, 143
- Strophantidin**, 260
- Structure agonist**, 660, 664
- Structure inhibitor**, 658, 665
- Subsarcolemmal**
 cisterna, 46
 space, 46
- Sudden cardiac death (SCD)**, 12, 465
- Sympathovagal drive**, 120
- Synchronization**, 102, 103, 107, 109, 113–115
- Syncope**, 72, 183, 339, 388, 395–398, 402, 432, 435, 455, 465, 656, 657
- T**
- Tail current**, 103, 202, 439, 454, 615, 629
- Tbx2***, 240–244
- Tbx3***, 68, 237, 239–244, 246, 247
 knock-out embryos, 243
- Tbx5***, 241–243
- Tbx18/Tbx18⁺***, 68, 238–240
- Tbx20***, 241
- TdP**, See Torsades de pointes
- Thallium flux assay**, 632
- Three-dimensional (3D) slab**, 269, 277
- Timothy syndrome**, 9, 388, 399–401, 403
- TNNP**, 271–281
- Torsades de pointes (TdP)**, 12, 400, 416, 431, 455, 616, 619, 639, 640, 642, 644–647, 652
- Transcriptional regulation**, 238–245
- Transcriptional repressors**, 244, 245, 247
- Transient outward K^+ current (I_{to})**, 11–12, 163–170, 176, 202, 204, 219, 225, 272, 287–288, 319, 355, 373, 377, 476, 480, 552, 599, 602, 611–612, 633, 658, 662
- $I_{to,fast}/I_{to,f}$, 12, 292, 355, 476, 480
- Transverse (t-) tubules**, 8, 9, 12, 18, 20, 46, 234, 255–264, 305, 316, 353, 375, 389, 462, 467, 589
- TRIAcD**, 639, 643–653
- Triangulation**, 635, 639, 642–645, 651
- Triggered activity**, 181, 183
- TRP channels**, 17, 19, 86, 340, 564–575, 605–606
- store operated Ca channel (SOCC), 17
- T-tubule membranes**, 467
- T-wave**, 4, 18, 140, 143, 184, 432, 436–439, 464, 467, 474, 644
- morphology, 432, 437, 439
 - over-sensing, 439
- Two-dimensional (2D) sheet**, 269, 274
- Type 4 long QT syndrome (type 4 LQTS)**, 464

U

Uncoupling, 526, 528, 529, 531, 532, 534, 536, 537
Upstroke, 5–9, 37, 86, 137, 164, 177, 181, 222, 226, 227, 287, 355, 409, 511, 527, 599, 651

V

Veins, pulmonary, 515
Ventricular arrhythmias, 10, 12, 14, 19, 61, 126, 176, 224, 298, 307, 327, 357, 388, 397, 432, 433, 438, 439, 464, 465, 467, 468, 513, 525–538, 543–557, 611
Ventricular conduction system, 234–236, 242, 243
Ventricular fibrillation (VF), 18, 140–146, 215, 224, 270, 394, 397, 435, 443, 464, 512, 517, 525, 532, 555, 611, 616, 639–642, 644–648
Ventricular premature beats (VPB), 532, 536
Ventricular refractory period, 432, 434, 438
Ventricular repolarisation, 432–436, 438

Ventricular tachycardia (VT), 16, 20, 72, 127, 140, 144–146, 188, 270, 296–297, 325, 387–398, 431, 437, 439, 516, 549, 555, 640, 641, 644–647, 662

Verapamil, 9, 635

Voltage-clamp, 103–108, 111, 112

Voltage-Gated K^+ (potassium/ K_V) channels, 10–12, 74, 176, 204, 218–219, 225, 292, 353, 373, 435, 476–477, 488, 564, 601, 613–618, 633, 656

Voltage-gated Na^+ (Na_V) channels, See Sodium channel

W

Wenckebach, 181
Window current, 38, 411–413, 420–422

Y

Yotiao (AKAP9), 453, 455

Z

Zatebradine, 68–70
ZD7288, 68, 71, 74
ZP123, 513